INAUGURAL – DISSERTATION

zur Erlangung der Doktorwürde der
Naturwissenschaftlich-Mathematischen
Gesamtfakultät der
Ruprecht-Karls-Universität
Heidelberg

vorgelegt von
Dipl.-Chem. Regina Berg
aus Hüttenfeld

Ausgeführt am Organisch-Chemischen Institut
der Ruprecht-Karls-Universität Heidelberg
unter der Betreuung von Prof. Dr. Bernd F. Straub

Tag der mündlichen Prüfung: 27. Juni 2013

Highly Active Dinuclear Copper Catalysts for Homogeneous Azide-Alkyne Cycloadditions

Gutachter:

Prof. Dr. Bernd F. Straub

Prof. Dr. Oliver Trapp

It is better to light a candle
than to curse the dark.

(Chinese proverb)

Danksagung

Herrn Professor B. F. Straub danke ich herzlich für die interessante und herausfordernde Themenstellung sowie die hervorragende fachliche Betreuung.

Der Studienstiftung des deutschen Volkes danke ich für ein Promotionsstipendium, das neben finanzieller auch wertvolle ideelle Förderung beinhaltete.

Ich möchte mich bei den Mitarbeitern in den analytischen Abteilungen der Chemischen Institute an der Ruprecht-Karls-Universität Heidelberg für die Aufnahme zahlreicher MS-, NMR- und IR-Spektren sowie für Elementar- und Röntgenstrukturanalysen bedanken.

Meinen Laborpartner(inne)n und Kolleg(inn)en aus dem Arbeitskreis danke ich für die freundliche Atmosphäre und die zahlreichen Gespräche.

Meinen beiden Forschungspraktikanten, Lena Hahn und Steffen Mader, sowie der Bachelor-Absolventin Christine Dietrich danke ich für ihr großes Interesse und die gute Zusammenarbeit.

Den zuverlässigen Korrekturlesern dieser Arbeit, Volker Berg, Janina Bucher, Daniel Hack und Achim Häußermann, danke ich für ihre Gewissenhaftigkeit und konstruktive Kritik.

Während der vergangenen Jahre war ich besonders dankbar für die Unterstützung, die ich durch meine Freunde erfahren habe. Ich danke daher denjenigen, die für mich da waren, wenn es mal nicht so gut lief, und mit mir Spaß hatten, wenn es etwas zu feiern gab. Ich danke besonders auch denjenen Freunden, die aus der Ferne, sei es aus Berlin oder Brisbane, Hamburg oder Freiburg, guten und regelmäßigen Kontakt gehalten haben. Danke!

Einen besonderen Dank möchte ich meinen Eltern Doris und Klaus-Rainer sowie meinen Brüdern Volker und Frank aussprechen. Ohne Eure Unterstützung wäre das alles nicht gegangen.

Table of Contents

Abbreviations

a	crystallographic *a*-axis of the unit cell
Å	Ångström (10^{-10} m)
AAC	azide-alkyne cycloaddition
Ac	acetyl group, $H_3C_2O_2$
aq.	aqueous
Ar	aryl group
ATRP	atom transfer radical polymerization
b	crystallographic *b*-axis of the unit cell
br	broad signal
BCN	bicyclo[6.1.0]nonyne derivatives
$(BimH)_3$	[tris(2-benzimidazolyl)methyl] amine, $C_{24}H_{21}N_7$
Bn	benzyl group, C_7H_7
Boc	*tert*-butyloxycarbonyl group, $C_5H_9O_2$
$(Bth)_3$	[tris(2-benzothiazolyl)methyl] amine, $C_{24}H_{18}N_4S_3$
c	crystallographic *c*-axis of the unit cell
C	Celsius
cat.	catalytic
CCD	charge-coupled device
COD	cyclooctadiene, C_8H_{12}
COSMO	Conductor-like Screening Model
CPCM	Conductor Polarized Continuum Model
CuAAC	copper-catalyzed azide-alkyne cycloaddition
Cy	cyclohexyl group, C_6H_{11}
$C18_6tren$	tris(2-dioctadecylaminoethyl) amine, N^1,N^1-bis(2-(dioctadecylamino)-ethyl)-N^2,N^2-dioctadecylethane-1,2-diamine, $C_{114}H_{234}N_4$
d	day
d	doublet
dba	dibenzylideneacetone, $C_{17}H_{14}O$
DCM	dichloromethane, CH_2Cl_2
dd	double doublet
D_e	bond-dissociation energy
deg	degrees
DFT	Density Functional Theory

DIBO	dibenzocyclooctynol derivatives
DIFO	difluorinated cyclooctyne
DIMAC	dimethoxyazacyclooctyne, $C_{11}H_{15}NO_3$
Dipp	2,6-diisopropylphenyl group, $C_{12}H_{17}$
DIPEA	*N,N*-diisopropylethylamine, $C_8H_{19}N$
DMF	*N,N*-dimethylformamide, C_3H_7NO
DMSO	dimethyl sulphoxide, C_2H_6OS
DNA	deoxyribonucleic acid
dppe	1,2-bis(diphenylphosphino)ethane, $C_{26}H_{24}P_2$
e	elementary charge
EA	elemental analysis
ECP	effective core potential
EI	electron impact
ESI	electrospray ionisation
Et	ethyl group, C_2H_5
et al.	*et alii*, and others
f	response factor
F	crystallographic structure factor
FAB	fast atom bombardment
FG	functional group
FID	flame ionization detector
Fmoc	9-fluorenylmethoxycarbonyl group, $C_{15}H_{11}O_2$
FT	Fourier transform
g	gram
G	Gibbs free energy
GC	gas chromatography
GC-MS	gas chromatography with mass spectrometry
Gly	glycine, $C_2H_5NO_2$
h	hours
h	crystallographic Bragg index *h*
H	enthalpy
HIV	human immunodeficiency virus
HIV-1 PR	human immunodeficiency virus protease
HMBA	4-hydroxymethylbenzoic acid, $C_8H_8O_3$

HMBC	heteronuclear multiple-bond correlation spectroscopy
HSQC	heteronuclear single quantum coherence spectroscopy
Hz	Hertz
ICy	1,3-bis(cyclohexyl)-imidazol-2-ylidene, $C_{15}H_{24}N_2$
I effect	inductive effect
Im	imidazole, $C_3H_4N_2$
IPr	1,3-bis(2,6-diisopropylphenyl)-imidazol-2-ylidene, $C_{27}H_{36}N_2$
^{i}Pr	isopropyl group, C_3H_7
IR	infrared spectroscopy
J	coupling constant
k	crystallographic Bragg index *k*
K	Kelvin
K	equilibrium constant
l	litre
l	crystallographic Bragg index *l*
LDA	lithium diisopropylamide, $C_6H_{14}LiN$
LCAO	linear combination of atomic orbitals
lit.	literature
M	molarity, 1 M = 1 mol l^{-1}
M	chemical formula weight
m	medium intensity
m	*meta*-
max.	maximum
min	minute
min.	minimum
m/*z*	mass/charge
Me	methyl group, CH_3
M effect	mesomeric effect
Mes	mesityl group, 2,4,6-trimethylphenyl group, C_9H_{11}
MHz	Megahertz
ml	millilitre
mmol	millimol
MO	molecular orbital
MOFO	monofluorinated cyclooctyne

MS	mass spectrometry
n	integer number
NBO	Natural Bond Orbital
NBS	*N*-bromosuccinimide, $C_4H_4BrNO_2$
^{n}Bu	*n*-butyl group, C_4H_9
NHC	*N*-heterocyclic carbene
NMR	nuclear magnetic resonance
NMP	*N*-methylpyrrolidone, C_5H_9NO
NOE	Nuclear Overhauser Effect
NPOE	1-(2-nitrophenoxy)octane, $C_{14}H_{21}NO_3$
o-	*ortho*-
p-	*para*-
p	pressure
PBF	Poisson Boltzmann finite element method
PEGA	poly[acryloyl-bis(aminopropyl)polyethylene glycol]
Ph	phenyl group, C_6H_5
Phe	phenylalanine, $C_9H_{11}NO_2$
phen	1,10-phenanthroline, $C_{12}H_8N_2$
PMDETA	*N*,*N*',*N*''-pentamethylethylenetriamine, $C_9H_{23}N_3$
Pov-ray	Persistence of Vision Raytracer
ppm	parts per million
Py	pyridine, C_5H_5N
$(Py)_3$	tris(2-pyridylmethyl) amine, $C_{18}H_{18}N_4$
pybox	bis(oxazoline) ligand with a pyridine linker
R	alkyl group
R	crystallographic reliability factor
R^2	coefficient of determination
RAFT	reversible addition-fragmentation chain transfer
RDS	rate-determining step
RT	room temperature
s	singlet
s	strong intensity
s	selectivity factor
S	entropy

SCFE	self-consistend field energy
sept	septet
SIPr	1,3-bis(2,6-diisopropylphenyl)-imidazolin-2-ylidene, $C_{27}H_{38}N_2$
stoich	stoichiometric
t	triplet
T	temperature
TBTA	tris[(1-benzyl-1*H*-1,2,3-triazol-4-yl)methyl] amine, $C_{30}H_{30}N_{10}$
^{t}Bu	*tert*-butyl group, C_4H_9
TCEP	tris(carboxyethyl)phosphine, $C_9H_{15}O_6P$
THF	tetrahydrofuran, C_4H_8O
TMEDA	tetramethylenediamine, $C_6H_{16}N_2$
TMS	tetramethylsilane, $C_4H_{12}Si$
TMS	trimethylsilyl group, $Si(CH_3)_3$
Tol	4-tolyl group, C_7H_7
tot	total
t_R	retention time
TRIP	2,4,6-triisopropylphenyl group, $C_{15}H_{23}$
TTTA	tris{[1-(*tert*-butyl)-1*H*-1,2,3-triazol-4-yl]methyl} amine, $C_{21}H_{36}N_{10}$
U	internal energy
V	volume
w	weak intensity
WCA	weakly coordinating anion
wR	weighted *R*-factor
X	halogen atom
Xyl	3,5-xylyl group, 3,5-dimethylphenyl group, C_8H_9
Z	number of formula units in the primitive cell
ZPE	zero point energy
α	angle α of the crystallographic unit cell
β	angle β of the crystallographic unit cell
γ	angle γ of the crystallographic unit cell
δ	chemical shift
λ	wave length
μ	absorption coefficient
σ	standard deviation

1 Abstract

The copper-catalyzed azide-alkyne cycloaddition for the synthesis of 1,4-disubstituted 1,2,3-triazoles (CuAAC) is a variant of Huisgen's 1,3-dipolar cycloaddition which disburdens the thermal reaction from its major drawbacks such as poor regioselectivity, long reaction times and harsh conditions. In contrast to the widely used "black box" reagent mixtures, a molecularly defined, highly active catalyst system for homogeneous CuAAC reactions has been developed in this PhD project. In dependence on the postulated stepwise mechanism, its most important structural feature is the presence of two copper(I) ions irreversibly bound in the same catalyst molecule.

A highly modular and profitable synthesis for bistriazolium hexafluorophosphate salts as precursors for the ancillary ligand system was devised. In analogy to the CuAAC catalyst systems of general formula $[(NHC)_2Cu]PF_6$ described in literature, novel dinuclear copper(I) complexes with a bistriazolylidene ligand backbone and 1,3-bis(2,6-diisopropylphenyl)-imidazol-2-ylidene (IPr) as sacrificial ligand were prepared.

However, these complexes did not show the expected high catalytic activity, most probably due to the strong coordination of the IPr ligands. In consequence, another family of dinuclear copper(I) complexes with μ-coordinated acetate as labile ligand was synthesized by reaction of the bistriazolium hexafluorophosphate ligand precursors with copper(I) acetate in the presence of a base.

The broad applicability and high catalytic activity of one of these bistriazolylidene dicopper acetate complexes was confirmed by a series of gaschromatographically monitored CuAAC reactions in different solvents and with various substrates. The order of reaction with respect to the initial concentration of the precatalyst was investigated by determination of the half value periods of reactions with different concentrations of the dinuclear copper acetate complex. The results of these kinetic experiments with phenylacetylene and ethyl propiolate were rationalized by postulating different catalyst resting states and rate-determining steps in dependence on the properties of the alkyne substrate.

Kurzzusammenfassung

Durch den Einsatz eines Kupferkatalysators in der Azid-Alkin-Cycloaddition zur Synthese von 1,4-disubstituierten 1,2,3-Triazolen (CuAAC-Reaktion) werden die schwerwiegenden Nachteile der thermischen 1,3-dipolaren Cycloaddition nach Huisgen wie deren geringe Regioselektivität, lange Reaktionszeiten und harsche Bedingungen aufgehoben. Im Unterschied zu den häufig zum Einsatz kommenden Mischungen aus Ligandenvorläufer und Kupfersalz, bei denen die Struktur der katalytisch aktiven Spezies unklar ist, wurde in der vorliegenden Doktorarbeit ein neues, molekular definiertes Katalysatorsystem entwickelt, welches hohe Aktivität in homogenen CuAAC-Reaktionen zeigt. Mit Blick auf den postulierten schrittweisen Mechanismus dieser Reaktion ist das entscheidende strukturelle Merkmal der neuen Katalysatoren die Anwesenheit zweier Kupfer(I)-Ionen, die irreversibel im selben Komplex gebunden sind.
Für die Synthese der Bis-1,2,4-triazoliumhexafluorophosphat-Ligandenvorläufer wurde eine modulare und effiziente Route ausgearbeitet. In Analogie zu den in der Literatur beschriebenen Katalysatorsystemen der allgemeinen Formel $[(NHC)_2Cu]PF_6$ wurden neuartige Bistriazolylidendikupfer(I)-Komplexe mit 1,3-Bis(2,6-diisopropylphenyl)-imidazol-2-yliden (IPr) als sogenanntem „Opferliganden“ hergestellt.
Jedoch zeigten diese Komplexe nicht die gewünschte hohe katalytische Aktivität. Dies lässt sich auf eine zu starke Koordination der IPr-Liganden zurückführen. Daher wurde eine Serie von dinuklearen Kupfer(I)-Komplexen mit μ-koordiniertem Acetat als labilem Liganden synthetisiert, indem die Bistriazoliumhexafluorophosphat-Ligandenvorläufer mit Kupferacetat in Gegenwart einer Base umgesetzt wurden.
Die breite Anwendbarkeit und hohe katalytische Aktivität dieser Bistriazolylidendikupferacetat-Komplexe in der CuAAC-Reaktion wurde mit Hilfe von gaschromatographisch verfolgten Experimenten in verschiedenen Solventien und mit unterschiedlichen Substraten belegt. Die Reaktionsordnung in Bezug auf den eingesetzten Präkatalysator wurde durch Bestimmung der Halbwertszeit von Reaktionen mit verschiedenen Konzentrationen an dinuklearem Kupferkomplex ermittelt. Die Ergebnisse dieser kinetischen Experimente mit Phenylacetylen und Ethylpropiolat wurden unter Annahme unterschiedlicher Katalysatorruhezustände und geschwindigkeitsbestimmender Schritte in Abhängigkeit von den Eigenschaften des jeweiligen Alkin-Substrats erklärt.

2 State of Knowledge

2.1 Click Chemistry

In 2001, Sharpless, Finn and Kolb published a ground-breaking essay reassessing the objectives and methods of organic synthesis.[1] First, the authors point out that bonds between carbon and a heteroatom are much more frequently occurring in nature than carbon-carbon bonds, which is plausible considering that carbon dioxide is nature's main building block and water the reaction medium. The most important structural units, nucleic acids, proteins and polysaccharides, are all condensates of monomers that are linked *via* carbon-heteroatom bonds. With a very limited reservoir of monomeric starting materials, for example the 22 proteinogenic amino acids or the five nucleic acids, a huge spectrum of biopolymers is created mainly by carbonyl chemistry, mostly aldol-type reactions. These are catalyzed by highly selective biopolymers called enzymes and energetically fuelled by the hydrolysis of triphosphates. However, nature had almost infinite resources of time and materials to create this fascinating universe of enzymatically controlled interdependent reaction pathways.

For chemists, who have very limited resources and no home-tailored enzymes to control their reactions, carbonyl chemistry is a very demanding field. On the one hand, there is hardly any thermodynamic driving force in carbonyl chemistry. Most aldol reactions, for example, are very close to equilibrium[2] so that "tricks" such as the azeotropic distillation of the by-product water need to be applied. Only with the advent of kinetically controlled enolate chemistry has aldol chemistry become a powerful and selective synthetic tool. However, the use of strong bases such as lithium diisopropylamide (LDA) necessitates the application of protecting groups for other functional groups. This development turned total synthesis into a complicated business.

Today, there is great competition among chemists for the preparation of complex natural products,[3] especially secondary metabolites, which requires long multi-step syntheses with elaborate protecting group strategies. Based on these observations, Sharpless and co-workers propose a renunciation from this path of applying complicated and long organic syntheses for the preparation of most challenging carbon frameworks, and ask for a return to the basic task of creating new substances with

the desired profile of properties and functions. This is the philosophy that triggered the development of “Click” chemistry.

Click reactions are defined as powerful and reliable transformations that can be easily performed on small and larger scales. A list of criteria for Click reactions is given below.

1) The synthesis should be modular, variable and applicable to a broad range of substrates.
2) Starting materials and reagents should be readily available.
3) The reaction procedures should be easy and not demand the exclusion of air and moisture.
4) Ideally, the reaction should be carried out in an environmentally benign solvent such as water.
5) The time needed to reach completion of the reaction should be short.
6) The transformation should proceed with high regio- and stereoselectivity.
7) If byproducts are formed in small amounts, they should be removable by applying uncomplicated and non-chromatographic methods.
8) The product should be easy to isolate from the reaction mixture, for example by filtration.
9) The yield of the desired product should be very high.
10) Either no purification procedures are necessary or the product can be purified by non-chromatographic methods such as re-crystallization.
11) The product should be stable under physiological conditions.

The fulfilment of many of these requirements is associated with a high thermodynamic driving force of the transformation. Highly exergonic reactions proceed fast and selectively to give only one product. There are four types of reactions that fulfil these criteria:

(I) cycloaddition reactions;
(II) nucleophilic substitutions, especially ring-opening reactions of strained electrophiles such as epoxides or aziridines;
(III) carbonyl chemistry of the non-aldol type, for example condensation reactions to give hydrazones, oximes or aromatic heterocycles;
(IV) additions to C-C multiple bonds, for example epoxidations or dihydroxylations.

These Click transformations are appropriate tools to create “diverse chemical function from a few good reactions”.[1] An example of three subsequent Click reactions for the synthesis of a tricyclic steroid-like scaffold is shown in Scheme 1.

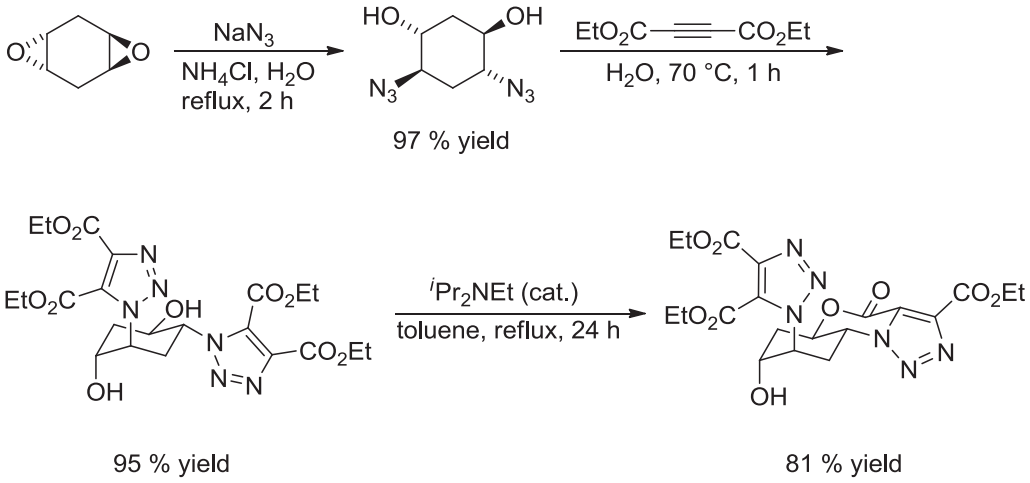

Scheme 1: Assembly of a complex tricyclic steroid-like framework by three subsequent Click reactions.[1]

2.2 From Huisgen’s Azide-Alkyne Cycloaddition to CuAAC

In 1893, Michael discovered a reaction between dimethyl but-2-ynedioate and azidobenzene at 100 °C in a sealed tube and suggested that regioisomeric triazoles were formed.[4] However, it was only in the 1960s that Huisgen recognized this type of reaction for its generality, scope and mechanism.[5] Following his studies of addition reactions between diazoalkanes and ring-strained olefins, Huisgen coined the term 1,3-dipolar cycloaddition. In a 1,3-dipolar cycloaddition, a 1,3-dipole (a-b-c) reacts with a multiple bond system (d-e), the so-called dipolarophile, to form a five-membered heterocycle (Scheme 2).

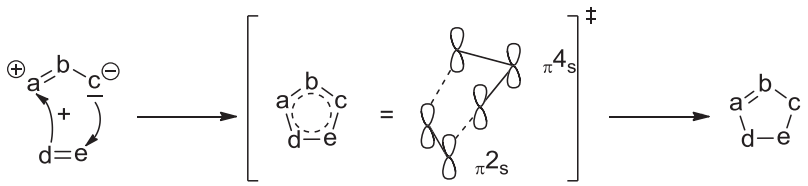

Scheme 2: Schematic representation of a 1,3-dipolar cycloaddition reaction.[5a-c]

1,3-Dipoles are defined as molecules that share four electrons in a π-system over three atoms. A 1,3-dipole a-b-c can be represented by a resonance structure with a positively charged atom a with an electron sextet and a lone pair at the negatively charged terminus c. There are two categories of 1,3-dipoles, *viz.* the bent allyl type dipoles (Table 1) and the linear propargyl-allenyl type dipoles (Table 2).

Table 1: Allyl type 1,3-dipoles.[5a] 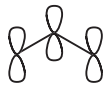

nitrogen as the centre atom

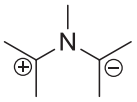 azomethine ylides

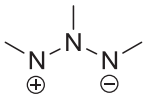 azonium imines

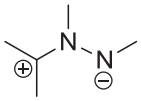 azomethine imines

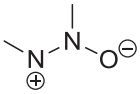 azoxy compounds

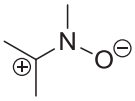 nitrones

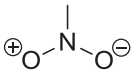 nitro compounds

oxygen as the centre atom

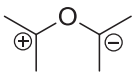 carbonyl ylides

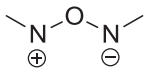 nitrosoimines

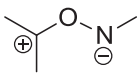 carbonyl imines

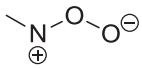 nitrosooxides

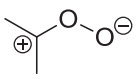 carbonyl oxides

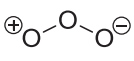 ozone

Table 2: Propargyl-allenyl type 1,3-dipoles.[5a]

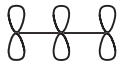

nitrilium betains		diazonium betains	
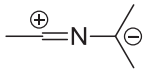	nitrile ylides	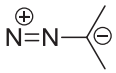	diazoalkanes
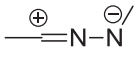	nitrile imines	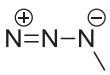	azides
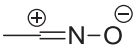	nitrile oxides	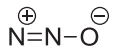	nitrous oxide

Huisgen compared the 1,3-dipolar cycloaddition with other “thermoreorganizations”[6] like the Claisen rearrangement, the Diels-Alder reaction and the Cope rearrangement. At that time, these reactions were known as “no mechanism” reactions because mechanistic studies did not give any results with respect to plausible mechanistic pathways of these transformations:[6] they did hardly respond to changes in the polarity of the medium, no intermediates could be isolated and no catalytic procedure had been developed. Stepwise mechanistic hypotheses were discussed,[7] but soon refuted in favour of a pericyclic concerted pathway (as shown in Scheme 2) by Huisgen and others on the basis of experimental observations[5c] and perturbational calculations.[8] Five criteria to address the question of pericyclic concerted or ionic stepwise mechanism were introduced: 1) influence of the solvent’s polarity on the rate of reaction; 2) stereospecifity in the formation of the product; 3) isolation of intermediates; 4) activation parameters; 5) substituent effects on the rate of reaction.[5c]

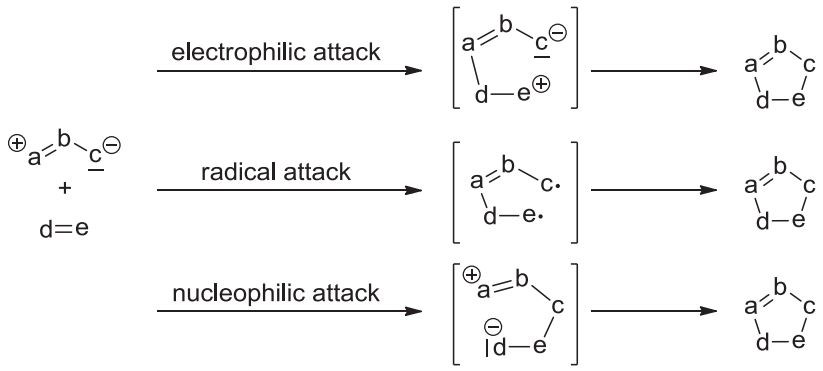

Scheme 3: Proposed mechanistic pathways for 1,3-dipolar cycloadditions that proved to be wrong.

If 1,3-dipolar cycloadditions proceeded by the electrophilic or the nucleophilic two-step mechanism shown in Scheme 3, the reaction should enormously profit from highly polar solvents due to stabilization of the highly polar transition state, as the intermediates are zwitterionic with charges far away from each other. Huisgen compared the dielectric constants of various reaction media with the observed rate constants for the cycloaddition of diphenyldiazomethane with dimethyl fumarate and showed that the choice of solvent did not take any significant influence on the rate of reaction. As for the stereochemistry of the reaction, all three intermediates shown in Scheme 3 allow for rotation around the single bond d-e. Consequently, if one of these proposals were realistic, scrambling could occur and a mixture of stereoisomers would be expected. However, all 1,3-dipolar cycloadditions proceed with the same stereoselectivity, *viz.* strict *syn*-addition of the 1,3-dipole to the dipolarophile. The stereospecifity of the reaction can only be explained by synchronous formation of the two newly generated σ-bonds as shown in Scheme 2. As no intermediates have ever been detected the evident conclusion for Huisgen and co-workers was that there simply are no intermediates in the course of the reaction, *i.e.* the reaction mechanism consists of only one elementary step. By determination of equilibrium constants, Huisgen was able to derive activation parameters such as the enthalpy of activation $\Delta H^{\neq}$ and the entropy of activation $\Delta S^{\neq}$. The latter value $\Delta S^{\neq}$ was extraordinarily large for all 1,3-dipolar cycloadditions investigated in this study. This is in accordance with the highly ordered four-centred transition state shown in Scheme 2 and typical for concerted pericyclic reactions. At last, differently substituted dipolarophiles have been compared with respect to their reactivity in 1,3-dipolar cycloadditions. The influence of substituents on the dipolarophile did not lead to clear-cut results. If the reaction were to proceed *via* an electrophilic attack, electron-donating groups on the dipolarophile should always exert a positive influence, and if the reaction started with a nucleophilic attack, the opposite would be true and electron-withdrawing substituents should be beneficial. However, the only tendency that Huisgen found when comparing the rates of reaction for different dipolarophiles was that the stronger the newly formed σ-bonds were, the higher the driving force of the 1,3-cycloaddition. The otherwise very divergent results do not support any of the hypotheses shown in Scheme 3. We will now focus on the reaction of organic azides with alkynes to give disubstituted 1,2,3-triazoles. The exemplary reaction of phenylacetylene with phenyl azide

proceeds in toluene under reflux conditions within 17 hours giving a mixture of the 1,4- and the 1,5-disubstituted 1,2,3-triazole in nearly equal amounts (Scheme 4).[9]
Although the reaction is highly exothermic (ΔH^0 = -50 to -65 kcal mol^{-1} = -209 to -272 kJ mol^{-1}),[10] it proceeds very slowly even at high temperatures, which is due to the large activation barrier, which was calculated to be 25.7 kcal mol^{-1} (= 107.6 kJ mol^{-1}) for the 1,4-addition and 26.0 kcal mol^{-1} (= 108.9 kJ mol^{-1}) for the 1,5-addition of propyne and methyl azide.[11]

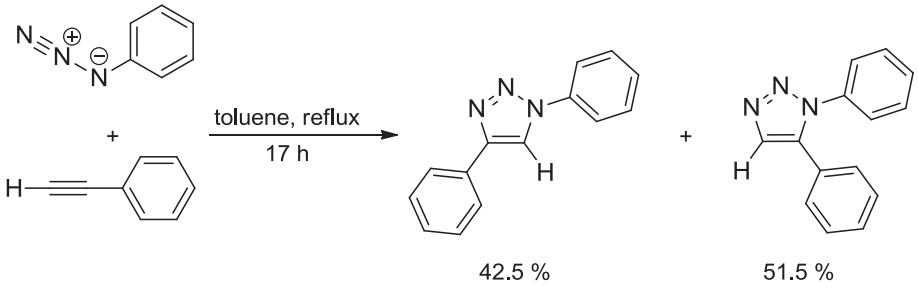

Scheme 4: Exemplary 1,3-cycloaddition of phenylacetylene with phenyl azide.[9]

This lack of regioselectivity can be explained by molecular orbital theory. Generally, in 1,3-dipolar cycloadditions the HOMO of the 1,3-dipole can react with the LUMO of the dipolarophile (type I), the LUMO of the 1,3-dipole can react with the HOMO of the dipolarophile (type III), or both interactions are involved (type II).[8] The energy gap between the HOMO-LUMO combinations is decisive for the kind of interaction (type I/II/III) that is dominant in a given cycloaddition. The regioselectivity, on the other hand, depends on the coefficients of the frontier orbitals in the 1,3-dipole and the dipolarophile, as the combination of the largest orbital coefficients is energetically most favourable.[12]
For the reaction of phenyl azide with styrene the regioselectivity is nearly perfect, as only the 1,5-disubstituted triazoline 1,5-diphenyl-4,5-dihydro-1*H*-1,2,3-triazole is formed. This can be explained by the fact that the energy gap between the LUMO of the 1,3-dipole phenyl azide and the HOMO of the dipolarophile styrene (8.8 eV) is significantly smaller than the difference between the energies of the styrene's LUMO and the HOMO of phenyl azide (10.5 eV). The reaction of phenyl azide and styrene thus proceeds by combination of the styrene's HOMO with the LUMO of phenyl azide. As the gain in energy is highest for the combination of the two large lobes, the orientation of the reactants and, as a consequence, the regioselectivity of the transformation is predetermined by the orbital energies (Figure 1).[13]

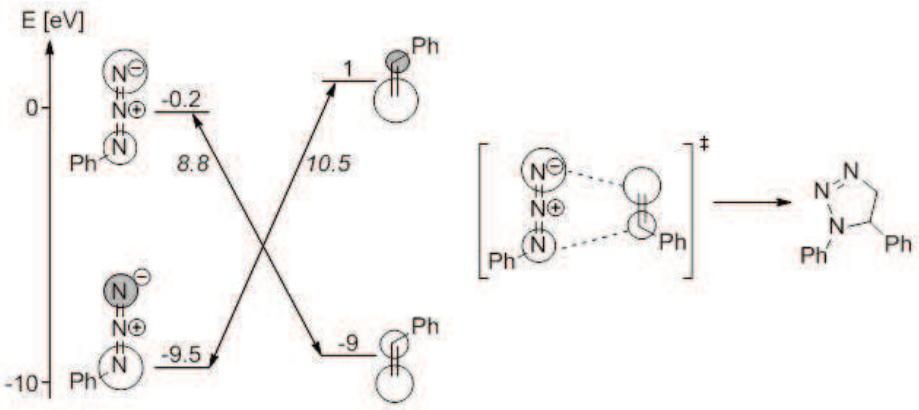

Figure 1: Energy diagram and schematic representation of the 1,3-dipolar cycloaddition between phenyl azide and styrene to give the 1,5-disubstituted triazoline.[13] The circles in this diagram do not represent orbitals, but the approximate size of the orbital lobes at the indicated positions: the diameter of a circle is roughly proportional to the molecular orbital's coefficient at the respective atom.

In the case of phenylacetylene, on the other hand, there is hardly any regioselectivity. This is due to the small difference between the HOMO-LUMO energy gaps. For the HOMO (phenyl azide)-LUMO (phenylacetylene) interaction, the energy difference is 9.3 eV, and for the alternative combination 10.0 eV (Figure 2). The difference of 0.7 eV is simply too small to induce a stereoselective reaction.[13]

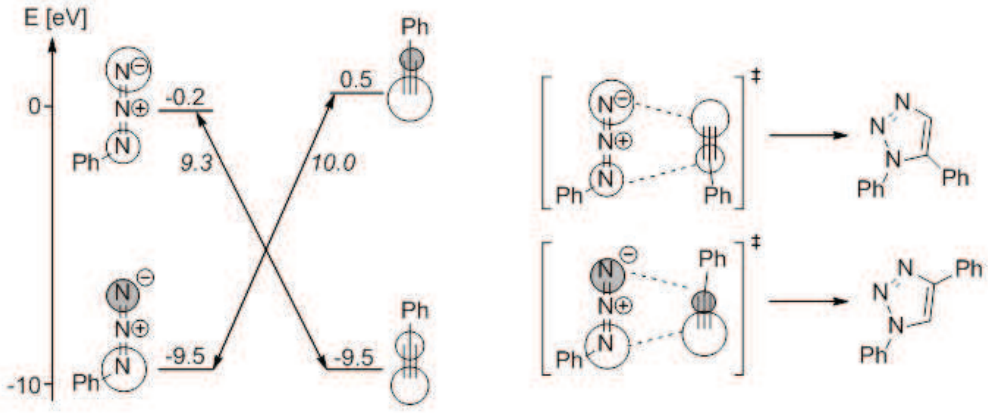

Figure 2: Energy diagram and schematic representation of the 1,3-dipolar cycloaddition between phenyl azide and phenylacetylene to give two regioisomeric disubstituted 1,2,3-triazoles.[13] The circles in this diagram do not represent orbitals, but the approximate size of the orbital lobes at the indicated positions: the diameter of a circle is roughly proportional to the molecular orbital's coefficient at the respective atom.

This finding has been supported by DFT calculations for the model cycloaddition between methyl azide and propyne.[11] The activation barriers for the formation of the 1,4- and the 1,5-disubstituted 1,2,3-triazole were found to be 25.7 and 26.0 kcal mol^{-1}

(107.6 kJ mol^{-1} and 108.9 kJ mol^{-1}, respectively), which means that the difference in activation enthalpies is too small to allow for a selective formation of one regioisomer. The lack of regioselectivity is one of the major drawbacks of Huisgen's 1,3-dipolar cycloaddition of azides and alkynes. The long reaction times and harsh conditions that do not tolerate sensitive functional groups in the substrates are other severe disadvantages of this reaction (Scheme 4). Nevertheless, Sharpless recognized the potential of this reaction when he considered it an optimal candidate for becoming a Click reaction due to its thermodynamic driving force and compatibility with most functional groups.[1]

In 2002, the groups of Meldal and Sharpless independently discovered a copper-catalyzed variant of Huisgen's azide-alkyne cycloaddtion, which was called CuAAC reaction. In fact, the catalytic effect of copper ions had first been mentioned by L'Abbé in 1984,[14] but had henceforth been overlooked until Meldal presented a copper(I)-catalyzed solid-phase synthesis of 1,2,3-triazoles. In this procedure, the terminal alkyne substrate was bound to a hydrophilic tertiary amide-poly(ethylene glycol) based resin *via* a peptide linker.[15] With copper(I) salts as catalysts, the corresponding triazole was formed under mild conditions upon addition of the azide. This reaction proceeds in a variety of organic solvents at room temperature with quantitative conversion to give the 1,4-disubstituted 1,2,3-triazole exclusively. Common side reactions such as the Glaser coupling were not observed. The presented reaction conditions are compatible with a variety of functional groups such as ester, ether, amide, thioether, Fmoc and Boc groups. Meldal *et al.* reported this reaction in the context of solid-supported peptide synthesis and expressed their hope for the synthesis of a library with triazole-containing peptides.
The group of Sharpless, on the other hand, presented a copper(I)-catalyzed azide-alkyne cycloaddition under solution-phase conditions (Scheme 5).[16] In their standard procedures, the cost-efficient salt copper(II) sulphate pentahydrate is reduced *in situ* by ascorbic acid or sodium ascorbate in a solvent mixture of water and alcohol. Alternatively, a copper(I) salt such as copper(I) iodide, copper(I) triflate or tetrakis(acetonitrile)copper(I) hexafluorophosphate can be used in the presence of a nitrogen base with acetonitrile as co-solvent. This reaction is applicable to a great variety of substrates with manifold functional groups, *e.g.* free hydroxyl, ester, carboxylic acid, amide, sulphonamide and amine substituents. The catalytic process is insensitive

towards the presence of air and pH changes between pH 4 and 12 in a solvent mixture of water and *tert*-butanol. This strictly regioselective stepwise process gives the 1,4-disubstituted 1,2,3-triazole only and speeds up the reaction by a factor of up to 10^7 in comparison to Huisgen's uncatalyzed procedure.[10-11]

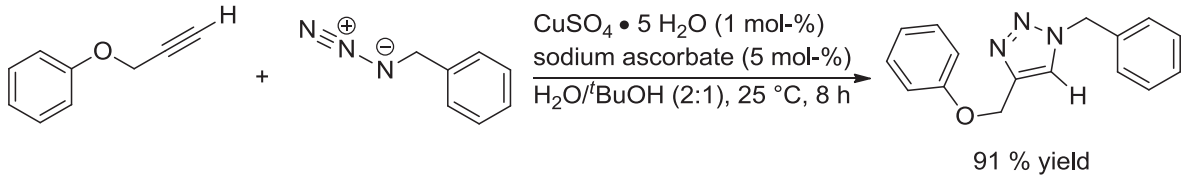

Scheme 5: CuAAC reaction of benzyl azide with (prop-2-yn-1-yloxy)benzene.[16]

2.3 Mechanistic Investigation of the CuAAC

In his seminal publication, Sharpless disclosed a first proposal for the CuAAC's mechanism.[16] As shown in Scheme 6, the alkyne substrate is deprotonated and σ-coordinates to the copper(I) centre of the active catalyst. If there is another free coordination site, the azide can coordinate to this copper(I) ion as well. The C-N bond is formed concomitantly to the formation of a double bond between the copper ion and the C1 atom of the acetylide. This unusual six-membered copper(III) metallacycle then undergoes a transannular ring contraction to give the copper triazolide. The latter can be protonated to release the triazole product.

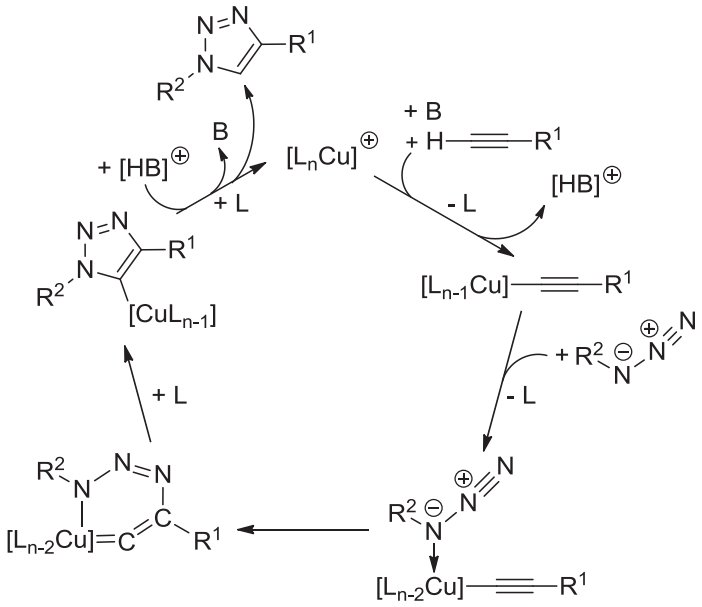

Scheme 6: Early mechanistic proposal by Sharpless.[16]

The groups of Fokin and Finn have tested different heterocyclic chelating ligands for CuAAC by fluorescence quenching in the reaction of dansyl azide fluorophore and dabsyl alkyne, and carried out kinetic measurements with a bis(bathophenanthroline-disulphonate) copper(I) complex formed *in situ* from copper(II) sulphate and bathophenanthrolinedisulphonic acid disodium salt in the presence of sodium ascorbate as reducing agent.[17] The authors found that the rate law of the reaction was second order with respect to the concentration of the copper(I) complex. As a consequence, they suggested two copper centres to be required for catalytic turnover.

Mechanistic studies for the ligand-free CuAAC followed.[18] The reaction of benzyl azide with phenylacetylene in dimethylsulphoxide/water in the presence of copper(II) sulphate pentahydrate and an excess of sodium ascorbate was monitored by taking aliquots at intervals from the reaction mixture by an automated liquid handler under inert gas atmosphere and subsequent LC-MS analysis. The authors found the reaction to be second order in the concentration of copper(I) ions under catalytic conditions. They also reported that the rate of reaction increases more slowly than suggested for rising copper concentrations, which hints at the formation of aggregates at high metal concentrations. This aggregation is prevented by addition of the fully deuterated product 1-benzyl-4-phenyl-1*H*-1,2,3-triazole so that a clean second order dependence on the copper concentration was observed. With excess copper concentrations the rate law was found to be between first and second order in the concentration of alkyne. The rate order of 1.3 ± 0.2 may either suggest that two pathways are

involved with participation of one or two alkyne molecules in the rate-determining step, respectively. Alternatively, there could be only one pathway including two acetylenes in the rate-determining step, which is inhibited by higher concentrations of the alkyne. The latter proposition is supported by the fact that commercially available copper acetylides are catalytically inactive, probably because they are coordinatively saturated by the preferentially bound alkyne, and binding of the azide substrate is inhibited.[19] The proposition that excess quantities of azide inhibit the CuAAC catalysis was later corrected,[20] for the inhibitory effect was caused by trace impurities in commercially available benzyl azide and was not observed when the azide was freshly distilled prior to use. All in all, it is an essential prerequisite for CuAAC catalysis to have labile ligands on the copper(I) that can easily dissociate to open free coordination sites for the substrates.

Based on these findings and the observation of polynuclear copper(I) alkyne complexes by the groups of Mykhalichko and García-Granda,[21] Fokin and Finn suggested the following mechanistic scheme (Scheme 7).[18] However, the precise structure of the putative dinuclear copper catalyst remains unknown[19] and is thus abbreviated by $[L_{2n}Cu_2]^{2+}$ (all charges and numbers of ligands have been consistently accounted for in a stoichiometric “book-keeping” fashion, but are not meaningful, as anionic ligands might also be present in the reaction mixture). In the first step, the alkyne π-coordinates to the copper(I) centre and can be easily deprotonated to give the acetylide complex, for example by sodium ascorbate,[22] which is needed in excess for the Sharpless-Fokin procedures.[16] A neighbouring copper(I) centre might also attract an acetylide ligand, which is shown in the equilibrium reaction on the right. However, this equilibrium is unproductive, as only the coordination of an azide molecule to the neighbouring copper(I) ion enables the formation of the copper(I) triazolide. The disputable intermediates for this step have been omitted in the article by Fokin and Finn,[18] whereas van Maarseeven suggested an intermediate[19] analogous to the highly strained metallacycle proposed by Sharpless (Scheme 6).[16] As this bicyclic intermediate is very implausible, Fokin and Finn have directly proceeded with the product of the ring contraction, *i.e.* the copper(I) triazolide that can be protonated to set free the triazole product and regenerate the active dinuclear catalyst.

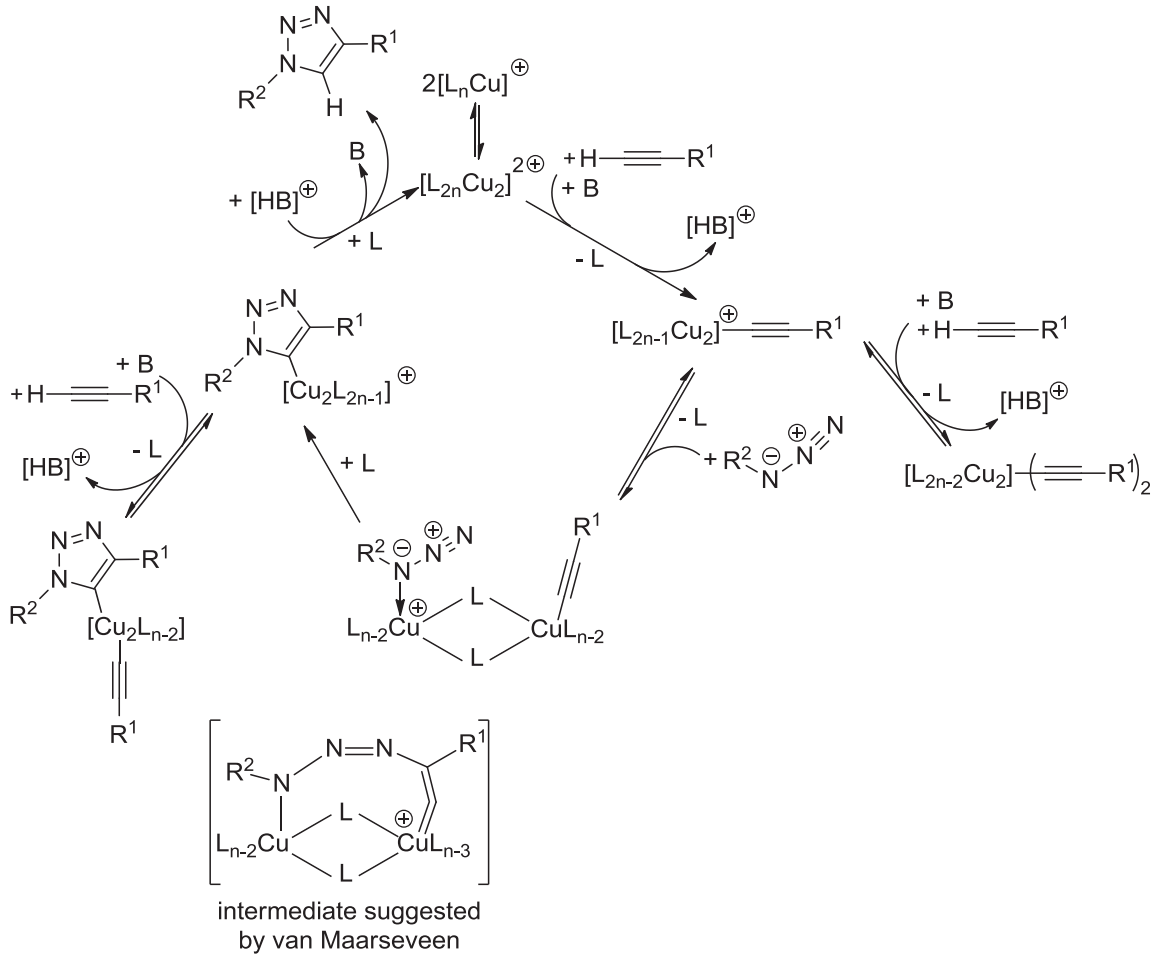

Scheme 7: Catalytic cycle of the CuAAC reaction on the basis of the proposed mechanistic scheme by Fokin and Finn in 2005[18] and an intermediate suggested by van Maarseveen.[19]

The first DFT study on the CuAAC's mechanism was carried out in 2005 by Sharpless and Fokin for the model reaction of propyne with methyl azide.[11] Geometry optimizations were carried out on the theoretical level B3LYP/6-311G(d,p) with subsequent single point energy calculations with 6-311+G(2d,2p). Solvation energies for an acetonitrile or water solvent environment were calculated with the COSMO model ("Conductor-like Screening Model") at the B3LYP/6-311G(d,p) level. All energies disclosed in this report are enthalpies to which solvation energies and zero-point energies were added. Albeit only the mechanistic pathway featuring mononuclear copper species shown in Scheme 6 was investigated, which is not in accordance with the kinetic studies described above, there are still some results worth mentioning. The calculations show that π-coordination of propyne to the copper(I) complex leads to a decrease in the pK_a value of 9.8 units, *i.e.* the alkyne is greatly acidified from pK_a (propyne) ≈ 25 to pK_a (copper-coordinated propyne) ≈ 15. Reaction of the copper-

alkyne π-complex with the azide in a concerted cycloaddition was shown to be very unlikely due to the high activation enthalpy of 27.8 kcal mol^{-1} (= 116.4 kJ mol^{-1}). Even the copper-free uncatalyzed concerted reaction has a lower enthalpy of activation (25.7 kcal mol^{-1} = 107.6 kJ mol^{-1}). Instead, the alkyne ligand is deprotonated to give the σ-acetylide complex. Such complexes are stable in aqueous solutions, even at acidic pH values.[21a] The σ-acetylide complex cannot undergo a concerted reaction with the azide either, as the activation barrier for this step is too high as well (23.7 kcal mol^{-1} = 99.2 kJ mol^{-1}). It has thus been proven that copper-catalyzed 1,3-dipolar cycloaddition reactions proceed *via* a stepwise mechanism. Indeed, the azide can replace one of the solvent ligands (acetonitrile or water) coordinating to the copper(I) centre. The ligator atom is the nitrogen next to the carbon. Starting from this resting state, the formation of the six-membered, highly strained copper(III) metallacycle (Scheme 6) was shown to be endothermic by 8.2 kcal mol^{-1} (34.3 kJ mol^{-1}) for L = acetonitrile and 12.6 kcal mol^{-1} (52.8 kJ mol^{-1}) for L = water. The activation barrier for this elementary step is 14.9 kcal mol^{-1} (62.4 kJ mol^{-1}) for L = acetonitrile and 18.7 kcal mol^{-1} (78.3 kJ mol^{-1}) for L = water, and is thus significantly lower than the barrier calculated for the uncatalyzed Huisgen cycloaddition (25.7 kcal mol^{-1} = 107.6 kJ mol^{-1}). Without any significant activation barrier, this highly strained intermediate undergoes a ring contraction to give the copper triazolide, from which the triazole product is released upon protonation. In fact, if this reaction is carried out in D_2O, deuterium is incorporated at the C5 position of the triazole. Although these calculations for the stepwise mechanism shown in Scheme 6 can account for the regioselectivity and the observed rate increase compared to the uncatalyzed concerted Huisgen cycloaddition, this proposal is not in accordance with the fact that the rate law is second order with respect to the concentration of copper(I) ions in solution.

The proposed intermediary formation of copper(I) acetylide as well as triazolide complexes has been experimentally supported by isolation and characterization of the NHC-copper(I) acetylide complexes [(IPr)Cu(C≡CPh)][23] and [(SIPr)Cu(C≡CPh)],[24] as well as the NHC-triazolide complex[24] of the reaction with 4,4'-(azidomethylene)-bis(methylbenzene) (Scheme 8).

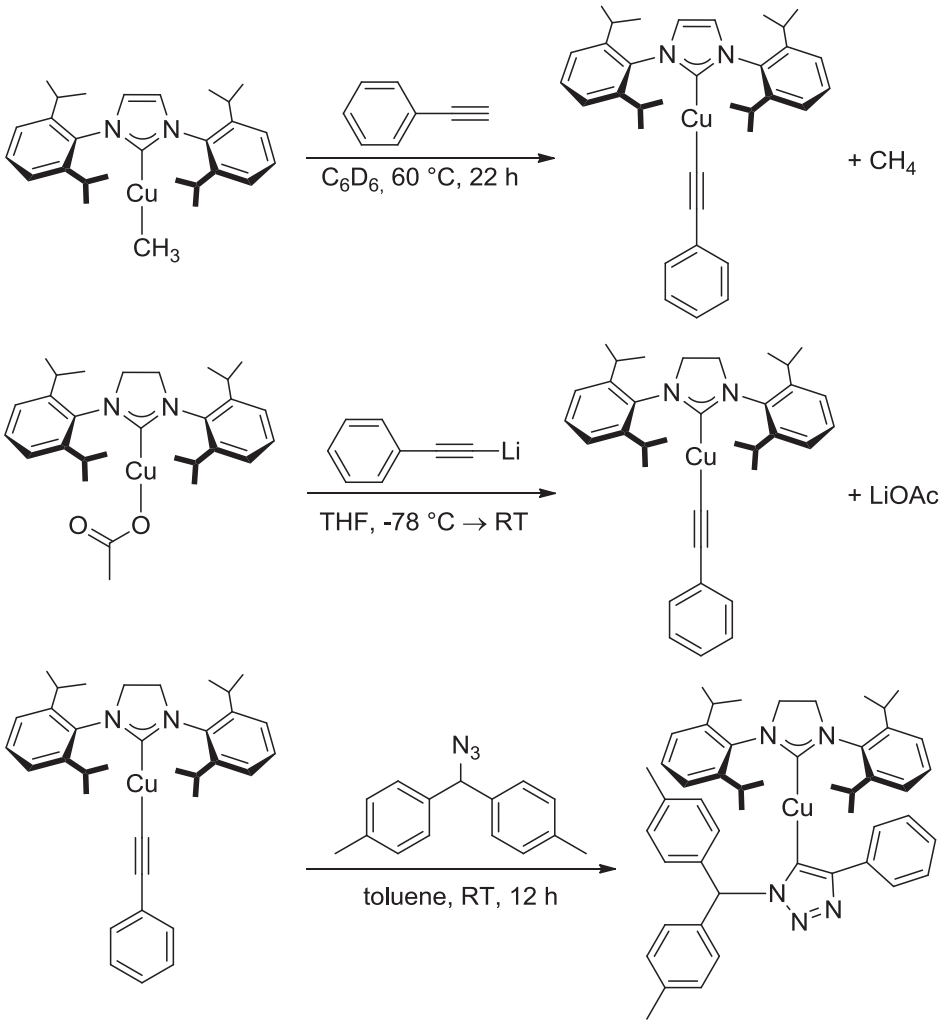

Scheme 8: Synthesis of supposed intermediates in the CuAAC's catalytic cycle.[23-24]

Supported by the isolation of these Click intermediates, it was suggested that the CuAAC can proceed *via* a mononuclear pathway when sterically encumbered copper(I) NHC-complexes are employed. This assumption has only recently been challenged.[25]

Usually, however, copper(I) acetylides are polynuclear structures in which the acetylide ligands coordinate to two copper centres either in the unsymmetric σ,π-coordination mode (μ_2-η^1,η^2) or in the symmetric σ,σ-coordination mode (μ_2-η^1,η^1).[21, 26] It is consensus in all mechanistic investigations that π-complexes of the alkyne substrate with the copper(I) centres need to be formed in order to enable facile deprotonation to give the σ-complexes. The group of Mykhalichko has structurally investigated both copper(I) alkyne and acetylide complexes.[21a] For the π-complexes, the authors found that the alkyne can either act as a bridging π-ligand for two copper centres

(μ_2-coordination mode), for example in the structure of $[Cu_2Cl_2(HC{\equiv}CCH_2OH)]$, or exclusively as a π-ligand for one copper(I) ion only, *e.g.* in [CuCl(HC≡CPh)]. According to the Chatt-Dewar-Duncanson model[27] the coordination of a copper(I) ion ($3d^{10}\,4s^0$) can be explained by a donating interaction L→M, in which electron density is transferred from the ligand to the metal centre, and a π-backdonation M→L from the metal to the ligand. In the case of a copper-alkyne π-complex, electron density is transferred from the bonding π-molecular orbital of acetylene to the unoccupied sp^3-hybridized orbital of the copper(I) centre (L→M donating interaction). On the other hand, a symmetrically suitable, fully occupied d-orbital of the copper ion can overlap with an antibonding π^*-molecular orbital of the alkyne ligand (M→L back donation). As a consequence of populating the antibonding π^*-MO of the alkyne, the C-C bond is elongated and the C-C-R geometry no longer linear, but bent. The transfer of electron density from the π-MO of the alkyne to the metal leads to positive partial charges on the alkyne's carbon atoms and to an elongation of the C-C bond as well. Donation and back donation interactions are synergistic, *i.e.* an increase in one component leads to an increase in the other component. The interaction of copper(I) ions with acetylene has also been studied computationally.[28] *Ab initio* calculations by Frenking *et al.* have shown the metal-ligand coordinative bond in $[Cu(HC{\equiv}CH)]^+$ to be stronger (D_e = 40.6 kcal mol^{-1} = 170.0 kJ mol^{-1}) than previously suspected.[28a-c] The C-C bond length was calculated to be 1.242 Å and the bending of the acetylene moiety C-C-H was found to be 168.7° in this C_{2v}-symmetric complex. In comparison, the bond length in free acetylene is 1.207 Å.[29] NBO analyses have shown that the metal-ligand interactions in $[Cu(HC{\equiv}CH)]^+$ are mainly electrostatic and that the electron density distribution is T-shaped. This means that the donating interaction L→M greatly prevails, which is in accordance with an ESR study by the group of Watanabe.[30]

The polarisation of the C-H bond of terminal alkynes or acetylene in copper π-complexes substantially facilitates the deprotonation and formation of the corresponding acetylide complex.[11] The resulting Cu-C bond is so strong that the copper acetylide is even formed in strongly acidic media, for example in Cu_2SO_4 solutions with up to 25 % H_2SO_4.[21a] The equilibrium between π-complex $[Cu(HC{\equiv}CH)]^+$, monocopper acetylide $[Cu(C{\equiv}CH)]$ and bisacetylide Cu_2C_2 is greatly influenced by the pH of the medium. The presence of halide ions and other ligands such as phosphanes has a strong impact on the speciation and nuclearity of these acetylide complexes, but they are in all cases complex polynuclear structures.[21, 26] This is why Straub chose a

tetranuclear model copper(I) acetylide and a dinuclear copper(I) acetylide complex with additional phenanthroline ligands as resting states for his DFT study.[31] Figure 3 shows two tetranuclear copper(I) acetylide complexes described in literature, which justify the choice of a tetranuclear copper(I) acetylide model as resting state.

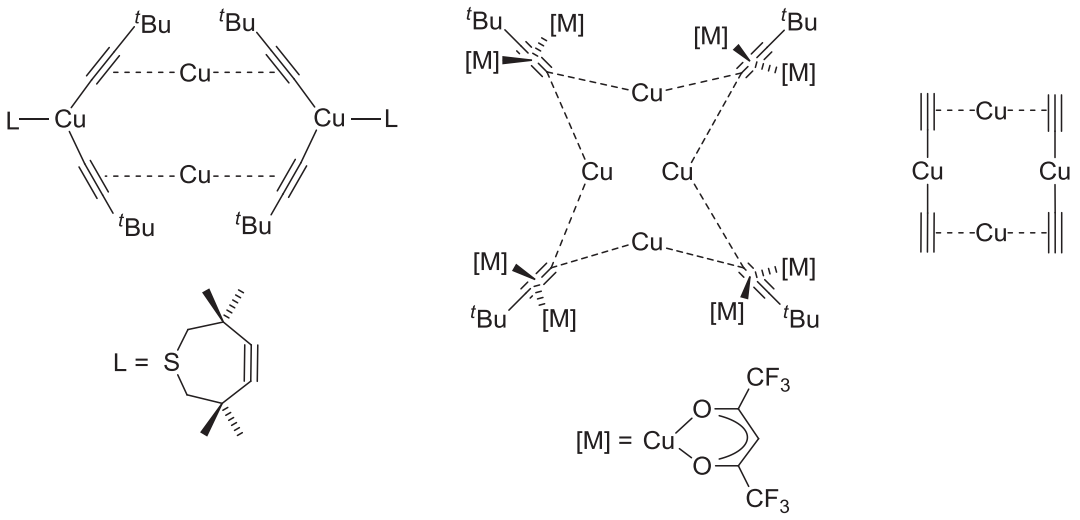

Figure 3: Tetranuclear copper acetylide complexes as reported by Weiss (left)[26l] and Tasker (middle)[26u] and Straub's model of tetranuclear copper(I) acetylides as resting state for mechanistic DFT studies.[31]

With these calculations, the author was able to show that the mononuclear pathway is greatly disfavoured due to the much higher Gibbs free energy of activation for the C-N bond forming elementary step: the barrier $\Delta G^{\neq}$ for the mononuclear pathway was calculated to be 173.1 kJ mol^{-1}, whereas the barrier for the putative pathway featuring tetranuclear complexes was only 86.9 kJ mol^{-1} (Figure 4). The high barrier of the mononuclear pathway is mainly due to the ring strain in the cyclic copper(III) intermediate: the sp-hybridized carbon atom in the fragment Cu=C=C prefers an angle of 180°, but this is impossible in a six-membered ring. The actual Cu=C=C angle was computed to be 131.4°. It is thus much more favourable for the alkenylidene carbon atom to bind to two copper(I) centres so that one Cu=C double bond is replaced by two Cu-C single bonds. However, the resulting six-membered copper(III) metallacycle is not stable and immediately undergoes reductive elimination to give the copper(I) triazolide complex.

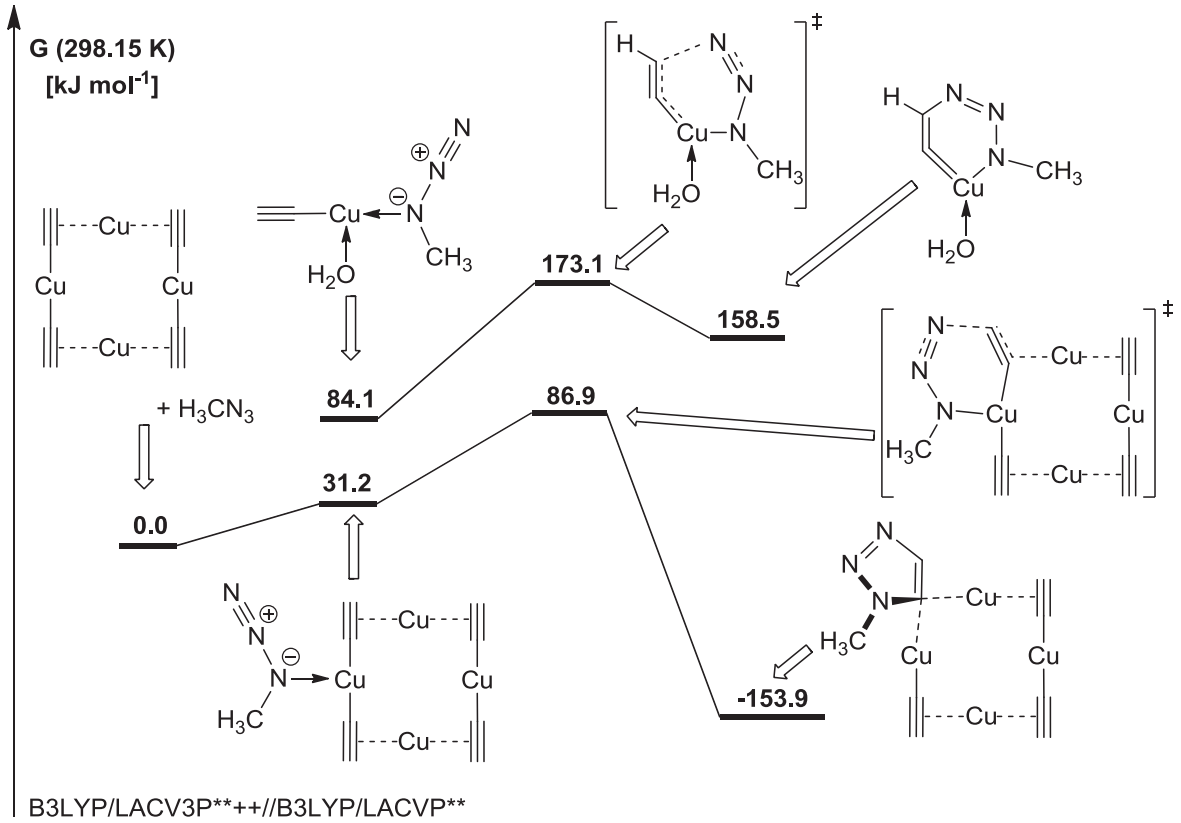

Figure 4: Gibbs free energy diagram for the computed mechanistic pathway of the CuAAC reaction starting from a tetranuclear copper(I) μ-acetylide model complex.[31]

Shortly after Straub's communication, Ahlquist and Fokin published a similar DFT study on the theoretical level B3LYP/LACV3P*+ applying the PBF solvent model for water and supported the picture of dinuclear copper(I) complexes playing a vital role in the CuAAC reaction mechanism.[32] All energies reported in their work are solution phase energies including zero point energy corrections. They found the overall energy barrier for a mononuclear pathway at 17 kcal mol^{-1} (= 71 kJ mol^{-1}), which is in good agreement with the result published by Himo *et al.* in 2005 (18.7 kcal mol^{-1} = 78.3 kJ mol^{-1} for L = water).[11] For the dinuclear pathway, they chose dicopper species with water and acetylide or chloride as spectator ligand. In the resting state, the acetylide is σ-coordinated to one copper(I) centre, to which an aqua ligand is coordinated as well. The second copper centre with an additional chloride or acetylide spectator ligand strongly interacts with the C1 atom of the acetylide, but less so with the C2 atom. Only in the presence of two identical spectator ligands was a strict μ_2-η^1,η^2 binding mode observed. The calculated energy of activation for the addition of

azide to the dicopper chloride complex was found to be 10.5 kcal mol^{-1} (= 43.9 kJ mol^{-1}) and thus significantly lower than for the mononuclear pathway.

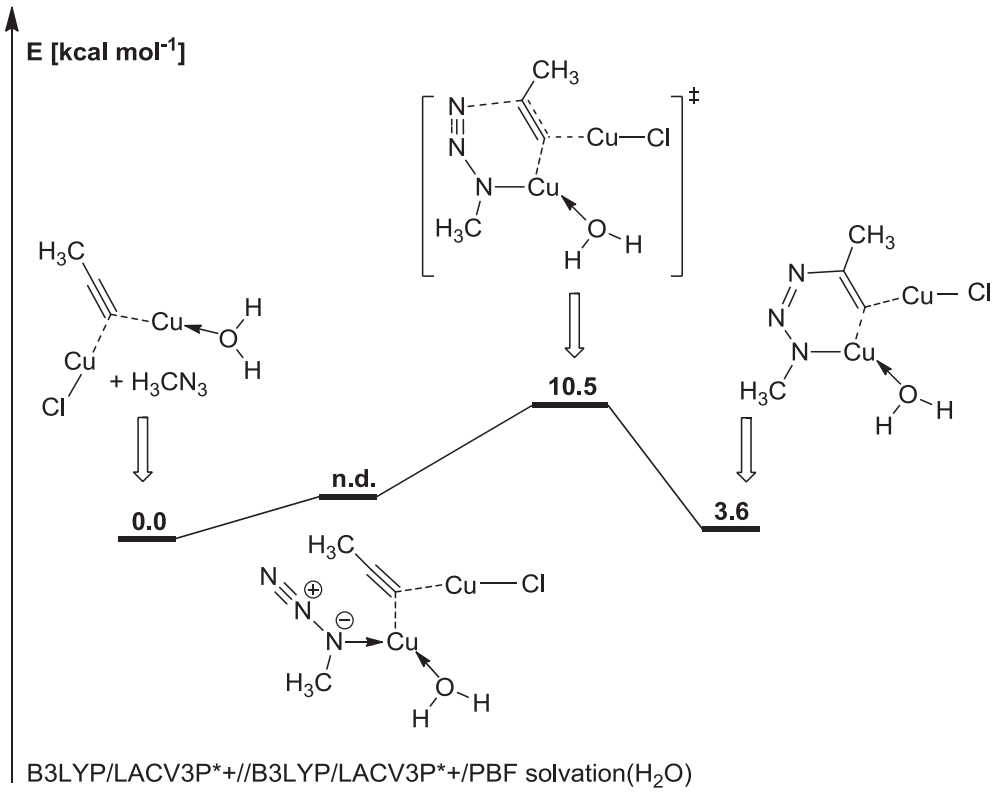

Figure 5: Energy diagram by Ahlquist and Fokin.[32]

These energy diagrams (Figure 4 and Figure 5) translate to the general mechanistic proposal shown in Scheme 9.

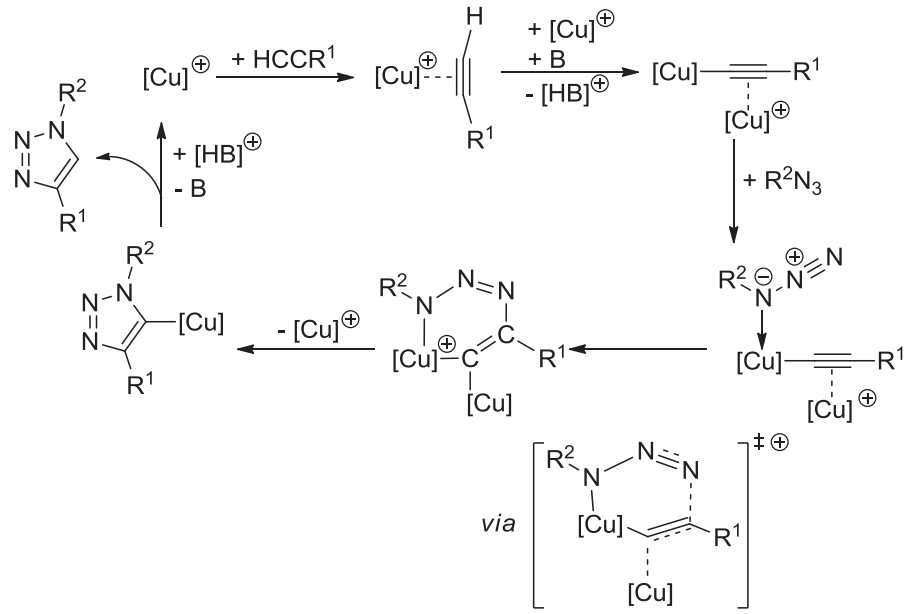

Scheme 9: Mechanistic proposal for the CuAAC reaction based on DFT calculations by Straub[31] and Fokin[32] ([Cu] stands for a copper(I) complex with the suitable number of ancillary ligands).

This mechanistic picture was supported by recent calculations carried out by the group of Cantillo.[33] In their DFT study, the authors compare different mechanistic proposals from literature on the same level of theory (B3LYP/LANL2DZ, solvent model CPCM for water). In conclusion, they confirm dinuclear copper acetylides to be the essential catalytic intermediates, whereas the corresponding copper alkyne π-complexes need to be deprotonated before the crucial C-N bond forming step can take place. The computed Gibbs free energy barrier was found to be 16.0 kcal mol^{-1} (= 70.0 kJ mol^{-1}) for the 1,4-addition and 20.4 kcal mol^{-1} (= 85.4 kJ mol^{-1}) for the 1,5-addition of methyl azide with propyne.

In 2010, the group of Heaney presented experimental evidence for the participation of dinuclear alkynyl copper(I) complexes in CuAAC reactions.[22] Aryl- and alkylethynyl copper(I) compounds usually form polymeric aggregates [(RC≡CCu)$_n$] of low solubility.[34] For example, X-ray powder diffraction studies have shown the insoluble yellow (phenylethynyl)copper(I) [(PhC≡CCu)$_n$] to consist of an infinite Cu-Cu ladder structure (n = ∞).[26t] Both copper ions in this ladder polymer [(PhC≡CCu)$_2$]$_n$ adopt the same μ-η^1,η^2-C≡C bridging mode.

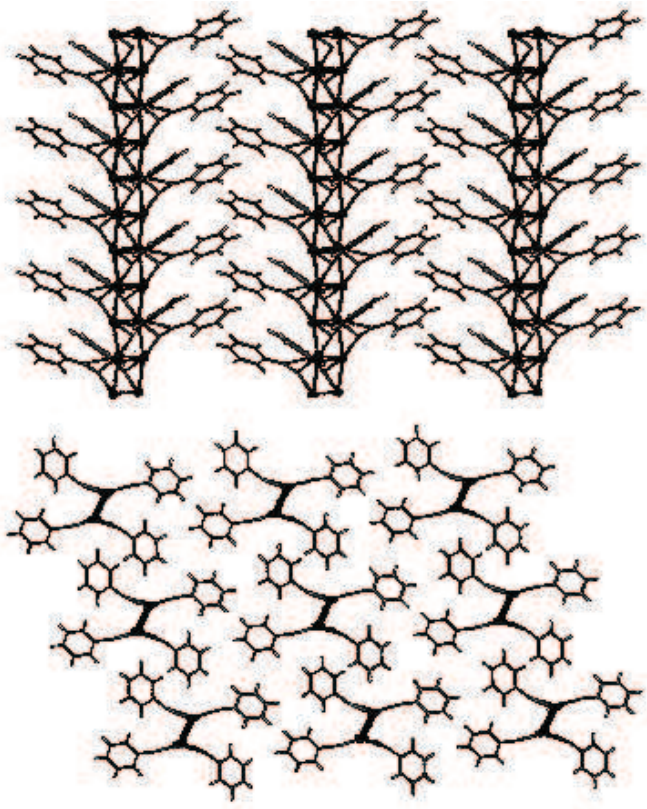

Figure 6: Structure of (phenylethynyl)copper(I) $[(PhC{\equiv}CCu)_2]_n$ (figure from the publication by Che *et al.*).[26t]

The distance between the two copper(I) ions was found to be between 2.49 and 2.83 Å. The group of Heaney recognized that this intermetallic distance was in the same range as calculated by Ahlquist and Fokin for the transition state in CuAAC reactions featuring dinuclear model structures (2.54 Å and 2.64 Å for chloride/water and acetylide/water as spectator ligands, respectively).[32] Heaney *et al.* concluded, that $[(PhC{\equiv}CCu)_2]_n$ should thus be a perfect catalyst for CuAAC reactions, as the two copper ions needed for the crucial elementary steps are extremely well positioned for catalytic performance.[35] Experiments were carried out in acetonitrile at 100 °C with microwave irradiation in order to facilitate the heterogeneous reaction. With 10 mol-% of catalyst $[(PhC{\equiv}CCu)_2]_n$, the reaction between phenylacetylene and benzyl azide reached 86 % conversion within ten minutes (Scheme 10). The $[(PhC{\equiv}CCu)_2]_n$ catalyst was recovered and re-used with similar results.

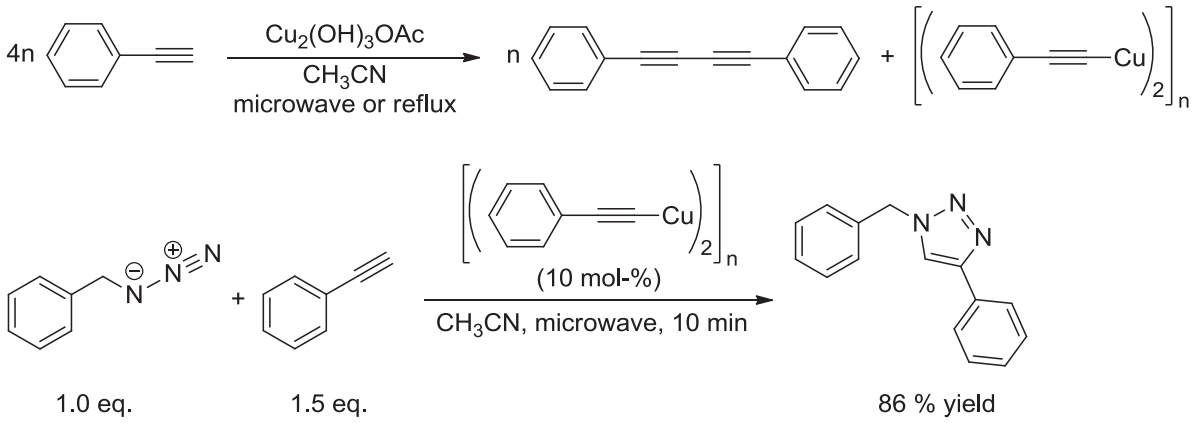

Scheme 10: Synthesis of $[(PhC{\equiv}CCu)_2]_n$ as co-product in the Glaser coupling of phenylacetylene in the presence of copper(II) hydroxyacetate in acetonitrile, and application of $[(PhC{\equiv}CCu)_2]_n$ as catalyst in the CuAAC test reaction of phenylacetylene with benzyl azide.[35]

When 4-tolylacetylene was used as substrate in combination with $[(PhC{\equiv}CCu)_2]_n$ as catalyst, ligand exchange at copper(I) took place and the product mixture contained 10 % 1-benzyl-4-phenyl-1*H*-1,2,3-triazole and 85 % 1-benzyl-4-(4-tolyl)-1*H*-1,2,3-triazole. The recovered yellow solid was used in the reaction of 4-tolylacetylene with benzyl azide thereafter and this reaction yielded 85 % 1-benzyl-4-(4-tolyl)-1*H*-1,2,3-triazole. When no alkyne substrate was added, the azide reacted with a stoichiometric amount of $[(PhC{\equiv}CCu)_2]_n$ to give 1-benzyl-4-phenyl-1*H*-1,2,3-triazole in 85 % yield, as well as a brown insoluble residue, which was regenerated to $[(PhC{\equiv}CCu)_2]_n$ by addition of phenylacetylene. It was also shown that under the given reaction conditions, the source of protons was the alkyne, as the reaction with 1-[D]-2-phenylacetylene proceeded with quantitative incorporation of deuterium at the triazole's C5 position. In a subsequent study, the group of Heaney carried out CuAAC reactions under the original Sharpless-Fokin-conditions.[16] Using 1 mol-% copper(II) sulphate in a solvent mixture of *tert*-butanol/water in the presence of 10 mol-% sodium ascorbate for the CuAAC test reaction of benzyl azide with phenylacetylene, the authors observed a transient yellow colour of the reaction mixture. With larger amounts of copper(II) sulphate, the known alkynyl copper(I) ladderane complexes[26t] could be isolated and identified.[22] It was also shown that the presence of a base is required for the formation of the catalytically active ethynylcopper ladderane complexes. For example, sodium ascorbate in the Sharpless-Fokin procedures is not only needed to reduce copper(II) to copper(I), but also for the deprotonation of the alkyne to facilitate the formation of the copper acetylide ladderane complex. Once the dinuclear

ladderane is formed, the presence of a base is not necessary anymore and $[(PhC{\equiv}CCu)_2]_n$ can be used under Sharpless-Fokin reaction conditions without the addition of an external base.
A detailed mechanistic report considering a variety of ligands was published by Fokin and Finn in 2007,[20] but its mechanistic implications will be discussed in the course of presenting different ligand systems in chapter 2.4.

Very recently, however, Fokin has presented direct evidence for the participation of a dinuclear copper intermediate in the CuAAC reaction mechanism.[25] In the first part of this study, the authors prepared the mononuclear σ-bound acetylide complex (SIPr)Cu(acetylide) by following the procedures reported by Straub.[24] With the help of real-time heat flow calorimetry, the authors monitored the progress of the reaction between this copper(I) acetylide complex and benzyl azide. The global heat output graph showed that there was no conversion at all after one hour at 35 °C with tetrahydrofuran as solvent. However, when 5 mol-% of $[Cu(PPh_3)_2]NO_3$ were added, the CuAAC reaction under these conditions was completed within 20 minutes under otherwise identical conditions. Similar results were obtained with $[Cu(PPh_3)_3]Br$, $[Cu(PPh_3)_3]NO_3$, CuI/TTTA and CuI/triethylamine as soluble copper(I) species, and in chloroform and dimethylformamide as alternative solvents. These experiments show that monomeric copper(I) acetylide complexes are unreactive towards organic azides. In contrast, Straub and co-workers had observed the reaction of a similar complex (SIPr)Cu(acetylide) with the sterically encumbered 4,4'-(azidomethylene)bis-(methylbenzene) in their study on the isolation of a copper(I) triazolide complex in 2007 without the need for an additional source of copper(I) ions. Even though Straub had inferred that "dinuclear copper complexes are not mandatory for Huisgen-Sharpless Click reactions, since even mononuclear copper(I) acetylides with extreme steric shielding react with bulky organoazides at room temperature", the author does at the same time voice his concern that "NHC dissociation, acetylide ligand exchange and formation of dinuclear complexes" still need to be ruled out in order to verify this conclusion.[24] By means of crossover experiments with enantiomerically enriched $[(^{63}Cu)(H_3CCN)_4]PF_6$ (1 equivalent) and the aforementioned (SIPr)Cu(acetylide) complex with natural isotopic distribution, Fokin and co-workers have now indeed shown that dinuclear copper complexes are essential for the CuAAC reaction to take place. With benzyl azide as substrate, an isotopic enrichment of approximately 50 % was

observed, namely from the naturally occurring ratio of 69(^{63}Cu):31(^{65}Cu) in the substrate complex (SIPr)Cu(acetylide) to 85(^{63}Cu):15(^{65}Cu) in the triazolide product complex (SIPr)Cu(triazolide). In order to find out at which stage isotopic scrambling of ^{63}Cu and ^{65}Cu occurs, mixtures of [(^{63}Cu)($H_3CCN)_4$]PF_6 (1 equivalent) with the starting material acetylide (SIPr)Cu(acetylide) and with the triazolide product complex (SIPr)Cu(triazolide) were prepared, but with neither of them was any isotope exchange detected. Only in the presence of the azide was isotopic scrambling between the NHC-copper complex and [(^{63}Cu)($H_3CCN)_4$]PF_6 observed. It was thus suggested that two equivalent copper(I) centres participate in the rate-determining C-N bond-forming step of the CuAAC reaction mechanism and that the ligands on these copper(I) ions can exchange rapidly after the first C-N bond has been formed. This unusual dissociation of the copper-NHC bond can be explained by assuming a formal oxidation state of +III at the copper centre. Because of the low electron density at the copper(III) centre, the Cu→C(carbene) backbonding interaction is supposed to be substantially weakened, which allows for a “rapid exchange of the NHC ligand between the two copper atoms” in the intermediate shown in Scheme 11.[25]

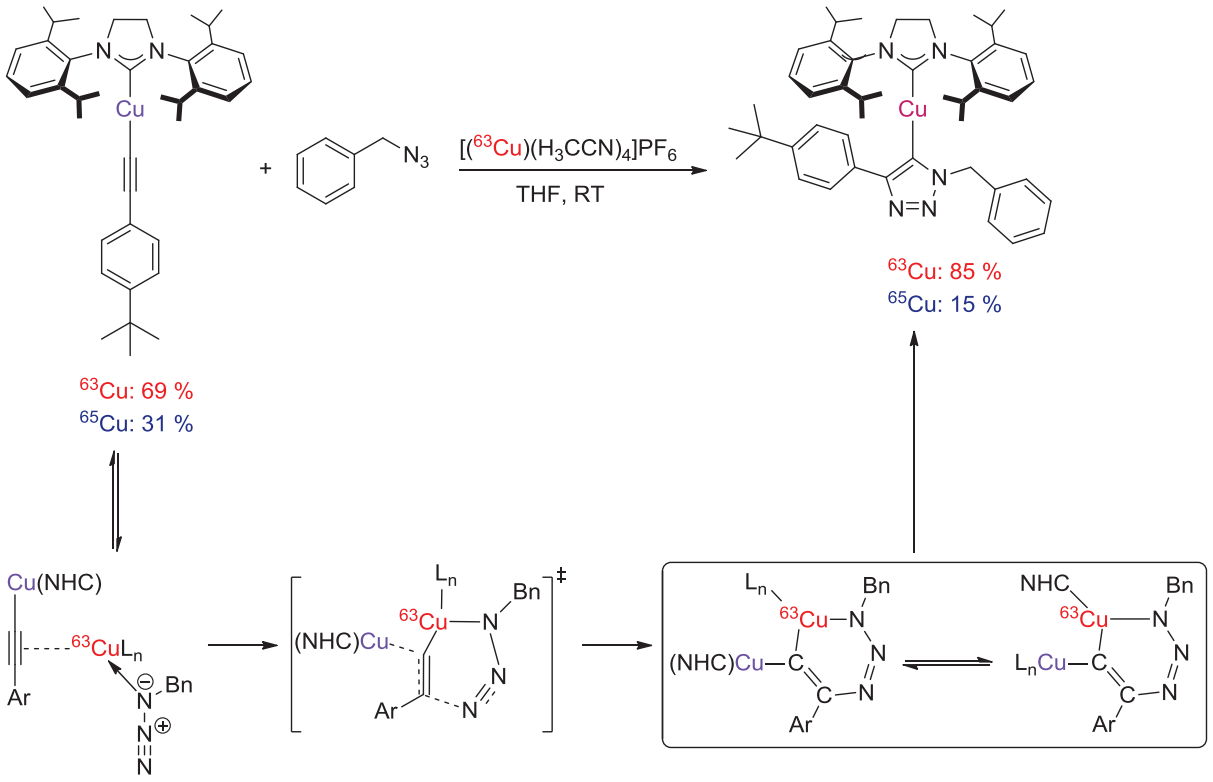

Scheme 11: Mechanistic explanation for the isotopic enrichment in the product triazolide in the presence of the isotopically pure exogenous catalyst [(^{63}Cu)($H_3CCN)_4$]PF_6 (with Ar = 4-^{t}BuPh, NHC = SIPr).[25]

Fokin thus draws the conclusion that these results do not only support the mechanistic picture given in Scheme 9, but also confirm that the CuAAC reaction can *only* take place when (at least) two copper(I) centres cooperate in the crucial mechanistic steps. It remains an unresolved question whether the formation of the triazolide species with 48 % yield after twelve hours reported by Straub (Scheme 8)[24] can be attributed to a very slow mechanistic pathway with mononuclear species or to catalysis with traces of a reactive dinuclear copper(I) species in analogy to Fokin's suggestion.

2.4 Catalysts for CuAAC Reactions

Since Meldal and Sharpless had first described the copper-catalyzed variant of Huisgen's 1,3-dipolar cycloaddition, a myriad of procedures employing different catalyst systems for CuAAC has been presented in literature.

The CuAAC reaction even proceeds in the presence of coiled copper metal turnings at room temperature by *in situ* oxidation to copper(I) species,[11, 16] even though this route takes longer for completion (12-48 hours) than with the standard catalyst systems, *i.e.* copper(II) salts plus reducing agent or copper(I) salts.[10] This method can be significantly sped up by applying microwave radiation.[36] It is also beneficial to add copper(II) sulphate, but this is usually not necessary as the patina on the metal surface is sufficient to start the catalysis.

The group of Rothenberg introduced nanometric copper clusters for ligand-free CuAAC.[37] These copper nanoclusters are prepared by reduction of cuprous chloride. Compared to other catalytic systems such as copper powder, copper shavings or copper(II) sulphate/ascorbate, the reaction with nanocluster catalysts proceeds faster, which is probably due to their higher surface area that favours heterogeneous catalysis. For example, the reaction of benzyl azide with phenylacetylene with a catalyst loading of 0.1 mol-% copper nanocluster takes 18 hours at room temperature to reach 82 % yield. Ponti *et al.* used mixed copper/copper oxide nanoparticles to effect a fast CuAAC reaction under mild conditions[38] and Lipshutz introduced a heterogeneous charcoal catalyst with copper nanoparticles adsorbed on its surface.[39]

The main advantage of using copper metal or nanoclusters is the high purity of the products, which contain only minute amounts of copper.

The most common source of copper for the CuAAC reaction are copper(II) salts. In the standard procedures introduced by Sharpless and Fokin (Scheme 5),[16] copper(II) sulphate pentahydrate is reduced *in situ* by sodium ascorbate, which is added in three- to ten-fold excess.[19] This procedure is tolerant towards most functional groups, even free amines, alcohols and carboxylic acids, and can be carried out in aqueous reaction media with organic co-solvents such as alcohols or dimethyl sulphoxide. As an alternative reducing agent, the water-soluble tris(2-carboxyethyl)-phosphane hydrochloride (TCEP) can be employed, which is especially suitable for applications in biological systems because it also protects cysteine residues in proteins from oxidative coupling.[40] However, the latter reagent should only be used in low quantities, as its binding to copper ions has an inhibitory effect.

The main advantages of reducing copper(II) salts *in situ* are the broad applicability of this procedure and the compatibility with oxygen and water, which means that no inert gas is needed.

Instead of forming the catalytically active copper(I) species *in situ*, a copper(I) salt can be added straightaway. Yet, this procedure is much less robust than the use of copper metal or copper(II) salts as precatalysts and usually demands an inert atmosphere and anhydrous solvents. In his seminal publication, Sharpless describes the use of copper(I) iodide, CuOTf • C_6H_6 and $[Cu(H_3CCN)_4][PF_6]$. However, acetonitrile as co-solvent and the presence of a nitrogen base such as triethylamine, *N,N*-diisopropylethylamine (DIPEA) or pyridine are required for these catalyses to work. The author also reports the formation of diacetylenes by alkyne-homocoupling as well as bistriazoles and 5-hydroxytriazoles as undesired by-products. Inert gas conditions and the application of 2,6-lutidine as base reduced this problem.[16]

For the solid-phase synthesis of peptidotriazoles, the group of Meldal used copper(I) iodide in combination with DIPEA as base (Scheme 12). The author pointed out that albeit copper(I) iodide was used in stoichiometric amounts (2 equivalents), this was only due to the small scale of the reactions – the catalysis was also effected by concentrations as low as 0.01 equivalents of copper(I) iodide.[15]

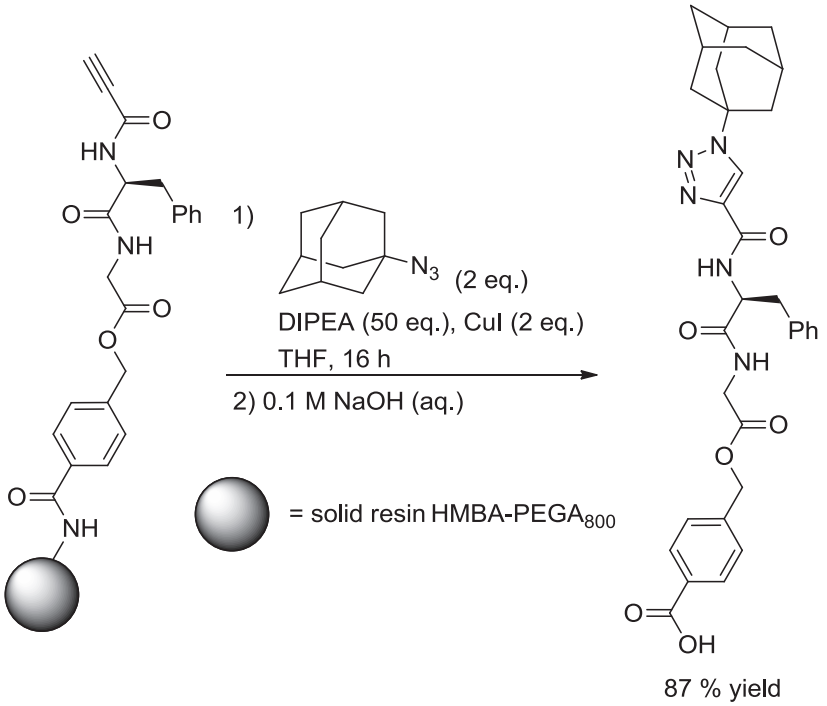

Scheme 12: Synthesis of 1-(adamant-1-yl)-1*H*-1,2,3-triazole-4-carbonyl-Phe-Gly-OH by solid-supported Click catalysis and subsequent release of the product from the resin by hydrolysis.[15]

The group of Wong has used copper(I) iodide for the synthesis of triazole-containing saccharides and their attachment to microtiter plates.[41] For the optimization of conditions, the reaction between 2-azidoethyl-β-D-galactopyranoside and *N*-tetradecylpropiolamide was carried out either without addition of a base or in the presence of triethylamine or DIPEA. In the absence of any base, the reaction proceeded very slowly. This is most probably due to the use of an aprotic solvent, which does not facilitate the deprotonation of the alkyne substrate. Usually when copper(II) precursors are used, protic solvents and basic reducing agents such as sodium ascorbate are present in the reaction mixture. Heaney has pointed out that ascorbate is needed in excess as it acts as a base in the deprotonation of the π-complexed alkyne.[22] Moreover, it is speculated that even in the absence of a basic reducing agent, *e.g.* by use of TCEP, the copper(I) ions formed *in situ* from copper(II) are more reactive towards the alkyne than copper(I) bromide or iodide, as the latter contain very stable cluster structures so that a minimum concentration of acetylide is needed for the reactive copper acetylide complex to form.[42]

However, when Wong used copper(I) iodide with triethylamine and acetonitrile as solvent, the reaction of 2-azidoethyl-β-D-galactopyranoside with *N*-tetradecylpropiolamide afforded only traces of product. On the other hand, the addition of DIPEA to the reaction mixture in acetonitrile gave the desired product in 38 % yield after 18 hours. In toluene, the reaction with triethylamine afforded 65 % conversion and 85 % with DIPEA. This illustrates the high sensitivity of the catalysis towards the choice of reaction conditions.

Generally, DIPEA and 2,6-lutidine seem to be best suited for CuAAC and an excess of base is favourable to the reaction as well. These nitrogen bases as well as acetonitrile as solvent may help stabilize the copper(I) oxidation state by preventing oxidation and disproportionation processes.[19]

Although the conditions described above are termed “ligand-free” it is obvious that solvent molecules as well as the nitrogen base can coordinate to the copper(I) ions. In order to avoid the use of inert gas and anhydrous solvents by protecting the copper(I) ions, to enhance their catalytic activity and to improve their applicability with a variety of substrates the search for suitable ligands started shortly after Sharpless’ and Meldal’s initial reports.[16]

Amine ligands are still very popular for CuAAC reactions. Triethylamine can even be used for reactions “on water”.[43] Although a variety of other tertiary amines such as propylamine[44] or tributylamine[45] has been employed, there is no comprehensive study about the influence of the nitrogen substituents. Based on Meldal’s[15] and Wong’s[41] reports, DIPEA has also become well-established in Click protocols.[42]

The triamine ligand PMDETA is preferably used in polymerization reactions in combination with copper(I) bromide.[46] For example, the group of Matyjaszewski reported the prepartation of α,ω-dihydroxy polystyrene by combination of ATRP and CuAAC.[47] In 2004, the group of Vincent first presented tris(2-dioctadecylaminoethyl) amine ($C18_6$tren), a sterically crowded tripodal ligand.[48] The corresponding copper(I) complex [Cu($C18_6$tren)]Br does not have to be prepared *in situ*, but can be isolated and handled in air. This is one of the few examples, where the copper(I) (pre-)catalyst complex is molecularly defined and characterized. As triazoles are more polar than the catalyst complex, CuAAC reactions can be conveniently carried out in toluene or *n*-octane, where the triazole product precipitates and can be easily isolated by filtration under aerobic conditions. On the other hand, the filtrate containing the catalyst can be re-used. As an example, the model reaction of benzyl azide with

phenylacetylene carried out in toluene at 60 °C with 0.05 mol-% [Cu(C18$_6$tren)]Br affords 86 % yield after 24 hours (Scheme 13).[49]

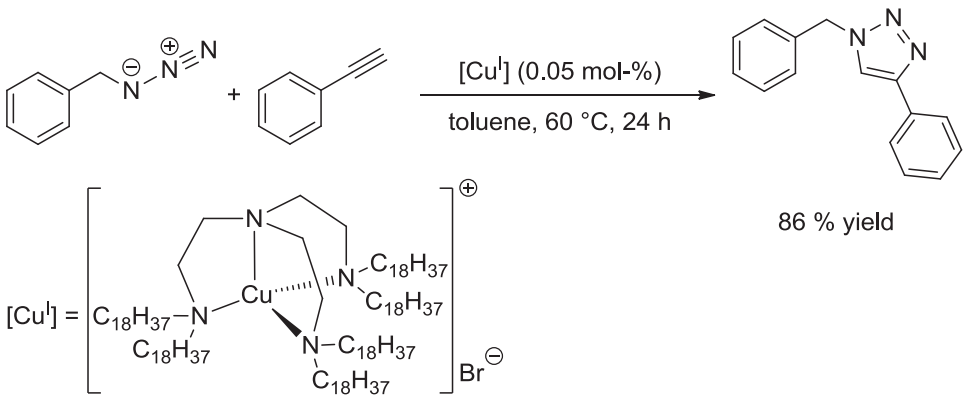

Scheme 13: CuAAC reaction with reusable copper(I)-tren catalyst.[49]

Imine ligands are rarely used as their copper(I) complexes are inherently unstable and need to be handled at below 0 °C under inert gas.[46] An exception are the copper(I) complexes of chiral pybox ligands, which were applied by Fokin and Finn in the kinetic resolution of α-chiral azides as well as in the desymmetrization of *gem*-diazides.[50] Scheme 14 shows the kinetic resolution of 1-(azidoethyl)benzene by reaction with phenylacetylene in the presence of a pybox ligand at 0 °C in dichloromethane to give predominantly the (*R*)-enantiomer of 4-phenyl-1-(1-phenylethyl)-1*H*-1,2,3-triazole. Although the stereodiscrimination is rather sluggish with a selectivity factor of $s = 8 \pm 0.4$, this report was a proof of principle that ligand-accelerated catalysis with chiral copper(I) complexes can facilitate asymmetric kinetic resolution by CuAAC.

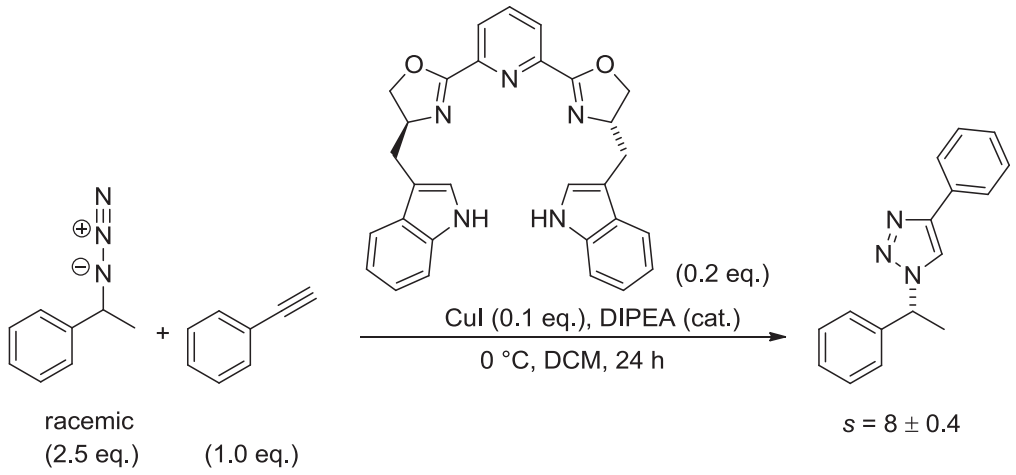

Scheme 14: Kinetic resolution of a racemic mixture of 1-(azidoethyl)benzene by a CuAAC reaction in the presence of a chiral pybox ligand ($s = k_{rel} = k_{fast}/k_{slow}$).[50]

Shortly after their seminal communication on the CuAAC reaction, the group of Sharpless reported the observation of an autocatalytic effect in the synthesis of tris-(triazolyl)amines, *i.e.* the tris(triazolyl)amine products act as rate-accelerating ligands for copper(I).[40a] The authors used the newly developed ligand system in a bioconjugation reaction with a virus. The exterior surface of the coat protein of cowpea mosaic virus was labelled with 60 azide groups as shown in Scheme 15.[40a] Then, the reaction with an alkyne-functionalized dye was carried out in the presence of copper(II) sulphate, TBTA as ligand and TCEP as reducing agent in a solution of potassium phosphate buffer (pH 8) and *tert*-butanol at 4 °C. Apart from acelerating the CuAAC process, the key advantage of TBTA is to stabilize the Cu(I) oxidation state in aqueous solution. This is important as Cu(II) ions are harmful to this experiment in two ways: on the one hand, Cu(II) ions catalyze the oxidative coupling of the alkyne substrates to give diynes; on the other hand, Cu(II)-triazole adducts on the protein surface of the virus induce the rapid decomposition of the capsid.

This communication by Sharpless *et al.* in 2003 triggered the search for other highly effective polytriazole ligands.

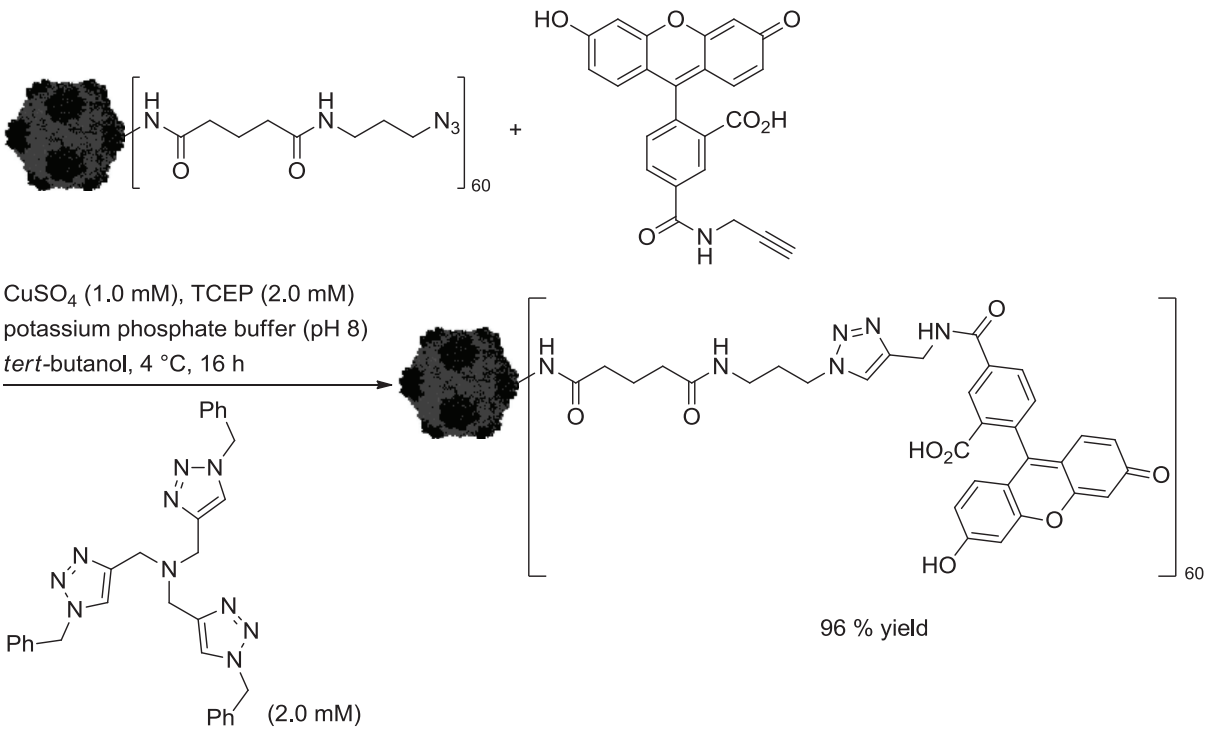

Scheme 15: Bioconjugation reaction of capsid-bound azide groups with alkinyl-functionalized dye molecules (cowpea mosaic virus is presented by the image of its crystal structure as published by the group of Lin in 1999).[40a, 51]

In 2004, Sharpless and Fokin compared a variety of polytriazoles as ligands in the CuAAC model reaction of benzyl azide with phenylacetylene in a solvent mixture of water and *tert*-butanol under aerobic conditions.[52] However, of all candidates tested, TBTA turned out to be the most potent additive for protecting the copper(I) ions with regard to oxidation and disproportionation. It was supposed that TBTA acts as a tetradentate ligand and blocks all coordination sites at the copper centre so that no oxidant can attack at the copper(I) ion. The tertiary amine's nitrogen atom was assumed to bind permanently to the metal centre, while the pendant triazole ligands might temporarily dissociate from the copper(I) ion to allow for the formation of the copper acetylide as starting point of the catalytic cycle (Scheme 9). The CuAAC reaction can even be carried out with tetrakis(acetonitrile)copper(I) hexafluorophosphate (1 mol-%) and TBTA (1 mol-%) under aerobic conditions. Cyclic voltammetry measurements have supported the hypothesis of TBTA influencing the redox activity of copper(I), as the redox potential of the Cu(I)/Cu(II) pair was shown to rise by approximately 300 mV when the water-soluble derivative tris(hydroxypropyltriazolylmethyl)-amine was present. Another water-soluble derivative, tris(1-benzyl-1*H*-1,2,3-triazol-4-yl)methanol, was found to be an excellent ligand for the preparation of air-stable

copper(I) complexes, which are highly active in CuAAC reactions on water or under neat conditions (Scheme 16).[53] Albeit no crystals could be grown, XRD and NMR measurements hint at the formation of a 1:1 complex between the ligand and copper(I) chloride.

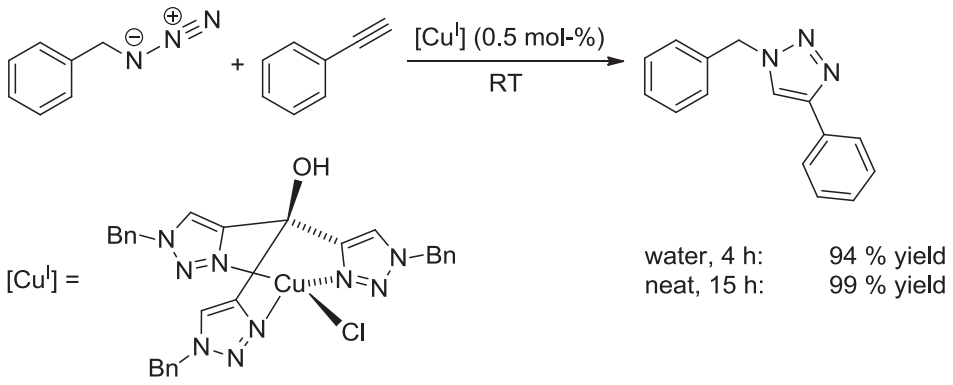

Scheme 16: CuAAC test reaction with chlorido[tris(1-benzyl-1*H*-1,2,3-triazol-4-yl)methanol-κ^3N^3]copper(I).[53]

In 2008, the group of Donnelly was able to crystallize a dinuclear copper(I)-TBTA complex from TBTA and tetrakis(acetonitrile)copper(I) tetrafluoroborate under anaerobic conditions in acetonitrile.[54] The single crystal X-ray structure shows a dinuclear dication $[Cu_2(\mu\text{-TBTA-}\kappa^4N^2,N^3,N^{3'},N^{3''})_2]^{2+}$, in which the coordination geometry at each copper(I) centre is a distorted tetrahedron. In contrast to the structural hypothesis by Sharpless and Fokin,[52] the central nitrogen of the tertiary amine does not coordinate to either copper(I) ion in the solid state. Instead the copper ions are bound to three proximal and one medial nitrogen atom each, *i.e.* one triazole ring in each TBTA molecule bridges the two copper ions as shown in Scheme 17. The air-sensitive salt $[Cu_2(\mu\text{-TBTA-}\kappa^4N^2,N^3,N^{3'},N^{3''})_2][BF_4]_2$ was shown to be an effective catalyst in the CuAAC test reaction of phenylacetylene with 2-azido-*N*-phenylacetamide even under aerobic conditions. With tetrakis(acetonitrile)copper(I) hexafluorophosphate in the absence of TBTA, no reaction was observed under identical conditions; only the addition of TBTA triggered the CuAAC catalysis.

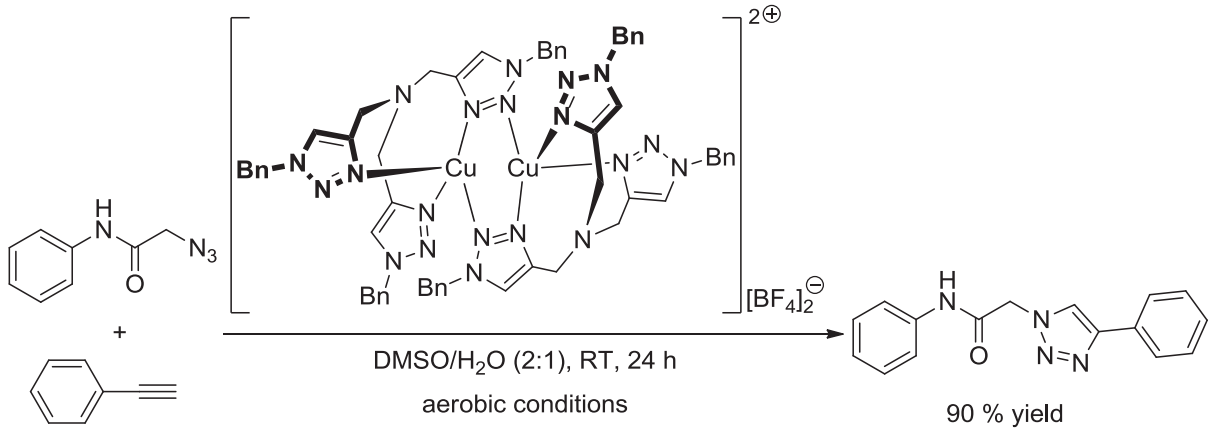

Scheme 17: CuAAC model reaction with $[Cu_2(\mu\text{-TBTA-}\kappa^4N^2,N^3,N^{3'},N^{3''})_2][BF_4]_2$.[54]

Albeit the crystal structure of the $[Cu_2(\mu\text{-TBTA-}\kappa^4N^2,N^3,N^{3'},N^{3''})_2][BF_4]_2$ precatalyst has been solved, the structural characteristics of the active species in solution remain unknown. A reaction calorimetry study by Finn gives no “clean” second order reaction profile in the CuAAC of benzyl azide (0.25 M) with phenylacetylene (0.45 M) in the presence of copper(II) sulphate pentahydrate (2 mM), sodium ascorbate (25 mM) and TBTA (4 mM) at 65 °C. Instead, the thermogram suggests different catalyst species to be involved.[55] In their subsequent mechanistic report,[20] Fokin and Finn kinetically investigated the reaction of phenylacetylene (1 mM; 10 - 50 mM) with benzyl azide (1 mM; 10 - 50 mM) in a solvent mixture of dimethyl sulphoxide and aqueous buffer in the presence of copper(II) sulphate (0.05 mM; 0.020 - 0.25 mM) and TBTA (2:1 ratio ligand:metal) at room temperature and pH 8 by varying the concentrations of the different reagents while keeping all other parameters constant. Surprisingly, they found a first-order dependence of the rate law with respect to the concentration of copper ions. As with other ligands tested in this study, the reaction was zero order in the concentration of the azide. The finding that the catalysis is inhibited by high concentrations of alkyne[18] was confirmed by determination of the alkyne’s rate order to be negative (-0.28 ± 0.2). However, in contrast to CuAAC reactions with other ligands, there was no “threshold” performance, *i.e.* kinetics was strictly continuous. Based on these findings, Donnelly suggested that the solid state complex $[Cu_2(\mu\text{-TBTA-}\kappa^4N^2,N^3,N^{3'},N^{3''})_2][BF_4]_2$ is only a catalyst precursor.[54] In his opinion the catalytic species is likely to be mononuclear as the bridging coordination of one of TBTA’s triazole groups is probably very labile, so that the dinuclear complex can easily dissociate in solution. Donnelly saw this idea in concordance with the isolation of a mononuclear

copper(I) triazolide as CuAAC intermediate by Straub.[24] Fokin and Finn, on the other hand, point out the “complex ways”,[20] in which the CuAAC catalysis responds to changes in concentration, type of ligand, presence of chloride ions, type of buffer and other parameters. In objection to Donnelly’s suggestion of a mononuclear pathway, they strongly emphasize the need for a second copper centre to assist the formation of the C-N bond between the azide and the acetylide as shown in Scheme 9 and in accordance with evidence from structural studies[21, 26] as well as quantumchemical calculations.[31-32] Fokin and Finn suggest that more than one mechanism might be operational under the conditions studied and stress that the first order rate dependence in the presence of TBTA is an exception, as a second order dependence was found for most other ligand systems.[20, 55] Although many questions remain unanswered, the authors conclude that the main advantage of TBTA is to “keep the metal coordination chemistry ‘cleaner’ by providing a high local concentration of weakly binding arms, while at the same time allowing access to open coordination sites”.[20]

Closely related to the tris(triazolylmethyl) amine ligands are the tris(pyridylmethyl) amines, tris(benzothiazolylmethyl) amines and tris(2-benzimidazolylmethyl) amines as well as hybrids of the latter.[20, 55-56] These ligands have the same structural motif of a central tertiary amine being surrounded by three nitrogen heterocycles, but provide for CuAAC reactions that are much faster than with tris(triazolylmethyl) amine ligands such as TBTA.[55]

Table 3: Structural variety of tris(2-benzimidazolylmethyl) amine and tris(benzothiazolylmethyl) amine ligands synthesized by the group of Finn (the same abbreviations as in the publication are used: BimY = benzimidazolylmethyl with Y substituent at the N atom; Bth = benzothiazolylmethyl; E = CO_2Et; E' = $CO_2{}^tBu$; A = $CO_2^-K^+$).[55]

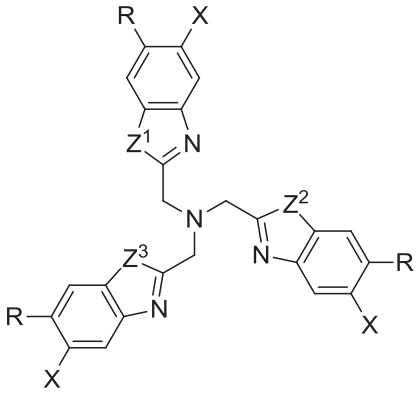

	Z^1	Z^2	Z^3	X	R
$(BimH)_3$	N-H	N-H	N-H	H	H
$(Bth)(BimH)_2$	S	N-H	N-H	H	H
$(Bth)_2(BimH)$	S	S	N-H	H	H
$(BimH/S)_3$	N-H	N-H	N-H	SO_3H	H
$(BimH/Me_2)_3$	N-H	N-H	N-H	CH_3	CH_3
$(BimC_1H)_3$	N-CH_3	N-CH_3	N-CH_3	H	H
$(BimC_3H)_3$	$N(CH_2)_2Me$	$N(CH_2)_2Me$	$N(CH_2)_2Me$	H	H
$(BimC_1E)_3$	$N(CH_2)CO_2Et$	$N(CH_2)CO_2Et$	$N(CH_2)CO_2Et$	H	H
$(BimC_1E')_3$	$N(CH_2)CO_2{}^tBu$	$N(CH_2)CO_2{}^tBu$	$N(CH_2)CO_2{}^tBu$	H	H
$(BimC_1A)_3$	$N(CH_2)CO_2K$	$N(CH_2)CO_2K$	$N(CH_2)CO_2K$	H	H
$(BimC_3A)_3$	$N(CH_2)_3CO_2K$	$N(CH_2)_3CO_2K$	$N(CH_2)_3CO_2K$	H	H
$(BimH)_2(BimC_4A)$	N-H	N-H	$N(CH_2)_4CO_2K$	H	H
$(Bth)(BimC_4A)_2$	S	$N(CH_2)_4CO_2K$	$N(CH_2)_4CO_2K$	H	H
$(BimC_4E)_3$	$N(CH_2)_4CO_2Et$	$N(CH_2)_4CO_2Et$	$N(CH_2)_4CO_2Et$	H	H
$(BimC_4A)_3$	$N(CH_2)_4CO_2K$	$N(CH_2)_4CO_2K$	$N(CH_2)_4CO_2K$	H	H
$(BimC_4A/Me_2)_3$	$N(CH_2)_4CO_2K$	$N(CH_2)_4CO_2K$	$N(CH_2)_4CO_2K$	CH_3	CH_3
$(BimH)(BimC_5A)_2$	N-H	$N(CH_2)_5CO_2K$	$N(CH_2)_5CO_2K$	H	H
$(BimC_5A)_3$	$N(CH_2)_5CO_2K$	$N(CH_2)_5CO_2K$	$N(CH_2)_5CO_2K$	H	H
$(Bth)_3$	S	S	S	H	H

As neither copper(I) alkynyl π-complexes nor acetylide complexes have been characterized for this class of ligands, mechanistic investigations have focused on kinetic measurements. The catalytic activity in the presence of the ligands (0.2 mM) presented in Table 3 was assessed in the test reaction of phenylacetylene (2 mM) with benzyl azide (1 mM) in a solvent mixture of dimethyl sulphoxide and aqueous buffer in the presence of sodium ascorbate (45 mM) and copper(II) sulphate pentahydrate (0.1 mM) at room temperature. Generally, all tris(2-benzimidazolylmethyl) amine ligands greatly accelerate this CuAAC reaction, but the rate is dependent on the nature of the heterocycle as well as on its substitution. As long as at least one benzimidazole ring is present in the ligand, the others can be replaced by benzothiazole rings. The rate of reaction in the CuAAC test reaction increases in the order $(Bth)_3$ << $(Bth)(BimH)_2$ < $(BimH)_3$ << $(Bth)_2(BimH)$.[55-56] With carboxylic acid or ester groups attached to the benzimidazole rings *via* alkyl chains $(CH_2)_4$ and $(CH_2)_5$ the CuAAC reaction was significantly accelerated [$(BimC_4A)_3$, $(BimC_3A)_3$, $(BimH)(BimC_5A)_2$, $(BimC_5A)_3$, $(BimC_4A/Me_2)_3$, $(BimC_4E)_3$]. On the other hand, $(BimC_1A)_3$ produced one of the worst performing catalysts as the acid group is directly attached to the benzimidazole by a CH_2-linker. Many of the observed reactions were sensitive towards the choice of pH and type of buffer, which might be due to a change in the rate-limiting step of the catalytic cycle or influences on structure and speciation. The water-soluble ligand $(BimC_4A)_3$ was found to be the most convenient for a variety of substrates in aqueous solutions with only 0.01 to 0.50 mol-% copper ions, as these reactions were found to be very fast, high-yielding and insensitive towards a wide range of pH values. On the other hand, tris(2-pyridylmethyl) amine $(Py)_3$, a secondary amine $H(BimH)_2$ and $[Py(BimC_4A)_2]$ were shown to slow down the reaction or have no effect on its rate.

As “ligand-free” CuAAC reactions have a second order rate law with respect to the concentration of copper ions,[18] the group of Finn has also prepared a “dimerized” version of $(BimH)_3$, namely $[(BimH)_2C_2(BimH)_2]$,[57] but for reasons that are not further discussed in their publication this ligand proved to be an inhibitor of the CuAAC reaction. Although the authors planned to explore “other binucleating systems” in future work,[55] no publication of any synthesis and CuAAC application of molecularly defined dinuclear copper complexes is known to us, except for the TBTA complex reported by Donnelly *et al.* (Scheme 17).[54]

Mechanistically, most ligand systems presented in Table 3 form copper catalysts with a “clean” second order rate profile with respect to the concentration of copper ions in reaction calorimetry experiments.[55] In their subsequent study, Fokin and Finn have examined the rate law for the CuAAC reaction in the presence of TBTA, $(BimH)_3$, $(BimC_4A)_3$, $(Bth)_3$ and $(Py)_3$. For the first time, the authors have experimentally obtained a rate law for the reaction of benzyl azide with phenylacetylene in the presence of Tris buffer, in which all participants, *i.e.* alkyne, azide and copper complex, have an integer exponent (Equation 1).[20]

Equation 1: Experimentally determined rate law for the reaction of benzyl azide with phenylacetylene in the presence of Tris buffer.[20]

$$\text{rate} = k\, c(BnN_3)\, c(PhC{\equiv}CH)\, c^2([Cu(BimH)_3])$$

It had already been shown that the presence of Tris buffer significantly decelerates the CuAAC reaction in the presence of $(BimH)_3$ and even more so with TBTA over a standard range of concentrations.[55] However, in the absence of buffer, the copper complexes of $(BimH)_3$ and $(BimC_4A)_3$ exhibited discontinuous kinetic behaviour: at low catalyst concentrations, the reaction stopped after a few turnovers, but at higher concentrations the usual high activity was observed, though it could only be marginally enhanced by further increasing the catalyst’s concentration. Similarly discontinuous behaviour was observed for the rate order with respect to the azide concentration. At low concentrations (10 - 20 mM) the observed rate order was 0.4, whereas the rate was independent of the azide’s concentration at higher concentrations (40 - 50 mM). When lowering the catalyst concentration, the rate was independent of the azide’s concentration throughout the given range of concentrations. This observation is attributed to the presence of chloride ions in the reaction mixture when Tris buffer is used, as the pH of the medium was identical for reactions in the presence and absence of Tris due to the buffer capacity of sodium ascorbate. A control experiment showed that addition of potassium chloride had an inhibitory effect on the catalysis as well (approximately by a factor of 3) and that the discontinuous kinetics with regard to the catalyst’s and the azide’s concentration was not observed anymore. As only the rate order of the azide and not of the alkyne was influenced by addition of potassium chloride, it is suggested that chloride ions and the azide substrate have approximately the same affinity for copper(I) centres. Alkyne or acetylide ligands, on the other

hand, coordinate much stronger to copper(I) ions and thus their rate order is not affected by the presence of chloride ions.

In another experiment, the concentration of copper ions was held constant and the concentration of ligand $(BimH)_3$ was increased. It was observed that the initial amount of rapid catalytic activity before steady state was reached was higher with low ligand concentrations, *i.e.* the lower the ligand concentration, the faster the reaction at the beginning. In fact, the ligands listed in Table 3 can be sorted in two categories, namely group 1 that shows best catalytic activity at a metal:ligand ratio 1:1 [$(BimH)_3$, $(BimC_1A)_3$, $(BimH/S)_3$], and group 2 whose ligands perform optimally at a metal:ligand ratio of 1:2 [$(BimC_1H)_3$, $(BimC_1E)_3$, $(BimC_1E')_3$, $(BimC_4A)_3$, $(BimH/Me_2)_3$]. However, even for group 1 ligands such as $(BimH)_3$ the rate of reaction does not dramatically drop when excess quantities of the ligand are present. If only one species were present, we would expect the activity to give a peak at a 1:1 ratio and then drop, as excess ligands block coordination sites for the substrates and thus create a much less active copper species. This means that the observed marginal loss of activity in the presence of excess ligand is either due to a low equilibrium constant for the formation of the less active catalyst species or that at least two mechanistic pathways for catalysis exist. It is suspected that a “complex set of equilibria” is involved in the speciation of catalytically active copper(I) complexes and that the formation of different multinuclear copper aggregates is decisive.[20, 55]

In 2010, Finn *et al.* published a comprehensive study comparing different (hybrid) tris(heterocyclemethyl) amine ligands regarding their binding abilities, kinetic rate orders and catalytic performance under various conditions by calorimetry measurements. The affinity of the heterocyclic arms to the copper(I) ions increases in the order triazole << pyridine < benzimidazole.[20] The different (hybrid) ligands are assigned to three different classes as shown in Figure 7.

Class I ligands

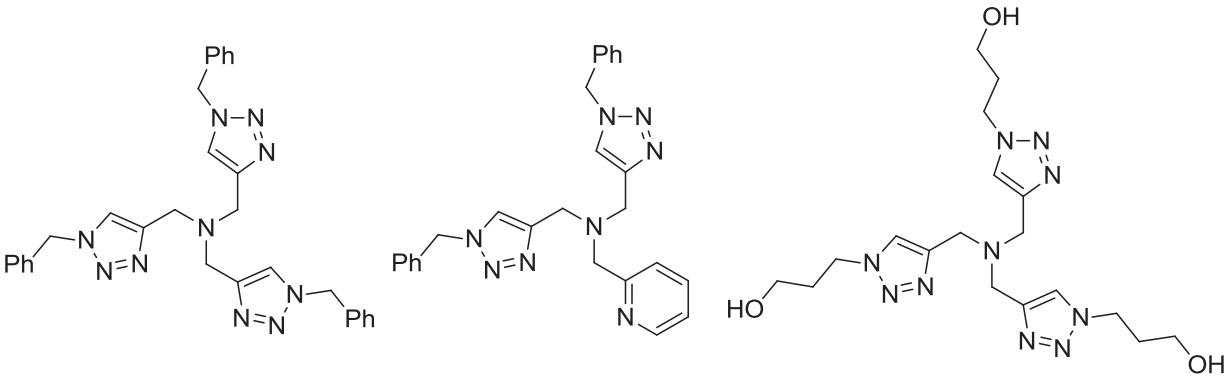

TBTA = $(Trz)_3$ $(Py)(Trz)_2$ $(TrzC_3OH)_3$

Class II ligands

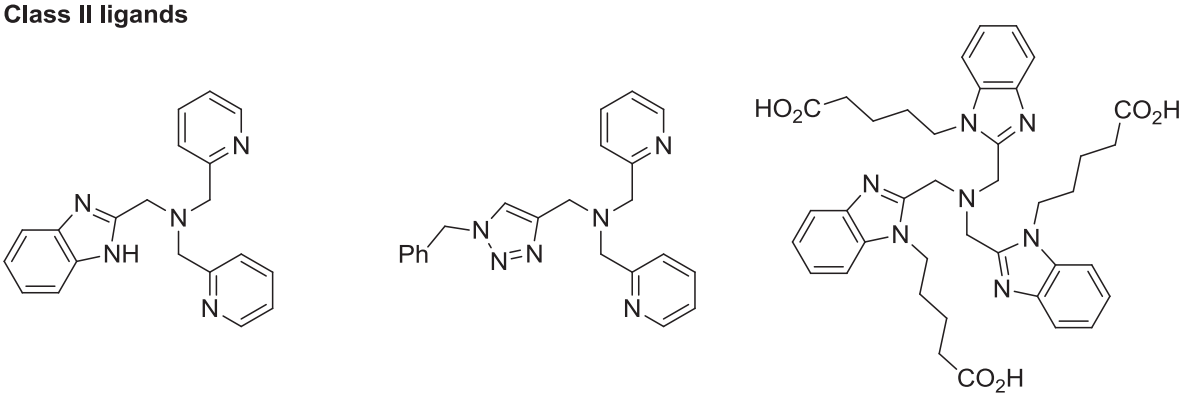

$(BimH)(Py)_2$ $(Py)_2(Trz)$ $(BimC_4A)_3$

Class III ligands

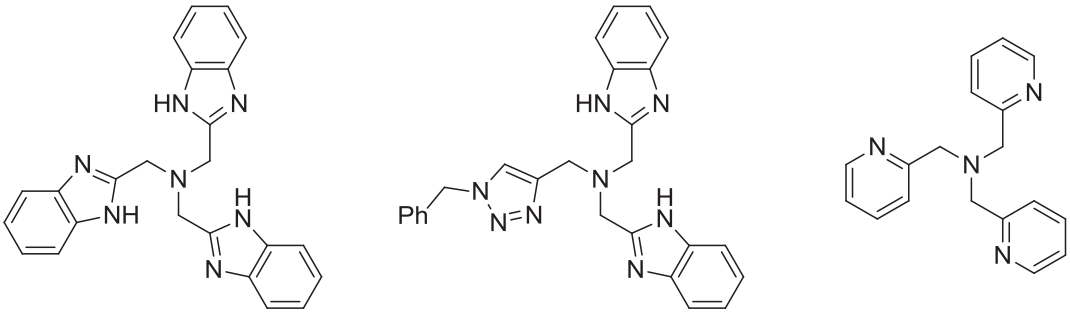

$(BimH)_3$ $(BimH)_2(Trz)$ $(Py)_3$

Figure 7: Categories of tris(heterocyclemethyl)amine ligands regarding their binding ability to copper(I) ions.

- *Class I* ligands do not contain benzimidazole groups and therefore coordinate weakly to copper(I) ions. Under aqueous conditions (H_2O:DMSO = 9:1) these ligands maintain their high catalytic activity even if the ligand is present in great

excess (ligand:metal ratios of 2:1 and 4:1). In contrast, the catalytic performance with these ligands is bad in DMSO. TBTA is an example for this class.

- *Class II* ligands contain two or more benzimidazole or pyridine groups and coordinate strongly to copper. The catalytic activity of the corresponding copper complexes is retained in DMSO. In aqueous solutions, however, optimal catalytic performance is observed at ligand:metal ratios of 0.5:1 or 1:1. Beyond this maximum, the catalytic activity decreases dramatically as the ligand is added in excess. An example for class II is $(BimH)(Py)_2$, an extremely active ligand in a 4:1 solvent mixture of DMSO and water at a ligand:metal ratio between 0.5:1 and 1:1. The rate order for the corresponding complex $[Cu(BimH)(Py)_2]$ was experimentally determined to be three in a 4:1 solvent mixture DMSO:H_2O and a first order rate law was found in an aqueous medium (DMSO:H_2O = 1:9). The rate order was the same for differrent metal:ligand ratios.
- *Class III* contains ligands that form relatively inactive copper complexes over all metal:ligand ratios tested, for example $(BimH)_3$ or $(Py)_3$.

These observations can be explained by considering the relative donor strengths of solvent molecules and ligands.

In strong donor solvents such as DMSO, DMF and NMP, the solvent molecules compete with the substrates and the *N*-donor ligands for binding sites at the metal centre. Thus, weak ligands categorized in class I are replaced by solvent molecules and ligand-accelerated catalysis is diminished. Class II ligands, on the other hand, coordinate much more strongly to copper(I) ions than solvent molecules, even if strong donor solvents such as DMSO are used. Reactions thus proceed well in both strongly and weakly coordinating solvents as long as the ligands are not present in excess. As soon as the ligand:metal ratio exceeds a certain threshold (0.5 or 1), the catalytic activity drops dramatically as very stable complexes are formed which do not have free coordination sites for binding the azide substrate. Class I ligands are not able to form such stable inhibitory complexes and can thus be used in great excess in weakly coordinating solvents like water.

To summarize their mechanistic picture for CuAAC reactions in the presence of tripodal tris(heterocyclemethyl)amine ligands also taking into account the coordinating solvent molecules and inhibitory species, Finn *et al.* proposed the mechanistic picture shown in Scheme 18.[56]

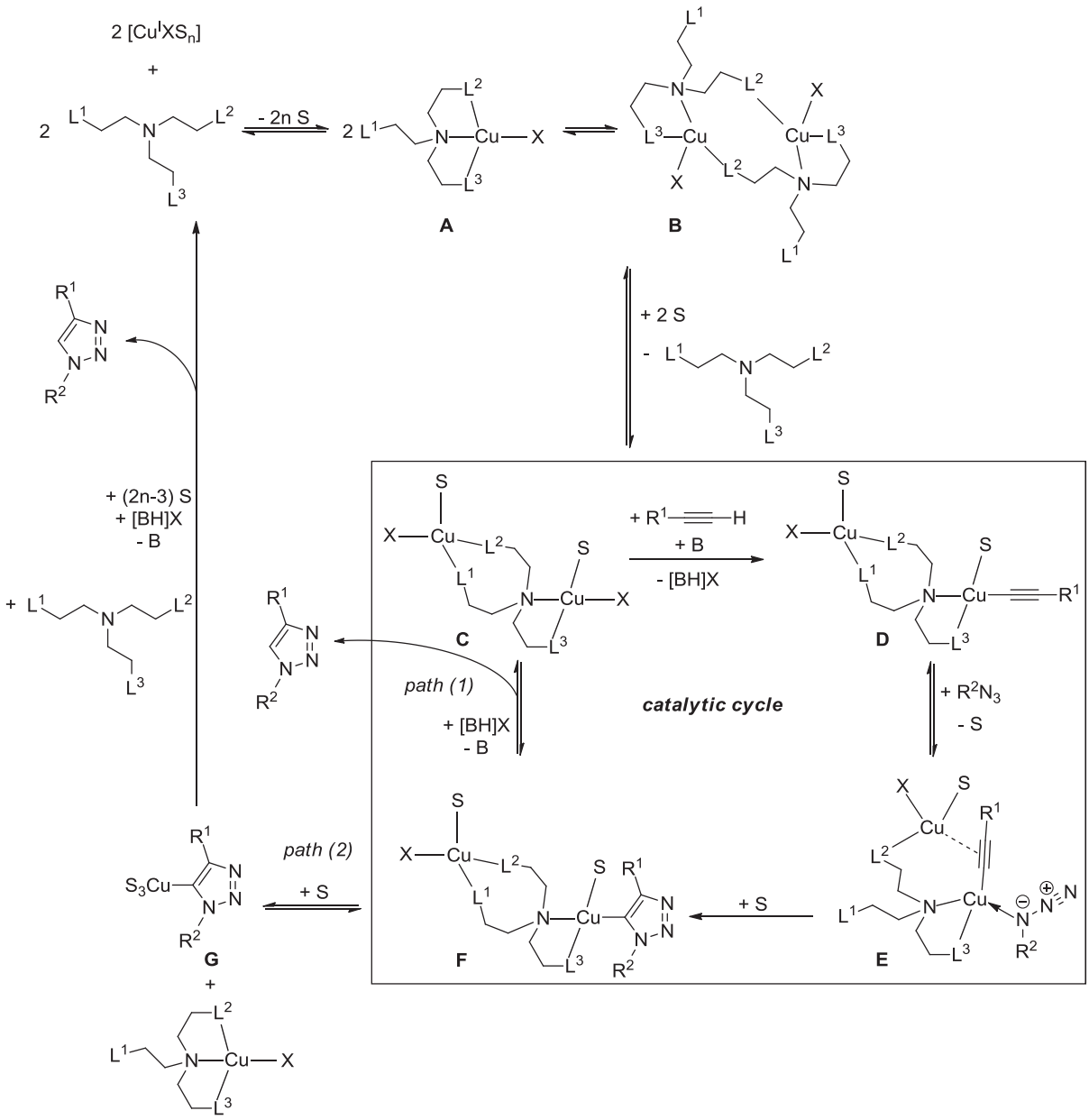

Scheme 18: Mechanistic scheme for ligand-accelerated catalysis with tripodal tris(heterocyclemethyl)amine ligands in consideration of solvent coordination and formation of inhibitory species (S = solvent molecule; B = base; X = halogen; n = integer number; L^1, L^2, L^3 = coordinating heterocycles in the tripodal ligand).[56]

The complexes **A** and **B** shown in the upper part of Scheme 18 are catalytically inactive: mononuclear complex **A** lacks a second copper centre to facilitate the C-N bond-forming step,[31-32] and in complex **B** both copper(I) ions are coordinatively saturated so that the azide substrate cannot be bound. These inhibitory complexes **A**/**B** are formed when strong ligands (class II) are used in equimolar or excess amounts in solvents which can only coordinate weakly to copper(I) ions. With only 0.5 molar equivalents of class II ligands or by dissociation of weakly binding class I ligands, the

catalytically active complex **C** can be formed, whose solvent ligands can be easily replaced to give the acetylide complex **D** and then complex **E**, in which both substrates are assembled for the crucial C-N bond-forming step. The pathway by which the copper triazolide complex **F** breaks down determines the overall rate order of reaction with respect to the concentration of copper(I) ions and ligand. In weak donor solvents, the dinuclear scaffold remains intact by regeneration of complex **C** (*path (1)*). As no change in the number of copper(I) ions present in the active species occurs in the catalytic cycle, this pathway would lead to a first-order dependence on the concentration of the dinuclear copper catalyst: rate = k • c([Cu_2L]) (L = tripodal ligand). However, in strong donor solvents, dinuclear complex **F** breaks up to give two mononuclear complexes **A** and **G** (*path (2)*). This pathway is in accordance with a second-order dependence on the concentration of copper(I) ions and a first-order dependence on the ligand's concentration, as one ligand and two copper centres need to be reassembled for one turnover: rate = k • $c^2(Cu^I)$ • c(L) (L = tripodal ligand). All in all, the following conclusions can be drawn: for CuAAC reactions in weak donor solvents, *e.g.* under aqueous conditions, weaker ligands (class I) are favourable in order to minimize the formation of inhibitory chelate complexes such as **B**. Stronger ligands (class II) are necessary in strong donor reaction media in order to facilitate the formation of dinuclear copper complexes needed for the mechanistic steps shown in Scheme 9.

In one of their first studies regarding the influence of additives, Fokin and Finn have presented 2,2'-bipyridine and 1,10-phenanthroline derivatives as effective ligands for CuAAC reactions (Figure 8).[17]

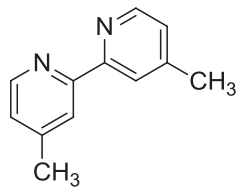

4,4'-dimethyl-2,2'-bipyridine

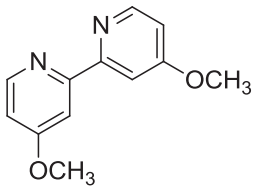

4,4'-dimethoxy-2,2'-bipyridine

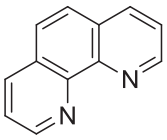

1,10-phenanthroline

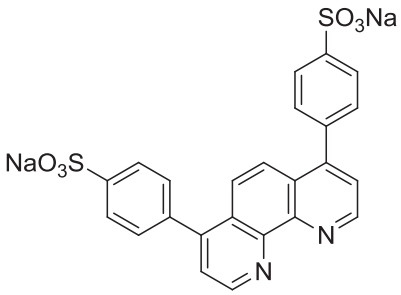

sodium 4,4'-(1,10-phenanthroline-4,7-diyl)dibenzenesulphonate

Figure 8: Derivatives of 2,2'-bipyridine and 1,10-phenanthroline, commonly used ligands in CuAAC reactions.

A two- to three-fold increase in the rate of reaction was observed with this class of ligands. Bathophenanthrolinedisulfonic acid disodium salt turned out to be an excellent ligand as it is water-soluble and allows for colorimetric detection. A ligand:copper ratio of 2:1 was found to be optimal, and under these conditions the rate order with respect to the complex [CuL_2] was found to be two. However, if these ligands are added in excess quantities (ligand:metal ratio > 2:1), the reaction is dramatically slowed down or does not work at all. As the rigid chelating ligands of this class bind so strongly to copper(I) ions, they form inhibitory species analogous to complex **B** in Scheme 18. Although even large excess quantities of strongly binding tris(heterocyclemethyl) amines only slow down the CuAAC reaction, catalysis is usually shut down completely when an excess of 2,2'-bipyridine or 1,10-phenanthroline derivatives is present in the reaction mixture.[55] Although the structural characteristics of the corresponding copper complexes remain elusive, these ligands are frequently applied in CuAAC reactions, especially in macromolecular chemistry.[46]

Sulphur-based ligands are rarely used for CuAAC catalysis. However, the copper(I) bromide dimethyl sulphide complex [$CuBr \cdot SMe_2]_2$ is well soluble in organic media, commercially available and shows good catalytic performance.[58] For example, the group of Nakamura used [$CuBr \cdot SMe_2]_2$ as catalyst in THF to synthesize triazole-

linked DNA analogues either in solution or on solid support.[59] Of the variety of sulphur-containing compounds tested by the group of Fu, thioanisole turned out to be a good ligand for CuAAC catalysis. With this ligand (30 mol-%) and copper(I) bromide (5 mol-%) the reaction of benzyl azide with phenylacetylene is completed within 10 minutes in aqueous solution at room temperature under aerobic conditions.[58] A homogeneous catalyst for CuAAC reactions in organic solvents was presented by van Koten *et al.* in 2009.[60] The (2-aminoarenethiolato)copper(I) complex reported in their work is an efficient catalyst for CuAAC reactions with a variety of substrates in dichloromethane or acetonitrile at room temperature. For example, the standard test reaction between benzyl azide and phenylacetylene in dichloromethane gives 91 % yield within 18 hours (Scheme 19). As copper(I) thiolate complexes show a high tendency to form aggregates,[61] speciation and nuclearity of the catalytically active species remain unknown.

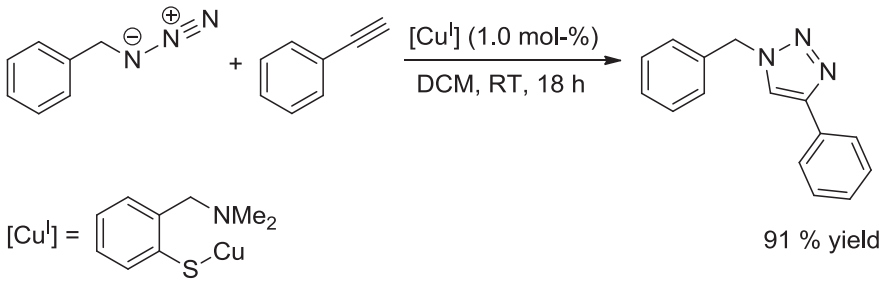

Scheme 19: Application of a (2-aminoarenethiolato)copper(I) complex as homogeneous catalyst for the CuAAC test reaction.[60]

Copper(I) complexes with phosphorus ligands, for example the commercially available air-stable salts [CuBr(PPh$_3$)$_3$] and {CuI[P(OEt)$_3$]}, are also well soluble in organic solvents and do thus allow for homogeneous CuAAC catalysis. They were first applied in the synthesis of neoglycoconjugates in the presence of DIPEA or DBU under microwave irradiation in toluene solution.[62] However, a recent study by Díez-González has shown, that neither irradiation nor any additive is necessary for [CuBr(PPh$_3$)$_3$] to be an effective CuAAC catalyst.[63] In a solvent mixture of water and *tert*-butanol, the test reaction of benzyl azide with phenylacetylene proceeded within two hours to give 95 % yield when 5 mol-% of [CuBr(PPh$_3$)$_3$] were present. Acetone, DMSO and acetonitrile also turned out to be suitable solvents for this catalyst system (Scheme 20). The catalyst loading for this reaction can be decreased to 500 ppm and full conversion is still reached within 24 hours under neat conditions.

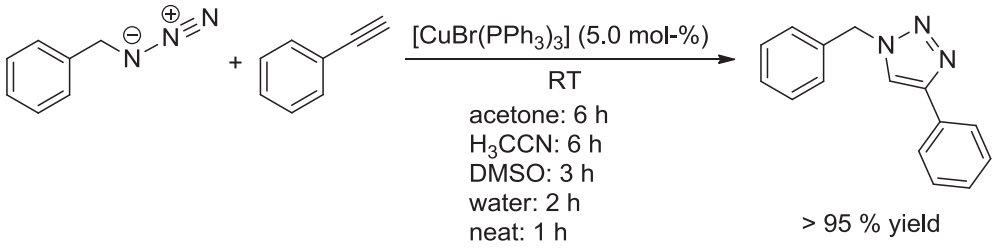

Scheme 20: Application of $[CuBr(PPh_3)_3]$ as homogeneous catalyst for the CuAAC test reaction of benzyl azide with phenylacetylene under homogeneous conditions in acetone, acetonitrile and DMSO, and as heterogeneous catalyst in water or under neat conditions.[63]

In this study, Díez-González also attempted the *in situ* preparation of the organoazide from the corresponding organic bromide and sodium azide. Albeit the organoazide was formed smoothly in DMSO or acetone, the cycloaddition reaction with phenylacetylene did not take place. A control experiment with benzyl azide, phenylacetylene and addition of sodium bromide showed that this salt exerts an inhibitory effect on the CuAAC catalysis with $[CuBr(PPh_3)_3]$. Only by applying high catalyst loadings and long reaction times could conversion to the triazole product be observed. However, this effect was not found when water was used as reaction medium. It is supposed that bromide ions can bind strongly to copper(I) ions in organic media, but due to a tight layer of solvent molecules they cannot do so in aqueous solution. Thus, the CuAAC reaction with *in situ* generated azides could only be carried out in water as reaction medium.

Chen *et al.* presented $[Cu(PPh_3)_2]NO_3$ as an effective CuAAC catalyst in toluene, water or under neat conditions. With 0.5 mol-% of this catalyst, the test reaction of phenylacetylene with benzyl azide in toluene proceeds within 40 minutes at room temperature to give 96 % yield. Under neat conditions, the amount of catalyst can be lowered to 50 ppm and the reaction still gives 81 % yield after 24 hours.[64] Recently, the authors of this report have shown that the phenanthroline complex $[Cu(phen)(PPh_3)_2]NO_3$ outperforms their original catalyst $[Cu(PPh_3)_2]NO_3$. With 2 mol-% $[Cu(phen)(PPh_3)_2]NO_3$ the model reaction of phenylacetylene and benzyl azide under neat conditions is finished after three minutes and gives 97 % yield.[65]

In 2011, Díez-González *et al.* introduced phosphinite and phosphonite copper(I) complexes (Figure 9) as novel molecularly defined catalysts for CuAAC reactions under Click conditions.[66]

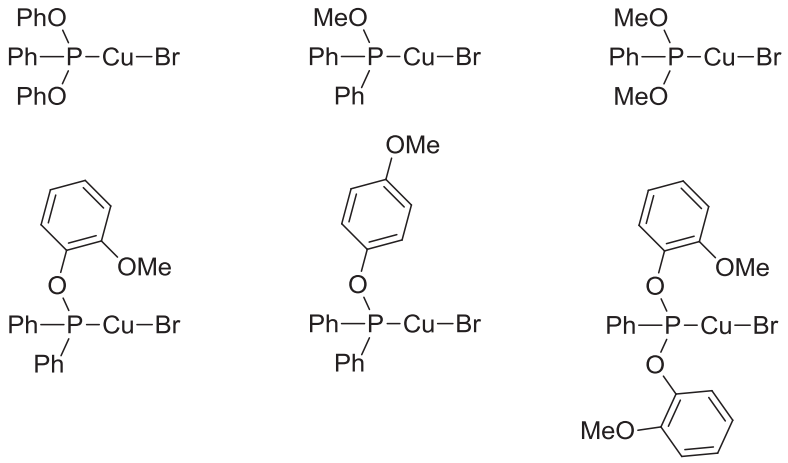

Figure 9: Phosphinite and phosphonite copper(I) complexes presented by Díez-González.[66]

These copper(I) complexes can be handled under aerobic conditions and have been fully characterized including single crystal X-ray structures, which show a cubane-like [Cu_4Br_4] scaffold. Their main advantages are the ease of preparation, the tolerance towards water and air, and that they are molecularly defined so that their characteristics can be tuned according to specific demands. In CuAAC reactions with these complexes, no additives are needed. For example, the model reaction of phenylacetylene with benzyl azide in the presence of 0.5 mol-% {CuBr[PPh_2(OPh-2-OMe)]} (Figure 9, second row, left) in water proceeds at room temperature to give > 95 % conversion after three hours.

In organometallic catalysis, *N*-heterocyclic carbene ligands (NHCs) have superseded phosphane ligands in many fields of application.[67] It was thus only a matter of time until NHC-copper complexes were first employed in CuAAC reactions. In 2006, the group of Nolan reported the application of air-stable complexes [(NHC)CuX] as efficient catalysts for CuAAC reactions with terminal and internal alkynes in aqueous solution or under neat conditions.[68] Also, the azide substrates could be prepared *in situ* by reaction of the corresponding bromide with sodium azide. For example, the reaction of benzylbromide with sodium azide and phenylacetylene in the presence of 2 mol-% [(SIMes)CuBr] in water gave 86 % 1-benzyl-4-phenyl-1*H*-1,2,3-triazole within 18 hours at room temperature. However, in organic solvents such as THF, dichloromethane or *tert*-butanol, only poor conversions were observed with these [(NHC)CuX] catalysts.

Table 4: CuAAC catalysts of type [(NHC)CuX] and their performance in the CuAAC test reaction.[68b]

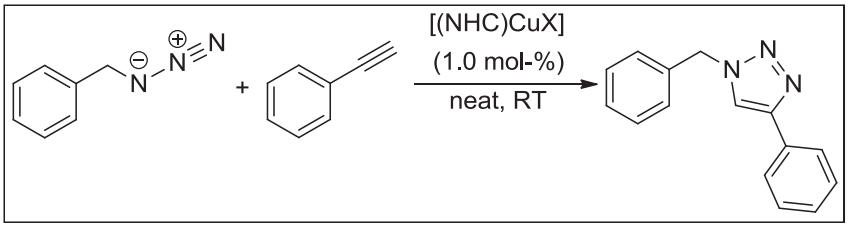

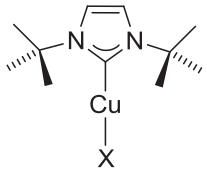

[(ItBu)CuX]
X = Cl, Br, I

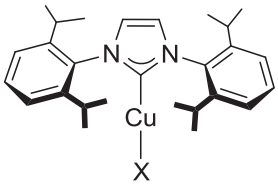

[(IPr)CuX]
X = Cl, Br, I

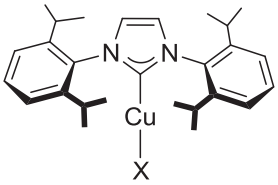

[(SIPr)CuX]
X = Cl, Br, I

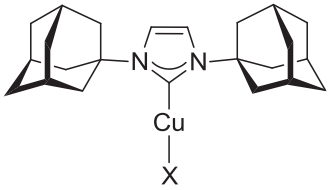

[(IAd)CuX]
X = Cl, Br, I

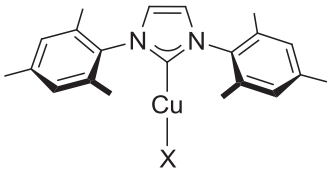

[(IMes)CuX]
X = Cl, Br

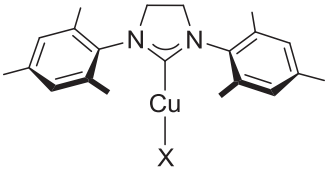

[(SIMes)CuX]
X = Cl, Br

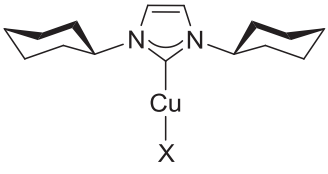

[(ICy)CuX]
X = Cl, Br, I

[(NHC)CuX]	reaction time	conv. [%]		[(NHC)CuX]	reaction time	conv. [%]
[(IPr)CuCl]	24 h	88		[(IMes)CuCl]	1 h	>99
[(IPr)CuBr]	24 h	63		[(IMes)CuBr]	30 min	>99
[(IPr)CuI]	4 h	95		[(SIMes)CuCl]	20 min	>99
[(SIPr)CuCl]	15 h	99		[(SIMes)CuBr]	20 min	>99
[(SIPr)CuBr]	10 h	96		[(ICy)CuCl]	10 min	>99
[(SIPr)CuI]	6 h	>99		[(ICy)CuBr]	1 h	>99
[(IAd)CuCl]	20 min	>99		[(ICy)CuI]	2 h	87
[(IAd)CuBr]	10 min	>99		[(ItBu)CuCl]	1 h	>99
[(IAd)CuI]	10 min	>99		[(ItBu)CuBr]	30 min	>99
				[(ItBu)CuI]	2 h	>99

Nolan *et al.* also report on the possibility of using [(SIPr)CuCl] as a latent catalyst.[69] With DMSO as solvent, complex [(SIPr)CuCl] (2 mol-%) does not facilitate the cycloaddition reaction of benzyl azide and phenylacetylene within one week. However, the latent catalyst could be activated by adding water and heating the reaction mixture to 60 °C for one hour, whereupon 99 % conversion was observed.
In 2009, Gautier *et al.* reported that the CuAAC catalysis with [(SIMes)CuCl] can be notably improved by addition of aromatic nitrogen donor ligands.[70] For example, fast homogeneous catalysis in water-alcohol solvent mixtures is possible with [(SIMes)CuCl] in the presence of 4-DMAP and 1,10-phenanthroline.

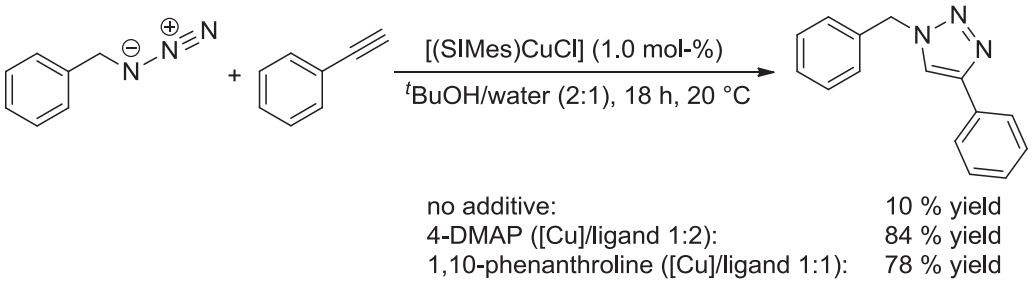

Scheme 21: Effect of additives on the CuAAC test reaction with [(SIMes)CuCl].[70]

The catalyst complex [(SIMes)CuCl(phen)] could be isolated as red crystals and a single crystal X-ray structure shows a distorted tetrahedral coordination geometry at the metal centre. Peak broadening indicative of ligand exchange was observed on the NMR time scale and the association constant of phenanthroline was determined to be approximately K = 250 M^{-1}. This relatively low value suggests that the phenanthroline ligand only binds weakly to the copper centre and can be easily replaced by the CuAAC's substrates. In an extended screening of *N*-donor additives, the efficiency in the CuAAC test reaction improved in the following order of ligands: neocuproine < 4,7-dimethoxy-1,10-phenanthroline < bathophenanthroline < 1,10-phenanthroline < 4,7-dichloro-1,10-phenanthroline.[71]

In 2006, the group of Nolan introduced a new family of monocationic copper(I) NHC-complexes of general formula $[(NHC)_2Cu]X$ (X = BF_4 or PF_6) as catalysts for hydrosilylation reactions of aldehydes, ketones and esters.[72] These complexes also display very high catalytic activity in CuAAC reactions in water, under neat conditions or as homogeneous catalysts in acetonitrile solution.[73]

Table 5: Performance of different $[(NHC)_2Cu]X$ (X = BF_4 or PF_6) precatalysts in the CuAAC test reaction of benzyl azide with phenylacetylene on water at room temperature.[73]

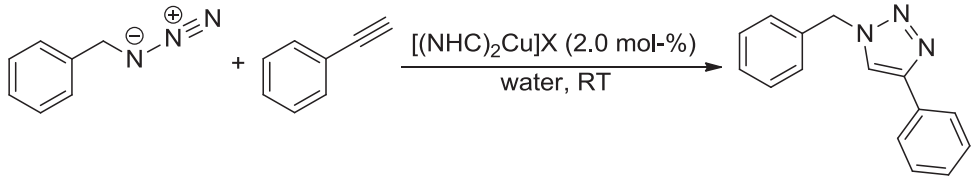

$[(NHC)_2Cu]X$	reaction time	conv. [%]		[(NHC)CuX]	reaction time	conv. [%]
$[(IPr)_2Cu]PF_6$	18 h	71		$[(IPr)_2Cu]BF_4$	8 h	100
$[(SIPr)_2Cu]PF_6$	5 h	100		$[(SIPr)_2Cu]BF_4$	5 h	100
$[(IMes)_2Cu]PF_6$	6 h	100		$[(IMes)_2Cu]BF_4$	6 h	100
$[(SIMes)_2Cu]PF_6$	18 h	5		$[(SIMes)_2Cu]BF_4$	18 h	13
$[(ICy)_2Cu]PF_6$	1.5 h	99		$[(ICy)_2Cu]BF_4$	5 h	95
$[(IAd)_2Cu]PF_6$	5 h	100		$[(IAd)_2Cu]BF_4$	3 h	100
$[(ItBu)_2Cu]PF_6$	18 h	76		$[(ItBu)_2Cu]BF_4$	18 h	35

$[(ICy)_2Cu]PF_6$ turned out to be the most efficient precatalyst (Table 5). It was thus tested in a variety of solvents and under neat conditions.

Table 6: Application of $[(ICy)_2Cu]PF_6$ in different organic solvents, water and under neat conditions.[73]

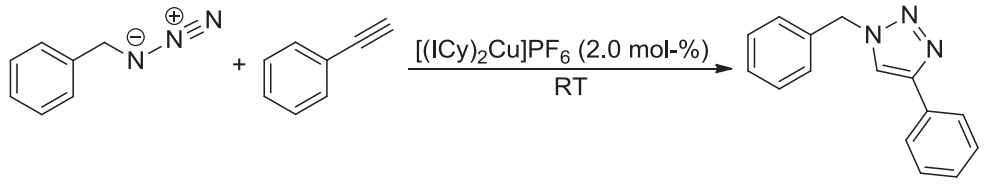

solvent	neat[b)]	water	DMSO	DMF	THF	acetone	acetonitrile
time[a)]	5 min	1.5 h	2 h	1.5 h	1 h	30 min	12 min

[a)]Reaction time until full conversion was observed by GC or NMR measurements.

[b)]The reaction under neat conditions was carried out with only 0.5 mol-% $[(ICy)_2Cu]PF_6$.

In alcoholic solvents, the reaction with $[(ICy)_2Cu]PF_6$ is sluggish, but in organic solvents such as acetone or acetonitrile, the CuAAC reaction proceeds even faster than in aqueous solution (Table 6). Neat conditions were found to be optimal as conversion was completed within five minutes with only 0.5 mol-% $[(ICy)_2Cu]PF_6$. As the

amount of catalyst was lowered to 50 ppm, still 80 % conversion was observed within 48 hours at room temperature.

Mechanistically, the second NHC ligand is supposed to play an active role in the catalytic cycle. After its dissociation from the precatalyst $[(NHC)_2Cu]X$, the free *N*-heterocyclic carbene can act as a base in the deprotonation of the alkyne substrate. As the protonation of the *N*-heterocyclic carbene is irreversible, the latter can no longer compete for the free coordination site at the copper(I) centre so that the formation of the copper acetylide complex is greatly facilitated. This "built-in" base, the irreversible deprotonation of the alkyne and the lack of species that can compete with the acetylide for free coordination sites at the copper(I) centre are probably the main factors why some complexes of type $[(NHC)_2Cu]X$ are catalytically more active than the [(NHC)CuX] family.

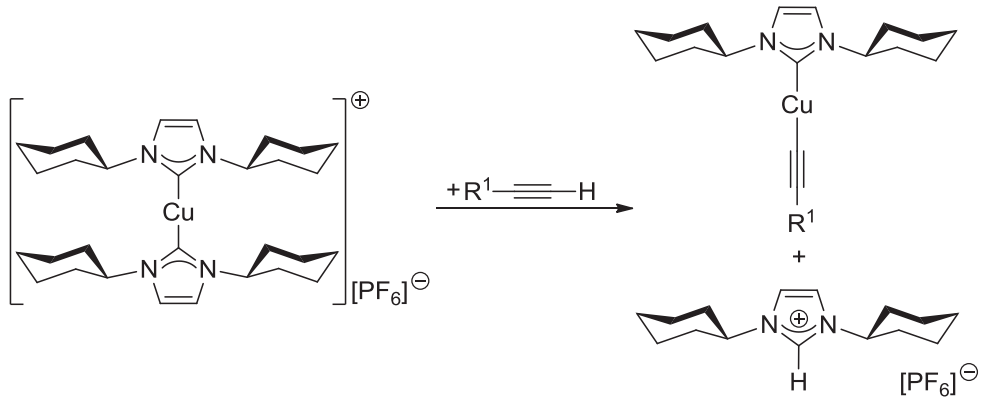

Scheme 22: Initiation of the catalytic cycle by formation of the copper acetylide intermediate from $[(ICy)_2Cu]PF_6$ and the alkyne substrate.[73]

Only recently, the potential of copper(I) acetate as heterogeneous catalyst for CuAAC reactions has been investigated by the group of Wang.[74] The authors of this study had noticed that the Cu-Cu distance found in polymeric copper(I) acetate $[(CuH_3CCO_2)_2]_n$ (2.556 Å) was in the same range as the distance for effective CuAAC catalysis with dinuclear copper(I) complexes as calculated in a DFT study by Ahlquist[32] (transition states with Cu-Cu distances of 2.54 Å for L = chloride and 2.64 Å for L = acetylide).[75] They tested copper(I) acetate in the CuAAC model reaction of benzyl azide with phenylacetylene and observed an excellence performance of this heterogeneous catalyst in a variety of solvents at room temperature under aerobic conditions (Table 7). At the beginning of each reaction, the authors observed a bright yellow color, which might be due to the formation of transient copper(I)

acetylide species.[76] And indeed did the isolation of this yellow compound in the absence of benzyl azide show that its elemental analysis and IR spectra are the same as for commercially available (phenylethynyl)copper PhC≡CCu.

Table 7: CuAAC reactions with copper(I) acetate as heterogeneous catalyst.[74]

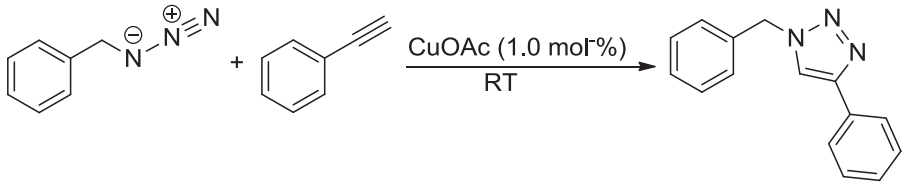

solvent	reaction time	yield
cyclohexane	8 min	98 %
dichloromethane	16 min	92 %
chloroform	15 min	93 %
toluene	10 min	98 %
water	11 min	95 %
acetonitrile	60 min	65 %
tetrahydrofuran	60 min	89 %

2.5 Applications of CuAAC Reactions

The CuAAC reaction is used in a plethora of fields such as preparative organic synthesis, bioconjugation, carbohydrate chemistry, polymer science, dendrimer synthesis, combinatorial chemistry, and materials science. In the following chapter, one example will be highlighted for each field of application.

2.5.1 Preparative Organic Synthesis

CuAAC reactions are valuable tools in the synthesis of triazole-containing compounds, as they are compatible with diverse functional groups and chemical conditions. It is thus recommendable to introduce the triazole groups as late as possible in the course of a complex synthetic pathway.[42]

As an example, a multicomponent reaction by combination of aldol, Wittig, Knoevenagel, Michael, Diels-Alder and CuAAC reaction is shown in Scheme 23.[77]

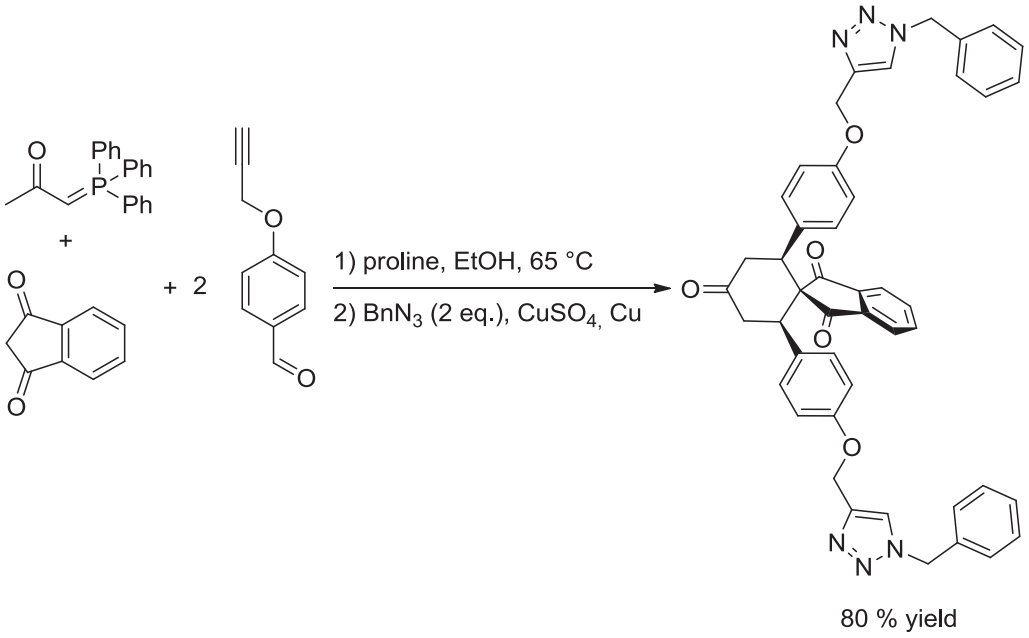

Scheme 23: Multicomponent reaction by combination of aldol, Wittig, Knoevenagel, Michael, Diels-Alder and CuAAC reaction in the synthesis of a polysubstituted spirotrione as reported by Barbas III.[77]

2.5.2 CuAAC for Bioconjugation

The aim of bioconjugation is to couple a biomolecule to another (bio)molecule *via* a covalent molecular linker. In the most common types of bioconjugate reactions, either a small molecule such as a fluorescent dye is coupled to a large biomolecule, or two proteins, for example an antibody and an enzyme, are conjugated to each other.[78]
The main advantage of CuAAC reactions in biological chemistry is the bioorthogonality of both substrates,[79] as neither the small and metabolically stable azide group nor the terminal alkyne interact or interfere with other molecules of the cellular environment. Both functional groups are nearly inert towards biological molecules and the reaction conditions found in living cells because they are neither basic or acidic nor strong electrophiles or nucleophiles.
The first example of a CuAAC bioconjugation, the reaction of virus-bound azide with alkinyl-functionalized dye as reported by Sharpless *et al.* in 2003, is shown in Scheme 15.[40a]

In 2006, the groups of Carell and Seela reported the postsynthetic functionalization of DNA derivatives by Click chemistry.[80] Carell used terminal alkyne groups as chemical reporters in oligodeoxyribonucleotides to carry out CuAAC reactions with azide-functionalized sugar or dye molecules (Scheme 24).

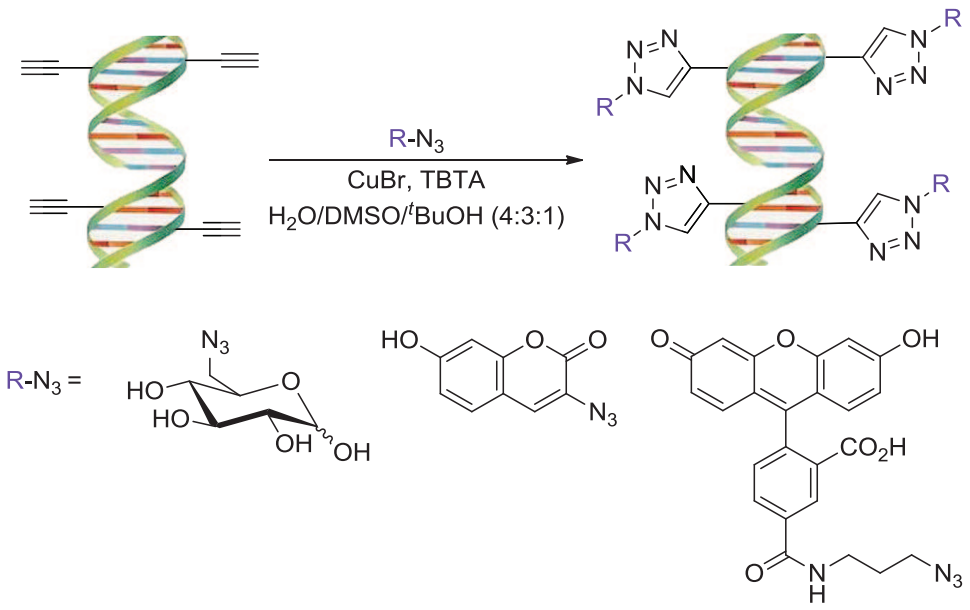

Scheme 24: Labelling of alkyne-modified DNA strands by CuAAC reactions with an azido sugar, 3-azido-7-hydroxycoumarin, and fluorescein azide.[80a]

The use of TBTA is extremely favourable in the context of bioorganic chemistry, as this additive protects the biomolecules from degradation, for example by preventing copper-mediated redox processes in aqueous solution.[81]

This methodology can also be applied *in vivo*, although milder copper-free 1,3-dipolar cycloaddition methodologies are on the rise in this field of chemical biology (see 2.8). As early as 2003, the group of Cravatt had introduced the CuAAC reaction for activity-based protein profiling *in vivo*.[40b] They site-specifically attached an azide group to the enzyme glutathione *S*-transferase and the functionalized protein was then reacted with a rhodamine-functionalized terminal alkyne in the presence of copper(II) sulphate, TCEP as reducing agent and TBTA as ligand for copper(I). Complete labelling was achieved within one hour.

Another example of this strategy was reported by the group of Tirrell, who was able to label newly synthesized proteins in *Escherichia coli* cells.[82] These proteins were co-translationally functionalized by the non-natural amino acids ethynylphenylalanine or homopropargylglycine, whose terminal alkyne group can then react with the dye

3-azido-7-hydroxycoumarin. As catalyst, either copper(II) sulphate pentahydrate was used in combination with TCEP and TBTA, or copper(I) bromide with TBTA.

2.5.3 CuAAC in Carbohydrate Chemistry

In glycochemistry, the CuAAC reaction is not only used for the preparation of glycoside mimetics, but also for the synthesis of glyco-macrocycles, glycopeptides, carbohydrate arrays and glycol-clusters.[83] Along with its efficiency, selectivity and robustness, the main advantage of the CuAAC in this field is the reaction's tolerance towards aqueous conditions and diverse functional groups. As an example, the preparation of a cyclodextrin analogue by cyclodimerization of functionalized trisaccharides is presented in Scheme 25.

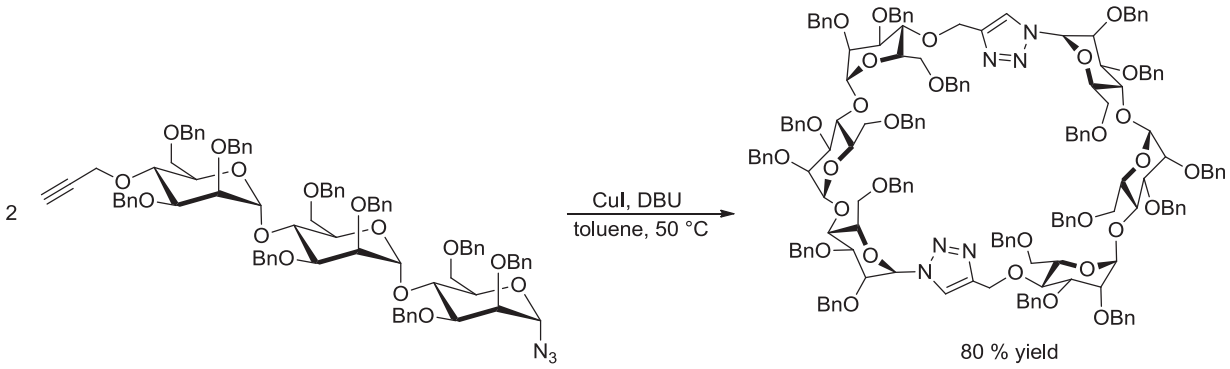

Scheme 25: Cyclodimerization of a trisaccharide in the synthesis of a cyclodextrin analogue.[84]

2.5.4 CuAAC in Polymer Science

The use of CuAAC reactions is not limited to low molecular-weight compounds, but has also become an effective tool in polymer chemistry, namely 1) for the derivatization of preformed polymers, 2) for the synthesis of linear polymers by triazole formation, and 3) for the formation of triazole-based solid supports.[42] The key advantage of CuAAC in this field is that the reaction proceeds quantitatively in most cases. Exclusion of oxygen is often beneficial. As an example the synthesis of triazole-functionalized polymers by combination of reversible addition-fragmentation chain transfer polymerization (RAFT) and the CuAAC reaction as reported by Benicewicz shall be presented (Scheme 26).[85] In this study, pre- and postfunctionalization have been compared and turned out to be equally successful strategies. This means that the

azido group in the monomer is inert towards the conditions of the polymerization reaction.

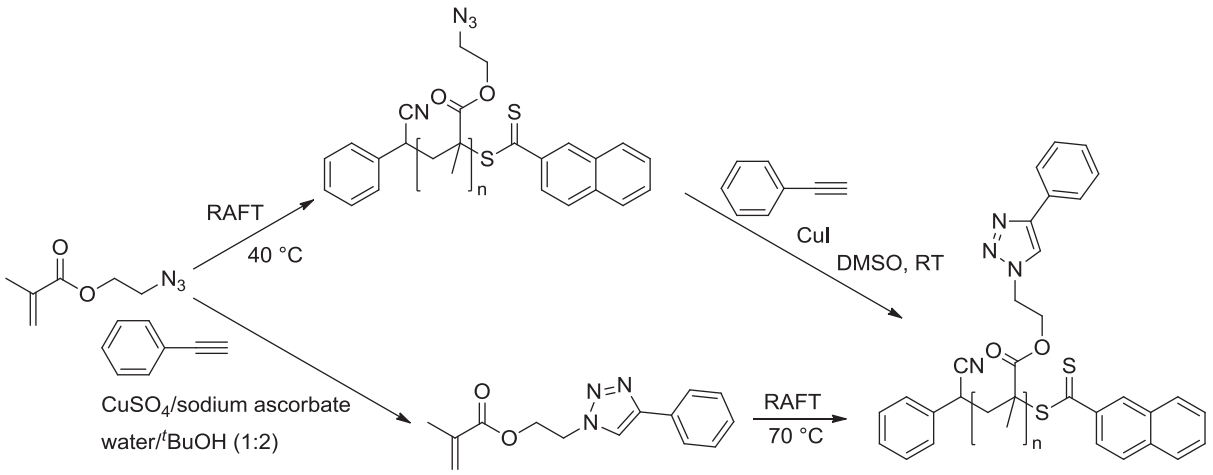

Scheme 26: Synthesis of triazole-functionalized polymethacrylate by either postfunctionalization (upper pathway) or prefunctionalization (lower pathway).[85]

2.5.5 CuAAC in Dendrimer Science

Dendrimers are highly regular, repetitively branched, tree-shaped molecules. For dendrimer synthesis, the CuAAC reaction is very suitable due to its high selectivity, the absence of byproducts, the simple procedure, the tolerance towards many functional groups, and the nearly quantitative yields. In 2004, Sharpless *et al.* reported a convergent approach for the synthesis of triazole dendrimers, in which the individual branches were synthesized sequentially and then coupled to a core in the last step.[86]

2.5.6 CuAAC in Materials and Surface Chemistry

CuAAC reactions are an excellent tool for the creation of new materials with specific properties. For the functionalization of surfaces, the triazole group presents a thermally and hydrolytically stable covalent linkage. For example, the group of Collman functionalized electrode surfaces with ferrocene units by decorating the electrode surface with 11-azidoundecane-1-thiol prior to a CuAAC reaction with 1-ferrocenylprop-2-yn-1-one (Scheme 27).

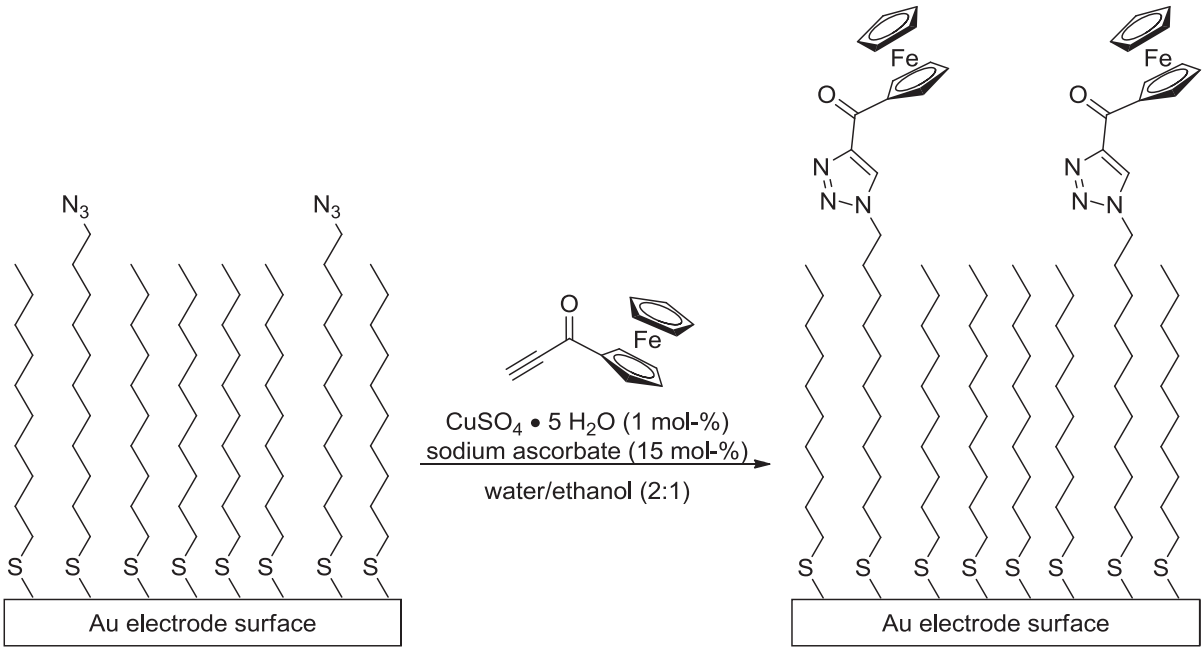

Scheme 27: Functionalization of an electrode surface by CuAAC reaction of surface-linked azide and 1-ferrocenylprop-2-yn-1-one.[87]

2.5.7 CuAAC in Combinatorial Chemistry

In line with Sharpless' initial thoughts on Click chemistry as a methodology to create a great variety of molecules by simple methods in order to have a large pool in which to fish for functionality (chapter 2.1), the modular and highly chemoselective CuAAC reaction is widely used for diversity-oriented synthesis of compound libraries by a combinatorial approach. Normally, each library compound is prepared by only few synthetic steps from key building blocks. In drug discovery, it is common practice to screen the libraries *in situ* with the biological target. This is easily possible as CuAAC reactions give no byproducts and purification steps for the triazoles are not necessary. For example, the group of Wong has synthesized a library of 100 compounds by CuAAC and tested their ability as HIV protease inhibitors *in situ*.[88] Scheme 28 shows the two different azide substrates used in this study, which were reacted in microtiter plates with fifty different alkynes each. The newly formed triazoles were assayed for their inhibition activity against HIV-1 PR and three mutants of the latter HIV protease. By this method, two highly active HIV-1 PR inhibitors were identified, which are shown in Scheme 28 as well.

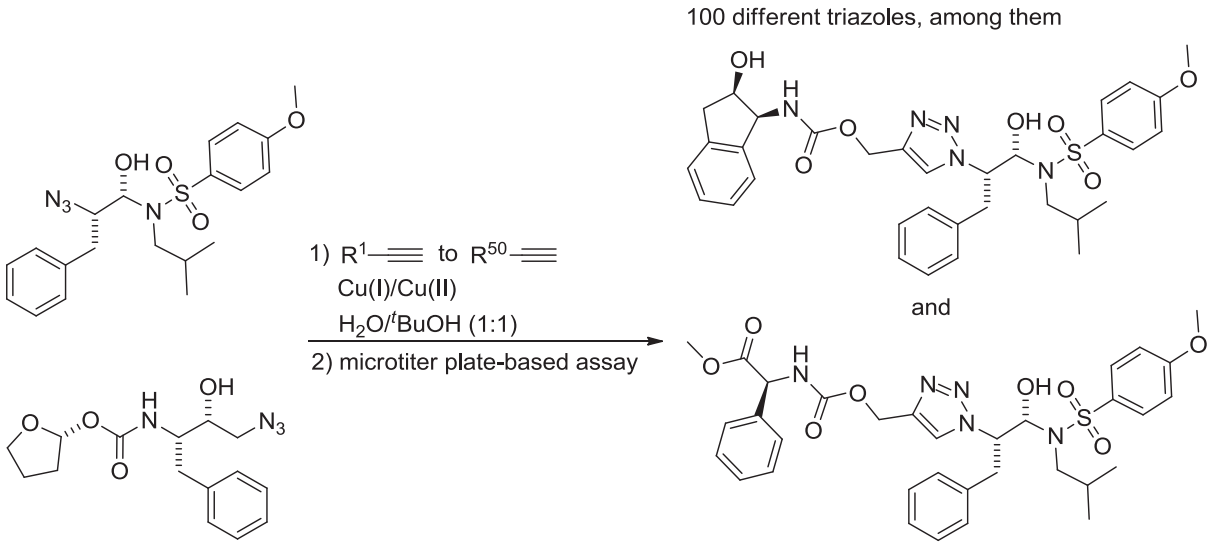

Scheme 28: Reaction of two azides with 50 different alkynes to form a compound library, from which two highly potent HIV-1 PR inhibitors were identified by an *in situ* assay.

2.6 CuAAC Reactions for the Synthesis of 1,4,5-Trisubstituted 1,2,3-Triazoles

1,4,5-Trisubstituted 1,2,3-triazoles are not accessible *via* CuAAC reactions that proceed by formation of a copper(I) acetylide, which then reacts with an azide in the coordination sphere of the copper catalyst, whereupon the copper triazolide is protonated to set free the 1,4-disubstituted triazole. However, in the last step of the catalytic cycle of the CuAAC with terminal alkynes (Scheme 9), instead of protonating the triazolide, it can also be trapped by other electrophiles under aprotic conditions. For example, the group of Wu presented the reaction of terminal alkynes with azides in the presence of stoichiometric amounts of the interhalogen ICl, copper(I) iodide (1 equivalent) and triethylamine (5 equivalents) to synthesize 5-iodo-1,4-disubstituted 1,2,3-triazoles.[89] Alternatively, allyliodide[90] or "I^+" ions prepared *in situ* from the reagent mixture NBS/CuI[91] can be used as electrophiles for trapping the triazolide.

The group of Rutjes reported the synthesis of 5-bromo-1,4-disubstituted 1,2,3-triazoles starting from 1-bromoalkynes. In their optimized procedure, the bromoalkyne reacts with an azide in the presence of 5 mol-% copper(I) iodide and 5 mol-% copper(II) acetate in THF at 50 °C to give the 5-bromo-1,4-disubstituted 1,2,3-triazoles with small quantities of the 5-iodo-1,4-disubstituted 1,2,3-triazole as byproduct.

Where necessary, the formation of this byproduct can be prevented by using copper(I) bromide instead of the iodide salt.

In order to further ameliorate this procedure, the groups of Sharpless and Fokin developed a system for the synthesis of 5-iodo-1,4-disubstituted 1,2,3-triazoles from 1-iodoalkynes.[92] The great advantage compared to the procedures of Wu,[89] Hsung[90] and Li[91] is that neither reactive electrophilic halogenating agents (such as NBS or iodine monochloride) nor stoichiometric amounts of copper salts need to be employed. Instead the presence of amine bases such as of triethylamine or tris[(*tert*-butyl)triazolylmethyl] amine (TTTA) greatly accelerates the highly selective formation of the 5-iodo-1,4-disubstituted 1,2,3-triazoles (Scheme 29).

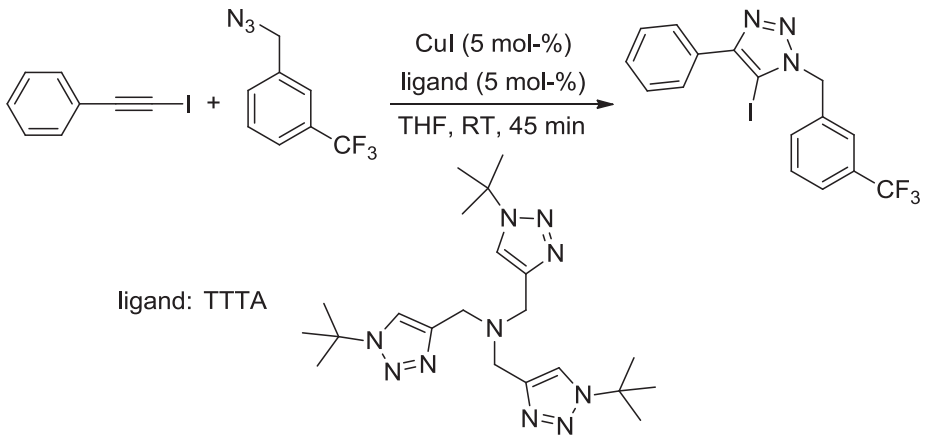

Scheme 29: Chemoselective synthesis of a 5-iodo-1,4-disubstituted 1,2,3-triazole.[92]

Despite the many similarities to the CuAAC reaction of terminal alkynes, the mechanism of the copper(I)-catalyzed azide-iodoalkyne cycloaddition needs to be significantly different from the CuAAC's mechanistic pathway shown in Scheme 9. Two catalytic cycles are currently discussed:[92-93] one the one hand, the formation of a copper(I) acetylide intermediate by copper-halogen exchange and trapping of the triazolide with "I^+" provided by ligand exchange with the 1-iodoalkyne (left side in Scheme 30); on the other hand, the copper(I) centre might only serve to activate the iodoalkyne by π-coordination, so that the cycloaddition process can then take place in the catalyst's coordination sphere (right side in Scheme 30). The latter pathway seems more probable, as even in protic media such as ethanol and water, only 5-iodo-1,4-disubstituted 1,2,3-triazoles are formed, which means that protonation of the copper(I) triazolide intermediate does not take place.

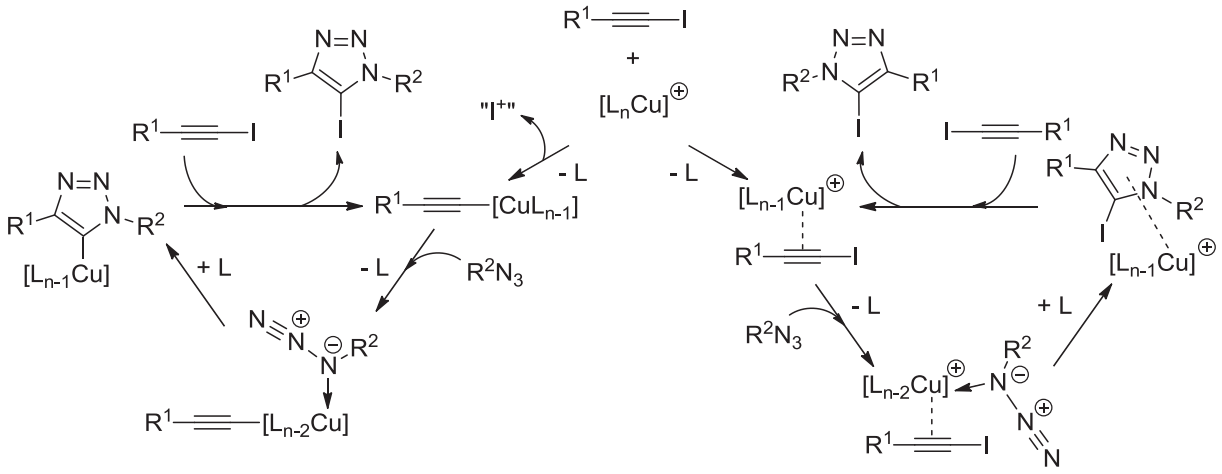

Scheme 30: Mechanistic proposals for the copper-catalyzed azide-iodoalkyne cycloaddition.[92]

In 2006, the group of Nolan presented the synthesis of 1,4,5-trisubstituted 1,2,3-triazoles by cycloaddition reactions between internal alkynes and azides using catalysts of general formula [(NHC)CuX].[68a] This unprecedented reactivity was tested with 3-hexyne and benzyl azide under neat conditions at 70 °C with 5 mol-% [(SIMes)CuBr] as catalyst (Scheme 31).

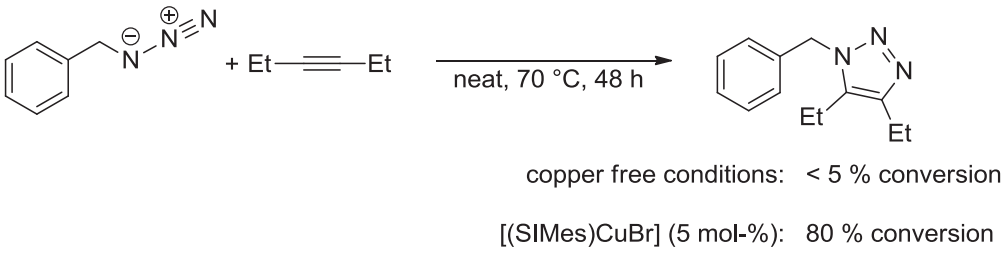

Scheme 31: 1,3-Dipolar cycloaddition of 3-hexyne catalyzed by [(SIMes)CuBr].[68a]

As for the mechanism of this transformation, Nolan proposes that the strong σ-donor NHC ligand facilitates the formation of a copper(I) π-complex with significant π-backbonding, and thus activates the alkyne for the cycloaddition reaction. Based on DFT calculations, the mechanism displayed in Scheme 32 was proposed, which is in analogy to the catalytic cycle presented on the right side of Scheme 30.

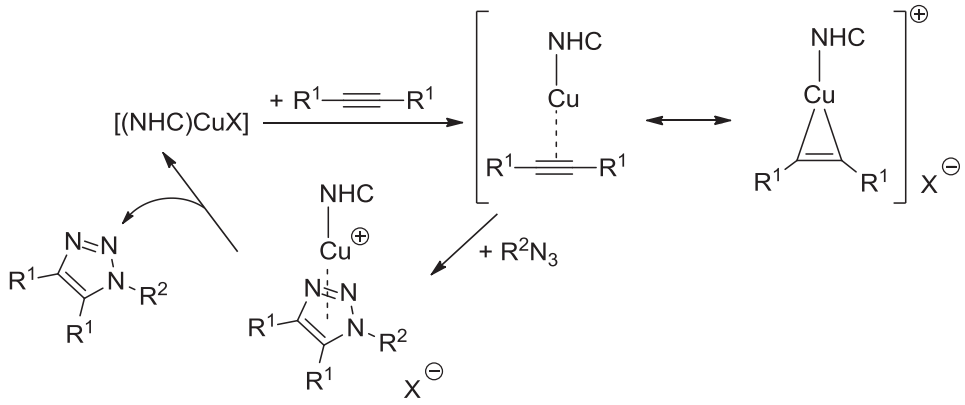

Scheme 32: Mechanistic picture for the cycloaddition of internal alkynes catalyzed by NHC-copper(I) complexes as proposed by Nolan.[68a]

Another popular method for the synthesis of 1,4,5-trisubstituted 1,2,3-triazoles is the ruthenium-catalyzed azide-alkyne cycloaddition presented in chapter 2.7.

2.7 RuAAC Reactions

In 2005, the groups of Jia and Fokin reported that 1,5-disubstituted 1,2,3-triazoles can be synthesized from azides and alkynes with the help of ruthenium(II) catalysts.[94] For example, the reaction of benzyl azide with phenylacetylene in refluxing THF proceeds to selectively give 100 % of the 1,5-disubstituted 1-benzyl-5-phenyl-1*H*-1,2,3-triazole when 2 mol-% of the complexes [Cp*RuCl(PPh_3)$_2$], [Cp*RuCl(COD)], or [Cp*RuCl]$_4$ are present in the reaction mixture (Scheme 33).[95] The key feature of the catalyst is the presence of the electron-rich Cp* ligand, which stabilizes higher oxidation states on the ruthenium centre. Other complexes without the Cp* ligand are either not reactive (for example [(COD)$RuCl_2$], [$RuCl_2$(PPh_3)$_3$] or [RuHCl(CO)(PPh_3)$_3$]), or product mixtures of 1,4- and 1,5-disubstituted triazoles are formed (for example with [CpRuCl(PPh_3)$_2$]).[94-95]

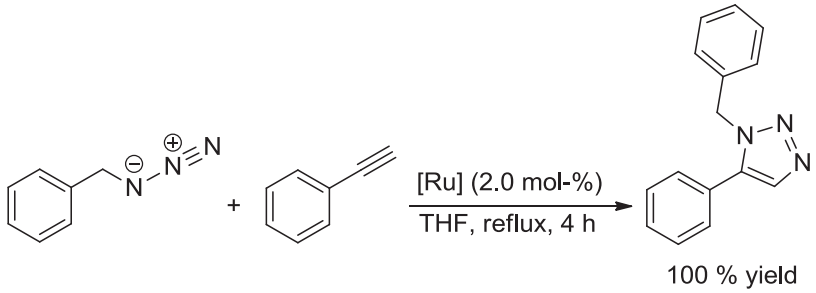

Scheme 33: RuAAC model reaction of phenylacetylene with benzyl azide.[95]

Very remarkably, internal alkynes can react in the RuAAC reaction with organic azides to form 1,4,5-trisubstituted 1,2,3-triazoles. For example, the reaction of 2-methyl-4-phenylbut-3-yn-2-ol with 1-azido-4-methylbenzene in toluene in the presence of [Cp*RuCl(COD)] yields 93 % 2-[4-phenyl-1-(4-tolyl)-1*H*-1,2,3-triazol-5-yl]propan-2-ol within 30 minutes at room temperature (Scheme 34).[95]

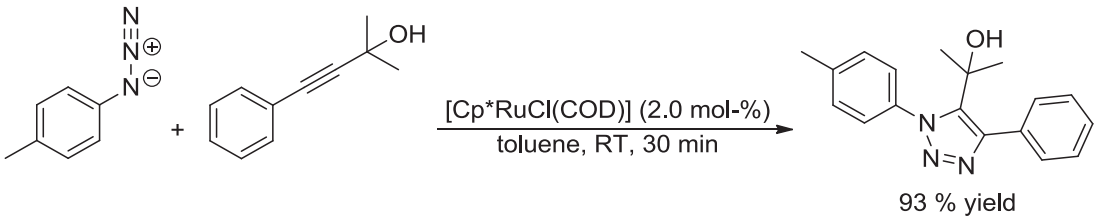

Scheme 34: RuAAC reaction of an internal alkyne with an azide to give the 1,4,5-trisubstituted 1,2,3-triazole.

The mechanistic proposal for the RuAAC reaction is shown in Scheme 35. The resting state of the catalysis is a neutral complex [Cp*RuCl]. This hypothesis is supported by the observations that an exchange of chloride for bromide or iodide leads to less active catalysts, that cationic complexes $[Cp^*Ru]^+$ are not active and that chelating diphosphine ligands prohibit catalysis. In the first step of the catalytic cycle, the ancillary ligands (COD; phosphines) are replaced by the substrates. Oxidative coupling leads to a ruthenacycle. This C-N bond forming step is decisive for the reaction's regioselectivity. When there are no anchor groups such as OH or NHR present, the C-N bond is normally formed between the terminal nitrogen atom of the azide and the more electronegative and sterically less encumbered carbon atom in the alkyne. In a reductive elimination, the triazole ring is set free.

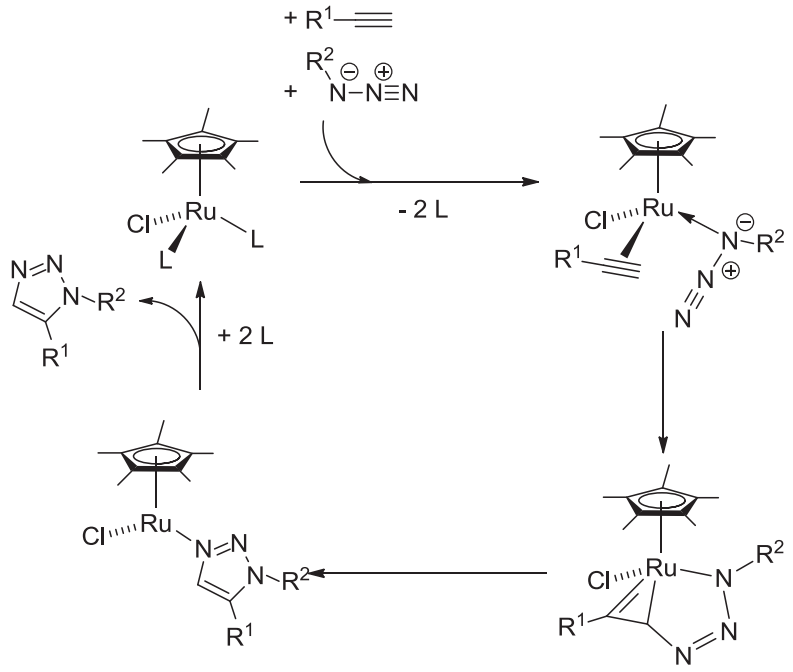

Scheme 35: Mechanistic pathway for the RuAAC reaction.[95]

2.8 Copper-Free Azide-Alkyne Cycloadditions (AAC)

2.8.1 Strain-Promoted [3+2]-Cycloadditions (SPAAC) of Cycloalkynes with Azides

Although there are some applications of CuAAC reactions with living cells in the presence of suitable ligands to "mask" the copper ions ,[40b, 82] the toxic nature of copper ions on the cell's metabolism generally impedes the application of CuAAC for the imaging of proteins and other biomolecules in live cells and animals.[96] Copper ions promote the formation of reactive oxygen species such as hydroxyl radicals, which exert oxidative stress and damage cellular structures, for example proteins, DNA and lipids.[97] Therefore, the group of Bertozzi started research on the development of bioorthogonal reactions for labelling applications within biological systems. The concept of bioorthogonality includes the conditions that the involved substances will neither react with any functional groups present in cells nor influence the cell's metabolism, but form covalent bonds with high selectivity under biological conditions, *i.e.* aqueous media, ambient temperatures and atmospheric pressure. Bertozzi's choice for AAC reactions with cyclooctyne derivatives as reactive alkyne substrates was fuelled by a report of Wittig and Krebs published in 1961, where the violent reaction of phenyl

azide with cyclooctyne is described.[98] The high driving force of this reaction is due to the partial release of ring strain.[99] In 2004, the first publication on strain-promoted azide-alkyne cycloadditions (SPAAC) described the facile reaction of a biotinylated cyclooctyne with benzyl azide, 2-azidoethanol and *N*-butyl α-azidoacetamide.[100] Next, an azide functionality was introduced into a glycoprotein and after incubation with the biotinylated cyclooctyne, Western blot analysis proved the successful biotinylation of the glycoprotein. Finally, reactions with immortalized T lymphocyte cells (Jurkat cell line) were carried out. After incorporation of an azide group into cell-surface glycoproteins, successful reaction with a solution of the biotinylated cyclooctyne without any physiological harm was observed (Scheme 36).

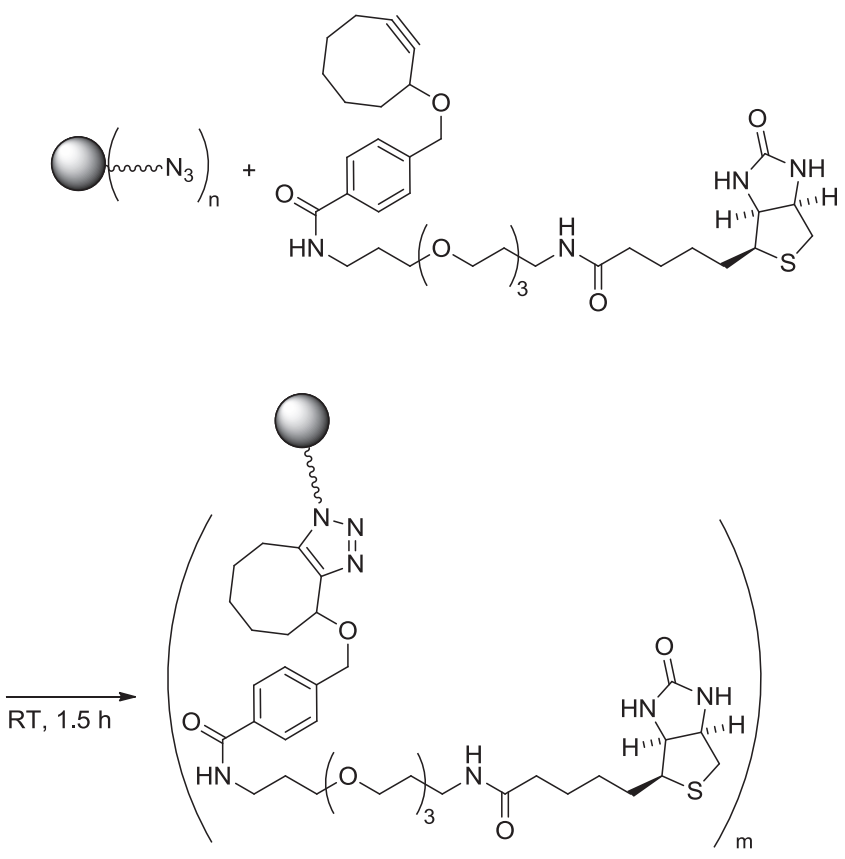

Scheme 36: Strain-promoted AAC reaction of biotinylated cyclooctyne with Jurkat cell surfaces decorated with azide groups (Jurkat cells are represented by grey balls).[100]

In the next stage, the kinetics of this reaction was improved by introducing fluoro substituents to the cyclooctyne.[101] These mono- and difluorinated cyclooctynes (referred to as MOFOs and DIFOs) reacted more rapidly than unsubstituted cyclooctyne derivatives, which is due to the electron-withdrawing characteristics of the fluoro substituents. To ameliorate the water solubility, heterocyclic dimethoxyazacyclooctyne

(DIMAC) has been developed.[102] The group of Boons introduced derivatives of dibenzocyclooctynol (DIBO), which are as active as Bertozzi's DIFO reagents.[103] The group of van Delft contributed bicyclo[6.1.0]nonyne derivatives (BCN), which have the advantage of an easier preparation and a symmetric scaffold so that there is no regioisomerism for the formed triazoles.[104] In 2007, Rutjes *et al.* presented a cyclonorbornadiene, which reacts with the azide in a [3+2]-cycloaddition with subsequent *retro*-Diels-Alder reaction, in which furane is released.[105]

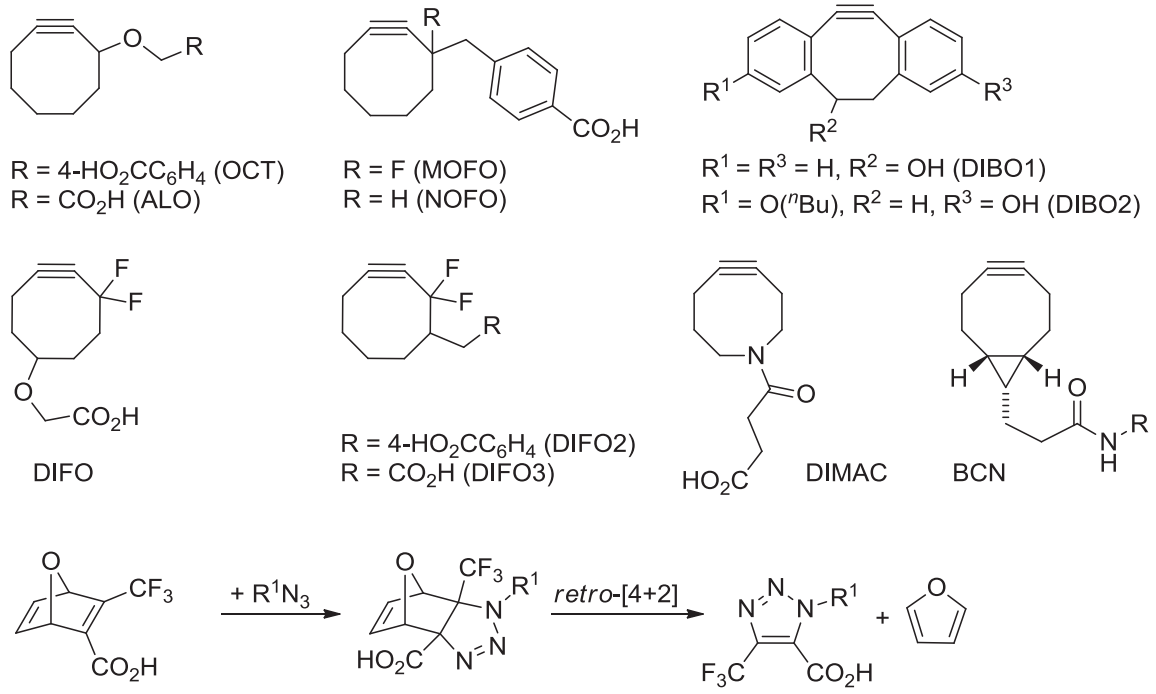

Figure 10: Strained alkyne substrates for SPAAC reactions and use of cyclonorbornadiene as a "masked" alkyne .[100-105]

An impressive application of SPAAC is the non-invasive *in vivo* imaging of membrane-associated glycans in living zebrafish embryos reported by the group of Bertozzi.[106] In this study, peracetylated *N*-azidoacetylgalactosamine was introduced in zebrafish glycoproteins. Reaction with a DIFO derivative containing a fluorescent dye led to fluorescent zebrafish embryos without any developmental abnormalities or signs of toxication.

2.8.2 *In Situ* Click Chemistry for Lead Identification

In target-guided synthesis, two fragments self-assemble in their own binding site. The term *in situ* Click chemistry describes 1,3-dipolar cycloaddition reactions between azides and alkynes when these substrates are assembled in a biomolecular “reaction vessel” that functions as template for the formation of the inhibitor. This means that the target biomolecule is incubated with a mixture of azide and alkyne substrates and only those which fit best into the binding sites of the biomolecule can react to form the triazole product (Scheme 37).[107] For example, potent inhibitors of acetylcholinesterase,[108] carbonic anhydrase,[109] HIV-protease[110] and chitinase[111] have been identified by this approach.

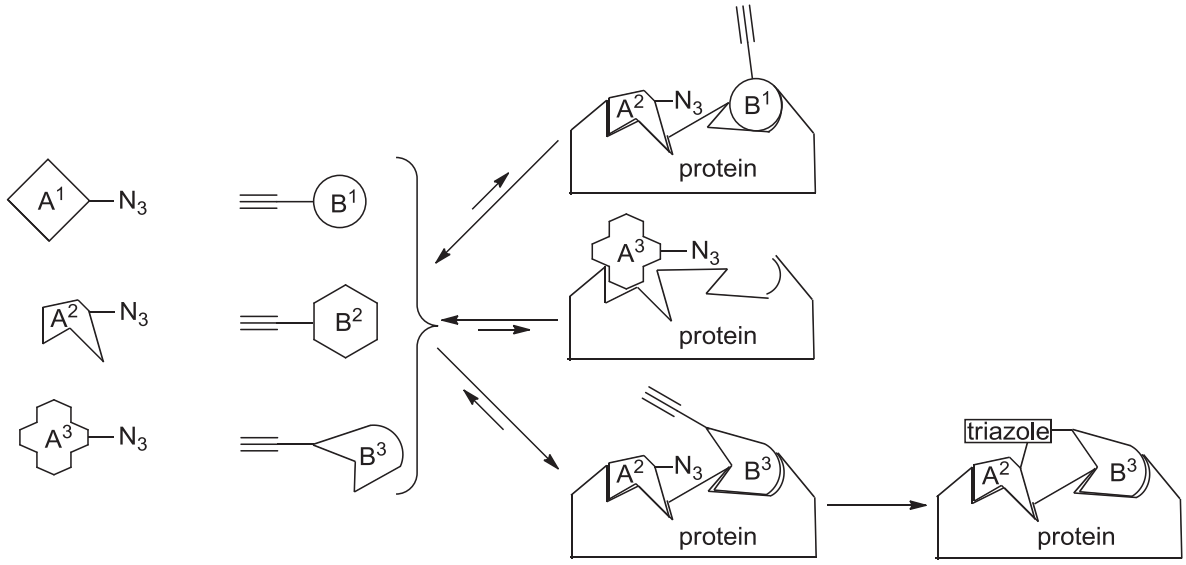

Scheme 37: Principle of *in situ* Click chemistry.[107]

3 Objectives

In the preceding section, various catalysts commonly applied in CuAAC reactions have been presented. Most of these catalyst systems are mixtures of a copper salt and an additive (Table 3, Figure 7 and Figure 8). The latter can act as a ligand to stabilize the catalytically active copper(I) ions with regard to oxidation and disproportionation and to help increase the salts' solubility. However, in only few cases, the structural characteristics of the active catalyst species have been elucidated.

In contrast to these widely used "black box" reagent mixtures, our aim was to rationally construct a molecularly defined, highly active catalyst system for homogeneous CuAAC reactions in organic solvents. In dependence on the postulated mechanism (Scheme 9), its most important structural feature is the presence of two copper(I) ions irreversibly bound in the same catalyst molecule in an adequate distance to each other. On the one hand, this feature should entropically favour the cooperation of the two copper(I) centres compared to mononuclear catalysts, which is particularly important with low catalyst concentrations. On the other hand, the enthalpically profitable formation of a bridged μ-acetylide intermediate is facilitated. It should thus be possible to effectively catalyze CuAAC reactions in aprotic solvents under homogeneous conditions with low catalyst loadings. A general structural outline of the envisioned precatalyst complexes is shown in Figure 11.

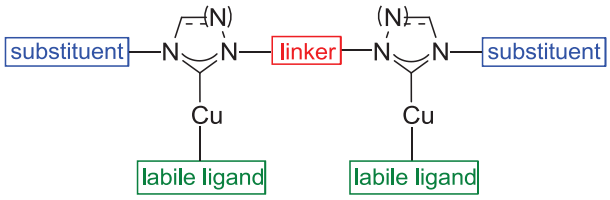

Figure 11: Structural features of target precatalyst system.

The key components of the envisioned ligand are two NHC units, which are bridged *via* a molecular linker (red). Additionally, a labile ligand (green) binds to each of the two copper(I) ions. These "sacrificial" ligands need to dissociate during the induction period in order to have free coordination sites for the substrates of the catalytic

reaction. Thus, these ligands should neither bind too strongly to the Cu(I) centres, as this would inhibit the catalytic performance, nor should they bind too weakly because in this case the precatalyst would not be stable.

As illustrated by Figure 11, the structural features of this catalyst system can be modularly adapted by exchanging single components. For example, the nature of the NHC units (imidazolylidene, imidazolinylidene, triazolylidene), their N-substituents (blue), the length and rigidity of the molecular linker and the nature of the sacrificial ligands can be independently varied to give a plethora of different combinations. Thus, there is much room for adaptation to specific substrates and reaction conditions.

In a previous PhD project in our group, a synthetic route for the modular preparation of symmetrically and unsymmetrically substituted bisimidazolinylidene ligand precursors had been developed.[112] The corresponding dinuclear copper complexes with chloride or bromide as sacrificial ligand were synthesized and characterized. However, their catalytic activity was not as high as expected, which might be due to the inhibiting effect of the halide ions present in the reaction mixture.[63, 112b] It was thus attempted to prepare a halide-free variant of the latter complexes by exchanging the sacrificial ligand. In his dissertation, Michael Bessel describes his experiments towards the synthesis of a dinuclear complex comprising two acetate sacrificial ligands. However, the low-yielding synthesis led to a very sensitive material that consisted of different species. Purification and full characterization of the desired complex was never achieved.[113] Catalytic tests showed low catalytic activity of this material. Thus, Bessel added IPr • HPF_6 as ligand precursor and did indeed obtain small quantities of the desired dicopper complex with IPr as sacrificial ligand. Albeit this dinuclear complex showed some catalytic activity in CuAAC test reactions, it was only synthesized in milligram amounts. The key flaw in its preparation is the sensitivity and irreproducible synthesis of the intermediate complex, which was never isolated in pure form and whose structure has not been elucidated unambiguously.

The major objectives for this PhD project were:

1) Quantum-chemical re-evaluation of supposable modules for the target catalyst system.

2) Reproducible and high-yielding synthesis of a stable dinuclear copper-complex based on the given structural outline (Figure 11) on a gram scale.
3) Catalytic testing in homogeneous CuAAC reactions in organic solvents.
4) Kinetic measurements to determine the order of reaction with respect to the dinuclear copper catalyst.

4 Results and Discussion

4.1 Synthesis of (IPr)CuOAc

In 2004, the group of Sadighi had reported the synthesis and characterization of the two coordinate NHC copper(I) acetate complex (IPr)CuOAc (**3**).[114] This complex seemed a good candidate for the introduction of the fragment (IPr)Cu by reaction with a bis-NHC ligand precursor. The literature protocol for the synthesis of (IPr)CuOAc (**3**) starts from the imidazolium salt IPr • HCl, which is deprotonated to give the free carbene IPr.[115] The latter is then reacted with copper(I) acetate to give the desired complex **3** in moderate yield.[114] In order to ensure the complete exclusion of halide ions, which are supposed to have an unfavourable effect on CuAAC catalysis due to their affinity to copper(I) ions,[63, 112b] and to avert the isolation of the sensitive free carbene, a modification of Sadighi's route was developed.
Following literature procedures by Hintermann,[116] 1,4-bis(2,6-diisopropylphenyl)-1,4-diazabutadiene (**1**) was prepared as a bright yellow crystalline solid. Instead of chloride, acetate was introduced as counterion in the next step by reaction with para-formaldehyde in glacial acetic acid as solvent (Scheme 38).

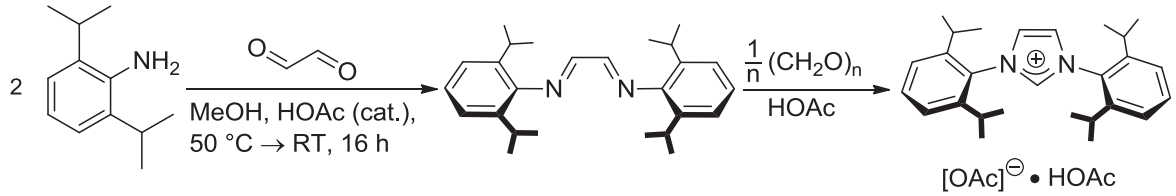

1

82 %
(lit.: 89.5 %)

2

Scheme 38: Synthesis of IPr • 2 HOAc.

Since a dark violet byproduct was formed, the reaction conditions were optimized in order to maximize the yield of the desired salt IPr • n HOAc (Table 8).

Table 8: Optimization of conditions for the preparation of imidazolium salt **2** from 1,4-bis(2,6-diisopropylphenyl)-1,4-diazabutadiene (**1**) and paraformaldehyde.

entry	temperature of the oil bath	reaction time	yield
1	120 °C	3 h	67 %
2	120 °C	5 h	53 %
3	120 °C	6 h	57 %
4	120 °C	24 h	55 %
5	80 °C	3 h	74 % - 84 %
6	60 °C	3 h	72 %

It was observed that the longer the reaction time and the higher the temperature, the darker turned the reaction mixture, which suggests that more of the undesired byproduct was formed. A hypothesis as to the formation and structure of the violet byproduct is formulated in Scheme 39, based on the resemblance to the triarylmethane dye crystal violet.[117] However, the exclusion of oxygen from the reaction mixture did not prevent the formation of the violet byproduct, which means that one of the reagents might also act as oxidant under anaerobic conditions.

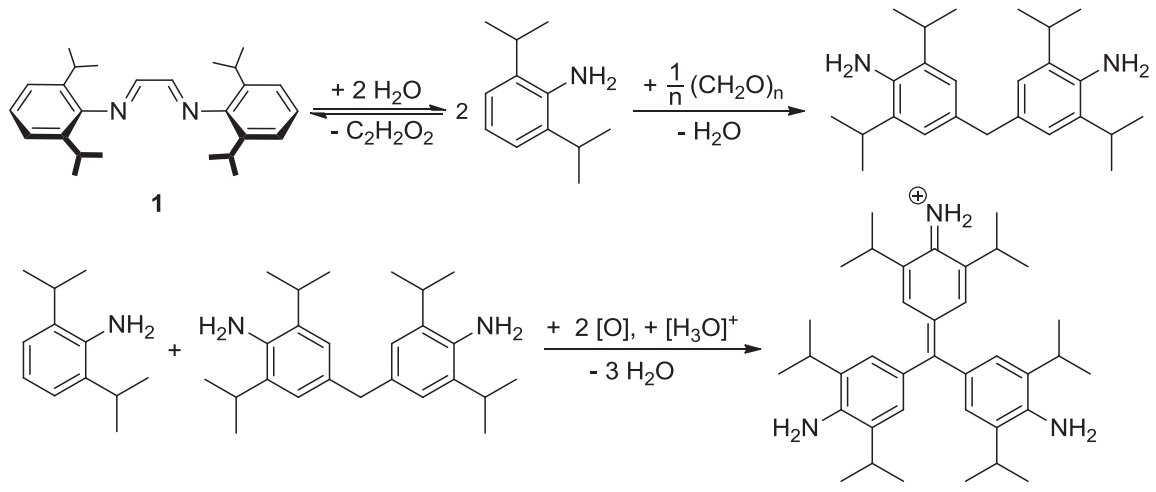

Scheme 39: Proposed pathway for the formation of a violet byproduct in the synthesis of IPr • 2 HOAc (**2**) shown in Scheme 38.

The complete removal of the byproduct was achieved by re-crystallization from THF, until a colourless salt was obtained. In the ^{1}H NMR spectrum, one additional equivalent of acetic acid per equivalent of IPr • HOAc was observed, *i.e.* the isolated product is IPr • 2 HOAc (**2**).

When the solution of the violet raw product in acetic acid was overlain by MTBE, crystals suitable for single crystal X-ray structure determination were grown. Figure 12 shows the ORTEP plot of this structure, in which an additional equivalent of acetic acid is attached by hydrogen bonding (IPr • 3 HOAc = **2** • HOAc).

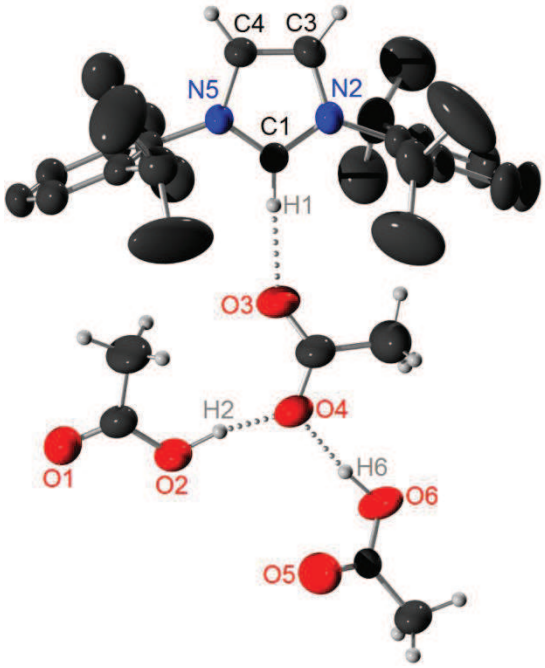

Figure 12: ORTEP plot of the single crystal X-ray structure of IPr • 3 HOAc (**2** • HOAc) (hydrogen atoms of the Dipp substituents are omitted for clarity).[118] Selected average bond lengths [Å], bond angles and dihedral angles: C1-N2 1.328, N2-C3 1.377, C3-C4 1.338, C4-N5 1.381, N5-C1 1.328, C1-O3 2.907; N2-C1-N5 108.13°; C1-N2-C11-C12 -93.06°, C1-N2-C11-C16 86.44°, C1-N5-C21-C22 -86.02°, C1-N5-C21-C26 92.34°.

As is typical for 2-protio-azolium salts, there is a hydrogen bond between the acidic hydrogen atom of the imidazolium heterocycle and the counterion, in this case acetate. The distance between C1 and O3 is 2.907 Å, and with the calculated position of the H1 proton this gives a hydrogen bond length of d(H1-O3) = 1.958 Å. The C1-H1-O3 angle was found to be 176.40°, which is a little larger than the Cl-H-C angle of 172° reported for IPr • HCl in literature.[115b] The acetate anion itself is stabilized by hydrogen bonds to two molecules of acetic acid. The C1-N2/5 distance was found to be 1.328 Å and the N2-C1-N5 angle 108.13°, which is in good accordance with the values reported for IPr • HCl with a C-N distance of 1.34 Å and an N-C-N angle of 107.6°. The planes of the Dipp substituents are twisted by approximately 90° with respect to the plane of the central imidazolium ring. In IPr • HCl, the planes of the Dipp substituents are twisted by only 73° to 80° with respect to the imidazolium

heterocycle's plane. This might be due to the observation that the acetate and the associated molecules of acetic acid are quite close to the heterocyclic cation so that the Dipp groups might need to be twisted more into the perpendicular plane in order to avoid steric repulsion between acetate and the isopropyl *ortho*-substituents.

The copper(I) complex (IPr)CuOAc (**3**) was synthesized by adding potassium hydride and copper(I) acetate to a suspension of IPr • 2 HOAc (**2**) in THF under inert gas conditions. After stirring at room temperature for one day and filtration of the dark grey reaction mixture, a yellow solution was obtained. Upon evaporation of the solvent, the raw product was washed with pentane and re-crystallized from THF/diethyl ether to give complex **3** as a colourless crystalline solid in 69 % yield. (IPr)CuOAc (**3**) is very air-sensitive in solution, but tolerates exposure to aerobic conditions as a solid for several days. The analytic data was in accordance with the data reported by the group of Sadighi.[114]

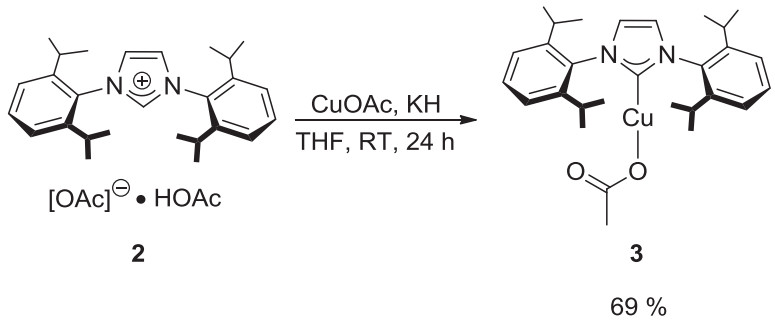

2 **3**

69 %

Scheme 40: Synthesis of (IPr)CuOAc (**3**) from IPr • 2 HOAc (**2**).

4.2 Attempted Synthesis of Dinuclear Bisimidazolinylidene Copper Complexes

Based on Michael Bessel's work on the synthesis of trimethylene-linked bisimidazolinium salts and their use as ligands in dinuclear copper(I) halide complexes,[112a] it was attempted to synthesize dinuclear copper complexes with bisimidazolinylidene ligands. 1-(2,6-Dimethylphenyl)-4,5-dihydro-1*H*-imidazole was used as a readily available starting material.[112] In order to introduce a xylylene-linker, the imidazoline was reacted with 1,3-bis(chloromethyl)benzene. The double S_N2 reaction proceeded

smoothly without solvent, as both substances have a low melting point: 1-(2,6-dimethylphenyl)imidazoline melts at 64 °C and 1,3-bis(chloromethyl)benzene at 35 °C. In order to prevent the presence of strongly coordinating halide ions in the following steps, an *in situ* salt metathesis with hexafluorophosphoric acid was carried out to obtain 3,3'-[1,3-phenylenebis(methylene)]bis[1-(2,6-dimethylphenyl)-4,5-dihydro-1*H*-imidazol-3-ium] bis(hexafluorophosphate) (**11**). In our group, the yield of this reaction has been increased to 82 %.[119]

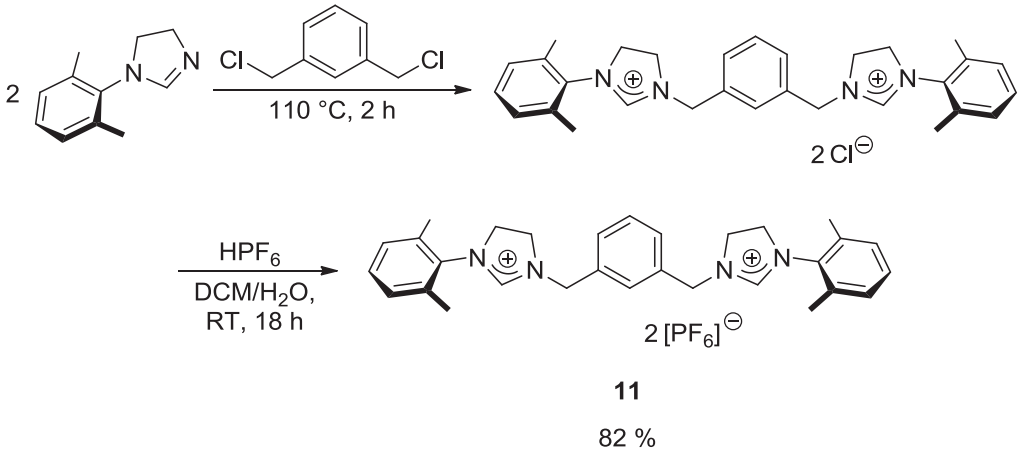

11

82 %

Scheme 41: Synthesis of 3,3'-[1,3-phenylenebis(methylene)]bis[1-(2,6-dimethylphenyl)-4,5-dihydro-1*H*-imidazol-3-ium] bis(hexafluorophosphate) (**11**).

With this material at hand, the synthesis of copper(I) complexes was attempted. In NMR or small-scale preparative experiments under inert gas conditions, the starting material **11** was mixed with a copper(I) precursor and a base in different solvents and stirred at room temperature (Table 9).

Table 9: Attempted syntheses of dicopper complexes from bisimidazolinium salt **11**.

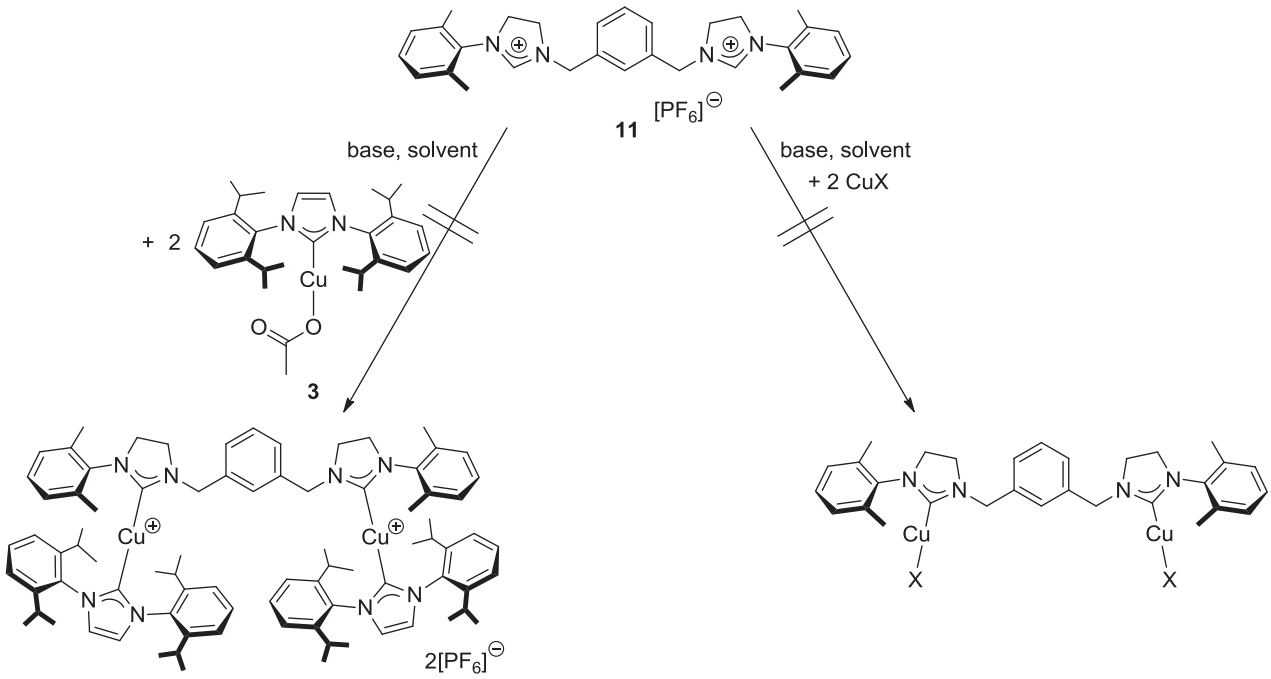

entry	solvent	base (eq.)	copper(I) precursor (eq.)	observation
1	d_6-acetone	DIPEA (excess)	(IPr)CuOAc (2.0 eq.)	decomposition of the imidazolinium heterocycle, probably due to traces of water in the reaction mixture
2	d_3-acetonitrile	NEt_3	(IPr)CuOAc (2.5 eq.)	no reaction at room temperature
3	d_3-acetonitrile	NEt_3	(IPr)CuOAc (2.5 eq.)	no reaction at 70 °C within 18 hours
4	d_3-acetonitrile	NaH (> 3 eq.)	(IPr)CuOAc (2.5 eq.)	decomposition of the starting material
5	THF	NaH (2.2 eq.)	CuOAc (2.3 eq.)	first greyish green suspension, then black precipitate; after filtration and re-crystallization from THF/diethyl ether very small amount of white crystals; mass spectrum shows peak at *m*/*z* = 513.20726 (Figure 13)

6	THF	KH (2.8 eq.)	CuOAc (2.2 eq.)	black solid residue, green solution: decomposition
7	d_6-acetone	K_2CO_3 (2.2 eq.)	CuOAc (5.3 eq.)	decomposition of the imidazolinium heterocycle, probably due to the presence of water
8	acetonitrile	NaH (2.2 eq.)	CuOAc (2.5 eq.)	black solid residue, dark grey solution; ^{1}H NMR of raw product in d_6-acetone: deprotonation almost complete, formation of a new species; acetone solution first turned green, then orange; no product isolated
9	d_3-acetonitrile	NaH (4.5 eq.)	$(H_3CCN)_4CuPF_6$ (2.5 eq.)	evolution of gas upon addition of NaH, black solid residue, colourless solution; ^{1}H NMR: deprotonation complete, various new species
10	d_3-acetonitrile	DIPEA (4.5 eq.)	$(H_3CCN)_4CuPF_6$ (2.5 eq.)	solution turns pink upon addition of DIPEA; ^{1}H NMR: deprotonation incomplete, various new species
11	acetonitrile	DIPEA (excess)	CuOAc (2.5 eq.)	solution turns pink upon addition of DIPEA and exposure to ultrasound; ^{1}H NMR: deprotonation complete, new peak at 11.2 ppm with integral 2 (protonated DIPEA); one product species (Figure 14)
12	d_3-acetonitrile	DIPEA (excess)	CuBr (2.2 eq.), copper powder	no reaction, starting material unaltered
13	d_3-acetonitrile	DIPEA (excess)	$(CuBr \bullet SMe_2)_2$ (1.1 eq.)	8 hours at 60 °C: mostly starting material; additional 6 hours at 75 °C: starting material and new species; additional 5 days at

				80 °C: starting material and product mixture
14	d_3-acetonitrile	NaH (8.8 eq.)	$(CuBr \cdot SMe_2)_2$ (1.1 eq.)	black precipitate, decomposition
15	d_3-acetonitrile	NEt_3 (excess)	$(CuBr \cdot SMe_2)_2$ (1.1 eq.)	homogeneous solution, starting material and unidentified product
16	d_3-acetonitrile	NaHMDS (2.2 eq.)	$(CuBr \cdot SMe_2)_2$ (1.1 eq.)	deprotonation complete, low solubility, species in ^{1}H NMR unidentified

Ligand precursor **11** was found to be very sensitive towards water under basic conditions as the presence of hydroxide ions in the basic reaction mixture leads to decomposition of the imidazolinium salt, probably by ring opening as depicted in Scheme 42.

This was confirmed by blind testing in the absence of copper species. The formation of the formamide decomposition product is indicated by a new peak at approximately 8.4 ppm in the ^{1}H NMR spectrum. It was thus necessary to strictly exclude any traces of water.

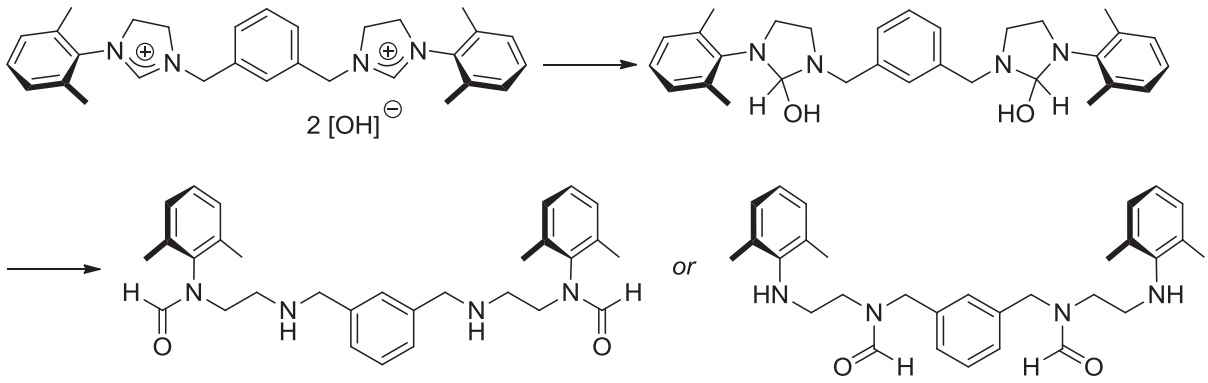

Scheme 42: Hypothesis regarding the decomposition pathway of bisimidazolinium salt **11** in basic media in the presence of water.

There were only two experiments that looked promising, namely entries 5 and 11 in Table 9. In an attempt to synthesize a dinuclear copper(I) complex with acetate as sacrificial ligand, the ligand precursor bisimidazolinium salt **11** was suspended in THF together with sodium hydride and copper(I) acetate. After some minutes of stirring at room temperature under inert gas conditions, the reaction mixture turned green and a

grey precipitate was formed. After 20 hours of stirring, the grey solution with black solid residue was filtered over a filter paper-capped canula and the residue was washed with THF. Diethyl ether was added to the solution and the Schlenk flask stored at -20 °C. After a few days, a small amount of colourless crystals had precipitated. Unfortunately, they were not suitable for single crystal X-ray analysis. As the quantity was not sufficient for taking an NMR spectrum, the crystals were subjected to mass spectrometry. In the ESI+ spectrum, the largest peak was observed at m/z = 513.20726. This peak is in accordance with the molecular formula of the monocation $[C_{30}H_{34}CuN_4]^+$ (structures **A** and **B** in Figure 13) with m/z (calculated) = 513.20740. In structural outline **B**, both NHC units coordinate to one copper ion, whereas a free carbene is supposed to be generated on one side under the conditions of ESI+ mass spectrometry to give species **A**. On the other hand, a dication of formula $[C_{60}H_{68}Cu_2N_8]^{2+}$ (structure **C** in Figure 13) would produce the observed m/z signal as well. However, this species itself can be excluded by the isotopic pattern, which indicates the presence of only one copper ion. Nevertheless, formation of species **C** in the reaction mixture cannot be ruled out completely, as the latter might decompose under the conditions of ESI+ mass spectrometry to give **A** or **B**. Thus, the structure of the product complex cannot be derived from the ESI+ mass spectrum.

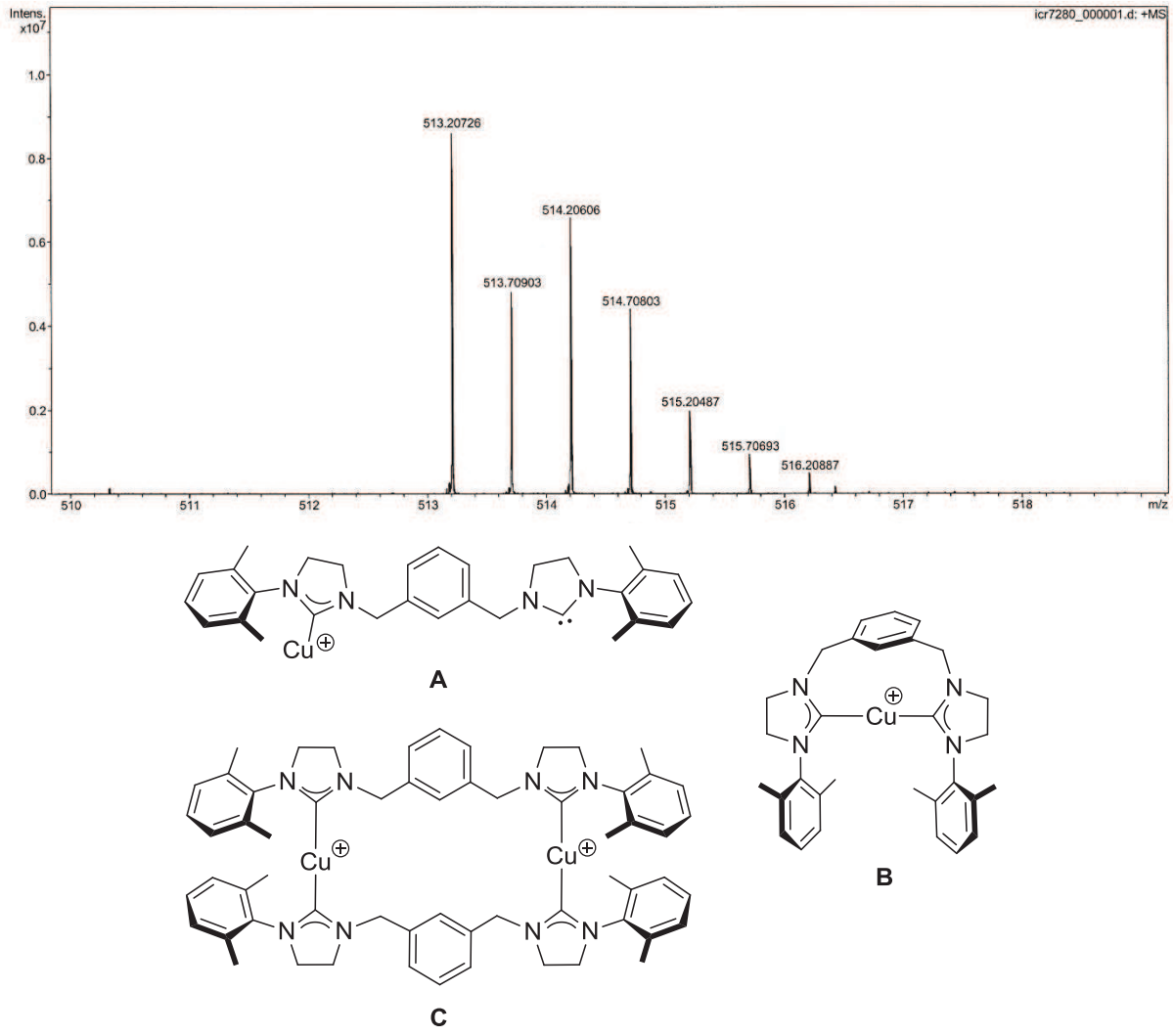

Figure 13: Detail from the ESI+ mass spectrum of the crystals obtained from the reaction mixture of entry 5 in Table 9 and plausible structures of copper complexes that fit to the signal at *m*/*z* = 513.20726.

In experiment 11, the deprotonation of the starting material by DIPEA was complete after ten minutes at room temperature with exposure to ultrasound. In the NMR spectrum in CD_3CN, one single product species was observed apart from the protonated base (peaks at 11.22, 3.10, 2.56 and 1.03 ppm). However, it is indecisive whether acetate (peak at 2.04 ppm) coordinates to the copper centres, *i.e.* whether the desired bis-NHC-dicopper diacetate complex is existent. Alternatively, a dinuclear complex containing two bis-NHC ligands (structure **C** in Figure 13) with acetate as counterion might be formed. This question could have only been decided by crystal structure analysis or elemental analysis.

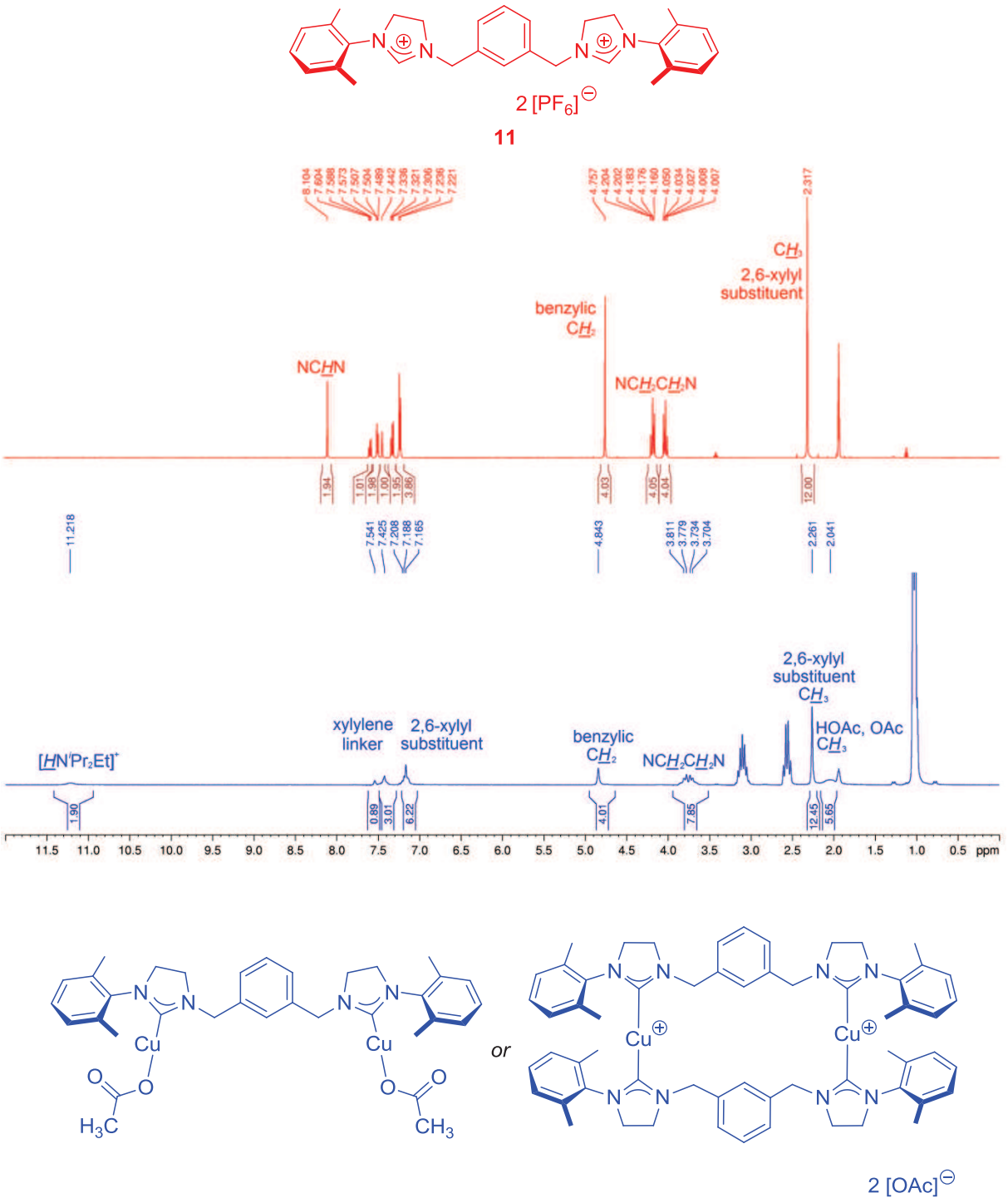

Figure 14: ^{1}H NMR spectra of the starting material bisimidazolinium salt **11** (upper part, red) and of the reaction mixture after ten minutes of ultrasound exposure at room temperature (lower part, blue) (spectra recorded in CD_3CN at 250 MHz).

While these studies were underway, thiol-functionalized triazolium salts were investigated by Stefanie Seitz in the Straub group.[120] These ligand precursors can be synthesized from easily available starting materials and are more acidic than the corresponding imidazolinium salts. Despite the hints on the formation of copper complexes

in the experiments summarized in Table 9, the work with bisimidazolinium salts was abandoned in favour of studies on bistriazolylidene ligands.

4.3 Calculations With Dinuclear Triazolylidene Copper Complexes

Accompanying the synthetic efforts to prepare bistriazolylidene dicopper(I) complexes, it was computationally investigated whether the mechanistic pathway shown in Scheme 9 was passable for bistriazolylidene dicopper(I) complexes with xylylene- or ethylene-linker units and different aryl substituents at the N4-position. All structures that have been modelled by DFT calculations are named by the letter **C** (indicating a calculated structure) plus a number; **x** stands for xylylene-linked model complexes, **e** for an ethylene-linker and the substituents on the 4-position of the triazolylidene ligands are given in parentheses. Calculations of thermodynamical data were carried out on the assumption of an ideal gas at standard conditions (T = 298.15 K, p = 1atm), if not explicitly stated otherwise.

It was supposed that the very stable μ_2-acetylido dicopper complex is the catalyst resting state. However, the bridging acetylide ligand can either be bound in the η^1,η^2-coordination mode with one copper ion forming a σ-bond with the C1 atom and the other copper centre interacting with both acetylide carbon atoms *via* a π-bond, or in the more symmetric η^1,η^1-coordination mode with both copper(I) ions interacting with the C1 atom of the ligand (Figure 15).

μ_2-η^1,η^2 μ_2-η^1,η^1

Figure 15: Modes of coordination of a μ_2-bridging acetylido ligand in a dinuclear copper complex.

It was thus necessary to calculate, whether complex **C01** (σ,π-coordination mode) or **C01iso** (σ,σ-coordination mode) was thermodynamically more stable. However, in

most geometry optimizations of **C01iso** structures, the result was a complex with σ,π-coordination, *i.e.* the more stable complex **C01** was "automatically" formed in the course of the geometry optimizations on **C01iso**. Only in the case of Ar = 4-tolyl was **C01iso** a minimum structure, but **C01x(Tol)iso** was found to be thermodynamically less stable than its isomer **C01x(Tol)** by 10 kJ mol^{-1} (Table 10). For the ethylene-linked bistriazolylidene model complex with Ar = Xyl and Ar' = Dipp, the geometry optimization of the starting structure **C01iso** ended with a transition state: the sole negative wave number ($\tilde{\nu}$ = -62.81 cm^{-1}) corresponds to the bending vibration of the acetylide group changing from one orientation to the other, *i.e.* from σ-coordination to Cu1 and concurrent π-coordination with Cu2 to the reverse binding situation with π-coordination to Cu1 and σ-coordination to Cu2.

Table 10: Thermodynamic stability of **C01** in comparison with **C01iso** on the theoretical level B3LYP/LACVP**//B3LYP/LACVP**.

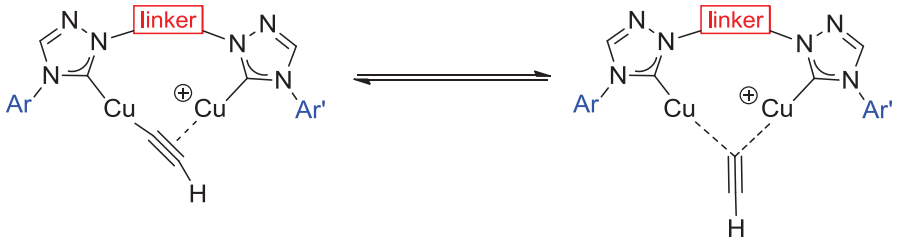

C01 **C01iso**

linker	Ar	ΔG (B3LYP/LACVP**//B3LYP/LACVP**)[a)]
xylylene	Ar = Ar' = 4-Tol	+ 10.1 kJ mol^{-1} (minimum)
ethylene	Ar = Xyl Ar' = Dipp	+ 9.2 kJ mol^{-1} (transition state)

[a)] with ΔG = G(**C01iso**) – G (**C01**)

Starting from the bridged dicopper acetylide complex, the azide coordinates to one of the copper(I) centres. For this structure it was checked as well whether the σ,π-coordination mode in **C02** was preferred over the σ,σ-coordination mode of the acetylide ligand in **C02iso**, but in the course of the geometry optimizations all complexes of

type **C02iso** with the μ_2-η^1,η^1-coordination mode did not turn out to represent minimum structures.

Altogether, the μ_2-η^1,η^1 dicopper acetylide complexes are thermodynamically less favourable than the corresponding μ_2-η^1,η^1 complexes. This finding is in accordance with the results of Ahlquist and Fokin who have also reported the preference for the μ_2-η^1,η^2-coordination mode if "two identical spectator ligands are present on both copper atoms".[32]
In consequence, only complexes of type **C01** and **C02** were considered in the formulation of the CuAAC reaction mechanism (Scheme 43).

With both the acetylide and the azide coordinated in structure **C02**, the C-N bond is formed. The transition state **C02TS03** of this supposedly rate-determining elementary step was unambiguously determined for all model complexes. The primary product would be the six-membered copper(III) metallacycle shown in curly brackets in Scheme 43. However, this structure was not found to be a stable intermediate, but immediately underwent reductive elimination to give the copper(I) triazolide complex **C03** in the course of the geometry optimizations. Complex **C03** can add another molecule of acetylene to give structure **C04**, whereupon the proton is transferred from the terminal alkyne to the triazolide giving the product 1-methyl-1*H*-1,2,3-triazole and the dicopper acetylide resting state **C01**. Complex **C04** containing both triazolide and alkyne ligand was found to be a stable species only in the case of the ethylene-linked series of dinuclear copper complexes; for the xylylene-linked complexes, the alkyne ligand dissociated in the course of the geometry optimizations.

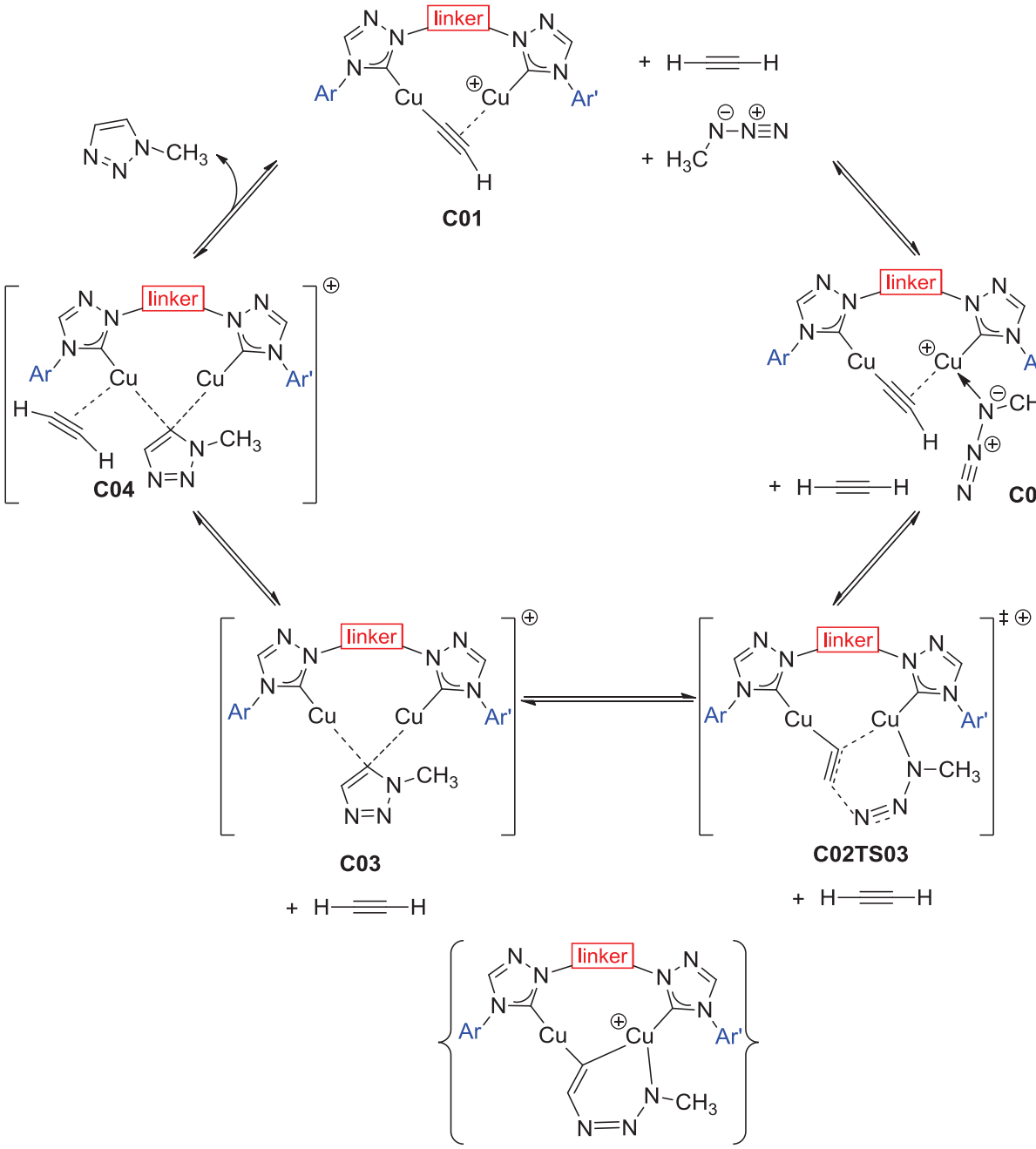

Scheme 43: Suggested mechanistic route for the CuAAC reaction of the model substrates methyl azide and ethyne with bistriazolylidene dicopper(I) complexes as catalysts.

First, geometry optimizations and frequency analyses under gas phase conditions were carried out on the theoretical level B3LYP/LACVP**. Single point energy calculations were then performed on the higher theoretical level B3LYP/LACV3P**++ with a triple zeta valence basis set. The difference $X^{LACVP^{**}}$ between the SCF energy and the Gibbs free energy as calculated on the level B3LYP/LACVP** was added to the SCF energy obtained by single point calculations on the higher level of theory (Equation 2). Furthermore, single point energies were determined on the level

B3LYP/LACVP** applying the PBF solvent model for dichloromethane. Again, the difference between the SCF energy and the Gibbs free energy obtained on the level B3LYP/LACVP** was added to the SCF solution phase energy calculated with B3LYP/LACVP**/PBF(dichloromethane) (Equation 2).

Equation 2: Estimation of the Gibbs free energy for calculations with basis set LACV3P**++ or with basis set LACVP** and PBF solvent model based on calculations including frequency analyses with LACVP** [with U(tot) = U + ZPE + SCFE; H(tot) = U(tot) + pV; G(tot) = H(tot)-TS = U + ZPE + SCFE + pV - TS].

$$G_{tot}^{LACVP^{**}} = SCFE^{LACVP^{**}} + ZPE + U + pV - TS = SCFE^{LACVP^{**}} + X^{LACVP^{**}}$$

$$G_{tot}^{LACV3P^{**}++} \approx SCFE^{LACV3P^{**}++} + X^{LACVP^{**}}$$

$$G_{tot}^{LACVP^{**}/PBF} \approx SCFE^{LACVP^{**}/PBF} + X^{LACVP^{**}}$$

The ΔG values thus obtained with the xylylene-linked model catalyst complexes in the reaction of methyl azide with acetylene as depicted in Scheme 43 are presented in Table 11.

Table 11: ΔG values [kJ mol^{-1}] for the catalytic cycle according to Scheme 43 with bistriazolylidene dicopper catalysts with a xylylene-linker; SCF energies [kJ mol^{-1}] are given in parentheses.

B3LYP/LACVP**// B3LYP/LACVP**	**C02x** + ethyne	**C02TS03x** + ethyne	**C03x** + ethyne	**C01x** + triazole
Ar = Ar' = Mes	46.8 (*-9.9*)	106.7 (*39.4*)	-156.2 (*-237.4*)	-243.0 (*-312.5*)
Ar = Ar' = 3,5-Xyl	29.6 (*-13.8*)	91.4 (*29.9*)	-150.7 (*-238.0*)	-243.0 (*-312.5*)
Ar = Ar' = Dipp	37.9 (*-17.5*)	128.2 (*59.9*)	-161.0 (*-243.2*)	-243.0 (*-312.5*)
Ar = Ar' = 4-Tol	21.7 (*-21.7*)	90.4 (*33.0*)	-153.3 (*-235.2*)	-243.0 (*-312.5*)
Ar = 3,5-Xyl Ar' = Dipp	35.1 (*-15.2*)	117.7 (*53.1*)	-158.3 (*-242.8*)	-243.0 (*-312.5*)

B3LYP/LACV3P**++// B3LYP/LACVP**	**C02x** + ethyne	**C02TS03x** + ethyne	**C03x** + ethyne	**C01x** + triazole
Ar = Ar' = Mes	59.6 (*2.9*)	123.3 (*55.9*)	-125.8 (*-207.0*)	-209.2 (*-278.7*)
Ar = Ar' = 3,5-Xyl	39.4 (*-4.0*)	105.1 (*43.6*)	-118.1 (*-205.5*)	-209.2 (*-278.7*)
Ar = Ar' = Dipp	53.6 (*-1.7*)	148.5 (*80.3*)	-131.0 (*-213.2*)	-209.2 (*-278.7*)
Ar = Ar' = 4-Tol	30.6 (*-12.8*)	102.7 (*45.3*)	-125.0 (*-207.0*)	-209.2 (*-278.7*)
Ar = 3,5-Xyl Ar' = Dipp	45.0 (*-5.3*)	132.3 (67.7)	-131.4 (*-215.8*)	-209.2 (*-278.7*)

B3LYP/LACVP**/ PBF(dichloromethane)// B3LYP/LACVP**	**C02x** + ethyne	**C02TS03x** + ethyne	**C03x** + ethyne	**C01x** + triazole
Ar = Ar' = Mes	66.9 (*10.2*)	122.7 (*55.3*)	-165.2 (*-246.4*)	-247.1 (*-316.6*)
Ar = Ar' = 3,5-Xyl	47.2 (*3.8*)	106.6 (*45.2*)	-158.3 (*-245.6*)	-247.1 (*-316.6*)
Ar = Ar' = Dipp	54.4 (*-0.9*)	144.3 (*76.1*)	-165.1 (*-247.3*)	-247.1 (*-316.6*)
Ar = Ar' = 4-Tol	37.9 (*-5.5*)	106.7 (*49.3*)	-162.1 (*-244.0*)	-247.1 (*-316.6*)
Ar = 3,5-Xyl Ar' = Dipp	50.1 (*-0.2*)	135.6 (71.0)	-160.8 (*-245.3*)	-247.1 (*-316.6*)

First, the influence of different aryl substituents was assessed for model complexes with xylylene-linked bistriazolylidene ligands. For all three levels of theory, the results showed the same tendencies, but the Gibbs free energies estimated after single point SCF calculations with the PBF solvent model or with the triple zeta basis set LACV3P**++ by applying Equation 2 were generally higher than with the original level of theory B3LYP/LACVP**. It is of course arguable, whether the procedure of adding the energy difference $X^{LACVP^{**}}$ to the SCF energy of single point calculations on higher levels of theory leads to significant errors. However, as the SCF energies (given in parentheses in Table 11) are higher for single point calculations with B3LYP/LACV3P**++ or B3LYP/LACVP**/PBF(dichloromethane) as well, this estimation of ΔG for B3LYP/LACV3P**++ and B3LYP/LACVP**/PBF(dichloromethane) seems reasonable, as geometry optimizations with frequency analyses on these higher levels of theory would have been too costly.

The Gibbs free energy of activation as well as the SCF energy for **C02TS03x** were highest for catalyst complexes with 2,6-diisopropylphenyl substituents (Dipp) on the N4-position, for example $\Delta E_{SCF}^{\neq}$ (B3LYP/LACVP**) = 59.9 kJ mol^{-1} and $\Delta G^{\neq}$ (B3LYP/LACVP**) = 128.2 kJ mol^{-1}. This is probably due to the steric hindrance by the isopropyl groups. The Gibbs free energies of activation were found to be very similar for the sterically less encumbered 3,5-xylyl and 4-tolyl substituted model catalyst complexes, for example $\Delta E_{SCF}^{\neq}$ (B3LYP/LACVP**) = 29.9 kJ mol^{-1} and

$\Delta G^{\neq}$ (B3LYP/LACVP**) = 91.4 kJ mol^{-1} with 3,5-xylyl substituents, and $\Delta E_{SCF}^{\neq}$ (B3LYP/LACVP**) = 33.0 kJ mol^{-1} and $\Delta G^{\neq}$ (B3LYP/LACVP**) = 90.4 kJ mol^{-1} for Ar = Ar' = 4-tolyl. The same tendencies are found when applying the higher levels of theory B3LYP/LACV3P**++ or B3LYP/LACVP**/PBF(dichloromethane). In conclusion, it can be pointed out that the activation energy is greatly dependent on the steric encumbrance of the aryl substituents on the triazolylidene ligands and rises in the order 4-tolyl ≈ 3,5-xylyl < mesityl < 2,6-diisopropylphenyl. With the unsymmetrically substituted ligand system Ar = 3,5-xylyl and Ar' = 2,6-diisopropylphenyl, the energy of transition state **C02TS03x** was calculated to be between the transition state energies with Ar = Ar' = 3,5-xylyl and Ar = Ar' = 2,6-diisopropylphenyl.

Compared to the calculations with tetranuclear model complexes reported by Straub,[31] the Gibbs free energies of activation obtained in this work are rather high. In Straub's calculations on the theoretical level B3LYP/LACV3P**++// B3LYP/LACVP**, the transition state analogous to **C02TS03** was found to have a Gibbs free energies of 86.9 kJ mol^{-1} relative to the sum of Gibbs energies of the tetranuclear copper(I) μ-acetylide model complex and free methyl azide (Figure 4). On the same level of theory, the lowest barrier in this work was found to be $\Delta G^{\neq}$ (B3LYP/LACV3P**++//B3LYP/LACVP**) = 102.7 kJ mol^{-1} with 4-tolyl substituents on the N4-positions of the bistriazolylidene ligand, *i.e.* the transition state of the optimal catalyst would be 15.8 kJ mol^{-1} higher in Gibbs free energy than calculated with the theoretical model by Straub (Figure 4).

A comparison of the calculational results obtained in this work with the report of Ahlquist and Fokin[32] seems inappropriate, as these authors have investigated model complexes with acetylide and chloride as spectator ligands and only the acetylide substrate acting as μ-bridging ligand. Applying the PBF solvent model for water, they calculated an overall barrier of $\Delta G^{\neq}$ [B3LYP/LACVP**/PBF(water)] = 10.5 kcal mol^{-1} (43.9 kJ mol^{-1}) for chloride as spectator ligand and $\Delta G^{\neq}$ [B3LYP/LACVP**/PBF (water)] = 12.9 kcal mol^{-1} (54.0 kJ mol^{-1}) for acetylide as spectator ligand. These values are much lower than the barriers calculated in this work and in Straub's report from 2007.[31] This might be due to the highly polar transition state postulated by Ahlquist and Fokin, which is well stabilized by the PBF solvent model for water.

As the calculated activation energies were comparably high, it was investigated whether an ethylene linkage might be a better choice for obtaining more active bistriazolylidene dicopper catalyst systems. The results for these model complexes are summarized in Table 12. Again, the Gibbs free energy of activation increases in the order 3,5-xylyl ≈ 4-tolyl < mesityl < 2,6-diisopropylphenyl. The general trend that the relative energies calculated on the theoretical level B3LYP/LACVP** are higher than for B3LYP/LACV3P**++//B3LYP/LACVP** and B3LYP/LACVP**/PBF(dichloromethane)//B3LYP/LACVP** is observed as well. A comparison of the results in Table 12 with those presented in Table 11 shows that regardless of the level of theory, no substantial decrease in activation energies is achieved when the xylylene-linker is replaced by an ethylene-linker. For example, the free energy of activation for 3,5-xylyl substituted catalysts is $\Delta G^{\neq}$ (B3LYP/LACVP**) = 91.4 kJ mol^{-1} with a xylylene-linker and $\Delta G^{\neq}$ (B3LYP/LACVP**) = 87.1 kJ mol^{-1} for the ethylene-linked dicopper complex. Moreover, the corresponding structures show that the acetylide can very well act as a bridging ligand regardless of whether ethylene or xylylene is present as linker unit.

Table 12: ΔG values [kJ mol^{-1}] for the catalytic cycle according to Scheme 43 with bistriazolylidene dicopper catalysts with an ethylene-linker; SCF energies [kJ mol^{-1}] are given in parentheses.

B3LYP/LACVP**// B3LYP/LACVP**	**C02e** + ethyne	**C02TS03e** + ethyne	**C03e** + ethyne	**C04e**	**C01e** + triazole
Ar = Ar' = Mes	35.8 (*-17.1*)	109.1 (*37.9*)	-154.1 (*-236.8*)	-135.1 (*-257.8*)	-243.0 (*-312.5*)
Ar = Ar' = Xyl	32.1 (*-15.7*)	87.1 (*24.2*)	-153.6 (*-233.7*)	-136.0 (*-259.3*)	-243.0 (*-312.5*)
Ar = Ar' = Dipp	38.1 (*-15.4*)	116.5 (*48.9*)	-150.8 (*-236.3*)	-121.7 (*-250.6*)	-243.0 (*-312.5*)
Ar = Ar' = 4-Tol	25.0 (*-29.0*)	88.3 (*26.1*)	-162.3 (*-235.8*)	-146.3 (*-257.5*)	-243.0 (*-312.5*)
Ar = Xyl Ar' = Dipp	33.3 (*-19.8*)	104.6 (*35.3*)	-154.5 (*-238.8*)	-119.7 (*-246.5*)	-243.0 (*-312.5*)

B3LYP/LACV3P**++// B3LYP/LACVP**	**C02e** + ethyne	**C02TS03e** + ethyne	**C03e** + ethyne	**C04e**	**C01e** + triazole
Ar = Ar' = Mes	45.8 (*-7.1*)	124.8 (*53.6*)	-126.8 (*-209.5*)	-88.6 (*-211.4*)	-209.2 (*-278.7*)
Ar = Ar' = 3,5-Xyl	40.7 (*-7.0*)	98.9 (*35.9*)	-126.9 (*-207.0*)	-88.7 (*-212.1*)	-209.2 (*-278.7*)
Ar = Ar' = Dipp	47.8 (*-5.2*)	128.1 (*61.0*)	-123.7 (*-208.6*)	-77.0 (*-205.3*)	-209.2 (*278.7*)
Ar = Ar' = 4-Tol	38.7 (*-15.2*)	99.8 (*37.6*)	-136.4 (*-209.6*)	-101.9 (*-213.0*)	-209.2 (*278.7*)
Ar = 3,5-Xyl Ar' = Dipp	42.5 (*-10.6*)	117.4 (*48.1*)	-128.5 (*-212.7*)	-72.8 (*-199.5*)	-209.2 (*278.7*)

B3LYP/LACVP**/ PBF(dichloromethane)// B3LYP/LACVP**	**C02x** + ethyne	**C02TS03x** + ethyne	**C03x** + ethyne	**C04e**	**C01x** + triazole
Ar = Ar' = Mes	49.3 (*-3.5*)	126.5 (*55.3*)	-158.4 (*-241.1*)	-121.8 (*-244.6*)	-247.1 (*-316.6)*
Ar = Ar' = 3,5-Xyl	45.7 (*-2.1*)	105.3 (*42.3*)	-156.2 (*-236.3*)	-119.2 (*-242.6*)	-247.1 (*-316.6)*
Ar = Ar' = Dipp	51.1 (*-1.8*)	129.6 (*62.5*)	-158.5 (*-243.4*)	-111.1 (*-239.4*)	-247.1 (*-316.6)*
Ar = Ar' = 4-Tol	45.1 (*-8.9*)	106.1 (*44.0*)	-167.8 (*-241.0*)	-132.3 (*-243.4*)	-247.1 (*-316.6)*
Ar = 3,5-Xyl Ar' = Dipp	48.6 (*-4.6*)	123.9 (*54.6*)	-157.2 (*-241.4*)	-103.7 (*-230.4*)	-247.1 (*-316.6)*

A representative energy diagram for the CuAAC reaction of ethyne with methyl azide with the ethylene-linked 3,5-xylyl substituted bistriazolylidene dicopper catalyst including structural representations is displayed in Figure 16. The corresponding ORTEP plots of the calculated structures involved are shown in Scheme 44.

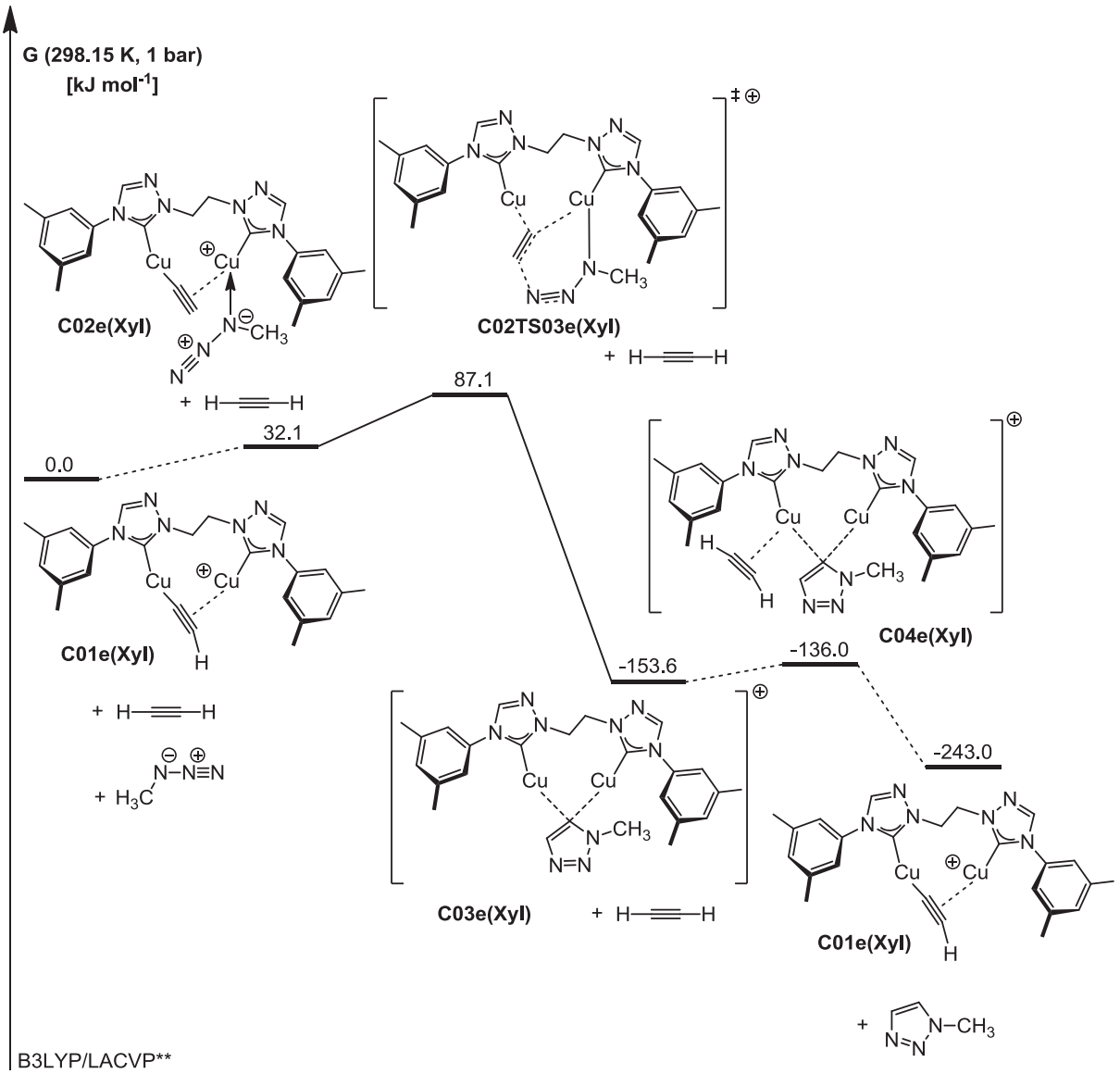

Figure 16: Gibbs free energy diagram of the CuAAC reaction between methyl azide and ethyne with the cationic complex μ-acetylido-μ-{1,1'-(ethane-1,2-diyl)bis[4-(3,5-dimethylphenyl)-1*H*-1,2,4-triazol-5-ylidene]}-κC,$\kappa C'$-dicopper(I) **C01e(Xyl)** as resting state.

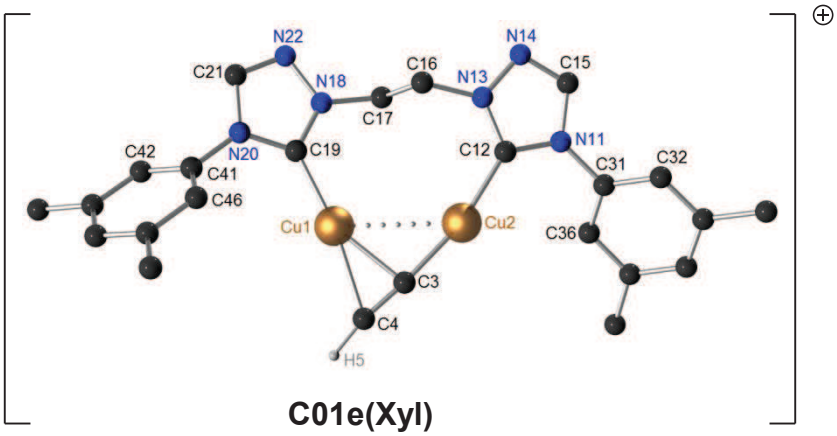

C01e(Xyl)

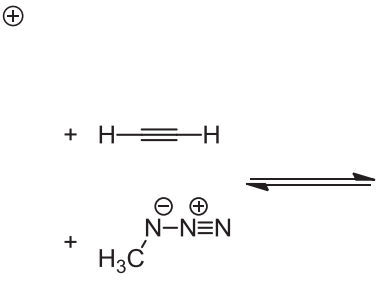

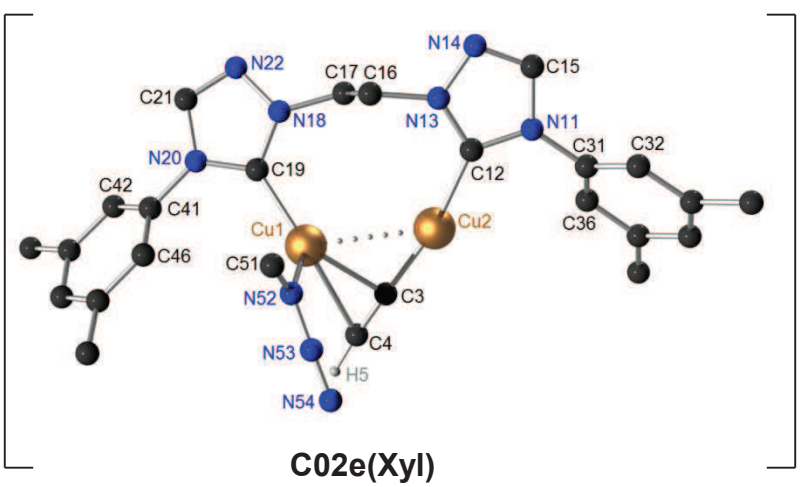

C02e(Xyl)

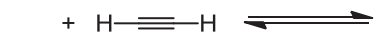

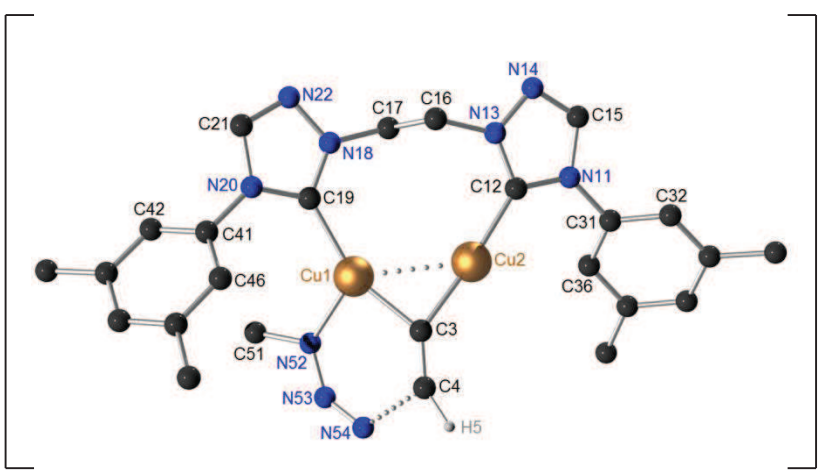

C02TS03e(Xyl)

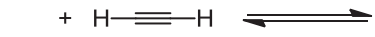

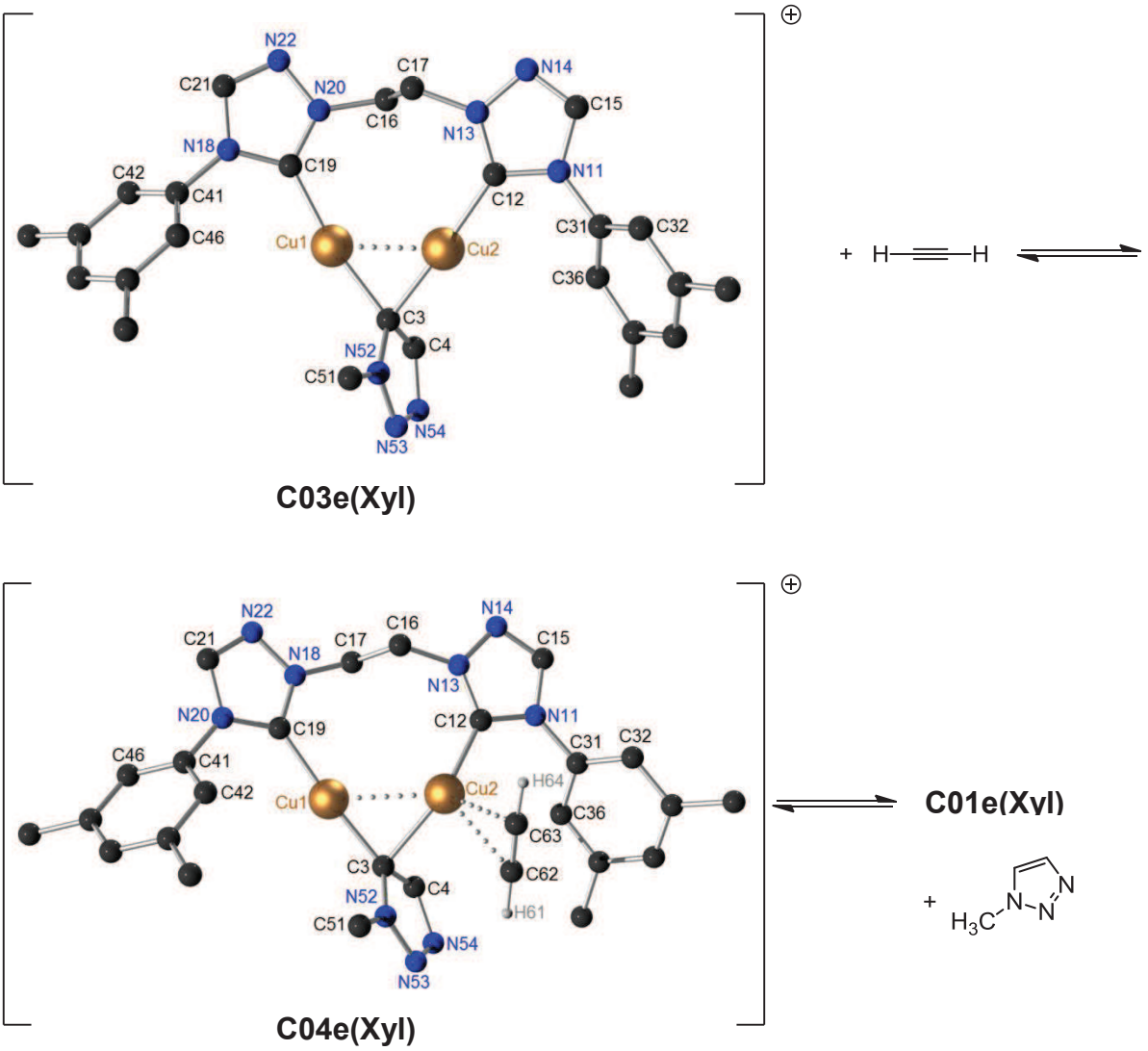

Scheme 44: ORTEP plots of the calculated structures in the catalytic cycle of the CuAAC reaction between methyl azide and ethyne with the cationic complex μ-acetylido-μ-{1,1'-(ethane-1,2-diyl)bis[4-(3,5-dimethylphenyl)-1*H*-1,2,4-triazol-5-ylidene]}-$\kappa C,\kappa C'$-dicopper(I) **C01e(Xyl)** as resting state (most hydrogen atoms are omitted for clarity).[118] Selected average bond lengths [Å], bond angles and dihedral angles for **C01e(Xyl)**: Cu1-Cu2 2.911, C3-C4 1.239, Cu1-C3 2.058, Cu1-C4 2.228, Cu2-C3 1.901, C4-H5 1.071; C3-C4-H5 170.83°, C12-Cu2-C3 167.68°, C19-Cu1-C3 155.81°, C19-Cu1-C4 170.90°; C12-Cu2-Cu1-C19 -1.30°, C19-N20-C41-C46 55.54°, C12-N11-C31-C36 48.21°. Selected average bond lengths [Å], bond angles and dihedral angles for **C02e(Xyl)**: Cu1-C3 2.106, Cu1-C4 2.509, Cu2-C3 1.900, Cu2-C4 1.939, C3-C4 1.232, Cu1-N52 2.286, C4-H5 1.069, C19-Cu1 1.981, N52-N53 1.136, N53-N54 1.249; N52-N53-N54 171.91°, C3-C4-H5 175.86°. Selected average bond lengths [Å], bond angles and dihedral angles for **C02TS03e(Xyl)**: Cu1-C3 1.944, C3-C4 1.265, C4-N44 1.834, N44-N43 1.186, N43-N42 1.270, N42-Cu1 2.071, Cu1-Cu2 2.653; N42-N43-N44 140.72°, C3-C4-H5 146.92°; N44-C4-C3-Cu1 24.74°, N44-N43-N42-Cu1 -12.40°. Selected average bond lengths [Å], bond angles and dihedral angles for **C03e(Xyl)**: Cu1-C19 1.942, Cu1-Cu2 2.500, Cu2-C12 1.941, Cu1-C3 1.986, Cu2-C28 2.011, N52-C3 1.388, C3-C4 1.406, C4-N54 1.357; Cu1-C3-Cu2 77.44°, Cu1-Cu2-C3 50.83°, C3-Cu1-Cu2 51.73°; Cu1-Cu2-C3-C4 119.21°, C12-Cu2-Cu1-C19 -2.24°, C19-Cu1-C3-N52 138.18°. Selected average bond lengths [Å], bond angles and dihedral angles for **C04e(Xyl)**: Cu1-Cu2 2.605,Cu1-C19 1.934, Cu2-C12 1.947, Cu1-C3 1.944, Cu2-C3 2.142, Cu2-C63 2.729, Cu2-C62 2.713, C62-C63 1.211; Cu2-C62-C63 77.89°, Cu2-C63-C62 76.40°; Cu1-Cu2-C3-C4 128.92°.

In the calculated resting state of the 3,5-xylyl substituted ethylene-linked bistriazolylidene dicopper acetylide model complex **C01e(Xyl)** the distance between the two copper(I) centres was found to be 2.911 Å. For comparison, the interatomic distance in copper metal is 2.556 Å,[121] and the Cu(I)-Cu(I) distance in the infinite ladder polymer (phenylethynyl)copper(I) [$(PhC{\equiv}CCu)_n$] (Figure 6) was found to be between 2.49 and 2.83 Å by applying powder diffraction methods.[26t] This result might mean that the bistriazolylidene ligand's "bite size" forces the copper(I) ions Cu1 and Cu2 in the resting state **C01e(Xyl)** to stand slightly farther apart than they would in an acetylide complex in the absence of the bridging bistriazolylidene ligand. On the other hand, the greater than expected distance between the metal ions might be attributed to the neglect of attractive cuprophilic interactions[122] in the geometry optimizations and energy calculations on the theoretical level applied in this work. In all complexes displayed in Scheme 44, dotted lines have been drawn in order to indicate the plausibility of "non-classical" d^{10}-d^{10} interactions between the closed-shell copper(I) ions in these dinuclear complexes. Compared to other systems, in which cuprophilic interactions are proposed either with or without the influence of a bridging ligand and its characteristic "bite size", the distances between the two copper ions are shorter than in the calculated structures shown in Scheme 44,[121, 122b, 123] so that the copper(I) centres are expected to be positioned closer to each other than the calculational results irrespective of cuprophilic interactions suggest.

In a review from 2000, structural data of polynuclear σ,π-acetylide complexes of copper(I) halides have been compiled by Mykhalichko.[21a] The C≡C bond lengths in the bridging acetylide ligands of these complexes were found to range between 1.19 Å in $(PyH)_4Cu_9Cl_{12}(C{\equiv}CH)$ and 1.29 Å in $(ImH)_4Cu_4Cl_4(C{\equiv}CCH_2OH) \cdot H_2O$ and $(NH_4)_2Cu_4Cl_5(C{\equiv}CCH_2OH) \cdot H_2O$. The calculated C≡C distance in model complex **C01e(Xyl)** is 1.239 Å and thus in the same range as the experimental values. However, the acetylide ligand's coordination mode in the acetylide complexes described by Mykhalichko is μ_2-η^1, η^1, whereas the μ_2-η^1, η^2-coordination mode was shown to be thermodynamically preferred for the model complexes presented herein (Table 10). The C≡C bond length in gaseous acetylene was calculated to be 1.205 Å, which is in good accordance with the value reported in literature (1.207 Å).[29] Thus, the alkyne bond is slightly weakened and elongated upon coordination as 4e-donor σ,π-ligand in **C01e(Xyl)**. Also, the C≡C-H bond angle is reduced from 180° to φ(C3-C4-H5) = 170.83°, which can be explained by the metallacyclopropene

interpretation of the bonding situation, *i.e.* a resonance structure with two σ-bonds between Cu1-C3 and Cu1-C4.[124] The C3-Cu1-C4 "metallacyclopropene" structure is slightly unsymmetric with a greater distance between Cu1 and C4 (2.228 Å) than between Cu1 and Cu3 (2.058 Å).

Upon coordination of methyl azide to the copper ion which forms the π-bond with the acetylide, the unsymmetry is increased as the Cu1-C4 distance (2.509 Å) is now much larger than the Cu1-C3 distance (2.106 Å). The azide is only weakly bound in model complex **C02e(Xyl)** with a Cu1-N52 distance of 2.286 Å. The N_3 unit is nearly linear with φ(N52-N53-N54) = 171.91°, which is almost identical to the geometry in free methyl azide (172.901°).

This changes significantly as the transition state **C02TS03e(Xyl)** of the C-N bond forming step is reached. In the six-membered cycle (Cu1-C3-C4-N54-N53-N52), the angle φ(N52-N53-N54) is reduced to 140.72°. Also, the acetylide ligand is already significantly bent towards the geometry of the product triazole with φ(C3-C4-H5) = 146.92°. The six-membered cycle is almost planar with torsion angles of only τ(N54-C4-C3-Cu1) = 24.74° and τ(N54-N53-N52-Cu1) = -12.40°. The Cu-Cu distance is 2.653 Å and thus only slightly larger than in the model transition state with water and acetylide as spectator ligands with d(Cu-Cu) = 2.64 Å as reported by Ahlquist and Fokin.[32]

As pointed out before, the six-membered cycle that is expected as the primary product in this mechanistic picture (shown in curly brackets in Scheme 43) was not found to be a minimum structure, but directly underwent reductive elimination in the course of the geometry optimizations to give complex **C03e(Xyl)** with an aromatic triazolide ligand in a highly exergonic step. In this complex, the triazolide is coordinated to both copper(I) centres by σ-bonds. The resulting triangle Cu1-C3-Cu2 is nearly planar and the distances d(Cu1-C3) = 1.986 Å and d(Cu2-C3) = 2.011 Å are very similar to each other. The plane of the triazolide heterocyle is nearly perpendicular with respect to the plane of the Cu1-C3-Cu2 triangle with τ(Cu1-Cu2-C3-C4) = 119.21°.

In structure **C04e(Xyl)**, an additional ethyne molecule "coordinates" to copper centre Cu2. However, this π-bond is quite loose as the Cu-C distance is large with d(Cu2-C62) = 2.713 Å and d(Cu2-C63) = 2.729 Å. It is thus disputable whether the addition of this ethyne molecule can be termed a coordinative bond at all. With all xylylene-linked model complexes, this contact is so weak that the alkyne removes itself from the dicopper species in the course of the geometry optimizations. The calcula-

tions thus cannot give an answer as to whether the deprotonation of the alkyne substrate takes place in the coordination sphere of the dicopper triazolide complex with the triazolide acting as a base. An experimental study shows that the CuAAC test reaction of benzyl azide with 1-[D]-2-phenylacetylene carried out in acetonitrile with $[(PhC{\equiv}CCu)_2]_n$ as catalyst exclusively afforded the C5-deuterated triazole product in 65 % yield.[35] This confirms the suggestion that the coordinated alkyne protonates the triazolide in the coordination sphere of the dicopper complex. In protic media, however, the triazolide ligand is rather protonated by the solvent, as the C5-deuterated triazole product was obtained in nearly quantitative yield when the reaction was carried out in D_2O with copper(II) sulphate pentahydrate as precatalyst and sodium ascorbate as reducing agent.[11] Under the experimental conditions described in section 4.7, the copper triazolide intermediate will most probably be protonated by acetic acid, which is present in the reaction mixture. Calculations to investigate the protonation of dicopper triazolide complex **C03** by a coordinated molecule of acetic acid as shown in Scheme 56 are envisaged for future work.
In any case, the triazole is finally set free and the dicopper acetylide complex **C01e(Xyl)** recovered.

All in all, these calculations have shown that the geometric characteristics of the projected bistriazolylidene catalyst complexes are adequate to enable CuAAC catalysis by the proposed mechanistic pathway shown in Scheme 43. It was taken for granted that the dicopper acetylide complex is thermodynamically very stable and constitutes the resting state of the catalytic cycle. However, calculations on alternative resting states such as dimerized tetranuclear species as proposed in paragraph 4.7.5 are planned to prove this assumption. The Gibbs free energy for the crucial transition state of the C-N bond forming step was found to be unexpectedly high, in some cases more than 100 kJ mol^{-1} above the sum of the Gibbs free energies of the substrates and the resting state. Complexes featuring an ethylene-linker were found to be slightly more advantageous than those with a xylylene molecular linker. Moreover, sterically demanding aryl substituents at the N4-position of the triazolylidene ligands turned out to impede catalysis. Thus, large substituents such as Dipp should be avoided.

4.4 Synthesis of Bistriazolium Hexafluorophosphate Salts

Due to their greater acidity, bistriazolium salts seemed more convenient precursors for the synthesis of bis-NHC dicopper complexes than bisimidazolinium salts (see paragraph 4.2). Moreover, the preliminary calculations presented in section 4.3 suggest that once the μ-bridged acetylide complex is formed, the catalytic pathway shown in Scheme 43 is passable. With regard to these expected advantages, a variety of bistriazolium hexafluorophosphate ligand precursors was prepared.

In 2009, a new protocol for the synthesis of aryl-substituted 1,2,4-triazoles was developed in our group.[120, 125] This synthetic procedure was used for the preparation of 1,2,4-triazolium salts with a thiophenol substituent by Stefanie Seitz in the course of her PhD thesis.[126] Based on these results, a variety of 1,2,4-triazoles was synthesized in analogy to the procedures reported by Alexander Siegle in his bachelor thesis.[125] The linkage of these 1,2,4-triazoles by double S_N2 reaction with a bis-electrophile under neat conditions analogous to literature reports[120, 125] was planned as the second step on the way towards bistriazolylidene dicopper(I) complexes. However, the 4-aryl substituted 1,2,4-triazoles used in this work had a much higher melting point than the thiophenol-substituted triazoles in the PhD project of Stefanie Seitz.[126] It was thus necessary to work out a new procedure for combining the triazole derivatives *via* an ethylene or a xylylene molecular bridge. Having established this route, a variety of symmetrically and unsymmetrically substituted bistriazolium halides was prepared and characterized. In order to avoid the presence of halide anions in the following steps, salt metathesis reactions were carried out in order to replace the halide by a weakly coordinating anion.

4.4.1 Synthesis of 4-Aryl-1,2,4-triazoles

4-Aryl-1,2,4-triazoles were synthesized by heating *N*,*N*-dimethylformamide azine dihydrochloride with the corresponding anilines under neat conditions. In order to allow for the testing of different substitution patterns, 1,2,4-triazoles with mesityl (Mes), 3,5-xylyl (Xyl), 2,6-diisopropylphenyl (Dipp) and 4-tolyl (4-Tol) groups at the N4-position were prepared (**21** - **24**, Table 13).

Table 13: Synthesis of 4-aryl-1,2,4-triazoles **21** - **24**.

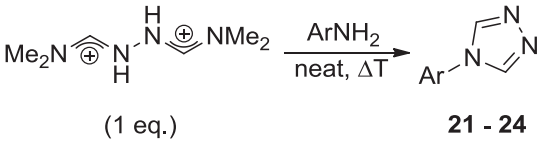

entry	Ar	equivalents of aniline	reaction conditions	yield	product	melting point of the product triazole
1	Mes	1	130 °C, 24 h	68 %	**21**	234 °C
2	Xyl	1	130 °C, 3 d	69 %	**22**	151 °C
3	4-Tol	2	140 °C, 3 d	43 %	**23**	118 °C
4	Dipp	2	150 °C, 8 d	39 %	**24**	228 °C

As the 3,5-xylyl substituted derivative **22** had not been described in literature so far, it was fully characterized including single crystal X-ray structure analysis (Figure 17).

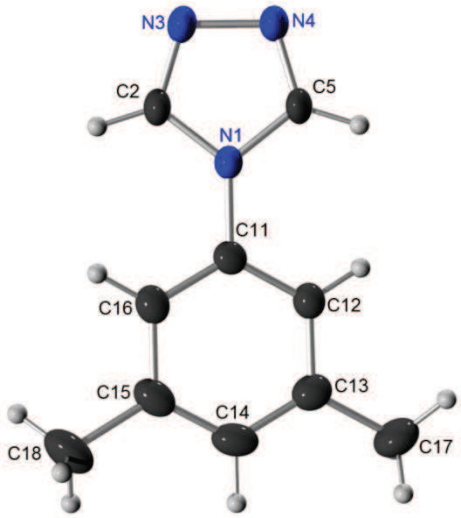

Figure 17: ORTEP plot of the single crystal X-ray structure of 4-(3,5-dimethylphenyl)-4*H*-1,2,4-triazole (**22**).[118, 127] Selected average bond lengths [Å], bond angles and dihedral angles: N1-C11 1.434, N1-C2 1.358, C2-N3 1.299, N3-N4 1.389, N4-C5 1.302, C5-N1 1.361; C2-N1-C5 103.49°; C2-N1-C11-C12 -12.56°, C2-N1-C11-C16 167.98°, C5-N1-C11-C12 166.90°, C5-N1-C11-C16 -12.55°.

In contrast to the structure of 4-(2,6-dimethylphenyl)-4*H*-1,2,4-triazole described in literature,[120] the planes of the triazole ring and the phenyl substituent are only slightly twisted by approximately 12° with respect to each other, as the steric bulk of the

methyl groups in the 3,5-xylyl groups is farther apart from the triazole heterocycle than with the *ortho*-disubstituted 2,6-dimethylphenyl substituents.

4.4.2 Synthesis of Symmetrically Substituted Xylylene-Linked Bistriazolium Halides

In order to molecularly link the 4-substituted 1,2,4-triazoles, a double S_N2 reaction with 1,3-bis(chloromethyl)- or 1,3-bis(bromomethyl)benzene was envisaged. However, the procedure reported in literature[120] was not applicable to this problem, as the 4-aryl substituted 1,2,4-triazoles of this work have a melting point which is too high for applying neat reaction conditions (Table 13). It was thus necessary to devise a new protocol for this transformation under solution phase conditions. The main difficulty was the need for a clean double S_N2 reaction. The ratio of monosubstitution *versus* disubstitution could be determined by NMR spectroscopy of samples taken from the reaction mixture. The peaks of the triazolium cation in the downfield region of the spectrum were used for determining the product ratio (Figure 18). The monosubstituted product was formed even when the triazole substrate was used in excess. Only with refluxing glacial acetic acid as solvent were satisfactory results obtained. The advantages of this solvent are its polarity and hydrogen bond donor ability, to which the good solubility of the salts involved in this reaction can be attributed, as well as its high boiling point, which allows for reactions at temperatures as high as 118 °C.

Table 14: Solvent screening for the double S_N2 reaction of 4-(2,4,6-trimethylphenyl)-4*H*-1,2,4-triazole **21** with 1,3-bis(chloromethyl)benzene or 1,3-bis(bromomethyl)benzene.

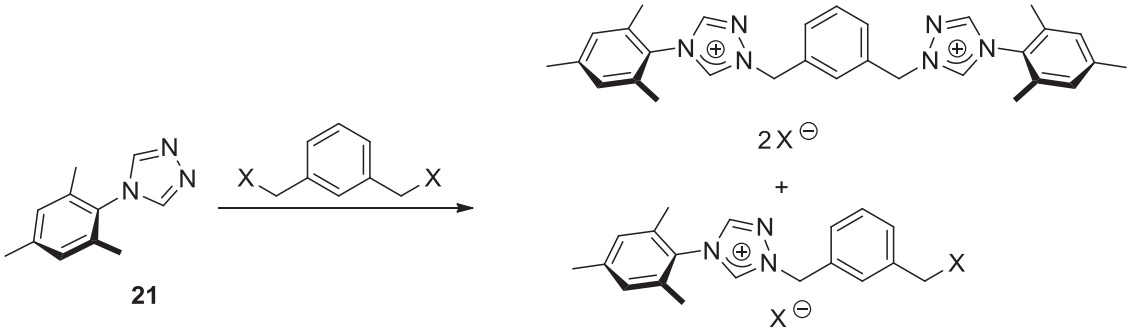

entry	solvent	X	equivalents of triazole	reaction conditions	approximate ratio disubstitution *vs.* monosubstitution
1	methanol	Cl	2.2	2 d, reflux	3 : 1
			3.1	7 d, reflux	3 : 1
2	methanol	Br	2.2	2 d, reflux	3.5 : 1
			3.3	6 d, reflux	3.6 : 1
3	isopropanol	Cl	2.2	3 d, reflux	1 : 1
4	acetonitrile	Cl	2.2	1 d, reflux	1.2 : 1
5	DMF	Cl	2.2	3 d, reflux	decomposition; ^{1}H NMR: complicated mixture
6	water	Cl	3.0	5 d, reflux	decomposition; ^{1}H NMR: complicated mixture
7	acetic acid	Cl	3.0	5 d, reflux	10 : 1

Figure 18 shows part of the ^{1}H NMR spectrum of the raw product from entry 7 in d_6-DMSO. The peaks at 11.33 and 9.64 ppm belong to the desired bistriazolium salt, whereas the peaks at 11.20 and at 9.60 ppm can be assigned to the undesired monotriazolium salt. The ^{1}H resonances of the NCHN groups in the triazole substrate (**21**), which was used in excess, are observed at 8.73 ppm.

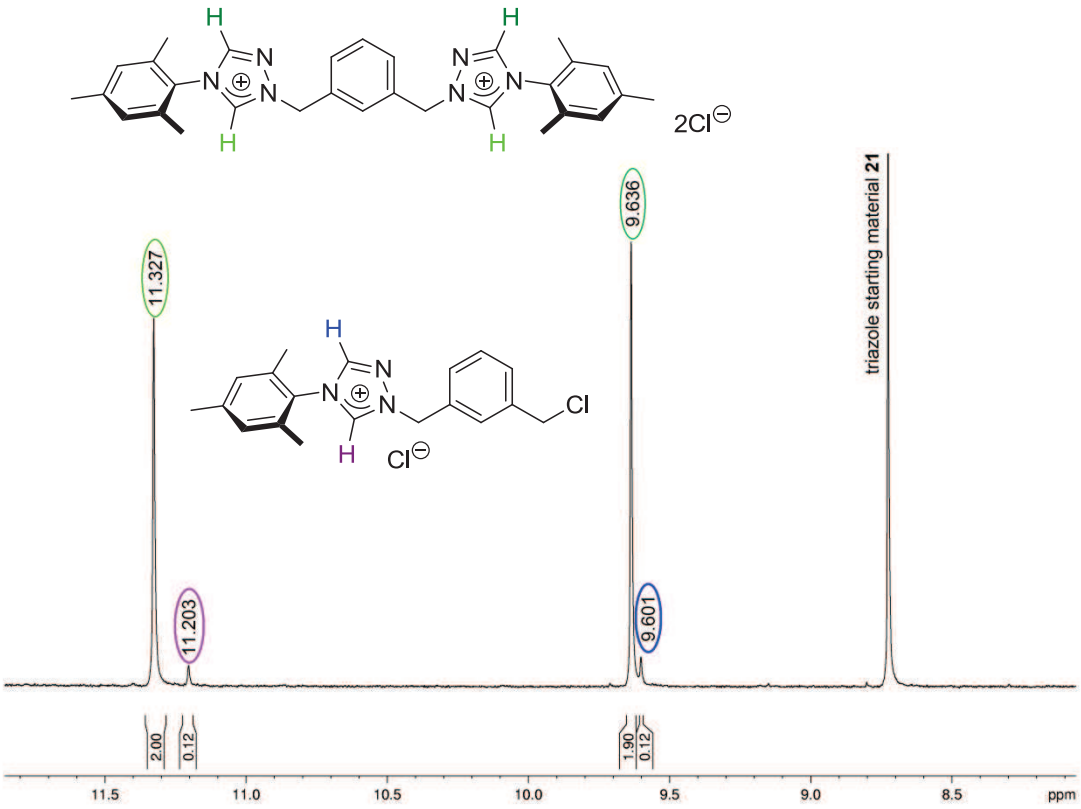

Figure 18: Downfield region of the ^{1}H NMR spectrum of the raw reaction mixture containing the mono-and disubstituted product as well as unaltered triazole starting material **21** (recorded in d_6-DMSO at 250 MHz; green: disubstitution product; blue/violet: monosubstitution product).

Based on these findings, xylylene-linked bistriazolium salts of different 1,2,4-triazoles were synthesized (**31** - **34**). The undesired monosubstitution product was only formed in minor amounts when applying the procedures reported in Table 14, entry 7.

Table 15: Synthesis of 1,1'-[1,3-phenylenebis(methylene)]bis(4-aryl-1*H*-1,2,4-triazolium) dichloride salts **31** - **34**.

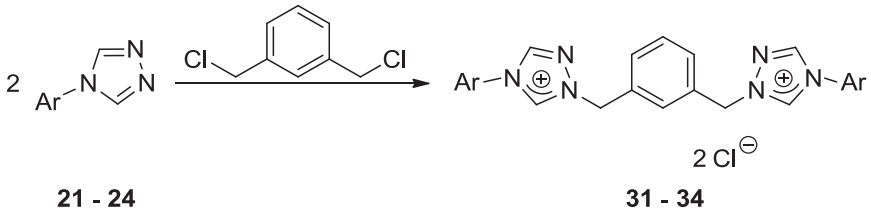

21 - 24 **31 - 34**

entry	Ar	equivalents of triazole	reaction conditions	yield	product
1	Mes	3.0	3 d, HOAc, reflux	90 %	**31**
2	Xyl	3.0	8 d, HOAc, reflux	88 %	**32**
3	4-Tol	2.6	8 d, HOAc, reflux	quant.	**33**
4	Dipp	2.3	4 d, HOAc, reflux	quant.	**34**

The excess triazole substrate was removed by extracting the raw product with hot toluene. The colourless salt was then washed with diethyl ether, in order to remove traces of toluene as well as acetic acid. In the case of 1,1'-[1,3-phenylenebis(methylene)]bis[4-(2,4,6-trimethylphenyl)-1*H*-1,2,4-triazolium] dichloride, one equivalent of acetic acid could not be detached from the product. For all other salts, only substoichiometric amounts of acetic acid were detected in the product after work-up. Together with traces of monosubstitution product, this prevented obtaining correct elemental analyses for these 1,1'-[1,3-phenylenebis(methylene)]bis(4-aryl-1*H*-1,2,4-triazolium) dichloride salts (**31** - **34**).

Due to the positive charge of the triazolium heterocycle, quaternization on N1 is indicated by signals in the far downfield region of the ^{1}H NMR spectrum. The two CH groups on the triazole ring are no longer equivalent and the ^{1}H resonance for the CH group in 5-position is observed at larger δ-values than for the CH group in 3-position: in d_6-DMSO, H3 proton resonances were observed between 9.66 and 9.84 ppm for the differently substituted bistriazolium chloride salts **31** - **34**, and resonances for the H5 protons between 11.23 and 11.61 ppm. The downfield shift of the CH_2 protons' resonance from 4.77 ppm in 1,3-bis(chloromethyl)benzene to 5.73 to 5.91 ppm in the xylylene-bridged bistriazolium salts is indicative of product formation as well. A representative ^{1}H NMR spectrum is shown in Figure 19.

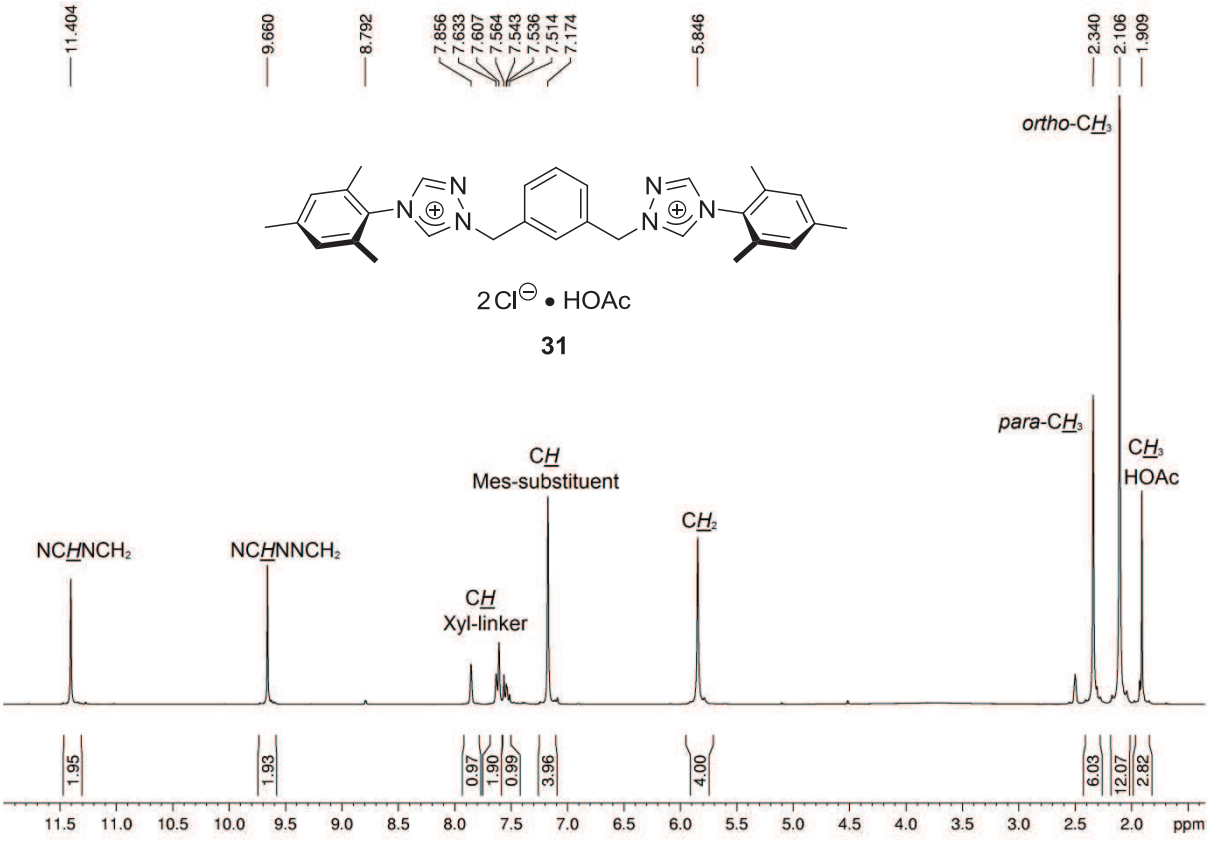

Figure 19: ^{1}H NMR spectrum of bistriazolium salt **31** (recorded in d_6-DMSO at 300 MHz).

For all xylylene-linked bistriazolium chloride salts, the C3 carbon atom is less shielded than the C5 carbon so that the order of peaks in the ^{13}C and the ^{1}H NMR spectrum is opposite to each other. With the help of a two-dimensional HSQC spectrum of bistriazolium salt **31**, it was found that the acidic triazolium CH group with its ^{1}H resonance at 11.40 ppm gives a ^{13}C signal at 144.3 ppm, whereas the CH group at the triazolium's 3-position has a ^{1}H resonance more upfield at 9.66 ppm and a ^{13}C peak more downfield at 145.7 ppm. All 1,1'-[1,3-phenylenebis(methylene)]bis(4-aryl-1*H*-1,2,4-triazolium) dichloride salts were soluble in DMSO, water and methanol, except for the 4-tolyl substituted derivative **33**, which was hardly soluble in any of these solvents. In ESI+ mass spectra, signals corresponding to the dication $[M\text{-}2Cl]^{2+}$, the monocation $[M\text{-}Cl]^{+}$ as well as the split-off of the aryl substituent $[M\text{-}Ar\text{-}2Cl]^{+}$ were observed.

4.4.3 Synthesis of Symmetrically Substituted Ethylene-Linked Bistriazolium Halides

In order to definitely prevent the formation of bis-NHC monocopper(I) complexes by bending of the bis-NHC ligand according to structure **IV** in Scheme 50, an ethylene-linker was introduced as an alternative to xylylene. With 1,2-dibromoethane as bis-electrophile, the bistriazolium salts were obtained in good to excellent yield by applying procedures analogous to those described for the synthesis of 1,1'-[1,3-phenylene-bis(methylene)]bis(4-aryl-1*H*-1,2,4-triazolium) salts **31** - **34** in section 4.4.2. No traces of monosubstitution product could be detected at all. For the 4-tolyl substituted triazole with its melting point at 118 °C it was also possible to alternatively carry out the reaction under neat conditions analogous to the procedure reported in literature.[120, 125] This route has the advantage of shorter reaction times and no impurities of acetic acid in the product, so that a correct elemental analysis was obtained for 1,1'-(ethane-1,2-diyl)bis[4-(4-methylphenyl)-1*H*-1,2,4-triazolium] dibromide (**43**).

Table 16: Synthesis of 1,1'-(ethane-1,2-diyl)bis(4-aryl-1*H*-1,2,4-triazolium) dibromide salts **41** - **44**.

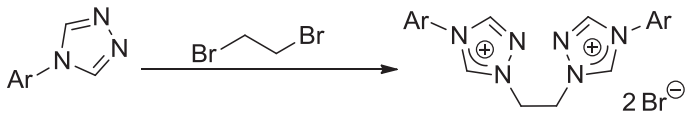

21 - 24 **41 - 44**

entry	Ar	equivalents of triazole	reaction conditions	yield	product
1	Mes	2.2	5 d, HOAc, reflux	90 %	**41**
2	Xyl[128]	3.0	6 d, HOAc, reflux	97 %	**42**
3	4-Tol	2.2	16 h, neat	82 %	**43**
4	Dipp	2.2	3 d, HOAc, reflux	30 %[129]	**44**

As a representative example, the ^{1}H NMR spectrum of 1,1'-(ethane-1,2-diyl)bis[4-(2,4,6-trimethylphenyl)-1*H*-1,2,4-triazolium] dibromide (**41**) is shown in Figure 20. As the aliphatic linker is less electron-withdrawing than the aromatic linker and the bromide counterion less electronegative than chloride, the triazolium resonances as well as the CH_2 groups' resonance are observed more upfield than with the xylylene-linked bistriazolium salts. The signals corresponding to the H5-position on the

heterocyclic ring in ethylene-linked bistriazolium bromide salts are found between 10.86 and 11.12 ppm, and the H3 resonances between 9.64 and 9.90 ppm. The methylene groups' signals are observed between 5.16 and 5.37 ppm. For example, in the ^{1}H NMR spectrum of **41** (Figure 20) the signal for the acidic triazolium proton H5 is observed at 10.86 ppm, the H3 proton gives a peak at 9.64 ppm, and the methylene group at 5.27 ppm. As with xylylene-linked bistriazolium chloride salts (paragraph 4.4.2), the C3 carbon atom is less shielded than C5 so that the order of peaks in the ^{13}C and the ^{1}H NMR spectrum of ethylene-linked bistriazolium bromide salts is reversed. As derived from the two-dimensional HSQC spectrum of bistriazolium bromide salt **41**, the peak of the acidic triazolium CH group with its ^{1}H resonance at 10.86 ppm gives a ^{13}C signal at 144.8 ppm, whereas the CH group at the triazolium's 3-position has a ^{1}H resonance more upfield at 9.64 ppm and a ^{13}C peak more downfield at 145.5 ppm.

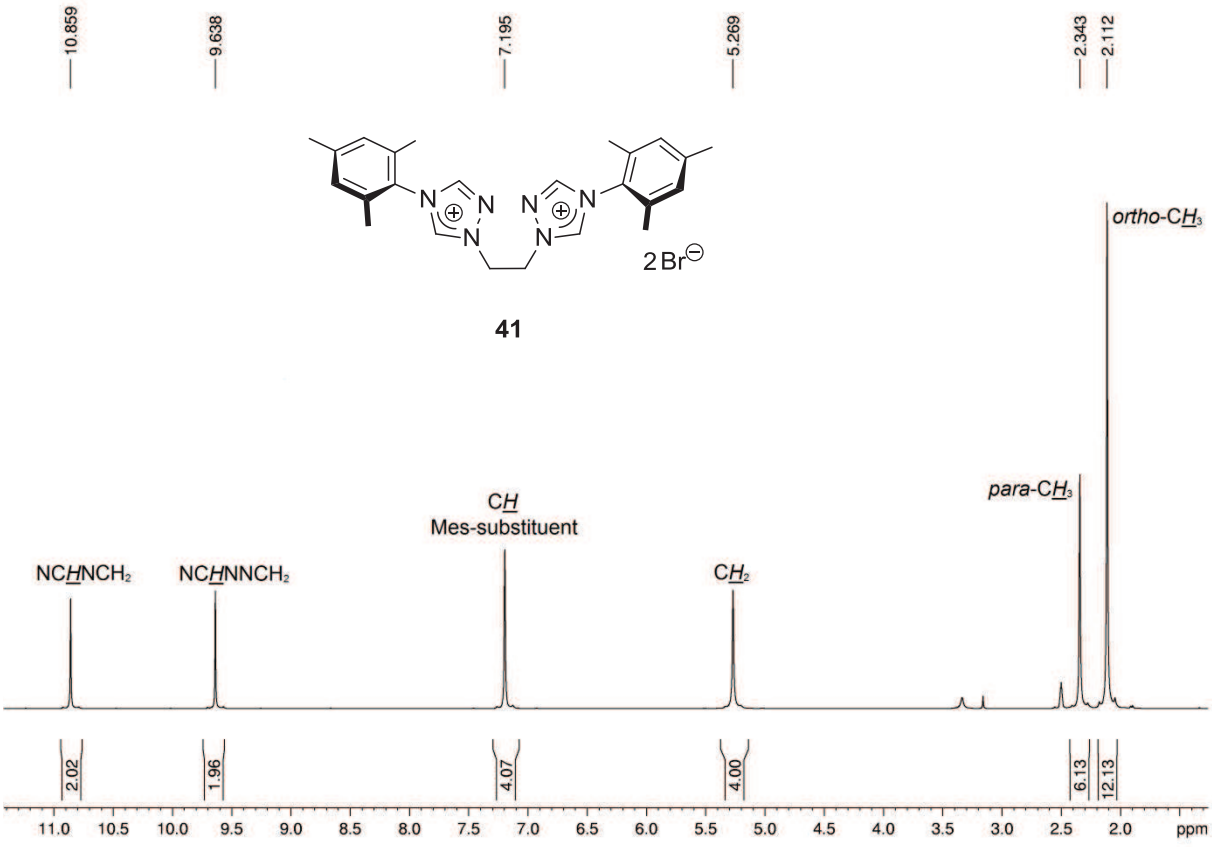

Figure 20: ^{1}H NMR spectrum of 1,1'-(ethane-1,2-diyl)bis[4-(2,4,6-trimethylphenyl)-1*H*-1,2,4-triazolium] dibromide (**41**) (recorded in d_6-DMSO at 300 MHz).

A crystal of bistriazolium bromide **41** suitable for X-ray diffraction analysis was obtained by re-crystallization from isopropanol (Figure 21).

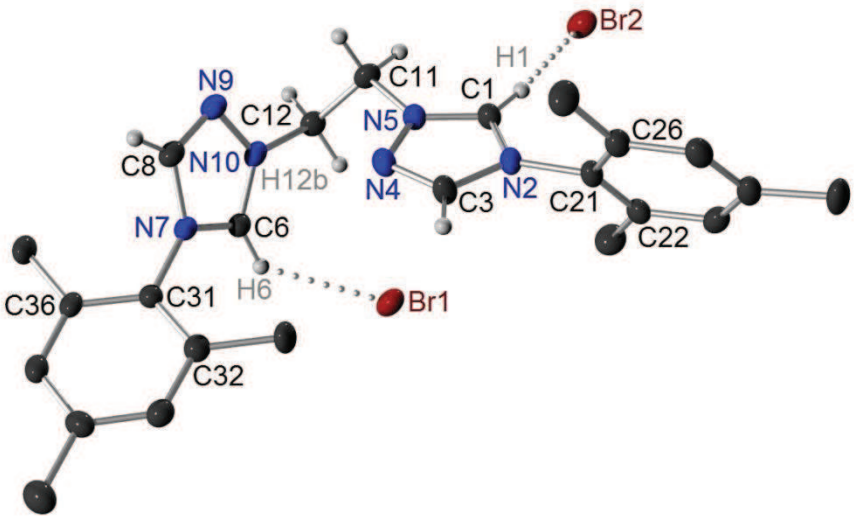

Figure 21: ORTEP plot of the single crystal X-ray structure of 1,1'-(ethane-1,2-diyl)bis[4-(2,4,6-trimethylphenyl)-1*H*-1,2,4-triazolium] dibromide (**41**) (hydrogen atoms on the mesityl substituents as well as co-crystallized solvent molecules are omitted for clarity).[118] Selected average bond lengths [Å], bond angles and dihedral angles: C1-N2 1.341, N2-C3 1.359, C3-N4 1.305, N4-N5 1.373, N5-C1 1.319, C1-Br2 3.354, C6-Br1 3.500; N2-C1-N5 106.33°, N7-C6-N10 107.51°; N5-C11-C12-N10 66.24°, C1-N2-C21-C22 -65.96°, C6-N7-C31-C32 62.51°.

The triazolium substituents on the ethylene-linker adopt a synclinal conformation with τ(N5-C11-C12-N10) = 66.24°. The mesityl substituents at the N4-positions are twisted with respect to the plane of the triazolium rings with torsion angles of τ(C1-N2-C21-C22) = -65.96° and τ(C6-N7-C31-C32) = 62.51° to avoid steric interactions of the triazolium rings with the methyl groups at the mesityl substituents' *ortho*-positions. It is arguable whether hydrogen bonds between the acidic triazolium proton and the bromide counterion as indicated by dotted lines in Figure 21 exist. In a recent review on hydrogen bonds in the solid state, Steiner points out that the "van der Waals cutoff" criterium, which demands the distance between the hydrogen atom and the electronegative partner of a hydrogen bond to be significantly below the sum of the van der Waals radii, might be too restrictive for the identification of hydrogen bonds based on crystal structural data. Instead, he proposes a rule of thumb according to which the hydrogen bond length should not exceed 3.0 or 3.2 Å with an angle X-H···Y of at least > 90°.[130] The distances between C1 and Br2 and C6 and Br1 in the crystal structure of **41** are 3.354 Å and 3.500 Å, respectively. With the calculated

positions for the acidic protons, this gives distances of d(H1-Br2) = 2.414 Å and d(H6-Br1) = 2.729 Å. Together with the angles φ(C1-H1-Br2) = 170.24° and φ(C6-H6-Br1) = 138.74°, this indicates that hydrogen bonds are present according to Steiner's rule of thumb, but that the interaction between H1 and Br2 is much stronger than between H6 and Br1. As the distance between the calculated position of H12b and Br1 is only 2.701 Å and the angle φ(C12-H12b-Br1) = 151.96°, the difference can be explained by an additional electrostatic attraction between the ethylene-linker's H12b proton and the bromide anion Br1.

In the group of Strassner, an alternative method for the synthesis of ethylene-linked bistriazolium salts was developed in 2010.[131] In their procedures, which were only published in a PhD thesis after the work described in sections 4.4.2 and 4.4.3 had been completed, 4-(4-methoxyphenyl)-4*H*-1,2,4-triazole as well as its *ortho*-isomer were reacted with 1,2-dibromoethane in acetonitrile at 90 °C in a pressure pipe. Applying these harsh conditions, only the disubstitution product 1,1'-(ethane-1,2-diyl)-bis[4-(4-methoxyphenyl)-1*H*-1,2,4-triazolium] dibromide was isolated in 72 % yield (*ortho*-isomer: 65 % yield). However, the products of these reactions were not obtained in high purity, the general applicability has not been shown and the yields were generally lower than with the procedures reported herein, so that Strassner's protocol does not seem to be superior to the one presented in sections 4.4.2 and 4.4.3.

4.4.4 Synthesis of Unsymmetrically Substituted Bistriazolium Halides

As the steric encumbrance at the two copper(I) centres in the envisaged dicopper catalyst is different upon coordination of the acetylide and the azide (Scheme 43), it was also planned to synthesize complementarily unsymmetric dicopper complexes: a sterically less demanding aryl substituent should be bound to one triazolylidene moiety in the corresponding dicopper complex, so that there would be enough room for the binding of azide and acetylide ligand; the other NHC ligand should be substituted by a larger aryl substituent so that only the acetylide could bind on this side. Part of this work was carried out in cooperation with Christine Dietrich in the course of her bachelor thesis.[132]

By using a large excess of the α,ω-dihalides 1,3-bis(chloromethyl)benzene and 1,2-dibromoethane, a single S_N1 substitution was carried out. As 1,2-dibromoethane is a liquid and 1,3-bis(chloromethyl)benzene has a very low melting point (35 °C), both reactions were carried out under neat conditions in analogy to the protocol for the synthesis of 1-(3-chloropropyl)-4-(2,6-dimethylphenyl)-4*H*-1,2,4-triazolium bromide reported in literature.[120] The reaction mixture of nine equivalents 1,3-bis(chloromethyl)benzene with 4-(3,5-dimethylphenyl)-1*H*-1,2,4-triazole (**22**) was stirred at 120 °C for 90 minutes. The resulting solid was broken to pieces and extracted with diethyl ether in order to remove excess 1,3-bis(chloromethyl)benzene, which was re-isolated by evaporating the diethyl ether. The synthesis of 1-(2-bromoethyl)-4-(3,5-dimethylphenyl)-1*H*-1,2,4-triazolium bromide (**45**) was achieved by stirring 25 equivalents of 1,2-dibromoethane with triazole **22** at 45 °C for seven days.

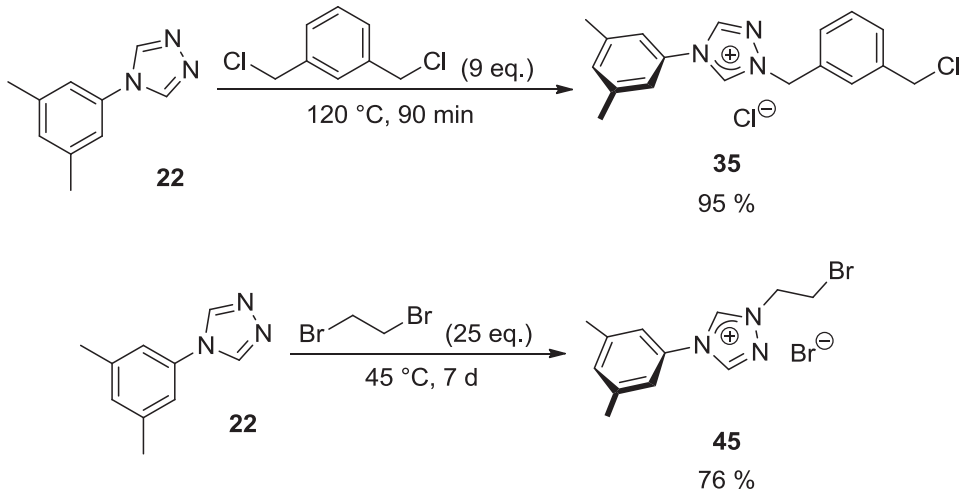

Scheme 45: Monosubstitution of 1,3-bis(chloromethyl)benzene and 1,2-dibromoethane with 4-(3,5-dimethylphenyl)-1*H*-1,2,4-triazole (**22**).

In the ^{1}H NMR spectra, the most obvious difference in comparison to the symmetrically substituted bistriazolium salts of paragraphs 4.4.2 and 4.4.3 is the observation of two peaks for the chemically inequivalent CH_2 groups. The deshielding effect of the cationic heterocyclic ring is stronger than of the halide. The signals for the CH_2 protons in monotriazolium chloride **35** are observed at 5.77 ppm (NCH_2) and 4.78 ppm (CH_2Cl) in d_6-DMSO. For monotriazolium bromide salt **45**, the methylene resonances are triplets at 4.91 ppm (NCH_2) and 4.06 ppm (CH_2Br).

In the next step, these monosubstitution products were reacted with the sterically more encumbering 4-(2,6-diisopropylphenyl)-4*H*-1,2,4-triazole (**24**). As tested before (4.4.2, 4.4.3), the S_N2 reaction on the cationic monotriazolium salts can be accomplished in acetic acid under reflux conditions.

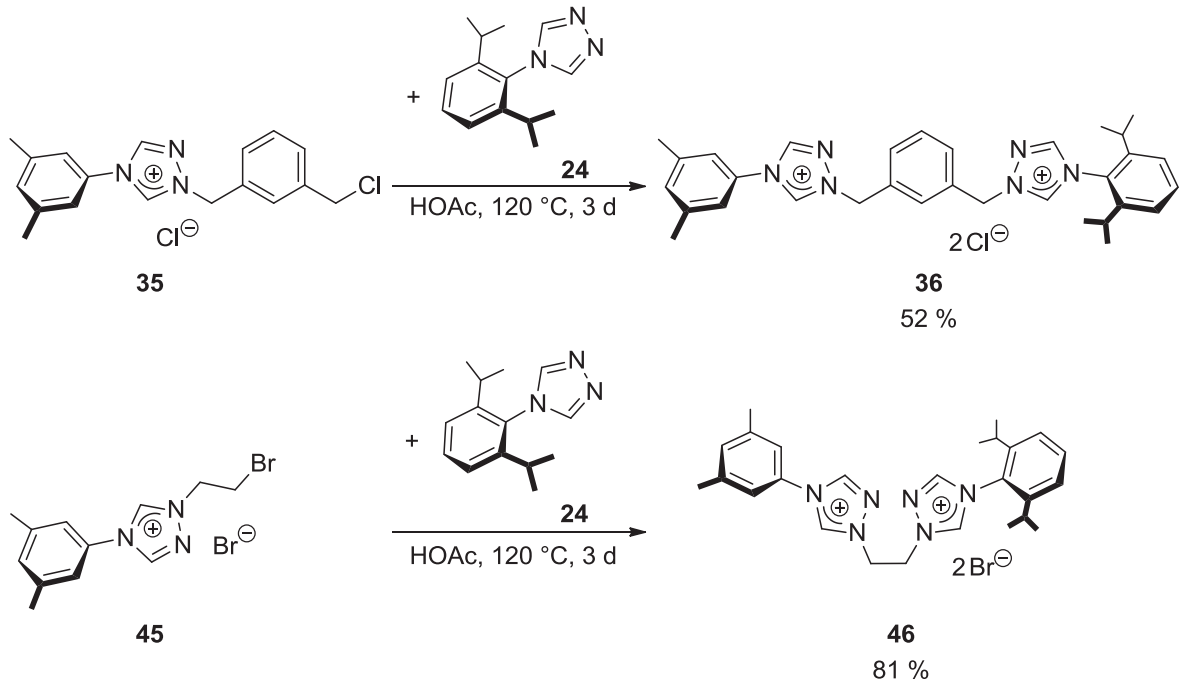

Scheme 46: Synthesis of unsymmetrically substituted bistriazolium halide salts **36** and **46**.

Figure 22 shows the ^{1}H NMR spectrum of 4-(2,6-diisopropylphenyl)-1-{3-[4-(3,5-dimethylphenyl)-1*H*-1,2,4-triazolium-1-ylmethyl]benzyl}-1*H*-1,2,4-triazolium dichloride (**36**) in d_6-DMSO. As the assignment of the ^{1}H and ^{13}C NMR spectra is much less apparent than for the symmetrically disubstituted salts, two-dimensional NMR spectra and comparison with the spectra of the symmetric congeners were necessary for detailed interpretation. The resonances for the 2,6-diisopropylphenyl substituted triazolium ring and its adjacent methylene group were found more downfield than the signals for the 3,5-xylyl substituted triazolium ring and the latter's adjacent methylene group. This is probably due to the less electron-donating influence of the Dipp-substituent, whose orbitals cannot overlap well with the ones of the triazolium ring as the Dipp-substituent's plane stands nearly perpendicular to the plane of the triazolium heterocycle to avoid steric repulsion. The plane of the sterically less encumbering Xyl-substituent, on the other hand, is only marginally twisted by an average dihedral angle of about 16° with respect to the plane of the triazolium ring, which allows for good overlap between the p-orbitals on the two aromatic rings. The latter information was gained from the single crystal X-Ray structure of **36**, which was obtained by recrystallization from acetonitrile (Figure 23).

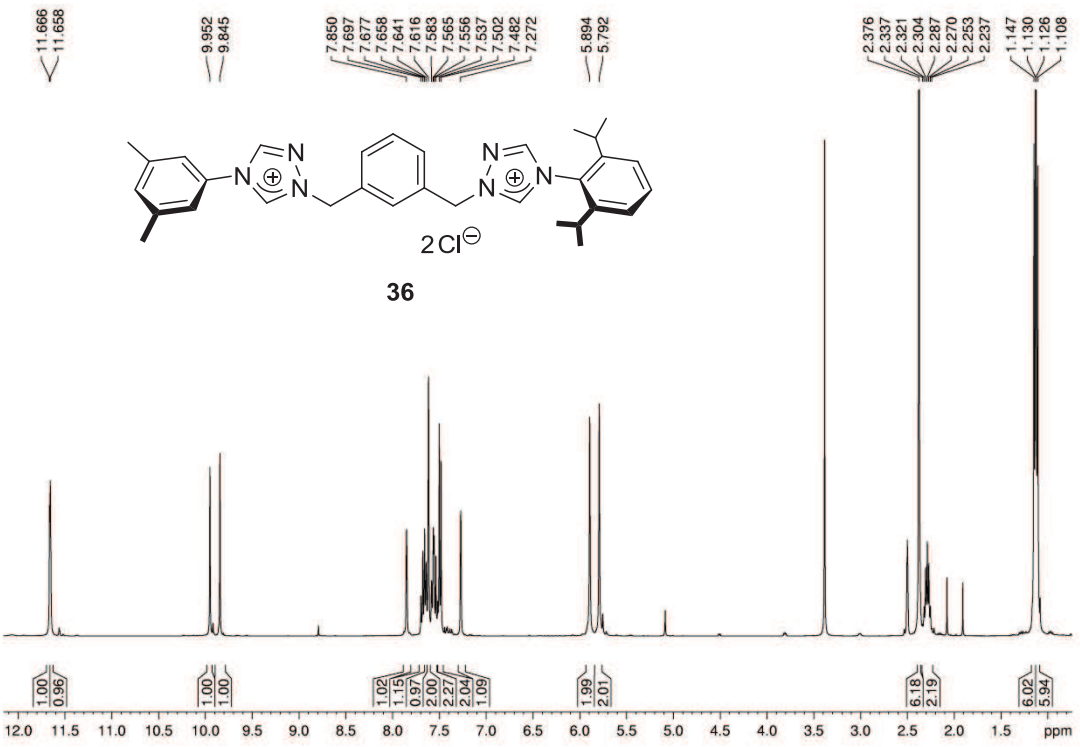

Figure 22: ^{1}H NMR spectrum of 4-(2,6-diisopropylphenyl)-1-{3-[(4-(3,5-dimethylphenyl)-1*H*-1,2,4-triazolium-1-yl)methyl]benzyl}-1*H*-1,2,4-triazolium dichloride (**36**) (recorded in d_6-DMSO at 400 MHz).

The chloride ions form hydrogen bonds with the acidic triazolium protons. One of these hydrogen bonds is indicated by a dotted line between H1 and Cl1 in Figure 23.

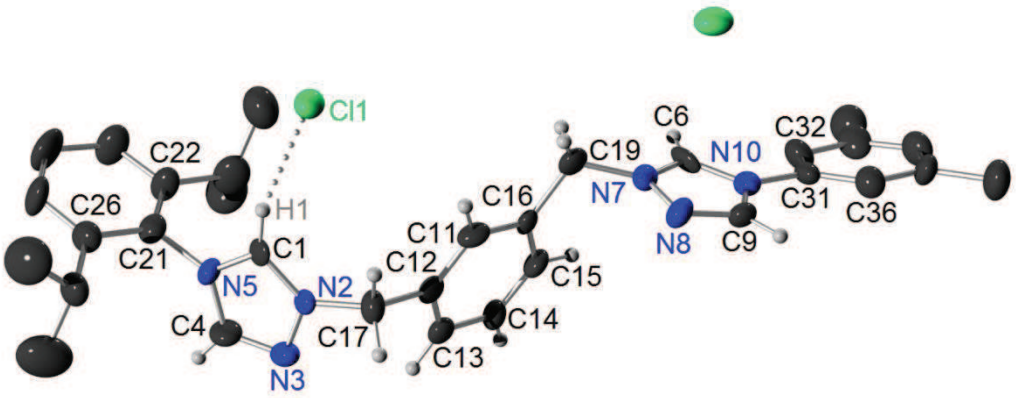

Figure 23: ORTEP plot of the single crystal X-ray structure of 4-(2,6-diisopropylphenyl)-1-{3-[4-(3,5-dimethylphenyl)-1*H*-1,2,4-triazolium-1-ylmethyl]benzyl}-1*H*-1,2,4-triazolium dichloride (**36**) (hydrogen atoms on the 4-aryl substituents and co-crystallized solvent molecules are omitted for clarity).[118] Selected average bond lengths [Å], bond angles and dihedral angles: C1-N2 1.312, N2-N3 1.362, N3-C4 1.324, C4-N5 1.346, N5-C1 1.321, C6-N7 1.334, N7-N8 1.382, N8-C9 1.297, C9-N10 1.377, N10-C6 1.355, N2-C17 1.468, N7-C19 1.461; N2-C1-N5 106.74°, N7-C6-N10 104.81°; C6-N10-C31-C32 -18.85°, C6-N10-C31-C36 160.82°, N7-C19-C16-C11 133.08°, N2-C17-C12-C11 119.17°, C1-N5-C21-C22 80.84°, C4-N5-C21-C26 87.09°.

4.4.5 Synthesis of Symmetrically Substituted Xylylene-Linked Bistriazolium Hexafluorophosphate Salts

In order to replace the strongly coordinating chloride counterions by a weakly coordinating anion, salt metathesis reactions with hexafluorophosphoric acid were carried out. Reaction conditions and yields are summarized in Table 17. The great advantage of these salt metatheses lies in the side effect that the resulting hexafluorophosphate salts crystallize very well and can be synthesized without any trace impurities.

Table 17: Salt metathesis reactions of 1,1'-[1,3-phenylenebis(methylene)]bis(4-aryl-1*H*-1,2,4-triazolium) dichloride salts **31** - **34** with hexafluorophosphoric acid.

31 - 34 **51 - 54**

entry	Ar	equivalents of HPF_6	reaction conditions	yield	product
1	Mes	3.0	DCM/H_2O, RT, 2 h	quant.	**51**
2	Xyl	2.6	DCM/H_2O, RT, 4 h	87 %	**52**
3	4-Tol	3.0	H_2O, RT, 4 h	82 %	**53**
4	Dipp	2.5	^{i}PrOH, RT, 2 h	75 %	**54**

The ^{1}H NMR spectra are very similar to the ones for the corresponding chloride salts except for all signals to be shifted upfield, which is probably due to weaker hydrogen bonds with the hexafluorophosphate anion than with the halide. For example, the triazole protons' resonances of bistriazolium dichloride salt **31** were observed at 11.40 and 9.66 ppm in d_6-DMSO, whereas in the spectrum of the corresponding hexafluorophosphate salt **51**, these signals were found at 10.58 and 9.52 ppm, respectively. The hexafluorophosphate salts crystallized much better than the corresponding halides. As an example, the crystal structure of bistriazolium hexafluorophosphate salt **53** is shown in Figure 24. The hydrogen bonds between H1 and F26 as well as H9 and F16 are marked by dotted lines.

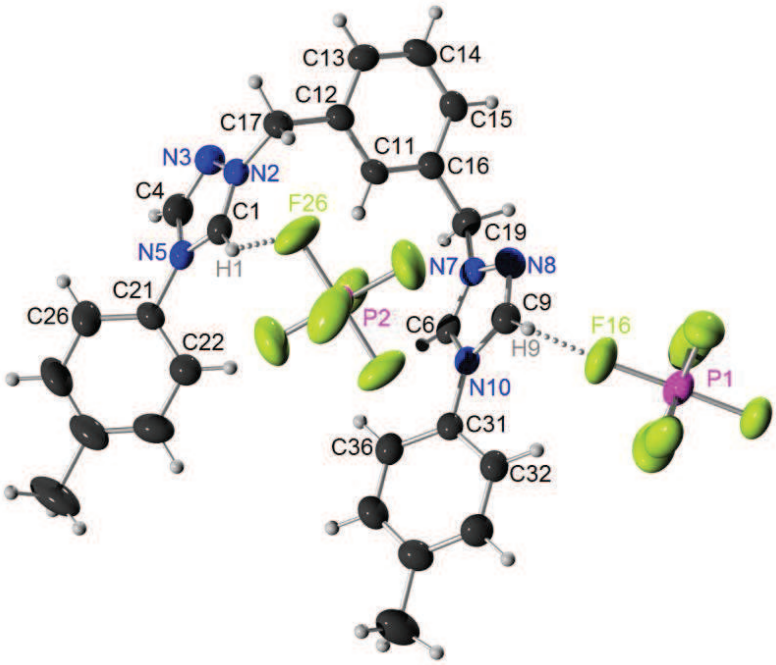

Figure 24: ORTEP plot of the single crystal X-ray structure of 1,1'-[1,3-phenylenebis(methylene)]bis[4-(4-methylphenyl)-1*H*-1,2,4-triazolium bis(hexafluorophosphate) (**53**) (co-crystallized solvent molecules are omitted for clarity).[118] Selected average bond lengths [Å], bond angles and dihedral angles: C1-N2 1.308, N2-N3 1.365, N3-C4 1.298, C4-N5 1.362, N5-C1 1.343, N2-C17 1.462; N2-N3-C4 103.56°, C1-N2-N3 111.41°, N2-N3-C4 103.56°, N3-C4-N5 112.39°, C4-N5-C1 105.11°, N5-C1-N2 107.54°, N7-C6-N10 108.02°; C1-N2-C17-C12 111.44°, N2-C17-C12-C13 132.90°, C6-N7-C19-C16 115.14°, N7-C19-C16-C15 135.68°, C4-N5-C21-C22 132.59°, C6-N10-C31-C32 147.17°.

4.4.6 Synthesis of Symmetrically Substituted Ethylene-Linked Bistriazolium Hexafluorophosphate Salts

With analogous procedures, the 1,1'-(ethane-1,2-diyl)bis(4-aryl-1*H*-1,2,4-triazolium) dibromide salts **41** - **43** were converted into hexafluorophosphate salts **61** - **63**. Again, the latter crystallized very well and did not contain any impurities.

Table 18: Salt metathesis reactions of 1,1'-(ethane-1,2-diyl)bis(4-aryl-1*H*-1,2,4-triazolium) dibromide salts **41** - **43** with hexafluorophosphoric acid.

41 - 43 **61 - 63**

entry	Ar	equivalents of HPF_6	reaction conditions	yield	product
1	Mes	2.5	MeOH, RT, 4 h	98 %	**61**
2	Xyl[133]	2.5	DCM/H_2O, RT, 4 h	93 %	**62**
3	4-Tol	2.7	MeOH, RT, 2 h	82 %	**63**

As an example, the crystal structure of bistriazolium hexafluorophosphate salt **61** is shown in Figure 25. The cation is symmetric with respect to the inversion centre between the two methylene groups (C11, C11b), and the triazolium substituents on the central ethylene unit have a torsion angle of τ(N2-C11-C11a-N2a) = 180.00° with respect to each other. In contrast, the dihedral angle τ(N5-C11-C12-N10) in the corresponding bromide salt shown in Figure 21 is 66.24°, which means that the conformation at the ethylene molecular bridge changes from synclinal to antiperiplanar when the bromide counterion is exchanged for hexafluorophosphate. The orientation of the aryl-substituents on the N4-position is approximately the same for the bromide and the hexafluorophosphate salt. In both species, the 4-aryl substituents adopt a synclinal conformation with τ(C1-N2-C21-C22) = -65.96° with bromide as counterion and τ(C1-N5-C21-C26) = -68.81° in the hexafluorophosphate salt .

There are no hydrogen bonds within one asymmetric unit of crystalline **61**, only between the hexafluorophosphate anions and the acidic triazolium protons of different asymmetric units.

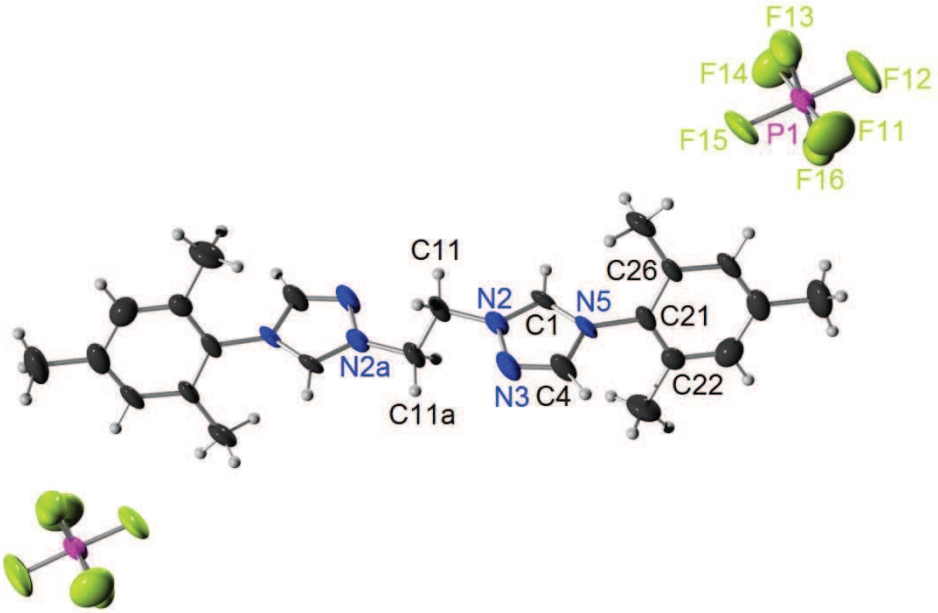

Figure 25: ORTEP plot of the single crystal X-ray structure of 1,1'-(ethane-1,2-diyl)bis[4-(2,4,6-trimethylphenyl)-1*H*-1,2,4-triazolium] bis(hexafluorophosphate) (**61**).[118, 134] Selected average bond lengths [Å], bond and dihedral angles: C1-N2 1.317, N2-N3 1.363, N3-C4 1.302, C4-N5 1.393, C1-F13 3.090, C1-F14 3.090, C1-F15 3.099; N3-C4-N5 111.45°, N2-C1-N5 107.82°; C1-N5-C21-C26 -68.81°, C1-N5-C21-C22 110.83°, C4-N5-C21-C22 -66.59°, C4-N5-C21-C26 113.77°, C1-N2-C11-C11a 110.38°, N2-C11-C11a-N2a 180.00°.

4.4.7 Synthesis of Unsymmetrically Substituted Bistriazolium Hexafluorophosphate Salts

In the same manner, the unsymmetrically substituted ethylene- and xylylene-linked bistriazolium halides **36** and **46** were converted into the corresponding hexafluorophosphate salts **56** and **66** (Scheme 47).

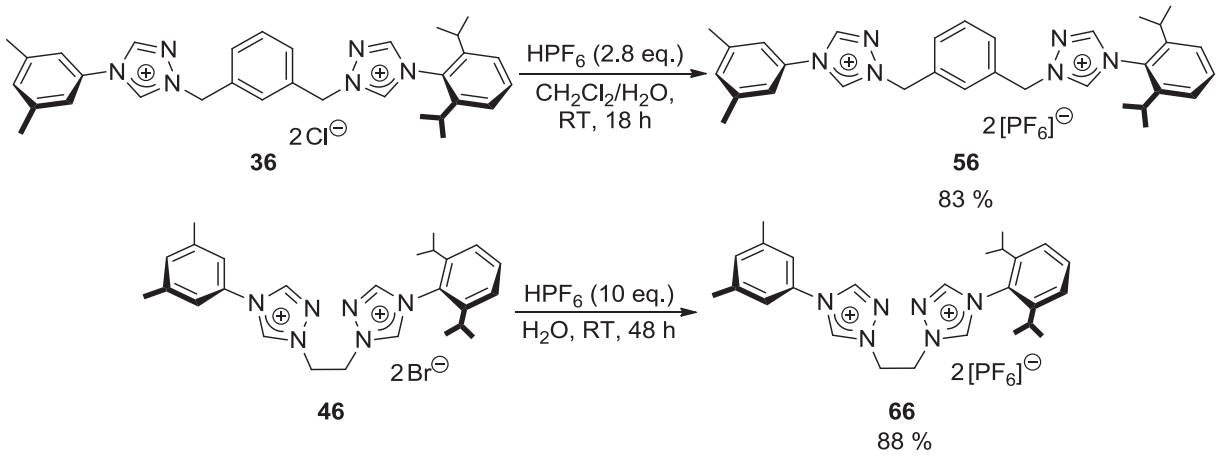

Scheme 47: Salt metathesis reactions of unsymmetrically substituted bistriazolium halides.

The single crystal X-ray structure of **56** shows that the Dipp-substituent's plane is twisted by approximately 75° with respect to the plane of the triazolium ring. The Xyl-substituent, on the other hand, is only slightly twisted by an average torsion angle of about 37° with respect to the other triazolium moiety, which is due to its lesser steric hindrance. As the Xyl-substituent does not have sterically encumbering *ortho*-substituents, there is also the possibility of forming hydrogen bonds between the hexafluorophosphate ion and the triazolium proton H9. The phenyl ring of the xylylene-linker is twisted as well so that the central molecular unit triazolium ring - xylylene-linker - triazolium ring adopts a Z-shaped conformation.

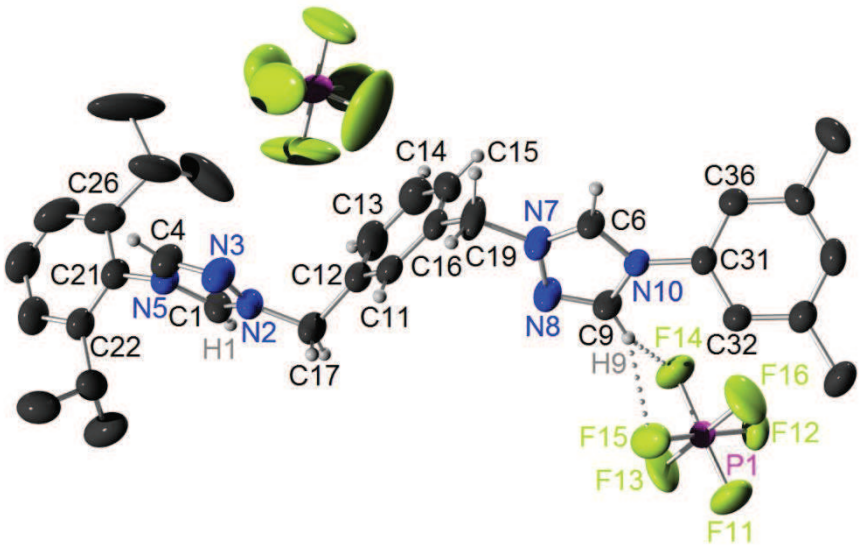

Figure 26: ORTEP plot of the single crystal X-ray structure of 4-(2,6-diisopropylphenyl)-1-{3-[4-(3,5-dimethylphenyl)-1*H*-1,2,4-triazolium-1-ylmethyl]benzyl}-1*H*-1,2,4-triazolium bis(hexafluorophosphate) (**56**) (hydrogen atoms on the 4-aryl substituents and co-crystallized solvent molecules are omitted for clarity).[118] Selected average bond lengths [Å], bond angles and dihedral angles: N8-C9 1.294, C9-N10 1.362, C1-N5 1.333, C1-N2 1.300; N2-C1-N5 107.95°, N8-C9-N10 112.06°; C1-N5-C21-C22 75.34°, C6-N10-C31-C32 142.63°, C6-N7-C19-C16 148.69°, C1-N2-C17-C12 111.32°, N2-C17-C12-C11 116.23°, N7-C19-C16-C11 106.08°, N2-C17-C19-N7 -166.98°.

4.5 Synthesis and Catalytic Testing of Dinuclear Bistriazolylidene Copper(I) Complexes with IPr as Sacrificial Ligand

In analogy to Nolan's complexes $[(NHC)_2Cu]PF_6$, for example $[(IPr)_2Cu]PF_6$,[72-73] our idea was to replace one of the mono-NHC ligands by a bistriazolylidene ligand so that dinuclear complexes of the general structural outline shown in Figure 27 could be obtained.

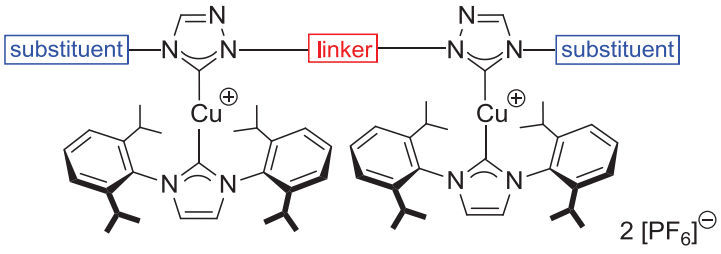

Figure 27: Structural outline of dinuclear bistriazolylidene copper(I) complexes with IPr as sacrificial ligand.

As triazolium are more acidic than imidazolium cations, the imidazolylidene was supposed to dissociate from the dinuclear copper(I) complex and act as a base in the deprotonation of the alkyne substrate. The more strongly coordinating bistriazolylidene ligand, on the other hand, should keep on binding to the two copper ions and keep them at a distance advantageous for their interplay in the CuAAC reaction.

4.5.1 Synthesis of Dinuclear Copper(I) Complexes with IPr as Sacrificial Ligand

In preliminary NMR experiments, the monocopper complex (IPr)CuOAc was reacted with the bistriazolium salt 1,1'-[1,3-phenylenebis(methylene)]bis[4-(2,4,6-trimethylphenyl)-1*H*-1,2,4-triazolium] bis(hexafluorophosphate) (**51**) in the presence of a base. With triethylamine as well as with potassium hydride, the NMR spectra hinted at the decomposition of the starting material. However, with sodium hydride, the ^{1}H NMR spectrum of the raw reaction mixture looked more promising. Thus, a small preparative experiment was carried out. One equivalent of the bistriazolium salt was mixed with (IPr)CuOAc (**3**, 2.1 equivalents) under inert gas and the two solids were dissolved in THF. However, after approximately two minutes of stirring, a colourless

precipitate was formed. Sodium hydride (2.2 equivalents) was added and the evolution of gas observed. After stirring the reaction mixture for one day at room temperature, the solution was filtrated over a filter paper-capped canula under inert gas conditions. After evaporation of THF, the remaining solid was analyzed by NMR spectroscopy, but the spectrum showed a variety of different species, probably decomposition products. The grey precipitate from the reaction mixture turned out to be partly soluble in acetonitrile as well as in acetone, and was analyzed by NMR spectroscopy as well. The ^{1}H NMR spectrum in acetonitrile showed the desired product without any impurities except for THF. This means that the product complex is hardly soluble in THF, but well soluble in acetonitrile and can be isolated from the reaction mixture by suspending the precipitate in acetonitrile. The most significant indicators for product formation in the ^{1}H NMR spectrum of the reaction mixture are the disappearance of the starting material's resonance for the acidic triazolium proton at 9.50 ppm upon deprotonation, the upfield shift of the remaining triazole proton's signal from 8.75 ppm to 8.21 ppm as well as the upfield shift of the methylene group's signal from 5.70 ppm in the bistriazolium salt to 4.72 ppm in the product complex.

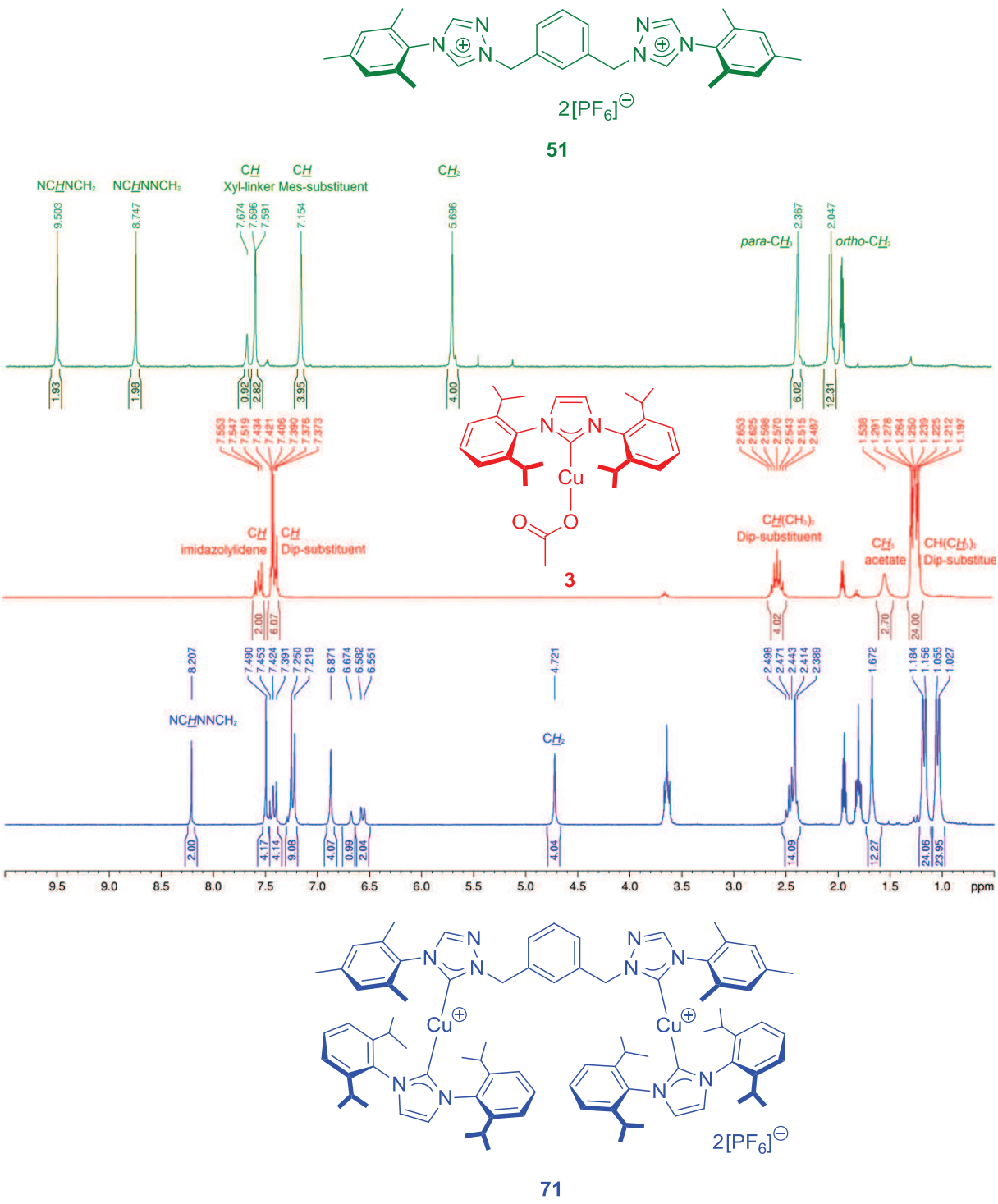

Figure 28: ^{1}H NMR spectra of both starting materials **51** (upper part, green) and **3** (middle, red) and product complex **71** (lower part, blue) (all spectra recorded in d_3-acetonitrile at 250 MHz).

Based on the observation that a colourless precipitate had already been formed before addition of the base, the reaction was next carried out in the absence of sodium hydride. The monocopper complex (IPr)CuOAc (**3**, 2.1 equivalents) was again mixed with bistriazolium hexafluorophosphate **51** (1.0 equivalents) and the two solids were dissolved in THF under inert gas. After a couple of minutes, a crystalline precipitate

began to form, and after 24 hours of stirring at room temperature, the reaction mixture was filtrated. The solid raw product was analyzed by NMR spectroscopy. The spectrum recorded in d_3-acetonitrile was identical to the one obtained with the previously described procedures. This proves that the addition of base is unnecessary for the synthesis of **71** from (IPr)CuOAc (**3**) and bistriazolium hexafluorophosphate **51**. After re-crystallization from acetonitrile/diethyl ether, the pure product was obtained in 62 % yield.

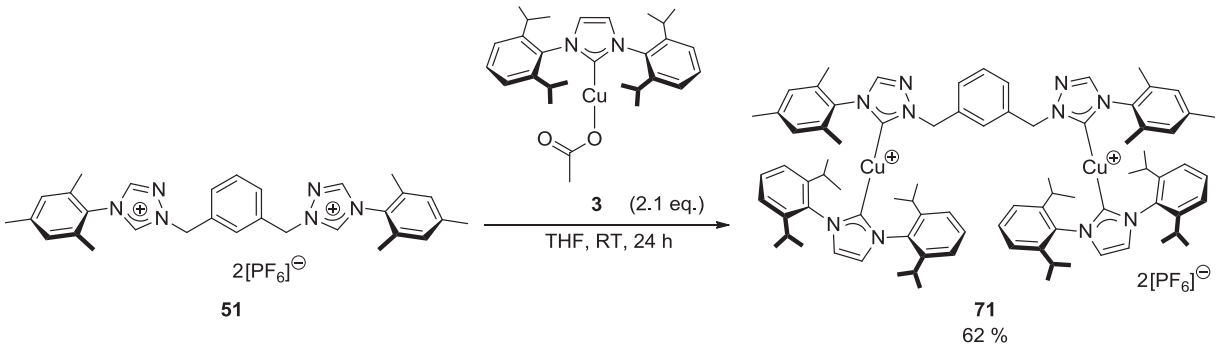

Scheme 48: Synthesis of μ-[1,1'-(benzene-1,3-diyldimethanediyl)bis[4-(2,4,6-trimethylphenyl)-1*H*-1,2,4-triazol-5-ylidene]-κ*C*,κ*C'*-bis{[1,3-bis(2,6-diisopropylphenyl)imidazol-2-ylidene]copper(I)} bis(hexafluorophosphate) (**71**).

As acetic acid is formed as byproduct in the synthesis of this dinuclear copper(I) complex (Scheme 48), the latter must be reasonably stable towards acidic conditions. Also, this complex was found to be tolerant towards air and moisture.

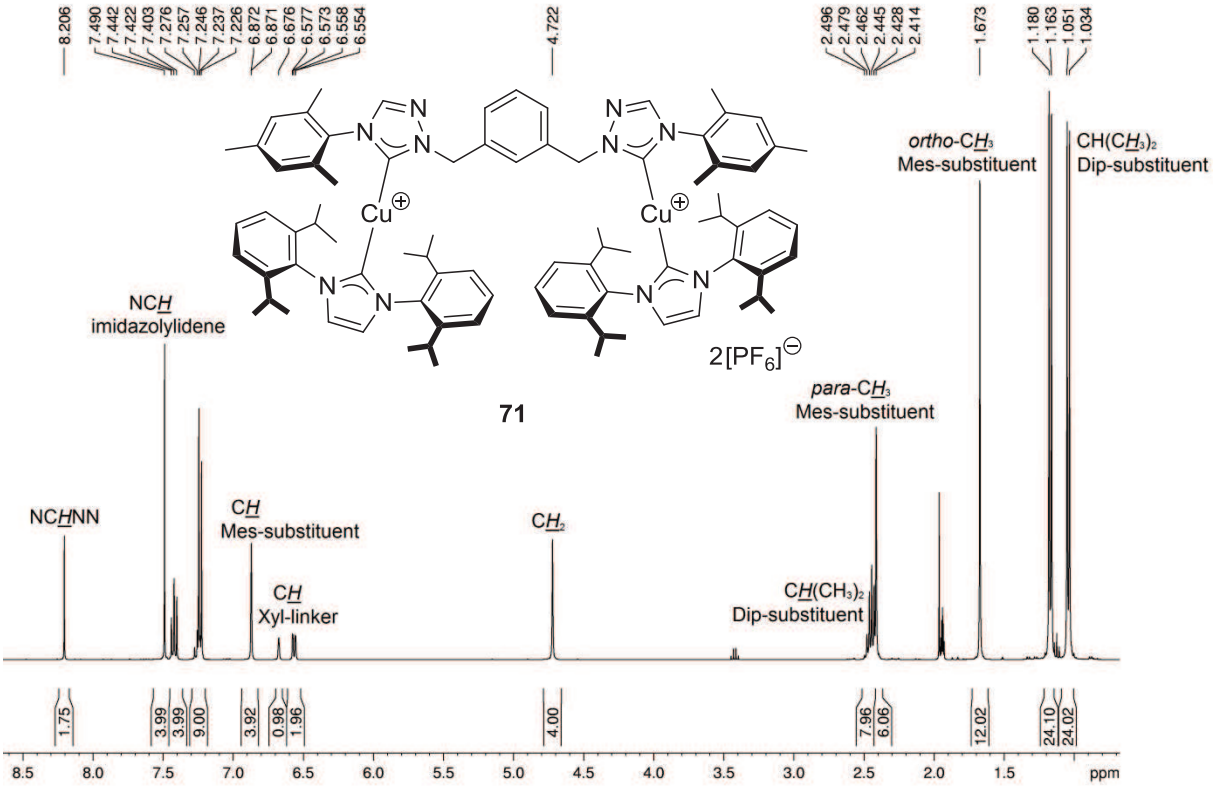

Figure 29: ^{1}H NMR spectrum of **71** (recorded in d_3-acetonitrile at 400 MHz).

In the ^{1}H NMR spectrum of **71** (Figure 29), the CH peaks of the triazolylidene rings are at 8.21 ppm. The more electron-rich imidazolylidene's ^{1}H resonances are observed at 7.49 ppm. The ^{13}C NMR spectrum shows the characteristic signal for the carbene C-atoms at 179.0 ppm for the imidazolylidene, and at 178.2 ppm for the triazolylidene ligands. These NMR shifts for the triazolylidene ligands are in the same range as those reported by Stefanie Seitz[126] for similar copper complexes, and the resonances of the imidazolylidene ligands are very close to those observed by Nolan *et al.* for $[(IPr)_2Cu]PF_6$ (Figure 30).[72a] In the ESI+ mass spectrum, only the *m*/*z* signal of the dication $[M\text{-}2PF_6]^+$ was observed.

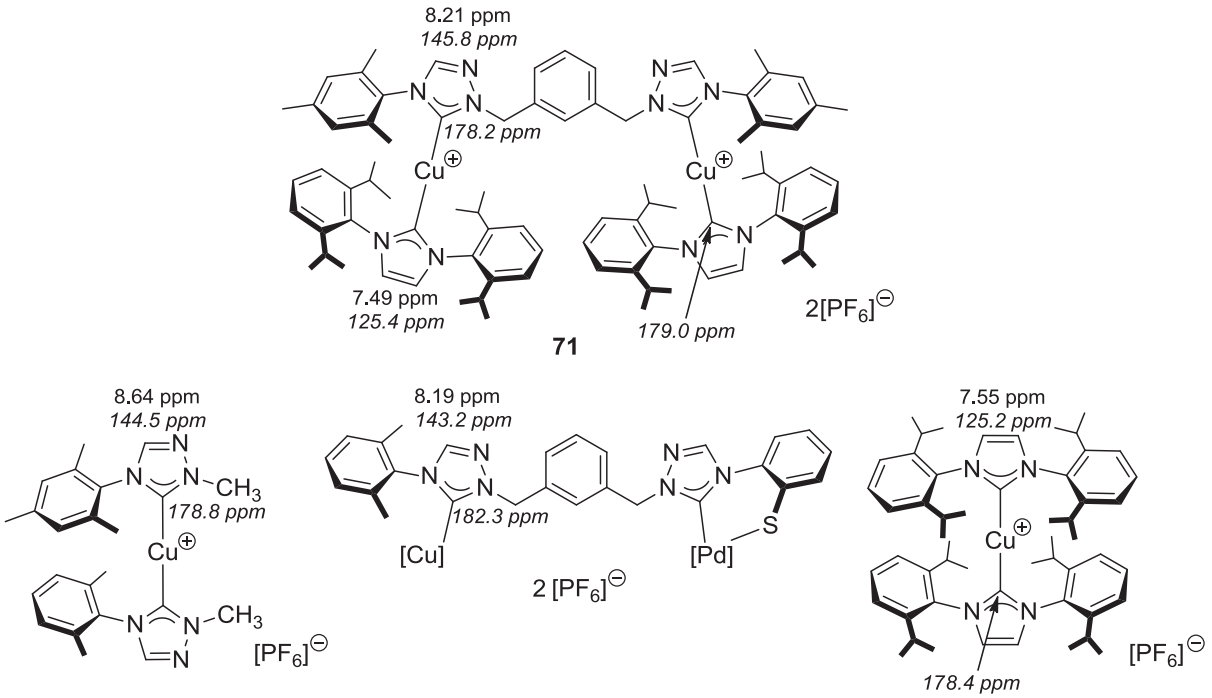

Figure 30: Comparison of ^{1}H and ^{13}C NMR (*italicized*) shifts of the NHC ligands in complex **71** (in d_3-acetonitrile) and the three literature-known complexes bis[4-(2,6-dimethylphenyl)-1-methyl-1,2,4-1*H*-triazolylidene]copper(I) hexafluorophosphate (in d_6-acetone; left side), *cis*-bis{1,1'-[1,3-phenylenedi(methylene)]-[4-(2,6-dimethylphenyl)-1,2,4-1*H*-triazolylidene]-[4-(2-thiophenyl)-1,2,4-1*H*-triazolylidene]}dicopper(I)palladium(II) bis(hexafluorophosphate) (in d_3-acetonitrile; middle, schematic representation) and $[(IPr)_2Cu]PF_6$ (in d_6-acetone, right side).

For comparison, the single crystal X-ray structure of the starting material bistriazolium hexafluorophosphate salt **51** is shown in Figure 31 and the crystal structure of dicopper complex **71** in Figure 32. The xylylene-bridged bistriazolium dication in Figure 31 is U-shaped with dihedral angles of τ(N11-C10-C20-N21) = 3.50° and τ(N11-C2-C6-N21) = 1.33°. Both triazolium rings are oriented so that the acidic CH groups (C12H and C22H) point away from the inside of the U-shape. The plane of the linker's phenyl ring is significantly twisted with respect to the planes of the triazolium heterocycles. Due to the steric encumbrance of their *ortho*-substituents, the 4-aryl groups are oriented almost perpendicular with respect to the plane of the adjacent triazolium rings with τ(C12-N13-C31-C32) = 95.71° and τ(C22-N23-C41-C42) = -72.12°. The bonds between the partially carbocationic C5-position and N4 in the triazolium rings are generally longer than between the C5-atom and N1: d(N11-C12) = 1.311 Å < d(C12-N13) = 1.327 Å and d(N21-C22) = 1.305 Å < d(C22-N23) = 1.334 Å. This observation hints at a greater double bond character between the N1-atom next to the linker and the C5-position than between the C5-atom and the aryl-substituted N4-atom.

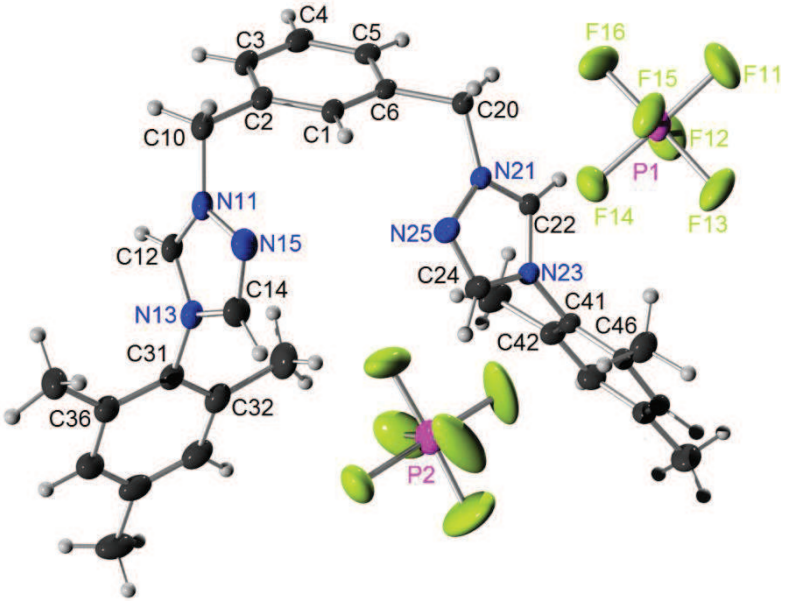

Figure 31: ORTEP plot of the single crystal X-ray structure of 1,1'-[1,3-phenylenebis(methylene)]bis[4-(2,4,6-trimethylphenyl)-1*H*-1,2,4-triazolium] bis(hexafluorophosphate) (**51**).[118] Selected average bond lengths [Å], bond angles and dihedral angles: N11-C12 1.311, C12-N13 1.327, N13-C14 1.366, C14-N15 1.303, N15-N11 1.361, N21-C22 1.305, C22-N23 1.334; N11-C12-N13 107.87°, N21-C22-N23 107.87°; N11-C10-C20-N21 3.50°, N11-C10-C2-C1 -65.33°, N21-C20-C6-C1 73.00°, C12-N13-C31-C32 95.71°, C22-N23-C41-C42 -72.12°.

Very similar to the U-shape of the xylylene-linked bistriazolium cation in **51** (Figure 31), the xylylene-bridged bistriazolylidene ligand in dinuclear complex **71** (Figure 32) adopts a bowl-like conformation in the solid state with dihedral angles τ(N2-C12-C16-N7) = -6.27° and τ(N3-C12-C16-N8) = -16.58°. The plane of the phenyl ring in the linker unit is oriented almost perpendicular with respect to the triazolylidene rings. As for the C-N bond lengths within the triazolylidene fragments, there is no consistent tendency as to which of the two C(carbene)-N bonds is stronger: d(C1-N2) = 1.339 Å < d(C1-N5) = 1.371 Å and d(C6-N7) = 1.363 Å > d(C6-N10) = 1.355 Å. The distance between the copper ions and the imidazolylidene carbene atoms is almost identical to the distance to the triazolylidene carbene atoms, *viz.* d(Cu1-C1) = 1.889 Å and d(Cu1-C41) = 1.886 Å. The bond angles in the IPr ligands φ(N47-C46-N50) = 102.62° and φ(N42-C41-N45) = 104.33° are in the same range as reported for $[(IPr)_2Cu]PF_6$ by the group of Nolan.[72a] However, the distance between the carbene C-atom and the copper centre in $[(IPr)_2Cu]PF_6$ (1.938 Å) is significantly longer than the distance between Cu1 and C41 (1.886 Å) or Cu2 and C46 (1.887 Å). This is most probably due to the reduced steric hindrance by the Mes-substituent and the

xylylene-linker as compared to the Dipp-substituent in $[(IPr)_2Cu]PF_6$. In the mononuclear complex prepared by Stefanie Seitz (Figure 30), the Cu-C(carbene) bond length is 1.889 Å, and in the dinuclear Cu,Pd-complex shown in Figure 30, the Cu-C distance is 1.913 Å, which is again in the same range as for the dinuclear copper(I) complex **71** (Figure 32). In the latter, the copper(I) centres are coordinated almost linearly with φ(C1-Cu1-C41) = 174.04° and φ(C6-Cu2-C46) = 175.62°, which is the typical coordination geometry for copper(I) ions (d^{10}-ML_2).

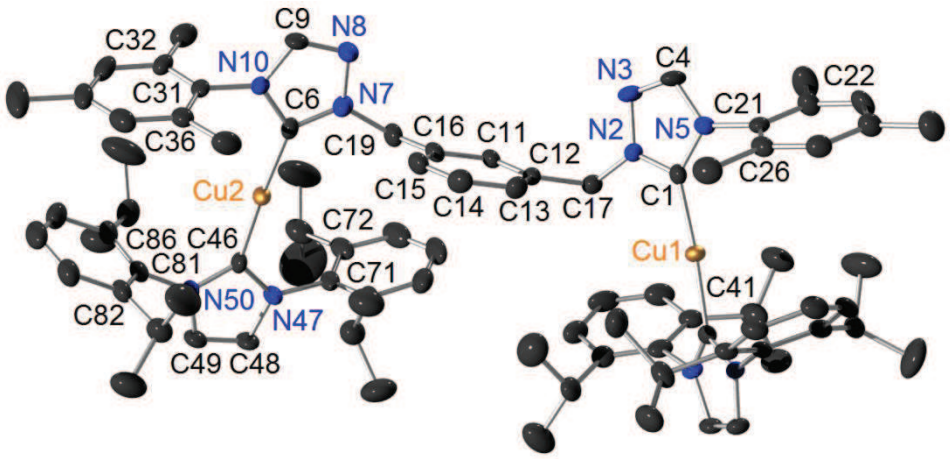

Figure 32: ORTEP plot of the single crystal X-ray structure of μ-[1,1'-(benzene-1,3-diyldimethanediyl)bis[4-(2,4,6-trimethylphenyl)-1*H*-1,2,4-triazol-5-ylidene]-κ*C*,κ*C'*-bis{[1,3-bis(2,6-diisopropylphenyl)imidazol-2-ylidene]copper(I)} bis(hexafluorophosphate) (**71**) (hydrogen atoms, hexafluorophosphate counterions and co-crystallized solvent molecules are omitted for clarity).[118] Selected average distances [Å], bond angles and dihedral angles: Cu1-Cu2 10.676, Cu1-C1 1.889, Cu1-C41 1.886, C1-N2 1.339, N2-N3 1.369, N3-C4 1.285, C4-N5 1.376, N5-C1 1.371, C6-N7 1.363, C6-N10 1.355, C46-N47 1.352, C46-N50 1.356; N2-C1-N5 102.63°, N7-C6-N10 101.54°, N45-C41-N42 104.33°, N47-C46-N50 102.62°, C1-Cu1-C41 174.04°, C6-Cu2-C46 175.62°; C1-N5-C21-C22 106.67°, C1-N5-C21-C26 -72.04°, N2-C17-C12-C11 126.35°, C46-N47-C71-C72 -89.37°, C46-N50-C81-C82 -96.45°, N3-C17-C19-N8 -21.36°, N3-N2-C12-C11 -50.19°.

In Fokin's DFT calculations of CuAAC transition states featuring dinuclear model structures, the distance between the two copper ions was found to be 2.54 Å and 2.64 Å for chloride/water or acetylide/water as spectator ligands, respectively.[32] In this work (section 4.3), the Cu-Cu distance in the transition state **C02TS03x(Mes)**, which comprises the same ligand system as precatalyst complex **71**, was calculated to be d(Cu1-Cu2) = 2.764 Å. In the solid state crystal structure of **71** (Figure 32), the distance between Cu1 and Cu2 is 10.676 Å. This means that for an optimal interplay, the two copper(I) centres need to approach each other, which is probably facilitated by dissociation of the IPr ligands.

Two additional complexes with the structural outline shown in Figure 27 have been synthesized. In the hope to decrease the distance between the two copper(I) centres, the xylylene-linker was replaced by an ethylene-linker. With mesityl-substituted bistriazolium hexafluorophosphate salt **61**, the base-free synthesis shown in Scheme 48 worked well. For the 4-tolyl substituted bistriazolium salt **63**, the addition of sodium hydride as base was essential. This hints at a lower acidity of the 4-tolyl substituted ligand precursor **63** as compared to **61**, *i.e.* better stabilization of the triazolium cation's charge by the 4-tolyl group. This observation might be explained by a better overlap of the π-system in the 4-aryl substituent with the π-electron system of the triazolium heterocycle as the less sterically encumbering 4-tolyl substituents' planes in **63** are only twisted by approximately 31° and 46° with respect to the triazolium heterocycle's plane. In the case of the mesityl substituent on the N4-position in ligand precursor **61**, the average torsion angle is 68° (Figure 25) and the overlap more impeded, which means that the stabilizing effect of the positive charge in the triazolium heterocycle by the +M-substituent is weaker than for the 4-tolyl substituent.

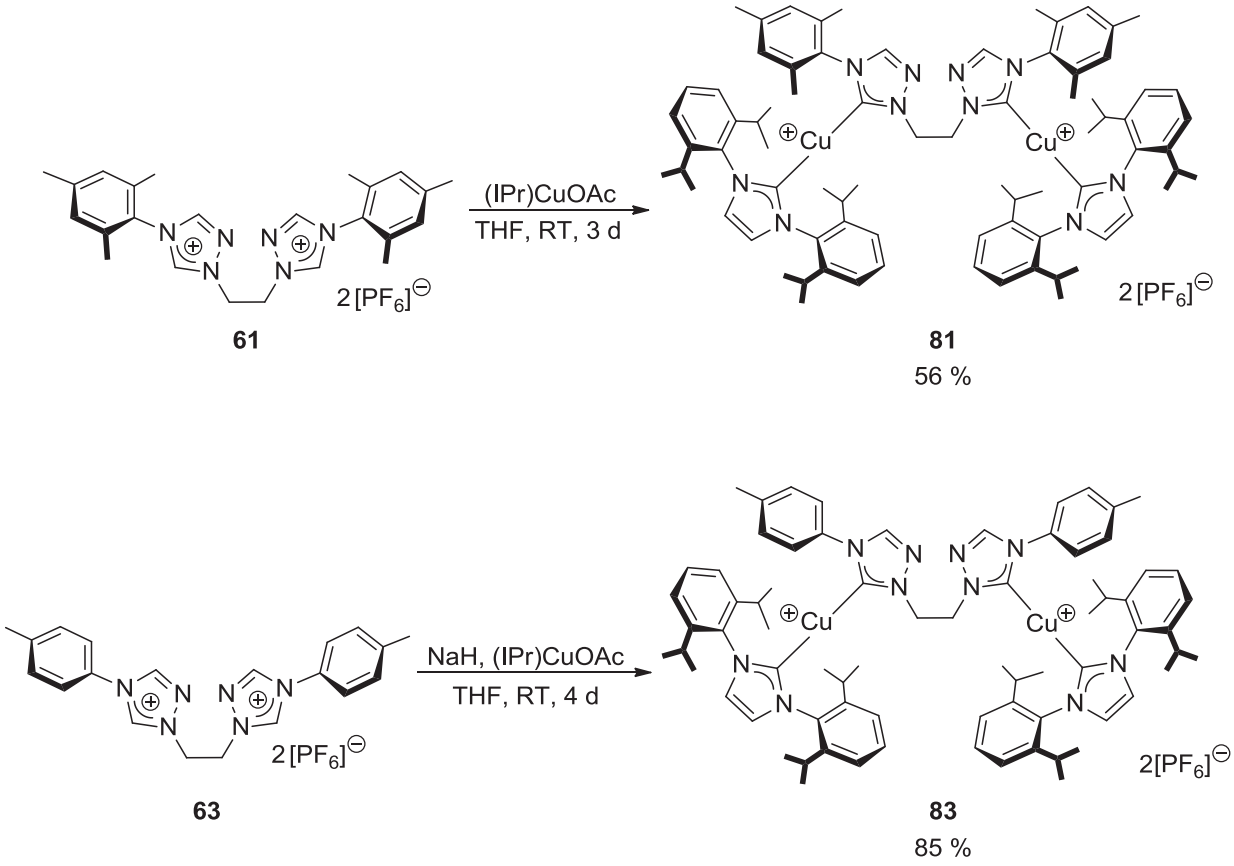

Scheme 49: Synthesis of dicopper complexes **81** (upper part) and **83** (lower part).

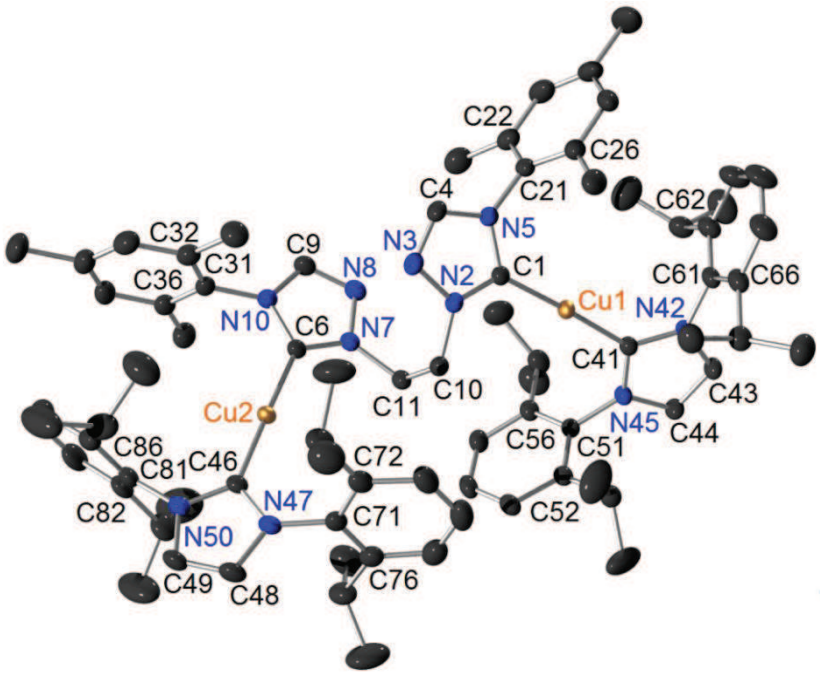

Figure 33: ORTEP plot of the single crystal X-ray structure of μ-[1,1'-(ethane-1,2-diyl)bis[4-(2,4,6-trimethylphenyl)-1*H*-1,2,4-triazol-5-ylidene]–κ*C*,κ*C*'-bis{[1,3-bis(2,6-diisopropylphenyl)-imidazol-2-ylidene]copper(I)} bis(hexafluorophosphate) (**81**) (hydrogen atoms, hexafluoro-phosphate counterions and co-crystallized solvent molecules are omitted for clarity).[118] Selected average distances [Å], bond angles and dihedral angles: Cu1-Cu2 7.304, Cu1-C1 1.898, Cu2-C6 1.892, Cu1-C41 1.903, Cu2-C46 1.894, C1-N2 1.338, N2-N3 1.377, N3-C4 1.295, C4-N5 1.369, N5-C1 1.362, C41-N42 1.354, N42-C43 1.383, C43-C44 1.337, C44-N45 1.387, N45-C41 1.348; N2-C1-N5 102.40°, N45-C41-N42 103.79°, C1-Cu1-C41 177.32°; C1-N5-C21-C22 98.00°, C4-N5-C21-C26 95.62°, C41-C42-C51-C56 83.32°, C43-N42-C51-C52 83.76°, N2-C10-C11-N7 -52.71°, N3-C10-C11-N8 10.84°.

In contrast to the structure of bistriazolium precursor **61** (Figure 25), the conformation at the ethylene linker in dicopper complex **81** (Figure 33) is synclinal with τ(N2-C10-C11-N7) = -52.71°. Thus, the bistriazolium ligand backbone is U-shaped as in the corresponding xylylene-bridged complex **71** shown in Figure 32 instead of Z-shaped as in the analogous complex with 4-tolyl substituents and an ethylene-linker (**83**, Figure 34). In dinuclear complex **81**, the distance between the two copper ions is 7.304 Å and thus significantly shorter than in the xylylene-linked complex **71** (10.676 Å, Figure 32). Apart from the shorter distance between the two halves of the dinuclear complex, there are only few structural differences between the xylylene- and the ethylene-linked complexes **71** and **81** with mesityl-substituents at the N4-position (Figure 32, Figure 33). The planes of the triazolium heterocycle and the mesityl-substituent in complex **81** are oriented approximately perpendicular to each other with τ(C1-N5-C21-C22) = 98.00°, which is a slightly greater twist than in the

substrate bistriazolium salt **61** with τ(C1-N5-C21-C22) = -110.83° (Figure 25) and in the xylylene-linked complex **71** with τ(C1-N5-C21-C22) = 106.67° (Figure 32).

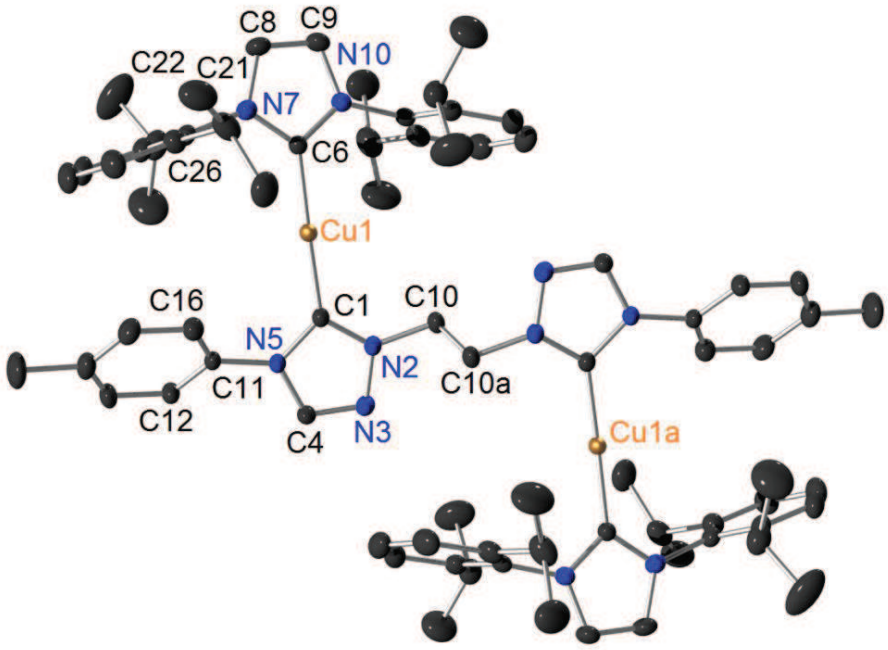

Figure 34: ORTEP plot of the single crystal X-ray structure of μ-[1,1'-(ethane-1,2-diyl)bis[4-(4-methylphenyl)-1*H*-1,2,4-triazol-5-ylidene]–κ*C*,κ*C*'-bis{[1,3-bis(2,6-diisopropylphenyl)imidazol-2-ylidene]copper(I)} bis(hexafluorophosphate) (**83**) (hydrogen atoms, hexafluorophosphate counterions and co-crystallized solvent molecules are omitted for clarity).[118] Selected average distances [Å], bond angles and dihedral angles: Cu1-Cu1a 7.751, Cu1-C1 1.893, Cu1-C6 1.895, C1-N2 1.344, N2-N3 1.377, N3-C4 1.305, C4-N5 1.368, N5-C1 1.372, C6-N7 1.353, N7-C8 1.389, C8-C9 1.346, C9-N10 1.382, N10-C6 1.364; N2-C1-N5 101.78°, N7-C6-N10 103.98°, C1-Cu1-C6 172.25°; C1-N5-C11-C16 34.69°, C6-N7-C21-C22 90.42°.

In the dinuclear copper complex with 4-tolyl substituents at the triazolium rings (**83**, Figure 34), the sterically encumbering IPr ligands optimally avoid each other. The dinuclear complex has an inversion centre and the IPr ligands are located in the second and the fourth quadrant. As in the substrate bistriazolium salt **63**, the plane of the 4-tolyl substituents is only slightly twisted with respect to the triazolium heterocycle's plane with τ(C1-N5-C11-C16) = 34.69°.

For all three dinuclear complexes presented so far, the distance between the copper centres and the triazolylidene carbene atoms is approximately 1.89 Å.

The catalytic activity of these dinuclear complexes with IPr as sacrificial ligand was tested in CuAAC test reactions with the standard substrates benzyl azide and phenylacetylene.

4.5.2 Catalytic Tests of Dinuclear Complexes with IPr as Sacrificial Ligand

The three dinuclear copper(I) complexes **71**, **81** and **83** presented in section 4.5.1 were tested for their catalytic activity in the CuAAC reaction of benzyl azide (**131**) with phenylacetylene. As these complexes are well soluble only in dichloromethane, acetone and acetonitrile, the choice of solvents was limited. Preliminary NMR experiments in d_2-dichloromethane showed that the reaction with 1 mol-% of ethylene-linked mesityl-substituted dicopper complex **81** did not show any conversion after 30 hours, but was completed within one week. With 1 mol-% of the ethylene-linked 4-tolyl substituted complex **83**, on the other hand, the reaction was completed within 50 hours. In d_3-acetonitrile, the reactions proceeded sluggishly as well. The reactions were carried out under inert gas and under aerobic conditions, and it was found that the presence of air did not impede the catalysis. As NMR spectroscopic measurements could not be carried out in regular intervals due to the service mode of the NMR facilities, gas chromatography was used as a means to monitor the progress of CuAAC catalysis more closely. All details as for the use of an internal standard and the determination of response factors are found in the experimental section and in the appendix to this work. With 2 mol-% of catalyst, full conversion was observed after 112 hours with complex **71**, and 97 % conversion with complex **83** after 22 hours (Figure 35). With complex **81**, no conversion was observed within three days, but the alkyne substrate was totally consumed after 154 hours. The left-over azide is attributed to loss of alkyne by evaporation in the course of this experiment.

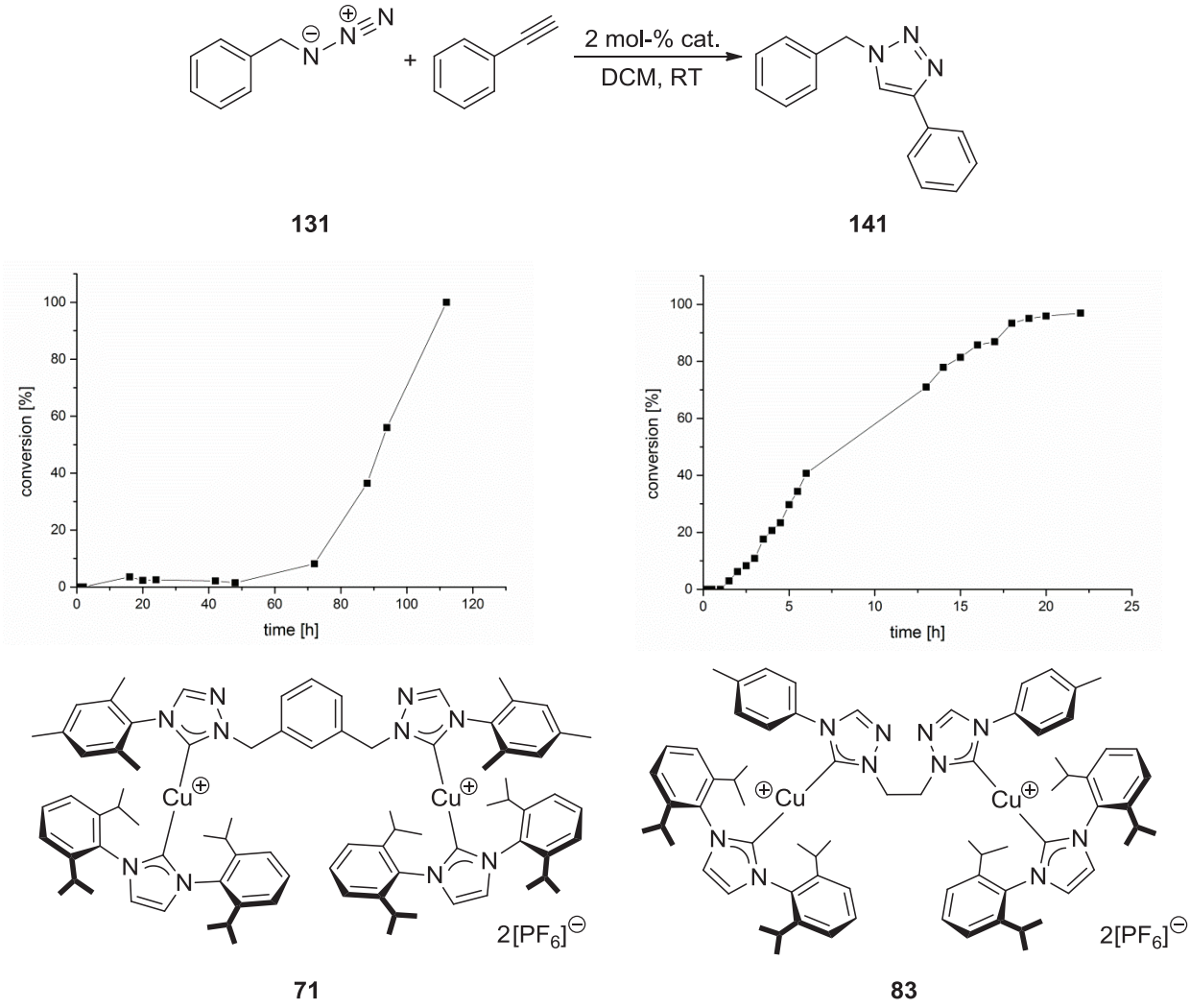

Figure 35: Diagrams of conversion with catalyst complexes **71** (2 mol-%, left side) and **83** (2 mol-%, right side) in the test reaction of benzyl azide with phenylacetylene in dichloromethane monitored by gaschromatography.

This very sluggish catalytic activity was attributed to the strong binding of the sacrificial NHC ligand IPr. It was thus attempted to introduce less strongly coordinating sacrificial ligands instead.

4.6 Synthesis of Dinuclear Bistriazolylidene Copper(I) Complexes with Acetate as Sacrificial Ligand

Based on the experience with the synthesis of (IPr)CuOAc (**3**, section 4.1), it was attempted to introduce acetate as a less strongly binding sacrificial ligand instead of the NHC ligand IPr (section 4.5). However, in the reaction of the ligand precursor bis-triazolium salt with copper(I) acetate in the presence of a base, a variety of products can be formed, which is illustrated by Scheme 50.

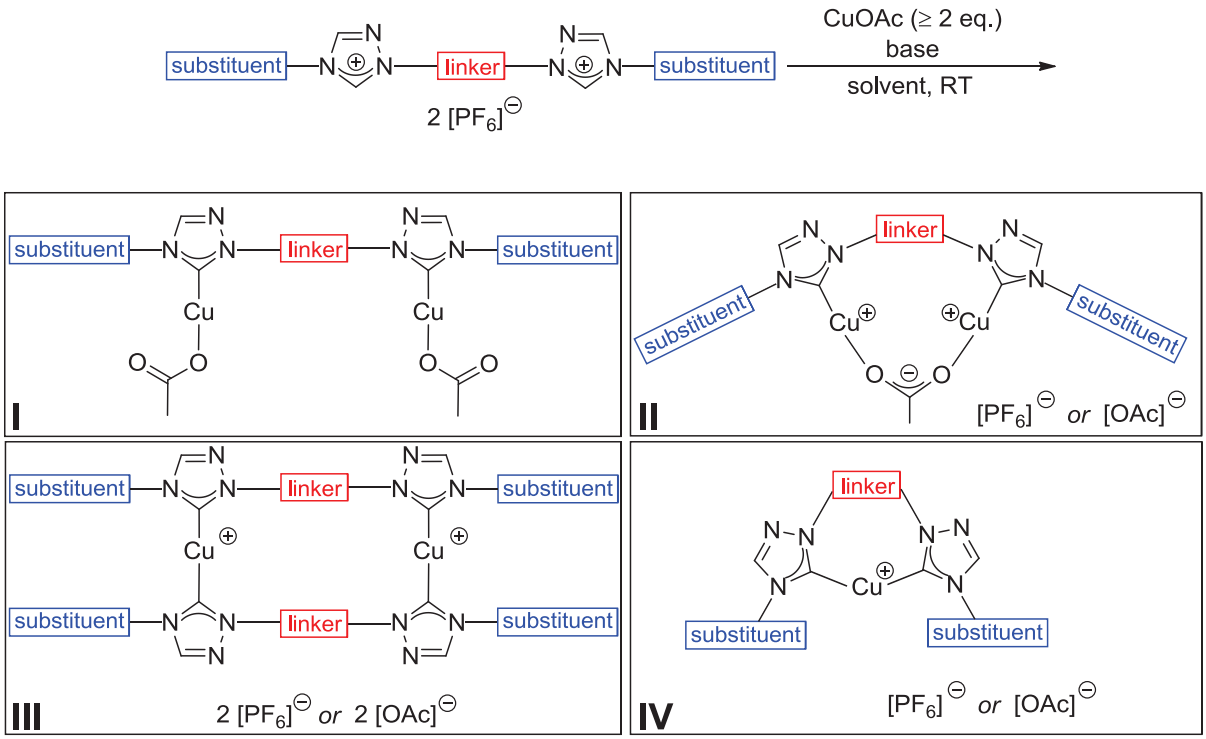

Scheme 50: Palette of products that might be formed in the reaction of the bistriazolium precursor with CuOAc in the presence of base.

Different bases and reaction conditions were first tested on the NMR scale and in small-scale preparative experiments. All reactions described in Table 19 were carried out under strict exclusion of air and moisture. In entries 1, 3, 4, 6, 7 and 8 CuOAc was added in excess to function not only as a source of copper(I) ions, but also as a base for the deprotonation of the bistriazolium salt.

Table 19: Attempts for the synthesis of bistriazolylidene dicopper(I) complexes with acetate as sacrificial ligand.

entry	conditions and observations
1	*ligand precursor*: **51** *conditions*: CD_3CN, CuOAc (4.5 eq.), 72 h, RT *observations*: reaction mixture turned slightly green with red precipitate *^{1}H NMR spectrum* of the reaction mixture: broad peaks, deprotonation complete, single new species with integrals fitting the bis-NHC ligand, no peak for acetate's methyl group
2	*ligand precursor*: **51** *conditions*: CD_3CN, 1) NaH (5.0 eq.), 24 h, RT, 2) CuOAc (4.5 eq.), 16 h, RT *observations*: reaction mixture turned orange with red precipitate *^{1}H NMR spectrum* of soluble fraction: broad peaks, deprotonation complete, single new species with integrals fitting the bis-NHC ligand, no peak for acetate's methyl group
3	*ligand precursor*: **51** *conditions*: CH_3CN, CuOAc (4.5 eq.), 5 d, RT *observations*: reaction mixture turned slightly green with colourless precipitate *^{1}H NMR spectrum* of soluble fraction in CD_3CN: broad peaks, deprotonation complete, very broad peak at 10.42 ppm, single new species with peaks of the ligand, alkyl region: peaks overlap each other strongly, no peak for acetate's methyl group *^{13}C NMR spectrum* of soluble fraction in CD_3CN: peak for carbene C-atom at 182.0 ppm, peaks for bistriazolylidene ligand present, no peaks for acetate *^{1}H NMR spectrum* of insoluble fraction in d_8-THF: dark green solution, single new species, peaks fit with the ligand, no peaks for acetate's methyl group *ESI+ mass spectrum*: single peak at *m*/*z* = 539.19670 corresponding to the bistriazolylidene ligand with one copper atom (isotopic pattern) *elemental analysis*: C – 45.69 %, H – 4.46 %, N – 9.94 % (calculated for bis-NHC monocopper acetate hexafluorophosphate complex $C_{32}H_{35}Cu_2F_6N_6O_2P$: C – 47.58 %, H – 4.37 %, N – 10.40 %)
4	*ligand precursor*: **51** *conditions*: THF, CuOAc (4.5 eq.), 2 d, RT *observations*: reaction mixture turned blue with colourless precipitate

	^{1}H NMR spectrum of soluble fraction in d_8-THF: variety of species, non-interpretable *^{1}H NMR spectrum* of insoluble fraction in CD_3CN: pinkish solution, deprotonation complete, single new species with peaks of the ligand, no peak for acetate's methyl group, very broad peaks at 13.02 and 3.20 ppm
5	*ligand precursor*: **61** *conditions*: d_8-THF, CuOAc (2.0 eq.), NaH (2.1 eq.) *observations*: evolution of gas upon addition of NaH, solution turned grey *^{1}H NMR spectrum* of the reaction mixture: very broad peaks, deprotonation complete, single new species with integrals fitting the bis-NHC ligand, peak for acetate's methyl group present (integral: 3)
6	*ligand precursor*: **61** *conditions*: CD_3CN, CuOAc (4.5 eq.), 2 d, RT *observations*: reaction mixture turned blue with colourless precipitate *^{1}H NMR spectrum* of the reaction mixture: deprotonation complete, single new species with peaks of the ligand, broad peak for methyl group of acetate/acetic acid at 2.08 ppm (integral: 12)
7	*ligand precursor*: **61** *conditions*: CH_3CN, CuOAc (4.4 eq.), 18 h, RT *observations*: reaction mixture turned slightly green with greenish brown precipitate *^{1}H NMR spectrum* of raw product in CD_3CN: deprotonation complete, single new species with peaks of the ligand, broad peak for CH_3 group in acetate/acetic acid at 2.25 ppm (integral: 8), broad peak at 13.20 ppm *^{13}C NMR spectrum* of raw product in CD_3CN: peak for carbene C-atom at 180.9 ppm, peaks for bistriazolylidene ligand present, no peaks for acetate *^{1}H NMR spectrum* of raw product in d_8-THF: deprotonation complete, single new species with peaks of the ligand, broad peak for CH_3 group in acetate/acetic acid 1.81 ppm (integral: 4.6), very broad peak at 12.52 ppm *^{13}C NMR spectrum* of raw product in d_8-THF: peak for carbene C-atom at 178.9 ppm, peaks for bistriazolylidene ligand present, no peaks for acetate *ESI+ mass spectrum*: single peak at *m*/*z* = 463.16675 corresponding to the bistriazolylidene ligand with one copper atom (isotopic pattern) *crystal structure*: Figure 37

8	*ligand precursor*: **54** *conditions*: d_8-THF, CuOAc (4.5 eq.), 18 h, 60 °C *observations*: reaction mixture turned violet with precipitate *^{1}H NMR spectrum* of soluble fraction: deprotonation incomplete, starting material still present, new species with peaks of the ligand, no peak for acetate's methyl group
9	*ligand precursor*: **54** *conditions*: d_8-THF, CuOAc (2.2 eq.), KH (2.0 eq.), 6 h *observations*: gas evolution upon addition of KH, grey precipitate *^{1}H NMR spectrum* of soluble fraction: deprotonation complete, single new species with peaks of the ligand, peak of the methyl group in acetate/acetic acid at 1.67 ppm (integral: 6) *ESI+ mass spectrum*: single peak at *m*/*z* = 623.29141 corresponding to the bistriazolylidene ligand with one copper atom (isotopic pattern)

In neither of the experiments listed in Table 19, the desired bis-NHC dicopper diacetate complex or the bis-NHC dicopper monoacetate complex with hexafluorophosphate or acetate as counterion (structural outlines **I** and **II** in Scheme 50) has been isolated as a pure compound. Most of all, it was hard to decide whether acetate was present in the product at all as the acetate's peaks were found neither in the ^{1}H nor in the ^{13}C NMR spectra of reaction mixtures 1, 2, 3, 4 and 8 in Table 19. At first sight, the spectra of these experiments would have better fitted with a dinuclear copper(I) complex containing two bis-NHC ligands or a bis-NHC monocopper complex (structural outlines **III** and **IV** in Scheme 50). Figure 36 shows the ^{1}H NMR spectra of the bistriazolium hexafluorophosphate starting material **51** and of the material obtained from the soluble fraction. Complete deprotonation of the triazolium cations by acetate is indicated by the disappearance of the peak at 9.52 ppm. A new and very broad peak at 10.42 ppm might be the resonance for the acidic proton of acetic acid. The peak at 1.96 ppm most probably corresponds to the methyl group of acetic acid. It is not clear whether there is another peak for the methyl group of an acetate ligand, as the peaks in the alkyl region strongly overlap each other. The formation of a new species is also apparent by the upfield shift of the resonance for the heterocycle's CH group from 8.75 ppm in triazolium salt **51** to 8.20 ppm in the product, and of the methylene group's signal from 5.70 ppm in the starting material to 5.48 ppm in the product.

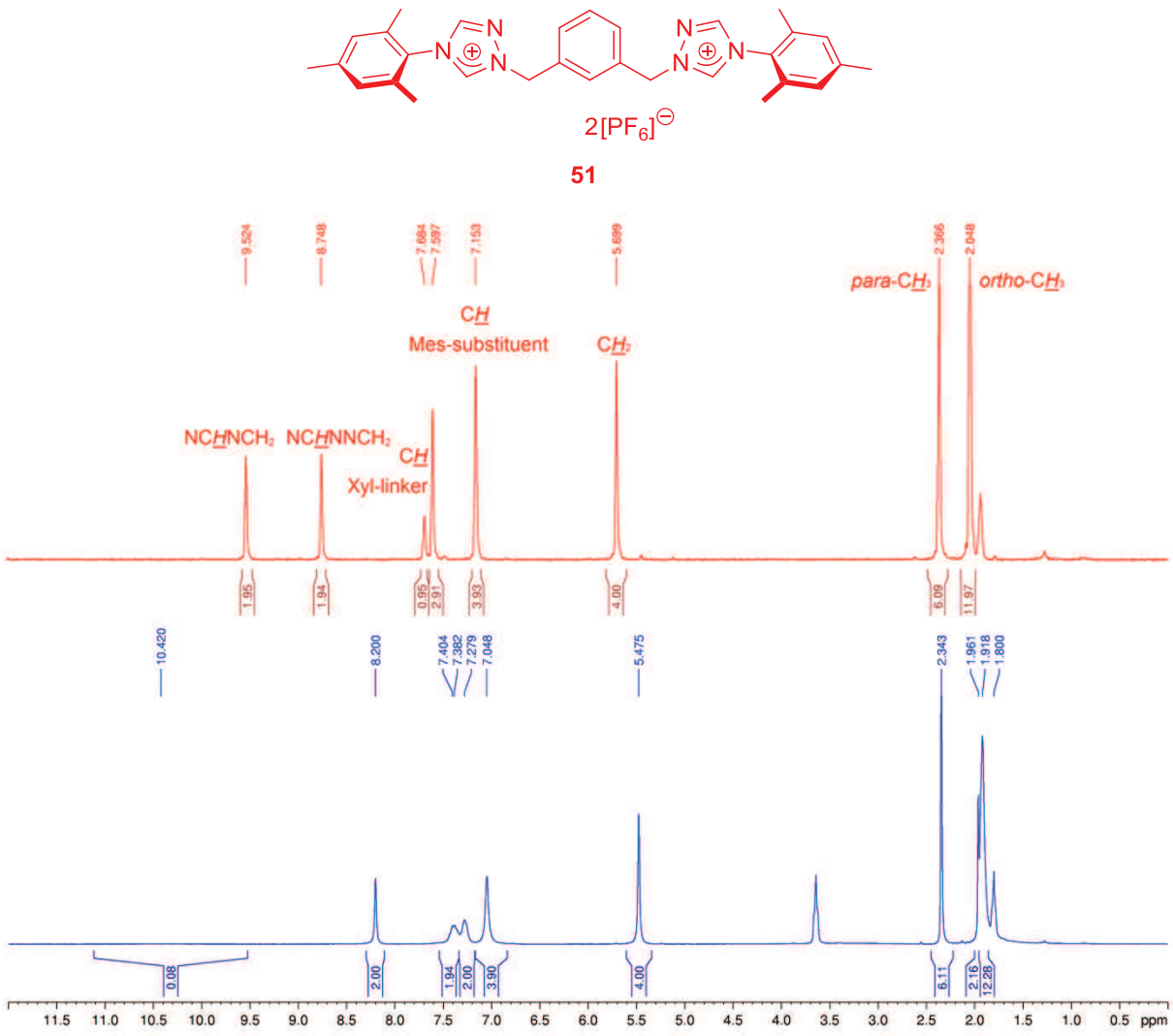

Figure 36: ^{1}H NMR spectrum of the soluble fraction of experiment 3 (Table 19) (lower part, blue) in comparison with the spectrum of the starting material bistriazolium hexafluorophosphate salt **51** (upper part, red) (spectra recorded in CD_3CN at 250 MHz).

Moreover, the ESI+ spectra of the (raw) products only showed a peak corresponding to the bistriazolylidene ligand with one coordinated copper(I) ion [Cu(bis-NHC ligand)]$^{+}$ (entries 3, 7, 9 in Table 19), and confirmed neither any dinuclear species nor the presence of acetate. Another problem in these syntheses was the sensitivity of the raw product. Even when the reaction was entirely carried out in the glovebox, the reaction mixture was found to turn green or blue, indicating the formation of copper(II) species. Together with the orange or violet precipitate observed in reaction mixtures 1, 2 and 8 in Table 19, this hints at the disproportionation of copper(I) to give copper(II) and a metallic precipitate under the reported reaction conditions. However, the sensitivity greatly depended on the choice of bistriazolium precursor, solvent, base

and reaction time. For example, it was found that xylylene-linked precursors lead to more sensitive reaction mixtures than ethylene-linked precursor salts. As for the substituents on the N4-position, mesityl turned out to facilitate decomposition more than 3,5-xylyl or 4-tolyl substituents.

Only by means of crystal structure analysis could the presence of acetate as ligand be proved. Several months after a crystal from experiment 7 (Table 19) had been handed in for X-ray analysis, the crystal structure displayed in Figure 37 was obtained, which corresponds to structural outline **I** in Scheme 50 (except for the bridging coordination mode of both acetate ligands). It is unknown whether this bis-NHC dicopper diacetate complex (**91d**; **d** stands for diacetate) was the only product in this reaction mixture. However, from this point on it seemed more realistic to isolate one of the complexes **I** or **II**, even if the analytical data from the ESI+ mass spectra did not suggest their formation. Most probably, these complexes decompose under the conditions in the ESI mass spectrometer so that only the [Cu(bistriazolylidene)]$^+$ peak is observed.

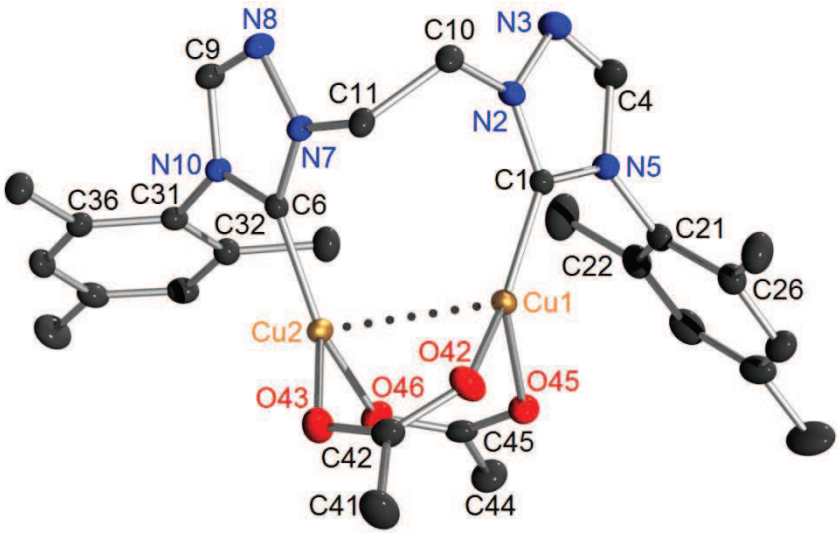

Figure 37: ORTEP plot of the single crystal X-ray structure of bis(μ-acetato-$\kappa O,\kappa O'$)-μ-{1,1'-(ethane-1,2-diyl)bis[4-(2,4,6-trimethylphenyl)-1*H*-1,2,4-triazol-5-ylidene]-$\kappa C,\kappa C'$}dicopper(I) (**91d**) from the reaction mixture of entry 7 in Table 19 (hydrogen atoms and hexafluorophosphate counterions are omitted for clarity).[118] Selected average distances [Å], bond angles and dihedral angles: Cu1-Cu2 2.712, C1-Cu1 1.888, Cu2-C6 1.879, Cu1-O42 1.947, Cu2-O43 2.017, Cu1-O45 2.100, Cu2-O46 2.000, C1-N2 1.334, N2-N3 1.380, N3-C4 1.290, C4-N5 1.364, N5-C1 1.368; C1-Cu1-O42 147.29°, C6-Cu2-O46 130.95°, C1-Cu1-O45 113.20°, C6-Cu2-O43 132.53°, O42-Cu1-O45 98.61°, O43-Cu2-O46 96.43°, N7-C6-N10 101.31°, N2-C1-N5 101.77°, O42-C42-O43 125.67°; N2-C10-C11-N7 -62.26°, C1-N5-C21-C22 107.86°, C1-N5-C21-C26 -71.37°, C4-N5-C21-C26 105.84°, C6-N10-C31-C36 114.05°, C6-N10-C31-C32 -69.22°, C9-N10-C31-C36 -67.47°, C9-N10-C31-C32 109.27°.

In the crystal structure of the neutral dinuclear complex **91d** shown in Figure 37, both acetate ligands coordinate in a μ_2-bridging mode. The distance between the two copper(I) centres is 2.712 Å. For comparison, the interatomic distance in copper metal is 2.556 Å,[121] and the Cu(I)-Cu(I) distance in crystalline polymeric copper(I) acetate was reported to be 2.544 Å by Drew[75b] and 2.556 Å by Fernando.[75a, 75c] The observation that the Cu(I)-Cu(I) distance in dinuclear complex **91d** displayed in Figure 37 is longer than in copper(I) acetate may thus be attributed to the influence of the bistriazolylidene ligand, which "forces" the copper(I) ions to be farther apart from each other than in copper(I) acetate. Nevertheless, a dotted line has been drawn between the two copper(I) centres in order to indicate the possibility of cuprophilic interactions. These "non-classical" d^{10}-d^{10} interactions[122] between closed-shell copper(I) ions have for example been discussed with regard to triazenido complexes such as tetrakis[1,3-dimethyltriazenidocopper(I)] reported by Corey *et al.* with Cu(I)-Cu(I) distances of 2.64 to 2.68 Å,[123d] and tetrakis[1,3-bis(4-fluorophenyl)triazenido)copper(I) with interionic distances of 2.6070 and 2.6098 Å disclosed by the group of Strähle.[123e] The shortest Cu(I)-Cu(I) distance, *viz.* 2.348 Å, was found in the related trinuclear complex tris[1,5-di(4-tolyl)pentaazadienidocopper(I)].[123f] However, for all these complexes, the short Cu(I)-Cu(I) distance might also be attributed to the "bite size" of the bridging ligands which connect the two copper(I) centres.[122b, 123g] Examples for unsupported Cu(I)-Cu(I) contacts are scarce.[121, 123a, 123b] For example, in a recent publication by Fackler *et al.* a dicopper complex with a neutral guanidine ligand was presented, in whose two polymorphs the distance between the metal centres was found to be 2.6725 and 2.6517 Å in the absence of any bridging ligands.[123c]

The Cu(I)-Cu(I) distance found in the neutral dicopper complex **91d** (2.712 Å) is only slightly greater than the interionic distances of 2.54 Å and 2.64 Å in the calculated transition states of CuAAC reactions featuring dinuclear model structures with chloride/water and acetylide/water as spectator ligands, respectively.[32] In the course of the DFT calculations presented in section 4.3, the Cu-Cu distance in the corresponding model transition state **C02TS03e(Mes)** was calculated to be d(Cu1-Cu2) = 2.69805 Å, which is very close to the interionic distance in the neutral diacetate complex **91d** shown in Figure 37. The coordination geometry on the copper(I) centres is distorted trigonal planar. The angle between the two oxygen ligator atoms is smaller

[φ (O42-Cu1-O45) = 98.61°] than between the carbene C-atom and one of the oxygen atoms [φ (C1-Cu1-O42) = 147.29°, φ (C1-Cu1-O45) = 113.20°].
The shape of the bistriazolylidene ligand system is bowl-like with the two triazolylidene rings slightly bent towards each other [τ (C1-N2-N7-C6) = -24.61°]. Again, the planes of the aryl-substituents at the N4-position are twisted with respect to the planes of the adjacent triazolium heterocycles, for example τ (C1-N5-C21-C22) = 107.86°.

Having obtained the crystal structure of bis(μ-acetato-κO,κO')-μ-{1,1'-(ethane-1,2-diyl)bis[4-(2,4,6-trimethylphenyl)-1*H*-1,2,4-triazol-5-ylidene]-κC,κC'}dicopper(I) (**91d**), further efforts on the isolation and purification of dinuclear copper(I) complexes with acetate as sacrificial ligand were concentrated on the synthesis of bistriazolylidene complexes with an ethylene-linker. The experiments summarized in Table 19 showed that in principle, acetate is a strong enough base for the deprotonation of the ligand precursor. This had also been shown by the base-free synthesis of dinuclear bistriazolylidene copper(I) complexes **71** and **81** as described in paragraph 4.5.1. However, copper(I) acetate obviously has the tendency to disproportionate, which was indicated by the green or blue colour of the reaction mixtures (presence of Cu^{2+} ions) and the sometimes observed formation of a reddish precipitate (copper metal). In the following experiments, copper(I) acetate was only used as the source for the metal ion and sodium acetate was chosen as an "external" base, as Crabtree *et al.* had already reported on the use of sodium acetate for the deprotonation of triazolium salts in the synthesis of iridium triazolylidene complexes.[135]

Table 20: Optimization of reaction conditions for the synthesis of dinuclear copper(I) complexes with acetate as sacrificial ligand.

entry	conditions and observations
1	*ligand precursor*: **61** *conditions*: CD_3CN, CuOAc (2.0 eq.), NaOAc (4.9 eq.), ultrasound *observations*: solution turned light blue *^{1}H NMR spectrum* of reaction mixture in CD_3CN: deprotonation complete, single new species with peaks of the ligand, alkyl integrals do not fit
2	*ligand precursor*: **61** *conditions*: THF, CuOAc (2.0 eq.), NaOAc (3.0 eq.), 5 h, RT; ultrasound *observations*: colourless solution with purple precipitate; the amount of precipitate increased in the ultrasound bath *^{1}H NMR spectrum* of the soluble fraction in d_8-THF: deprotonation complete, single species with peaks of the ligand, acetate methyl peak at 1.83 ppm (integral: 5.9), broad peak at 10.55 ppm (acetic acid) *elemental analysis*: C – 45.17 %, H – 4.89 %, N – 11.57 % (calculated for bis-NHC dicopper monoacetate hexafluorophosphate complex $C_{26}H_{31}Cu_2F_6N_6PO_2$: C – 42.68 %, H – 4.27 %, N – 11.49 %)
3	*ligand precursor*: **61** *conditions*: THF, CuOAc (2.0 eq.), NaOAc (1.1 eq.), 5 h, RT; ultrasound *observations*: turquoise solution with violet precipitate *^{1}H NMR spectrum* of the soluble fraction in d_8-THF: deprotonation complete, single species with peaks of the ligand, acetate methyl peak at 1.80 ppm (integral: 5.8), broad peak at 10.51 ppm (acetic acid) *^{1}H NMR spectrum* after work-up in d_8-THF: single species with peaks of the ligand, acetate methyl peak at 1.81 ppm (integral: 3.0) *elemental analysis*: C – 42.35 %, H – 4.63 %, N – 11.09 % (calculated for bis-NHC dicopper monoacetate hexafluorophosphate complex $C_{26}H_{31}Cu_2F_6N_6PO_2$: C – 42.68 %, H – 4.27 %, N – 11.49 %)
4	*ligand precursor*: **61** *conditions*: d_6-acetone, CuOAc (2.2 eq.), NaOAc (1.1 eq.), 2 h, RT; ultrasound *observations*: grey solution with grey precipitate *^{1}H NMR spectrum* of the raw mixture: deprotonation complete, single species with peaks of the ligand, acetate methyl peak at 1.92 ppm (integral: 9), broad

	peak at 10.43 ppm (acetic acid)
5	*ligand precursor*: **61** *conditions*: acetone, CuOAc (2.0 eq.), NaOAc (1.1 eq.), ultrasound, 2 h *observations*: turquoise solution with red precipitate *^{1}H NMR spectrum* of the soluble fraction in d_8-THF: deprotonation complete, single species with peaks of the ligand, acetate methyl peak at 1.83 ppm (integral: 4.6), broad peak at 10.53 ppm (acetic acid) *crystal structure*: Figure 38
6	*ligand precursor*: **63** *conditions*: dichloromethane, CuOAc (2.1 eq.), NaOAc (1.1 eq.), RT, 6 d *observations*: slightly yellow solution with violet precipitate *^{1}H NMR spectrum* product after work-up in d_6-dmso: deprotonation complete, single species with peaks of the ligand, acetate methyl peak at 2.01 ppm (integral: 2.8) *^{13}C NMR spectrum* product after work-up in d_6-dmso: peak for carbene C-atom at 176.6 ppm, no peaks for the acetate ligand *yield*: 22 %
7	*ligand precursor*: **63** *conditions*: THF, 1) NaOAc (2.3 eq.), RT, 2 d; 2) CuOAc (2.2 eq.), RT, 5 d *observations*: slightly yellow solution with violet precipitate *^{1}H NMR spectrum* product after work-up in CD_2Cl_2: deprotonation complete, single species with peaks of the ligand, acetate methyl peak at 2.06 ppm (integral: 3.0) *^{13}C NMR spectrum* product after work-up in CD_2Cl_2: peak for carbene C-atom at 176.6 ppm, no peaks for the acetate ligand *HSQC spectrum*: ^{13}C resonance for the acetate's methyl group at 23.0 ppm *yield*: 39 %
8	*ligand precursor*: **61** *conditions*: dichloromethane, CuOAc (3.0 eq.), NaOAc (2.3 eq.), 4 d *observations*: turquoise solution with red precipitate *^{1}H NMR spectrum* of the reaction product in d_8-THF: deprotonation complete, single species with peaks of the ligand, acetate methyl peak at 1.80 ppm (integral: 3.1)

	ESI+ mass spectrum: peak at *m*/*z* = 463.16645 corresponding to the bistriazolylidene ligand with one copper atom (isotopic pattern), Figure 38
9	*ligand precursor*: **61** *conditions*: dichloromethane, 1) NaOAc (2.3 eq.), 2 h, 2) CuOAc (2.2 eq.), 4 d *observations*: slightly turquoise solution with reddish precipitate *^{1}H NMR spectrum* of the reaction product in CD_2Cl_2: deprotonation complete, single species with peaks of the ligand, acetate methyl peak at 1.99 ppm (integral: 2.6) *elemental analysis*: C – 42.80 %, H – 4.34 %, N – 11.40 % (calculated for bis-NHC dicopper monoacetate hexafluorophosphate complex $C_{26}H_{31}Cu_2F_6N_6PO_2$: C – 42.68 %, H – 4.27 %, N – 11.49 %) *yield*: 68 %

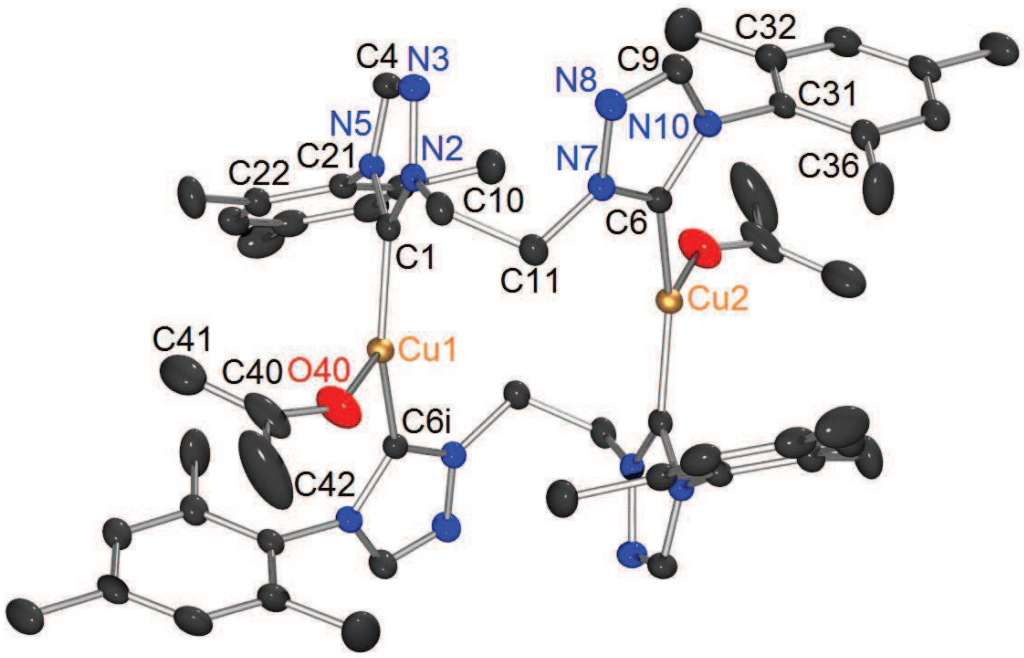

Figure 38: ORTEP plot of the single crystal X-ray structure of bis{μ-[1,1'-(ethane-1,2-diyl)bis-(4-(2,4,6-trimethylphenyl)-1*H*-1,2,4-triazol-5-ylidene)]-κC,κC'}dicopper(I) bis(hexafluorophosphate) (**111** • 2 acetone) from the reaction mixture of entry 5 in Table 19 (hydrogen atoms and hexafluorophosphate counterions are omitted for clarity).[118] Selected average distances [Å], bond angles and dihedral angles: Cu1-Cu2 4.502, C1-Cu1 1.912, C6-Cu2 1.916, Cu1-O40 2.204; C1-Cu1-C6i 150.46°, C1-Cu1-O40 104.50°, O40-Cu1-C6i 104.93°, N2-C1-N5 101.93°, N7-C6-N10 101.99°; N2-C10-C11-N7 -59.16°, C4-N5-C21-C22 99.21°, C4-N5-C21-C26 -80.60°.

The attempted synthesis of a bis-NHC dicopper acetate complex with acetone as solvent (entry 5 in Table 20) and subsequent crystallization from acetone/diethyl ether led to the isolation of a tetra-NHC dicopper complex (**111** • 2 acetone) shown in Figure 38. Most probably due to the influence of the coordinating solvent acetone, a tetra-NHC dicopper complex corresponding to structural outline **III** in Scheme 50 was isolated instead of the desired complexes **I** or **II**. In this complex, two bistriazolylidene ligands bind to two copper(I) centres. The complex cation is symmetric with respect to a centre of inversion. Both copper(I) ions are additionally coordinated by acetone. The coordination geometry at the copper(I) ions is not trigonal-planar, but rather T-shaped. The angle formed by the two coordinating carbene atoms and the central copper ion is φ(C1-Cu1-C6i) = 150.46°. In contrast, the angles formed with the oxygen ligator atom are φ(C1-Cu1-O40) = 104.50° and φ(O40-Cu1-C6i) = 104.93°. The distance between the carbene C-atom and the copper centre is slightly elongated in comparison to the Cu-C bonds in the complexes displayed in Figure 33 (**81**), Figure 34 (**83**) and Figure 37 (**91d**), for example d(C1-Cu1) = 1.912 Å. The bonds to the oxygen ligator atoms are even longer, for example d(Cu1-O40) = 2.204 Å, which hints at a weak coordination of the solvent molecules. The distance between the two copper(I) centres is 4.502 Å and thus cuprophilic interactions are beyond all question. Again, the mesityl substituent's aryl plane is strongly twisted with respect to the plane of the triazolylidene heterocycles, for example τ(C1-N5-C21-C22) = 99.72°. The ligand adopts a distorted bowl-shape with a dihedral angle of τ(N2-C10-C11-N7) = 59.16°.

Applying the optimized reaction conditions acquired in this work (Table 19 and Table 20) and by M. Sc. Ella Schreiner in her master thesis,[136] three examples of the desired bis-NHC dicopper monoacetate hexafluorophosphate complexes following structural outline **II** in Figure 27 were synthesized and fully characterized. After work-up of the raw mixtures including complete removal of acetic acid, the resulting solid products **91** - **93** were stable towards air. Even in solution these complexes did not decompose rapidly.

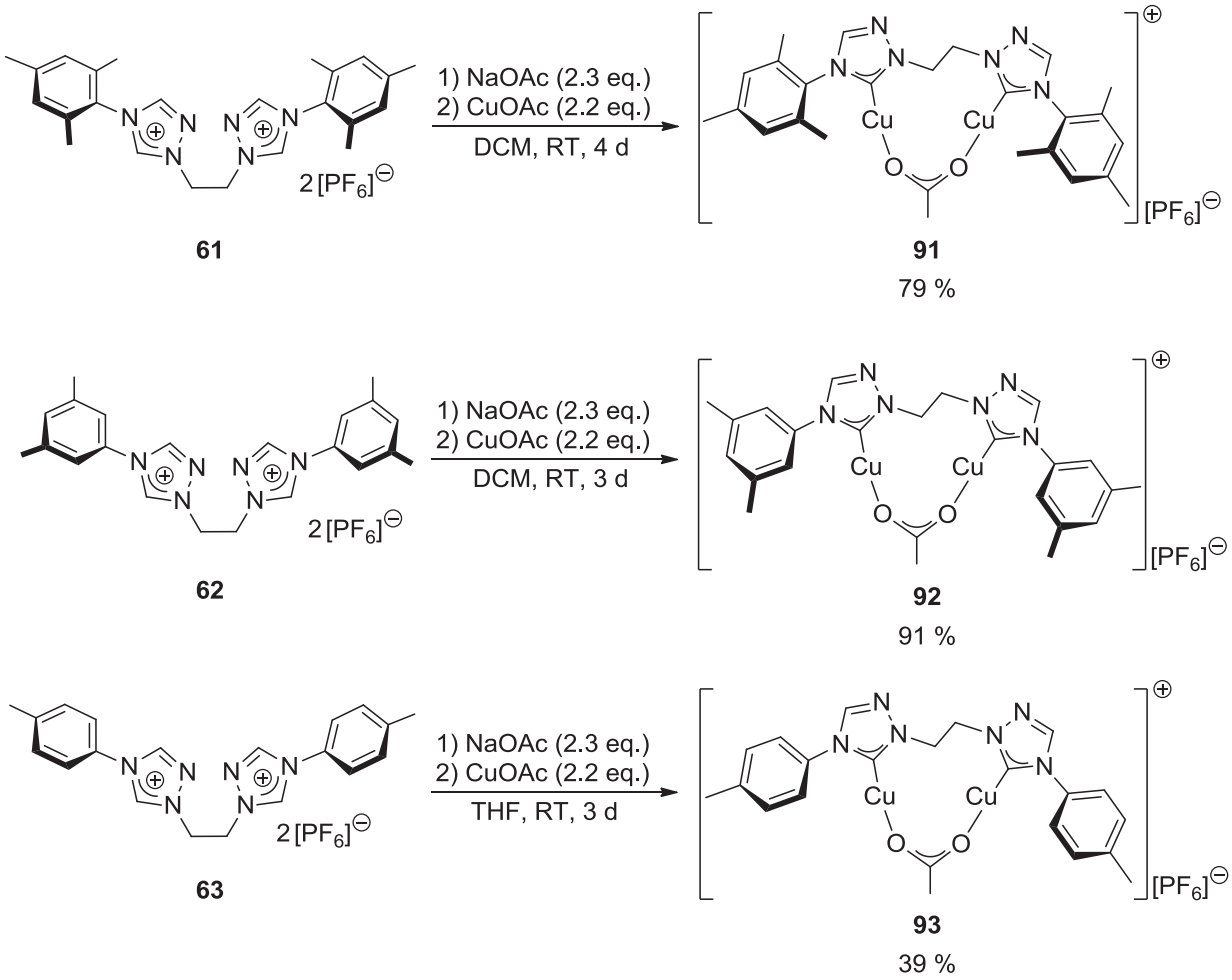

Scheme 51: Optimized procedures and yields for the synthesis of ethylene-linked bistriazolylidene dicopper acetate hexafluorophosphate complexes **91** - **93**.[137]

In the optimized procedures, dichloromethane was used as solvent and the external base sodium acetate applied in slight excess. Then, copper(I) acetate was added to the reaction mixture, which was stirred in the glovebox for several days at room temperature. The colourless or slightly yellow reaction mixtures were then filtered over a frit under inert gas. The solvent was evaporated and the colourless solid washed with diethyl ether several times in order to remove the acetic acid formed as byproduct. Attempts on re-crystallization were not successful. In the case of the 3,5-xylyl substituted complex **92**, re-crystallization from acetonitrile/diethyl ether afforded a coordination polymer (**92p**), whose single crystal X-ray structure is shown in Figure 37. As can be deduced from the shown excerpt of the crystal structure, the bistriazolylidene species acts as a μ_2-bridging ligand between two copper(I) centres which are not bridgingly μ_2-coordinated by acetate ligands. Instead, two acetate ligands bridge two copper(I) centres which are bound by different bistriazolylidene ligands.

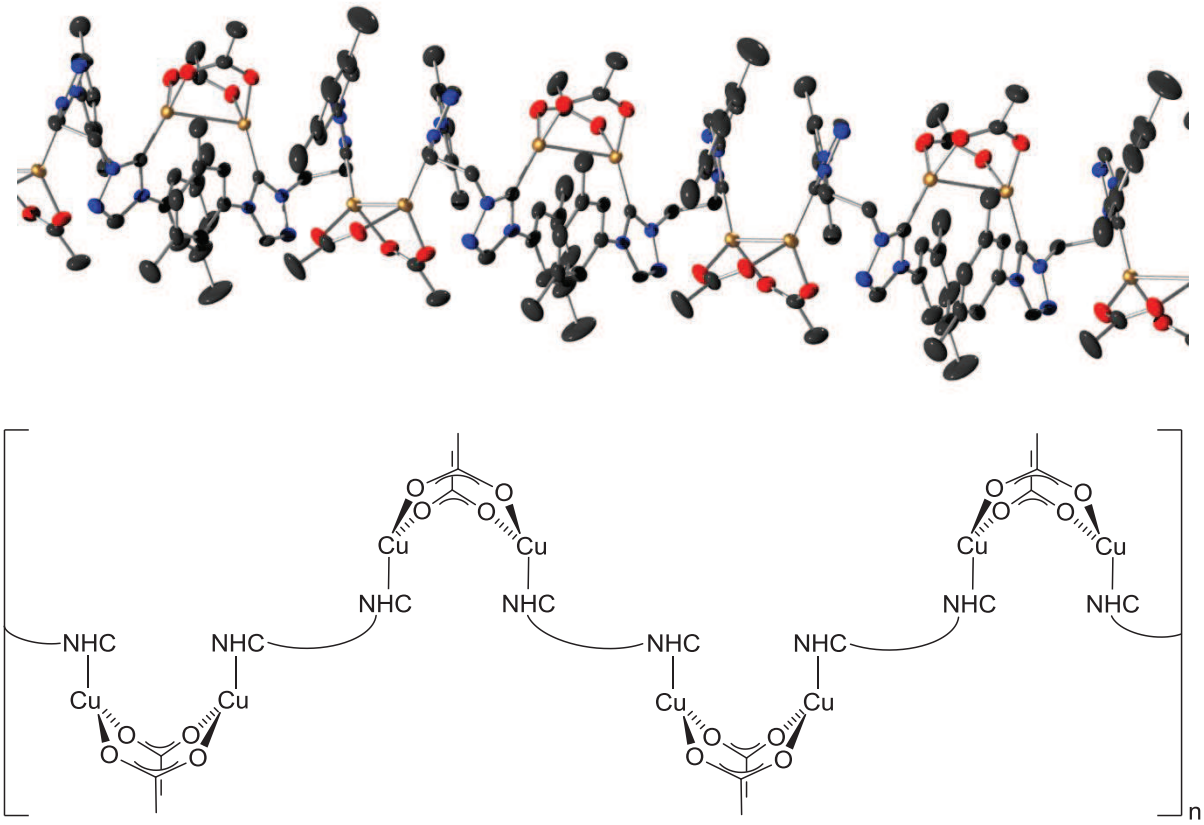

Figure 39: ORTEP plot of the single crystal X-ray structure of polymeric bis(μ-acetato-κ*O*,κ*O*')-μ-{1,1'-(ethane-1,2-diyl)bis[4-(3,5-dimethylphenyl)-1*H*-1,2,4-triazol-5-ylidene]-κ*C*,κ*C*'}dicopper(I) (**92p**) obtained from a re-crystallization assay of complex **92** (hydrogen atoms and hexafluorophosphate counterions are omitted for clarity)[118] and schematic representation of its structure with NHC ⌒ NHC = 1,1'-(ethane-1,2-diyl)bis[4-(3,5-dimethylphenyl)-1*H*-1,2,4-triazol-5-ylidene].

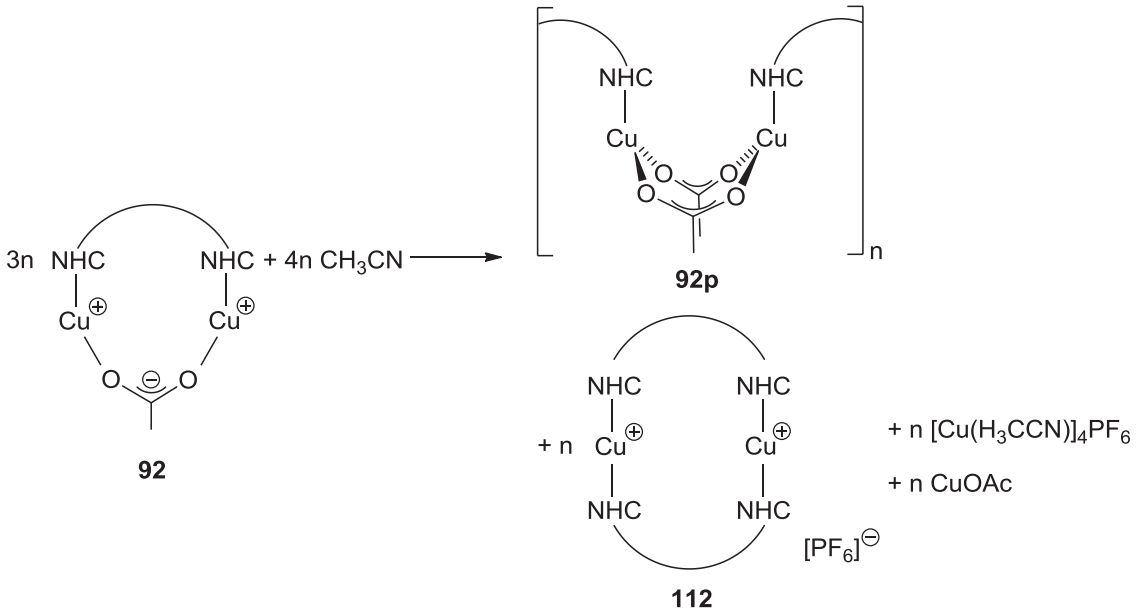

Scheme 52: Schematic representation of the hypothesized route for decomposition of complex **92** in acetonitrile.

Scheme 52 shows a possible route for the formation of the polymeric species **92p** in acetonitrile. However, this decomposition of complex **92** does not occur immediately, but was only observed in a crystallization assay after some weeks.

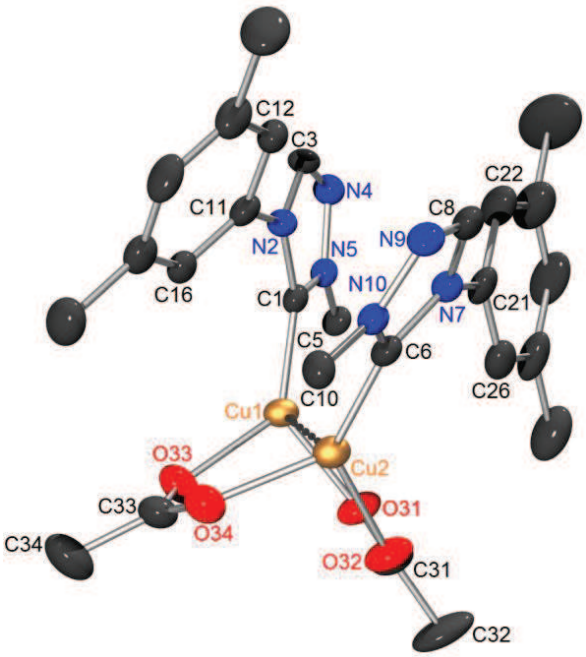

Figure 40: ORTEP plot of the monomeric unit in the coordination polymer **92p** (hydrogen atoms are omitted for clarity).[118] Selected average distances [Å], bond angles and dihedral angles: Cu1-Cu2 2.684, C1-Cu1 1.885, C6-Cu2 1.874, Cu1-O31 2.036, Cu2-O32 2.021, Cu1-O33 2.009, Cu2-O34 2.032; C1-Cu1-O31 127.19°, C6-Cu2-O32 129.35°, C1-Cu1-O33 133.39°, C6-Cu2-O34 130.65°, O31-Cu1-O33 97.41°, O32-Cu2-O34 98.32°; C1-N2-C11-C12 149.06°, C3-N2-C11-C16 143.93°.

In the monomeric unit of the coordination polymer bis(*μ*-acetato-κ*O*,κ*O*')-*μ*-{1,1'-(ethane-1,2-diyl)bis[4-(3,5-dimethylphenyl)-1*H*-1,2,4-triazol-5-ylidene]-κ*C*,κ*C*'}dicopper(I) (**92p**), the distance between the two copper(I) centres is only 2.684 Å, which is smaller than in the similar complex bis(*μ*-acetato-κ*O*,κ*O*')-*μ*-{1,1'-(ethane-1,2-diyl)bis-[4-(2,4,6-trimethylphenyl)-1*H*-1,2,4-triazol-5-ylidene]-κ*C*,κ*C*'}dicopper(I) (**91d**) shown in Figure 37. This might be due to the bonding of the bistriazolylidene ligand to different copper(I) centres so that it cannot "force" the copper ions to stand farther apart from each other than they would prefer based on the "bite size" of acetate in combination with cuprophilic interactions. However, the Cu(I)-Cu(I) distance is still substantially larger than in copper(I) acetate (2.544 Å to 2.556 Å).[75] The coordination geometry of the copper centres is distorted trigonal-planar. The angle between the two oxygen ligator atoms is much smaller than between the carbene C-atom and one

of the oxygen ligator atoms, for example φ (O31-Cu1-O33) = 97.41° and φ (C1-Cu1-O31) = 127.19°. The xylyl substituents' aryl plane is only slightly distorted with respect to the triazolylidene heterocycle as its steric hindrance is much smaller than for *ortho*-substituted aryl substituents such as mesityl. In the polymeric species **92p** shown in Figure 39, the ethylene-linked bistriazolylidene ligand adopts a bowl-shaped conformation with τ (N5-C5-C10-N10) = -60.10°. The polymeric chain has a zick-zack structure with the dicopper unit alternately located on the upper and lower side, as schematically represented in Figure 39.

During her master thesis in the Straub group, M. Sc. Ella Schreiner obtained a single-crystal X-ray structure by re-crystallization of complex **92** from THF/diethyl ether, which shows the coordination polymer of the bis-NHC dicopper monoacetate complex itself (Figure 41).[136, 138] In comparison to the structure of the polymeric decomposition product **92p** shown in Figure 39 and Figure 40, the copper(I) centres are farther apart from each other so that no cuprophilic interactions are possible. Due to further association to adjacent coordination units on one side, the monomeric cationic complex shown in the upper part of Figure 41 is quite unsymmetric and the two copper(I) centres nonequivalent. For example, the 3,5-xylyl ring at N5 is considerably twisted with respect to the plane of the triazolylidene heterocycle with τ (C1-N5-C21-C22) = -106.25°, whereas the xylyl-substituent at N10 is only slightly twisted by τ (C6-N10-C31-C32) = 45.52°, which is very similar to the analogous torsion in the polymeric decomposition product **92p** (Figure 39, Figure 40). Moreover, the coordination geometry at the Cu1 centre is almost linear with φ (C1-Cu1-O11) = 172.83°, whereas the angle at the Cu2 centre is φ (C6-Cu2-O12) = 146.03°. This bend is due to the coordination of another triazolylidene heterocycle *via* the nitrogen lone pair at the N2-position. Similarly to the situation in the crystal structure of the dicopper tetra-NHC complex with two coordinating acetone molecules (**111** • 2 acetone, Figure 38), the copper(I) centre Cu2 in the crystal structure of **92** is tricoordinate with two strong contacts to the acetate's oxygen atom [d(Cu2-O12) = 1.979 Å] and the carbene ligand [d(Cu2-C6) = 1.894 Å] and a weaker bond to the N8a atom of an adjacent coordination unit [d(Cu2-N8a) = 2.128 Å]. The coordination geometry at the Cu2 centre is T-shaped with φ (N8a-Cu2-C6) = 121.00° and φ (N8a-Cu2-O12) = 90.35°. The resulting coordination polymer is shown in the lower part of Figure 41.

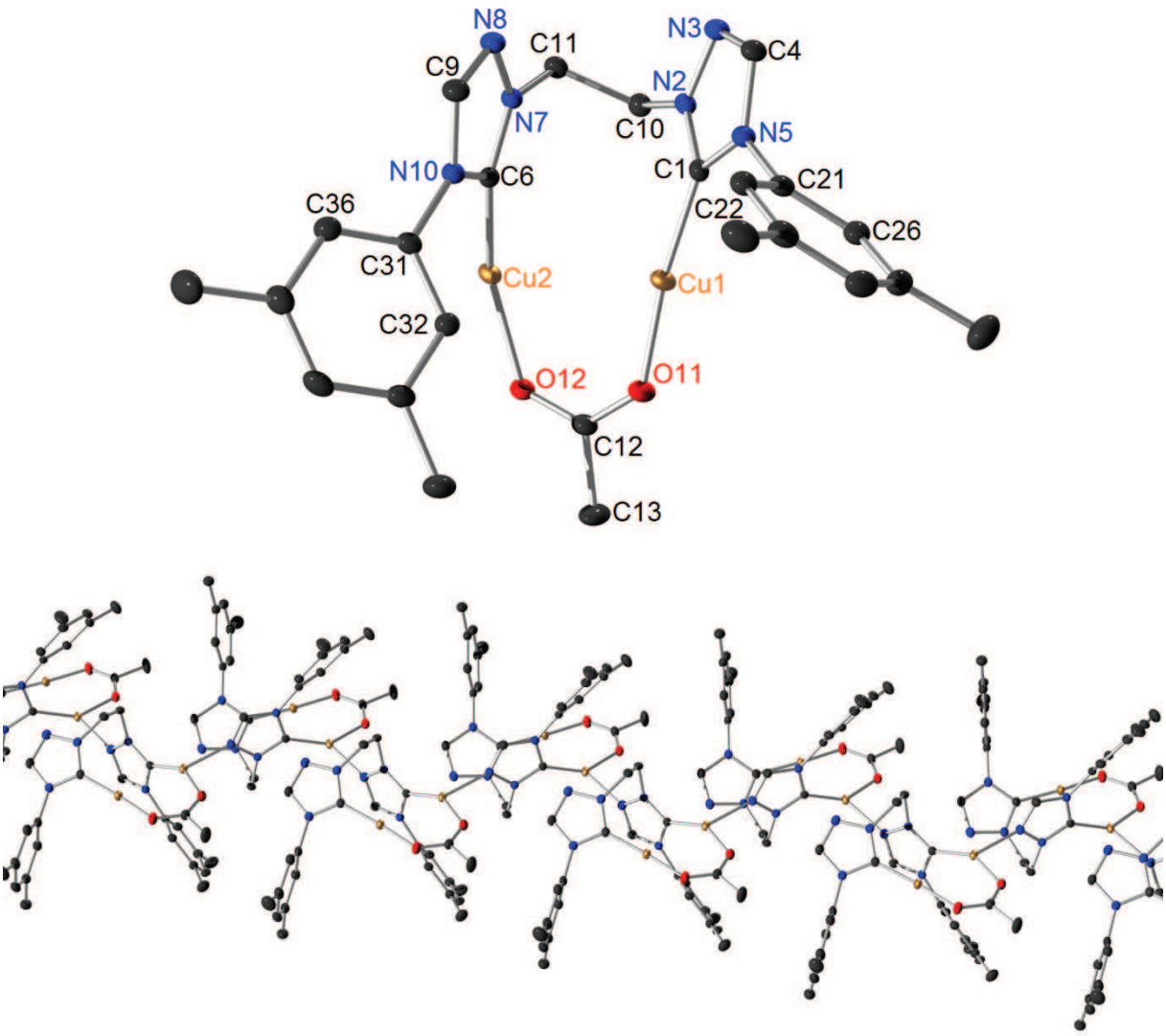

Figure 41: ORTEP plot of the single crystal X-ray structure of complex **92** obtained by M. Sc. Ella Schreiner (hydrogen atoms and the hexafluorophosphate counterion are omitted for clarity).[118, 136, 138]

Complete analytic data including elemental analyses were obtained for the three bis-NHC dicopper(I) monoacetate hexafluorophosphate complexes **91** - **93** shown in Scheme 51. As for the mass spectra, although a dicopper complex had never been observed in an ESI+ spectrum, the FAB+ spectra did show the corresponding signals for the cations $[M\text{-}PF_6]^+$ including two copper(I) ions (as confirmed by the isotopic pattern) as well as the acetate ligand. As an example, the FAB+ mass spectrum of complex **91** is shown in Figure 42.

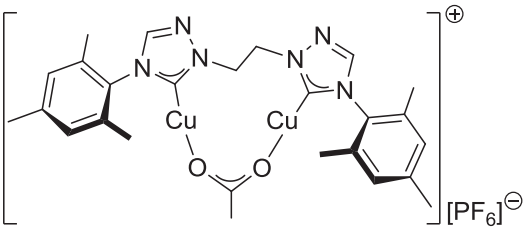

91

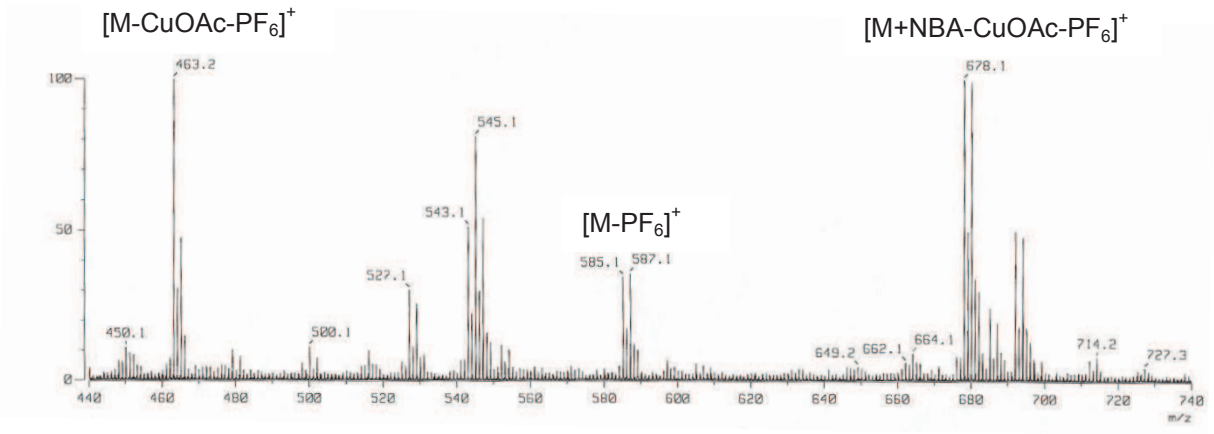

Figure 42: Excerpt of the FAB+ mass spectrum of complex **91** and assignment of the most prominent peaks.

The peak with the greatest intensity is observed at *m*/*z* = 678.1 and can be assigned to the cationic species $[M(^{63}Cu,^{63}Cu)+C_7H_6NO_3(NBA\text{-}matrix)\text{-}OAc\text{-}PF_6]^+$, *i.e.* an adduct of the dicopper species (without acetate and hexafluorophosphate) and nitrobenzyl alcohol from the FAB matrix. The signal at *m*/*z* = 463.2, which is the base peak in the ESI+ spectrum of the same substance, has an intensity of 81 % and its isotopic pattern indicates the presence of one copper(I) atom. The signal of the dinuclear ($^{63}Cu,^{63}Cu$)-complex $[M\text{-}PF_6]^+$ is observed at *m*/*z* = 585.1 with an intensity of 35 %. Its isotopologues, the ($^{63}Cu,^{65}Cu$)-complex and the ($^{65}Cu,^{65}Cu$)-complex, give signals at *m*/*z* = 587.1 and 589.1 with intensities of 36 % and 10 %, respectively, which is in accordance with the calculated isotopic pattern. A high-resolution FAB+ spectrum further confirms these assignments.

As for the NMR spectra, high concentrations and numerous scans allow for the observation of all peaks, although the signal for the acetate's methyl group is of very low intensity in the ^{13}C NMR spectrum. This can be explained by exchange of the weakly binding acetate ligand so that the intensity of this peak is very low, even in deuterated dichloromethane as non-coordinating solvent. The assignment of the

acetate ligands' peaks in the one-dimensional ^{13}C NMR spectrum could be carried out unambiguously with the help of a two-dimensional HSQC spectrum.

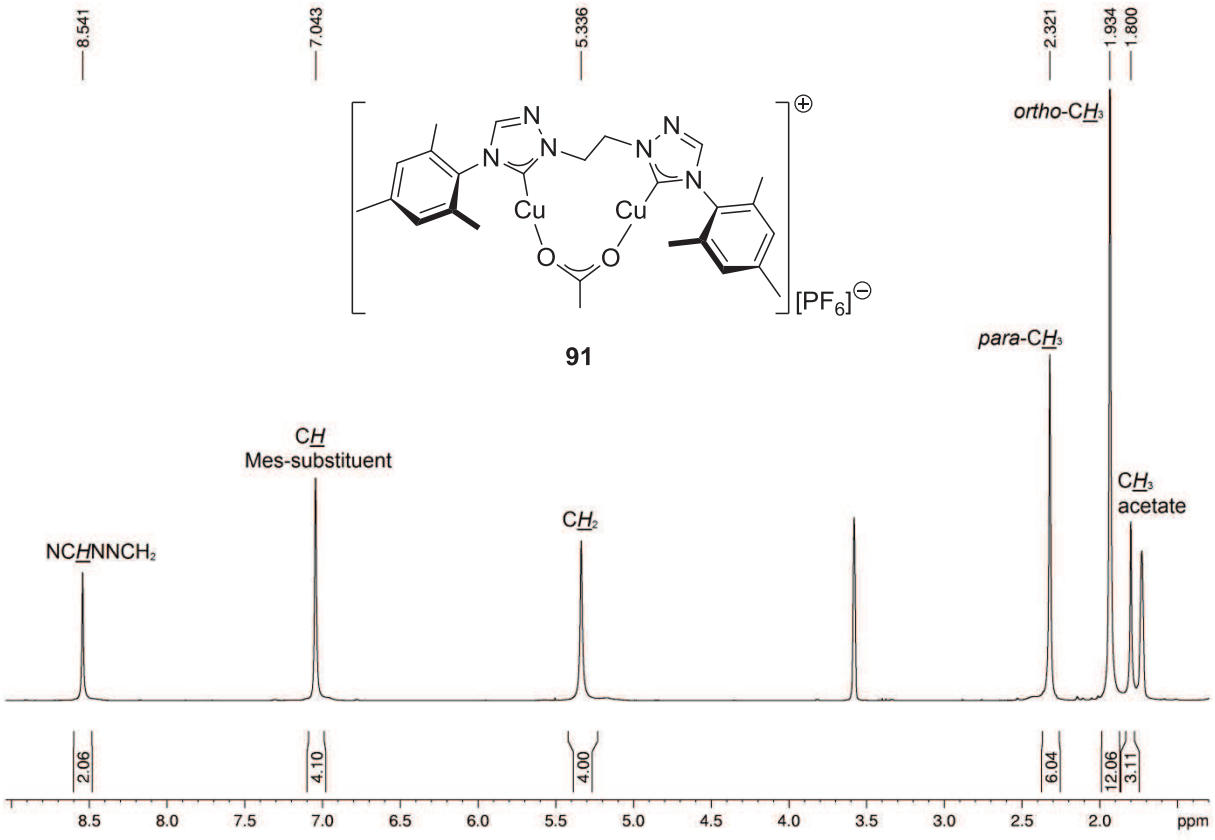

Figure 43: ^{1}H NMR spectrum of dinuclear copper(I) acetate complex **91** (recorded in d_8-THF at 250 MHz).

In the ^{1}H NMR spectrum of complex **91** (Figure 43), the resonance of the triazolylidene proton is observed at 8.54 ppm. There is only one aryl resonance at 7.04 ppm. In comparison to the substrate hexafluorophosphate salt **61**, the signal for the methylene group is shifted upfield from 5.80 ppm (in d_8-THF) to 5.34 ppm. The peak corresponding to the acetate ligand's methyl group is observed at 1.80 ppm with the expected intensity of three protons.

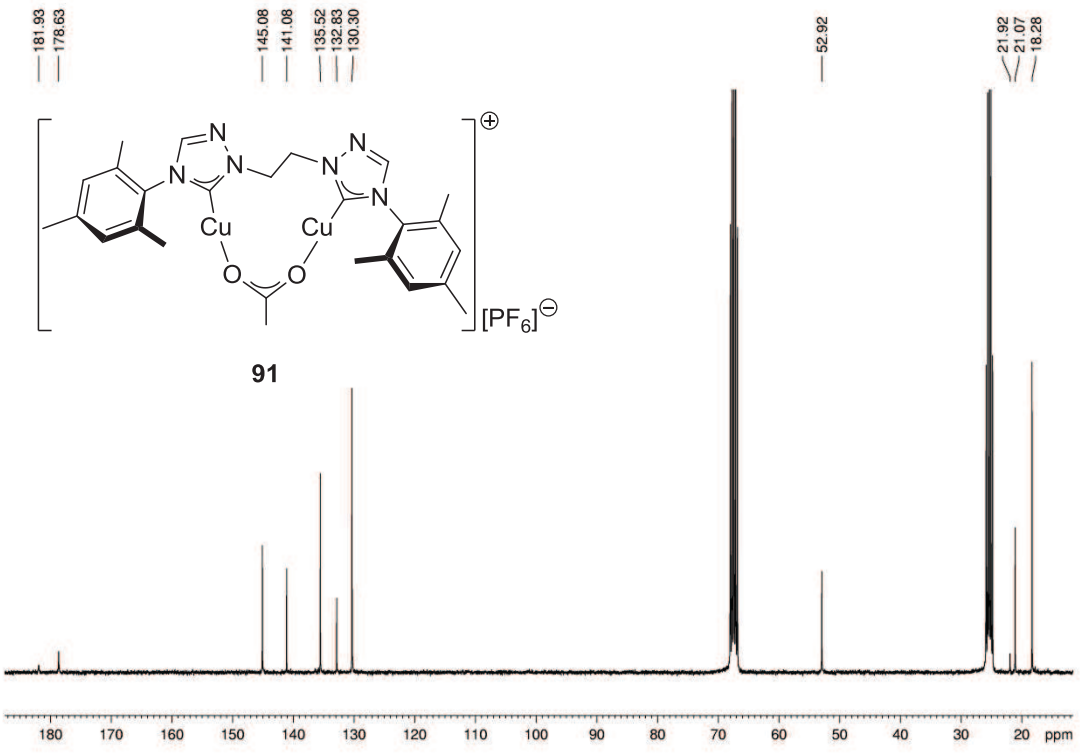

Figure 44: ^{13}C NMR spectrum of dinuclear copper(I) acetate complex **91** (recorded in d_8-THF at 75 MHz).

In the ^{13}C NMR spectrum of complex **91** (Figure 44), the signals for the acetate ligand are observed at 181.9 ppm (carboxylate) and 21.9 ppm (methyl group). They are both of very low intensity. The carbene C-atom's resonance is at 178.6 ppm, which is the typical range for triazolylidene carbene signals (compare to Figure 30, although these chemical shifts were observed in spectra recorded in d_3-acetonitrile). The peaks of the triazolylidene CH-group (145.1 ppm) and the aryl C-atoms follow. The methylene groups' resonance is observed at 52.9 ppm and the CH_3 groups of the mesityl-substituent in the typical alkyl region.

In the final experimental stage of this PhD project, the synthesis of two xylylene-linked bis-NHC dicopper monoacetate complexes finally succeeded (Scheme 53). Applying the optimized conditions described in Scheme 51, μ-acetato-κO,κO'-μ-{1,1'-(benzene-1,3-diyldimethanediyl)bis[4-(3,5-dimethylphenyl)-1*H*-1,2,4-triazol-5-ylidene]}-κC,$\kappa C'$-dicopper(I) hexafluorophosphate (**102**) was synthesized and completely characterized. However, this complex has only been obtained in low yield (22 %) and turned out to be extremely sensitive so that it was oxidized even as a solid when

exposed to air. Also, this complex displays very low solubility in organic solvents so that it was not used in catalytic test reactions.

Similarly, μ-acetato-$\kappa O,\kappa O'$-μ-{1,1'-(benzene-1,3-diyldimethanediyl)bis[4-(2,4,6-trimethylphenyl)-1*H*-1,2,4-triazol-5-ylidene]}-$\kappa C,\kappa C'$-dicopper(I) hexafluorophosphate (**101**) was synthesized in DCM. However, the complete characterization of this compound including elemental analysis remains to be done.

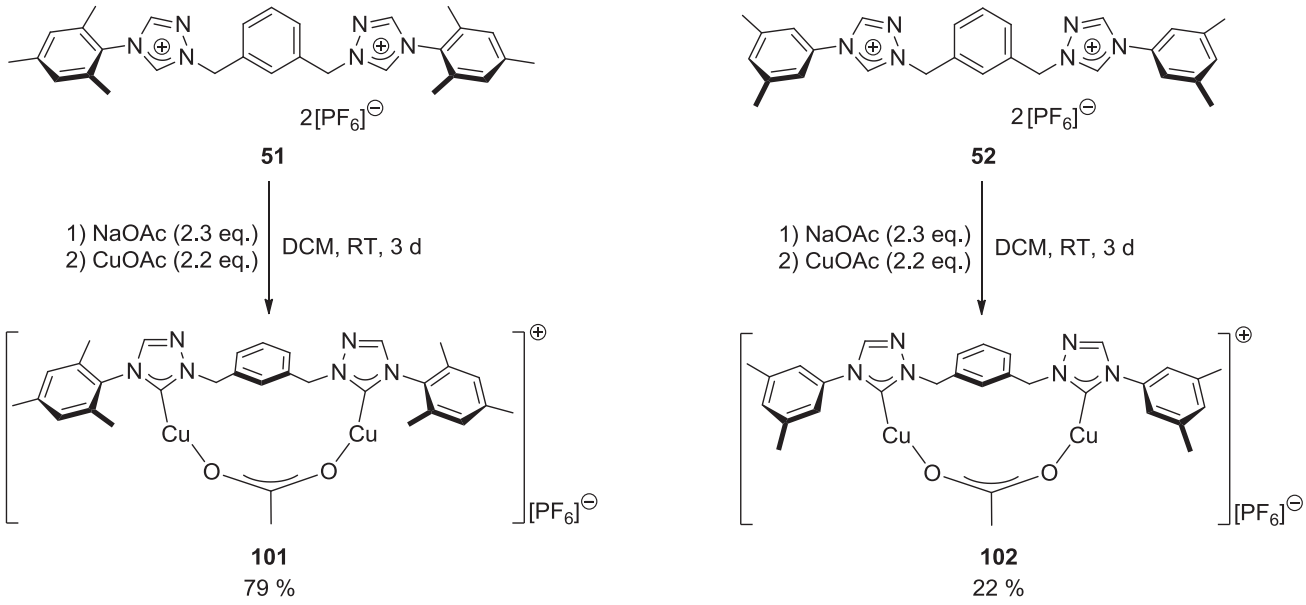

Scheme 53: Synthesis of xylylene-linked dicopper acetate complexes **101** and **102**.

Complex **101** was very sensitive as well. For reasons of comparison, a ^{1}H NMR spectrum was recorded in d_3-acetonitrile. Indeed, the signal for the acetate ligand's protons, which had been observed as a broad peak at 1.79 ppm in d_6-DMSO, could not be identified in the spectrum with d_3-acetonitrile as solvent. Most probably, this strongly coordinating solvent replaces the acetate ligand or the acetate complex decomposes to give the corresponding tetra-NHC dicopper complex analogous to structural outline **III** in Scheme 50. Figure 45 shows the ^{1}H NMR spectra of complex **101** in d_6-DMSO (green), in d_3-acetonitrile (red) and the spectrum of the product from entry 3 in Table 19 (blue). It thus becomes obvious that complex **101** decomposes in d_3-acetonitrile to give the same species that had been isolated at an earlier stage of this project. Obviously, acetonitrile had not been an adequate solvent for the synthesis of these highly sensitive and labile complexes containing a xylylene-linked bistriazolylidene ligand.

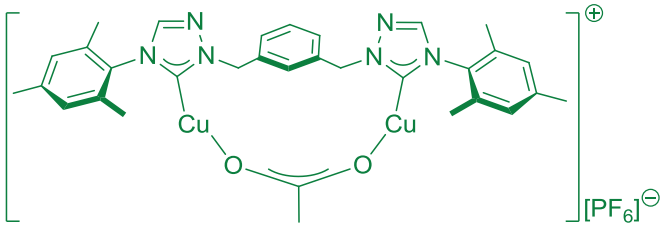

101

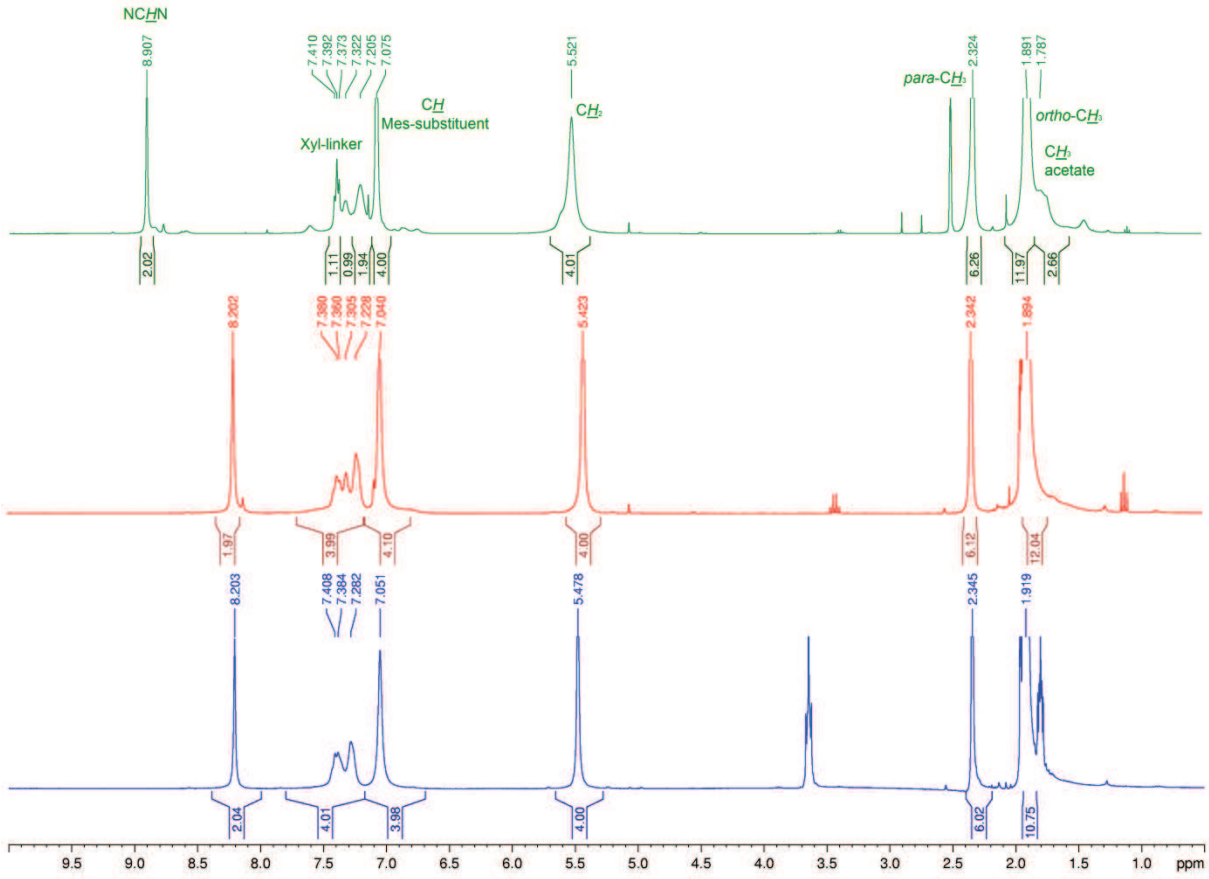

Figure 45: ^{1}H NMR spectra of complex **101** in d_6-DMSO (green, upper part), in d_3-acetonitrile (red, middle) and of the reaction product from Table 19, entry 3, in d_3-acetonitrile (blue, lower part).

The ^{1}H NMR spectrum of complex **102** in d_6-DMSO is shown in Figure 46. Compared to the corresponding complex with an ethylene-linker (**92**), all signals are slightly shifted downfield, which is due to the more electron-withdrawing characteristics of the central xylylene moiety compared to an ethylene group. The ^{1}H resonance of the triazolium ring's CH group is observed at 9.14 ppm and the signal corresponding to the isolated position of the linker unit at 7.59 ppm. The other protons of the linker unit and the *ortho*-hydrogen atoms of the xylyl-substituents are isochronous and give a signal with an intensity corresponding to seven protons at 7.41 ppm. The chemical

shift of the *para*-CH groups in complex **102** is identical to the corresponding signal's position in the ethylene-linked complex **92** in d_6-DMSO. The signal for the benzylic CH_2 groups is observed at 5.58 ppm (**92**: 5.04 ppm) and the acetate ligand's methyl group gives a very broad peak at 1.99 ppm with an intensity of three protons.

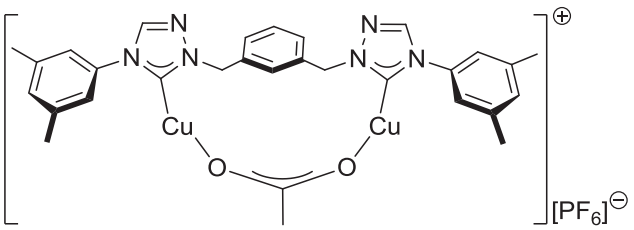

102

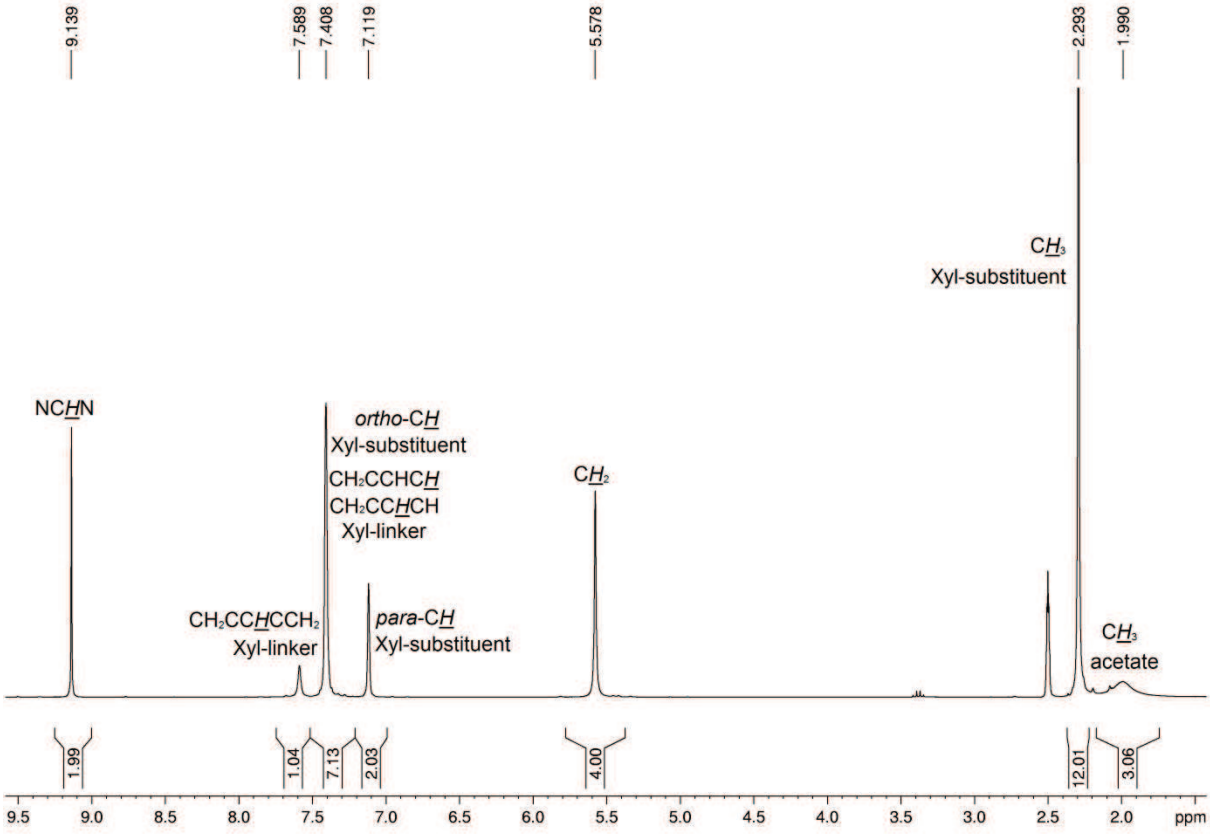

Figure 46: ^{1}H NMR spectrum of xylylene-linked dicopper acetate complex **102** (recorded in d_6-DMSO at 300 MHz).

In the FAB+ spectrum of **102**, the base peak is the monocationic dicopper complex $[M(^{63}Cu,^{63}Cu)\text{-}PF_6]^+$. In the ESI+ spectrum, there are again no signals for dinuclear copper complexes.

All in all, the work with bistriazolylidene dicopper acetate complexes described in this paragraph (4.6) had been very challenging, as analytic means such as NMR spectroscopy and mass spectrometry produced ambiguous results. The isolation of the desired complexes containing acetate as ligand could neither be verified by ESI+ mass spectrometry, which had been used before as an appropriate technique for the detection of the dinuclear copper complexes presented in section 4.5.1, nor by NMR spectroscopy with coordinating solvents such as acetone or acetonitrile. Only by means of FAB+ mass spectrometry, NMR spectroscopy with high concentrations and an increased number of scans in weakly coordinating solvents, and elemental analysis was the succesful synthesis and structural identity of complexes **91** - **93** and **101** - **102** unambiguously confirmed.

4.7 Catalytic Tests in CuAAC Reactions

In preliminary catalytic experiments, the progress of the CuAAC test reaction with catalysts **91** and **92** synthesized by the author was monitored NMR spectroscopically by Johannes Straub in the course of his master thesis.[139] For comparative experiments, the author also synthesized Nolan's catalyst $[(ICy)_2Cu]PF_6$ (**123**). The preparation of the ligand precursor ICy • HCl (**121**) was carried out by applying literature procedures reported by the group of Herrmann. However, the synthesis of $[(ICy)_2Cu]PF_6$ (**123**) starting from ICy • HCl (**121**) and tetrakis(acetonitrile)copper hexafluorophosphate as reported in *Angew. Chem.* **2008**, *120*, 9013 - 9016 did not lead to the pure product as indicated by elemental analysis, most probably because chloride was still present. Thus, an alternative procedure with ICy • HBF_4 (**122**) as substrate described in a preceding publication on catalytic hydrosilylation reactions with $[(ICy)_2Cu]PF_6$ was applied.[72b] The ligand precursor ICy • HBF_4 (**122**) was prepared by subjecting ICy • HCl (**121**) to a salt metathesis reaction with HBF_4. The procedure presented in Scheme 54 finally gave the desired complex **123** as a pure product.

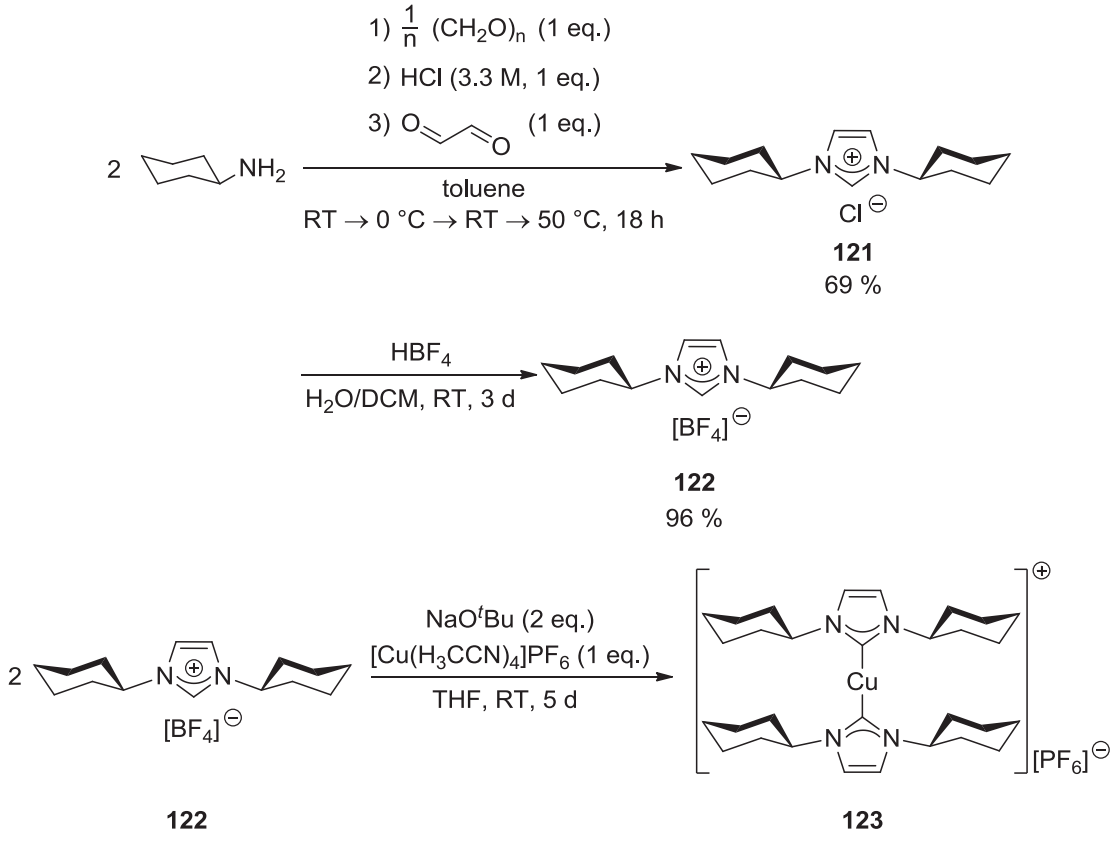

Scheme 54: Synthesis of $[(ICy)_2Cu]PF_6$ (**123**) according to a procedure reported in literature.[72b]

By re-crystallization from THF/pentane, crystals suitable for single crystal X-ray analysis were obtained. Although complex $[(ICy)_2Cu]PF_6$ (**123**) had first been described in literature as early as 2007, its crystal structure had not been published yet. As can be seen in the ORTEP plot displayed in Figure 47, the NHC ligands are twisted with respect to each other. The alignment of the carbene C-atoms and the central copper ion is nearly linear with φ(C1-Cu1-C6) = 172.58°. With respect to the axis C1-C6, the planes of the imidazolylidene rings are twisted by a torsion angle of τ(N2-C1-C6-N7) = -40.77°, most probably due to the steric hindrance of the cyclohexyl substituents.

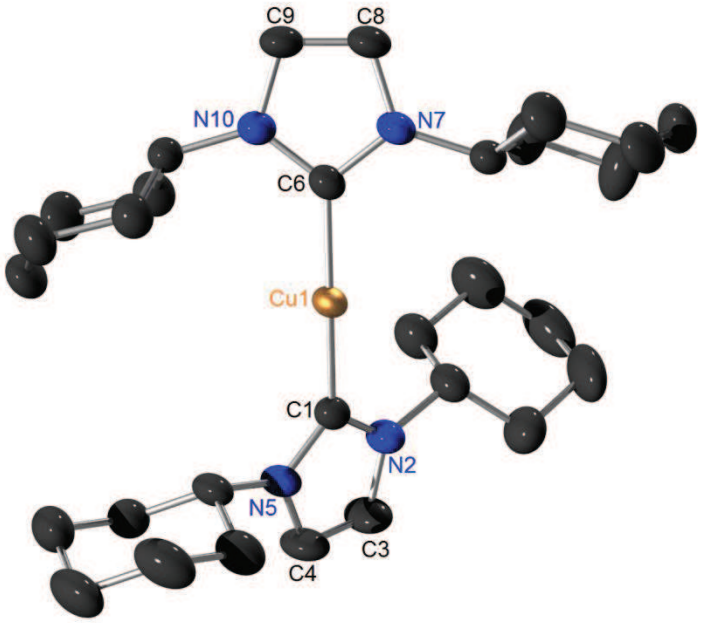

Figure 47: ORTEP plot of the single crystal X-ray structure of $[(ICy)_2Cu]PF_6$ (**123**) (hydrogen atoms, the hexafluorophosphate counterion and co-crystallized solvent molecules are omitted for clarity).[118, 140] Selected average bond lengths [Å], bond and dihedral angles: Cu1-C1 1.902, Cu1-C6 1.906, C1-N2 1.354, N2-C3 1.376, C3-N4 1.331, C4-N5 1.382, N5-C1 1.352; C1-Cu1-N6 172.58°, N2-C1-N5 104.40°; N2-C1-C6-N7 -40.77°.

4.7.1 General Experimental Setup for Catalytic Test Reactions Monitored by Gaschromatography

Catalytic CuAAC test reactions with the dinuclear copper(I) complexes shown in Scheme 51 were carried out at room temperature and monitored by use of gas chromatography. For quantitation, all peak areas in the chromatogram were determined by integration. In order to compensate for varying sample volumes, the analytes' peak areas were divided by the peak area of the internal standard, whose relative

concentration was constant for all samples. Quantitative analysis of conversion was enabled by determination of response factors for the azide substrate and the product triazole with respect to the internal standard dodecane in separate experiments carried out before the actual catalytic tests: different quantities of dodecane and the analyte in question were weighed into GC vials, which were then filled up with dichloromethane and subjected to the same GC method as the corresponding reaction mixture. In a diagram, the ratio of the weighed in amounts of substance was plotted against the ratio of the measured GC integrals. The slope of the resulting line is the response factor for this analyte with respect to dodecane. All normalized integrals do thus have to be multiplied by this factor. As calibration factors were only determined for dodecane as internal standard, no diagrams of conversion could be obtained for measurements carried out in DMSO and acetonitrile, as these solvents are not miscible with dodecane. However, apart from determining the reaction time, which was defined as the point when none of the substrates could be detected anymore, the conversion can be estimated by the increase in the product signal's integral.

The substrate stock solutions consisting of the alkyne, the azide, dodecane (or toluene) as internal standard and the solvent were stored at 4 °C and analyzed by gas chromatography before each catalytic experiment to ensure their purity and especially the absence of product triazole before the addition of the catalyst. Catalyst stock solutions were prepared and stored under inert gas.

For catalytic experiments, an aliquot of the catalyst stock solution was filled into a glass vial equipped with a magnetic stir bar and diluted with anhydrous solvent. The experiment started when the substrate mixture was added. The reaction mixture was stirred at room temperature and samples were taken in regular intervals by microliter syringe. These samples were diluted with a great excess of solvent and filtered over pipettes filled with cotton and Celite in order to stop the reaction process by removal of the catalyst. Aliquots of the diluted samples were filled into 1.5 ml clear glass vials and subjected to gas chromatographic analysis applying a suitable temperature program.

4.7.2 Variation of Catalyst

In the first stage of catalytic testing, the three dinuclear copper(I) complexes **91** - **93** were compared to each other in the standard test reaction of phenylacetylene with benzyl azide in dichloromethane. Benzyl azide was synthesized according to a procedure reported in literature,[141] phenylacetylene was distilled prior to use and stored under inert gas. Dichloromethane was chosen as solvent as the solubility of the dinuclear complexes in dichloromethane is reasonably good and there were no solubility issues in the preparation of dichloromethane stock solutions with the desired concentrations. Moreover, the catalyst stock solutions were stored for several weeks at -30 °C without decomposition of the dicopper complexes, which had turned out to be stable in this non-coordinating solvent. Table 21 summarizes the results of these measurements. The catalytic performance of the three different catalysts was very similar. At the very beginning of the reaction, the mesityl-substituted catalyst **91** was the fastest reaching 50 % conversion after approximately 12 minutes, whereas the 4-tolyl substituted catalyst **93** reached 50 % conversion after about 15 minutes and the 3,5-xylyl substituted catalyst **92** after 19 minutes. However, the slope of the conversion diagram for the mesityl-substituted catalyst **91** flattens significantly from about 35 minutes on and this catalyst was out-performed by the other two catalysts. Full conversion was defined as the point where neither of the two substrate peaks was observed in the chromatogram anymore. With the mesityl-substituted catalyst **91**, full conversion was reached after one hour, whereas the 3,5-xylyl substituted catalyst **92** and the 4-tolyl substituted catalyst **93** gave full conversion after 45 and 50 minutes, respectively.

Table 21: Catalytic performance of dinuclear copper acetate catalysts in the CuAAC test reaction in dichloromethane (0.5 mol-% catalyst, room temperature, GC monitoring).

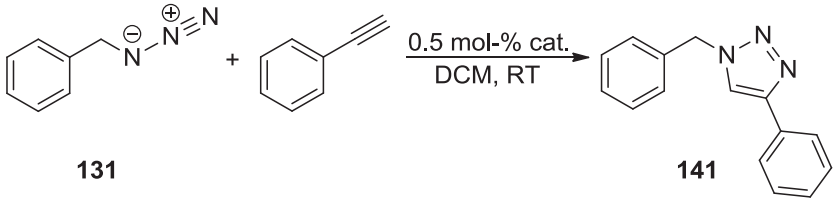

131 **141**

catalyst	conversion diagram	time[a)] [min]
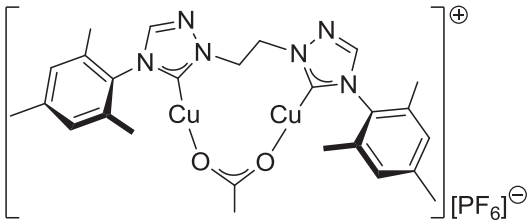 **91**	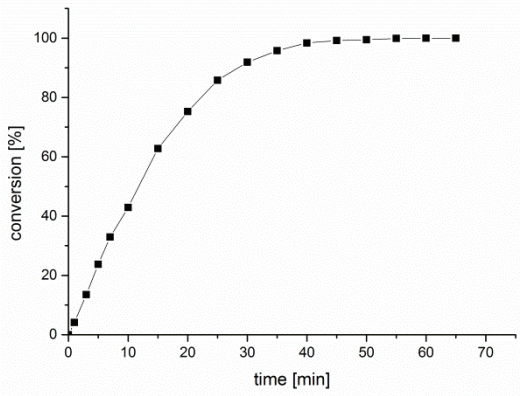	60
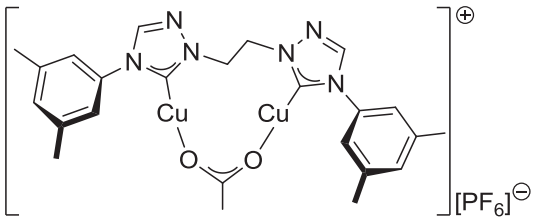 **92**	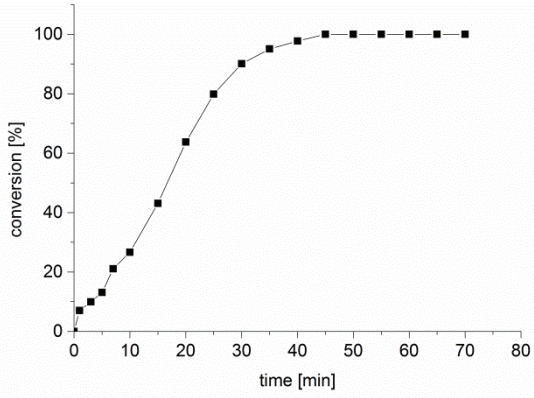	45
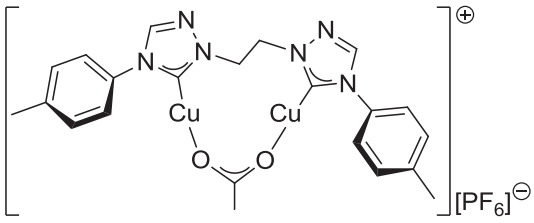 **93**	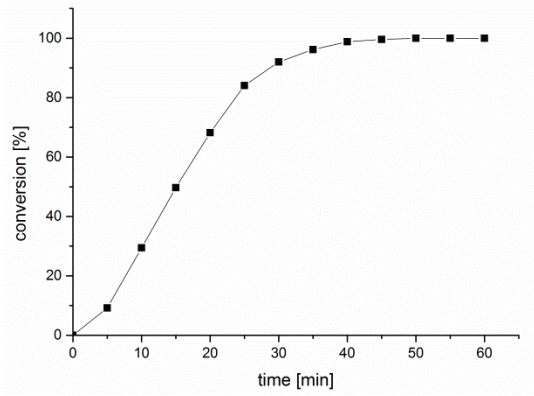	50

[a)]Reaction time until full conversion was observed by gas chromatography, *i.e.* none of the starting materials' peaks was detected anymore after the reaction time listed in this column.

The reaction mixtures remained homogeneous throughout the experiments. However, immediately after addition of the substrates, the solution turned yellow for up to approximately one minute and then returned to being colourless again. Such a change in colour has also been reported for CuAAC catalyses with copper(I) acetate[74] and is attributed to the formation of transient alkyne or acetylide copper complexes,[35, 74, 76] which have not been structurally identified. However, in the course of the reaction, 1,2,3-triazoles are formed, which can substitute the alkyne ligands. If dicopper alkyne complexes were yellow and the corresponding triazole complexes colourless, this would explain the fading of the reaction mixture's colour as the catalytic reaction progresses.

The dinuclear complexes **92** and **93** were found to be similarly active catalysts in the CuAAC test reaction, but as the 3,5-xylyl substituted catalyst **92** was easier to synthesize in very good yield (Scheme 51), this species was used for all subsequent experiments.

4.7.3 Variation of Substrates

Besides phenylacetylene, alkyne substrates with different electronic properties were used in CuAAC test reactions. With ethyl propiolate, the test reaction in dichloromethane proceeded faster than with phenylacetylene, probably due to the electron-withdrawing characteristics of the substituent, which might cause a change in the rate-determining step and the catalyst resting state of the CuAAC catalysis (see section 4.7.5). After 15 minutes, none of the starting materials could be detected by gas chromatography anymore. The reactions with 1-octyne and 2-methylbut-3-yn-2-ol, on the other hand, were slower due to the electron-donating properties of the substituents. With 1-octyne, the reaction was finished after 50 minutes and with 2-methylbut-3-yn-2-ol after 70 minutes.

As sterically demanding azide, 4,4'-(azidomethylene)bis(methylbenzene) was synthesized by variation of a procedure reported in literature.[24] In the reaction with phenyl acetylene, full conversion was observed after 225 minutes. Obviously, the steric hindrance of the azide strongly influences the rate of reaction. On the other hand, the reaction of 4,4'-(azidomethylene)bis(methylbenzene) with ethyl propiolate proceeded as fast as the latter's reaction with benzyl azide, most probably because the steric

encumbrance of the azide does not play a significant role in the reaction with a sterically uncritical alkyne.

In preparative experiments under identical reaction conditions, but without extraction of samples for GC analysis, the isolated yield was determined. The reaction mixture was diluted with dichloromethane and filtered over a Pasteur pipette filled with Celite. After evaporation of the solvent, ^{1}H NMR spectra showed the pure product. However, in order to remove inorganic impurities not visible in the NMR spectra, the product triazoles were subjected to short column chromatography. The values given in the fifth column of Table 22 are averages of two independent runs. These values prove that when full conversion is indicated by gas chromatographic measurements, the product has indeed been formed quantitatively.

Table 22: Catalytic performance of complex **92** in CuAAC reactions with different substrates.

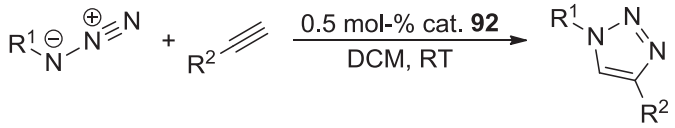

entry	R^1	R^2	reaction time[a)]	conversion	yield[b)]
1	Ph	Bn	45 min	quant.	96 %
2	*n*-hexyl	Bn	50 min	quant.	96 %
3	CMe_2OH	Bn	70 min	quant.	96 %
4	CO_2Et	Bn	15 min	quant.	98 %
5	Ph	$CH(Tol)_2$	225 min	quant.	98 %
6	CO_2Et	$CH(Tol)_2$	13 min	quant.	98 %

[a)] Reaction time until full conversion was observed by gas chromatography, *i.e.* none of the starting materials' peaks was detected anymore after the reaction time listed in this column. [b)]Isolated yield after purification by short column chromatography; average of two independent runs.

4.7.4 Variation of Solvent

In order to assess the range of solvents suitable for homogeneous CuAAC with dinuclear complex **92**, catalyst and substrate stock solutions in acetone, acetonitrile, THF and DMSO were prepared. As dodecane does not mix with the polar solvents

DMSO and acetonitrile, toluene was added instead of dodecane. However, as the response factors were based on dodecane, a quantitative interpretation of conversion was not possible and thus, only the reaction time was determined in the case of these solvents. As the product triazole **141** precipitated during the course of the reaction when acetone or acetonitrile were used as solvents, quantitative determination of conversion was not feasible with these solvents, as the relative concentration of the product in the aliquots taken for GC analysis was too small. Again, only the end of the reaction could be determined by the absence of both starting materials' peaks in the gas chromatograms.

Table 23: Catalytic performance of complex **92** in the CuAAC test reaction of benzyl azide with phenylacetylene in different organic solvents.

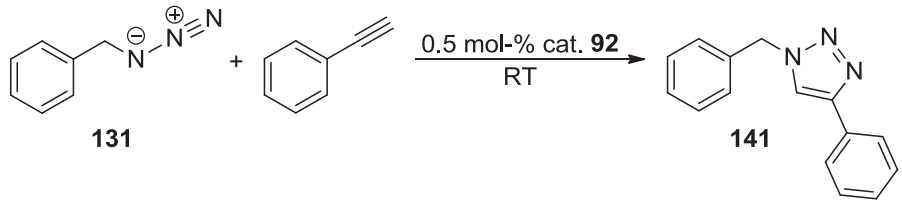

131 **141**

entry	solvent	reaction time[a)]	conversion
1	acetone[c)]	135 min	quant.
2	acetonitrile[b), c)]	35 min	quant.
3	DCM	45 min	quant.
4	DMSO[b)]	> 720 min	quant.
5	THF	270 min	quant.

[a)] Reaction time until full conversion was observed by gas chromatography, *i.e.* none of the starting materials' peaks was detected anymore after the reaction time listed in this column. [b)]Due to the immiscibility with dodecane, toluene was added as standard. [c)]The product triazole precipitated.

The reaction in DMSO proceeded very slowly and traces of the starting material could still be detected after twelve hours reaction time. In THF the reaction was completed within 270 minutes and the reaction in acetone was twice as fast with full conversion after 135 minutes. These observations are in accordance with Nolan's report regarding the catalytic performance of $[(ICy)_2Cu]PF_6$ in different organic solvents.[73] With 2 mol-% $[(ICy)_2Cu]PF_6$, the test reaction of phenylacetylene with benzyl azide at

room temperature reached full conversion within two hours in DMSO, after one hour in THF and after 30 minutes in acetone.

The best catalytic performance was observed in DCM and acetonitrile. However, as described in paragraph 4.6, crystallization of complex **92** from acetonitrile/diethyl ether led to decomposition of this complex and formation of the coordination polymer **92p** shown in Figure 39. It is thus not definitely clear, which is the catalytically active species in this reaction carried out in acetonitrile. However, the reaction mixture remains colourless during the course of the reaction and the precipitate formed was identified to be the product. As the crystalline coordination polymer was only obtained from a re-crystallization assay after months, in the course of which the solution had turned yellow-green, it is rather improbable that decomposition takes place within 35 minutes and it does thus seem justifiable to assume that decomposition products are not the reason for the very good catalytic activity in acetonitrile solution. Otherwise a better catalytic activity would also be expected for reactions in acetone solution, as the dinuclear complex **91** had also been shown to decompose in this solvent after several weeks (Figure 38).

4.7.5 Variation of Catalyst Concentration

As the energetically most favourable mechanistic pathway of the CuAAC reaction was suggested to proceed with participation of dinuclear copper species, the order of reaction with respect to the concentration of dinuclear copper(I) catalysts was expected to be one, as the resting state as well as the transition state of the rate-determining step were assumed to contain the same number of copper(I) ions, namely two (Scheme 43). In order to determine the order of reaction with respect to dinuclear complex **92** experimentally, reactions with different concentrations of **92** were carried out in dichloromethane at room temperature. At intervals, samples of the reaction mixture were taken and analyzed by gas chromatography. The stoppage of the catalysis in these samples was ensured by dilution with a great excess of solvent and filtration over a Pasteur pipette filled with Celite. From the integral of the triazole peak in the chromatograms, the half value period, *i.e.* the time after which 50 % conversion had been reached, was determined by intrapolation.

Equation 3 gives the relationship between the half value period and the concentration of the catalyst. In the first line, the rate law is expressed in a general way with k being

the rate constant and n and m real numbers, which represent the order of reaction with respect to the concentration of substrate and to the concentration of catalyst, respectively. This equation is integrated starting from the initial concentration c_0(substrate) of the substrates at t = 0 and ending with half of the starting concentration $c_{1/2}$(substrate) at the half value period $t_{1/2}$. If the substrates' concentration is identical for a series of experiments, the half value periods measured in these experiments should be proportional to the inverse of the catalyst concentration to the m-th power. Thus, if the reaction were first order in the catalyst concentration, the half value period should be inversely proportional to c(cat.).

Equation 3: General kinetic relationship between the half value period $t_{1/2}$ and the catalyst concentration (c = concentration, k = rate constant, n = rate order with respect to the substrate, m = rate order with respect to the catalyst resting state concentration; for calculating the indefinite integral in line 2 for n = 1, $\int \frac{1}{c}\, dc = \ln c$ needs to be considered).

$$\frac{d\, c(\text{substrate})}{dt} = -k\, c^n(\text{substrate})\, c^m(\text{cat.})$$

$$\int_{c_0(\text{substrate})}^{c_{1/2}(\text{substrate})=\frac{1}{2}c_0(\text{substrate})} \frac{1}{c^n(\text{substrate})\; c^m(\text{cat.})}\, d\, c(\text{substrate}) = -\int_{t=0}^{t_{1/2}} k\, dt$$

$$\frac{1}{c^m(\text{cat.})} \left[\frac{1}{(1-n)}\, c^{1-n}(\text{substrate})\right]_{c_0(\text{substrate})}^{c_{1/2}(\text{substrate})} = -k\, t_{1/2}$$

As c_0(substrate) and therefore $c_{1/2}$(substrate) are the same for all experiments in this study, it follows:

$$\frac{1}{c^m(\text{cat.})} \sim t_{1/2}$$

Each serial dilution was carried out with the same catalyst and substrates' stock solution. The results of different series cannot be compared to each other and no mean values and standard deviations have been calculated, as the measured half value periods differ significantly from each other, but are coherent within one series of experiments. However, the errors regarding the weighting in of substrates and catalyst,

the volumetric error in the preparation of the GC assays, the error regarding the integration of peaks in the GC chromatogram and the error in the moment of sample taking are probably large. In consequence, the results presented herein can only be considered as a mark of distinction between different reaction orders.

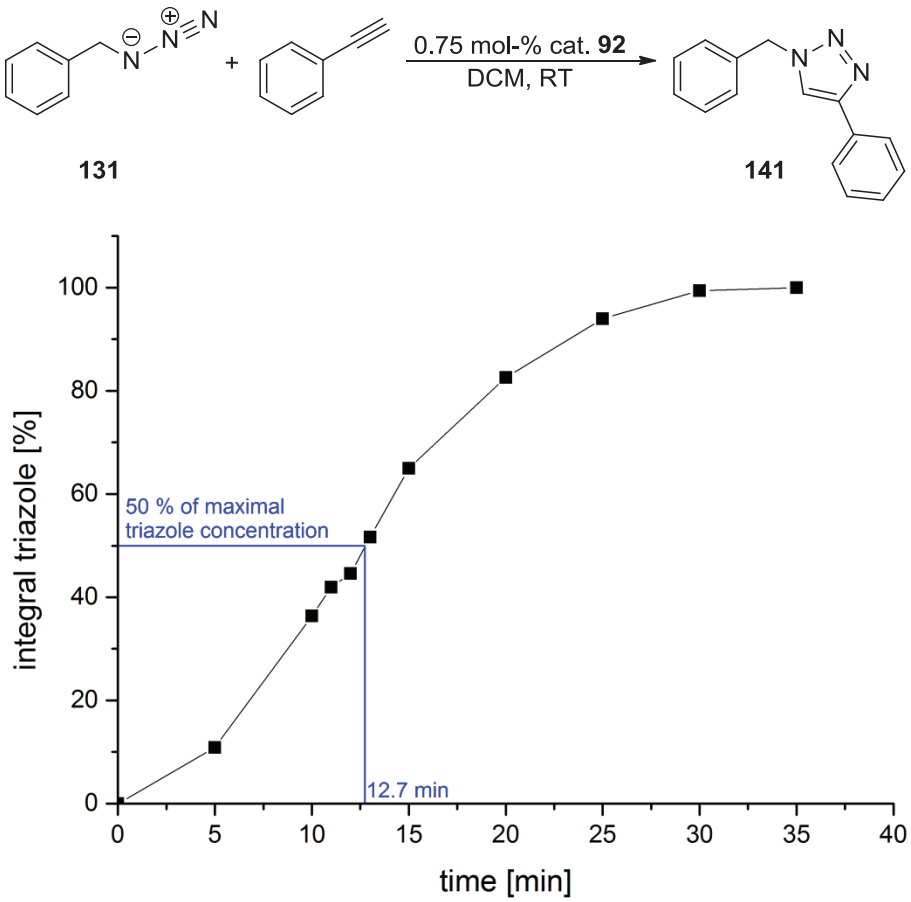

Figure 48: Graphical determination of the half value period for the reaction of benzyl azide with phenylacetylene in DCM at room temperature in the presence of 0.75 mol-% **92**.

Figure 48 shows exemplarily how the half value periods have been determined. The largest normalized product integral measured was set 100 %. At half the value of this normalized integral, the two nearest points on the slope were connected by a line and the time of the 50 % value read off. All half value periods determined by this method in one series of experiments are presented in Table 24.

Table 24: Half value periods determined for different concentrations of complex **92** in the CuAAC test reaction of benzyl azide with phenylacetylene in DCM at room termperature.

concentration of complex **92** [mol-%]	concentration of complex **92** [μmol ml^{-1}]	half value period $t_{1/2}$ [a)] [min]
0.75	2.98	12.7
0.62	2.49	15.4
0.50	1.99	18.6
0.37	1.49	23.0
0.25	0.99	29.3
0.12	0.50	46.4

[a)]The half value period was determined by intrapolation between the two data points nearest to 50 % in the diagram that represents the measured integrals [%] of the triazole product in the reaction mixture (Figure 48).

According to Equation 3 for m = 1, a linear correlation between the measured half value periods and the inverse of the concentration is expected for a series of experiments with the same substrate concentrations. Figure 49 displays a diagram in which the measured half value periods (ordinate) are plotted against the inverse concentration of complex **92** (abscissa). It is obvious that there is no linear correlation between these two parameters.

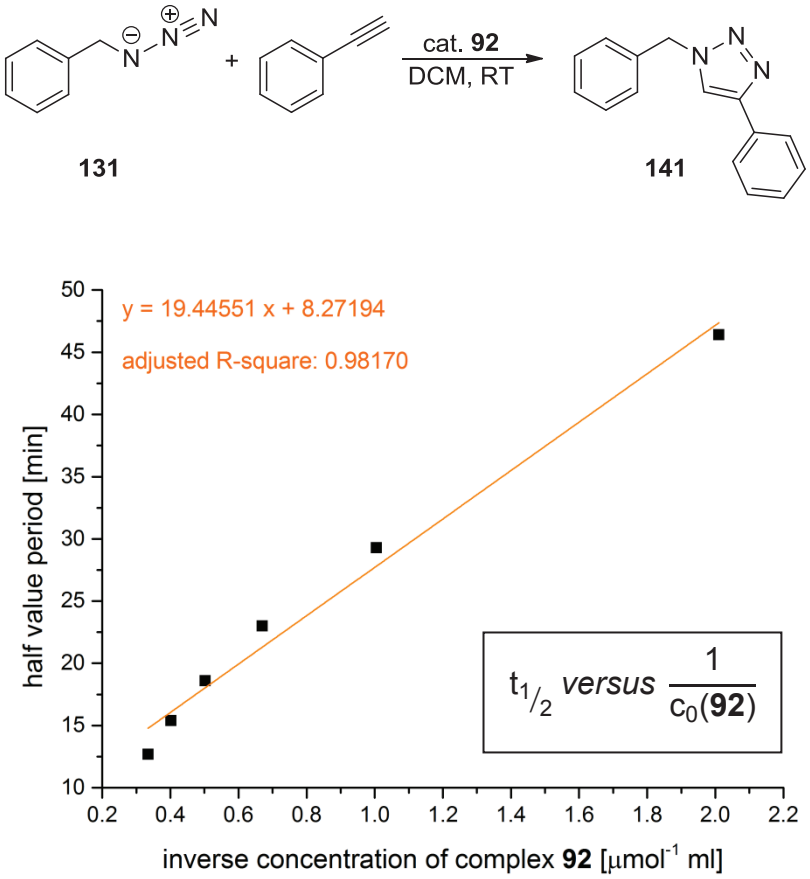

Figure 49: Plot of the experimentally determined half value periods of the CuAAC reaction between benzyl azide and phenylacetylene (Table 24) against the inverse initial concentration of dicopper complex **92**.

In order to determine the order of reaction m with respect to the concentration of the dinuclear copper complex **92**, the half value periods were plotted against c^{-m}(**92**) with different values for m. It turned out that the best correlation was found for m = 0.5. Figure 50 shows the plot of the experimentally determined half value periods against the square root of the inverse catalyst concentration.

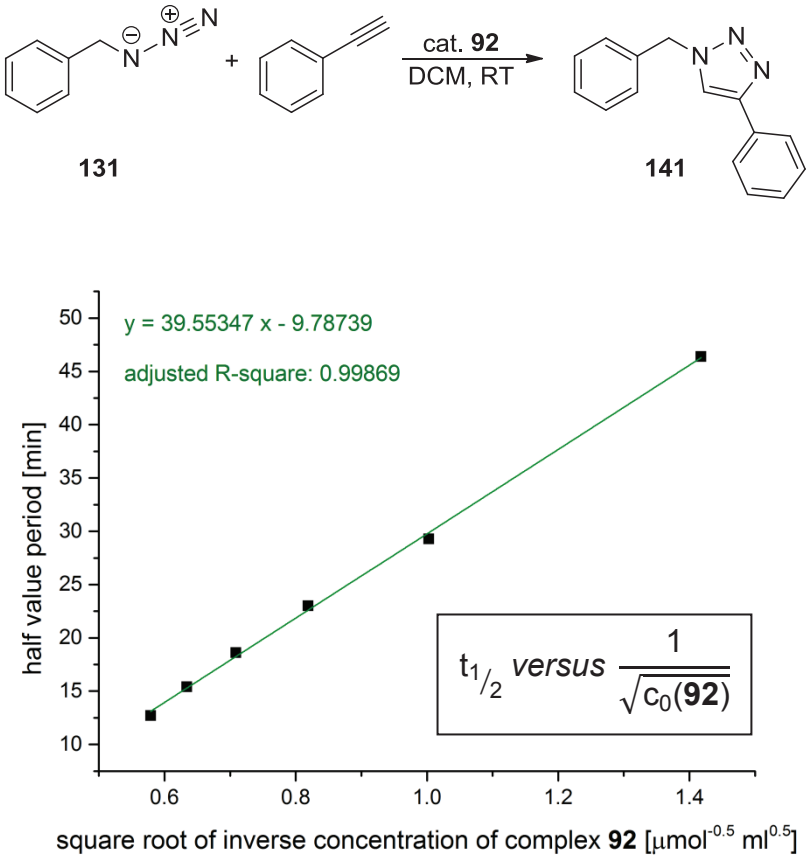

Figure 50: Plot of the experimentally determined half value periods of the CuAAC reaction between benzyl azide and phenylacetylene (Table 24) against the square root of the inverse initial concentration of dicopper complex **92**.

These findings hint at an order of reaction of m = 0.5 with respect to the initial concentration of dinuclear copper complex **92** for the CuAAC reaction between phenylacetylene and benzyl azide in dichloromethane:

$$t_{1/2} \sim \frac{1}{\sqrt{c_0(\mathbf{92})}}$$

Having obtained this unexpected result, a similar series of measurements was carried out with ethyl propiolate as alkyne substrate. The half value period was determined by the same procedure as illustrated in Figure 48. However, due to the faster reaction the measurements were not as accurate as in the case of phenylacetylene. Again, the experimentally determined half value periods (ordinate) were plotted against the inverse catalyst concentration (abscissa). However, the correlation between these two parameters was not satisfying (Figure 51, upper part).

Table 25: Half value periods determined for different concentrations of catalyst complex **92** in the CuAAC test reaction of benzyl azide with ethyl propiolate in DCM at room termperature.

concentration of complex **92** [mol-%]	concentration of complex **92** [μmol ml^{-1}]	half value period $t_{1/2}$ [a)] [min]
0.74	2.98	2.3
0.62	2.49	3.3
0.49	1.99	5.6
0.37	1.49	8.0
0.25	0.99	16.4
0.12	0.50	50.2

[a)]The half value period was determined by intrapolation between the two data points nearest to 50 % in the diagram that represents the measured integrals [%] of the triazole product in the reaction mixture (Figure 48).

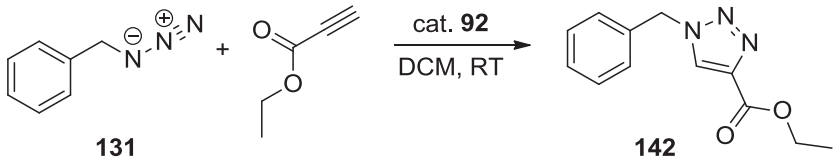

131 142

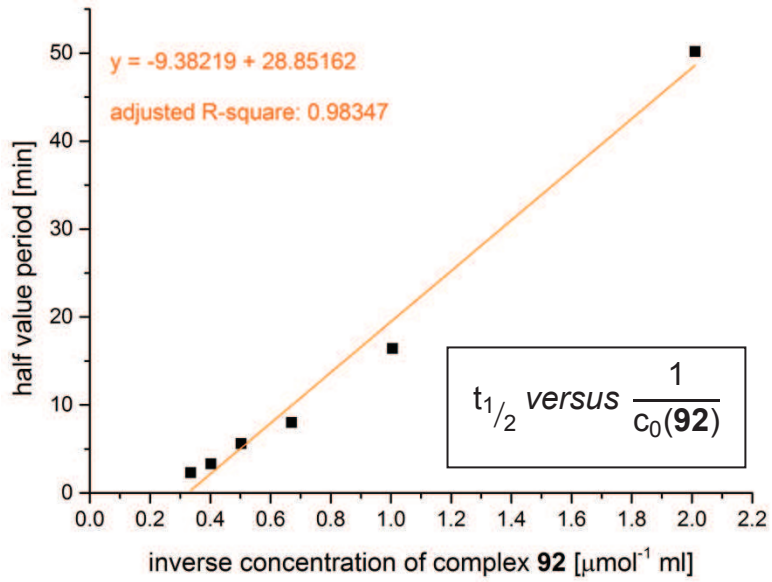

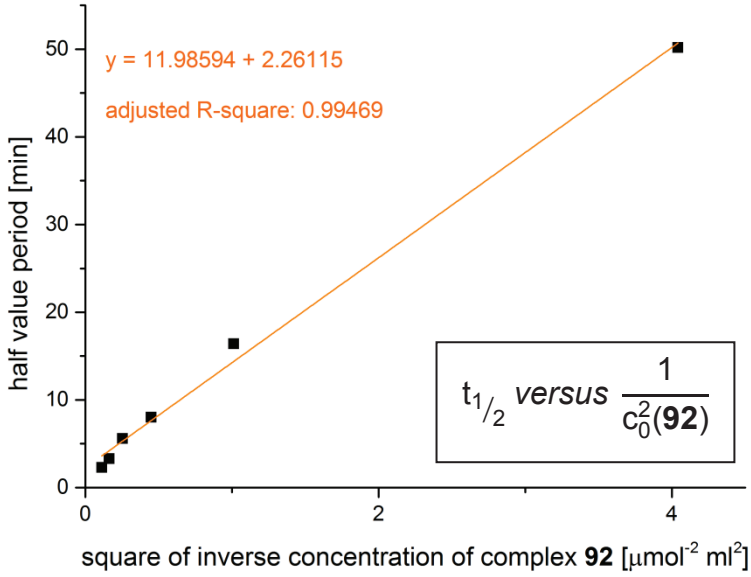

Figure 51: Plots of the experimentally determined half value periods of the CuAAC reaction between benzyl azide and ethyl propiolate (Table 25) against the inverse initial concentration of complex **92** (m = 1, upper part) and the square of the inverse concentration (m = 2, lower part).

Assuming an order of m = 2, the graph shown in the lower part of Figure 51 was obtained. Although the correlation is slightly better than for m = 1, it is still unsatisfac-

tory. The best fit to the experimental data was found with m = 1.5, *i.e.* a one and a half order rate dependence on the initial concentration of dinuclear complex **92**.

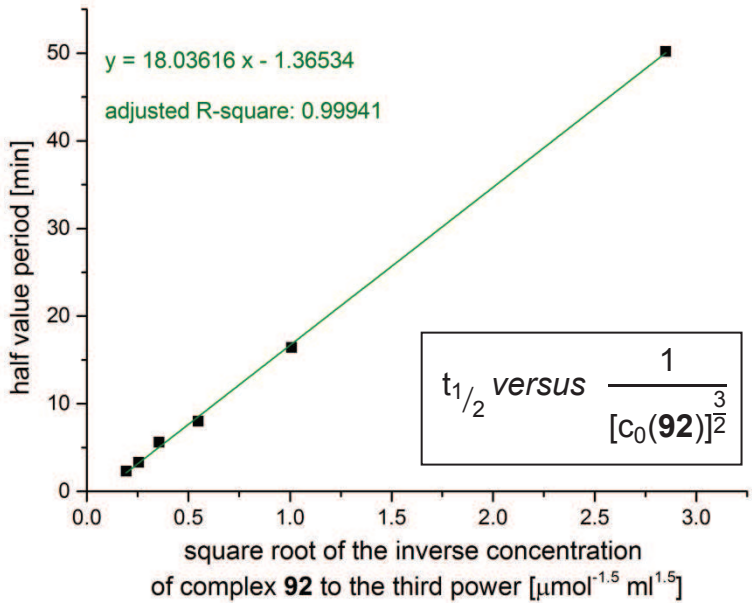

Figure 52: Plots of the experimentally determined half value periods of the CuAAC reaction between benzyl azide and ethyl propiolate (Table 25) against the square root of the inverse initial concentration of complex **92**.

In contrast to the analogous reaction with phenylacetylene, the experimentally determined order of reaction with respect to the concentration of dinuclear copper complex **92** is approximately m = 1.5 when ethyl propiolate is the alkyne starting material:

$$t_{1/2} \sim \frac{1}{[c_0(\mathbf{92})]^{\frac{3}{2}}}$$

Even though the error in this series of reactions is larger due to the higher rate and the hence less precise determination of half value periods, the difference between the reactions with phenylacetylene on the one hand and ethyl propiolate on the other hand is obvious. This change in the order of reaction with respect to the initial concentration of dinuclear complex **92** might be explained by proposing different resting states and rate-determining steps for CuAAC reactions with ethyl propiolate and phenylacetylene as alkyne substrates (Scheme 55).

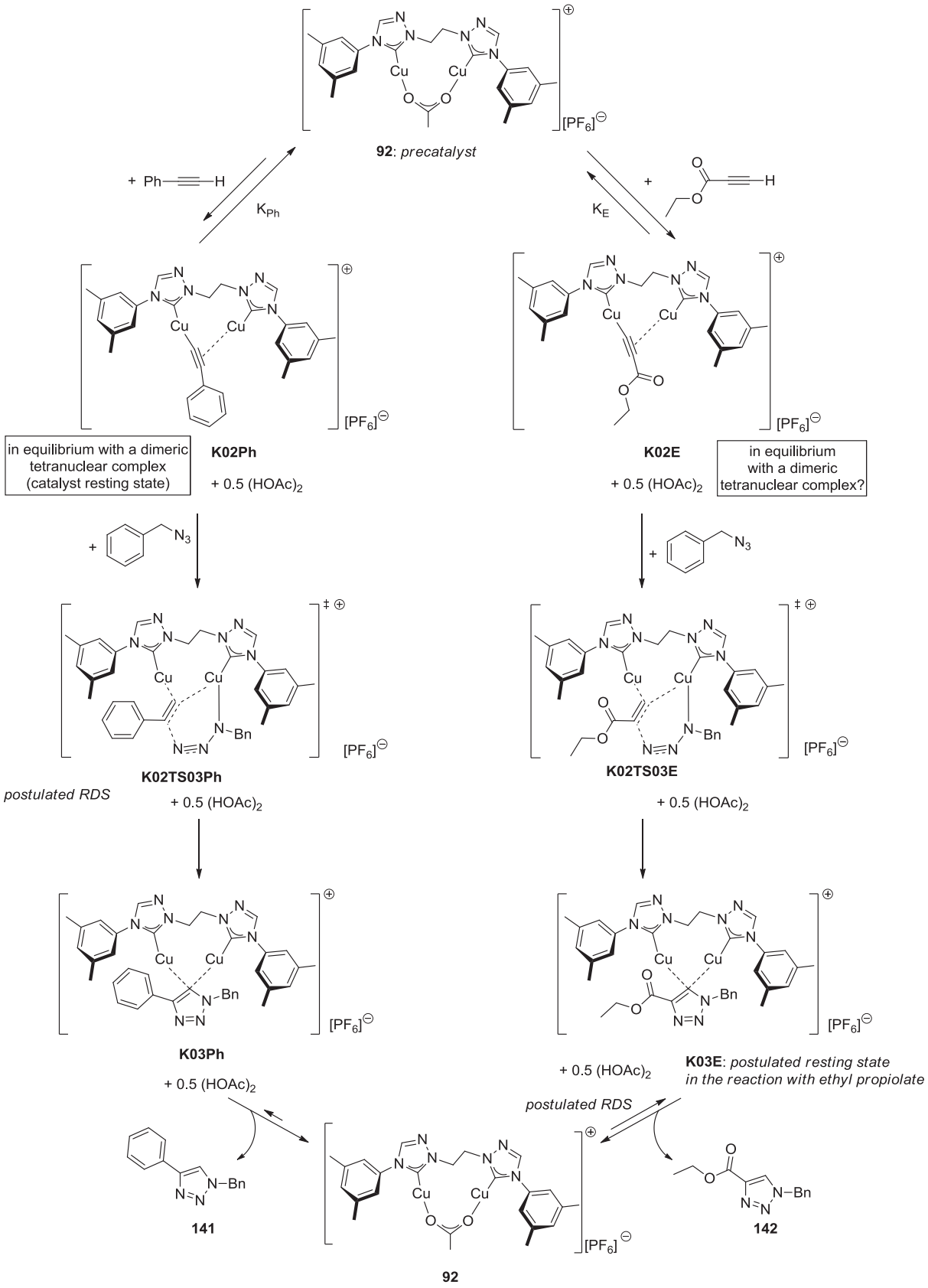

Scheme 55: Mechanistic hypothesis for explaining the results from kinetic measurements.

Scheme 55 displays the proposed reaction mechanism for the CuAAC reaction with dinuclear complex **92** for phenylacetylene (left) and ethyl propiolate (right) as alkyne substrates. In the first step of the mechanism, dicopper acetate precatalyst **92** reacts with the alkyne substrate to give the corresponding bridged acetylide complex **K02** in an equilibrium reaction. Due to the -M effect of the ester group -CO_2Et, ethyl propiolate is more acidic than phenylacetylene (PhC≡CH: pK_a^{DMSO} = 28.7).[142] In consequence, the formation of the acetylide complex and acetic acid (dimeric) is more favourable for ethyl propiolate as substrate than the deprotonation of phenylacetylene. The acetylide complexes **K02** shown in Scheme 55 might well dimerize to give the tetranuclear species analogous to the model complexes suggested by Straub.[31] In the case of phenylacetylene as substrate, the C-N bond-forming step is supposed to be rate-determining, as has been proposed by calculational studies reported in literature.[31-32] With ethyl propiolate, on the other hand, the C-N bond-forming reaction is supposed to proceed fast relative to the protonation of the copper triazolide intermediate **K03E**. Triazolide complex **K03E** is proposed to be the resting state of this transformation and its protonation by a coordinated molecule of acetic acid assumed to be the rate determining elementary step (Scheme 56), because this protonation is disadvantaged due to the ester group's -M effect that substantially lowers the electron density at the C5-position of the heterocycle. All in all, Scheme 55 summarizes the presumptions for explaining the experimentally determined orders of reaction for CuAAC reactions with ethyl propiolate and phenylacetylene in dichloromethane with dinuclear complex **92** as precatalyst: 1) with phenylacetylene, a tetranuclear acetylide complex is the assumed catalyst resting state and the C-N bond formation the rate-determining step; 2) with ethyl propiolate as substrate, dinuclear copper triazolide complex **K03E** is the catalyst's resting state and its protonation the rate-determining elementary step.

In order to explain the observed order of reaction m = 0.5 for the CuAAC reaction of phenylacetylene with dinuclear complex **92** as precatalyst, we must assume that the catalyst resting state contains twice the number of bis-NHC dicopper fragments as the transition state of the rate-determining step. A plausible equilibrium reaction for the dimerization of **K02Ph** is shown in Figure 53. The proposed dimeric resting state **(K02Ph)$_2$** needs to dissociate in order to arrive at the transition state **K02TS03** of the rate-determining elementary step.

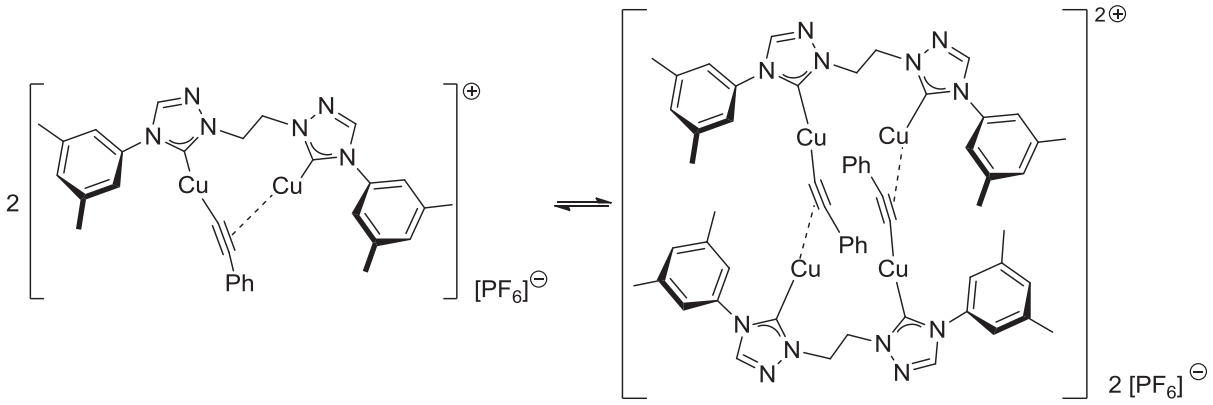

K02Ph **(K02Ph)$_2$**

Figure 53: Dimerization of **K02Ph** to give the resting state **(K02Ph)$_2$**.

Equation 4: Postulated rate law of the CuAAC reaction of phenylacetylene and benzyl azide in dichloromethane with precatalyst **92** and the C-N bond formation as rate-determining elementary step.

$$\frac{-d\,c(\text{phenylacetylene})}{dt} = k\,c^{n}(\text{azide})\sqrt{c[(\mathbf{K02Ph})_2]}$$

with $c[(\mathbf{K02Ph})_2] = \frac{1}{2}c_0(\mathbf{92})$:

$$\frac{-d\,c(\text{phenylacetylene})}{dt} = k\,c^{n}(\text{azide})\sqrt{\frac{1}{2}c_0(\mathbf{92})}$$

In contrast, the -M effect of the ester group has a two-fold significance for the CuAAC reaction's mechanism in the case of ethyl propiolate as substrate. On the one hand, the deprotonation of the alkyne substrate is facilitated so that the product side of the pre-equilibrium reaction is favoured even more strongly than for the reaction with phenylacetylene. On the other hand, the electron density at the C5-position of the heterocycle in the copper triazolide complex **K03E** is lower. As a consequence, the protonation of this intermediate is impeded. It is thus postulated that **K03E** is the resting state and the protonation of **K03E** by a coordinated molecule of acetic acid as shown in Scheme 56 the rate-determining step in the CuAAC reaction of ethyl propiolate in dichloromethane as aprotic solvent. Equation 5 states the rate law of the CuAAC reaction with ethyl propiolate on the basis of these assumptions.

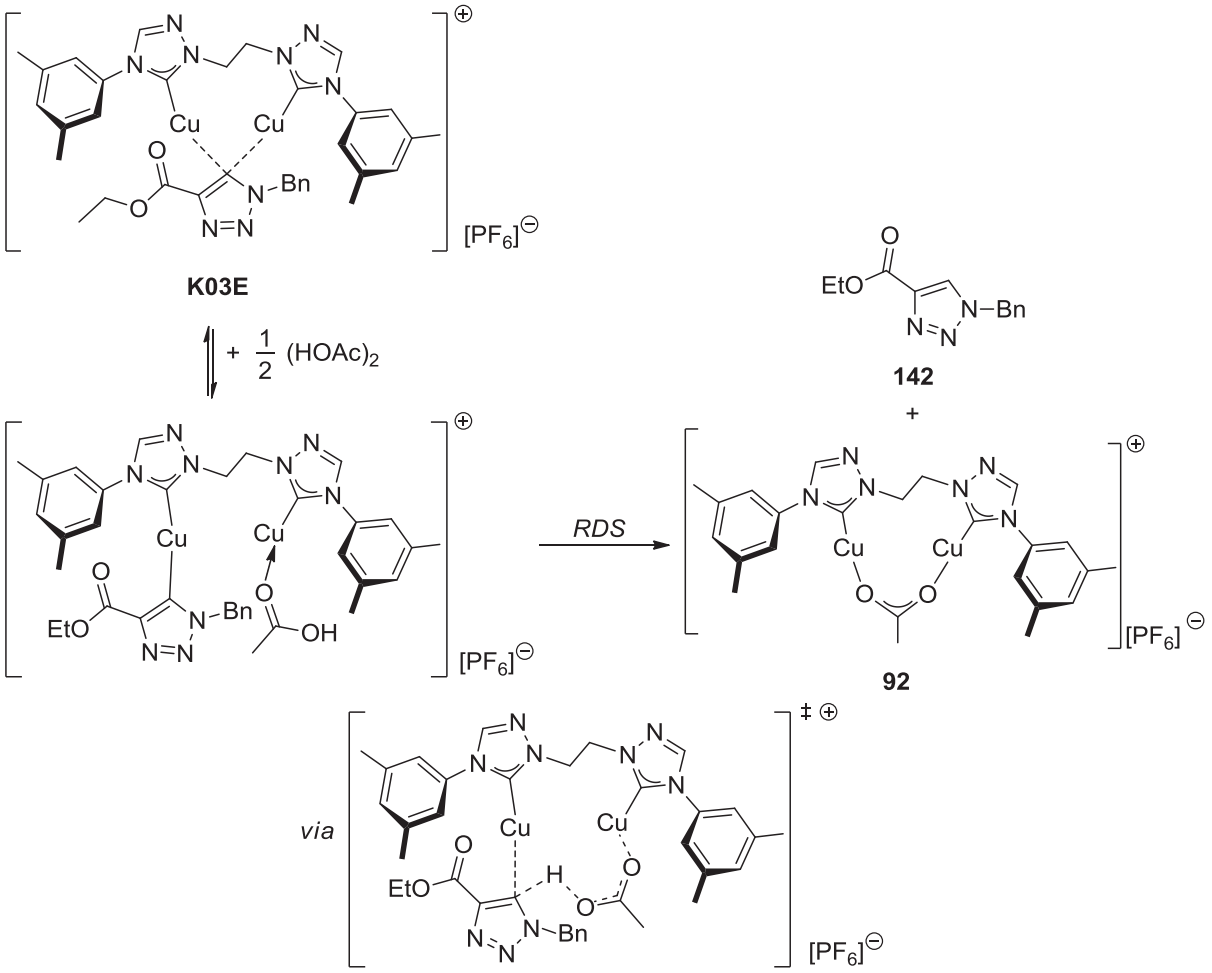

Scheme 56: Supposed rate-determining step for the CuAAC reaction with ethyl propiolate.

Equation 5: Postulated rate law of the CuAAC reaction of ethyl propiolate and benzyl azide in dichloromethane with complex **92** and the protonation of the triazolide complex as rate-determining elementary step.

$$\frac{-\mathrm{d}\,c(\text{ethyl propiolate})}{\mathrm{dt}} = k\,c(\mathbf{K03E})\sqrt{c[(HOAc)_2]}$$

The question that arises now is how the experimentally determined order m = 1.5 with respect to the initial concentration of dinuclear complex **92** can be explained. Assuming that the pre-equilibrium deprotonation of ethyl propiolate as well as the C-N bond forming reaction proceed fast, the concentration of the supposed resting state **K03E** can be substituted by the initial concentration of dinuclear precatalyst complex **92**. The stoichiometry of the fast pre-equilibrium deprotonation is 1:1, which means that the concentration of acetic acid is as high as the initial concentration of precatalyst complex **92**. However, as acetic acid mainly exists as a hydrogen-bonded

dimer in dichloromethane solution,[143] one equivalent of complex **92** gives 0.5 equivalents of this dimer $(HOAc)_2$. It thus follows that the rate of reaction would have an order of m = 1.5 with respect to the initial concentration of precatalyst complex **92** if acetylide complex **K03E** were the resting state and its protonation by a molecule of coordinated acetic acid the rate-determining elementary step (Equation 6).

Equation 6: Postulated rate law of the CuAAC reaction of ethyl propiolate and benzyl azide in dichloromethane with complex **92** as catalyst if complex **K03E** were the resting state.

$$c(\mathbf{K03E}) = c_0(\mathbf{92})$$

$$2\ c[(HOAc)_2] = c_0(\mathbf{92})$$

$$\frac{-d\ c(\text{ethyl propiolate})}{dt} = k\ c_0(\mathbf{92})\ \sqrt{\frac{1}{2}c_0(\mathbf{92})]}$$

$$\frac{-d\ c(\text{ethyl propiolate})}{dt} = \frac{1}{\sqrt{2}}\ k\ c_0^{\frac{3}{2}}(\mathbf{92})$$

The hypothesis of an equilibrium reaction between ethyl propiolate and complex **92** has been tested by an NMR experiment, in which ethyl propiolate (1 equivalent) has been added to a solution of complex **92** in dichloromethane in the absence of the azide substrate. A comparison of the NMR spectra shown in Figure 60 confirms that the reaction mixture does indeed contain acetic acid, some unaltered ethyl propiolate as well as at least two new species. In the presence of the azide, the deprotonation reaction of the alkyne substrate will be greatly favoured as the acetylide complex **K02E** reacts with the azide in a fast and irreversible elementary step, so that the concentration of **K02E** is steadily kept low.

4.8 Attempts for the Synthesis and Isolation of a Dinuclear Copper Acetylide Complex

At several stages of this project, it was attempted to isolate a molecularly defined dicopper complex with a μ-coordinated acetylide ligand.

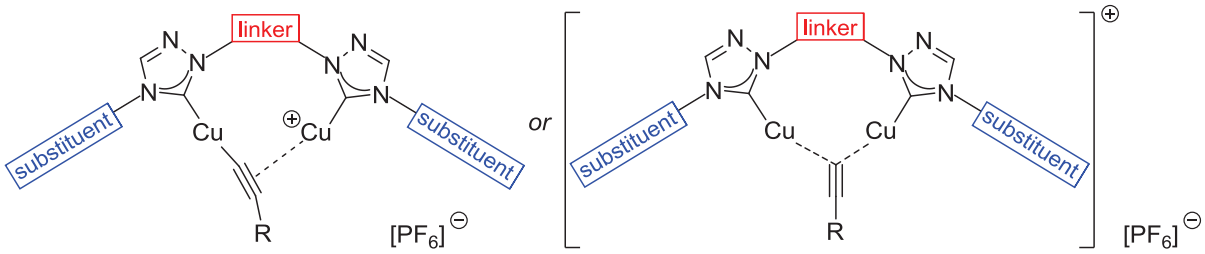

Figure 54: Structural outline of the desired acetylide dicopper(I) complex formulated with the acetylide ligand bound in a μ_2-η^1,η^2- (left) and μ_2-η^1,η^1-coordination mode (right).

Such a dicopper acetylide complex is supposed to be an important intermediate in the proposed mechanism of the CuAAC reaction shown in Scheme 9 and its isolation and characterization would further support this mechanistic picture. In consideration of the successful characterization of the monomeric NHC-copper(I) acetylide complexes [(IPr)Cu(C≡CPh)][23] and [(SIPr)Cu(C≡CPh)][24] it was hoped for the isolation of a molecularly defined and well soluble species instead of polynuclear insoluble material. In the report on the synthesis of [(SIPr)Cu(C≡CPh)],[24] the authors have also pointed out that this NHC copper(I) acetylide complex is only moderately stable and decomposes to polymeric copper phenylacetylide.

It was first attempted to synthesize copper(I) acetylide complexes directly from the ligand precursor bistriazolium salts and (phenylethynyl)copper(I) PhC≡CCu or (3,3-dimethylbut-1-yn-1-yl)copper(I) ^{t}BuC≡CCu. (Phenylethynyl)copper(I) was synthesized from copper(II) sulphate pentahydrate and phenylacetylene with hydroxylammonium sulphate as reducing agent following the procedures reported by Owsley and Castro.[76a] The obtained yellow solid was characterized by EI+ mass spectrometry and infrared spectroscopy. The elemental analysis showed traces of nitrogen in the (phenylethynyl)copper(I) sample, which indicates the presence of ammonia since the synthesis had been carried out in ammonia water. In an NMR experiment, four equivalents of this material were added to a solution of bistriazolium hexafluorophosphate

salt **51** in CD_3CN under inert gas. However, (phenylethynyl)copper(I) was completely insoluble and did not react with the bistriazolium salt. The reaction mixture was heated to 75 °C for 18 hours. After centrifugation of the yellow solid, the NMR spectrum of the acetonitrile solution showed complete deprotonation of the starting material as well as the formation of a new species. However, the ^{13}C spectrum did not show a signal in the downfield region (>160 ppm), where the resonance for carbene C-atoms would be expected. Moreover, the ESI+ spectrum only showed a peak at *m*/*z* = 539.19829 with the isotopic pattern of a single copper atom, which is in accordance with the formation of the bis-NHC monocopper complex $[C_{30}H_{32}CuN_6]^+$ under the experimental conditions in the mass spectrometer. At this stage, it had not been known yet that ESI+ mass spectrometry is not an equivalent method to decide whether dinuclear complexes are present in the product mixture, as it had only been observed after the successful synthesis of dinuclear copper(I) complexes that the ESI spectra do only show decomposition products of the latter.

Similar experiments were carried out with the more reactive acetylide (3,3-dimethyl-but-1-yn-1-yl)copper(I). Due to its greater instability, this reagent was not isolated, but prepared *in situ* by variation of the procedures reported by House and Umen.[144] The alkyne substrate *tert*-butylacetylene was reacted with methyllithium in ethereal solution to give the lithium acetylide. After the evolution of methane had ceased, this solution was transferred to a solution of tetrakis(acetonitrile)copper(I) hexafluorophosphate in acetonitrile at 0 °C. To this solution, the ligand precursor salt **51** dissolved in acetonitrile was added *via* syringe (Scheme 57).

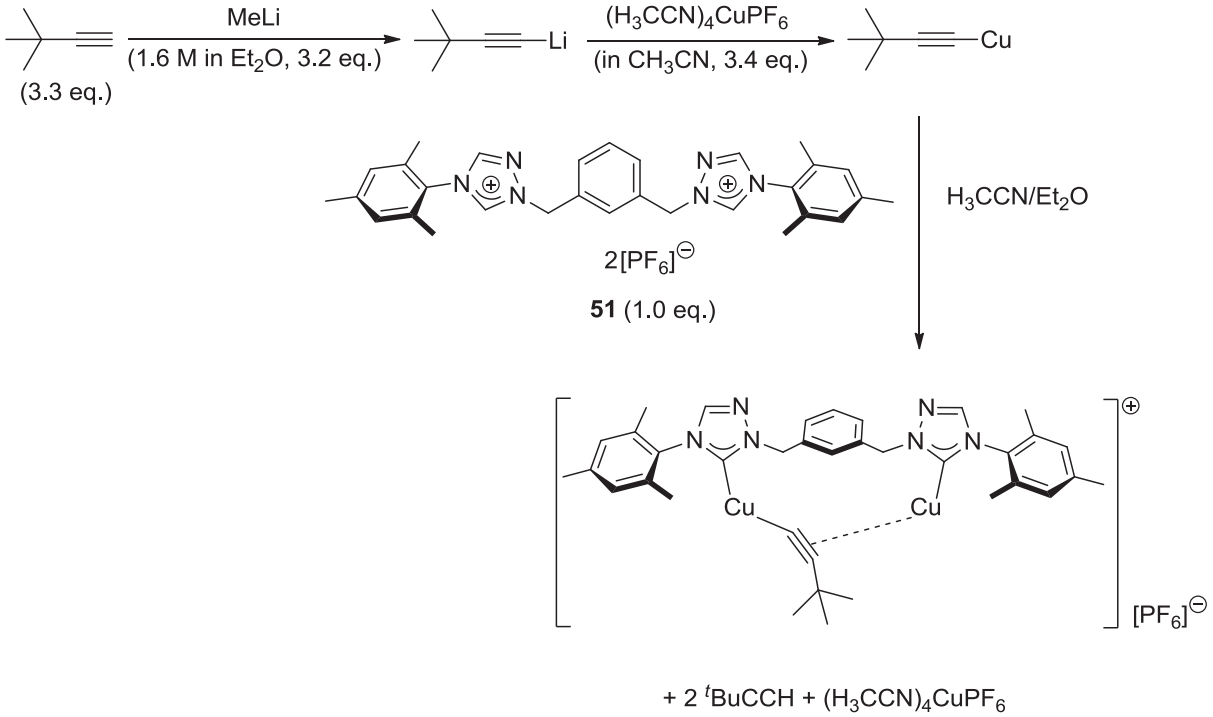

Scheme 57: Attempted synthesis of a bis-NHC dicopper acetylide species by reaction of the bistriazolium ligand precursor **51** with (3,3-dimethylbut-1-yn-1-yl)copper(I).

In the ^{1}H NMR spectrum of the raw product, complete deprotonation of the bistriazolium salt and the formation of a single new species were observed (Figure 55). However, the integrals in the alkyl region did not fit the desired product, even when considering that copper(I) *tert*-butylacetylide was used in excess. Again, the ESI+ spectrum only showed one peak at *m*/*z* = 539.19810 with the isotopic pattern of a single copper atom.

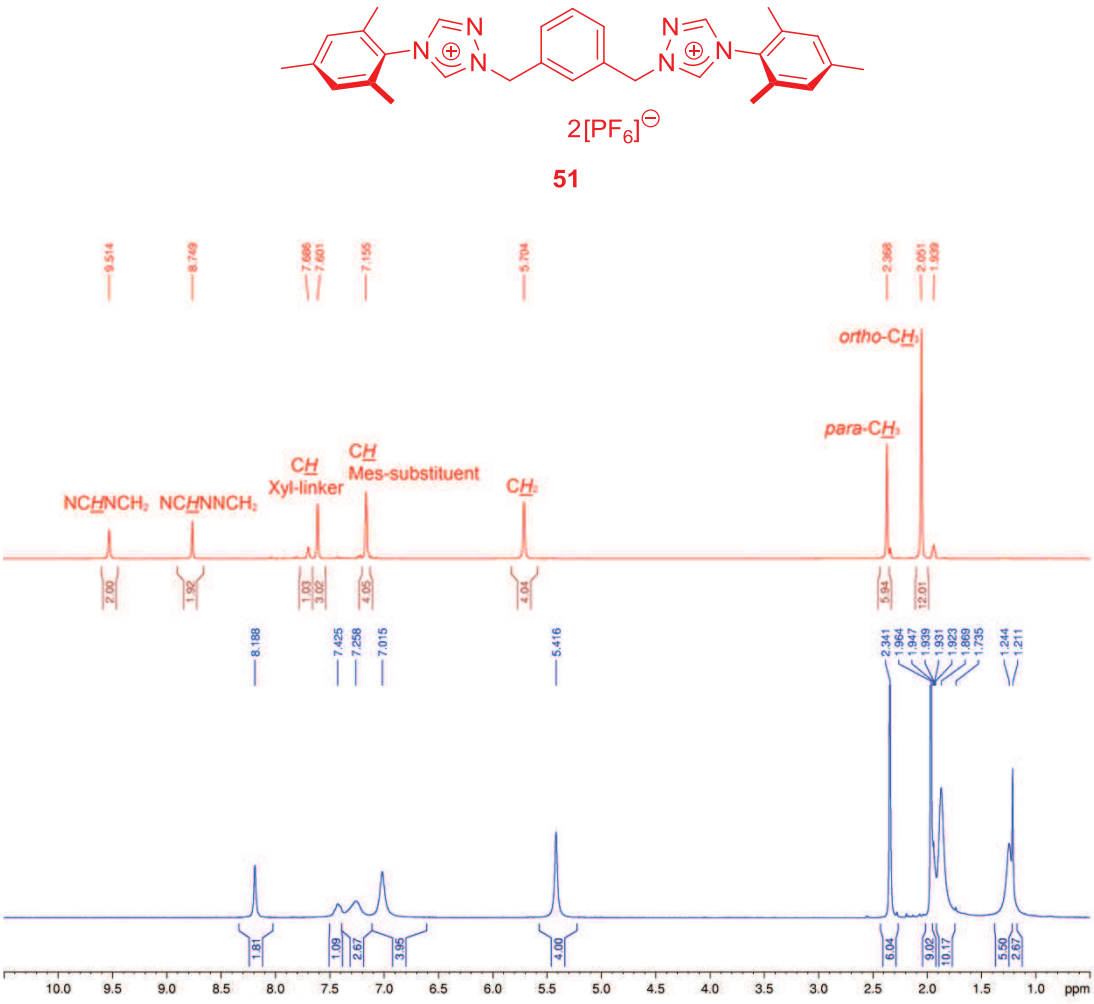

Figure 55: ^{1}H NMR spectra of the raw product in the reaction of bistriazolium hexafluorophosphate salt **51** with 3.2 equivalents of (3,3-dimethylbut-1-yn-1-yl)copper(I) (lower part, blue) in comparison with the reaction's starting material (upper part, red) (recorded in CD_3CN at 250 MHz).

As it was suspected that the linker length might be decisive for the stability of the μ_2-acetylide complex, a similar experiment was carried out with ethylene-linked bistriazolium salt **61** as ligand precursor. Five equivalents of *tert*-butylacetylene were reacted with 4.5 equivalents of methyllithium in ethereal solution. After the evolution of methane had stopped, this solution was transferred to a flask charged with an acetonitrile solution of tetrakis(acetonitrile)copper(I) hexafluorophosphate (2.5 equivalents) at 0 °C. The slightly yellow, cloudy solution was allowed to warm to room temperature and stirred for five minutes before an acetonitrile solution of **61** (1.0 equivalents) was added *via* syringe. The reaction mixture was stirred at room temperature for 18 hours. The ESI+ spectrum of the raw reaction mixture showed many signals, among them *m*/*z* = 479.16263, which stands for the bis-NHC monocopper species $[C_{25}H_{32}CuN_6]^+$. However, none of the peaks had the correct isotopic pattern for a

dicopper species. The ^{1}H NMR spectrum was inconclusive as well: a single new species was formed but the signals in the ^{1}H NMR spectrum were very broad, especially for the methylene protons, and the NCHN protons of the triazolylidene ligands were not equivalent anymore, but gave two signals with the intensity of one proton each. However, the intensities of the peaks in the alkyl region did not fit at all.

After the synthesis of dinuclear copper(I) complexes with acetate as sacrificial ligand had been achieved, a series of experiments was carried out in order to synthesize the corresponding dicopper acetylide complex. When mixing phenylacetylene with complex **91** in d_8-THF in the absence or in the presence of triethylamine, a bright yellow precipitate was formed immediately. Comparison of the ^{1}H NMR spectra of the acetate complex (**91**, Figure 56, upper part, green) and the raw product shows that a reaction giving a single new species had taken place: the resonances of the triazolium heterocycle, the mesityl substituent and the methylene group are shifted upfield from 8.54 ppm to 8.42 ppm, from 7.04 ppm to 6.93 ppm and from 5.34 ppm to 5.17 ppm, respectively.

For reference, the tetra-NHC complex corresponding to structural outline **III** in Scheme 50 was synthesized by mixing one equivalent of the bistriazolium hexafluorophosphate ligand precursor **61** with four equivalents of sodium acetate and only one equivalent of copper(I) acetate in THF and stirring this suspension for twelve days. Due to the shortfall of copper(I), tetra-NHC complex **111** was isolated as the sole product. Its ^{1}H NMR spectrum in d_8-THF is shown in the lower part of Scheme 51 (blue).

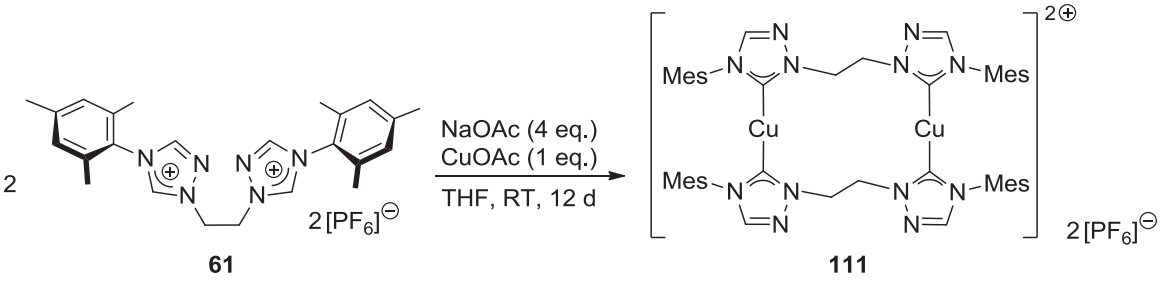

61 111

Scheme 58: Synthesis of the reference tetra-NHC complex bis-{μ-{1,1'-(ethane-1,2-diyl)bis[4-(2,4,6-trimethylphenyl-1*H*-1,2,4-triazol-5-ylidene]}-$\kappa C,\kappa C'$}dicopper(I) bis(hexafluorophosphate) (**111**).

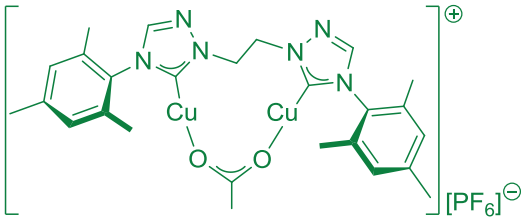

91

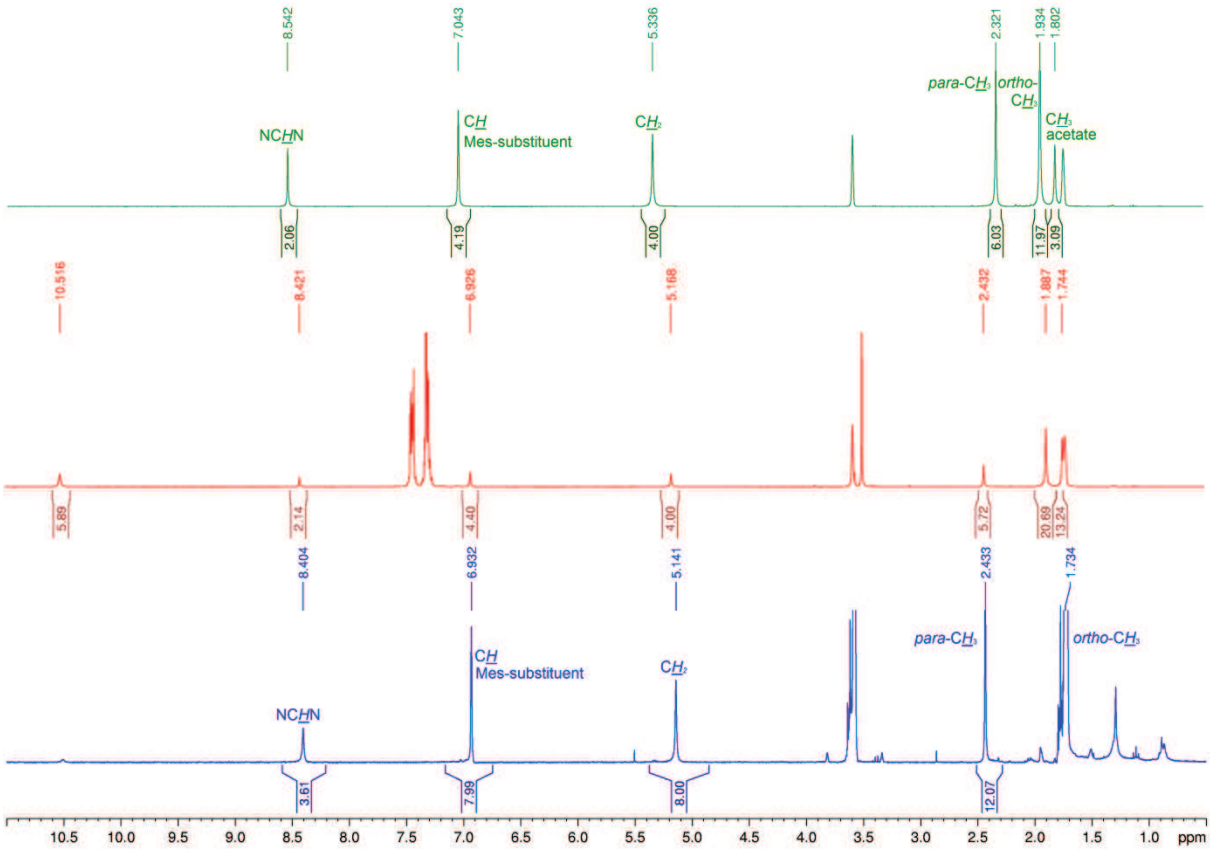

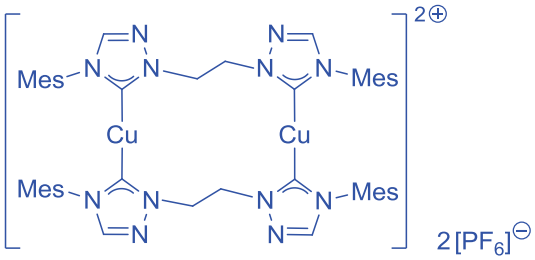

111

Figure 56: ^{1}H NMR of the raw product in the reaction of dicopper acetate complex **91** with phenylacetylene (middle, red) and comparison with the ^{1}H NMR spectra of the reaction's starting material (**91**, top, green) and the reference tetra-NHC dicopper complex (**111**, bottom, blue) (all spectra recorded in d_8-THF at 250 MHz or 300 MHz).

By comparison of the spectra in Figure 56 it becomes obvious that instead of the desired dicopper acetylide complex, tetra-NHC dicopper complex **111** was formed, probably by the equation given in Scheme 59.

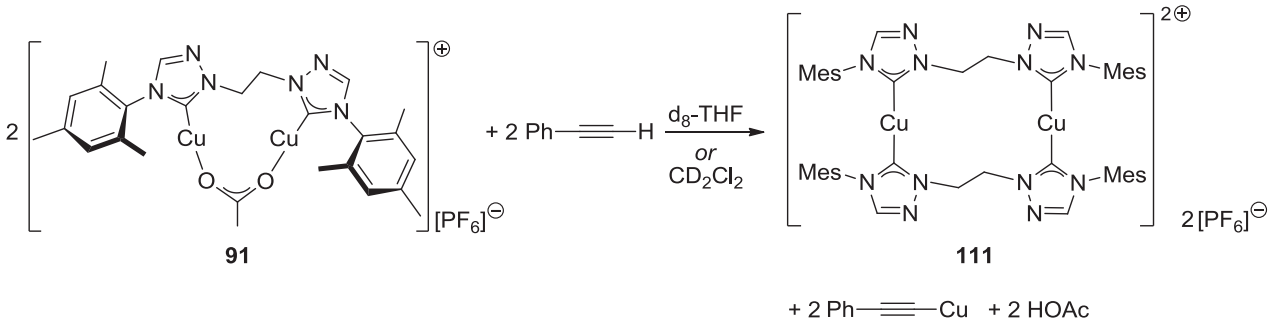

Scheme 59: Proposed equation to describe the formation of tetra-NHC dicopper complex **111** in the reaction mixture of dicopper acetate complex **91** with phenylacetylene in THF or dichloromethane.

The same experiment was carried out with *tert*-butylacetylene. Immediately after addition of the alkyne to the d_8-THF solution of complex **91**, the solution turned bright yellow and cloudy. The ^{1}H NMR spectrum of the reaction mixture was compared to the spectrum of the tetra-NHC dicopper complex **111** shown in Figure 56 (lower part, blue) and it was obvious that this complex had again been formed instead of the desired dicopper acetylide complex.

As coordinating solvents might be disadvantageous to this reaction, dicopper complex **91** was reacted with *tert*-butylacetylene and phenylacetylene in dichloromethane. With both alkyne substrates, the reaction mixture immediately turned bright yellow, but there was no precipitation. In the ^{1}H NMR spectra of the reaction mixtures the starting material as well as the tetra-NHC dicopper species shown in Scheme 59 were identified.

As further experiments with the alkyne itself did not seem to be promising, the corresponding lithium acetylide species were used from then on. When complex **91** was mixed with 2.5 equivalents of lithium phenylacetylide in d_8-THF, the solution immediately turned orange, but there was no precipitation. In the ^{1}H NMR spectrum of the reaction mixture, the formation of a new species was observed, but the peaks were very broad and due to the excess of lithium phenylacetylide, it could not be determined whether the acetylide ligand was present. In the corresponding ^{13}C NMR

spectrum, the carbene C-atom's resonance disappeared and the peak of the triazolium heterocycle's CH group was small and very broad. All other peaks of the ligand system were only slightly shifted, for example the methylene group's signal from 52.9 ppm in the starting material to 52.6 ppm in the reaction mixture. Altogether it remained unclear whether the desired dicopper acetylide was formed. However, for the first time the formation of the undesired tetra-NHC dicopper complex was not observed.

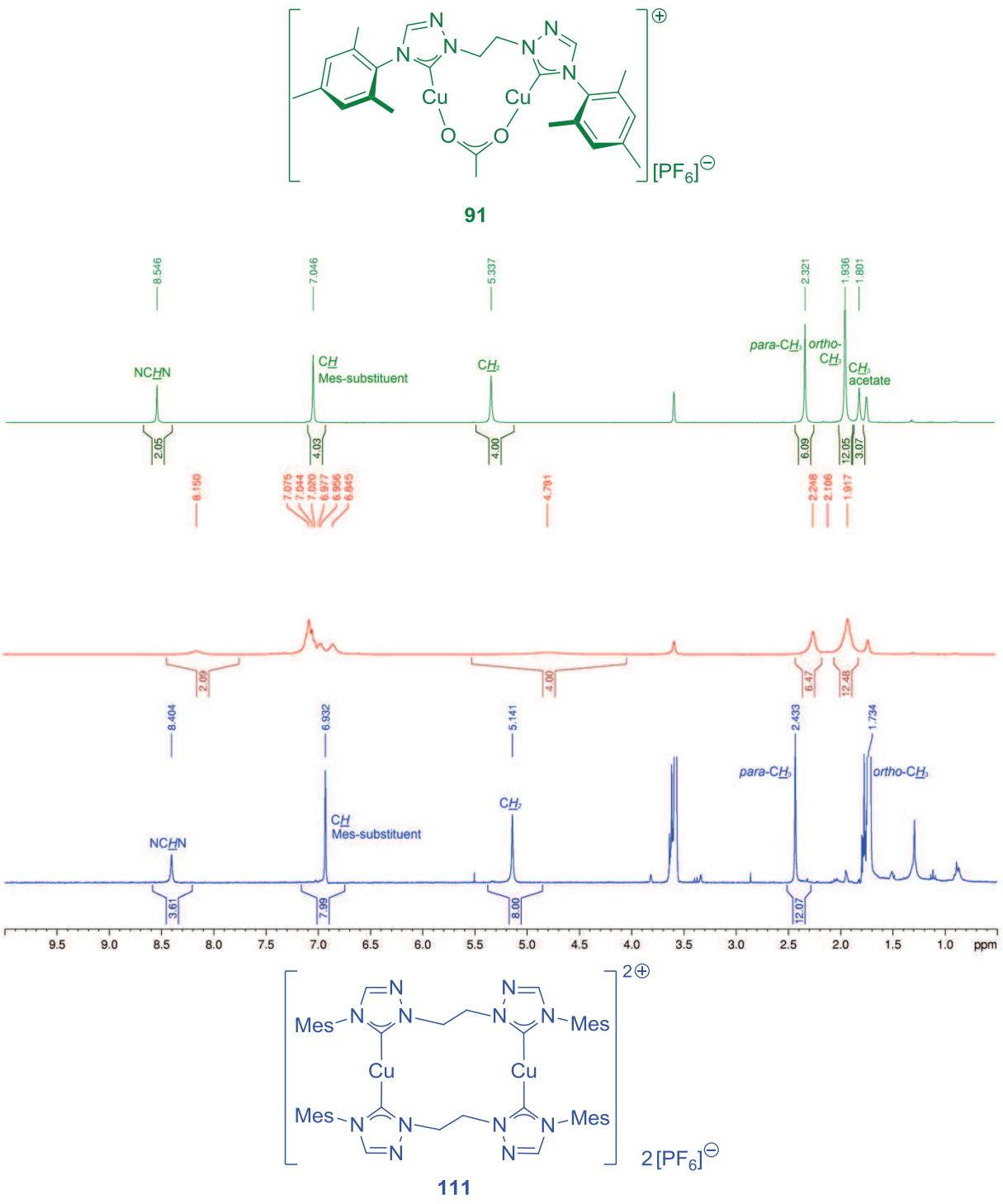

Figure 57: ^{1}H NMR spectrum of the raw product in the reaction of dicopper acetate complex **91** with lithium phenylacetylide (middle, red) and comparison with the ^{1}H NMR spectra of the reaction's starting material (**91**, top, green) and the reference tetra-NHC dicopper complex (**111**, bottom, blue) (spectra recorded in d_8-THF at 250 MHz and at 300 MHz).

The experiment was repeated with xylyl-subsituted complex **92** and lithium phenylacetylide. Complex **92** was hardly soluble in d_8-THF, but when a solution of lithium phenylacetylide was added, the reaction mixture turned orange and the precipitate

dissolved. The ^{1}H NMR spectrum of the reaction mixture shows that a conversion has taken place, but again the peaks are very broad. In comparison with the ^{1}H NMR spectrum of lithium phenylacetylide it also becomes clear that the acetylide has reacted as well since the peaks have significantly shifted. The corresponding tetra-NHC complex **112** is very poorly soluble in THF so that it is improbable that this undesired product was formed. A comparison of the NMR spectra of the starting material **92**, the complex formed in the reaction with lithium phenylacetylide and reference tetra-NHC complex **112** is shown in Figure 58. Although the spectrum of **112** has a very bad signal-to-noise ratio due to the complex' low solubility in THF, it is obvious that **112** is not the product of the reaction between **92** and lithium phenylacetylide. Instead, one of the "unstable, non-isolable intermediates" containing two copper(I) centres "that have to date eluded more conventional mechanistic studies" postulated by Fokin[25] based on *in situ* reaction calorimetry and metal isotope crossover experiments has probably been formed.

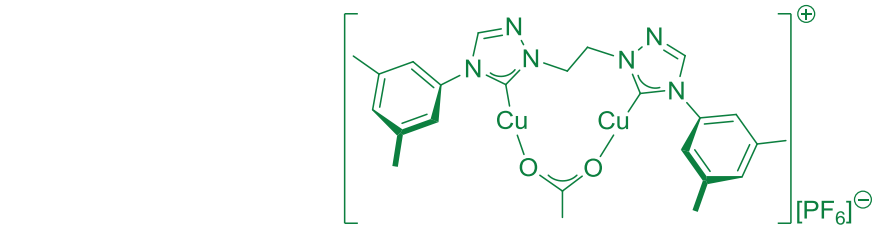

92

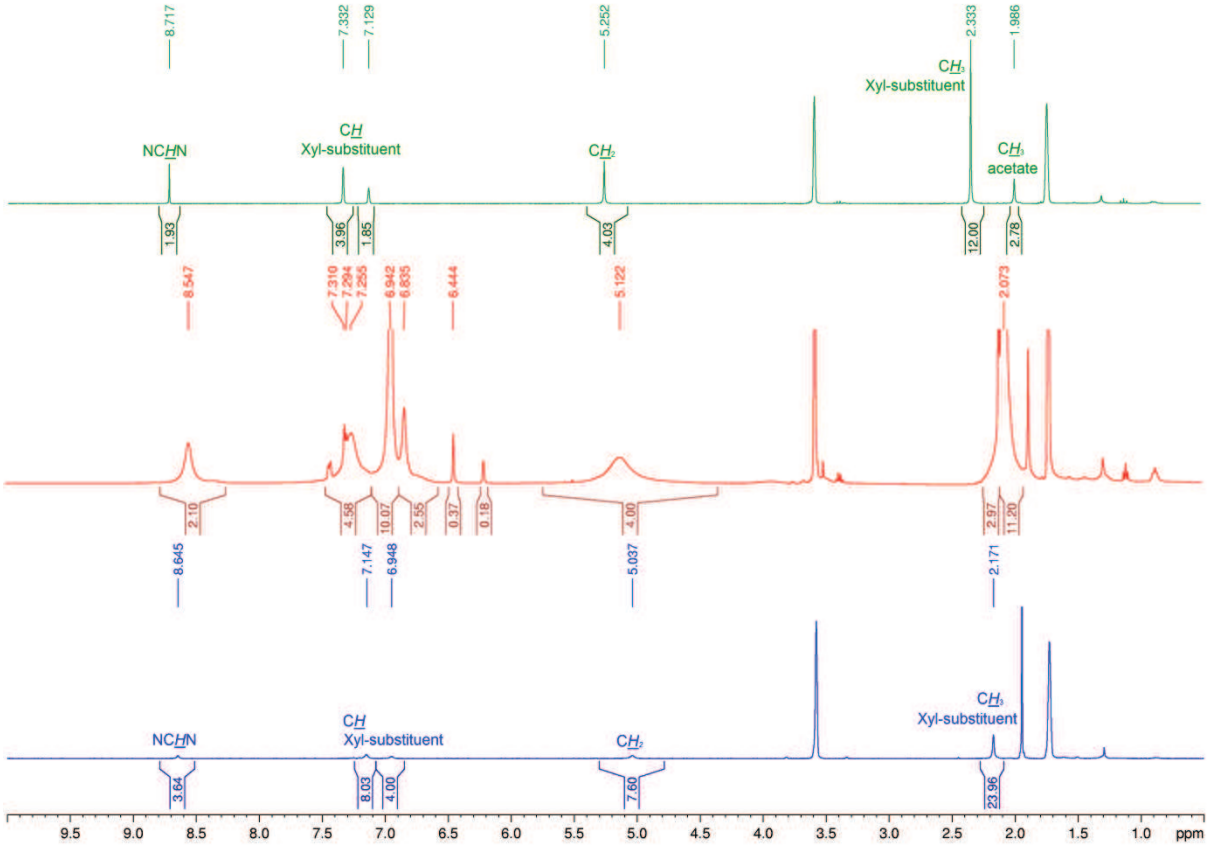

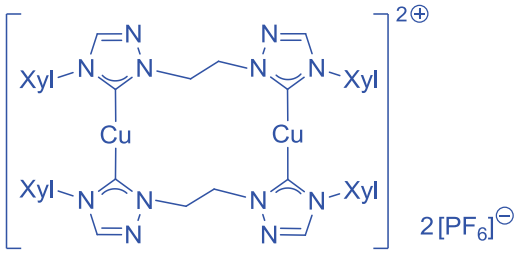

112

Figure 58: ^{1}H NMR spectrum of the raw product in the reaction of complex **92** with lithium phenylacetylide (in d_8-THF at 400 MHz, middle, red) and comparison with the ^{1}H NMR spectra of the reaction's starting material **92** (in d_8-THF at 250 MHz, top, green) and reference tetra-NHC dicopper complex **112** (in d_8-THF at 250 MHz, bottom, blue).

In an attempt to identify this new species, an ESI+ mass spectrum was taken. Although the base peak *m*/*z* = 435.13571 is again the signal corresponding to the

bis-NHC monocopper complex $[C_{22}H_{24}N_6(^{63}Cu)]^+$, the cationic monoacetylide complex gives a signal with 42 % intensity at *m*/*z* = 599.10486. The calculated mass for $[C_{30}H_{29}(^{63}Cu)_2N_6]^+$ is 599.10402 and thus fits well with the experimental value. Also, the observed isotopic pattern indicates that a dicopper complex is present.

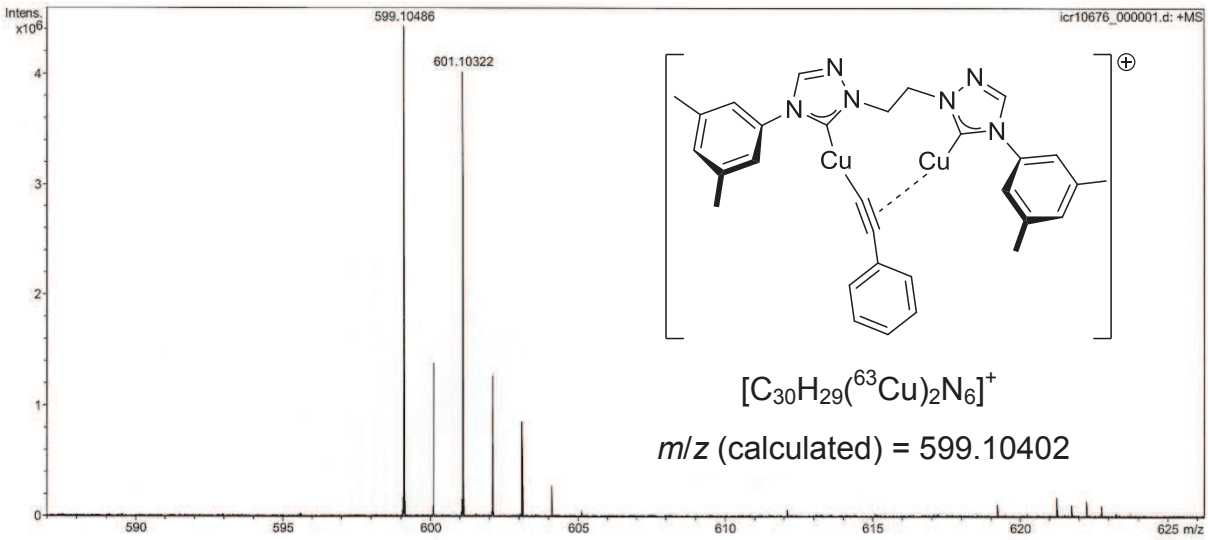

Figure 59: Excerpt from the ESI+ mass spectrum of the raw reaction mixture in the reaction of μ-acetato-$\kappa O,\kappa O'$- μ-{1,1'-(ethane-1,2-diyl)bis[4-(3,5-dimethylphenyl)-1*H*-1,2,4-triazol-5-ylidene]}-$\kappa C,\kappa C'$-dicopper(I) hexafluorophosphate (**92**) and lithium phenylacetylide.

In preparative assays, however, the desired bis-NHC dicopper acetylide complex shown in Figure 59 has not been isolated and fully characterized so far. Attempts to crystallize this compound always led to oxidation of the copper(I) species, which was indicated by the green or blue colour of the solution. Nevertheless, the results presented herein show that it might be possible to synthesize and fully characterize bis-NHC dicopper complexes with a bridging acetylide ligand analogous to the structural outline shown in Figure 54.

In the context of the kinetic experiments carried out in this work (section 4.7.5), it was tested whether a reaction takes place in the mixture of ethyl propiolate and complex **92** in dichloromethane at room temperature. It had been speculated that there is a pre-equilibrium between the starting materials ethyl propiolate and complex **92** and dinuclear copper acetylide complex **K02E**. In an NMR experiment, ethyl propiolate (1 equivalent) was added to dinuclear complex **92** in deuterated dichloromethane under inert gas conditions. Complex **92** is only partly soluble in dichloromethane,

which is the reason for the very broad signals observed in its ^{1}H NMR spectrum (Figure 60, upper part). However, upon addition of ethyl propiolate, the precipitate was completely dissolved and a yellow solution obtained. The ^{1}H NMR spectrum of this homogeneous mixture shows some left-over ethyl propiolate (peaks marked by red circles), but also acetic acid (broad peak at δ > 10 ppm) and at least two new species containing the ester group -CO_2Et, which is indicated by the signals in the alkyl region marked by light blue rectangles (Figure 60). For example, at least two new triplets are observed between 0.90 and 1.12 ppm and two new quartets between 3.68 and 4.14 ppm. Together with the remaining ethyl propiolate, this supports the idea of an equilibrium deprotonation reaction between complex **92** and substrate ethyl propiolate on the one side and acetic acid and a dicopper acetylide complex of unknown composition on the other side (Scheme 60).

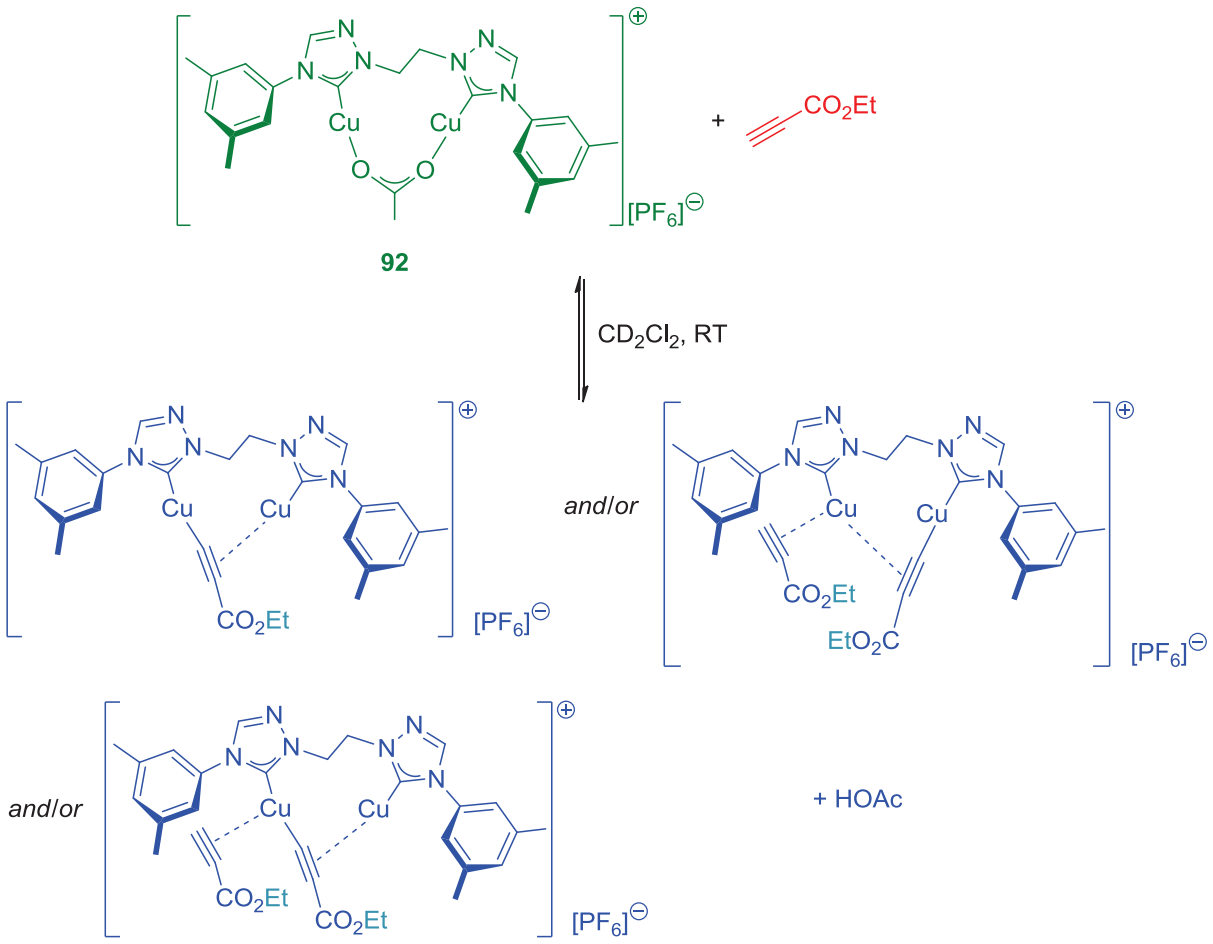

Scheme 60: Proposed equilibrium reaction between dinuclear complex **92** and ethyl propiolate in CD_2Cl_2 at room temperature.

After several hours, a greenish precipitate was observed in the reaction mixture, which hints at decomposition of copper(I) complexes in favour of the formation of copper(II) species.

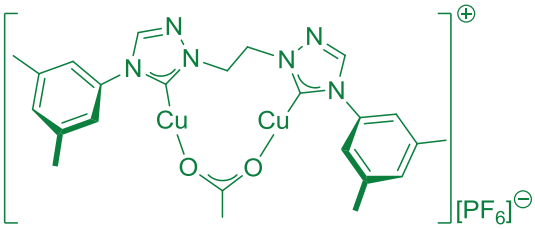

92

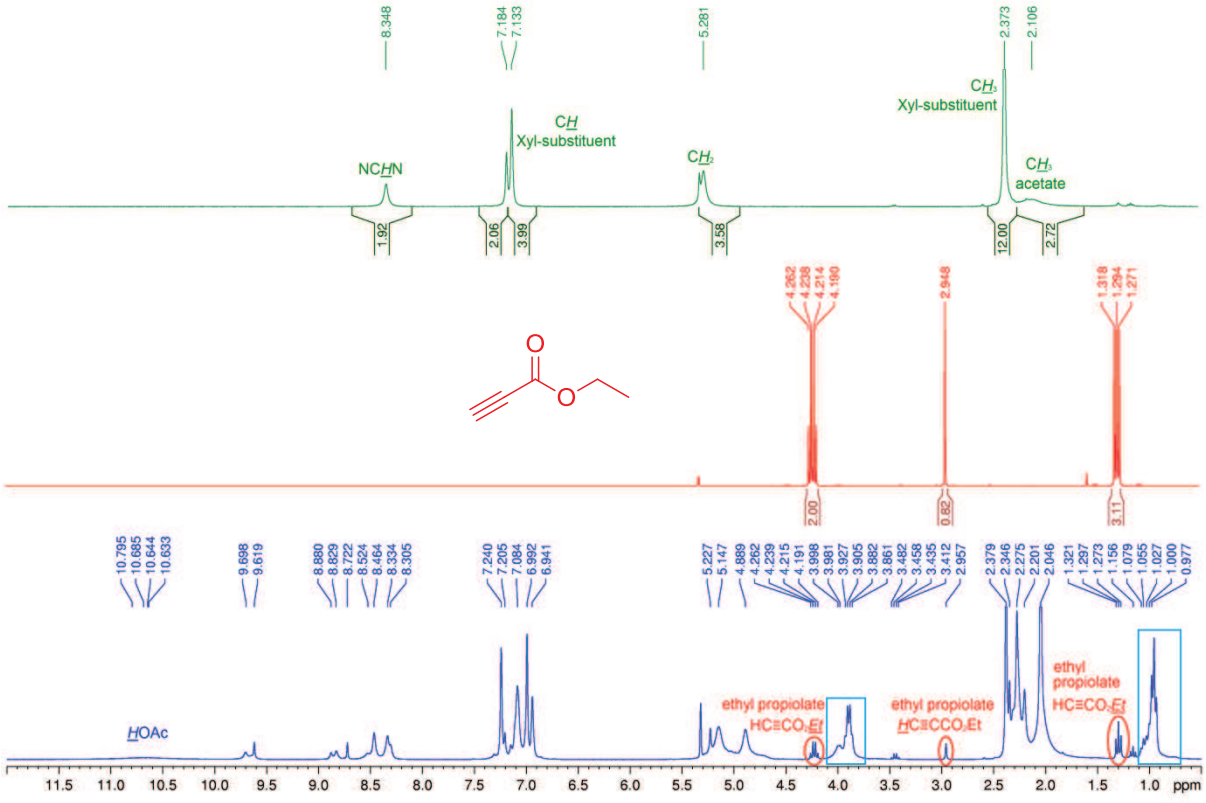

Figure 60: ^{1}H NMR spectrum of the raw product in the reaction of complex **92** with ethyl propiolate (in CD_2Cl_2 at 300 MHz, lower part, blue) and comparison with the ^{1}H NMR spectra of the reaction's starting material **92** (in CD_2Cl_2 at 300 MHz, top, green) and ethyl propiolate (in CD_2Cl_2 at 300 MHz, middle, red).

An important goal for future work on this project is the isolation and characterization of bistriazolylidene dicopper acetylide complexes derived from complex **92**. In order to establish suitable reaction conditions, dinuclear copper complex **92** will be combined with different alkyne substrates (ethyl propiolate, phenylacetylene, *tert*-butylacetylene) in various solvents (tetrahydrofuran, dichloromethane, pyridine) at ambient

and at low temperatures. Alternatively, the corresponding lithium acetylides will be formed *in situ* and combined with **92** as well. It is aspired to unambiguously characterize the dicopper acetylide species formed in one of these reactions by applying NMR spectroscopy, mass spectrometry as well as single crystal X-ray analysis.

5 Perspective

5.1 Scope and Applicability

As dinuclear copper(I) acetate complex **92** had turned out to be a potent homogeneous catalyst for the copper-catalyzed [3+2]-cycloaddition between alkynes and azides, the substrate spectrum of this catalytic transformation can be expanded to other 1,3-dipoles in future work. In Table 1 and Table 2, a variety of 1,3-dipoles is displayed whose reactions with dipolarophiles such as alkynes in the presence of the dinuclear copper(I) catalyst might be interesting to examine. For example, nitrones were reported to react with copper(I) phenylacetylide to form β-lactams by 1,3-dipolar cycloaddition of the nitrone with the acetylide and subsequent rearrangement of the resulting organocopper species *via* a ketene intermediate.[145] This so-called Kinugasa reaction[146] had first been described as early as 1972 and was later adapted to proceed with terminal alkynes in the presence of substoichiometric amounts of copper(I) iodide (Scheme 61, upper part).[147] Recently, various asymmetric variants of this reaction have been presented by the groups of Basak,[148] Tang[149] and Fu.[150] β-Lactams are well known for their biological activity as antibiotics (cephalosporins, penicillins, carbapenems, and monobactams).[151] Bicyclic [3.3.0]-fused pyrazolidinones also show antibacterial activity with the pyrazolidinone ring formally surrogating the β-lactam unit.[152] They are synthesized by 1,3-dipolar cycloaddition of azomethine imines with alkynes.[153] However, as with the uncatalyzed synthesis of triazoles from azides and alkynes, this reaction requires elevated temperatures and often gives a mixture of regioisomeric products.[153c, 153d, 154] Only in 2003 has the group of Fu presented a copper(I)-catalyzed variant of this reaction (Scheme 61, lower part), whose main advantages are high regioselectivity, good yield, mild reaction conditions and the possibility of asymmetric catalysis by employing chiral copper(I) complexes as catalysts.[155] Although the interplay of two copper(I) centres is not as essential as in the CuAAC reaction, where the formation of an sp-hybridized carbon atom in a highly strained six-membered cycle is avoided (Scheme 9), it might be interesting to test the catalytic activity of complex **92** in these [3+2]-cycloadditions

in order to expand its scope of applicability and to examine whether the assumed formation of a bridged μ-acetylide dicopper complex has a positive effect on catalysis.

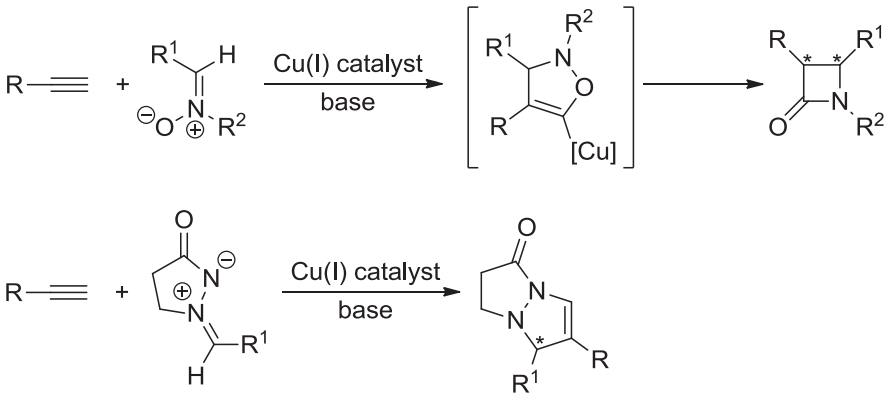

Scheme 61: Synthesis of pharmacologically active agents by copper(I)-catalyzed [3+2]-cycloadditions.

5.2 Mechanistic Studies

In this work, a series of kinetic experiments with dinuclear copper acetate complex **92** has been carried out in order to determine the order of reaction with respect to the concentration of precatalyst **92** in CuAAC reactions of benzyl azide with phenylacetylene or ethyl propiolate as alkyne substrate. For the standard test reaction of benzyl azide with phenylacetylene in dichloromethane, it was unexpectedly observed that the best correlation with the experimental results was found for an order of 0.5 with respect to the initial concentration of dicopper precatalyst **92**, which can be explained by postulating a tetranuclear copper acetylide complex as resting state. In order to account for the observation that the experimentally determined order of reaction with respect to the initial concentration of the dinuclear copper complex is 1.5 with ethyl propiolate as alkyne substrate, it is proposed that the protonation of the dinuclear copper triazolide intermediate by a coordinated molecule of acetic acid is the rate-determining step.

All in all, the great advantage of precatalyst system **92** is the possibility to carry out kinetic studies with molecularly defined species in solution. As has been evidenced in this work, no polynuclear copper acetylide aggregates of low solubility are formed in CuAAC test reactions with precatalyst **92** in dichloromethane as reaction medium. It

is thus possible to rationally explain the results of these experiments. To gain further insight into the mechanism of the CuAAC reaction with dinuclear copper complex **92** as precatalyst, more kinetic experiments are planned in order to determine the order of reaction with respect to the concentration of the azide and the alkyne substrate and to investigate the influence of acetic acid.

All kinetic measurements presented in this work were monitored by applying gas chromatographic methods. It might be interesting to further examine the kinetics of CuAAC reactions with dinuclear complex **92** as catalyst by applying more accurate analytic techniques. For example, stopped flow Fourier transform infrared spectroscopy (SF-FTIR)[156] could be employed in order to monitor the progress of the CuAAC reaction more precisely. Time-resolved infrared spectroscopy appears to be the method of choice as the disappearance of the characteristic signals for the C-N_3 asymmetric stretch of the azide (for example, $\tilde{\nu}$ (film) = 2096 cm^{-1} for benzyl azide) and the C≡C stretch vibration of the alkyne starting material (for example, $\tilde{\nu} \approx 2110$ cm^{-1} for phenylacetylene)[157] is an excellent marker for the progress of the reaction. Alternatively, 3-azidocoumarin[158] can be used as azide in order to enable the better established combination of fluorescence spectroscopy with stopped-flow kinetic measurements.[159]

Apart from kinetic studies, the elucidation of the reaction mechanism of the CuAAC reaction with dinuclear copper(I) catalysts can be spurred by the isolation and characterization of the μ_2-acetylide intermediate with the structural outline shown in Figure 54. Attempts for its synthesis have been summarized in paragraph 4.8, but the isolation and complete characterization of this complex has not succeeded so far. However, there are some obvious experiments that should be carried out in future work with dinuclear copper complex **92** as starting material. Reactions with the alkyne substrates ethyl propiolate, phenylacetylene and *tert*-butylacetylene in tetrahydrofuran, dichloromethane and pyridine with varying stoichiometric ratios are planned. Alternatively, the alkyne substrates will be deprotonated by methyl lithium to give the corresponding lithium acetylides. These can be isolated (as in the case of lithium phenylacetylide) or used *in situ* for the reaction with dicopper complex **92** in dichloromethane or tetrahydrofuran. As the resulting dicopper acetylide species might

be thermally instable, these reactions will be carried out at ambient and at low temperatures.

The ultimative goal is to obtain a crystal suitable for single crystal X-ray analysis. Although this task seems very demanding in the light of the high sensitivity of these complexes, the preliminary experiments carried out in this work indicate that the isolation of μ-acetylide-$\kappa O,\kappa O'$- μ-{1,1'-(ethane-1,2-diyl)bis[4-(3,5-dimethylphenyl)-1*H*-1,2,4-triazol-5-ylidene]}-$\kappa C,\kappa C'$-dicopper(I) hexafluorophosphate is a realistic goal for future work. If this attempt finally succeeded, this would be the first example of the dinuclear "intermediates that have to date eluded more conventional mechanistic studies", as Fokin points out in his latest article.[25] With this dicopper acetylide species at hand, experiments should then be carried out that prove the intermediacy of this complex in the CuAAC reaction by adding an azide substrate and isolating the corresponding triazole product.

5.3 Modifications on the Ligand System

For applications in bioorganic chemistry, a water-soluble CuAAC catalyst without leaching of copper(I) ions is much sought-after. For homogeneous catalysis in aqueous media, the addition of polar groups to the ligand backbone is essential. Based on Santini's work on the synthesis of sulfonate- or carboxylate-substituted bis-NHC ligands and their water-soluble silver complexes,[160] an analogous route is suggested for the synthesis of water-soluble dicopper complexes for CuAAC reactions. As the synthesis of the bistriazolium ligand precursors has been described in literature with the sole difference of a methylene instead of an ethylene-linker, the first two steps shown in Scheme 62 might be reproduced by applying the given literature procedures.[160a] The critical step will most probably be the formation of the dinuclear copper(I) complexes.

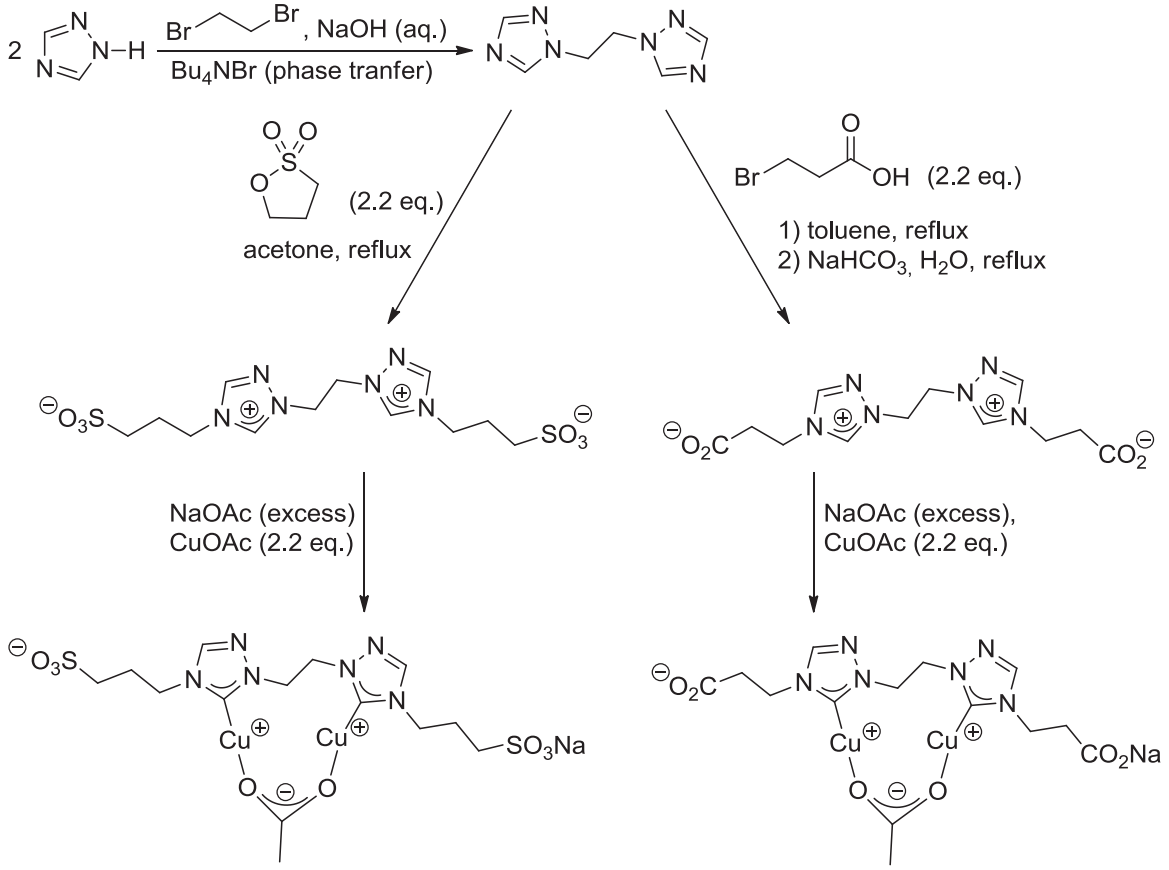

Scheme 62: Suggested route for the synthesis of water-soluble dinuclear copper complexes for CuAAC reactions in aqueous media.

In his PhD thesis, Michael Bessel has computationally examined the influence of pendant alkyl carboxylate groups on CuAAC reactions with bisimidazolinylidene dicopper complexes.[112b] The main advantage of this catalyst design is the presence of a Brønsted base within the catalyst complex in order to facilitate the deprotonation of the coordinating alkyne. In Bessel's work, $(CH_2)_4COO^-$ was found to be the optimal substituent on the N4-position of a model bisimidazolinylidene ligand. With this side chain derived from valeric acid, effective coordination and thus stabilization of the copper(I) ions by the carboxylate group as well as deprotonation of coordinatively bound terminal alkynes should be feasible. It might thus be possible to replace the acetate sacrificial ligand in complexes **91** - **93** by a carboxylate ligand present in the side chain of the chelate ligand. Again, the most critical step in this synthesis will be the introducetion of the metal.

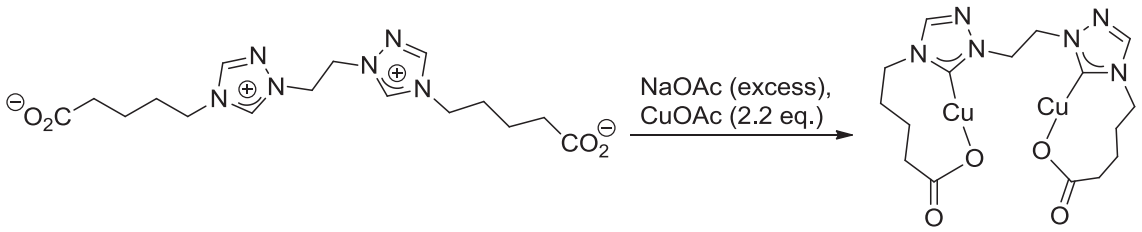

Scheme 63: Catalyst outline with pendant carboxylic acid substituents analogous to the bis-imidazolinylidene catalyst systems suggested by Bessel.[112b]

In a bachelor thesis carried out in our group, first steps on the route towards water-soluble dicopper complexes included the synthesis of bistriazolium salts with (di)ethylene glycol ether substituents.[161]

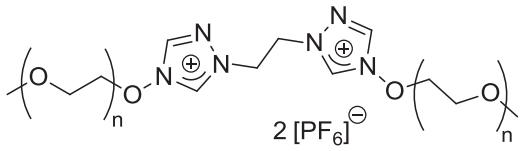

Figure 61: New ligand precursors (n= 1,2) for the synthesis of dinuclear copper(I) complexes prepared by Tobias Fischer in the group of Straub.[161]

Experiments on the synthesis of water-soluble dinuclear copper catalysts from these ligand precursors are underway in the Straub group.

6 Experimental Section

6.1 General Experimental Methodology

Reagents and Solvents

Chemicals and solvents used in this work were supplied by the Department of Chemistry at the Ruprecht-Karls-University Heidelberg or bought directly from Acros Organics, Fisher Scientific, Sigma Aldrich, Strem Chemicals, and TCI. Phenylacetylene was distilled before use. Reactions involving air-sensitive reagents were carried out in an atmosphere of nitrogen or argon using standard Schlenk techniques or an MBraun LABmaster 130 glovebox operated with nitrogen.[162] Anhydrous solvents were taken from an MBraun MB SCS-800 solvent purification system containing appropriate drying agents. Deuterated solvents for the use of NMR spectroscopy were supplied by Deutero GmbH and Euriso-top. All reported yields are isolated yields, unless otherwise indicated.

Column Chromatography and Thin Layer Chromatography

For column chromatography silica gel with grain size between 0.040 and 0.063 mm was used as stationary phase.

Thin layer chromatograms were generated with commercially available ready-to-use plates supplied by Macherey & Nagel (POLYGRAM© SIL G/UV_{254}) as stationary phase. The spots could be observed under a UV lamp (λ = 254 nm). Substances were characterized by their retardation factors R_f, *i.e.* the ratio between the distance of the substance's spot from the starting point and the distance of the solvent front from the starting point.

Nuclear Magnetic Resonance (NMR)

^{1}H NMR spectra were recorded at room temperature. The following instruments were employed: Bruker Avance DRX (300 MHz), Bruker Avance III (400 MHz), Bruker ARX (250 MHz), Bruker Avance III (300 MHz), Bruker Avance DRX (500 MHz), Bruker Avance III (500 MHz), and Bruker Avance III (600 MHz). Chemical shifts δ are reported in ppm relative to TMS and were determined by reference to the residual ^{1}H solvent peaks (acetone: 2.05 ppm; acetonitrile: 1.94 ppm; dichloromethane: 5.32 ppm;

chloroform: 7.26 ppm; DMSO: 2.50 ppm; tetrahydrofuran: 1.72 ppm, 3.58 ppm);[163] coupling constants *J* are given in Hz. The following abbreviations were used for describing the signals' multiplicities: s - singlet, d - doublet, t – triplet, quin - quintet, sept - septet, m - multiplet. $^{13}C\{^{1}H\}$ NMR spectra were recorded at room temperature with the following spectrometers: Bruker Avance 300 (75 MHz) and Bruker Avance 500 (126 MHz). The spectra were calibrated with respect to the solvent (acetone: 29.84 ppm, 206.26 ppm; acetonitrile: 1.32 ppm, 118.26 ppm; chloroform: 77.16 ppm; dichloromethane: 53.84 ppm; DMSO: 39.52 ppm; tetrahydrofuran: 25.31 ppm, 67.21 ppm).[163] The assignment of signals in the $^{13}C\{^{1}H\}$ NMR spectra was achieved by interpretation of two-dimensional NMR spectra (HMBC, HSQC). For processing, analysis and interpretation of NMR spectra, the program TopSpin 3.1 by Bruker was used.

Infrared Spectroscopy (IR)

Infrared spectra were recorded on an infrared spectrometer Vector 22 FTIR by Bruker. Measurements were carried out with KBr-pellets or with a thin film of the analyte. The following abbreviations were used to describe both the intensity and profile of the signals: w (weak), m (medium), s (strong), br (broad). The assignment of the hexafluorophosphate and tetrafluoroborate anions' vibrational frequencies was based on literature data.[164]

Mass Spectrometry (MS)

Mass spectra were recorded by the Mass Spectrometry Service Facility of the Department of Chemistry at the Ruprecht-Karls-University Heidelberg. The following machines were employed: Bruker ApexQe hybrid 9.4 T FT-ICR (HR-ESI) and JEOL JMS-700 magnetic sector (EI, FAB). Apart from the method of ionization and the peak of the molecular ion, the base peak and characteristic fragmentation peaks with their relative intensities are reported.

Elemental Analysis (EA)

Elemental analyses were carried out by the Laboratory of Microanalysis in the Department of Chemistry at the Ruprecht-Karls-University Heidelberg on the instruments vario EL and vario MICRO cube by Elementar Analysensysteme GmbH.

Melting Point Analysis

Determination of melting points was carried out in open capillaries using a Gallenkamp hot-stage microscope.

Crystal Structure Analysis

X-ray analyses were carried out in the Department of Chemistry at the Ruprecht-Karls-University Heidelberg by Dr. Rominger and co-workers using the following hardware: Bruker Smart Apex Diffractometer and Bruker Smart 1000 Diffractometer. For analysis and graphic representation, the programs Ortep[3] and POV-Ray[4] were used.

Gas Chromatography (GC)

Gas chromatograms were recorded on a Shimadzu GC-2010 instrument with a capillary column (FSSE 54CB025) with an inner diameter of 0.32 mm and a polyphenylmethylsiloxane film thickness of 0.25 µm. Helium was used as carrier gas with a total flow of 21.8 ml min^{-1}. The analytes were detected by FID (flame ionization detector; hydrogen flow: 40.0 ml min^{-1}, air flow: 400.0 ml min^{-1}). An internal standard was used for quantitative analyses. Processing of the chromatograms was carried out with the help of the program GCsolution (version 2.3000SU) by Shimadzu.

6.2 Syntheses

6.2.1 Synthesis of (IPr)CuOAc

6.2.1.1 1,4-Bis(2,6-diisopropylphenyl)-1,4-diazabutadiene (**1**)

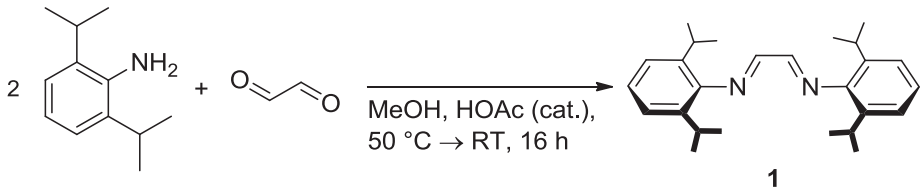

1

1,4-Bis(2,6-diisopropylphenyl)-1,4-diazabutadiene (**1**) was synthesized according to a procedure reported in literature.[116] In a 500 ml three-necked flask equipped with a thermometer and a dropping funnel, 2,6-diisopropylaniline (92 % pure, ρ = 0.94 g cm^{-3}, 70 ml, 61 g 2,6-diisopropylaniline, 0.34 mol) and glacial acetic acid (0.4 ml) were dissolved in methanol (85 ml) and heated to 50 °C while stirring. After removal of the heat source, a solution of glyoxal (40 weight-% in water, ρ = 1.265 g cm^{-3}, 19.6 ml, 9.91 g glyoxal, 0.171 mmol) in methanol (80 ml) was added to the warm reaction mixture. After ten minutes, crystallization of a bright yellow solid commenced. The reaction mixture was stirred at room temperature for 16 hours. The yellow precipitate was filtered and washed with methanol until the solution was bright yellow. The solid residue was dried *in vacuo*. The methanol solution was concentrated and stored at 8 °C for a second crystallization. The crystalline product fractions were combined and dried *in vacuo* (52.64 g, 0.1398 mol, 82 %; lit.: 89.5 %).

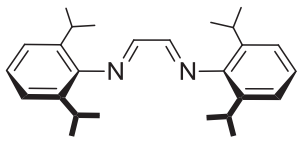

1

$C_{26}H_{36}N_2$

M ($C_{26}H_{36}N_2$) = 376.58 g mol^{-1}

^{1}H NMR (300.190 MHz, $CDCl_3$, 27 °C): δ = 8.13 (s, 2H, NC<u>H</u>), 7.25 - 7.15 (m, 6H, *meta*-C<u>H</u> and *ortho*-C<u>H</u>), 2.97 (sept, $^3J_{H\text{-}H}$ = 6.9 Hz, 4H, C<u>H</u>(CH_3)$_2$), 1.23 (d, $^3J_{H\text{-}H}$ = 6.9 Hz, 24H, C<u>H</u>$_3$).

$^{13}C\{^1H\}$ NMR (75.483 MHz, $CDCl_3$, 27 °C): δ = 163.2 (N<u>C</u>H), 148.2 (*ipso*-<u>C</u>N), 136.9 (*ortho*-<u>C</u>CH(CH_3)$_2$), 125.3 (*para*-<u>C</u>H), 123.3 (*meta*-<u>C</u>H), 28.2 (<u>C</u>H(CH_3)$_2$), 23.5 (CH(<u>C</u>H_3)$_2$).

HR-MS (EI+, methanol) *m*/*z* (%): 188.1454 (97.2) $[M\text{-}C_{13}H_{18}N]^{\bullet+}$, 333.2309 (100.0) $[M\text{-}C_3H_7]^{\bullet+}$, 361.2624 (10.4) $[M\text{-}CH_3]^{\bullet+}$, 375.2761 (1.7) $[M\text{-}H]^{\bullet+}$, 376.2858 (2.9) $[M]^{\bullet+}$.

calculated for $[C_{26}H_{36}N_2]^{\bullet+}$:	376.2873
found:	376.2858

Melting Point: 110 °C

6.2.1.2 1,3-Bis(2,6-diisopropylphenyl)imidazolium Acetate (**2**)

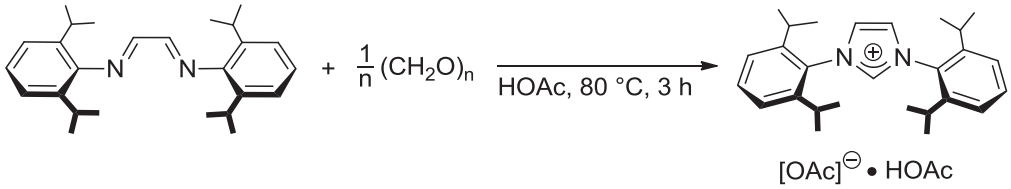

1 **2**

In a 250 ml round-bottomed flask, 1,4-bis(2,6-diisopropylphenyl)-1,4-diazabutadiene (12.088 g, 32.100 mmol) and paraformaldehyde (97 % pure, 1.068 g $(CH_2O)_n$, 35.57 mmol) were dissolved in glacial acetic acid (130 ml). While the reaction mixture was stirred at 80 °C for three hours, it turned dark purple. After the solvent had been removed *in vacuo*, the slimy dark solid was washed with diethyl ether (7 × 150 ml). The resulting violet solid was dried *in vacuo* and dissolved in hot tetrahydrofuran. At 8 °C, the slightly yellow product crystallized from the solution. The solvent was decanted and the solid residue washed with diethyl ether (5 × 100 ml). The mother liquor was concentrated and stored at -20 °C for a second crystallization process. The combined fractions of colourless crystalline product **2** were dried *in vacuo* (13.744 g, 27.038 mmol, 84 %).

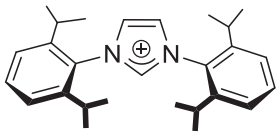

$[OAc]^{\ominus} \bullet HOAc$

2

$C_{31}H_{44}N_2O_4$

M ($C_{31}H_{44}N_2O_4$) = 508.69 g mol^{-1}

^{1}H NMR (400.180 MHz, $CDCl_3$, 25 °C): δ = 15.88 (br, s, 1H, *H*OAc), 10.19 (t, $^4J_{H\text{-}H}$ = 1.5 Hz, 1H, NC*H*N*)*, 7.91 (d, $^4J_{H\text{-}H}$ = 1.5 Hz, 2H, NC*H*), 7.51 (t, $^3J_{H\text{-}H}$ = 7.8 Hz, 2H, *para*-C*H*), 7.29 (d, $^3J_{H\text{-}H}$ = 7.8 Hz, 4H, *meta*-C*H*), 2.38 (sept, $^3J_{H\text{-}H}$ = 6.8 Hz, 4H, C*H*(CH_3)$_2$), 1.56 (s, 6H, [H_3CCOO]$^-$, H_3CCOOH), 1.23 (d, $^3J_{H\text{-}H}$ = 6.8 Hz, 12H, CH(CH_3)$_2$), 1.17 (d, $^3J_{H\text{-}H}$ = 6.8 Hz, 12H, CH(CH_3)$_2$).

^{13}C{^{1}H} NMR (100.625 MHz, $CDCl_3$, 25 °C): δ = 175.8 (H_3C*C*OO), 145.1 (*ortho*-*C*CH(CH_3)$_2$), 140.0 (N*C*HN), 132.1 (*para*-*C*H), 130.2 (*ipso*-*C*N), 126.3 (N*C*H), 124.7 (*meta*-*C*H), 29.2 (*C*H(CH_3)$_2$), 24.5 (CH(*C*H_3)$_2$), 23.8 (CH(*C*H_3)$_2$), 23.0 ([H_3*C*COO]$^-$, H_3*C*COOH).

HR-MS (ESI+, methanol) *m*/*z* (%): 389.29513 (100.0) [M-OAc-HOAc]$^+$.

calculated for [$C_{27}H_{37}N_2$]$^+$:	389.29513
found:	389.29513

Infrared Spectroscopy (KBr): $\tilde{\nu}$ [cm^{-1}] = 3414 (br, m), 3158 (w), 3068 (w), 2967 (s), 2929 (m), 2872 (m), 1715 (m), 1636 (m), 1580 (m), 1535 (m), 1458 (m), 1448 (m), 1404 (m), 1389 (m), 1367 (m), 1332 (w), 1257 (m), 1206 (w), 1062 (m), 809 (m), 760 (m), 749 (m).

Elemental Analysis (No. 28723)

calculated for $C_{31}H_{44}N_2O_4$:	C 73.19 %, H 8.72 %, N 5.51 %
found:	C 73.18 %, H 8.75 %, N 5.64 %

Crystal Structure: Crystallographic data and structure refinements for reb1, formula $C_{29}H_{40}N_2O_2$+2HOAc, M ($C_{33}H_{48}N_2O_6$) = 568.74 g mol^{-1}: colourless crystal (polyhedron), dimensions 0.39 × 0.19 × 0.18 mm^3, crystal system monoclinic, space group

$P2_1/n$, Z = 4, a = 12.7921(14) Å, b = 22.331(3) Å, c = 12.9295(14) Å, α = 90°, β = 111.033(2)°, γ = 90°, V = 3447.3(7) Å^3, ρ = 1.096 g cm^{-3}, T = 200(2) K, Θ_{max} = 25.35°, radiation Mo K_α, λ = 0.71073 Å, 0.3° ω-scans with CCD area detector, covering a whole sphere in reciprocal space, 29090 reflections measured, 6314 unique (R(int)= 0.0453), 4643 observed ($I > 2\sigma(I)$), intensities were corrected for Lorentz and polarization effects, an empirical absorption correction was applied using SADABS[165] based on the Laue symmetry of the reciprocal space, μ = 0.08 mm^{-1}, T_{min} = 0.97, T_{max} = 0.99, structure solved by direct methods and refined against F^2 with a full-matrix least-squares algorithm using the SHELXTL (version 2008/4) software package,[166] 403 parameters refined, hydrogen atoms were treated using appropriate riding models, except for the acetic acid protons H2 and H6, which were refined isotropically, goodness of fit 1.03 for observed reflections, final residual values $R1(F)$ = 0.056, $wR(F^2)$ = 0.148 for observed reflections, residual electron density -0.22 to 0.35 eÅ^{-3}.

Melting Point: 169 °C

6.2.1.3 (IPr)CuOAc (**3**)[167]

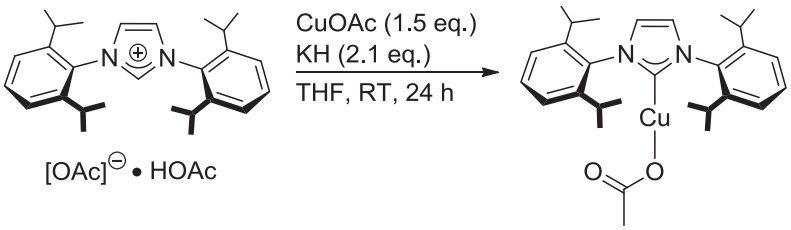

2 **3**

A flame-dried Schlenk flask was charged with 1,3-bis(2,6-diisopropylphenyl)imidazolium acetate (2.640 g, 5.190 mmol) and taken into the glovebox. The substrate was suspended in tetrahydrofuran (40 ml). Potassium hydride (0.437 g, 10.9 mmol) and copper acetate (0.960 g, 7.83 mmol) were added to the reaction mixture. The formation of gas was observed. While stirring the suspension for 24 hours at room temperature under an atmosphere of inert gas, the reaction mixture turned from olive-green to dark brown. The reaction mixture was filtered over a filter paper-capped canula resulting in a yellow solution. The solvent was removed *in vacuo* and the raw product

washed with pentane (3 × 20 ml). After re-crystallization from tetrahydrofuran/diethyl ether, the product was obtained as a colourless solid (1.817 g, 3.555 mmol, 69 %).

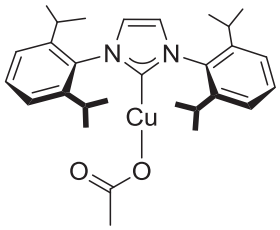

3

$C_{29}H_{39}CuN_2O_2$

M = 511.18 g mol^{-1}

^{1}H NMR (300.510 MHz, CD_3CN, 27 °C): δ = 7.56 (t, $^3J_{H\text{-}H}$ = 7.7 Hz, 2H, *para*-C*H*), 7.45 (s, 2H, NC*H*), 7.41 (d, $^3J_{H\text{-}H}$ = 7.7 Hz, 4H, *meta*-C*H*), 2.60 (sept, $^3J_{H\text{-}H}$ = 6.9 Hz, 4H, C*H*(CH_3)$_2$), 1.53 (s, 3H, *H*$_3$CCOO), 1.29 (d, $^3J_{H\text{-}H}$ = 6.9 Hz, 12H, CH(C*H*$_3$)$_2$), 1.25 (d, $^3J_{H\text{-}H}$ = 6.9 Hz, 12H, CH(C*H*$_3$)$_2$).

^{13}C{^{1}H} NMR (75.468 MHz, CD_3CN, 27 °C): δ = 180.5 (N*C*N), 176.9 (H_3C*C*OO), 146.9 (*ortho*-*C*CH(CH_3)$_2$), 135.7 (*ipso*-*C*N), 131.4 (*para*-*C*H), 125.0 (*meta*-*C*H), 124.8 (N*C*H), 29.1 (*C*H(CH_3)$_2$), 25.0 (CH(*C*H$_3$)$_2$), 23.9 (H_3*C*COO, CH(*C*H$_3$)$_2$).

^{1}H NMR (400.180 MHz, C_6D_6, 25 °C): δ = 7.23 - 7.15 (m, br, 2H, *para*-C*H*), 7.07 (d, $^3J_{H\text{-}H}$ = 7.8 Hz, 4H, *meta*-C*H*), 6.37 (s, 2H, NC*H*), 2.60 (sept, $^3J_{H\text{-}H}$ = 6.9 Hz, 4H, C*H*(CH_3)$_2$), 1.89 (s, 3H, *H*$_3$CCOO), 1.44 (d, $^3J_{H\text{-}H}$ = 6.9 Hz, 12H, CH(C*H*$_3$)$_2$), 1.08 (d, $^3J_{H\text{-}H}$ = 6.9 Hz, 12H, CH(C*H*$_3$)$_2$).

^{13}C{^{1}H} NMR (75.476 MHz, C_6D_6, 25 °C): δ = 182.2 (N*C*N), 177.3 (H_3C*C*OO), 145.8 (*ortho*-*C*CH(CH_3)$_2$), 135.0 (*ipso*-*C*N), 130.7 (*para*-*C*H), 124.3 (*meta*-*C*H), 122.9 (N*C*H), 29.1 (*C*H(CH_3)$_2$), 25.0 (CH(*C*H$_3$)$_2$), 23.9 (CH(*C*H$_3$)$_2$), 23.3 (H_3*C*COO).

HR-MS (ESI+, methanol) *m*/*z* (%): 483.24341 (100.0) [M(^{63}Cu)-OAc+H_3COH]$^+$, 485.24171 (100.0) [M(^{65}Cu)-OAc+H_3COH]$^+$.

calculated for [$C_{28}H_{40}$(^{63}Cu)N_2O]$^+$: 483.24312

found: 483.24341

Infrared Spectroscopy (KBr): $\tilde{\nu}$ [cm^{-1}] = 3428 (br, s), 3159 (w), 3136 (w), 3071 (w), 2966 (s), 2927 (m), 2869 (m), 1579 (br, s), 1470 (s), 1457 (s), 1408 (s), 1385 (m), 1365 (m), 1327 (m), 1282 (m), 1255 (w), 1214 (w), 1179 (w), 1115 (w), 1106 (w), 1059 (w), 947 (w), 937 (w), 808 (m), 763 (m), 742 (m), 700 (w), 682 (w), 638 (w), 549 (w), 450 (w).

Elemental Analysis (No. 229447)

calculated for $C_{29}H_{39}CuN_2O_2$:	C 68.14 %,	H 7.69 %,	N 5.48 %
found:	C 68.26 %,	H 7.79 %,	N 5.51 %

Decomposition Temperature: 236 °C (dark brown liquid).

6.2.2 Synthesis of 3,3'-[1,3-Phenylenebis(methylene)]bis[1-(2,6-dimethylphenyl)-4,5-dihydro-1*H*-imidazol-3-ium] Bis(hexafluorophosphate)

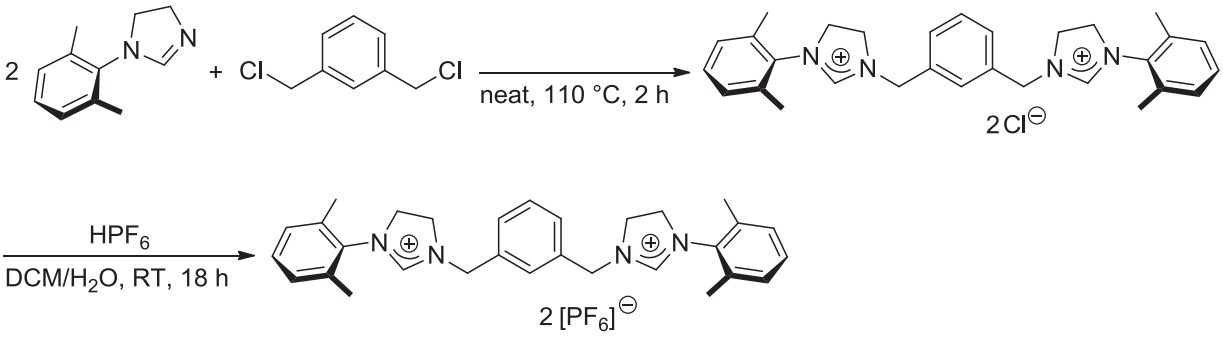

11

1-(2,6-Dimethylphenyl)-4,5-dihydro-1*H*-imidazole had been synthesized in our group following a procedure reported in literature.[112a] In a 100 ml round-bottomed flask, a mixture of 1-(2,6-dimethylphenyl)-4,5-dihydro-1*H*-imidazole (1.742 g, 10.00 mmol) and 1,3-bis(chloromethyl)benzene (0.875 g, 5.00 mmol) was heated to 110 °C for two hours. The mixture had already turned solid at 60 °C. After cooling down to room temperature, dichloromethane (50 ml) was added. In a separate flask, a solution of hexafluorophosphoric acid (60 weight-% solution in water, ρ = 1.6510 g cm^{-3}, 2.2 ml, 15 mmol) in water (20 ml) and dichloromethane (5 ml) was prepared. The dichloromethane solution of intermediate was added to the hexafluorophosphoric acid solution while stirring. The biphasic mixture was vigorously stirred for 18 hours. The volatile dichloromethane was removed at the rotary evaporator. A colourless solid precipitated from the aqueous solution. After filtration, the solid was washed with diethyl ether (3 × 100 ml) and dried *in vacuo* (3.223 g, 4.341 mmol, 43 %).[119]

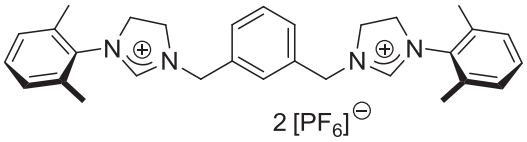

11

$C_{30}H_{36}F_{12}N_4P_2$

M ($C_{30}H_{36}F_{12}N_4P_2$) = 742.56 g mol^{-1}

^{1}H NMR (500.130 MHz, CD_3CN, 25 °C): δ = 8.10 (s, 2H, NC*H*N), 7.59 (t, $^3J_{H\text{-}H}$ = 7.6 Hz, 1H, Xyl-linker, NCH_2CCHCH), 7.50 (dd, $^3J_{H\text{-}H}$ = 7.6 Hz, $^4J_{H\text{-}H}$ = 1.5 Hz, 2H, Xyl-linker, NCH_2CCHCH), 7.44 (br, s, 1H, Xyl-linker, $NCH_2CCHCCH_2N$), 7.32 (t,

$^{3}J_{H\text{-}H}$ = 7.6 Hz, 2H, *para*-C<u>*H*</u>), 7.23 (d, $^{3}J_{H\text{-}H}$ = 7.6 Hz, 4H, *meta*-C<u>*H*</u>), 4.76 (s, 4H, benzyl-C<u>*H*</u>$_2$), 4.18 (m, 4H, NC<u>*H*</u>$_2$), 4.03 (m, 4H, NC<u>*H*</u>$_2$), 2.32 (s, 12H, C<u>*H*</u>$_3$).

^{13}C{^{1}H} NMR (125.758 MHz, CD_3CN, 25 °C): δ = 159.1 (N<u>*C*</u>HN), 137.1 (<u>*C*</u>CH$_3$), 134.9 (Xyl-linker, NCH$_2$<u>*C*</u>CH), 134.2 (*ipso*-<u>*C*</u>N), 131.2 (*para*-<u>*C*</u>H), 131.1 (Xyl-linker, NCH$_2$CCH<u>*C*</u>H), 130.4 (Xyl-linker, NCH$_2$C<u>*C*</u>HCCH$_2$N), 130.3 (Xyl-linker, NCH$_2$C-<u>*C*</u>HCH), 130.1 (*meta*-<u>*C*</u>H), 52.6 (benzyl-<u>*C*</u>H$_2$), 51.8 (N<u>*C*</u>H$_2$), 49.5 (N<u>*C*</u>H$_2$), 17.8 (<u>*C*</u>H$_3$).

^{31}P{^{1}H} NMR (121.495 MHz, CD_3CN, 25 °C): δ = -143.35 (sept, $^{1}J_{P\text{-}F}$ = 706.8 Hz).

HR-MS (ESI+, methanol) *m*/*z* (%): 597.25609 (100.0) [M-PF$_6$]$^+$.

calculated for [C$_{30}$H$_{36}$F$_6$N$_4$P]$^+$:	597.25763
found:	597.25609

Infrared Spectroscopy (KBr): $\tilde{\nu}$ [cm^{-1}] = 3446 (br, s), 3098 (w), 2965 (w), 1645 (s), 1592 (w), 1511 (w), 1471 (m), 1447 (m), 1368 (w), 1305 (m), 1275 (m), 1254 (m), 1215 (m), 1168 (w), 1094 (w), 842 (s, hexafluorophosphate, asymmetric stretching mode), 783 (m), 708 (w), 558 (s, hexafluorophosphate, bending mode), 496 (m), 458 (m).

Elemental Analysis (No. 29106)

calculated for C$_{30}$H$_{36}$F$_{12}$N$_4$P$_2$:	C	48.52 %,	H	4.89 %,	N	7.55 %,	P 8.34
found:	C	48.47 %,	H	4.90 %,	N	7.78 %,	P 8.09

Melting Point: 264 - 266 °C.

6.2.3 Synthesis of 4-Aryl-1,2,4-triazoles

*6.2.3.1 4-(2,4,6-Trimethylphenyl)-4*H*-1,2,4-triazole* (**21**)

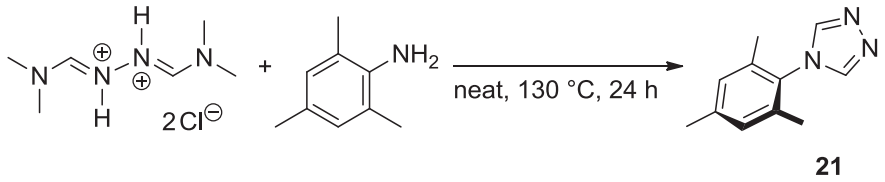

21

4-(2,4,6-Trimethylphenyl)-4*H*-1,2,4-triazole was synthesized according to a procedure reported in literature.[120] A flame-dried Schlenk flask was charged with *N*,*N*-dimethylformamide azine dihydrochloride (4.30 g, 20.0 mmol) and 2,4,6-trimethylaniline (2.8 ml, 2.9 g, 22 mmol) was added *via* syringe. The reaction mixture was stirred at 130 °C for 24 hours resulting in a beige coloured solid. After cooling down to room temperature, an aqueous solution of sodium hydroxide (1.0 mol l^{-1}, 100 ml) and toluene (500 ml, portion-wise) were added, and the aqueous phase was extracted with toluene (3 × 100 ml). The combined organic phases were dried over magnesium sulphate. After filtration of the drying agent, the solvent was removed *in vacuo*. The raw product was purified by sublimation (130 °C, 0.2 mbar) to give a colourless crystalline solid (2.53 g, 13.5 mmol, 68 %; lit.: 56 %).

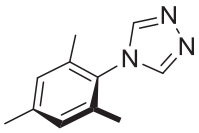

21

$C_{11}H_{13}N_3$

M ($C_{11}H_{13}N_3$) = 187.24 g mol^{-1}

^{1}H NMR (300.190 MHz, $CDCl_3$, 27 °C): δ = 8.12 (s, 2H, NC*H*N), 6.98 (s, 2H, *meta*-C*H*), 2.32 (s, 3H, *para*-CH_3), 1.96 (s, 6H, *ortho*-CH_3).

^{13}C{^{1}H} NMR (75.483 MHz, $CDCl_3$, 27 °C): δ = 143.1 (N*C*HN), 140.1 (*para*-*C*CH_3), 135.0 (*ortho*-*C*CH_3), 129.6 (*ipso*-*C*N), 129.5 (*meta*-*C*H), 21.1 (*para*-*C*H_3), 17.5 (*ortho*-*C*H_3).

HR-MS (EI+) *m*/*z* (%): 159.0926 (23.5) $[M\text{-}CH_2N]^{\bullet+}$, 187.1111 (100.0) $[M]^{\bullet+}$.
calculated for $[C_{11}H_{13}N_3]^{\bullet+}$: 187.1104
found: 187.1111

Elemental Analysis (No. 29363)
calculated for $C_{11}H_{13}N_3$: C 70.56 %, H 7.00 %, N 22.44 %
found: C 70.35 %, H 6.73 %, N 22.19 %

Melting Point: 234 °C.

*6.2.3.2 4-(3,5-Dimethylphenyl)-4*H*-1,2,4-triazole* (**22**)

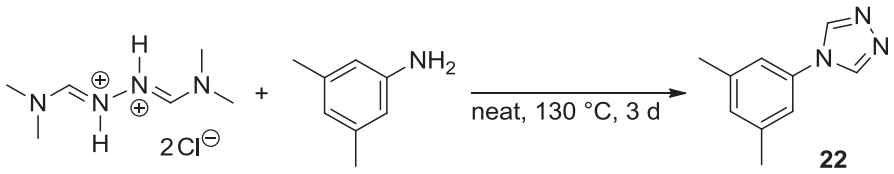

A flame-dried Schlenk flask was charged with *N*,*N*-dimethylformamide azine dihydrochloride (25.81 g, 120.0 mmol) and 3,5-dimethylaniline (15.0 ml, 14.5 g, 120 mmol) was added *via* syringe. The reaction mixture was stirred at 130 °C for three days resulting in a brown oil. After cooling down to room temperature, an aqueous solution of sodium hydroxide (1.0 mol l^{-1}, 250 ml) and toluene (700 ml, portion-wise) were added, and the aqueous phase was extracted with toluene (5 × 100 ml). The combined organic phases were dried over magnesium sulphate. After filtration of the drying agent, the solvent was removed *in vacuo*. The raw product was purified by sublimation (130 °C, 0.2 mbar) to give a colourless crystalline solid (14.3 g, 82.6 mmol, 69 %).

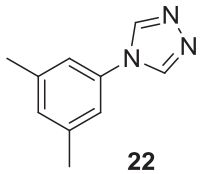

22

$C_{10}H_{11}N_3$

M ($C_{10}H_{11}N_3$) = 173.21 g mol^{-1}

^{1}H NMR (300.190 MHz, $CDCl_3$, 27 °C): δ = 8.42 (s, 2H, NC*H*N), 7.06 (s, 1H, *para*-C*H*), 6.97 (s, 2H, *ortho*-C*H*), 2.37 (s, 6H, CH_3).

^{13}C{^{1}H} NMR (75.483 MHz, $CDCl_3$, 27 °C): δ = 141.5 (N*C*HN), 140.4 (*meta*-*C*CH_3), 133.8 (*ipso*-*C*N), 130.6 (*para*-*C*H), 119.9 (*ortho*-*C*H), 21.3 (*C*H_3).

HR-MS (EI+) *m*/*z* (%): 131.0597 (20.6) [M-C_2H_4N]$^{\bullet+}$, 145.0796 (19.0) [M-CH_2N]$^{\bullet+}$, 146.0838 (12.0) [M-CHN]$^{\bullet+}$, 173.0937 (100) [M]$^{\bullet+}$.

calculated for [$C_{10}H_{11}N_3$]$^{\bullet+}$:	173.0947
found:	173.0937

Infrared Spectroscopy (KBr)**:** $\tilde{\nu}$ [cm^{-1}] = 3103 (s), 2918 (m), 1618 (s), 1601 (s), 1521 (s), 1455 (m), 1368 (m), 1298 (s), 1270 (w), 1259 (m), 1224 (s), 1111 (s), 1060 (s), 898 (s), 880 (m), 870 (m), 850 (s), 817 (s), 685 (s), 643 (s).

Elemental Analysis (No. 30630)

calculated for $C_{10}H_{11}N_3$:	C 69.34 %, H 6.40 %, N 24.26 %
found:	C 69.38 %, H 6.52 %, N 24.33 %

Melting Point: 151 °C.

Crystal Structure: Crystallographic data and structure refinements for reb2, formula $C_{10}H_{11}N_3$, M = 173.21 g mol^{-1}: colourless crystal (polyhedron), dimensions 0.33 × 0.21 × 0.17 mm^3, crystal system: tetragonal, space group $P4_2/n$, Z = 8, a = 14.110(2) Å, b = 14.110(2) Å, c = 9.3589(16) Å, α = 90°, β =90°, γ=90°, V = 1863.4(5) Å^3, ρ = 1.235 g cm^{-3}, T = 200(2) K, Θ_{max}= 25.07°, radiation Mo K$_\alpha$, λ = 0.71073 Å, 0.3° ω-scans with CCD area detector, covering a whole sphere in

reciprocal space, 11555 reflections measured, 1657 unique (R(int) = 0.0409), 1255 observed ($I > 2\sigma(I)$), intensities were corrected for Lorentz and polarization effects, an empirical absorption correction was applied using SADABS[165] based on the Laue symmetry of the reciprocal space, μ = 0.08 mm^{-1}, T_{min} = 0.97, T_{max} = 0.99, structure solved by direct methods and refined against F^2 with a full-matrix least-squares algorithm using the SHELXTL (version 2008/4) software package,[166] 120 parameters refined, hydrogen atoms were treated using appropriate riding models, goodness of fit 1.11 for observed reflections, final residual values $R1(F)$ = 0.047, $wR(F^2)$ = 0.112 for observed reflections, residual electron density -0.18 to 0.20 eÅ^{-3}. CCDC 869464 contains the supplementary crystallographic data for this strcuture. This data can be obtained free of charge from the Cambridge Crystallographic Data Centre *via* www.ccdc.cam.ac.uk/data_request/cif.

*6.2.3.3 4-(4-Methylphenyl)-4*H*-1,2,4-triazole* (**23**)

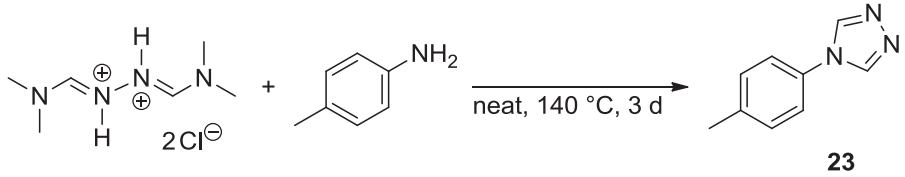

23

4-(4-Methylphenyl)-4*H*-1,2,4-triazole was synthesized according to a procedure reported in literature.[120] A flame-dried Schlenk flask was charged with *N*,*N*-dimethylformamide azine dihydrochloride (18.06 g, 83.95 mmol) and 4-methylaniline (18.00 g, 168.0 mmol). The melted reaction mixture was stirred at 140 °C for three days. After cooling down to room temperature, an aqueous solution of sodium hydroxide (1.0 mol l^{-1}, 100 ml) and toluene (500 ml, portion-wise) were added, and the aqueous phase was extracted with toluene (5 × 100 ml). The combined organic phases were dried over magnesium sulphate. After filtration of the drying agent, the solvent was removed *in vacuo*. The raw product was a brown oil. Upon addition of diethyl ether, a beige solid precipitated. After filtration and drying *in vacuo*, the raw product was purified by sublimation (125 °C, 0.3 mbar) to give a colourless crystalline solid (5.69 g, 35.7 mmol, 43 %; lit.: 58 %).

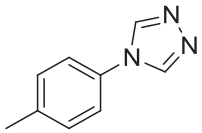

23

$C_9H_9N_3$

M ($C_9H_9N_3$) = 159.19 g mol^{-1}

^{1}H NMR (600.244 MHz, $CDCl_3$, 22 °C): δ = 8.40 (s, 2H, NC*H*N), 7.28 (d, $^3J_{H\text{-}H}$ = 8.3 Hz, 2H, *meta*-C*H*), 7.23 (d, $^3J_{H\text{-}H}$ = 8.3 Hz, 2H, *ortho*-C*H*), 2.37 (s, 3H, CH_3).

^{13}C{^{1}H} NMR (150.931 MHz, $CDCl_3$, 22 °C): δ = 141.5 (N*C*HN), 139.2 (*para*-*C*CH_3), 131.4 (*ipso*-*C*N), 130.7 (*meta*-*C*H), 122.1 (*ortho*-*C*H), 21.0 (*C*H_3).

HR-MS (EI+) *m*/*z* (%): 91.0538 (51.4) $[M\text{-}C_2H_2N_3]^{\bullet+}$, 104.0503 (23.9) $[M\text{-}C_2H_3N_2]^{\bullet+}$, 105.0587 (25.0) $[M\text{-}C_2H_2N_2]^{\bullet+}$, 131.0611 (60.1) $[M\text{-}C_2H_2N]^{\bullet+}$, 159.0780 (100.0) $[M]^{\bullet+}$.

calculated for $[C_9H_9N_3]^{\bullet+}$:	159.0791
found:	159.0780

Elemental Analysis (No. 30829)

calculated for $C_9H_9N_3$:	C 67.90 %,	H 5.70 %,	N 26.40 %
found:	C 67.93 %,	H 5.56 %,	N 26.25 %

Melting Point: 118 °C.

*6.2.3.4 4-(2,6-Diisopropylphenyl)-4*H*-1,2,4-triazole* (**24**)

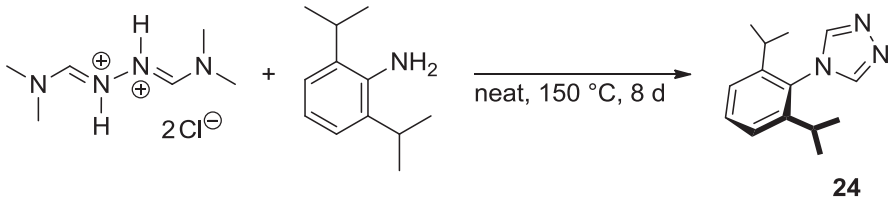

24

4-(2,6-Diisopropylphenyl)-4*H*-1,2,4-triazole was synthesized according to a procedure reported in literature.[120] A flame-dried Schlenk flask was charged with *N*,*N*-dimethylformamide azine dihydrochloride (5.39 g, 25.1 mmol) and 2,6-diisopropylaniline (92 %, 10.3 ml, 8.91 g 2,6-diisopropylaniline , 50.24 mmol) was added *via* syringe. The reaction mixture was stirred at 150 °C for eight days resulting in a dark violet solid. After cooling down to room temperature, an aqueous solution of sodium hydroxide (1.0 mol l^{-1}, 100 ml) and toluene (300 ml, portion-wise) were added, and the aqueous phase was extracted with toluene (3 × 100 ml). The combined organic phases were dried over magnesium sulphate. After filtration of the drying agent, the solvent was removed *in vacuo* and the raw product purified by sublimation (160 °C, 0.2 mbar) to give a slightly violet crystalline solid (2.26 g, 9.86 mmol, 39 %; lit.: 42 %).

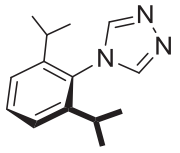

24

$C_{14}H_{19}N_3$

M ($C_{14}H_{19}N_3$) = 229.32 g mol^{-1}

^{1}H NMR (400.180 MHz, $CDCl_3$, 25 °C): δ = 8.15 (s, 2H, NC*H*N), 7.46 (t, $^3J_{H\text{-}H}$ = 7.8 Hz, 1H, *para*-C*H*), 7.26 (d, $^3J_{H\text{-}H}$ = 7.8 Hz, 2H, *meta*-C*H*), 2.30 (sept, $^3J_{H\text{-}H}$ = 6.9 Hz, 2H, C*H*(CH_3)$_2$), 1.10 (d, $^3J_{H\text{-}H}$ = 6.9 Hz, 12H, CH(C*H*$_3$)$_2$).

^{13}C{^{1}H} NMR (100.625 MHz, $CDCl_3$, 25 °C): δ = 146.2 (*ortho*-*C*CH(CH_3)$_2$), 144.0 (N*C*HN), 130.9 (*para*-*C*H), 129.0 (*ipso*-*C*N), 124.3 (*meta*-*C*H), 28.3 (C*H*(CH_3)$_2$), 24.2 (CH(C*H*$_3$)$_2$).

HR-MS (ESI+, methanol) *m*/*z* (%): 230.16522 (47.8) $[M+H]^+$, 252.14718 (39.3) $[M+Na]^+$, 268.12112 (38.8) $[M+K]^+$, 289.23874 (100) $[M+C_3H_{10}N]^+$, 481.30533 (53.9) $[2M+Na]^+$.

calculated for $[C_{14}H_{20}N_3]^+$: 230.16517

found: 230.16522

Elemental Analysis (No. 30041)

calculated for $C_{14}H_{19}N_3$: C 73.33 %, H 8.35 %, N 18.32 %

found: C 73.48 %, H 8.33 %, N 18.34 %

Melting Point: 228 °C.

6.2.4 Synthesis of Symmetrically Substituted Bistriazolium Halide Salts

*6.2.4.1 1,1'-[1,3-Phenylenebis(methylene)]bis[4-(2,4,6-trimethylphenyl)-1*H*-1,2,4-triazolium] Dichloride • Acetic Acid* (**31**)

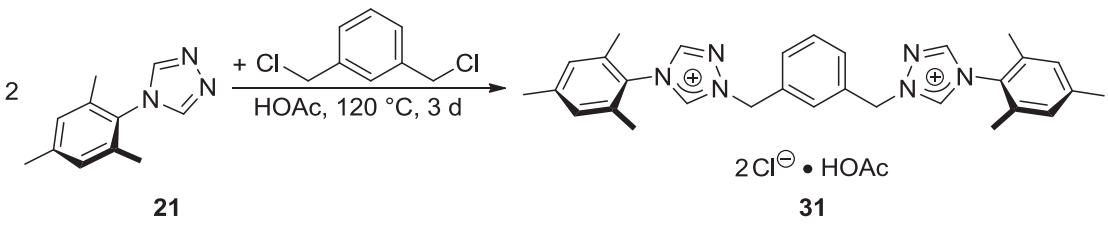

21 **31**

A 100 ml Schlenk flask under an atmosphere of inert gas was charged with 4-(2,4,6-trimethylphenyl)-4*H*-1,2,4-triazole (**21**, 7.510 g, 40.11 mmol) and 1,3-bis(chloromethyl)benzene (2.340 g, 13.37 mmol). The solid substrates were dissolved in glacial acetic acid (10 ml). The reaction mixture was stirred under reflux conditions for three days. The solvent was removed *in vacuo*. The solid residue was washed with hot toluene (90 °C, 3 × 100 ml) and diethyl ether (3 × 100 ml). The colourless powdery product was dried *in vacuo* (7.306 g, 11.99 mmol, 90 % with respect to the adduct with acetic acid $C_{32}H_{38}Cl_2N_6O_2$). The excess triazole was isolated from the toluene solution by evaporating the solvent *in vacuo* and washing the resulting solid with diethyl ether.

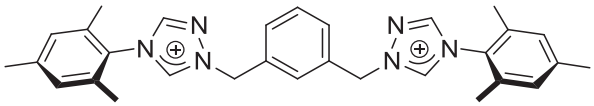

$2\,Cl^{\ominus}$ • HOAc

31

$C_{30}H_{34}Cl_2N_6$ • HOAc

M ($C_{30}H_{34}Cl_2N_6$) = 549.54 g mol^{-1}

M ($C_{32}H_{38}Cl_2N_6O_2$) = 609.59 g mol^{-1}

^{1}H NMR (300.190 MHz, d_6-DMSO, 27 °C): δ = 11.40 (s, 2H, MesNC*H*NCH$_2$), 9.66 (s, 2H, MesNC*H*NNCH$_2$), 7.86 (br, s, 1H, Xyl-linker, CH$_2$CC*H*CCH$_2$), 7.62 (br, m, 2H, Xyl-linker, CH$_2$CC*H*CH), 7.54 (br, m, 1H, Xyl-linker, CH$_2$CCHC*H*), 7.17 (s, 4H, Mes-substituent, *meta*-C*H*), 5.85 (s, 4H, C*H*$_2$), 2.34 (s, 6H, *para*-C*H*$_3$), 2.11 (s, 12H, *ortho*-C*H*$_3$), 1.91 (s, 3H, *H*$_3$CCOOH).

^{13}C{^{1}H} NMR (75.483 MHz, d_6-DMSO, 27 °C): δ = 171.9 (H$_3$C*C*OOH), 145.7 (MesN*C*HNNCH$_2$), 144.3 (MesN*C*HNCH$_2$), 141.0 (Mes-substituent, *para*-*C*CH$_3$), 134.3 (Xyl-linker, *ipso*-*C*CH$_2$), 133.9 (Mes-substituent, *ortho*-*C*CH$_3$), 129.7 (Xyl-linker, CH$_2$C*C*HCCH$_2$), 129.6 (Xyl-linker, CH$_2$C*C*HCH or CH$_2$CCH*C*H), 129.5 (Mes-substituent, *meta*-*C*H), 129.5 (Xyl-linker, CH$_2$C*C*HCH or CH$_2$CCH*C*H), 128.0 (Mes-substituent, *ipso*-*C*N), 54.7 (*C*H$_2$), 21.1 (*para*-*C*H$_3$), 20.6 (*ortho*-*C*H$_3$), 17.3 (H$_3$*C*COOH).

HR-MS (ESI+, methanol) *m*/*z* (%): 239.14167 (31.7) [M-HOAc-2Cl]$^{2+}$, 359.19806 (4.9) [M-HOAc-C$_9$H$_{11}$-2Cl]$^+$, 513.25277 (100.0) [M(^{35}Cl)-HOAc-Cl]$^+$, 513.25277 (35.7) [M(^{37}Cl)-HOAc-Cl]$^+$.

calculated for [C$_{30}$H$_{34}$(^{35}Cl)N$_6$]$^+$:	513.25280
found:	513.25277

Infrared Spectroscopy (KBr): $\tilde{\nu}$ [cm^{-1}] = 3423 (br, m), 2982 (br, m), 1715 (m), 1608 (w), 1559 (m), 1517 (w), 1486 (w), 1452 (w), 1383 (w), 1316 (w), 1232 (w), 1203 (w), 1155 (w), 1091 (w), 1001 (w), 858 (w), 736 (w), 678 (w), 577 (w), 443 (w).

Melting Point: 240 °C.

*6.2.4.2 1,1'-(Ethane-1,2-diyl)bis[4-(2,4,6-trimethylphenyl)-1*H*-1,2,4-triazolium] Dibromide* (**41**)

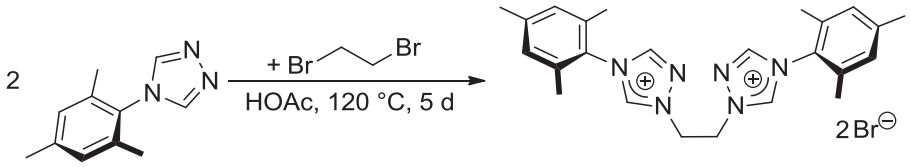

21 **41**

In a 100 ml Schlenk flask flushed with inert gas, 4-(2,4,6-trimethylphenyl)-4*H*-1,2,4-triazole (**21**, 3.091 g, 16.51 mmol) was dissolved in glacial acetic acid (8 ml) and 1,2-dibromoethane (1.422 g, 7.569 mmol) was added *via* syringe. The reaction mixture was stirred under reflux conditions (120 °C) for five days. The solvent was removed *in vacuo*. The light yellow solid residue was washed with hot toluene (90 °C, 3 × 100 ml) and diethyl ether (3 × 30 ml). The colourless solid was dried *in vacuo* (3.828 g, 6.807 mmol, 90 %). The excess triazole was isolated from the toluene solution by evaporating the solvent *in vacuo* and washing the resulting solid with diethyl ether.

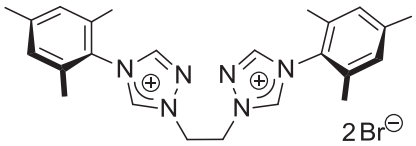

41

$C_{24}H_{30}Br_2N_6$

M ($C_{24}H_{30}Br_2N_6$) = 562.34 g mol^{-1}

^{1}H NMR (300.190 MHz, d_6-DMSO, 27 °C): δ = 10.86 (s, 2H, MesNC*H*NCH$_2$) 9.64 (s, 2H, MesNC*H*NNCH$_2$), 7.20 (s, 4H, *meta*-C*H*), 5.27 (s, 4H, C*H*$_2$), 2.34 (s, 6H, *para*-C*H*$_3$), 2.11 (s, 12H, *ortho*-C*H*$_3$).

^{13}C{^{1}H} NMR (75.483 MHz, d_6-DMSO, 27 °C): δ = 145.5 (MesN*C*HNNCH$_2$), 144.8 (MesN*C*HNCH$_2$), 141.1 (*para*-*C*CH$_3$), 134.4 (*ortho*-*C*CH$_3$), 129.5 (*meta*-*C*H), 127.9 (*ipso*-*C*N), 50.2 (*C*H$_2$), 20.6 (*para*-*C*H$_3$), 17.3 (*ortho*-*C*H$_3$).

HR-MS (ESI+, methanol) *m*/*z* (%): 188.11824 (1.1) $[M\text{-}C_{13}H_{16}N_3\text{-}2Br]^+$, 201.12605 (23.3) $[M\text{-}2Br]^{2+}$, 214.13385 (29.3) $[M\text{-}C_{11}H_{14}N_3\text{-}2Br]^+$, 274.15499 (41.9) $[M\text{-}C_9H_{10}N_3\text{-}2Br\text{+}O_2]^+$, 283.16656 (77.3) $[M\text{-}C_9H_{11}\text{-}2Br]^+$, 374.23395 (100.0) $[M\text{-}H_2CN\text{-}2Br]^+$, 401.24487 (30.3) $[M\text{-}H\text{-}2Br]^+$.

calculated for $[C_{24}H_{30}N_6]^{2+}$:	201.12605
found:	201.12605

Infrared Spectroscopy (KBr)**:** $\tilde{\nu}$ [cm^{-1}] = 3406 (br, m), 3001 (br, s), 1718 (s), 1607 (m), 1561 (s), 1520 (m), 1486 (m), 1447 (m), 1380 (m), 1313 (m), 1208 (m, br), 1227 (m), 1161 (m), 1091 (m), 1038 (m), 1003 (m), 991 (m), 857 (m), 679 (m), 578 (m), 557 (m).

Decomposition Temperature: 277 °C (black solid).

Crystal Strcuture: Crystallographic data and structure refinements for reb21, formula $C_{24}H_{30}Br_2N_6$, *M* ($C_{24}H_{30}Br_2N_6$) = 562.34 g mol^{-1}: colourless crystal (polyhedron), dimensions 0.18 × 0.17 × 0.15 mm^3, crystal system monoclinic, space group $P2_1/c$, $Z = 4$, a = 12.0668(12) Å, b = 15.4462(14) Å, c = 14.4654(14) Å, α = 90°, β = 95.580(3)°, γ = 90°, V = 2683.4(4) $Å^3$, ρ = 1.432 g cm^{-3}, T = 200(2) K, Θ_{max} = 25.03°, radiation Mo K_α, λ = 0.71073 Å, 0.5° ω-scans with CCD area detector, covering the asymmetric unit in reciprocal space with a mean redundancy of 3.64 and a completeness of 100.0 % to a resolution of 0.84 Å, 17545 reflections measured, 4743 unique (R(int)= 0.0631), 3290 observed ($I > 2\sigma(I)$), intensities were corrected for Lorentz and polarization effects, an empirical absorption correction was applied using SADABS[165] based on the Laue symmetry of the reciprocal space, μ = 3.05 mm^{-1}, T_{min} = 0.61, T_{max} = 0.66, structure solved by direct methods and refined against F^2 with a full-matrix least-squares algorithm using the SHELXTL (version 2008/4) software package,[166] 314 parameters refined, hydrogen atoms were treated using appropriate riding models, goodness of fit 1.04 for observed reflections, final residual values $R1(F)$ = 0.056, $wR(F^2)$ = 0.141 for observed reflections, residual electron density -0.88 to 0.89 $eÅ^{-3}$.

*6.2.4.3 1,1'-[1,3-Phenylenebis(methylene)]bis[4-(3,5-dimethylphenyl)-1*H*-1,2,4-triazolium] Dichloride* (**32**)

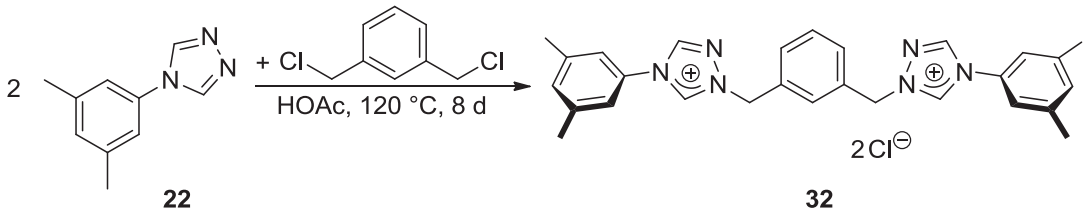

22 **32**

A 100 ml Schlenk flask under an atmosphere of inert gas was charged with 4-(3,5-dimethylphenyl)-4*H*-1,2,4-triazole (**22**, 3.454 g, 19.94 mmol) and 1,3-bis(chloromethyl)-benzene (1.164 g, 6.649 mmol). The solid substrates were dissolved in glacial acetic acid (8 ml). The reaction mixture was stirred under reflux conditions (120 °C) for eight days. The solvent was removed *in vacuo*. The solid residue was washed with hot toluene (90 °C, 3 × 100 ml), with isopropanol (2 × 100 ml) and with diethyl ether (3 × 100 ml). The colourless powdery product was dried *in vacuo* (3.037 g, 5.824 mmol, 88 %). The excess triazole was isolated from the toluene solution by evaporating the solvent *in vacuo* and washing the resulting solid with diethyl ether.

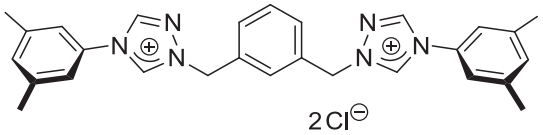

32

$C_{28}H_{30}Cl_2N_6$

M ($C_{28}H_{30}Cl_2N_6$) = 521.48 g mol^{-1}

^{1}H NMR (400.180 MHz, d_6-DMSO, 25 °C): δ = 11.23 (s, 2H, XylNC*H*NCH$_2$), 9.80 (s, 2H, XylNC*H*NNCH$_2$), 7.79 (s, 1H, Xyl-linker, CH$_2$CC*H*CCH$_2$), 7.70 - 7.40 (m, 7H, Xyl-linker, CH$_2$CC*H*CH and CH$_2$CCHC*H*, and Xyl-substituent, *ortho*-C*H*), 7.29 (s, 2H, Xyl-substituent, *para*-C*H*), 5.73 (s, 4H, C*H*$_2$), 2.38 (s, 12H, C*H*$_3$).

^{1}H NMR (400.180 MHz, CD_3OD, 25 °C): δ = 10.75 (s, 2H, XylNC*H*NCH$_2$), 9.48 (s, 2H, XylNC*H*NNCH$_2$), 7.89 (s, 1H, Xyl-linker, CH$_2$CC*H*CCH$_2$), 7.68 (dd, $^3J_{H\text{-}H}$ = 7.7 Hz, $^4J_{H\text{-}H}$ = 1.2 Hz, 2H, Xyl-linker, CH$_2$CC*H*CH), 7.57 (t, $^3J_{H\text{-}H}$ = 7.7 Hz, 1H, Xyl-linker,

$CH_2CCHC\underline{H}$), 7.45 (s, 4H, Xyl-substituent, *ortho*-C$\underline{H}$), 7.31 (s, 2H, Xyl-substituent, *para*-C$\underline{H}$), 5.79 (s, 4H, C$\underline{H_2}$), 2.44 (s, 12H, C$\underline{H_3}$).

$^{13}C\{^1H\}$ NMR (100.625 MHz, CD_3OD, 25 °C): δ = 144.6 (XylN$\underline{C}$HNNCH$_2$), 142.8 (XylN$\underline{C}$*H*NCH$_2$), 142.2 (Xyl-substituent, $\underline{C}CH_3$), 134.8 (Xyl-linker, *ipso*-$\underline{C}CH_2$), 133.4 (Xyl-substituent, *para*-$\underline{C}$H), 131.5 (Xyl-linker, $CH_2C\underline{C}HCH$), 131.5 (Xyl-linker, $CH_2C\underline{C}HCCH_2$), 131.1 (Xyl-linker, $CH_2CCH\underline{C}H$), 121.2 (Xyl-substituent, *ortho*-$\underline{C}$H), 56.8 ($\underline{C}H_2$), 21.2 ($\underline{C}H_3$).
A signal for the quaternary *ipso*-C-atom of the xylyl-substituent next to the triazolium's N-atom is missing in the $^{13}C\{^1H\}$ NMR spectrum: it might either be concealed by another peak or its intensity is too low, possibly due the electric quadrupole moment of the neighbouring ^{14}N-atom.

HR-MS (ESI+, methanol) *m*/*z* (%): 225.12613 (19.1) $[M\text{-}2Cl]^{2+}$, 345.18242 (2.4) $[M\text{-}C_8H_9\text{-}2Cl]^+$, 422.23422 (2.3) $[M\text{-}CH_2N\text{-}2Cl]^+$, 449.24499 (100.0) $[M\text{-}H\text{-}2Cl]^+$, 485.22174 (35.8) $[M(^{35}Cl)\text{-}Cl]^+$, 487.21883 (12.0) $[M(^{37}Cl)\text{-}Cl]^+$.
calculated for $[C_{28}H_{30}(^{35}Cl)N_6]^+$: 485.22150
found: 485.22174

Infrared Spectroscopy (KBr): $\tilde{\nu}$ [cm^{-1}] = 3425 (s), 3012 (br, s), 1620 (s), 1599 (m), 1566 (s), 1476 (w), 1440 (w), 1377 (m), 1310 (w), 1270 (m), 1206 (w), 1106 (m), 1053 (w), 1004 (w), 849 (w), 821 (m), 733 (w), 683 (m), 661 (w), 638 (w).

Elemental Analysis (No. 32462)
calculated for $C_{28}H_{30}Cl_2N_6$: C 64.49 %, H 5.80 %, N 16.12 %
found: C 63.89 %, H 5.94 %, N 15.80 %

Decomposition Temperature: 266 °C - 269 °C (dark brown liquid).

*6.2.4.4 1,1'-(Ethane-1,2-diyl)bis[4-(3,5-dimethylphenyl)-1*H*-1,2,4-triazolium] Dibromide* (**42**)[128]

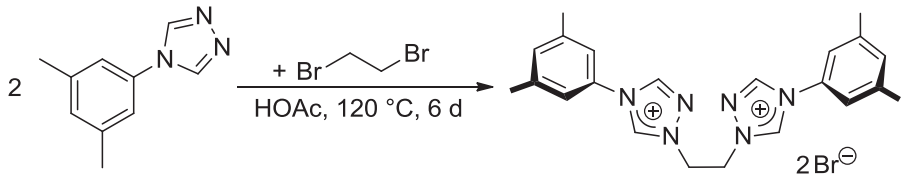

22 **42**

In a 100 ml Schlenk flask flushed with inert gas, 4-(3,5-dimethylphenyl)-4*H*-1,2,4-triazole (**22**, 5.196 g, 30.00 mmol) was dissolved in glacial acetic acid (5 ml) and 1,2-dibromoethane (1.879 g, 10.00 mmol) was added *via* syringe. The reaction mixture was stirred under reflux conditions (120 °C) for six days. The solvent was removed *in vacuo*. The light yellow solid residue was washed with acetone (3 × 30 ml), hot toluene (90 °C, 2 × 100 ml) and diethyl ether (3 × 30 ml). The colourless solid was dried *in vacuo* (5.180 g, 9.695 mmol, 97 %). The excess triazole was isolated from the toluene solution by evaporating the solvent *in vacuo* and washing the resulting solid with diethyl ether.

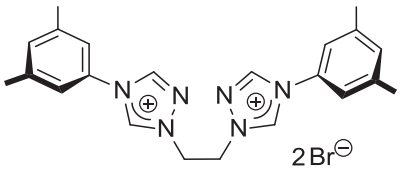

42

$C_{22}H_{26}Br_2N_6$

M ($C_{22}H_{26}Br_2N_6$) = 534.29 g mol^{-1}

^{1}H NMR (500.130 MHz, d_6-DMSO, 25 °C): δ = 11.09 (s, 2H, XylNC*H*NCH$_2$), 9.90 (s, 2H, XylNC*H*NNCH$_2$), 7.52 (s, 4H, *ortho*-C*H*), 7.29 (s, 2H, *para*-C*H*), 5.16 (s, 4H, C*H*$_2$), 2.38 (s, 12H, C*H*$_3$).

^{13}C{^{1}H} NMR (125.758 MHz, d_6-DMSO, 25 °C): δ = 143.0 (XylN*C*HNNCH$_2$), 142.7 (XylN*C*HNCH$_2$), 139.9 (*C*CH$_3$), 131.8 (*ipso*-*C*N), 131.7 (*para*-*C*H), 119.7 (*ortho*-*C*H), 49.8 (*C*H$_2$), 20.7 (*C*H$_3$).

HR-MS (ESI+, methanol) *m*/*z* (%): 269.15081 (13.8) $[M\text{-}2Br\text{-}C_8H_9]^+$, 346.20246 (7.9) $[M\text{-}2Br\text{-}CH_2N]^+$, 373.21328 (100.0) $[M\text{-}2Br\text{-}H]^+$, 453.13938 (61.1) $[M(^{79}Br)\text{-}Br]^+$, 455.13731 (61.8) $[M(^{81}Br)\text{-}Br]^+$, 985.19706 (3.1) $[2M(^{79}Br,^{79}Br,^{79}Br)\text{-}Br]^+$, 987.19478 (9.2) $[2M(^{79}Br,^{79}Br,^{81}Br)\text{-}Br]^+$, 989.19272 (9.2) $[2M(^{79}Br,^{81}Br,^{81}Br)\text{-}Br]^+$, 991.19073 (3.1) $[2M(^{81}Br,^{81}Br,^{81}Br)\text{-}Br]^+$.

calculated for $[C_{22}H_{25}N_6]^+$: 373.21352

found: 373.21328

Infrared Spectroscopy (KBr): $\tilde{\nu}$ [cm^{-1}] = 3422 (br, m), 3018 (w), 1620 (m), 1570 (m), 1527 (w), 1477 (w), 1442 (w), 1309 (w), 1270 (w), 1192 (w), 1106 (w), 1054 (w), 999 (w), 849 (w), 821 (w), 683 (w), 636 (w).

Elemental Analysis (No. 31567)

calculated for $C_{22}H_{26}Br_2N_6$: C 49.46 %, H 4.90 %, N 15.73 %

found: C 49.42 %, H 4.92 %, N 15.53 %

Decomposition Temperature: 300 – 307 °C (black liquid).

*6.2.4.5 1,1'-[1,3-Phenylenebis(methylene)]bis[4-(4-methylphenyl)-1*H*-1,2,4-triazolium Dichloride* (**33**)

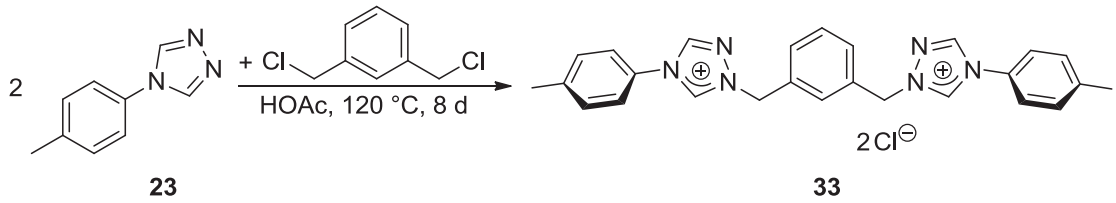

23 **33**

A 100 ml Schlenk flask under an atmosphere of inert gas was charged with 4-(4-methylphenyl)-4*H*-1,2,4-triazole (**23**, 1.988 g, 12.49 mmol) and 1,3-bis(chloromethyl)-benzene (0.841 g, 4.80 mmol). The solid substrates were dissolved in glacial acetic acid (6 ml). The reaction mixture was stirred under reflux conditions (120 °C) for eight days. The solvent was removed *in vacuo*. The solid residue was washed with hot toluene (90 °C, 3 × 100 ml), with isopropanol (2 × 100 ml) and with diethyl ether (3 × 100 ml). The colourless powdery product was dried *in vacuo* (2.367 g, 4.797 mmol, quantitative yield). The excess triazole was isolated from the toluene solution by evaporating the solvent *in vacuo* and washing the resulting solid with diethyl ether.

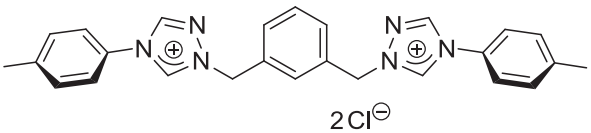

33

$C_{26}H_{26}Cl_2N_6$

M ($C_{26}H_{26}Cl_2N_6$) = 492.16 g mol^{-1}

^{1}H NMR (400.180 MHz, D_2O, 25 °C): δ = 9.24 (s, 2H, TolNC*H*NNCH_2), 7.74 (s, 1H, Xyl-linker, CH_2CC*H*CCH_2), 7.70 - 7.58 (m, 3H, Xyl-linker, CH_2CC*H*CH and CH_2CCHC*H*), 7.52 (d, $^3J_{H\text{-}H}$ = 8.5 Hz, 4H, Tol-substituent, *meta*-C*H*), 7.47 (d, $^3J_{H\text{-}H}$ = 8.5 Hz, 4H, Tol-substituent, *ortho*-C*H*), 5.78 (s, 4H, CH_2), 2.43 (s, 6H, CH_3).
The signals for the acidic protons of the triazolium rings cannot be observed in the ^{1}H NMR spectrum due to proton exchange with the solvent D_2O.

^{13}C{^{1}H} NMR (100.625 MHz, D_2O, 25 °C): δ = 143.5 (TolN*C*HNNCH_2), 142.1 (Tol-substituent, *C*CH_3), 140.8 (t, $^1J_{C\text{-}D}$ = 34.8 Hz, TolN*C*HNCH_2), 132.8 (Xyl-linker, *ipso*-

CCH_2), 130.9 (Tol-substituent, *ortho*-*C*H), 130.5 (Xyl-linker, CH_2C*C*HCH), 130.4 (Xyl-linker, CH_2CCH*C*H), 130.1 (Xyl-linker, CH_2C*C*$HCCH_2$), 129.0 (Tol-substituent, *ipso*-*C*N), 122.2 (Tol-substituent, *meta*-*C*H), 55.7 (*C*H_2), 20.3 (*C*H_3).
The exchange of the acidic triazolium proton against deuterium is complete and the corresponding signal in the $^{13}C\{^1H\}$ NMR spectrum is observed as a triplet at 140.8 ppm.

HR-MS (ESI+, methanol) *m*/*z* (%): 211.11069 (3.8) $[M\text{-}2Cl]^{2+}$, 394.20308 (2.7) $[M\text{-}CH_2N\text{-}2Cl]^+$, 421.21380 (100.0) $[M\text{-}H\text{-}2Cl]^+$, 457.19065 (25.0) $[M(^{35}Cl)\text{-}Cl]^+$, 459.18778 (8.6) $[M(^{37}Cl)\text{-}Cl]^+$

calculated for $[C_{26}H_{26}(^{35}Cl)N_6]^+$:	457.19020
found:	457.19065

Infrared Spectroscopy (KBr): $\tilde{\nu}$ [cm^{-1}] = 3441 (br, m), 3003 (m), 1719 (w), 1568 (s), 1515 (w), 1443 (w), 1372 (w), 1335 (w), 1304 (w), 1278 (w), 1227 (w), 1094 (m), 1008 (w), 817 (m), 738 (w), 629 (w), 523 (w).

Decomposition Temperature: 274 - 276 °C (dark brown solid).

*6.2.4.6 1,1'-(Ethane-1,2-diyl)bis[4-(4-methyl)-1*H*-1,2,4-triazolium] Dibromide* (**43**)[168]

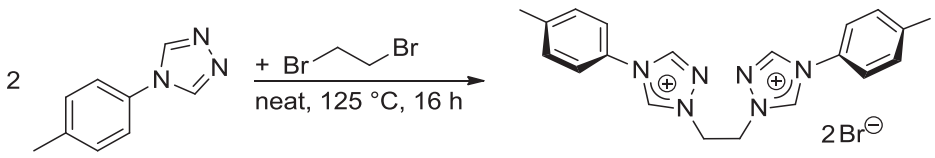

23 **43**

A 100 ml Schlenk flask flushed with inert gas was charged with 4-(4-methylphenyl)-4*H*-1,2,4-triazole (**23**, 2.430 g, 15.27 mmol) and 1,2-dibromoethane (1.303 g, 6.936 mmol). The neat reaction mixture was stirred at 125 °C for 16 hours. The resulting colourless solid was washed with hot toluene (90 °C, 3 × 100 ml) and diethyl ether (3 × 30 ml) and then dried *in vacuo* (3.188 g, 5.669 mmol, 82 %). The excess triazole was isolated from the toluene solution by evaporating the solvent *in vacuo* and washing the resulting solid with diethyl ether.

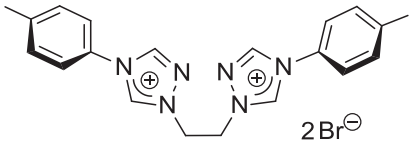

43

$C_{20}H_{22}Br_2N_6$

M ($C_{20}H_{22}Br_2N_6$) = 506.24 g mol^{-1}

^{1}H NMR (300.190 MHz, d_6-DMSO, 27 °C): δ = 11.14 (s, 2H, TolNC*H*NCH$_2$), 9.91 (s, 2H, TolNC*H*NNCH$_2$), 7.76 (d, $^3J_{H\text{-}H}$ = 8.3 Hz, 4H, *meta*-C*H*), 7.50 (d, $^3J_{H\text{-}H}$ = 8.3 Hz, 4H, *ortho*-C*H*), 5.18 (s, 4H, CH$_2$), 2.40 (s, 6H, CH$_3$).

^{13}C{^{1}H} NMR (75.483 MHz, d_6-DMSO, 27 °C): δ = 143.1 (TolNCHNNCH$_2$), 142.7 (TolNCHNCH$_2$), 140.6 (CCH$_3$), 130.5 (*ortho*-CH), 129.6 (*ipso*-CN), 122.2 (*meta*-CH), 49.8 (CH$_2$), 20.6 (CH$_3$).

HR-MS (ESI+, methanol) *m*/*z* (%): 255.13525 (19.6) [M-C$_7$H$_7$-2Br]$^+$, 345.18216 (100.0) [M-H-2Br]$^+$, 425.10838 (35.3) [M(^{79}Br)-Br]$^+$, 427.10631 (36.9) [M(^{81}Br)-Br]$^+$.

calculated for [C$_{20}$H$_{22}$(^{79}Br)N$_6$]$^+$:	425.10838
found:	425.10838

Infrared Spectroscopy (KBr): $\tilde{\nu}$ [cm^{-1}] = 3423 (s), 3009 (m), 2954 (m), 1621 (w), 1571 (s), 1512 (m), 1438 (w), 1336 (w), 1304 (w), 1280 (w), 1253 (w), 1211 (w), 1094 (m), 1042 (w), 995 (w), 818 (m), 648 (w), 626 (w), 523 (w), 465 (w).

Elemental Analysis (No. 30979)

calculated for $C_{20}H_{22}Br_2N_6$:	C 47.45 %,	H 4.38 %,	N 16.60 %
found:	C 47.28 %,	H 4.47 %,	N 16.38 %

Melting Point: 250 - 252 °C.

*6.2.4.7 1,1'-[1,3-Phenylenebis(methylene)]bis[4-(2,6-diisopropylphenyl)-1*H*-1,2,4-triazolium] Dichloride* (**34**)

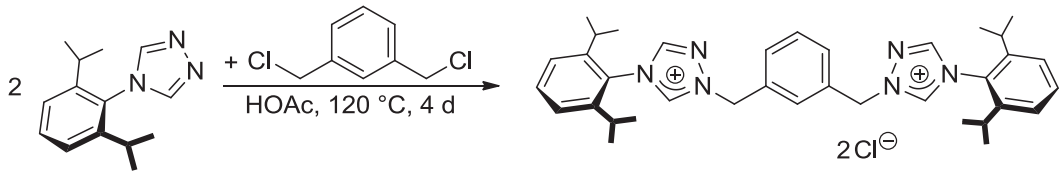

24 **34**

A 100 ml Schlenk flask under an atmosphere of inert gas was charged with 4-(2,6-diisopropylphenyl)-4*H*-1,2,4-triazole (**24**, 3.004 g, 13.10 mmol) and 1,3-bis(chloromethyl)benzene (0.996 g, 5.69 mmol). The solid substrates were dissolved in glacial acetic acid (5 ml). The reaction mixture was stirred under reflux conditions (120 °C) for four days. The solvent was removed *in vacuo*. The solid residue was washed with hot toluene (90 °C, 3 × 100 ml) and diethyl ether (3 × 100 ml). The colourless powdery product was dried *in vacuo* (3.595 g, 5.673 mmol, quantitative yield). The excess triazole was isolated from the toluene solution by evaporating the solvent *in vacuo* and washing the resulting solid with diethyl ether.

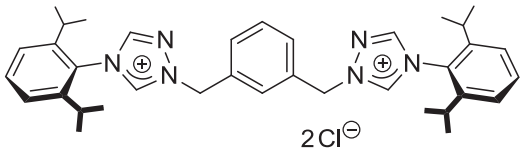

34

$C_{36}H_{46}Cl_2N_6$

M ($C_{36}H_{46}Cl_2N_6$) = 633.70 g mol^{-1}

^{1}H NMR (400.180 MHz, d_6-DMSO, 25 °C): δ = 11.61 (s, 2H, DippNC*H*NCH$_2$), 9.84 (s, 2H, DippNC*H*NNCH$_2$), 7.81 (s, 1H, Xyl-linker, CH$_2$CC*H*CCH$_2$), 7.69 (t, $^3J_{H\text{-}H}$ = 7.8 Hz, 2H, Dipp-substituent, *para*-C*H*), 7.62 - 7.55 (m, 3H, Xyl-linker, CH$_2$CC*H*CH and CH$_2$CCHC*H*), 7.50 (d, $^3J_{H\text{-}H}$ = 7.8 Hz, 4H, Dipp-substituent, *meta*-C*H*), 5.91 (s, 4H, C*H*$_2$), 2.30 (sept, $^3J_{H\text{-}H}$ = 6.8 Hz, 4H, C*H*(CH$_3$)$_2$), 1.16 (d, $^3J_{H\text{-}H}$ = 6.8 Hz, 12H, CH(C*H*$_3$)$_2$), 1.13 (d, $^3J_{H\text{-}H}$ = 6.8 Hz, 12H, CH(C*H*$_3$)$_2$).

$^{13}C\{^{1}H\}$ NMR (100.625 MHz, d_6-DMSO, 25 °C): δ = 146.2 (DippN<u>C</u>HNNCH$_2$), 145.1 (Dipp-substituent, *ortho*-<u>C</u>CH(CH$_3$)$_2$), 144.6 (DippN<u>C</u>HNCH$_2$), 134.1 (Xyl-linker, *ipso*-<u>C</u>CH$_2$), 132.2 (Dipp-substituent, *para*-<u>C</u>H), 129.8 (Xyl-linker, CH$_2$C<u>C</u>HCH or CH$_2$C-CH<u>C</u>H), 129.7 (Xyl-linker, CH$_2$C<u>C</u>HCH or CH$_2$CCH<u>C</u>H), 129.3 (Xyl-linker, CH$_2$C<u>C</u>H-CCH$_2$), 127.2 (Dipp-substituent, *ipso*-<u>C</u>N), 124.7 (Dipp-substituent, *meta*-<u>C</u>H), 55.0 (<u>C</u>H$_2$), 28.1 (<u>C</u>H(CH$_3$)$_2$), 23.6 (CH(<u>C</u>H$_3$)$_2$), 23.6 (CH(<u>C</u>H$_3$)$_2$).

HR-MS (ESI+, methanol) *m*/*z* (%): 281.18879 (59.4) [M-2Cl]$^{2+}$, 401.24516 (8.5) [M-$C_{12}H_{17}$-2Cl]$^{+}$, 561.37029 (100.0) [M-H-2Cl]$^{+}$, 597.34724 (41.7) [M(^{35}Cl)-Cl]$^{+}$, 599.34436 (13.3) [M(^{37}Cl)-Cl]$^{+}$.

calculated for [$C_{36}H_{46}N_6$]$^{2+}$:	281.18865
found:	281.18879

Infrared Spectroscopy (KBr): $\tilde{\nu}$ [cm^{-1}] = 3425 (br, s), 2966 (s), 2929 (s), 2871 (m), 1716 (w), 1619 (w), 1589 (w), 1556 (m), 1462 (m), 1388 (w), 1368 (w), 1304 (w), 1192 (w), 1118 (w), 1088 (w), 1060 (w), 807 (m), 757 (w), 746 (w), 680 (w).

Melting Point: 250 °C.

6.2.4.8 1,1'-(Ethane-1,2-diyl)bis[4-(2,6-diisopropylphenyl)-1H-1,2,4-triazolium] Dibromide (**44**)[129]

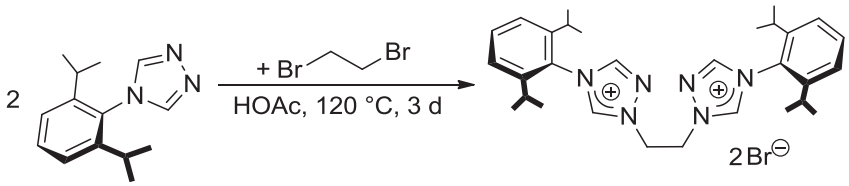

24 **44**

In a 100 ml Schlenk flask flushed with inert gas, 4-(2,6-diisopropylphenyl)-4*H*-1,2,4-triazole (**24**, 0.300 g, 1.31 mmol) was dissolved in glacial acetic acid (1.3 ml) and 1,2-dibromoethane (0.112 g, 0.596 mmol) was added *via* syringe. The reaction mixture was stirred under reflux conditions (120 °C) for three days. The solvent was removed *in vacuo*. The light yellow solid residue was washed with hot toluene (90 °C, 2 × 100 ml) and diethyl ether (3 × 30 ml). The colourless solid was dried *in vacuo*

(0.114 g, 0.176 mmol, 30 %), but still contained traces of acetic acid. The excess triazole was isolated from the toluene solution by evaporating the solvent *in vacuo* and washing the resulting solid with diethyl ether.

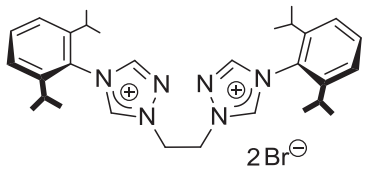

44

$C_{30}H_{42}Br_2N_6$

M ($C_{30}H_{42}Br_2N_6$) = 646.50 g mol^{-1}

^{1}H NMR (500.130 MHz, d_6-DMSO, 25 °C): δ = 11.12 (s, 2H, DippNC*H*NCH$_2$), 9.82 (s, 2H, DippNC*H*NNCH$_2$), 7.69 (t, $^3J_{H\text{-}H}$ = 7.8 Hz, 2H, *para*-C*H*), 7.51 (d, $^3J_{H\text{-}H}$ = 7.8 Hz, 4H, *meta*-C*H*), 5.37 (s, 4H, C*H*$_2$), 2.41 (sept, $^3J_{H\text{-}H}$ = 6.7 Hz, 4H, C*H*(CH$_3$)$_2$), 1.18 (d, $^3J_{H\text{-}H}$ = 6.7 Hz, 12H, CH(C*H*$_3$)$_2$), 1.13 (d, $^3J_{H\text{-}H}$ = 6.7 Hz, 12H, CH(C*H*$_3$)$_2$).

^{13}C{^{1}H} NMR (125.758 MHz, d_6-DMSO, 25 °C): δ = 145.9 (DippN*C*HNNCH$_2$), 145.3 (*ortho*-*C*CH(CH$_3$)$_2$), 145.0 (DippN*C*HNCH$_2$), 132.2 (*para*-*C*H), 127.1 (*ipso*-*C*N), 124.7 (*meta*-*C*H), 50.4 (*C*H$_2$), 27.9 (*C*H(CH$_3$)$_2$), 23.9 (CH(*C*H$_3$)$_2$), 23.6 (CH(*C*H$_3$)$_2$).

HR-MS (ESI+, methanol) *m*/*z* (%): 243.17307 (10.3) [M-2Br]$^{2+}$, 325.21364 (14.5) [M-$C_{12}H_{17}$-2Br]$^+$, 485.33901 (100.0) [M-H-2Br]$^+$, 565.26538 (16.4) [M(^{79}Br)-Br]$^+$, 567.26337 (16.4) [M(^{81}Br)-Br]$^+$.

calculated for [$C_{30}H_{41}N_6$]$^+$:	485.33872
found:	485.33901

Infrared Spectroscopy (KBr): $\tilde{\nu}$ [cm^{-1}] = 3440 (br, s), 2966 (s), 2871 (w), 1717 (w), 1627 (w), 1589 (w), 1559 (w), 1464 (w), 1387 (w), 1368 (w), 1302 (w), 1222 (w), 1182 (w), 1089 (w), 1060 (w), 991 (w), 805 (w), 757 (w), 677 (w), 552 (w).

Melting Point: 253 - 255 °C.

6.2.5 Synthesis of Unsymmetrically Substituted Bistriazolium Halide Salts

*6.2.5.1 1-[3-(Chloromethyl)benzyl]-4-(3,5-dimethylphenyl)-1*H*-1,2,4-triazolium Chloride* (**35**)

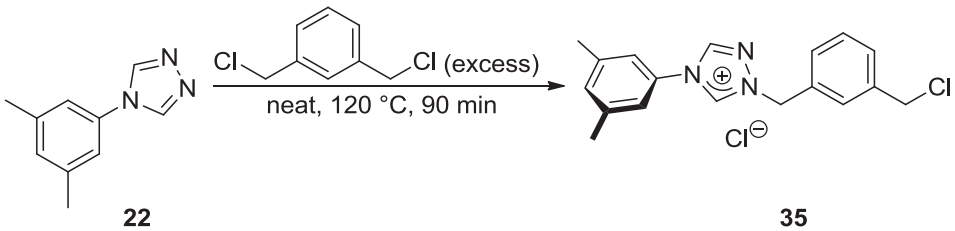

22 **35**

A flame-dried 50 ml Schlenk flask was charged with 4-(3,5-dimethylphenyl)-1*H*-1,2,4-triazole (**22**, 0.750 g, 4.33 mmol) and 1,3-bis(chloromethyl)benzene (6.821 g, 38.96 mmol). The reaction mixture was heated to 120 °C for 90 minutes. After cooling off, the resulting solid was broken to pieces and diethyl ether was added. After stirring this mixture for 18 hours, the ether solution was filtered and the resulting colourless solid dried *in vacuo* (1.427 g, 4.097 mmol, 95 %). The excess 1,3-bis(chloromethyl)benzene was re-isolated from the diethyl ether solution by evaporating the solvent.

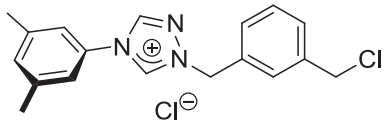

35

$C_{18}H_{19}Cl_2N_3$

M ($C_{18}H_{19}Cl_2N_3$) = 348.27 g mol^{-1}

^{1}H NMR (300.080 MHz, d_6-DMSO, 25 °C): δ = 11.64 (s, 1H, XylNC*H*NCH$_2$), 9.96 (s, 1H, XylNC*H*NNCH$_2$), 7.64 (s, 1H, Xyl-linker, CH$_2$CC*H*CCH$_2$), 7.60 (s, 2H, Xyl-substituent, *ortho*-C*H*), 7.59 - 7.37 (m, 3H, Xyl-linker, NCH$_2$CC*H*CHCHCCH$_2$Cl and NCH$_2$CCHC*H*CHCCH$_2$Cl and NCH$_2$CCHCHC*H*CCH$_2$Cl), 7.26 (s, 1H, Xyl-substituent, *para*-C*H*), 5.77 (s, 2H, NC*H*$_2$), 4.78 (s, 2H, C*H*$_2$Cl), 2.38 (s, 6H, C*H*$_3$).

^{13}C{^{1}H} NMR (75.455 MHz, d_6-DMSO, 25 °C): δ = 143.1 (XylN*C*HNNCH$_2$), 142.0 (XylN*C*HNCH$_2$), 139.7 (Xyl-substituent, *C*CH$_3$), 138.2 (Xyl-linker, *C*CH$_2$Cl),

133.6 (Xyl-linker, $NCH_2\underline{C}$) 132.0 (Xyl-substituent, *ipso*-$\underline{C}$N), 131.5 (Xyl-substituent, *para*-$\underline{C}$H), 129.4 (Xyl-linker, $NCH_2C\underline{C}HCHCHCCH_2Cl$ or $NCH_2CCH\underline{C}HCHCCH_2Cl$ or $NCH_2CCHCH\underline{C}HCCH_2Cl$), 129.3 (Xyl-linker, $CH_2C\underline{C}HCCH_2$), 129.2 (Xyl-linker, $NCH_2C\underline{C}HCHCHCCH_2Cl$ or $NCH_2CCH\underline{C}HCHCCH_2Cl$ or $NCH_2CCHCH\underline{C}HCCH_2Cl$), 129.0 (Xyl-linker, $NCH_2C\underline{C}HCHCHCH_2Cl$ or $NCH_2CCH\underline{C}HCHCH_2Cl$ or $NCH_2CCHCH\underline{C}HCHCH_2Cl$), 119.6 (Xyl-substituent, *ortho*-$\underline{C}$H), 54.5 ($N\underline{C}H_2$), 45.7 ($\underline{C}H_2Cl$), 20.7 ($\underline{C}H_3$).

HR-MS (ESI+, methanol) *m*/*z* (%): 312.12632 (100) $[M(^{35}Cl)\text{-}Cl]^+$, 314.12333 (34.4) $[M(^{37}Cl)\text{-}Cl]^+$.

calculated for $[C_{18}H_{19}(^{35}Cl)N_3]^+$:	312.12620
found:	312.12632

Infrared Spectroscopy (KBr)**:** $\tilde{\nu}$ [cm^{-1}] = 3420 (br, s), 3004 (br, s), 1620 (s), 1599 (m), 1566 (s), 1476 (w), 1441 (m), 1368 (w), 1310 (m), 1271 (m), 1204 (w), 1174 (w), 1106 (m), 849 (w), 821 (m), 762 (w), 711 (w), 682 (s, C-Cl stretch), 662 (m, C-Cl stretch), 638 (m).

Elemental Analysis (No. 30177)

calculated for $C_{18}H_{19}Cl_2N_3$:	C	62.08 %,	H	5.50 %,	N 12.07 %
found:	C	61.81 %,	H	5.49 %,	N 11.90 %

Melting Point: 265 °C.

*6.2.5.2 4-(2,6-Diisopropylphenyl)-1-{3-[4-(3,5-dimethylphenyl)-1*H*-1,2,4-triazolium-1-ylmethyl]benzyl}-1*H*-1,2,4-triazolium Dichloride* (**36**)

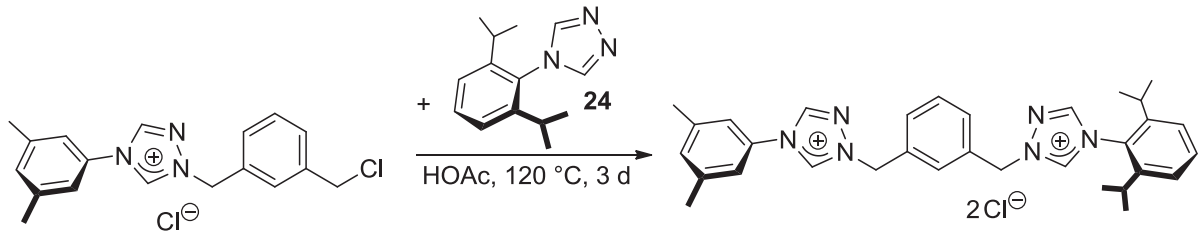

35 **36**

In a 100 ml Schlenk flask flushed with inert gas, 1-[3-(chloromethyl)benzyl]-4-(3,5-dimethylphenyl)-1*H*-1,2,4-triazolium chloride (**35**, 0.311 g, 0.893 mmol) and 4-(2,6-diisopropylphenyl)-4*H*-1,2,4-triazole (**24**, 0.410 g, 1.79 mmol) were dissolved in glacial acetic acid (3 ml). The reaction mixture was stirred under reflux conditions (120 °C) for three days. The solvent was removed *in vacuo*. The solid residue was washed with hot toluene (90 °C, 3 × 100 ml) and diethyl ether (3 × 30 ml). The colourless powdery product was dried *in vacuo* (0.270 g, 0.468 mmol, 52 %). Traces of acetic acid in the product could not be eliminated, but did not affect the subsequent reaction.

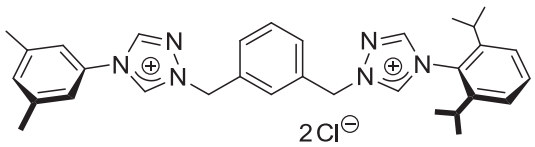

36

$C_{32}H_{38}Cl_2N_6$

M ($C_{32}H_{38}Cl_2N_6$) = 577.59 g mol^{-1}

^{1}H NMR (400.180 MHz, d_6-DMSO, 25 °C): δ = 11.67 (s, 1H, $CH_2NC\underline{H}NDipp$), 11.66 (s, 1H, $XylNC\underline{H}NCH_2$), 9.95 (s, 1H, $CH_2NNC\underline{H}NDipp$), 9.84 (s, 1H, $XylNC\underline{H}NNCH_2$), 7.85 (s, 1H, Xyl-linker, $CH_2CC\underline{H}CCH_2$), 7.68 (t, $^3J_{H\text{-}H}$ = 7.8 Hz, 1H, Dipp-substituent, *para*-C$\underline{H}$), 7.66 - 7.63 (m, 1H, Xyl-linker, $XylNCHNCH_2CCHC\underline{H}CH\text{-}CCH_2NCHNDipp$), 7.62 (s, 2H, Xyl-substituent, *ortho*-C$\underline{H}$), 7.60 - 7.52 (2H, Xyl-linker, $XylNCHNCH_2CC\underline{H}CHCHCCH_2NCHNDipp$ and $XylNCHNCH_2CCHCHC\underline{H}CCH_2N\text{-}CHNDipp$), 7.49 (d, $^3J_{H\text{-}H}$ = 7.8 Hz, 2H, Dipp-substituent, *meta*-C$\underline{H}$), 7.27 (s, 1H, Xyl-

substituent, *para*-C<u>*H*</u>), 5.89 (s, 2H, C<u>*H*</u>$_2$NCHNDipp), 5.79 (s, 2H, XylNCHNC<u>*H*</u>$_2$), 2.38 (s, 6H, Xyl-substituent, C<u>*H*</u>$_3$), 2.29 (sept, $^3J_{H\text{-}H}$ = 6.9 Hz, 2H, C<u>*H*</u>(CH$_3$)$_2$), 1.14 (d, $^3J_{H\text{-}H}$ = 6.9 Hz, 6H, CH(C<u>*H*</u>$_3$)$_2$), 1.12 (d, $^3J_{H\text{-}H}$ = 6.9 Hz, 6H, CH(C<u>*H*</u>$_3$)$_2$).

^{13}C{^{1}H} NMR (100.625 MHz, d$_6$-DMSO, 25 °C): δ = 146.2 (CH$_2$NN<u>*C*</u>HNDipp), 145.1 (Dipp-substituent, *ortho*-<u>*C*</u>CH(CH$_3$)$_2$), 144.5 (CH$_2$N<u>*C*</u>HNDipp), 143.1 (XylN<u>*C*</u>HN-NCH$_2$), 142.1 (XylN<u>*C*</u>HNCH$_2$), 139.7 (Xyl-substituent, <u>*C*</u>CH$_3$), 134.0 (Xyl-linker, XylN-CHNCH$_2$<u>*C*</u>), 133.9 (Xyl-linker, <u>*C*</u>CH$_2$NCHNDipp), 132.2 (Dipp-substituent, *para*-<u>*C*</u>H), 132.0 (Xyl-substituent, *ipso*-<u>*C*</u>N), 131.5 (Xyl-substituent, *para*-<u>*C*</u>H), 129.7 (Xyl-linker, XylNCHNCH$_2$CCHC<u>*H*</u>CHCCH$_2$NCHNDipp), 129.6 (Xyl-linker, CH$_2$C<u>*C*</u>HCCH$_2$), 129.5 (Xyl-linker, XylNCHNCH$_2$C<u>*C*</u>HCHCHCCH$_2$NCHNDipp or XylNCHNCH$_2$CCH-CH<u>*C*</u>HCCH$_2$NCHNDipp), 129.2 (Xyl-linker, XylNCHNCH$_2$C<u>*C*</u>HCHCHCCH$_2$NCHNDipp or XylNCHNCH$_2$CCHCH<u>*C*</u>HCCH$_2$NCHNDipp), 127.2 (Dipp-substituent, *ipso*-<u>*C*</u>N), 124.7 (Dipp-substituent, *meta*-<u>*C*</u>H), 119.7 (Xyl-substituent, *ortho*-<u>*C*</u>H), 55.0 (<u>*C*</u>H$_2$N-CHNDipp), 54.5 (XylNCHN<u>*C*</u>H$_2$), 28.1 (<u>*C*</u>H(CH$_3$)$_2$), 23.6 (CH(<u>*C*</u>H$_3$)$_2$), 23.6 (CH(<u>*C*</u>H$_3$)$_2$), 20.7 (Xyl-substituent, <u>*C*</u>H$_3$).

HR-MS (ESI+, methanol) *m*/*z* (%): 253.15739 (100.0) [M-2Cl]$^{2+}$, 345.18253 (6.4) [M-C$_{12}$H$_{17}$-2Cl]$^+$, 505.30799 (41.2) [M-H-2Cl]$^+$, 541.28475 (26.8) [M(^{35}Cl)-Cl]$^+$, 543.28186 (8.6) [M(^{37}Cl)-Cl]$^+$, 568.30377 (9.5) [M+NO$_3$-2Cl]$^+$.

calculated for [C$_{32}$H$_{38}$N$_6$]$^{2+}$:	253.15735
found:	253.15739

Infrared Spectroscopy (KBr): $\tilde{\nu}$ [cm^{-1}] = 3421 (br, s), 2966 (br, s), 1717 (m), 1620 (m), 1598 (w), 1562 (s), 1441 (w), 1368 (w), 1309 (m), 1225 (w), 1195 (w), 1160 (w), 1105 (w), 1003 (w), 850 (w), 810 (w), 757 (w), 741 (w), 728 (w), 683 (w).

Melting Point: 245 °C.

Crystal Structure: Crystallographic data and structure refinements for reb5, formula C$_{32}$H$_{38}$Cl$_2$N$_6$+ H$_2$O+CH$_3$CN, *M* (C$_{34}$H$_{43}$Cl$_2$N$_7$O) = 636.67 g mol^{-1}: colourless crystal (plate), dimensions 0.33 × 0.20 × 0.04 mm^3, crystal system triclinic, space group $P\bar{1}$, *Z* = 2, *a* = 8.717(4) Å, *b* = 10.138(5) Å, *c* = 20.249(10) Å, α = 86.845(12)°, β = 78.926(11)°, γ = 89.511(12)°, *V* = 1753.5(15) Å^3, ρ = 1.206 g cm^{-3}, *T* = 200(2) K,

Θ_{max} = 23.26°, radiation Mo K_α, λ = 0.71073 Å, 0.3° ω-scans with CCD area detector, covering a whole sphere in reciprocal space, 12245 reflections measured, 5041 unique (R(int) = 0.0907), 3272 observed ($I > 2\sigma(I)$), intensities were corrected for Lorentz and polarization effects, an empirical absorption correction was applied using SADABS[165] based on the Laue symmetry of the reciprocal space, μ = 0.22 mm^{-1}, T_{min} = 0.93, T_{max} = 0.99, structure solved by direct methods and refined against F^2 with a full-matrix least-squares algorithm using the SHELXTL (version 2008/4) software package,[166] 400 parameters refined, hydrogen atoms were treated using appropriate riding models, except of those of the crystal water which were not considered, goodness of fit 1.11 for observed reflections, final residual values $R1(F)$ = 0.146, $wR(F^2)$ = 0.327 for observed reflections, residual electron density -0.64 to 0.72 eÅ^{-3}.

*6.2.5.3 1-(2-Bromoethyl)-4-(3,5-dimethylphenyl)-1*H*-1,2,4-triazolium Bromide* (**45**)[168]

22 **45**

A flame-dried Schlenk flask flushed with inert gas was charged with 4-(3,5-dimethylphenyl)-4*H*-1,2,4-triazole (**22**, 1.960 g, 11.3 mmol) and 1,2-dibromoethane (52.800 g, 281.1 mmol). The reaction mixture was stirred at 45 °C for seven days. The product was filtrated, washed with diethyl ether (5 × 50 ml) and dried *in vacuo* (3.100 g, 8.6 mmol, 76 %).

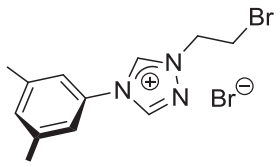

45

$C_{12}H_{15}Br_2N_3$

M ($C_{12}H_{15}Br_2N_3$) = 361.08 g mol^{-1}

^{1}H NMR (400.180 MHz, d_6-DMSO, 25 °C): δ = 11.13 (s, 1H, NC*H*NCH$_2$), 9.92 (s, 1H, NC*H*NNCH$_2$), 7.55 (s, 2H, *ortho*-C*H*), 7.30 (s, 1H, *para*-C*H*), 4.92 (t, $^3J_{H\text{-}H}$ = 5.9 Hz, 2H, NC*H*$_2$CH$_2$Br), 4.06 (t, $^3J_{H\text{-}H}$ = 5.9 Hz, 2H, NCH$_2$C*H*$_2$Br), 2.39 (s, 6H, C*H*$_3$).

^{13}C{^{1}H} NMR (100.625 MHz, d_6-DMSO, 25 °C): δ = 143.0 (N*C*HNNCH$_2$), 142.1 (N*C*HNCH$_2$), 139.9 (*C*CH$_3$), 131.8 (*ipso*-*C*N), 131.7 (*para*-*C*H), 119.7 (*ortho*-*C*H), 53.3 (N*C*H$_2$CH$_2$Br), 29.3 (NCH$_2$*C*H$_2$Br), 20.7 (*C*H$_3$).

HR-MS (ESI+, methanol) *m*/*z* (%): 280.04447 (90.0) [M(^{79}Br)-Br]$^+$, 282.04242 (100.0) [M(^{81}Br)-Br]$^+$.

calculated for [$C_{12}H_{15}(^{79}Br)N_3$]$^+$:	280.04439
found:	280.04447

Infrared Spectroscopy (KBr): $\tilde{\nu}$ [cm^{-1}] = 3470 (br, m), 3037 (m), 2995 (m), 1951 (s), 2822 (w), 1622 (m), 1602 (m), 1477 (w), 1451 (w), 1313 (w), 1250 (w), 1225 (w), 1208 (w), 1172 (w), 1110 (w), 850 (w), 680 (m, C-Br stretch), 646 (m), 622 (w).

Elemental Analysis (No. 30156)

calculated for $C_{12}H_{15}Br_2N_3$:	C 39.92 %,	H 4.19 %,	N 11.64 %
found:	C 39.91 %,	H 4.11 %,	N 11.59 %

Melting Point: 256 °C.

*6.2.5.4 4-(2,6-Diisopropylphenyl)-1-{2-[4-(3,5-dimethylphenyl)-1*H*-1,2,4-triazolium-1-yl]ethyl}-1*H*-1,2,4-triazol-1-ium Dibromide* (**46**)

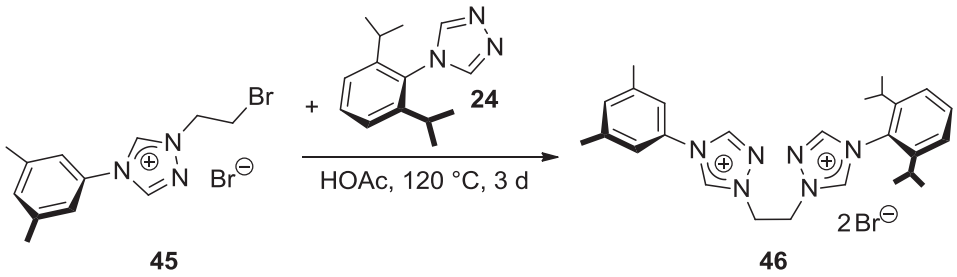

45 **46**

In a 100 ml Schlenk flask flushed with inert gas, 1-(2-bromoethyl)-4-(3,5-dimethylphenyl)-1*H*-1,2,4-triazolium bromide (**45**, 3.100 g, 8.586 mmol) and 4-(2,6-diisopropylphenyl)-4*H*-1,2,4-triazole (**24**, 2.756 g, 12.02 mmol) were dissolved in glacial acetic acid (8 ml). The reaction mixture was stirred under reflux conditions (120 °C) for three days. The solvent was removed *in vacuo*. The yellow solid residue was washed with hot toluene (90 °C, 3 × 100 ml) and diethyl ether (3 × 50 ml). The colourless product was dried *in vacuo* (4.100 g, 6.945 mmol, 81 %). Traces of acetic acid in the product could not be eliminated, but did not affect the subsequent reaction.

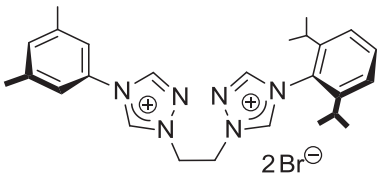

46

$C_{26}H_{34}Br_2N_6$

M ($C_{26}H_{34}Br_2N_6$) = 590.40 g mol^{-1}

^{1}H NMR (300.190 MHz, d_6-DMSO, 27 °C): δ = 11.22 (s, 1H, $CH_2NC\underline{H}NDipp$), 10.94 (s, 1H, $XylNC\underline{H}NCH_2$), 9.87 (s, 1H, $CH_2NNC\underline{H}NDipp$), 9.84 (s, 1H, $XylNC\underline{H}N$-NCH_2), 7.68 (t, $^3J_{H\text{-}H}$ = 7.7 Hz, 1H, Dipp-substituent, *para*-C$\underline{H}$), 7.55 (s, 2H, Xyl-substituent, *ortho*-C$\underline{H}$), 7.49 (d, $^3J_{H\text{-}H}$ = 7.7 Hz, 2H, Dipp-substituent, *meta*-C$\underline{H}$), 7.30 (s, 1H, Xyl-substituent, *para*-C$\underline{H}$), 5.31 (m, 2H, $C\underline{H}_2NCHNDipp$), 5.24 (m, 2H, $XylNCH$-$NC\underline{H}_2$), 2.39 (s, 6H, Xyl-substituent, $C\underline{H}_3$), 2.36 (sept, $^3J_{H\text{-}H}$ = 6.6 Hz, 2H, Dipp-substituent, $C\underline{H}(CH_3)_2$), 1.14 (d, $^3J_{H\text{-}H}$ = 6.6 Hz, 12H, $CH(C\underline{H}_3)_2$).

$^{13}C\{^1H\}$ NMR (75.483 MHz, d_6-DMSO, 27 °C): δ = 146.0 ($CH_2NN\underline{C}HNDipp$), 145.2 (*ortho*-$\underline{C}CH(CH_3)_2$), 144.8 ($XylN\underline{C}HNCH_2$), 142.9 ($CH_2N\underline{C}HNDipp$), 142.8 ($XylN\underline{C}HNNCH_2$), 139.8 (Xyl-substituent, $\underline{C}CH_3$), 132.2 (Dipp-substituent, *para*-$\underline{C}H$), 131.7 (Xyl-substituent, *para*-$\underline{C}H$), 127.0 (Dipp-substituent, *ipso*-$\underline{C}N$), 124.7 (Dipp-substituent, *meta*-$\underline{C}H$), 119.8 (Xyl-substituent, *ortho*-$\underline{C}H$), 50.8 ($\underline{C}H_2N$-CHNDipp), 49.7 ($XylNCHN\underline{C}H_2$), 27.8 (Dipp-substituent, $\underline{C}H(CH_3)_2$), 23.9 (Dipp-substituent, $CH(\underline{C}H_3)_2$), 23.5 (Dipp-substituent, $CH(\underline{C}H_3)_2$), 20.7 (Xyl-substituent, $\underline{C}H_3$).
A signal for the quaternary *ipso*-C-atom of the xylyl-substituent next to the triazolium's N-atom is missing in the $^{13}C\{^1H\}$ NMR spectrum: it might either be concealed by another peak or its intensity is too low, possibly due the electric quadrupole moment of the neighbouring ^{14}N-atom.

HR-MS (ESI+, methanol) *m*/*z* (%): 200.11829 (2.2) $[M\text{-}C_{14}H_{20}N_3\text{-}2Br]^+$, 215.14177 (33.9) $[M\text{-}2Br]^{2+}$, 256.18091 (24.9) $[M\text{-}C_{10}H_{12}N_3\text{-}2Br]^+$, 269.15101 (44.0) $[M\text{-}C_{12}H_{17}\text{-}2Br]^+$, 325.21366 (2.0) $[M\text{-}C_8H_9\text{-}2Br]^+$, 402.26548 (96.0) $[M\text{-}CH_2N\text{-}2Br]^+$, 429.27640 (100.0) $[M\text{-}H\text{-}2Br]^+$.

calculated for $[C_{26}H_{34}N_6]^{2+}$:	215.14170
found:	215.14177

Infrared Spectroscopy (KBr): $\tilde{\nu}$ [cm^{-1}] = 3422 (br, m), 2965 (s), 1619 (m), 1565 (s), 1465 (m), 1386 (w), 1304 (m), 1250 (m), 1182 (m), 1119 (m), 1087 (w), 1048 (m), 872 (s), 843 (s), 823 (w), 807 (w), 760 (m), 684 (m), 652 (w).

Melting Point: 288 °C.

6.2.6 Synthesis of Symmetrically Substituted Bistriazolium Hexafluorophosphate Salts

*6.2.6.1 1,1'-[1,3-Phenylenebis(methylene)]bis[4-(2,4,6-trimethylphenyl)-1*H*-1,2,4-triazolium] Bis(hexafluorophosphate)* (**51**)

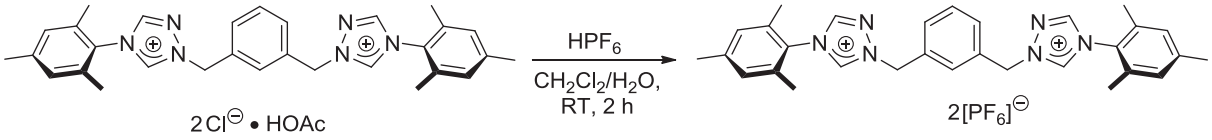

31 **51**

In a 100 ml round-bottomed flask, a solution of hexafluorophosphoric acid (60 weight-% solution in water, ρ = 1.6510 g cm^{-3}, 0.5 ml, 3 mmol) in de-ionized water (10 ml) was prepared. A solution of 1,1'-[1,3-phenylenebis(methylene)]bis[4-(2,4,6-trimethylphenyl)-1*H*-1,2,4-triazolium] dichloride (containing one equivalent of acetic acid; **31**, 0.624 g, 1.02 mmol) in dichloromethane (50 ml) was added. The reaction mixture was vigorously stirred for two hours. De-ionized water (100 ml) was added and the phases were separated. The aqueous phase was extracted with dichloromethane (2 × 100 ml). The combined organic phases were dried over magnesium sulphate. After filtration of the drying agent, the solvent was removed *in vacuo* to give the product as a colourless crystalline solid (0.562 g, 1.02 mmol, quantitative yield).

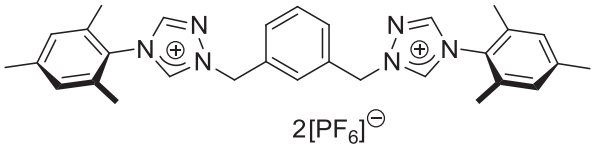

51

$C_{30}H_{34}F_{12}N_6P_2$

M ($C_{30}H_{34}F_{12}N_6P_2$) = 768.56 g mol^{-1}

^{1}H NMR (300.130 MHz, CD_3CN, 25 °C): δ = 9.50 (s, 2H, MesNC*H*NCH$_2$), 8.75 (s, 2H, MesNC*H*NNCH$_2$), 7.68 (br, s, 1H, Xyl-linker, CH$_2$CC*H*CCH$_2$), 7.65 - 7.52 (m, 3H, Xyl-linker, CH$_2$CC*H*CH and CH$_2$CCHC*H*), 7.15 (s, Mes-substituent, *meta*-C*H*), 5.70 (s, 4H, C*H*$_2$), 2.37 (s, 6H, *para*-C*H*$_3$), 2.05 (s, 12H, *ortho*-C*H*$_3$).

$^{13}C\{^1H\}$ NMR (125.758 MHz, CD_3CN, 25 °C): δ = 146.3 (MesN<u>C</u>HNNCH$_2$), 143.5 (MesN<u>C</u>HNCH$_2$), 143.1 (Mes-substituent, *para*-<u>C</u>CH$_3$), 135.6 (Mes-substituent, *ortho*-<u>C</u>CH$_3$), 133.9 (Xyl-linker, *ipso*-<u>C</u>CH$_2$), 131.4 (Xyl-linker, CH$_2$C<u>C</u>HCH), 131.4 (Xyl-linker, CH$_2$C<u>C</u>HCCH$_2$ or CH$_2$CCH<u>C</u>H), 131.1 (Xyl-linker, CH$_2$C<u>C</u>HCCH$_2$ or CH$_2$C-CH<u>C</u>H), 130.7 (Mes-substituent, *meta*-<u>C</u>H), 128.5 (Mes-substituent, *ipso*-<u>C</u>N), 56.9 (<u>C</u>H$_2$), 21.0 (*para*-<u>C</u>H$_3$), 17.6 (*ortho*-<u>C</u>H$_3$).

$^{31}P\{^1H\}$ NMR (202.456 MHz, CD_3CN, 25 °C): δ = -144.56 (sept, $^1J_{P\text{-}F}$ = 707.1 Hz).

^1H NMR (300.190 MHz, d_6-DMSO, 25 °C): δ = 10.58 (s, 2H, MesNC<u>H</u>NCH$_2$), 9.52 (s, 2H, MesNC<u>H</u>NNCH$_2$), 7.68 (s, 1H, Xyl-linker, CH$_2$CC<u>H</u>CCH$_2$), 7.53 - 7.58 (m, 3H, Xyl-linker, CH$_2$CC<u>H</u>CH and CH$_2$CCHC<u>H</u>), 7.20 (s, 4H, Mes-substituent, *meta*-C<u>H</u>), 5.75 (s, 4H, C<u>H</u>$_2$), 2.35 (s, 6H, *para*-C<u>H</u>$_3$), 2.07 (s, 12H, *ortho*-C<u>H</u>$_3$).

^1H NMR (500.130 MHz, d_8-THF, 25 °C): δ = 10.02 (s, 2H, MesNC<u>H</u>NCH$_2$), 9.06 (s, 2H, MesNC<u>H</u>NNCH$_2$), 7.86 (s, 1H, Xyl-linker, CH$_2$CC<u>H</u>CCH$_2$), 7.67 (d, $^3J_{H\text{-}H}$ = 7.7 Hz, 2H, Xyl-linker, CH$_2$CC<u>H</u>CH), 7.54 (t, $^3J_{H\text{-}H}$ = 7.7 Hz, 1H, Xyl-linker, CH$_2$CCHC<u>H</u>), 7.10 (s, 4H, Mes-substituent, *meta*-C<u>H</u>), 5.80 (s, 4H, C<u>H</u>$_2$), 2.34 (s, 6H, *para*-C<u>H</u>$_3$), 2.08 (s, 12H, *ortho*-C<u>H</u>$_3$).

$^{13}C\{^1H\}$ NMR (75.483 MHz, d_8-THF, 25 °C): δ = 146.2 (MesN<u>C</u>HNNCH$_2$), 144.2 (MesN<u>C</u>HNCH$_2$), 142.4 (Mes-substituent, *para*-<u>C</u>CH$_3$), 135.7 (Mes-substituent, *ortho*-<u>C</u>CH$_3$), 134.4 (Xyl-linker, *ipso*-<u>C</u>CH$_2$), 131.2 (Xyl-linker, CH$_2$C<u>C</u>HCCH$_2$ and CH$_2$C-<u>C</u>HCH), 130.5 (Xyl-linker, CH$_2$CCH<u>C</u>H), 130.4 (Mes-substituent, *meta*-<u>C</u>H), 128.9 (Mes-substituent, *ipso*-<u>C</u>N), 56.6 (<u>C</u>H$_2$), 20.9 (*para*-<u>C</u>H$_3$), 17.2 (*ortho*-<u>C</u>H$_3$).

$^{31}P\{^1H\}$ NMR (75.476 MHz, d_8-THF, 25 °C): δ = -144.23 (sept, $^1J_{P\text{-}F}$ = 711.4 Hz).

HR-MS (ESI+, methanol) *m*/*z* (%): 239.14166 (11.3) $[M\text{-}2PF_6]^{2+}$; 359.19801 (2.9) $[M\text{-}C_9H_{11}\text{-}2PF_6]^+$, 623.24751 (100.00) $[M\text{-}PF_6]^+$.

calculated for $[C_{30}H_{34}F_6N_6P]^+$:	623.24813
found:	623.24751

Infrared Spectroscopy (KBr): $\tilde{\nu}$ [cm^{-1}] = 3442 (br, w), 3145 (w), 3008 (w), 2924 (w), 2128 (w), 1597 (w), 1562 (w), 1485 (w), 1456 (w), 1304 (w), 1267 (w), 1196 (w), 1154 (w), 1116 (w), 1096 (w), 1001 (w), 843 (s, hexafluorophosphate, asymmetric stretching mode), 777 (w), 740 (w), 678 (w), 558 (s, hexafluorophosphate, bending mode).

Elemental Analysis (No. 29478)

calculated for $C_{30}H_{34}F_{12}N_6P_2$:	C	46.88 %,	H	4.46 %,	N	10.93 %,	P 8.06 %
found:	C	47.05 %,	H	4.58 %,	N	10.94 %,	P 7.99 %

Decomposition Temperature: 247 °C (dark brown solid).

Crystal Structure: Crystallographic data and structure refinements for reb3, formula $C_{30}H_{34}F_{12}N_6P_2$, M ($C_{30}H_{34}F_{12}N_6P_2$) = 768.56 g mol^{-1}: colourless crystal (polyhedron), dimensions 0.37 × 0.34 × 0.26 mm^3, crystal system monoclinic, space group $P2_1/n$, Z = 4, a = 9.9410(8) Å, b = 12.0982(9) Å, c = 29.191(2) Å, α = 90°, β = 96.334(2)°, γ=90°, V = 3489.3(5) $Å^3$, ρ = 1.463 g cm^{-3}, T = 200(2) K, Θ_{max} = 28.31°, radiation Mo K_α, λ = 0.71073 Å, 0.3° ω-scans with CCD area detector, covering a whole sphere in reciprocal space, 36293 reflections measured, 8651 unique (R(int)= 0.0291), 6853 observed ($I > 2\sigma(I)$), intensities were corrected for Lorentz and polarization effects, an empirical absorption correction was applied using SADABS[165] based on the Laue symmetry of the reciprocal space, μ = 0.22 mm^{-1}, T_{min} = 0.92, T_{max} = 0.94, structure solved by direct methods and refined against F^2 with a full-matrix least-squares algorithm using the SHELXTL (version 2008/4) software package,[166] 486 parameters refined, hydrogen atoms were treated using appropriate riding models, goodness of fit 1.03 for observed reflections, final residual values $R1(F)$ = 0.060, $wR(F^2)$ = 0.160 for observed reflections, residual electron density -0.37 to 0.65 $eÅ^{-3}$.

*6.2.6.2 1,1'-(Ethane-1,2-diyl)bis[4-(2,4,6-trimethylphenyl)-1*H*-1,2,4-triazolium] Bis(hexafluorophosphate)* (**61**)

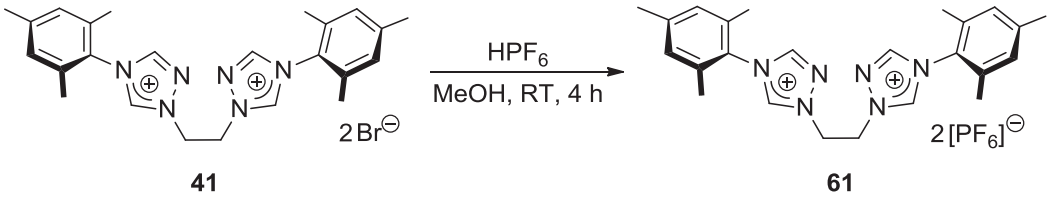

41 **61**

In a 100 ml round-bottomed flask, a solution of hexafluorophosphoric acid (60 weight-% solution in water, ρ = 1.6510 g cm^{-3}, 2.5 ml, 18 mmol) in methanol (20 ml) was prepared. 1,1'-(Ethane-1,2-diyl)bis(4-(2,4,6-trimethylphenyl)-1*H*-1,2,4-triazolium) dibromide (**41**, 4.000 g, 7.113 mmol) was dissolved in methanol (50 ml) in an Erlenmeyer flask. This solution was added to the solution of hexafluorophosphoric acid in methanol at room temperature. After several minutes of stirring, the solution turned cloudy and the product began to crystallize. After four hours of vigorous stirring, the flask was stored at -20 °C for 18 hours. The solid product was isolated by filtration, washed with diethyl ether (3 × 50 ml) and dried *in vacuo* (3.925 g, 6.981 mmol, 98 %).

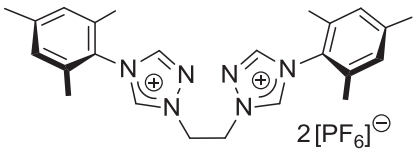

61

$C_{24}H_{30}F_{12}N_6P_2$

M ($C_{24}H_{30}F_{12}N_6P_2$) = 692.46 g mol^{-1}

^{1}H NMR (300.510 MHz, d_6-acetone, 25 °C): δ = 10.35 (s, 2H, MesNC*H*NCH$_2$), 9.40 (s, 2H, MesNC*H*NNCH$_2$), 7.19 (s, 4H, *meta*-C*H*), 5.55 (s, 4H, C*H*$_2$), 2.37 (s, 6H, *para*-C*H*$_3$), 2.17 (s, 12H, *ortho*-C*H*$_3$).

^{1}H NMR (300.511 MHz, CD_3CN, 27 °C): δ = 9.59 (s, 2H, MesNC*H*NCH$_2$), 8.78 (s, 2H, MesNC*H*NNCH$_2$), 7.17 (s, 4H, *meta*-C*H*), 5.16 (s, 4H, C*H*$_2$), 2.38 (s, 6H, *para*-C*H*$_3$), 2.08 (s, 12H, *ortho*-C*H*$_3$).

$^{13}C\{^1H\}$ NMR (75.455 MHz, CD_3CN, 27 °C): δ = 146.5 (MesN<u>C</u>HNNCH$_2$), 144.8 (MesN<u>C</u>HNCH$_2$), 143.2 (*para*-<u>C</u>CH$_3$), 135.6 (*ortho*-<u>C</u>CH$_3$), 130.6 (*meta*-<u>C</u>H), 128.4 (*ipso*-<u>C</u>N), 51.2 (<u>C</u>H$_2$), 21.0 (*para*-<u>C</u>H$_3$), 17.6 (*ortho*-<u>C</u>H$_3$).

$^{31}P\{^1H\}$ NMR (121.475 MHz, CD_3CN, 27 °C): δ = -144.61 (sept, $^1J_{P\text{-}F}$ = 707.0 Hz).

^{1}H NMR (300.510 MHz, d_6-DMSO, 25 °C): δ = 10.52 (s, 2H, MesNC<u>H</u>NCH$_2$), 9.57 (s, 2H, MesNC<u>H</u>NNCH$_2$), 7.21 (s, 4H, *meta*-C<u>H</u>), 5.18 (s, 4H, C<u>H$_2$</u>), 2.35 (s, 6H, *para*-C<u>H$_3$</u>), 2.08 (s, 12H, *ortho*-C<u>H$_3$</u>).

^{1}H NMR (300.509 MHz, d_8-THF, 25 °C): δ = 10.07 (s, 2H, MesNC<u>H</u>NCH$_2$), 9.14 (s, 2H, MesNC<u>H</u>NNCH$_2$), 7.13 (s, 4H, *meta*-C<u>H</u>), 5.35 (s, 4H, C<u>H$_2$</u>), 2.35 (s, 6H, *para*-C<u>H$_3$</u>), 2.15 (s, 12H, *ortho*-C<u>H$_3$</u>).
$^{31}P\{^1H\}$ NMR (121.649 MHz, d_8-THF, 25 °C): δ = -146.20 (sept, $^1J_{P\text{-}F}$ = 711.0 Hz).

HR-MS (ESI+, methanol) *m*/*z* (%): 214.13390 (1.7) [M-$C_{11}H_{14}N_3$-2PF_6]$^+$, 283.16660 (14.8) [M-C_9H_{11}-2PF_6]$^+$, 401.24501 (5.0) [M-H-2PF_6]$^+$, 547.21713 (100.0) [M-PF_6]$^+$.
calculated for $[C_{24}H_{30}F_6N_6P]^+$: 547.21683
found: 547.21713

Infrared Spectroscopy (KBr): $\tilde{\nu}$ [cm^{-1}] = 3421 (br, m), 3149 (m), 2965 (br, w), 1608 (w), 1565 (s), 1485 (w), 1448 (w), 1309 (w), 1227 (m), 1201 (w), 1161 (w), 1096 (m), 1004 (m), 992 (m), 839 (s, hexafluorophosphate, asymmetric stretching mode), 740 (w), 679 (w), 576 (w), 558 (s, hexafluorophosphate, bending mode).

Elemental Analysis (No.29969)

calculated for $C_{24}H_{30}F_{12}N_6P_2$:	C 41.63 %,	H 4.37 %,	N 12.14 %
found:	C 41.66 %,	H 4.42 %,	N 11.96 %

Decomposition Temperature: 251 °C (dark brown solid).

Crystal Structure: Crystallographic data and structure refinements for reb7, formula $C_{24}H_{30}F_{12}N_6P_2$, *M* ($C_{24}H_{30}F_{12}N_6P_2$) = 692.46 g mol^{-1}: colourless crystal (plate), dimensions 0.30 × 0.12 × 0.01 mm^3, crystal system monoclinic, space group $P2_1/c$, *Z* = 4,

a = 24.885(9) Å, *b* = 7.395(3) Å, *c* = 17.665(6) Å, α = 90°, β = 109.768(4)°, γ = 90°, *V* = 3059.2(19) Å^3, ρ = 1.504 g cm^{-3}, *T* = 200(2) K, Θ_{max} = 21.49°, radiation Mo K$_\alpha$, λ = 0.71073 Å, 0.3° ω-scans with CCD area detector, covering the asymmetric unit in reciprocal space with a mean redundancy of 2.84 and a completeness of 99.8 % to a resolution of 0.97Å, 10424 reflections measured, 3512 unique (*R*(int)= 0.0624), 2380 observed ($I > 2\sigma(I)$), intensities were corrected for Lorentz and polarization effects, an empirical absorption correction was applied using SADABS[165] based on the Laue symmetry of the reciprocal space, μ = 0.24 mm^{-1}, T_{min} = 0.93, T_{max} = 1.00, structure solved by direct methods and refined against F^2 with a full-matrix least-squares algorithm using the SHELXTL (version 2008/4) software package,[166] 403 parameters refined, hydrogen atoms were treated using appropriate riding models, goodness of fit 1.05 for observed reflections, final residual values *R*1(*F*) = 0.076, *wR*(F^2) = 0.188 for observed reflections, residual electron density -0.40 to 0.62 eÅ^{-3}. CCDC 869465 contains the supplementary crystallographic data for this strucure. This data can be obtained free of charge from the Cambridge Crystallographic Data Centre *via* www.ccdc.cam.ac.uk/data_request/cif.

*6.2.6.3 1,1'-[1,3-Phenylenebis(methylene)]bis[4-(3,5-dimethylphenyl)-1*H*-1,2,4-triazolium] Bis(hexafluorophosphate)* (**52**)

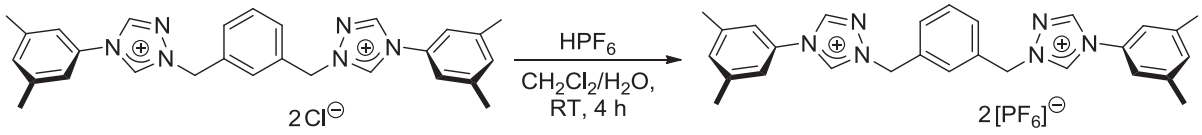

32 **52**

In a 100 ml round-bottomed flask, a solution of hexafluorophosphoric acid (65 weight-% solution in water, ρ = 1.6510 g cm^{-3}, 0.15 ml, 1.1 mmol) in de-ionized water (20 ml) was prepared. A solution of 1,1'-[1,3-phenylenebis(methylene)]bis[4-(3,5-dimethylphenyl)-1*H*-1,2,4-triazolium] dichloride (**32**, 0.217 g, 0.416 mmol) in dichloromethane (50 ml) was added. The reaction mixture was vigorously stirred for four hours. The colourless solid product was filtered off, washed with diethyl ether (3 × 30 ml) and dried *in vacuo* (0.189 g, 0.362 mmol, 87 %).

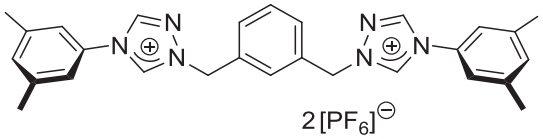

52

$C_{28}H_{30}F_{12}N_6P_2$

M ($C_{28}H_{30}F_{12}N_6P_2$) = 740.51 g mol^{-1}

^{1}H NMR (300.080 MHz, d_6-DMSO, 25 °C): δ = 10.86 (s, 2H, XylNC*H*NCH$_2$), 9.76 (s, 2H, XylNC*H*NNCH$_2$), 7.68 (br, s, 1H, Xyl-linker, CH$_2$CC*H*CCH$_2$), 7.56 (m, 3H, Xyl-linker, CH$_2$CC*H*CH and CH$_2$CCHC*H*), 7.48 (s, 4H, Xyl-substituent, *ortho*-C*H*), 7.31 (s, 2H, Xyl-substituent, *para*-C*H*), 5.71 (s, 4H, C*H*$_2$), 2.40 (s, 12H, C*H*$_3$).

^{13}C{^{1}H} NMR (75.455 MHz, d_6-DMSO, 25 °C): δ = 143.2 (XylNCHNNCH$_2$), 141.9 (XylNCHNCH$_2$), 139.8 (Xyl-substituent, CCH$_3$), 133.6 (Xyl-linker, *ipso*-CCH$_2$), 132.0 (Xyl-substituent, *ipso*-CN), 131.7 (Xyl-substituent, *para*-CH), 129.5 (Xyl-linker, CH$_2$CCHCCH$_2$ and CH$_2$CCHCH and CH$_2$CCHCH), 119.8 (Xyl-substituent, *ortho*-CH), 54.8 (CH$_2$), 20.7 (CH$_3$).

^{31}P{^{1}H} NMR (121.475 MHz, d_6-DMSO, 25 °C): δ = -144.19 (sept, $^1J_{P\text{-}F}$ = 711.3 Hz).

HR-MS (ESI+, methanol) *m*/*z* (%): 449.24545 (6.6) [M-H-2PF$_6$]$^+$, 595.21722 (100.0) [M-PF$_6$]$^+$.

calculated for [$C_{28}H_{30}F_6N_6P$]$^+$:	595.21683
found:	595.21722

Infrared Spectroscopy (KBr): $\tilde{\nu}$ [cm^{-1}] = 3431 (br, w), 3153 (m), 2925 (w), 1621 (s), 1598 (s), 1570 (w), 1477 (w), 1442 (m), 1365 (w), 1313 (w), 1270 (w), 1178 (w), 1107 (s), 1058 (w), 1004 (m), 828 (br, s, hexafluorophosphate, asymmetric stretching mode), 740 (w), 684 (m), 664 (w), 648 (m), 558 (s, hexafluorophosphate, bending mode), 490 (w).

Elemental Analysis (No. 31495)

calculated for $C_{28}H_{30}F_{12}N_6P_2$:	C 45.41 %,	H 4.08 %,	N 11.35 %
found:	C 45.51 %,	H 4.13 %,	N 11.44 %

Melting Point: 256 °C.

Crystal Structure: Crystallographic data and structure refinements for reb17, formula $C_{28}H_{30}F_{12}N_6P_2$, M ($C_{28}H_{30}F_{12}N_6P_2$) = 740.51 g mol^{-1}: colourless crystal (polyhedron), dimensions 0.10 × 0.05 × 0.05 mm^3, crystal system monoclinic, space group $P2_1/n$, Z = 4, a = 7.4295(5) Å, b = 23.5205(14) Å, c = 18.3700(12) Å, α = 90°, β = 93.535(2)°, γ = 90°, V = 3204.0(4) Å^3, ρ = 1.535 g cm^{-3}, T = 200(2) K, Θ_{max} = 21.04°, radiation Mo K$_\alpha$, λ = 0.71073 Å, 0.3° ω-scans with CCD area detector, covering the asymmetric unit in reciprocal space with a mean redundancy of 7.0 and a completeness of 99.9 %, 28095 reflections measured, 3463 unique (R(int) = 0.0812), 2538 observed ($I > 2\sigma(I)$), intensities were corrected for Lorentz and polarization effects, an empirical absorption correction was applied using SADABS[165] based on the Laue symmetry of the reciprocal space, μ = 0.24 mm^{-1}, T_{min} = 0.98, T_{max} = 0.99, structure solved by direct methods and refined against F^2 with a full-matrix least-squares algorithm using the SHELXTL (version 2008/4) software package,[166] 470 parameters refined, hydrogen atoms were treated using appropriate riding models, goodness of fit 1.03 for observed reflections, final residual values $R1(F)$ = 0.061, $wR(F^2)$ = 0.149 for observed reflections, residual electron density -0.37 to 0.69 eÅ^{-3}.

*6.2.6.4 1,1'-(Ethane-1,2-diyl)bis[4-(3,5-dimethylphenyl)-1*H*-1,2,4-triazolium] Bis(hexafluorophosphate)* (**62**)[133]

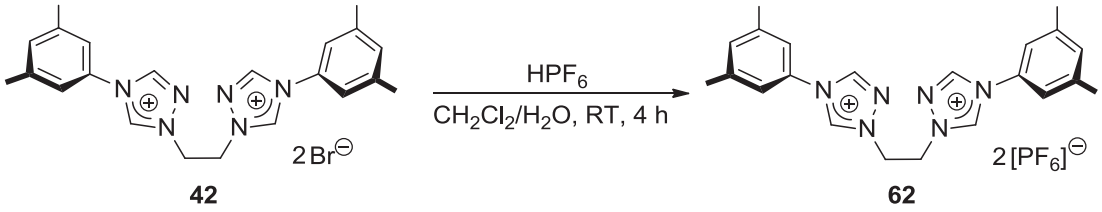

42 **62**

In a 100 ml round-bottomed flask, 1,1'-(ethane-1,2-diyl)bis[4-(3,5-dimethylphenyl)-1*H*-1,2,4-triazolium] dibromide (**42**, 2.032 g, 3.803 mmol) was suspended in dichloromethane (75 ml). A solution of hexafluorophosphoric acid (65 weight-% solution in water, ρ = 1.6510 g cm^{-3}, 1.3 ml, 9.6 mmol) in de-ionized water (15 ml) was added *via* syringe. The reaction mixture was vigorously stirred for four hours at room temperature. The colourless product was filtered off the reaction mixture, washed with diethyl ether (4 × 20 ml) and dried *in vacuo* (2.341 g, 3.523 mmol, 93 %).

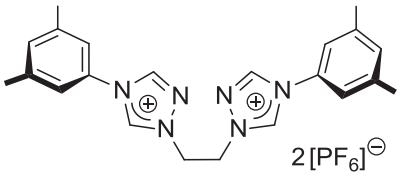

62

$C_{22}H_{26}F_{12}N_6P_2$

M ($C_{22}H_{26}F_{12}N_6P_2$) = 664.41 g mol^{-1}

^{1}H NMR (300.080 MHz, d_6-DMSO, 25 °C): δ = 10.76 (s, 2H, XylNC*H*NCH$_2$), 9.84 (s, 2H, XylNC*H*NNCH$_2$), 7.42 (s, 4H, *ortho*-C*H*), 7.32 (s, 2H, *para*-C*H*), 5.09 (s, 4H, C*H*$_2$), 2.40 (s, 12H, C*H*$_3$).

^{13}C{^{1}H} NMR (75.455 MHz, d_6-DMSO, 25 °C): δ = 143.2 (XylN*C*HNNCH$_2$), 142.6 (XylN*C*HNCH$_2$), 140.1 (*meta*-*C*CH$_3$), 131.9 (*para*-*C*H), 131.8 (*ipso*-*C*N), 119.6 (*ortho*-*C*H), 49.8 (*C*H$_2$), 20.7 (*C*H$_3$).

^{31}P{^{1}H} NMR (121.649 MHz, d_6-DMSO, 27 °C): δ = -144.19 (sept, $^1J_{P\text{-}F}$ = 711.3 Hz).

HR-MS (ESI+, methanol) *m*/*z* (%): 373.21362 (5.9) $[M\text{-}H\text{-}2PF_6]^+$, 519.18517 (100.0) $[M\text{-}PF_6]^+$, 1183.33449 (5.6) $[2M\text{-}PF_6]^+$.

calculated for $[C_{22}H_{26}F_6N_6P]^+$: 519.18553

found: 519.18517

Infrared Spectroscopy (KBr): $\tilde{\nu}$ [cm^{-1}] = 3430 (br, w), 3153 (s), 2927 (w), 1621 (s), 1574 (s), 1477 (m), 1440 (m), 1382 (w), 1366 (w), 1313 (m), 1279 (w), 1188 (m), 1108 (s), 1059 (w), 1001 (m), 831 (br, s, hexafluorophosphate, asymmetric stretching mode), 740 (w), 686 (s), 648 (m), 558 (s, hexafluorophosphate, bending mode).

Elemental Analysis (No. 31566)

calculated for $C_{22}H_{26}F_{12}N_6P_2$: C 39.77 %, H 3.94 %, N 12.65 %

found: C 39.75 %, H 4.24 %, N 12.52 %

Melting Point: 220 °C.

*6.2.6.5 1,1'-[1,3-Phenylenebis(methylene)]bis[4-(4-methylphenyl)-1*H*-1,2,4-triazolium Bis(hexafluorophosphate)* (**53**)

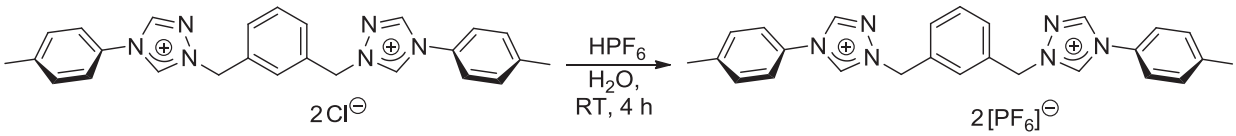

33 **53**

In a 100 ml round-bottomed flask, a solution of 1,1'-[1,3-phenylenebis(methylene)]-bis[4-(4-methylphenyl)-1*H*-1,2,4-triazolium] dichloride (**33**, 0.505 g, 1.02 mmol) in de-ionized water (50 ml) was prepared. A solution of hexafluorophosphoric acid (65 weight-% solution in water, ρ = 1.6510 g cm^{-3}, 0.35 ml, 2.6 mmol) in de-ionized water (10 ml) was added *via* syringe while vigorously stirring the solution. Immediately, a colourless solid precipitated. After stirring for two hours at room temperature, the solid product was filtered off the reaction mixture, washed with ethanol (3 × 30 ml) and diethyl ether (3 × 30 ml) and dried *in vacuo* (0.595 g, 0.835 mmol, 82 %).

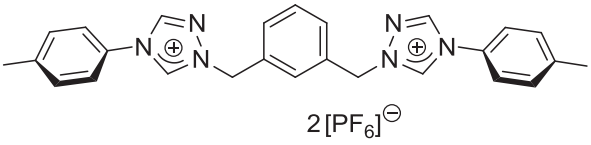

$2\,[PF_6]^{\ominus}$

53

$C_{26}H_{26}F_{12}N_6P_2$

M ($C_{26}H_{26}F_{12}N_6P_2$) = 712.45 g mol^{-1}

^{1}H NMR (600.244 MHz, d_6-DMSO, 22 °C): δ = 10.81 (s, 2H, TolNC*H*NCH$_2$), 9.75 (s, 2H, TolNC*H*NNCH$_2$), 7.71 (s, 1H, Xyl-linker, CH$_2$C*C*HCCH$_2$), 7.71 (d, $^3J_{H\text{-}H}$ = 7.7 Hz, 4H, Tol-substituent, *meta*-C*H*), 7.61 - 7.53 (m, 3H, Xyl-linker, CH$_2$CC*H*CH and CH$_2$CCHC*H*), 7.51 (d, $^3J_{H\text{-}H}$ = 7.7 Hz, 4H, Tol-substituent, *ortho*-C*H*), 5.71 (s, 4H, C*H*$_2$), 2.43 (s, 6H, C*H*$_3$).

^{13}C{^{1}H} NMR (150.932 MHz, d_6-DMSO, 22 °C): δ = 143.3 (TolN*C*HNNCH$_2$), 141.9 (TolN*C*HNCH$_2$), 140.6 (Tol-substituent, *C*CH$_3$), 133.5 (Xyl-linker, *ipso*-*C*CH$_2$), 130.5 (Tol-substituent, *ortho*-*C*H), 129.7 (Tol-substituent, *ipso*-*C*N), 129.6 (Xyl-linker, CH$_2$C*C*HCCH$_2$), 129.5 (Xyl-linker, CH$_2$C*C*HCH and CH$_2$CCH*C*H), 122.3 (Tol-substituent, *meta*-*C*H), 54.8 (*C*H$_2$), 20.6 (*C*H$_3$).

^{31}P{^{1}H} NMR (242.983 MHz, d_6-DMSO, 22 °C): δ = -144.18 (sept, $^1J_{P\text{-}F}$ = 711.4 Hz).

HR-MS (ESI+, methanol) *m*/*z* (%): 567.18565 (100.0) [M-PF$_6$]$^+$.

calculated for [$C_{26}H_{26}F_6N_6P$]$^+$:	567.18553
found:	567.18565

Infrared Spectroscopy (KBr): $\tilde{\nu}$ [cm^{-1}] = 3391 (br, s), 3345 (br, s), 3156 (s), 1571 (s), 1514 (m), 1443 (m), 1335 (w), 1305 (m), 1242 (m), 1200 (m), 1099 (s), 1007 (m), 838 (br, s, hexafluorophosphate, asymmetric stretching mode), 738 (m), 665 (w), 628 (w), 559 (s, hexafluorophosphate, bending mode), 528 (w).

Melting Point: 244 °C.

Crystal Structure: Crystallographic data and structure refinements for reb20, formula $C_{26}H_{26}F_{12}N_6P_2$+H_3CCN, M ($C_{28}H_{29}F_{12}N_7P_2$) = 753.51 g mol^{-1}: colourless crystal

(plate), dimensions 0.13 × 0.13 × 0.03 mm^3, crystal system monoclinic, space group $P2_1/n$, Z = 4, a = 12.6321(4) Å, b = 20.5013(7) Å, c = 13.0096(5) Å, α = 90°, β = 101.471(1)°, γ = 90°, V = 3301.9(2) $Å^3$, ρ = 1.516 g cm^{-3}, T = 200(2) K, Θ_{max} = 24.11°, radiation Mo K_α, λ = 0.71073 Å, 0.5° ω-scans with CCD area detector, covering the asymmetric unit in reciprocal space with a mean redundancy of 6.39 and a completeness of 99.9 % to a resolution of 0.87 Å, 34007 reflections measured, 5252 unique (R(int) = 0.0606), 3446 observed ($I > 2\sigma(I)$), intensities were corrected for Lorentz and polarization effects, an empirical absorption correction was applied using SADABS[165] based on the Laue symmetry of the reciprocal space, μ = 0.23 mm^{-1}, T_{min} = 0.97, T_{max} = 0.99, structure solved by direct methods and refined against F^2 with a full-matrix least-squares algorithm using the SHELXTL (version 2008/4) software package,[166] 510 parameters refined, hydrogen atoms were treated using appropriate riding models, goodness of fit 1.03 for observed reflections, final residual values $R1(F)$ = 0.052, $wR(F^2)$ = 0.115 for observed reflections, residual electron density -0.33 to 0.42 e$Å^{-3}$.

6.2.6.6 *1,1'-(Ethane-1,2-diyl)bis[4-(4-methylphenyl)-1*H*-1,2,4-triazolium] Bis(hexafluorophosphate)* (**63**)

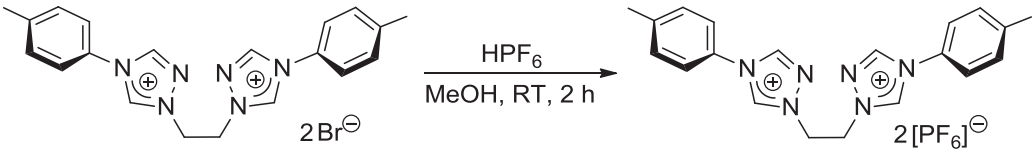

43 **63**

In a 100 ml round-bottomed flask, a solution of hexafluorophosphoric acid (65 weight-% solution in water, ρ = 1.6510 g cm^{-3}, 1.0 ml, 7.9 mmol) in methanol (20 ml) was prepared. 1,1'-(Ethane-1,2-diyl)bis[4-(4-methylphenyl)-1*H*-1,2,4-triazolium] dibromide (**43**, 1.500 g, 2.963 mmol) was dissolved in methanol (20 ml) in an Erlenmeyer flask. This solution was added to the solution of hexafluorophosphoric acid in methanol at room temperature. After several minutes of stirring, the solution turned cloudy and the product began to crystallize. After two hours of vigorous stirring, the flask was stored at -20 °C for 18 hours. The solid colourless product was

isolated by filtration, washed with diethyl ether (3 × 50 ml) and dried *in vacuo* (1.545 g, 2.428 mmol, 82 %).

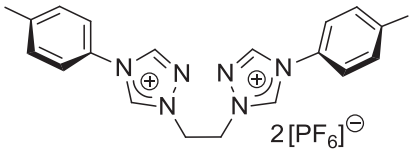

63

$C_{20}H_{22}F_{12}N_6P_2$

M ($C_{20}H_{22}F_{12}N_6P_2$) = 636.36 g mol^{-1}

^{1}H NMR (500.130 MHz, d_6-acetone, 25 °C): δ = 10.42 (s, 2H, TolNC*H*NCH$_2$), 9.56 (s, 2H, TolNC*H*NNCH$_2$), 7.69 (d, $^3J_{H\text{-}H}$ = 7.8 Hz, 4H, *meta*-C*H*), 7.52 (d, $^3J_{H\text{-}H}$ = 7.8 Hz, 4H, *ortho*-C*H*), 5.44 (s, 4H, CH$_2$), 2.45 (s, 6H, CH$_3$).

^{13}C{^{1}H} NMR (125.758 MHz, d_6-acetone, 25 °C): δ = 144.7 (TolNCHNNCH$_2$), 143.5 (CCH$_3$), 142.7 (TolNCHNCH$_2$), 131.7 (*ortho*-CH), 130.5 (*ipso*-CN), 123.8 (*meta*-CH), 51.3 (CH$_2$), 21.1 (CH$_3$).

^{31}P{^{1}H} NMR (202.456 MHz, d_6-acetone, 25 °C): δ = -144.40 (sept, $^1J_{P\text{-}F}$ = 708.6 Hz).

^{1}H NMR (300.080 MHz, CD_3CN, 26 °C): δ = 9.68 (s, 2H, TolNC*H*NCH$_2$), 8.99 (s, 2H, TolNC*H*NNCH$_2$), 7.50 (m, 8H, *ortho*-C*H* and *meta*-C*H*), 5.11 (s, 4H, CH$_2$), 2.45 (s, 6H, CH$_3$).

^{13}C{^{1}H} NMR (75.455 MHz, CD_3CN, 26 °C): δ = 144.5 (TolNCHNNCH$_2$), 143.1 (CCH$_3$), 142.9 (TolNCHNCH$_2$), 131.8 (*ortho*-CH), 130.0 (*ipso*-CN), 123.7 (*meta*-CH), 50.8 (CH$_2$), 21.1 (CH$_3$).

^{31}P{^{1}H} NMR (121.649 MHz, CD_3CN, 27 °C): δ = -144.62 (sept, $^1J_{P\text{-}F}$ = 707.2 Hz).

^{1}H NMR (300.510 MHz, d_6-DMSO, 25 °C): δ = 10.73 (s, 2H, TolNC*H*NCH$_2$), 9.83 (s, 2H, TolNC*H*NNCH$_2$), 7.67 (d, $^3J_{H\text{-}H}$ = 8.5 Hz, 4H, *meta*-C*H*), 7.53 (d, $^3J_{H\text{-}H}$ = 8.5 Hz, 4H, *ortho*-C*H*), 5.10 (s, 4H, CH$_2$), 2.42 (s, 6H, CH$_3$).

$^{31}P\{^{1}H\}$ NMR (121.649 MHz, d_6-DMSO, 27 °C): δ = -144.19 (sept, $^{1}J_{P\text{-}F}$ = 711.3 Hz).

HR-MS (ESI+, methanol) *m*/*z* (%): 255.13522 (5.8) $[M\text{-}C_7H_7\text{-}2PF_6]^+$, 345.18214 (14.1) $[M\text{-}H\text{-}2PF_6]^+$, 491.15414 (100.0) $[M\text{-}PF_6]^+$.

calculated for $[C_{20}H_{22}F_6N_6P]^+$:	491.15423
found:	491.15414

Infrared Spectroscopy (KBr): $\tilde{\nu}$ [cm^{-1}] = 3425 (br, m), 3155 (m), 3046 (w), 2964 (w), 1575 (s), 1513 (s), 1440 (w), 1414 (w), 1338 (w), 1305 (w), 1244 (w), 1205 (m), 1100 (s), 996 (m), 841 (br, s, hexafluorophosphate, asymmetric stretching mode), 741 (w), 656 (w), 628 (m), 559 (s, hexafluorophosphate, bending mode), 529 (m).

Elemental Analysis (No. 30859)

calculated for $C_{20}H_{22}F_{12}N_6P_2$:	C 37.75 %,	H 3.48 %,	N 13.21 %
found:	C 37.69 %,	H 3.66 %,	N 13.14 %

Melting Point: 242 - 244 °C.

Crystal Structure: Crystallographic data and structure refinements for reb12, formula $C_{20}H_{22}F_{12}N_6P_2$, *M* ($C_{20}H_{22}F_{12}N_6P_2$) = 636.36 g mol^{-1}: colourless crystal (polyhedron), dimensions 0.40 × 0.25 × 0.08 mm^3, crystal system monoclinic, space group $P2_1/n$, *Z* = 4, *a* = 10.981(3) Å, *b* = 9.825(3) Å, *c* = 24.298(6) Å, α = 90°, β = 96.673(5)°, γ = 90°, *V* = 2603.7(11) $Å^3$, ρ = 1.623 g cm^{-3}, *T* = 200(2) K, Θ_{max} = 28.31°, radiation Mo K_α, λ = 0.71073 Å, 0.3° ω-scans with CCD area detector, covering a whole sphere in reciprocal space, 26875 reflections measured, 6449 unique (*R*(int)= 0.0266), 5316 observed ($I > 2\sigma(I)$), intensities were corrected for Lorentz and polarization effects, an empirical absorption correction was applied using SADABS[165] based on the Laue symmetry of the reciprocal space, μ = 0.28 mm^{-1}, T_{min} = 0.90, T_{max} = 0.98, structure solved by direct methods and refined against F^2 with a full-matrix least-squares algorithm using the SHELXTL (version 2008/4) software package,[166] 491 parameters refined, hydrogen atoms were treated using appropriate riding models, goodness of fit 1.04 for observed reflections, final residual values *R*1(*F*) = 0.038, *wR*(F^2) = 0.092 for observed reflections, residual electron density -0.23 to 0.26 e$Å^{-3}$.

*6.2.6.7 1,1'-[1,3-Phenylenebis(methylene)]bis[4-(2,6-diisopropylphenyl)-1*H*-1,2,4-triazolium] Bis(hexafluorophosphate)* (**54**)

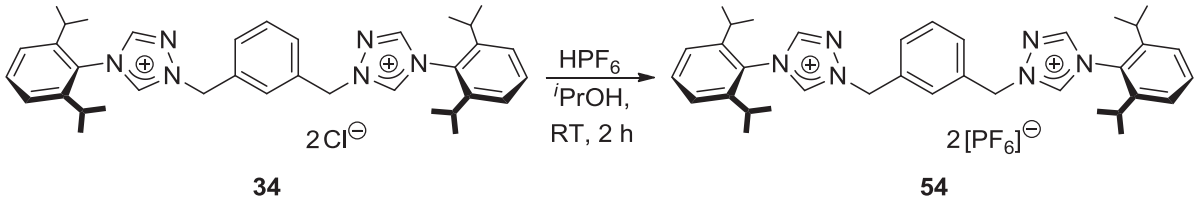

34 **54**

In a 250 ml round-bottomed flask, a solution of hexafluorophosphoric acid (60 weight-% solution in water, ρ = 1.6510 g cm^{-3}, 2.1 ml, 14 mmol) in isopropanol (50 ml) was prepared. 1,1'-[1,3-Phenylenebis(methylene)]bis[4-(2,6-diisopropylphenyl)-1*H*-1,2,4-triazolium] dichloride (**34**, 3.575 g, 5.642 mmol) was dissolved in isopropanol (100 ml) in an Erlenmeyer flask. This solution was added to the solution of hexafluorophosphoric acid at room temperature. After several minutes of stirring, the solution turned cloudy and the product began to crystallize. After two hours of vigorous stirring, the solid product was isolated by filtration, washed with isopropanol (2 × 50 ml) and diethyl ether (3 × 50 ml), and dried *in vacuo* (3.590 g, 4.210 mmol, 75 %).

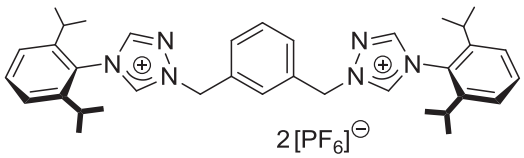

54

$C_{36}H_{46}F_{12}N_6P_2$

M ($C_{36}H_{46}F_{12}N_6P_2$) = 852.31 g mol^{-1}

^{1}H NMR (300.080 MHz, d_6-DMSO, 25 °C): δ = 10.79 (s, 2H, DippNC*H*NCH$_2$), 9.74 (s, 2H, DippNC*H*NNCH$_2$), 7.74 - 7.51 (m, 10H, Xyl-linker, CH$_2$CC*H*CCH$_2$, CH$_2$CC*H*CH and CH$_2$CCHC*H*; Dipp-substituent, *para*-C*H* and *meta*-C*H*), 5.84 (s, 4H, C*H*$_2$), 2.31 (sept, $^3J_{H\text{-}H}$ = 6.7 Hz, 4H, C*H*(CH$_3$)$_2$), 1.18 - 1.13 (m, 24H, CH(C*H*$_3$)$_2$).

^{13}C{^{1}H} NMR (75.455 MHz, d_6-DMSO, 25 °C): δ = 146.3 (DippN*C*HNNCH$_2$), 145.1 (Dipp-substituent, *ortho*-*C*CH(CH$_3$)$_2$), 144.3 (DippN*C*HNCH$_2$), 133.9 (Xyl-linker, *ipso*-*C*CH$_2$), 132.3 (Dipp-substituent, *para*-*C*H), 130.0 (Xyl-linker, CH$_2$C*C*HCH or

$CH_2CCH\underline{C}H$), 129.6 (Xyl-linker, $CH_2C\underline{C}HCH$ or $CH_2CCH\underline{C}H$), 129.3 (Xyl-linker, $CH_2C\underline{C}HCCH_2$), 127.3 (Dipp-substituent, *ipso*-$\underline{C}$N), 124.8 (Dipp-substituent, *meta*-$\underline{C}$H), 55.4 ($\underline{C}H_2$), 28.1 ($\underline{C}H(CH_3)_2$), 23.6 ($CH(\underline{C}H_3)_2$), 23.5 ($CH(\underline{C}H_3)_2$).

$^{31}P\{^1H\}$ NMR (121.475 MHz, d_6-DMSO, 25 °C): δ = -144.18 (sept, $^1J_{P\text{-}F}$ = 711.2 Hz).

^1H NMR (300.080 MHz, d_8-THF, 25 °C): δ = 10.06 (s, 2H, DippNC$\underline{H}$NCH_2), 9.19 (s, 2H, DippNC$\underline{H}$NNCH_2), 7.94 (s, 1H, Xyl-linker, $CH_2CC\underline{H}CCH_2$), 7.70 (d, $^3J_{H\text{-}H}$ = 7.7 Hz, 2H, Xyl-linker, $CH_2CC\underline{H}CH$), 7.61 (t, $^3J_{H\text{-}H}$ = 7.8 Hz, 2H, Dipp-substituent, *para*-C$\underline{H}$), 7.57 (t, $^3J_{H\text{-}H}$ = 7.7 Hz, 1H, Xyl-linker, $CH_2CCHC\underline{H}$), 7.43 (d, $^3J_{H\text{-}H}$ = 7.8 Hz, 4H, Dipp-substituent, *meta*-C$\underline{H}$), 5.86 (s, 4H, C$\underline{H}_2$), 2.40 (sept, $^3J_{H\text{-}H}$ = 6.8 Hz, 4H, C$\underline{H}(CH_3)_2$), 1.18 (d, $^3J_{H\text{-}H}$ = 6.8 Hz, 12H, $CH(C\underline{H}_3)_2$), 1.15 (d, $^3J_{H\text{-}H}$ = 6.8 Hz, 12H, $CH(C\underline{H}_3)_2$).

$^{13}C\{^1H\}$ NMR (75.455 MHz, d_8-THF, 25 °C): δ = 146.7 (DippN$\underline{C}$HNCH_2 and Dipp-substituent, *ortho*-$\underline{C}CH(CH_3)_2$), 144.2 (DippN$\underline{C}$HNCH_2), 134.2 (Xyl-linker, *ipso*-$\underline{C}CH_2$), 133.0 (Dipp-substituent, *para*-$\underline{C}$H), 131.8 (Xyl-linker, $CH_2C\underline{C}HCCH_2$), 131.4 (Xyl-linker, $CH_2C\underline{C}HCH$), 130.8 (Xyl-linker, $CH_2CCH\underline{C}H$), 128.2 (Dipp-substituent, *ipso*-$\underline{C}$N), 125.4 (Dipp-substituent, *meta*-$\underline{C}$H), 56.8 ($\underline{C}H_2$), 29.2 ($\underline{C}H(CH_3)_2$), 24.1 ($CH(\underline{C}H_3)_2$), 23.7 ($CH(\underline{C}H_3)_2$).

HR-MS (ESI+, methanol) *m*/*z* (%): 281.18875 (43.8) $[M\text{-}2PF_6]^{2+}$, 401.24510 (11.4) $[M\text{-}C_{12}H_{17}\text{-}2PF_6]^+$, 561.37058 (20.2) $[M\text{-}H\text{-}2PF_6]^+$, 597.34731 (4.9) $[M+(^{35}Cl)\text{-}2PF_6]^+$, 707.34269 (100.0) $[M\text{-}PF_6]^+$.

calculated for $[C_{36}H_{46}F_6N_6P]^+$:	707.34203
found:	707.34269

Infrared Spectroscopy (KBr): $\tilde{\nu}$ [cm^{-1}] = 3443 (br, w), 3141 (m), 2970 (s), 2933 (m), 2875 (w), 1590 (w), 1559 (m), 1464 (m), 1369 (w), 1312 (w), 1185 (w), 1118 (w), 1093 (m), 1061 (w), 1002 (w), 843 (br, s, hexafluorophosphate, asymmetric stretching mode), 756 (w), 745 (w), 680 (w), 558 (s, hexafluorophosphate, bending mode).

Elemental Analysis (No. 30163)

calculated for $C_{36}H_{46}F_{12}N_6P_2$:	C	50.71 %,	H	5.44 %,	N 9.86 %
found:	C	50.80 %,	H	5.51 %,	N 9.93 %

Melting Point: 232 °C.

Crystal Structure: Crystallographic data and structure refinements for reb11, formula $C_{36}H_{46}F_{12}N_6P_2$, M ($C_{36}H_{46}F_{12}N_6P_2$) = 852.31 g mol^{-1}: colourless crystal (polyhedron), dimensions 0.37 × 0.11 × 0.07 mm^3, crystal system monoclinic, space group C2/c, Z = 8, a = 38.072(2) Å, b = 12.4742(8) Å, c = 17.3018(11) Å, α = 90°, β = 103.158(1)°, γ = 90°, V = 8001.2(9) Å^3, ρ = 1.416 g cm^{-3}, T = 200(2) K, Θ_{max} = 26.73°, radiation Mo K$_\alpha$, λ = 0.71073 Å, 0.3° ω-scans with CCD area detector, covering the asymmetric unit in reciprocal space with a mean redundancy of 8.07 and a completeness of 99.8 % to a resolution of 0.79 Å, 69843 reflections measured, 8482 unique (R(int)= 0.0454), 6138 observed ($I > 2\sigma(I)$), intensities were corrected for Lorentz and polarization effects, an empirical absorption correction was applied using SADABS[165] based on the Laue symmetry of the reciprocal space, μ = 0.20 mm^{-1}, T_{min} = 0.93, T_{max} = 0.99, structure solved by direct methods and refined against F^2 with a full-matrix least-squares algorithm using the SHELXTL (version 2008/4) software package,[166] 633 parameters refined, hydrogen atoms were treated using appropriate riding models, goodness of fit 1.04 for observed reflections, final residual values $R1(F)$ = 0.061, $wR(F^2)$ = 0.146 for observed reflections, residual electron density -0.42 to 0.46 eÅ^{-3}.

6.2.7 Synthesis of Unsymmetrically Substituted Bistriazolium Hexafluorophosphate Salts

*6.2.7.1 4-(2,6-Diisopropylphenyl)-1-{3-[(4-(3,5-dimethylphenyl)-1*H*-1,2,4-triazolium-1-yl)methyl]benzyl}-1*H*-1,2,4-triazolium Bis(hexafluorophosphate)* (**56**)

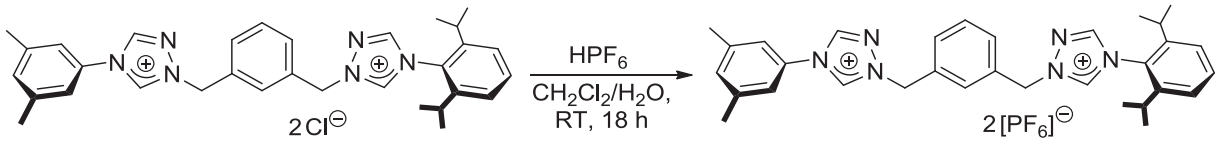

36 **56**

In a 100 ml round-bottomed flask, a solution of hexafluorophosphoric acid (60 weight-% solution in water, ρ = 1.6510 g cm^{-3}, 0.7 ml, 5 mmol) in de-ionized water (25 ml) was prepared. A solution of 4-(2,6-diisopropylphenyl)-1-{3-[(4-(3,5-dimethylphenyl)-1*H*-1,2,4-triazolium-1-yl)methyl]benzyl}-1*H*-1,2,4-triazolium dichloride (**36**, 0.964 g, 1.67 mmol) in dichloromethane (40 ml) was added. The reaction mixture was vigorously stirred for 18 hours. De-ionized water (100 ml) was added and the phases were separated. The organic phase was washed with water (2 × 100 ml). The aqueous phases were extracted with dichloromethane (2 × 100 ml). The combined organic phases were dried over magnesium sulphate. After filtration of the drying agent, the solvent was removed *in vacuo* to give the product as a colourless crystalline solid (1.103 g, 1.384 mmol, 83 %).

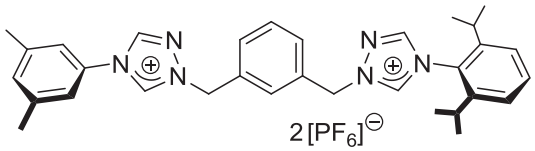

56

$C_{32}H_{38}F_{12}N_6P_2$

M ($C_{32}H_{38}F_{12}N_6P_2$) = 796.61 g mol^{-1}

^{1}H NMR (500.130 MHz, CD_3CN, 25 °C): δ = 10.39 (s, 1H, $CH_2NC\underline{H}NDipp$), 10.36 (s, 1H, $XylNC\underline{H}NCH_2$), 8.97 (s, 1H, $CH_2NNC\underline{H}NDipp$), 8.84 (s, 1H, $XylNC\underline{H}NNCH_2$), 7.88 (s, 1H, Xyl-linker, $CH_2CC\underline{H}CCH_2$), 7.67 - 7.54 (m, 4H, Xyl-linker, XylNCHN-$CH_2CC\underline{H}CHCH$ and $XylNCHNCH_2CCHC\underline{H}CH$ and $XylNCHNCH_2CCHCHC\underline{H}$, and Dipp-substituent, *para*-C$\underline{H}$), 7.43 (d, $^3J_{H\text{-}H}$ = 7.8 Hz, 2H, Dipp-substituent, *meta*-C$\underline{H}$), 7.34 (s, 2H, Xyl-substituent, *ortho*-C$\underline{H}$), 7.28 (s, 1H, Xyl-substituent, *para*-C$\underline{H}$), 5.75 (m, 2H, $C\underline{H}_2NCHNDipp$), 5.67 (m, 2H, $XylNCHNC\underline{H}_2$), 2.38 (s, 6 H, Xyl-substituent, $C\underline{H}_3$), 2.28 (sept, $^3J_{H\text{-}H}$ = 6.8 Hz, 2H, $C\underline{H}(CH_3)_2$), 1.14 (d, $^3J_{H\text{-}H}$ = 6.8 Hz, 6H, $CH(C\underline{H}_3)_2$), 1.11 (d, $^3J_{H\text{-}H}$ = 6.8 Hz, 6H, $CH(C\underline{H}_3)_2$).

^{13}C{^{1}H} NMR (125.758 MHz, CD_3CN, 25 °C): δ = 146.5 ($CH_2NN\underline{C}HNDipp$), 146.5 (Dipp-substituent, *ortho*-$\underline{C}CH(CH_3)_2$), 144.4 ($CH_2N\underline{C}HNDipp$), 143.8 ($XylN\underline{C}HN-NCH_2$), 142.1 ($XylN\underline{C}HNCH_2$), 141.8 (Xyl-substituent, *meta*-$\underline{C}CH_3$), 134.2 (Xyl-linker, $XylNCHNCH_2C\underline{C}HCHCH$ or $XylNCHNCH_2CCH\underline{C}HCH$ or $XylNCHNCH_2CCHCH\underline{C}H$), 134.1 (Xyl-linker, $XylNCHNCH_2C\underline{C}HCHCH$ or $XylNCHNCH_2CCH\underline{C}HCH$ or $XylNCH-NCH_2CCHCH\underline{C}H$), 133.5 (Xyl-substituent, *para*-$\underline{C}$H), 133.3 (Xyl-linker, $XylNCHNCH_2-C\underline{C}HCHCH$ or $XylNCHNCH_2CCH\underline{C}HCH$ or $XylNCHNCH_2CCHCH\underline{C}H$), 132.6 (Xyl-substituent, *ipso*-$\underline{C}$N), 131.7 (Xyl-linker, $\underline{C}CH_2NCHNDipp$ or $XylNCHNCH_2\underline{C}$), 131.6 (Xyl-linker, $CH_2C\underline{C}HCCH_2$), 131.3 (Dipp-substituent, *para*-$\underline{C}$H), 131.0 (Xyl-linker, $XylNCHNCH_2\underline{C}$ or $\underline{C}CH_2NCHNDipp$), 127.9 (Dipp-substituent, *ipso*-$\underline{C}$N), 125.8 (Dipp-substituent, *meta*-$\underline{C}$H), 121.0 (Xyl-substituent, *ortho*-$\underline{C}$H), 57.0 ($\underline{C}H_2NCHNDipp$), 56.6 ($XylNCHN\underline{C}H_2$), 29.4 ($\underline{C}H(CH_3)_2$), 24.0 ($CH(\underline{C}H_3)_2$), 23.9 ($CH(\underline{C}H_3)_2$), 21.1 (Xyl-substituent, $\underline{C}H_3$).

^{31}P{^{1}H} NMR (202.456 MHz, CD_3CN, 25 °C): δ = -144.56 (sept, $^1J_{P\text{-}F}$ = 707.0 Hz).

HR-MS (ESI+, methanol) *m*/*z* (%): 253.15729 (6.9) $[M\text{-}2PF_6]^{2+}$, 505.30764 (8.1) $[M\text{-}H\text{-}2PF_6]^{+}$, 651.27927 (100) $[M\text{-}PF_6]^{+}$.

calculated for $[C_{32}H_{38}F_6N_6P]^{+}$:	651.28002
found:	651.27927

Infrared Spectroscopy (KBr): $\tilde{\nu}$ [cm^{-1}] = 3431 (br, m), 3146 (s), 2970 (s), 2932 (m), 2184 (w), 1621 (s), 1597 (m), 1568 (s), 1445 (s), 1369 (m), 1313 (m), 1185 (m), 1106 (s), 1060 (m), 1003 (m), 836 (br, s, hexafluorophosphate, asymmetric stretching mode), 757 (m), 740 (s), 727 (m), 685 (s), 558 (s, hexafluorophosphate, bending mode).

Elemental Analysis (No. 30367)

calculated for $C_{32}H_{38}F_{12}N_6P_2$:	C 48.25 %,	H 4.81 %,	N 10.55 %
found:	C 48.48 %,	H 5.02 %,	N 10.25 %

Melting Point: 184 °C.

Crystal Structure: Crystallographic data and structure refinements for reb10, formula $C_{32}H_{38}F_{12}N_6P_2$, *M* ($C_{32}H_{38}F_{12}N_6P_2$) = 796.61 g mol^{-1}: colourless crystal (polyhedron), dimensions 0.26 × 0.12 × 0.06 mm^3, crystal system triclinic, space group $P\bar{1}$, *Z* = 2, *a* = 10.2433(3) Å, *b* = 10.2978(3) Å, *c* = 19.2667(6) Å, α = 92.245(1)°, β = 102.215(1)°, γ = 109.934(1)°, *V* = 1853.55(10) $Å^3$, ρ = 1.456 g cm^{-3}, *T* = 200(2) K, Θ_{max} = 23.76°, radiation Mo K_α, λ = 0.71073 Å, 0.3° ω-scans with CCD area detector, covering the asymmetric unit in reciprocal space with a mean redundancy of 4.09 and a completeness of 99.5 % to a resolution of 0.88 Å, 23202 reflections measured, 5652 unique (*R*(int)= 0.0399), 4346 observed ($I > 2\sigma(I)$), intensities were corrected for Lorentz and polarization effects, an empirical absorption correction was applied using SADABS[165] based on the Laue symmetry of the reciprocal space, μ = 0.21 mm^{-1}, T_{min} = 0.95, T_{max} = 0.99, structure solved by direct methods and refined against F^2 with a full-matrix least-squares algorithm using the SHELXTL (version 2008/4) software package,[166] 631 parameters refined, hydrogen atoms were treated using appropriate riding models, goodness of fit 1.02 for observed reflections, final residual values *R*1(*F*) = 0.056, *wR*(F^2) = 0.134 for observed reflections, residual electron density -0.28 to 0.39 e$Å^{-3}$.

*6.2.7.2 4-(2,6-Diisopropylphenyl)-1-{2-[4-(3,5-dimethylphenyl)-1*H*-1,2,4-triazolium-1-yl]ethyl}-1*H*-1,2,4-triazol-1-ium Bis(hexafluorophosphate)* (**66**)

46 **66**

In a 100 ml round-bottomed flask, a solution of hexafluorophosphoric acid (60 weight-% solution in water, ρ = 1.6510 g cm^{-3}, 7.5 ml, 51 mmol) in de-ionized water (40 ml) was prepared. 4-(2,6-Diisopropylphenyl)-1-{2-[4-(3,5-dimethylphenyl)-1*H*-1,2,4-triazolium-1-yl]ethyl}-1*H*-1,2,4-triazol-1-ium dibromide (**46**, 2.897 g, 4.907 mmol) was added as a powdery solid. The reaction mixture was vigorously stirred for 48 hours. After filtration the colourless crystalline solid was washed with de-ionized water (3 × 50 ml) and diethyl ether (3 × 100 ml) and dried *in vacuo* (3.098 g, 4.300 mmol, 88 %).

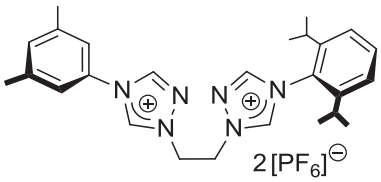

66

$C_{26}H_{34}F_{12}N_6P_2$

M ($C_{26}H_{34}F_{12}N_6P_2$) = 796.61 g mol^{-1}

^{1}H NMR (300.190 MHz, d$_6$-DMSO, 27 °C): δ = 10.94 (s, 1H, $CH_2NC\underline{H}NDipp$), 10.59 (s, 1H, $XylNC\underline{H}NCH_2$), 9.81 ($CH_2NNC\underline{H}NDipp$), 9.78 (s, 1H, $XylNC\underline{H}NNCH_2$), 7.69 (t, $^3J_{H\text{-}H}$ = 7.8 Hz, 1H, Dipp-substituent, *para*-C$\underline{H}$), 7.51 (d, $^3J_{H\text{-}H}$ = 7.8 Hz, 2H, Dipp-substituent, *meta*-C$\underline{H}$), 7.45 (s, 2H, Xyl-substituent, *ortho*-C$\underline{H}$), 7.33 (s, 1H, Xyl-substituent, *para*-C$\underline{H}$), 5.19 (br, 4H, $XylNCHNC\underline{H}_2$ and $C\underline{H}_2NCHNDipp$), 2.41 (s, 6H, Xyl-substituent, C$\underline{H}_3$), 2.34 (sept, $^3J_{H\text{-}H}$ = 6.7 Hz, 2H, Dipp-substituent, C$\underline{H}(CH_3)_2$), 1.16 - 1.14 (br, d, $^3J_{H\text{-}H}$ = 6.7 Hz, 12H, $CH(C\underline{H}_3)_2$).

$^{13}C\{^1H\}$ NMR (75.483 MHz, d_6-DMSO, 27 °C): δ = 146.1 ($CH_2NN\underline{C}HNDipp$), 145.2 (Dipp-substituent, *ortho*-$\underline{C}CH(CH_3)_2$), 144.8 ($CH_2N\underline{C}HNDipp$), 143.0 ($XylN\underline{C}HNNCH_2$), 142.8 ($XylN\underline{C}HNCH_2$), 140.0 (Xyl-substituent, $\underline{C}CH_3$), 132.3 (Xyl-substituent, *ipso*-$\underline{C}N$), 131.9 (Dipp-substituent, *para*-$\underline{C}H$), 131.7 (Xyl-substituent, *para*-$\underline{C}H$), 127.1 (Dipp-substituent, *ipso*-$\underline{C}N$), 124.8 (Dipp-substituent, *meta*-$\underline{C}H$), 119.7 (Xyl-substituent, *ortho*-$\underline{C}H$), 51.0 ($\underline{C}H_2NCHNDipp$), 49.7 ($XylNCHN\underline{C}H_2$), 27.9 (Dipp-substituent, $\underline{C}H(CH_3)_2$), 23.9 (Dipp-substituent, $CH(\underline{C}H_3)_2$), 23.4 (Dipp-substituent, $CH(\underline{C}H_3)_2$), 20.7 (Xyl-substituent, $\underline{C}H_3$).

$^{31}P\{^1H\}$ NMR (121.649 MHz, d_6-DMSO, 27 °C): δ = -144.18 (sept, $^1J_{P\text{-}F}$ = 711.3 Hz).

HR-MS (ESI+, methanol) *m*/*z* (%): 269.15087 (6.3) $[M\text{-}C_{12}H_{17}\text{-}2PF_6]^+$, 429.27624 (27.3) $[M\text{-}H\text{-}2PF_6]^+$, 575.24796 (100.0) $[M\text{-}PF_6]^+$.

calculated for $[C_{26}H_{34}F_6N_6P]^+$:	575.24813
found:	575.24796

Infrared Spectroscopy (KBr): $\tilde{\nu}$ [cm^{-1}] = 3144 (br, s), 3144 (w), 2969 (s), 1620 (m), 1568 (s), 1521 (w), 1465 (m), 1368 (w), 1339 (w), 1306 (w), 1279 (w), 1185 (w), 1106 (m), 1060 (w), 990 (w), 844 (br, s, hexafluorophosphate, asymmetric stretching mode), 740 (w), 684 (m), 653 (w) 558 (s, hexafluorophosphate, bending mode).

Melting Point: 261 °C.

6.2.8 Synthesis of Dinuclear Copper Complexes Containing IPr-Ligands

6.2.8.1 μ-*[1,1'-(Benzene-1,3-diyldimethanediyl)bis[4-(2,4,6-trimethylphenyl)-1*H-*1,2,4-triazol-5-ylidene]-*κC,κC'*-bis{[1,3-bis(2,6-diisopropylphenyl)imidazol-2-ylidene]copper(I)} Bis(hexafluorophosphate)* (**71**)

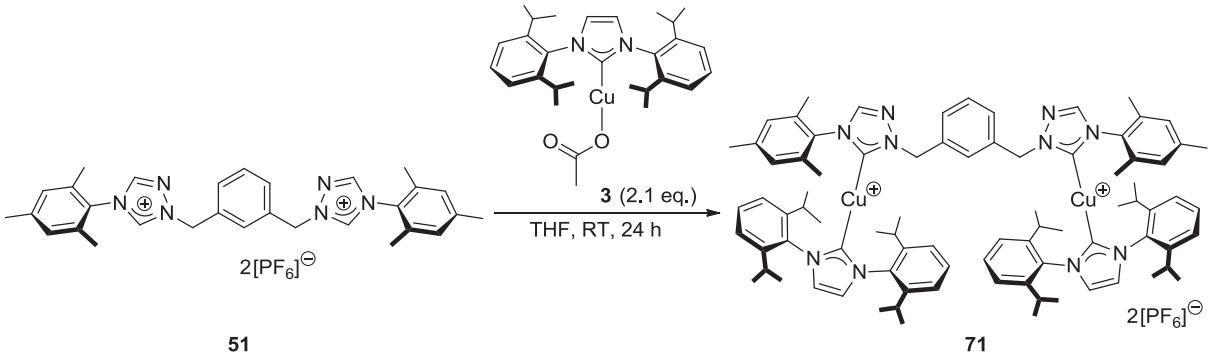

51 **71**

A flame-dried Schlenk flask was charged with 1,1'-[1,3-phenylenebis(methylene)]bis-(4-mesityl-1*H*-1,2,4-triazolium) bis(hexafluorophosphate) (**51**, 0.214 g, 0.278 mmol). In the glovebox, (IPr)CuOAc (**3**, 0.300 g, 0.587 mmol) was added and the solid starting materials were dissolved in tetrahydrofuran (15 ml). After five minutes, precipitation of a colourless solid commenced. The reaction mixture was stirred for 24 hours at room temperature. After filtration, the raw product was washed with diethyl ether (2 × 10 ml) and re-crystallized from acetonitrile/diethyl ether. The colourless crystalline product was air-stable (0.288 g, 0.172 mmol, 62 %).

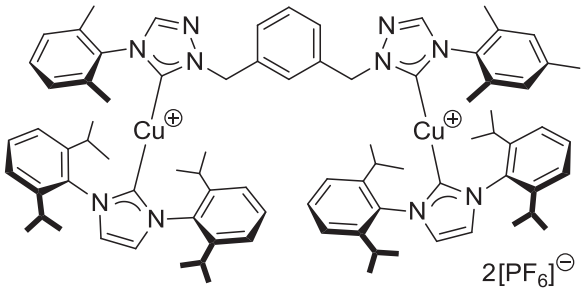

71

$C_{84}H_{104}Cu_2F_{12}N_{10}P_2$

M ($C_{84}H_{104}Cu_2F_{12}N_{10}P_2$) = 1670.81 g mol^{-1}

^{1}H NMR (400.180 MHz, CD_3CN, 25 °C): δ = 8.21 (s, 2H, triazolylidene, NC*H*NN), 7.49 (s, 4H, imidazolylidene, NC*H*), 7.42 (t, $^3J_{H\text{-}H}$ = 7.8 Hz, 4H, Dipp-substituent, *para*-C*H*), 7.26 (t, $^3J_{H\text{-}H}$ = 7.7 Hz, 1H, Xyl-linker, CH_2CCHCH), 7.24 (d, $^3J_{H\text{-}H}$ = 7.8 Hz, 8H, Dipp-substituent, *meta*-C*H*), 6.87 (s, 4H, Mes-substituent, *meta*-C*H*), 6.67 (s, 1H, Xyl-linker, $CH_2CCHCCH_2$), 6.57 (dd, $^3J_{H\text{-}H}$ = 7.7 Hz, $^4J_{H\text{-}H}$ = 1.6 Hz, 2H, Xyl-linker, CH_2CCHCH), 4.72 (s, 4H, CH_2), 2.44 (sept, $^3J_{H\text{-}H}$ = 6.9 Hz, 8H, Dipp-substituent, CH(CH_3)$_2$), 2.41 (s, 6H, Mes-substituent, *para*-CH_3), 1.67 (s, 12H, Mes-substituent, *ortho*-CH_3), 1.17 (d, $^3J_{H\text{-}H}$ = 6.9 Hz, 24H, Dipp-substituent, CH(CH_3)$_2$), 1.04 (d, $^3J_{H\text{-}H}$ = 6.9 Hz, 24H, Dipp-substituent, CH(CH_3)$_2$).

^{13}C{^{1}H} NMR (100.625 MHz, CD_3CN, 25 °C): δ = 179.0 (imidazolylidene, NCN), 178.2 (triazolylidene, NCN), 146.5 (Dipp-substituent, *ortho*-CCH(CH_3)$_2$), 145.8 (triazolylidene, NCHNN), 141.1 (Mes-substituent, *para*-$C$$CH_3$), 136.1 (Xyl-linker, $C$$CH_2$), 135.0 (Mes-substituent, *ortho*-$C$$CH_3$), 134.9 (Dipp-substituent, *ipso*-CN), 131.7 (Dipp-substituent, *para*-CH), 131.5 (Mes-substituent, *ipso*-CN), 130.7 (Mes-substituent, *meta*-CH), 130.4 (Xyl-linker, CH_2CCHCH), 127.7 (Xyl-linker, CH_2CCHCH), 127.7 (Xyl-linker, $CH_2CCHCCH_2$), 125.4 (imidazolylidene, NCH), 125.0 (Dipp-substituent, *meta*-CH), 56.7 ($C$$H_2$), 29.4 (Dipp-substituent, CH(CH_3)$_2$), 25.0 (Dipp-substituent, CH($C$$H_3$)$_2$), 23.9 (Dipp-substituent, CH($C$$H_3$)$_2$), 21.3 (Mes-substituent, *para*-$C$$H_3$), 17.8 (Mes-substituent, *ortho*-$C$$H_3$).

^{31}P{^{1}H} NMR (121.475 MHz, CD_3CN, 25 °C): δ = -144.60 (sept, $^1J_{P\text{-}F}$ = 706.4 Hz).

HR-MS (ESI+, methanol) *m*/*z* (%): 689.35132 (100.0) $[M(^{63}Cu,^{63}Cu)\text{-}2PF_6]^{2+}$, 691.35405 (40.1) $[M(^{63}Cu,^{65}Cu)\text{-}2PF_6]^{2+}$.

calculated for $[C_{84}H_{104}(^{63}Cu)_2N_{10}]^{2+}$: 689.35133

found: 689.35132

Infrared Spectroscopy (KBr)*: $\tilde{\nu}$* [cm^{-1}] = 3441 (br, m), 3143 (w), 2964 (m), 2872 (w), 1612 (w), 1525 (m), 1469 (w), 1412 (w), 1386 (w), 1365 (w), 1330 (w), 1309 (w), 1218 (w), 1061 (w), 988 (w), 949 (w), 843 (br, s, hexafluorophosphate, asymmetric stretching mode), 807 (w), 761 (w), 558 (s, hexafluorophosphate, bending mode).

Elemental Analysis (No. 31857)

calculated for $C_{84}H_{104}Cu_2F_{12}N_{10}P_2$: C 60.38 %, H 6.27 %, N 8.38 %

found: C 60.44 %, H 6.44 %, N 8.16 %

Decomposition Temperature: 272 °C (red, then brown solid).

Crystal Structure: Crystallographic data and structure refinements for reg4, formula $C_{84}H_{104}Cu_2F_{12}N_{10}P_2$+$CH_3CN$, *M* ($C_{86}H_{107}Cu_2F_{12}N_{11}P_2$) = 1711.90 g mol^{-1}: colourless crystal (plate), dimensions 0.27 × 0.17 × 0.03 mm^3, crystal system triclinic, space group $P\bar{1}$, *Z* = 2, *a* = 10.638(3) Å, *b* = 12.542(4) Å, *c* = 36.392(12) Å, α = 81.661(7)°, β = 85.315(8)°, γ = 69.104(7)°, *V* = 4486(2) $Å^3$, ρ = 1.267 g cm^{-3}, *T* = 200(2) K, Θ_{max} = 20.83°, radiation Mo K_α, λ = 0.71073 Å, 0.3° ω-scans with CCD area detector, covering a whole sphere in reciprocal space, 24440 reflections measured, 9392 unique (*R*(int) = 0.0662), 6299 observed ($I > 2\sigma(I)$), intensities were corrected for Lorentz and polarization effects, an empirical absorption correction was applied using SADABS[165] based on the Laue symmetry of the reciprocal space, μ = 0.58 mm^{-1}, T_{min} = 0.86, T_{max} = 0.98, structure solved by direct methods and refined against F^2 with a full-matrix least-squares algorithm using the SHELXTL (version 2008/4) software package,[166] 1135 parameters refined, hydrogen atoms were treated using appropriate riding models, goodness of fit 1.04 for observed reflections, final residual values *R*1(*F*) = 0.062, *wR*(F^2) = 0.158 for observed reflections, residual electron density -0.43 to 0.82 e$Å^{-3}$.

6.2.8.2 μ-*[1,1'-(Ethane-1,2-diyl)bis[4-(2,4,6-trimethylphenyl)-1*H*-1,2,4-triazol-5-ylidene]*–κC,κC'-*bis{[1,3-bis(2,6-diisopropylphenyl)imidazol-2-ylidene]copper(I)} Bis(hexafluorophosphate)* (**81**)

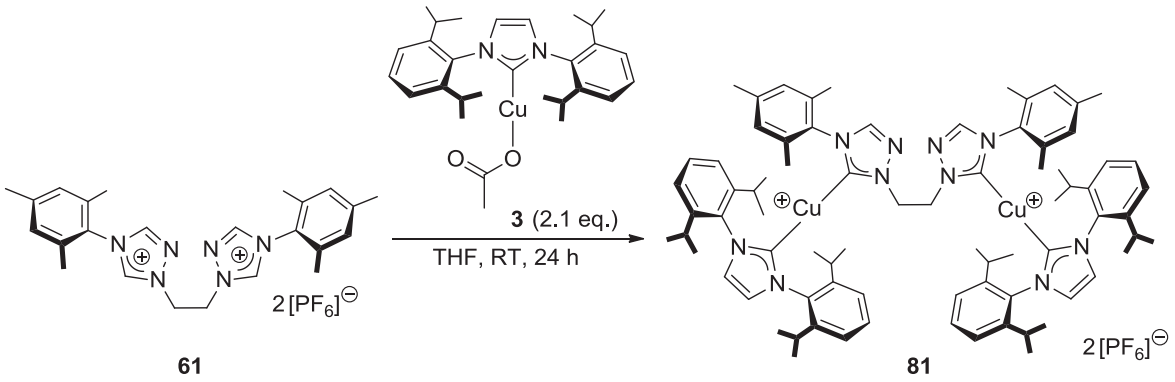

A flame-dried Schlenk flask was charged with 1,1'-(ethane-1,2-diyl)bis[4-(2,4,6-trimethylphenyl)-1*H*-1,2,4-triazolium] bis(hexafluorophosphate) (**51**, 0.600 g, 0.866 mmol). In the glovebox, (IPr)CuOAc (**3**, 0.974 g, 1.91 mmol) was added and the solid starting materials were dissolved in tetrahydrofuran (10 ml). After five minutes, the precipitation of a colourless solid commenced. The reaction mixture was stirred for three days at room temperature. After filtration, the raw product was washed with tetrahydrofuran (10 ml) and diethyl ether (2 × 10 ml). The colourless crystalline product was air-stable (0.774 g, 0.485 mmol, 56 %).

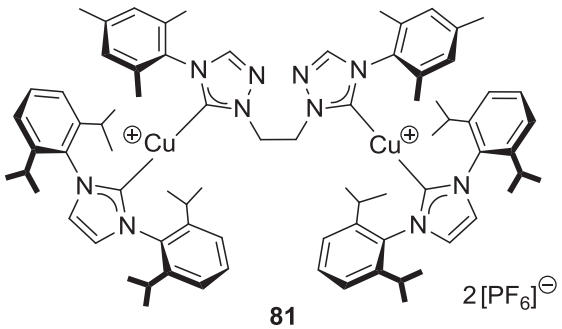

81

$C_{78}H_{100}Cu_2F_{12}N_{10}P_2$

M ($C_{78}H_{100}Cu_2F_{12}N_{10}P_2$) = 1594.72 g mol^{-1}

^{1}H NMR (300.190 MHz, CD_3CN, 27 °C): δ = 7.79 (s, 2H, triazolylidene, NC*H*NN), 7.57 (t, $^3J_{H\text{-}H}$ = 7.8 Hz, 4H, Dipp-substituent, *para*-C*H*), 7.51 (s, 4H, imidazolylidene, NC*H*), 7.35 (d, $^3J_{H\text{-}H}$ = 7.8 Hz, 8H, Dipp-substituent, *meta*-C*H*), 6.81 (s, 4H, Mes-

substituent, *meta*-C*H*), 3.55 (s, 4H, CH_2), 2.48 (sept, $^3J_{H\text{-}H}$ = 6.9 Hz, 8H, Dipp-substituent, C*H*(CH_3)$_2$), 2.38 (s, 6H, Mes-substituent, *para*-CH_3), 1.53 (s, 12H, Mes-substituent, *ortho*-CH_3), 1.21 (d, $^3J_{H\text{-}H}$ = 6.9 Hz, 24H, Dipp-substituent, CH(CH_3)$_2$), 1.11 (d, $^3J_{H\text{-}H}$ = 6.9 Hz, 24H, Dipp-substituent, CH(CH_3)$_2$).

^{13}C{^{1}H} NMR (75.483 MHz, CD_3CN, 27 °C): δ = 178.9 (imidazolylidene, N*C*N), 178.6 (triazolylidene, N*C*N), 146.7 (Dipp-substituent, *ortho*-*C*$CH(CH_3)_2$), 144.4 (triazolylidene, N*C*HNN), 141.2 (Mes-substituent, *para*-*C*CH_3), 135.1 (Mes-substituent, *ipso*-*C*N), 135.0 (Dipp-substituent, *ipso*-*C*N), 131.8 (Dipp-substituent, *para*-*C*H), 131.4 (Mes-substituent, *ortho*-*C*CH_3), 130.7 (Mes-substituent, *meta*-*C*H), 125.5 (imidazolylidene, N*C*H), 125.2 (Dipp-substituent, *meta*-*C*H), 52.2 (*C*H_2), 29.5 (Dipp-substituent, *C*H(CH_3)$_2$), 25.2 (Dipp-substituent, CH(*C*H_3)$_2$), 23.9 (Dipp-substituent, CH(*C*H_3)$_2$), 21.2 (Mes-substituent, *para*-*C*H_3), 17.7 (Mes-substituent, *ortho*-*C*H_3).

^{31}P{^{1}H} NMR (121.649 MHz, CD_3CN, 26 °C): δ = -144.58 (sept, $^1J_{P\text{-}F}$ = 706.6 Hz).

HR-MS (ESI+, acetonitrile) *m*/*z* (%): 389.29528 (100.0) [M-$C_{51}H_{63}N_8Cu_2$-2PF_6]$^+$, 401.24505 (2.2) [M-2$C_{27}H_{35}Cu_2N_2$-H-2PF_6]$^+$, 492.24365 (96.9) [M(^{63}Cu)-$C_{51}H_{64}CuN_8$-2PF_6+H_3CCN]$^+$, 494.24188 (44.0) [M(^{65}Cu)-$C_{51}H_{64}CuN_8$-2PF_6+H_3CCN]$^+$, 651.33508 (77.3) [M(^{63}Cu,^{63}Cu)-2PF_6]$^{2+}$, 653.33791 (24.6) [M(^{63}Cu,^{65}Cu)-2PF_6]$^{2+}$.

calculated for [$C_{78}H_{100}$(^{63}Cu)$_2N_{10}$]$^{2+}$:	651.33568
found:	651.33508

Infrared Spectroscopy (KBr): $\tilde{\nu}$ [cm^{-1}] = 3439 (br, m), 3145 (w), 2964 (m), 2927 (m), 2871 (w), 1627 (br, w), 1527 (w), 1458 (m), 1411 (w), 1386 (w), 1365 (w), 1330 (w), 1061 (w), 982 (w), 843 (br, s, hexafluorophosphate, asymmetric stretching mode), 808 (m), 761 (m), 704 (w), 558 (s, hexafluorophosphate, bending mode), 454 (w).

Elemental Analysis (No. 30707)

calculated for $C_{84}H_{104}Cu_2F_{12}N_{10}P_2$:	C 58.75 %, H 6.32 %,
	N 8.78 %, P 3.88 %
found:	C 58.82 %, H 6.40 %,
	N 8.80 %, P 3.88 %

Decomposition Temperature: 264 °C (black solid).

Crystal Structure: Crystallographic data and structure refinements for reb9, formula $C_{78}H_{100}Cu_2F_{12}N_{10}P_2$+3$CH_3CN$, *M* ($C_{84}H_{109}Cu_2F_{12}N_{13}P_2$) = 1717.90 g mol^{-1}: colourless crystal (polyhedron), dimensions 0.23 × 0.23 × 0.09 mm^3, crystal system triclinic, space group $P\bar{1}$, *Z* = 2, *a* = 11.1914(4) Å, *b* = 19.6953(7) Å, *c* = 21.0620(7) Å, α = 80.413(2)°, β = 82.312(2)°, γ = 79.050(2)°, *V* = 4469.2(3) $Å^3$, ρ = 1.277 g cm^{-3}, *T* = 200(2) K, Θ_{max} = 26.94°, radiation Mo K_α, λ = 0.71073 Å, 0.3° ω-scans with CCD area detector, covering the asymmetric unit in reciprocal space with a mean redundancy of 3.98 and a completeness of 99.6 % to a resolution of 0.78 Å, 77147 reflections measured, 19304 unique (*R*(int)= 0.0456), 14421 observed ($I > 2\sigma(I)$), intensities were corrected for Lorentz and polarization effects, an empirical absorption correction was applied using SADABS[165] based on the Laue symmetry of the reciprocal space, μ = 0.59 mm^{-1}, T_{min} = 0.88, T_{max} = 0.95, structure solved by direct methods and refined against F^2 with a full-matrix least-squares algorithm using the SHELXTL (version 2008/4) software package,[166] 1091 parameters refined, hydrogen atoms were treated using appropriate riding models, goodness of fit 1.01 for observed reflections, final residual values *R*1(*F*) = 0.046, *wR*(F^2) = 0.115 for observed reflections, residual electron density -0.37 to 0.60 e$Å^{-3}$.

6.2.8.3 μ-*{1,1'-(Ethane-1,2-diyl)bis[4-(4-methylphenyl)-1*H*-1,2,4-triazol-5-ylidene}-*κC,*κC'-bis{[1,3-bis(2,6-diisopropylphenyl)imidazol-2-ylidene]copper(I)} Bis(hexafluorophosphate)* (**83**)

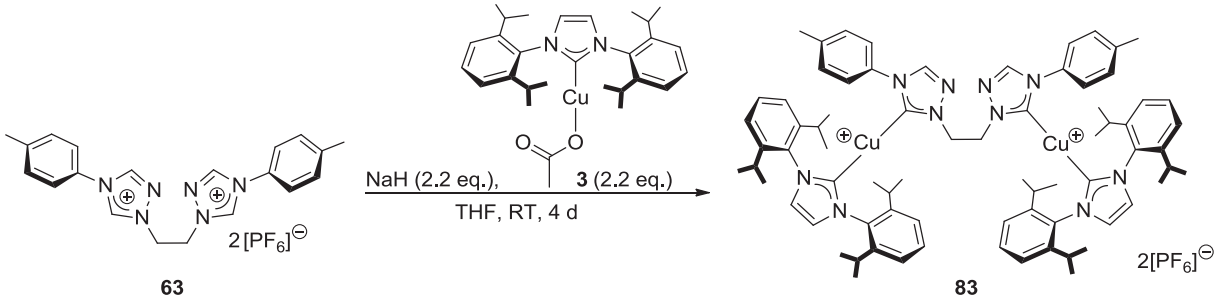

63 **83**

A flame-dried Schlenk flask was charged with 1,1'-(ethane-1,2-diyl)bis[4-(4-methylphenyl)-1*H*-1,2,4-triazolium] bis(hexafluorophosphate) (**63**, 0.865 g, 1.36 mmol). In the glovebox, (IPr)CuOAc (**3**, 1.529 g, 2.991 mmol) was added and the solid starting materials were dissolved in tetrahydrofuran (10 ml). Sodium hydride (0.072 g, 3.0 mmol) was added to the reaction mixture and the evolution of gas was observed. The reaction mixture was stirred for four days at room temperature. After filtration, the raw product was washed with tetrahydrofuran (2 × 10 ml). Acetonitrile (35 ml) was added and the mixture was filtered over a filter paper-capped canula. The colourless air-stable product was isolated by evaporation of the solvent *in vacuo* (1.775 g, 1.154 mmol, 85 %).

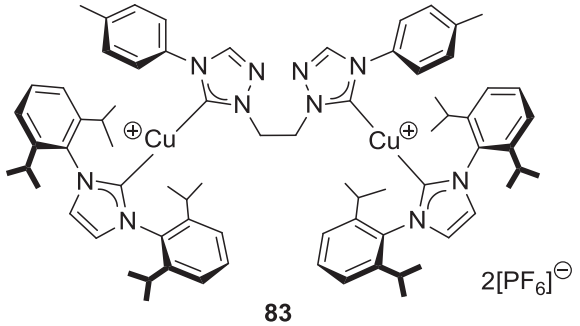

83

$C_{74}H_{92}Cu_2F_{12}N_{10}P_2$

M ($C_{74}H_{92}Cu_2F_{12}N_{10}P_2$) = 1538.61 g mol^{-1}

^{1}H NMR (300.190 MHz, CD_3CN, 27 °C): δ = 8.12 (s, 2H, triazolylidene, NC*H*NN), 7.56 (t, $^3J_{H\text{-}H}$ = 7.8 Hz, 4H, Dipp-substituent, *para*-C*H*), 7.46 (s, 4H, imidazolylidene, NC*H*), 7.36 (d, $^3J_{H\text{-}H}$ = 7.8 Hz, 8H, Dipp-substituent, *meta*-C*H*), 6.96 (d, $^3J_{H\text{-}H}$ = 8.3 Hz, 4H, Tol-substituent, *meta*-C*H*), 6.87 (d, $^3J_{H\text{-}H}$ = 8.3 Hz, 4H, Tol-substituent, *ortho*-C*H*), 3.57 (s, 4H, CH_2), 2.52 (sept, $^3J_{H\text{-}H}$ = 6.9 Hz, 8H, Dipp-substituent, C*H*(CH_3)$_2$), 2.40 (s, 6H, Tol-substituent, CH_3), 1.19 (d, $^3J_{H\text{-}H}$ = 6.9 Hz, 24H, Dipp-substituent, CH(CH_3)$_2$), 1.06 (d, $^3J_{H\text{-}H}$ = 6.9 Hz, 24H, Dipp-substituent, CH(CH_3)$_2$).

^{13}C{^{1}H} NMR (75.483 MHz, CD_3CN, 27 °C): δ = 179.9 (imidazolylidene, N*C*N), 178.0 (triazolylidene, N*C*N), 146.9 (Dipp-substituent, *ortho*-*C*CH(CH_3)$_2$), 143.2 (triazolylidene, N*C*HNN), 140.7 (Tol-substituent, *C*CH_3), 135.5 (Dipp-substituent, *ipso*-*C*N), 133.6 (Tol-substituent, *ipso*-*C*N), 131.6 (Dipp-substituent, *para*-*C*H), 131.5 (Tol-substituent, *meta*-*C*H), 125.5 (imidazolylidene, N*C*H), 125.3 (Dipp-substituent, *meta*-*C*H), 124.0 (Tol-substituent, *ortho*-*C*H), 50.3 (*C*H_2), 29.5 (Dipp-substituent, *C*H(CH_3)$_2$), 24.8 (Dipp-substituent, CH(*C*H_3)$_2$), 24.0 (Dipp-substituent, CH(*C*H_3)$_2$), 21.1 (Tol-substituent, *C*H_3).

^{31}P{^{1}H} NMR (121.649 MHz, CD_3CN, 27 °C): δ = -144.59 (sept, $^1J_{P\text{-}F}$ = 706.5 Hz).

HR-MS (ESI+, acetonitrile) *m*/*z* (%): 623.30442 (99.4) [M(^{63}Cu,^{63}Cu)-2PF_6]$^{2+}$, 625.30702 (28.6) [M(^{63}Cu,^{65}Cu)-2PF_6]$^{2+}$, 795.39359 (18.5) [M(^{63}Cu)-$C_{27}H_{36}CuN_2$-2PF_6]$^+$, 797.39221 (7.9) [M(^{65}Cu)-$C_{27}H_{36}CuN_2$-2PF_6]$^+$, 941.36636 (16.2) [M(^{63}Cu)-$C_{27}H_{35}CuN_2$-PF_6]$^+$, 943.36521 (6.5) [M(^{65}Cu)-$C_{27}H_{35}CuN_2$-PF_6]$^+$, 1391.57953 (15.6) [M(^{63}Cu,^{63}Cu)-PF_6]$^+$, 1393.57860 (19.7) [M(^{63}Cu,^{65}Cu)-PF_6]$^+$, 1395.58011 (6.5) [M(^{65}Cu,^{65}Cu)-PF_6]$^+$.

calculated for $[C_{74}H_{92}(^{63}Cu)_2N_{10}]^{2+}$: 623.30438
found: 623.30423

Infrared Spectroscopy (KBr): $\tilde{\nu}$ [cm^{-1}] = 3428 (br, m), 3144 (w), 2964 (m), 2871 (w), 1579 (s), 1517 (m), 1459 (m), 1412 (m), 1365 (m), 1329 (w), 1257 (w), 1215 (w), 1119 (w), 1061 (w), 983 (w), 845 (br, s, hexafluorophosphate, asymmetric stretching mode), 760 (m), 702 (w), 650 (w), 558 (m, hexafluorophosphate, bending mode).

Elemental Analysis (No. 31568)
calculated for $C_{74}H_{92}Cu_2F_{12}N_{10}P_2$: C 57.77 %, H 6.03 %, N 9.10 %
found: C 57.65 %, H 6.23 %, N 9.13 %

Decomposition Temperature: 264 °C (black solid).

Crystal Structure: Crystallographic data and structure refinements for reb16, formula $C_{74}H_{92}Cu_2F_{12}N_{10}P_2$+2$CH_3CN$, M ($C_{78}H_{98}Cu_2F_{12}N_{12}P_2$) = 1620.74 g mol^{-1}: colourless crystal (polyhedron), dimensions 0.28 × 0.17 × 0.05 mm^3, crystal system triclinic, space group $P\bar{1}$, Z = 1, a = 10.4897(12), b = 12.3247(15) Å, c = 16.933(2) Å, α = 73.652(2)°, β = 87.851(2)°, γ = 87.666(2)°, V = 2098.1(4) $Å^3$, ρ = 1.283 g cm^{-3}, T = 200(2) K, Θ_{max} = 28.95°, radiation Mo K_α, λ = 0.71073 Å, 0.3° ω-scans with CCD area detector, covering the asymmetric unit in reciprocal space with a mean redundancy of 3.71 and a completeness of 97.7 % to a resolution of 0.73 Å, 7318 reflections measured, 10858 unique (R(int)= 0.0667), 14421 observed ($I > 2\sigma(I)$), intensities were corrected for Lorentz and polarization effects, an empirical absorption correction was applied using SADABS[165] based on the Laue symmetry of the reciprocal space, μ = 0.62 mm^{-1}, T_{min} = 0.85, T_{max} = 0.97, structure solved by direct methods and refined against F^2 with a full-matrix least-squares algorithm using the SHELXTL (version 2008/4) software package,[166] 544 parameters refined, hydrogen atoms were treated using appropriate riding models, goodness of fit 1.02 for observed reflections, final residual values $R1(F)$ = 0.056, $wR(F^2)$ = 0.141 for observed reflections, residual electron density -0.60 to 1.28 e$Å^{-3}$.

6.2.9 Synthesis of Dinuclear Copper Acetate Complexes

6.2.9.1 μ-*Acetato-*κ*O,*κ*O'-*μ*-{1,1'-(ethane-1,2-diyl)bis[4-(2,4,6-trimethylphenyl)-1*H*-1,2,4-triazol-5-ylidene]}-*κ*C,*κ*C'-dicopper(I) Hexafluorophosphate* (**91**)

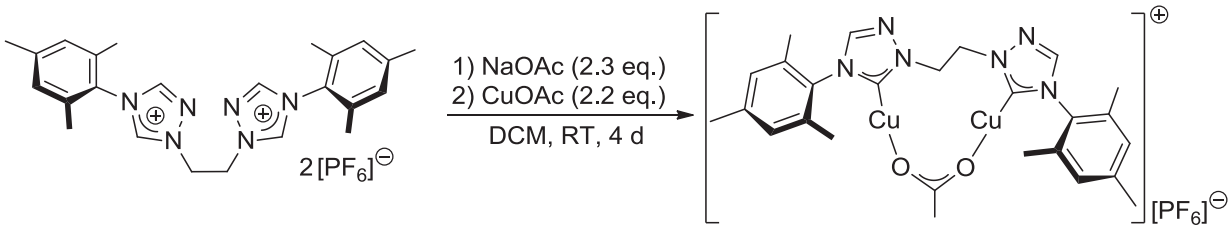

61 **91**

A flame-dried Schlenk flask was charged with 1,1'-(ethane-1,2-diyl)bis[4-(2,4,6-trimethylphenyl)-1*H*-1,2,4-triazolium] bishexafluorophosphate (**61**, 1.049 g, 1.515 mmol) under an atmosphere of inert gas and sodium acetate (0.286 g, 3.49 mmol) was added. In the glovebox, the mixture was suspended in dichloromethane (15 ml) and stirred for two hours at room temperature. Copper(I) acetate (0.409 g, 3.34 mmol) and dichloromethane (10 ml) were added. The reaction mixture was stirred for four days. After filtration over a frit under inert gas, the solvent was removed *in vacuo*. The colourless solid residue was washed with diethyl ether (4 × 20 ml) and dried *in vacuo*. The colourless product was obtained as a crystalline solid (0.880 g, 1.20 mmol, 79 %).

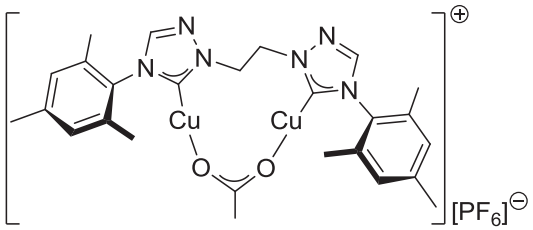

91

$C_{26}H_{31}Cu_2F_6N_6O_2P$

M ($C_{26}H_{31}Cu_2F_6N_6O_2P$) = 731.62 g mol^{-1}

^{1}H NMR (300.510 MHz, CD_2Cl_2, 27 °C): δ = 8.12 (s, 2H, NC*H*N), 7.05 (s, 4H, *meta*-C*H*), 5.38 (s, 4H, CH_2), 2.36 (s, 6H, *para*-CH_3), 1.97 (s, 3H, H_3CCOO), 1.93 (s, 12H, *ortho*-CH_3).

^{13}C{^{1}H} NMR (125.758 MHz, CD_2Cl_2, 25 °C): δ = 183.5 (H_3C*C*OO), 177.1 (N*C*N), 144.3 (N*C*HN), 141.5 (*para*-*C*CH_3), 134.7 (*ortho*-*C*CH_3), 131.3 (*ipso*-*C*N), 130.3 (*meta*-*C*H), 52.3 (*C*H_2), 21.2 (*para*-*C*H_3), 17.7 (H_3*C*COO), 18.3 (*ortho*-*C*H_3).
The signal for the acetate ligand's methyl group is of very low intensity in the ^{13}C{^{1}H} NMR spectrum, but can be identified with the help of a HSQC spectrum.

^{31}P{^{1}H} NMR (202.456 MHz, CD_2Cl_2, 25 °C): δ = -144.49 (sept, $^1J_{P\text{-}F}$ = 711.8 Hz).

^{1}H NMR (300.509 MHz, d_8-THF, 27 °C): δ = 8.54 (s, 2H, NC*H*N), 7.04 (s, 4H, *meta*-C*H*), 5.34 (s, 4H, CH_2), 2.32 (s, 6H, *para*-CH_3), 1.93 (s, 12H, *ortho*-CH_3), 1.80 (s, 3H, H_3CCOO).

^{13}C{^{1}H} NMR (75.483 MHz, d_8-THF, 27 °C): δ = 181.9 (H_3C*C*OO), 178.6 (N*C*N), 145.1 (N*C*HN), 141.1 (*para*-*C*CH_3), 135.5 (*ortho*-*C*CH_3), 132.8 (*ipso*-*C*N), 130.3 (*meta*-*C*H), 52.9 (*C*H_2), 21.9 (H_3*C*COO), 21.1 (*para*-*C*H_3), 18.3 (*ortho*-*C*H_3).

^{31}P{^{1}H} NMR (121.475 MHz, d_8-THF, 27 °C): δ = -144.27 (sept, $^1J_{P\text{-}F}$ = 710.8 Hz).

HR-MS (ESI+, methanol) *m*/*z* (%): 463.16690 (100.0) [M(^{63}Cu)-CuOAc-PF_6]$^+$, 465.16541 (23.8) [M(^{65}Cu)-CuOAc-PF_6]$^+$, 961.30335 (40.4) [2M(^{63}Cu,^{63}Cu)-2CuOAc-2PF_6+^{35}Cl]$^+$, 963.30212 (51.3) [2M(^{63}Cu,^{65}Cu)-2CuOAc-2PF_6+^{35}Cl]$^+$ or

[2M(^{63}Cu,^{63}Cu)-2CuOAc-2PF_6+^{37}Cl]$^+$, 965.30088 (21.8) [2M(^{65}Cu,^{63}Cu)-2CuOAc-2PF_6+^{37}Cl]$^+$ or [2M(^{65}Cu,^{65}Cu)-2CuOAc-2PF_6+^{35}Cl]$^+$, 967.29912 (3.2) [2M(^{65}Cu,^{65}Cu)-2CuOAc-2PF_6+^{37}Cl]$^+$, 1071.29701 (79.4) [2M(^{63}Cu,^{63}Cu)-2CuOAc-PF_6]$^+$, 1073.29667 (93.6) [2M(^{63}Cu,^{65}Cu)-2CuOAc-PF_6]$^+$, 1075.29996 (22.5) [2M(^{65}Cu,^{65}Cu)-2CuOAc-PF_6]$^+$.

HR-MS (FAB+, NBA matrix) *m*/*z* (%): 436.1675 (86.8) [M(^{63}Cu)-HCN-CuOAc-PF_6]$^+$, 438.1635 (46.9) [M(^{65}Cu)-HCN-CuOAc-PF_6]$^+$, 463.1775 (81.0) [M(^{63}Cu)-CuOAc-PF_6]$^+$, 465.1870 (33.1) [M(^{65}Cu)-CuOAc-PF_6]$^+$, 543.1194 (45.3) [M(^{63}Cu,^{63}Cu)-2H-PF_5-OAc]$^+$, 545.1281 (48.5) [M(^{63}Cu,^{65}Cu)-2H-PF_5-OAc]$^+$, 547.1 (33.8) [M(^{65}Cu,^{65}Cu)-2H-PF_5-OAc]$^+$, 585.1094 (34.6) [M(^{63}Cu,^{63}Cu)-PF_6]$^+$, 587.1082 (35.6) [M(^{63}Cu,^{65}Cu)-PF_6]$^+$, 589.0934 (10.2) [M(^{65}Cu,^{65}Cu)-PF_6]$^+$, 678.1314 (100.0) [M(^{63}Cu,^{63}Cu)+$C_7H_6NO_3$(NBA-matrix)-OAc-PF_6]$^+$, 680.1259 (99.0) [M(^{63}Cu,^{65}Cu)+$C_7H_6NO_3$(NBA-matrix)-OAc-PF_6]$^+$, 682.1274 (29.9) [M(^{65}Cu,^{65}Cu)+$C_7H_6NO_3$ (NBA-matrix)-OAc-PF_6]$^+$.

calculated for [$C_{26}H_{31}(^{63}Cu)_2N_6O_2$]$^+$: 585.1095
found: 585.1094

Infrared Spectroscopy (KBr): $\tilde{\nu}$ [cm^{-1}] = 3142 (br, w), 2922 (w), 1590 (m), 1530 (m), 1489 (m), 1441 (m), 1317 (w), 1226 (w), 1160 (w), 1034 (w), 986 (w), 947 (w), 842 (br, s), 741 (w), 672 (w), 583 (w), 559 (s).

Elemental Analysis (No. 31476)

calculated for $C_{26}H_{31}Cu_2F_6N_6PO_2$: C 42.68 %, H 4.27 %, N 11.49 %
found: C 42.80 %, H 4.34 %, N 11.40 %

Decomposition Temperature: 236 °C (reddish brown solid).

Crystal Structure: μ-Acetato-$\kappa O,\kappa O'$-μ-{1,1'-(ethane-1,2-diyl)bis[4-(2,4,6-trimethylphenyl)-1*H*-1,2,4-triazol-5-ylidene]}-$\kappa C,\kappa C'$-dicopper(I) hexafluorophosphate is not stable in solution. The single crystal X-ray structure shows a neutral complex, in which two acetate ligands μ-coordinate to the two copper centres.

Crystallographic data and structure refinements for reb8, formula $C_{28}H_{34}Cu_2N_6O_4$, *M* ($C_{28}H_{34}Cu_2N_6O_4$) = 645.71 g mol^{-1}: colourless crystal (polyhedron), dimensions

0.26 × 0.06 × 0.05 mm^3, crystal system monoclinic, space group $P2_1/c$, Z = 4, a = 9.569(2), b = 18.170(4) Å, c = 17.100(4) Å, α = 90°, β = 102.822(6)°, γ = 90°, V = 2899.0(12) $Å^3$, ρ = 1.479 g cm^{-3}, T = 200(2) K, Θ_{max} = 28.39°, radiation Mo K_α, λ = 0.71073 Å, 0.3° ω-scans with CCD area detector, covering a whole sphere in reciprocal space, 30742 reflections measured, 7248 unique (R(int)= 0.0524), 5474 observed ($I > 2\sigma(I)$), intensities were corrected for Lorentz and polarization effects, an empirical absorption correction was applied using SADABS[165] based on the Laue symmetry of the reciprocal space, μ = 1.51 mm^{-1}, T_{min} = 0.69, T_{max} = 0.93, structure solved by direct methods and refined against F^2 with a full-matrix least-squares algorithm using the SHELXTL (version 2008/4) software package,[166] 369 parameters refined, hydrogen atoms were treated using appropriate riding models, goodness of fit 1.02 for observed reflections, final residual values $R1(F)$ = 0.043, $wR(F^2)$ = 0.090 for observed reflections, residual electron density -0.36 to 0.48 e$Å^{-3}$.

6.2.9.2 μ-*Acetato-κO,κO'-μ-{1,1'-(ethane-1,2-diyl)bis[4-(3,5-dimethylphenyl)-1*H*-1,2,4-triazol-5-ylidene]}-κC,κC'-dicopper(I) Hexafluorophosphate* (**92**)[137]

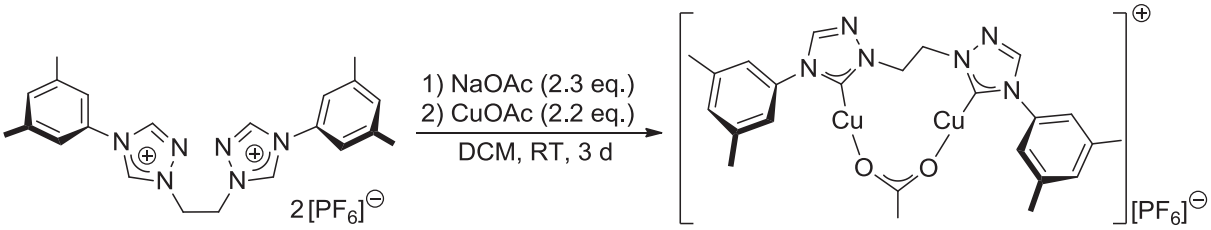

62 **92**

A flame-dried Schlenk flask was charged with 1,1'-(ethane-1,2-diyl)bis[4-(3,5-dimethylphenyl)-1*H*-1,2,4-triazolium] bis(hexafluorophosphate) (**62**, 1.040 g, 1.565 mmol) under an atmosphere of inert gas and sodium acetate (0.295 g, 3.60 mmol) was added. In the glovebox, the mixture was suspended in dichloromethane (10 ml) and stirred for five hours at room temperature. Copper(I) acetate (0.422 g, 3.44 mmol) as well as dichloromethane (20 ml) were added. The reaction mixture was stirred for three days at room temperature and then diluted with dichloromethane (50 ml). After filtration over a frit under inert gas, the solvent was removed *in vacuo*. The solid

residue was washed with diethyl ether (4 × 20 ml). The colourless product was obtained as a crystalline solid (0.998 mg, 1.42 mmol, 91 %).

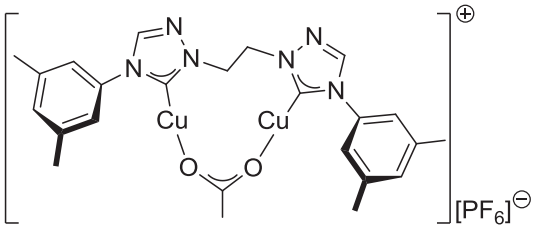

92

$C_{24}H_{27}Cu_2F_6N_6O_2P$

M ($C_{24}H_{27}Cu_2F_6N_6O_2P$) = 703.57 g mol^{-1}

^{1}H NMR (300.510 MHz, d_6-acetone, 27 °C): δ = 8.85 (s, 2H, NC*H*N), 7.31 (s, 4H, *ortho*-C*H*), 7.21 (s, 2H, *para*-C*H*), 5.36 (s, 4H, CH_2), 2.34 (s, 12H, CH_3), 1.98 (s, 3H, H_3CCOO).

^{1}H NMR (500.130 MHz, CD_2Cl_2, 25 °C): δ = 8.35 (br, s, 2H, NC*H*N), 7.19 (br, s, 2H, *para*-C*H*), 7.13 (br, s, 4H, *ortho*-C*H*), 5.29 (s, 4H, CH_2), 2.38 (br, s, 12H, CH_3), 2.09 (br, s, 3H, H_3CCOO).

^{13}C{^{1}H} NMR (125.758 MHz, CD_2Cl_2, 25 °C): δ = 175.7 (N*C*N), 142.7 (N*C*HN), 141.2 (*C*CH_3), 135.9 (*ipso*-*C*N), 132.2 (*para*-*C*H), 121.8 (*ortho*-*C*H), 52.0 (*C*H_2), 21.3 (*C*H_3).
Signals for the acetate ligand are missing in the ^{13}C{^{1}H} NMR spectrum. Due to ligand exchange, some peaks are broadened and the acetate ligand's signal intensities might be too low.

^{31}P{^{1}H} NMR (202.456 MHz, CD_2Cl_2, 25 °C): δ = -144.49 (sept, $^1J_{P\text{-}F}$ = 711.7 Hz).

^{1}H NMR (300.190 MHz, d_6-DMSO, 27 °C): δ = 9.10 (br, s, 2H, NC*H*N), 7.25 (br, s, 4H, *ortho*-C*H*), 7.12 (br, s, 2H, *para*-C*H*), 5.04 (s, 4H, CH_2), 2.25 (br, s, 12H, CH_3), 1.97 (br, s, 3H, H_3CCOO).

$^{13}C\{^1H\}$ NMR (75.483 MHz, d_6-DMSO, 27 °C): δ = 176.9 (N<u>C</u>N), 142.4 (N<u>C</u>HN), 139.2 (<u>C</u>CH_3), 135.9 (*ipso*-<u>C</u>N), 130.2 (*para*-<u>C</u>H), 121.0 (*ortho*-<u>C</u>H), 51.6 (<u>C</u>H_2), 22.9 (H_3<u>C</u>COO), 20.7 (<u>C</u>H_3).
The signal for the acetate carboxylate C-atom is missing in the $^{13}C\{^1H\}$ NMR spectrum, the signal for its CH_3 group can only be observed in the HSQC spectrum.

$^{31}P\{^1H\}$ NMR (121.649 MHz, d_6-DMSO, 27 °C): δ = -141.33 (sept, $^1J_{P\text{-}F}$ = 711.2 Hz).

^1H NMR (300.509 MHz, d_8-THF, 25 °C): δ = 8.72 (s, 2H, NC<u>H</u>N), 7.33 (s, 4H, *ortho*-C<u>H</u>), 7.13 (s, 2H, *para*-C<u>H</u>), 5.25 (s, 4H, C<u>H_2</u>), 2.33 (s, 12H, C<u>H_3</u>), 1.99 (s, 3H, <u>H_3</u>CCOO).

HR-MS (ESI+, CH_2Cl_2) *m*/*z* (%): 905.23833 (74.8) [2M(^{63}Cu,^{63}Cu)-2CuOAc-2PF_6+^{35}Cl]$^+$, 907.23684 (100.0) [2M(^{63}Cu,^{65}Cu)-2CuOAc-2PF_6+^{35}Cl]$^+$ or [2M(^{63}Cu,^{63}Cu)-2CuOAc-2PF_6+^{37}Cl]$^+$, 909.23475 (43.3) [2M(^{65}Cu,^{65}Cu)-2CuOAc-2PF_6+^{35}Cl]$^+$ or [2M(^{63}Cu,^{65}Cu)-2CuOAc-2PF_6+^{37}Cl]$^+$, 911.23190 (6.1) [2M(^{65}Cu,^{65}Cu)-2CuOAc-2PF_6+^{37}Cl]$^+$, 949.18871 (31.4) [2M(^{63}Cu,^{63}Cu)-2CuOAc-2PF_6+^{79}Br]$^+$, 951.18630 (61.7) [2M(^{63}Cu,^{65}Cu)-2CuOAc-2PF_6+^{79}Br]$^+$ or [2M(^{63}Cu,^{63}Cu)-2CuOAc-2PF_6+^{81}Br]$^+$, 953.18469 (37.3) [2M(^{65}Cu,^{65}Cu)-2CuOAc-2PF_6+^{79}Br]$^+$ or [2M(^{63}Cu,^{65}Cu)-2CuOAc-2PF_6+^{81}Br]$^+$, 955.18298 (7.3) [2M(^{65}Cu,^{65}Cu)-2CuOAc-2PF_6+^{81}Br]$^+$.

HR-MS (FAB+, NBA matrix) *m*/*z* (%): 408.1300 (100.0) [M(^{63}Cu)-CuOAc-HCN-PF_6]$^+$, 410.1251 (49.9) [M(^{65}Cu)-CuOAc-HCN-PF_6]$^+$, 435.1479 (98.0) [M(^{63}Cu)-CuOAc-PF_6]$^+$, 437.1468 (49.0) [M(^{65}Cu)-CuOAc-PF_6]$^+$, 517.0668 (66.2) [M(^{63}Cu, ^{63}Cu)-OAc-PF_5]$^+$, 519.0642 (41.6) [M(^{63}Cu,^{65}Cu)-OAc-PF_5]$^+$, 557.0811 (47.0) [M(^{63}Cu,^{63}Cu)-PF_6]$^+$, 559.0789 (44.8) [M(^{63}Cu,^{65}Cu)-PF_6]$^+$, 561.0776 (13.0) [M(^{65}Cu,^{65}Cu)-PF_6]$^+$.
calculated for [$C_{24}H_{27}$(^{63}Cu)$_2N_6O_2$]$^+$: 557.0782
found: 557.0811

Infrared Spectroscopy (KBr): $\tilde{\nu}$ [cm^{-1}] = 3428 (br, w), 3147 (w), 3015 (w), 2958 (w), 2923 (w), 1616 (s), 1598 (s), 1559 (s), 1475 (m), 1444 (s), 1318 (m), 1255 (w), 1212 (w), 1124 (w), 1041 (w), 999 (w), 843 (br, s, hexafluorophosphate, asymmetric stretching mode), 692 (m), 668 (w), 558 (s, hexafluorophosphate, bending mode).

Elemental Analysis (No. 31868)

calculated for $C_{24}H_{27}Cu_2F_6N_6O_2P$:	C 40.97 %,	H 3.87 %,	N 11.94 %
found:	C 41.05 %,	H 4.08 %,	N 11.85 %

Decomposition Temperature: 206 °C (black solid).

Crystal Structure: μ-Acetato-$\kappa O,\kappa O'$-μ-{1,1'-(ethane-1,2-diyl)bis[4-(3,5-xylyl)-1*H*-1,2,4-triazol-5-ylidene]}$\kappa C,\kappa C'$-dicopper(I) hexafluorophosphate was crystallized from acetonitrile/diethyl ether. In this solvent mixture, a coordination polymer was formed, in which two acetate ligands coordinate two copper ions which are bound by separate NHC ligands.

Crystallographic data and structure refinements for reb19, formula $[C_{24}H_{27}Cu_2N_6O_2]^+ + [OAc]^- + 2.5CH_3CN$, M ($C_{31}H_{37.50}Cu_2N_{8.50}O_4$) = 720.29 g mol^{-1}: colourless crystal (needle), dimensions 0.70 × 0.06 × 0.05 mm^3, crystal system monoclinic, space group $P2_1/n$, Z = 4, a = 13.0903(15) Å, b = 13.1366(14) Å, c = 20.261(2) Å, α = 90°, β = 94.839(3)°, γ = 90°, V = 3471.7(7) Å^3, ρ = 1.378 g cm^{-3}, T = 200(2) K, Θ_{max} = 25.43°, radiation Mo K$_\alpha$, λ = 0.71073 Å, 0.5° ω-scans with CCD area detector, covering the asymmetric unit in reciprocal space with a mean redundancy of 5.51 and a completeness of 98.4 % to a resolution of 0.84 Å, 35181 reflections measured, 6317 unique (R(int) = 0.0725), 4063 observed ($I > 2\sigma(I)$), intensities were corrected for Lorentz and polarization effects, an empirical absorption correction was applied using SADABS[165] based on the Laue symmetry of the reciprocal space, μ = 1.27 mm^{-1}, T_{min} = 0.47, T_{max} = 0.94, structure solved by direct methods and refined against F^2 with a full-matrix least-squares algorithm using the SHELXTL (version 2008/4) software package,[166] 457 parameters refined, hydrogen atoms were treated using appropriate riding models, goodness of fit 1.06 for observed reflections, final residual values $R1(F)$ = 0.075, $wR(F^2)$ = 0.187 for observed reflections, residual electron density -0.49 to 1.18 eÅ^{-3}.

During the course of her master thesis, M. Sc. Ella Schreiner was able to crystallize complex **92** as a coordination polymer. CCDC 869467 contains the supplementary crystallographic data for this structure. This data can be obtained free of charge from The Cambridge Crystallographic Data Centre *via* www.ccdc.cam.ac.uk/data_request/cif.

6.2.9.3 μ-*Acetato-κO,κO'-* μ-*{1,1'-(ethane-1,2-diyl)bis[4-(4-methylphenyl)-1*H-*1,2,4-triazol-5-ylidene]}-κC,κC'-dicopper(I) Hexafluorophosphate* (**93**)

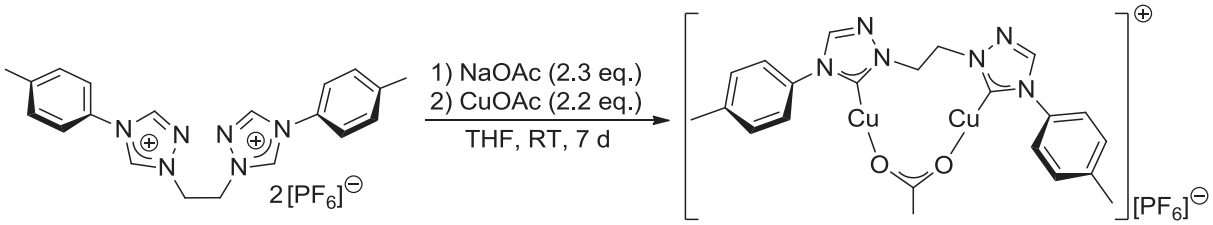

63 **93**

A flame-dried Schlenk flask was charged with 1,1'-(ethane-1,2-diyl)bis[4-(4-methylphenyl)-1*H*-1,2,4-triazolium] bis(hexafluorophosphate) (**63**, 0.848 g, 1.33 mmol) under an atmosphere of inert gas and sodium acetate (0.251 g, 3.06 mmol) was added. In the glovebox, the mixture was suspended in tetrahydrofuran (18 ml) and stirred for two days at room temperature. Copper(I) acetate (0.360 g, 2.94 mmol) was added and the reaction mixture stirred for five days at room temperature. The slightly yellow solution was filtered over a filter paper-capped canula and the solvent removed *in vacuo*. The raw product was dissolved in dichloromethane (100 ml), filtrated over a filter paper-capped canula and overlain with diethyl ether to allow for crystallization at -20 °C. After filtration, the resulting colourless solid was dried *in vacuo* (0.350 mg, 0.518 mmol, 39 %).

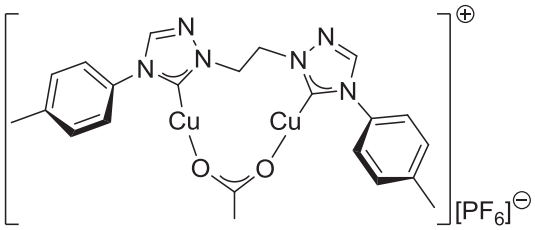

93

$C_{22}H_{23}Cu_2F_6N_6O_2P$

M ($C_{22}H_{23}Cu_2F_6N_6O_2P$) = 675.51 g mol^{-1}

^{1}H NMR (500.130 MHz, CD_2Cl_2, 25 °C): δ = 8.34 (s, 2H, NC*H*N), 7.45 – 7.32 (m, 8H, *ortho*-C*H*, *meta*-C*H*), 5.30 (s, 4H, CH_2), 2.44 (s, 6H, CH_3), 2.06 (s, 3H, H_3CCOO).

^{13}C{^{1}H} NMR (125.758 MHz, CD_2Cl_2, 25 °C): δ = 175.5 (N*C*N), 142.9 (N*C*HN), 141.4 (*C*CH_3), 133.5 (*ipso*-*C*N), 131.3 (*meta*-*C*H), 124.0 (*ortho*-*C*H), 52.0 (*C*H_2), 23.0 (H_3*C*COO), 21.3 (*C*H_3).
The signal for the acetate carboxyl group is missing in the ^{13}C{^{1}H} NMR spectrum. The signal for the acetate ligand's methyl group is of very low intensity in the ^{13}C{^{1}H} NMR spectrum, but can be identified with the help of a HSQC spectrum.

^{31}P{^{1}H} NMR (202.456 MHz, CD_2Cl_2, 23 °C): δ = -144.55 (sept, $^1J_{P\text{-}F}$ = 711.7 Hz).

^{1}H NMR (500.130 MHz, d_6-DMSO, 25 °C): δ = 9.07 (s, 2H, NC*H*N), 7.54 (d, $^3J_{H\text{-}H}$ = 7.8 Hz, 4H, *ortho*-C*H*), 7.36 (d, $^3J_{H\text{-}H}$ = 7.8 Hz, 4H, *meta*-C*H*), 5.06 (s, 4H, *C*H_2), 2.37 (s, 6H, CH_3), 2.01 (s, 3H, H_3CCOO).

^{13}C{^{1}H} NMR (125.758 MHz, d_6-DMSO, 25 °C): δ = 176.6 (N*C*N), 142.5 (N*C*HN), 138.9 (*C*CH_3), 133.8 (*ipso*-*C*N), 130.0 (*meta*-*C*H), 123.5 (*ortho*-*C*H), 52.6 (*C*H_2), 21.0 (*C*H_3).
The signals for the acetate group are missing in the ^{13}C{^{1}H} NMR spectrum.

^{1}H NMR (300.509 MHz, d_8-THF, 27 °C): δ = 8.72 (s, 2H, NC*H*N), 7.54 (d, $^3J_{H\text{-}H}$ = 7.8 Hz, 4H, *ortho*-C*H*), 7.34 (d, $^3J_{H\text{-}H}$ = 7.8 Hz, 4H, *meta*-C*H*), 5.27 (s, 4H, CH_2), 2.38 (s, 6H, CH_3), 1.96 (s, 3H, H_3CCOO).

$^{13}C\{^1H\}$ NMR (75.563 MHz, d_8-THF, 24 °C): δ = 143.4 (N<u>C</u>HN), 140.5 (<u>C</u>CH_3), 135.0 (*ipso*-<u>C</u>N), 131.2 (*meta*-<u>C</u>H), 124.5 (*ortho*-<u>C</u>H), 52.6 (<u>C</u>H_2), 21.0 (<u>C</u>H_3).
Signals for the carbene C-atom and the C-atoms of the acetate ligand are missing in the $^{13}C\{^1H\}$ NMR spectrum. Due to ligand exchange and only slight solubility, peaks are broadened and intensities low.

$^{31}P\{^1H\}$ NMR (121.649 MHz, d_8-THF, 24 °C): δ = -144.28 (sept, $^1J_{P\text{-}F}$ = 710.6 Hz).

HR-MS (ESI+, methanol) *m*/*z* (%): 345.18216 (2.4) [M-CuOAc-Cu-PF_6+H]$^+$, 361.17707 (14.1) [M-CuOAc-Cu-PF_6+OH]$^+$, 407.10372 (100.0) [M(^{63}Cu -CuOAc)-PF_6]$^+$, 409.10206 (30.8) [M(^{65}Cu)-CuOAc-PF_6]$^+$.

HR-MS (FAB+, NBA matrix) *m*/*z* (%): 407.1103 (22.7) [M(^{63}Cu)-CuOAc-PF_6]$^+$, 409.1111 (12.2) [M(^{65}Cu)-CuOAc-PF_6]$^+$, 529.0461 (100.0) [M(^{63}Cu,^{63}Cu)-PF_6]$^+$, 531.0441 (87.6) [M(^{63}Cu,^{65}Cu)-PF_6]$^+$, 533.0410 (23.1) [M(^{65}Cu,^{65}Cu)-PF_6]$^+$.
calculated for [$C_{22}H_{23}(^{63}Cu)_2N_6O_2$]$^+$: 529.0469
found: 529.0461

Infrared Spectroscopy (KBr): $\tilde{\nu}$ [cm^{-1}] = 3440 (br, w), 3146 (w), 1576 (m), 1534 (m), 1516 (s), 1410 (m), 1325 (w), 1261 (w), 1112 (w), 987 (w), 848 (br, s, hexafluorophosphate, asymmetric stretching mode), 739 (w), 710 (w), 559 (s, hexafluorophosphate, bending mode), 509 (w).

Elemental Analysis (No. 31418)

calculated for $C_{22}H_{23}Cu_2F_6N_6O_2P$:	C 39.12 %,	H 3.43 %,	N 12.44 %
found:	C 38.84 %,	H 3.56 %,	N 12.14 %

Decomposition Temperature: 202 °C (dark brown solid).

6.2.9.4 μ-*Acetato-*κ*O,*κ*O'-*μ*-{1,1'-(benzene-1,3-diyldimethanediyl)bis[4-(2,4,6-trimethylphenyl)-1*H*-1,2,4-triazol-5-ylidene]}-*κ*C,*κ*C'-dicopper(I) Hexafluorophosphate* (**101**)

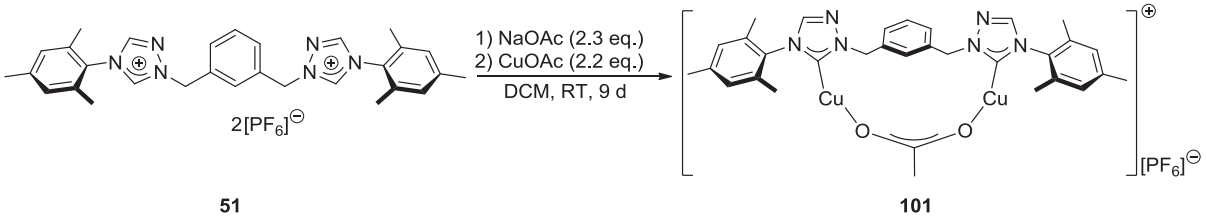

51 **101**

A flame-dried Schlenk flask was charged with 1,1'-[1,3-phenylenebis(methylene)]bis-[4-(2,4,6-trimethylphenyl)-1*H*-1,2,4-triazolium] bis(hexafluorophosphate) (**51**, 1.016 g, 1.322 mmol) under an atmosphere of inert gas and sodium acetate (0.254 g, 3.04 mmol) was added. In the glovebox, the mixture was suspended in dichloromethane (15 ml) and stirred for four hours at room temperature. Copper(I) acetate (0.357 g, 2.91 mmol) as well as dichloromethane (5 ml) were added. The reaction mixture was stirred for nine days at room temperature. After dilution with dichloromethane (50 ml) and filtration of the suspension over a frit under inert gas, the solvent was removed *in vacuo*. The solid residue was washed with diethyl ether (3 × 50 ml). The colourless product was obtained as a crystalline solid (0.810 g, 1.04 mmol, 79 %).

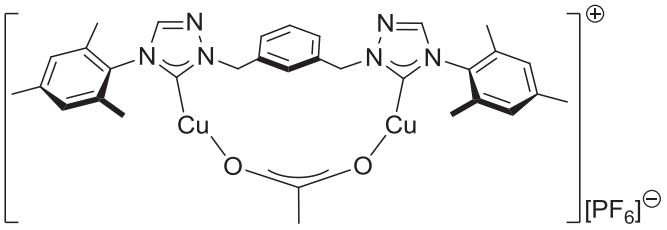

101

$C_{32}H_{35}Cu_2F_6N_6O_2P$

M ($C_{32}H_{35}Cu_2F_6N_6O_2P$) = 807.72 g mol^{-1}

^{1}H NMR (400.180 MHz, d_6-DMSO, 20 °C): δ = 8.91 (s, 2H, NC*H*N), 7.39 (t, 1H, $^3J_{H\text{-}H}$ = 7.4 Hz, Xyl-linker, CH_2CCHCH), 7.32 (br, m, 1H, Xyl-linker, $CH_2CCHCCH_2$), 7.21 (br, m, 2H, Xyl-linker, CH_2CCHCH), 7.08 (s, 4H, Mes-substituent, *meta*-C*H*),

5.52 (s, 4H, C$\underline{H_2}$), 2.32 (s, 6H, Mes-substituent, *para*-C$\underline{H_3}$), 1.89 (s, 12H, Mes-substituent, *ortho*-C$\underline{H_3}$), 1.79 (br, s, 3H, $\underline{H_3}$CCOO).

^{13}C{^{1}H} NMR (100.625 MHz, d_6-DMSO, 20 °C): δ = 179.3 (N$\underline{C}$N), 144.5 (N$\underline{C}$HN), 139.4 (Mes-substituent, *para*-$\underline{C}$CH$_3$), 136.7 (Xyl-linker, CH$_2\underline{C}$), 135.6 (Mes-substituent, *ortho*-$\underline{C}$CH$_3$), 132.1 (Mes-substituent, *ipso*-$\underline{C}$N), 129.3 (Xyl-linker, CH$_2$CH$\underline{C}$H), 129.1 (Mes-substituent, *meta*-$\underline{C}$H), 127.1 (Xyl-linker, CH$_2$C$\underline{C}$HCH and CH$_2$C$\underline{C}$HCCH$_2$), 55.3 ($\underline{C}$H$_2$), 20.7 (Mes-substituent, *para*-$\underline{C}$H$_3$), 17.4 (Mes-substituent, *ortho*-$\underline{C}$H$_3$), 17.0 (H$_3\underline{C}$COO).
The signals for the acetate's carboxylate group are missing in the ^{13}C{^{1}H} NMR spectrum.

^{31}P{^{1}H} NMR (121.649 MHz, d_6-DMSO, 27 °C): δ = -144.16 (sept, $^1J_{P\text{-}F}$ = 711.2 Hz).

HR-MS (FAB+, NPOE matrix): 539.1959 (100.0) [M(^{63}Cu)-CuOAc-PF$_6$]$^+$, 541.1960 (50.5) [M(^{65}Cu)-CuOAc-PF$_6$]$^+$, 661.1407 (7.9) [M(^{63}Cu,^{63}Cu)-PF$_6$]$^+$, 663.1431 (7.9) [M(^{63}Cu,^{65}Cu)-PF$_6$]$^+$, 665.1387 (1.9) [M(^{65}Cu,^{65}Cu)-PF$_6$]$^+$

calculated for [C$_{32}$H$_{35}$(^{63}Cu)$_2$N$_6$O$_2$]$^+$:	661.1408
found:	661.1407

Infrared Spectroscopy (KBr): $\tilde{\nu}$ [cm^{-1}] = 3445 (br, w), 3140 (w), 2923 (w), 1610 (m), 1527 (m), 1489 (m), 1446 (m), 1307 (w), 1227 (w), 1165 (w), 1016 (w), 988 (w), 948 (w), 842 (br, s, hexafluorophosphate, asymmetric stretching mode), 750 (w), 692 (w), 582 (w), 558 (s, hexafluorophosphate, bending mode), 464 (w).

6.2.9.5 μ-*Acetato-*κ*O,*κ*O'-*μ*-{1,1'-(benzene-1,3-diyldimethanediyl)bis[4-(3,5-dimethylphenyl)-1*H*-1,2,4-triazol-5-ylidene]}-*κ*C,*κ*C'-dicopper(I) Hexafluorophosphate* (**102**)

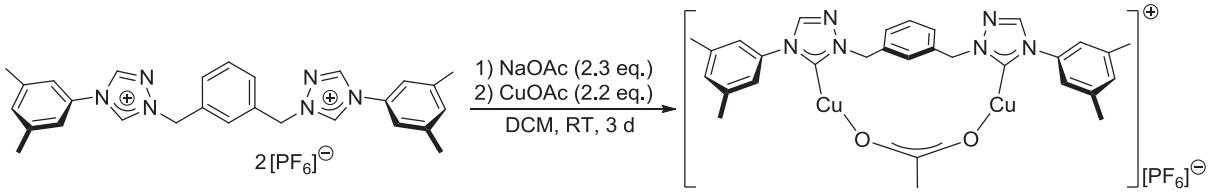

52 **102**

A flame-dried Schlenk flask was charged with 1,1'-[1,3-phenylenebis(methylene)]bis-[4-(3,5-dimethylphenyl)-1*H*-1,2,4-triazolium] bis(hexafluorophosphate) (**52**, 1.078 g, 1.456 mmol) under an atmosphere of inert gas and sodium acetate (0.275 g, 3.35 mmol) was added. In the glovebox, the mixture was suspended in dichloromethane (20 ml) and stirred for one day at room temperature. Copper(I) acetate (0.393 g, 3.21 mmol) as well as dichloromethane (20 ml) were added. The reaction mixture was stirred for three days at room temperature. After filtration of the suspension over a frit under inert gas, the solvent was removed *in vacuo*. The solid residue was washed with diethyl ether (4 × 20 ml). The colourless product was obtained as a crystalline solid (0.253 mg, 0.324 mmol, 22 %).

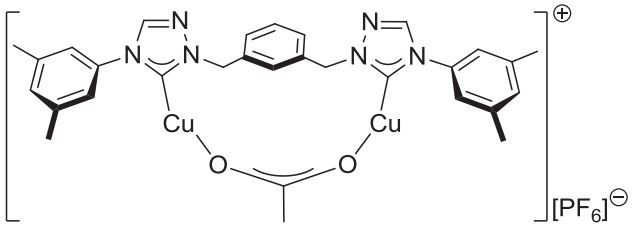

102

$C_{30}H_{31}Cu_2F_6N_6O_2P$

M ($C_{30}H_{31}Cu_2F_6N_6O_2P$) = 779.66 g mol^{-1}

^{1}H NMR (300.130 MHz, d_6-DMSO, 25 °C): δ = 9.14 (s, 2H, NC*H*N), 7.59 (s, 1H, Xyl-linker, CH_2CC*H*CCH_2), 7.41 (m, 7H, Xyl-substituent, *ortho*-C*H*, and Xyl-linker, CH_2CC*H*CH and CH_2CCHC*H*), 7.12 (s, 2H, Xyl-substituent, *para*-C*H*), 5.58 (s, 4H, CH_2), 2.29 (s, 6H, Xyl-substituent, CH_3), 1.99 (s, 3H, H_3CCOO).

$^{13}C\{^1H\}$ NMR (75.468 MHz, d_6-DMSO, 25 °C): δ = 176.4 (N<u>C</u>N), 142.7 (N<u>C</u>HN), 139.2 (Xyl-substituent, *meta*-<u>C</u>CH_3), 136.3 (Xyl-linker, CH_2<u>C</u>), 136.1 (Xyl-substituent, *ipso*-<u>C</u>N), 130.2 (Xyl-substituent, *para*-<u>C</u>H), 129.2 (Xyl-linker, CH_2C<u>C</u>HCH or CH_2CH<u>C</u>H), 128.1 (Xyl-linker, CH_2C<u>C</u>$HCCH_2$), 127.9 (Xyl-linker, CH_2C<u>C</u>HCH or CH_2CH<u>C</u>H), 121.1 (Xyl-substituent, *ortho*-<u>C</u>H), 55.6 (<u>C</u>H_2), 20.7 (<u>C</u>H_3).
The signals for the acetate group are missing in the $^{13}C\{^1H\}$ NMR spectrum.

$^{31}P\{^1H\}$ NMR (121.495 MHz, d_6-DMSO, 25 °C): δ = -144.19 (sept, $^1J_{P\text{-}F}$ = 711.2 Hz).

HR-MS (ESI+, methanol) *m*/*z* (%): 511.16636 (100.0) $[M(^{63}Cu)\text{-}CuOAc\text{-}PF_6]^+$, 513.16458 (46.4) $[M(^{65}Cu)\text{-}CuOAc\text{-}PF_6]^+$.

calculated for $[C_{28}H_{28}CuN_6]^+$:	511.16660
found:	511.16636

Infrared Spectroscopy (KBr): $\tilde{\nu}$ [cm^{-1}] = 3429 (br, m), 3149 (w), 2923 (w), 1615 (s), 1597 (s), 1529 (s), 1475 (m), 1408 (s), 1347 (m), 1311 (w), 1254 (w), 1210 (w), 1157 (w), 1125 (w), 1039 (w), 1017 (w), 955 (w), 847 (br, s, hexafluorophosphate, asymmetric stretching mode), 738 (m), 692 (m), 662 (m), 619 (w), 558 (s, hexafluorophosphate, bending mode), 427 (w).

Elemental Analysis (No. 32464)

calculated for $C_{30}H_{31}Cu_2F_6N_6O_2P$:	C 46.22 %,	H 4.01 %,	N 10.78 %
found:	C 46.10 %,	H 4.17 %,	N 10.64 %

Decomposition Temperature: 240 °C (black solid).

6.2.10 Synthesis of Tetra-NHC Complexes for Reference Purposes

The tetra-NHC dicopper complexes were only prepared for reference purposes and thus not fully characterized except for the necessary NMR spectra.

*6.2.10.1 Bis-{μ-{1,1'-(ethane-1,2-diyl)bis[4-(2,4,6-trimethylphenyl)-1*H*-1,2,4-triazol-5-ylidene]}-κC,κC'}dicopper(I) Bis(hexafluorophosphate)* (**111**)

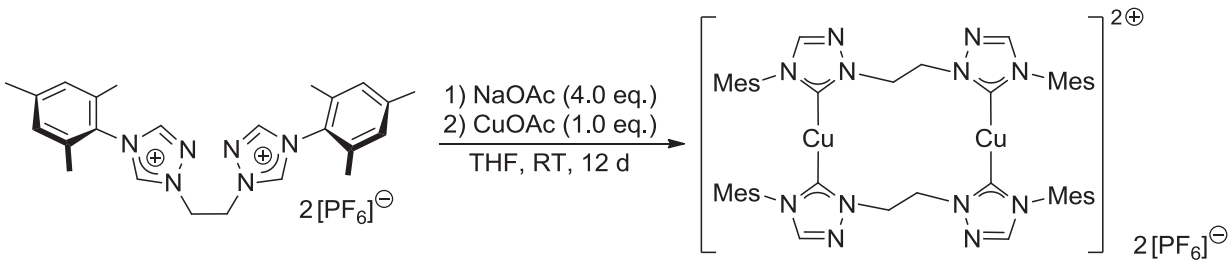

61 **111**

A flame-dried Schlenk flask was charged with 1,1'-(ethane-1,2-diyl)bis[4-(2,4,6-trimethylphenyl)-1*H*-1,2,4-triazolium] bis(hexafluorophosphate) (**61**, 0.301 g, 0.435 mmol) under an atmosphere of inert gas and sodium acetate (0.144 g, 1.76 mmol) was added. In the glovebox, the mixture was suspended in THF (10 ml) and stirred for 10 minutes at room temperature. Copper(I) acetate (0.053 g, 0.43 mmol) as well as THF (10 ml) were added. The reaction mixture was stirred for twelve days at room temperature. After filtration over a filter paper-capped canula under inert gas, the solvent was removed *in vacuo*. The colourless solid residue was washed with THF (2 × 5 ml) and dried *in vacuo*.

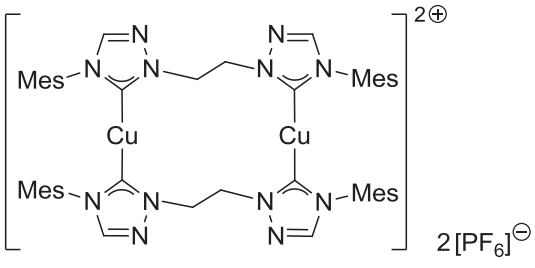

111

$C_{48}H_{56}Cu_2F_{12}N_{12}P_2$

M ($C_{48}H_{56}Cu_2F_{12}N_{12}P_2$) = 1218.06 g mol^{-1}

^{1}H NMR (300.510 MHz, CD_3CN, 27 °C): δ = 8.19 (s, 4H, NC*H*N), 7.01 (s, 8H, *meta*-C*H*), 4.76 (s, 8H, CH_2), 2.35 (s, 12H, *para*-CH_3), 1.76 (s, 24H, *ortho*-CH_3).

^{1}H NMR (300.510 MHz, CD_2Cl_2, 27 °C): δ = 8.00 (s, 4H, NC*H*N), 6.92 (s, 8H, *meta*-C*H*), 5.14 (s, 8H, CH_2), 2.45 (s, 12H, *para*-CH_3), 1.72 (s, 24H, *ortho*-CH_3).

^{1}H NMR (600.244 MHz, d_6-DMSO, 22 °C): δ = 8.73 (s, 4H, NC*H*N), 6.94 (s, 8H, *meta*-C*H*), 4.98 (s, 8H, CH_2), 2.37 (s, 12H, *para*-CH_3), 1.62 (s, 24H, *ortho*-CH_3).

^{13}C{^{1}H} NMR (150.932 MHz, d_6-DMSO, 22 °C): δ = 181.9 (N*C*N), 143.7 (N*C*HN), 138.7 (*para*-*C*CH_3), 134.2 (*ortho*-*C*CH_3), 132.0 (*ipso*-*C*N), 128.9 (*meta*-*C*H), 51.6 (*C*H_2), 20.7 (*para*-*C*H_3), 17.1 (*ortho*-*C*H_3).

^{31}P{^{1}H} NMR (242.983 MHz, d_6-DMSO, 22 °C): δ = -144.19 (sept, $^{1}J_{P-F}$ = 711.2 Hz).

^{1}H NMR (300.510 MHz, d_8-THF, 27 °C): δ = 8.40 (s, 4H, NC*H*N), 6.93 (s, 8H, *meta*-C*H*), 5.14 (s, 8H, CH_2), 2.43 (s, 12H, *para*-CH_3), 1.77 (s, 24H, *ortho*-CH_3).

HR-MS (ESI+, methanol) *m*/*z* (%): 463.16784 (27.5) [M(^{63}Cu)-$C_{24}H_{28}CuN_6$-2PF_6]$^+$, 465.16613 (7.2) [M(^{65}Cu)-$C_{24}H_{28}CuN_6$-2PF_6]$^+$, 961.30453 (66.6) [M(^{63}Cu,^{63}Cu)+^{35}Cl-2PF_6]$^+$, 963.30299 (100.0) [M(^{63}Cu,^{65}Cu)+^{35}Cl-2PF_6]$^+$ or [M(^{63}Cu,^{63}Cu)+^{37}Cl-2PF_6]$^+$, 965.30155 (43.9) [M(^{65}Cu,^{65}Cu)+^{35}Cl-2PF_6]$^+$ or [M(^{63}Cu,^{65}Cu)+^{37}Cl-2PF_6]$^+$, 967.29963 (5.9) [M(^{65}Cu,^{65}Cu)+^{37}Cl-2PF_6]$^+$,1071.30098 (34.6) [M(^{63}Cu,^{63}Cu)-PF_6]$^+$, 1073.29926 (35.8) [M(^{63}Cu,^{65}Cu)-PF_6]$^+$, 1075.29837 (7.7) [M(^{65}Cu,^{65}Cu)-PF_6]$^+$.
calculated for [$C_{48}H_{56}$(^{63}Cu)$_2F_6N_{12}P$]$^+$: 1071.29792
found: 1071.30098

Infrared Spectroscopy (KBr): $\tilde{\nu}$ [cm^{-1}] = 3436 (br, w), 3140 (br, w), 2923 (br, w), 2861 (br, w), 1579 (s), 1533 (m), 1489 (m), 1420 (s), 1320 (w), 1265 (w), 1226 (w), 1044 (w), 1015 (w), 987 (w), 924 (w), 846 (br, s, hexafluorophosphate, asymmetric stretching mode), 741 (w), 651 (w), 583 (w), 558 (s, hexafluorophosphate, bending mode).

*6.2.10.2 Bis-{μ-{1,1'-(ethane-1,2-diyl)bis[4-(3,5-dimethylphenyl)-1*H*-1,2,4-triazol-5-ylidene]}-κC,κC'}dicopper(I) Bis(hexafluorophosphate)* (**112**)

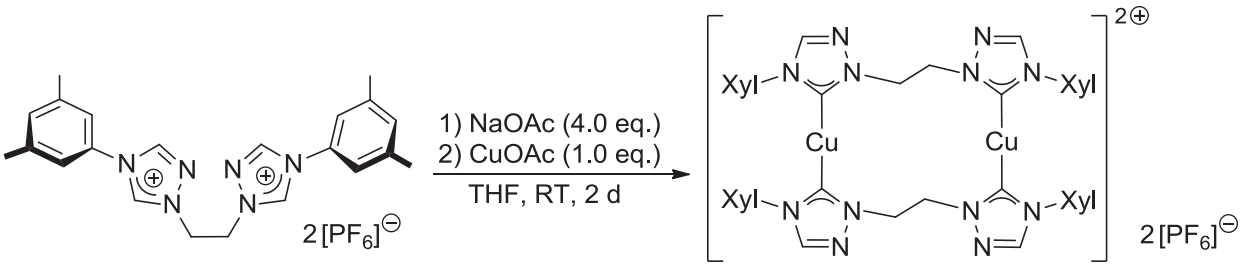

62 **112**

A flame-dried Schlenk flask was charged with 1,1'-(ethane-1,2-diyl)bis[4-(3,5-dimethylphenyl)-1*H*-1,2,4-triazolium] bis(hexafluorophosphate) (**62**, 0.362 g, 0.545 mmol) under an atmosphere of inert gas and sodium acetate (0.179 g, 2.18 mmol) was added. In the glovebox, the mixture was suspended in THF (10 ml) and stirred for 15 minutes at room temperature. Copper(I) acetate (0.067 g, 0.55 mmol) as well as THF (20 ml) were added. The reaction mixture was stirred for two days at room temperature. After filtration over a filter paper-capped canula under inert gas, the solvent was removed *in vacuo*. The solid residue was washed with THF (2 × 5 ml) and dried *in vacuo*. Acetonitrile (20 ml) was added and the solution filtrated over a filter paper-capped canula. The solution was concentrated and overlain by diethyl ether to allow for crystallization at -20 °C. The colourless product was obtained as a crystalline solid (0.173 mg, 0.149 mmol, 27 %).

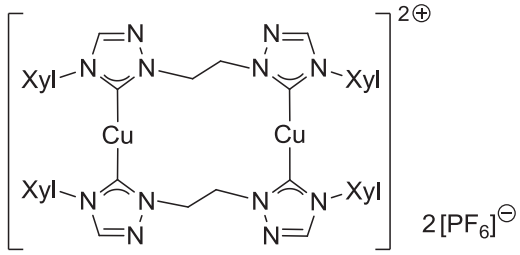

112

$C_{44}H_{48}Cu_2F_{12}N_{12}P_2$

M ($C_{44}H_{48}Cu_2F_{12}N_{12}P_2$) = 1161.95 g mol^{-1}

^{1}H NMR (300.510 MHz, CD_3CN, 27 °C): δ = 8.47 (s, 2H, NC*H*N), 7.03 (s, 2H, *para*-C*H*), 6.92 (s, 4H, *ortho*-C*H*), 4.75 (s, 4H, CH_2), 2.16 (s, 12H, CH_3).

^{31}P{^{1}H} NMR (121.649 MHz, CD_3CN, 27 °C): δ = -144.59 (s, $^1J_{P\text{-}F}$ = 706.7 Hz)

^{1}H NMR (600.244 MHz, d_6-DMSO, 22 °C): δ = 9.25 (s, 4H, NC*H*N), 6.95 (s, 8H, *ortho*-C*H*), 6.90 (s, 4H, *para*-C*H*), 5.09 (s, 8H, CH_2), 1.99 (s, 24H, CH_3).

^{13}C{^{1}H} NMR (150.932 MHz, d_6-DMSO, 22 °C): δ = 177.9 (N*C*N), 142.4 (N*C*HN), 139.0 (*meta*-*C*CH_3), 135.4 (*ipso*-*C*N), 130.1 (*para*-*C*H), 120.1 (*ortho*-*C*H), 52.9 (*C*H_2), 20.5 (*C*H_3).

^{31}P{^{1}H} NMR (121.475 MHz, d_6-DMSO, 27 °C): δ = -144.17 (sept, $^1J_{P\text{–}F}$ = 711.3 Hz).

^{1}H NMR (300.509 MHz, d_8-THF, 27 °C): δ = 8.65 (s, 4H, NC*H*N), 7.15 (s, 8H, *ortho*-C*H*), 6.95 (s, 4H, *para*-C*H*), 5.04 (s, 8H, CH_2), 2.17 (s, 24H, CH_3).

HR-MS (ESI+, methanol) *m*/*z* (%): 435.13598 (28.4) [M(^{63}Cu)-$C_{22}H_{24}CuN_6$-2PF_6]$^+$, 437.13431 (8.0) [M(^{65}Cu)-$C_{22}H_{24}CuN_6$-2PF_6]$^+$, 905.23987 (73.9) [M(^{63}Cu,^{63}Cu)+^{35}Cl-2PF_6]$^+$, 907.23805 (100.0) [M(^{63}Cu,^{65}Cu)+^{35}Cl-2PF_6]$^+$ or [M(^{63}Cu,^{63}Cu)+^{37}Cl-2PF_6]$^+$, 909.23720 (41.8) [M(^{65}Cu,^{65}Cu)+^{35}Cl-2PF_6]$^+$ or [M(^{63}Cu,^{65}Cu)+^{37}Cl-2PF_6]$^+$, 911.23463 (5.6) [M(^{65}Cu,^{65}Cu)+^{37}Cl-2PF_6]$^+$, 1015.23749 (17.6) [M(^{63}Cu,^{63}Cu)-PF_6]$^+$, 1017.23604 (16.1) [M(^{63}Cu,^{65}Cu)-PF_6]$^+$.

calculated for [$C_{44}H_{48}$(^{63}Cu)$_2F_6N_{12}P$]$^+$: 1015.23532

found: 1015.23749

Infrared Spectroscopy (KBr): $\tilde{\nu}$ [cm^{-1}] = 3448 (br, w), 3148 (w), 2923 (w), 2254 (w), 1616 (s), 1599 (m), 1534 (m), 1475 (m), 1447 (m), 1379 (w), 1311 (w), 1250 (w), 1211 (w), 1160 (w), 1122 (w), 1040 (w), 984 (w), 838 (br, s, hexafluorophosphate, asymmetric stretching mode), 740 (w), 692 (m), 665 (w), 558 (s, hexafluorophosphate, bending mode), 464 (w).

Elemental Analysis (No. 31856)

calculated for $C_{44}H_{48}Cu_2F_{12}N_{12}P_2$:	C 45.48 %,	H 4.16 %,	N 14.47 %
found:	C 45.60 %,	H 4.44 %,	N 15.01 %

Decomposition Temperature: 190 °C (brown solid).

6.2.11 Synthesis of $[(ICy)_2Cu]PF_6$

6.2.11.1 1,3-Dicyclohexylimidazolium Chloride (**121**)

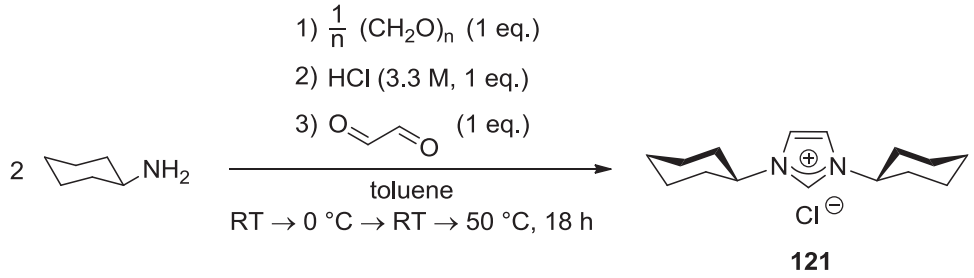

121

1,3-Dicyclohexylimidazolium chloride was synthesized according to a procedure reported in literature.[169] A 500 ml three-necked flask was equipped with an interior thermometer and a dropping funnel. To a solution of freshly distilled cyclohexylamine (11.4 ml, 9.92 g, 100 mmol) in toluene (100 ml), solid paraformaldehyde was added (3.00 g, 100 mmol). The suspension was vigorously stirred for 30 minutes at room temperature. After cooling the reaction mixture to 0 °C, the second equivalent of cyclohexylamine (11.4 ml, 9.92 g, 100 mmol) was added *via* syringe. The reaction mixture was stirred at 0 °C for ten minutes. An aqueous solution of hydrochloric acid (3.30 M, 30.0 ml, 3.61 g HCl, 100 mmol) was added *via* the dropping funnel and the reaction mixture was allowed to warm to room temperature. An aqueous solution of glyoxal (40 weight-%, ρ = 1.265 g ml^{-1}, 11.5 ml, 5.80 g glyoxal, 100 mmol) was slowly added *via* another dropping funnel. The dropping funnel was removed and a reflux condenser was put on. The reaction mixture was stirred at 50 °C for 18 hours. An aqueous solution of sodium carbonate (saturated solution, 100 ml) as well as diethyl ether (100 ml) were added. After separation of the phases, the product was in the aqueous phase. The latter was extracted with dichloromethane (3 × 150 ml) and the combined organic phases were dried over magnesium sulphate. After filtration, the solvent was removed *in vacuo* to give the product as a colourless hygroscopic solid (18.65 g, 69.38 mmol, 69 %; lit.: 75 %).

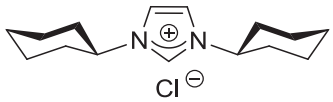

121

$C_{15}H_{25}ClN_2$

M ($C_{15}H_{25}ClN_2$) = 268.83 g mol^{-1}

^{1}H NMR (300.080 MHz, $CDCl_3$, 25 °C): δ = 10.69 (br, s, 1H, NC*H*N), 7.46 (d, $^4J_{H\text{-}H}$ = 1.4 Hz, 2H, NC*H*C*H*N), 4.43 (tt, $^3J_{axial\text{-}axial}$ = 11.7 Hz, $^3J_{axial\text{-}equatorial}$ = 3.8 Hz, 2H, NC*H*CH_2), 2.17 – 2.00 (m, 4H, C*H*$_2$), 1.87 – 1.51 (m, 10H, C*H*$_2$), 1.48 – 1.26 (m, 4H, C*H*$_2$), 1.25 – 1.07 (m, 2H, C*H*$_2$).

^{13}C{^{1}H} NMR (75.455 MHz, $CDCl_3$, 25 °C): δ = 135.6 (N*C*HN), 119.8 (N*C*H*C*HN), 59.7 (N*C*HCH_2), 33.4 (*C*H_2), 24.9 (*C*H_2), 24.5 (*C*H_2).

HR-MS (ESI+, methanol) *m*/*z* (%): 233.20116 (100) [M-Cl]$^+$, 501.37204 (4.3) [2M(^{35}Cl)-Cl]$^+$.

calculated for $[C_{15}H_{25}N_2]^+$:	233.20123
found:	233.20116

Elemental Analysis (No. 30895)

calculated for $C_{15}H_{25}ClN_2$:	C 67.02 %, H 9.37 %, N 10.42 %
found:	C 67.04 %, H 9.53 %, N 10.44 %

6.2.11.2 1,3-Dicyclohexylimidazolium Tetrafluoroborate (**122**)

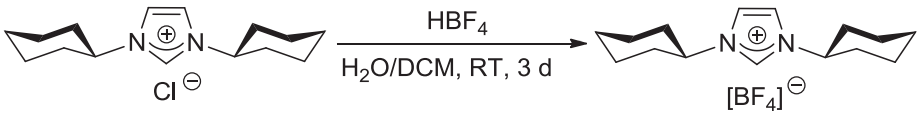

121 **122**

In a 100 ml round-bottomed flask, tetrafluoroboric acid (48 weight-% in water, ρ = 1.4 g cm^{-3}, 16.4 mmol) was dissolved in water (20 ml). In an Erlenmeyer flask, 1,3-dicyclohexylimidazolium chloride (**121**, 2.000 g, 7.440 mmol) was dissolved in water (20 ml). After adding this solution to the diluted tetrafluoroboric acid, a colourless precipitate was formed immediately. The suspension was stirred for two hours at

room temperature. Dichloromethane (50 ml) was added and after stirring this solution for three days, the phases were separated. The aqueous phase was extracted with dichloromethane (3 × 50 ml) and the combined organic phases were dried over magnesium sulphate. After filtration of the drying agent, the solvent was removed *in vacuo*. The product was isolated as a colourless crystalline solid (2.289 g, 7.149 mmol, 96 %). The analytical data was in accordance with the data reported in literature.[170]

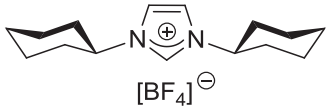

$[BF_4]^{\ominus}$

122

$C_{15}H_{25}BF_4N_2$

M ($C_{15}H_{25}BF_4N_2$) = 320.18 g mol^{-1}

^{1}H NMR (300.510 MHz, d_6-DMSO, 27 °C): δ = 9.22 (br, s, 1H, NC*H*N), 7.89 (d, $^4J_{H\text{-}H}$ = 1.3 Hz, 2H, NC*H*C*H*N), 4.26 (tt, $^3J_{axial\text{-}axial}$ = 11.6 Hz, $^3J_{axial\text{-}equatorial}$ = 3.8 Hz, 2H, NC*H*CH_2), 2.21 – 1.96 (m, 4H, CH_2), 1.94 – 1.78 (m, 4H, CH_2), 1.78 – 1.54 (m, 6H, CH_2), 1.51 – 1.30 (m, 4H, CH_2), 1.30 – 1.11 (m, 2H, CH_2).

^{13}C{^{1}H} NMR (75.563 MHz, d_6-DMSO, 27 °C): δ = 135.6 (N*C*HN), 119.8 (N*C*H*C*HN), 59.7 (N*C*HCH_2), 33.4 (*C*H_2), 24.9 (*C*H_2), 24.5 (*C*H_2).

^{19}F{^{1}H} NMR (282.762 MHz, d_6-DMSO, 27 °C): δ = -148.33 ($[^{11}BF_4]^-$), -148.28 ($[^{10}BF_4]^-$).

HR-MS (ESI+, methanol) *m*/*z* (%): 233.20136 (100.0) $[M\text{-}BF_4]^+$.

calculated for $[C_{15}H_{25}N_2]^+$:	233.20123
found:	233.20136

Infrared Spectroscopy (KBr): $\tilde{\nu}$ [cm^{-1}] = 3426 (br, m), 3149 (m), 3058 (m), 2937 (s), 2860 (s), 1555 (s), 1455 (s), 1434 (m), 1367 (w), 1270 (m), 1193 (s), 1164 (s), 1066 (br, s, tetrafluoroborate, antisymmetric stretching mode), 991 (m), 897 (m), 850 (m), 757 (m, tetrafluoroborate, symmetric stretching mode), 651 (m), 522 (m, tetrafluoroborate, bending mode).

Elemental Analysis (No. 31078)

calculated for $C_{15}H_{25}BF_4N_2$:	C	56.27 %,	H	7.87 %,	N 8.75 %
found:	C	56.30 %,	H	7.85 %,	N 8.73 %

Melting Point: 181 °C.

6.2.11.3 [(ICy)$_2$Cu]PF$_6$ (**123**)

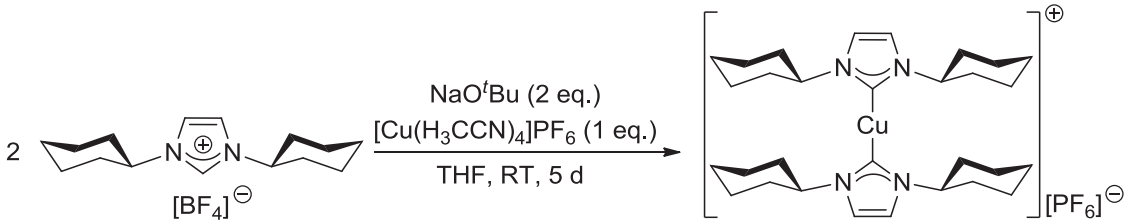

122 **123**

[ICy$_2$Cu]PF$_6$ (**123**) was synthesized according to a procedure reported in literature.[72b] In the glovebox, a flame-dried Schlenk flask was charged with 1,3-dicyclohexylimidazolium tetrafluoroborate (**122**, 0.321 g, 1.003 mmol), tetrakis(acetonitrile)copper(I) hexafluorophosphate (0.188 g, 0.504 mmol) and sodium-*tert*-butoxide (0.097 g, 1.01 mmol). The solids were suspended in anhydrous tetrahydrofuran (12 ml) and stirred for five days at room temperature. The reaction mixture was filtered over a frit filled with Celite under inert gas. Anhydrous tetrahydrofuran was used to rinse the filter material and the resulting solution was overlain by pentane. The product crystallized from the reaction mixture when stored at -20 °C overnight. The solution was removed *via* a paper-capped canula and the crystalline solid washed with anhydrous diethyl ether (3 × 10 ml). The colourless crystalline product was dried *in vacuo* (yield not determined).

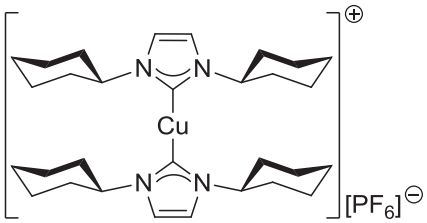

123

$C_{30}H_{48}CuF_6N_4P$

M ($C_{30}H_{48}CuF_6N_4P$) = 673.24 g mol^{-1}

^{1}H NMR (300.190 MHz, d_6-acetone, 27 °C): δ = 7.33 (s, 4H, NC*H*), 4.21 (tt, $^3J_{axial\text{-}axial}$ = 11.8 Hz, $^3J_{axial–equatorial}$ = 3.7 Hz, 4H, NC*H*CH_2), 2.99 - 1.59 (m, 28H, C*H*$_2$), 1.35 - 0.98 (m, 12H, C*H*$_2$).

^{13}C{^{1}H} NMR (75.483 MHz, d_6-acetone, 27 °C): δ = 186.2 (N*C*N), 117.6 (N*C*H), 60.5 (N*C*HCH_2), 34.9 (*C*H_2), 26.3 (*C*H_2), 25.6 (*C*H_2).

^{31}P{^{1}H} NMR (121.475 MHz, d_6-acetone, 27 °C): δ = -144.22 (sept, $^1J_{P–F}$ = 707.9 Hz).

^{1}H NMR (300.510 MHz, CD_2Cl_2, 27 °C): δ = 7.10 (s, 4H, NC*H*), 4.20 (tt, 4H, $^3J_{axial\text{-}axial}$ = 12.0 Hz, $^3J_{axial\text{-}equatorial}$ = 3.9 Hz, NC*H*CH_2), 2.23 - 2.05 (m, 8H, C*H*$_2$), 2.01 - 1.69 (m, 20H, C*H*$_2$), 1.50 - 1.16 (m, 12H, C*H*$_2$).

^{13}C{^{1}H} NMR (75.563 MHz, CD_2Cl_2, 27 °C): δ = 118.9 (N*C*H), 62.2 (N*C*HCH_2), 35.5 (*C*H_2), 26.1 (*C*H_2), 25.5 (*C*H_2).
The signal of the carbene C-atom is not observed in the ^{13}C{^{1}H} NMR spectrum.

^{31}P{^{1}H} NMR (121.649 MHz, CD_2Cl_2, 27 °C): δ = -144.45 (s, $^1J_{P\text{-}F}$ = 710.6 Hz)

HR-MS (ESI+, methanol) *m*/*z* (%): 527.31689 (100.0) [M-PF_6]$^+$.

calculated for [$C_{30}H_{48}CuN_4$]$^+$:	527.31695
found:	527.31689

Elemental Analysis (No. 31127)

calculated for $C_{30}H_{48}CuF_6N_4P$:	C 53.52 %, H 7.19 %, N 8.32 %
found:	C 53.01 %, H 7.37 %, N 8.19 %

Crystal Structure

Crystallographic data and structure refinements for reb15, formula $C_{30}H_{48}CuF_6N_4P$+ C_4H_8O, M ($C_{34}H_{56}CuF_6N_4PO$) = 745.35 g mol^{-1}: colourless crystal (polyhedron), dimensions 0.15 × 0.14 × 0.06 mm^3, crystal system monoclinic, space group $P2_1/n$, Z = 4, a = 10.1187(11) Å, b = 18.1662(19) Å, c = 20.410(2) Å, α = 90°, β = 95.786(2), γ = 90°, V = 3732.6(7) Å^3, ρ = 1.326 g cm^{-3}, T = 200(2) K, Θ_{max} = 25.87°, radiation Mo K_α, λ = 0.71073 Å, 0.5° ω-scans with CCD area detector, covering the asymmetric unit in reciprocal space with a mean redundancy of 6.67 and a completeness of 99.7 % to a resolution of 0.81 Å, 48953 reflections measured, 7223 unique (R(int) = 0.0404), 5430 observed ($I > 2\sigma(I)$), intensities were corrected for Lorentz and polarization effects, an empirical absorption correction was applied using SADABS[165] based on the Laue symmetry of the reciprocal space, μ = 0.69 mm^{-1}, T_{min} = 0.90, T_{max} = 0.96, structure solved by direct methods and refined against F^2 with a full-matrix least-squares algorithm using the SHELXTL (version 2008/4) software package,[166] 453 parameters refined, hydrogen atoms were treated using appropriate riding models, goodness of fit 1.03 for observed reflections, final residual values $R1(F)$ = 0.046, $wR(F^2)$ = 0.114 for observed reflections, residual electron density -0.30 to 0.65 eÅ^{-3}. CCDC 869468 contains the supplementary crystallographic data for this paper. This data can be obtained free of charge from The Cambridge Crystallographic Data Centre *via* www.ccdc.cam.ac.uk/data_request/cif.

6.3 Catalytic Studies

6.3.1 Syntheses of Organoazides

6.3.1.1 Benzyl Azide (**131**)

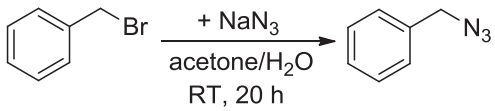

131

Benzyl azide was synthesized according to a procedure reported in literature. [141, 171] Benzyl bromide (98 %, 1.767 g benzyl bromide, 10.12 mmol) and sodium azide (0.987 g, 15.2 mmol) were dissolved in a mixture of acetone (40 ml) and water (10 ml). The reaction mixture was stirred for 20 hours at room temperature. Dichloromethane (50 ml) and water (50 ml) were added and the phases separated. The aqueous phase was extracted with dichloromethane (2 × 30 ml) and the combined organic phases dried over magnesium sulphate. After filtration of the drying agent, the solvent was removed *in vacuo* to give a yellow oil (1.292 g, 9.703 mmol, 96 %).

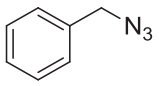

131

$C_7H_7N_3$

M ($C_7H_7N_3$) = 133.15 g mol^{-1}

^{1}H NMR (300.080 MHz, $CDCl_3$, 25 °C): δ = 7.47 - 7.27 (m, 5H, aryl-C*H*), 4.35 (s, 2H, CH_2).

^{13}C{^{1}H} NMR (75.455 MHz, $CDCl_3$, 25 °C): δ = 135.5 (*ipso*–*C*), 129.0 (*meta*–*C*H), 128.4 (*ortho*–*C*H), 128.3 (*para*–*C*H), 54.9 (*C*H_2).

HR-MS (EI+): *m*/*z* (%): 91.0550 (100.0) $[M–N_3]^{\bullet+}$, 104.0514 (42.6) $[M–HN_2]^{\bullet+}$, 133.0645 (52.4) $[M]^{\bullet+}$.

calculated for $[C_7H_7N_3]^{\bullet+}$: 133.0640

found: 133.0645

Infrared Spectroscopy (film): $\tilde{\nu}$ [cm^{-1}] = 3347 (w), 3066 (w), 3032 (w), 2928 (w), 2096 (s, C–N_3 asymmetric stretch), 1496 (w), 1455 (m), 1350 (w), 1256 (m), 1202 (m), 1078 (w), 1029 (w), 877 (m), 750 (m), 699 (s), 569 (w), 462 (w).

Elemental Analysis (No. 32308)

calculated for $C_7H_7N_3$: C 63.14 %, H 5.30 %, N 31.56 %

found: C 63.05 %, H 5.48 %, N 31.70 %

6.3.1.2 4,4'-(Chloromethylene)bis(methylbenzene) (**132**)

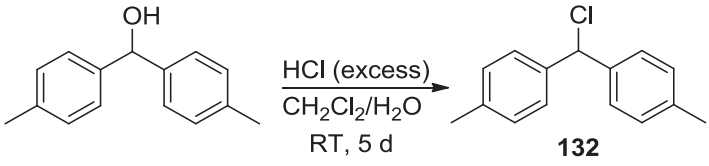

132

4,4'–(Chloromethylene)bis(methylbenzene) was synthesized by variation of a procedure reported in literature.[172] In a 100 ml round–bottomed flask, di-*p*-tolylmethanol[173] (10.0 g, 47.1 mmol) was dissolved in dichloromethane (35 ml) giving a light yellow solution. An aqueous solution of hydrochloric acid (37 weight-% solution in water, 20 ml, 0.24 mol) was added. The mixture was stirred at room temperature for five days. The phases were separated and the organic phase was washed with water (3 × 100 ml). The aqueous phase was extracted with dichloromethane (100 ml) and the combined organic phases were dried over potassium carbonate. After filtration, the solvent was removed *in vacuo*, giving an oily reddish substance. Pentane was added and the flask stored at –50 °C for two days to allow for crystallization of the product. The solvent was decanted and the obtained white crystals dried *in vacuo* (9.52 g, 41.3 mmol, 88 %).

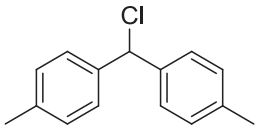

132

$C_{15}H_{15}Cl$

M ($C_{15}H_{15}Cl$) = 230.73 g mol^{-1}

^{1}H NMR (300.510 MHz, $CDCl_3$, 27 °C): δ = 7.33 (d, $^{3}J_{H-H}$ = 8.1 Hz, 4H, *ortho*–C<u>*H*</u>), 7.17 (d, $^{3}J_{H-H}$ = 8.1 Hz, 4H, *meta*–C<u>*H*</u>), 6.13 (s, 1H, C<u>*H*</u>Cl), 2.36 (s, 6H, C<u>*H*</u>$_3$).

^{13}C{^{1}H} NMR (75.563 MHz, $CDCl_3$, 27 °C): δ = 138.5 (*ipso*–<u>*C*</u>CHCl), 137.9 (*para*–<u>*C*</u>CH_3), 129.3 (*meta*–<u>*C*</u>H), 127.8 (*ortho*–<u>*C*</u>H), 64.4 (<u>*C*</u>HCl), 21.2 (<u>*C*</u>H_3).

HR-MS (EI+): *m*/*z* (%): 195.1204 (100.0) [M-Cl]$^{\bullet+}$, 230.0856 (3.4) [M(^{35}Cl)]$^{\bullet+}$, 232.0841 (1.3) [M(^{37}Cl)]$^{\bullet+}$.

calculated for [$C_{15}H_{15}$(^{35}Cl)]$^{\bullet+}$:	230.0857
found:	230.0856

Elemental Analysis (No. 29536)

calculated for $C_{15}H_{15}Cl$:	C 78.08 %, H 6.55 %
found:	C 78.37 %, H 6.66 %

Melting Point: 46-48 °C.

6.3.1.3 4,4'-(Azidomethylene)bis(methylbenzene) (**133**)

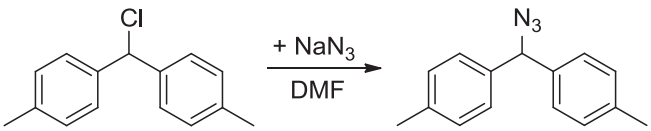

132 **133**

4,4'-(Azidomethylene)bis(methylbenzene) was synthesized by variation of a procedure reported in literature.[24] In a 50 ml round-bottomed flask, 4,4'–(chloromethylene)bis(methylbenzene) (4.415 g, 20.80 mmol) was dissolved in dimethylformamide

(99.5 %, 10 ml). Sodium azide was added (1.352 g, 20.80 mmol) and the reaction mixture stirred for 23 hours at room temperature. Dichloromethane was added (20 ml) and the resulting precipitate removed by filtration. The solvent was removed *in vacuo* and the raw product was dissolved in diethyl ether (50 ml). The diethyl ether solution was washed with water (4 × 100 ml) and the combined aqueous phases were extracted with diethyl ether (100 ml). The combined organic phases were dried over magnesium sulphate. After filtration of the drying agent, the solvent was removed *in vacuo* and the product obtained as a yellow oil (3.69 g, 15.5 mmol, 75 %).

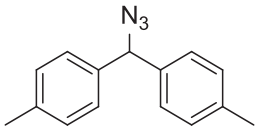

133

$C_{15}H_{15}N_3$

M ($C_{15}H_{15}N_3$) = 237.30 g mol^{-1}

^{1}H NMR (300.130 MHz, $CDCl_3$, 25 °C): δ = 7.27 (d, $^3J_{H\text{-}H}$ = 8.2 Hz, 4H, *ortho*-C<u>*H*</u>), 7.22 (d, $^3J_{H\text{-}H}$ = 8.2 Hz, 4H, *meta*-C<u>*H*</u>), 5.71 (s, 1H, C<u>*H*</u>N_3), 2.40 (s, 6H, C<u>*H*</u>$_3$).

^{13}C{^{1}H} NMR (75.468 MHz, $CDCl_3$, 25 °C): δ = 137.8 (*para*-<u>*C*</u>CH_3), 136.9 (*ipso*-<u>*C*</u>CN_3), 129.4 (*meta*-<u>*C*</u>H), 127.4 (*ortho*-<u>*C*</u>H*)*, 68.3 (<u>*C*</u>HN_3), 21.2 (<u>*C*</u>H_3).

HR-MS (EI+): *m*/*z* (%): 165.0726 (14.6) [M-2CH_3-N_3]$^{\bullet+}$, 180.0925 (15.6) [M-CH_3-N_3]$^{\bullet+}$, 195.1202 (100.0) [M-N_3]$^{\bullet+}$, 208.1120 [M-H-N_2]$^{\bullet+}$; 237.1241 (5.3) [M]$^{\bullet+}$.

calculated for [$C_{15}H_{15}N_3$]$^{\bullet+}$:	237.1260
found:	237.1241

Infrared Spectroscopy (film): $\tilde{\nu}$ [cm^{-1}] = 3310 (w), 3025 (m), 2924 (m), 2472 (w), 2102 (s, C–N_3 asymmetric stretch), 1909 (w), 1614 (w), 1512 (s), 1451 (w), 1413 (w), 1379 (w), 1242 (br, s), 1182 (m), 1042 (w), 1022 (w), 924 (w), 882 (w), 810 (s), 776 (s), 762 (s), 723 (w), 666 (w), 631 (w), 582 (w), 559 (m), 536 (w), 478 (w).

Elemental Analysis (No. 29528)

calculated for $C_{15}H_{15}N_3$:	C 75.92 %, H 6.37 %, N 17.71 %
found:	C 75.77 %, H 6.44 %, N 17.13 %

6.3.2 Preparation of Stock Solutions

Catalyst Stock Solution A: μ-Acetato-κO, $\kappa O'$-μ-{1,1'-(ethane-1,2-diyl)bis[4-(2,4,6-trimethylphenyl)-1*H*-1,2,4-triazol-5-ylidene]}-κC,$\kappa C'$-dicopper(I) hexafluorophosphate (**91**, 14.68 mg, 20.07 μmol) was dissolved in dichloromethane (4.0 ml) in a Schlenk flask under inert gas ($c_{catalyst}$ = 0.005 mmol ml^{-1}).

Catalyst Stock Solution B (i-v): μ-Acetato-κO, $\kappa O'$-μ-{1,1'-(ethane-1,2-diyl)bis[4-(3,5-dimethylphenyl)-1*H*-1,2,4-triazol-5-ylidene]}-κC,κC'-dicopper(I) hexafluorophosphate (**92**, 14.00 mg, 19.90 μmol) was dissolved in the solvent (4.00 ml; **i**: tetrahydrofuran; **ii**: acetonitrile; **iii**: acetone; **iv**: dichloromethane, **v**: dimethyl sulphoxide) in a Schlenk flask under inert gas ($c_{catalyst}$ = 0.005 mmol ml^{-1}).

Catalyst Stock Solution C: μ-Acetato-κO,$\kappa O'$-μ-{1,1'-(ethane-1,2-diyl)bis[4-(4-methylphenyl)-1*H*-1,2,4-triazol-5-ylidene]}-κC,$\kappa C'$-dicopper(I) hexafluorophosphate (**93**, 13.50 mg, 19.98 μmol) was dissolved in dichloromethane (4.0 ml) in a Schlenk flask under inert gas ($c_{catalyst}$ = 0.005 mmol ml^{-1}).

Catalyst Stock Solution D: μ-{1,1'-(Benzene-1,3-diyldimethanediyl)bis[4-(2,4,6-trimethylphenyl)-1*H*-1,2,4-triazol-5-ylidene]}-κC,$\kappa C'$-bis{[1,3-bis(2,6-diisopropylphenyl)-imidazol-2-ylidene]copper(I)} bis(hexafluorophosphate) (**71**, 44.50 mg, 26.63 μmol) was dissolved in dichloromethane (2.0 ml) in a Schlenk flask under inert gas ($c_{catalyst}$ = 0.013 mmol ml^{-1}).

Catalyst Stock Solution E: μ-{1,1'-(Ethane-1,2-diyl)bis[4-(2,4,6-trimethylphenyl)-1*H*-1,2,4-triazol-5-ylidene]}–κC,$\kappa C'$-bis{[1,3-bis(2,6-diisopropylphenyl)imidazol-2-ylidene]copper(I)} bis(hexafluorophosphate) (**81**, 42.50 mg, 26.65 μmol) was dissolved in dichloromethane (2.0 ml) in a Schlenk flask under inert gas ($c_{catalyst}$ = 0.013 mmol ml^{-1}).

Catalyst Stock Solution F: μ-{1,1'-(Ethane-1,2-diyl)bis[4-(4-methylphenyl)-1*H*-1,2,4-triazol-5-ylidene}- κC,$\kappa C'$-bis{[1,3-bis(2,6-diisopropylphenyl)imidazol-2-ylidene]-

copper(I)} bis(hexafluorophosphate) (**83**, 82.00 mg, 53.29 μmol) was dissolved in dichloromethane (4.0 ml) in a Schlenk flask under inert gas ($c_{catalyst}$ = 0.013 mmol ml^{-1}).

Substrate Solution 1 (i-v): Phenylacetylene (310 µl, 288 mg, 2.82 mmol), benzyl azide (**131**, 350 µl, 373 mg, 2.80 mmol) and dodecane (350 µl) were dissolved in the solvent (1.80 ml; **i**: tetrahydrofuran; **ii**: acetonitrile (use of toluene instead of dodecane); **iii**: acetone; **iv**: dichloromethane, **v**: dimethyl sulphoxide) (c_{alkyne} = c_{azide} = 1.00 mmol ml^{-1}).

Substrate Solution 2: Ethyl propiolate (284 µl, 275 mg, 2.80 mmol), benzyl azide (**131**, 350 µl, 373 mg, 2.80 mmol) and dodecane (350 µl) were dissolved in dichloromethane (1.80 ml) (c_{alkyne} = c_{azide} = 1.01 mmol ml^{-1}).

Substrate Solution 3: 1-Octyne (410 µl, 308 mg, 2.82 mmol), benzyl azide (**131**, 350 µl, 373 mg, 2.80 mmol) and dodecane (350 µl) were dissolved in dichloromethane (1.80 ml) (c_{alkyne} = c_{azide} = 1.00 mmol ml^{-1}).

Substrate Solution 4: 2-Methylbut-3-yn-2-ol (274 µl, 236 mg, 2.80 mmol), benzyl azide (**131**, 350 µl, 373 mg, 2.80 mmol) and dodecane (350 µl) were dissolved in dichloromethane (1.80 ml) (c_{alkyne} = c_{azide} = 1.01 mmol ml^{-1}).

Substrate Solution 5: Phenylacetylene (160 µl, 149 mg, 1.46 mmol), 4,4'-(azidomethylene)bis(methylbenzene) (**133**, 320 µl, 347 mg, 1.46 mmol) and dodecane (280 µl) were dissolved in dichloromethane (700 µl) (c_{alkyne} = c_{azide} = 1.00 mmol ml^{-1}).

Substrate Solution 6: Ethyl propiolate (150 µl, 145 mg, 1.48 mmol), 4,4'-(azidomethylene)bis(methylbenzene) (**133**, 320 µl, 339 mg, 1.43 mmol) and dodecane (250 µl) were dissolved in dichloromethane (710 µl) (c_{alkyne} = 1.03 mmol ml^{-1}, c_{azide} = 1.00 mmol ml^{-1}).

All catalyst stock solutions were stored under inert gas at -30 °C. All substrate stock solutions were analyzed by gas chromatography directly before the start of each catalytic test reaction in order to ensure the purity of the substrate solution and especially the absence of product triazole before the start of the catalytic reaction.

6.3.3 GC Methods

All GC samples were filled into 1.5 ml clear glass vials by Shimadzu to be closed with a screw cap equipped with a septum. The GC instrument was operated in the split mode with a split ratio of ten. Injection was carried out by an autosampling unit. The injection volume was always 1 µl of sample solution. The following temperature programs were used for GC analyses (Table 26).

Table 26: Temperature programs used for GC measurements.

*Method 1: Catalytic Tests with Substrate Solutions **1i-iv***

rate [°C min^{-1}]	temperature [°C]	hold time [min]
–	60	3.50
8.00	260	8.00
40.00	300	3.00

*Method 2: Catalytic Tests with Substrate Solutions **2** - **4***

rate [°C min^{-1}]	temperature [°C]	hold time [min]
–	60	3.50
10.00	250	3.00

*Method 3: Catalytic Tests with Substrate Solutions **5** - **6***

rate [°C min^{-1}]	temperature [°C]	hold time [min]
–	60	3.50
10.00	250	10.00
15.00	295	5.00

For quantitation, all peak areas in the chromatogram were measured. In order to compensate for varying sample volumes, the analytes' peak areas were divided by the peak area of the internal standard, whose relative concentration was constant for all samples.

6.3.4 Determination of Response Factors

As the normalized peak areas are not directly proportional to the amount of substance, it was necessary, to determine response factors for azides and triazoles with respect to the internal standard dodecane, whose response factor was arbitrarily set one.

General Procedure: In separate experiments carried out before the actual catalytic tests, different quantities of dodecane and the analyte in question were weighed into GC vials, which were then filled up with dichloromethane and subjected to the same GC method as the corresponding reaction mixture. In a diagram, the ratio of the weighed in amounts of substance was plotted against the ratio of the measured integrals. The slope of the resulting line is the response factor for this analyte with respect to dodecane. All normalized integrals do thus have to be multiplied by this factor. The results of all calibration measurements are summarized below (Table 27).

Table 27: Response factors for analytes with respect to dodecane.

substance	method	response factor *f*
benzyl azide	*1*	1.8271
benzyl azide	*2*	1.8494
1-benzyl-4-phenyl-1*H*-1,2,3-triazole	*1*	0.8044
1-benzyl-4-ethanoat-1*H*-1,2,3-triazole	*2*	1.5633
1-benzyl-4-hexyl-1*H*-1,2,3-triazole	*2*	1.1662
2-(1-benzyl-1*H*-1,2,3-triazol-4-yl)propan-2-ol	*2*	1.4774
4,4'-(azidomethylene)bis(methylbenzene)	*3*	1.2893
1-(di-4-tolylmethyl)-4-phenyl-1*H*-1,2,3-triazole	*3*	1.3338
ethyl-1-(di-4-tolylmethyl)-1*H*-1,2,3-triazole-4-carboxylate	*3*	2.1949

6.3.5 Catalytic Test Reactions With Dinuclear Copper Complexes

All catalytic test reactions were carried out at least twice. The graphs shown in the below section represent measurements from one experiment. If reaction times were slightly varying, the worst result is presented herein. The original data can be found in the appendix.

6.3.5.1 Variation of Catalyst

Reaction of Phenylacetylene and Benzyl Azide with 0.5 mol-% of Catalyst Complex 91

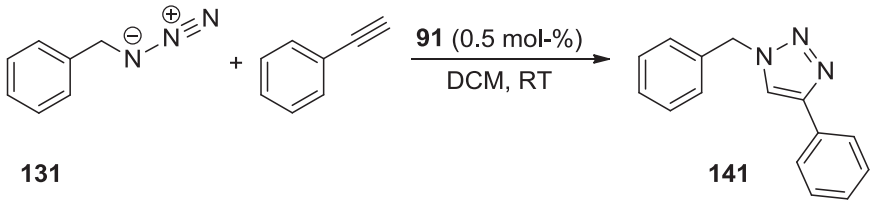

131 **141**

An aliquot of catalyst stock solution **A** (200 μl, 1.00 μmol) was filled into a GC vial equipped with a magnetic stir bar and diluted with anhydrous dichloromethane (100 μl) under inert gas. At *t* = 0, substrate mixture **1(iv)** (200 μl, 0.200 mmol) was added *via* syringe. The reaction mixture was stirred at room temperature. In regular intervals, samples (10 μl) of this reaction mixture were taken over the septum by microlitre syringe.

These samples were diluted with dichloromethane (5 ml per sample), filtered over glass Pasteur pipettes filled with cotton and Celite (approximate height in a 2 ml pipette: 1.5 cm) and analyzed by gas chromatography using temperature program 1. The reaction with 0.5 mol–% catalyst was finished, *i.e.* neither substrate was detectable anymore, after 60 minutes.

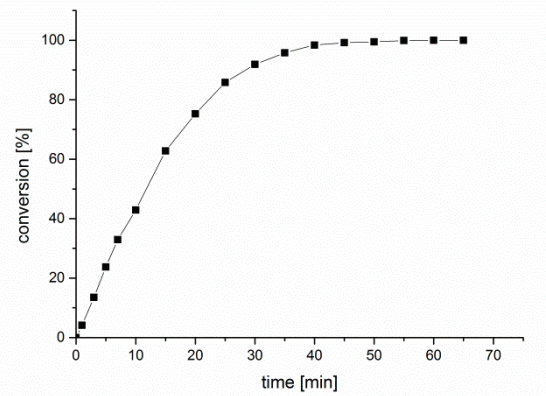

Reaction of Phenylacetylene and Benzyl Azide with 0.5 mol-% of Catalyst Complex 92

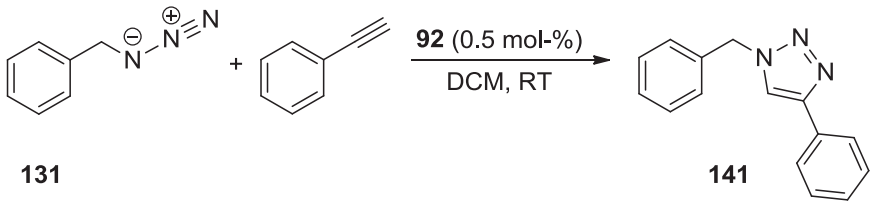

131 141

An aliquot of catalyst stock solution **B(iv)** (200 μl, 0.995 μmol) was filled into a GC vial equipped with a magnetic stir bar and diluted with anhydrous dichloromethane (100 μl) under inert gas. At *t* = 0, substrate mixture **1(iv)** (200 μl, 0.200 mmol) was added *via* syringe. The reaction mixture was stirred at room temperature. In regular intervals, samples (10 μl) of this reaction mixture were taken over the septum by microlitre syringe.

These samples were diluted with dichloromethane (5 ml per sample), filtered over glass Pasteur pipettes filled with cotton and Celite (approximate height in a 2 ml pipette: 1.5 cm) and analyzed by gas chromatography using temperature program 1. The reaction with 0.5 mol–% catalyst was finished, *i.e.* neither substrate was detectable anymore, after 45 minutes.

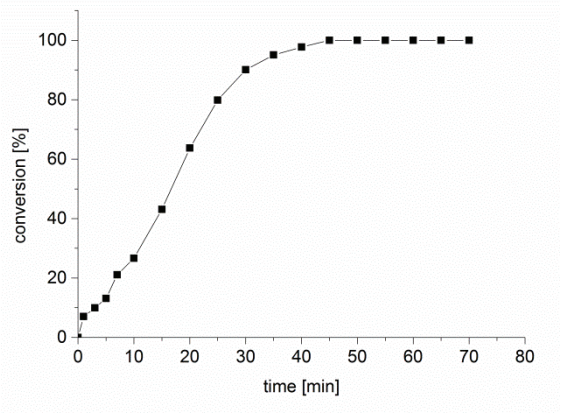

Reaction of Phenylacetylene and Benzyl Azide with 0.5 mol-% of Catalyst Complex 93

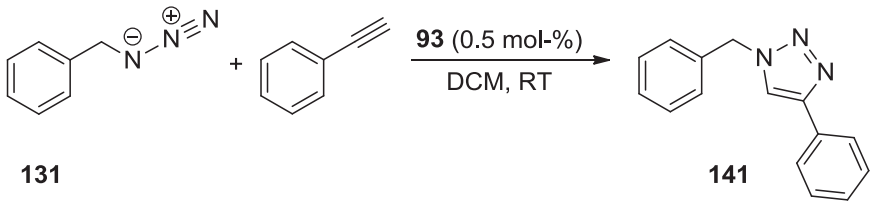

131 141

An aliquot of catalyst stock solution **C** (200 μl, 1.00 μmol) was filled into a GC vial equipped with a magnetic stir bar and diluted with anhydrous dichloromethane (100 μl) under inert gas. At *t* = 0, substrate mixture **1(iv)** (200 μl, 0.200 mmol) was added *via* syringe. The reaction mixture was stirred at room temperature. In regular intervals, samples (10 μl) of this reaction mixture were taken over the septum by microlitre syringe.

These samples were diluted with dichloromethane (5 ml per sample), filtered over glass Pasteur pipettes filled with cotton and Celite (approximate height in a 2 ml pipette: 1.5 cm) and analyzed by gas chromatography using temperature program 1. The reaction with 0.5 mol-% catalyst was finished, *i.e.* neither substrate was detectable anymore, after 45 minutes.

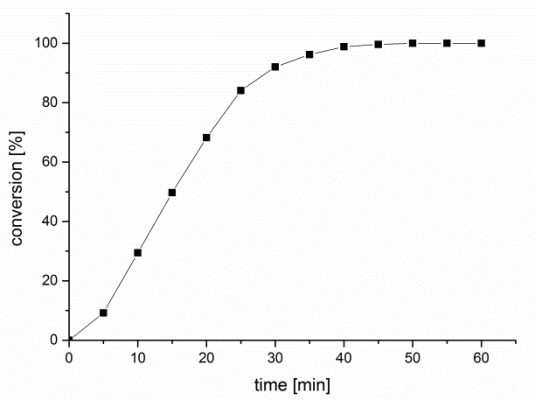

Reaction of Phenylacetylene and Benzyl Azide with 2.0 mol-% *of* Catalyst Complex 71

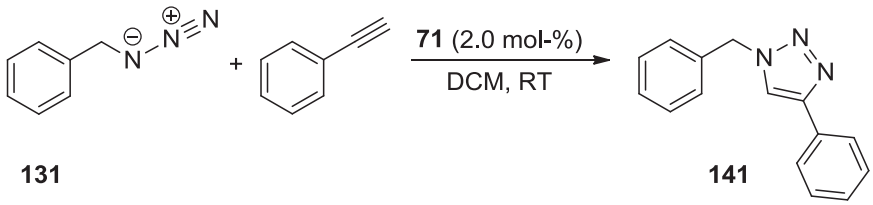

131 **141**

An aliquot of catalyst stock solution **D** (300 μl, 4.00 μmol) was filled into a GC vial equipped with a magnetic stir bar under inert gas. At *t* = 0, substrate mixture **1(iv)** (200 μl, 0.200 mmol) was added *via* syringe. The reaction mixture was stirred at room temperature. In regular intervals, samples (10 μl) of this reaction mixture were taken over the septum by microlitre syringe.

These samples were diluted with dichloromethane (5 ml per sample), filtered over glass Pasteur pipettes filled with cotton and Celite (approximate height in a 2 ml pipette: 1.5 cm) and analyzed by gas chromatography using temperature program 1. The reaction with 2.0 mol-% catalyst was finished, *i.e.* neither substrate was detectable anymore, after 112 hours.

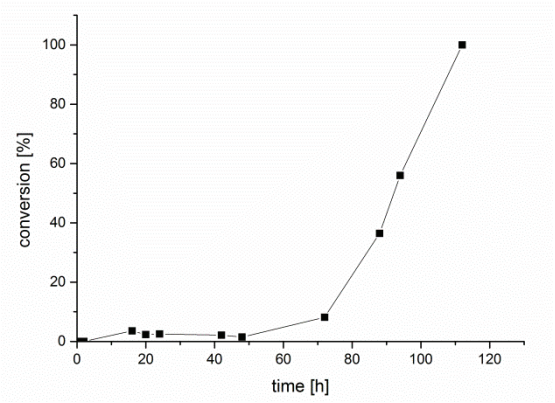

Reaction of Phenylacetylene and Benzyl Azide with 2.0 mol-% *of* Catalyst Complex 81

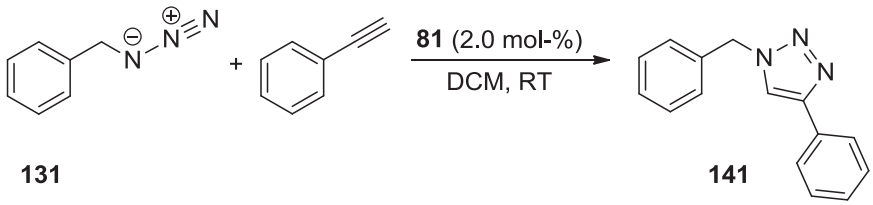

131 **141**

An aliquot of catalyst stock solution **E** (300 μl, 4.00 μmol) was filled into a GC vial equipped with a magnetic stir bar under inert gas. At *t* = 0, substrate mixture **1(iv)** (200 μl, 0.200 mmol) was added *via* syringe. The reaction mixture was stirred at room temperature. In regular intervals, samples (10 μl) of this reaction mixture were taken over the septum by microlitre syringe. These samples were diluted with dichloromethane (5 ml per sample), filtered over glass Pasteur pipettes filled with cotton and Celite (approximate height in a 2 ml pipette: 1.5 cm) and analyzed by gas chromatography using temperature program 1. After three days, still no conversion was observed. As the volume of DCM solvent was reduced due to evaporation, more DCM was added. However, although consumption of the substrates was observed, the alkyne substrate also evaporated. After 154 hours, 88 % conversion was observed based on the concentration of the azide, but there was no phenylacetylene left due to losses by evaporation.

Reaction of Phenylacetylene and Benzyl Azide with 2.0 mol-% *of* Catalyst Complex 83

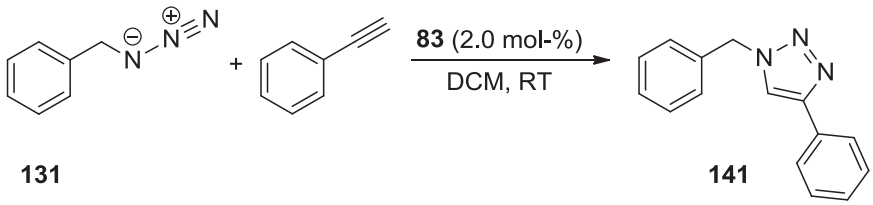

131 141

An aliquot of catalyst stock solution **F** (300 μl, 4.00 μmol) was filled into a GC vial equipped with a magnetic stir bar under inert gas. At *t* = 0, substrate mixture **1(iv)** (200 μl, 0.200 mmol) was added *via* syringe. The reaction mixture was stirred at room temperature. In regular intervals, samples (10 μl) of this reaction mixture were taken over the septum by microlitre syringe.

These samples were diluted with dichloromethane (5 ml per sample), filtered over glass Pasteur pipettes filled with cotton and Celite (approximate height in a 2 ml pipette: 1.5 cm) and analyzed by gas chromatography using temperature program 1. After 22 hours the reaction had reached 97 % conversion.

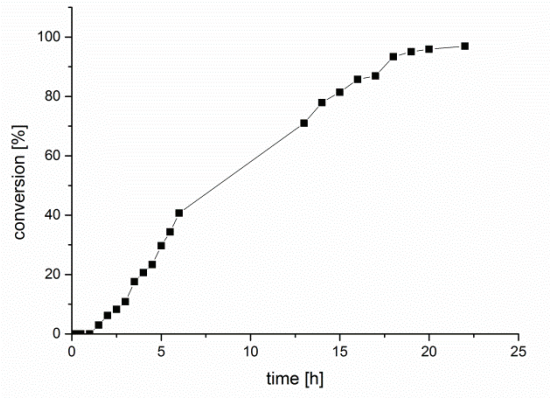

6.3.5.2 Variation of Substrates

Reaction of Ethyl Propiolate and Benzyl Azide with 0.5 mol-% of Catalyst Complex 92

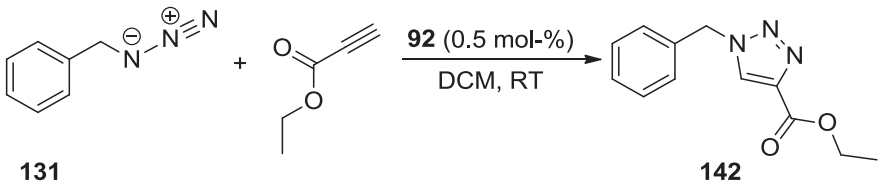

131 **142**

An aliquot of catalyst stock solution **B(iv)** (200 μl, 0.995 μmol) was filled into a GC vial equipped with a magnetic stir bar and diluted with anhydrous dichloromethane (100 μl) under inert gas. At *t* = 0, substrate mixture **2** (200 μl, 0.201 mmol) was added *via* syringe. The reaction mixture was stirred at room temperature. In regular intervals, samples (10 μl) of this reaction mixture were taken over the septum by microlitre syringe.

These samples were diluted with dichloromethane (5 ml per sample), filtered over glass Pasteur pipettes filled with cotton and Celite (approximate height in a 2 ml pipette: 1.5 cm) and analyzed by gas chromatography using temperature program *2*. The reaction with 0.5 mol-% catalyst was finished, *i.e*. neither substrate was detectable anymore, after 13 minutes.

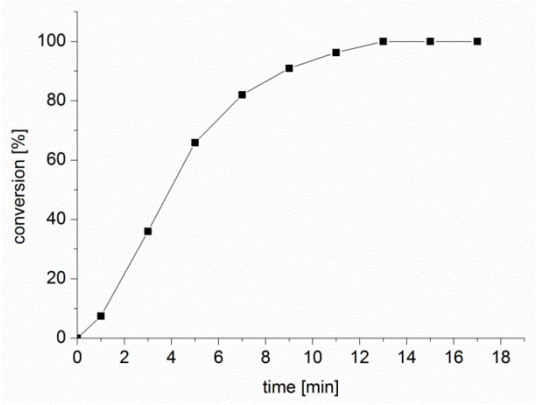

Reaction of 1-Octyne and Benzyl Azide with 0.5 mol-% of Catalyst Complex 92

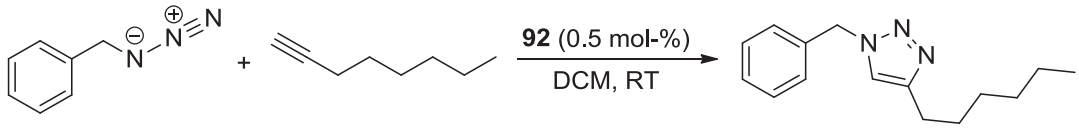

131 **143**

An aliquot of catalyst stock solution **B(iv)** (200 μl, 0.995 μmol) was filled into a GC vial equipped with a magnetic stir bar and diluted with anhydrous dichloromethane (100 μl) under inert gas. At *t* = 0, substrate mixture **3** (200 μl, 0.199 mmol benzyl azide, 0.200 mmol 1-octyne) was added *via* syringe. The reaction mixture was stirred at room temperature. In regular intervals, samples (10 μl) of this reaction mixture were taken over the septum by microlitre syringe.

These samples were diluted with dichloromethane (5 ml per sample), filtered over glass Pasteur pipettes filled with cotton and Celite (approximate height in a 2 ml pipette: 1.5 cm) and analyzed by gas chromatography using temperature program *2*. The reaction with 0.5 mol-% catalyst was finished, *i.e.* neither substrate was detectable anymore, after 50 minutes.

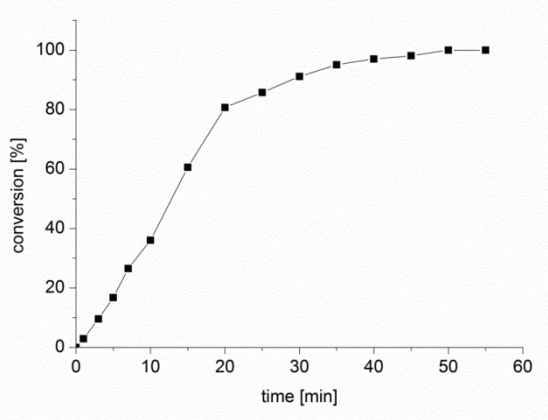

Reaction of 2-Methylbut-3-yn-2-ol and Benzyl Azide with 0.5 mol-% of Catalyst Complex 92

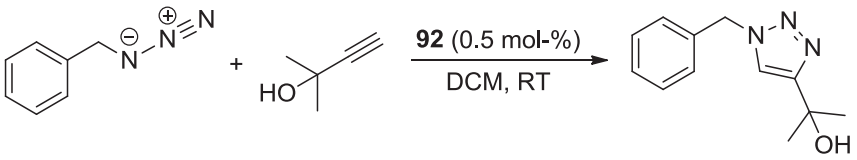

131 **144**

An aliquot of catalyst stock solution **B(iv)** (200 μl, 0.995 μmol) was filled into a GC vial equipped with a magnetic stir bar and diluted with anhydrous dichloromethane (100 μl) under inert gas. At *t* = 0, substrate mixture **4** (200 μl, 0.202 mmol) was added *via* syringe. The reaction mixture was stirred at room temperature. In regular intervals, samples (10 μl) of this reaction mixture were taken over the septum by microlitre syringe.

These samples were diluted with dichloromethane (5 ml per sample), filtered over glass Pasteur pipettes filled with cotton and Celite (approximate height in a 2 ml pipette: 1.5 cm) and analyzed by gas chromatography using temperature program *2*. The reaction with 0.5 mol-% catalyst was finished, *i.e.* neither substrate was detectable anymore, after 70 minutes.

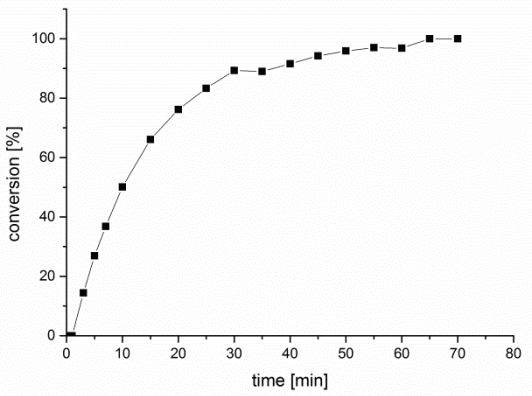

Reaction of Phenylacetylene and 4,4'-(Azidomethylene)bis(methylbenzene) with 0.5 mol-% of Catalyst Complex 92

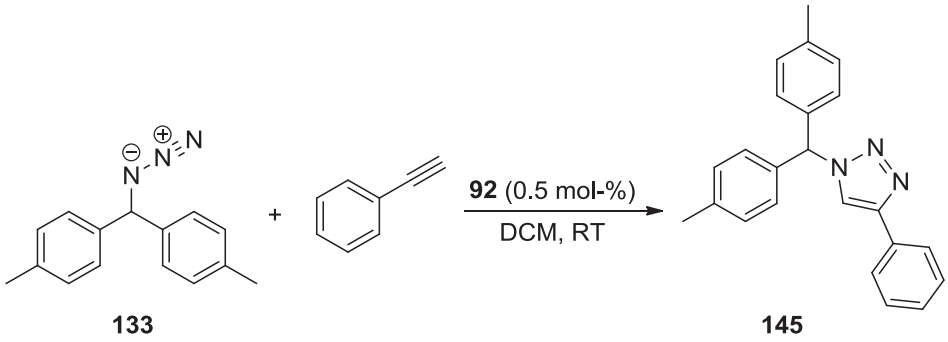

133 **145**

An aliquot of catalyst stock solution **B(iv)** (200 µl, 0.995 µmol) was filled into a GC vial equipped with a magnetic stir bar and diluted with absolute dichloromethane (100 µl) under inert gas. At *t* = 0, substrate mixture **5** (200 µl, 0.200 mmol) was added *via* syringe. The reaction mixture was stirred at room temperature. In regular intervals, samples (10 µl) of this reaction mixture were taken over the septum by microlitre syringe.

These samples were diluted with dichloromethane (5 ml per sample), filtered over glass Pasteur pipettes filled with cotton and Celite (approximate height in a 2 ml pipette: 1.5 cm) and analyzed by gas chromatography using temperature program *3*. The reaction with 0.5 mol-% catalyst was finished, *i.e.* neither substrate was detectable anymore, after 225 minutes.

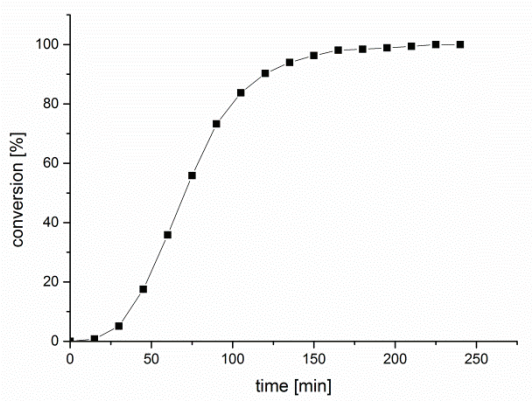

Reaction of Ethyl Propiolate and 4,4'-(Azidomethylene)bis(methylbenzene) with 0.5 mol-% of Catalyst Complex 92

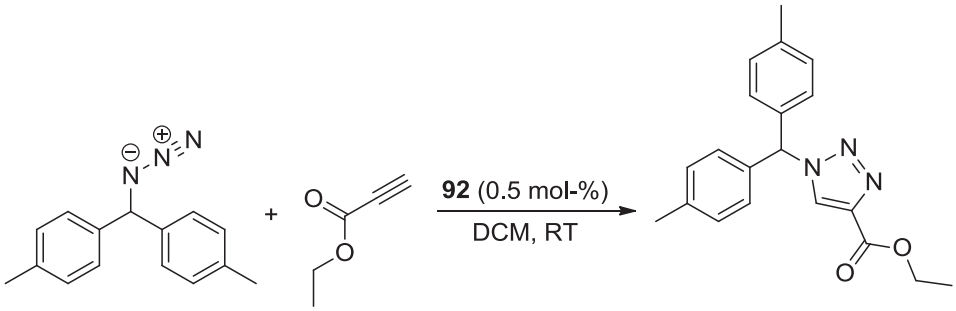

133 **146**

An aliquot of catalyst stock solution **B(iv)** (200 µl, 0.995 µmol) was filled into a GC vial equipped with a magnetic stir bar and diluted with absolute dichloromethane (100 µl) under inert gas. At *t* = 0, substrate mixture **6** (200 µl, 0.200 mmol 4,4'-(azidomethylene)bis(methylbenzene), 0.207 mmol ethyl propiolate) was added *via* syringe. The reaction mixture was stirred at room temperature. In regular intervals, samples (10 µl) of this reaction mixture were taken over the septum by microlitre syringe. These samples were diluted with dichloromethane (5 ml per sample), filtered over glass Pasteur pipettes filled with cotton and Celite (approximate height in a 2 ml pipette: 1.5 cm) and analyzed by gas chromatography using temperature program *3*. The reaction with 0.5 mol-% catalyst was finished, *i.e.* neither substrate was detectable anymore, after 13 minutes.

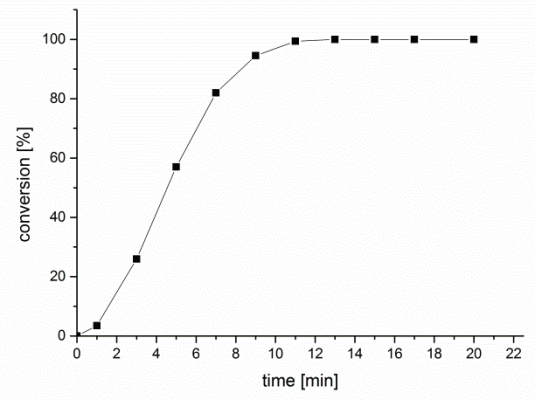

6.3.5.3 Variation of Solvent

Reaction of Phenylacetylene and Benzyl Azide in Tetrahydrofuran with 0.5 mol-% of Catalyst Complex 92

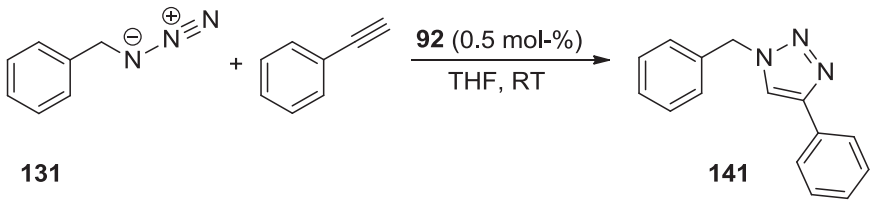

131 **141**

An aliquot of catalyst stock solution **B(i)** (200 μl, 0.995 μmol) was filled into a GC vial equipped with a magnetic stir bar and diluted with anhydrous tetrahydrofuran (100 μl) under inert gas. At *t* = 0, substrate mixture **1(i)** (200 μl, 0.200 mmol) was added *via* syringe. The reaction mixture was stirred at room temperature. In regular intervals, samples (10 μl) of this reaction mixture were taken over the septum by microlitre syringe.

These samples were diluted with dichloromethane (5 ml per sample), filtered over glass Pasteur pipettes filled with cotton and Celite (approximate height in a 2 ml pipette: 1.5 cm) and analyzed by gas chromatography using temperature program *1*. The reaction with 0.5 mol-% catalyst was finished, *i.e.* neither substrate was detectable anymore, after 270 minutes.

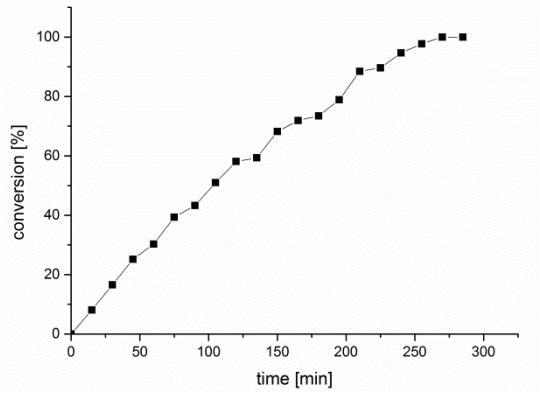

Reaction of Phenylacetylene and Benzyl Azide in Acetonitrile with 0.5 mol-% of Catalyst Complex 92

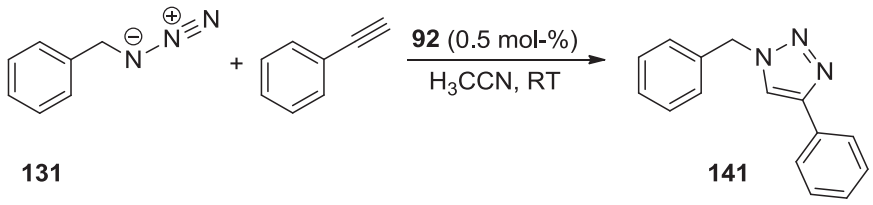

131 141

Catalyst stock solution **B(ii)** as well as substrate solution **1(ii)** were prepared according to the above procedures using anhydrous acetonitrile as solvent. As dodecane is not miscible with acetonitrile, toluene was used as internal standard instead. The response factors listed in Table 27 cannot be applied in this case, as they had been determined relative to dodecane as standard. An aliquot of the catalyst stock solution (200 μl, 0.995 μmol) was filled into a GC vial equipped with a magnetic stir bar and diluted with anhydrous acetonitrile (100 μl) under inert gas. At t = 0, substrate mixture **1(ii)** (200 μl, 0.200 mmol) was added *via* syringe. The reaction mixture was stirred at room temperature and after a couple of minutes, the product started to precipitate. In regular intervals, samples (10 μl) of this reaction mixture were taken over the septum by microlitre syringe. These samples were diluted with dichloromethane (5 ml per sample), filtered over glass Pasteur pipettes filled with cotton and Celite (approximate height in a 2 ml pipette: 1.5 cm) and analyzed by gas chromatography using temperature program *1*. The reaction with 0.5 mol-% catalyst was finished, *i.e.* neither substrate was detectable anymore, after 35 minutes. However, due to its precipitation during the course of the reaction, the concentration of the product triazole in the regularly extracted samples will always be too low and thus, a reliable time-conversion relationship cannot be established.

Reaction of Phenylacetylene and Benzyl Azide in Acetone with 0.5 mol-% of Catalyst Complex 92

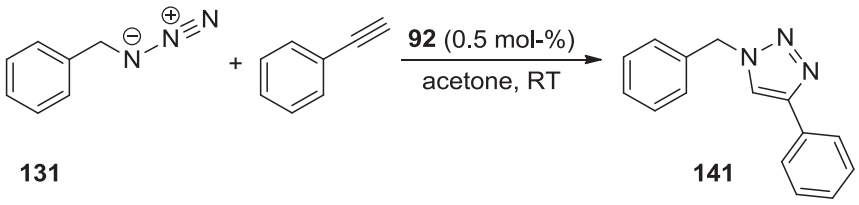

131 **141**

An aliquot of catalyst stock solution **B(iii)** (200 μl, 0.995 μmol) was filled into a GC vial equipped with a magnetic stir bar and diluted with anhydrous acetone (100 μl) under inert gas. At *t* = 0, substrate mixture **1(iii)** (200 μl, 0.200 mmol) was added *via* syringe. The reaction mixture was stirred at room temperature and after a couple of minutes, the product started to precipitate. In regular intervals, samples (10 μl) of this reaction mixture were taken over the septum by microlitre syringe. These samples were diluted with dichloromethane (5 ml per sample), filtered over glass Pasteur pipettes filled with cotton and Celite (approximate height in a 2 ml pipette: 1.5 cm) and analyzed by gas chromatography using temperature program *2*. The reaction with 0.5 mol-% catalyst was finished, *i.e.* neither substrate was detectable anymore, after 120 minutes. However, due to its precipitation during the course of the reaction, the concentration of the product triazole in the regularly extracted samples will always be too low and thus, a reliable time-conversion relationship cannot be established.

Reaction of Phenylacetylene and Benzyl Azide in Dimethyl Sulphoxide with 0.5 mol-% of Catalyst Complex 92

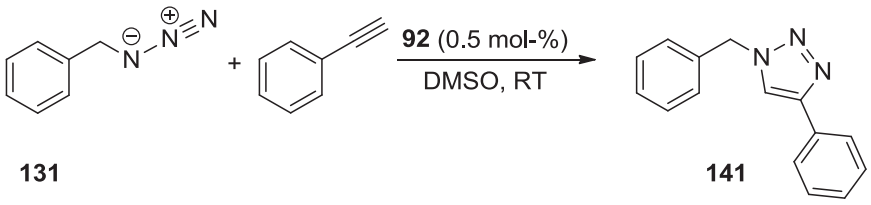

131 141

Catalyst stock solution **B(v)** as well as substrate solution **1(v)** were prepared according to the above procedures using anhydrous dimethyl sulphoxide as solvent. As dodecane is not miscible with dimethyl sulphoxide, toluene was used as internal standard instead. The response factors listed in Table 27 cannot be applied in this case, as they had been determined relative to dodecane as standard. An aliquot of the catalyst stock solution (200 μl, 0.995 μmol) was filled into a GC vial equipped with a magnetic stir bar and diluted with anhydrous dimethyl sulphoxide (100 μl) under inert gas. At *t* = 0, substrate mixture **1(v)** (200 μl, 0.200 mmol) was added *via* syringe. The reaction mixture was stirred at room temperature. In regular intervals, samples (10 μl) of this reaction mixture were taken over the septum by microlitre syringe. These samples were diluted with dichloromethane (5 ml per sample), filtered over glass Pasteur pipettes filled with cotton and Celite (approximate height in a 2 ml pipette: 1.5 cm) and analyzed by gas chromatography using temperature program *1*. The reaction with 0.5 mol-% catalyst has not reached full conversion after eleven hours.

6.3.5.4 Variation of Catalyst Concentration

Catalytic Reaction of Phenylacetylene and Benzyl Azide with 0.75 mol-% of Catalyst Complex 92

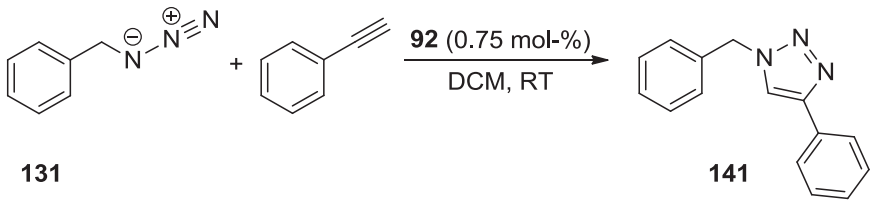

131 **141**

An aliquot of catalyst stock solution **B(iv)** (300 μl, 1.49 μmol) was filled into a GC vial equipped with a magnetic stir bar under inert gas. At *t* = 0, substrate mixture **1(iv)** (200 μl, 0.200 mmol) was added *via* syringe. The reaction mixture was stirred at room temperature. In regular intervals, samples (10 μl) of this reaction mixture were taken over the septum by microlitre syringe.

These samples were diluted with dichloromethane (5 ml per sample), filtered over glass Pasteur pipettes filled with cotton and Celite (approximate height in a 2 ml pipette: 1.5 cm) and analyzed by gas chromatography using temperature program 1. The reaction with 0.75 mol-% catalyst was finished, *i.e.* neither substrate was detectable anymore, after 30 minutes. The integral of the product triazole (**141**) reached half of its maximum value after 12.7 minutes.

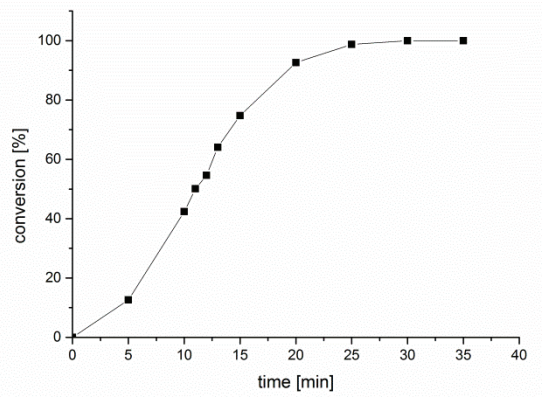

Reaction of Phenylacetylene and Benzyl Azide with 0.62 mol-% of Catalyst Complex 92

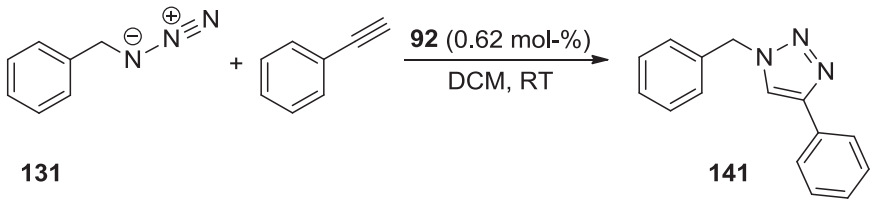

131 141

An aliquot of catalyst stock solution **B(iv)** (250 μl, 1.24 μmol) was filled into a GC vial equipped with a magnetic stir bar and diluted with anhydrous dichloromethane (50 μl) under inert gas. At *t* = 0, substrate mixture **1(iv)** (200 μl, 0.200 mmol) was added *via* syringe. The reaction mixture was stirred at room temperature. In regular intervals, samples (10 μl) of this reaction mixture were taken over the septum by microlitre syringe.

These samples were diluted with dichloromethane (5 ml per sample), filtered over glass Pasteur pipettes filled with cotton and Celite (approximate height in a 2 ml pipette: 1.5 cm) and analyzed by gas chromatography using temperature program 1. The reaction with 0.62 mol-% catalyst was finished, *i.e.* neither substrate was detectable anymore, after 40 minutes. The integral of the product triazole (**141**) reached half of its maximum value after 15.4 minutes.

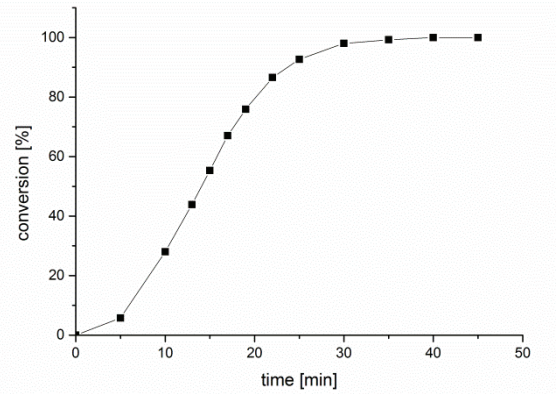

Reaction of Phenylacetylene and Benzyl Azide with 0.50 mol-% of Catalyst Complex 92

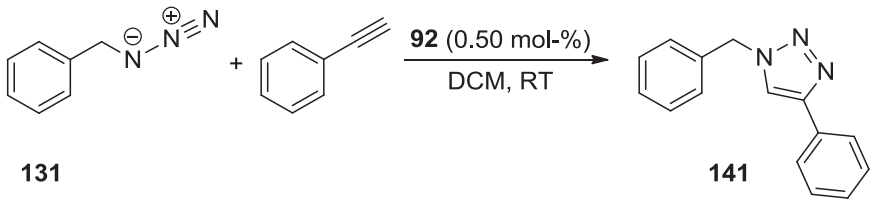

131 141

An aliquot of catalyst stock solution **B(iv)** (200 μl, 0.995 μmol) was filled into a GC vial equipped with a magnetic stir bar and diluted with anhydrous dichloromethane (100 μl) under inert gas. At *t* = 0, substrate mixture **1(iv)** (200 μl, 0.200 mmol) was added *via* syringe. The reaction mixture was stirred at room temperature. In regular intervals, samples (10 μl) of this reaction mixture were taken over the septum by microlitre syringe.

These samples were diluted with dichloromethane (5 ml per sample), filtered over glass Pasteur pipettes filled with cotton and Celite (approximate height in a 2 ml pipette: 1.5 cm) and analyzed by gas chromatography using temperature program 1. The reaction with 0.50 mol-% catalyst was finished, *i.e.* neither substrate was detectable anymore, after 45 minutes. The integral of the product triazole (**141**) reached half of its maximum value after 18.6 minutes.

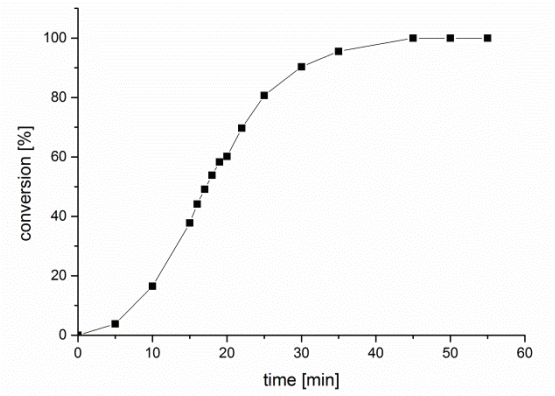

Catalytic Reaction of Phenylacetylene and Benzyl Azide with 0.37 mol-% of Catalyst Complex 92

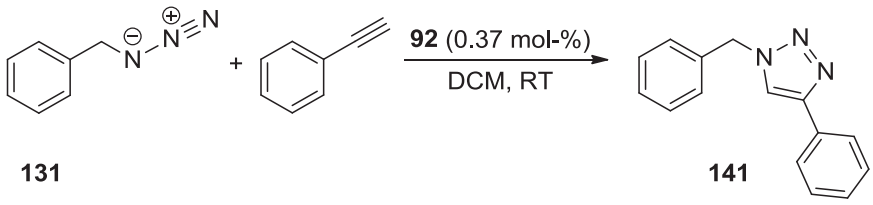

131 141

An aliquot of catalyst stock solution **B(iv)** (150 μl, 0.746 μmol) was filled into a GC vial equipped with a magnetic stir bar and diluted with anhydrous dichloromethane (150 μl) under inert gas. At *t* = 0, substrate mixture **1(iv)** (200 μl, 0.200 mmol) was added *via* syringe. The reaction mixture was stirred at room temperature. In regular intervals, samples (10 μl) of this reaction mixture were taken over the septum by microlitre syringe.

These samples were diluted with dichloromethane (5 ml per sample), filtered over glass Pasteur pipettes filled with cotton and Celite (approximate height in a 2 ml pipette: 1.5 cm) and analyzed by gas chromatography using temperature program 1. The reaction with 0.37 mol-% catalyst was finished, *i.e.* neither substrate was detectable anymore, after 50 minutes. The integral of the product triazole (**141**) reached half of its maximum value after 23.0 minutes.

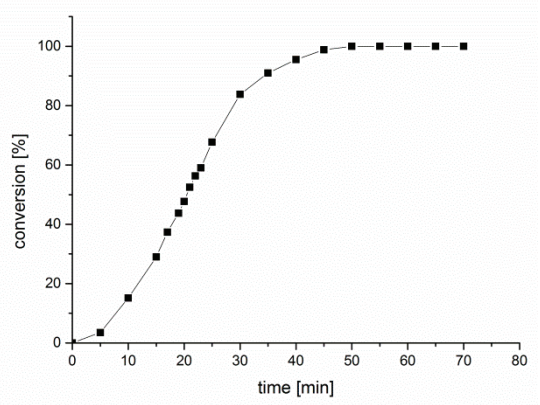

Reaction of Phenylacetylene and Benzyl Azide with 0.25 mol-% of Catalyst Complex *92*

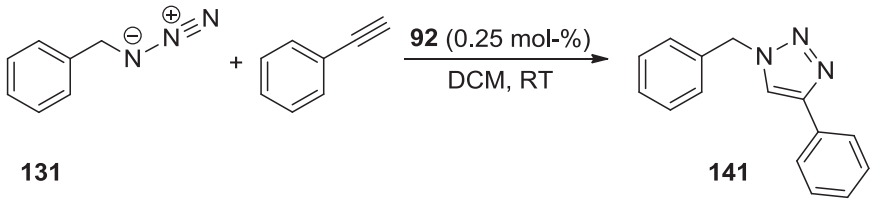

131 **141**

An aliquot of catalyst stock solution **B(iv)** (100 μl, 0.498 μmol) was filled into a GC vial equipped with a magnetic stir bar and diluted with anhydrous dichloromethane (200 μl) under inert gas. At *t* = 0, substrate mixture **1(iv)** (200 μl, 0.200 mmol) was added *via* syringe. The reaction mixture was stirred at room temperature. In regular intervals, samples (10 μl) of this reaction mixture were taken over the septum by microlitre syringe.

These samples were diluted with dichloromethane (5 ml per sample), filtered over glass Pasteur pipettes filled with cotton and Celite (approximate height in a 2 ml pipette: 1.5 cm) and analyzed by gas chromatography using temperature program 1. The reaction with 0.25 mol-% catalyst was finished, *i.e.* neither substrate was detectable anymore, after 80 minutes. The integral of the product triazole (**141**) reached half of its maximum value after 29.3 minutes.

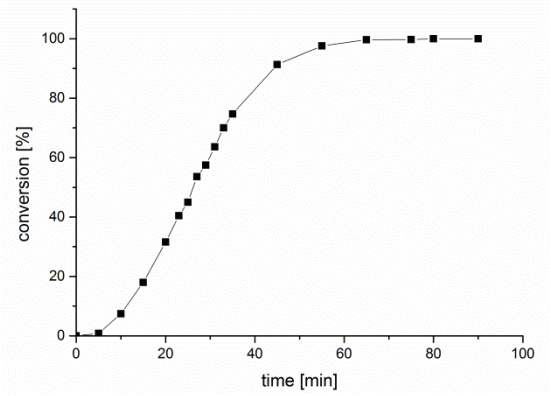

Reaction of Phenylacetylene and Benzyl Azide with 0.12 mol-% of Catalyst Complex 92

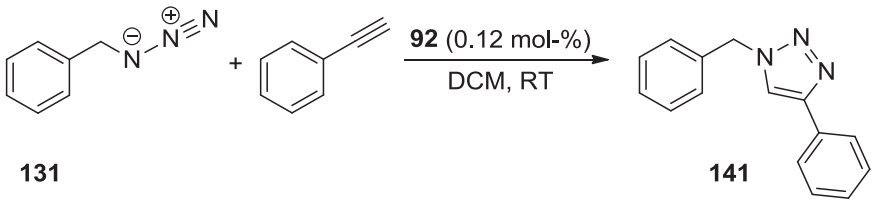

131 141

An aliquot of catalyst stock solution **B(iv)** (50 μl, 0.25 μmol) was filled into a GC vial equipped with a magnetic stir bar and diluted with anhydrous dichloromethane (250 μl) under inert gas. At *t* = 0, substrate mixture **1(iv)** (200 μl, 0.200 mmol) was added *via* syringe. The reaction mixture was stirred at room temperature. In regular intervals, samples (10 μl) of this reaction mixture were taken over the septum by microlitre syringe.

These samples were diluted with dichloromethane (5 ml per sample), filtered over glass Pasteur pipettes filled with cotton and Celite (approximate height in a 2 ml pipette: 1.5 cm) and analyzed by gas chromatography using temperature program 1. The reaction with 0.12 mol-% catalyst was finished, *i.e.* neither substrate was detectable anymore, after 130 minutes. The integral of the product triazole (**141**) reached half of its maximum value after 46.4 minutes.

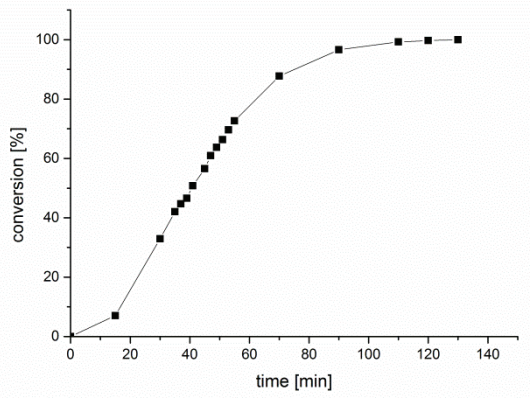

Catalytic Reaction of Ethyl Propiolate and Benzyl Azide with 0.74 mol-% of Catalyst Complex 92

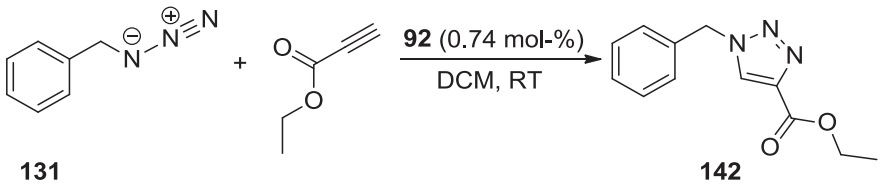

131 142

An aliquot of catalyst stock solution **B(iv)** (300 μl, 1.49 μmol) was filled into a GC vial equipped with a magnetic stir bar under inert gas. At *t* = 0, substrate mixture **2** (200 μl, 0.201 mmol) was added *via* syringe. The reaction mixture was stirred at room temperature. In regular intervals, samples (10 μl) of this reaction mixture were taken over the septum by microlitre syringe.

These samples were diluted with dichloromethane (5 ml per sample), filtered over glass Pasteur pipettes filled with cotton and Celite (approximate height in a 2 ml pipette: 1.5 cm) and analyzed by gas chromatography using temperature program 2. The reaction with 0.74 mol-% catalyst was finished, *i.e*. neither substrate was detectable anymore, after five minutes. The integral of the product triazole (**142**) reached half of its maximum value after 2.3 minutes.

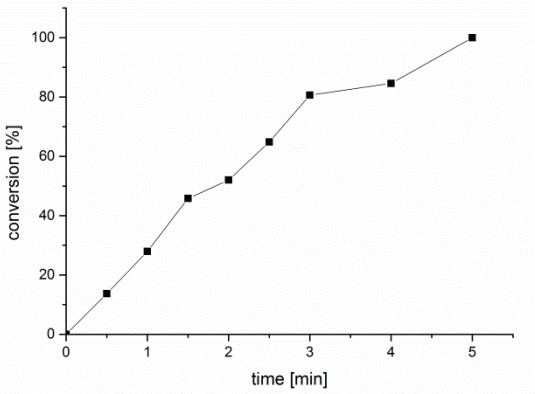

Catalytic Reaction of Ethyl Propiolate and Benzyl Azide with 0.62 mol-% of Catalyst Complex 92

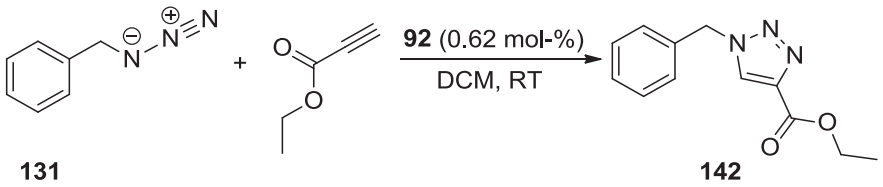

131 142

An aliquot of catalyst stock solution **B(iv)** (250 μl, 1.24 μmol) was filled into a GC vial equipped with a magnetic stir bar and diluted with anhydrous dichloromethane (50 μl) under inert gas. At *t* = 0, substrate mixture **2** (200 μl, 0.201 mmol) was added *via* syringe. The reaction mixture was stirred at room temperature. In regular intervals, samples (10 μl) of this reaction mixture were taken over the septum by microlitre syringe.

These samples were diluted with dichloromethane (5 ml per sample), filtered over glass Pasteur pipettes filled with cotton and Celite (approximate height in a 2 ml pipette: 1.5 cm) and analyzed by gas chromatography using temperature program *2*. The reaction with 0.62 mol-% catalyst was finished, *i.e*. neither substrate was detectable anymore, after seven minutes. The integral of the product triazole (**142**) reached half of its maximum value after 3.3 minutes.

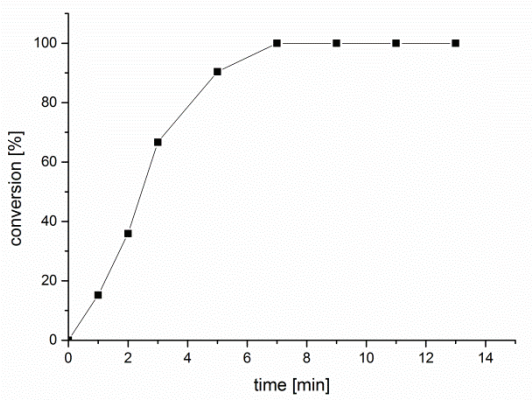

Catalytic Reaction of Ethyl Propiolate and Benzyl Azide with 0.49 mol-% of Catalyst Complex 92

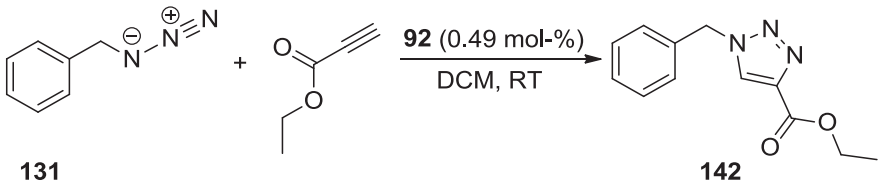

131 142

An aliquot of catalyst stock solution **B(iv)** (200 μl, 0.995 μmol) was filled into a GC vial equipped with a magnetic stir bar and diluted with anhydrous dichloromethane (100 μl) under inert gas. At *t* = 0, substrate mixture **2** (200 μl, 0.201 mmol) was added *via* syringe. The reaction mixture was stirred at room temperature. In regular intervals, samples (10 μl) of this reaction mixture were taken over the septum by microlitre syringe.

These samples were diluted with dichloromethane (5 ml per sample), filtered over glass Pasteur pipettes filled with cotton and Celite (approximate height in a 2 ml pipette: 1.5 cm) and analyzed by gas chromatography using temperature program 2. The reaction with 0.49 mol-% catalyst was finished, *i.e*. neither substrate was detectable anymore, after 13 minutes. The integral of the product triazole (**142**) reached half of its maximum value after 5.6 minutes.

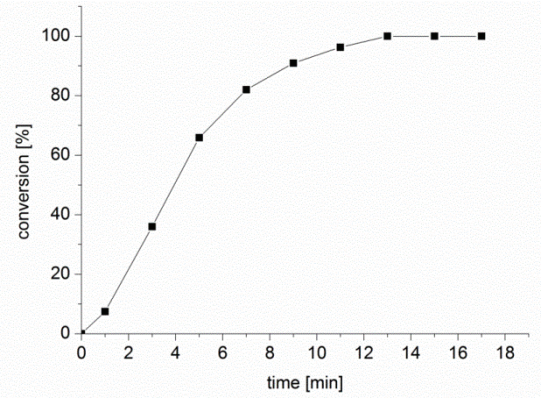

Catalytic Reaction of Ethyl Propiolate and Benzyl Azide with 0.37 mol-% of Catalyst Complex *92*

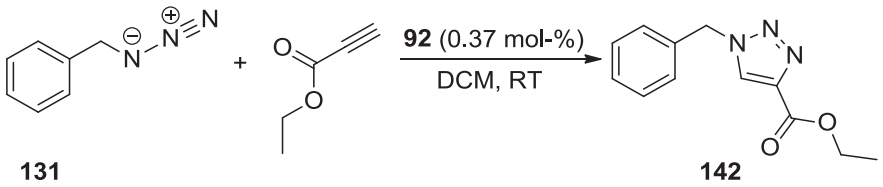

131 **142**

An aliquot of the catalyst stock solution **B(iv)** (150 μl, 0.746 μmol) was filled into a GC vial equipped with a magnetic stir bar and diluted with anhydrous dichloromethane (150 μl) under inert gas. At *t* = 0, substrate mixture **2** (200 μl, 0.201 mmol) was added *via* syringe. The reaction mixture was stirred at room temperature. In regular intervals, samples (10 μl) of this reaction mixture were taken over the septum by microlitre syringe.

These samples were diluted with dichloromethane (5 ml per sample), filtered over glass Pasteur pipettes filled with cotton and Celite (approximate height in a 2 ml pipette: 1.5 cm) and analyzed by gas chromatography using temperature program *2*. The reaction with 0.37 mol-% catalyst was finished, *i.e*. neither substrate was detectable anymore, after 15 minutes. The integral of the product triazole (**142**) reached half of its maximum value after 8.0 minutes.

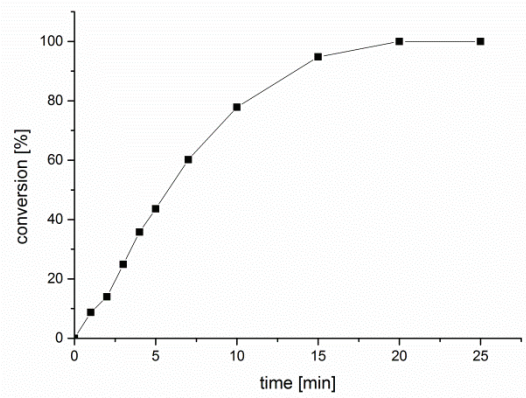

Reaction of Ethyl Propiolate and Benzyl Azide with 0.25 mol-% of Catalyst Complex 92

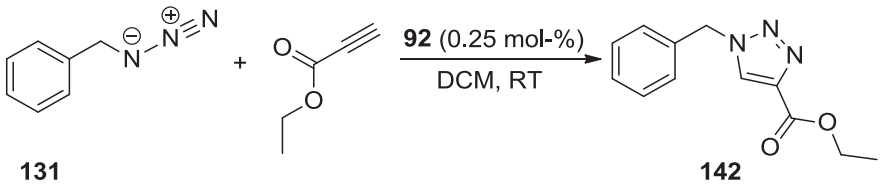

131 142

An aliquot of catalyst stock solution **B(iv)** (100 μl, 0.498 μmol) was filled into a GC vial equipped with a magnetic stir bar and diluted with anhydrous dichloromethane (200 μl) under inert gas. At *t* = 0, substrate mixture **2** (200 μl, 0.201 mmol) was added *via* syringe. The reaction mixture was stirred at room temperature. In regular intervals, samples (10 μl) of this reaction mixture were taken over the septum by microlitre syringe.

These samples were diluted with dichloromethane (5 ml per sample), filtered over glass Pasteur pipettes filled with cotton and Celite (approximate height in a 2 ml pipette: 1.5 cm) and analyzed by gas chromatography using temperature program *2*. The reaction with 0.25 mol-% catalyst was finished, *i.e*. neither substrate was detectable anymore, after 40 minutes. The integral of the product triazole (**142**) reached half of its maximum value after 16.4 minutes.

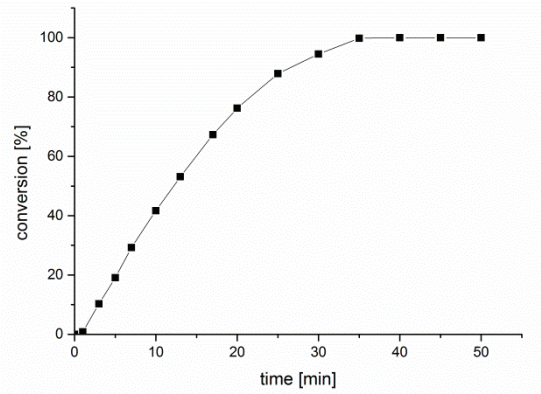

Reaction of Ethyl Propiolate and Benzyl Azide with 0.12 mol-% of Catalyst Complex 92

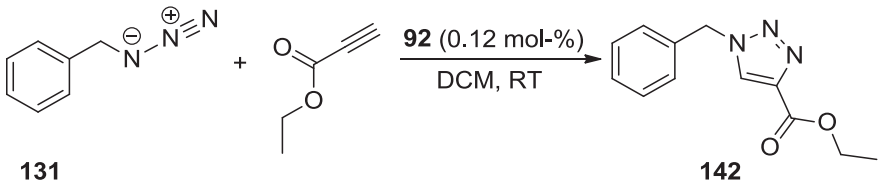

131 142

An aliquot of the catalyst stock solution **B(iv)** (50 μl, 0.25 μmol) was filled into a GC vial equipped with a magnetic stir bar and diluted with anhydrous dichloromethane (250 μl) under inert gas. At *t* = 0, substrate mixture **2** (200 μl, 0.201 mmol) was added *via* syringe. The reaction mixture was stirred at room temperature. In regular intervals, samples (10 μl) of this reaction mixture were taken over the septum by microlitre syringe.

These samples were diluted with dichloromethane (5 ml per sample), filtered over glass Pasteur pipettes filled with cotton and Celite (approximate height in a 2 ml pipette: 1.5 cm) and analyzed by gas chromatography using temperature program *2*. The reaction with 0.12 mol-% catalyst was finished, *i.e*. neither substrate was detectable anymore, after 105 minutes. The integral of the product triazole (**142**) reached half of its maximum value after 50.2 minutes.

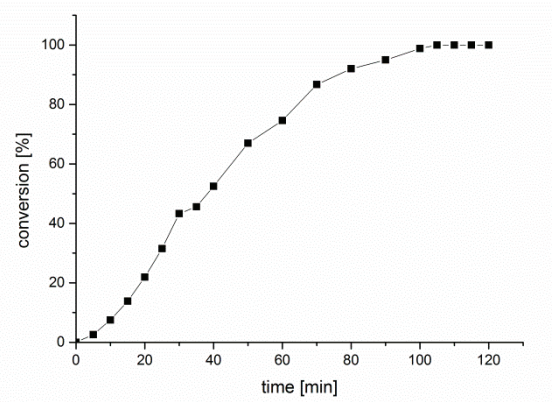

6.3.6 Isolation and Characterization of Product Triazoles

Product triazoles were isolated by diluting the reaction mixtures with dichloromethane and filtering over a Pasteur pipette filled with cotton and Celite. After removal of the solvent, the NMR spectra of the obtained raw products showed pure substances. In order to remove traces of copper species, short column chromatographies were carried out.

*6.3.6.1 1-Benzyl-4-phenyl-1*H*-1,2,3-triazole* (**141**)

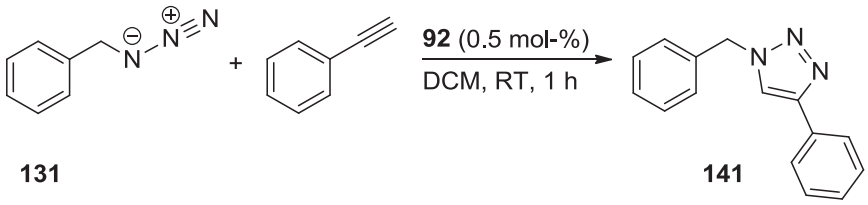

131 **141**

An aliquot of the catalyst stock solution **B(iv)** (200 µl, 0.995 µmol) was filled into a GC vial equipped with a magnetic stir bar and diluted with absolute dichloromethane (100 µl) under inert gas. Substrate mixture **1(iv)** (200 µl, 0.200 mmol) was added *via* syringe. The reaction mixture was stirred at room temperature for one hour. The reaction mixture was diluted with dichloromethane (10 ml) and filtered over a glass Pasteur pipette filled with cotton and Celite (approximate height in a 2 ml pipette: 3 cm; rinsing with dichloromethane). The solvent was removed *in vacuo*. The NMR spectrum of the resulting solid showed a pure substance. In order to remove traces of inorganic impurities, the product was purified by column chromatography (silica gel, isopropanol:dichloromethane = 1:30, R_f = 0.22) to give a white crystalline solid (average yield of two independent runs: 45.1 mg, 0.191 mmol, 96 %). The analytical data was in accordance with the data presented in literature.[36, 174]

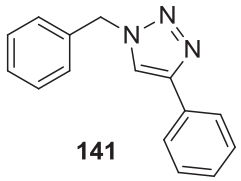

141

$C_{15}H_{13}N_3$

M ($C_{15}H_{13}N_3$) = 235.28 g mol^{-1}

^{1}H NMR (300.080 MHz, d_6-acetone, 25 °C): δ = 8.36 (s, 1H, NC*H*CN), 7.93 - 7.84 (m, 2H, phenyl, *ortho*-C*H*), 7.73 - 6.99 (m, 8H, aryl-C*H*), 5.67 (s, 2H, CH_2).

^{13}C{^{1}H} NMR (75.455 MHz, d_6-acetone, 25 °C): δ = 148.2 (phenyl, *ipso*-*C*), 136.9 (benzyl, *ipso*-*C*), 132.1 (triazolyl, *ipso*-*C*), 129.6 (aryl-*C*H), 129.5 (aryl-*C*H), 129.1 (aryl-*C*H), 128.8 (aryl-*C*H), 128.6 (aryl-*C*H), 126.2 (phenyl, *ortho*-*C*H), 121.4 (N*C*HCN), 54.3 (*C*H_2).

HR-MS (ESI+, methanol) *m*/*z* (%): 236.11831 (1.6) $[M+H]^+$, 258.10028 (2.8) $[M+Na]^+$, 274.07421 (3.1) $[M+K]^+$, 493.21126 (100.0) $[2M+Na]^+$, 509.18534 (19.3) $[2M+K]^+$.

calculated for $[C_{30}H_{26}N_6Na]^+$:	493.21111
found:	493.21126

Infrared Spectroscopy (KBr): $\tilde{\nu}$ [cm^{-1}] = 3445 (br, m), 3143 (w), 3122 (w), 3096 (w), 1608 (w), 1559 (w), 1507 (w), 1496 (w), 1483 (w), 1469 (w), 1483 (w), 1469 (w), 1454 (w), 1442 (w), 1428 (w), 1362 (w), 1334 (w), 1224 (w), 1209 (w), 1195 (w), 1158 (w), 1141 (w), 1076 (w), 1047 (w), 1028 (w), 1003 (w), 973 (w), 913 (w), 827 (w), 807 (w), 768 (s), 731 (s), 708 (w), 696 (s), 589 (w), 580 (w), 508 (w), 482 (w), 474 (w).

Elemental Analysis (No. 31834)

calculated for $C_{15}H_{13}N_3$:	C 76.57 %, H 5.57 %, N 17.86 %
found:	C 76.56 %, H 5.39 %, N 17.91 %

Melting Point: 130 °C.

*6.3.6.2 1-Benzyl-4-ethanoate-1*H*-1,2,3-triazole* (**142**)

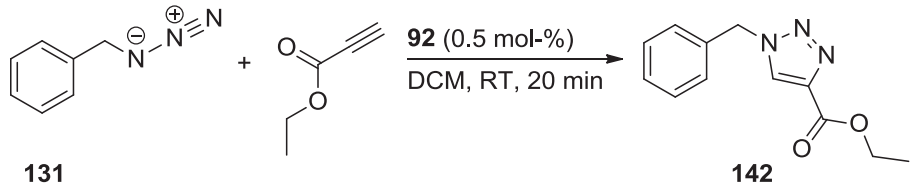

131 **142**

An aliquot of catalyst stock solution **B(iv)** (200 µl, 0.995 µmol) was filled into a GC vial equipped with a magnetic stir bar and diluted with absolute dichloromethane (100 µl) under inert gas. Substrate mixture **2** (200 µl, 0.201 mmol) was added *via* syringe. The reaction mixture was stirred at room temperature for 20 minutes. Then, the reaction mixture was diluted with dichloromethane (10 ml) and filtered over a glass Pasteur pipette filled with cotton and Celite (approximate height in a 2 ml pipette: 3 cm; rinsing with dichloromethane). The solvent was removed *in vacuo*. The NMR spectrum of the resulting solid showed a pure substance. In order to remove traces of inorganic impurities in the product, it was purified by column chromatography (silica gel, isopropanol:dichloromethane = 1:30, R_f = 0.51) to give a white crystalline solid (average yield of two independent runs: 45.4 mg, 0.196 mmol, 98 %). The analytic data was in accordance with the data presented in literature.[16, 175]

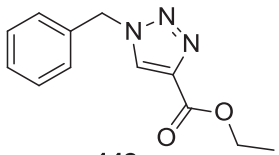

142

$C_{12}H_{13}N_3O_2$

M ($C_{12}H_{13}N_3O_2$) = 231.25 g mol^{-1}

^{1}H NMR (300.510 MHz, CD_2Cl_2, 27 °C): δ = 8.02 (s, 1H, NC*H*CN), 7.65 - 7.01 (m, 5H, aryl-C*H*), 5.57 (s, 2H, CH_2N), 4.34 (q, $^3J_{H-H}$ = 7.1 Hz, 2H, CH_2O), 1.35 (t, $^3J_{H-H}$ = 7.1 Hz, 3H, CH_3).

$^{13}C\{^1H\}$ NMR (75.563 MHz, CD_2Cl_2, 27 °C): δ = 161.0 (<u>C</u>OO), 140.8 (NCH<u>C</u>N), 134.6 (phenyl, *ipso*-<u>C</u>), 129.5 (aryl-<u>C</u>H), 129.3 (aryl-<u>C</u>H), 128.6 (aryl-<u>C</u>H), 127.8 (N<u>C</u>HCN), 61.4 (<u>C</u>H_2O), 54.7 (<u>C</u>H_2N), 14.4 (<u>C</u>H_3).

HR–MS (ESI+, MeOH) : *m/z* (%): 270.06423 (4.0) $[M+K]^+$, 463.20962 (9.1) $[2M+H]^+$, 485.19111 (100.0) $[2M+Na]^+$, 501.16523 (52.3) $[2M+K]^+$.

calculated for $[C_{24}H_{26}N_6O_4Na]^+$:	485.19077
found:	485.19111

Elemental Analysis (No. 31875)

calculated for $C_{12}H_{13}N_3O_2$:	C 62.33 %, H 5.67 %, N 18.17 %
found:	C 62.22 %, H 5.46 %, N 18.08 %

Melting Point: 95 °C.

*6.3.6.3 1-Benzyl-4-hexyl-1*H*-1,2,3-triazole* (**143**)

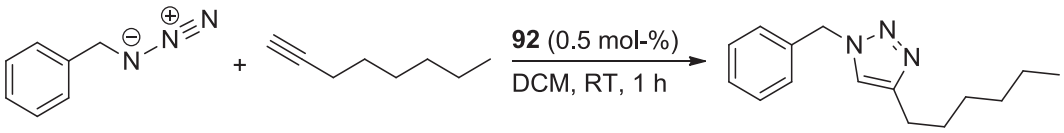

131 **143**

An aliquot of catalyst stock solution **B**(**iv)** (200 µl, 0.995 µmol) was filled into a GC vial equipped with a magnetic stir bar and diluted with absolute dichloromethane (100 µl) under inert gas. Substrate mixture **3** (200 µl, 0.200 mmol) was added *via* syringe. The reaction mixture was stirred at room temperature for one hour. Then, the reaction mixture was diluted with dichloromethane (10 ml) and filtered over a glass Pasteur pipette filled with cotton and Celite (approximate height in a 2 ml pipette: 3 cm; rinsing with dichloromethane). The solvent was removed *in vacuo*. The NMR spectrum of the resulting solid showed a pure substance. In order to remove traces of inorganic impurities in the product, it was purified by column chromatography (silica gel, dichloromethane:ethyl acetate:petroleum ether = 1:1:3, R_f = 0.50) to give a white crystalline solid (average yield of two independent runs: 46.8 mg, 0.192 mmol, 96 %). The analytic data was in accordance with the data presented in literature.[176]

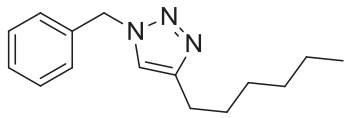

143

$C_{15}H_{21}N_3$

M ($C_{15}H_{21}N_3$) = 243.35 g mol^{-1}

^{1}H NMR (300.510 MHz, $CDCl_3$, 27 °C): δ = 7.42 - 7.29 (m, 3H, aryl-C<u>*H*</u>), 7.29 - 7.20 (m, 2H, aryl-C<u>*H*</u>), 7.18 (s, 1H, NC<u>*H*</u>CN), 5.48 (s, 2H, benzyl, C<u>H_2</u>N), 2.68 (t, $^3J_{H\text{-}H}$ = 7.6 Hz, 2H, CH_2C<u>H_2</u>CN), 1.63 (quint, $^3J_{H\text{–}H}$ = 7.6 Hz, 2H, C<u>H_2</u>CH_2CN), 1.42 - 1.14 (m, 6H, hexyl, C<u>H_2</u>), 0.86 (t, $^3J_{H\text{–}H}$ = 6.7 Hz, 3H, C<u>H_3</u>).

^{13}C{^{1}H} NMR (75.563 MHz, $CDCl_3$, 27 °C): δ = 149.1 (N<u>*C*</u>CH_2), 135.2 (benzyl, *ipso*-<u>*C*</u>), 129.1 (aryl–<u>*C*</u>H), 128.6 (aryl–<u>*C*</u>H), 128.0 (aryl–<u>*C*</u>H), 120.6 (N<u>*C*</u>HCN), 54.0 (benzyl, <u>*C*</u>H_2N), 31.6 (hexyl, <u>*C*</u>H_2), 29.5 (NCCH_2<u>*C*</u>H_2), 29.0 (hexyl, <u>*C*</u>H_2), 25.8 (NC<u>*C*</u>H_2CH_2), 22.6 (hexyl, <u>*C*</u>H_2), 14.1 (<u>*C*</u>H_3).

HR–MS (ESI+, MeOH): *m*/*z* (%): 244.18076 (6.9) $[M+H]^+$, 266.16271 (6.4) $[M+Na]^+$, 282.13665 (9.3) $[M+K]^+$, 487.35414 (54.1) $[2M+H]^+$, 509.33594 (100.0) $[2M+Na]^+$, 525.31001 (31.9) $[2M+K]^+$.

calculated for $[C_{30}H_{42}N_6Na]^+$:	509.33631
found:	509.33594

Elemental Analysis (No. 31890)

calculated for $C_{15}H_{21}N_3$:	C 74.03 %, H 8.70 %, N 17.27 %
found:	C 74.12 %, H 8.80 %, N 17.25 %

Melting Point: 60 °C.

*6.3.6.4 2-(1-Benzyl-1*H*-1,2,3-triazol-4-yl)propan-2-ol* (**144**)

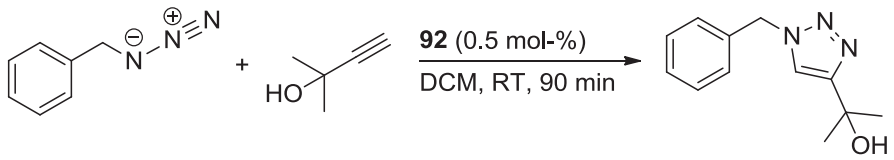

131 **144**

An aliquot of catalyst stock solution **B(iv)** (200 µl, 0.995 µmol) was filled into a GC vial equipped with a magnetic stir bar and diluted with absolute dichloromethane (100 µl) under inert gas. Substrate mixture **4** (200 µl, 0.202 mmol) was added *via* syringe. The reaction mixture was stirred at room temperature for 90 minutes. Then, the reaction mixture was diluted with dichloromethane (10 ml) and filtered over a glass Pasteur pipette filled with cotton and Celite (approximate height in a 2 ml pipette: 3 cm; rinsing with dichloromethane). The solvent was removed *in vacuo*. The NMR spectrum of the resulting solid showed a pure substance. In order to remove traces of inorganic impurities in the product, it was purified by column chromatography (silica gel, isopropanol:dichloromethane = 1:30, R_f = 0.38) to give a white crystalline solid (average yield of two independent runs: 42.0 mg, 0.193 mmol, 96 %). The analytic data was in accordance with the data presented in literature.[36, 177]

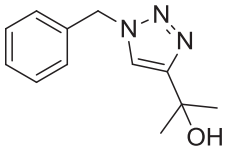

144

$C_{12}H_{15}N_3O$

M ($C_{12}H_{15}N_3O$) = 217.27 g mol^{-1}

^{1}H NMR (400.180 MHz, CD_2Cl_2, 25 °C): δ = 7.42 (s, 1H, NC*H*CN), 7.40 - 7.31 (m, 3H, aryl-C*H*), 7.31 - 7.12 (m, 2H, aryl-C*H*), 5.48 (s, 2H, CH_2), 2.83 (s, 1H, O*H*), 1.56 (s, 6H, CH_3)

^{13}C{^{1}H} NMR (100.625 MHz, CD_2Cl_2, 26 °C): δ = 156.4 (NCH*C*N), 135.5 (*ipso*-*C*, benzyl), 129.4 (aryl-*C*H), 128.9 (aryl-*C*H), 128.5 (aryl-*C*H), 119.6 (N*C*HCN), 68.6 (*C*(CH_3)$_2$OH), 54.4 (*C*H_2), 30.6 (*C*H_3)

The methylene group's ^{13}C signal coincides with the solvent signal, but can be identified with the help of a HSQC spectrum.

HR–MS (ESI+, MeOH): *m*/*z* (%): 218.12887 (0.5) $[M+H]^+$, 240.11087 (1.1) $[M+Na]^+$, 256.08490 (3.5) $[M+K]^+$, 457.23315 (100.0) $[2M+Na]^+$, 473.20754 (5.6) $[2M+K]^+$.

calculated for $[C_{24}H_{30}N_6O_2Na]^+$:	457.23224
found:	457.23315

Elemental Analysis (No. 31941)

calculated for $C_{12}H_{15}N_3O$:	C 66.34 %, H 6.96 %, N 19.34 %
found:	C 66.00 %, H 6.84 %, N 19.11 %

Melting Point: 83 °C.

*6.3.6.5 1-(Di-4-tolylmethyl)-4-phenyl-1*H*-1,2,3-triazole* (**145**)

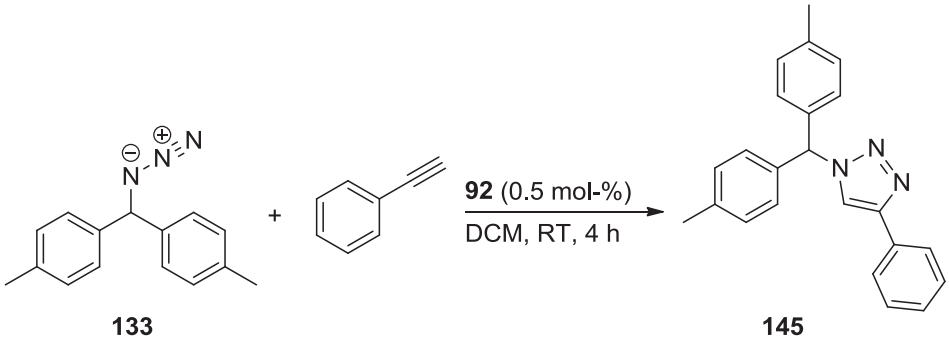

133 **145**

An aliquot of catalyst stock solution **B(iv)** (200 µl, 0.99 µmol) was filled into a GC vial equipped with a magnetic stir bar and diluted with absolute dichloromethane (100 µl) under inert gas. Substrate mixture **5** (200 µl, 0.203 mmol azide, 0.200 mmol alkyne) was added *via syringe*. The reaction mixture was stirred at room temperature for four hours. Then, the reaction mixture was diluted with dichloromethane (10 ml) and filtered over a glass Pasteur pipette filled with cotton and Celite (approximate height in a 2 ml pipette: 3 cm; rinsing with dichloromethane). The solvent was removed *in vacuo*. The NMR spectrum of the resulting solid showed a pure substance. In order to remove traces of inorganic impurities in the product, it was purified by column chromatography (silica gel, dichloromethane:petroleum ether = 10:1, R_f = 0.20) to give a white crystalline solid (average yield of two independent runs: 66.6 mg,

0.196 mmol, 98 %). The analytic data was in accordance with the data presented in literature.[24]

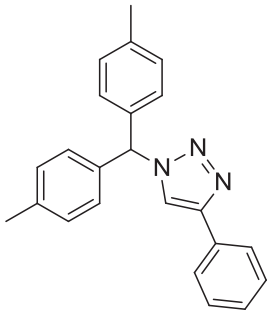

145

$C_{23}H_{21}N_3$

M ($C_{23}H_{21}N_3$) = 339.43 g mol^{-1}

^{1}H NMR (400.180 MHz, CD_2Cl_2, 26 °C)

δ = 7.80 (d, $^3J_{H–H}$ = 7.7 Hz, 2H, phenyl, *ortho*-C*H*), 7.69 (s, 1H, NC*H*CN), 7.41 (t, $^3J_{H-H}$ = 7.5 Hz, 2H, phenyl, *meta*-C*H*), 7.32 (t, $^3J_{H–H}$ = 7.3 Hz, 1H, phenyl, *para*-C*H*), 7.21 (d, $^3J_{H–H}$ = 7.8 Hz, 4H, tolyl, *ortho*-C*H*), 7.08 (d, $^3J_{H–H}$ = 7.8 Hz, 4H, tolyl, *meta*-C*H*), 7.04 (s, 1H, Tol_2C*H*), 2.37 (s, 6H, CH_3).

^{13}C{^{1}H} NMR (100.625 MHz, CD_2Cl_2, 26 °C)

δ = 147.5 (NCH*C*N), 138.9 (tolyl, *C*CH_3), 135.9 (tolyl, *ipso*–*C*), 131.2 (phenyl, *ipso*–*C*), 129.9 (tolyl, *meta*–*C*H), 129.2 (phenyl, *meta*-*C*H), 128.4 (phenyl, *para*-*C*H), 128.4 (tolyl, *ortho*–*C*H), 125.9 (phenyl, *ortho*–*C*H), 120.3 (N*C*HCN), 68.2 (Tol_2*C*H), 21.2 (*C*H_3).

HR–MS (ESI+, MeOH): *m*/*z* (%): 340.18100 (43.8) $[M+H]^+$, 362.16300 (37.0) $[M+Na]^+$, 378.13699 (19.0) $[M+K]^+$, 679.35513 (100.0) $[2M+H]^+$, 701.33697 (76.4) $[2M+Na]^+$, 717.31089 (77.7) $[2M+K]^+$.

calculated for $[C_{23}H_{22}N_3]^+$:	340.18137
found:	340.18100

Melting Point: 160 °C.

*6.3.6.6 Ethyl-1-(di-4-tolylmethyl)-1*H*-1,2,3-triazole-4-carboxylate* (**146**)

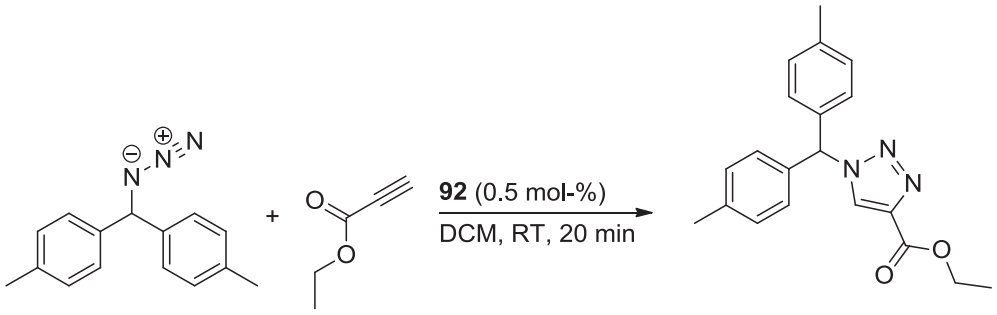

133 **146**

An aliquot of catalyst stock solution **B(iv)** (200 µl, 0.99 µmol) was filled into a GC vial equipped with a magnetic stir bar and diluted with absolute dichloromethane (100 µl) under inert gas. Substrate mixture **6** (200 µl, 0.20 mmol) was added *via syringe*. The reaction mixture was stirred at room temperature for 20 minutes. Then, the reaction mixture was diluted with dichloromethane (10 ml) and filtered over a glass Pasteur pipette filled with cotton and Celite (approximate height in a 2 ml pipette: 3 cm; rinsing with dichloromethane). The solvent was removed *in vacuo*. The NMR spectrum of the resulting solid showed a pure substance. In order to remove traces of inorganic impurities in the product, it was purified by column chromatography (silica gel, dichloromethane:petroleum ether = 10:1, R_f = 0.19) to give a colourless crystalline solid (average yield of two independent runs: 66.2 mg, 0.197 mmol, 95 %).

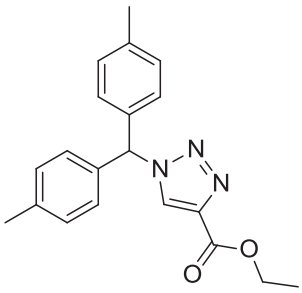

146

$C_{20}H_{21}N_3O_2$

M ($C_{20}H_{21}N_3O_2$) = 335.39964 g mol^{-1}

^{1}H NMR (400.180 MHz, CD_2Cl_2, 26 °C): δ = 7.92 (s, 1H, NC<u>H</u>CN), 7.20 (d, $^3J_{H\text{-}H}$ = 7.8 Hz, 4H, tolyl, *meta*-C<u>H</u>), 7.04 (s, 1H, Tol$_2$C<u>H</u>), 7.02 (d, $^3J_{H\text{-}H}$ = 7.8 Hz, 4H, tolyl, *ortho*–C<u>H</u>), 4.35 (q, $^3J_{H\text{-}H}$ = 7.1 Hz, 2H, H$_3$CC<u>H$_2$</u>), 2.36 (s, 6H, tolyl, C<u>H$_3$</u>), 1.35 (t, $^3J_{H\text{-}H}$ = 7.1 Hz, 3H, <u>H$_3$</u>CCH$_2$).

$^{13}C\{^1H\}$ NMR (100.625 MHz, CD_2Cl_2, 26 °C): δ = 161.0 (<u>C</u>OO), 140.1 (NCH<u>C</u>N), 139.2 (tolyl, <u>C</u>CH_3), 135.2 (tolyl, *ipso*-<u>C</u>), 130.0 (tolyl, *meta*-<u>C</u>H), 128.3 (tolyl, *ortho*-<u>C</u>H), 128.0 (N<u>C</u>HCN), 68.4 (Tol$_2$<u>C</u>H), 61.5 (H_3C<u>C</u>H_2), 21.2 (tolyl, <u>C</u>H_3), 14.5 (H_3<u>C</u>CH_2).

HR–MS (ESI+, MeOH): *m*/*z* (%):165.0695 (36.0) $[M\text{-}C_7H_{12}N_3O_2]^+$, 195.1164 (100.0) $[M\text{-}CO_2C_2H_5\text{-}HC_2N_3]^+$, 234.1281 (17.3) $[M\text{-}CO_2C_2H_5\text{-}N_2]^+$, 278.1182 (26.4) $[M\text{-}C_2H_5\text{-}N_2]^+$, 292.1338 (16.7) $[M\text{-}CH_3\text{-}N_2]^+$, 306.1443 (92.0) $[M\text{-}H\text{-}N_2]^+$, 320.1373 (1.1) $[M\text{-}CH_3]^+$, 335.1650 (0.8) $[M]^{\bullet+}$.

calculated for $[C_{20}H_{21}N_3O_2]^+$:	335.1628
found:	335.1650

IR (KBr) $\tilde{\nu}$ [cm^{-1}] = 3427 (br, m), 3117 (m), 3032 (w), 2981 (m), 2924 (w), 1902 (w), 1726 (s, C=O stretching mode), 1543 (m), 1514 (m), 1446 (m), 1394 (m), 1331 (m), 1300 (w), 1230 (s, C–O stretching mode), 1186 (m), 1155 (m), 1097 (w), 1043 (s, C-O stretching mode), 871 (w), 843 (w), 807 (w), 768 (s), 583 (w), 541 (w), 525 (w), 479 (w).

Elemental analysis (No. 32262)

calculated for $C_{20}H_{21}N_3O_2$:	C 71.62 %, H 6.31 %, N 12.53 %
found:	C 71.90 %, H 6.16 %, N 12.41 %

Melting Point: 118 °C.

7 Bibliography

[1] H. C. Kolb, M. G. Finn, K. B. Sharpless, *Angew. Chem.* **2001**, *113*, 2056-2075; *Angew. Chem. Int. Ed.* **2001**, *40*, 2004-2021.

[2] J. P. Guthrie, *Can. J. Chem.* **1978**, *56*, 962-973.

[3] a) K. C. Nicolaou, E. J. Sorensen, *Classics in Total Synthesis: Targets, Strategies, Methods*, VCH, Weinheim, New York, Basel **1996**; b) K. C. Nicolaou, S. A. Snyder, *Classics in Total Synthesis: More Targets, Strategies, Methods*, Wiley-VCH, Weinheim, **2003**.

[4] A. Michael, *Journal für Praktische Chemie* **1893**, *48*, 94-95.

[5] a) R. Huisgen, *Proceedings of the Chemical Society* **1961**, 357-396; b) R. Huisgen, *Angew. Chem.* **1963**, *75*, 604-637; *Angew. Chem. Int. Ed.* **1963**, *2*, 565-598; c) R. Huisgen, *Angew. Chem.* **1963**, *75*, 742-754; *Angew. Chem. Int. Ed.* **1963**, *2*, 633-645; d) R. Huisgen, G. Szeimies, L. Möbius, *Chem. Ber.* **1967**, *100*, 2494-2507.

[6] W. v. E. Doering, W. R. Roth, *Tetrahedron* **1962**, *18*, 67-74.

[7] R. A. Firestone, *J. Org. Chem.* **1968**, *33*, 2285-2290.

[8] R. Sustmann, *Pure Appl. Chem.* **1974**, *40*, 569-593.

[9] W. Kirmse, L. Horner, *Liebigs Ann. Chem.* **1958**, *614*, 1-3.

[10] J. E. Hein, V. V. Fokin, *Chem. Soc. Rev.* **2010**, *39*, 1302-1315.

[11] F. Himo, T. Lovell, R. Hilgraf, V. V. Rostovtsev, L. Noodleman, K. B. Sharpless, V. V. Fokin, *J. Am. Chem. Soc.* **2005**, *127*, 210-216.

[12] I. Fleming, *Molecular Orbitals and Organic Chemical Reactions*, reference ed., Wiley, Chichester, **2010**, pp. 303-307.

[13] I. Fleming, *Molecular Orbitals and Organic Chemical Reactions*, reference ed., Wiley, Chichester, **2010**, pp. 329-331.

[14] G. L'Abbé, *Bull. Soc. Chim. Belg.* **1984**, *93*, 579-592.

[15] C. W. Tornøe, C. Christensen, M. Meldal, *J. Org. Chem.* **2002**, *67*, 3057-3064.

[16] V. V. Rostovtsev, L. G. Green, V. V. Fokin, K. B. Sharpless, *Angew. Chem.* **2002**, *114*, 2708-2711; *Angew. Chem. Int. Ed.* **2002**, *41*, 2596-2599.

[17] W. G. Lewis, F. G. Magallon, V. V. Fokin, M. G. Finn, *J. Am. Chem. Soc.* **2004**, *126*, 9152-9153.

[18] V. O. Rodionov, V. V. Fokin, M. G. Finn, *Angew. Chem.* **2005**, *117*, 2250-2255; *Angew. Chem. Int. Ed.* **2005**, *44*, 2210-2215.

[19] V. D. Bock, H. Hiemstra, J. H. v. Maarseveen, *Eur. J. Org. Chem.* **2006**, 51-68.

[20] V. O. Rodionov, S. I. Presolski, D. Díaz Díaz, V. V. Fokin, M. G. Finn, *J. Am. Chem. Soc.* **2007**, *129*, 12705-12712.

[21] a) B. M. Mykhalichko, O. N. Temkin, M. G. Mys'kiv, *Russian Chemical Reviews* **2000**, *69*, 957-984; b) J. Diez, M. P. Gamasa, J. Gimeno, E. Lastra, A. Aguirre, S. García-Granda, *Organometallics* **1993**, *12*, 2213-2220.

[22] B. R. Buckley, S. E. Dann, H. Heaney, *Chem. Eur. J.* **2010**, *16*, 6278-6284.

[23] L. A. Goj, E. D. Blue, C. Munro-Leighton, T. B. Gunnoe, J. L. Petersen, *Inorg. Chem.* **2005**, *44*, 8647-8649.

[24] C. Nolte, P. Mayer, B. F. Straub, *Angew. Chemie* **2007**, *119*, 2147-2149; *Angew. Chem. Int. Ed.* **2007**, *46*, 2101-2103.

[25] B. T. Worrell, J. A. Malik, V. V. Fokin, *Science Express*, **2013**, DOI:10.1126/science.1229506.

[26] a) R. W. M. ten Hoedt, J. G. Noltes, G. van Koten, A. L. Spek, *J. Chem. Soc., Dalton Trans.* **1978**, 1800-1806; b) M. G. B. Drew, F. S. Esho, S. M. Nelson, *J. Chem. Soc., Chem. Commun.* **1982**, 1347-1348; c) L. Naldini, F. Demartin, M.

Manassero, M. Sansoni, G. Rassu, M. A. Zoroddu, *J. Organomet. Chem.* **1985**, *279*, c42-c44; d) M. P. Gamasa, J. Gimeno, E. Lastra, X. Solans, *J. Organomet. Chem.* **1988**, *346*, 277-286; e) D. M. Knotter, A. L. Spek, G. van Koten, *J. Chem. Soc., Chem. Commun.* **1989**, 1738-1740; f) M. P. Gamasa, J. Gimeno, E. Lastra, A. Aguirre, S. García-Granda, *J. Organomet. Chem.* **1989**, *378*, C11-C14; g) J. Diez, M. P. Gamasa, J. Gimeno, A. Aguirre, S. García-Granda, *Organometallics* **1991**, *10*, 380-382; h) D. M. Knotter, A. L. Spek, D. M. Grove, G. Van Koten, *Organometallics* **1992**, *11*, 4083-4090; i) V. W. W. Yam, W. K. Lee, T. F. Lai, *Organometallics* **1993**, *12*, 2383-2387; j) F. Olbrich, J. Kopf, E. Weiss, *Angew. Chem.* **1993**, *105*, 1136-1138; *Angew. Chem. Int. Ed.* **1993**, *32*, 1077-1079; k) A. J. Edwards, M. A. Paver, P. R. Raithby, M.-A. Rennie, C. A. Russell, D. S. Wright, *Organometallics* **1994**, *13*, 4967-4972; l) F. Olbrich, U. Behrens, E. Weiss, *J. Organomet. Chem.* **1994**, *472*, 365-370; m) K. Osakada, T. Takizawa, T. Yamamoto, *Organometallics* **1995**, *14*, 3531-3538; n) D. L. Reger, J. E. Collins, M. F. Huff, A. L. Rheingold, G. P. A. Yap, *Organometallics* **1995**, *14*, 5475-5477; o) M. D. Janssen, J. G. Donkervoort, S. B. van Berlekom, A. L. Spek, D. M. Grove, G. van Koten, *Inorg. Chem.* **1996**, *35*, 4752-4763; p) V. W.-W. Yam, W.-K. Lee, K.-K. Cheung, B. Crystall, D. Phillips, *J. Chem. Soc., Dalton Trans.* **1996**, 3283-3287; q) V. W.-W. Yam, W.-K. Lee, K.-K. Cheung, *J. Chem. Soc., Dalton Trans.* **1996**, 2335-2339; r) V. W.-W. Yam, S. W.-K. Choi, C.-L. Chan, K.-K. Cheung, *Chem. Commun.* **1996**, 2067-2068; s) V. W.-W. Yam, W.-K. Lee, K. K. Cheung, H.-K. Lee, W.-P. Leung, *J. Chem. Soc., Dalton Trans.* **1996**, 2889-2891; t) S. S. Y. Chui, M. F. Y. Ng, C.-M. Che, *Chem. Eur. J.* **2005**, *11*, 1739-1749; u) C. W. Baxter, T. C. Higgs, P. J. Bailey, S. Parsons, F. McLachlan, M. McPartlin, P. A. Tasker, *Chem. Eur. J.* **2006**, *12*, 6166-6174.

[27] C. E. Housecroft, A. G. Sharpe, *Inorganic Chemistry*, 2nd ed., Pearson, Prentice Hall, Harlow, England, **2005**.

[28] a) J. Miralles-Sabater, M. Merchan, I. Nebot-Gil, P. M. Viruela-Martin, *J. Phys. Chem.* **1988**, *92*, 4853-4859; b) M. Sodupe, C. W. Bauschlicher, *J. Phys. Chem.* **1991**, *95*, 8640-8645; c) Y. D. Hill, B. S. Freiser, C. W. Bauschlicher, *J. Am. Chem. Soc.* **1991**, *113*, 1507-1510; d) M. Böhme, T. Wagener, G. Frenking, *J. Organomet. Chem.* **1996**, *520*, 31-43.

[29] a) A. F. Holleman, E. Wiberg, *Lehrbuch der Anorganischen Chemie*, 101st ed., Walter de Gruyter, Berlin, New York, **1995**, p. 1842; b) H. Beyer, W. Walter, W. Francke, *Lehrbuch der Organischen Chemie*, 24th ed., S. Hirzel Verlag, Stuttgart, Leipzig, **2004**, pp. 98-100.

[30] P. H. Kasai, D. McLeod, T. Watanabe, *J. Am. Chem. Soc.* **1980**, *102*, 179-190.

[31] B. F. Straub, *Chem. Commun.* **2007**, 3868-3870.

[32] M. Ahlquist, V. V. Fokin, *Organometallics* **2007**, *26*, 4389-4391.

[33] D. Cantillo, M. Avalos, R. Babiano, P. Cintas, J. L. Jimenez, J. C. Palacios, *Organic & Biomolecular Chemistry* **2011**, *9*, 2952-2958.

[34] a) R. Nast, W. Pfab, *Chem. Ber.* **1956**, *89*, 415-421; b) D. Blake, G. Calvin, G. E. Coates, *Proceedings of the Chemical Society* **1959**, 396-397.

[35] B. R. Buckley, S. E. Dann, D. P. Harris, H. Heaney, E. C. Stubbs, *Chem. Commun.* **2010**, *46*, 2274-2276.

[36] P. Appukkuttan, W. Dehaen, V. V. Fokin, E. Van der Eycken, *Org. Lett.* **2004**, *6*, 4223-4225.

[37] G. Rothenberg, L. D. Pachón, J. H. van Maarseveen, *Adv. Synth. Catal.* **2005**, *347*, 811-815.

[38] G. Molteni, C. L. Bianchi, G. Marinoni, N. Santo, A. Ponti, *New J. Chem.* **2006**, *30*, 1137-1139.
[39] B. H. Lipshutz, B. R. Taft, *Angew. Chem.* **2006**, *118*, 8415-8418; *Angew. Chem. Int. Ed.* **2006**, *45*, 8235-8238.
[40] a) Q. Wang, T. R. Chan, R. Hilgraf, V. V. Fokin, K. B. Sharpless, M. G. Finn, *J. Am. Chem. Soc.* **2003**, *125*, 3192-3193; b) A. E. Speers, G. C. Adam, B. F. Cravatt, *J. Am. Chem. Soc.* **2003**, *125*, 4686-4687.
[41] F. Fazio, M. C. Bryan, O. Blixt, J. C. Paulson, C.-H. Wong, *J. Am. Chem. Soc.* **2002**, *124*, 14397-14402.
[42] M. Meldal, C. W. Tornøe, *Chem. Rev.* **2008**, *108*, 2952-3015.
[43] a) Z.-Y. Yan, Y.-B. Zhao, M.-J. Fan, W.-M. Liu, Y.-M. Liang, *Tetrahedron* **2005**, *61*, 9331-9337; b) Y.-M. Wu, J. Deng, X. Fang, Q.-Y. Chen, *J. Fluorine Chem.* **2004**, *125*, 1415-1423.
[44] a) T. Hasegawa, M. Umeda, M. Numata, T. Fujisawa, S. Haraguchi, K. Sakurai, S. Shinkai, *Chem. Lett.* **2006**, *35*, 82-83; b) T. Hasegawa, M. Umeda, M. Numata, C. Li, A.-H. Bae, T. Fujisawa, S. Haraguchi, K. Sakurai, S. Shinkai, *Carbohydr. Res.* **2006**, *341*, 35-40.
[45] K. A. Kalesh, K. Liu, S. Q. Yao, *Organic & Biomolecular Chemistry* **2009**, *7*, 5129-5136.
[46] S. Díez-González, *Catal. Sci. Technol.* **2011**, *1*, 166-178.
[47] H. Gao, G. Louche, B. S. Sumerlin, N. Jahed, P. Golas, K. Matyjaszewski, *Macromolecules* **2005**, *38*, 8979-8982.
[48] G. Barré, D. Taton, D. Lastécouères, J.-M. Vincent, *J. Am. Chem. Soc.* **2004**, *126*, 7764-7765.
[49] N. Candelon, D. Lastécouères, A. K. Diallo, J. R. Aranzaez, D. Astruc, J.-M. Vincent, *Chem. Commun.* **2008**, 741-743.
[50] J.-C. Meng, V. V. Fokin, M. G. Finn, *Tetrahedron Lett.* **2005**, *46*, 4543-4546.
[51] T. Lin, Z. Chen, R. Usha, C. V. Stauffacher, J.-B. Dai, T. Schmidt, J. E. Johnson, *Virology* **1999**, *265*, 20-34.
[52] K. B. Sharpless, T. R. Chan, R. Hilgraf, V. V. Fokin, *Org. Lett.* **2004**, *6*, 2853-2855.
[53] S. Özçubukçu, E. Ozkal, C. Jimeno, M. A. Pericàs, *Org. Lett.* **2009**, *11*, 4680-4683.
[54] P. S. Donnelly, S. D. Zanatta, S. C. Zammit, J. M. White, S. J. Williams, *Chem. Commun.* **2008**, 2459-2461.
[55] V. O. Rodionov, S. I. Presolski, S. Gardinier, Y.-H. Lim, M. G. Finn, *J. Am. Chem. Soc.* **2007**, *129*, 12696-12704.
[56] S. I. Presolski, V. Hong, S.-H. Cho, M. G. Finn, *J. Am. Chem. Soc.* **2010**, *132*, 14570-14576.
[57] H. M. J. Hendriks, J. M. W. L. Birker, J. Van Rijn, G. C. Verschoor, J. Reedijk, *J. Am. Chem. Soc.* **1982**, *104*, 3607-3617.
[58] F. Wang, H. Fu, Y. Jiang, Y. Zhao, *Green Chemistry* **2008**, *10*, 452-456.
[59] H. Isobe, T. Fujino, N. Yamazaki, M. Guillot-Nieckowski, E. Nakamura, *Org. Lett.* **2008**, *10*, 3729-3732.
[60] P. Fabbrizzi, S. Cicchi, A. Brandi, E. Sperotto, G. v. Koten, *Eur. J. Org. Chem.* **2009**, 5423-5430.
[61] a) I. G. Dance, *Polyhedron* **1986**, *5*, 1037-1104; b) R. V. Parish, Z. Salehi, R. G. Pritchard, *Angew. Chem.* **1997**, *109*, 276-278; *Angew. Chem. Int. Ed.* **1997**, *36*, 251-253; c) K. Fujisawa, S. Imai, N. Kitajima, Y. Moro-oka, *Inorg. Chem.* **1998**, *37*, 168-169; d) D. Li, T. Wu, X.-P. Zhou, R. Zhou, X.-C. Huang, *Angew. Chem.* **2005**, *117*, 4247-4250; *Angew. Chem. Int. Ed.* **2005**, *44*, 4175-4178.

[62] F. Pérez-Balderas, M. Ortega-Muñoz, J. Morales-Sanfrutos, F. Hernández-Mateo, F. G. Calvo-Flores, J. A. Calvo-Asín, J. Isac-García, F. Santoyo-González, *Org. Lett.* **2003**, *5*, 1951-1954.
[63] S. Lal, S. Díez-González, *J. Org. Chem.* **2011**, *76*, 2367-2373.
[64] D. Wang, N. Li, M. Zhao, W. Shi, C. Ma, B. Chen, *Green Chemistry* **2010**, *12*, 2120-2123.
[65] D. Wang, M. Zhao, X. Liu, Y. Chen, N. Li, B. Chen, *Organic & Biomolecular Chemistry* **2012**, *10*, 229-231.
[66] S. Lal, J. McNally, A. J. P. White, S. Díez-González, *Organometallics* **2011**, *30*, 6225-6232.
[67] W. A. Herrmann, *Angew. Chem.* **2002**, *114*, 1342-1363; *Angew. Chem. Int. Ed.* **2002**, *41*, 1290-1309.
[68] a) S. P. Nolan, S. Díez-González, A. Correa, L. Cavallo, *Chem. Eur. J.* **2006**, *12*, 7558-7564; b) S. Díez-González, E. C. Escudero-Adán, J. Benet-Buchholz, E. D. Stevens, A. M. Z. Slawin, S. P. Nolan, *Dalton Trans.* **2010**, *39*, 7595-7606.
[69] S. Díez-González, E. D. Stevens, S. P. Nolan, *Chem. Commun.* **2008**, 4747-4749.
[70] M.-L. Teyssot, A. Chevry, M. Traïkia, M. El-Ghozzi, D. Avignant, A. Gautier, *Chem. Eur. J.* **2009**, *15*, 6322-6326.
[71] M.-L. Teyssot, L. Nauton, J.-L. Canet, F. Cisnetti, A. Chevry, A. Gautier, *Eur. J. Org. Chem.* **2010**, *2010*, 3507-03515.
[72] a) S. Díez-González, N. M. Scott, S. P. Nolan, *Organometallics* **2006**, *25*, 2355-2358; b) S. Díez-González, E. D. Stevens, N. M. Scott, J. L. Petersen, S. P. Nolan, *Chem. Eur. J.* **2008**, *14*, 158-168.
[73] S. Díez-González, S. P. Nolan, *Angew. Chem.* **2008**, *120*, 9013-9016; *Angew. Chem. Int. Ed.* **2008**, *47*, 8881-8884.
[74] C. Shao, G. Cheng, D. Su, J. Xu, X. Wang, Y. Hu, *Adv. Synth. Catal.* **2010**, *352*, 1587-1592.
[75] a) R. D. Mounts, T. Ogura, Q. Fernando, *Inorg. Chem.* **1974**, *13*, 802-805; b) M. G. B. Drew, D. A. Edwards, R. Richards, *J. Chem. Soc., Chem. Commun.* **1973**, 124-125; c) T. Ogura, R. D. Mounts, Q. Fernando, *J. Am. Chem. Soc.* **1973**, *95*, 949-951.
[76] a) D. C. Owsley, C. E. Castro, *Organic Synthesis* **1972**, *52*, 128-130; b) I. Bae, H. Han, S. Chang, *J. Am. Chem. Soc.* **2005**, *127*, 2038-2039.
[77] D. B. Ramachary, C. F. Barbas, *Chem. Eur. J.* **2004**, *10*, 5323-5331.
[78] a) N. Stephanopoulos, M. B. Francis, *Nat Chem Biol* **2011**, *7*, 876-884; b) J. Kalia, R. T. Raines, *Curr. Org. Chem.* **2010**, *14*, 138-147.
[79] a) E. M. Sletten, C. R. Bertozzi, *Acc. Chem. Res.* **2011**, *44*, 666-676; b) E. M. Sletten, C. R. Bertozzi, *Angew. Chem.* **2009**, *121*, 7108-7133; *Angew. Chem. Int. Ed.* **2008**, *48*, 6974–6998.
[80] a) T. Carell, J. Gierlich, G. A. Burley, P. M. E. Gramlich, D. M. Hammond, *Org. Lett.* **2006**, *8*, 3639-3642; b) F. Seela, V. R. Sirivolu, *Chem. Biodiversity* **2006**, *3*, 509-514; c) P. M. E. Gramlich, S. Warncke, J. Gierlich, T. Carell, *Angew. Chem.* **2008**, *120*, 3491-3493; *Angew. Chem. Int. Ed*. **2008**, *47*, 3442-3444.
[81] a) N. K. Devaraj, G. P. Miller, W. Ebina, B. Kakaradov, J. P. Collman, E. T. Kool, C. E. D. Chidsey, *J. Am. Chem. Soc.* **2005**, *127*, 8600-8601; b) R. L. Weller, S. R. Rajski, *Org. Lett.* **2005**, *7*, 2141-2144.
[82] K. E. Beatty, F. Xie, Q. Wang, D. A. Tirrell, *J. Am. Chem. Soc.* **2005**, *127*, 14150-14151.

[83] S. Dedola, S. A. Nepogodiev, R. A. Field, *Organic & Biomolecular Chemistry* **2007**, *5*, 1006-1017.
[84] K. D. Bodine, D. Y. Gin, M. S. Gin, *J. Am. Chem. Soc.* **2004**, *126*, 1638-1639.
[85] Y. Li, J. Yang, B. C. Benicewicz, *J. Polym. Sci., Part A: Polym. Chem.* **2007**, *45*, 4300-4308.
[86] P. Wu, A. K. Feldman, A. K. Nugent, C. J. Hawker, A. Scheel, B. Voit, J. Pyun, J. M. J. Fréchet, K. B. Sharpless, V. V. Fokin, *Angew. Chem.* **2004**, *116*, 4018-4022; *Angew. Chem. Int. Ed.* **2004**, *43*, 3928–3932.
[87] J. P. Collman, N. K. Devaraj, C. E. D. Chidsey, *Langmuir* **2004**, *20*, 1051-1053.
[88] A. Brik, J. Muldoon, Y.-C. Lin, J. H. Elder, D. S. Goodsell, A. J. Olson, V. V. Fokin, K. B. Sharpless, C.-H. Wong, *ChemBioChem* **2003**, *4*, 1246-1248.
[89] Y.-M. Wu, J. Deng, Y. Li, Q.-Y. Chen, *Synthesis* **2005**, 1314-1318.
[90] X. Zhang, R. P. Hsung, H. Li, *Chem. Commun.* **2007**, 2420-2422.
[91] L. Li, G. Zhang, A. Zhu, L. Zhang, *J. Org. Chem.* **2008**, *73*, 3630-3633.
[92] J. E. Hein, J. C. Tripp, L. B. Krasnova, K. B. Sharpless, V. V. Fokin, *Angew. Chem.* **2009**, *121*, 8162-8165; *Angew. Chem. Int. Ed.* **2009**, *48*, 8018-8021.
[93] B. H. M. Kuijpers, G. C. T. Dijkmans, S. Groothuys, P. J. L. M. Quaedflieg, R. H. Blaauw, F. L. van Delft, F. P. J. T. Rutjes, *Synlett* **2005**, *2005*, 3059-3062.
[94] L. Zhang, X. Chen, P. Xue, H. H. Y. Sun, I. D. Williams, K. B. Sharpless, V. V. Fokin, G. Jia, *J. Am. Chem. Soc.* **2005**, *127*, 15998-15999.
[95] B. C. Boren, S. Narayan, L. K. Rasmussen, L. Zhang, H. Zhao, Z. Lin, G. Jia, V. V. Fokin, *J. Am. Chem. Soc.* **2008**, *130*, 8923-8930.
[96] a) S. Schoffelen, M. H. L. Lambermon, M. B. v. Eldijk, J. C. M. v. Hest, *Bioconjugate Chem.* **2008**, *19*, 1127-1131; b) E. Lallana, R. Riguera, E. Fernandez-Megia, *Angew. Chem.* **2011**, *123*, 8956-8966; *Angew. Chem. Int. Ed.* **2011**, *50*, 8794–8804; c) A. Kumar, K. Li, C. Cai, *Chem. Commun.* **2011**, *47*, 3186-3188.
[97] G. J. Brewer, *Chem. Res. Toxicol.* **2009**, *23*, 319-326.
[98] G. Wittig, A. Krebs, *Chem. Ber.* **1961**, *94*, 3260-3275.
[99] a) H. Meier, H. Petersen, H. Kolshorn, *Chem. Ber.* **1980**, *113*, 2398-2409; b) R. B. Turner, A. D. Jarrett, P. Goebel, B. J. Mallon, *J. Am. Chem. Soc.* **1973**, *95*, 790-792; c) K. J. Shea, J. S. Kim, *J. Am. Chem. Soc.* **1992**, *114*, 4846-4855.
[100] N. J. Agard, J. A. Prescher, C. R. Bertozzi, *J. Am. Chem. Soc.* **2004**, *126*, 15046-15047.
[101] a) N. J. Agard, J. M. Baskin, J. A. Prescher, A. Lo, C. R. Bertozzi, *ACS Chemical Biology* **2006**, *1*, 644-648; b) J. M. Baskin, J. A. Prescher, S. T. Laughlin, N. J. Agard, P. V. Chang, I. A. Miller, A. Lo, J. A. Codelli, C. R. Bertozzi, *Proceedings of the National Academy of Sciences* **2007**, *104*, 16793-16797; c) J. A. Codelli, J. M. Baskin, N. J. Agard, C. R. Bertozzi, *J. Am. Chem. Soc.* **2008**, *130*, 11486-11493.
[102] E. M. Sletten, C. R. Bertozzi, *Org. Lett.* **2008**, *10*, 3097-3099.
[103] X. Ning, J. Guo, M. A. Wolfert, G.-J. Boons, *Angew. Chem.* **2008**, *120*, 2285-2287; *Angew. Chem. Int. Ed.* **2008**, *47*, 2253-2255.
[104] J. Dommerholt, S. Schmidt, R. Temming, L. J. A. Hendriks, F. P. J. T. Rutjes, J. C. M. van Hest, D. J. Lefeber, P. Friedl, F. L. van Delft, *Angew. Chem.* **2010**, *122*, 9612-9615; *Angew. Chem. Int.. Ed.* **2010**, *49*, 9422-9425.
[105] S. S. van Berkel, A. J. Dirks, M. F. Debets, F. L. van Delft, J. J. L. M. Cornelissen, R. J. M. Nolte, F. P. J. T. Rutjes, *ChemBioChem* **2007**, *8*, 1504-1508.

[106] S. T. Laughlin, J. M. Baskin, S. L. Amacher, C. R. Bertozzi, *Science* **2008**, *320*, 664-667.
[107] S. K. Mamidyala, M. G. Finn, *Chem. Soc. Rev.* **2010**, *39*, 1252-1261.
[108] a) W. G. Lewis, L. G. Green, F. Grynszpan, Z. Radić, P. R. Carlier, P. Taylor, M. G. Finn, K. B. Sharpless, *Angew. Chem.* **2002**, *114*, 1095-1099; *Angew. Chem. Int. Ed.* **2002**, *41*, 1053-1057; b) R. Manetsch, A. Krasiński, Z. Radić, J. Raushel, P. Taylor, K. B. Sharpless, H. C. Kolb, *J. Am. Chem. Soc.* **2004**, *126*, 12809-12818.
[109] a) V. P. Mocharla, B. Colasson, L. V. Lee, S. Röper, K. B. Sharpless, C.-H. Wong, H. C. Kolb, *Angew. Chem.* **2005**, *117*, 118-122; *Angew. Chem. Int. Ed.* **2005**, *44*, 116-120; b) J. Wang, G. Sui, V. P. Mocharla, R. J. Lin, M. E. Phelps, H. C. Kolb, H.-R. Tseng, *Angew. Chem.* **2006**, *118*, 5402-5407; *Angew. Chem. Int. Ed.* **2006**, *45*, 5276-5281.
[110] M. Whiting, J. Muldoon, Y.-C. Lin, S. M. Silverman, W. Lindstrom, A. J. Olson, H. C. Kolb, M. G. Finn, K. B. Sharpless, J. H. Elder, V. V. Fokin, *Angew. Chem.* **2006**, *118*, 1463-1467; *Angew. Chem. Int. Ed.* **2006**, *45*, 1435–1439.
[111] T. Hirose, T. Sunazuka, A. Sugawara, A. Endo, K. Iguchi, T. Yamamoto, H. Ui, K. Shiomi, T. Watanabe, K. B. Sharpless, S. Omura, *J. Antibiot.* **2009**, *62*, 277-282.
[112] a) M. Bessel, B. F. Straub, F. Rominger, *Synthesis* **2010**, *9*, 1459-1466; b) M. Bessel, *PhD Thesis*, *Rationales Design von Katalysatoren für die Kupfer-katalysierte Azid-Alkin-Cycloaddition*, Prof. B. F. Straub, Ruprecht-Karls-University Heidelberg (Germany), **2013**.
[113] "Eine eindeutige Charakterisierung der Substanz war nicht möglich, weil die Reinigung der Verbindung nicht gelang und deshalb Nebenprodukte mitgeführt wurden." (M. Bessel, *PhD thesis*, Ruprecht-Karls-Universität Heidelberg (Germany), **2010**, p. 236).
[114] N. P. Mankad, T. G. Gray, D. S. Laitar, J. P. Sadighi, *Organometallics* **2004**, *23*, 1191-1193.
[115] a) L. Jafarpour, E. D. Stevens, S. P. Nolan, *J. Organomet. Chem.* **2000**, *606*, 49-54; b) A. J. Arduengo, R. Krafczyk, R. Schmutzler, H. A. Craig, J. R. Goerlich, W. J. Marshall, M. Unverzagt, *Tetrahedron* **1999**, *55*, 14523-14534.
[116] L. Hintermann, *Beilstein Journal of Organic Chemistry* **2007**, *3*, 22.
[117] H. Beyer, W. Walter, W. Francke, *Lehrbuch der Organischen Chemie*, 24th ed., S. Hirzel Verlag, Stuttgart, Leipzig, **2004**, pp. 648-650.
[118] a) L. Farrugia, *J. Appl. Crystallogr.* **1997**, *30*, 565; b)
[119] The author has only obtained 43 % yield, but the yield of this reaction could be increased to 82 % by C. Loos in the group of Prof. B. F. Straub.
[120] S. C. Holm, A. F. Siegle, C. Loos, F. Rominger, B. F. Straub, *Synthesis* **2010**, 2278-2286.
[121] K. Singh, J. R. Long, P. Stavropoulos, *J. Am. Chem. Soc.* **1997**, *119*, 2942-2943.
[122] a) P. K. Mehrotra, R. Hoffmann, *Inorg. Chem.* **1978**, *17*, 2187-2189; b) C. Kölmel, R. Ahlrichs, *J. Phys. Chem.* **1990**, *94*, 5536-5542.
[123] a) R. D. Köhn, G. Seifert, Z. Pan, M. F. Mahon, G. Kociok-Köhn, *Angew. Chem.* **2003**, *115*, 818-820; *Angew. Chem. Int. Ed.* **2003**, *42*, 793-796; b) X.-M. Zhang, Z.-M. Hao, H.-S. Wu, *Inorg. Chem.* **2005**, *44*, 7301-7303; c) G. M. Chiarella, D. Y. Melgarejo, A. Rozanski, P. Hempte, L. M. Perez, C. Reber, J. P. Fackler Jr, *Chem. Commun.* **2010**, *46*, 136-138; d) J. E. O'Connor, G. A. Janusonis, E. R. Corey, *Chemical Communications (London)* **1968**, 445-446; e) E. Hartmann, J. Strähle, *Z. Anorg. Allg. Chem.* **1990**, *583*, 31-40; f) J. Beck,

J. Strähle, *Angew. Chem.* **1985**, *97*, 419-420; *Angew. Chem. Int. Ed.* **1985**, *24*, 409-410; g) K. M. Merz, R. Hoffmann, *Inorg. Chem.* **1988**, *27*, 2120-2127.
[124] C. Janiak, *Moderne Anorganische Chemie*, 3rd ed. (Ed.: E. Riedel), Walter de Gruyter, Berlin, New York, **2007**, pp. 695-696.
[125] A. Siegle, *Bachelor Thesis*, Prof. B. F. Straub, Ruprecht-Karls-Universität Heidelberg (Germany), **2009**.
[126] S. Seitz, *PhD Thesis*, *Thiolfunktionalisierte 1,2,4-Triazoliumsalze als NHC-Vorläufer*, Prof. B. F. Straub, Ruprecht-Karls-University Heidelberg (Germany), **2013**.
[127] CCDC 869464 contains the supplementary crystallographic data for this strcuture. This data can be obtained free of charge from the Cambridge Crystallographic Data Centre *via* www.ccdc.cam.ac.uk/data_request/cif.
[128] This compound had first been synthesized by M. Sc. Ella Schreiner in the course of her master thesis (June - November 2011) by applying the author's procedure for the synthesis of 1,1'-[1,3-phenylenebis(methylene)]-bis[4-(2,4,6-trimethylphenyl)-1*H*-1,2,4-triazolium] dichloride to the reaction of 4-(3,5-dimethylphenyl)-4*H*-1,2,4-triazole with 1,2-dibromoethane (E. Schreiner, *Master Thesis*, Prof. B. F. Straub, Ruprecht-Karls-Universität Heidelberg (Germany), **2011**, 56-57).
[129] This procedure has not been optimized and the author is of the opinion that major improvements are feasible.
[130] T. Steiner, *Angew. Chem.* **2002**, *114*, 50-80; *Angew. Chem. Int. Ed.* **2002**, *41*, 48-76.
[131] M. Kirsten, *PhD Thesis*, *Organokatalyse: Theoretische Untersuchungen zur Claisen-Umlagerung und zum Einfluss von Azolen auf die Morita-Baylis-Hillman-Reaktion sowie neuartige Bis(carben)metallkomplexe auf der Basis von Triazolen*, Prof. T. Straßner, Technische Universität Dresden (Germany), **2010**.
[132] C. Dietrich, *Bachelor Thesis*, Prof. B. F. Straub, Ruprecht-Karls-Universität Heidelberg (Germany), **2011**.
[133] This compound had first been synthesized by M. Sc. Ella Schreiner in the course of her master thesis (E. Schreiner, *Master Thesis*, Prof. B. F. Straub, Ruprecht-Karls-Universität Heidelberg (Germany), **2011**, 61-62). CCDC 869466 contains the supplementary crystallographic data for this structure. This data can be obtained free of charge from the Cambridge Crystallographic Data Centre *via* www.ccdc.cam.ac.uk/data_request/cif.
[134] CCDC 869465 contains the supplementary crystallographic data for this strucure. This data can be obtained free of charge from the Cambridge Crystallographic Data Centre *via* www.ccdc.cam.ac.uk/data_request/cif.
[135] J. R. Miecznikowski, R. H. Crabtree, *Organometallics* **2004**, *23*, 629-631.
[136] E. Schreiner, *Master Thesis*, Prof. B. F. Straub, Ruprecht-Karls-Universität Heidelberg (Germany), **2011**.
[137] This compound had first been synthesized by M. Sc. Ella Schreiner in the course of her master thesis (E. Schreiner, *Master Thesis*, Prof. B. F. Straub, Ruprecht-Karls-Universität Heidelberg (Germany), **2011**, 64-65). CCDC 869467 contains the supplementary crystallographic data for this structure. This data can be obtained free of charge from the Cambridge Crystallographic Data Centre *via* www.ccdc.cam.ac.uk/data_request/cif.
[138] CCDC 869467 contains the supplementary crystallographic data for this structure. This data can be obtained free of charge from The Cambridge Crystallographic Data Centre *via* www.ccdc.cam.ac.uk/data_request/cif.

[139] J. Straub, *Master Thesis*, Prof. B. F. Straub, Ruprecht-Karls-Universität Heidelberg (Germany), **2012**.
[140] CCDC 869468 contains the supplementary crystallographic data for this strucure. This data can be obtained free of charge from the Cambridge Crystallographic Data Centre *via* www.ccdc.cam.ac.uk/data_request/cif.
[141] Commercially available benzyl azide is reported to contain unidentified trace impurities with an inhibitory effect on CuAAC reactions (*J. Am. Chem. Soc.* **2007**, *129*, 12705-12712). Therefore, benzyl azide was synthesized following the procedures in *Org. Biomol. Chem*. **2008**, *6*, 3461-3463 and stored at 4 °C under inert gas in the dark.
[142] F. G. Bordwell, *Acc. Chem. Res.* **1988**, *21*, 456-463.
[143] Y. Fujii, H. Yamada, M. Mizuta, *J. Phys. Chem.* **1988**, *92*, 6768-6772.
[144] H. O. House, M. J. Umen, *J. Org. Chem.* **1973**, *38*, 3893-3901.
[145] a) M. Kinugasa, S. Hashimoto, *J. Chem. Soc., Chem. Commun.* **1972**, 466-467; b) L. K. Ding, W. J. Irwin, *J. Chem. Soc., Perkin Trans. 1* **1976**, 2382-2386.
[146] J. Marco-Contelles, *Angew. Chem.* **2004**, *116*, 2248-2250; *Angew. Chem. Int. Ed.* **2004**, *43*, 2198-2200.
[147] M. Miura, M. Enna, K. Okuro, M. Nomura, *J. Org. Chem.* **1995**, *60*, 4999-5004.
[148] A. Basak, S. C. Ghosh, T. Bhowmich, A. K. Das, V. Bertolasi, *Tetrahedron Lett.* **2002**, *43*, 5499-5501.
[149] M.-C. Ye, J. Zhou, Z.-Z. Huang, Y. Tang, *Chem. Commun.* **2003**, 2554-2555.
[150] a) M. M. C. Lo, G. C. Fu, *J. Am. Chem. Soc.* **2002**, *124*, 4572-4573; b) R. Shintani, G. C. Fu, *Angew. Chem.* **2003**, *115*, 4216-4219; *Angew. Chem. Int. Ed.* **2003**, *42*, 4082-4085.
[151] M. I. Page, *The Chemistry of β-Lactams*, Blackie Academic & Professional, **1992**.
[152] a) R. M. Claramunt, J. Elguero, *Org. Prep. Proced. Int.* **1991**, *23*, 273-320; b) L. N. Jungheim, S. K. Sigmund, *J. Org. Chem.* **1987**, *52*, 4007-4013.
[153] a) R. Huisgen, R. Fleischmann, A. Eckell, *Tetrahedron Lett.* **1960**, *1*, 1-4; b) R. Huisgen, A. Eckell, *Tetrahedron Lett.* **1960**, *1*, 5-8; c) H. Dorn, A. Otto, *Chem. Ber.* **1968**, *101*, 3287-3301; d) H. Dorn, A. Otto, *Angew. Chem.* **1968**, *80*, 196; *Angew. Chem. Int. Ed.* **1968**, *7*, 214-215.
[154] a) T.-H. Chuang, K. B. Sharpless, *Helv. Chim. Acta* **2000**, *83*, 1734-1743; b) C. Turk, J. Svete, B. Stanovnik, L. Golič, S. Golič-Grdadolnik, A. Golobič, L. Selič, *Helv. Chim. Acta* **2001**, *84*, 146-156; c) I. Panfil, Z. Urbańczyk-Lipkowska, K. Suwińska, J. Solecka, M. Chmielewski, *Tetrahedron* **2002**, *58*, 1199-1212.
[155] a) R. Shintani, G. C. Fu, *J. Am. Chem. Soc.* **2003**, *125*, 10778-10779; b) L. M. Stanley, M. P. Sibi, *Chem. Rev.* **2008**, *108*, 2887-2902.
[156] a) S. J. George, Z. Cui, M. Razavet, C. J. Pickett, *Chem. Eur. J.* **2002**, *8*, 4037-4046; b) J. A. Wright, L. Webster, A. Jablonskyte, P. M. Woi, S. K. Ibrahim, C. J. Pickett, *Faraday Discuss.* **2011**, *148*, 359-371; c) M. Muthusamy, E. A. Ambundo, S. J. George, S. J. Lippard, R. N. F. Thorneley, *J. Am. Chem. Soc.* **2003**, *125*, 11150-11151; d) S. J. George, G. A. Ashby, C. W. Wharton, R. N. F. Thorneley, *J. Am. Chem. Soc.* **1997**, *119*, 6450-6451; e) *Optics & Laser Technology* **1996**, *28*, iii-viii.
[157] R. A. Nyquist, S. Fiedler, *Vib. Spectrosc.* **1994**, *7*, 149-162.
[158] K. Sivakumar, F. Xie, B. M. Cash, S. Long, H. N. Barnhill, Q. Wang, *Org. Lett.* **2004**, *6*, 4603-4606.

[159] M. G. Gore, S. P. Bottomley, *Spectrophotometry And Spectrofluorimetry: A Practical Approach*, 2nd ed. (Ed.: M. G. Gore), Oxford University Press, Oxford, **2000**, pp. 209-264.
[160] a) G. Papini, M. Pellei, G. Gioia Lobbia, A. Burini, C. Santini, *Dalton Transactions* **2009**, 6985-6990; b) L.-A. Schaper, S. J. Hock, W. A. Herrmann, F. E. Kühn, *Angew. Chem.* **2013**, *125*, 284-304; *Angew. Chem. Int. Ed.* **2013**, *52*, 270–289.
[161] T. Fischer, *Bachelor Thesis*, Prof. B. F. Straub, Ruprecht-Karls-Universität Heidelberg (Germany), **2012**.
[162] D. F. Shriver, M. A. Drezdon, *The Manipulation of Air-Sensitive Compounds, Vol. 2*, John Wiley & Sons, **1986**.
[163] G. R. Fulmer, A. J. M. Miller, N. H. Sherden, H. E. Gottlieb, A. Nudelman, B. M. Stoltz, J. E. Bercaw, K. I. Goldberg, *Organometallics* **2010**, *29*, 2176-2179.
[164] a) A. M. Heyns, *Spectrochim. Acta* **1977**, *33A*, 315-322; b) I. S. Perelygin, M. A. Klimchuk, *Zhurnal Prikladnoi Spektroskopii* **1989**, *50*, 280-285.
[165] G. M. Sheldrick, *Bruker Analytical X-Ray-Division*, Madison, Wisconsin **2008**.
[166] G. M. Sheldrick, *Acta Cryst.* **2008**, *A64*, 112-122.
[167] (IPr)CuOAc was first synthesized by the group of J. P. Sadighi. However, the herein presented synthesis differs from their route presented in Organometallics **2004**, *23*, 1191-1193.
[168] This procedure was developed on the basis of the synthesis of 1-(3-chloropropyl)-4-(2,6-dimethylphenyl)-1*H*-1,2,4-triazolium bromide as reported in S. C. Holm, A. F. Siegle, C. Loos, F. Rominger, B. F. Straub, *Synthesis* **2010**, 2278-2286.
[169] W. A. Herrmann, C. Köcher, L. J. Gooßen, G. R. J. Artus, *Chem. Eur. J.* **1996**, *2*, 1627-1636.
[170] R. H. Archer, J. R. Carpenter, S.-J. Hwang, A. W. Burton, C.-Y. Chen, S. I. Zones, M. E. Davis, *Chem. Mater.* **2010**, *22*, 2563-2572.
[171] L. Campbell-Verduyn, P. H. Elsinga, L. Mirfeizi, R. A. Dierckx, B. L. Feringa, *Organic & Biomolecular Chemistry* **2008**, *6*, 3461-3463.
[172] J. F. Norris, C. Banta, *J. Am. Chem. Soc.* **1928**, *50*, 1804-1808.
[173] Di-4-tolylmethanol was synthesized by M. Bessel in the course of his PhD project in the group of Prof. B. F. Straub, Ruprecht-Karls-Universität Heidelberg (Germany).
[174] a) R. Gompper, *Chem. Ber.* **1957**, *90*, 382-386; b) K. Kacprzak, *Synlett* **2005**, 943-946.
[175] S. T. Abu-Orabi, M. A. Atfah, I. Jibril, F. M. Mari'i, A. A.-S. Ali, *J. Heterocycl. Chem.* **1989**, *26*, 1461-1468.
[176] M. Iwasaki, H. Yorimitsu, K. Oshima, *Chem. As. J.* **2007**, *2*, 1430-1435.
[177] F. Moulin, *Helv. Chim. Acta* **1952**, *35*, 167-180.

Highly Active Dinuclear Copper Catalysts for Homogeneous Azide-Alkyne Cycloadditions

Supplementary Information

Forschungspraktika und Bachelorarbeit

Im Verlauf dieser Doktorarbeit wurden M. Sc. Lena Hahn (Organisch-Chemisches Fortgeschrittenenpraktikum, November 2010 - Januar 2011, “Synthesis of a Dinuclear Bis-NHC-Copper(I) Complex as Potential Catalyst for the Azide-Alkyne-Cycloaddition“, Kürzel: LH) und M. Sc. Steffen Mader (Organisch-Chemisches Fortgeschrittenenpraktikum, August 2011 - November 2011, „Dinukleare Kupferkomplexe als Katalysatoren für die Azid-Alkin-Cycloaddition“, Kürzel: SM) als Forschungspraktikanten sowie die Bachelorarbeit von B. Sc. Christine Dietrich (Mai - Juni 2011, „Ligandensynthese für die Klick-Reaktion“, Kürzel: CC) betreut.

Supplementary Information

1 NMR Spectra

1.1 Synthesis of (IPr)CuOAc

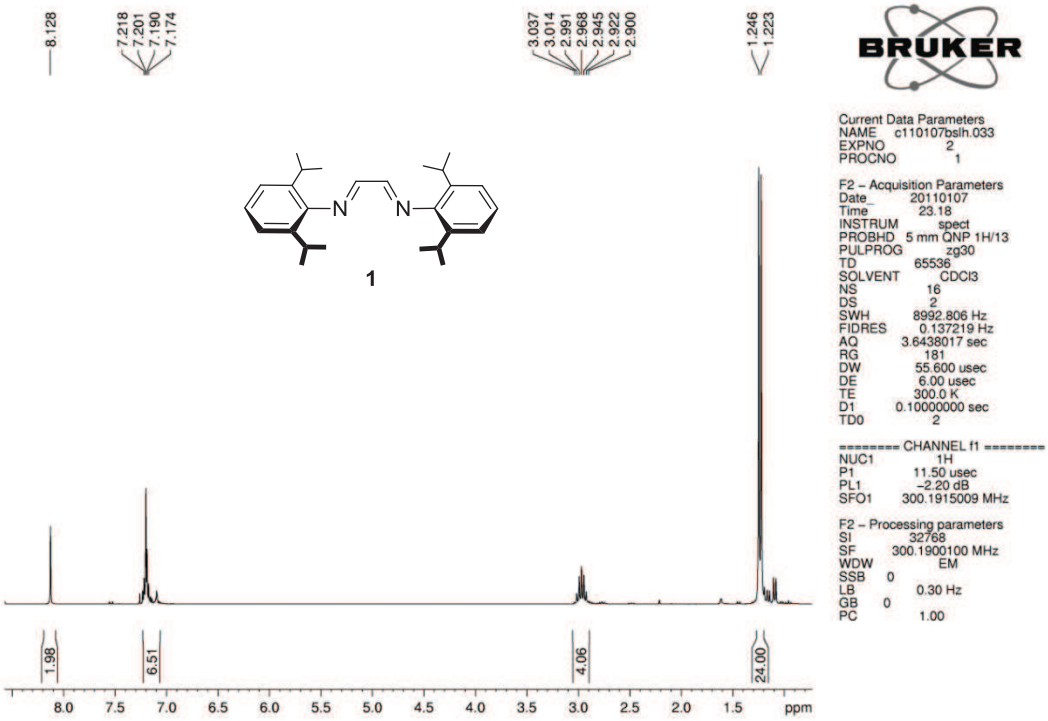

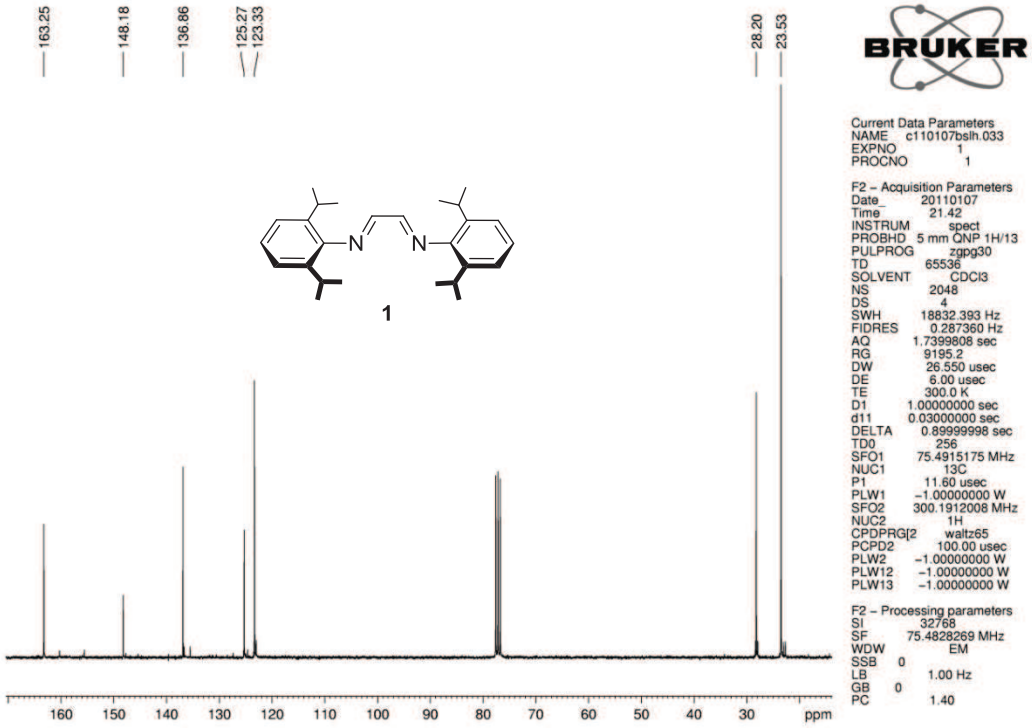

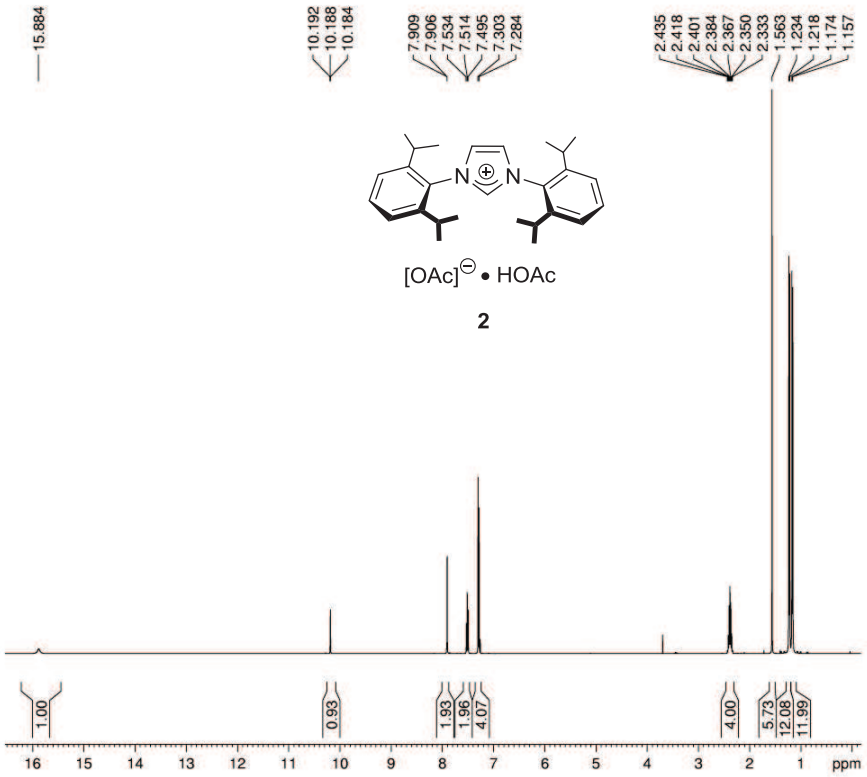

$[OAc]^{\ominus} \bullet HOAc$

2

BRUKER

Current Data Parameters
NAME c121102bsrb.053
EXPNO 2
PROCNO 1

F2 – Acquisition Parameters
Date_ 20121102
Time 8.51
INSTRUM spect
PROBHD 5 mm CPPBBO BB
PULPROG zg30
TD 65536
SOLVENT CDCl3
NS 40
DS 2
SWH 12019.230 Hz
FIDRES 0.183399 Hz
AQ 2.7262976 sec
RG 40.3
DW 41.600 usec
DE 12.00 usec
TE 298.0 K
D1 0.50000000 sec
TD0 5

======== CHANNEL f1 ========
SFO1 400.1820009 MHz
NUC1 1H
P1 11.50 usec
PLW1 10.00000000 W

F2 – Processing parameters
SI 65536
SF 400.1800137 MHz
WDW EM
SSB 0
LB 0.30 Hz
GB 0
PC 1.00

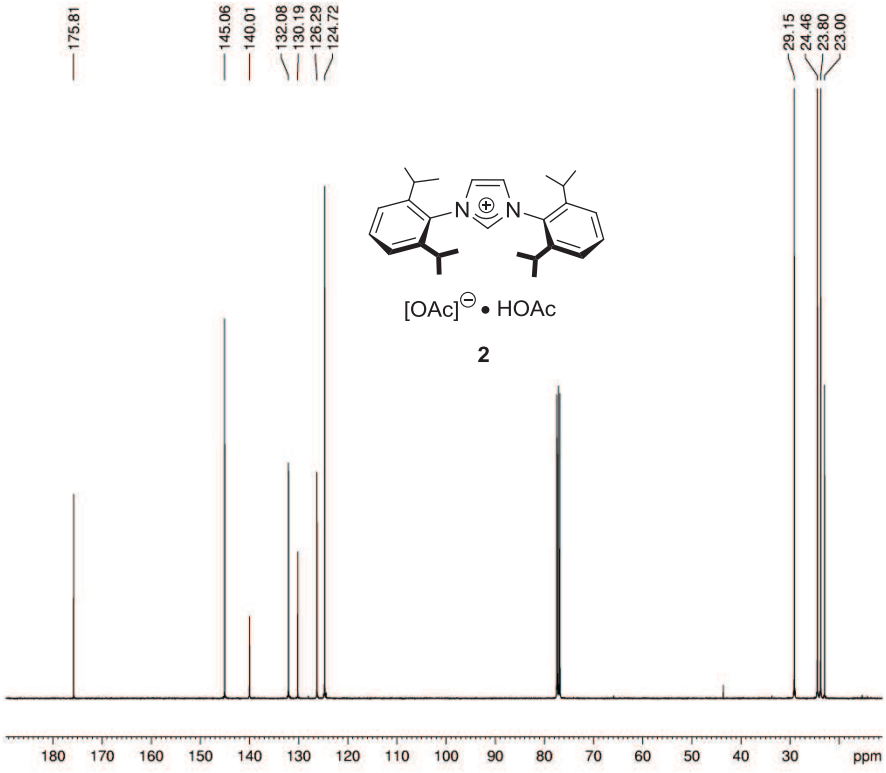

$[OAc]^{\ominus} \bullet HOAc$

2

BRUKER

Current Data Parameters
NAME c121102bsrb.053
EXPNO 1
PROCNO 1

F2 – Acquisition Parameters
Date_ 20121102
Time 7.02
INSTRUM spect
PROBHD 5 mm CPPBBO BB
PULPROG zgpg30
TD 98132
SOLVENT CDCl3
NS 2048
DS 2
SWH 30864.197 Hz
FIDRES 0.314517 Hz
AQ 1.5897384 sec
RG 2050
DW 16.200 usec
DE 20.00 usec
TE 298.0 K
D1 1.50000000 sec
D11 0.03000000 sec
TD0 256

======== CHANNEL f1 ========
SFO1 100.6364098 MHz
NUC1 13C
P1 10.00 usec
PLW1 45.00000000 W

======== CHANNEL f2 ========
SFO2 400.1816007 MHz
NUC2 1H
CPDPRG[2 waltz65
PCPD2 90.00 usec
PLW2 10.00000000 W
PLW12 0.16327000 W
PLW13 0.13225000 W

F2 – Processing parameters
SI 65536
SF 100.6253341 MHz
WDW EM
SSB 0
LB 1.00 Hz
GB 0
PC 1.40

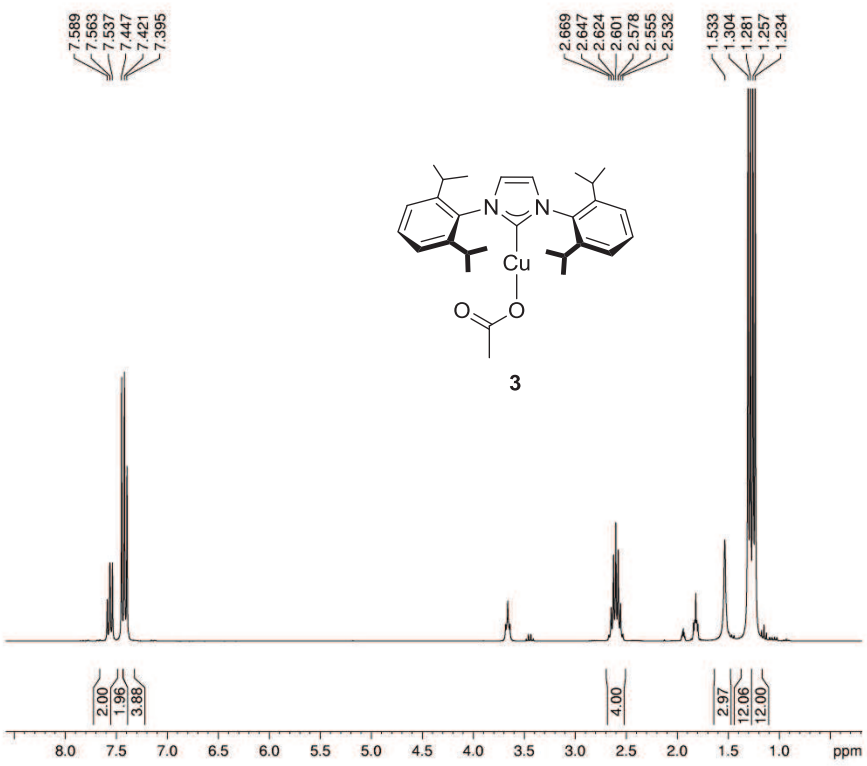

BRUKER

Current Data Parameters
NAME a120301bsrb316
EXPNO 1
PROCNO 1

F2 – Acquisition Parameters
Date_ 20120301
Time 21.53
INSTRUM spect
PROBHD 5 mm PABBO BB–
PULPROG zg30
TD 65536
SOLVENT CD3CN
NS 16
DS 2
SWH 9014.423 Hz
FIDRES 0.137549 Hz
AQ 3.6350634 sec
RG 40.3
DW 55.467 usec
DE 6.50 usec
TE 300.0 K
D1 0.10000000 sec
TD0 2

======== CHANNEL f1 ========
NUC1 1H
P1 9.80 usec
PLW1 16.00000000 W
SFO1 300.5115025 MHz

F2 – Processing parameters
SI 65536
SF 300.5100119 MHz
WDW EM
SSB 0
LB 0.30 Hz
GB 0
PC 1.00

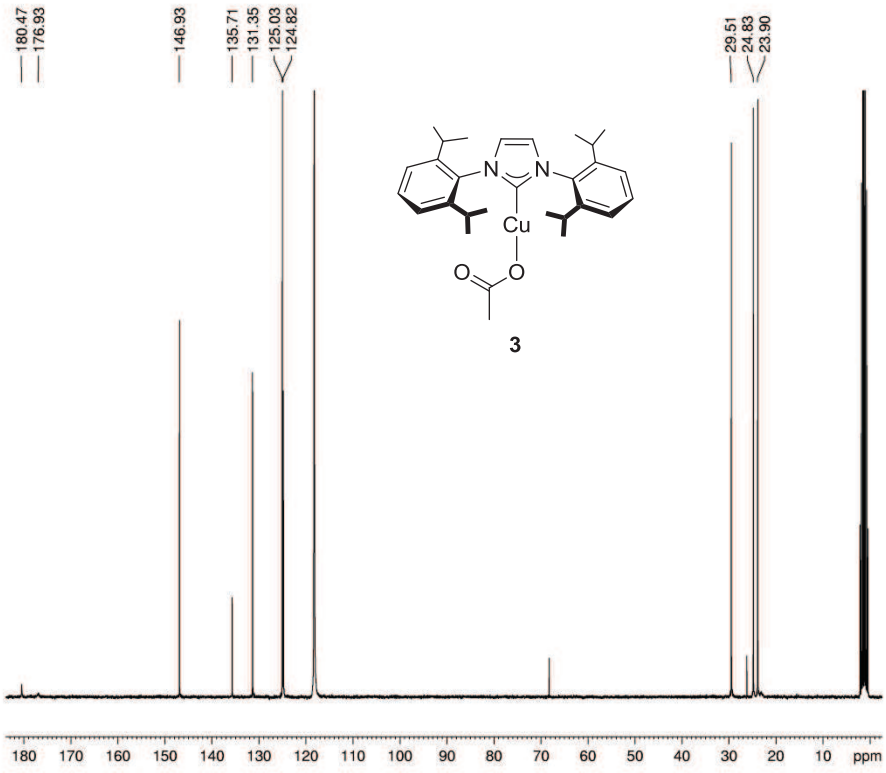

BRUKER

Current Data Parameters
NAME b121203bsrb.316
EXPNO 1
PROCNO 1

F2 – Processing parameters
SI 65536
SF 75.4676772 MHz
WDW EM
SSB 0
LB 1.00 Hz
GB 0
PC 1.40

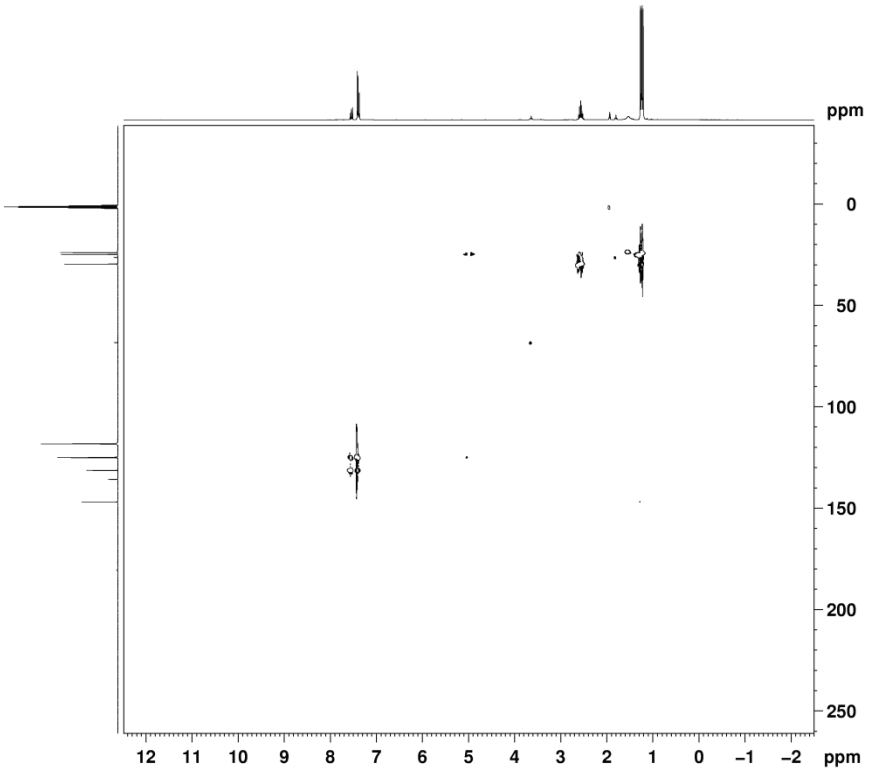

Current Data Parameters
NAME b121203bsrb.316
EXPNO 3
PROCNO 1

F1 – Acquisition parameters
TD 256
SFO1 75.47605 MHz
FIDRES 88.376694 Hz
SW 299.756 ppm
FnMODE Echo–Antiecho

F2 – Processing parameters
SI 1024
SF 300.1300029 MHz
WDW QSINE
SSB 2
LB 0 Hz
GB 0
PC 1.40

F1 – Processing parameters
SI 1024
MC2 echo–antiecho
SF 75.4676604 MHz
WDW QSINE
SSB 2
LB 0 Hz
GB 0

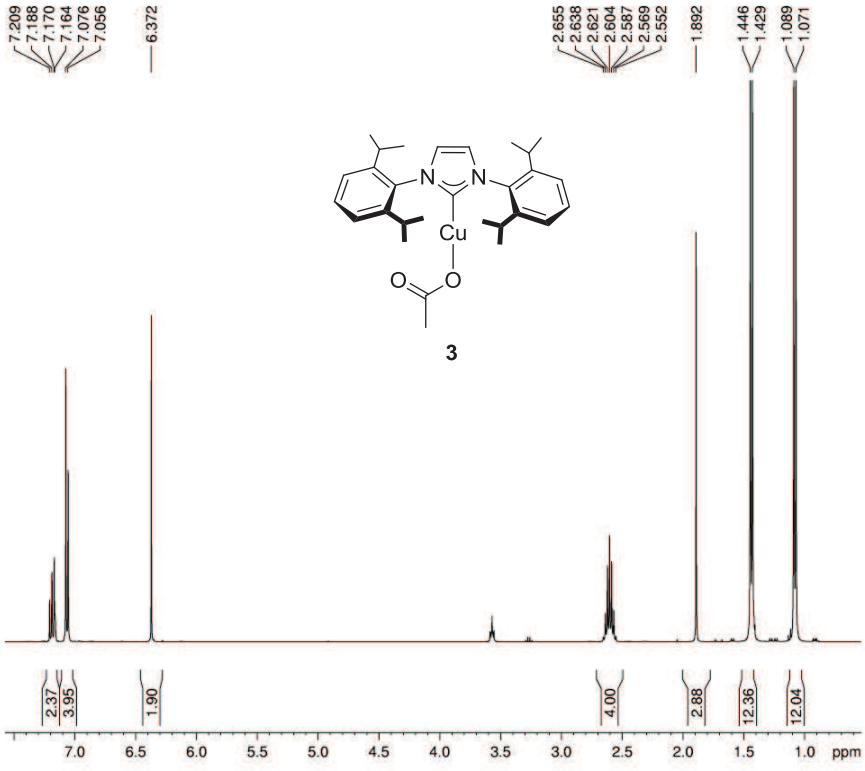

Current Data Parameters
NAME c130118bsrb.316
EXPNO 2
PROCNO 1

F2 – Acquisition Parameters
Date_ 20130120
Time 17.33
INSTRUM spect
PROBHD 5 mm CPPBBO BB
PULPROG zg30
TD 65536
SOLVENT C6D6
NS 128
DS 2
SWH 12019.230 Hz
FIDRES 0.183399 Hz
AQ 2.7262976 sec
RG 40.3
DW 41.600 usec
DE 12.00 usec
TE 298.0 K
D1 0.50000000 sec
TD0 16

======== CHANNEL f1 ========
SFO1 400.1820009 MHz
NUC1 1H
P1 11.50 usec
PLW1 10.00000000 W

F2 – Processing parameters
SI 65536
SF 400.1799990 MHz
WDW EM
SSB 0
LB 0.30 Hz
GB 0
PC 1.00

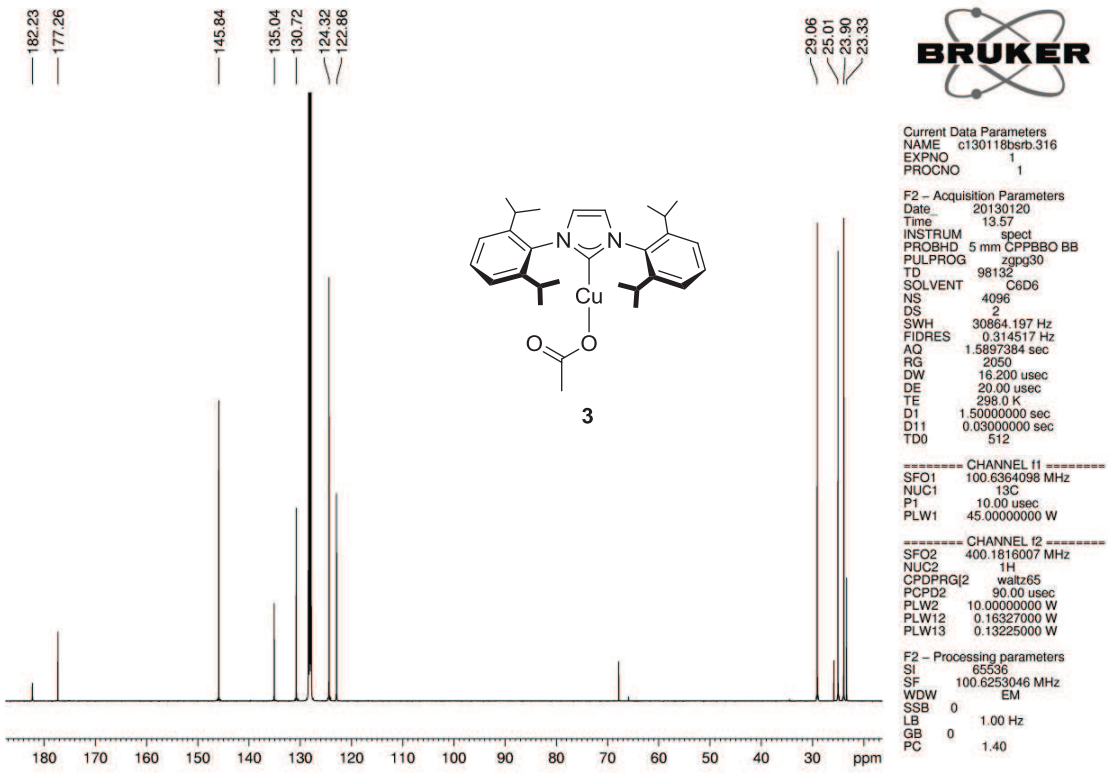
182.23
177.26
145.84
135.04
130.72
124.32
122.86
29.06
25.01
23.90
23.33
Cu
O
O
N
N
3
180 170 160 150 140 130 120 110 100 90 80 70 60 50 40 30 ppm
BRUKER
Current Data Parameters
NAME c130118bsrb.316
EXPNO 1
PROCNO 1
F2 – Acquisition Parameters
Date_ 20130120
Time 13.57
INSTRUM spect
PROBHD 5 mm CPPBBO BB
PULPROG zgpg30
TD 98132
SOLVENT C6D6
NS 4096
DS 2
SWH 30864.197 Hz
FIDRES 0.314517 Hz
AQ 1.5897384 sec
RG 2050
DW 16.200 usec
DE 20.00 usec
TE 298.0 K
D1 1.50000000 sec
D11 0.03000000 sec
TD0 512
======== CHANNEL f1 ========
SFO1 100.6364098 MHz
NUC1 13C
P1 10.00 usec
PLW1 45.00000000 W
======== CHANNEL f2 ========
SFO2 400.1816007 MHz
NUC2 1H
CPDPRG[2 waltz65
PCPD2 90.00 usec
PLW2 10.00000000 W
PLW12 0.16327000 W
PLW13 0.13225000 W
F2 – Processing parameters
SI 65536
SF 100.6253046 MHz
WDW EM
SSB 0
LB 1.00 Hz
GB 0
PC 1.40

1.2 3,3'-[1,3-Phenylenebis(methylene)]bis[1-(2,6-dimethylphenyl)-4,5-dihydro-1*H*-imidazol-3-ium] Bis(hexafluorophosphate)

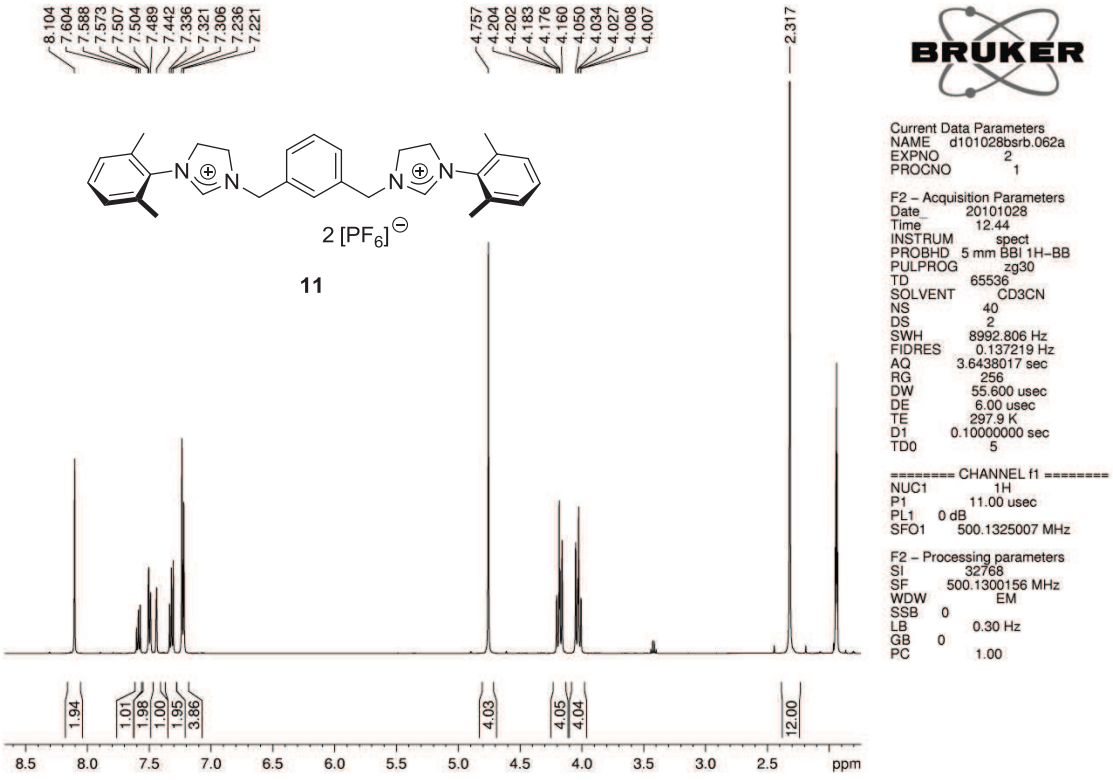

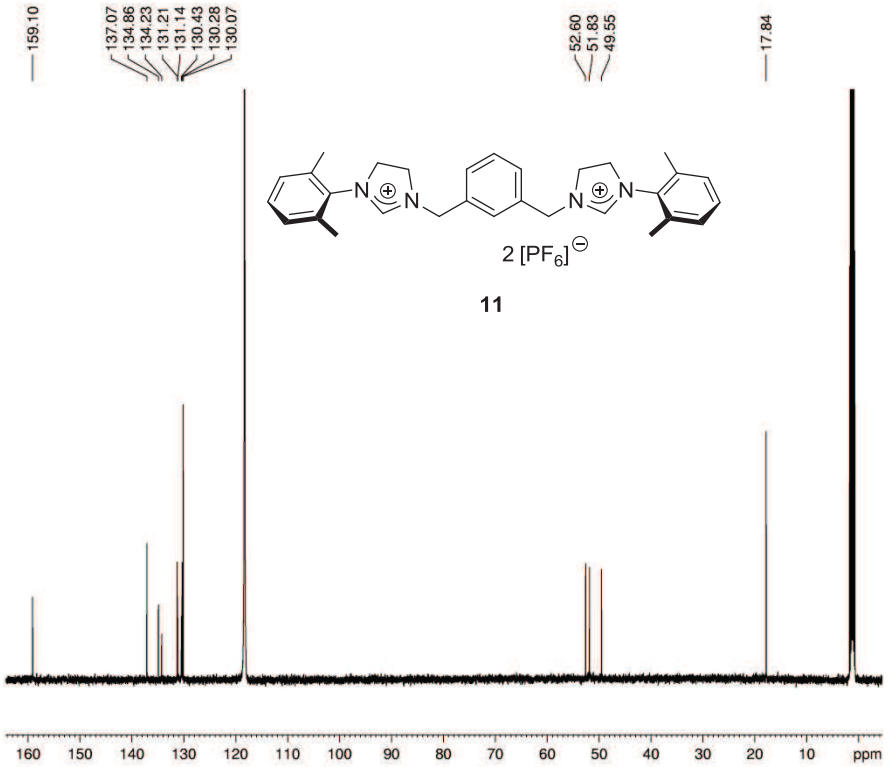

Current Data Parameters
NAME d101028bsrb.062a
EXPNO 1
PROCNO 1

F2 – Acquisition Parameters
Date_ 20101028
Time 10.25
INSTRUM spect
PROBHD 5 mm BBI 1H-BB
PULPROG zgpg30
TD 131072
SOLVENT CD3CN
NS 2600
DS 4
SWH 31446.541 Hz
FIDRES 0.239918 Hz
AQ 2.0840447 sec
RG 8192
DW 15.900 usec
DE 20.00 usec
TE 298.0 K
D1 1.00000000 sec
d11 0.03000000 sec
DELTA 0.89999998 sec
TD0 512
SFO1 125.7716224 MHz
NUC1 13C
P1 16.45 usec
PLW1 −1.00000000 W
SFO2 500.1320005 MHz
NUC2 1H
CPDPRG[2 waltz16
PCPD2 80.00 usec
PLW2 −1.00000000 W
PLW12 −1.00000000 W
PLW13 −1.00000000 W

F2 – Processing parameters
SI 65536
SF 125.7576688 MHz
WDW EM
SSB 0
LB 1.00 Hz
GB 0
PC 1.40

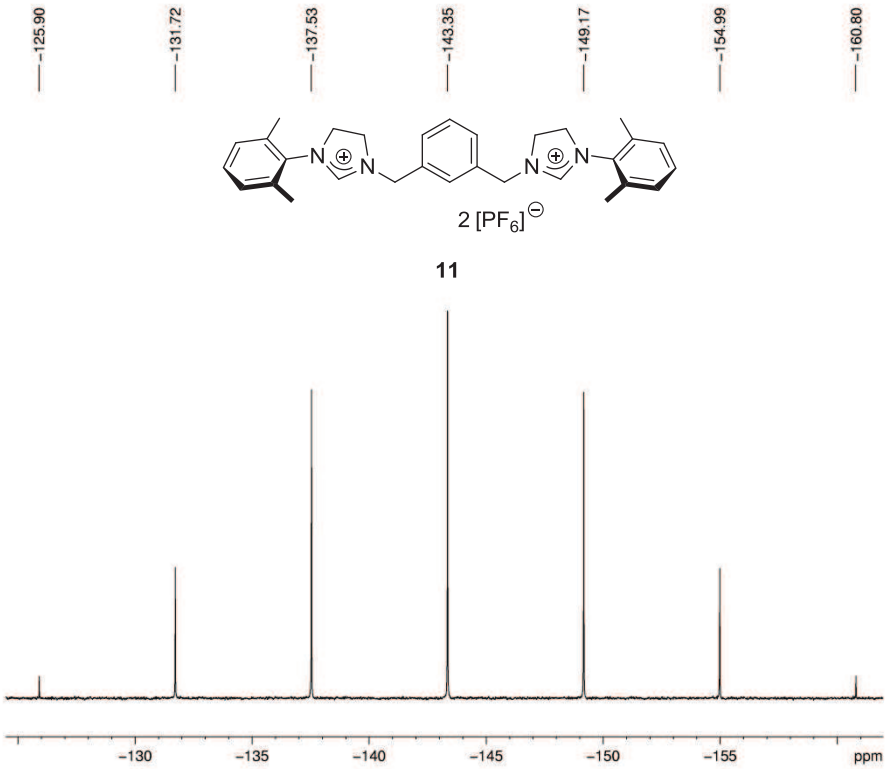

Current Data Parameters
NAME b101001bsrb.054
EXPNO 1
PROCNO 1

F2 – Processing parameters
SI 65536
SF 121.4947010 MHz
WDW EM
SSB 0
LB 1.00 Hz
GB 0
PC 1.40

1.3 4-Aryl-1,2,4-triazoles

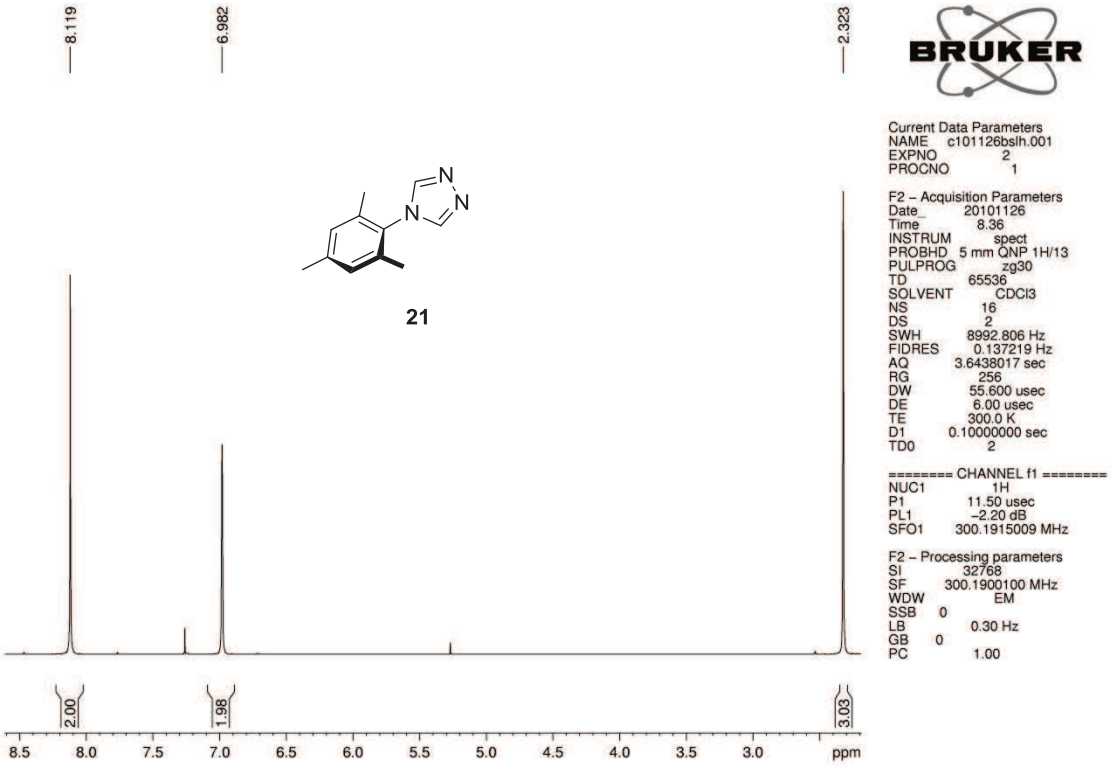

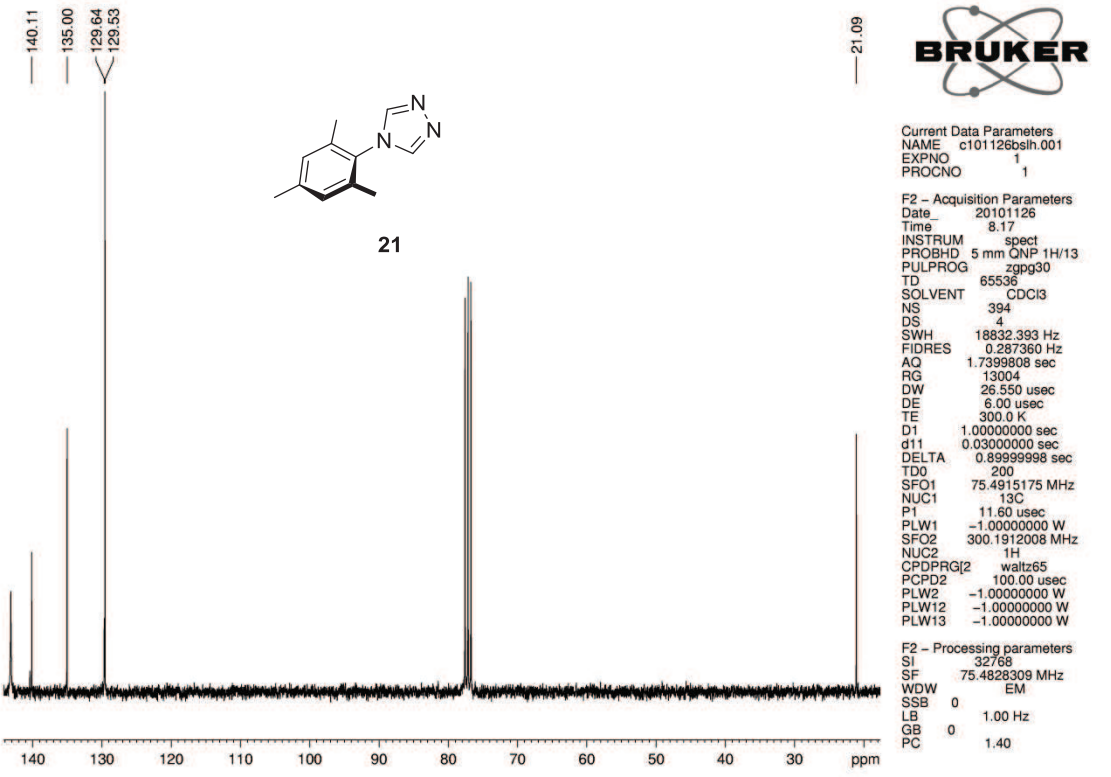

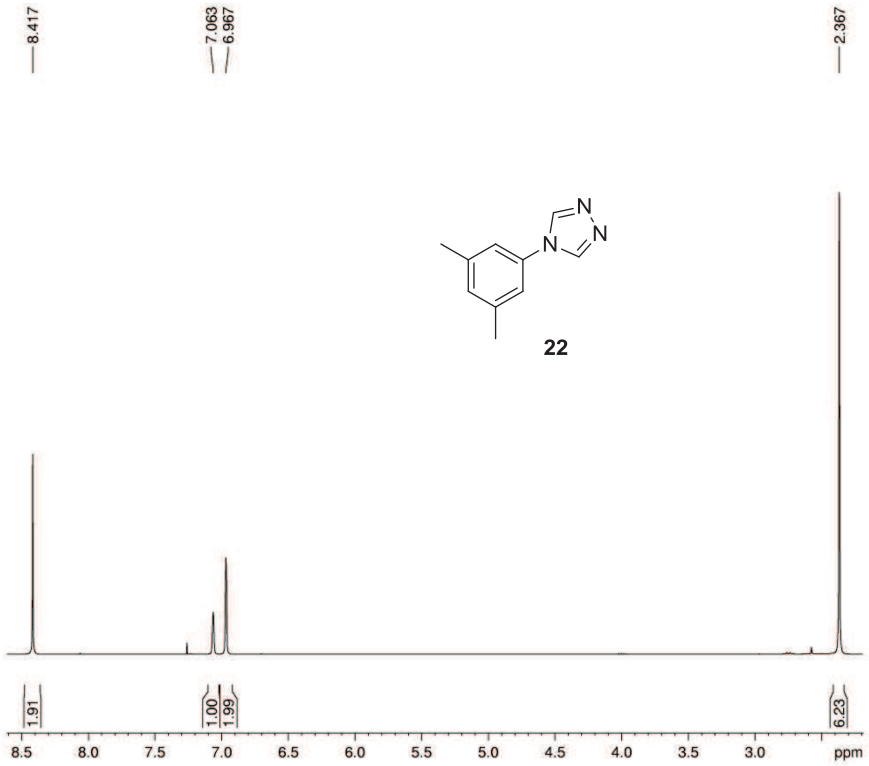

22

BRUKER

Current Data Parameters
NAME c101210bslh.007
EXPNO 2
PROCNO 1

F2 – Acquisition Parameters
Date_ 20101211
Time 10.53
INSTRUM spect
PROBHD 5 mm QNP 1H/13
PULPROG zg30
TD 65536
SOLVENT CDCl3
NS 32
DS 2
SWH 8992.806 Hz
FIDRES 0.137219 Hz
AQ 3.6438017 sec
RG 287.4
DW 55.600 usec
DE 6.00 usec
TE 300.0 K
D1 0.10000000 sec
TD0 4

======== CHANNEL f1 ========
NUC1 1H
P1 11.50 usec
PL1 -2.20 dB
SFO1 300.1915009 MHz

F2 – Processing parameters
SI 32768
SF 300.1900103 MHz
WDW EM
SSB 0
LB 0.30 Hz
GB 0
PC 1.00

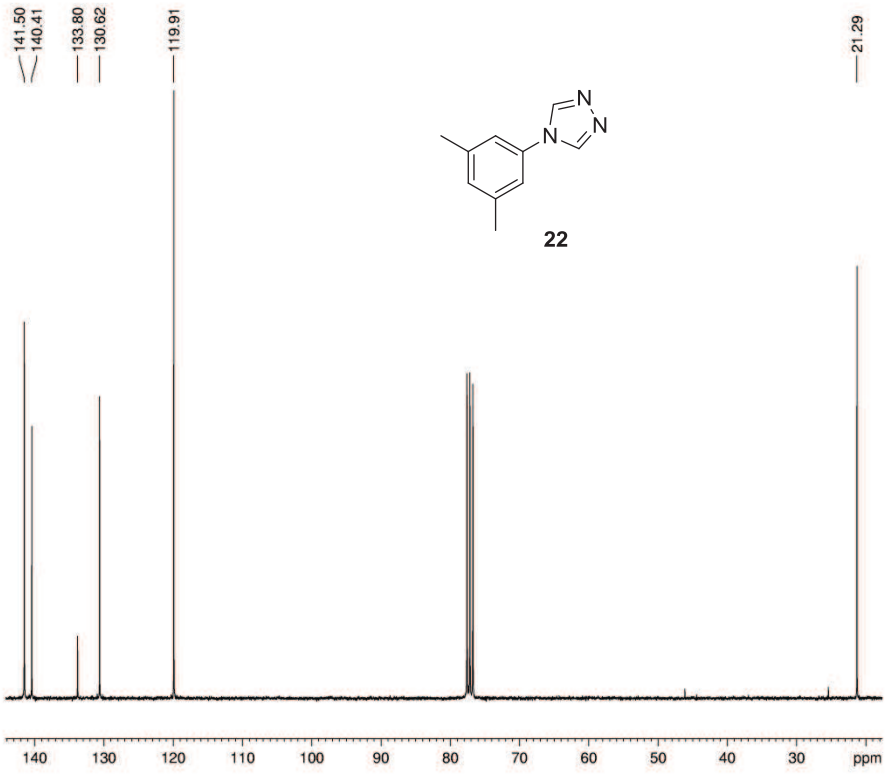

22

BRUKER

Current Data Parameters
NAME c101210bslh.007
EXPNO 1
PROCNO 1

F2 – Acquisition Parameters
Date_ 20101211
Time 7.41
INSTRUM spect
PROBHD 5 mm QNP 1H/13
PULPROG zgpg30
TD 65536
SOLVENT CDCl3
NS 4096
DS 4
SWH 18832.393 Hz
FIDRES 0.287360 Hz
AQ 1.7399808 sec
RG 13004
DW 26.550 usec
DE 6.00 usec
TE 300.0 K
D1 1.00000000 sec
d11 0.03000000 sec
DELTA 0.89999998 sec
TD0 512
SFO1 75.4915175 MHz
NUC1 13C
P1 11.60 usec
PLW1 -1.00000000 W
SFO2 300.1912008 MHz
NUC2 1H
CPDPRG[2 waltz65
PCPD2 100.00 usec
PLW2 -1.00000000 W
PLW12 -1.00000000 W
PLW13 -1.00000000 W

F2 – Processing parameters
SI 32768
SF 75.4828314 MHz
WDW EM
SSB 0
LB 1.00 Hz
GB 0
PC 1.40

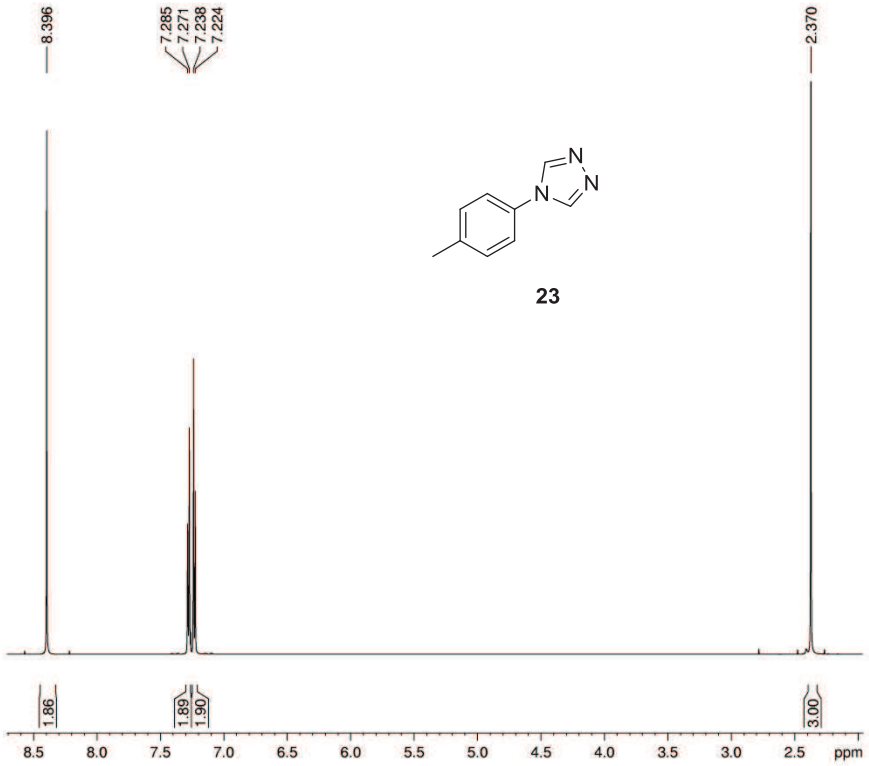

23

Current Data Parameters
NAME e121017bsrb.211
EXPNO 2
PROCNO 1

F2 – Acquisition Parameters
Date_ 20121017
Time 8.51
INSTRUM spect
PROBHD 5 mm CPQCI 1H–
PULPROG zg30
TD 131072
SOLVENT CDCl3
NS 24
DS 2
SWH 18028.846 Hz
FIDRES 0.137549 Hz
AQ 3.6350634 sec
RG 7.02
DW 27.733 usec
DE 12.00 usec
TE 295.0 K
D1 0.10000000 sec
TD0 3

======== CHANNEL f1 ========
SFO1 600.2468302 MHz
NUC1 1H
P1 7.63 usec
PLW1 7.50000000 W

F2 – Processing parameters
SI 65536
SF 600.2438430 MHz
WDW EM
SSB 0
LB 0.30 Hz
GB 0
PC 1.00

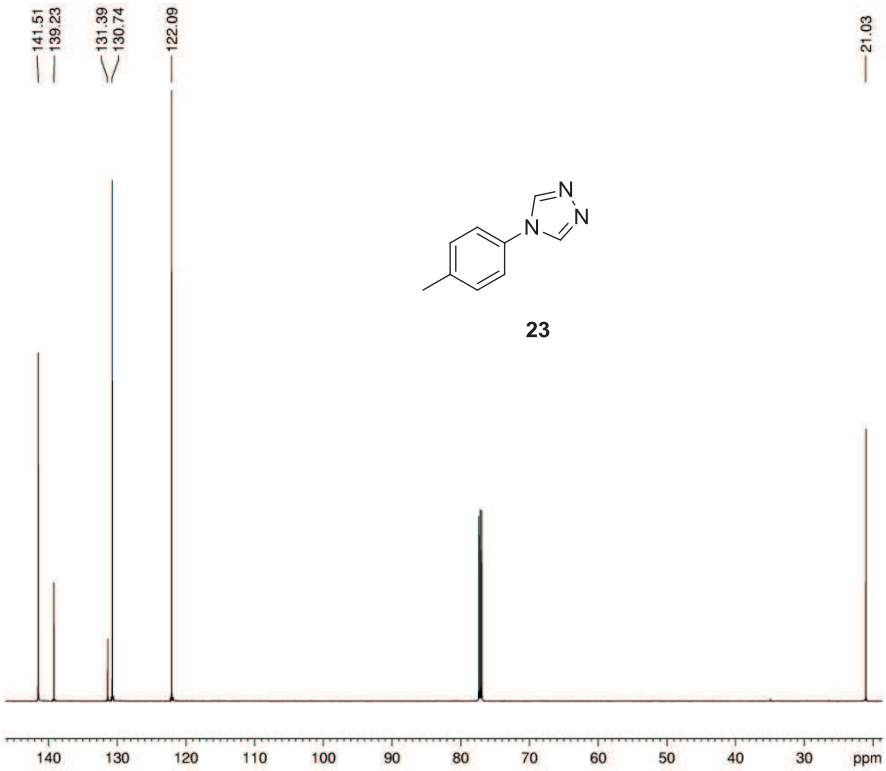

23

Current Data Parameters
NAME e121017bsrb.211
EXPNO 1
PROCNO 1

F2 – Acquisition Parameters
Date_ 20121017
Time 7.56
INSTRUM spect
PROBHD 5 mm CPQCI 1H–
PULPROG zgpg30
TD 98132
SOLVENT CDCl3
NS 1024
DS 4
SWH 45454.547 Hz
FIDRES 0.463198 Hz
AQ 1.0794520 sec
RG 1820
DW 11.000 usec
DE 16.00 usec
TE 295.0 K
D1 2.00000000 sec
D11 0.03000000 sec
TD0 128

======== CHANNEL f1 ========
SFO1 150.9480335 MHz
NUC1 13C
P1 12.50 usec
PLW1 87.00000000 W

======== CHANNEL f2 ========
SFO2 600.2462301 MHz
NUC2 1H
CPDPRG[2 waltz64
PCPD2 70.00 usec
PLW2 7.50000000 W
PLW12 0.08899100 W
PLW13 0.04360500 W

F2 – Processing parameters
SI 65536
SF 150.9314309 MHz
WDW EM
SSB 0
LB 1.00 Hz
GB 0
PC 1.40

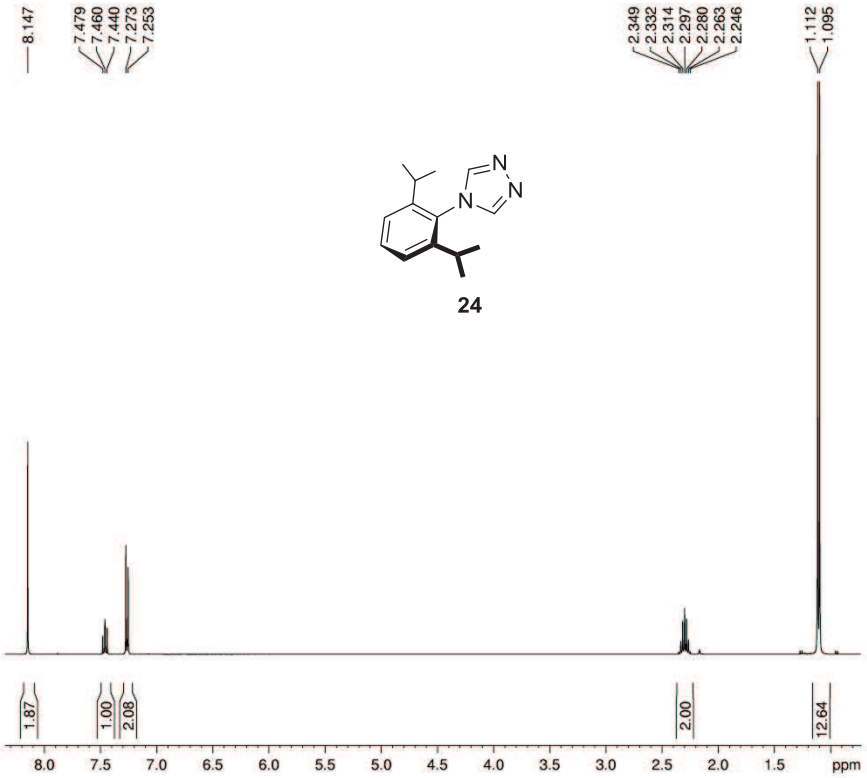

24

Current Data Parameters
NAME c121017bsrb.156
EXPNO 2
PROCNO 1

F2 – Acquisition Parameters
Date_ 20121017
Time 9.27
INSTRUM spect
PROBHD 5 mm CPPBBO BB
PULPROG zg30
TD 65536
SOLVENT CDCl3
NS 40
DS 2
SWH 12019.230 Hz
FIDRES 0.183399 Hz
AQ 2.7262976 sec
RG 36
DW 41.600 usec
DE 12.00 usec
TE 298.0 K
D1 0.50000000 sec
TD0 5

======== CHANNEL f1 ========
SFO1 400.1820009 MHz
NUC1 1H
P1 11.50 usec
PLW1 10.00000000 W

F2 – Processing parameters
SI 65536
SF 400.1800136 MHz
WDW EM
SSB 0
LB 0.30 Hz
GB 0
PC 1.00

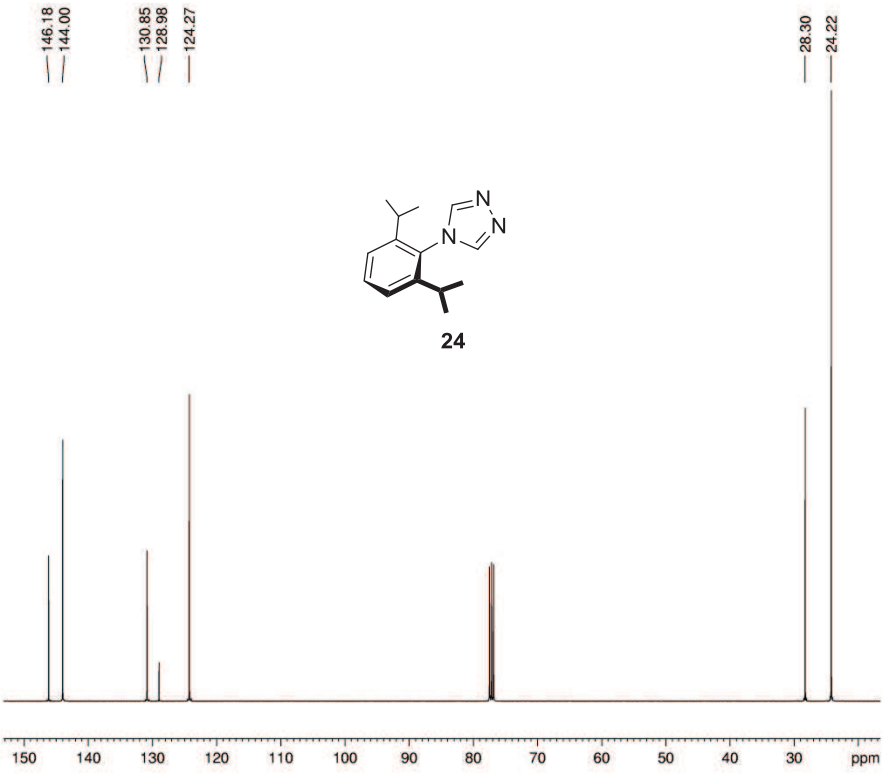

24

Current Data Parameters
NAME c121017bsrb.156
EXPNO 1
PROCNO 1

F2 – Acquisition Parameters
Date_ 20121017
Time 7.38
INSTRUM spect
PROBHD 5 mm CPPBBO BB
PULPROG zgpg30
TD 98132
SOLVENT CDCl3
NS 2048
DS 2
SWH 30864.197 Hz
FIDRES 0.314517 Hz
AQ 1.5897384 sec
RG 2050
DW 16.200 usec
DE 20.00 usec
TE 298.0 K
D1 1.50000000 sec
D11 0.03000000 sec
TD0 256

======== CHANNEL f1 ========
SFO1 100.6364098 MHz
NUC1 13C
P1 10.00 usec
PLW1 45.00000000 W

======== CHANNEL f2 ========
SFO2 400.1816007 MHz
NUC2 1H
CPDPRG[2 waltz65
PCPD2 90.00 usec
PLW2 10.00000000 W
PLW12 0.16327000 W
PLW13 0.13225000 W

F2 – Processing parameters
SI 65536
SF 100.6253354 MHz
WDW EM
SSB 0
LB 1.00 Hz
GB 0
PC 1.40

1.4 Symmetrically Substituted Bistriazolium Halide Salts

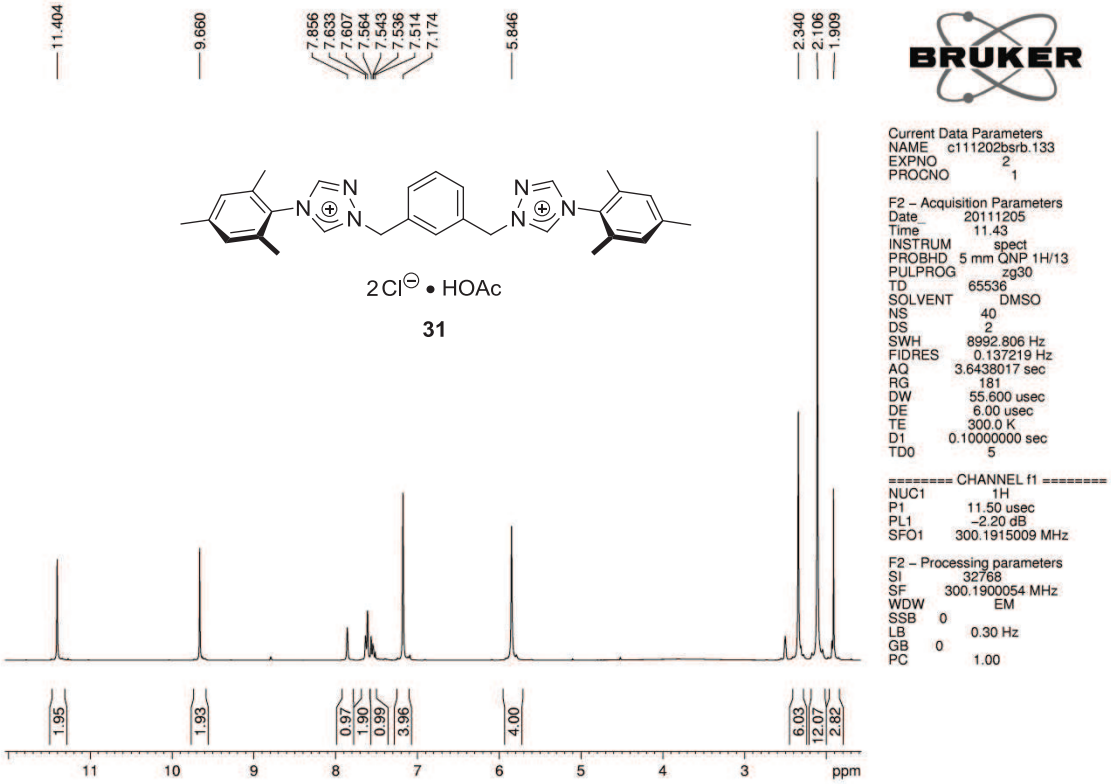

$2\,Cl^{\ominus} \bullet HOAc$

31

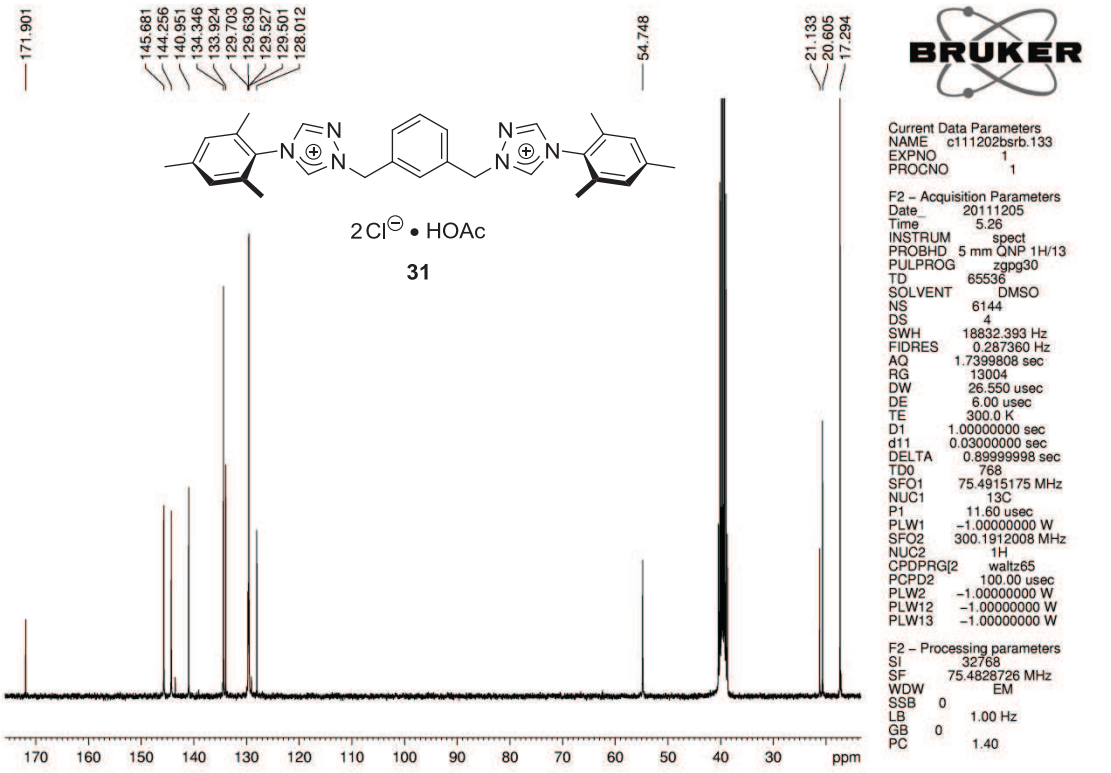

$2\,Cl^{\ominus} \bullet HOAc$

31

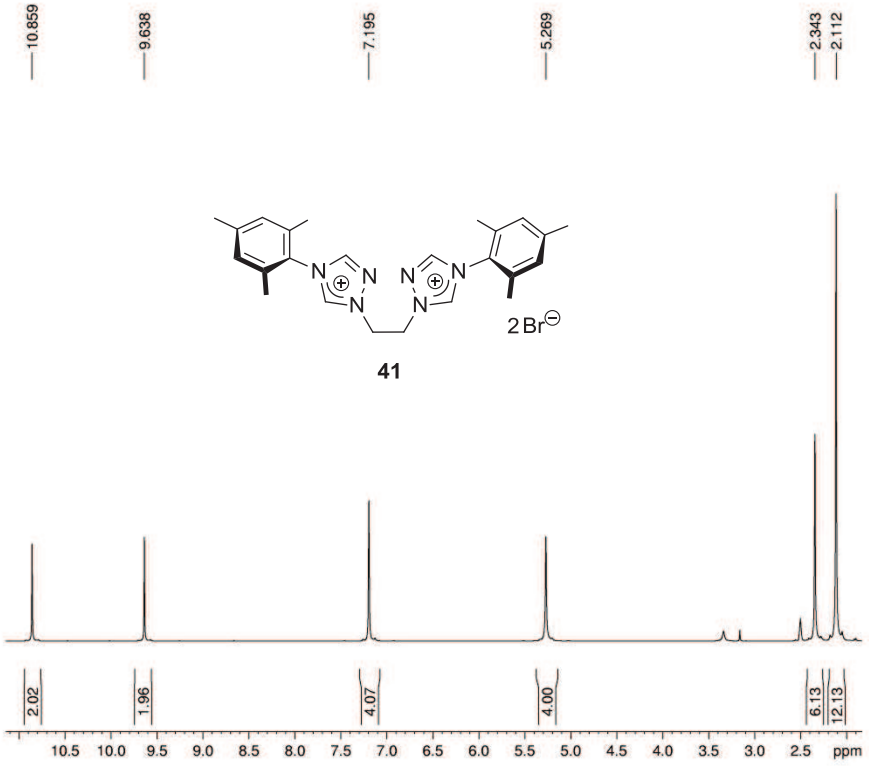

41

BRUKER

Current Data Parameters
NAME c120118bsrb.275
EXPNO 2
PROCNO 1

F2 – Acquisition Parameters
Date_ 20120118
Time 19.37
INSTRUM spect
PROBHD 5 mm QNP 1H/13
PULPROG zg30
TD 65536
SOLVENT DMSO
NS 128
DS 2
SWH 8992.806 Hz
FIDRES 0.137219 Hz
AQ 3.6438017 sec
RG 287.4
DW 55.600 usec
DE 6.00 usec
TE 300.0 K
D1 0.10000000 sec
TD0 16

======== CHANNEL f1 ========
NUC1 1H
P1 11.50 usec
PL1 −2.20 dB
SFO1 300.1915009 MHz

F2 – Processing parameters
SI 32768
SF 300.1900051 MHz
WDW EM
SSB 0
LB 0.30 Hz
GB 0
PC 1.00

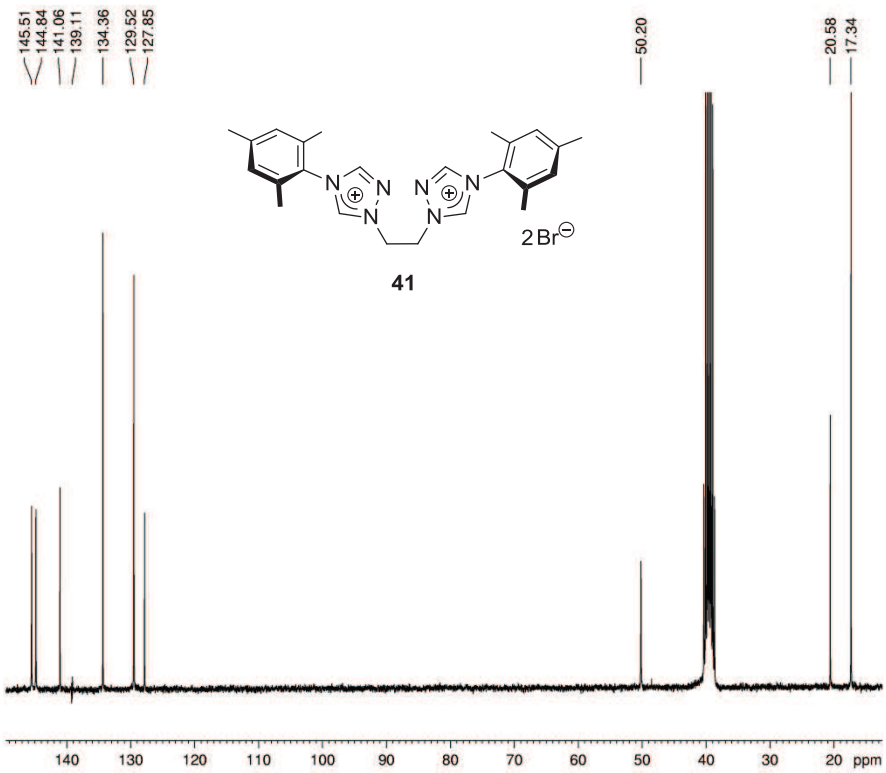

41

BRUKER

Current Data Parameters
NAME c120118bsrb.275
EXPNO 5
PROCNO 1

F2 – Acquisition Parameters
Date_ 20120119
Time 2.22
INSTRUM spect
PROBHD 5 mm QNP 1H/13
PULPROG zgpg30
TD 65536
SOLVENT DMSO
NS 6440
DS 4
SWH 18832.393 Hz
FIDRES 0.287360 Hz
AQ 1.7399808 sec
RG 13004
DW 26.550 usec
DE 6.00 usec
TE 300.0 K
D1 1.00000000 sec
d11 0.03000000 sec
DELTA 0.89999998 sec
TD0 128
SFO1 75.4915175 MHz
NUC1 13C
P1 11.60 usec
PLW1 −1.00000000 W
SFO2 300.1912008 MHz
NUC2 1H
CPDPRG[2 waltz65
PCPD2 100.00 usec
PLW2 −1.00000000 W
PLW12 −1.00000000 W
PLW13 −1.00000000 W

F2 – Processing parameters
SI 32768
SF 75.4828747 MHz
WDW EM
SSB 0
LB 1.00 Hz
GB 0
PC 1.40

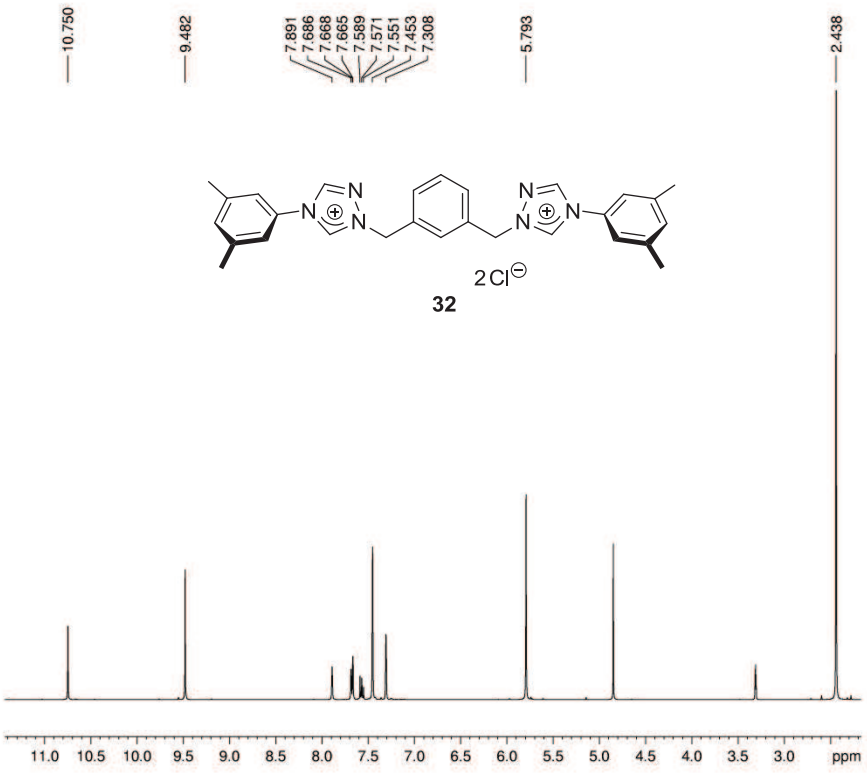

BRUKER

Current Data Parameters
NAME c120903bsrb.441
EXPNO 2
PROCNO 1

F2 – Acquisition Parameters
Date_ 20120903
Time 17.39
INSTRUM spect
PROBHD 5 mm CPPBBO BB
PULPROG zg30
TD 65536
SOLVENT MeOD
NS 40
DS 2
SWH 12019.230 Hz
FIDRES 0.183399 Hz
AQ 2.7262976 sec
RG 90.5
DW 41.600 usec
DE 12.00 usec
TE 298.0 K
D1 0.50000000 sec
TD0 5

======== CHANNEL f1 ========
SFO1 400.1820009 MHz
NUC1 1H
P1 11.50 usec
PLW1 10.00000000 W

F2 – Processing parameters
SI 65536
SF 400.1800118 MHz
WDW EM
SSB 0
LB 0.30 Hz
GB 0
PC 1.00

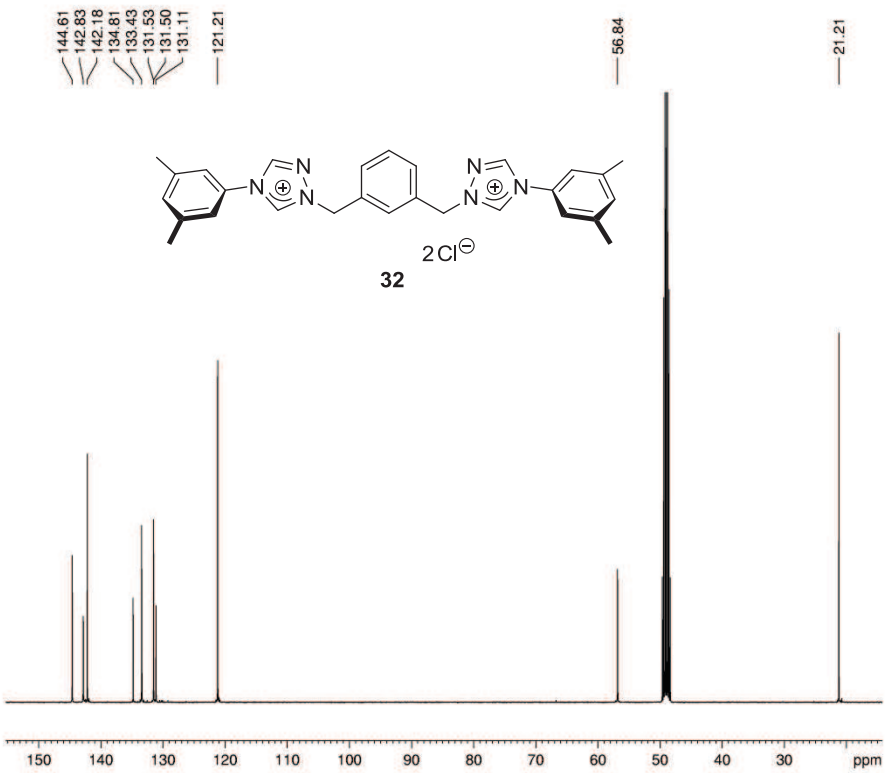

BRUKER

Current Data Parameters
NAME c120903bsrb.441
EXPNO 1
PROCNO 1

F2 – Acquisition Parameters
Date_ 20120903
Time 14.50
INSTRUM spect
PROBHD 5 mm CPPBBO BB
PULPROG zgpg30
TD 98132
SOLVENT MeOD
NS 3200
DS 2
SWH 30864.197 Hz
FIDRES 0.314517 Hz
AQ 1.5897384 sec
RG 2050
DW 16.200 usec
DE 20.00 usec
TE 298.0 K
D1 1.50000000 sec
D11 0.03000000 sec
TD0 400

======== CHANNEL f1 ========
SFO1 100.6364098 MHz
NUC1 13C
P1 10.00 usec
PLW1 45.00000000 W

======== CHANNEL f2 ========
SFO2 400.1816007 MHz
NUC2 1H
CPDPRG[2 waltz65
PCPD2 90.00 usec
PLW2 10.00000000 W
PLW12 0.16327000 W
PLW13 0.13225000 W

F2 – Processing parameters
SI 65536
SF 100.6252030 MHz
WDW EM
SSB 0
LB 1.00 Hz
GB 0
PC 1.40

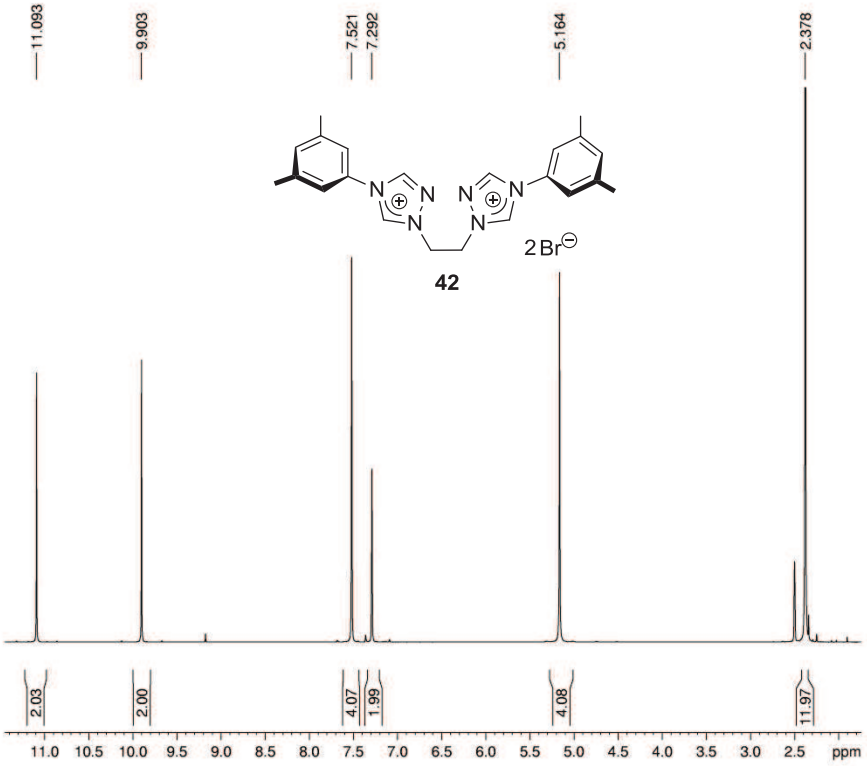

BRUKER

Current Data Parameters
NAME d120105bsrb.285
EXPNO 2
PROCNO 1

F2 – Acquisition Parameters
Date_ 20120105
Time 12.00
INSTRUM spect
PROBHD 5 mm BBI 1H–BB
PULPROG zg30
TD 65536
SOLVENT DMSO
NS 128
DS 2
SWH 8992.806 Hz
FIDRES 0.137219 Hz
AQ 3.6438017 sec
RG 114
DW 55.600 usec
DE 6.00 usec
TE 298.0 K
D1 0.10000000 sec
TD0 16

======== CHANNEL f1 ========
NUC1 1H
P1 11.00 usec
PL1 0 dB
SFO1 500.1325007 MHz

F2 – Processing parameters
SI 32768
SF 500.1300063 MHz
WDW EM
SSB 0
LB 0.30 Hz
GB 0
PC 1.00

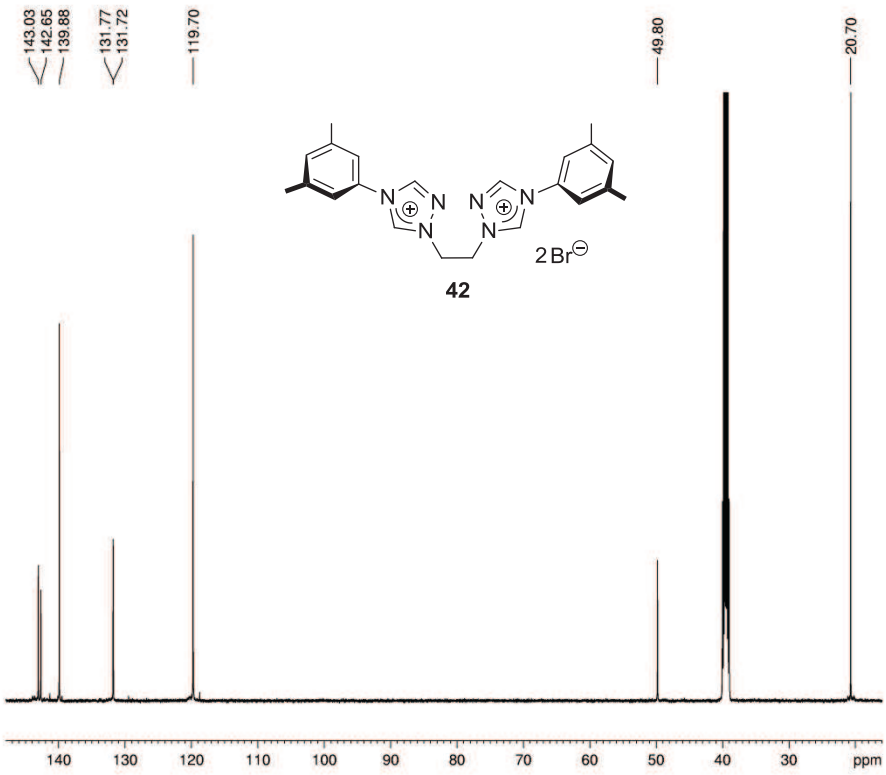

BRUKER

Current Data Parameters
NAME d120105bsrb.285
EXPNO 5
PROCNO 1

F2 – Acquisition Parameters
Date_ 20120106
Time 16.30
INSTRUM spect
PROBHD 5 mm BBI 1H–BB
PULPROG zgpg30
TD 131072
SOLVENT DMSO
NS 10240
DS 4
SWH 31446.541 Hz
FIDRES 0.239918 Hz
AQ 2.0840447 sec
RG 7298.2
DW 15.900 usec
DE 20.00 usec
TE 298.0 K
D1 1.00000000 sec
d11 0.03000000 sec
DELTA 0.89999998 sec
TD0 1280
SFO1 125.7716224 MHz
NUC1 13C
P1 16.45 usec
PLW1 –1.00000000 W
SFO2 500.1320005 MHz
NUC2 1H
CPDPRG[2 waltz16
PCPD2 80.00 usec
PLW2 –1.00000000 W
PLW12 –1.00000000 W
PLW13 –1.00000000 W

F2 – Processing parameters
SI 65536
SF 125.7578535 MHz
WDW EM
SSB 0
LB 1.00 Hz
GB 0
PC 1.40

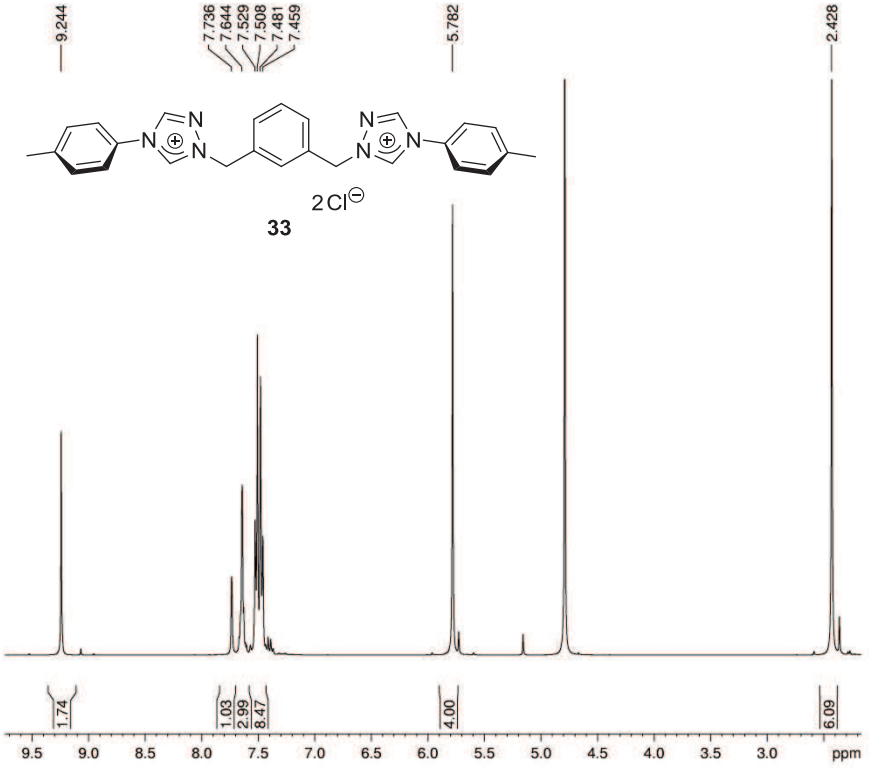

BRUKER

Current Data Parameters
NAME c121019bsrb.479
EXPNO 2
PROCNO 1

F2 – Acquisition Parameters
Date_ 20121021
Time 2.02
INSTRUM spect
PROBHD 5 mm CPPBBO BB
PULPROG zg30
TD 65536
SOLVENT D2O
NS 128
DS 2
SWH 12019.230 Hz
FIDRES 0.183399 Hz
AQ 2.7262976 sec
RG 128
DW 41.600 usec
DE 12.00 usec
TE 298.0 K
D1 0.50000000 sec
TD0 16

======== CHANNEL f1 ========
SFO1 400.1820009 MHz
NUC1 1H
P1 11.50 usec
PLW1 10.00000000 W

F2 – Processing parameters
SI 65536
SF 400.1799675 MHz
WDW EM
SSB 0
LB 0.30 Hz
GB 0
PC 1.00

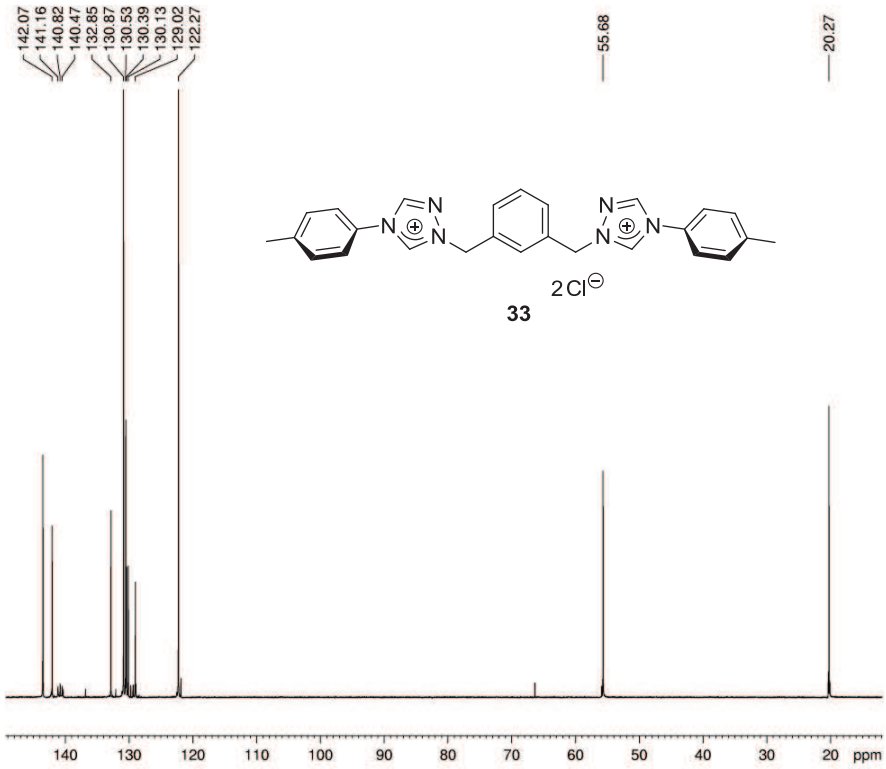

BRUKER

Current Data Parameters
NAME c121019bsrb.479
EXPNO 1
PROCNO 1

F2 – Acquisition Parameters
Date_ 20121020
Time 17.02
INSTRUM spect
PROBHD 5 mm CPPBBO BB
PULPROG zgpg30
TD 98132
SOLVENT D2O
NS 10240
DS 2
SWH 30864.197 Hz
FIDRES 0.314517 Hz
AQ 1.5897384 sec
RG 2050
DW 16.200 usec
DE 20.00 usec
TE 298.0 K
D1 1.50000000 sec
D11 0.03000000 sec
TD0 1280

======== CHANNEL f1 ========
SFO1 100.6364098 MHz
NUC1 13C
P1 10.00 usec
PLW1 45.00000000 W

======== CHANNEL f2 ========
SFO2 400.1816007 MHz
NUC2 1H
CPDPRG[2 waltz65
PCPD2 90.00 usec
PLW2 10.00000000 W
PLW12 0.16327000 W
PLW13 0.13225000 W

F2 – Processing parameters
SI 65536
SF 100.6253410 MHz
WDW EM
SSB 0
LB 1.00 Hz
GB 0
PC 1.40

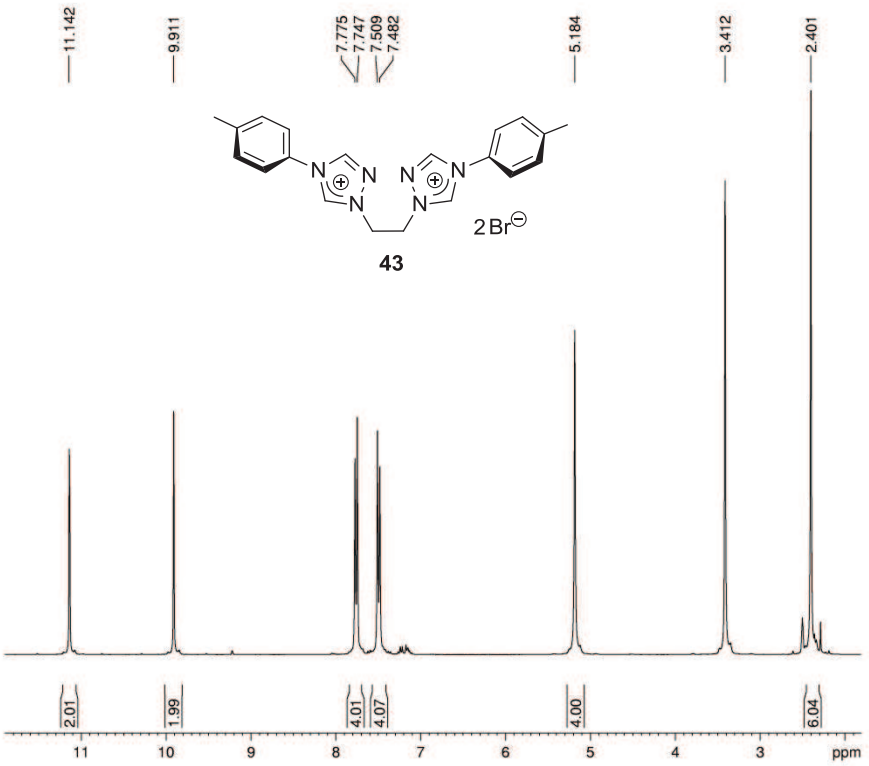


```
Current Data Parameters
NAME    c110913bsrb.219
EXPNO              2
PROCNO             1

F2 – Acquisition Parameters
Date_        20110913
Time             19.53
INSTRUM          spect
PROBHD  5 mm QNP 1H/13
PULPROG          zg30
TD              65536
SOLVENT          DMSO
NS                 40
DS                  2
SWH           8992.806 Hz
FIDRES        0.137219 Hz
AQ            3.6438017 sec
RG                181
DW             55.600 usec
DE              6.00 usec
TE              300.0 K
D1          0.10000000 sec
TD0                 5

======== CHANNEL f1 ========
NUC1               1H
P1              11.50 usec
PL1             -2.20 dB
SFO1       300.1915009 MHz

F2 – Processing parameters
SI              32768
SF         300.1900053 MHz
WDW                EM
SSB     0
LB              0.30 Hz
GB      0
PC              1.00
```

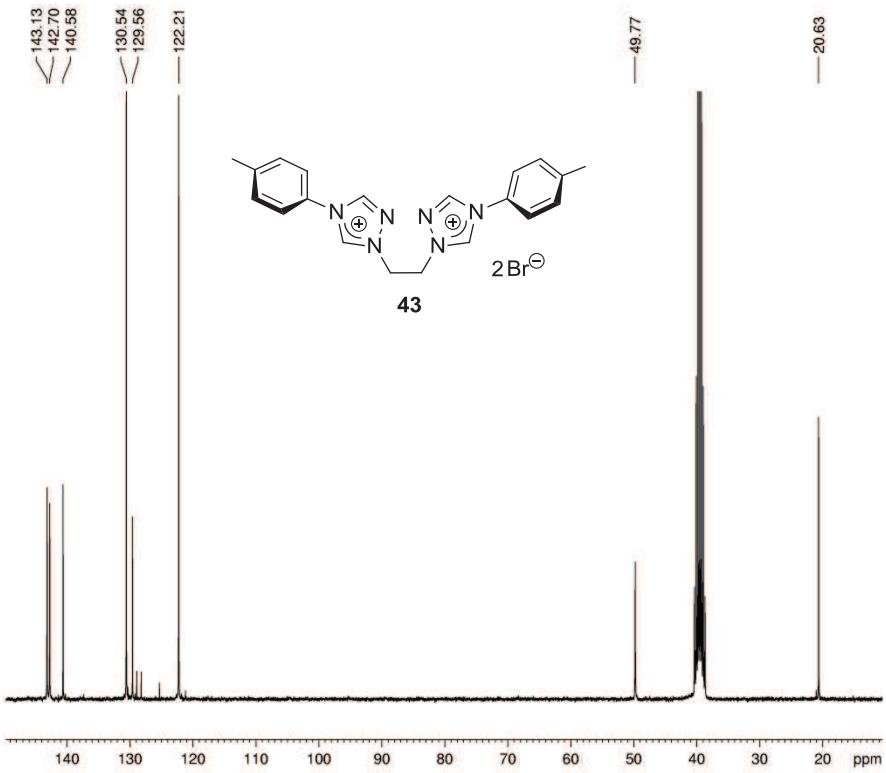


```
Current Data Parameters
NAME    c110913bsrb.219
EXPNO              1
PROCNO             1

F2 – Acquisition Parameters
Date_        20110913
Time             15.06
INSTRUM          spect
PROBHD  5 mm QNP 1H/13
PULPROG        zgpg30
TD              65536
SOLVENT          DMSO
NS               6144
DS                  4
SWH          18832.393 Hz
FIDRES        0.287360 Hz
AQ            1.7399808 sec
RG                13004
DW             26.550 usec
DE              6.00 usec
TE              300.0 K
D1          1.00000000 sec
d11         0.03000000 sec
DELTA       0.89999998 sec
TD0               768
SFO1       75.4915175 MHz
NUC1               13C
P1              11.60 usec
PLW1        -1.00000000 W
SFO2       300.1912008 MHz
NUC2               1H
CPDPRG[2        waltz65
PCPD2          100.00 usec
PLW2        -1.00000000 W
PLW12       -1.00000000 W
PLW13       -1.00000000 W

F2 – Processing parameters
SI              32768
SF         75.4828740 MHz
WDW                EM
SSB     0
LB              1.00 Hz
GB      0
PC              1.40
```

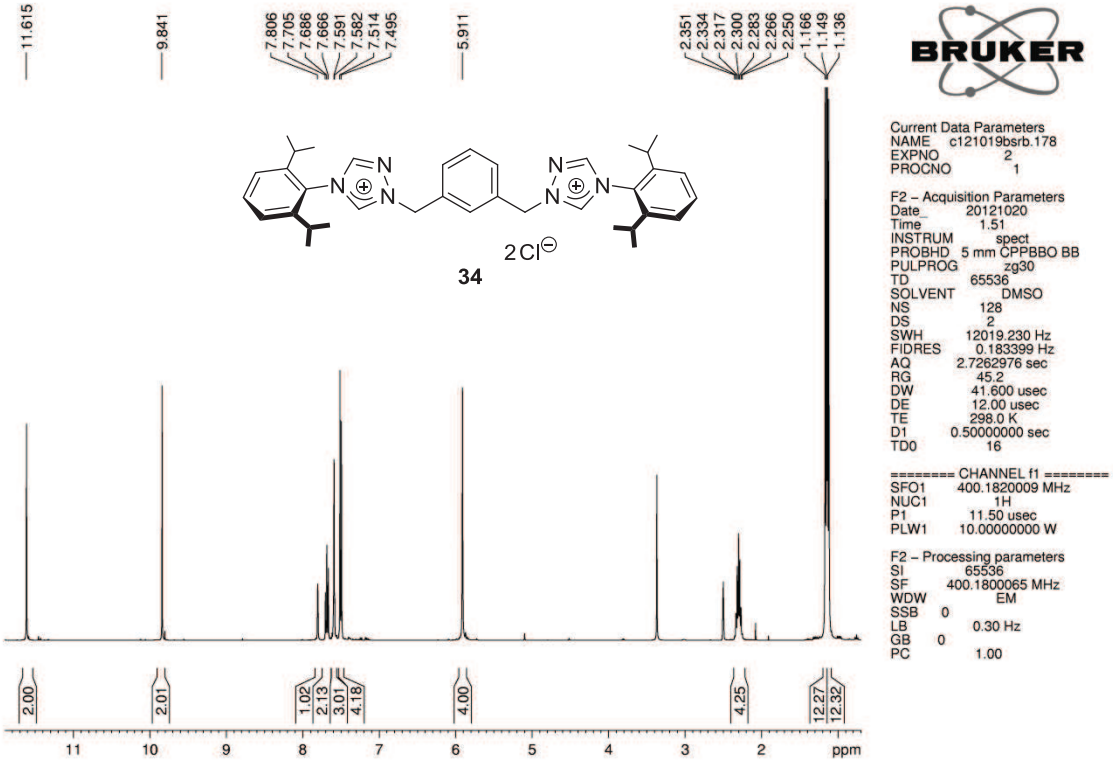
11.615
9.841
7.806
7.705
7.686
7.666
7.591
7.582
7.514
7.495
5.911
2.351
2.334
2.317
2.300
2.283
2.266
2.250
1.166
1.149
1.136
2.00
2.01
1.02
2.13
3.01
4.18
4.00
4.25
12.27
12.32
11 10 9 8 7 6 5 4 3 2 ppm
2 Cl⊖
34
BRUKER
Current Data Parameters
NAME c121019bsrb.178
EXPNO 2
PROCNO 1
F2 – Acquisition Parameters
Date_ 20121020
Time 1.51
INSTRUM spect
PROBHD 5 mm CPPBBO BB
PULPROG zg30
TD 65536
SOLVENT DMSO
NS 128
DS 2
SWH 12019.230 Hz
FIDRES 0.183399 Hz
AQ 2.7262976 sec
RG 45.2
DW 41.600 usec
DE 12.00 usec
TE 298.0 K
D1 0.50000000 sec
TD0 16
======== CHANNEL f1 ========
SFO1 400.1820009 MHz
NUC1 1H
P1 11.50 usec
PLW1 10.00000000 W
F2 – Processing parameters
SI 65536
SF 400.1800065 MHz
WDW EM
SSB 0
LB 0.30 Hz
GB 0
PC 1.00

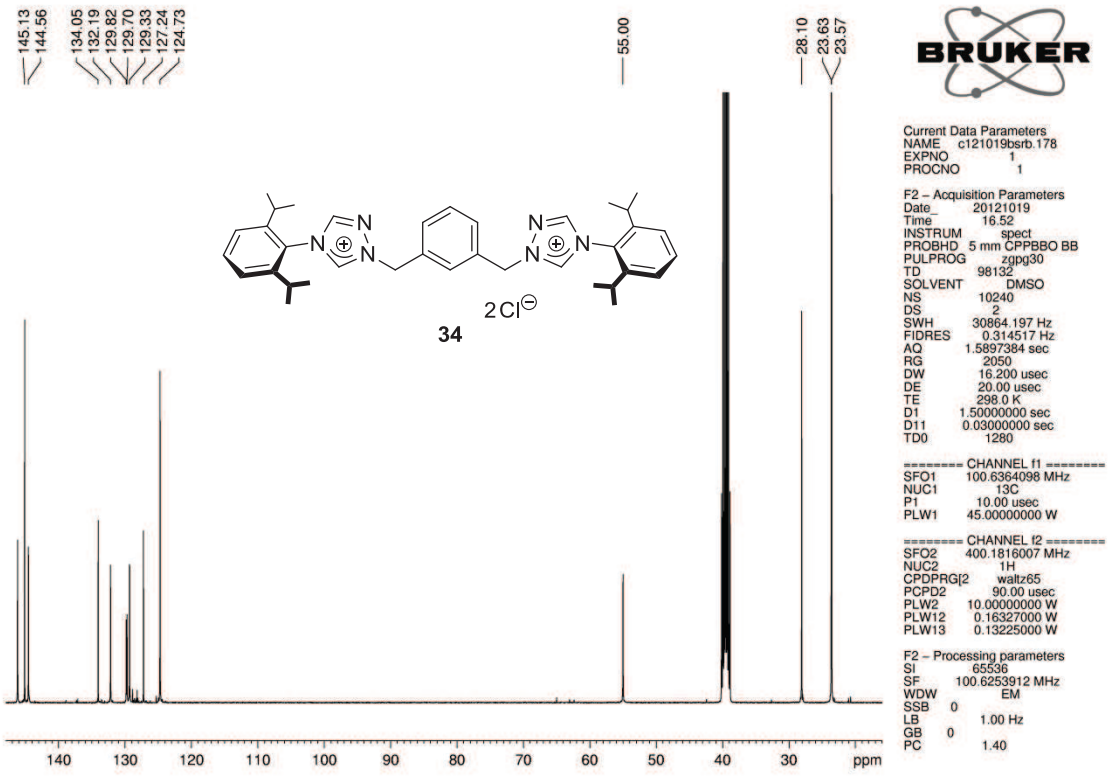
145.13
144.56
134.05
132.19
129.82
129.70
129.33
127.24
124.73
55.00
28.10
23.63
23.57
140 130 120 110 100 90 80 70 60 50 40 30 ppm
2 Cl⊖
34
BRUKER
Current Data Parameters
NAME c121019bsrb.178
EXPNO 1
PROCNO 1
F2 – Acquisition Parameters
Date_ 20121019
Time 16.52
INSTRUM spect
PROBHD 5 mm CPPBBO BB
PULPROG zgpg30
TD 98132
SOLVENT DMSO
NS 10240
DS 2
SWH 30864.197 Hz
FIDRES 0.314517 Hz
AQ 1.5897384 sec
RG 2050
DW 16.200 usec
DE 20.00 usec
TE 298.0 K
D1 1.50000000 sec
D11 0.03000000 sec
TD0 1280
======== CHANNEL f1 ========
SFO1 100.6364098 MHz
NUC1 13C
P1 10.00 usec
PLW1 45.00000000 W
======== CHANNEL f2 ========
SFO2 400.1816007 MHz
NUC2 1H
CPDPRG[2 waltz65
PCPD2 90.00 usec
PLW2 10.00000000 W
PLW12 0.16327000 W
PLW13 0.13225000 W
F2 – Processing parameters
SI 65536
SF 100.6253912 MHz
WDW EM
SSB 0
LB 1.00 Hz
GB 0
PC 1.40

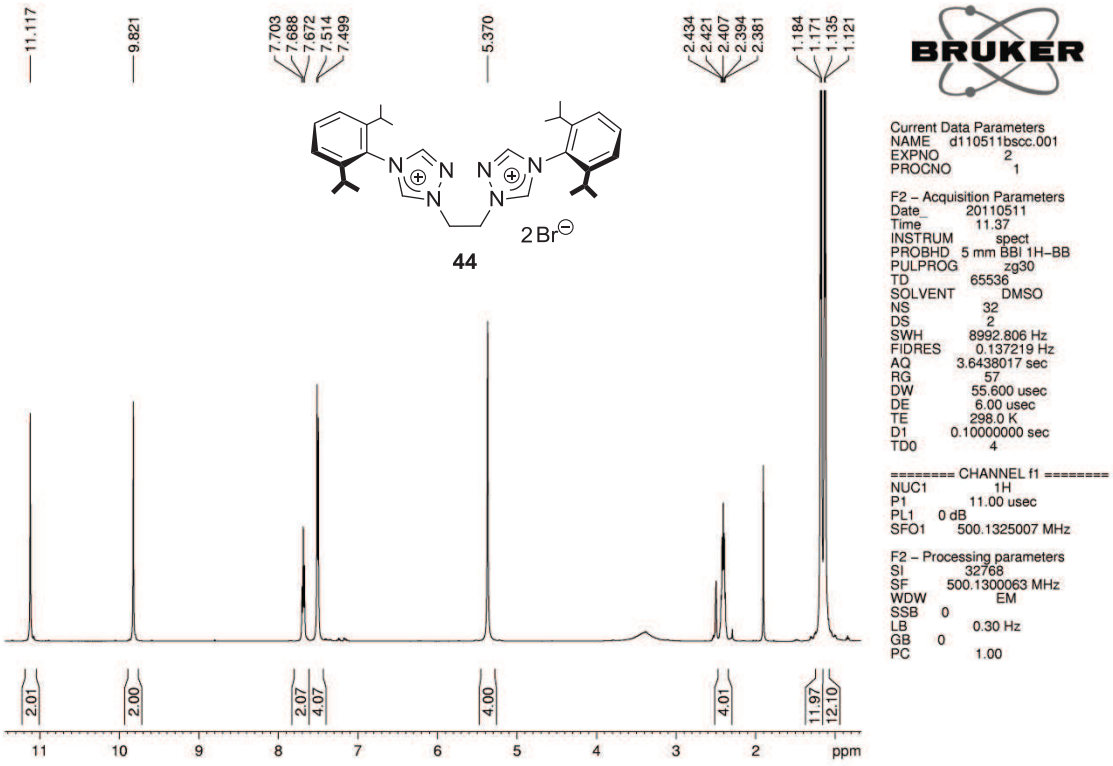
11.117
9.821
7.703
7.688
7.672
7.514
7.499
5.370
2.434
2.421
2.407
2.394
2.381
1.184
1.171
1.135
1.121
2Br⊖
44
2.01
2.00
2.07
4.07
4.00
4.01
11.97
12.10
11
10
9
8
7
6
5
4
3
2
ppm
BRUKER
Current Data Parameters
NAME d110511bscc.001
EXPNO 2
PROCNO 1
F2 – Acquisition Parameters
Date_ 20110511
Time 11.37
INSTRUM spect
PROBHD 5 mm BBI 1H–BB
PULPROG zg30
TD 65536
SOLVENT DMSO
NS 32
DS 2
SWH 8992.806 Hz
FIDRES 0.137219 Hz
AQ 3.6438017 sec
RG 57
DW 55.600 usec
DE 6.00 usec
TE 298.0 K
D1 0.10000000 sec
TD0 4
======== CHANNEL f1 ========
NUC1 1H
P1 11.00 usec
PL1 0 dB
SFO1 500.1325007 MHz
F2 – Processing parameters
SI 32768
SF 500.1300063 MHz
WDW EM
SSB 0
LB 0.30 Hz
GB 0
PC 1.00

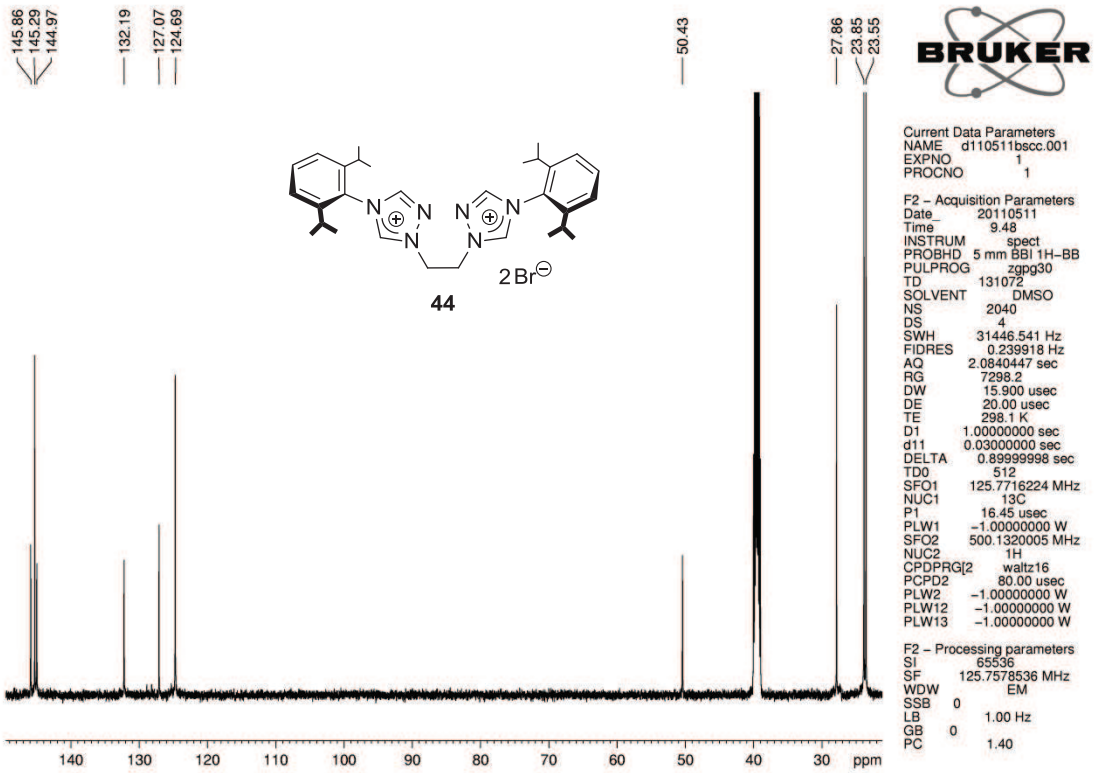
145.86
145.29
144.97
132.19
127.07
124.69
50.43
27.86
23.85
23.55
2Br⊖
44
140
130
120
110
100
90
80
70
60
50
40
30
ppm
BRUKER
Current Data Parameters
NAME d110511bscc.001
EXPNO 1
PROCNO 1
F2 – Acquisition Parameters
Date_ 20110511
Time 9.48
INSTRUM spect
PROBHD 5 mm BBI 1H–BB
PULPROG zgpg30
TD 131072
SOLVENT DMSO
NS 2040
DS 4
SWH 31446.541 Hz
FIDRES 0.239918 Hz
AQ 2.0840447 sec
RG 7298.2
DW 15.900 usec
DE 20.00 usec
TE 298.1 K
D1 1.00000000 sec
d11 0.03000000 sec
DELTA 0.89999998 sec
TD0 512
SFO1 125.7716224 MHz
NUC1 13C
P1 16.45 usec
PLW1 –1.00000000 W
SFO2 500.1320005 MHz
NUC2 1H
CPDPRG[2 waltz16
PCPD2 80.00 usec
PLW2 –1.00000000 W
PLW12 –1.00000000 W
PLW13 –1.00000000 W
F2 – Processing parameters
SI 65536
SF 125.7578536 MHz
WDW EM
SSB 0
LB 1.00 Hz
GB 0
PC 1.40

1.5 Synthesis of Unsymmetrically Substituted Bistriazolium Halide Salts

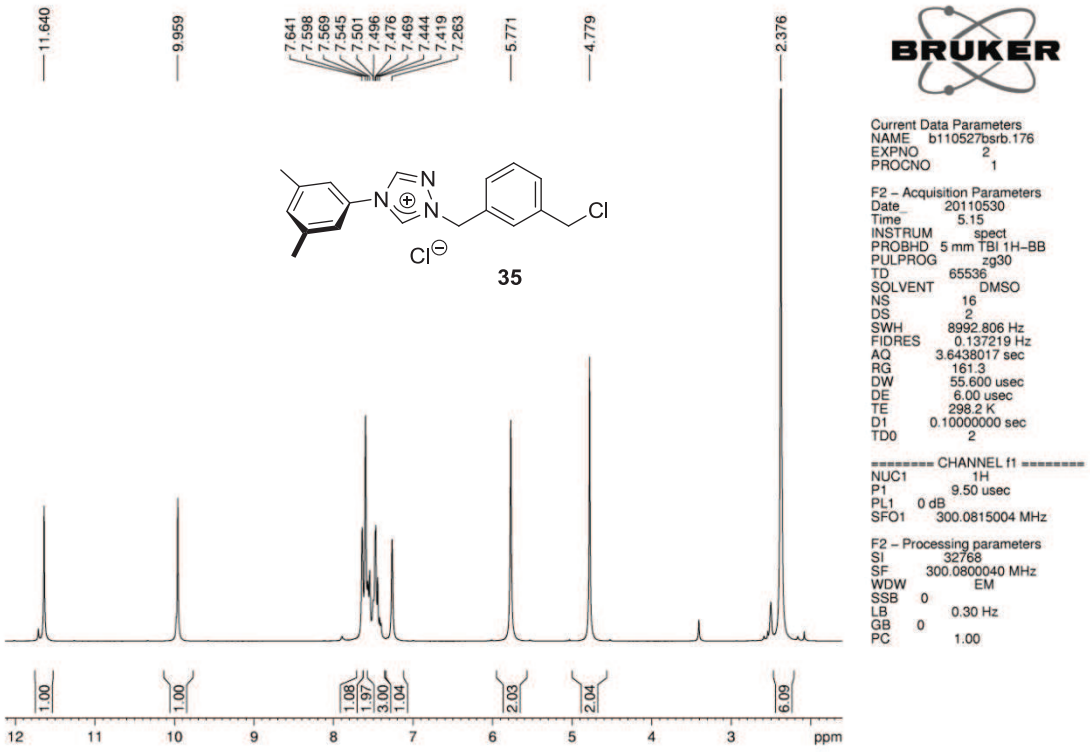

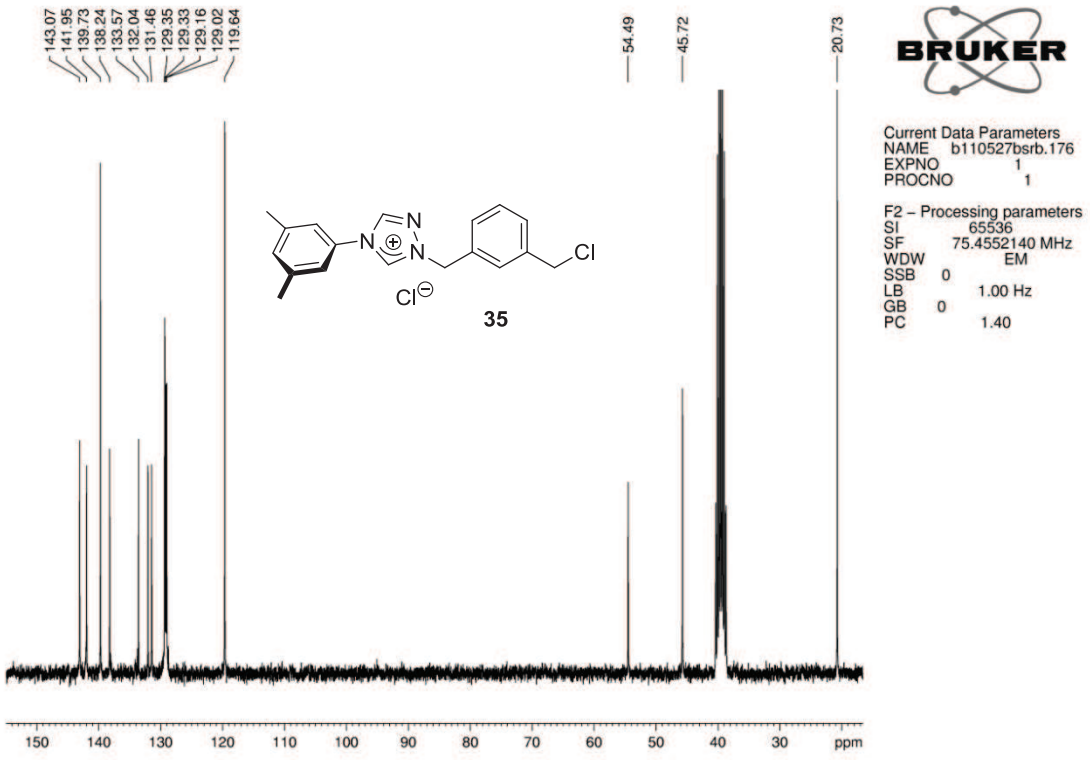

BRUKER

Current Data Parameters
NAME c121022bsrb.177
EXPNO 2
PROCNO 1

F2 – Acquisition Parameters
Date_ 20121022
Time 10.01
INSTRUM spect
PROBHD 5 mm CPPBBO BB
PULPROG zg30
TD 65536
SOLVENT DMSO
NS 16
DS 2
SWH 12019.230 Hz
FIDRES 0.183399 Hz
AQ 2.7262976 sec
RG 45.2
DW 41.600 usec
DE 12.00 usec
TE 298.0 K
D1 0.50000000 sec
TD0 2

======== CHANNEL f1 ========
SFO1 400.1820009 MHz
NUC1 1H
P1 11.50 usec
PLW1 10.00000000 W

F2 – Processing parameters
SI 65536
SF 400.1800063 MHz
WDW EM
SSB 0
LB 0.30 Hz
GB 0
PC 1.00

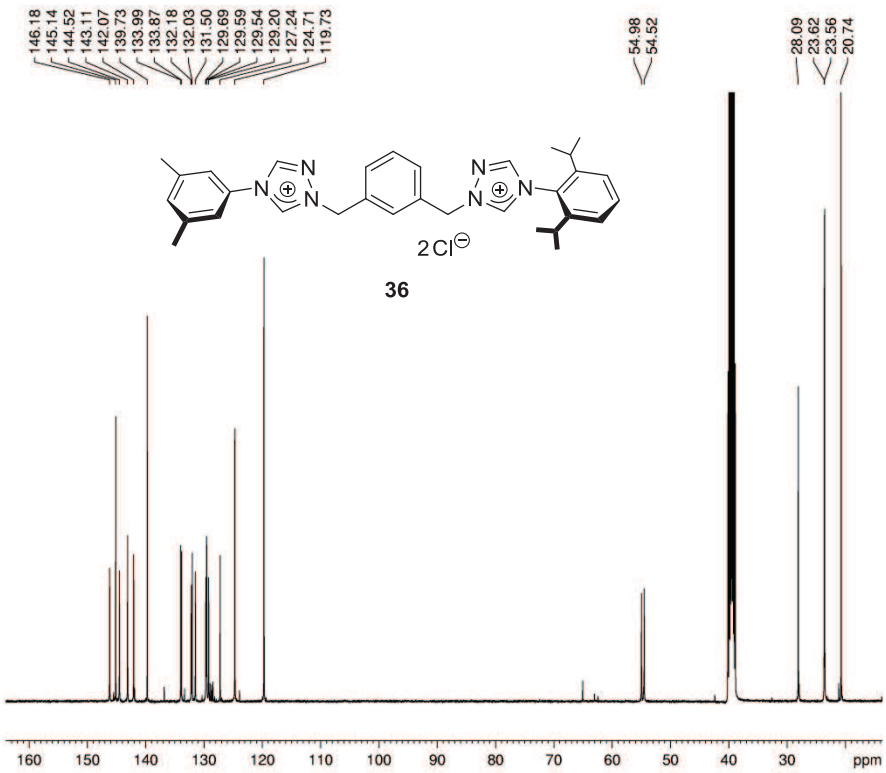

BRUKER

Current Data Parameters
NAME c121022bsrb.177
EXPNO 1
PROCNO 1

F2 – Acquisition Parameters
Date_ 20121022
Time 7.11
INSTRUM spect
PROBHD 5 mm CPPBBO BB
PULPROG zgpg30
TD 98132
SOLVENT DMSO
NS 3200
DS 2
SWH 30864.197 Hz
FIDRES 0.314517 Hz
AQ 1.5897384 sec
RG 2050
DW 16.200 usec
DE 20.00 usec
TE 298.0 K
D1 1.50000000 sec
D11 0.03000000 sec
TD0 400

======== CHANNEL f1 ========
SFO1 100.6364098 MHz
NUC1 13C
P1 10.00 usec
PLW1 45.00000000 W

======== CHANNEL f2 ========
SFO2 400.1816007 MHz
NUC2 1H
CPDPRG[2 waltz65
PCPD2 90.00 usec
PLW2 10.00000000 W
PLW12 0.16327000 W
PLW13 0.13225000 W

F2 – Processing parameters
SI 65536
SF 100.6253907 MHz
WDW EM
SSB 0
LB 1.00 Hz
GB 0
PC 1.40

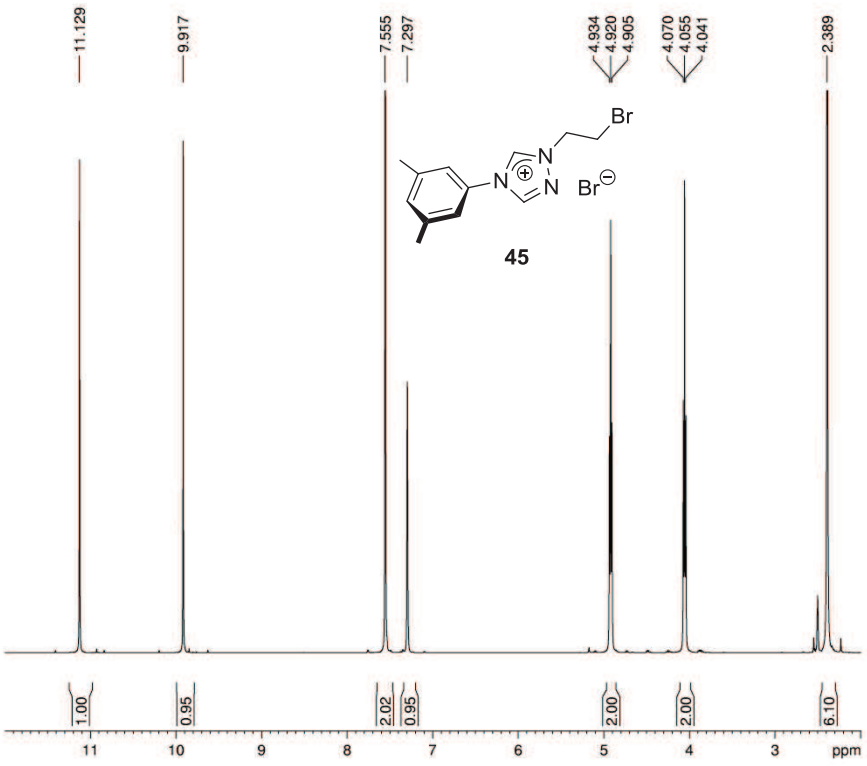

45

Current Data Parameters
NAME c121022bsrb.299
EXPNO 2
PROCNO 1

F2 – Acquisition Parameters
Date_ 20121022
Time 18.05
INSTRUM spect
PROBHD 5 mm CPPBBO BB
PULPROG zg30
TD 65536
SOLVENT DMSO
NS 16
DS 2
SWH 12019.230 Hz
FIDRES 0.183399 Hz
AQ 2.7262976 sec
RG 57
DW 41.600 usec
DE 12.00 usec
TE 298.0 K
D1 0.50000000 sec
TD0 2

======== CHANNEL f1 ========
SFO1 400.1820009 MHz
NUC1 1H
P1 11.50 usec
PLW1 10.00000000 W

F2 – Processing parameters
SI 65536
SF 400.1800065 MHz
WDW EM
SSB 0
LB 0.30 Hz
GB 0
PC 1.00

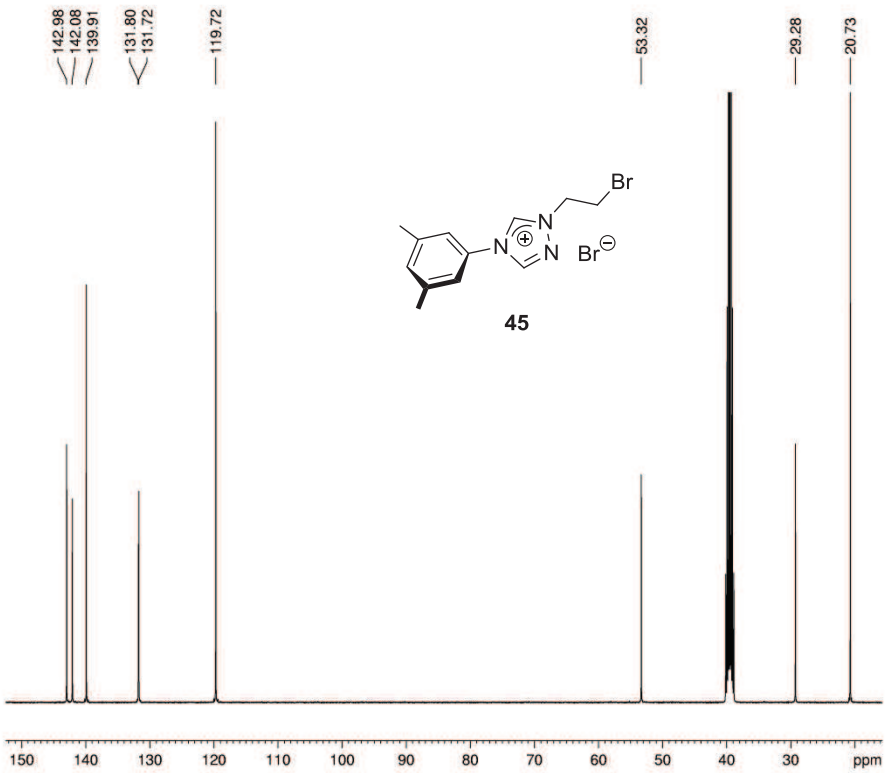

45

Current Data Parameters
NAME c121022bsrb.299
EXPNO 1
PROCNO 1

F2 – Acquisition Parameters
Date_ 20121022
Time 15.16
INSTRUM spect
PROBHD 5 mm CPPBBO BB
PULPROG zgpg30
TD 98132
SOLVENT DMSO
NS 3200
DS 2
SWH 30864.197 Hz
FIDRES 0.314517 Hz
AQ 1.5897384 sec
RG 2050
DW 16.200 usec
DE 20.00 usec
TE 298.0 K
D1 1.50000000 sec
D11 0.03000000 sec
TD0 400

======== CHANNEL f1 ========
SFO1 100.6364098 MHz
NUC1 13C
P1 10.00 usec
PLW1 45.00000000 W

======== CHANNEL f2 ========
SFO2 400.1816007 MHz
NUC2 1H
CPDPRG[2 waltz65
PCPD2 90.00 usec
PLW2 10.00000000 W
PLW12 0.16327000 W
PLW13 0.13225000 W

F2 – Processing parameters
SI 65536
SF 100.6253919 MHz
WDW EM
SSB 0
LB 1.00 Hz
GB 0
PC 1.40

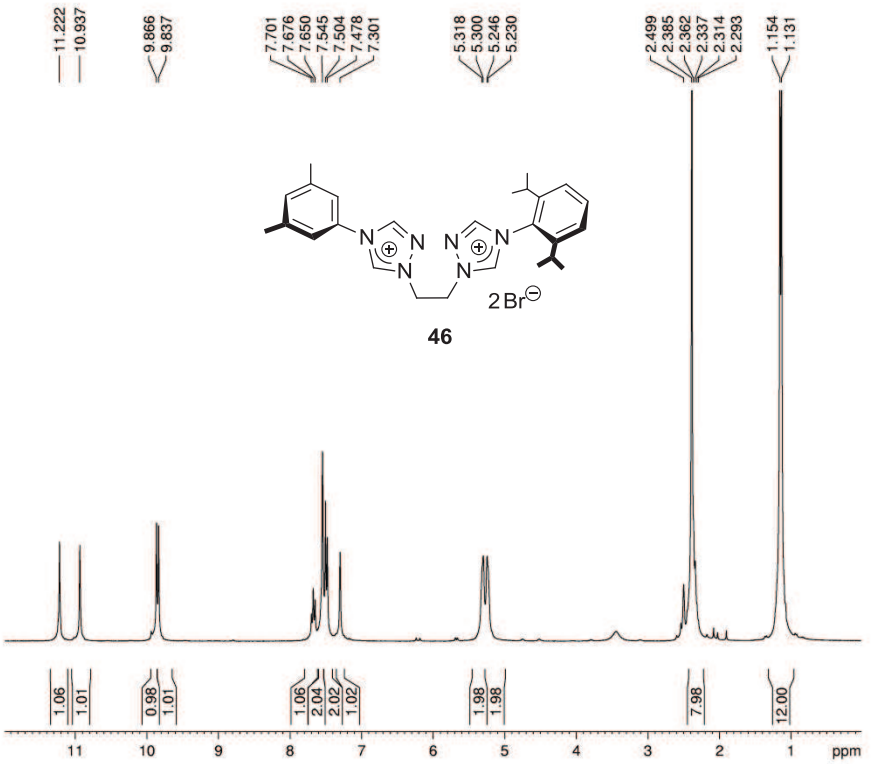

46

Current Data Parameters
NAME c110530bscc.CD008
EXPNO 2
PROCNO 1

F2 – Acquisition Parameters
Date_ 20110530
Time 10.52
INSTRUM spect
PROBHD 5 mm QNP 1H/13
PULPROG zg30
TD 65536
SOLVENT DMSO
NS 16
DS 2
SWH 8992.806 Hz
FIDRES 0.137219 Hz
AQ 3.6438017 sec
RG 181
DW 55.600 usec
DE 6.00 usec
TE 300.0 K
D1 0.10000000 sec
TD0 2

======== CHANNEL f1 ========
NUC1 1H
P1 11.50 usec
PL1 −2.20 dB
SFO1 300.1915009 MHz

F2 – Processing parameters
SI 32768
SF 300.1900057 MHz
WDW EM
SSB 0
LB 0.30 Hz
GB 0
PC 1.00

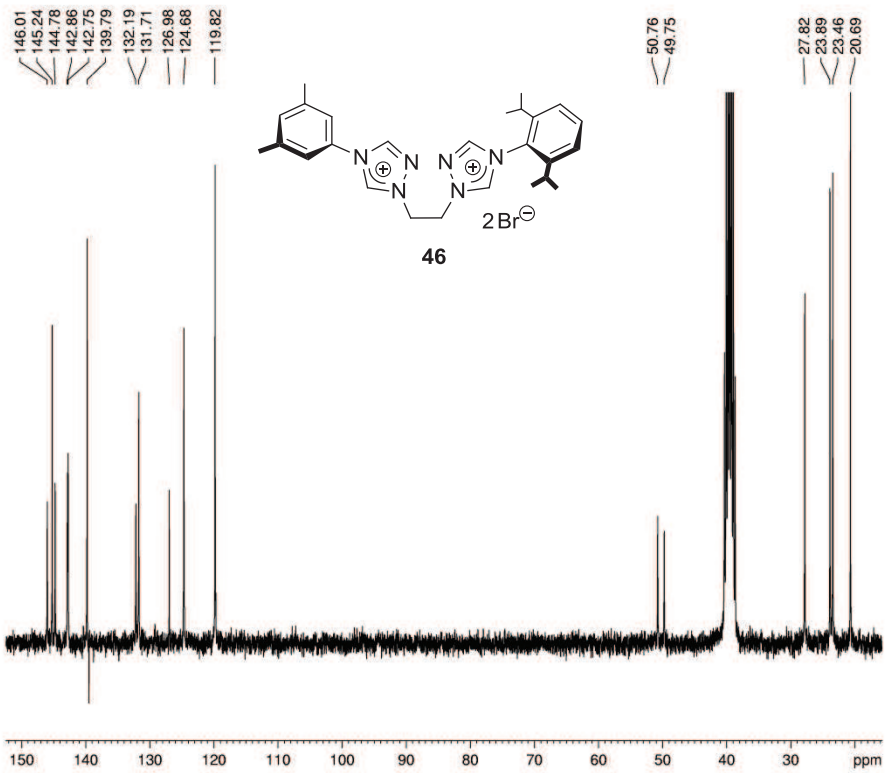

46

Current Data Parameters
NAME c110530bscc.CD008
EXPNO 1
PROCNO 1

F2 – Acquisition Parameters
Date_ 20110530
Time 9.16
INSTRUM spect
PROBHD 5 mm QNP 1H/13
PULPROG zgpg30
TD 65536
SOLVENT DMSO
NS 2048
DS 4
SWH 18832.393 Hz
FIDRES 0.287360 Hz
AQ 1.7399808 sec
RG 13004
DW 26.550 usec
DE 6.00 usec
TE 300.0 K
D1 1.00000000 sec
d11 0.03000000 sec
DELTA 0.89999998 sec
TD0 256
SFO1 75.4915175 MHz
NUC1 13C
P1 11.60 usec
PLW1 −1.00000000 W
SFO2 300.1912008 MHz
NUC2 1H
CPDPRG[2 waltz65
PCPD2 100.00 usec
PLW2 −1.00000000 W
PLW12 −1.00000000 W
PLW13 −1.00000000 W

F2 – Processing parameters
SI 32768
SF 75.4828765 MHz
WDW EM
SSB 0
LB 1.00 Hz
GB 0
PC 1.40

1.6 Symmetrically Substituted Bistriazolium Hexafluorophosphate Salts

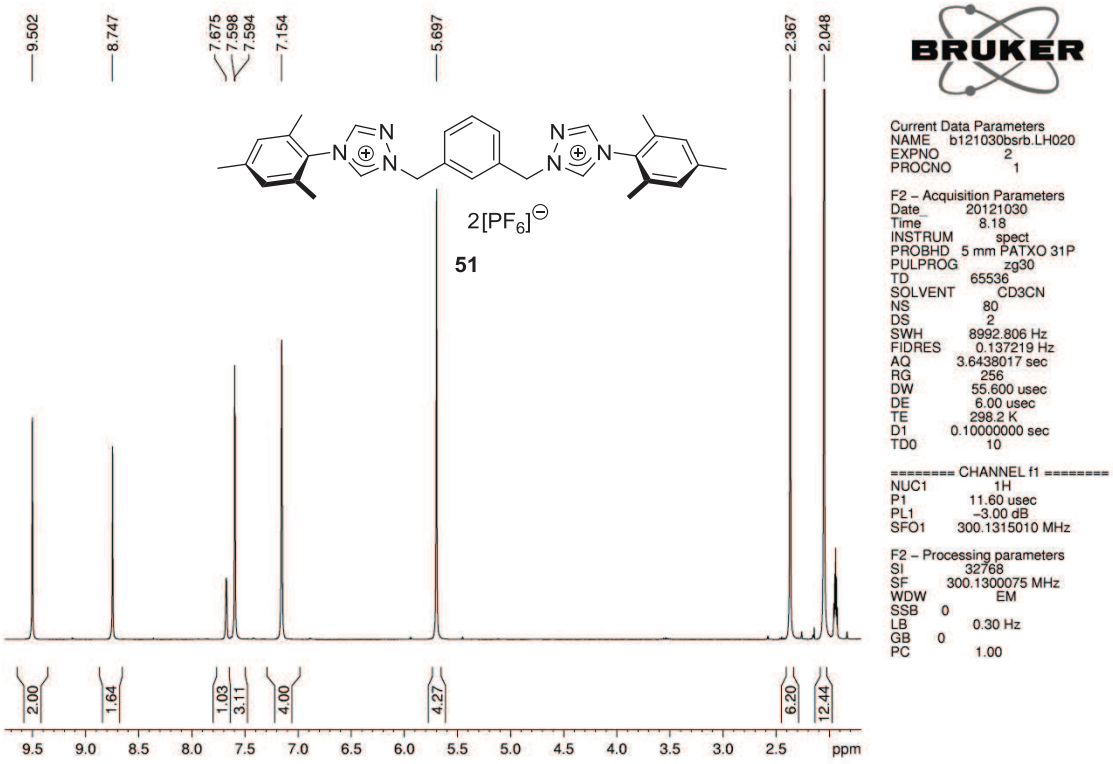

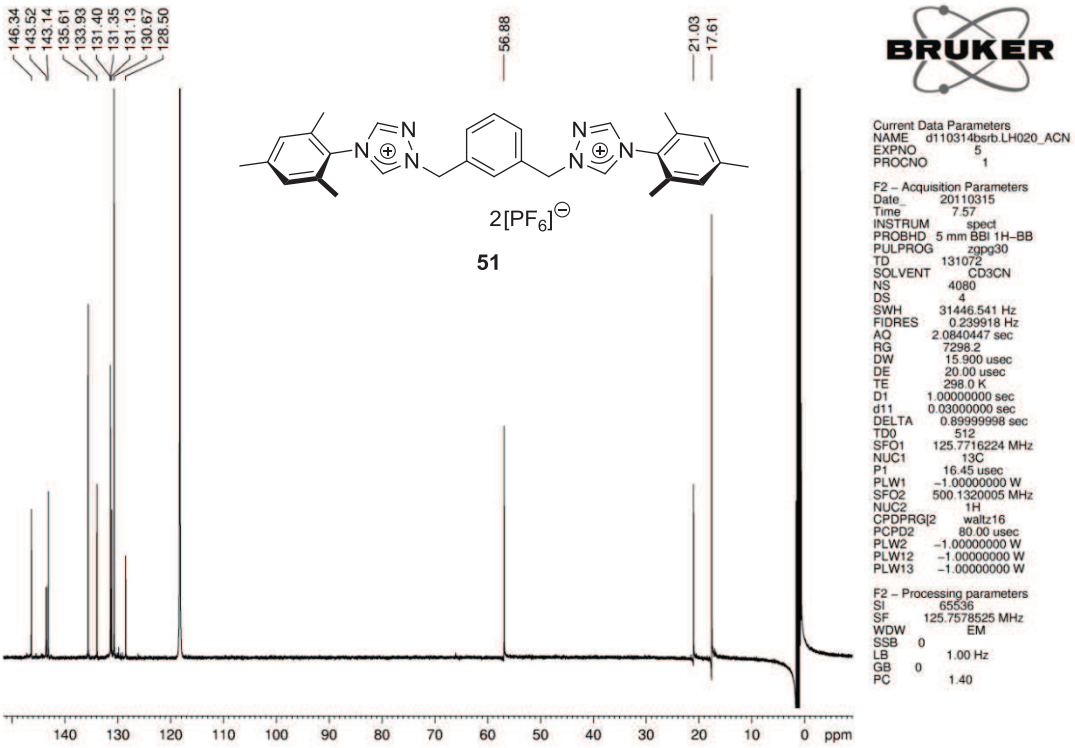

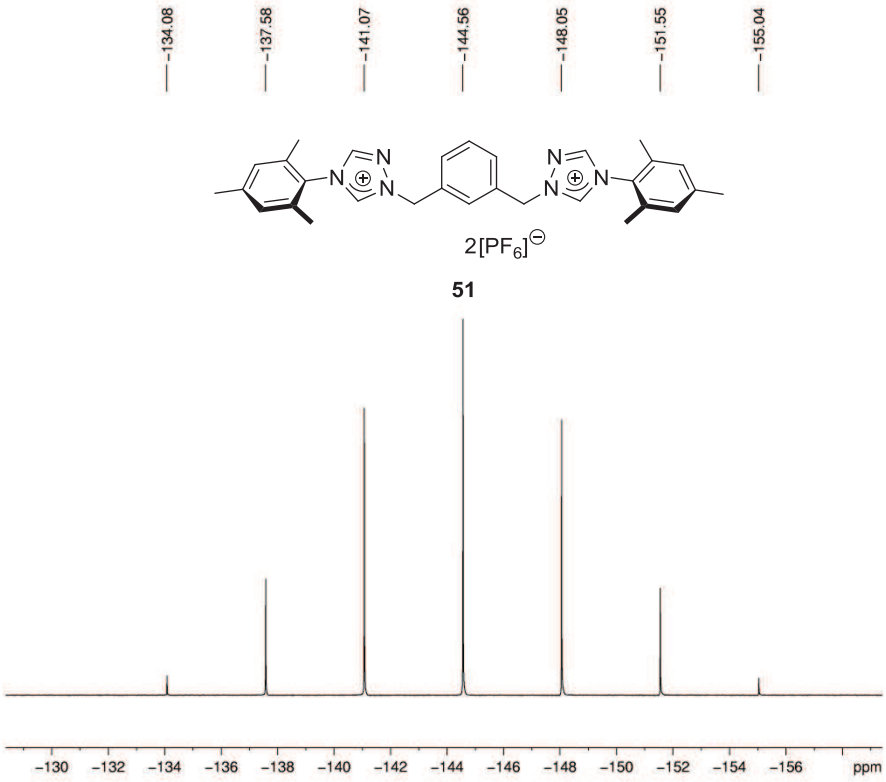
−134.08
−137.58
−141.07
−144.56
−148.05
−151.55
−155.04
2[PF6]⊖
51
−130 −132 −134 −136 −138 −140 −142 −144 −146 −148 −150 −152 −154 −156 ppm

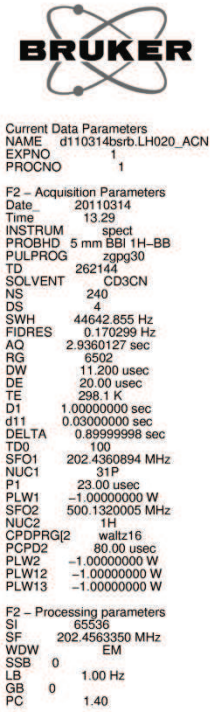
BRUKER
Current Data Parameters
NAME d110314bsrb.LH020_ACN
EXPNO 1
PROCNO 1
F2 – Acquisition Parameters
Date_ 20110314
Time 13.29
INSTRUM spect
PROBHD 5 mm BBI 1H–BB
PULPROG zgpg30
TD 262144
SOLVENT CD3CN
NS 240
DS 4
SWH 44642.855 Hz
FIDRES 0.170299 Hz
AQ 2.9360127 sec
RG 6502
DW 11.200 usec
DE 20.00 usec
TE 298.1 K
D1 1.00000000 sec
d11 0.03000000 sec
DELTA 0.89999998 sec
TD0 100
SFO1 202.4360894 MHz
NUC1 31P
P1 23.00 usec
PLW1 −1.00000000 W
SFO2 500.1320005 MHz
NUC2 1H
CPDPRG[2 waltz16
PCPD2 80.00 usec
PLW2 −1.00000000 W
PLW12 −1.00000000 W
PLW13 −1.00000000 W
F2 – Processing parameters
SI 65536
SF 202.4563350 MHz
WDW EM
SSB 0
LB 1.00 Hz
GB 0
PC 1.40

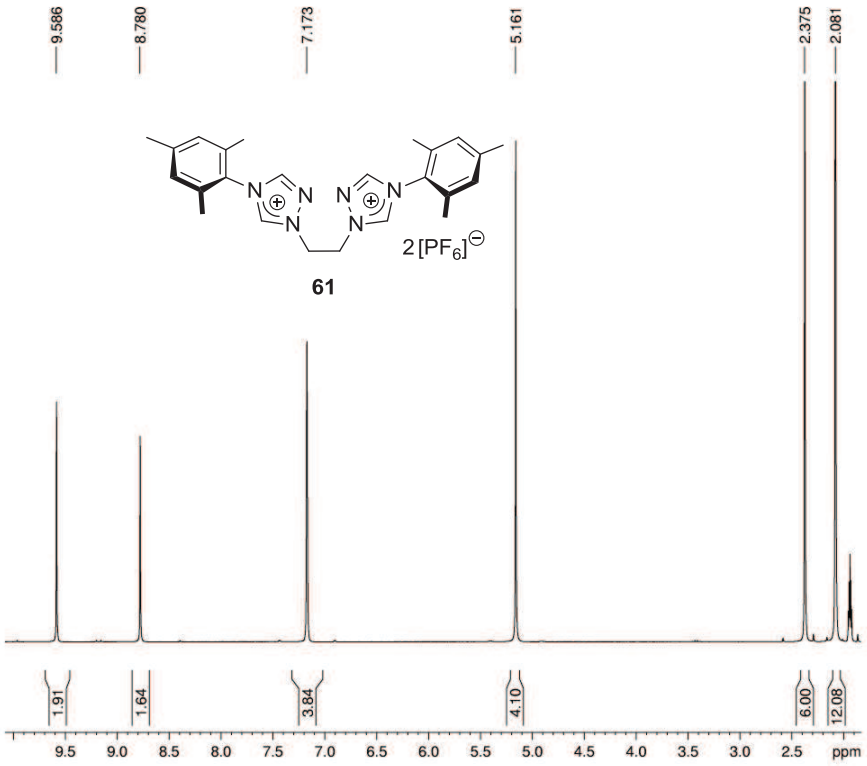
9.586
8.780
7.173
5.161
2.375
2.081
2[PF6]⊖
61
1.91
1.64
3.84
4.10
6.00
12.08
9.5 9.0 8.5 8.0 7.5 7.0 6.5 6.0 5.5 5.0 4.5 4.0 3.5 3.0 2.5 ppm

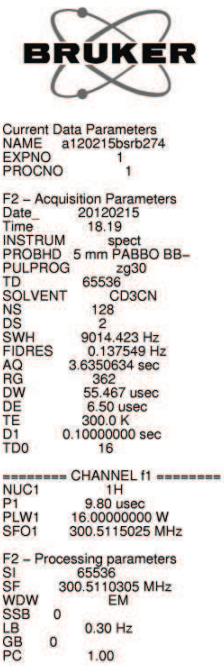
BRUKER
Current Data Parameters
NAME a120215bsrb274
EXPNO 1
PROCNO 1
F2 – Acquisition Parameters
Date_ 20120215
Time 18.19
INSTRUM spect
PROBHD 5 mm PABBO BB–
PULPROG zg30
TD 65536
SOLVENT CD3CN
NS 128
DS 2
SWH 9014.423 Hz
FIDRES 0.137549 Hz
AQ 3.6350634 sec
RG 362
DW 55.467 usec
DE 6.50 usec
TE 300.0 K
D1 0.10000000 sec
TD0 16
======== CHANNEL f1 ========
NUC1 1H
P1 9.80 usec
PLW1 16.00000000 W
SFO1 300.5115025 MHz
F2 – Processing parameters
SI 65536
SF 300.5110305 MHz
WDW EM
SSB 0
LB 0.30 Hz
GB 0
PC 1.00

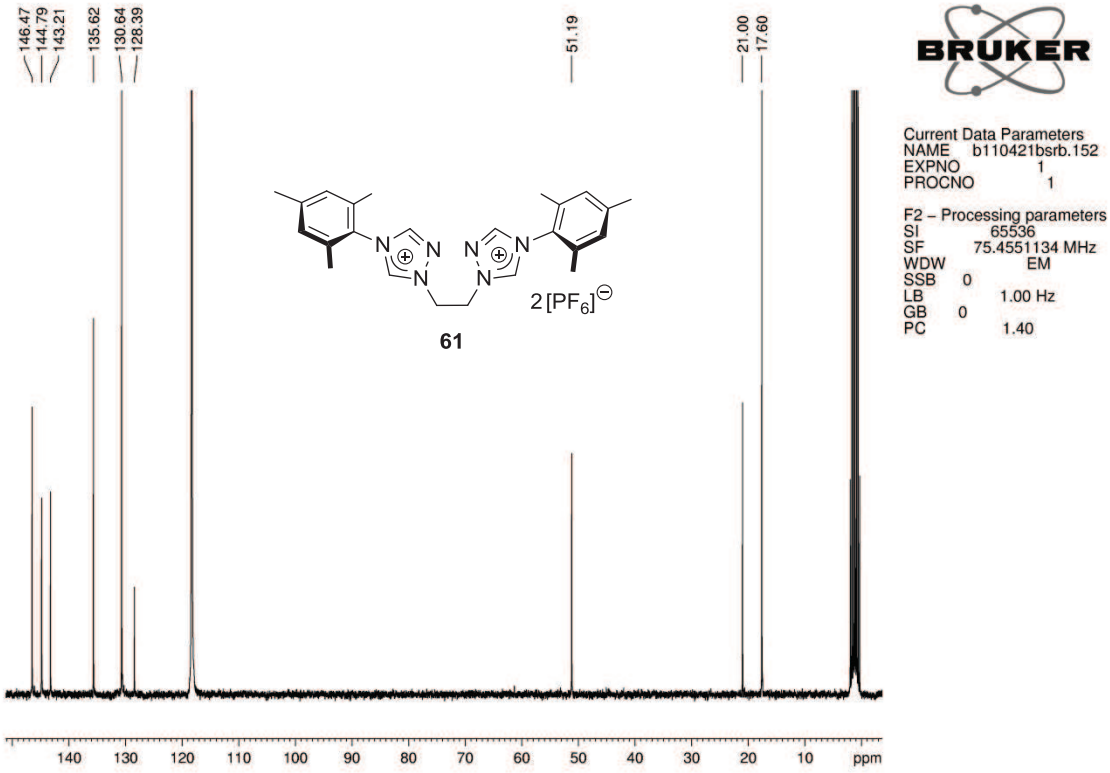
146.47
144.79
143.21
135.62
130.64
128.39
51.19
21.00
17.60
2 [PF6]⊖
61
BRUKER
Current Data Parameters
NAME b110421bsrb.152
EXPNO 1
PROCNO 1
F2 – Processing parameters
SI 65536
SF 75.4551134 MHz
WDW EM
SSB 0
LB 1.00 Hz
GB 0
PC 1.40
140 130 120 110 100 90 80 70 60 50 40 30 20 10 ppm

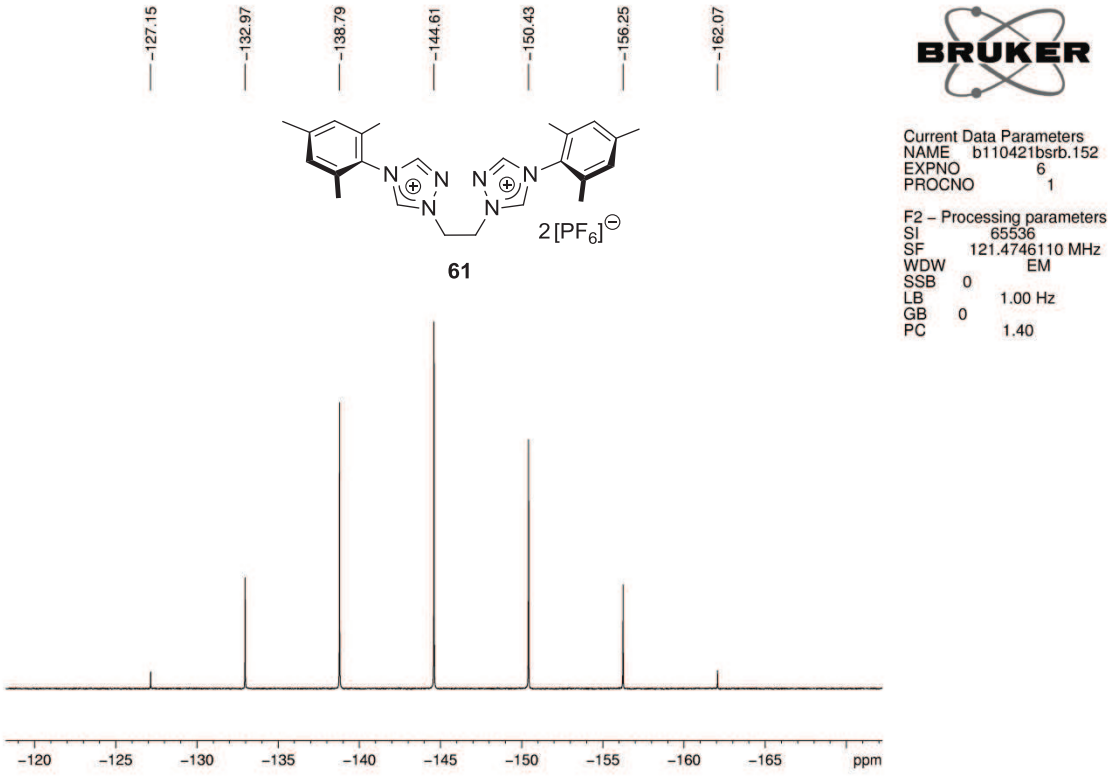
−127.15
−132.97
−138.79
−144.61
−150.43
−156.25
−162.07
2 [PF6]⊖
61
BRUKER
Current Data Parameters
NAME b110421bsrb.152
EXPNO 6
PROCNO 1
F2 – Processing parameters
SI 65536
SF 121.4746110 MHz
WDW EM
SSB 0
LB 1.00 Hz
GB 0
PC 1.40
−120 −125 −130 −135 −140 −145 −150 −155 −160 −165 ppm

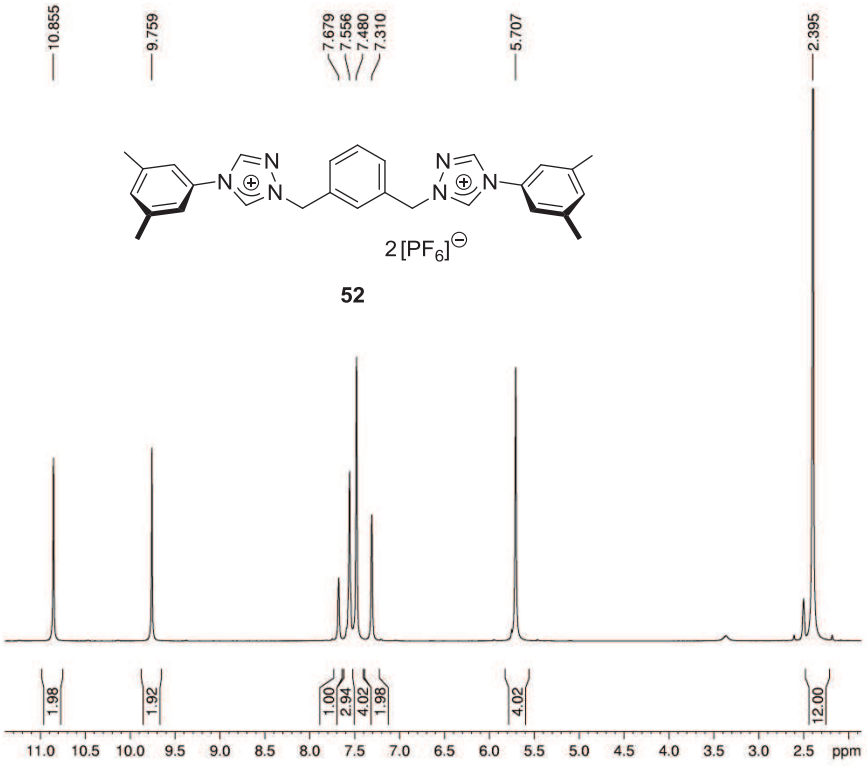

BRUKER

Current Data Parameters
NAME b120316bsrb.332
EXPNO 2
PROCNO 1

F2 – Acquisition Parameters
Date_ 20120316
Time 9.06
INSTRUM spect
PROBHD 5 mm TBI 1H–BB
PULPROG zg30
TD 65536
SOLVENT DMSO
NS 40
DS 2
SWH 8992.806 Hz
FIDRES 0.137219 Hz
AQ 3.6438017 sec
RG 256
DW 55.600 usec
DE 6.00 usec
TE 298.2 K
D1 0.10000000 sec
TD0 5

======== CHANNEL f1 ========
NUC1 1H
P1 8.40 usec
PL1 0 dB
SFO1 300.0815004 MHz

F2 – Processing parameters
SI 32768
SF 300.0800038 MHz
WDW EM
SSB 0
LB 0.30 Hz
GB 0
PC 1.00

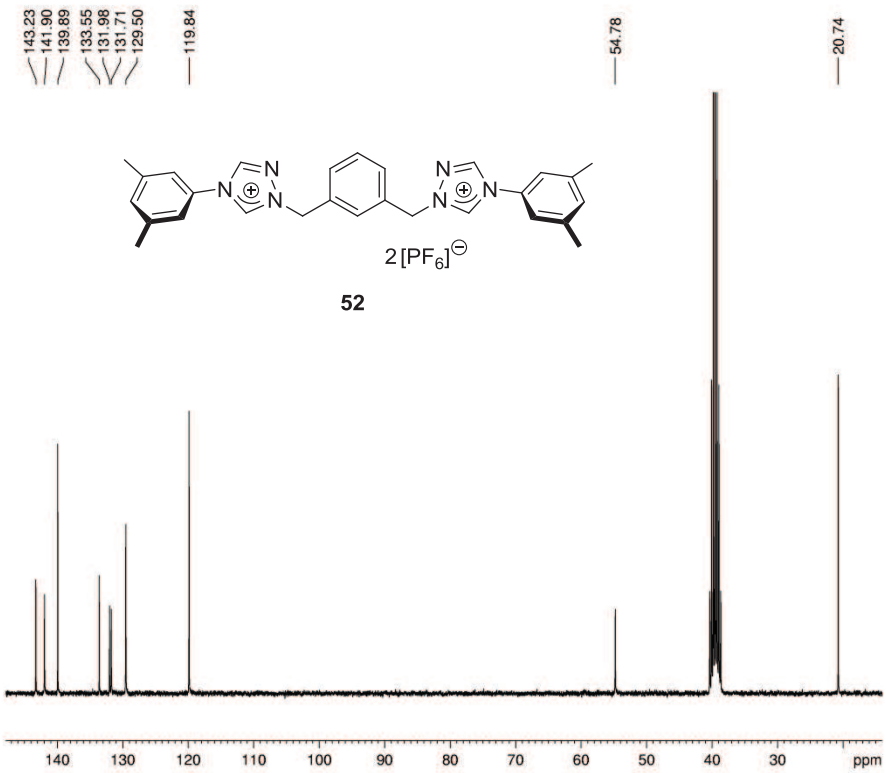

BRUKER

Current Data Parameters
NAME b120316bsrb.332
EXPNO 3
PROCNO 1

F2 – Processing parameters
SI 65536
SF 75.4552115 MHz
WDW EM
SSB 0
LB 1.00 Hz
GB 0
PC 1.40

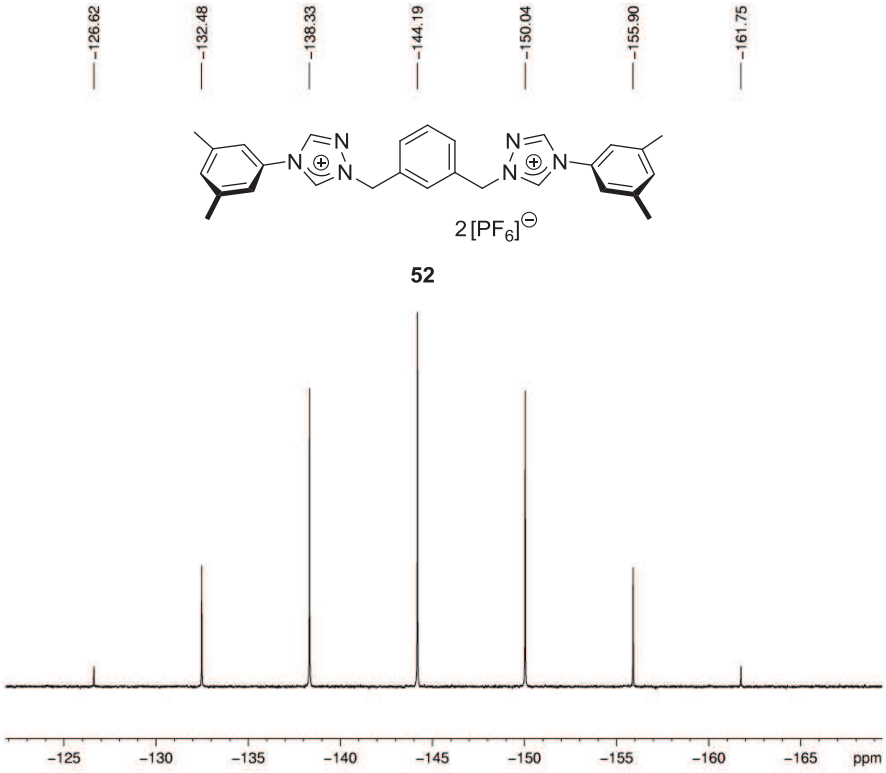

Current Data Parameters
NAME b120316bsrb.332
EXPNO 1
PROCNO 1

F2 – Processing parameters
SI 65536
SF 121.4746110 MHz
WDW EM
SSB 0
LB 1.00 Hz
GB 0
PC 1.40

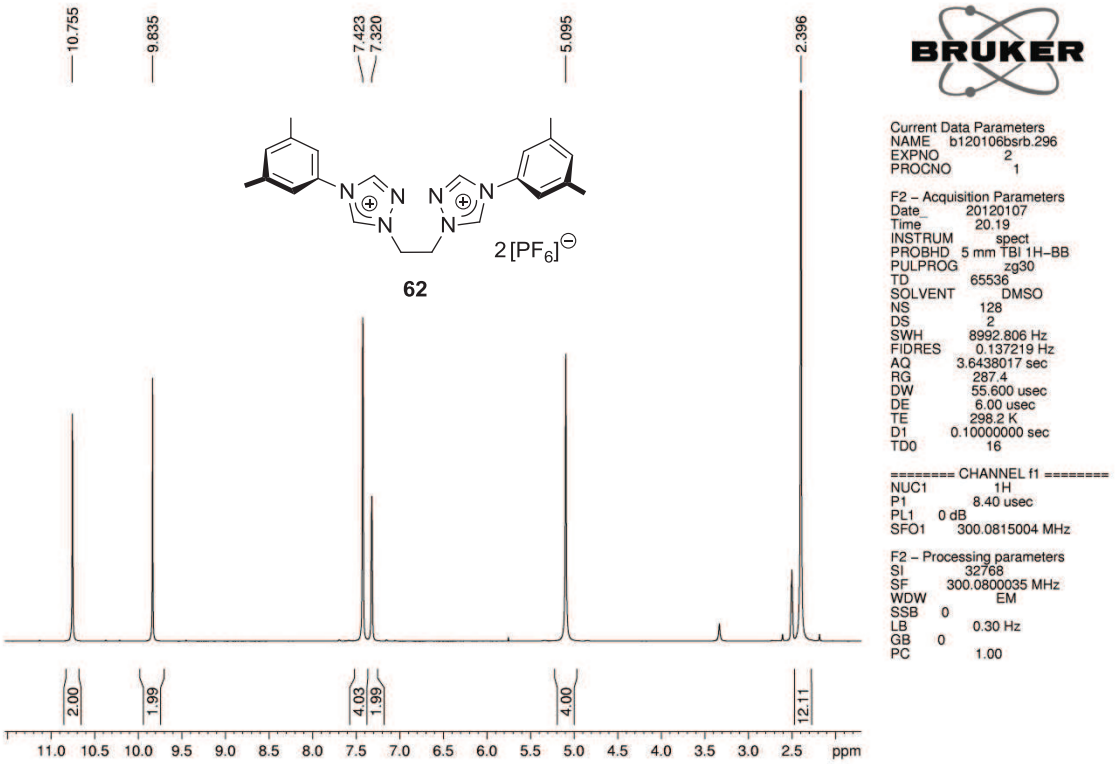

Current Data Parameters
NAME b120106bsrb.296
EXPNO 2
PROCNO 1

F2 – Acquisition Parameters
Date_ 20120107
Time 20.19
INSTRUM spect
PROBHD 5 mm TBI 1H-BB
PULPROG zg30
TD 65536
SOLVENT DMSO
NS 128
DS 2
SWH 8992.806 Hz
FIDRES 0.137219 Hz
AQ 3.6438017 sec
RG 287.4
DW 55.600 usec
DE 6.00 usec
TE 298.2 K
D1 0.10000000 sec
TD0 16

======== CHANNEL f1 ========
NUC1 1H
P1 8.40 usec
PL1 0 dB
SFO1 300.0815004 MHz

F2 – Processing parameters
SI 32768
SF 300.0800035 MHz
WDW EM
SSB 0
LB 0.30 Hz
GB 0
PC 1.00

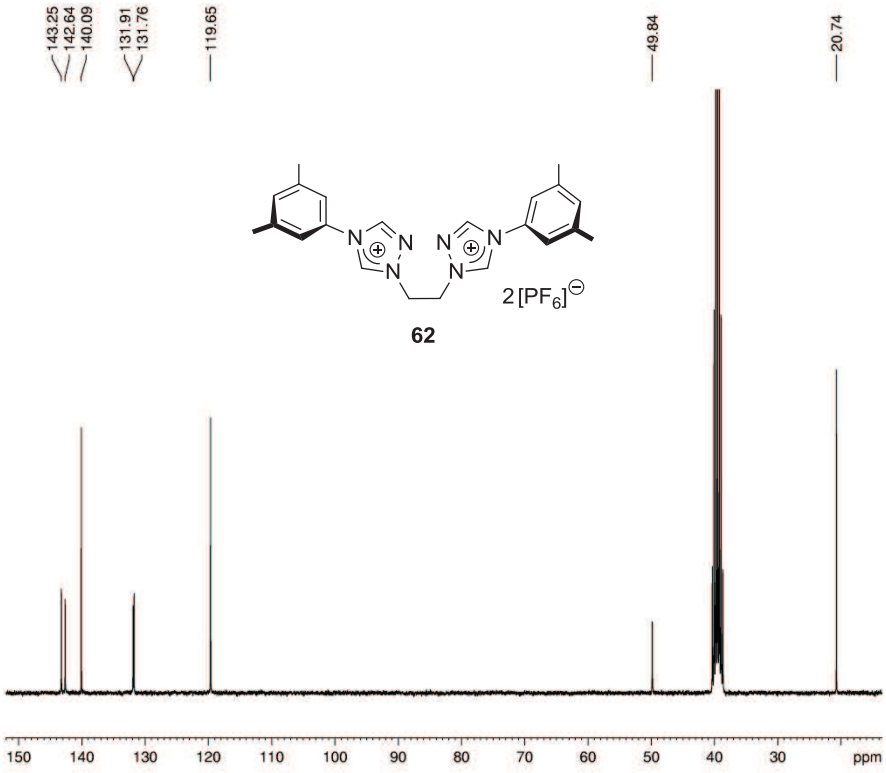

62

Current Data Parameters
NAME b120106bsrb.296
EXPNO 1
PROCNO 1

F2 – Processing parameters
SI 65536
SF 75.4552114 MHz
WDW EM
SSB 0
LB 1.00 Hz
GB 0
PC 1.40

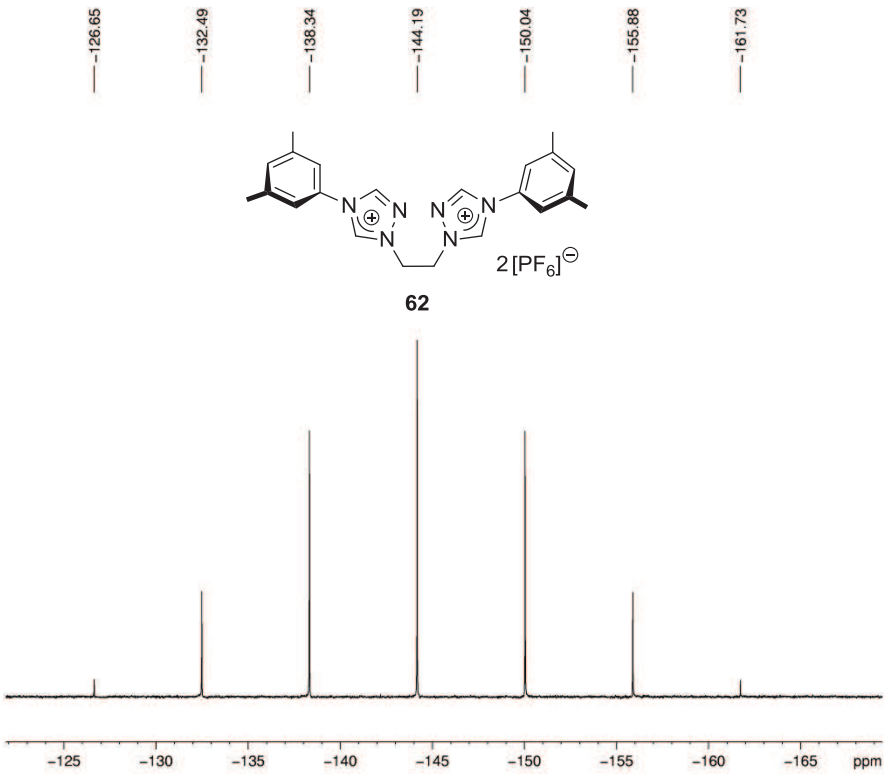

62

Current Data Parameters
NAME a120104bsrb296
EXPNO 2
PROCNO 1

F2 – Acquisition Parameters
Date_ 20120104
Time 18.50
INSTRUM spect
PROBHD 5 mm PABBO BB–
PULPROG zgpg30
TD 135168
SOLVENT DMSO
NS 64
DS 4
SWH 49019.609 Hz
FIDRES 0.362657 Hz
AQ 1.3787136 sec
RG 1820
DW 10.200 usec
DE 10.00 usec
TE 300.1 K
D1 1.00000000 sec
d11 0.03000000 sec
DELTA 0.89999998 sec
TD0 8
SFO1 121.6425956 MHz
NUC1 31P
P1 11.30 usec
PLW1 16.00000000 W
SFO2 300.5115025 MHz
NUC2 1H
CPDPRG[2 waltz65
PCPD2 80.00 usec
PLW2 16.00000000 W
PLW12 0.25000000 W
PLW13 0.16000000 W

F2 – Processing parameters
SI 65536
SF 121.6486780 MHz
WDW EM
SSB 0
LB 1.00 Hz
GB 0
PC 1.40

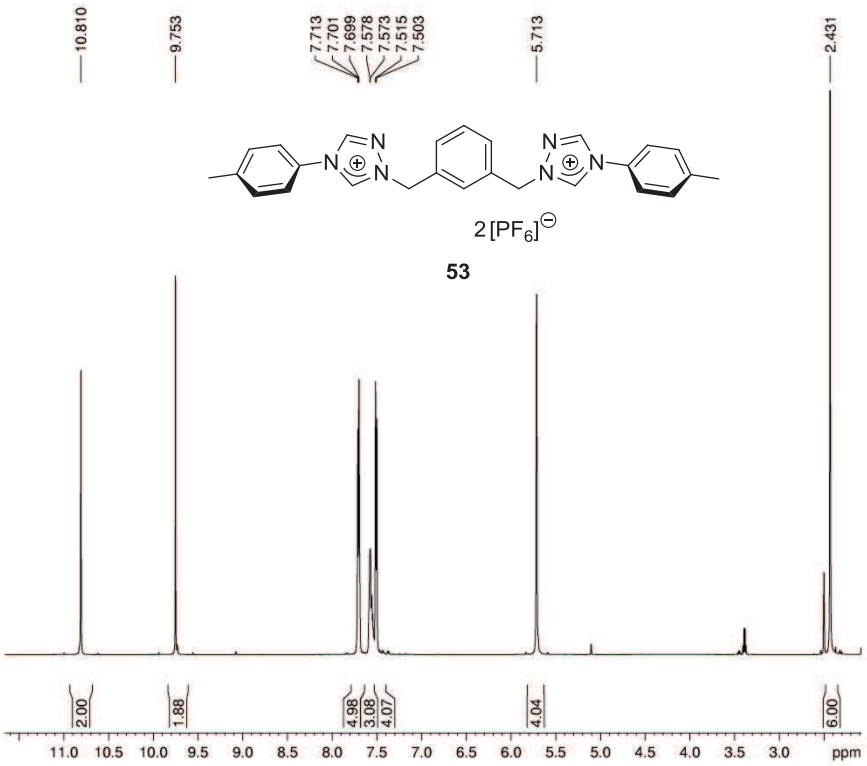

$2\,[PF_6]^{\ominus}$

53

BRUKER

Current Data Parameters
NAME e121022bsrb.482
EXPNO 2
PROCNO 1

F2 – Acquisition Parameters
Date_ 20121022
Time 10.54
INSTRUM spect
PROBHD 5 mm CPQCI 1H–
PULPROG zg30
TD 131072
SOLVENT DMSO
NS 128
DS 2
SWH 18028.846 Hz
FIDRES 0.137549 Hz
AQ 3.6350634 sec
RG 15.35
DW 27.733 usec
DE 12.00 usec
TE 295.0 K
D1 0.10000000 sec
TD0 16

======== CHANNEL f1 ========
SFO1 600.2468302 MHz
NUC1 1H
P1 7.63 usec
PLW1 7.50000000 W

F2 – Processing parameters
SI 65536
SF 600.2438331 MHz
WDW EM
SSB 0
LB 0.30 Hz
GB 0
PC 1.00

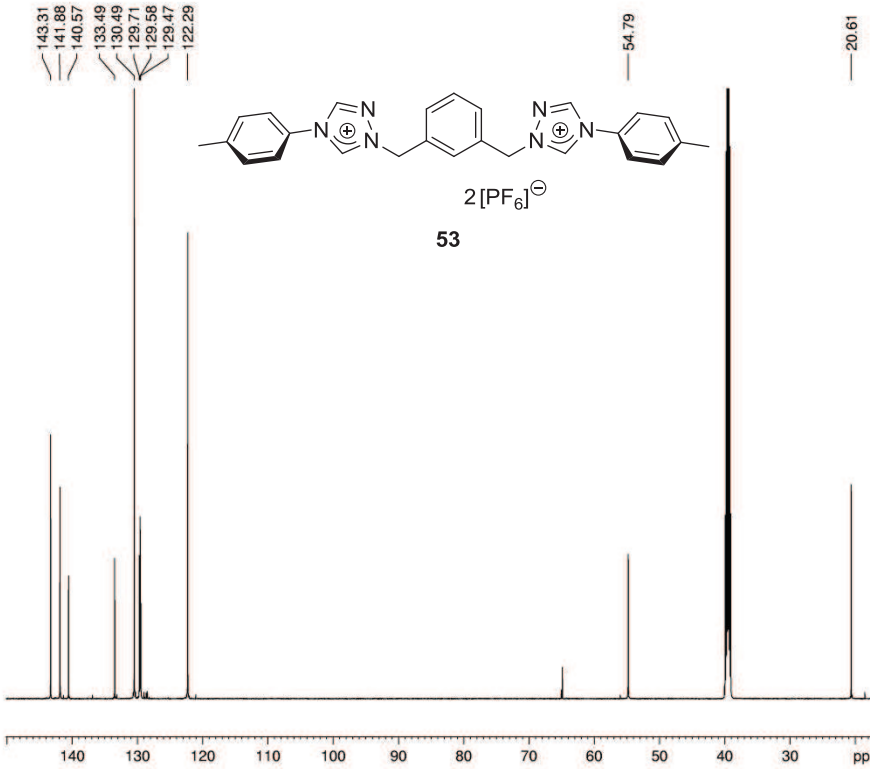

$2\,[PF_6]^{\ominus}$

53

BRUKER

Current Data Parameters
NAME e121022bsrb.482
EXPNO 1
PROCNO 1

F2 – Acquisition Parameters
Date_ 20121022
Time 7.18
INSTRUM spect
PROBHD 5 mm CPQCI 1H–
PULPROG zgpg30
TD 98132
SOLVENT DMSO
NS 4096
DS 4
SWH 45454.547 Hz
FIDRES 0.463198 Hz
AQ 1.0794520 sec
RG 1820
DW 11.000 usec
DE 16.00 usec
TE 295.0 K
D1 2.00000000 sec
D11 0.03000000 sec
TD0 512

======== CHANNEL f1 ========
SFO1 150.9480335 MHz
NUC1 13C
P1 12.50 usec
PLW1 87.00000000 W

======== CHANNEL f2 ========
SFO2 600.2462301 MHz
NUC2 1H
CPDPRG[2 waltz64
PCPD2 70.00 usec
PLW2 7.50000000 W
PLW12 0.08899100 W
PLW13 0.04360500 W

F2 – Processing parameters
SI 65536
SF 150.9315043 MHz
WDW EM
SSB 0
LB 1.00 Hz
GB 0
PC 1.40

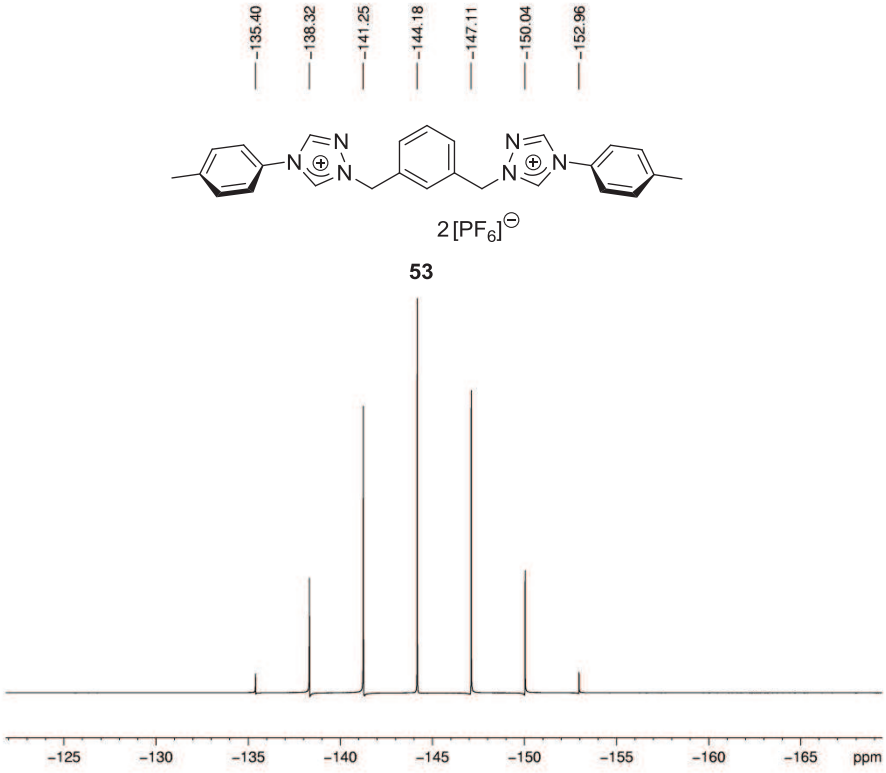

BRUKER

Current Data Parameters
NAME e121022bsrb.482
EXPNO 6
PROCNO 1

F2 – Acquisition Parameters
Date_ 20121022
Time 17.06
INSTRUM spect
PROBHD 5 mm CPQCI 1H–
PULPROG zgig30
TD 131072
SOLVENT DMSO
NS 512
DS 4
SWH 49019.609 Hz
FIDRES 0.373990 Hz
AQ 1.3369344 sec
RG 1620
DW 10.200 usec
DE 20.00 usec
TE 295.0 K
D1 2.00000000 sec
D11 0.03000000 sec
TD0 64

======== CHANNEL f1 ========
SFO1 242.9588577 MHz
NUC1 31P
P1 41.25 usec
PLW1 16.00000000 W

======== CHANNEL f2 ========
SFO2 600.2462301 MHz
NUC2 1H
CPDPRG[2 waltz64
PCPD2 70.00 usec
PLW2 7.50000000 W
PLW12 0.08899100 W

F2 – Processing parameters
SI 65536
SF 242.9831560 MHz
WDW EM
SSB 0
LB 1.00 Hz
GB 0
PC 1.40

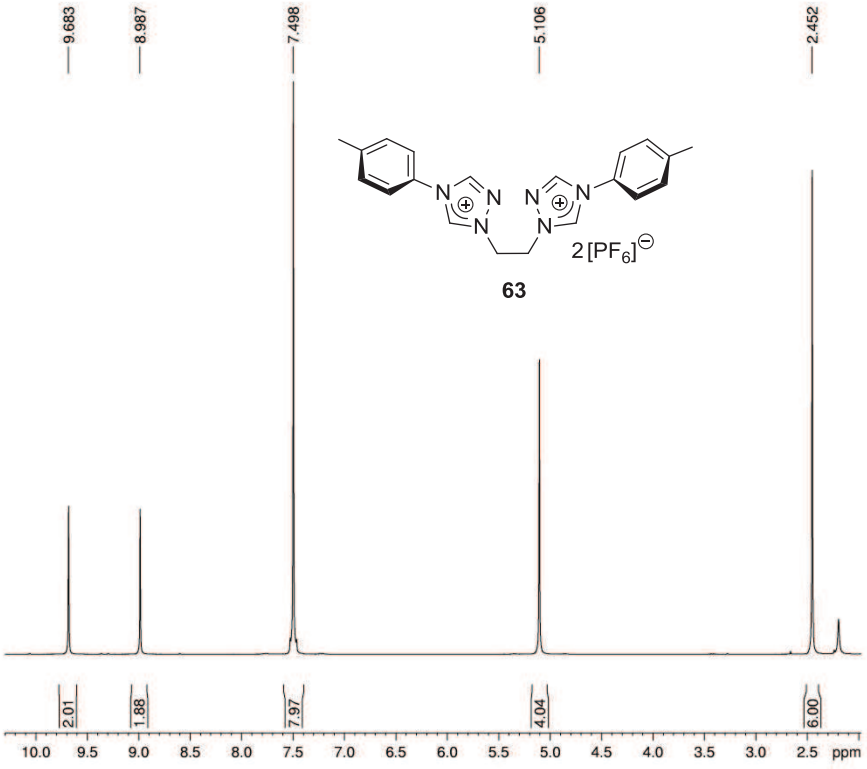

BRUKER

Current Data Parameters
NAME b110913bsrb.220
EXPNO 2
PROCNO 1

F2 – Acquisition Parameters
Date_ 20110913
Time 12.06
INSTRUM spect
PROBHD 5 mm TBI 1H–BB
PULPROG zg30
TD 65536
SOLVENT CD3CN
NS 40
DS 2
SWH 8992.806 Hz
FIDRES 0.137219 Hz
AQ 3.6438017 sec
RG 287.4
DW 55.600 usec
DE 6.00 usec
TE 299.2 K
D1 0.10000000 sec
TD0 5

======== CHANNEL f1 ========
NUC1 1H
P1 9.50 usec
PL1 0 dB
SFO1 300.0815004 MHz

F2 – Processing parameters
SI 32768
SF 300.0800094 MHz
WDW EM
SSB 0
LB 0.30 Hz
GB 0
PC 1.00

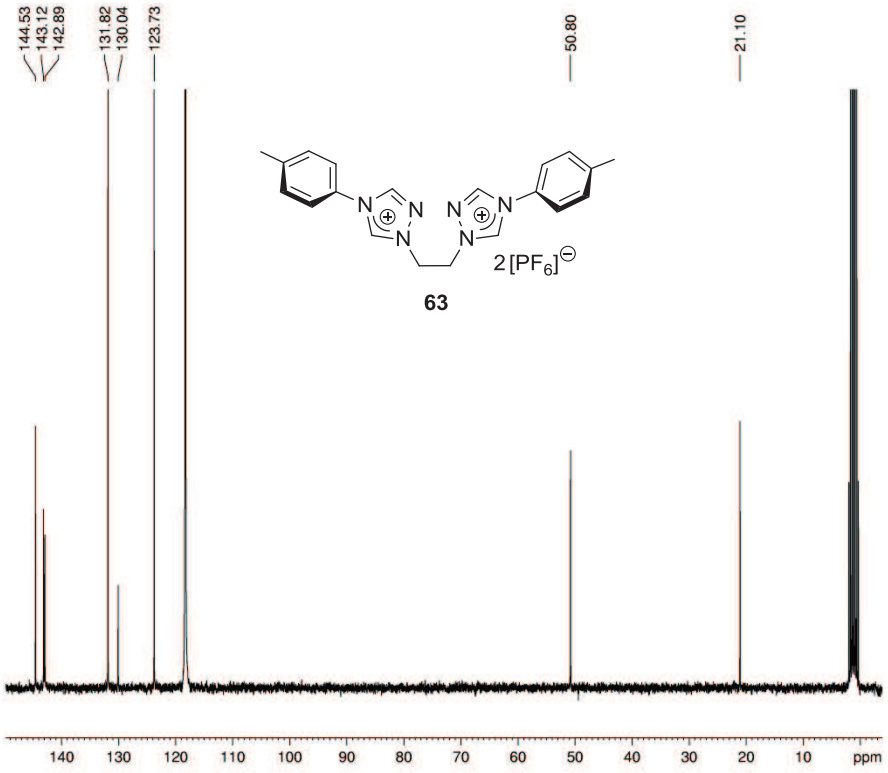

Current Data Parameters
NAME b110913bsrb.220
EXPNO 1
PROCNO 1

F2 – Processing parameters
SI 65536
SF 75.4551117 MHz
WDW EM
SSB 0
LB 1.00 Hz
GB 0
PC 1.40

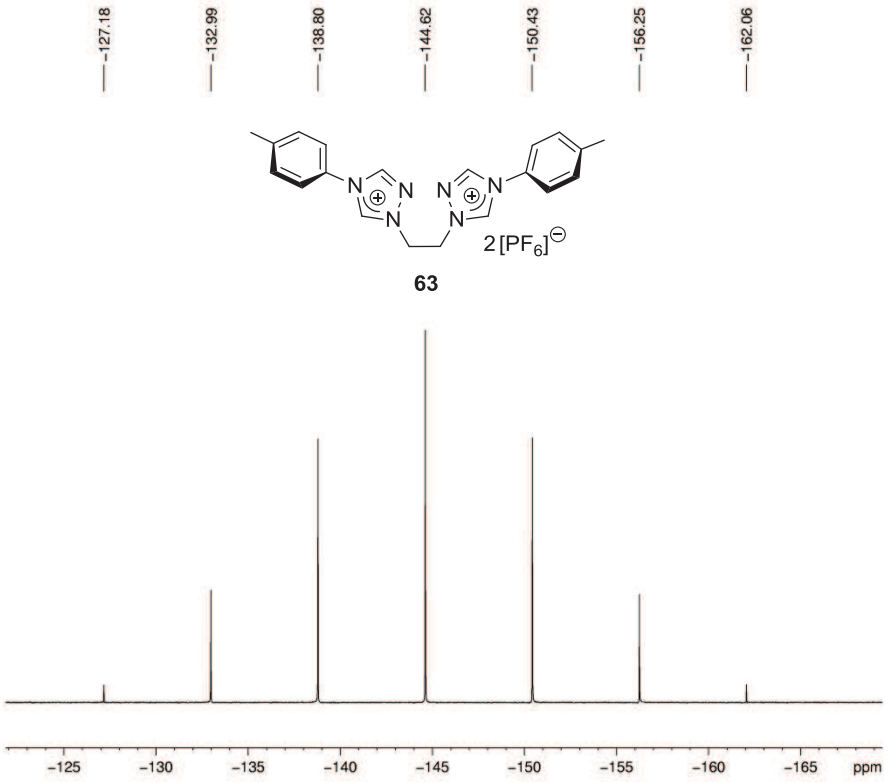

Current Data Parameters
NAME a110919bsrb220
EXPNO 2
PROCNO 1

F2 – Acquisition Parameters
Date_ 20110919
Time 15.26
INSTRUM spect
PROBHD 5 mm PABBO BB–
PULPROG zgpg30
TD 135168
SOLVENT CD3CN
NS 64
DS 4
SWH 49019.609 Hz
FIDRES 0.362657 Hz
AQ 1.3787136 sec
RG 2050
DW 10.200 usec
DE 10.00 usec
TE 300.1 K
D1 1.00000000 sec
d11 0.03000000 sec
DELTA 0.89999998 sec
TD0 8
SFO1 121.6425956 MHz
NUC1 31P
P1 11.30 usec
PLW1 16.00000000 W
SFO2 300.5115025 MHz
NUC2 1H
CPDPRG[2 waltz65
PCPD2 80.00 usec
PLW2 16.00000000 W
PLW12 0.25000000 W
PLW13 0.16000000 W

F2 – Processing parameters
SI 65536
SF 121.6486780 MHz
WDW EM
SSB 0
LB 1.00 Hz
GB 0
PC 1.40

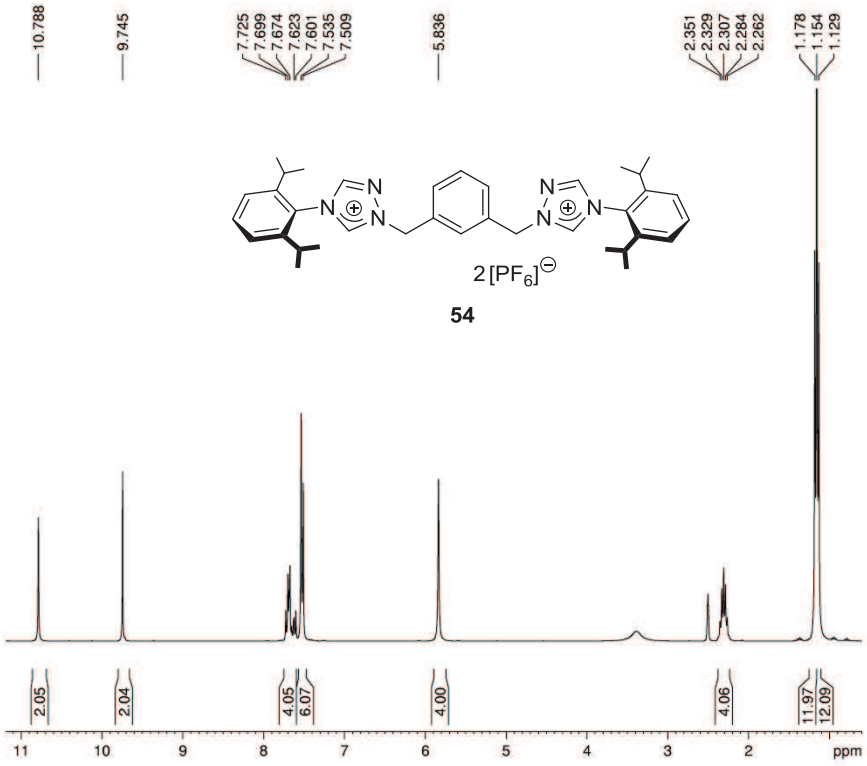

$2\,[PF_6]^{\ominus}$

54

Current Data Parameters
NAME b110610bscc.CD006
EXPNO 2
PROCNO 1

F2 – Acquisition Parameters
Date_ 20110612
Time 15.29
INSTRUM spect
PROBHD 5 mm TBI 1H–BB
PULPROG zg30
TD 65536
SOLVENT DMSO
NS 40
DS 2
SWH 8992.806 Hz
FIDRES 0.137219 Hz
AQ 3.6438017 sec
RG 161.3
DW 55.600 usec
DE 6.00 usec
TE 298.2 K
D1 0.10000000 sec
TD0 5

======== CHANNEL f1 ========
NUC1 1H
P1 9.50 usec
PL1 0 dB
SFO1 300.0815004 MHz

F2 – Processing parameters
SI 32768
SF 300.0800035 MHz
WDW EM
SSB 0
LB 0.30 Hz
GB 0
PC 1.00

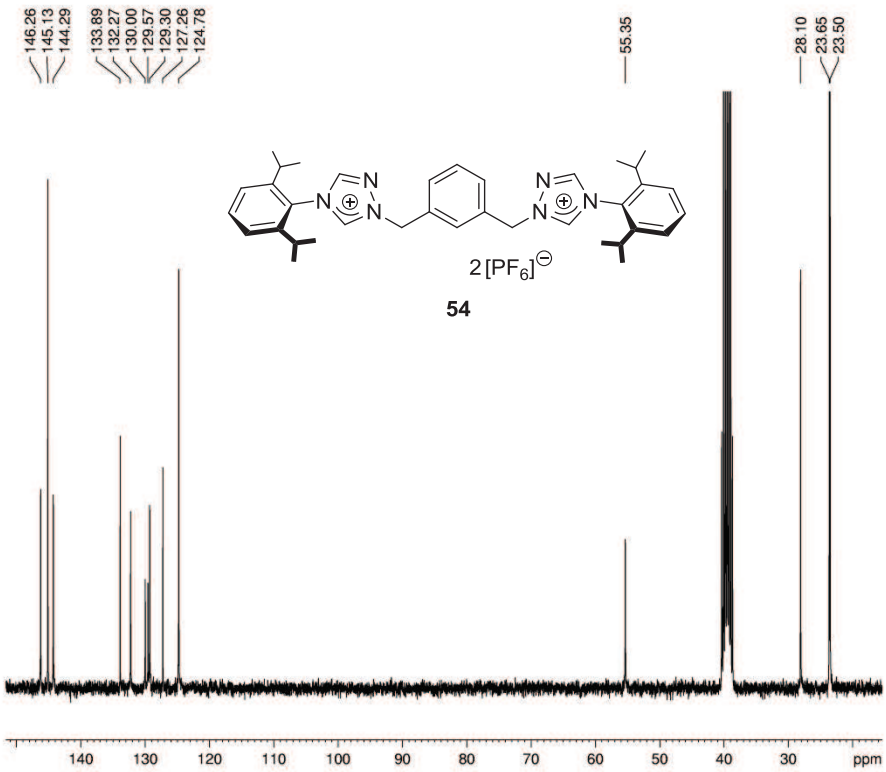

$2\,[PF_6]^{\ominus}$

54

Current Data Parameters
NAME b110610bscc.CD006
EXPNO 1
PROCNO 1

F2 – Processing parameters
SI 65536
SF 75.4552116 MHz
WDW EM
SSB 0
LB 1.00 Hz
GB 0
PC 1.40

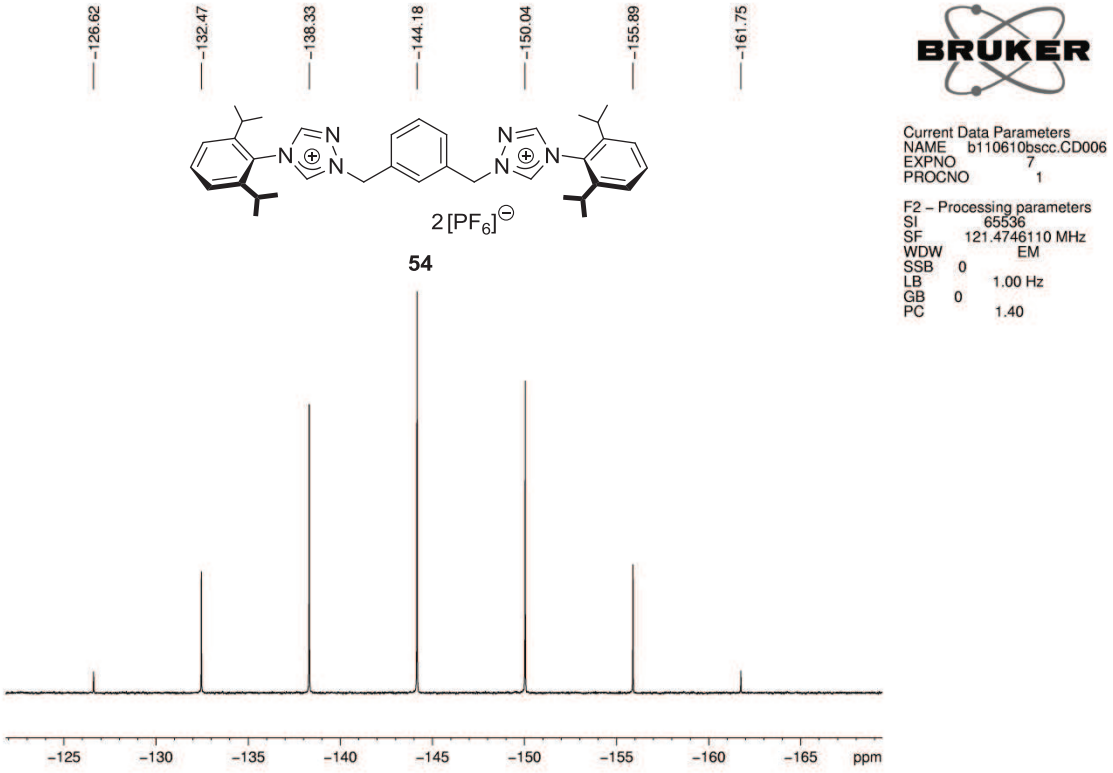
126.62
132.47
138.33
144.18
150.04
155.89
161.75
2 [PF6]⊖
54
BRUKER
Current Data Parameters
NAME b110610bscc.CD006
EXPNO 7
PROCNO 1
F2 – Processing parameters
SI 65536
SF 121.4746110 MHz
WDW EM
SSB 0
LB 1.00 Hz
GB 0
PC 1.40
−125
−130
−135
−140
−145
−150
−155
−160
−165
ppm

1.7 Unsymmetrically Substituted Bistriazolium Hexafluorophosphate Salts

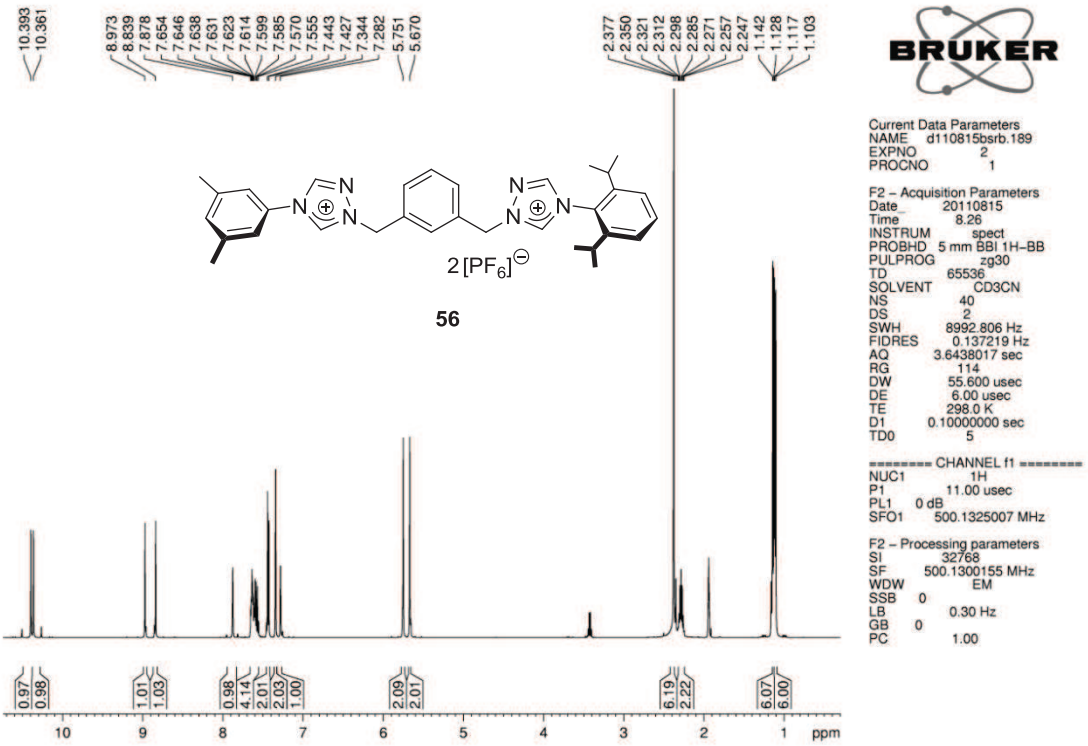

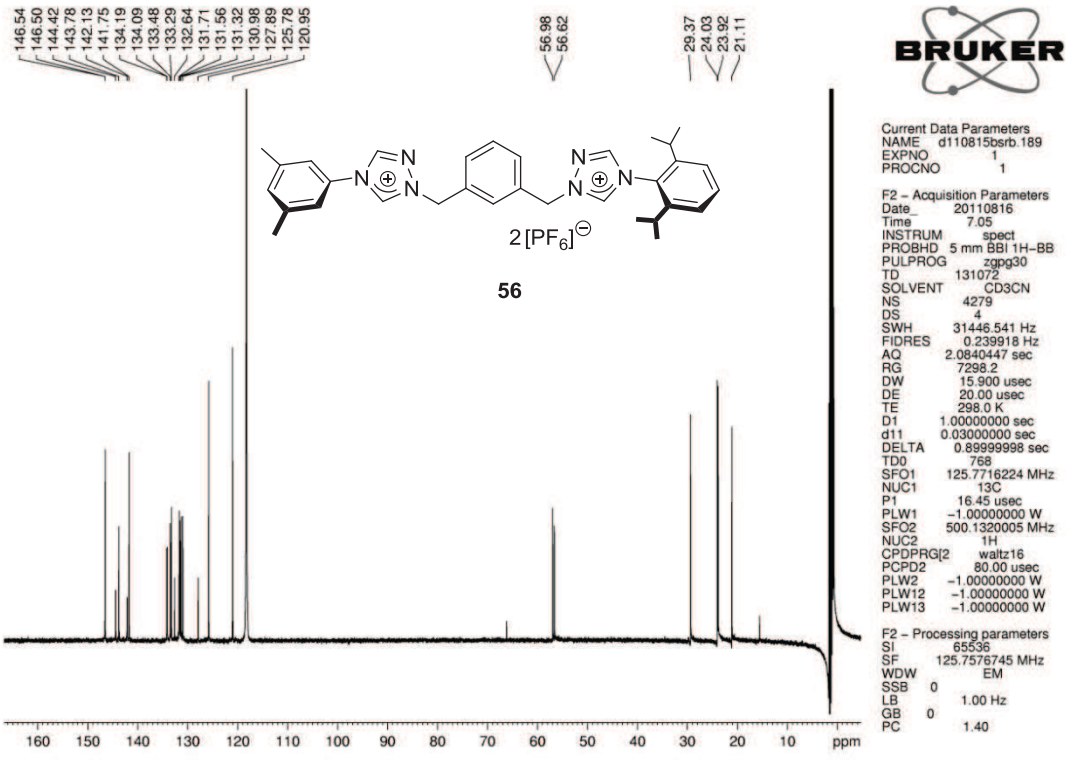

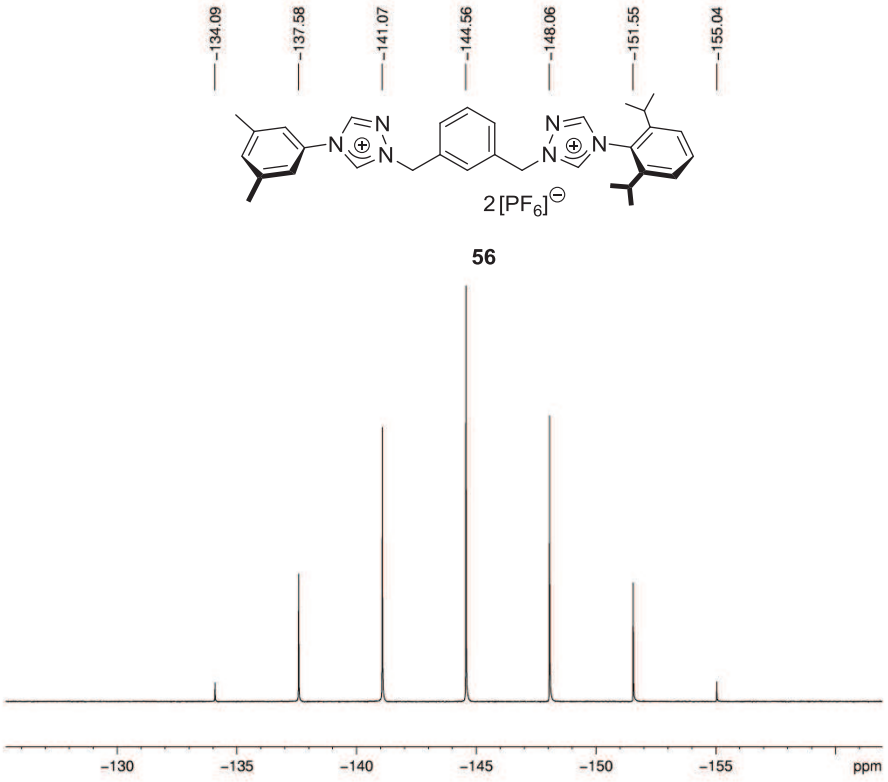

56

Current Data Parameters
NAME d110815bsrb.189
EXPNO 7
PROCNO 1

F2 – Acquisition Parameters
Date_ 20110815
Time 8.31
INSTRUM spect
PROBHD 5 mm BBI 1H–BB
PULPROG zgpg30
TD 262144
SOLVENT CD3CN
NS 408
DS 4
SWH 60606.063 Hz
FIDRES 0.231194 Hz
AQ 2.1626880 sec
RG 8192
DW 8.250 usec
DE 20.00 usec
TE 298.0 K
D1 1.00000000 sec
d11 0.03000000 sec
DELTA 0.89999998 sec
TD0 100
SFO1 202.4360894 MHz
NUC1 31P
P1 23.00 usec
PLW1 −1.00000000 W
SFO2 500.1320005 MHz
NUC2 1H
CPDPRG[2 waltz16
PCPD2 80.00 usec
PLW2 −1.00000000 W
PLW12 −1.00000000 W
PLW13 −1.00000000 W

F2 – Processing parameters
SI 65536
SF 202.4563350 MHz
WDW EM
SSB 0
LB 1.00 Hz
GB 0
PC 1.40

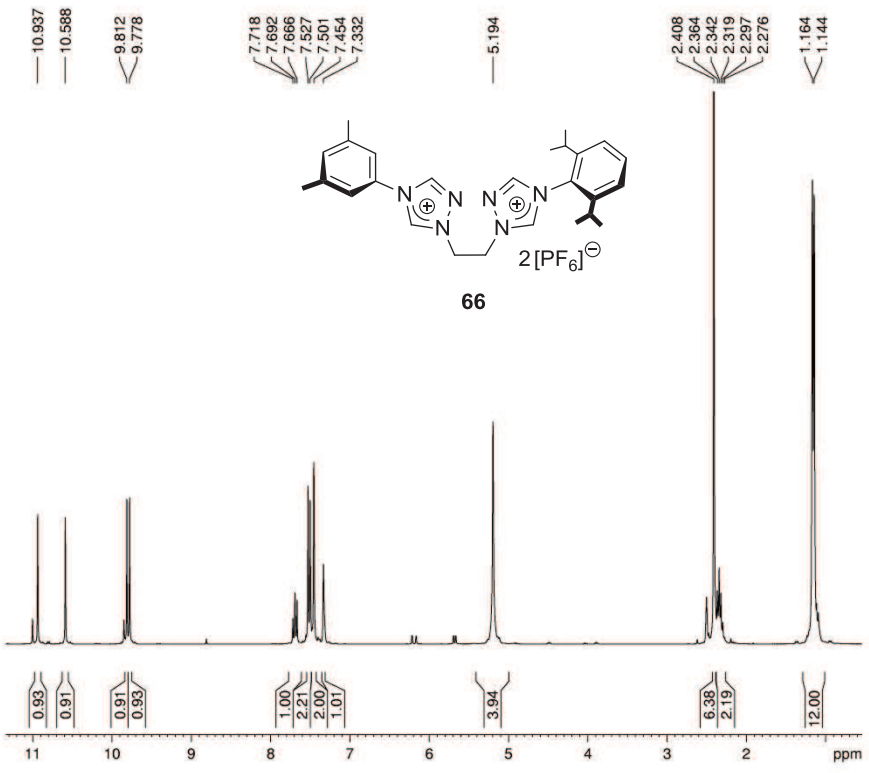

66

Current Data Parameters
NAME c110809bsrb.197
EXPNO 2
PROCNO 1

F2 – Acquisition Parameters
Date_ 20110809
Time 15.47
INSTRUM spect
PROBHD 5 mm QNP 1H/13
PULPROG zg30
TD 65536
SOLVENT DMSO
NS 40
DS 2
SWH 8992.806 Hz
FIDRES 0.137219 Hz
AQ 3.6438017 sec
RG 256
DW 55.600 usec
DE 6.00 usec
TE 300.0 K
D1 0.10000000 sec
TD0 5

======== CHANNEL f1 ========
NUC1 1H
P1 11.50 usec
PL1 −2.20 dB
SFO1 300.1915009 MHz

F2 – Processing parameters
SI 32768
SF 300.1900051 MHz
WDW EM
SSB 0
LB 0.30 Hz
GB 0
PC 1.00

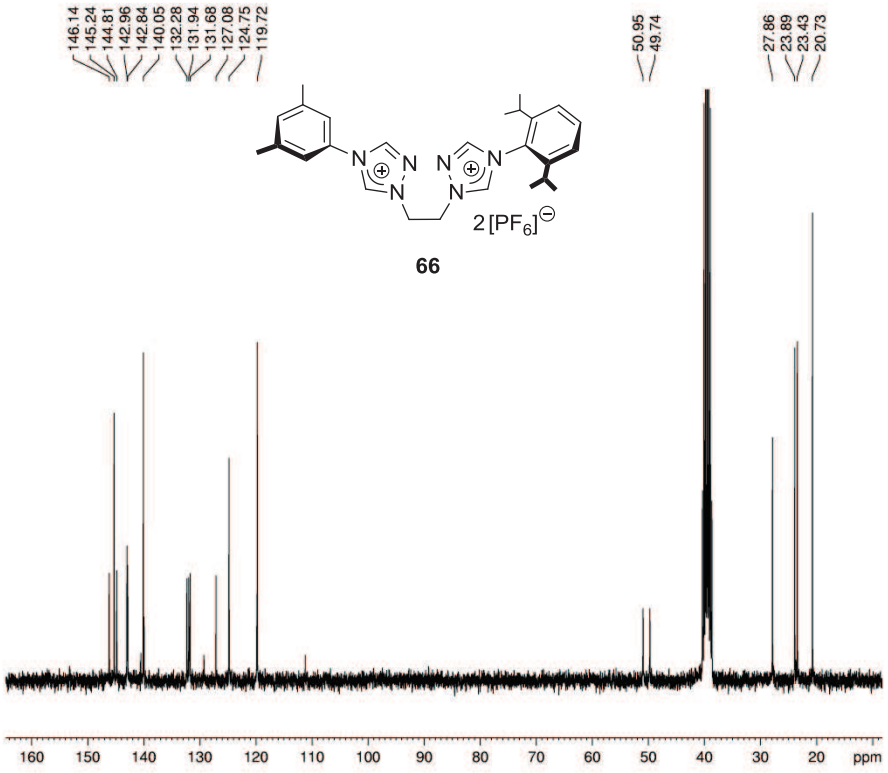

66

BRUKER

Current Data Parameters
NAME c110809bsrb.197
EXPNO 1
PROCNO 1

F2 – Acquisition Parameters
Date_ 20110809
Time 14.58
INSTRUM spect
PROBHD 5 mm QNP 1H/13
PULPROG zgpg30
TD 65536
SOLVENT DMSO
NS 1024
DS 4
SWH 18832.393 Hz
FIDRES 0.287360 Hz
AQ 1.7399808 sec
RG 13004
DW 26.550 usec
DE 6.00 usec
TE 300.0 K
D1 1.00000000 sec
d11 0.03000000 sec
DELTA 0.89999998 sec
TD0 128
SFO1 75.4915175 MHz
NUC1 13C
P1 11.60 usec
PLW1 –1.00000000 W
SFO2 300.1912008 MHz
NUC2 1H
CPDPRG[2 waltz65
PCPD2 100.00 usec
PLW2 –1.00000000 W
PLW12 –1.00000000 W
PLW13 –1.00000000 W

F2 – Processing parameters
SI 32768
SF 75.4828720 MHz
WDW EM
SSB 0
LB 1.00 Hz
GB 0
PC 1.40

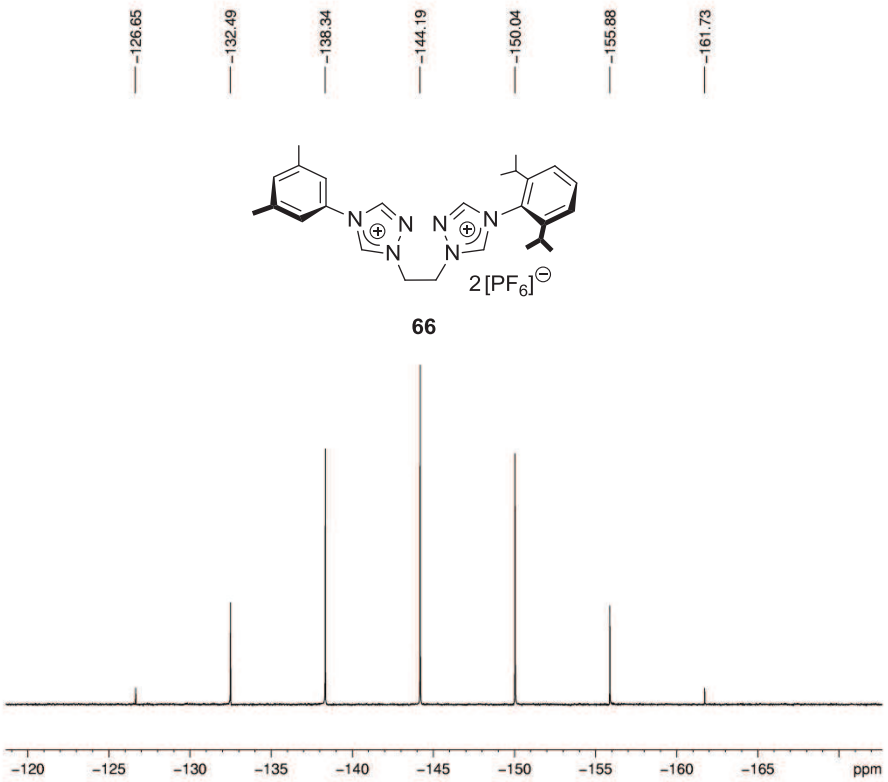

66

BRUKER

Current Data Parameters
NAME a110707bsrb192
EXPNO 2
PROCNO 1

F2 – Acquisition Parameters
Date_ 20110707
Time 15.07
INSTRUM spect
PROBHD 5 mm PABBO BB–
PULPROG zgpg30
TD 135168
SOLVENT DMSO
NS 64
DS 4
SWH 49019.609 Hz
FIDRES 0.362657 Hz
AQ 1.3787136 sec
RG 2050
DW 10.200 usec
DE 10.00 usec
TE 0 K
D1 1.00000000 sec
d11 0.03000000 sec
DELTA 0.89999998 sec
TD0 8
SFO1 121.6425956 MHz
NUC1 31P
P1 11.30 usec
PLW1 16.00000000 W
SFO2 300.5115025 MHz
NUC2 1H
CPDPRG[2 waltz65
PCPD2 80.00 usec
PLW2 16.00000000 W
PLW12 0.25000000 W
PLW13 0.16000000 W

F2 – Processing parameters
SI 65536
SF 121.6486780 MHz
WDW EM
SSB 0
LB 1.00 Hz
GB 0
PC 1.40

1.8 Dinuclear Copper Complexes Containing IPr-Ligands

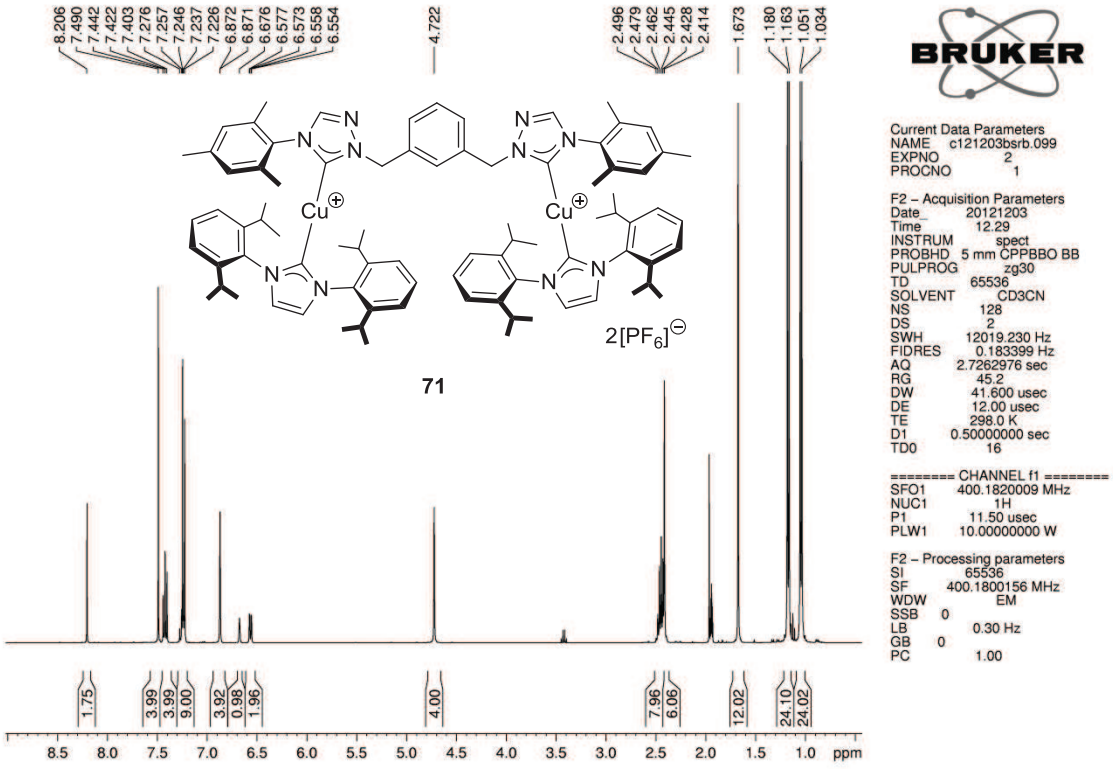

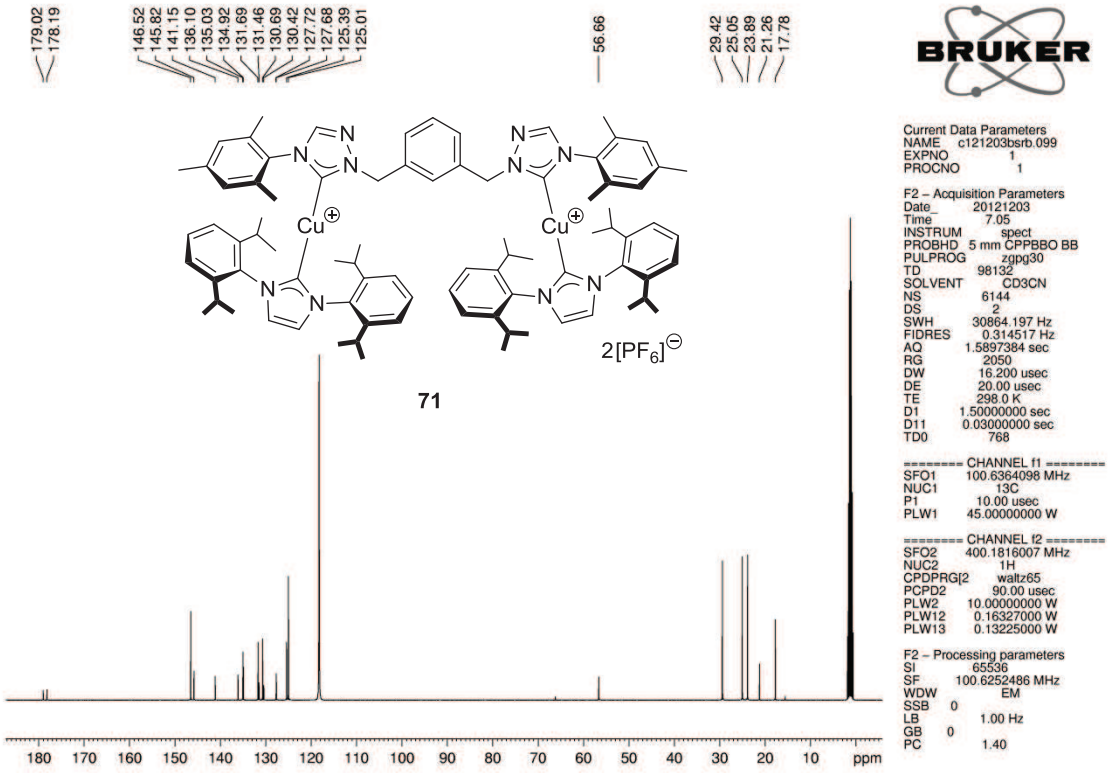

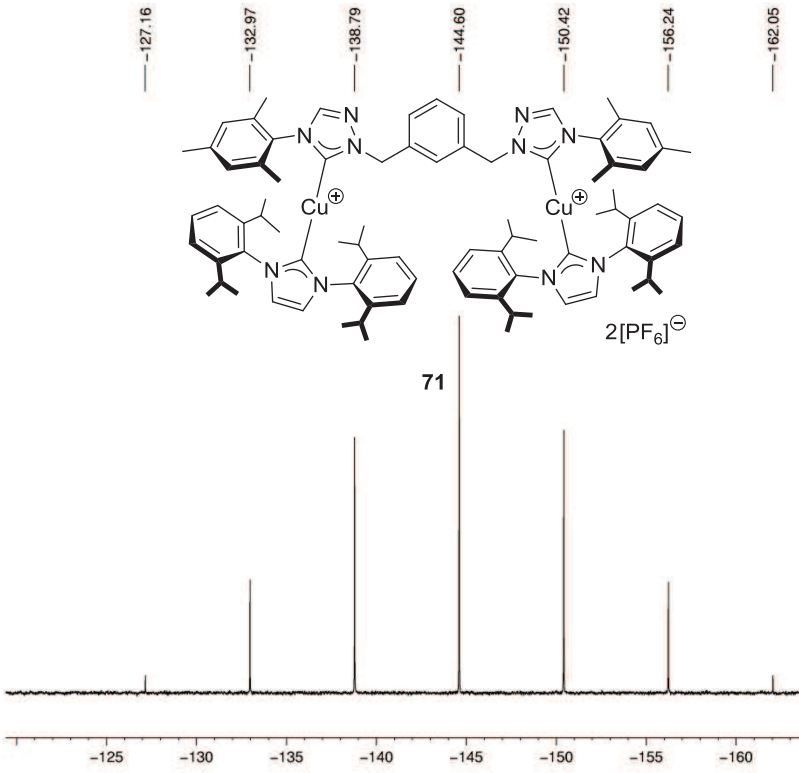

Current Data Parameters
NAME b111208bsrb.099UK
EXPNO 1
PROCNO 1

F2 – Processing parameters
SI 65536
SF 121.4746110 MHz
WDW EM
SSB 0
LB 1.00 Hz
GB 0
PC 1.40

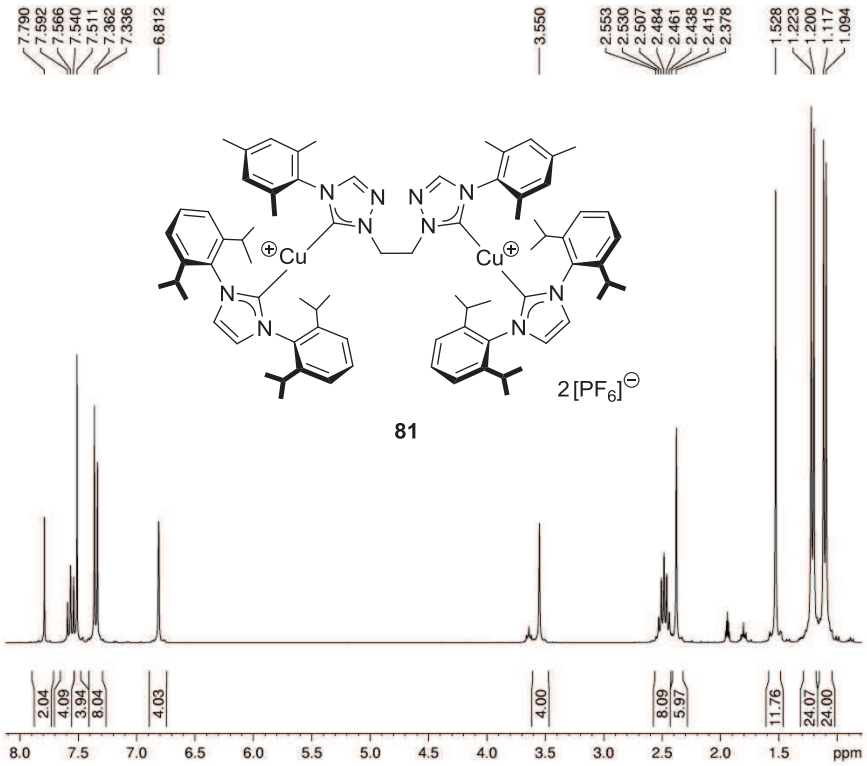

Current Data Parameters
NAME c110513bsrb.170
EXPNO 2
PROCNO 1

F2 – Acquisition Parameters
Date_ 20110514
Time 23.12
INSTRUM spect
PROBHD 5 mm QNP 1H/13
PULPROG zg30
TD 65536
SOLVENT CD3CN
NS 128
DS 2
SWH 8992.806 Hz
FIDRES 0.137219 Hz
AQ 3.6438017 sec
RG 181
DW 55.600 usec
DE 6.00 usec
TE 300.0 K
D1 0.10000000 sec
TD0 16

======== CHANNEL f1 ========
NUC1 1H
P1 11.50 usec
PL1 −2.20 dB
SFO1 300.1915009 MHz

F2 – Processing parameters
SI 32768
SF 300.1900114 MHz
WDW EM
SSB 0
LB 0.30 Hz
GB 0
PC 1.00

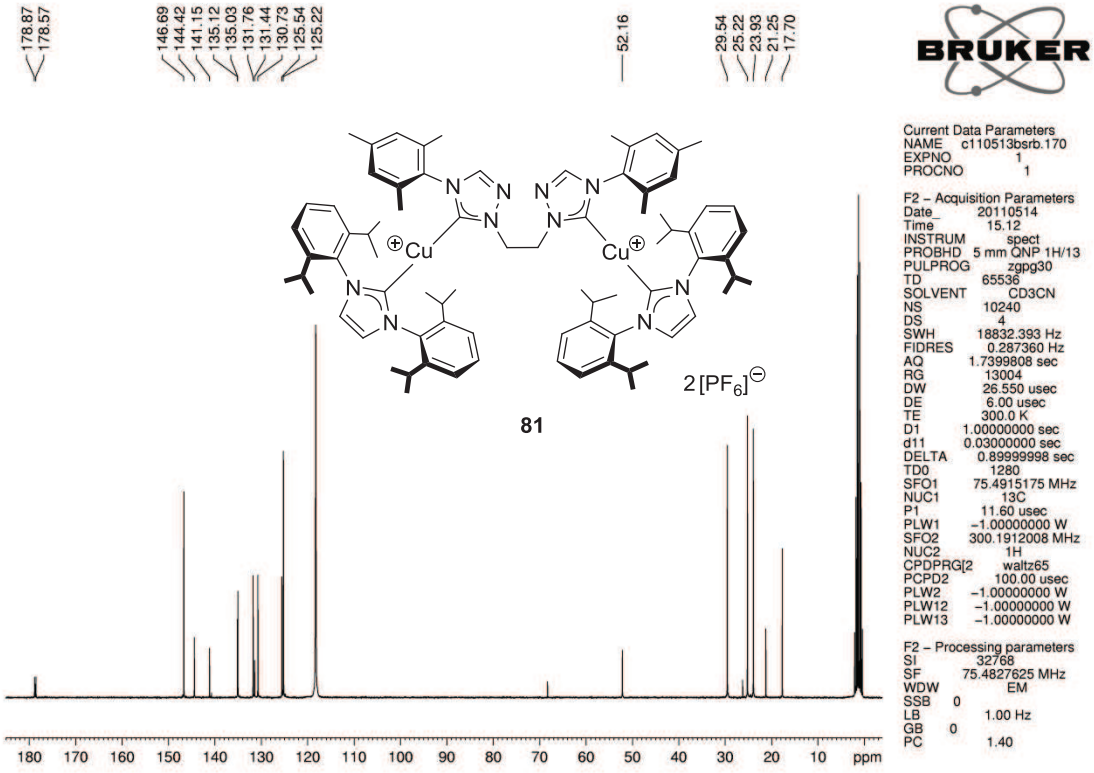
178.87
178.57
146.69
144.42
141.15
135.12
135.03
131.76
131.44
130.73
125.54
125.22
52.16
29.54
25.22
23.93
21.25
17.70
BRUKER
Cu
Cu
2 [PF6]⊖
81
180 170 160 150 140 130 120 110 100 90 80 70 60 50 40 30 20 10 ppm
Current Data Parameters
NAME c110513bsrb.170
EXPNO 1
PROCNO 1
F2 – Acquisition Parameters
Date_ 20110514
Time 15.12
INSTRUM spect
PROBHD 5 mm QNP 1H/13
PULPROG zgpg30
TD 65536
SOLVENT CD3CN
NS 10240
DS 4
SWH 18832.393 Hz
FIDRES 0.287360 Hz
AQ 1.7399808 sec
RG 13004
DW 26.550 usec
DE 6.00 usec
TE 300.0 K
D1 1.00000000 sec
d11 0.03000000 sec
DELTA 0.89999998 sec
TD0 1280
SFO1 75.4915175 MHz
NUC1 13C
P1 11.60 usec
PLW1 −1.00000000 W
SFO2 300.1912008 MHz
NUC2 1H
CPDPRG[2 waltz65
PCPD2 100.00 usec
PLW2 −1.00000000 W
PLW12 −1.00000000 W
PLW13 −1.00000000 W
F2 – Processing parameters
SI 32768
SF 75.4827625 MHz
WDW EM
SSB 0
LB 1.00 Hz
GB 0
PC 1.40

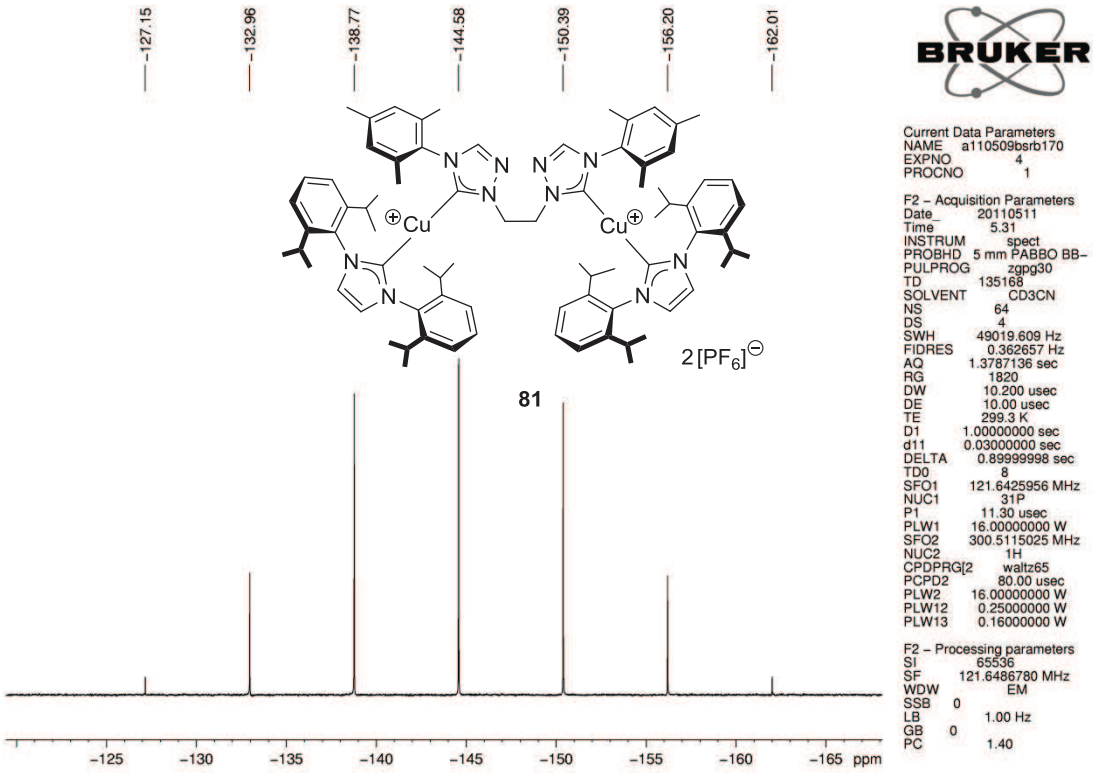
−127.15
−132.96
−138.77
−144.58
−150.39
−156.20
−162.01
BRUKER
Cu
Cu
2 [PF6]⊖
81
−125 −130 −135 −140 −145 −150 −155 −160 −165 ppm
Current Data Parameters
NAME a110509bsrb170
EXPNO 4
PROCNO 1
F2 – Acquisition Parameters
Date_ 20110511
Time 5.31
INSTRUM spect
PROBHD 5 mm PABBO BB−
PULPROG zgpg30
TD 135168
SOLVENT CD3CN
NS 64
DS 4
SWH 49019.609 Hz
FIDRES 0.362657 Hz
AQ 1.3787136 sec
RG 1820
DW 10.200 usec
DE 10.00 usec
TE 299.3 K
D1 1.00000000 sec
d11 0.03000000 sec
DELTA 0.89999998 sec
TD0 8
SFO1 121.6425956 MHz
NUC1 31P
P1 11.30 usec
PLW1 16.00000000 W
SFO2 300.5115025 MHz
NUC2 1H
CPDPRG[2 waltz65
PCPD2 80.00 usec
PLW2 16.00000000 W
PLW12 0.25000000 W
PLW13 0.16000000 W
F2 – Processing parameters
SI 65536
SF 121.6486780 MHz
WDW EM
SSB 0
LB 1.00 Hz
GB 0
PC 1.40

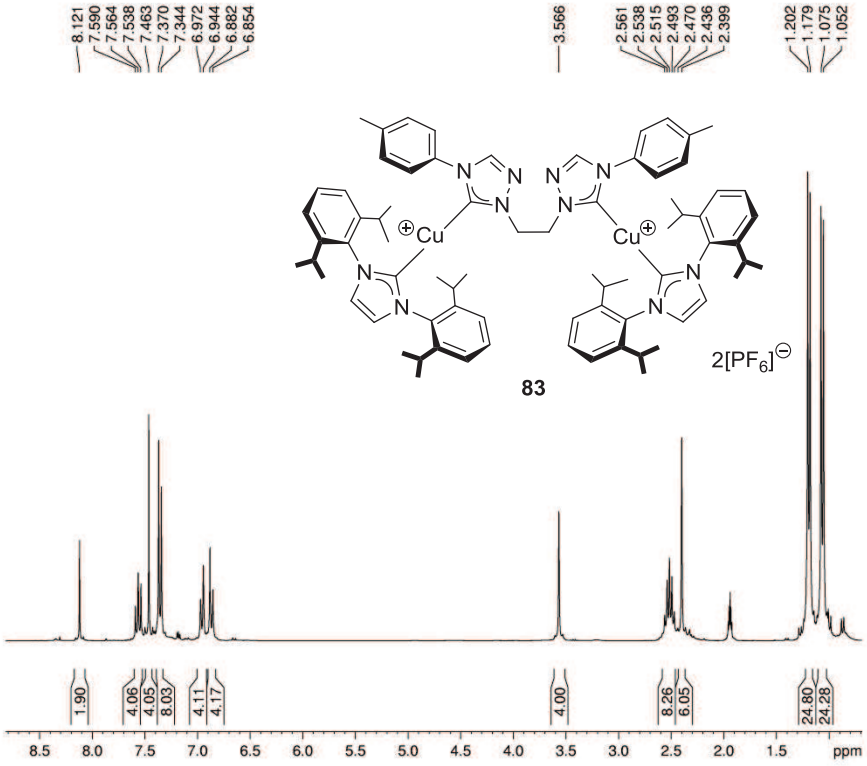

Current Data Parameters
NAME c120106bsrb.286
EXPNO 2
PROCNO 1

F2 – Acquisition Parameters
Date_ 20120108
Time 8.00
INSTRUM spect
PROBHD 5 mm QNP 1H/13
PULPROG zg30
TD 65536
SOLVENT CD3CN
NS 128
DS 2
SWH 8992.806 Hz
FIDRES 0.137219 Hz
AQ 3.6438017 sec
RG 181
DW 55.600 usec
DE 6.00 usec
TE 300.0 K
D1 0.10000000 sec
TD0 16

======== CHANNEL f1 ========
NUC1 1H
P1 11.50 usec
PL1 –2.20 dB
SFO1 300.1915009 MHz

F2 – Processing parameters
SI 32768
SF 300.1900115 MHz
WDW EM
SSB 0
LB 0.30 Hz
GB 0
PC 1.00

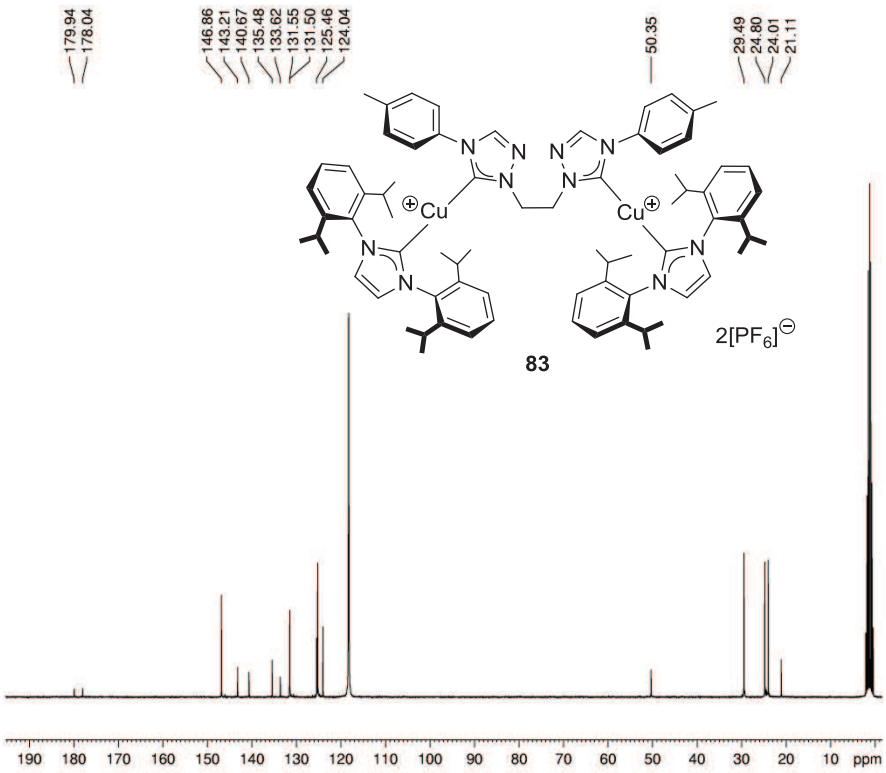

Current Data Parameters
NAME c120106bsrb.286
EXPNO 1
PROCNO 1

F2 – Acquisition Parameters
Date_ 20120108
Time 0
INSTRUM spect
PROBHD 5 mm QNP 1H/13
PULPROG zgpg30
TD 65536
SOLVENT CD3CN
NS 10240
DS 4
SWH 18832.393 Hz
FIDRES 0.287360 Hz
AQ 1.7399808 sec
RG 13004
DW 26.550 usec
DE 6.00 usec
TE 300.0 K
D1 1.00000000 sec
d11 0.03000000 sec
DELTA 0.89999998 sec
TD0 1280
SFO1 75.4915175 MHz
NUC1 13C
P1 11.60 usec
PLW1 –1.00000000 W
SFO2 300.1912008 MHz
NUC2 1H
CPDPRG[2 waltz65
PCPD2 100.00 usec
PLW2 –1.00000000 W
PLW12 –1.00000000 W
PLW13 –1.00000000 W

F2 – Processing parameters
SI 32768
SF 75.4827641 MHz
WDW EM
SSB 0
LB 1.00 Hz
GB 0
PC 1.40

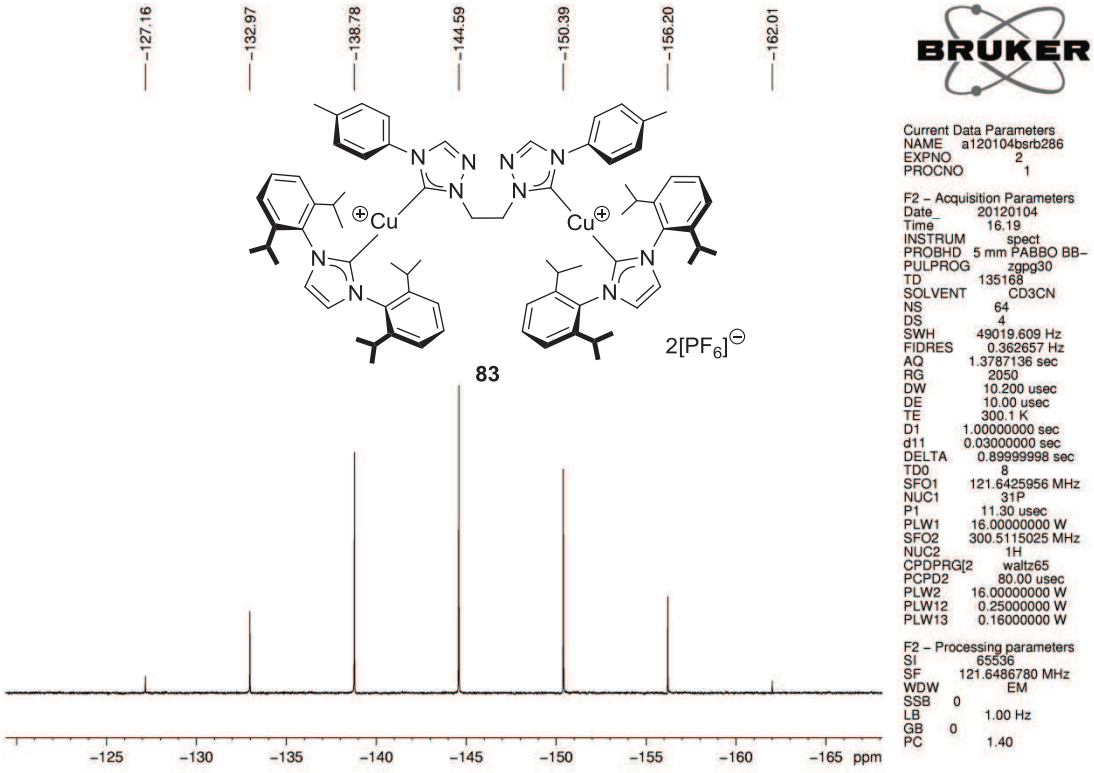
127.16
132.97
138.78
144.59
150.39
156.20
162.01
Cu
Cu
2[PF6]
83
−125
−130
−135
−140
−145
−150
−155
−160
−165 ppm
BRUKER
Current Data Parameters
NAME a120104bsrb286
EXPNO 2
PROCNO 1
F2 – Acquisition Parameters
Date_ 20120104
Time 16.19
INSTRUM spect
PROBHD 5 mm PABBO BB–
PULPROG zgpg30
TD 135168
SOLVENT CD3CN
NS 64
DS 4
SWH 49019.609 Hz
FIDRES 0.362657 Hz
AQ 1.3787136 sec
RG 2050
DW 10.200 usec
DE 10.00 usec
TE 300.1 K
D1 1.00000000 sec
d11 0.03000000 sec
DELTA 0.89999998 sec
TD0 8
SFO1 121.6425956 MHz
NUC1 31P
P1 11.30 usec
PLW1 16.00000000 W
SFO2 300.5115025 MHz
NUC2 1H
CPDPRG[2 waltz65
PCPD2 80.00 usec
PLW2 16.00000000 W
PLW12 0.25000000 W
PLW13 0.16000000 W
F2 – Processing parameters
SI 65536
SF 121.6486780 MHz
WDW EM
SSB 0
LB 1.00 Hz
GB 0
PC 1.40

1.9 Dinuclear Copper Acetate Complexes

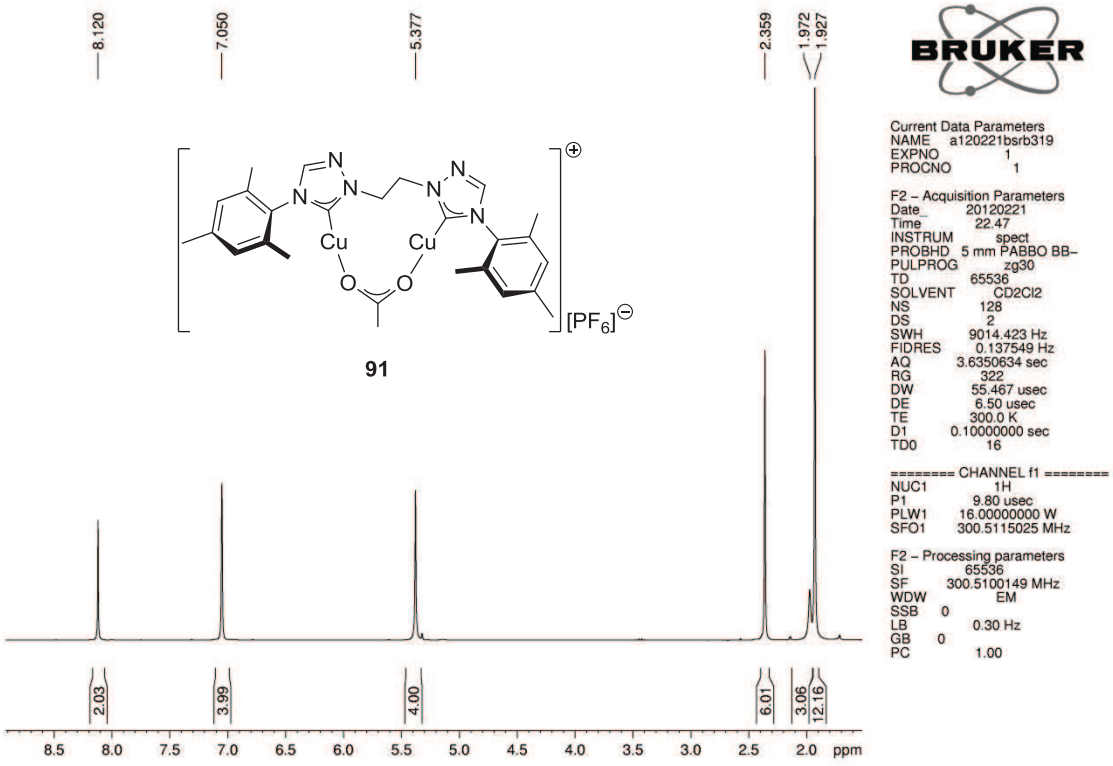

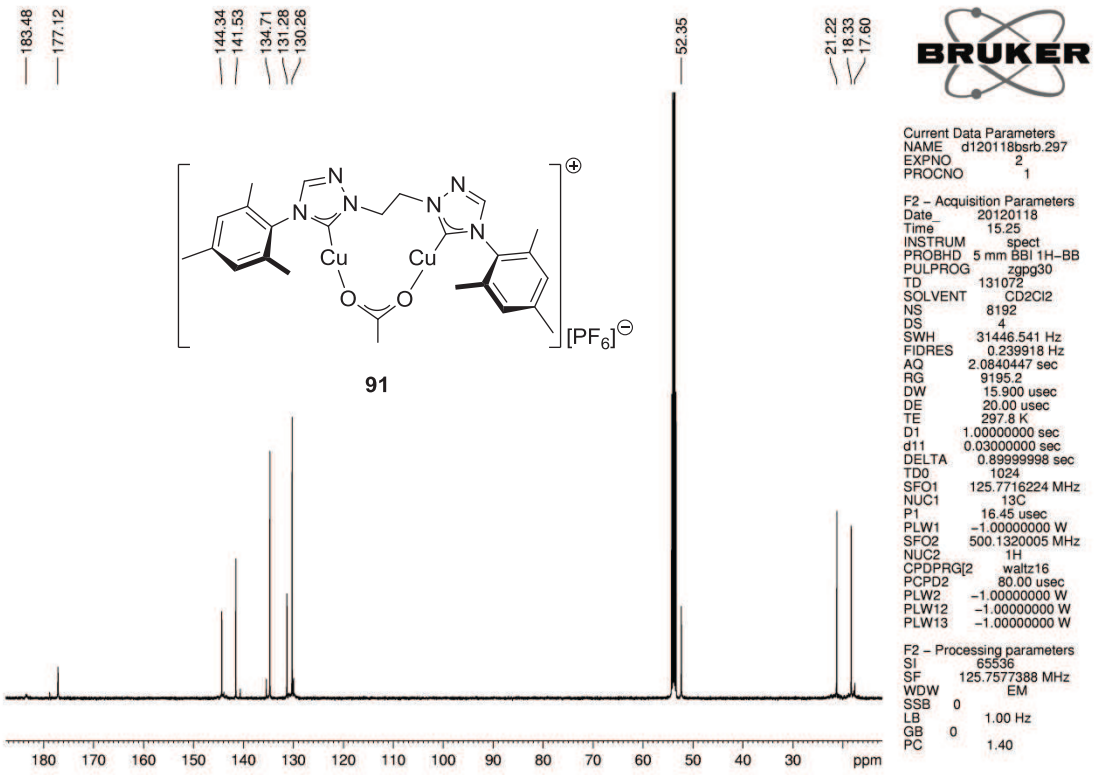

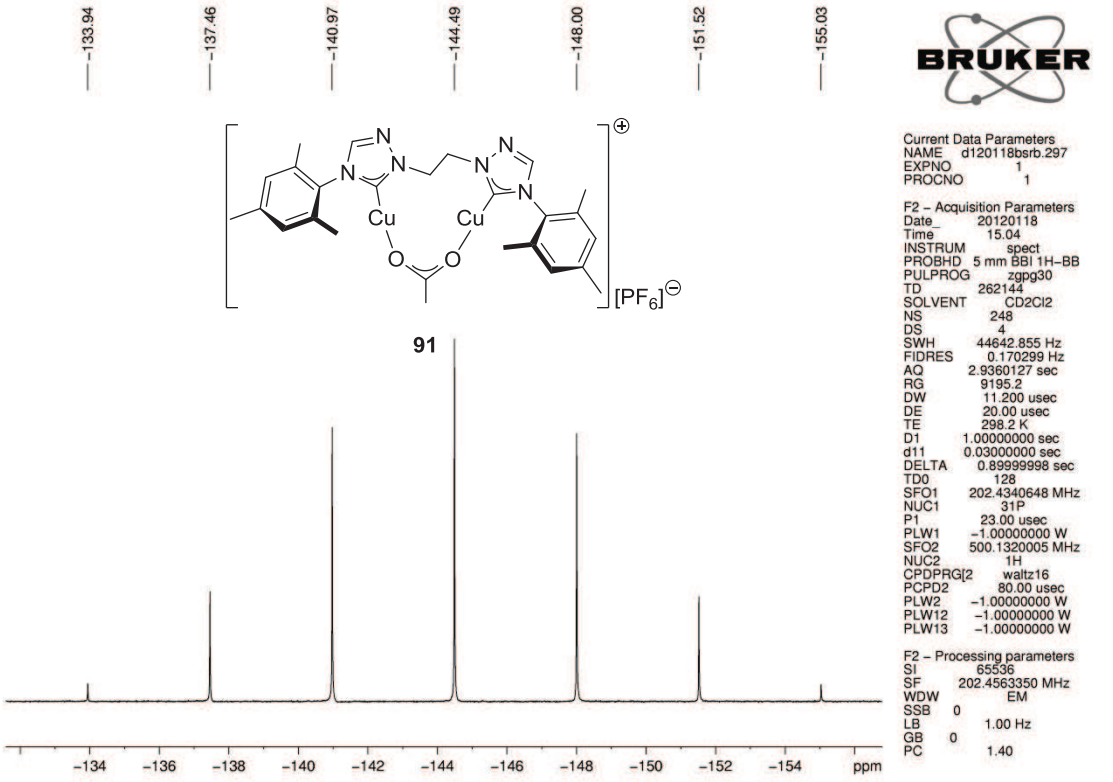
−133.94
−137.46
−140.97
−144.49
−148.00
−151.52
−155.03
Cu
Cu
O
O
[PF6]⊖
91
−134
−136
−138
−140
−142
−144
−146
−148
−150
−152
−154
ppm
BRUKER
Current Data Parameters
NAME d120118bsrb.297
EXPNO 1
PROCNO 1
F2 – Acquisition Parameters
Date_ 20120118
Time 15.04
INSTRUM spect
PROBHD 5 mm BBI 1H–BB
PULPROG zgpg30
TD 262144
SOLVENT CD2Cl2
NS 248
DS 4
SWH 44642.855 Hz
FIDRES 0.170299 Hz
AQ 2.9360127 sec
RG 9195.2
DW 11.200 usec
DE 20.00 usec
TE 298.2 K
D1 1.00000000 sec
d11 0.03000000 sec
DELTA 0.89999998 sec
TD0 128
SFO1 202.4340648 MHz
NUC1 31P
P1 23.00 usec
PLW1 −1.00000000 W
SFO2 500.1320005 MHz
NUC2 1H
CPDPRG[2 waltz16
PCPD2 80.00 usec
PLW2 −1.00000000 W
PLW12 −1.00000000 W
PLW13 −1.00000000 W
F2 – Processing parameters
SI 65536
SF 202.4563350 MHz
WDW EM
SSB 0
LB 1.00 Hz
GB 0
PC 1.40

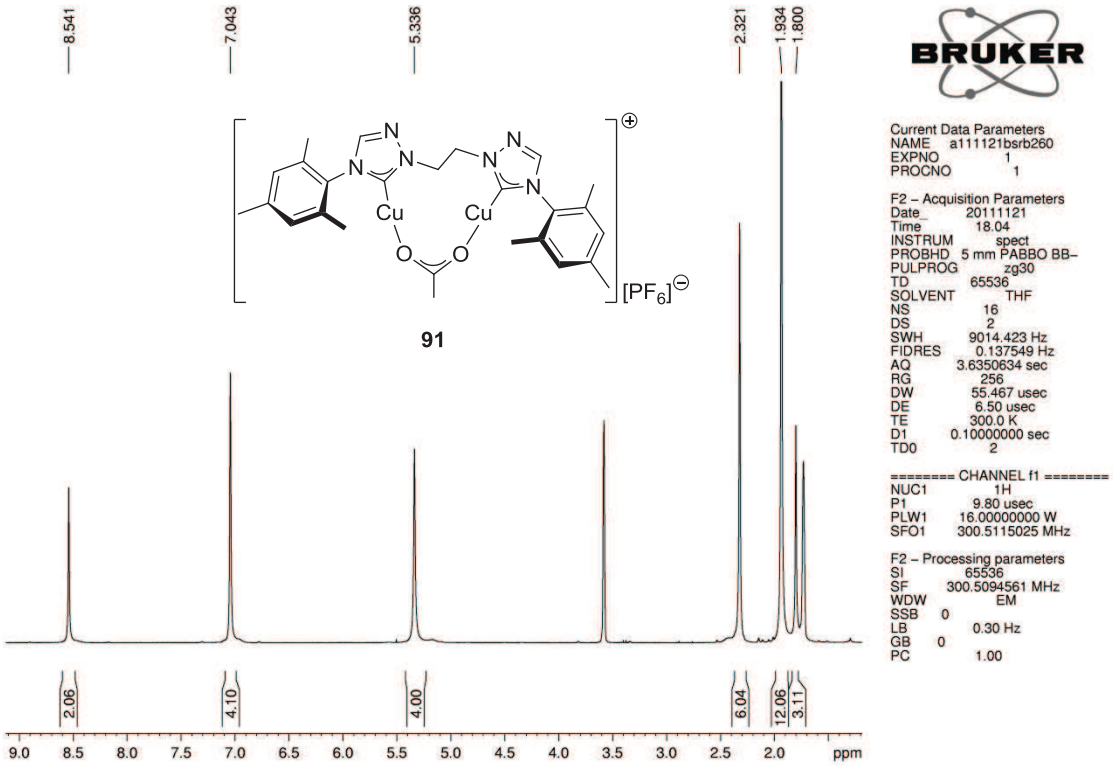
8.541
7.043
5.336
2.321
1.934
1.800
Cu
Cu
O
O
[PF6]⊖
91
2.06
4.10
4.00
6.04
12.06
3.11
9.0
8.5
8.0
7.5
7.0
6.5
6.0
5.5
5.0
4.5
4.0
3.5
3.0
2.5
2.0
ppm
BRUKER
Current Data Parameters
NAME a111121bsrb260
EXPNO 1
PROCNO 1
F2 – Acquisition Parameters
Date_ 20111121
Time 18.04
INSTRUM spect
PROBHD 5 mm PABBO BB–
PULPROG zg30
TD 65536
SOLVENT THF
NS 16
DS 2
SWH 9014.423 Hz
FIDRES 0.137549 Hz
AQ 3.6350634 sec
RG 256
DW 55.467 usec
DE 6.50 usec
TE 300.0 K
D1 0.10000000 sec
TD0 2
======== CHANNEL f1 ========
NUC1 1H
P1 9.80 usec
PLW1 16.00000000 W
SFO1 300.5115025 MHz
F2 – Processing parameters
SI 65536
SF 300.5094561 MHz
WDW EM
SSB 0
LB 0.30 Hz
GB 0
PC 1.00

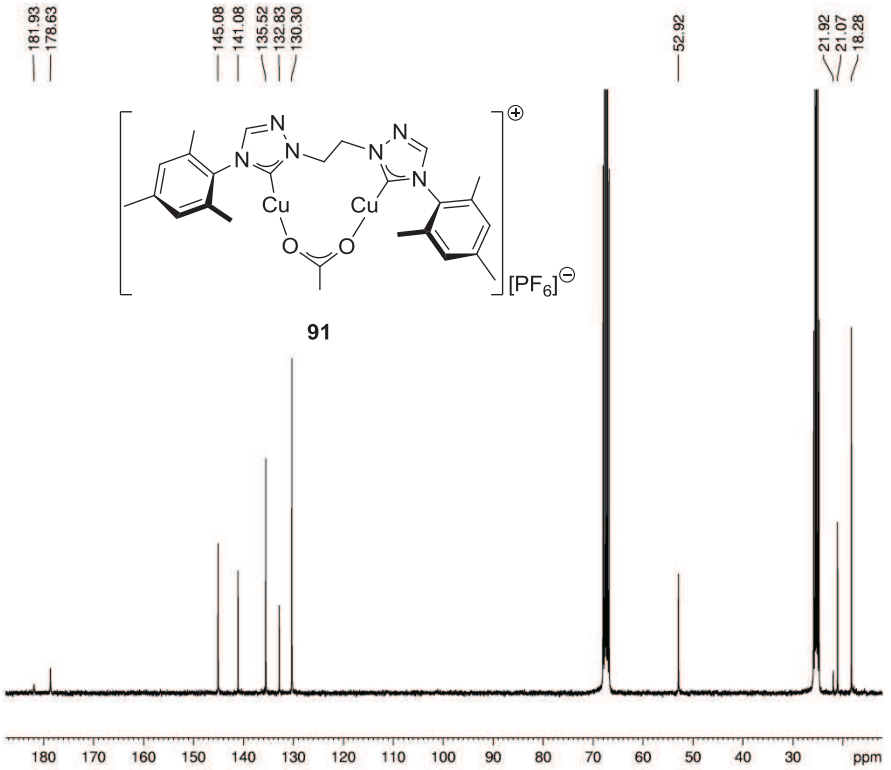

Current Data Parameters
NAME c111025bsrb.242UK
EXPNO 5
PROCNO 1

F2 – Acquisition Parameters
Date_ 20111025
Time 19.57
INSTRUM spect
PROBHD 5 mm QNP 1H/13
PULPROG zgpg30
TD 65536
SOLVENT THF
NS 8192
DS 4
SWH 18832.393 Hz
FIDRES 0.287360 Hz
AQ 1.7399808 sec
RG 13004
DW 26.550 usec
DE 6.00 usec
TE 300.0 K
D1 1.00000000 sec
d11 0.03000000 sec
DELTA 0.89999998 sec
TD0 1024
SFO1 75.4915175 MHz
NUC1 13C
P1 11.60 usec
PLW1 −1.00000000 W
SFO2 300.1912008 MHz
NUC2 1H
CPDPRG[2 waltz65
PCPD2 100.00 usec
PLW2 −1.00000000 W
PLW12 −1.00000000 W
PLW13 −1.00000000 W

F2 – Processing parameters
SI 32768
SF 75.4827624 MHz
WDW EM
SSB 0
LB 1.00 Hz
GB 0
PC 1.40

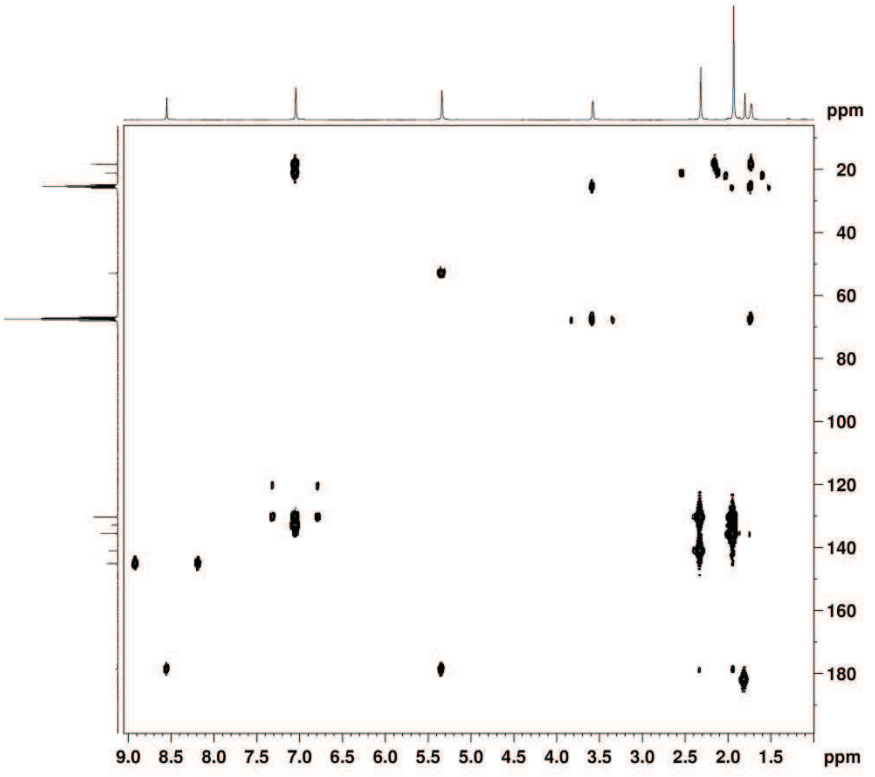

Current Data Parameters
NAME c111025bsrb.242UK
EXPNO 4
PROCNO 1

F2 – Acquisition Parameters
Date_ 20111025
Time 17.40
INSTRUM spect
PROBHD 5 mm QNP 1H/13
PULPROG hmbcgplpndqf
TD 4096
SOLVENT THF
NS 40
DS 16
SWH 3906.250 Hz
FIDRES 0.953674 Hz
AQ 0.5242880 sec
RG 16384
DW 128.000 usec
DE 6.00 usec
TE 300.0 K
CNST2 145.0000000
CNST13 8.0000000
d0 0.00000300 sec
D1 1.00000000 sec
d2 0.00344829 sec
d6 0.06250000 sec
D16 0.00010000 sec
in0 0 sec
ST1CNT 0
d0orig 0.00000300 sec
ph1loop 0
t1loop 0
SFO1 300.1915009 MHz
NUC1 1H
P1 11.50 usec
p2 23.00 usec
PLW1 −1.00000000 W
SFO2 75.4915175 MHz
NUC2 13C
P3 11.40 usec
PLW2 −1.00000000 W
GPNAM[1] SINE.100
GPNAM[2] SINE.100
GPNAM[3] SINE.100
GPZ1 50.00 %
GPZ2 30.00 %
GPZ3 40.10 %
P16 1000.00 usec

F1 – Acquisition parameters
TD 128
SFO1 75.49152 MHz
FIDRES 147.405655 Hz
SW 249.934 ppm
FnMODE QF

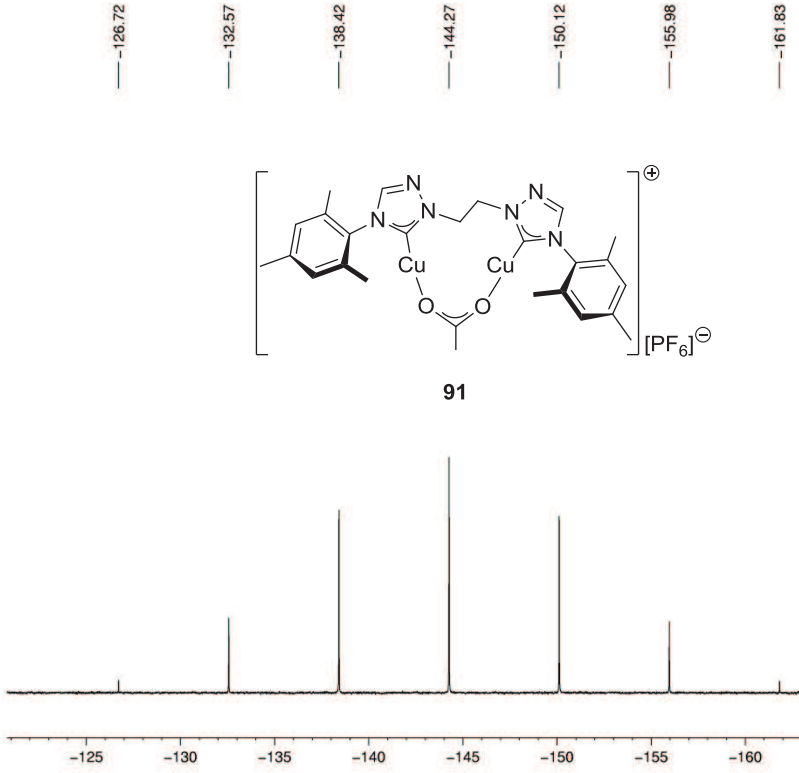

91

BRUKER

Current Data Parameters
NAME b111026bsrb.242UK
EXPNO 1
PROCNO 1

F2 – Processing parameters
SI 65536
SF 121.4746110 MHz
WDW EM
SSB 0
LB 1.00 Hz
GB 0
PC 1.40

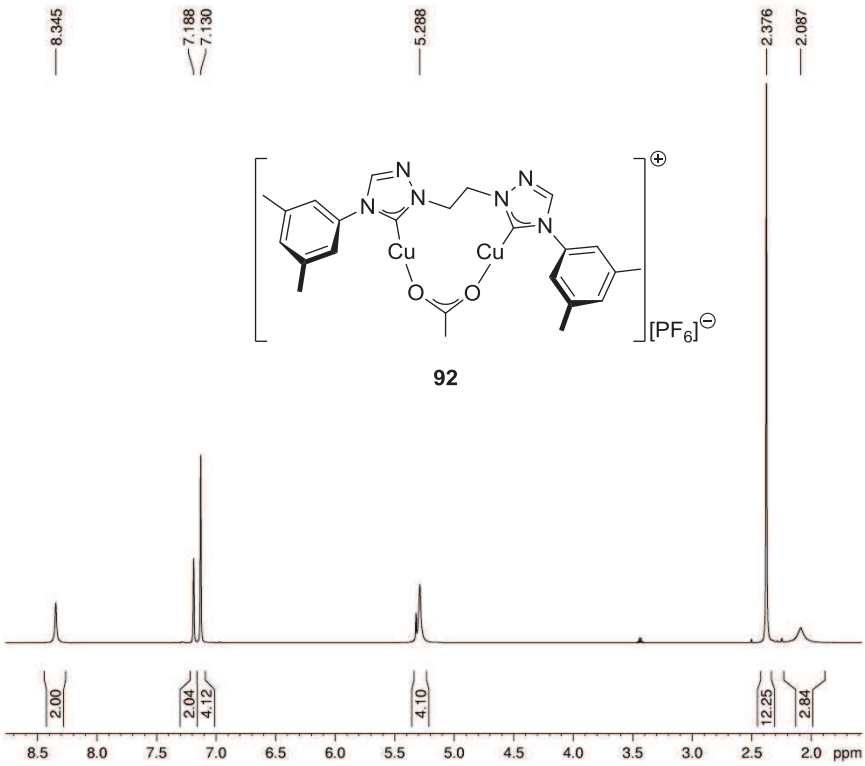

92

BRUKER

Current Data Parameters
NAME d120127bsrb.301
EXPNO 2
PROCNO 1

F2 – Acquisition Parameters
Date_ 20120127
Time 22.03
INSTRUM spect
PROBHD 5 mm BBI 1H-BB
PULPROG zg30
TD 65536
SOLVENT CD2Cl2
NS 128
DS 2
SWH 8992.806 Hz
FIDRES 0.137219 Hz
AQ 3.6438017 sec
RG 256
DW 55.600 usec
DE 6.00 usec
TE 297.9 K
D1 0.10000000 sec
TD0 16

======== CHANNEL f1 ========
NUC1 1H
P1 11.00 usec
PL1 0 dB
SFO1 500.1325007 MHz

F2 – Processing parameters
SI 32768
SF 500.1300207 MHz
WDW EM
SSB 0
LB 0.30 Hz
GB 0
PC 1.00

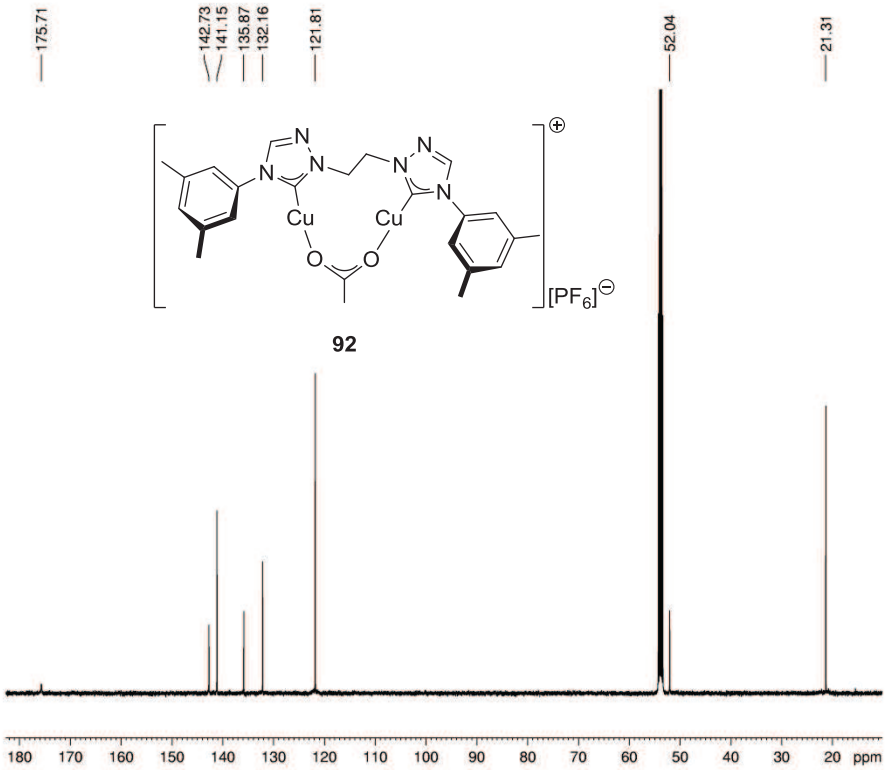

Current Data Parameters
NAME d120127bsrb.301
EXPNO 1
PROCNO 1

F2 – Acquisition Parameters
Date_ 20120127
Time 14.53
INSTRUM spect
PROBHD 5 mm BBI 1H–BB
PULPROG zgpg30
TD 131072
SOLVENT CD2Cl2
NS 8192
DS 4
SWH 31446.541 Hz
FIDRES 0.239918 Hz
AQ 2.0840447 sec
RG 9195.2
DW 15.900 usec
DE 20.00 usec
TE 298.0 K
D1 1.00000000 sec
d11 0.03000000 sec
DELTA 0.89999998 sec
TD0 1024
SFO1 125.7716224 MHz
NUC1 13C
P1 16.45 usec
PLW1 −1.00000000 W
SFO2 500.1320005 MHz
NUC2 1H
CPDPRG[2 waltz16
PCPD2 80.00 usec
PLW2 −1.00000000 W
PLW12 −1.00000000 W
PLW13 −1.00000000 W

F2 – Processing parameters
SI 65536
SF 125.7577353 MHz
WDW EM
SSB 0
LB 1.00 Hz
GB 0
PC 1.40

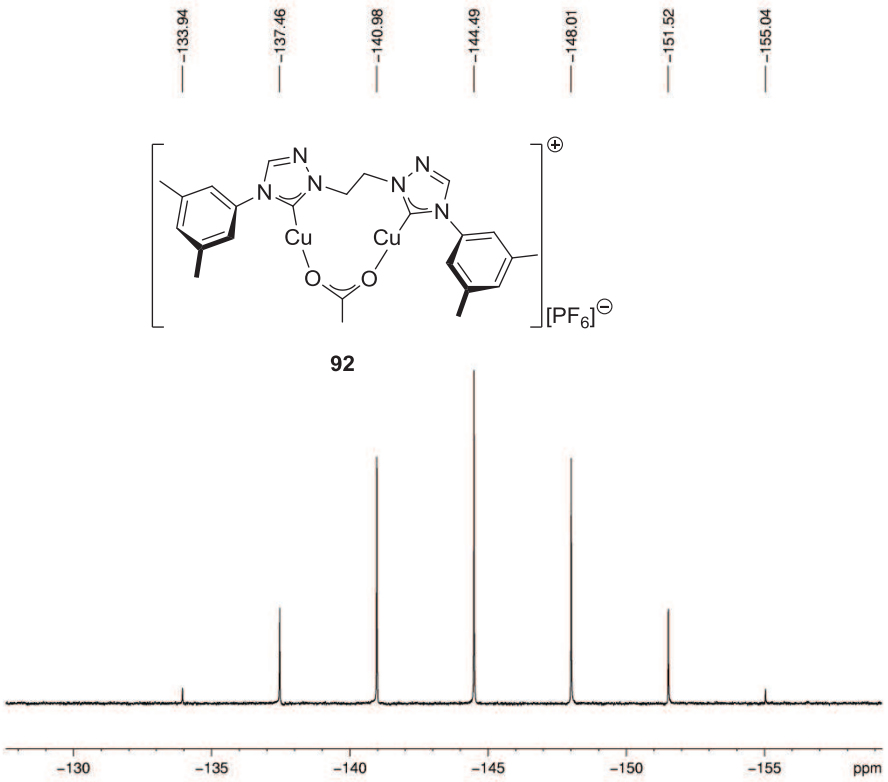

Current Data Parameters
NAME d120127bsrb.301
EXPNO 6
PROCNO 1

F2 – Acquisition Parameters
Date_ 20120127
Time 14.28
INSTRUM spect
PROBHD 5 mm BBI 1H–BB
PULPROG zgpg30
TD 262144
SOLVENT CD2Cl2
NS 336
DS 4
SWH 44642.855 Hz
FIDRES 0.170299 Hz
AQ 2.9360127 sec
RG 10321.3
DW 11.200 usec
DE 20.00 usec
TE 298.1 K
D1 1.00000000 sec
d11 0.03000000 sec
DELTA 0.89999998 sec
TD0 64
SFO1 202.4360894 MHz
NUC1 31P
P1 23.00 usec
PLW1 −1.00000000 W
SFO2 500.1320005 MHz
NUC2 1H
CPDPRG[2 waltz16
PCPD2 80.00 usec
PLW2 −1.00000000 W
PLW12 −1.00000000 W
PLW13 −1.00000000 W

F2 – Processing parameters
SI 65536
SF 202.4563350 MHz
WDW EM
SSB 0
LB 1.00 Hz
GB 0
PC 1.40

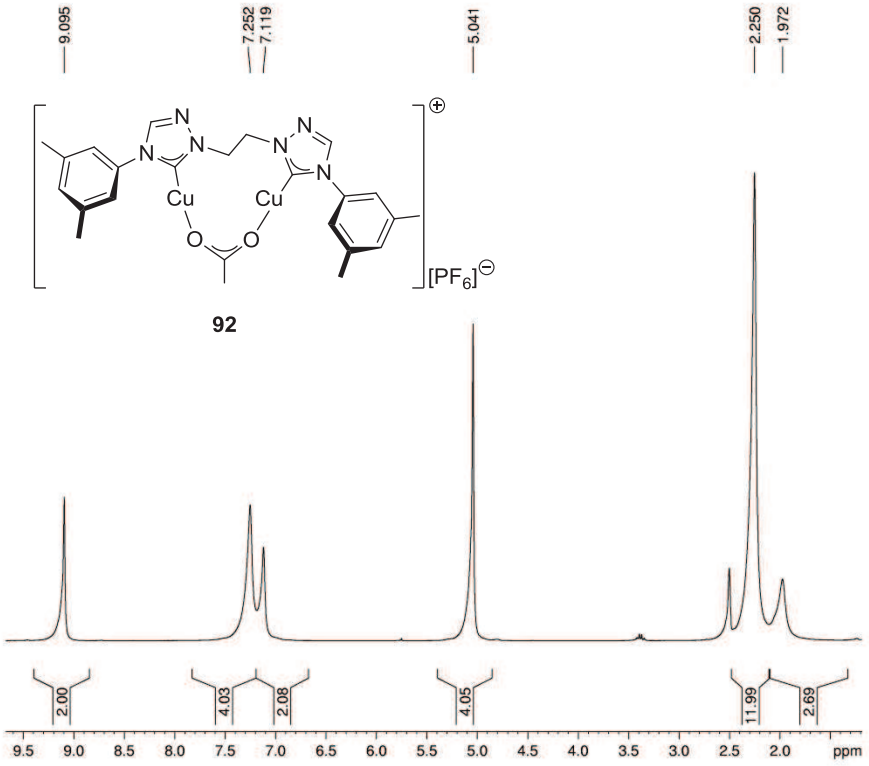

92

BRUKER

Current Data Parameters
NAME c120210bsrb.302
EXPNO 2
PROCNO 1

F2 – Acquisition Parameters
Date_ 20120212
Time 21.52
INSTRUM spect
PROBHD 5 mm QNP 1H/13
PULPROG zg30
TD 65536
SOLVENT DMSO
NS 128
DS 2
SWH 8992.806 Hz
FIDRES 0.137219 Hz
AQ 3.6438017 sec
RG 287.4
DW 55.600 usec
DE 6.00 usec
TE 300.0 K
D1 0.10000000 sec
TD0 16

======== CHANNEL f1 ========
NUC1 1H
P1 11.50 usec
PL1 −2.20 dB
SFO1 300.1915009 MHz

F2 – Processing parameters
SI 32768
SF 300.1900047 MHz
WDW EM
SSB 0
LB 0.30 Hz
GB 0
PC 1.00

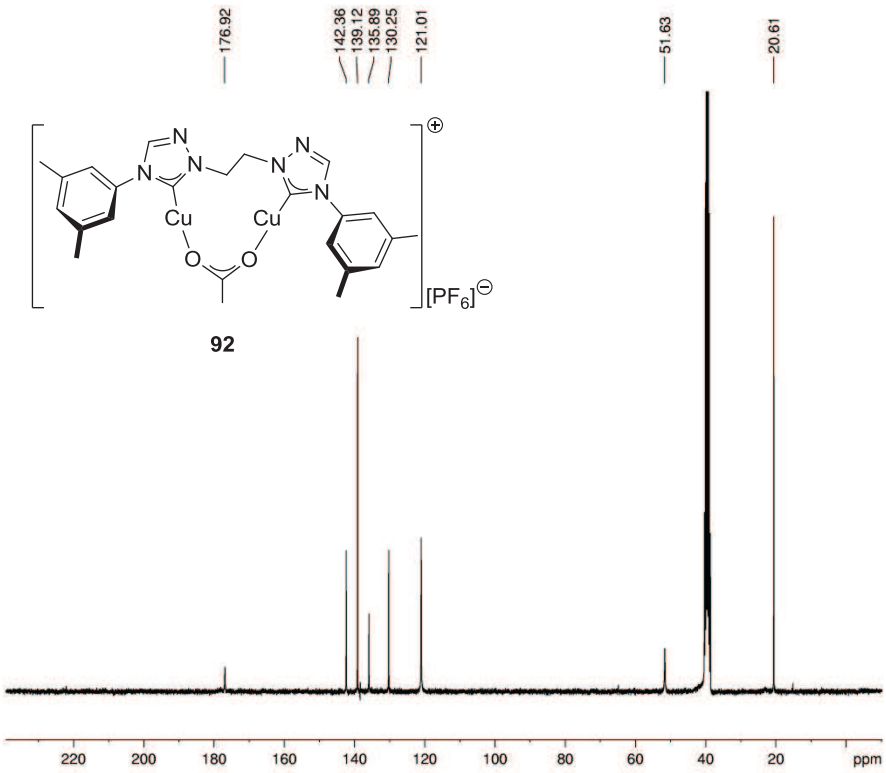

92

BRUKER

Current Data Parameters
NAME c120210bsrb.302
EXPNO 1
PROCNO 1

F2 – Acquisition Parameters
Date_ 20120212
Time 13.53
INSTRUM spect
PROBHD 5 mm QNP 1H/13
PULPROG zgpg30
TD 65536
SOLVENT DMSO
NS 10240
DS 4
SWH 18832.393 Hz
FIDRES 0.287360 Hz
AQ 1.7399808 sec
RG 20642.5
DW 26.550 usec
DE 6.00 usec
TE 300.0 K
D1 1.00000000 sec
d11 0.03000000 sec
DELTA 0.89999998 sec
TD0 1280
SFO1 75.4915175 MHz
NUC1 13C
P1 11.60 usec
PLW1 −1.00000000 W
SFO2 300.1912008 MHz
NUC2 1H
CPDPRG[2 waltz65
PCPD2 100.00 usec
PLW2 −1.00000000 W
PLW12 −1.00000000 W
PLW13 −1.00000000 W

F2 – Processing parameters
SI 32768
SF 75.4828735 MHz
WDW EM
SSB 0
LB 1.00 Hz
GB 0
PC 1.40

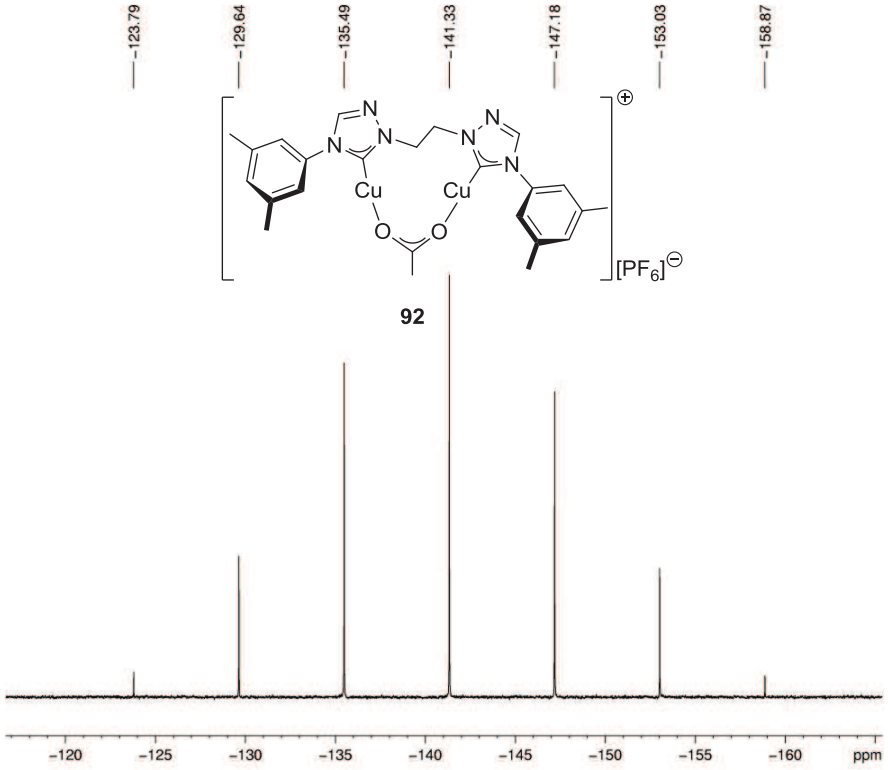

BRUKER

Current Data Parameters
NAME a120208bsrb302dmso
EXPNO 2
PROCNO 1

F2 – Acquisition Parameters
Date_ 20120208
Time 19.12
INSTRUM spect
PROBHD 5 mm PABBO BB–
PULPROG zgpg30
TD 135168
SOLVENT DMSO
NS 64
DS 4
SWH 49019.609 Hz
FIDRES 0.362657 Hz
AQ 1.3787136 sec
RG 1820
DW 10.200 usec
DE 10.00 usec
TE 300.1 K
D1 1.00000000 sec
d11 0.03000000 sec
DELTA 0.89999998 sec
TD0 8
SFO1 121.6425956 MHz
NUC1 31P
P1 11.30 usec
PLW1 16.00000000 W
SFO2 300.5115025 MHz
NUC2 1H
CPDPRG[2 waltz65
PCPD2 80.00 usec
PLW2 16.00000000 W
PLW12 0.25000000 W
PLW13 0.16000000 W

F2 – Processing parameters
SI 65536
SF 121.6486780 MHz
WDW EM
SSB 0
LB 1.00 Hz
GB 0
PC 1.40

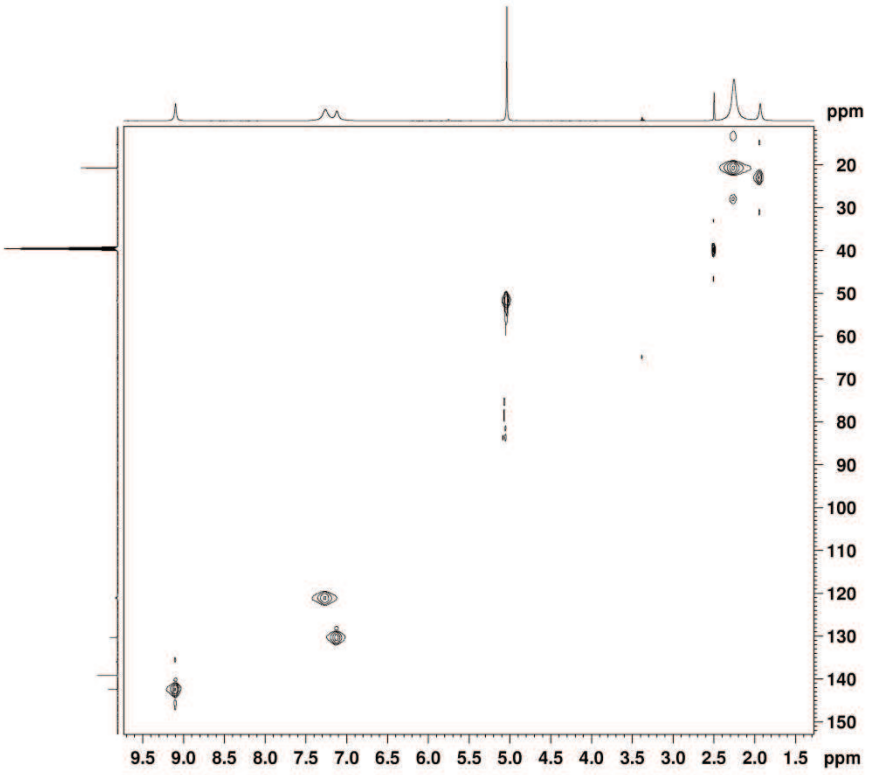

BRUKER

Current Data Parameters
NAME st_rb302
EXPNO 60013
PROCNO 1

F2 – Acquisition Parameters
Date_ 20120209
Time 16.21
INSTRUM spect
PROBHD 5 mm CPQNP 1H/
PULPROG hsqcetgpsisp2.2
TD 2048
SOLVENT DMSO
NS 2
DS 16
SWH 9615.385 Hz
FIDRES 4.695012 Hz
AQ 0.1064960 sec
RG 2050
DW 52.000 usec
DE 10.00 usec
TE 295.0 K
CNST2 145.0000000
CNST17 −0.5000000
d0 0.00000300 sec
D1 1.50000000 sec
d4 0.00172414 sec
d11 0.03000000 sec
D16 0.00020000 sec
D24 0.00086207 sec
DELTA 0.00123120 sec
DELTA1 0.00120661 sec
DELTA2 0.00147014 sec
DELTA3 0.00055807 sec
DELTA4 0.00027014 sec
in0 0 sec
ST1CNT 64
d0orig 0.00000300 sec
ph1loop 0
t1loop 0
SFO1 600.1336008 MHz
NUC1 1H
P1 14.60 usec
p2 29.20 usec
P28 1000.00 usec
PLW1 −1.00000000 W
SFO2 150.9148812 MHz
NUC2 13C
CPDPRG[2 garp4
P3 12.00 usec
P14 500.00 usec
P24 2000.00 usec
PCPD2 60.00 usec
PLW0 −1.00000000 W
PLW2 −1.00000000 W
PLW12 −1.00000000 W
SPNAM[3] Gp80 0.5 20.1

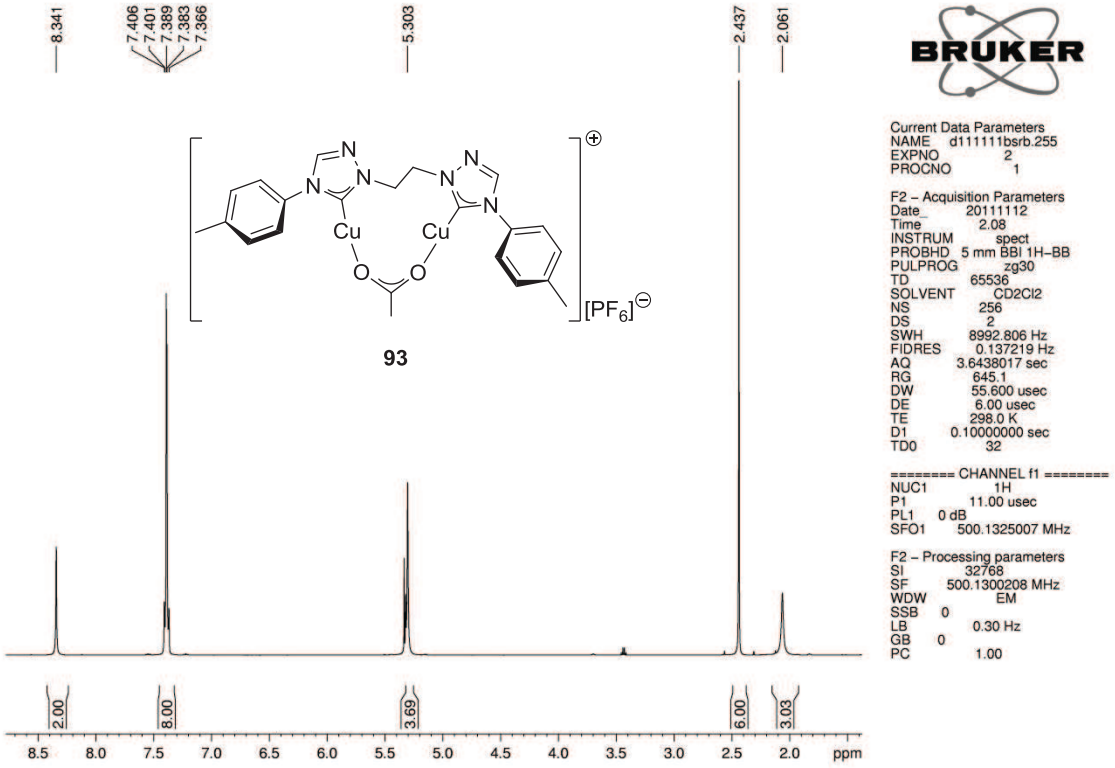
8.341
7.406
7.401
7.389
7.383
7.366
5.303
2.437
2.061
Cu
Cu
O
O
[PF6]⊖
93
2.00
8.00
3.69
6.00
3.03
8.5 8.0 7.5 7.0 6.5 6.0 5.5 5.0 4.5 4.0 3.5 3.0 2.5 2.0 ppm
BRUKER
Current Data Parameters
NAME d111111bsrb.255
EXPNO 2
PROCNO 1
F2 – Acquisition Parameters
Date_ 20111112
Time 2.08
INSTRUM spect
PROBHD 5 mm BBI 1H–BB
PULPROG zg30
TD 65536
SOLVENT CD2Cl2
NS 256
DS 2
SWH 8992.806 Hz
FIDRES 0.137219 Hz
AQ 3.6438017 sec
RG 645.1
DW 55.600 usec
DE 6.00 usec
TE 298.0 K
D1 0.10000000 sec
TD0 32
======== CHANNEL f1 ========
NUC1 1H
P1 11.00 usec
PL1 0 dB
SFO1 500.1325007 MHz
F2 – Processing parameters
SI 32768
SF 500.1300208 MHz
WDW EM
SSB 0
LB 0.30 Hz
GB 0
PC 1.00

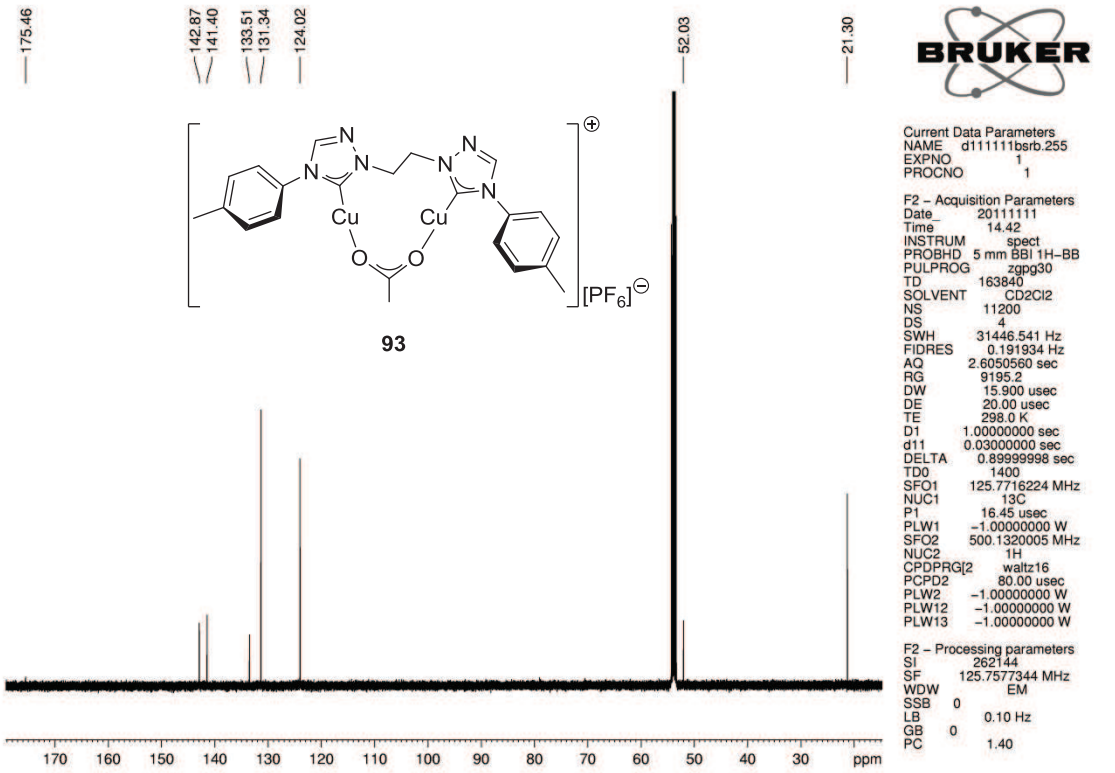
175.46
142.87
141.40
133.51
131.34
124.02
52.03
21.30
Cu
Cu
O
O
[PF6]⊖
93
170 160 150 140 130 120 110 100 90 80 70 60 50 40 30 ppm
BRUKER
Current Data Parameters
NAME d111111bsrb.255
EXPNO 1
PROCNO 1
F2 – Acquisition Parameters
Date_ 20111111
Time 14.42
INSTRUM spect
PROBHD 5 mm BBI 1H–BB
PULPROG zgpg30
TD 163840
SOLVENT CD2Cl2
NS 11200
DS 4
SWH 31446.541 Hz
FIDRES 0.191934 Hz
AQ 2.6050560 sec
RG 9195.2
DW 15.900 usec
DE 20.00 usec
TE 298.0 K
D1 1.00000000 sec
d11 0.03000000 sec
DELTA 0.89999998 sec
TD0 1400
SFO1 125.7716224 MHz
NUC1 13C
P1 16.45 usec
PLW1 –1.00000000 W
SFO2 500.1320005 MHz
NUC2 1H
CPDPRG[2 waltz16
PCPD2 80.00 usec
PLW2 –1.00000000 W
PLW12 –1.00000000 W
PLW13 –1.00000000 W
F2 – Processing parameters
SI 262144
SF 125.7577344 MHz
WDW EM
SSB 0
LB 0.10 Hz
GB 0
PC 1.40

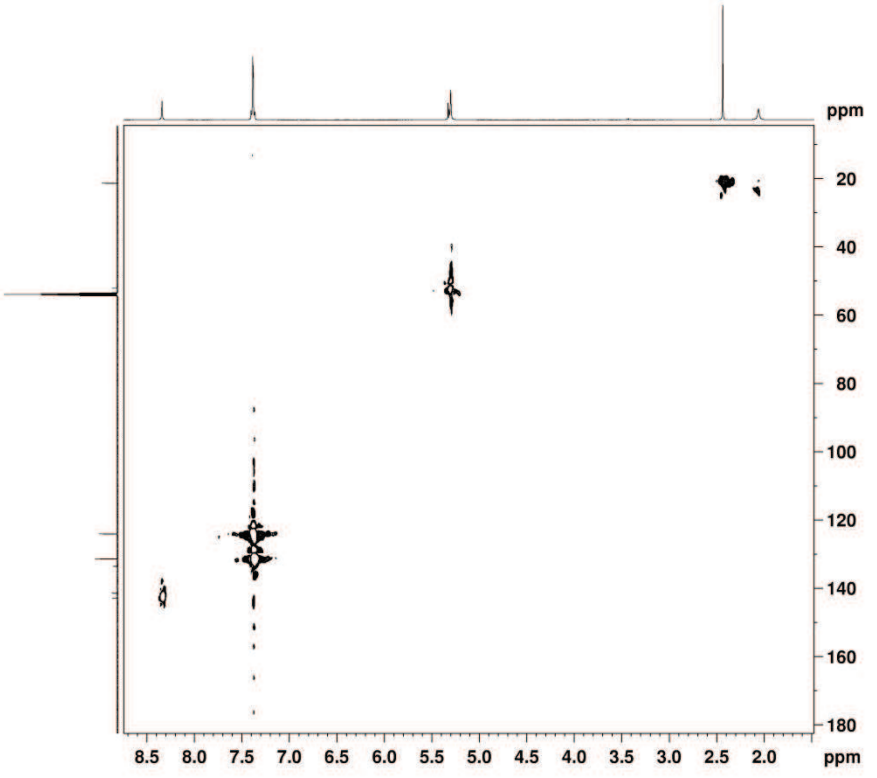

BRUKER

Current Data Parameters
NAME d111111bsrb.255
EXPNO 3
PROCNO 1

F2 – Acquisition Parameters
Date_ 20111112
Time 2.35
INSTRUM spect
PROBHD 5 mm BBI 1H–BB
PULPROG hsqcedetgpsisp2.2
TD 1024
SOLVENT CD2Cl2
NS 512
DS 16
SWH 6510.417 Hz
FIDRES 6.357829 Hz
AQ 0.0786432 sec
RG 5792.6
DW 76.800 usec
DE 6.00 usec
TE 298.1 K
CNST2 145.0000000
CNST17 −0.5000000
d0 0.00000300 sec
D1 1.00000000 sec
d4 0.00172414 sec
d11 0.03000000 sec
D16 0.00030000 sec
D21 0.00344828 sec
D24 0.00086207 sec
DELTA 0.00262028 sec
DELTA1 0.00130542 sec
DELTA2 0.00147414 sec
DELTA3 0.00056207 sec
DELTA4 0.00017414 sec
DELTA5 0.00394828 sec
in0 0 sec
ST1CNT 0
d0orig 0.00000300 sec
ph1loop 0
t1loop 0
SFO1 500.1325007 MHz
NUC1 1H
P1 11.00 usec
p2 22.00 usec
P28 1000.00 usec
PLW1 −1.00000000 W
SFO2 125.7722511 MHz
NUC2 13C
CPDPRG[2 garp4
P3 14.40 usec
P14 500.00 usec
P24 2000.00 usec
PCPD2 80.00 usec
PLW0 −1.00000000 W
PLW2 −1.00000000 W

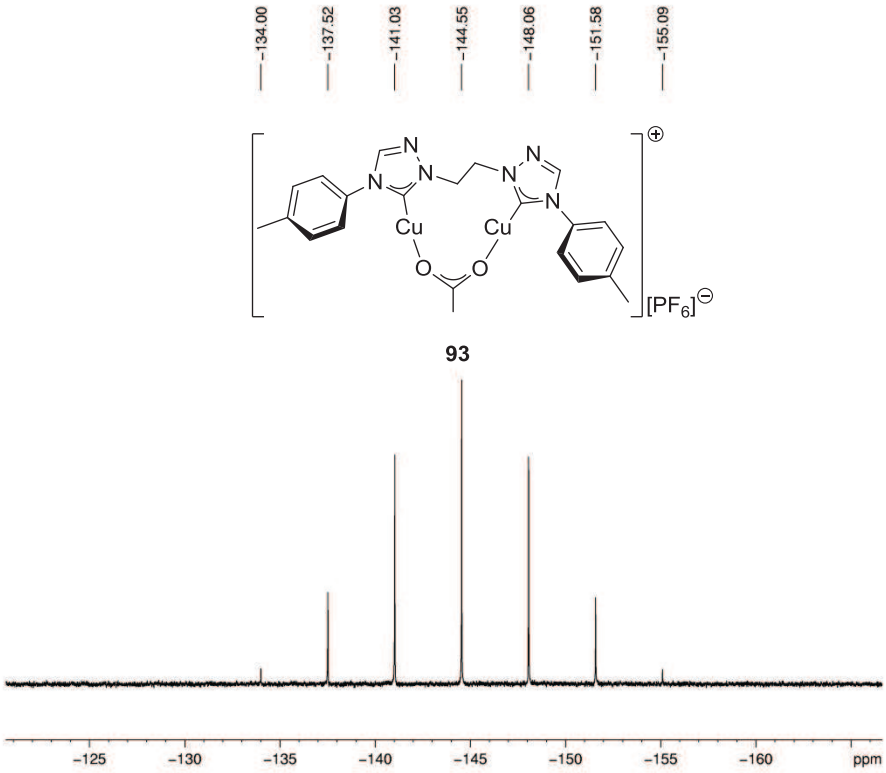

BRUKER

Current Data Parameters
NAME d111104bsrb.246
EXPNO 6
PROCNO 1

F2 – Acquisition Parameters
Date_ 20111104
Time 14.23
INSTRUM spect
PROBHD 5 mm BBI 1H–BB
PULPROG zgpg30
TD 262144
SOLVENT CD2Cl2
NS 1024
DS 4
SWH 40650.406 Hz
FIDRES 0.155069 Hz
AQ 3.2243712 sec
RG 10321.3
DW 12.300 usec
DE 20.00 usec
TE 296.3 K
D1 1.00000000 sec
d11 0.03000000 sec
DELTA 0.89999998 sec
TD0 128
SFO1 202.4360894 MHz
NUC1 31P
P1 23.00 usec
PLW1 −1.00000000 W
SFO2 500.1320005 MHz
NUC2 1H
CPDPRG[2 waltz16
PCPD2 80.00 usec
PLW2 −1.00000000 W
PLW12 −1.00000000 W
PLW13 −1.00000000 W

F2 – Processing parameters
SI 65536
SF 202.4563350 MHz
WDW EM
SSB 0
LB 1.00 Hz
GB 0
PC 1.40

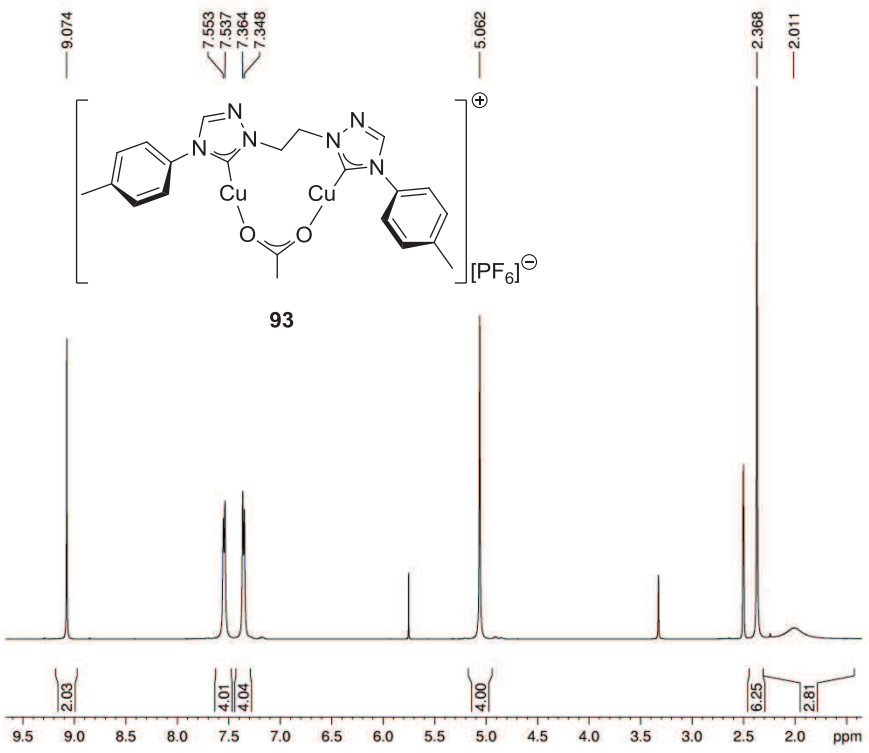

93

BRUKER

Current Data Parameters
NAME d111214bsrb.236UK
EXPNO 2
PROCNO 1

F2 – Acquisition Parameters
Date_ 20111213
Time 13.21
INSTRUM spect
PROBHD 5 mm BBI 1H–BB
PULPROG zg30
TD 65536
SOLVENT DMSO
NS 40
DS 2
SWH 8992.806 Hz
FIDRES 0.137219 Hz
AQ 3.6438017 sec
RG 143.7
DW 55.600 usec
DE 6.00 usec
TE 298.0 K
D1 0.10000000 sec
TD0 5

======== CHANNEL f1 ========
NUC1 1H
P1 11.00 usec
PL1 0 dB
SFO1 500.1325007 MHz

F2 – Processing parameters
SI 32768
SF 500.1300059 MHz
WDW EM
SSB 0
LB 0.30 Hz
GB 0
PC 1.00

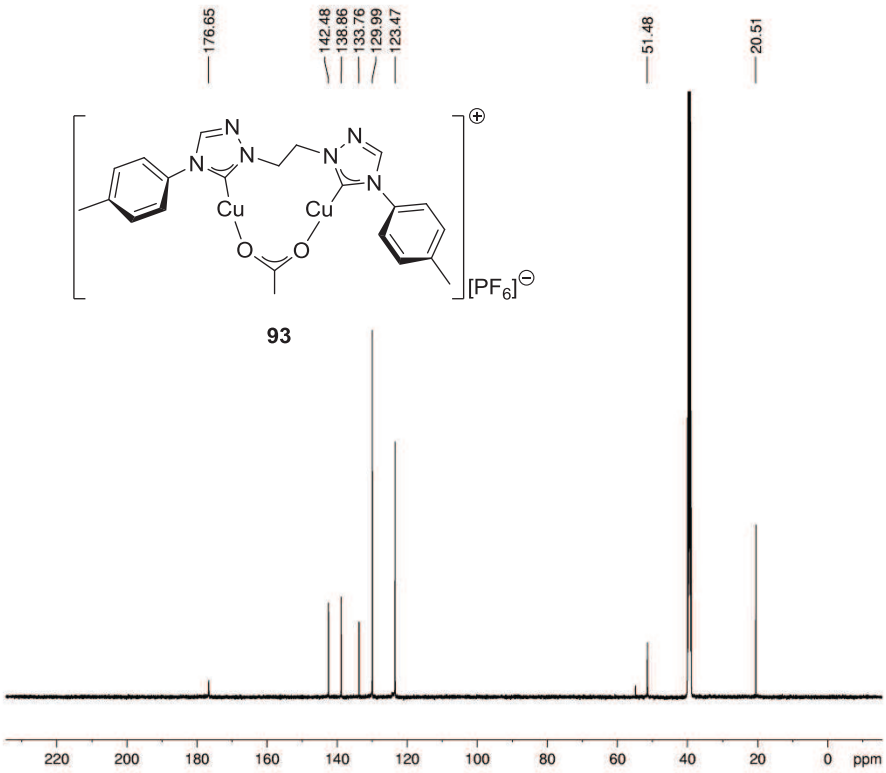

93

BRUKER

Current Data Parameters
NAME d111214bsrb.236UK
EXPNO 3
PROCNO 1

F2 – Acquisition Parameters
Date_ 20111214
Time 15.02
INSTRUM spect
PROBHD 5 mm BBI 1H–BB
PULPROG zgpg30
TD 131072
SOLVENT DMSO
NS 10240
DS 4
SWH 31446.541 Hz
FIDRES 0.239918 Hz
AQ 2.0840447 sec
RG 9195.2
DW 15.900 usec
DE 20.00 usec
TE 298.1 K
D1 1.00000000 sec
d11 0.03000000 sec
DELTA 0.89999998 sec
TD0 1280
SFO1 125.7716224 MHz
NUC1 13C
P1 16.45 usec
PLW1 −1.00000000 W
SFO2 500.1320005 MHz
NUC2 1H
CPDPRG[2 waltz16
PCPD2 80.00 usec
PLW2 −1.00000000 W
PLW12 −1.00000000 W
PLW13 −1.00000000 W

F2 – Processing parameters
SI 65536
SF 125.7578502 MHz
WDW EM
SSB 0
LB 1.00 Hz
GB 0
PC 1.40

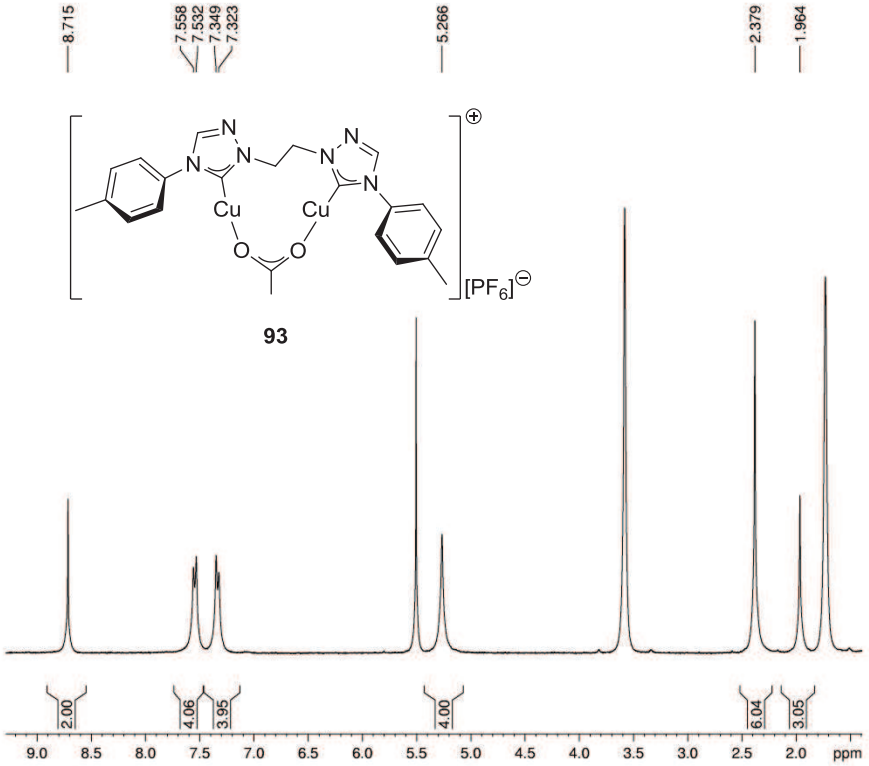

BRUKER

Current Data Parameters
NAME a111018bsrb236UK
EXPNO 1
PROCNO 1

F2 – Acquisition Parameters
Date_ 20111018
Time 13.37
INSTRUM spect
PROBHD 5 mm PABBO BB–
PULPROG zg30
TD 65536
SOLVENT THF
NS 16
DS 2
SWH 9014.423 Hz
FIDRES 0.137549 Hz
AQ 3.6350634 sec
RG 322
DW 55.467 usec
DE 6.50 usec
TE 300.0 K
D1 0.10000000 sec
TD0 2

======== CHANNEL f1 ========
NUC1 1H
P1 9.80 usec
PLW1 16.00000000 W
SFO1 300.5115025 MHz

F2 – Processing parameters
SI 65536
SF 300.5094562 MHz
WDW EM
SSB 0
LB 0.30 Hz
GB 0
PC 1.00

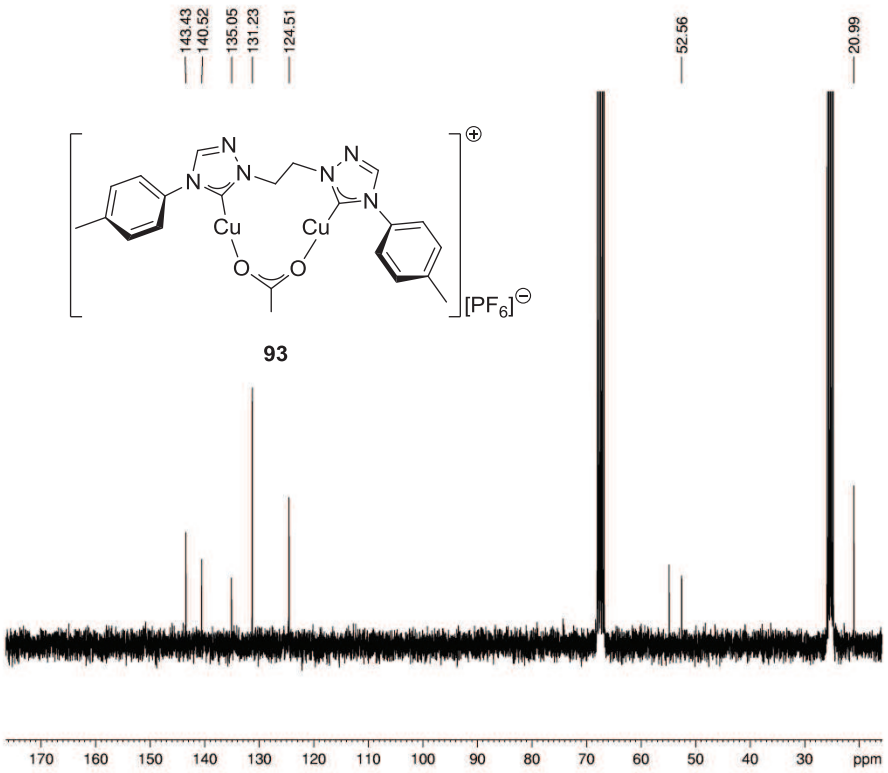

BRUKER

Current Data Parameters
NAME a111018bsrb236UK
EXPNO 2
PROCNO 1

F2 – Acquisition Parameters
Date_ 20111022
Time 4.44
INSTRUM spect
PROBHD 5 mm PABBO BB–
PULPROG zgpg30
TD 65536
SOLVENT THF
NS 1024
DS 4
SWH 18939.395 Hz
FIDRES 0.288992 Hz
AQ 1.7301503 sec
RG 2050
DW 26.400 usec
DE 10.00 usec
TE 296.7 K
D1 1.00000000 sec
d11 0.03000000 sec
DELTA 0.89999998 sec
TD0 128
SFO1 75.5719898 MHz
NUC1 13C
P1 8.00 usec
PLW1 42.00000000 W
SFO2 300.5115025 MHz
NUC2 1H
CPDPRG[2 waltz65
PCPD2 80.00 usec
PLW2 16.00000000 W
PLW12 0.25000000 W
PLW13 0.16000000 W

F2 – Processing parameters
SI 65536
SF 75.5632270 MHz
WDW EM
SSB 0
LB 0.70 Hz
GB 0
PC 1.40

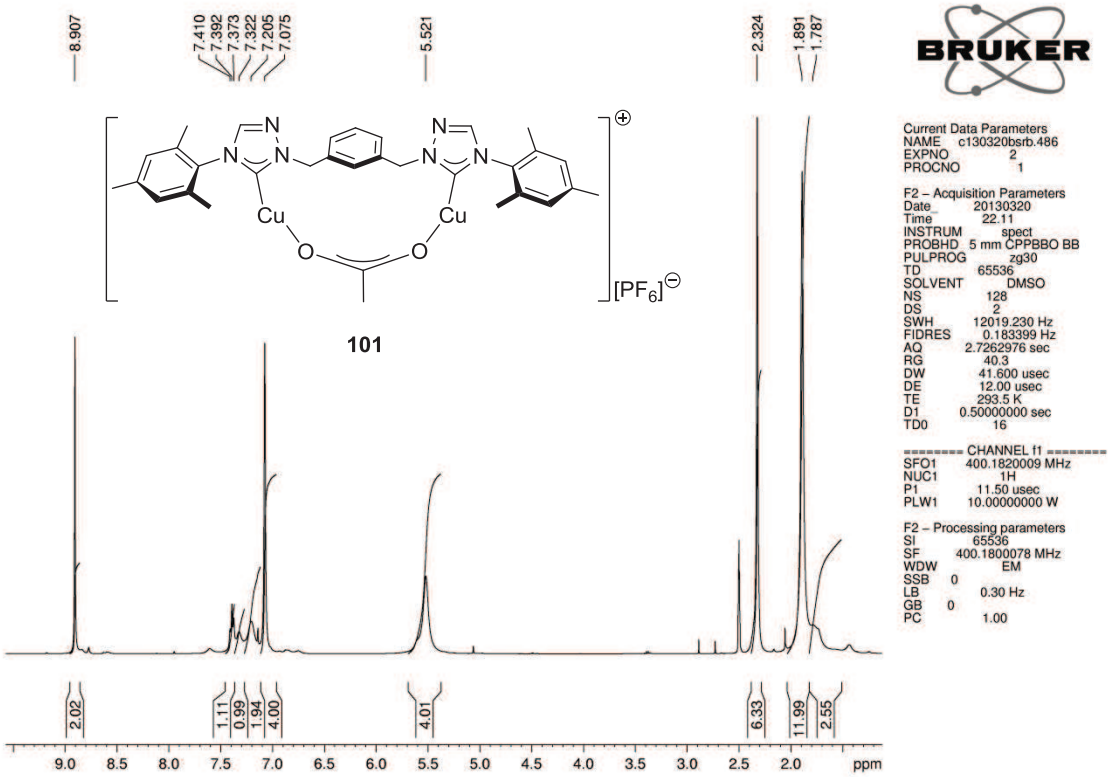
8.907
7.410
7.392
7.373
7.322
7.205
7.075
5.521
2.324
1.891
1.787
Cu
Cu
O
O
[PF6]⊖
101
2.02
1.11
0.99
1.94
4.00
4.01
6.33
11.99
2.55
9.0 8.5 8.0 7.5 7.0 6.5 6.0 5.5 5.0 4.5 4.0 3.5 3.0 2.5 2.0 ppm
BRUKER
Current Data Parameters
NAME c130320bsrb.486
EXPNO 2
PROCNO 1
F2 – Acquisition Parameters
Date_ 20130320
Time 22.11
INSTRUM spect
PROBHD 5 mm CPPBBO BB
PULPROG zg30
TD 65536
SOLVENT DMSO
NS 128
DS 2
SWH 12019.230 Hz
FIDRES 0.183399 Hz
AQ 2.7262976 sec
RG 40.3
DW 41.600 usec
DE 12.00 usec
TE 293.5 K
D1 0.50000000 sec
TD0 16
======== CHANNEL f1 ========
SFO1 400.1820009 MHz
NUC1 1H
P1 11.50 usec
PLW1 10.00000000 W
F2 – Processing parameters
SI 65536
SF 400.1800078 MHz
WDW EM
SSB 0
LB 0.30 Hz
GB 0
PC 1.00

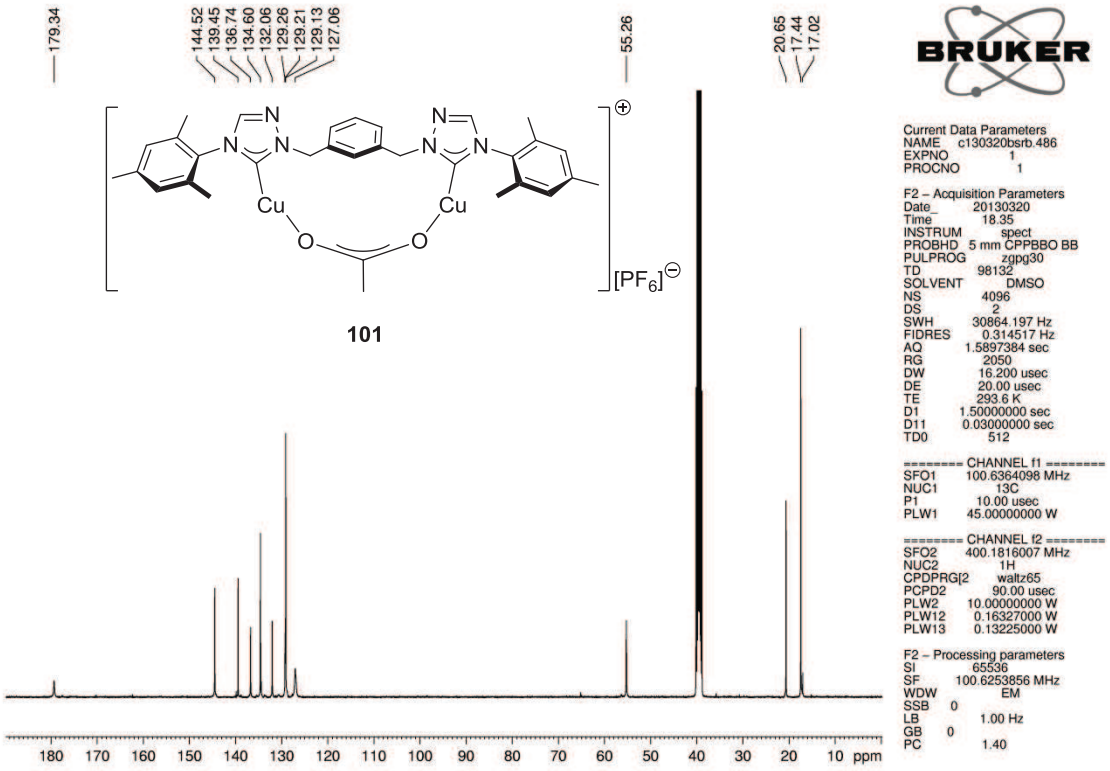
179.34
144.52
139.45
136.74
134.60
132.06
129.26
129.21
129.13
127.06
55.26
20.65
17.44
17.02
Cu
Cu
O
O
[PF6]⊖
101
180 170 160 150 140 130 120 110 100 90 80 70 60 50 40 30 20 10 ppm
BRUKER
Current Data Parameters
NAME c130320bsrb.486
EXPNO 1
PROCNO 1
F2 – Acquisition Parameters
Date_ 20130320
Time 18.35
INSTRUM spect
PROBHD 5 mm CPPBBO BB
PULPROG zgpg30
TD 98132
SOLVENT DMSO
NS 4096
DS 2
SWH 30864.197 Hz
FIDRES 0.314517 Hz
AQ 1.5897384 sec
RG 2050
DW 16.200 usec
DE 20.00 usec
TE 293.6 K
D1 1.50000000 sec
D11 0.03000000 sec
TD0 512
======== CHANNEL f1 ========
SFO1 100.6364098 MHz
NUC1 13C
P1 10.00 usec
PLW1 45.00000000 W
======== CHANNEL f2 ========
SFO2 400.1816007 MHz
NUC2 1H
CPDPRG[2 waltz65
PCPD2 90.00 usec
PLW2 10.00000000 W
PLW12 0.16327000 W
PLW13 0.13225000 W
F2 – Processing parameters
SI 65536
SF 100.6253856 MHz
WDW EM
SSB 0
LB 1.00 Hz
GB 0
PC 1.40

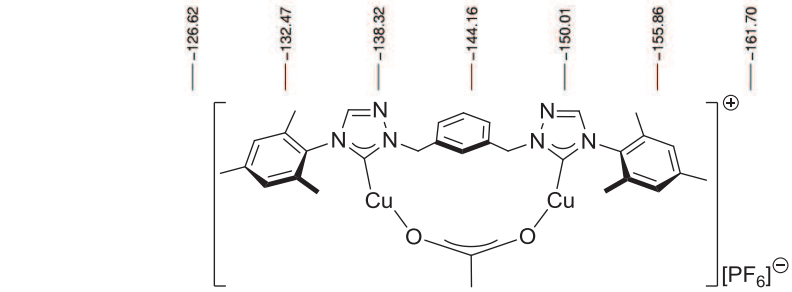

101

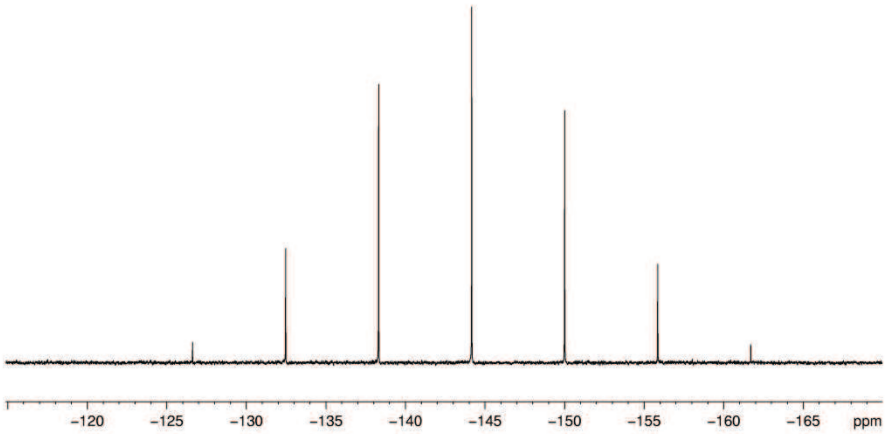

BRUKER

```
Current Data Parameters
NAME      a130315bsrb486DMSO
EXPNO              2
PROCNO             1

F2 - Acquisition Parameters
Date_          20130315
Time              18.55
INSTRUM           spect
PROBHD   5 mm PABBO BB-
PULPROG          zgpg30
TD              135168
SOLVENT           DMSO
NS                  64
DS                   4
SWH           49019.609 Hz
FIDRES        0.362657 Hz
AQ            1.3787136 sec
RG                1820
DW              10.200 usec
DE              10.00 usec
TE              300.1 K
D1          1.00000000 sec
D11         0.03000000 sec
TD0                  8

======== CHANNEL f1 ========
SFO1        121.6425956 MHz
NUC1               31P
P1              11.30 usec
PLW1        16.00000000 W

======== CHANNEL f2 ========
SFO2        300.5115025 MHz
NUC2               1H
CPDPRG[2         waltz65
PCPD2           80.00 usec
PLW2        16.00000000 W
PLW12        0.25000000 W
PLW13        0.16000000 W

F2 - Processing parameters
SI                65536
SF          121.6486780 MHz
WDW                EM
SSB                0
LB              1.00 Hz
GB                 0
PC              1.40
```

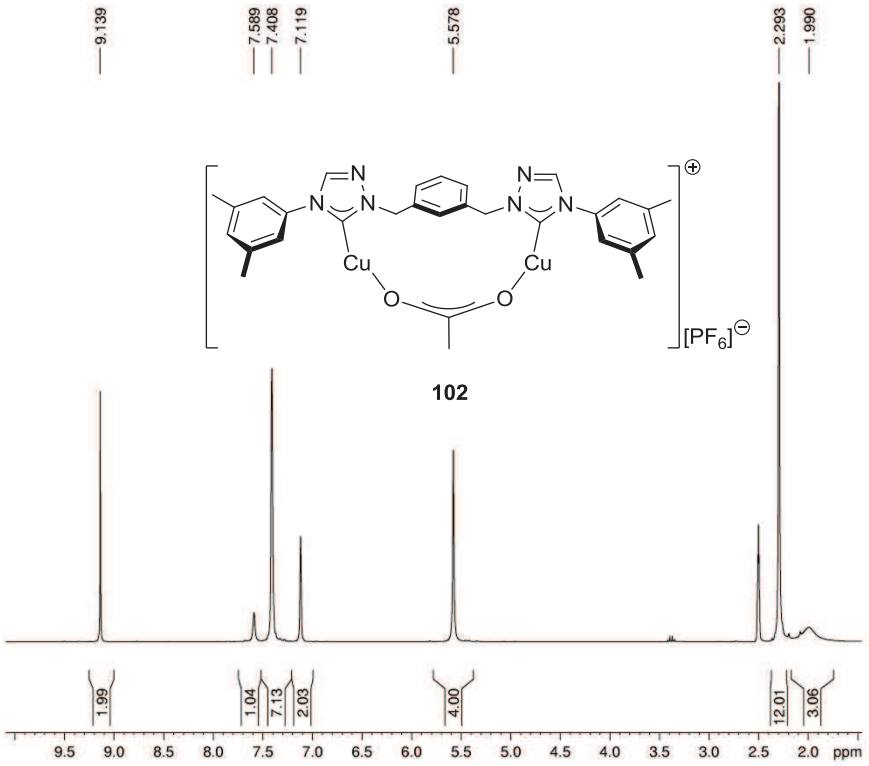

102

BRUKER

```
Current Data Parameters
NAME      b120822bsrb.437
EXPNO              2
PROCNO             1

F2 - Acquisition Parameters
Date_          20120822
Time              20.17
INSTRUM           spect
PROBHD   5 mm PATXO 31P
PULPROG           zg30
TD                65536
SOLVENT           DMSO
NS                  80
DS                   2
SWH           8992.806 Hz
FIDRES        0.137219 Hz
AQ            3.6438017 sec
RG                 362
DW              55.600 usec
DE               6.00 usec
TE              298.2 K
D1          0.10000000 sec
TD0                 10

======== CHANNEL f1 ========
NUC1               1H
P1              11.60 usec
PL1             -3.00 dB
SFO1        300.1315010 MHz

F2 - Processing parameters
SI                32768
SF          300.1300012 MHz
WDW                EM
SSB                0
LB              0.30 Hz
GB                 0
PC              1.00
```

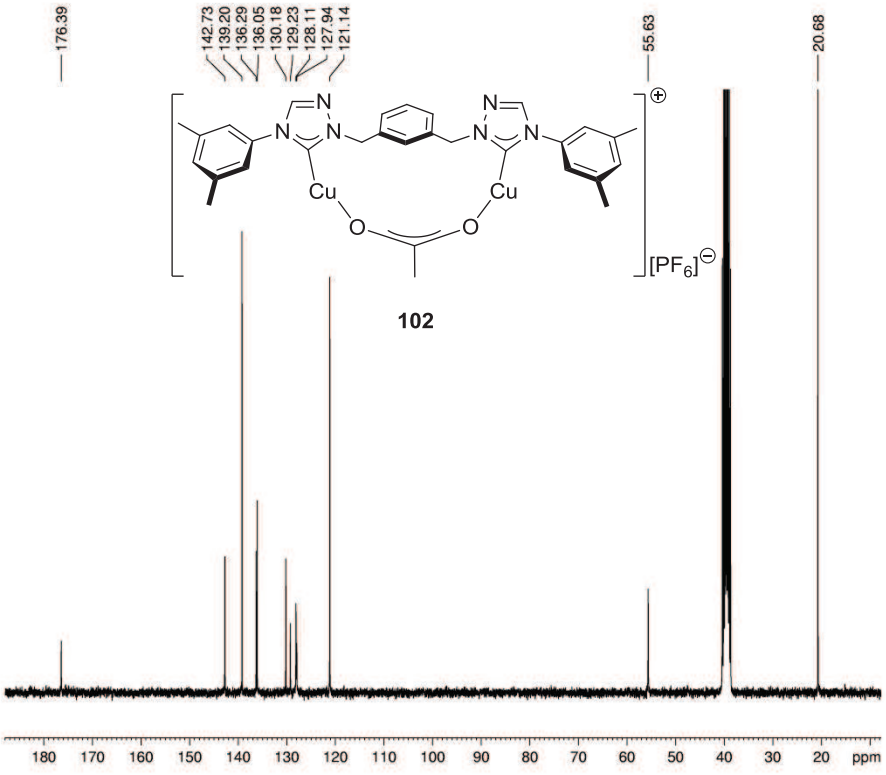

102

Current Data Parameters
NAME b120822bsrb.437
EXPNO 1
PROCNO 1

F2 – Processing parameters
SI 65536
SF 75.4677842 MHz
WDW EM
SSB 0
LB 1.00 Hz
GB 0
PC 1.40

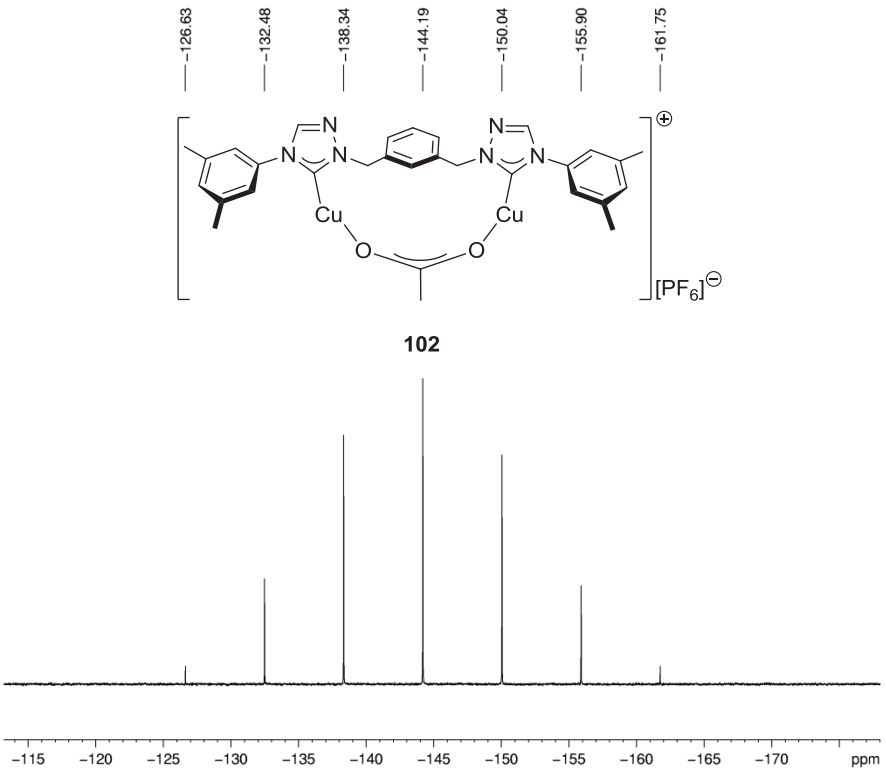

102

Current Data Parameters
NAME b120822bsrb.437
EXPNO 7
PROCNO 1

F2 – Processing parameters
SI 65536
SF 121.4948510 MHz
WDW EM
SSB 0
LB 1.00 Hz
GB 0
PC 1.40

1.10 Synthesis of Tetra-NHC Complexes for Reference Purposes

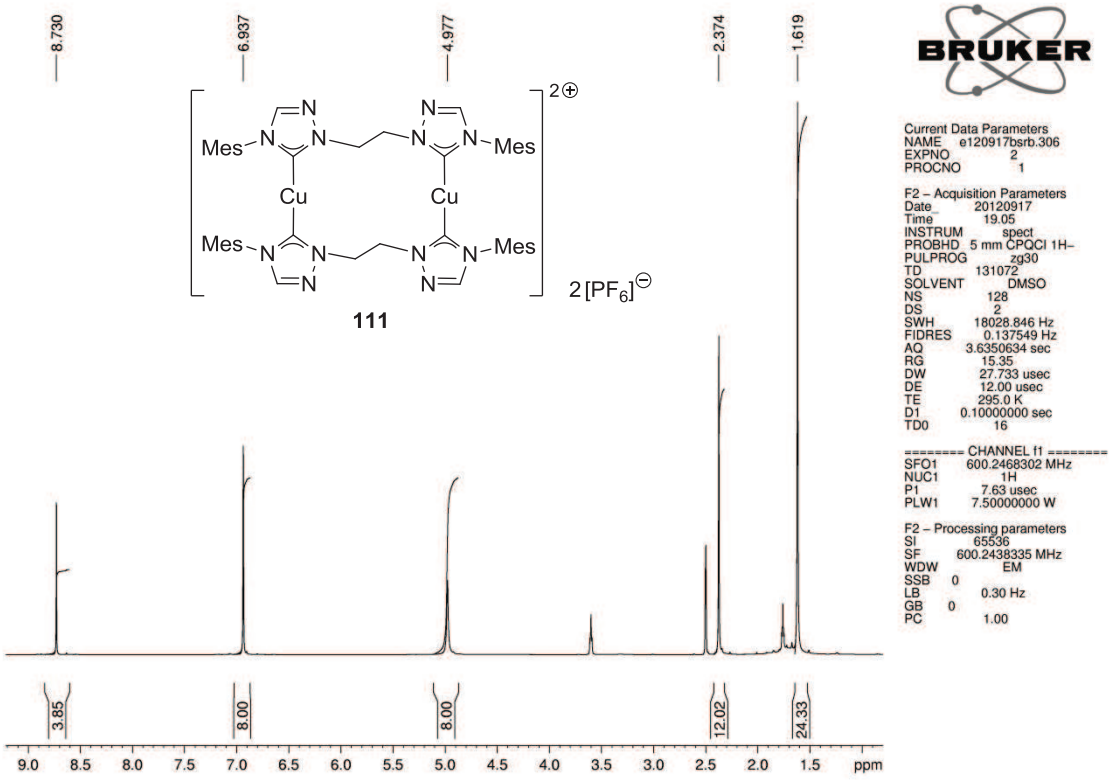

111

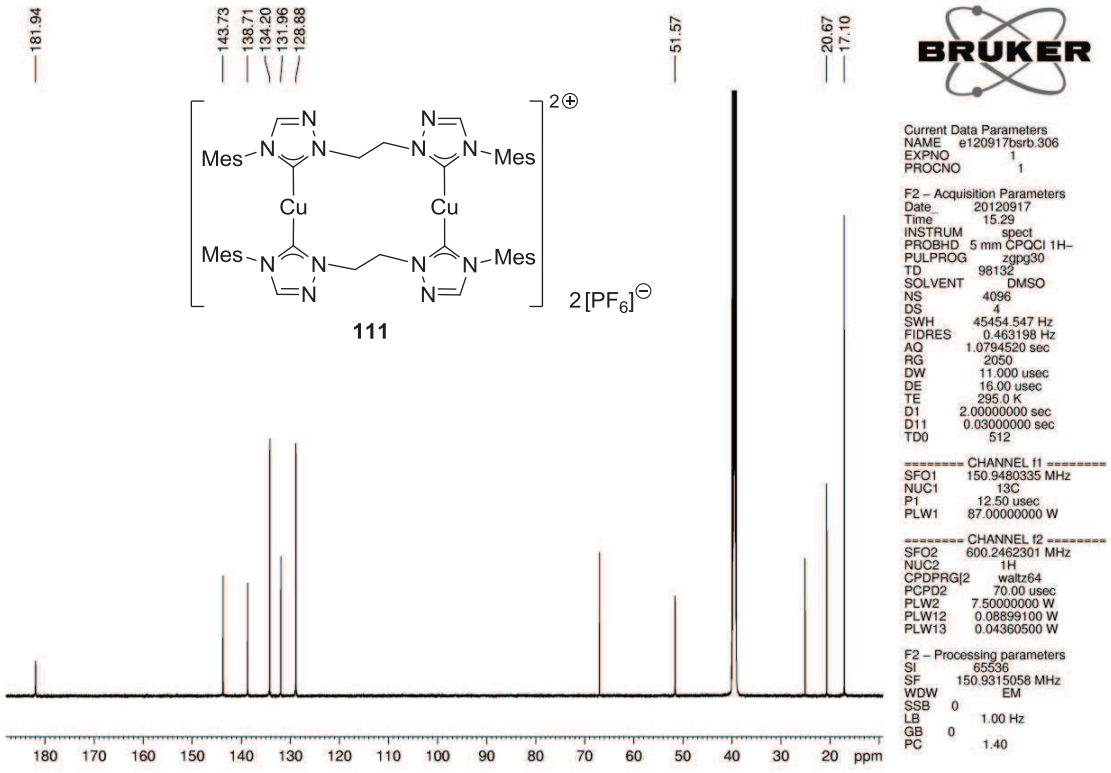

111

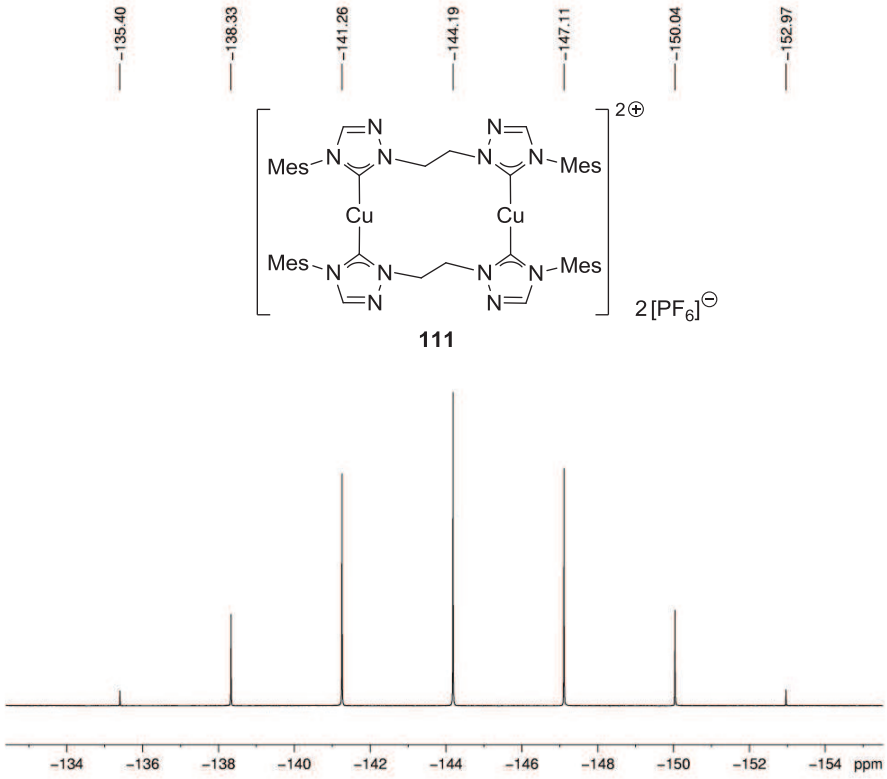

111

Current Data Parameters
NAME e120917bsrb.306
EXPNO 6
PROCNO 1

F2 – Acquisition Parameters
Date_ 20120918
Time 0.27
INSTRUM spect
PROBHD 5 mm CPQCI 1H–
PULPROG zgig30
TD 131072
SOLVENT DMSO
NS 800
DS 4
SWH 53571.430 Hz
FIDRES 0.408718 Hz
AQ 1.2233387 sec
RG 1030
DW 9.333 usec
DE 20.00 usec
TE 295.0 K
D1 2.00000000 sec
D11 0.03000000 sec
TD0 100

======== CHANNEL f1 ========
SFO1 242.9588577 MHz
NUC1 31P
P1 41.25 usec
PLW1 16.00000000 W

======== CHANNEL f2 ========
SFO2 600.2462301 MHz
NUC2 1H
CPDPRG[2 waltz64
PCPD2 70.00 usec
PLW2 7.50000000 W
PLW12 0.08899100 W

F2 – Processing parameters
SI 65536
SF 242.9831560 MHz
WDW EM
SSB 0
LB 1.00 Hz
GB 0
PC 1.40

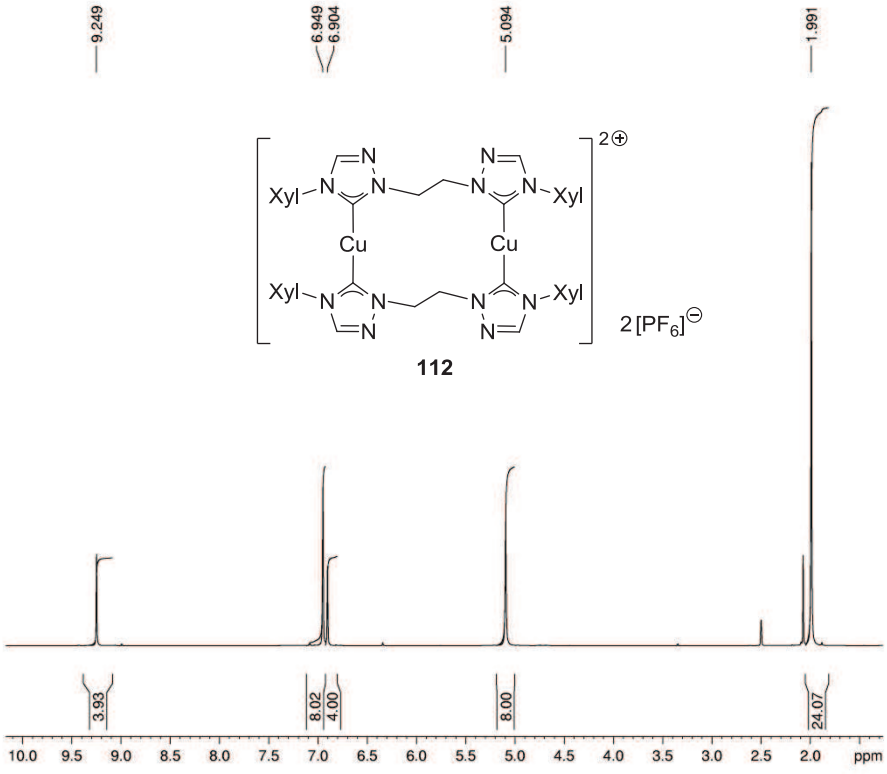

112

Current Data Parameters
NAME e130325bsrb.325
EXPNO 2
PROCNO 1

F2 – Acquisition Parameters
Date_ 20130326
Time 0.58
INSTRUM spect
PROBHD 5 mm CPQCI 1H–
PULPROG zg30
TD 131072
SOLVENT DMSO
NS 128
DS 2
SWH 18028.846 Hz
FIDRES 0.137549 Hz
AQ 3.6350634 sec
RG 13.85
DW 27.733 usec
DE 12.00 usec
TE 295.0 K
D1 0.10000000 sec
TD0 16

======== CHANNEL f1 ========
SFO1 600.2468302 MHz
NUC1 1H
P1 7.63 usec
PLW1 7.50000000 W

F2 – Processing parameters
SI 65536
SF 600.2438337 MHz
WDW EM
SSB 0
LB 0.30 Hz
GB 0
PC 1.00

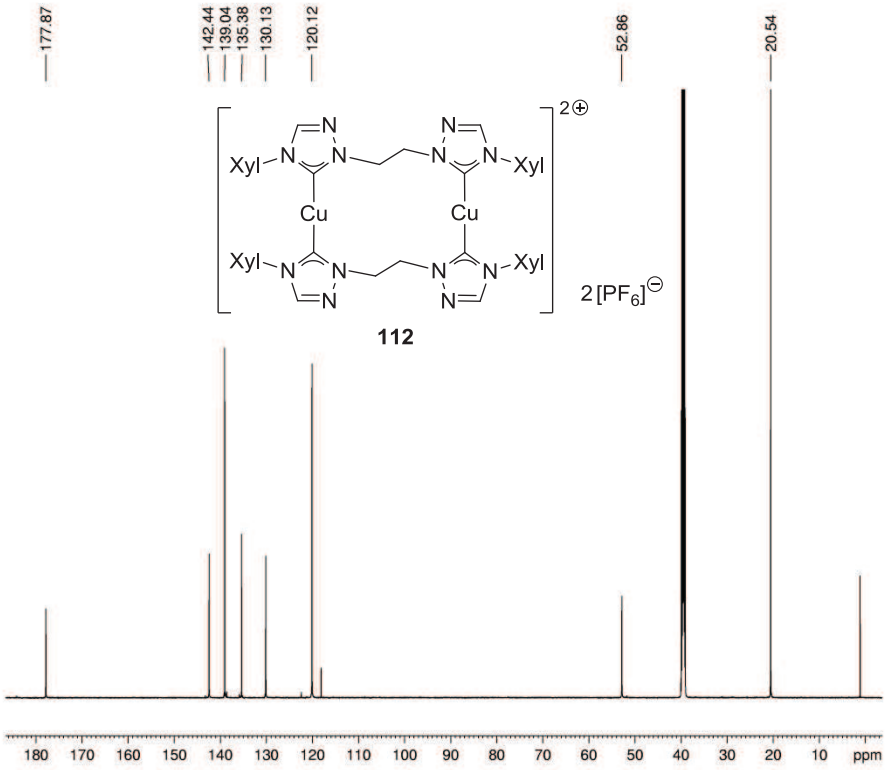

112

Current Data Parameters
NAME e130325bsrb.325
EXPNO 1
PROCNO 1

F2 – Acquisition Parameters
Date_ 20130325
Time 21.23
INSTRUM spect
PROBHD 5 mm CPQCI 1H–
PULPROG zgpg30
TD 98132
SOLVENT DMSO
NS 4096
DS 4
SWH 45454.547 Hz
FIDRES 0.463198 Hz
AQ 1.0794520 sec
RG 2050
DW 11.000 usec
DE 16.00 usec
TE 295.0 K
D1 2.00000000 sec
D11 0.03000000 sec
TD0 512

======== CHANNEL f1 ========
SFO1 150.9480335 MHz
NUC1 13C
P1 12.50 usec
PLW1 87.00000000 W

======== CHANNEL f2 ========
SFO2 600.2462301 MHz
NUC2 1H
CPDPRG[2 waltz64
PCPD2 70.00 usec
PLW2 7.50000000 W
PLW12 0.08899100 W
PLW13 0.04360500 W

F2 – Processing parameters
SI 65536
SF 150.9314981 MHz
WDW EM
SSB 0
LB 1.00 Hz
GB 0
PC 1.40

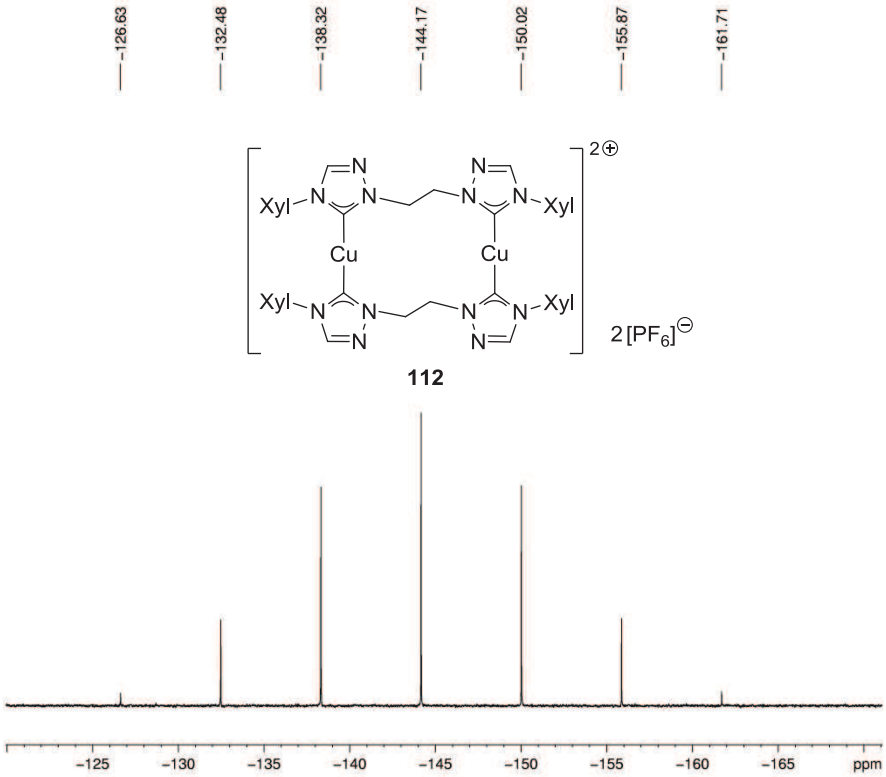

112

Current Data Parameters
NAME a130325bsrb325DMSO
EXPNO 2
PROCNO 1

F2 – Acquisition Parameters
Date_ 20130325
Time 14.39
INSTRUM spect
PROBHD 5 mm PABBO BB–
PULPROG zgpg30
TD 135168
SOLVENT DMSO
NS 64
DS 4
SWH 49019.609 Hz
FIDRES 0.362657 Hz
AQ 1.3787136 sec
RG 2050
DW 10.200 usec
DE 10.00 usec
TE 300.1 K
D1 1.00000000 sec
D11 0.03000000 sec
TD0 8

======== CHANNEL f1 ========
SFO1 121.6425956 MHz
NUC1 31P
P1 11.30 usec
PLW1 16.00000000 W

======== CHANNEL f2 ========
SFO2 300.5115025 MHz
NUC2 1H
CPDPRG[2 waltz65
PCPD2 80.00 usec
PLW2 16.00000000 W
PLW12 0.25000000 W
PLW13 0.16000000 W

F2 – Processing parameters
SI 65536
SF 121.6486780 MHz
WDW EM
SSB 0
LB 1.00 Hz
GB 0
PC 1.40

1.11 Synthesis of $[(ICy)_2Cu]PF_6$

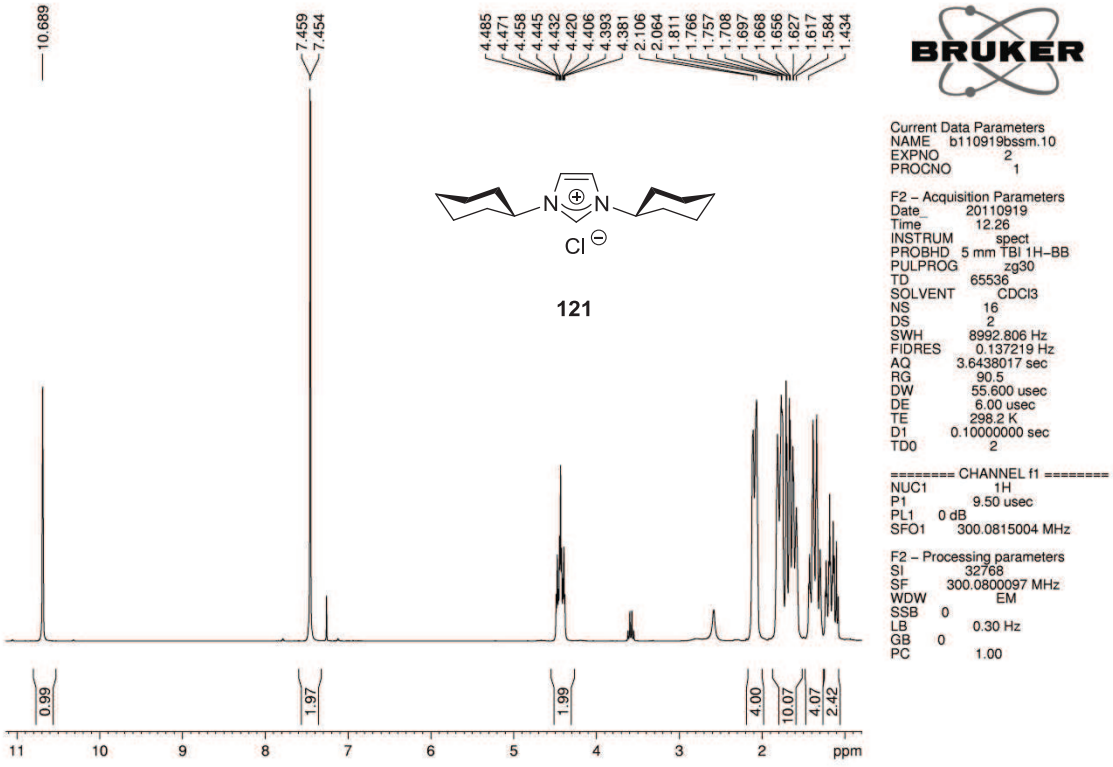

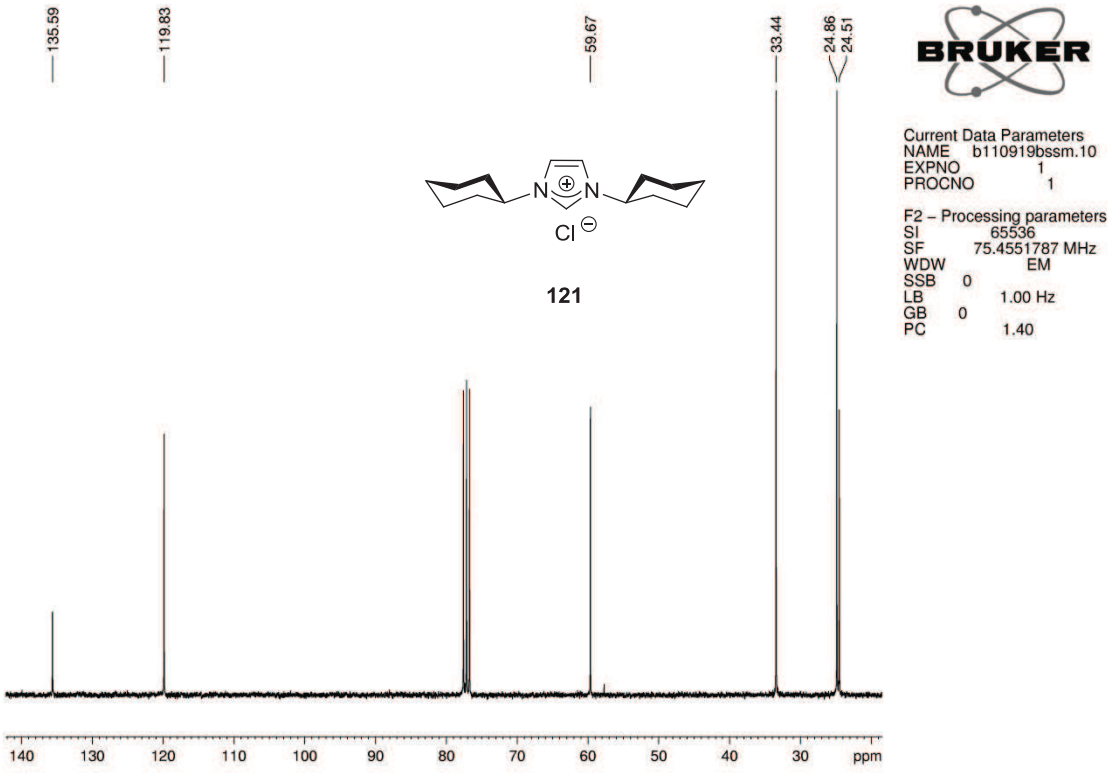

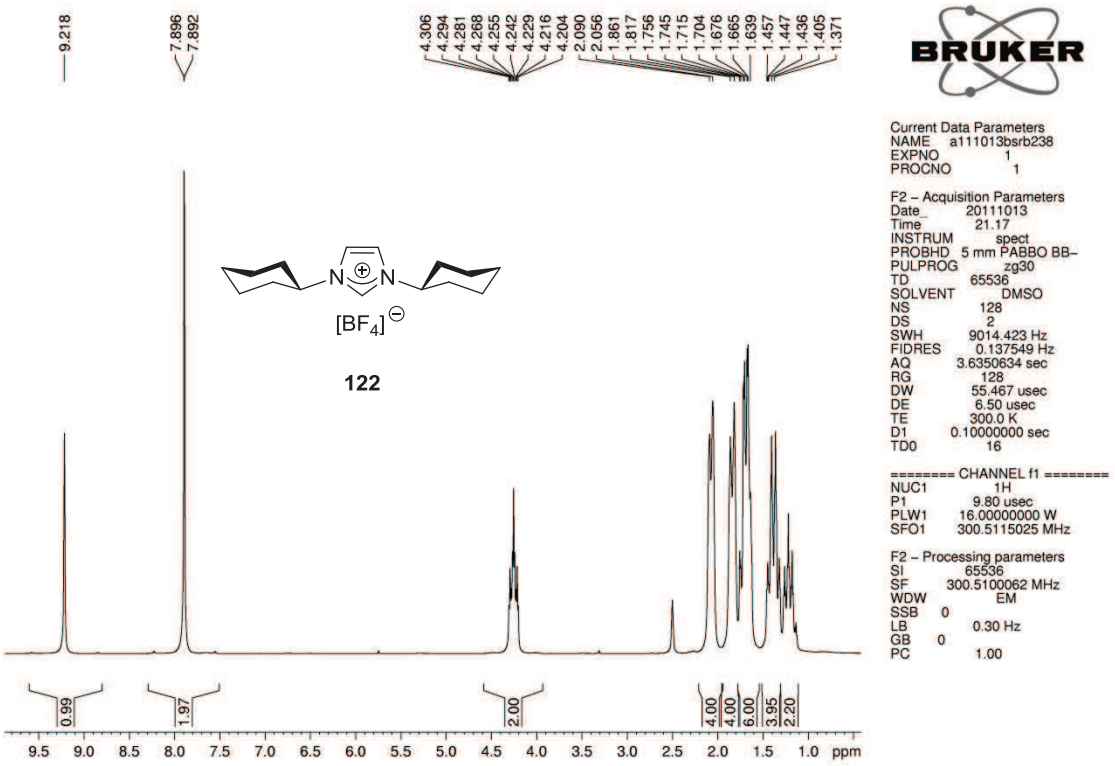
9.218
7.896
7.892
4.306
4.294
4.281
4.268
4.255
4.242
4.229
4.216
4.204
2.090
2.056
1.861
1.817
1.756
1.745
1.715
1.704
1.676
1.665
1.639
1.457
1.447
1.436
1.405
1.371
BRUKER
Current Data Parameters
NAME a111013bsrb238
EXPNO 1
PROCNO 1
F2 – Acquisition Parameters
Date_ 20111013
Time 21.17
INSTRUM spect
PROBHD 5 mm PABBO BB–
PULPROG zg30
TD 65536
SOLVENT DMSO
NS 128
DS 2
SWH 9014.423 Hz
FIDRES 0.137549 Hz
AQ 3.6350634 sec
RG 128
DW 55.467 usec
DE 6.50 usec
TE 300.0 K
D1 0.10000000 sec
TD0 16
======== CHANNEL f1 ========
NUC1 1H
P1 9.80 usec
PLW1 16.00000000 W
SFO1 300.5115025 MHz
F2 – Processing parameters
SI 65536
SF 300.5100062 MHz
WDW EM
SSB 0
LB 0.30 Hz
GB 0
PC 1.00
[BF4]⊖
122
0.99
1.97
2.00
4.00
4.00
6.00
3.95
2.20
9.5 9.0 8.5 8.0 7.5 7.0 6.5 6.0 5.5 5.0 4.5 4.0 3.5 3.0 2.5 2.0 1.5 1.0 ppm

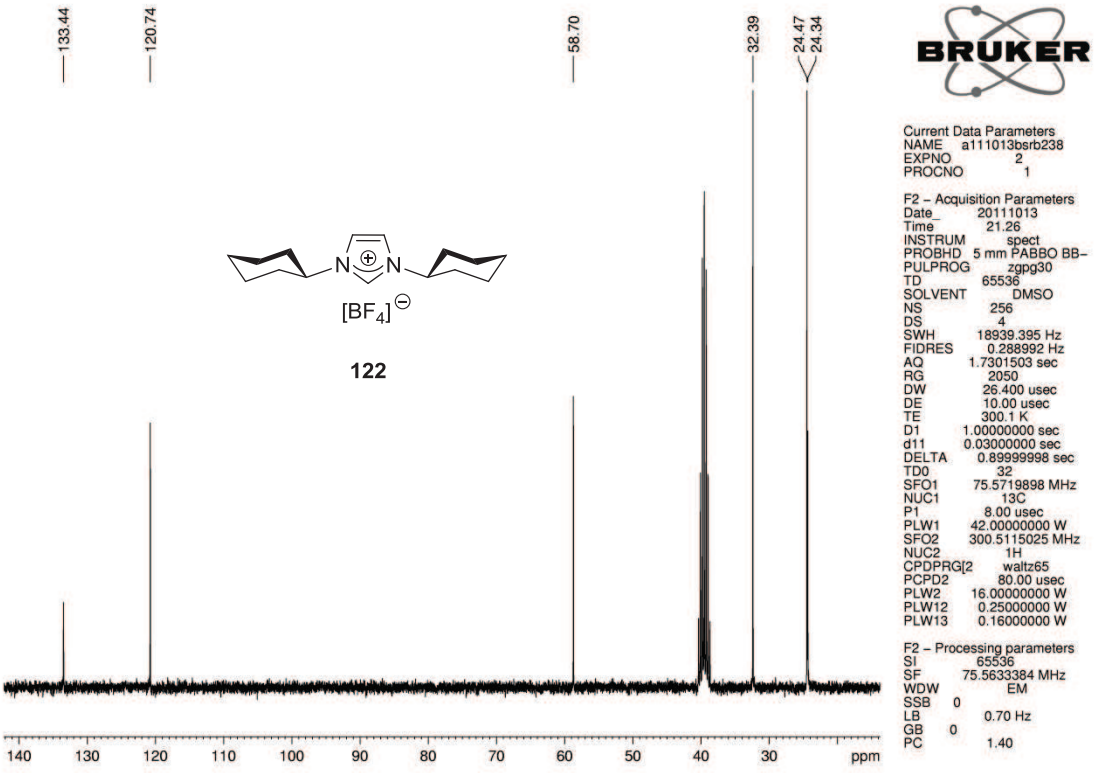
133.44
120.74
58.70
32.39
24.47
24.34
BRUKER
Current Data Parameters
NAME a111013bsrb238
EXPNO 2
PROCNO 1
F2 – Acquisition Parameters
Date_ 20111013
Time 21.26
INSTRUM spect
PROBHD 5 mm PABBO BB–
PULPROG zgpg30
TD 65536
SOLVENT DMSO
NS 256
DS 4
SWH 18939.395 Hz
FIDRES 0.288992 Hz
AQ 1.7301503 sec
RG 2050
DW 26.400 usec
DE 10.00 usec
TE 300.1 K
D1 1.00000000 sec
d11 0.03000000 sec
DELTA 0.89999998 sec
TD0 32
SFO1 75.5719898 MHz
NUC1 13C
P1 8.00 usec
PLW1 42.00000000 W
SFO2 300.5115025 MHz
NUC2 1H
CPDPRG[2 waltz65
PCPD2 80.00 usec
PLW2 16.00000000 W
PLW12 0.25000000 W
PLW13 0.16000000 W
F2 – Processing parameters
SI 65536
SF 75.5633384 MHz
WDW EM
SSB 0
LB 0.70 Hz
GB 0
PC 1.40
[BF4]⊖
122
140 130 120 110 100 90 80 70 60 50 40 30 ppm

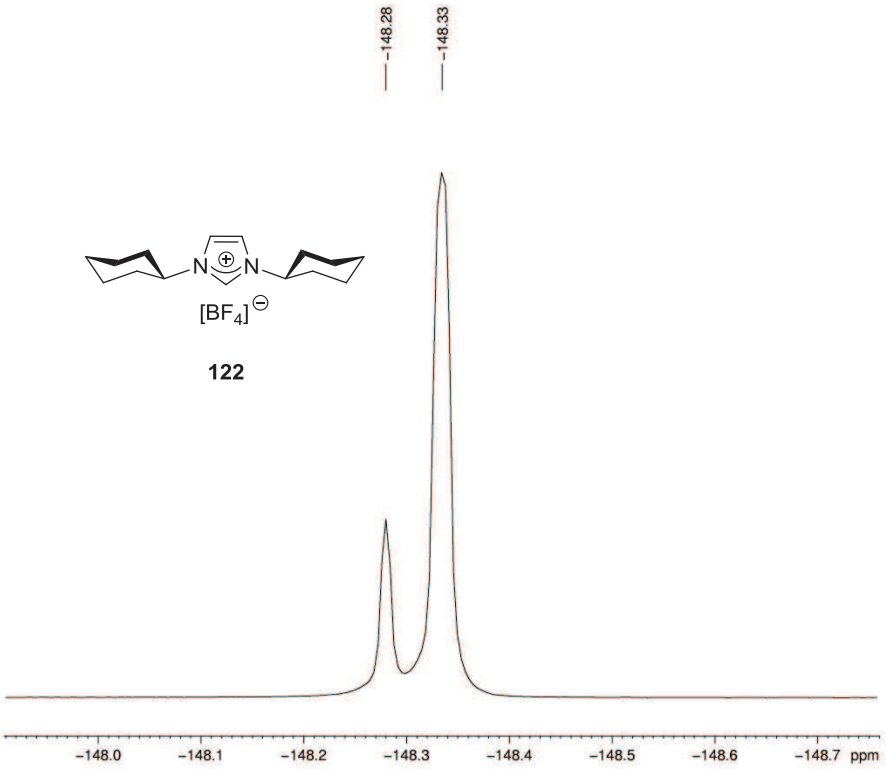

$[BF_4]^{\ominus}$

122

Current Data Parameters
NAME a111013bsrb238
EXPNO 3
PROCNO 1

F2 – Acquisition Parameters
Date_ 20111013
Time 21.40
INSTRUM spect
PROBHD 5 mm PABBO BB–
PULPROG zgfhigqn.2
TD 262144
SOLVENT DMSO
NS 16
DS 4
SWH 71428.570 Hz
FIDRES 0.272478 Hz
AQ 1.8350080 sec
RG 1150
DW 7.000 usec
DE 10.00 usec
TE 300.1 K
D1 1.50000000 sec
d11 0.03000000 sec
d12 0.00002000 sec
TD0 2
rde1 0.00000800 sec
SFO1 282.7491877 MHz
NUC1 19F
P1 12.20 usec
PLW1 11.00000000 W
SFO2 300.5115025 MHz
NUC2 1H
CPDPRG[2 waltz65
PCPD2 80.00 usec
PLW2 16.00000000 W
PLW12 0.25000000 W

F2 – Processing parameters
SI 65536
SF 282.7619120 MHz
WDW EM
SSB 0
LB 0.30 Hz
GB 0
PC 1.00

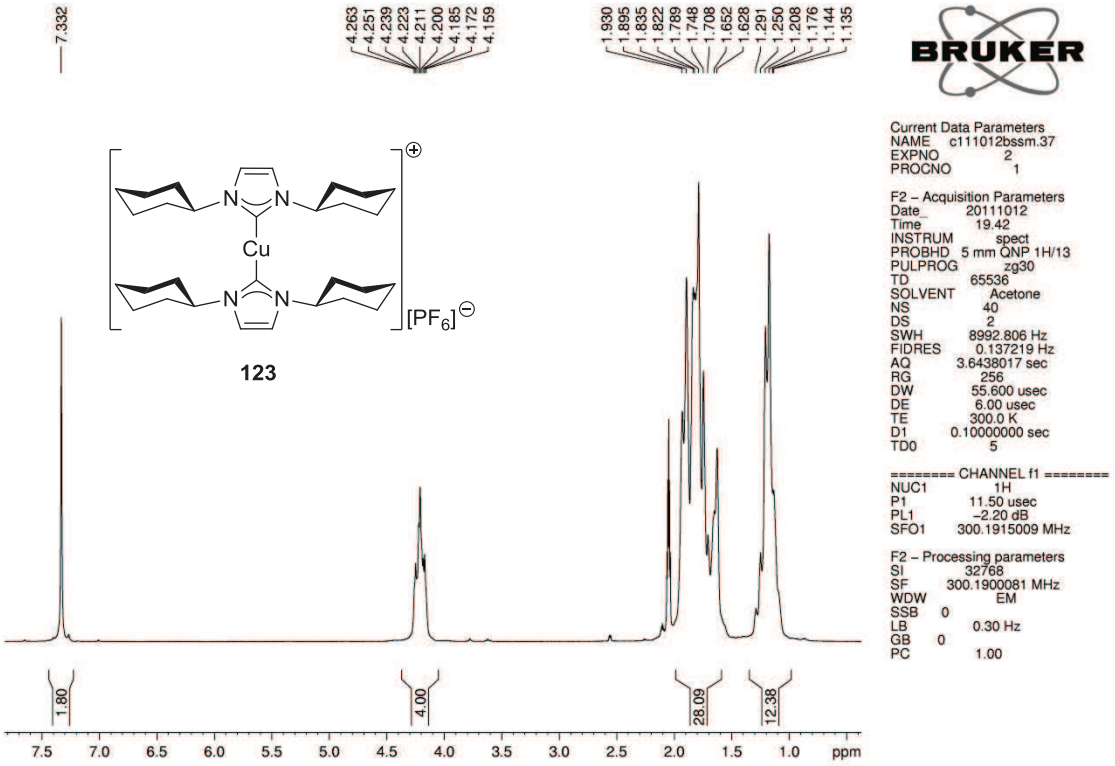
7.332
4.263
4.251
4.239
4.223
4.211
4.200
4.185
4.172
4.159
1.930
1.895
1.835
1.822
1.789
1.748
1.708
1.652
1.628
1.291
1.250
1.208
1.176
1.144
1.135
Cu
[PF6]
123
1.80
4.00
28.09
12.38
7.5 7.0 6.5 6.0 5.5 5.0 4.5 4.0 3.5 3.0 2.5 2.0 1.5 1.0 ppm
BRUKER
Current Data Parameters
NAME c111012bssm.37
EXPNO 2
PROCNO 1
F2 – Acquisition Parameters
Date_ 20111012
Time 19.42
INSTRUM spect
PROBHD 5 mm QNP 1H/13
PULPROG zg30
TD 65536
SOLVENT Acetone
NS 40
DS 2
SWH 8992.806 Hz
FIDRES 0.137219 Hz
AQ 3.6438017 sec
RG 256
DW 55.600 usec
DE 6.00 usec
TE 300.0 K
D1 0.10000000 sec
TD0 5
======== CHANNEL f1 ========
NUC1 1H
P1 11.50 usec
PL1 –2.20 dB
SFO1 300.1915009 MHz
F2 – Processing parameters
SI 32768
SF 300.1900081 MHz
WDW EM
SSB 0
LB 0.30 Hz
GB 0
PC 1.00

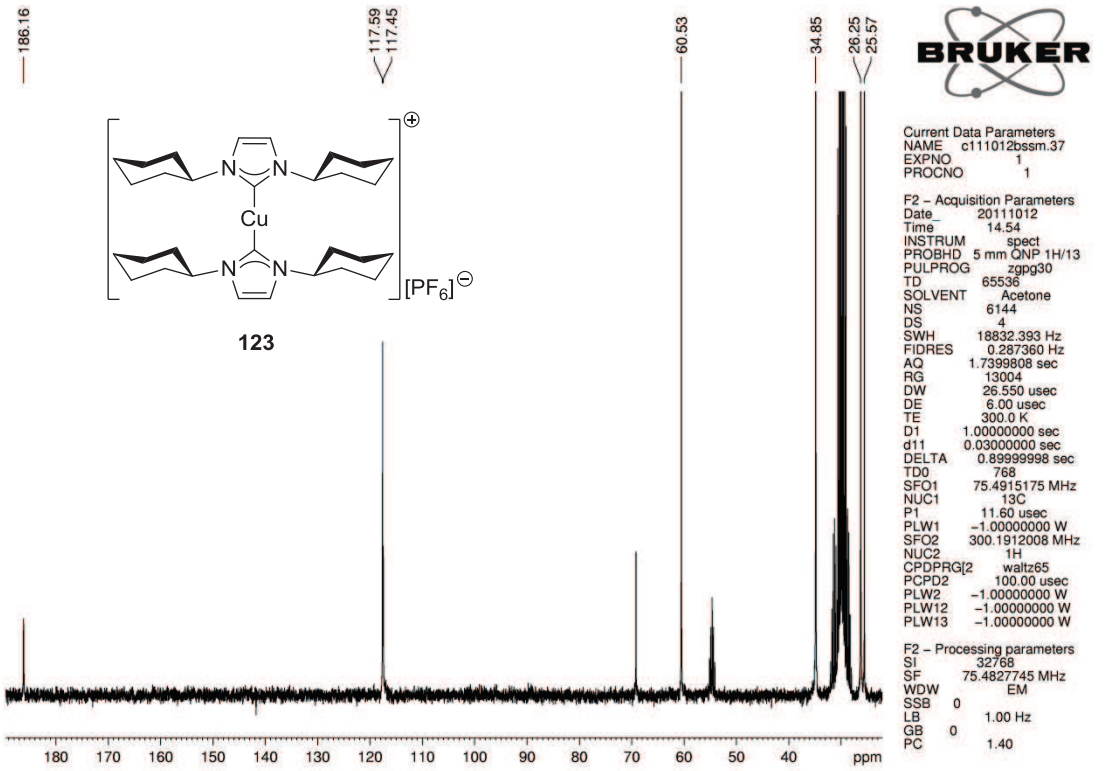
186.16
117.59
117.45
60.53
34.85
26.25
25.57
Cu
[PF6]
123
180 170 160 150 140 130 120 110 100 90 80 70 60 50 40 ppm
BRUKER
Current Data Parameters
NAME c111012bssm.37
EXPNO 1
PROCNO 1
F2 – Acquisition Parameters
Date_ 20111012
Time 14.54
INSTRUM spect
PROBHD 5 mm QNP 1H/13
PULPROG zgpg30
TD 65536
SOLVENT Acetone
NS 6144
DS 4
SWH 18832.393 Hz
FIDRES 0.287360 Hz
AQ 1.7399808 sec
RG 13004
DW 26.550 usec
DE 6.00 usec
TE 300.0 K
D1 1.00000000 sec
d11 0.03000000 sec
DELTA 0.89999998 sec
TD0 768
SFO1 75.4915175 MHz
NUC1 13C
P1 11.60 usec
PLW1 –1.00000000 W
SFO2 300.1912008 MHz
NUC2 1H
CPDPRG[2 waltz65
PCPD2 100.00 usec
PLW2 –1.00000000 W
PLW12 –1.00000000 W
PLW13 –1.00000000 W
F2 – Processing parameters
SI 32768
SF 75.4827745 MHz
WDW EM
SSB 0
LB 1.00 Hz
GB 0
PC 1.40

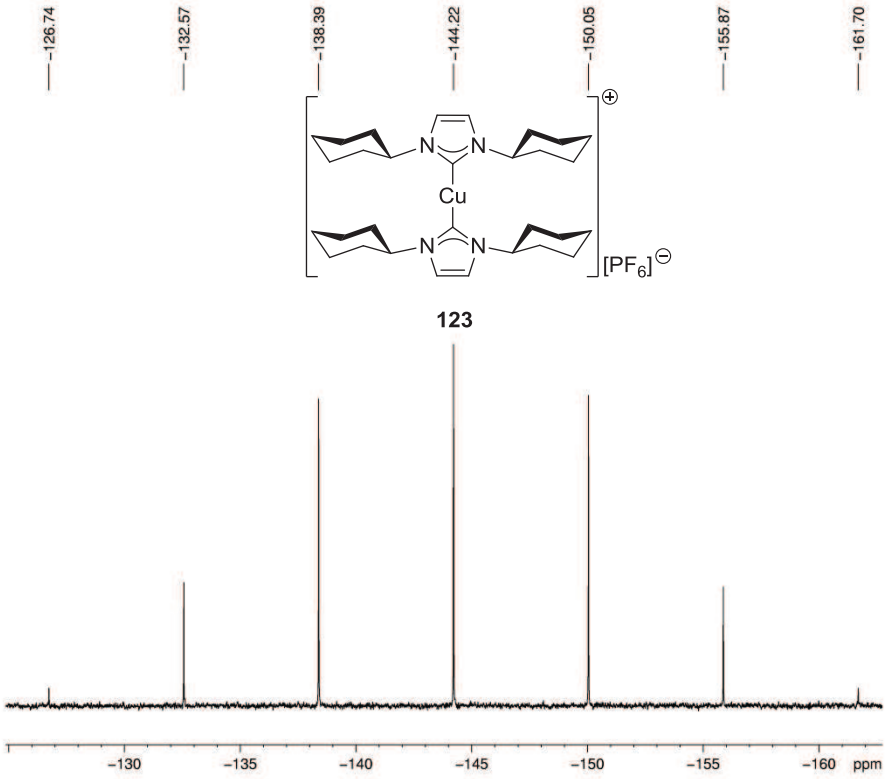

123

BRUKER

Current Data Parameters
NAME b111012bssm.37
EXPNO 1
PROCNO 1

F2 – Processing parameters
SI 65536
SF 121.4746110 MHz
WDW EM
SSB 0
LB 1.00 Hz
GB 0
PC 1.40

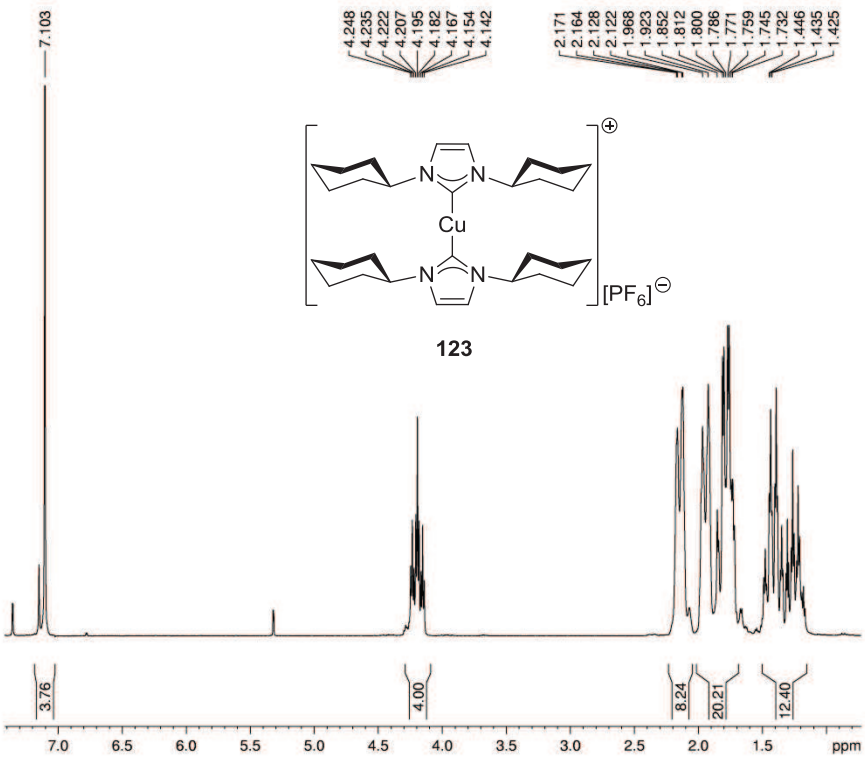

123

BRUKER

Current Data Parameters
NAME a111017bsrb239
EXPNO 1
PROCNO 1

F2 – Acquisition Parameters
Date_ 20111017
Time 13.14
INSTRUM spect
PROBHD 5 mm PABBO BB–
PULPROG zg30
TD 65536
SOLVENT CD2Cl2
NS 16
DS 2
SWH 9014.423 Hz
FIDRES 0.137549 Hz
AQ 3.6350634 sec
RG 256
DW 55.467 usec
DE 6.50 usec
TE 300.0 K
D1 0.10000000 sec
TD0 2

======== CHANNEL f1 ========
NUC1 1H
P1 9.80 usec
PLW1 16.00000000 W
SFO1 300.5115025 MHz

F2 – Processing parameters
SI 65536
SF 300.5100149 MHz
WDW EM
SSB 0
LB 0.30 Hz
GB 0
PC 1.00

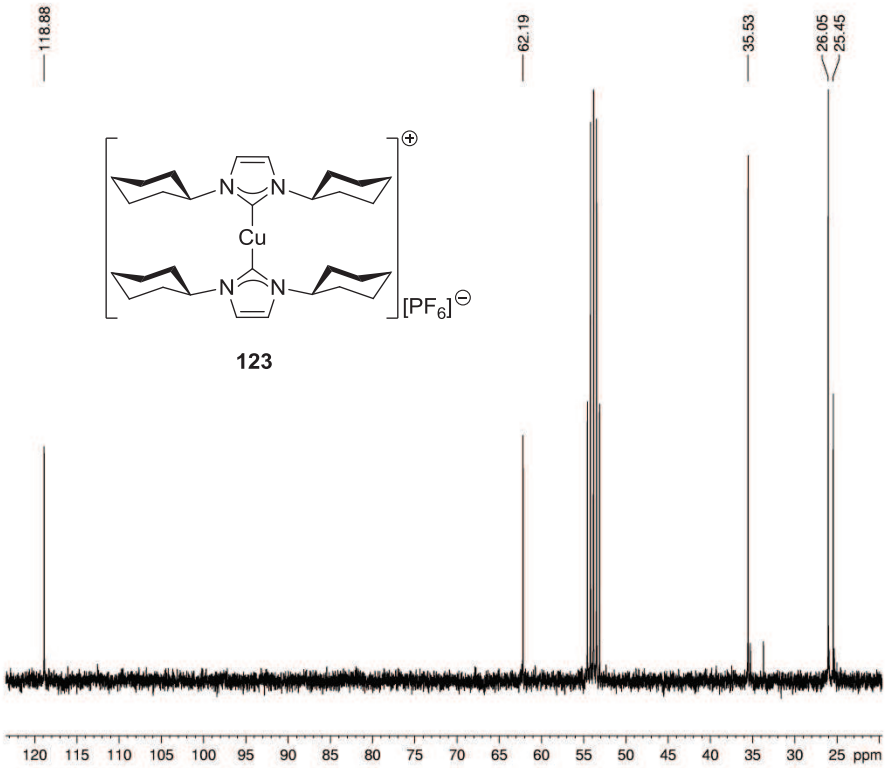

123

```
Current Data Parameters
NAME      a111017bsrb239
EXPNO              3
PROCNO             1

F2 - Acquisition Parameters
Date_          20111018
Time              5.00
INSTRUM           spect
PROBHD  5 mm PABBO BB-
PULPROG          zgpg30
TD              65536
SOLVENT          CD2Cl2
NS                256
DS                  4
SWH           18939.395 Hz
FIDRES        0.288992 Hz
AQ            1.7301503 sec
RG                2050
DW             26.400 usec
DE             10.00 usec
TE               300.1 K
D1            1.00000000 sec
d11           0.03000000 sec
DELTA         0.89999998 sec
TD0                 32
SFO1          75.5719898 MHz
NUC1                13C
P1              8.00 usec
PLW1          42.00000000 W
SFO2          300.5115025 MHz
NUC2                1H
CPDPRG[2         waltz65
PCPD2           80.00 usec
PLW2          16.00000000 W
PLW12          0.25000000 W
PLW13          0.16000000 W

F2 - Processing parameters
SI              65536
SF          75.5632684 MHz
WDW                EM
SSB     0
LB              0.70 Hz
GB      0
PC              1.40
```

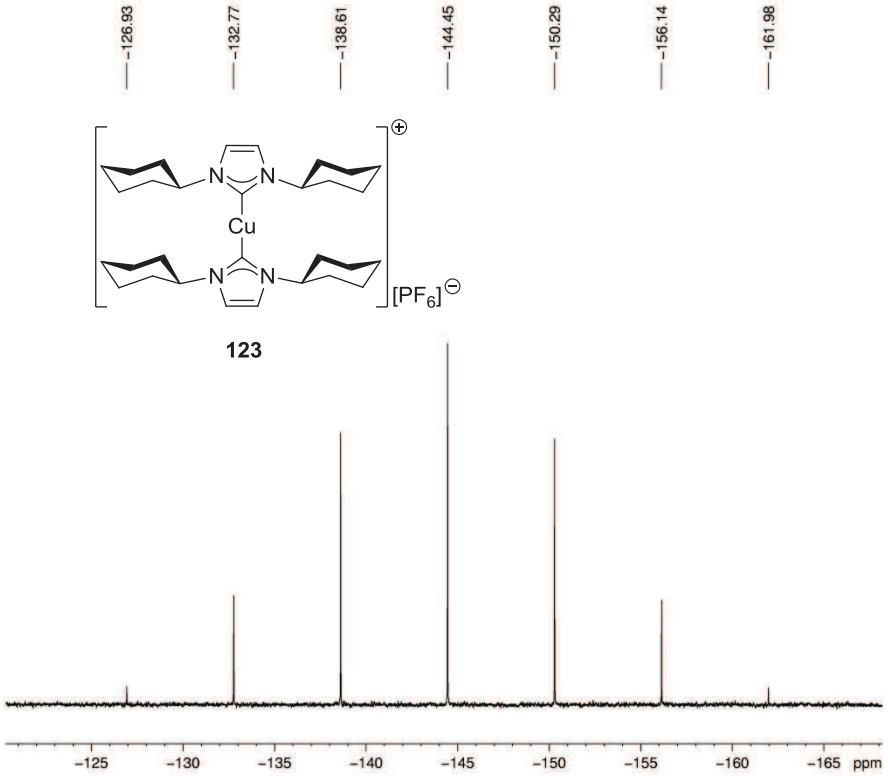

123

```
Current Data Parameters
NAME      a111017bsrb239
EXPNO              2
PROCNO             1

F2 - Acquisition Parameters
Date_          20111017
Time             13.16
INSTRUM           spect
PROBHD  5 mm PABBO BB-
PULPROG          zgpg30
TD             135168
SOLVENT          CD2Cl2
NS                64
DS                 4
SWH           49019.609 Hz
FIDRES        0.362657 Hz
AQ            1.3787136 sec
RG                2050
DW             10.200 usec
DE             10.00 usec
TE               300.1 K
D1            1.00000000 sec
d11           0.03000000 sec
DELTA         0.89999998 sec
TD0                 8
SFO1          121.6425956 MHz
NUC1                31P
P1             11.30 usec
PLW1          16.00000000 W
SFO2          300.5115025 MHz
NUC2                1H
CPDPRG[2         waltz65
PCPD2           80.00 usec
PLW2          16.00000000 W
PLW12          0.25000000 W
PLW13          0.16000000 W

F2 - Processing parameters
SI              65536
SF          121.6486780 MHz
WDW                EM
SSB     0
LB              1.00 Hz
GB      0
PC              1.40
```

1.12 Organoazides

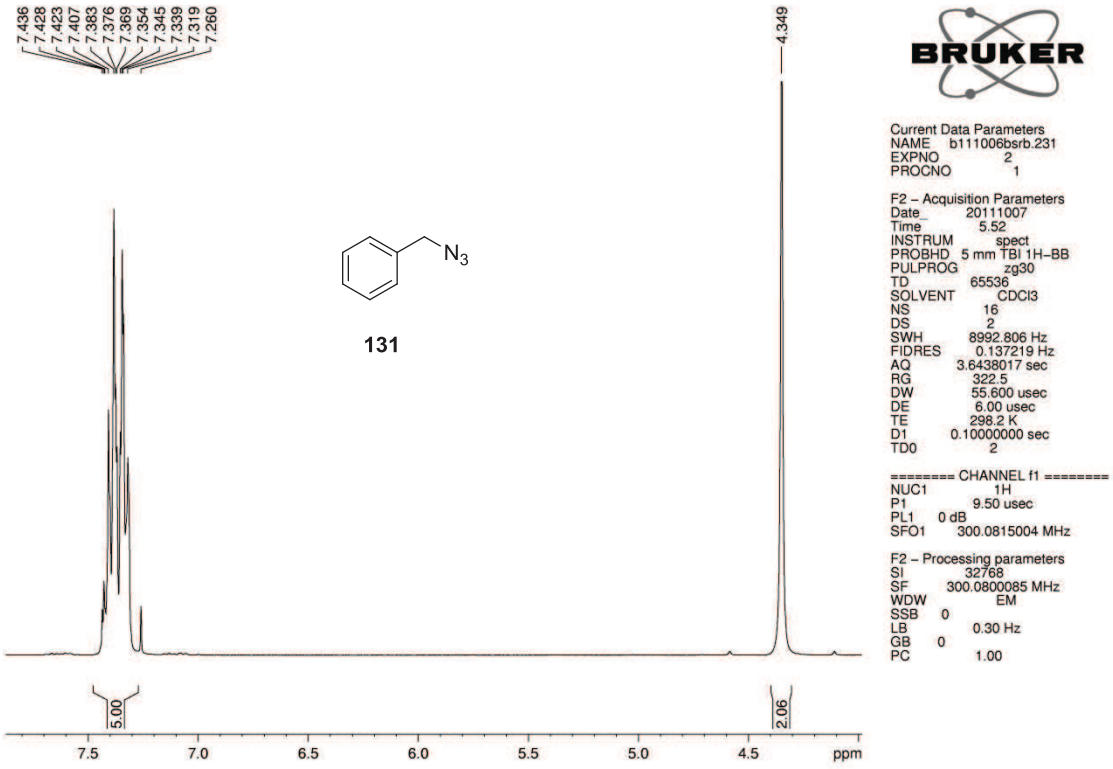

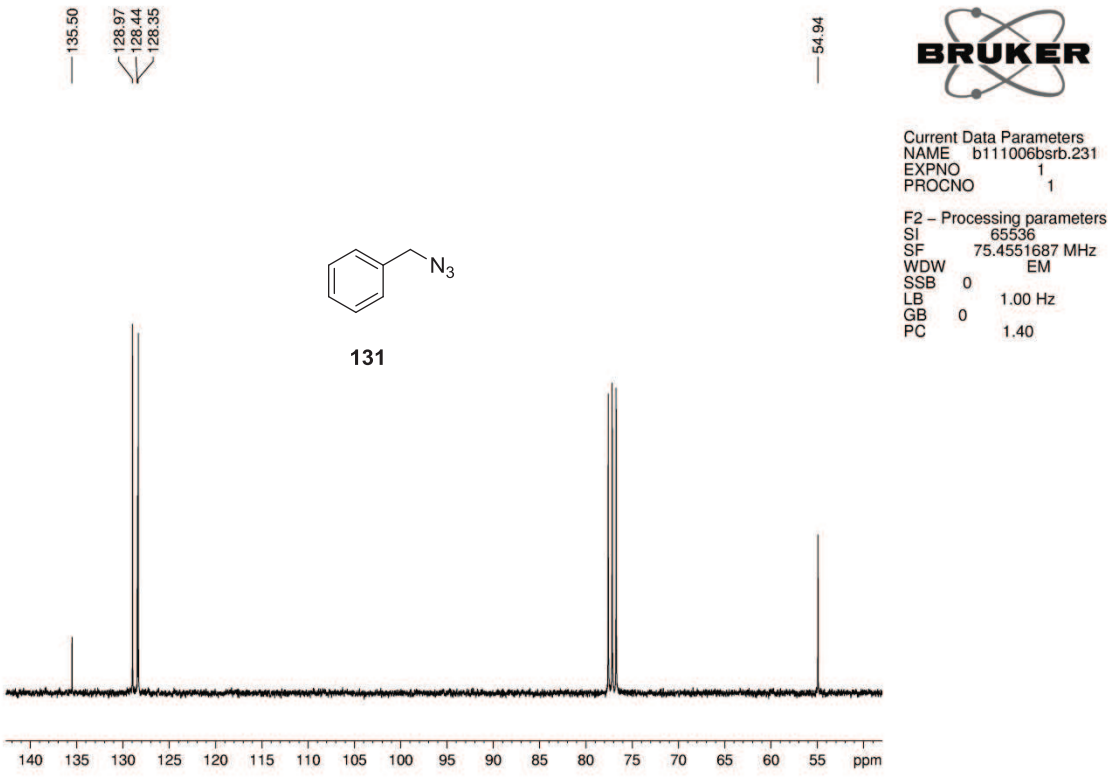

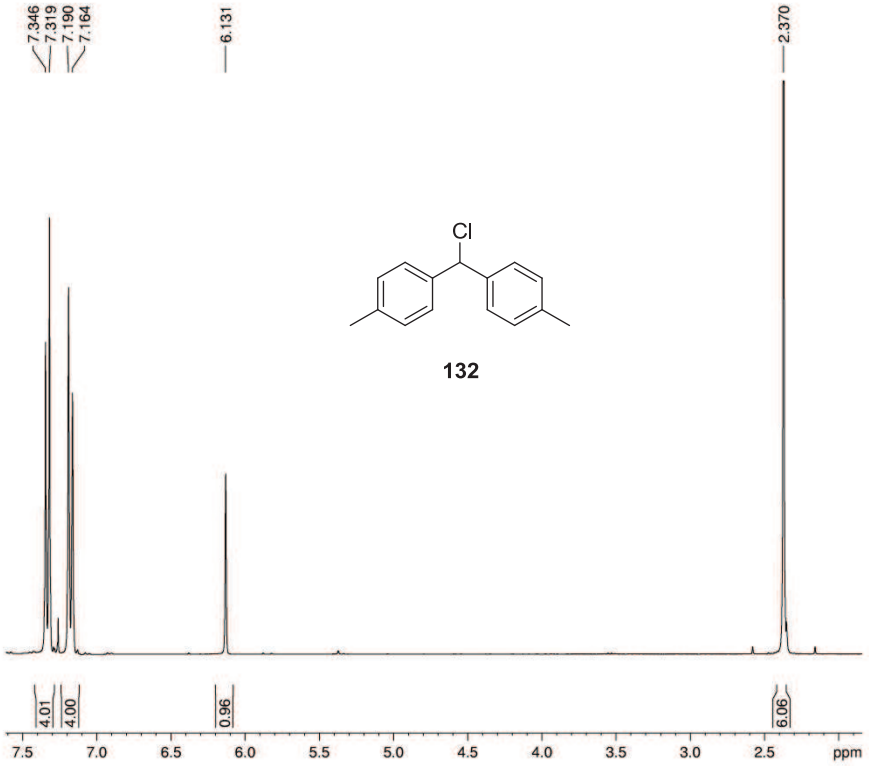

132

Current Data Parameters
NAME a120815bsrb.375
EXPNO 2
PROCNO 1

F2 – Acquisition Parameters
Date_ 20120815
Time 23.55
INSTRUM spect
PROBHD 5 mm PABBO BB–
PULPROG zg30
TD 65536
SOLVENT CDCl3
NS 16
DS 2
SWH 9014.423 Hz
FIDRES 0.137549 Hz
AQ 3.6350634 sec
RG 203
DW 55.467 usec
DE 6.50 usec
TE 299.9 K
D1 0.10000000 sec
TD0 2

======== CHANNEL f1 ========
SFO1 300.5115025 MHz
NUC1 1H
P1 9.80 usec
PLW1 16.00000000 W

F2 – Processing parameters
SI 65536
SF 300.5100105 MHz
WDW EM
SSB 0
LB 0.30 Hz
GB 0
PC 1.00

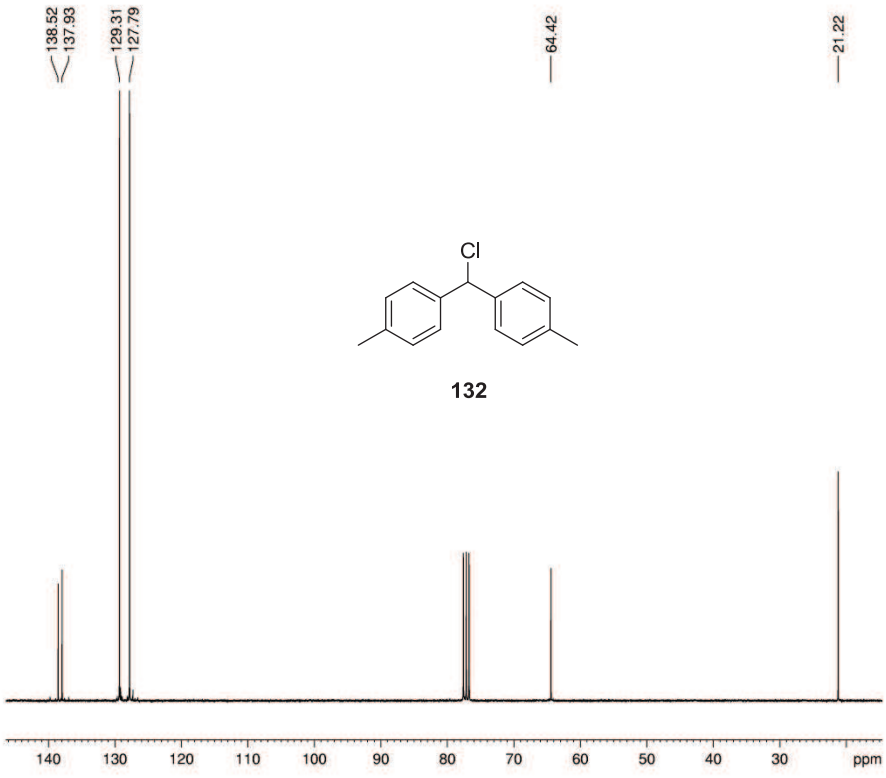

132

Current Data Parameters
NAME a120815bsrb.375
EXPNO 1
PROCNO 1

F2 – Acquisition Parameters
Date_ 20120815
Time 22.40
INSTRUM spect
PROBHD 5 mm PABBO BB–
PULPROG zgpg30
TD 65536
SOLVENT CDCl3
NS 1600
DS 4
SWH 18939.395 Hz
FIDRES 0.288992 Hz
AQ 1.7301503 sec
RG 2050
DW 26.400 usec
DE 10.00 usec
TE 300.1 K
D1 1.00000000 sec
D11 0.03000000 sec
TD0 200

======== CHANNEL f1 ========
SFO1 75.5719898 MHz
NUC1 13C
P1 8.00 usec
PLW1 42.00000000 W

======== CHANNEL f2 ========
SFO2 300.5115025 MHz
NUC2 1H
CPDPRG[2 waltz65
PCPD2 80.00 usec
PLW2 16.00000000 W
PLW12 0.25000000 W
PLW13 0.16000000 W

F2 – Processing parameters
SI 65536
SF 75.5632940 MHz
WDW EM
SSB 0
LB 0.70 Hz
GB 0
PC 1.40

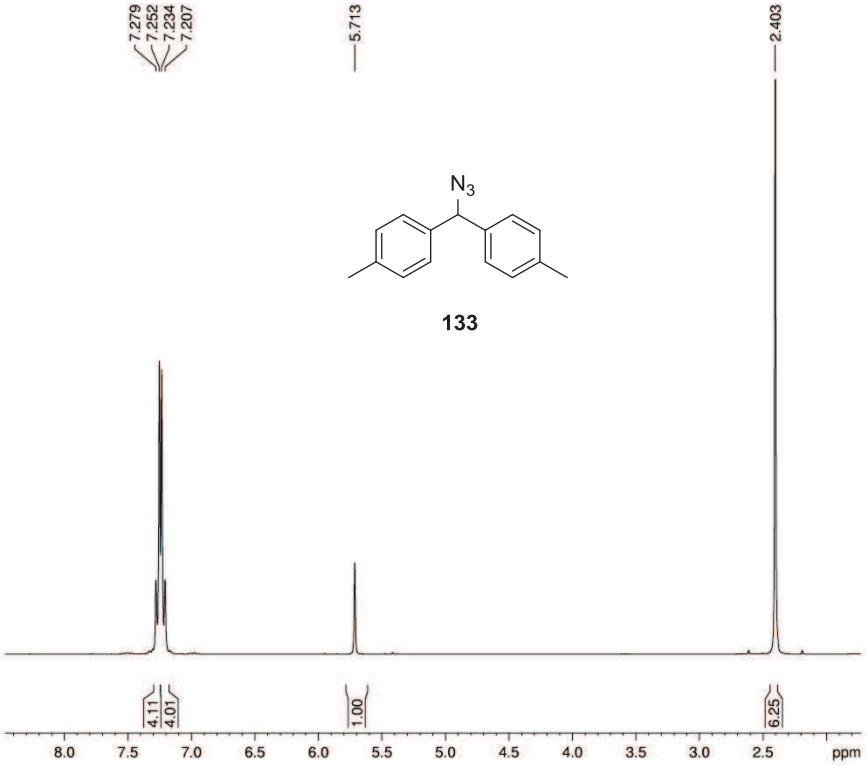

BRUKER

Current Data Parameters
NAME b120807bsrb.385
EXPNO 1
PROCNO 1

F2 – Acquisition Parameters
Date_ 20120808
Time 4.13
INSTRUM spect
PROBHD 5 mm PATXO 31P
PULPROG zg30
TD 65536
SOLVENT CDCl3
NS 16
DS 2
SWH 8992.806 Hz
FIDRES 0.137219 Hz
AQ 3.6438017 sec
RG 101.6
DW 55.600 usec
DE 6.00 usec
TE 298.2 K
D1 0.10000000 sec
TD0 2

======== CHANNEL f1 ========
NUC1 1H
P1 11.60 usec
PL1 –3.00 dB
SFO1 300.1315010 MHz

F2 – Processing parameters
SI 32768
SF 300.1299990 MHz
WDW EM
SSB 0
LB 0.30 Hz
GB 0
PC 1.00

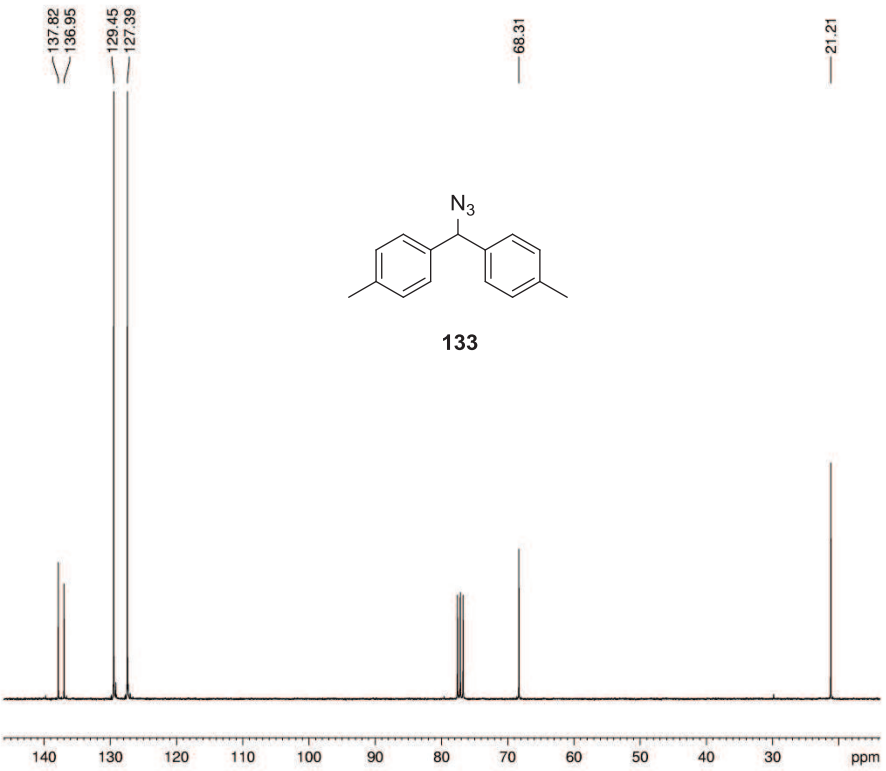

BRUKER

Current Data Parameters
NAME b120807bsrb.385
EXPNO 4
PROCNO 1

F2 – Processing parameters
SI 65536
SF 75.4677445 MHz
WDW EM
SSB 0
LB 1.00 Hz
GB 0
PC 1.40

1.13 1,4-Disubstituted 1,2,3-Triazoles

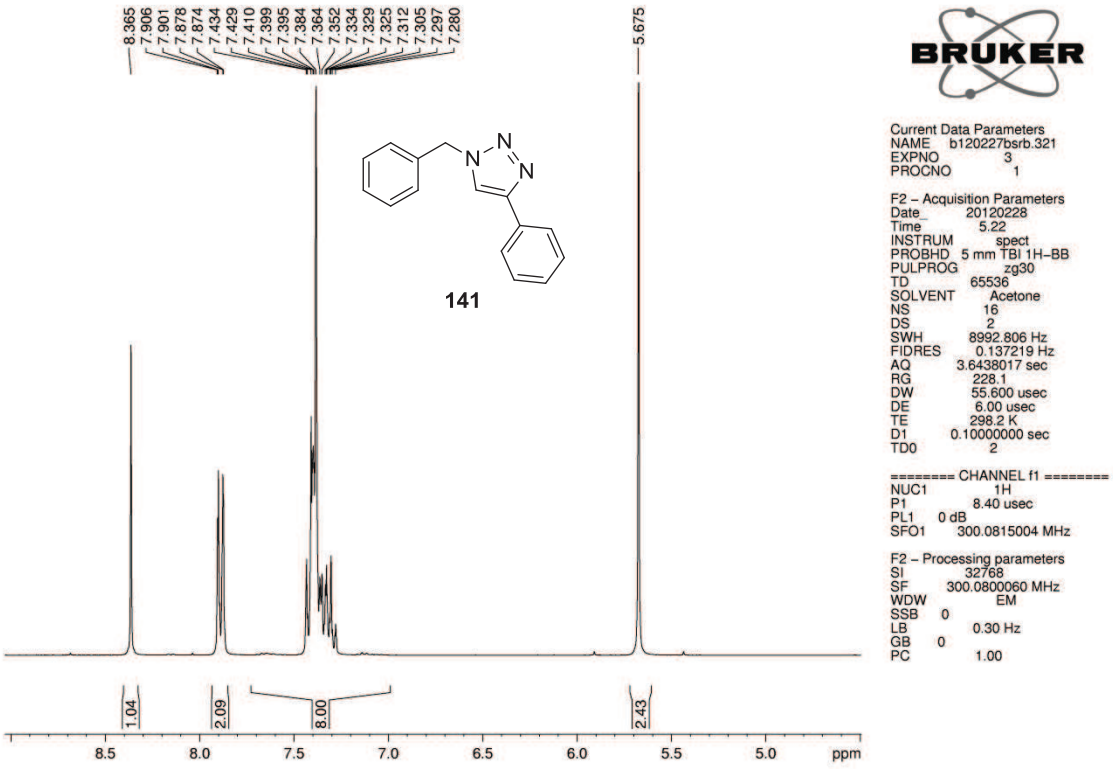

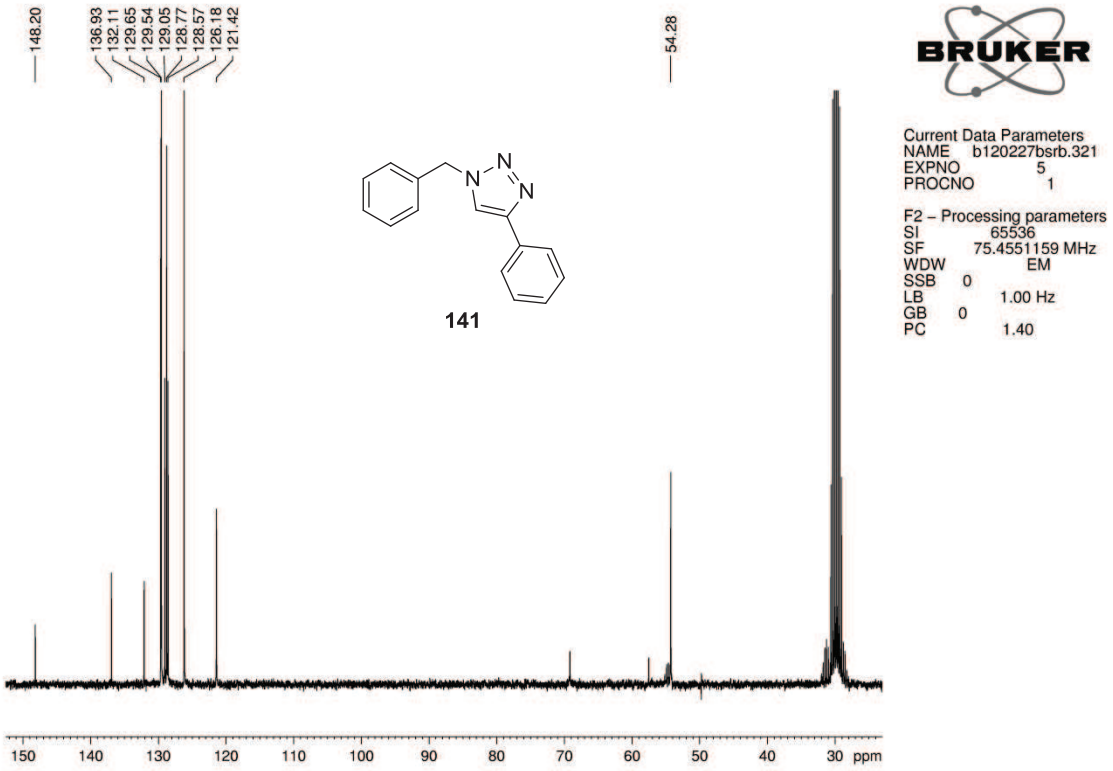

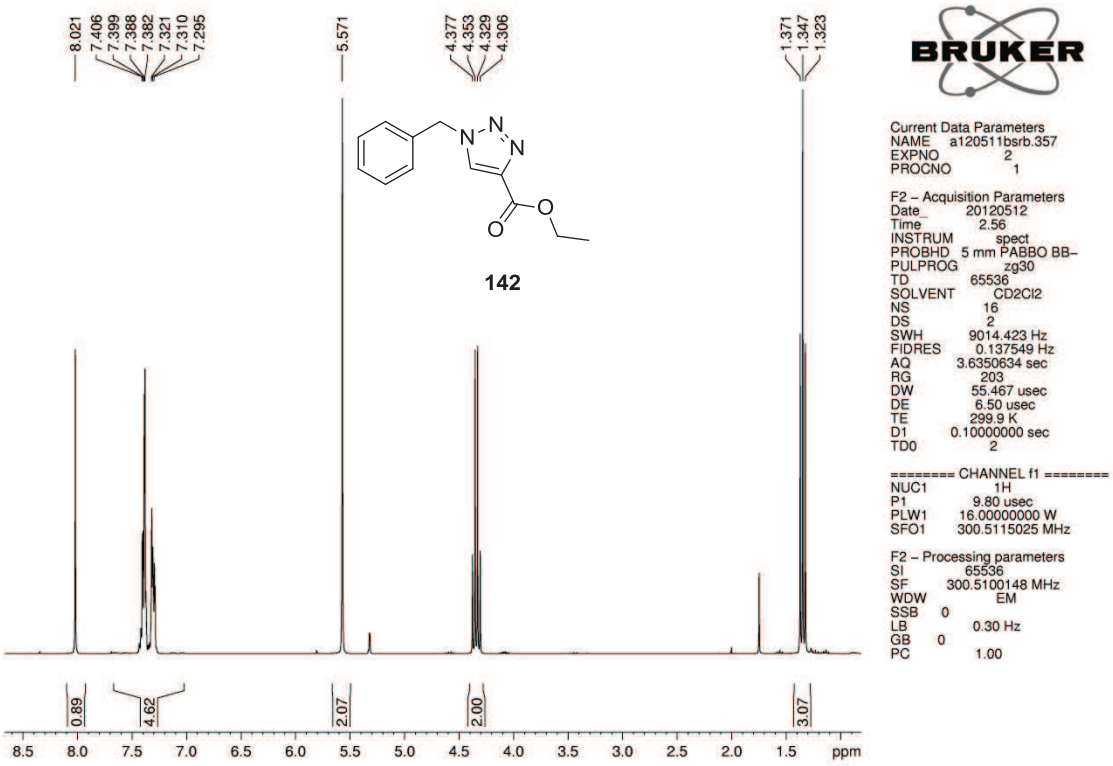
8.021
7.406
7.399
7.388
7.382
7.321
7.310
7.295
5.571
4.377
4.353
4.329
4.306
1.371
1.347
1.323
142
0.89
4.62
2.07
2.00
3.07
8.5 8.0 7.5 7.0 6.5 6.0 5.5 5.0 4.5 4.0 3.5 3.0 2.5 2.0 1.5 ppm
BRUKER
Current Data Parameters
NAME a120511bsrb.357
EXPNO 2
PROCNO 1
F2 – Acquisition Parameters
Date_ 20120512
Time 2.56
INSTRUM spect
PROBHD 5 mm PABBO BB–
PULPROG zg30
TD 65536
SOLVENT CD2Cl2
NS 16
DS 2
SWH 9014.423 Hz
FIDRES 0.137549 Hz
AQ 3.6350634 sec
RG 203
DW 55.467 usec
DE 6.50 usec
TE 299.9 K
D1 0.10000000 sec
TD0 2
======== CHANNEL f1 ========
NUC1 1H
P1 9.80 usec
PLW1 16.00000000 W
SFO1 300.5115025 MHz
F2 – Processing parameters
SI 65536
SF 300.5100148 MHz
WDW EM
SSB 0
LB 0.30 Hz
GB 0
PC 1.00

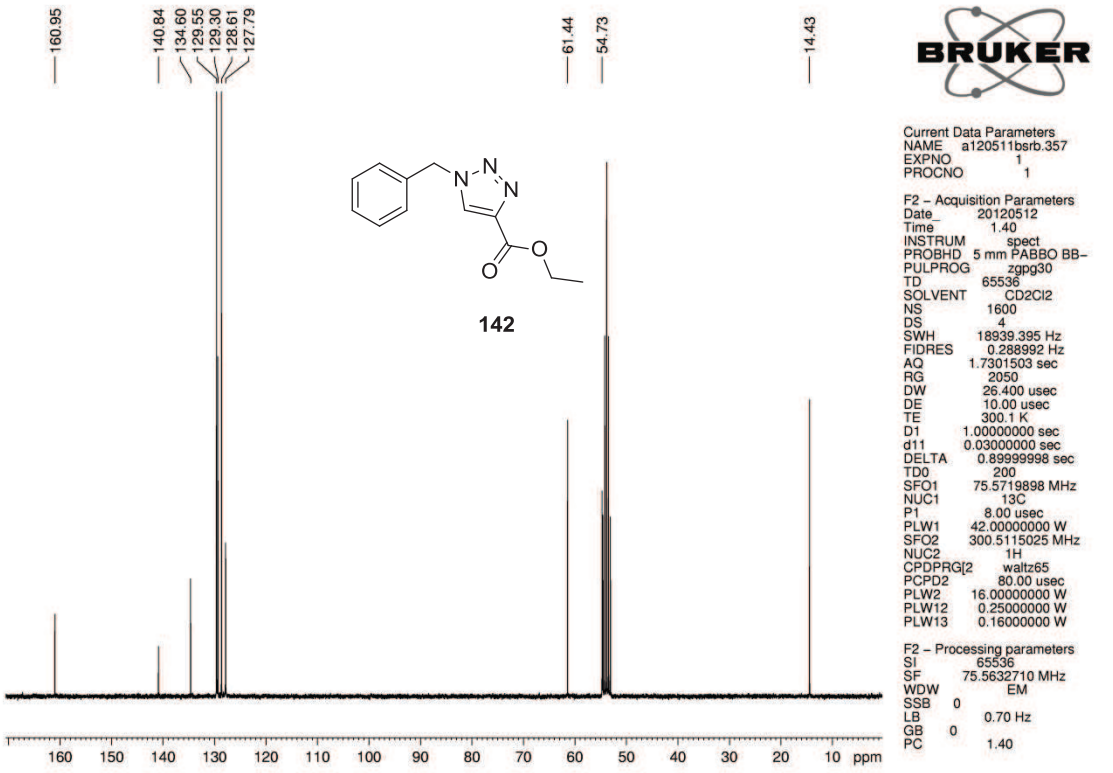
160.95
140.84
134.60
129.55
129.30
128.61
127.79
61.44
54.73
14.43
142
160 150 140 130 120 110 100 90 80 70 60 50 40 30 20 10 ppm
BRUKER
Current Data Parameters
NAME a120511bsrb.357
EXPNO 1
PROCNO 1
F2 – Acquisition Parameters
Date_ 20120512
Time 1.40
INSTRUM spect
PROBHD 5 mm PABBO BB–
PULPROG zgpg30
TD 65536
SOLVENT CD2Cl2
NS 1600
DS 4
SWH 18939.395 Hz
FIDRES 0.288992 Hz
AQ 1.7301503 sec
RG 2050
DW 26.400 usec
DE 10.00 usec
TE 300.1 K
D1 1.00000000 sec
d11 0.03000000 sec
DELTA 0.89999998 sec
TD0 200
SFO1 75.5719898 MHz
NUC1 13C
P1 8.00 usec
PLW1 42.00000000 W
SFO2 300.5115025 MHz
NUC2 1H
CPDPRG[2 waltz65
PCPD2 80.00 usec
PLW2 16.00000000 W
PLW12 0.25000000 W
PLW13 0.16000000 W
F2 – Processing parameters
SI 65536
SF 75.5632710 MHz
WDW EM
SSB 0
LB 0.70 Hz
GB 0
PC 1.40

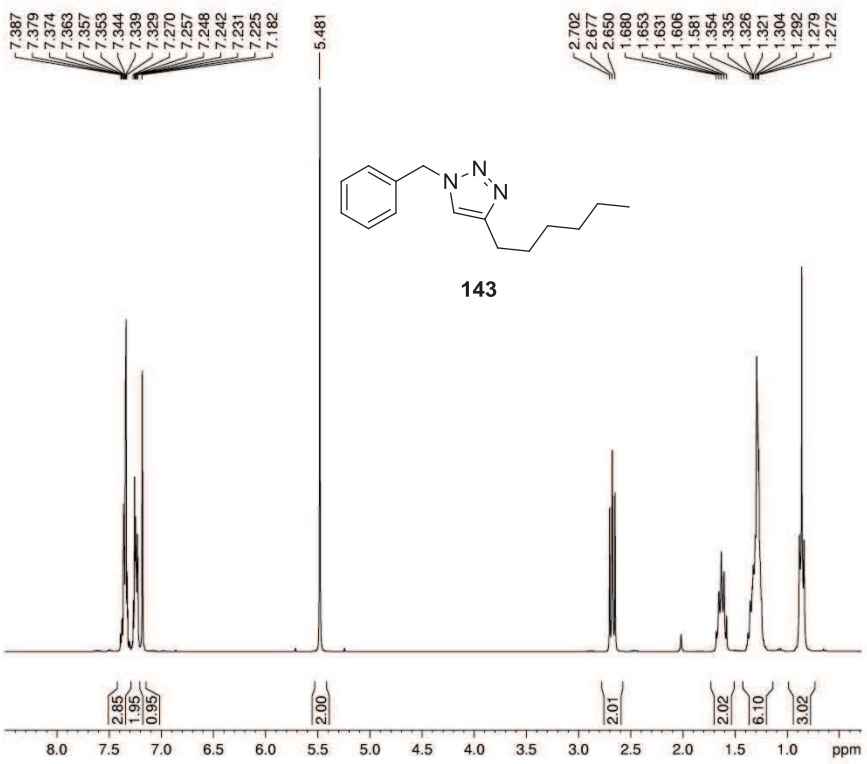

BRUKER

Current Data Parameters
NAME a120813bsrb366
EXPNO 1
PROCNO 1

F2 – Acquisition Parameters
Date_ 20120813
Time 10.22
INSTRUM spect
PROBHD 5 mm PABBO BB–
PULPROG zg30
TD 65536
SOLVENT CDCl3
NS 128
DS 2
SWH 9014.423 Hz
FIDRES 0.137549 Hz
AQ 3.6350634 sec
RG 128
DW 55.467 usec
DE 6.50 usec
TE 300.0 K
D1 0.10000000 sec
TD0 16

======== CHANNEL f1 ========
SFO1 300.5115025 MHz
NUC1 1H
P1 9.80 usec
PLW1 16.00000000 W

F2 – Processing parameters
SI 65536
SF 300.5100076 MHz
WDW EM
SSB 0
LB 0.30 Hz
GB 0
PC 1.00

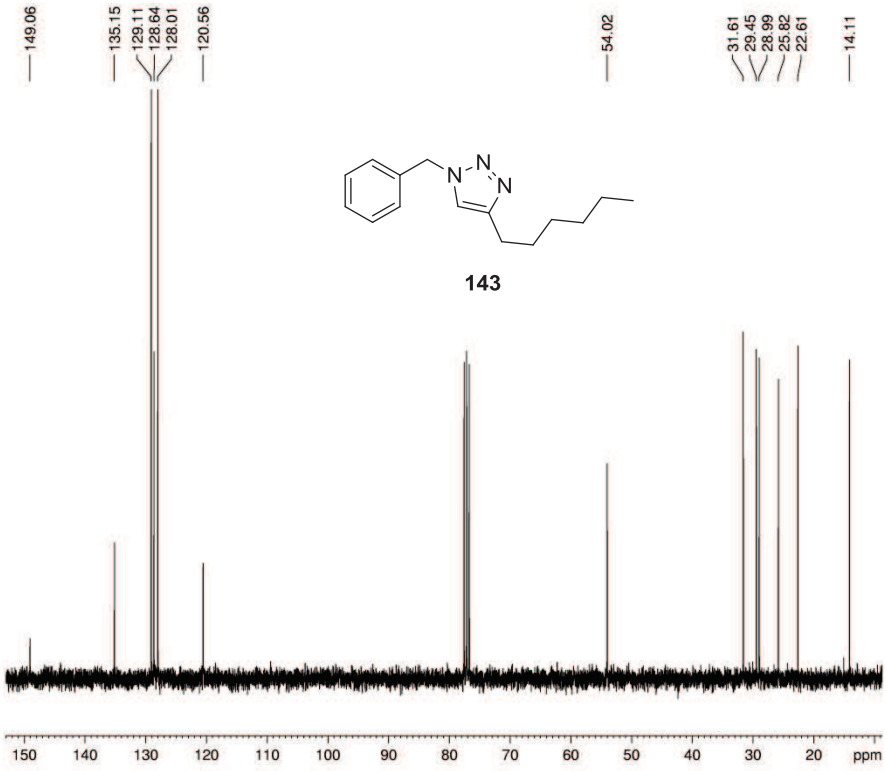

BRUKER

Current Data Parameters
NAME a120813bsrb366
EXPNO 2
PROCNO 1

F2 – Acquisition Parameters
Date_ 20120813
Time 10.31
INSTRUM spect
PROBHD 5 mm PABBO BB–
PULPROG zgpg30
TD 65536
SOLVENT CDCl3
NS 64
DS 4
SWH 18939.395 Hz
FIDRES 0.288992 Hz
AQ 1.7301503 sec
RG 2050
DW 26.400 usec
DE 10.00 usec
TE 300.1 K
D1 1.00000000 sec
D11 0.03000000 sec
TD0 8

======== CHANNEL f1 ========
SFO1 75.5719898 MHz
NUC1 13C
P1 8.00 usec
PLW1 42.00000000 W

======== CHANNEL f2 ========
SFO2 300.5115025 MHz
NUC2 1H
CPDPRG[2 waltz65
PCPD2 80.00 usec
PLW2 16.00000000 W
PLW12 0.25000000 W
PLW13 0.16000000 W

F2 – Processing parameters
SI 65536
SF 75.5632946 MHz
WDW EM
SSB 0
LB 0.70 Hz
GB 0
PC 1.40

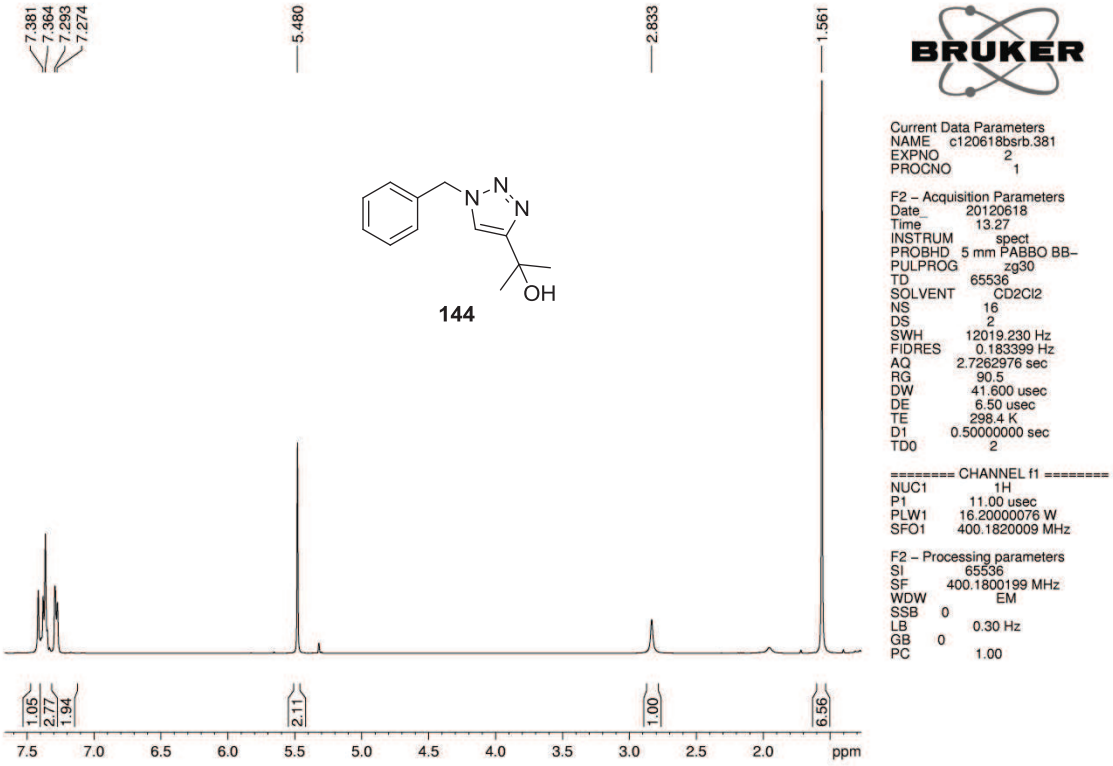
7.381
7.364
7.293
7.274
5.480
2.833
1.561
1.05
2.77
1.94
2.11
1.00
6.56
7.5
7.0
6.5
6.0
5.5
5.0
4.5
4.0
3.5
3.0
2.5
2.0
ppm
N
N
N
OH
144
BRUKER
Current Data Parameters
NAME c120618bsrb.381
EXPNO 2
PROCNO 1
F2 – Acquisition Parameters
Date_ 20120618
Time 13.27
INSTRUM spect
PROBHD 5 mm PABBO BB–
PULPROG zg30
TD 65536
SOLVENT CD2Cl2
NS 16
DS 2
SWH 12019.230 Hz
FIDRES 0.183399 Hz
AQ 2.7262976 sec
RG 90.5
DW 41.600 usec
DE 6.50 usec
TE 298.4 K
D1 0.50000000 sec
TD0 2
======== CHANNEL f1 ========
NUC1 1H
P1 11.00 usec
PLW1 16.20000076 W
SFO1 400.1820009 MHz
F2 – Processing parameters
SI 65536
SF 400.1800199 MHz
WDW EM
SSB 0
LB 0.30 Hz
GB 0
PC 1.00

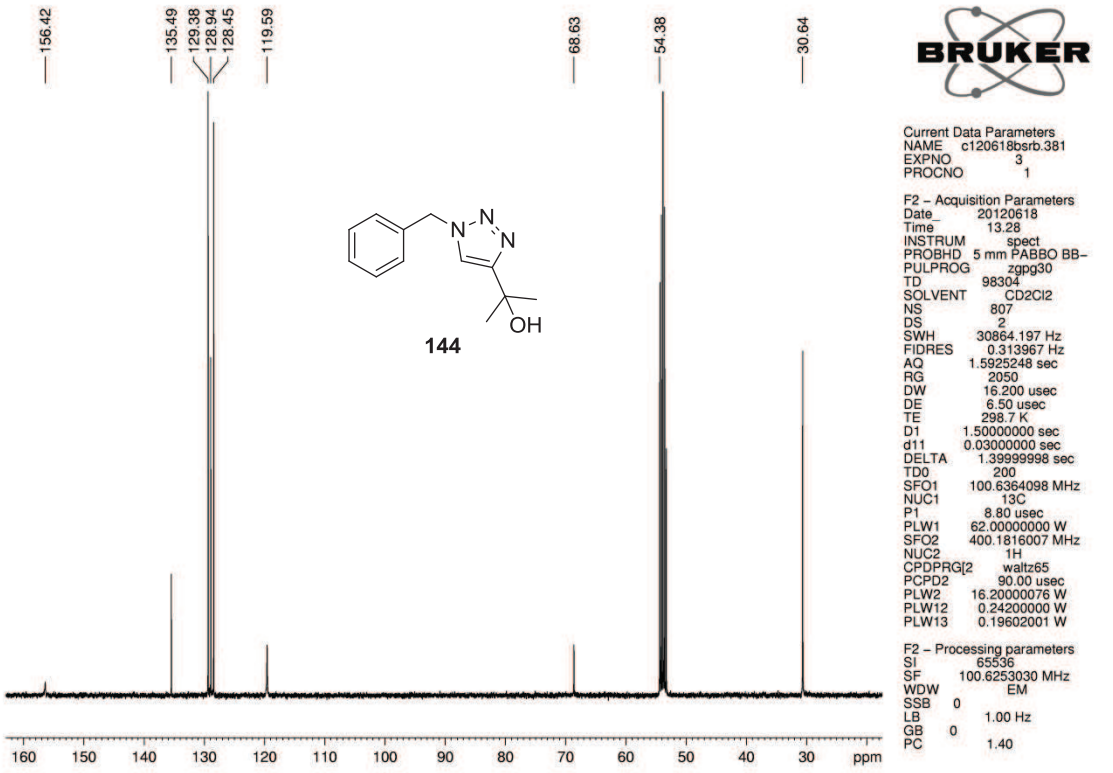
156.42
135.49
129.38
128.94
128.45
119.59
68.63
54.38
30.64
160
150
140
130
120
110
100
90
80
70
60
50
40
30
ppm
N
N
N
OH
144
BRUKER
Current Data Parameters
NAME c120618bsrb.381
EXPNO 3
PROCNO 1
F2 – Acquisition Parameters
Date_ 20120618
Time 13.28
INSTRUM spect
PROBHD 5 mm PABBO BB–
PULPROG zgpg30
TD 98304
SOLVENT CD2Cl2
NS 807
DS 2
SWH 30864.197 Hz
FIDRES 0.313967 Hz
AQ 1.5925248 sec
RG 2050
DW 16.200 usec
DE 6.50 usec
TE 298.7 K
D1 1.50000000 sec
d11 0.03000000 sec
DELTA 1.39999998 sec
TD0 200
SFO1 100.6364098 MHz
NUC1 13C
P1 8.80 usec
PLW1 62.00000000 W
SFO2 400.1816007 MHz
NUC2 1H
CPDPRG[2 waltz65
PCPD2 90.00 usec
PLW2 16.20000076 W
PLW12 0.24200000 W
PLW13 0.19602001 W
F2 – Processing parameters
SI 65536
SF 100.6253030 MHz
WDW EM
SSB 0
LB 1.00 Hz
GB 0
PC 1.40

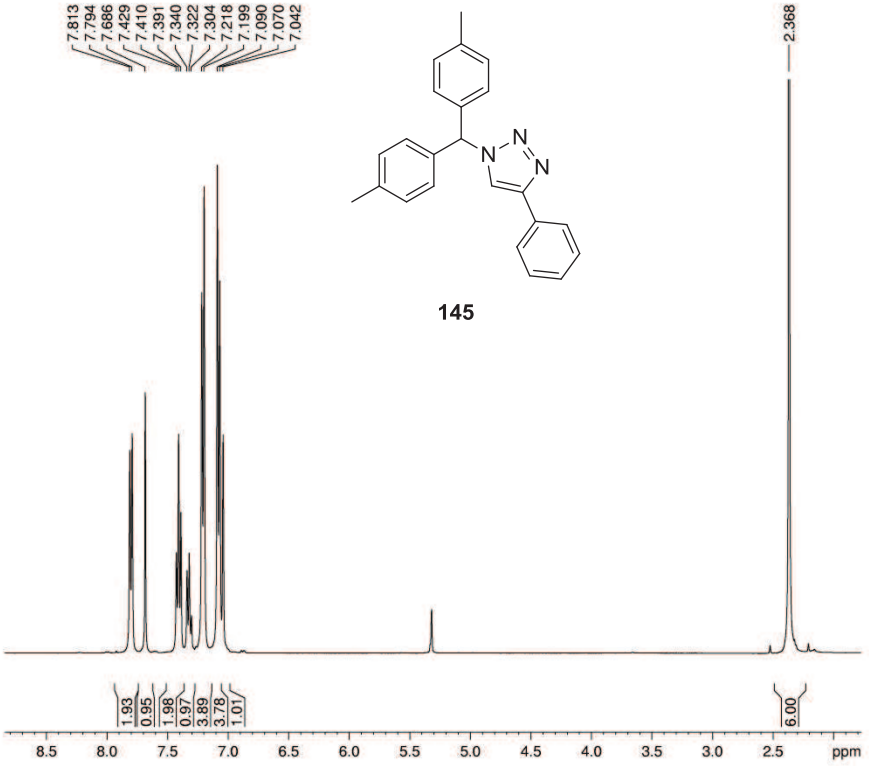

145

BRUKER

Current Data Parameters
NAME c120705bsrb.413C
EXPNO 2
PROCNO 1

F2 – Acquisition Parameters
Date_ 20120705
Time 10.19
INSTRUM spect
PROBHD 5 mm PABBO BB–
PULPROG zg30
TD 65536
SOLVENT CD2Cl2
NS 16
DS 2
SWH 12019.230 Hz
FIDRES 0.183399 Hz
AQ 2.7262976 sec
RG 90.5
DW 41.600 usec
DE 6.50 usec
TE 298.7 K
D1 0.50000000 sec
TD0 2

======== CHANNEL f1 ========
NUC1 1H
P1 11.00 usec
PLW1 16.20000076 W
SFO1 400.1820009 MHz

F2 – Processing parameters
SI 65536
SF 400.1800199 MHz
WDW EM
SSB 0
LB 0.30 Hz
GB 0
PC 1.00

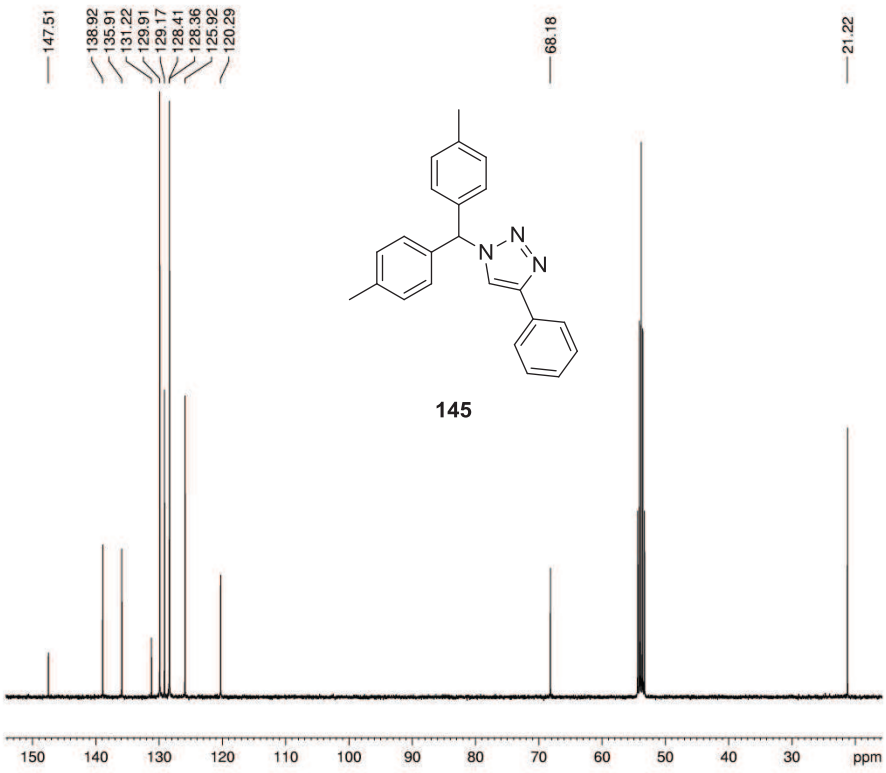

145

BRUKER

Current Data Parameters
NAME c120705bsrb.413C
EXPNO 1
PROCNO 1

F2 – Acquisition Parameters
Date_ 20120705
Time 9.31
INSTRUM spect
PROBHD 5 mm PABBO BB–
PULPROG zgpg30
TD 98304
SOLVENT CD2Cl2
NS 887
DS 2
SWH 30864.197 Hz
FIDRES 0.313967 Hz
AQ 1.5925248 sec
RG 2050
DW 16.200 usec
DE 6.50 usec
TE 298.7 K
D1 1.50000000 sec
d11 0.03000000 sec
DELTA 1.39999998 sec
TD0 200
SFO1 100.6364098 MHz
NUC1 13C
P1 8.80 usec
PLW1 62.00000000 W
SFO2 400.1816007 MHz
NUC2 1H
CPDPRG[2 waltz65
PCPD2 90.00 usec
PLW2 16.20000076 W
PLW12 0.24200000 W
PLW13 0.19602001 W

F2 – Processing parameters
SI 65536
SF 100.6253026 MHz
WDW EM
SSB 0
LB 1.00 Hz
GB 0
PC 1.40

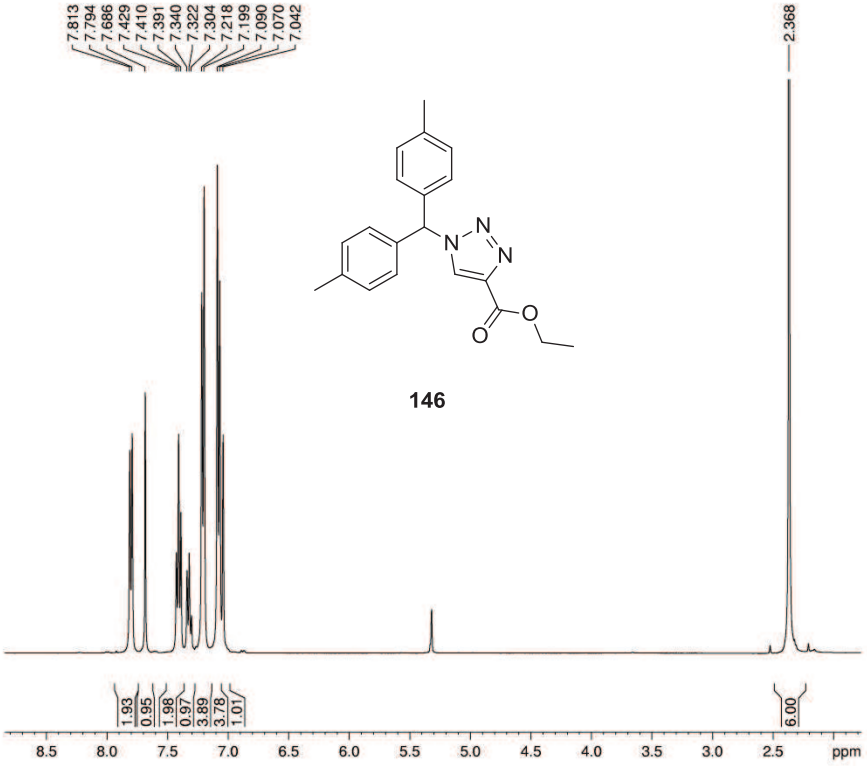

146

Current Data Parameters
NAME c120705bsrb.413C
EXPNO 2
PROCNO 1

F2 – Acquisition Parameters
Date_ 20120705
Time 10.19
INSTRUM spect
PROBHD 5 mm PABBO BB–
PULPROG zg30
TD 65536
SOLVENT CD2Cl2
NS 16
DS 2
SWH 12019.230 Hz
FIDRES 0.183399 Hz
AQ 2.7262976 sec
RG 90.5
DW 41.600 usec
DE 6.50 usec
TE 298.7 K
D1 0.50000000 sec
TD0 2

======== CHANNEL f1 ========
NUC1 1H
P1 11.00 usec
PLW1 16.20000076 W
SFO1 400.1820009 MHz

F2 – Processing parameters
SI 65536
SF 400.1800199 MHz
WDW EM
SSB 0
LB 0.30 Hz
GB 0
PC 1.00

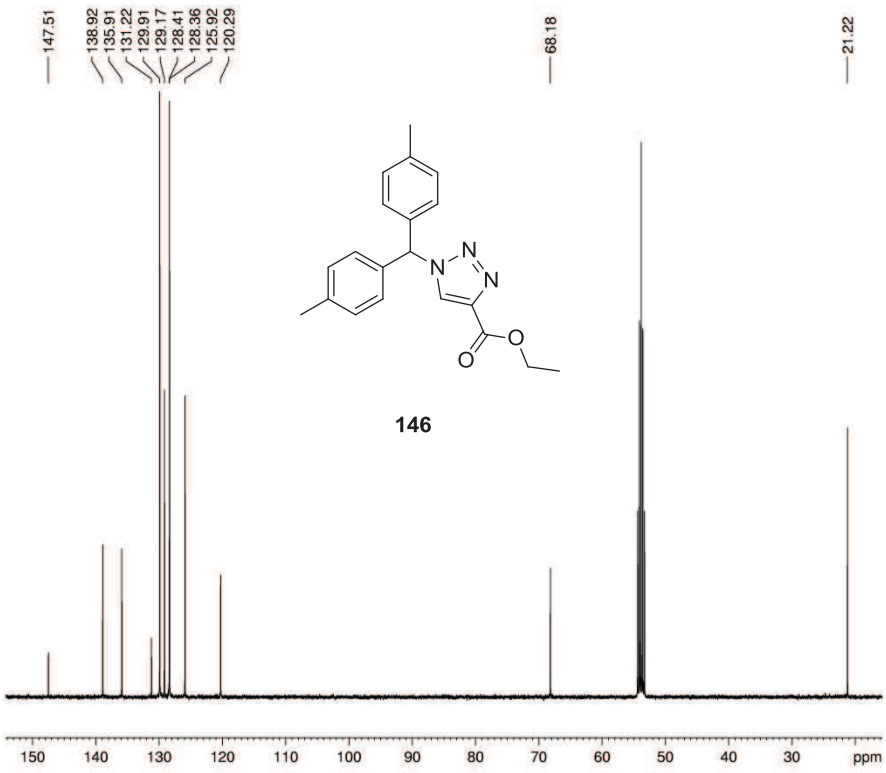

146

Current Data Parameters
NAME c120705bsrb.413C
EXPNO 1
PROCNO 1

F2 – Acquisition Parameters
Date_ 20120705
Time 9.31
INSTRUM spect
PROBHD 5 mm PABBO BB–
PULPROG zgpg30
TD 98304
SOLVENT CD2Cl2
NS 887
DS 2
SWH 30864.197 Hz
FIDRES 0.313967 Hz
AQ 1.5925248 sec
RG 2050
DW 16.200 usec
DE 6.50 usec
TE 298.7 K
D1 1.50000000 sec
d11 0.03000000 sec
DELTA 1.39999998 sec
TD0 200
SFO1 100.6364098 MHz
NUC1 13C
P1 8.80 usec
PLW1 62.00000000 W
SFO2 400.1816007 MHz
NUC2 1H
CPDPRG[2 waltz65
PCPD2 90.00 usec
PLW2 16.20000076 W
PLW12 0.24200000 W
PLW13 0.19602001 W

F2 – Processing parameters
SI 65536
SF 100.6253026 MHz
WDW EM
SSB 0
LB 1.00 Hz
GB 0
PC 1.40

2 X-Ray Diffraction Data

2.1 1,3-Bis(2,6-diisopropylphenyl)imidazolium Acetate • 2 HOAc (2 • HOAc)

Name: Regina Berg (AK Straub)
Sample: rb036
File Name: reb1.*
Operator: F. Rominger (AK Hofmann)
Instrument: Bruker APEX

Table 2.1.1: Crystal data and structure refinement for reb1.

Identification code	reb1
Empirical formula	$C_{33}H_{48}N_2O_6$
Formula weight	568.73
Temperature	200(2) K
Wavelength	0.71073 Å
Crystal system	monoclinic
Space group	$P2_1/n$
Z	4
Unit cell dimensions	*a* = 12.7921(14) Å α = 90 deg.
	b = 22.331(3) Å β = 111.033(2) deg.
	c = 12.9295(14) Å γ = 90 deg.
Volume	3447.3(7) Å^3
Density (calculated)	1.10 g/cm^3
Absorption coefficient	0.08 mm^{-1}
Crystal shape	polyhedron
Crystal size	0.39 x 0.19 x 0.18 mm^3
Crystal colour	colourless
Theta range for data collection	1.9 to 25.4 deg.
Index ranges	$-15 \le h \le 15$, $-26 \le k \le 26$, $-15 \le l \le 15$
Reflections collected	29090
Independent reflections	6314 (R(int) = 0.0453)
Observed reflections	4643 ($I > 2\sigma(I)$)
Absorption correction	Semi-empirical from equivalents
Max. and min. transmission	0.99 and 0.97
Refinement method	Full-matrix least-squares on F^2
Data/restraints/parameters	6314 / 16 / 403
Goodness-of-fit on F^2	1.03
Final R indices ($I > 2\sigma(I)$)	*R1* = 0.056, *wR2* = 0.148
Largest diff. peak and hole	0.35 and -0.22 eÅ^{-3}

Table 2.1.2: Atomic coordinates and equivalent isotropic displacement parameters ($Å^2$) for reb1. (U_{eq} is defined as one third of the trace of the orthogonalized U_{ij} tensor.)

Atom	x	y	z	U_{eq}
C1	0.7980(1)	0.1286(1)	0.6959(1)	0.0373(4)
N2	0.8100(1)	0.0891(1)	0.6242(1)	0.0397(4)
C3	0.7817(2)	0.0332(1)	0.6505(2)	0.0479(5)
C4	0.7534(2)	0.0395(1)	0.7399(2)	0.0470(5)
N5	0.7636(1)	0.0995(1)	0.7674(1)	0.0381(3)
C11	0.8463(2)	0.1044(1)	0.5335(1)	0.0430(4)
C12	0.7639(2)	0.1164(1)	0.4310(2)	0.0535(5)
C13	0.8021(2)	0.1312(1)	0.3460(2)	0.0739(7)
C14	0.9137(3)	0.1337(1)	0.3638(2)	0.0829(8)
C15	0.9923(2)	0.1217(1)	0.4655(2)	0.0721(7)
C16	0.9603(2)	0.1067(1)	0.5537(2)	0.0533(5)
C17	0.6404(2)	0.1149(1)	0.4116(2)	0.0655(6)
C19	1.0491(2)	0.0934(1)	0.6657(2)	0.0685(7)
C21	0.7419(2)	0.1281(1)	0.8584(1)	0.0380(4)
C22	0.8316(2)	0.1359(1)	0.9574(2)	0.0436(4)
C23	0.8089(2)	0.1664(1)	1.0408(2)	0.0533(5)
C24	0.7031(2)	0.1866(1)	1.0258(2)	0.0555(5)
C25	0.6160(2)	0.1768(1)	0.9277(2)	0.0521(5)
C26	0.6331(2)	0.1474(1)	0.8405(2)	0.0442(4)
C27	0.9488(2)	0.1141(1)	0.9744(2)	0.0552(5)
C29	0.5362(2)	0.1373(1)	0.7318(2)	0.0556(5)
C171	0.5788(3)	0.0704(2)	0.3242(4)	0.1439(18)
C172	0.5875(3)	0.1758(2)	0.3857(4)	0.1311(15)
C191	1.1204(3)	0.0403(2)	0.6572(3)	0.1279(14)
C192	1.1230(3)	0.1470(2)	0.7118(3)	0.1165(12)
C271	1.0011(2)	0.0793(1)	1.0816(2)	0.0867(8)
C272	1.0230(2)	0.1663(1)	0.9676(3)	0.0850(8)
C291	0.4472(3)	0.0989(2)	0.7479(3)	0.1256(14)
C292	0.4884(4)	0.1949(2)	0.6774(3)	0.157(2)
O1	0.7487(2)	0.4006(1)	0.9503(2)	0.0726(5)
O2	0.7940(1)	0.4007(1)	0.8028(2)	0.0659(4)
H2	0.800(2)	0.3750(14)	0.738(3)	0.111(10)
C31	0.7565(2)	0.3738(1)	0.8720(2)	0.0543(5)
C32	0.7217(3)	0.3106(1)	0.8479(3)	0.0992(10)
O3	0.8360(2)	0.2565(1)	0.6861(2)	0.1004(7)
O4	0.8191(1)	0.3506(1)	0.6369(1)	0.0619(4)
C33	0.8392(2)	0.2966(1)	0.6228(2)	0.0602(6)
C34	0.8708(3)	0.2824(1)	0.5248(3)	0.0988(10)
O5	0.7398(3)	0.4834(1)	0.5339(3)	0.1052(15)
O6	0.8705(3)	0.4276(1)	0.5131(3)	0.0789(11)
H6	0.839(3)	0.4002(19)	0.558(3)	0.147(13)
C35	0.8144(4)	0.4770(3)	0.4976(4)	0.0453(12)
C36	0.8431(2)	0.5230(1)	0.4324(2)	0.0670(6)
O5B	0.8656(8)	0.4917(5)	0.6095(8)	0.083(2)
O6B	0.7988(11)	0.4263(5)	0.4730(9)	0.083(2)
C35B	0.8515(19)	0.4712(10)	0.5193(18)	0.083(2)
O5C	0.7059(13)	0.4485(7)	0.4398(12)	0.083(2)
O6C	0.8577(13)	0.4536(9)	0.5789(16)	0.083(2)
C35C	0.793(3)	0.475(3)	0.487(5)	0.083(2)

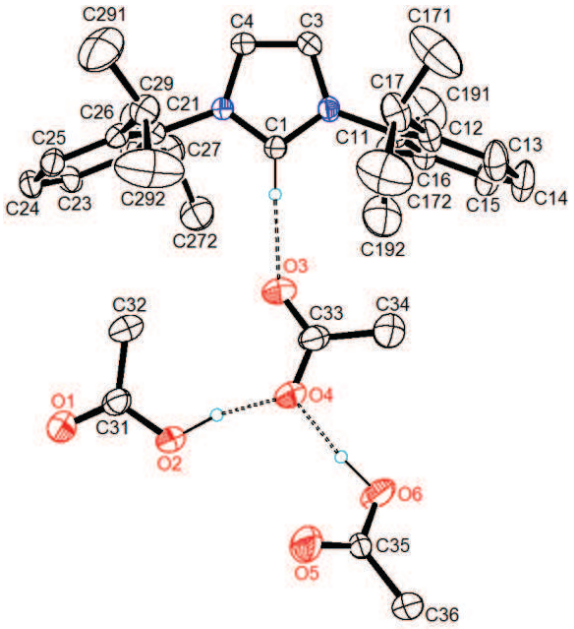

Figure 2.1.1: ORTEP plot of 1,3-bis(2,6-diisopropylphenyl)imidazolium acetate with two molecules of acetic acid (**2** • HOAc) (some hydrogen atoms are omitted for clarity).[1]

2.2 4-(3,5-Dimethylphenyl)-4*H*-1,2,4-triazole (22)

Name:	Lena Hahn / Regina Berg (AK Straub)
Sample:	LH007
File Name:	reb2.*
CCDC:	869464
Operator:	F. Rominger (AK Hofmann)
Instrument:	Bruker APEX

Table 2.2.1: Crystallographic data and structure refinement for reb2.

Identification code	reb2	
Empirical formula	$C_{10}H_{11}N_3$	
Formula weight	173.22	
Temperature	200(2) K	
Wavelength	0.71073 Å	
Crystal system	tetragonal	
Space group	$P4_2/n$	
Z	8	
Unit cell dimensions	*a* = 14.110(2) Å	α = 90 deg.
	b = 14.110(2) Å	β = 90 deg.
	c =9.3589(16) Å	γ = 90 deg.
Volume	1863.4(5) Å^3	
Density (calculated)	1.24 g/cm^3	
Absorption coefficient	0.08 mm^{-1}	
Crystal shape	polyhedron	
Crystal size	0.33 x 0.21 x 0.17 mm^3	
Crystal colour	colourless	
Theta range for data collection	2.0 to 25.1 deg.	

Index ranges	$-16 \le h \le 16$, $-16 \le k \le 16$, $-11 \le l \le 11$
Reflections collected	11555
Independent reflections	1657 (R(int) = 0.0409)
Observed reflections	1255 ($I > 2\sigma(I)$)
Absorption correction	Semi-empirical from equivalents
Max. and min. transmission	0.99 and 0.97
Refinement method	Full-matrix least-squares on F^2
Data/restraints/parameters	1657 / 0 / 120
Goodness-of-fit on F^2	1.11
Final R indices ($I > 2\sigma(I)$)	$R1$ = 0.047, $wR2$ = 0.112
Largest diff. peak and hole	0.20 and -0.18 eÅ^{-3}

Table 2.2.2: Atomic coordinates and equivalent isotropic displacement parameters (Å^2) for reb2. (U_{eq} is defined as one third of the trace of the orthogonalized U_{ij} tensor.)

Atom	x	y	z	U_{eq}
N1	0.8446(1)	0.3808(1)	0.1157(2)	0.0238(4)
C2	0.7829(2)	0.3733(2)	0.2265(2)	0.0315(5)
N3	0.6956(1)	0.3686(1)	0.1835(2)	0.0339(5)
N4	0.6985(1)	0.3731(1)	0.0352(2)	0.0320(5)
C5	0.7873(2)	0.3801(2)	-0.0012(2)	0.0293(5)
C11	0.9458(1)	0.3882(1)	0.1220(2)	0.0244(5)
C12	0.9883(2)	0.4069(1)	0.2524(2)	0.0285(5)
C13	1.0862(2)	0.4150(2)	0.2607(2)	0.0333(5)
C14	1.1393(2)	0.4038(2)	0.1372(3)	0.0364(6)
C15	1.0970(2)	0.3855(1)	0.0063(2)	0.0323(5)
C16	0.9987(2)	0.3776(1)	-0.0007(2)	0.0282(5)
C17	1.1323(2)	0.4369(2)	0.4023(3)	0.0489(7)
C18	1.1559(2)	0.3725(2)	-0.1271(3)	0.0485(7)

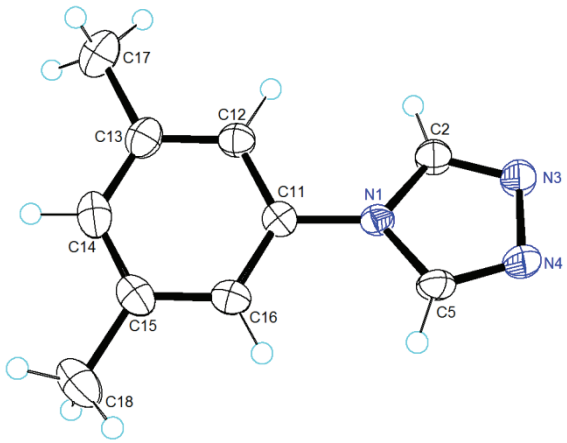

Figure 2.2.1: ORTEP plot of 4-(3,5-dimethylphenyl)-4*H*-1,2,4-triazole (**22**).[1a, 2]

2.3 1,1'-(Ethane-1,2-diyl)bis[4-(2,4,6-trimethylphenyl)-1*H*-1,2,4-triazolium] Dibromide (41)

Name: Regina Berg (AK Straub)
Sample: rb158
File Name: reb21.*
Operator: F. Rominger (AK Hofmann)
Instrument: Bruker APEX

Table 2.3.1: Crystal data and structure refinement for reb21.

Empirical formula	$C_{24}H_{34}Br_2N_6O_2$
Formula weight	598.38
Temperature	200(2) K
Wavelength	0.71073 Å
Crystal system	monoclinic
Space group	$P2_1/c$
Z	4
Unit cell dimensions	*a* = 12.0668(12) Å α = 90 deg.
	b = 15.4462(14) Å β = 95.580(3) deg.
	c = 14.4654(14) Å γ = 90 deg.
Volume	2683.4(4) Å^3
Density (calculated)	1.43 g/cm^3
Absorption coefficient	3.05 mm^{-1}
Crystal shape	polyhedron
Crystal size	0.18 x 0.17 x 0.15 mm^3
Crystal colour	colourless
Theta range for data collection	1.9 to 25.0 deg.
Index ranges	$-14 \le h \le 11$, $-18 \le k \le 17$, $-16 \le l \le 17$
Reflections collected	17545
Independent reflections	4743 (R(int) = 0.0631)
Observed reflections	3290 ($I > 2\sigma(I)$)
Absorption correction	Semi-empirical from equivalents
Max. and min. transmission	0.66 and 0.61
Refinement method	Full-matrix least-squares on F^2
Data/restraints/parameters	4743 / 0 / 314
Goodness-of-fit on F^2	1.04
Final R indices ($I > 2\sigma(I)$)	*R1* = 0.056, *wR2* = 0.141
Largest diff. peak and hole	0.89 and -0.88 eÅ^{-3}

Table 2.3.2: Atomic coordinates and equivalent isotropic displacement parameters (Å^2) for reb21. (U_{eq} is defined as one third of the trace of the orthogonalized U_{ij} tensor.)

Atom	x	y	z	U_{eq}
Br1	0.3461(1)	0.0742(1)	0.2795(1)	0.0487(2)
Br2	-0.1557(1)	-0.0058(1)	0.2853(1)	0.0450(2)
C1	0.0062(5)	0.1705(3)	0.3149(4)	0.0343(12)
N2	0.0197(4)	0.2410(3)	0.2631(3)	0.0332(10)
C3	0.1030(5)	0.2884(3)	0.3083(4)	0.0392(13)
N4	0.1400(4)	0.2521(3)	0.3867(3)	0.0386(11)
N5	0.0782(4)	0.1776(3)	0.3892(3)	0.0327(10)

C6	0.3717(4)	0.1888(3)	0.4892(3)	0.0329(12)
N7	0.4056(4)	0.2595(3)	0.5378(3)	0.0319(10)
C8	0.3309(5)	0.2697(3)	0.6028(4)	0.0368(13)
N9	0.2548(4)	0.2091(3)	0.5970(3)	0.0383(11)
N10	0.2824(4)	0.1592(3)	0.5242(3)	0.0329(10)
C11	0.0922(5)	0.1173(3)	0.4675(4)	0.0373(13)
C12	0.2096(5)	0.0868(3)	0.4900(4)	0.0345(12)
C21	-0.0478(4)	0.2610(3)	0.1759(4)	0.0343(12)
C22	-0.0391(5)	0.2064(4)	0.1008(4)	0.0378(13)
C23	-0.1078(5)	0.2249(4)	0.0201(4)	0.0438(14)
C24	-0.1830(5)	0.2929(4)	0.0151(4)	0.0456(15)
C25	-0.1873(5)	0.3460(4)	0.0929(4)	0.0448(14)
C26	-0.1197(5)	0.3302(3)	0.1756(4)	0.0377(13)
C27	0.0371(6)	0.1299(4)	0.1034(4)	0.0528(16)
C28	-0.2618(6)	0.3082(5)	-0.0714(4)	0.066(2)
C29	-0.1297(6)	0.3877(4)	0.2589(4)	0.0519(16)
C31	0.4970(4)	0.3167(3)	0.5229(3)	0.0321(12)
C32	0.4942(5)	0.3625(3)	0.4403(4)	0.0381(13)
C33	0.5806(5)	0.4193(3)	0.4302(4)	0.0415(14)
C34	0.6650(5)	0.4321(4)	0.5004(4)	0.0415(14)
C35	0.6639(5)	0.3854(4)	0.5823(4)	0.0391(13)
C36	0.5813(5)	0.3263(3)	0.5958(3)	0.0352(12)
C37	0.4011(5)	0.3519(4)	0.3621(4)	0.0490(15)
C38	0.7574(6)	0.4956(4)	0.4875(5)	0.0582(18)
C39	0.5835(5)	0.2751(4)	0.6842(4)	0.0475(15)
O2	0.4580(14)	-0.0561(9)	0.4698(11)	0.104(7)
O1	0.5762(7)	-0.0261(6)	0.3586(5)	0.076(3)

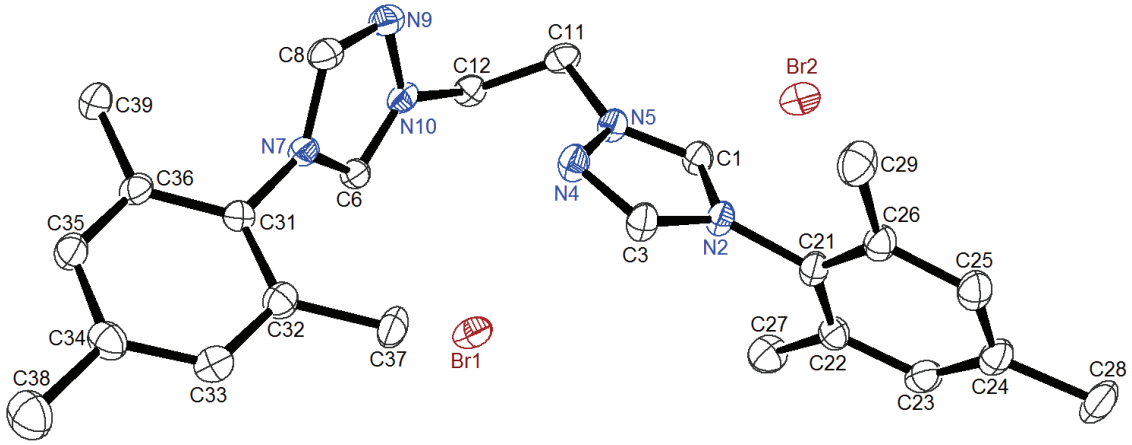

Figure 2.3.1: ORTEP plot of 1,1'-(ethane-1,2-diyl)bis[4-(2,4,6-trimethylphenyl)-1*H*-1,2,4-triazolium] dibromide (**41**) (hydrogen atoms and co-crystallized water molecules are omitted for clarity).[1a, 2]

2.4 4-(2,6-Diisopropylphenyl)-1-{3-[(4-(3,5-dimethylphenyl)-1*H*-1,2,4-triazolium-1-yl)methyl]benzyl}-1*H*-1,2,4-triazolium Dichloride (36)

Name: Regina Berg (AK Straub)
Sample: CD014
File Name: reb5.*
Operator: F. Rominger (AK Hofmann)
Instrument: Bruker APEX

Table 2.4.1: Crystal data and structure refinement for reb5.

Identification code	reb5	
Empirical formula	$C_{34}H_{43}Cl_2N_7O$	
Formula weight	636.65	
Temperature	200(2) K	
Wavelength	0.71073 Å	
Crystal system	triclinic	
Space group	$P\bar{1}$	
Z	2	
Unit cell dimensions	*a* =8.717(4) Å	α = 86.845(12) deg.
	b = 10.138(5) Å	β = 78.926(11) deg.
	c = 20.249(10) Å	γ = 89.511(12) deg.
Volume	1753.5(15) Å^3	
Density (calculated)	1.21 g/cm^3	
Absorption coefficient	0.22 mm^{-1}	
Crystal shape	plate	
Crystal size	0.33 x 0.20 x 0.04 mm^3	
Crystal colour	colourless	
Theta range for data collection	2.0 to 23.3 deg.	
Index ranges	$-9 \le h \le 9$, $-11 \le k \le 11$, $-22 \le l \le 22$	
Reflections collected	12245	
Independent reflections	5041 (R(int) = 0.0907)	
Observed reflections	3272 ($I > 2\sigma(I)$)	
Absorption correction	Semi-empirical from equivalents	
Max. and min. transmission	0.99 and 0.93	
Refinement method	Full-matrix least-squares on F^2	
Data/restraints/parameters	5041 / 0 / 400	
Goodness-of-fit on F^2	1.11	
Final R indices ($I > 2\sigma(I)$)	*R1* = 0.146, *wR2* = 0.327	
Largest diff. peak and hole	0.72 and -0.64 eÅ^{-3}	

Table 2.4.2: Atomic coordinates and equivalent isotropic displacement parameters ($Å^2$) for reb5. (U_{eq} is defined as one third of the trace of the orthogonalized U_{ij} tensor.)

Atom	x	y	z	U_{eq}
Cl1	0.6844(3)	0.9708(3)	0.2129(1)	0.0373(8)
Cl2	0.2564(3)	1.3903(3)	0.5334(2)	0.0466(9)
C1	1.0522(12)	0.9035(9)	0.2168(5)	0.025(2)
N2	1.0863(9)	0.8783(8)	0.2766(4)	0.0232(19)
N3	1.2435(11)	0.8753(9)	0.2744(5)	0.035(2)
C4	1.3011(13)	0.9001(11)	0.2096(6)	0.038(3)
N5	1.1865(10)	0.9174(8)	0.1738(4)	0.027(2)
C6	0.5842(12)	1.3464(10)	0.5600(6)	0.031(3)
N7	0.5947(9)	1.2299(9)	0.5318(4)	0.031(2)
N8	0.5490(11)	1.1263(9)	0.5785(4)	0.033(2)
C9	0.5098(12)	1.1826(10)	0.6353(5)	0.029(3)
N10	0.5317(10)	1.3172(9)	0.6266(5)	0.033(2)
C11	0.8184(12)	1.0363(10)	0.4013(5)	0.030(3)
C12	0.9642(12)	0.9810(10)	0.3833(5)	0.029(3)
C13	1.0927(13)	1.0281(10)	0.4041(5)	0.032(3)
C14	1.0733(13)	1.1411(11)	0.4438(5)	0.034(3)
C15	0.9288(13)	1.1935(11)	0.4627(5)	0.032(3)
C16	0.7982(12)	1.1422(9)	0.4416(5)	0.023(2)
C17	0.9816(13)	0.8579(11)	0.3423(5)	0.033(3)
C19	0.6404(14)	1.2063(11)	0.4602(5)	0.038(3)
C21	1.2027(13)	0.9606(11)	0.1026(5)	0.033(3)
C22	1.1945(15)	1.0963(10)	0.0876(6)	0.038(3)
C23	1.2083(17)	1.1343(12)	0.0203(6)	0.054(4)
C24	1.2370(18)	1.0445(14)	-0.0315(6)	0.061(4)
C25	1.2460(16)	0.9117(12)	-0.0119(6)	0.047(3)
C26	1.2315(14)	0.8655(11)	0.0527(6)	0.039(3)
C27	1.1618(18)	1.1974(12)	0.1398(7)	0.058(4)
C29	1.2420(14)	0.7206(11)	0.0722(6)	0.041(3)
C31	0.4937(12)	1.4140(11)	0.6774(5)	0.032(3)
C32	0.5537(13)	1.5421(11)	0.6624(6)	0.041(3)
C33	0.5097(14)	1.6357(12)	0.7098(7)	0.046(3)
C34	0.4117(14)	1.5997(12)	0.7712(6)	0.045(3)
C35	0.3592(14)	1.4703(12)	0.7858(5)	0.039(3)
C36	0.3987(13)	1.3757(11)	0.7386(6)	0.038(3)
C37	0.5720(17)	1.7712(13)	0.6973(7)	0.062(4)
C38	0.2565(17)	1.4291(14)	0.8533(6)	0.056(4)
C271	1.2976(18)	1.2965(16)	0.1304(8)	0.075(5)
C272	1.0061(18)	1.2642(15)	0.1417(8)	0.071(4)
C291	1.414(2)	0.6771(16)	0.0667(10)	0.088(6)
C292	1.1576(19)	0.6370(14)	0.0318(9)	0.075(5)
N40	1.078(2)	0.5941(12)	0.2365(7)	0.091(5)
C40	1.018(2)	0.5156(16)	0.2749(8)	0.077(5)
C41	0.938(2)	0.4143(16)	0.3219(8)	0.089(6)
O40	0.8998(14)	1.4454(12)	0.5742(6)	0.091(4)

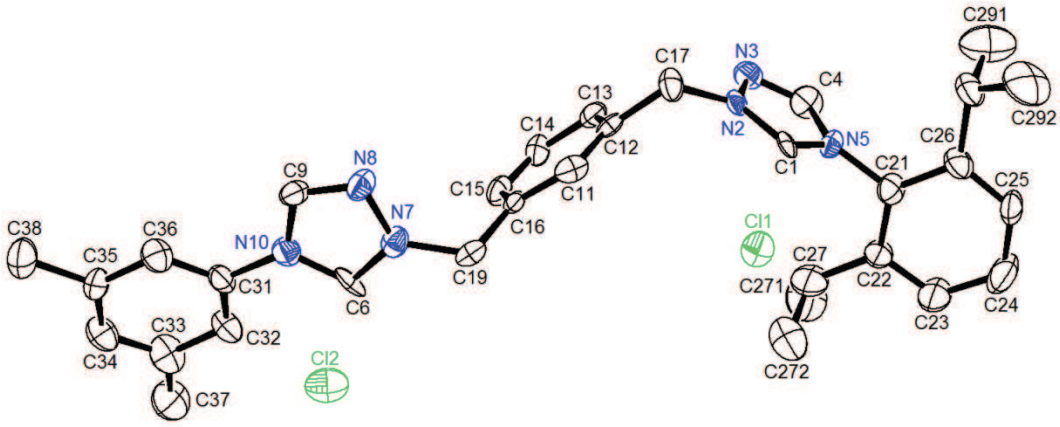

Figure 2.4.1: ORTEP plot of 4-(2,6-diisopropylphenyl)-1-{3-[(4-(3,5-dimethylphenyl)-1*H*-1,2,4-triazolium-1-yl)methyl]benzyl}-1*H*-1,2,4-triazolium dichloride (**36**) (hydrogen atoms and co-crystallized solvent molecules are omitted for clarity).[1a, 2]

2.5 1,1'-[1,3-Phenylenebis(methylene)]bis[4-(2,4,6-trimethylphenyl)-1*H*-1,2,4-triazolium] Bis(hexafluorophosphate) (51)

Name:	Lena Hahn / Regina Berg (AK Straub)
Sample:	LH020
File Name:	reb3.*
Operator:	F. Rominger (AK Hofmann)
Instrument:	Bruker APEX

Table 2.5.1: Crystal data and structure refinement for reb3.

Identification code	reb3	
Empirical formula	$C_{30}H_{34}F_{12}N_6P_2$	
Formula weight	768.57	
Temperature	200(2) K	
Wavelength	0.71073 Å	
Crystal system	monoclinic	
Space group	$P2_1/n$	
Z	4	
Unit cell dimensions	*a* =9.9410(8) Å	α = 90 deg.
	b = 12.0982(9) Å	β = 96.334(2) deg.
	c = 29.191(2) Å	γ = 90 deg.
Volume	3489.3(5) Å^3	
Density (calculated)	1.46 g/cm^3	
Absorption coefficient	0.22 mm^{-1}	
Crystal shape	polyhedron	
Crystal size	0.37 x 0.34 x 0.26 mm^3	
Crystal colour	colourless	
Theta range for data collection	2.1 to 28.3 deg.	
Index ranges	$-13 \le h \le 13$, $-16 \le k \le 16$, $-38 \le l \le 38$	
Reflections collected	36293	
Independent reflections	8651 (*R*(int) = 0.0291)	
Observed reflections	6853 ($I > 2\sigma(I)$)	

Absorption correction	Semi-empirical from equivalents
Max. and min. transmission	0.94 and 0.92
Refinement method	Full-matrix least-squares on F^2
Data/restraints/parameters	8651 / 861 / 486
Goodness-of-fit on F^2	1.03
Final R indices ($I>2\sigma(I)$)	$R1$ = 0.060, $wR2$ = 0.160
Largest diff. peak and hole	0.65 and -0.37 eÅ^{-3}

Table 2.5.2: Atomic coordinates and equivalent isotropic displacement parameters (Å^2) for reb3. (U_{eq} is defined as one third of the trace of the orthogonalized U_{ij} tensor.)

Atom	x	y	z	U_{eq}
C1	0.2963(3)	0.5768(2)	0.0211(1)	0.0334(5)
C2	0.2891(3)	0.6828(2)	0.0029(1)	0.0363(6)
C3	0.1706(3)	0.7425(2)	0.0025(1)	0.0433(7)
C4	0.0594(3)	0.6965(3)	0.0199(1)	0.0436(7)
C5	0.0675(3)	0.5922(2)	0.0391(1)	0.0365(6)
C6	0.1862(3)	0.5318(2)	0.0398(1)	0.0306(5)
C10	0.4122(3)	0.7313(3)	-0.0155(1)	0.0458(7)
N11	0.5222(3)	0.7466(2)	0.0222(1)	0.0399(5)
C12	0.5437(3)	0.8306(2)	0.0504(1)	0.0394(6)
N13	0.6460(3)	0.8045(2)	0.0817(1)	0.0395(5)
C14	0.6846(3)	0.7004(3)	0.0706(1)	0.0478(7)
N15	0.6108(3)	0.6630(2)	0.0342(1)	0.0484(6)
C20	0.1951(3)	0.4165(2)	0.0596(1)	0.0335(5)
N21	0.2815(2)	0.4117(2)	0.1039(1)	0.0325(5)
C22	0.2525(3)	0.3728(2)	0.1434(1)	0.0318(5)
N23	0.3634(2)	0.3808(2)	0.1734(1)	0.0335(5)
C24	0.4597(3)	0.4250(3)	0.1491(1)	0.0463(7)
N25	0.4137(2)	0.4442(2)	0.1066(1)	0.0476(6)
C31	0.7029(3)	0.8729(2)	0.1200(1)	0.0403(6)
C32	0.6568(3)	0.8558(3)	0.1629(1)	0.0487(7)
C33	0.7124(4)	0.9229(3)	0.1987(1)	0.0554(9)
C34	0.8069(4)	1.0032(3)	0.1923(1)	0.0541(9)
C35	0.8484(4)	1.0173(3)	0.1490(1)	0.0524(8)
C36	0.7976(3)	0.9526(3)	0.1119(1)	0.0443(7)
C37	0.5494(5)	0.7718(4)	0.1697(2)	0.0710(11)
C38	0.8641(5)	1.0762(4)	0.2318(1)	0.0716(12)
C39	0.8445(4)	0.9691(3)	0.0649(1)	0.0588(9)
C41	0.3771(3)	0.3535(2)	0.2221(1)	0.0327(5)
C42	0.3169(3)	0.4230(2)	0.2517(1)	0.0434(7)
C43	0.3289(4)	0.3945(3)	0.2979(1)	0.0499(7)
C44	0.4008(3)	0.3025(3)	0.3144(1)	0.0437(7)
C45	0.4634(3)	0.2382(2)	0.2839(1)	0.0375(6)
C46	0.4522(3)	0.2608(2)	0.2369(1)	0.0331(5)
C47	0.2431(4)	0.5269(3)	0.2350(1)	0.0666(11)
C48	0.4086(5)	0.2711(4)	0.3648(1)	0.0640(10)
C49	0.5153(3)	0.1866(3)	0.2042(1)	0.0497(8)
P1	0.2959(1)	0.0840(1)	0.0735(1)	0.0444(2)
F11	0.2008(3)	-0.0151(2)	0.0577(1)	0.1020(10)
F12	0.2040(3)	0.1202(2)	0.1115(1)	0.0935(9)
F13	0.3822(3)	0.0080(2)	0.1097(1)	0.0862(8)
F14	0.3918(3)	0.1866(2)	0.0879(1)	0.0723(6)
F15	0.3914(3)	0.0493(2)	0.0349(1)	0.0712(7)
F16	0.2152(3)	0.1618(2)	0.0361(1)	0.0899(9)
P2	0.8586(3)	0.4132(3)	0.1456(1)	0.0596(10)
F21	0.7469(4)	0.3267(4)	0.1508(3)	0.162(3)
F22	0.7816(5)	0.4519(4)	0.0990(2)	0.1311(19)

F23	0.7808(5)	0.5057(5)	0.1703(2)	0.1256(19)
F24	0.9773(3)	0.4984(2)	0.1393(1)	0.0732(10)
F25	0.9438(5)	0.3784(7)	0.1912(2)	0.174(3)
F26	0.9403(6)	0.3242(5)	0.1224(3)	0.150(3)
P2B	0.8589(11)	0.4117(8)	0.1434(3)	0.023(2)
F21B	0.7408(17)	0.3745(19)	0.1072(6)	0.094(7)
F22B	0.923(3)	0.490(2)	0.1088(9)	0.158(13)
F23B	0.7619(16)	0.5142(12)	0.1482(5)	0.051(4)
F24B	0.9620(17)	0.4530(18)	0.1838(7)	0.092(7)
F25B	0.7797(16)	0.3596(13)	0.1820(5)	0.061(5)
F26B	0.9422(18)	0.3195(13)	0.1196(5)	0.041(4)

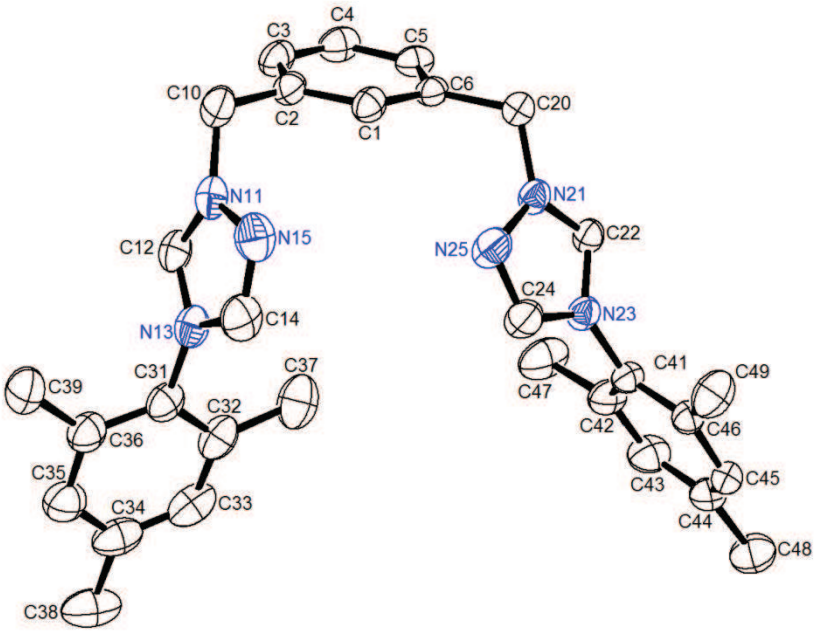

Figure 2.5.1: ORTEP plot of 1,1'-[1,3-phenylenebis(methylene)]bis[4-(2,4,6-trimethylphenyl)-1*H*-1,2,4-triazolium] bis(hexafluorophosphate) (**51**) (hydrogen atoms and counterions are omitted for clarity).[1a, 2]

2.6 1,1'-(Ethane-1,2-diyl)bis[4-(2,4,6-trimethylphenyl)-1*H*-1,2,4-triazolium] Bis(hexafluorophosphate) (61)

Name: Regina Berg (AK Straub)
Sample: would-be AF061, but true source of this crystal unknown
File Name: reb7.*
Operator: F. Rominger (AK Hofmann)
Instrument: Bruker APEX

Table 2.6.1: Crystal data and structure refinement for reb7.

Identification code	reb7	
Empirical formula	$C_{24}H_{30}F_{12}N_6P_2$	
Formula weight	692.48	
Temperature	200(2) K	
Wavelength	0.71073 Å	
Crystal system	monoclinic	
Space group	$P2_1/c$	
Z	4	
Unit cell dimensions	*a* = 24.885(9) Å	α = 90 deg.
	b =7.395(3) Å	β = 109.768(4) deg.
	c = 17.665(6) Å	γ = 90 deg.
Volume	3059.2(19) Å^3	
Density (calculated)	1.50 g/cm^3	
Absorption coefficient	0.24 mm^{-1}	
Crystal shape	plate	
Crystal size	0.30 x 0.12 x 0.01 mm^3	
Crystal colour	colourless	
Theta range for data collection	0.9 to 21.5 deg.	
Index ranges	$-22 \le h \le 25$, $-7 \le k \le 7$, $-18 \le l \le 18$	
Reflections collected	10424	
Independent reflections	3512 (*R*(int) = 0.0624)	
Observed reflections	2380 ($I > 2\sigma(I)$)	
Absorption correction	Semi-empirical from equivalents	
Max. and min. transmission	1.00 and 0.93	
Refinement method	Full-matrix least-squares on F^2	
Data/restraints/parameters	3512 / 0 / 403	
Goodness-of-fit on F^2	1.05	
Final *R* indices ($I > 2\sigma(I)$)	*R1* = 0.076, *wR2* = 0.188	
Largest diff. peak and hole	0.62 and -0.40 eÅ^{-3}	

Table 2.6.2: Atomic coordinates and equivalent isotropic displacement parameters (Å^2) for reb7. (U_{eq} is defined as one third of the trace of the orthogonalized U_{ij} tensor.)

Atom	x	y	z	U_{eq}
C11	0.4385(3)	0.7631(9)	0.3776(4)	0.0316(18)
N21	0.4642(3)	0.6049(7)	0.4006(3)	0.0314(15)
N31	0.4414(3)	0.4750(8)	0.3442(3)	0.0442(18)
C41	0.4016(4)	0.5591(10)	0.2882(4)	0.042(2)
N51	0.3981(3)	0.7389(7)	0.3076(3)	0.0290(15)
C111	0.5111(3)	0.5603(10)	0.4732(4)	0.0377(19)

C211	0.3567(3)	0.8715(9)	0.2601(4)	0.0301(18)
C221	0.3004(3)	0.8482(9)	0.2530(4)	0.0331(19)
C231	0.2607(4)	0.9662(11)	0.2047(5)	0.048(2)
C241	0.2776(4)	1.1085(10)	0.1641(4)	0.044(2)
C251	0.3346(4)	1.1251(9)	0.1745(4)	0.039(2)
C261	0.3760(3)	1.0094(9)	0.2226(4)	0.0319(18)
C271	0.2810(4)	0.7010(12)	0.2970(5)	0.061(3)
C281	0.2339(4)	1.2361(12)	0.1112(5)	0.068(3)
C291	0.4376(4)	1.0361(10)	0.2327(5)	0.050(2)
P11	0.4110(1)	1.5570(3)	0.0639(1)	0.0414(6)
F111	0.3900(3)	1.4486(10)	-0.0152(4)	0.120(3)
F121	0.3844(3)	1.7303(8)	0.0126(4)	0.104(2)
F131	0.4702(2)	1.5946(7)	0.0493(3)	0.0680(15)
F141	0.4345(3)	1.6696(9)	0.1436(4)	0.102(2)
F151	0.4396(2)	1.3851(7)	0.1142(4)	0.090(2)
F161	0.3535(2)	1.5279(8)	0.0818(3)	0.0803(18)
C12	0.0569(3)	0.7367(9)	-0.0695(4)	0.0311(19)
N22	0.0338(3)	0.8963(7)	-0.0681(3)	0.0291(15)
N32	0.0588(3)	1.0280(8)	-0.0988(4)	0.0413(17)
C42	0.0982(4)	0.9415(10)	-0.1174(4)	0.041(2)
N52	0.0983(3)	0.7580(7)	-0.0994(3)	0.0298(15)
C112	-0.0126(3)	0.9438(10)	-0.0382(4)	0.0354(19)
C212	0.1375(3)	0.6232(9)	-0.1092(4)	0.0313(18)
C222	0.1941(3)	0.6374(10)	-0.0607(4)	0.037(2)
C232	0.2320(4)	0.5089(10)	-0.0705(4)	0.043(2)
C242	0.2131(4)	0.3710(10)	-0.1273(4)	0.039(2)
C252	0.1571(3)	0.3629(9)	-0.1732(4)	0.0344(19)
C262	0.1163(3)	0.4870(9)	-0.1659(4)	0.0290(18)
C272	0.2162(4)	0.7810(12)	0.0036(5)	0.060(3)
C282	0.2561(4)	0.2310(11)	-0.1351(5)	0.056(2)
C292	0.0557(3)	0.4717(10)	-0.2159(4)	0.042(2)
P12	0.0934(1)	0.5580(3)	0.1406(1)	0.0370(6)
F112	0.0802(3)	0.6550(8)	0.2107(3)	0.0899(19)
F122	0.1548(2)	0.5091(7)	0.1995(3)	0.0735(16)
F132	0.1158(2)	0.7399(7)	0.1150(3)	0.0806(18)
F142	0.1042(2)	0.4597(8)	0.0680(3)	0.0844(18)
F152	0.0311(2)	0.6076(6)	0.0814(2)	0.0497(12)
F162	0.0682(2)	0.3765(6)	0.1631(3)	0.0781(17)

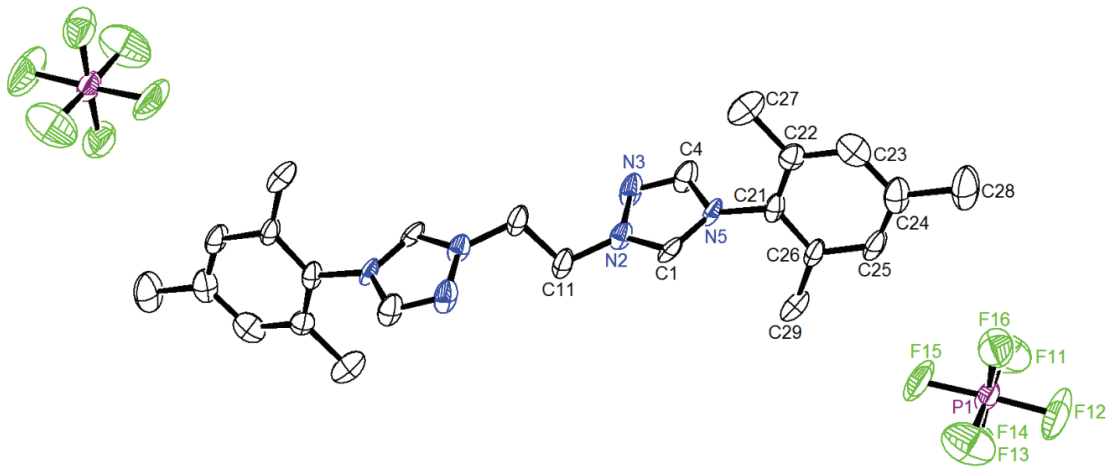

Figure 2.6.1: ORTEP plot of 1,1'-(ethane-1,2-diyl)bis[4-(2,4,6-trimethylphenyl)-1*H*-1,2,4-triazolium] bis(hexafluorophosphate) (**61**) (hydrogen atoms are omitted for clarity).[1a, 2]

2.7 1,1'-[1,3-Phenylenebis(methylene)]bis[4-(3,5-dimethylphenyl)-1*H*-1,2,4-triazolium] Bis(hexafluorophosphate) (52)

Name: Regina Berg (AK Straub)
Sample: rb332
File Name: reb17.*
Operator: T. Oeser
Instrument: Bruker Quazar

Table 2.7.1: Crystal data and structure refinement for reb17.

Identification code	reb17
Empirical formula	$C_{28}H_{30}F_{12}N_6P_2$
Formula weight	740.52
Temperature	200(2) K
Wavelength	0.71073 Å
Crystal system	monoclinic
Space group	$P2_1/n$
Z	4
Unit cell dimensions	*a* =7.4295(5) Å α = 90 deg. *b* = 23.5205(14) Å β = 93.535(2) deg. *c* = 18.3700(12) Å γ = 90 deg.
Volume	3204.0(4) Å^3
Density (calculated)	1.53 g/cm^3
Absorption coefficient	0.24 mm^{-1}
Crystal shape	polyhedron
Crystal size	0.10 x 0.05 x 0.05 mm^3
Crystal colour	colourless
Theta range for data collection	1.4 to 21.0 deg.
Index ranges	$-7 \le h \le 7$, $-23 \le k \le 23$, $-18 \le l \le 18$
Reflections collected	28095
Independent reflections	3463 (*R*(int) = 0.0812)
Observed reflections	2538 ($I > 2\sigma(I)$)
Absorption correction	Semi-empirical from equivalents
Max. and min. transmission	0.99 and 0.98
Refinement method	Full-matrix least-squares on F^2
Data/restraints/parameters	3463 / 0 / 470
Goodness-of-fit on F^2	1.03
Final *R* indices ($I > 2\sigma(I)$)	*R1* = 0.061, *wR2* = 0.149
Largest diff. peak and hole	0.69 and -0.37 eÅ^{-3}

Table 2.7.2: Atomic coordinates and equivalent isotropic displacement parameters ($Å^2$) for reb17. (U_{eq} is defined as one third of the trace of the orthogonalized U_{ij} tensor.)

Atom	x	y	z	U_{eq}
N11	0.3268(6)	0.2106(2)	-0.2851(2)	0.0304(12)
N12	0.1619(6)	0.1851(2)	-0.2985(3)	0.0361(12)
N14	0.2378(6)	0.1910(2)	-0.1800(2)	0.0287(11)
N21	0.2179(6)	0.4374(2)	-0.3111(2)	0.0309(12)
N22	0.3881(7)	0.4581(2)	-0.3144(3)	0.0484(15)
N24	0.2931(6)	0.4667(2)	-0.2040(2)	0.0284(11)
C1	0.2810(7)	0.3210(2)	-0.3642(3)	0.0313(14)
C2	0.3493(7)	0.2721(2)	-0.3939(3)	0.0262(14)
C3	0.3428(7)	0.2657(2)	-0.4688(3)	0.0298(14)
C4	0.2729(7)	0.3087(2)	-0.5137(3)	0.0318(15)
C5	0.2055(7)	0.3577(3)	-0.4835(3)	0.0345(15)
C6	0.2072(7)	0.3637(2)	-0.4080(3)	0.0301(14)
C7	0.4357(8)	0.2265(2)	-0.3461(3)	0.0361(15)
C8	0.1198(8)	0.4156(2)	-0.3769(3)	0.0367(15)
C13	0.1122(8)	0.1743(2)	-0.2330(3)	0.0349(15)
C15	0.3712(8)	0.2135(2)	-0.2153(3)	0.0294(14)
C23	0.4304(9)	0.4756(3)	-0.2483(3)	0.0480(18)
C25	0.1614(8)	0.4430(2)	-0.2458(3)	0.0280(14)
C31	0.2364(7)	0.1811(2)	-0.1025(3)	0.0270(13)
C32	0.1875(7)	0.1282(2)	-0.0791(3)	0.0322(15)
C33	0.1885(7)	0.1172(2)	-0.0047(3)	0.0330(15)
C34	0.2414(7)	0.1605(2)	0.0429(3)	0.0332(15)
C35	0.2945(7)	0.2135(2)	0.0195(3)	0.0304(14)
C36	0.2891(7)	0.2239(2)	-0.0549(3)	0.0288(14)
C37	0.1390(10)	0.0592(3)	0.0214(4)	0.0559(19)
C38	0.3563(8)	0.2588(3)	0.0733(3)	0.0423(16)
C41	0.2845(7)	0.4830(2)	-0.1284(3)	0.0282(14)
C42	0.3282(7)	0.5376(2)	-0.1086(3)	0.0316(14)
C43	0.3168(7)	0.5544(2)	-0.0361(3)	0.0345(15)
C44	0.2589(7)	0.5147(3)	0.0125(3)	0.0369(16)
C45	0.2148(7)	0.4596(3)	-0.0066(3)	0.0345(15)
C46	0.2268(7)	0.4432(2)	-0.0787(3)	0.0321(14)
C47	0.3588(9)	0.6146(2)	-0.0132(3)	0.0468(17)
C48	0.1564(9)	0.4173(3)	0.0487(3)	0.0535(19)
P1	0.1946(2)	0.6772(1)	0.1936(1)	0.0451(5)
F1	0.2031(6)	0.7427(2)	0.2137(3)	0.0950(16)
F2	0.3695(18)	0.6830(7)	0.1500(11)	0.085(6)
F2A	0.227(9)	0.6989(7)	0.1199(11)	0.15(2)
F3	0.023(2)	0.6740(5)	0.2362(12)	0.096(7)
F3A	0.159(6)	0.6502(11)	0.2714(9)	0.124(11)
F4	0.079(2)	0.6853(6)	0.1199(8)	0.101(5)
F4A	-0.017(3)	0.6805(11)	0.184(3)	0.130(17)
F5	0.317(3)	0.6709(6)	0.2662(7)	0.120(8)
F5A	0.395(3)	0.6684(8)	0.213(3)	0.126(17)
F6	0.1865(6)	0.6118(2)	0.1744(2)	0.0829(14)
P2	0.1276(2)	0.4263(1)	0.2861(1)	0.0363(5)
F7	0.1633(8)	0.3799(2)	0.2263(2)	0.0984(17)
F8	0.3346(5)	0.4286(2)	0.3098(3)	0.1001(18)
F9	0.0876(7)	0.4713(2)	0.3448(3)	0.0987(17)
F10	-0.0798(5)	0.4235(2)	0.2619(3)	0.0845(15)
F11	0.1487(5)	0.4758(2)	0.2277(2)	0.0753(13)
F12	0.1049(5)	0.3759(2)	0.3418(2)	0.0608(11)

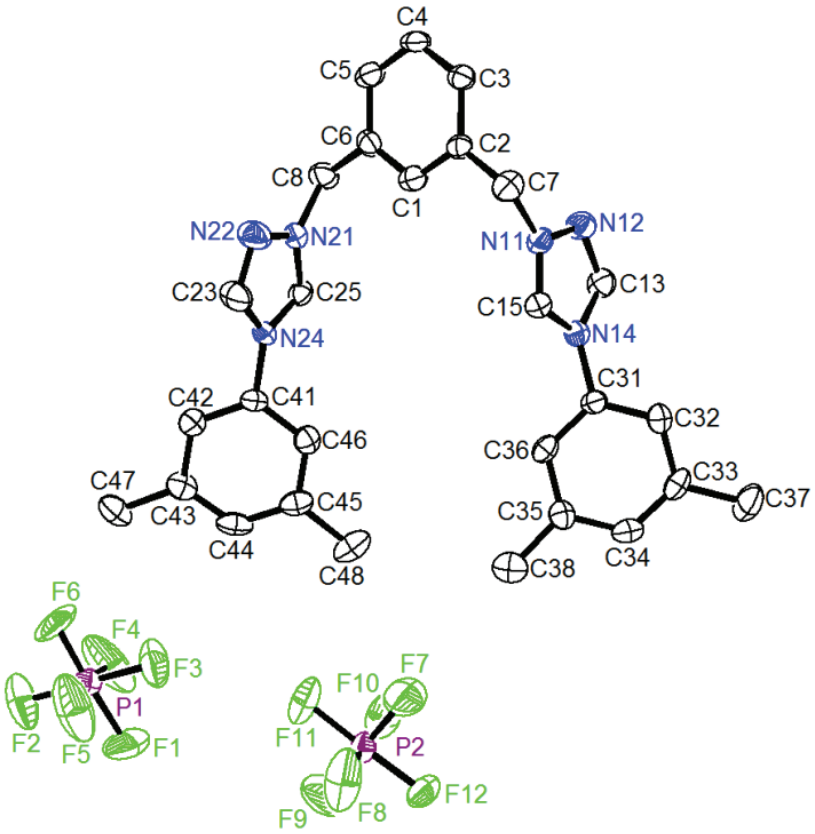

Figure 2.7.1: ORTEP plot of 1,1'-[1,3-phenylenebis(methylene)]bis[4-(3,5-dimethylphenyl)-1*H*-1,2,4-tri-azolium] bis(hexafluorophosphate) (**52**) (hydrogen atoms are omitted for clarity).[1a, 2]

2.8 1,1'-[1,3-Phenylenebis(methylene)]bis[4-(4-methylphenyl)-1*H*-1,2,4-triazolium] Bis(hexafluorophosphate) (53)

Name:	Regina Berg (AK Straub)
Sample:	rb482
File Name:	reb20.*
Operator:	F. Rominger (AK Hofmann)
Instrument:	Bruker APEX-II CCD

Table 2.8.1: Crystal data and structure refinement for reb20.

Identification code	reb20
Empirical formula	$C_{28}H_{29}F_{12}N_7P_2$
Formula weight	753.52
Temperature	200(2) K
Wavelength	0.71073 Å
Crystal system	monoclinic
Space group	$P2_1/n$

Z	4
Unit cell dimensions	*a* = 12.6321(4) Å α = 90 deg.
	b = 20.5013(7) Å β = 101.471(1) deg.
	c = 13.0096(5) Å γ = 90 deg.
Volume	3301.9(2) Å^3
Density (calculated)	1.52 g/cm^3
Absorption coefficient	0.23 mm^{-1}
Crystal shape	plate
Crystal size	0.13 x 0.13 x 0.03 mm^3
Crystal colour	colourless
Theta range for data collection	1.9 to 24.1 deg.
Index ranges	-14≤*h*≤14, -23≤*k*≤23, -13≤*l*≤14
Reflections collected	34007
Independent reflections	5252 (*R*(int) = 0.0606)
Observed reflections	3446 (*I*>2σ(*I*))
Absorption correction	Semi-empirical from equivalents
Max. and min. transmission	0.99 and 0.97
Refinement method	Full-matrix least-squares on F^2
Data/restraints/parameters	5252 / 921 / 510
Goodness-of-fit on F^2	1.03
Final *R* indices (*I*>2σ(*I*))	*R1* = 0.052, *wR2* = 0.115
Largest diff. peak and hole	0.42 and -0.33 eÅ^{-3}

Table 2.8.2: Atomic coordinates and equivalent isotropic displacement parameters (Å^2) for reb20. (U_{eq} is defined as one third of the trace of the orthogonalized U_{ij} tensor.)

Atom	x	y	z	U_{eq}
C1	0.7597(2)	0.2317(2)	0.5742(3)	0.0334(8)
N2	0.7659(2)	0.1757(1)	0.5279(2)	0.0343(7)
N3	0.8084(2)	0.1826(2)	0.4398(2)	0.0441(8)
C4	0.8265(3)	0.2448(2)	0.4363(3)	0.0461(10)
N5	0.7979(2)	0.2776(1)	0.5176(2)	0.0326(7)
C6	0.3317(2)	0.2461(2)	0.4537(3)	0.0342(8)
N7	0.3289(2)	0.1826(1)	0.4407(2)	0.0347(7)
N8	0.2915(2)	0.1523(1)	0.5206(2)	0.0420(7)
C9	0.2738(3)	0.2000(2)	0.5799(3)	0.0392(9)
N10	0.2978(2)	0.2594(1)	0.5419(2)	0.0321(7)
C11	0.5463(3)	0.1259(2)	0.4538(3)	0.0349(8)
C12	0.6367(3)	0.0861(2)	0.4832(3)	0.0331(8)
C13	0.6346(3)	0.0230(2)	0.4453(3)	0.0386(9)
C14	0.5430(3)	-0.0008(2)	0.3807(3)	0.0405(9)
C15	0.4528(3)	0.0383(2)	0.3527(3)	0.0377(9)
C16	0.4541(3)	0.1020(2)	0.3885(2)	0.0330(8)
C17	0.7340(3)	0.1114(2)	0.5596(3)	0.0407(9)
C19	0.3566(3)	0.1453(2)	0.3539(3)	0.0397(9)
C21	0.8096(3)	0.3460(2)	0.5411(3)	0.0359(8)
C22	0.7242(3)	0.3802(2)	0.5646(3)	0.0445(9)
C23	0.7387(4)	0.4459(2)	0.5895(3)	0.0553(11)
C24	0.8360(4)	0.4767(2)	0.5880(3)	0.0556(11)
C25	0.9193(4)	0.4406(2)	0.5645(3)	0.0627(12)
C26	0.9077(3)	0.3753(2)	0.5407(3)	0.0522(11)
C28	0.8503(4)	0.5486(2)	0.6157(4)	0.0844(17)
C31	0.2897(2)	0.3229(2)	0.5859(2)	0.0315(8)
C32	0.2093(3)	0.3354(2)	0.6405(3)	0.0393(9)
C33	0.2028(3)	0.3963(2)	0.6837(3)	0.0445(9)
C34	0.2745(3)	0.4461(2)	0.6710(3)	0.0450(9)

C35	0.3554(3)	0.4314(2)	0.6172(3)	0.0475(10)
C36	0.3642(3)	0.3704(2)	0.5748(3)	0.0418(9)
C38	0.2643(4)	0.5137(2)	0.7149(4)	0.0687(13)
P1	0.0236(5)	0.1779(3)	0.7736(4)	0.0423(13)
F11	0.0053(7)	0.1419(5)	0.6650(4)	0.096(3)
F12	0.0392(5)	0.1119(2)	0.8336(6)	0.0737(17)
F13	-0.1036(5)	0.1752(4)	0.7720(7)	0.0569(17)
F14	0.0420(4)	0.2147(3)	0.8830(4)	0.0647(17)
F15	0.0068(4)	0.2457(3)	0.7152(7)	0.094(2)
F16	0.1501(5)	0.1823(5)	0.7757(7)	0.064(2)
P1B	0.0289(14)	0.1812(8)	0.7633(10)	0.042(4)
F11B	0.007(2)	0.1171(8)	0.699(2)	0.119(9)
F12B	0.0344(14)	0.144(2)	0.8692(16)	0.188(13)
F13B	-0.0973(13)	0.1915(14)	0.7552(19)	0.075(7)
F14B	0.0490(13)	0.2479(13)	0.821(3)	0.159(11)
F15B	0.0197(11)	0.2178(12)	0.6556(14)	0.088(6)
F16B	0.1548(14)	0.1726(14)	0.771(2)	0.065(6)
P2	0.5566(1)	0.2309(1)	0.7693(1)	0.0378(3)
F21	0.5334(2)	0.2314(1)	0.6449(2)	0.0722(7)
F22	0.4810(2)	0.1706(1)	0.7712(2)	0.0945(9)
F23	0.4552(2)	0.2763(1)	0.7661(2)	0.0689(7)
F24	0.5806(2)	0.2319(2)	0.8930(2)	0.0816(8)
F25	0.6325(2)	0.2920(1)	0.7675(2)	0.0802(8)
F26	0.6592(2)	0.1863(1)	0.7725(2)	0.0779(8)
N40	1.1464(3)	0.0262(2)	0.3262(3)	0.0779(12)
C40	1.0843(4)	0.0517(2)	0.3631(4)	0.0606(12)
C41	1.0062(4)	0.0850(3)	0.4111(4)	0.0919(17)

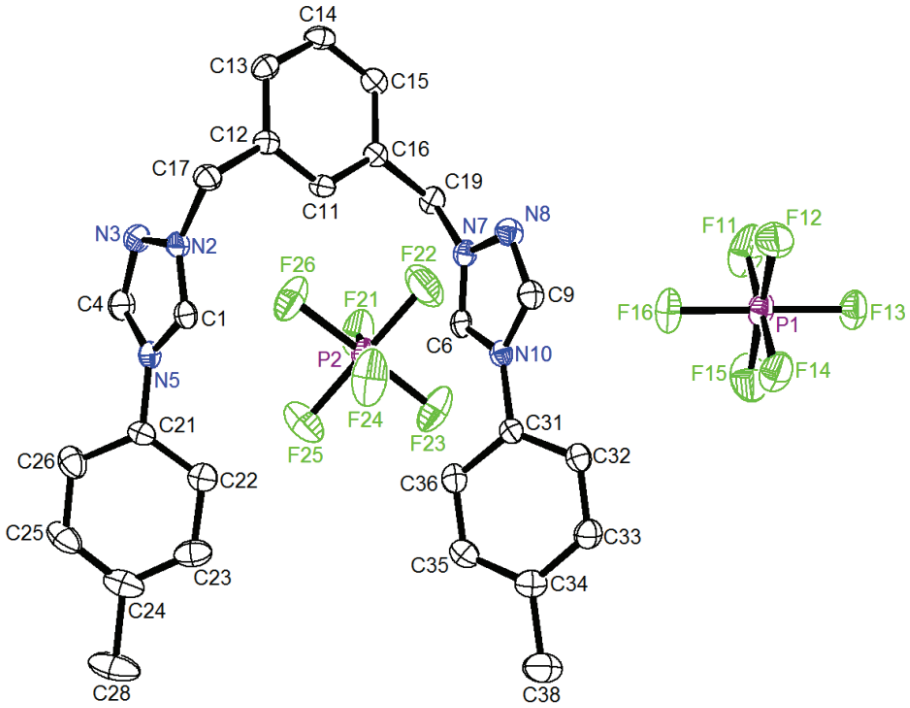

Figure 2.8.1: ORTEP plot of 1,1'-[1,3-phenylenebis(methylene)]bis[4-(4-methylphenyl)-1*H*-1,2,4-triazolium] bis(hexafluorophosphate) (**53**) (hydrogen atoms and co-crystallized solvent molecules are omitted for clarity).[1a, 2]

2.9 1,1'-(Ethane-1,2-diyl)bis[4-(4-methylphenyl)-1*H*-1,2,4-triazolium] Bis(hexafluorophosphate) (63)

Name: Regina Berg (AK Straub)
Sample: rb220
File Name: reb12.*
Operator: F. Rominger (AK Hofmann)
Instrument: Bruker APEX

Table 2.9.1: Crystal data and structure refinement for reb12.

Identification code	reb12	
Empirical formula	$C_{20}H_{22}F_{12}N_6P_2$	
Formula weight	636.38	
Temperature	200(2) K	
Wavelength	0.71073 Å	
Crystal system	monoclinic	
Space group	$P2_1/n$	
Z	4	
Unit cell dimensions	*a* = 10.981(3) Å	α = 90 deg.
	b =9.825(3) Å	β = 96.673(5) deg.
	c = 24.298(6) Å	γ = 90 deg.
Volume	2603.7(11) Å^3	
Density (calculated)	1.62 g/cm^3	
Absorption coefficient	0.28 mm^{-1}	
Crystal shape	polyhedron	
Crystal size	0.40 x 0.25 x 0.08 mm^3	
Crystal colour	colourless	
Theta range for data collection	1.7 to 28.3 deg.	
Index ranges	$-14 \le h \le 14$, $-13 \le k \le 13$, $-32 \le l \le 32$	
Reflections collected	26875	
Independent reflections	6449 (*R*(int) = 0.0266)	
Observed reflections	5316 ($I > 2\sigma(I)$)	
Absorption correction	Semi-empirical from equivalents	
Max. and min. transmission	0.98 and 0.90	
Refinement method	Full-matrix least-squares on F^2	
Data/restraints/parameters	6449 / 1554 / 491	
Goodness-of-fit on F^2	1.04	
Final *R* indices ($I > 2\sigma(I)$)	*R1* = 0.038, *wR2* = 0.092	
Largest diff. peak and hole	0.26 and -0.23 eÅ^{-3}	

Table 2.9.2: Atomic coordinates and equivalent isotropic displacement parameters ($Å^2$) for reb12. (U_{eq} is defined as one third of the trace of the orthogonalized U_{ij} tensor.)

Atom	x	y	z	U_{eq}
C1	0.2982(2)	0.4479(2)	0.1367(1)	0.0383(3)
N2	0.2013(1)	0.5228(2)	0.1405(1)	0.0421(3)
N3	0.2025(2)	0.5773(2)	0.1921(1)	0.0626(5)
C4	0.3035(2)	0.5311(2)	0.2186(1)	0.0601(6)
N5	0.3657(1)	0.4503(2)	0.1860(1)	0.0396(3)
C6	0.2025(2)	0.8066(2)	0.0074(1)	0.0424(4)
N7	0.2011(1)	0.7493(2)	0.0559(1)	0.0416(3)
N8	0.3172(1)	0.7376(2)	0.0830(1)	0.0480(4)
C9	0.3857(2)	0.7892(2)	0.0486(1)	0.0471(4)
N10	0.3192(1)	0.8345(1)	0.0010(1)	0.0404(3)
C10	0.1009(2)	0.5543(2)	0.0974(1)	0.0462(4)
C11	0.0959(2)	0.7044(2)	0.0827(1)	0.0469(4)
C21	0.4789(2)	0.3780(2)	0.2020(1)	0.0380(3)
C22	0.4916(2)	0.3074(2)	0.2513(1)	0.0507(4)
C23	0.5995(2)	0.2375(2)	0.2664(1)	0.0555(5)
C24	0.6926(2)	0.2356(2)	0.2327(1)	0.0474(4)
C25	0.6771(2)	0.3085(2)	0.1835(1)	0.0453(4)
C26	0.5702(2)	0.3810(2)	0.1679(1)	0.0412(4)
C28	0.8061(2)	0.1523(2)	0.2483(1)	0.0670(6)
C31	0.3659(2)	0.8941(2)	-0.0464(1)	0.0416(4)
C32	0.2957(2)	0.9868(2)	-0.0790(1)	0.0478(4)
C33	0.3414(2)	1.0406(2)	-0.1250(1)	0.0532(5)
C34	0.4565(2)	1.0050(2)	-0.1385(1)	0.0530(5)
C35	0.5254(2)	0.9139(2)	-0.1040(1)	0.0541(5)
C36	0.4814(2)	0.8570(2)	-0.0585(1)	0.0493(4)
C38	0.5062(2)	1.0647(3)	-0.1885(1)	0.0719(6)
P1	0.7395(1)	0.5749(2)	0.0484(1)	0.0241(6)
F11	0.8056(3)	0.7173(4)	0.0510(3)	0.0804(15)
F12	0.6787(8)	0.5994(8)	-0.0113(3)	0.0832(17)
F13	0.6256(6)	0.6391(7)	0.0735(3)	0.0645(13)
F14	0.6802(5)	0.4300(5)	0.0504(3)	0.0612(11)
F15	0.8039(6)	0.5485(6)	0.1110(2)	0.0646(12)
F16	0.8589(7)	0.5097(7)	0.0262(4)	0.0527(11)
P1B	0.7373(4)	0.5770(5)	0.0481(2)	0.0764(17)
F11B	0.749(2)	0.7287(6)	0.0294(6)	0.137(5)
F12B	0.6719(12)	0.5473(17)	-0.0140(4)	0.105(3)
F13B	0.6099(10)	0.6129(14)	0.0688(4)	0.074(3)
F14B	0.7178(16)	0.4250(8)	0.0611(6)	0.111(4)
F15B	0.8021(9)	0.6036(18)	0.1053(4)	0.105(4)
F16B	0.8612(11)	0.5415(17)	0.0240(7)	0.085(3)
P2	0.0859(2)	0.1190(2)	0.1167(1)	0.0323(5)
F21	0.0032(5)	0.0375(5)	0.1546(2)	0.0867(14)
F22	0.1869(4)	0.0101(6)	0.1303(3)	0.0930(18)
F23	0.1327(6)	0.2085(6)	0.1705(1)	0.0832(15)
F24	0.1661(4)	0.2059(3)	0.0822(2)	0.0807(12)
F25	-0.0246(4)	0.2273(5)	0.1036(2)	0.0807(12)
F26	0.0303(6)	0.0330(5)	0.0652(2)	0.0669(12)
P2B	0.0877(5)	0.1182(5)	0.1159(2)	0.0880(17)
F21B	-0.0019(10)	0.0910(19)	0.1558(5)	0.156(5)
F22B	0.1690(9)	-0.0080(9)	0.1399(3)	0.083(3)
F23B	0.1766(12)	0.2008(9)	0.1584(5)	0.121(4)
F24B	0.1863(7)	0.133(2)	0.0726(4)	0.191(6)
F25B	0.0215(13)	0.2421(8)	0.0905(6)	0.168(5)
F26B	0.0138(10)	0.0285(12)	0.0699(5)	0.104(3)

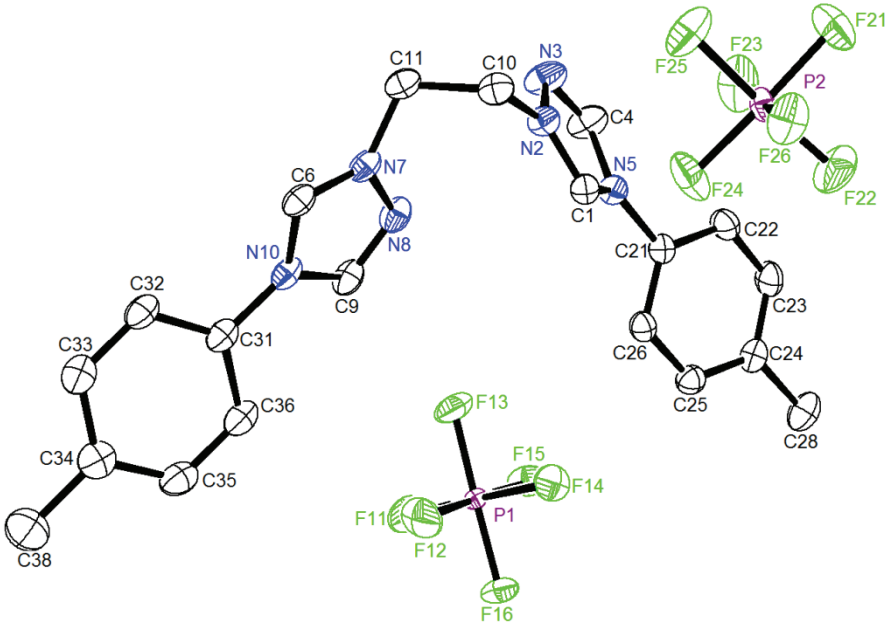

Figure 2.9.1: ORTEP plot of 1,1'-(ethane-1,2-diyl)bis[4-(4-methylphenyl)-1*H*-1,2,4-triazolium] bis(hexafluorophosphate) (**63**) (hydrogen atoms are omitted for clarity).[1a, 2]

2.10 1,1'-[1,3-Phenylenebis(methylene)]bis[4-(2,6-diisopropylphenyl)-1*H*-1,2,4-triazolium] Bis(hexafluorophosphate) (54)

Name:	Regina Berg (AK Straub)
Sample:	CD016
File Name:	reb11.*
Operator:	F. Rominger (AK Hofmann)
Instrument:	Bruker APEX II Quazar

Table 2.10.1: Crystal data and structure refinement for reb11.

Identification code	reb11	
Empirical formula	$C_{36}H_{46}F_{12}N_6P_2$	
Formula weight	852.73	
Temperature	200(2) K	
Wavelength	0.71073 Å	
Crystal system	monoclinic	
Space group	C2/c	
Z	8	
Unit cell dimensions	*a* = 38.072(2) Å	α = 90 deg.
	b = 12.4742(8) Å	β = 103.158(1) deg.
	c = 17.3018(11) Å	γ = 90 deg.
Volume	8001.2(9) Å^3	
Density (calculated)	1.42 g/cm^3	
Absorption coefficient	0.20 mm^{-1}	

Crystal shape	polyhedron
Crystal size	0.37 x 0.11 x 0.07 mm^3
Crystal colour	colourless
Theta range for data collection	2.4 to 26.7 deg.
Index ranges	$-48 \le h \le 48$, $-15 \le k \le 15$, $-21 \le l \le 21$
Reflections collected	69843
Independent reflections	8482 (R(int) = 0.0454)
Observed reflections	6138 ($I > 2\sigma(I)$)
Absorption correction	Semi-empirical from equivalents
Max. and min. transmission	0.99 and 0.93
Refinement method	Full-matrix least-squares on F^2
Data/restraints/parameters	8482 / 1554 / 633
Goodness-of-fit on F^2	1.04
Final R indices ($I > 2\sigma(I)$)	$R1$ = 0.061, $wR2$ = 0.146
Largest diff. peak and hole	0.46 and -0.42 $eÅ^{-3}$

Table 2.10.2: Atomic coordinates and equivalent isotropic displacement parameters ($Å^2$) for reb11. (U_{eq} is defined as one third of the trace of the orthogonalized U_{ij} tensor.)

Atom	x	y	z	U_{eq}
C1	0.1941(1)	0.0392(3)	0.4382(2)	0.0401(7)
N2	0.1703(1)	0.1153(2)	0.4152(2)	0.0390(6)
N3	0.1416(1)	0.1051(2)	0.4497(2)	0.0436(7)
C4	0.1492(1)	0.0201(3)	0.4935(2)	0.0401(7)
N5	0.1814(1)	-0.0235(2)	0.4882(2)	0.0369(6)
C6	0.0562(1)	-0.1669(3)	0.1123(2)	0.0433(8)
N7	0.0776(1)	-0.0864(2)	0.1384(1)	0.0328(5)
N8	0.1116(1)	-0.1079(2)	0.1316(2)	0.0470(7)
C9	0.1095(1)	-0.2034(3)	0.1006(2)	0.0465(8)
N10	0.0755(1)	-0.2425(2)	0.0873(2)	0.0355(6)
C11	0.1202(1)	0.1057(2)	0.2622(2)	0.0353(7)
C12	0.1480(1)	0.1810(2)	0.2773(2)	0.0347(7)
C13	0.1541(1)	0.2437(3)	0.2159(2)	0.0463(8)
C14	0.1322(1)	0.2344(3)	0.1409(2)	0.0563(10)
C15	0.1044(1)	0.1616(3)	0.1263(2)	0.0493(9)
C16	0.0984(1)	0.0957(2)	0.1862(2)	0.0365(7)
C17	0.1713(1)	0.2023(3)	0.3591(2)	0.0462(8)
C19	0.0677(1)	0.0173(3)	0.1703(2)	0.0415(8)
C21	0.1983(1)	-0.1181(3)	0.5296(2)	0.0385(7)
C22	0.1873(1)	-0.2179(3)	0.4962(2)	0.0433(8)
C23	0.2039(1)	-0.3064(3)	0.5373(2)	0.0544(9)
C24	0.2287(1)	-0.2947(3)	0.6089(2)	0.0581(10)
C25	0.2378(1)	-0.1946(3)	0.6414(2)	0.0523(9)
C26	0.2231(1)	-0.1024(3)	0.6016(2)	0.0419(7)
C27	0.1575(1)	-0.2295(3)	0.4209(2)	0.0512(9)
C29	0.2317(1)	0.0075(3)	0.6382(2)	0.0479(9)
C31	0.0638(1)	-0.3476(2)	0.0539(2)	0.0388(7)
C32	0.0495(1)	-0.3541(3)	-0.0276(2)	0.0452(8)
C33	0.0401(1)	-0.4570(3)	-0.0575(2)	0.0538(9)
C34	0.0451(1)	-0.5451(3)	-0.0088(3)	0.0579(10)
C35	0.0591(1)	-0.5343(3)	0.0712(3)	0.0558(10)
C36	0.0686(1)	-0.4348(3)	0.1056(2)	0.0457(8)
C37	0.0438(1)	-0.2580(3)	-0.0826(2)	0.0542(9)
C39	0.0821(1)	-0.4232(3)	0.1947(2)	0.0537(9)
C271	0.1372(1)	-0.3350(4)	0.4177(3)	0.0784(14)
C272	0.1711(1)	-0.2152(5)	0.3462(3)	0.0892(17)
C291	0.2116(1)	0.0253(3)	0.7041(3)	0.0620(11)

C292	0.2720(1)	0.0252(4)	0.6686(3)	0.0639(11)
C371	0.0040(1)	-0.2370(4)	-0.1156(3)	0.0885(16)
C372	0.0630(2)	-0.2716(5)	-0.1499(3)	0.0858(15)
C391	0.0503(1)	-0.4270(4)	0.2344(3)	0.0780(13)
C392	0.1106(2)	-0.5064(4)	0.2290(3)	0.0851(15)
P1	0.2044(2)	0.6446(5)	0.0872(4)	0.0722(19)
F11	0.2125(3)	0.7471(4)	0.0428(4)	0.114(3)
F12	0.1904(2)	0.7098(6)	0.1499(4)	0.111(3)
F13	0.1657(2)	0.6412(7)	0.0295(5)	0.107(3)
F14	0.1958(2)	0.5394(5)	0.1276(4)	0.115(3)
F15	0.2185(2)	0.5749(4)	0.0246(4)	0.0835(19)
F16	0.2436(2)	0.6516(8)	0.1417(4)	0.110(3)
P1B	0.2062(1)	0.6484(4)	0.0847(4)	0.0295(13)
F11B	0.1868(2)	0.7587(6)	0.0650(6)	0.089(3)
F12B	0.1751(4)	0.5956(11)	0.0283(11)	0.190(7)
F13B	0.1869(4)	0.6360(14)	0.1516(8)	0.168(7)
F14B	0.2281(2)	0.5446(5)	0.1073(8)	0.119(5)
F15B	0.2382(3)	0.7066(9)	0.1413(9)	0.143(5)
F16B	0.2274(4)	0.6680(16)	0.0191(7)	0.189(7)
P2	0.0458(1)	0.8927(3)	0.3890(2)	0.0510(11)
F21	0.0711(2)	0.9751(5)	0.4487(6)	0.136(4)
F22	0.0224(2)	0.9053(11)	0.4501(5)	0.157(5)
F23	0.0257(3)	0.9826(9)	0.3363(5)	0.150(4)
F24	0.0191(2)	0.8072(7)	0.3432(4)	0.113(3)
F25	0.0709(2)	0.8829(11)	0.3339(7)	0.168(5)
F26	0.0666(3)	0.8002(6)	0.4405(5)	0.139(4)
P2B	0.0466(2)	0.8915(8)	0.3885(6)	0.119(3)
F21B	0.0389(6)	0.9470(16)	0.4623(7)	0.229(9)
F22B	0.0792(3)	0.8340(14)	0.4382(7)	0.161(7)
F23B	0.0669(3)	0.9929(10)	0.3748(9)	0.147(5)
F24B	0.0582(4)	0.8423(10)	0.3121(6)	0.125(5)
F25B	0.0122(3)	0.9495(11)	0.3468(11)	0.146(6)
F26B	0.0253(3)	0.7956(10)	0.4044(14)	0.223(10)

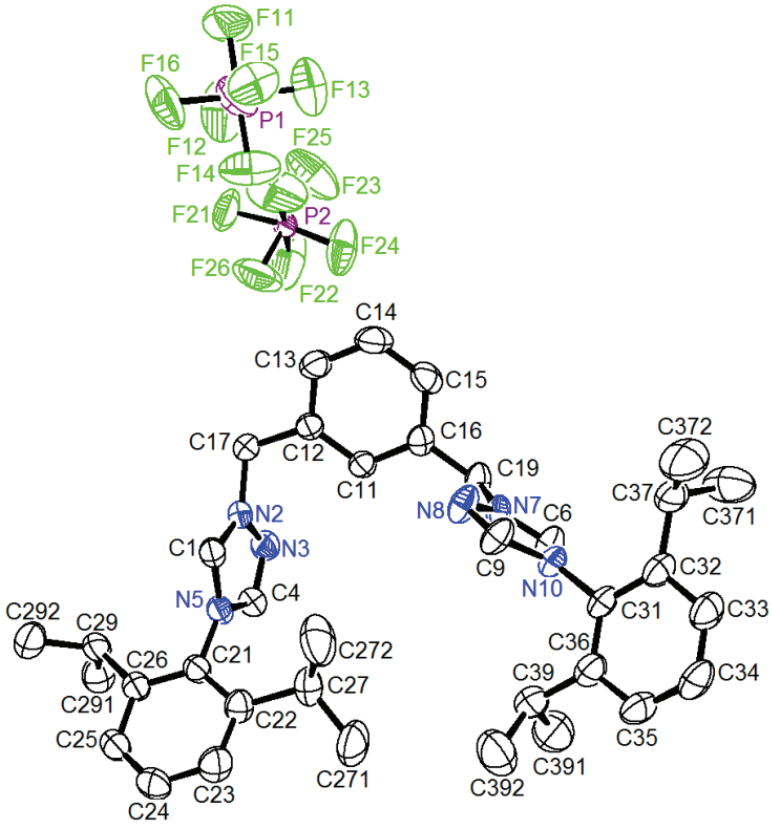

Figure 2.10.1: ORTEP plot of 1,1'-[1,3-phenylenebis(methylene)]bis[4-(2,6-diisopropylphenyl)-1*H*-1,2,4-triazolium] bis(hexafluorophosphate) (**54**) (hydrogen atoms are omitted for clarity).[1a, 2]

2.11 4-(2,6-Diisopropylphenyl)-1-{3-[(4-(3,5-dimethylphenyl)-1*H*-1,2,4-triazolium-1-yl)methyl]benzyl}-1*H*-1,2,4-triazolium Bis(hexafluorophosphate) (56)

Name:	Regina Berg (AK Straub)
Sample:	CD022
File Name:	reb10.*
Operator:	F. Rominger (AK Hofmann)
Instrument:	Bruker APEX II Quazar

Table 2.11.1: Crystal data and structure refinement for reb10.

Identification code	reb10
Empirical formula	$C_{32}H_{38}F_{12}N_6OP_2$
Formula weight	812.62
Temperature	200(2) K
Wavelength	0.71073 Å
Crystal system	triclinic
Space group	$P\bar{1}$

Z	2
Unit cell dimensions	*a* = 10.2433(3) Å α = 92.245(1) deg.
	b = 10.2978(3) Å β = 102.215(1) deg.
	c = 19.2667(6) Å γ = 109.934(1) deg.
Volume	1853.55(10) Å^3
Density (calculated)	1.46 g/cm^3
Absorption coefficient	0.21 mm^{-1}
Crystal shape	polyhedron
Crystal size	0.26 x 0.12 x 0.06 mm^3
Crystal colour	colourless
Theta range for data collection	2.2 to 23.8 deg.
Index ranges	$-11 \le h \le 11$, $-11 \le k \le 11$, $-21 \le l \le 21$
Reflections collected	23202
Independent reflections	5652 (R(int) = 0.0399)
Observed reflections	4346 ($I > 2\sigma(I)$)
Absorption correction	Semi-empirical from equivalents
Max. and min. transmission	0.99 and 0.95
Refinement method	Full-matrix least-squares on F^2
Data/restraints/parameters	5652 / 1578 / 631
Goodness-of-fit on F^2	1.02
Final R indices ($I > 2\sigma(I)$)	*R1* = 0.056, *wR2* = 0.134
Largest diff. peak and hole	0.39 and -0.28 eÅ^{-3}

Table 2.11.2: Atomic coordinates and equivalent isotropic displacement parameters (Å^2) for reb10. (U_{eq} is defined as one third of the trace of the orthogonalized U_{ij} tensor.)

Atom	x	y	z	U_{eq}
C1	1.0736(4)	-0.2347(4)	0.3133(3)	0.0530(11)
N2	1.1246(4)	-0.1585(3)	0.2661(2)	0.0505(9)
N3	1.2386(4)	-0.1837(4)	0.2519(2)	0.0564(10)
C4	1.2526(5)	-0.2771(5)	0.2930(2)	0.0515(11)
N5	1.1528(3)	-0.3127(3)	0.3321(2)	0.0426(8)
C6	1.3906(4)	0.6067(4)	0.1232(2)	0.0388(9)
N7	1.3324(3)	0.4854(3)	0.1441(2)	0.0445(8)
N8	1.1892(3)	0.4530(4)	0.1370(2)	0.0491(9)
C9	1.1658(4)	0.5598(4)	0.1120(2)	0.0439(10)
N10	1.2873(3)	0.6580(3)	0.1027(2)	0.0341(7)
C11	1.2446(4)	0.1652(4)	0.2033(2)	0.0425(9)
C12	1.1784(4)	0.0906(4)	0.2518(2)	0.0476(10)
C13	1.2023(6)	0.1535(5)	0.3198(3)	0.0650(13)
C14	1.2945(6)	0.2895(6)	0.3399(3)	0.0696(14)
C15	1.3616(5)	0.3642(5)	0.2915(3)	0.0577(12)
C16	1.3354(4)	0.3029(4)	0.2221(2)	0.0436(10)
C17	1.0737(5)	-0.0563(5)	0.2281(3)	0.0670(14)
C19	1.4010(5)	0.3839(5)	0.1672(3)	0.0638(14)
C21	1.1343(4)	-0.4171(4)	0.3819(2)	0.0450(10)
C22	1.0243(5)	-0.5449(4)	0.3590(2)	0.0494(10)
C23	1.0123(6)	-0.6440(5)	0.4069(3)	0.0643(13)
C24	1.1043(7)	-0.6159(6)	0.4726(3)	0.0737(15)
C25	1.2118(6)	-0.4903(7)	0.4933(3)	0.0772(17)
C26	1.2305(5)	-0.3845(6)	0.4482(2)	0.0624(13)
C27	0.9209(5)	-0.5791(5)	0.2864(2)	0.0572(12)
C271	0.7682(6)	-0.6118(7)	0.2930(3)	0.0881(18)
C272	0.9319(5)	-0.6974(6)	0.2408(3)	0.0718(14)
C29	1.3376(14)	-0.2255(17)	0.4689(7)	0.091(5)
C291	1.2635(15)	-0.1338(11)	0.4954(7)	0.127(6)

C292	1.4703(14)	-0.219(2)	0.5255(7)	0.171(9)
C31	1.3008(4)	0.7890(4)	0.0755(2)	0.0333(8)
C32	1.1902(4)	0.7945(4)	0.0213(2)	0.0399(9)
C33	1.2011(4)	0.9194(4)	-0.0053(2)	0.0440(10)
C34	1.3243(5)	1.0350(4)	0.0229(2)	0.0462(10)
C35	1.4349(4)	1.0292(4)	0.0770(2)	0.0421(9)
C36	1.4213(4)	0.9030(4)	0.1040(2)	0.0382(9)
C37	1.0841(5)	0.9271(5)	-0.0657(3)	0.0664(14)
C38	1.5665(5)	1.1545(4)	0.1066(3)	0.0628(13)
P1	0.7772(7)	0.6205(8)	0.0797(3)	0.0372(14)
F11	0.6737(8)	0.6121(9)	0.0059(3)	0.094(3)
F12	0.7275(11)	0.7370(8)	0.1095(4)	0.0605(19)
F13	0.6571(7)	0.5060(5)	0.1036(5)	0.089(3)
F14	0.8857(9)	0.6329(9)	0.1527(3)	0.088(3)
F15	0.8273(13)	0.5084(11)	0.0460(5)	0.075(2)
F16	0.8980(7)	0.7398(6)	0.0568(5)	0.093(3)
P2	1.2992(8)	0.1799(7)	0.6808(4)	0.0651(17)
F21	1.3597(15)	0.1033(15)	0.6350(7)	0.168(6)
F22	1.268(2)	0.2713(19)	0.6246(7)	0.243(9)
F23	1.1452(10)	0.0767(17)	0.6499(9)	0.231(8)
F24	1.2420(10)	0.2608(13)	0.7287(6)	0.140(4)
F25	1.3077(18)	0.0944(12)	0.7459(6)	0.181(6)
F26	1.4515(9)	0.2840(10)	0.7174(8)	0.134(5)
P1B	0.7712(13)	0.6002(15)	0.0788(7)	0.053(3)
F11B	0.797(2)	0.6730(18)	0.0111(7)	0.137(8)
F12B	0.708(2)	0.707(2)	0.1034(12)	0.121(6)
F13B	0.6224(9)	0.5002(16)	0.0368(10)	0.135(7)
F14B	0.747(2)	0.5311(16)	0.1468(8)	0.152(7)
F15B	0.837(2)	0.4927(19)	0.0587(12)	0.125(7)
F16B	0.9219(9)	0.6961(14)	0.1206(10)	0.098(7)
P2B	1.3195(11)	0.1835(11)	0.6665(6)	0.104(3)
F21B	1.4217(13)	0.2935(13)	0.6316(7)	0.161(5)
F22B	1.4040(19)	0.0879(18)	0.6672(14)	0.245(10)
F23B	1.4246(17)	0.250(2)	0.7369(7)	0.213(9)
F24B	1.2058(15)	0.079(2)	0.6956(13)	0.254(11)
F25B	1.2332(15)	0.2799(15)	0.6652(13)	0.197(8)
F26B	1.235(2)	0.121(2)	0.5893(7)	0.260(9)
C29B	1.361(3)	-0.271(3)	0.4759(11)	0.067(6)
C293	1.371(3)	-0.195(2)	0.5481(11)	0.110(8)
C294	1.4972(16)	-0.308(2)	0.4801(11)	0.097(6)
O1	1.073(2)	-0.044(2)	0.4601(11)	0.178(9)

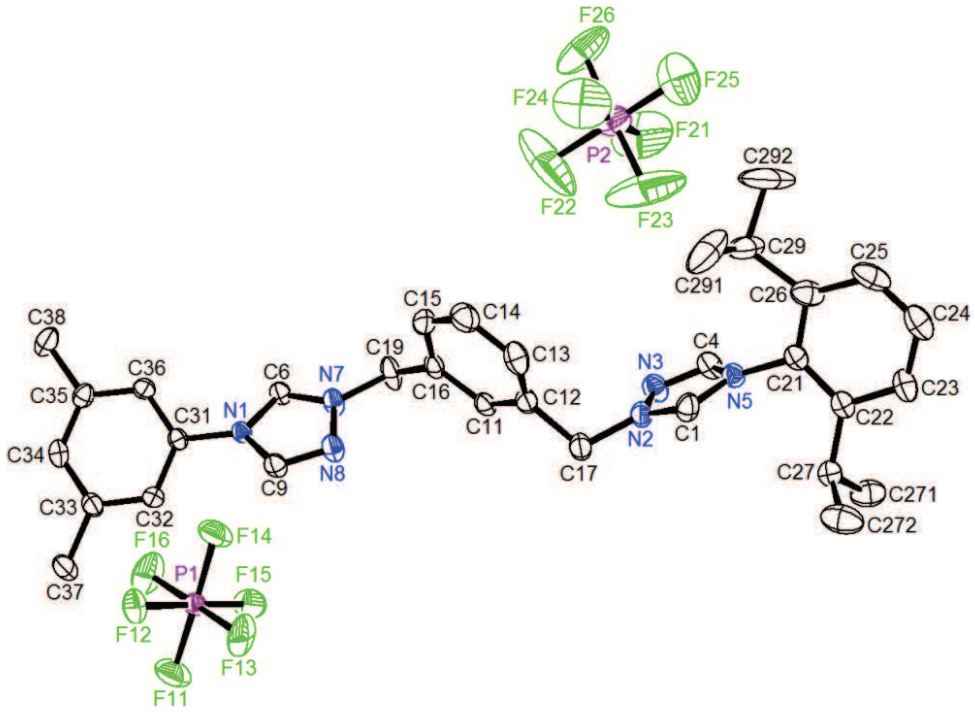

Figure 2.11.1: ORTEP plot of 4-(2,6-diisopropylphenyl)-1-{3-[(4-(3,5-dimethylphenyl)-1*H*-1,2,4-triazolium-1-yl)methyl]benzyl}-1*H*-1,2,4-triazolium bis(hexafluorophosphate) (**56**) (hydrogen atoms are omitted for clarity).[1a, 2]

2.12 μ-{1,1'-(Benzene-1,3-diyldimethanediyl)bis[4-(2,4,6-trimethylphenyl)-1*H*-1,2,4-triazol-5-ylidene]}-$\kappa C,\kappa C'$-bis{[1,3-bis(2,6-diisopropylphenyl)imidazol-2-ylidene]copper(I)} Bis(hexafluorophosphate) (71)

Name:	Regina Berg / Lena Hahn (AK Straub)
Sample:	LH029
File Name:	reg4.*
Operator:	F. Rominger (AK Hofmann)
Instrument:	Bruker APEX

Table 2.12.1: Crystal data and structure refinement for reg4.

Identification code	reg4
Empirical formula	$C_{86}H_{107}Cu_2F_{12}N_{11}P_2$
Formula weight	1711.85
Temperature	200(2) K
Wavelength	0.71073 Å
Crystal system	triclinic
Space group	$P\bar{1}$

Z	2	
Unit cell dimensions	*a* = 10.638(3) Å	α = 81.661(7) deg.
	b = 12.542(4) Å	β = 85.315(8) deg.
	c = 36.392(12) Å	γ = 69.104(7) deg.
Volume	4486(2) Å^3	
Density (calculated)	1.27 g/cm^3	
Absorption coefficient	0.58 mm^{-1}	
Crystal shape	plate	
Crystal size	0.27 x 0.17 x 0.03 mm^3	
Crystal colour	colourless	
Theta range for data collection	1.7 to 20.8 deg.	
Index ranges	$-10 \le h \le 10$, $-12 \le k \le 12$, $-36 \le l \le 36$	
Reflections collected	24440	
Independent reflections	9392 (R(int) = 0.0662)	
Observed reflections	6299 ($I > 2\sigma(I)$)	
Absorption correction	Semi-empirical from equivalents	
Max. and min. transmission	0.98 and 0.86	
Refinement method	Full-matrix least-squares on F^2	
Data/restraints/parameters	9392 / 1248 / 1135	
Goodness-of-fit on F^2	1.04	
Final R indices ($I > 2\sigma(I)$)	*R1* = 0.062, *wR2* = 0.158	
Largest diff. peak and hole	0.82 and -0.43 eÅ^{-3}	

Table 2.12.2: Atomic coordinates and equivalent isotropic displacement parameters (Å^2) for reg4. (U_{eq} is defined as one third of the trace of the orthogonalized U_{ij} tensor.)

Atom	x	y	z	U_{eq}
Cu1	-0.0144(1)	0.7165(1)	0.1333(1)	0.0350(3)
Cu2	0.6351(1)	0.2720(1)	0.3575(1)	0.0388(3)
C1	0.1667(7)	0.6914(6)	0.1182(2)	0.0358(18)
N2	0.2690(6)	0.6715(5)	0.1405(2)	0.0366(15)
N3	0.3914(6)	0.6520(6)	0.1223(2)	0.0487(17)
C4	0.3644(8)	0.6582(7)	0.0881(3)	0.051(2)
N5	0.2293(6)	0.6823(5)	0.0838(2)	0.0369(15)
C6	0.7321(7)	0.2586(6)	0.3117(2)	0.0395(19)
N7	0.7177(6)	0.3355(5)	0.2804(2)	0.0476(17)
N8	0.8143(7)	0.3003(6)	0.2527(2)	0.0537(18)
C9	0.8885(8)	0.2000(8)	0.2677(2)	0.049(2)
N10	0.8435(6)	0.1708(5)	0.3026(2)	0.0373(15)
C11	0.4352(7)	0.5530(6)	0.2260(2)	0.0401(19)
C12	0.3415(7)	0.5591(6)	0.2013(2)	0.0382(19)
C13	0.3214(8)	0.4585(7)	0.1955(2)	0.049(2)
C14	0.3936(8)	0.3553(7)	0.2146(2)	0.054(2)
C15	0.4879(8)	0.3487(7)	0.2399(2)	0.050(2)
C16	0.5092(7)	0.4476(6)	0.2456(2)	0.0395(19)
C17	0.2598(7)	0.6737(6)	0.1807(2)	0.042(2)
C19	0.6074(8)	0.4471(6)	0.2734(2)	0.050(2)
C21	0.1613(7)	0.7044(6)	0.0494(2)	0.0356(19)
C22	0.1524(8)	0.8053(7)	0.0259(2)	0.048(2)
C23	0.0870(9)	0.8267(7)	-0.0072(2)	0.054(2)
C24	0.0262(8)	0.7520(7)	-0.0171(2)	0.049(2)
C25	0.0369(8)	0.6550(7)	0.0073(2)	0.046(2)
C26	0.1038(8)	0.6272(6)	0.0404(2)	0.0398(19)
C27	0.2129(10)	0.8900(8)	0.0357(2)	0.075(3)
C28	-0.0488(9)	0.7789(8)	-0.0524(2)	0.065(3)
C29	0.1123(9)	0.5196(7)	0.0659(2)	0.061(2)

C31	0.9002(8)	0.0651(6)	0.3266(2)	0.039(2)
C32	0.8409(8)	-0.0191(7)	0.3278(2)	0.047(2)
C33	0.8966(10)	-0.1189(7)	0.3521(3)	0.061(3)
C34	1.0044(10)	-0.1363(8)	0.3737(2)	0.063(3)
C35	1.0587(9)	-0.0508(8)	0.3711(2)	0.065(3)
C36	1.0073(8)	0.0524(7)	0.3480(2)	0.049(2)
C37	0.7253(9)	-0.0019(8)	0.3035(2)	0.065(3)
C38	1.0646(12)	-0.2475(8)	0.3999(3)	0.106(4)
C39	1.0680(8)	0.1453(7)	0.3457(2)	0.064(2)
C41	-0.1914(7)	0.7448(6)	0.1531(2)	0.0331(18)
N42	-0.2980(6)	0.7279(5)	0.1400(2)	0.0306(14)
C43	-0.4117(7)	0.7713(6)	0.1621(2)	0.0391(19)
C44	-0.3776(7)	0.8148(6)	0.1897(2)	0.041(2)
N45	-0.2418(6)	0.7976(5)	0.1840(2)	0.0341(15)
C46	0.5331(7)	0.2978(6)	0.4024(2)	0.0394(19)
N47	0.4330(6)	0.3976(5)	0.4079(2)	0.0419(16)
C48	0.3707(8)	0.3931(7)	0.4421(2)	0.053(2)
C49	0.4325(8)	0.2876(8)	0.4595(2)	0.052(2)
N50	0.5317(6)	0.2307(5)	0.4351(2)	0.0420(16)
C51	-0.2911(7)	0.6773(6)	0.1065(2)	0.0323(18)
C52	-0.3148(7)	0.7508(7)	0.0731(2)	0.0398(19)
C53	-0.3062(8)	0.6985(8)	0.0409(2)	0.050(2)
C54	-0.2757(8)	0.5820(8)	0.0427(2)	0.052(2)
C55	-0.2526(8)	0.5128(7)	0.0764(2)	0.049(2)
C56	-0.2598(7)	0.5581(6)	0.1099(2)	0.0369(19)
C57	-0.3461(7)	0.8791(6)	0.0710(2)	0.045(2)
C59	-0.2351(8)	0.4825(6)	0.1462(2)	0.049(2)
C61	-0.1551(7)	0.8256(7)	0.2070(2)	0.042(2)
C62	-0.1049(8)	0.7518(7)	0.2381(2)	0.046(2)
C63	-0.0145(8)	0.7797(9)	0.2579(2)	0.061(2)
C64	0.0233(9)	0.8734(9)	0.2456(3)	0.066(3)
C65	-0.0299(9)	0.9439(8)	0.2141(3)	0.062(3)
C66	-0.1246(8)	0.9259(7)	0.1940(2)	0.046(2)
C67	-0.1404(8)	0.6462(7)	0.2505(2)	0.053(2)
C69	-0.1917(9)	1.0097(7)	0.1614(3)	0.060(2)
C71	0.3993(8)	0.4946(6)	0.3790(2)	0.046(2)
C72	0.4665(9)	0.5733(7)	0.3778(3)	0.058(2)
C73	0.4318(12)	0.6635(8)	0.3485(3)	0.081(3)
C74	0.3400(13)	0.6725(9)	0.3226(3)	0.086(4)
C75	0.2812(9)	0.5906(9)	0.3242(3)	0.076(3)
C76	0.3073(9)	0.5002(7)	0.3531(2)	0.057(2)
C77	0.5679(10)	0.5601(8)	0.4062(3)	0.069(3)
C79	0.2406(9)	0.4104(8)	0.3548(3)	0.069(3)
C81	0.6232(9)	0.1161(7)	0.4434(2)	0.046(2)
C82	0.5840(9)	0.0242(7)	0.4384(2)	0.050(2)
C83	0.6744(11)	-0.0869(8)	0.4484(2)	0.064(3)
C84	0.7990(12)	-0.1050(8)	0.4612(3)	0.077(3)
C85	0.8369(10)	-0.0137(9)	0.4647(2)	0.074(3)
C86	0.7511(9)	0.1008(7)	0.4555(2)	0.057(2)
C87	0.4507(9)	0.0440(7)	0.4222(2)	0.061(2)
C89	0.7911(9)	0.2023(8)	0.4600(3)	0.073(3)
C571	-0.2286(10)	0.9106(8)	0.0536(3)	0.100(4)
C572	-0.4737(10)	0.9475(8)	0.0510(3)	0.099(4)
C591	-0.0850(9)	0.4184(8)	0.1521(3)	0.075(3)
C592	-0.3097(9)	0.3979(7)	0.1509(2)	0.065(3)
C671	-0.0208(11)	0.5386(8)	0.2460(3)	0.092(3)
C672	-0.2004(11)	0.6487(10)	0.2900(3)	0.094(4)
C691	-0.1003(11)	1.0578(9)	0.1356(3)	0.093(3)
C692	-0.3109(9)	1.1089(8)	0.1761(3)	0.086(3)
C771	0.6970(14)	0.5613(18)	0.3892(4)	0.192(9)
C772	0.5116(19)	0.6477(14)	0.4337(4)	0.203(8)
C791	0.2736(11)	0.3498(9)	0.3207(3)	0.095(3)

C792	0.0899(10)	0.4620(10)	0.3623(3)	0.107(4)
C871	0.4705(12)	0.0061(12)	0.3838(3)	0.118(5)
C872	0.3691(11)	-0.0163(10)	0.4470(3)	0.095(4)
C891	0.9313(14)	0.1901(12)	0.4428(3)	0.134(5)
C892	0.7869(11)	0.2218(10)	0.4998(3)	0.102(4)
P1	0.0000	0.5000	0.5000	0.0644(10)
F11	0.013(3)	0.441(3)	0.4645(6)	0.133(10)
F12	-0.1367(12)	0.5952(18)	0.4879(7)	0.112(9)
F13	0.082(2)	0.5712(16)	0.4797(7)	0.113(8)
F11B	-0.047(4)	0.447(3)	0.5366(9)	0.20(2)
F12B	0.075(4)	0.3797(17)	0.4878(14)	0.156(16)
F13B	-0.131(3)	0.512(6)	0.4817(12)	0.24(2)
P2	0.5076(5)	0.3094(4)	0.0527(1)	0.0641(14)
F21	0.5504(11)	0.2727(14)	0.0143(3)	0.146(5)
F22	0.5768(16)	0.1880(9)	0.0724(4)	0.172(6)
F23	0.6356(13)	0.3347(14)	0.0538(5)	0.188(7)
F24	0.4593(13)	0.3409(12)	0.0915(3)	0.131(4)
F25	0.4412(16)	0.4302(9)	0.0345(3)	0.152(5)
F26	0.3821(9)	0.2764(9)	0.0526(3)	0.098(3)
P3	0.3389(2)	0.0055(2)	0.2587(1)	0.0666(7)
F31	0.1989(13)	0.0778(16)	0.2426(6)	0.175(7)
F32	0.261(2)	-0.0350(17)	0.2926(5)	0.199(10)
F33	0.337(2)	0.1080(14)	0.2786(5)	0.141(7)
F34	0.4725(16)	-0.0733(16)	0.2763(6)	0.179(8)
F35	0.4135(19)	0.0460(16)	0.2243(5)	0.116(5)
F36	0.3413(15)	-0.0994(11)	0.2392(4)	0.085(5)
F31B	0.319(3)	-0.055(3)	0.2264(7)	0.138(13)
F32B	0.439(3)	0.050(3)	0.2327(9)	0.154(14)
F33B	0.4621(19)	-0.102(2)	0.2706(6)	0.101(9)
F34B	0.360(3)	0.068(3)	0.2898(8)	0.119(11)
F35B	0.237(2)	-0.036(2)	0.2836(6)	0.082(8)
F36B	0.222(3)	0.117(2)	0.2444(8)	0.176(15)
N90	0.2601(14)	0.9388(13)	0.1314(4)	0.149(5)
C90	0.2809(15)	1.0216(16)	0.1351(4)	0.121(5)
C91	0.3052(18)	1.1350(14)	0.1376(5)	0.180(7)

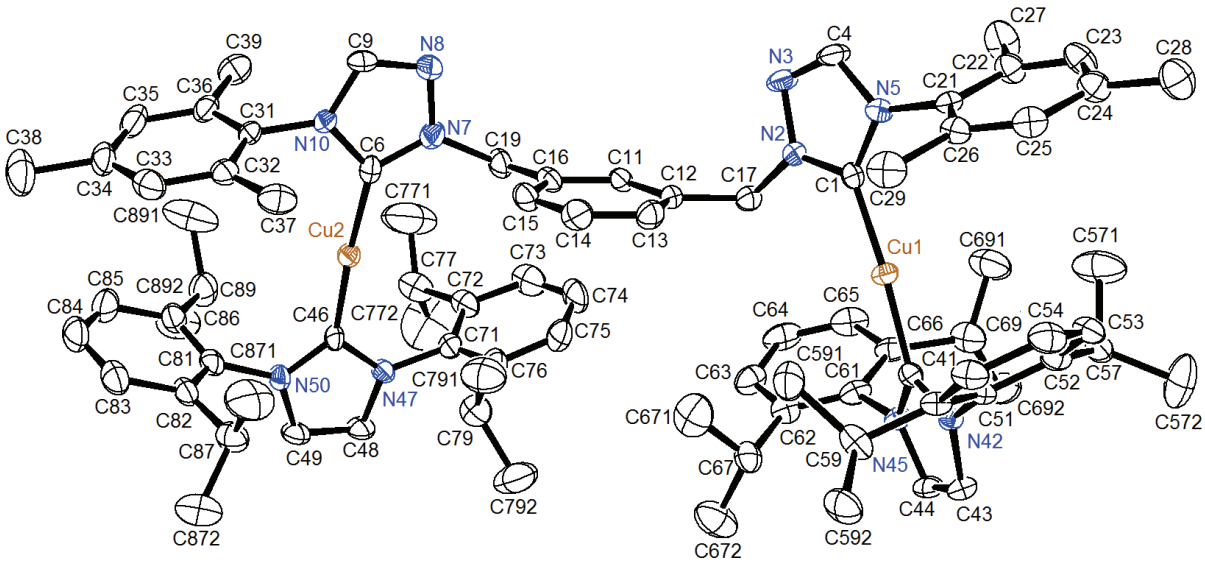

Figure 2.12.1: ORTEP plot of μ-{1,1'-(benzene-1,3-diyldimethanediyl)bis[4-(2,4,6-trimethylphenyl)-1*H*-1,2,4-triazol-5-ylidene]}-κ*C*,κ*C*'-bis{[1,3-bis(2,6-diisopropylphenyl)imidazol-2-ylidene]copper(I)} bis(hexafluorophosphate) (**71**) (hydrogen atoms and co-crystallized solvent molecules are omitted for clarity).[1a, 2]

2.13 μ-{1,1'-(Ethane-1,2-diyl)bis[4-(2,4,6-trimethylphenyl)-1*H*-1,2,4-triazol-5-ylidene]}-κ*C*,κ*C'*-bis{[1,3-bis(2,6-diisopropylphenyl)-imidazol-2-ylidene]copper(I)} Bis(hexafluorophosphate) (81)

Name:	Regina Berg (AK Straub)
Sample:	rb170
File Name:	reb9.*
Operator:	F. Rominger (AK Hofmann)
Instrument:	Bruker APEX II Quazar

Table 2.13.1: Crystal data and structure refinement for reb9.

Identification code	reb9	
Empirical formula	$C_{84}H_{109}Cu_2F_{12}N_{13}P_2$	
Formula weight	1717.86	
Temperature	200(2) K	
Wavelength	0.71073 Å	
Crystal system	triclinic	
Space group	$P\bar{1}$	
Z	2	
Unit cell dimensions	*a* = 11.1914(4) Å	α = 80.413(2) deg.
	b = 19.6953(7) Å	β = 82.312(2) deg.
	c = 21.0620(7) Å	γ = 79.050(2) deg.
Volume	4469.2(3) Å^3	
Density (calculated)	1.28 g/cm^3	

Absorption coefficient	0.59 mm^{-1}
Crystal shape	polyhedron
Crystal size	0.23 x 0.23 x 0.09 mm^3
Crystal colour	colourless
Theta range for data collection	1.0 to 26.9 deg.
Index ranges	$-14 \le h \le 14$, $-24 \le k \le 25$, $-26 \le l \le 26$
Reflections collected	77147
Independent reflections	19304 (R(int) = 0.0456)
Observed reflections	14421 ($I > 2\sigma(I)$)
Absorption correction	Semi-empirical from equivalents
Max. and min. transmission	0.95 and 0.88
Refinement method	Full-matrix least-squares on F^2
Data/restraints/parameters	19304 / 861 / 1091
Goodness-of-fit on F^2	1.01
Final R indices ($I > 2\sigma(I)$)	$R1$ = 0.046, $wR2$ = 0.115
Largest diff. peak and hole	0.60 and -0.37 $eÅ^{-3}$

Table 2.13.2: Atomic coordinates and equivalent isotropic displacement parameters ($Å^2$) for reb9. (U_{eq} is defined as one third of the trace of the orthogonalized U_{ij} tensor.)

Atom	x	y	z	U_{eq}
Cu1	-0.1214(1)	0.4480(1)	0.2601(1)	0.0331(1)
Cu2	-0.0006(1)	0.0740(1)	0.2400(1)	0.0329(1)
C1	-0.0428(2)	0.3919(1)	0.1965(1)	0.0334(5)
N2	-0.0539(2)	0.3269(1)	0.1903(1)	0.0347(4)
N3	0.0122(2)	0.3024(1)	0.1363(1)	0.0417(5)
C4	0.0656(2)	0.3543(1)	0.1090(1)	0.0419(6)
N5	0.0357(2)	0.4092(1)	0.1436(1)	0.0366(5)
C6	0.1027(2)	0.1414(1)	0.2323(1)	0.0329(5)
N7	0.0811(2)	0.2025(1)	0.2547(1)	0.0349(4)
N8	0.1791(2)	0.2377(1)	0.2425(1)	0.0430(5)
C9	0.2616(2)	0.1965(1)	0.2114(1)	0.0430(6)
N10	0.2199(2)	0.1376(1)	0.2041(1)	0.0354(4)
C10	-0.1173(2)	0.2784(1)	0.2365(1)	0.0390(6)
C11	-0.0335(2)	0.2365(1)	0.2856(1)	0.0403(6)
C21	0.0794(3)	0.4749(1)	0.1261(1)	0.0435(6)
C22	0.1941(3)	0.4793(2)	0.1425(2)	0.0532(8)
C23	0.2352(3)	0.5426(2)	0.1216(2)	0.0731(11)
C24	0.1668(4)	0.5986(2)	0.0875(2)	0.0829(13)
C25	0.0527(4)	0.5927(2)	0.0737(2)	0.0727(11)
C26	0.0062(3)	0.5303(2)	0.0922(2)	0.0539(8)
C27	0.2687(3)	0.4198(2)	0.1820(2)	0.0661(9)
C28	0.2133(5)	0.6675(2)	0.0668(3)	0.136(3)
C29	-0.1176(3)	0.5244(2)	0.0756(2)	0.0676(9)
C31	0.2908(2)	0.0786(1)	0.1757(1)	0.0383(6)
C32	0.3600(2)	0.0268(1)	0.2157(1)	0.0433(6)
C33	0.4277(3)	-0.0300(2)	0.1880(2)	0.0525(7)
C34	0.4284(3)	-0.0345(2)	0.1229(2)	0.0587(8)
C35	0.3588(3)	0.0184(2)	0.0852(2)	0.0587(8)
C36	0.2876(3)	0.0761(2)	0.1103(1)	0.0475(7)
C37	0.3640(3)	0.0319(2)	0.2857(2)	0.0561(8)
C38	0.5048(4)	-0.0971(2)	0.0943(2)	0.0852(13)
C39	0.2115(3)	0.1323(2)	0.0682(2)	0.0616(8)
N42	-0.2301(2)	0.4730(1)	0.3889(1)	0.0331(4)
C43	-0.2851(2)	0.5246(1)	0.4259(1)	0.0389(6)
C44	-0.2916(2)	0.5854(1)	0.3862(1)	0.0397(6)
N45	-0.2405(2)	0.5696(1)	0.3256(1)	0.0350(4)
C46	-0.1062(2)	0.0075(1)	0.2498(1)	0.0340(5)

N47	-0.2299(2)	0.0199(1)	0.2559(1)	0.0371(5)
C48	-0.2761(3)	-0.0417(2)	0.2635(1)	0.0473(7)
C49	-0.1802(3)	-0.0935(2)	0.2621(1)	0.0457(6)
N50	-0.0773(2)	-0.0628(1)	0.2535(1)	0.0375(5)
C51	-0.2063(2)	0.3991(1)	0.4121(1)	0.0344(5)
C52	-0.3010(2)	0.3613(1)	0.4149(1)	0.0385(6)
C53	-0.2736(3)	0.2894(1)	0.4342(1)	0.0472(7)
C54	-0.1583(3)	0.2580(1)	0.4502(1)	0.0488(7)
C55	-0.0684(3)	0.2970(1)	0.4483(1)	0.0460(6)
C56	-0.0892(2)	0.3691(1)	0.4290(1)	0.0394(6)
C57	-0.4280(2)	0.3956(2)	0.3979(1)	0.0457(6)
C59	0.0117(3)	0.4110(2)	0.4272(2)	0.0511(7)
C61	-0.2280(3)	0.6208(1)	0.2682(1)	0.0392(6)
C62	-0.1240(3)	0.6518(2)	0.2573(1)	0.0484(7)
C63	-0.1137(4)	0.7003(2)	0.2013(2)	0.0680(9)
C64	-0.2038(4)	0.7160(2)	0.1600(2)	0.0743(11)
C65	-0.3057(3)	0.6853(2)	0.1725(2)	0.0622(9)
C66	-0.3220(3)	0.6367(1)	0.2279(1)	0.0459(6)
C67	-0.0249(3)	0.6338(2)	0.3027(2)	0.0530(7)
C69	-0.4341(3)	0.6022(2)	0.2420(1)	0.0494(7)
C71	-0.3027(2)	0.0884(1)	0.2571(1)	0.0393(6)
C72	-0.3481(3)	0.1076(2)	0.3180(2)	0.0486(7)
C73	-0.4186(3)	0.1737(2)	0.3179(2)	0.0629(9)
C74	-0.4420(3)	0.2172(2)	0.2603(2)	0.0671(10)
C75	-0.3949(3)	0.1968(2)	0.2016(2)	0.0573(8)
C76	-0.3229(2)	0.1312(2)	0.1982(1)	0.0457(6)
C77	-0.3169(3)	0.0602(2)	0.3800(2)	0.0592(8)
C79	-0.2693(3)	0.1094(2)	0.1336(2)	0.0546(8)
C81	0.0467(3)	-0.0999(1)	0.2487(1)	0.0436(6)
C82	0.1086(3)	-0.1134(1)	0.3036(2)	0.0525(7)
C83	0.2300(3)	-0.1484(2)	0.2960(2)	0.0734(11)
C84	0.2804(4)	-0.1683(2)	0.2373(3)	0.0840(13)
C85	0.2161(4)	-0.1548(2)	0.1848(2)	0.0790(12)
C86	0.0968(3)	-0.1192(2)	0.1884(2)	0.0570(8)
C87	0.0492(3)	-0.0926(2)	0.3682(2)	0.0599(8)
C89	0.0262(4)	-0.0983(2)	0.1299(2)	0.0742(11)
C111	-0.2017(2)	0.5003(1)	0.3266(1)	0.0320(5)
C571	-0.5258(4)	0.3748(3)	0.4499(2)	0.1106(19)
C572	-0.4510(4)	0.3801(3)	0.3341(2)	0.1060(17)
C591	0.0582(4)	0.4030(2)	0.4931(2)	0.0808(11)
C592	0.1160(3)	0.3920(2)	0.3755(2)	0.0775(11)
C671	-0.0009(4)	0.6985(2)	0.3257(2)	0.0900(13)
C672	0.0896(4)	0.5931(3)	0.2723(2)	0.0962(14)
C691	-0.5512(3)	0.6537(2)	0.2304(2)	0.0798(11)
C692	-0.4217(3)	0.5436(2)	0.2010(2)	0.0631(9)
C771	-0.4266(5)	0.0535(3)	0.4289(2)	0.1165(19)
C772	-0.2168(4)	0.0835(2)	0.4080(2)	0.0891(13)
C782	0.1275(6)	-0.0653(4)	0.4057(3)	0.161(3)
C791	-0.3681(4)	0.1053(2)	0.0915(2)	0.0836(12)
C792	-0.1844(4)	0.1584(3)	0.0980(2)	0.0936(14)
C871	-0.0049(6)	-0.1506(3)	0.4094(2)	0.128(2)
C891	0.0463(6)	-0.1539(3)	0.0853(2)	0.125(2)
C892	0.0539(5)	-0.0303(2)	0.0922(2)	0.0978(14)
P1	0.5904(1)	0.6942(1)	-0.0134(1)	0.0491(2)
F11	0.5460(2)	0.6485(1)	0.0514(1)	0.0963(8)
F12	0.6444(2)	0.6223(1)	-0.0409(1)	0.1025(8)
F13	0.7200(2)	0.6909(1)	0.0118(1)	0.0774(6)
F14	0.6383(2)	0.7346(1)	-0.0799(1)	0.0967(8)
F15	0.5412(2)	0.7616(1)	0.0162(2)	0.1105(9)
F16	0.4638(2)	0.6966(1)	-0.0403(1)	0.0770(6)
P2	0.5615(6)	-0.1830(3)	0.4025(3)	0.0684(13)
F21	0.5527(10)	-0.1545(5)	0.3294(3)	0.114(3)

F22	0.5659(14)	-0.1082(4)	0.4126(5)	0.178(5)
F23	0.7022(6)	-0.1961(7)	0.3867(6)	0.182(5)
F24	0.5691(9)	-0.2073(6)	0.4762(3)	0.149(4)
F25	0.5600(10)	-0.2596(4)	0.3921(7)	0.153(4)
F26	0.4215(5)	-0.1752(6)	0.4160(4)	0.146(3)
P2B	0.5815(7)	-0.1935(4)	0.3960(4)	0.083(2)
F21B	0.6551(10)	-0.2541(3)	0.4378(5)	0.144(4)
F22B	0.6866(11)	-0.2056(6)	0.3415(6)	0.161(5)
F23B	0.6475(11)	-0.1385(4)	0.4141(5)	0.136(4)
F24B	0.5099(13)	-0.1349(7)	0.3512(9)	0.236(8)
F25B	0.4845(16)	-0.1845(6)	0.4545(9)	0.283(9)
F26B	0.5175(12)	-0.2483(6)	0.3759(8)	0.188(6)
N90	0.0931(5)	0.1259(3)	0.4039(2)	0.1108(14)
C90	0.1690(5)	0.1397(3)	0.4199(3)	0.109(2)
C91	0.2658(6)	0.1696(6)	0.4368(6)	0.247(6)
N92	-0.6952(6)	0.5422(2)	0.4104(2)	0.1367(19)
C92	-0.6904(4)	0.5990(3)	0.4057(2)	0.0756(11)
C93	-0.6876(4)	0.6720(2)	0.3992(2)	0.0875(12)
N94	0.3306(4)	0.6285(2)	-0.1576(2)	0.0927(11)
C94	0.3605(3)	0.5935(2)	-0.1125(2)	0.0627(9)
C95	0.4024(4)	0.5465(2)	-0.0563(2)	0.0736(10)

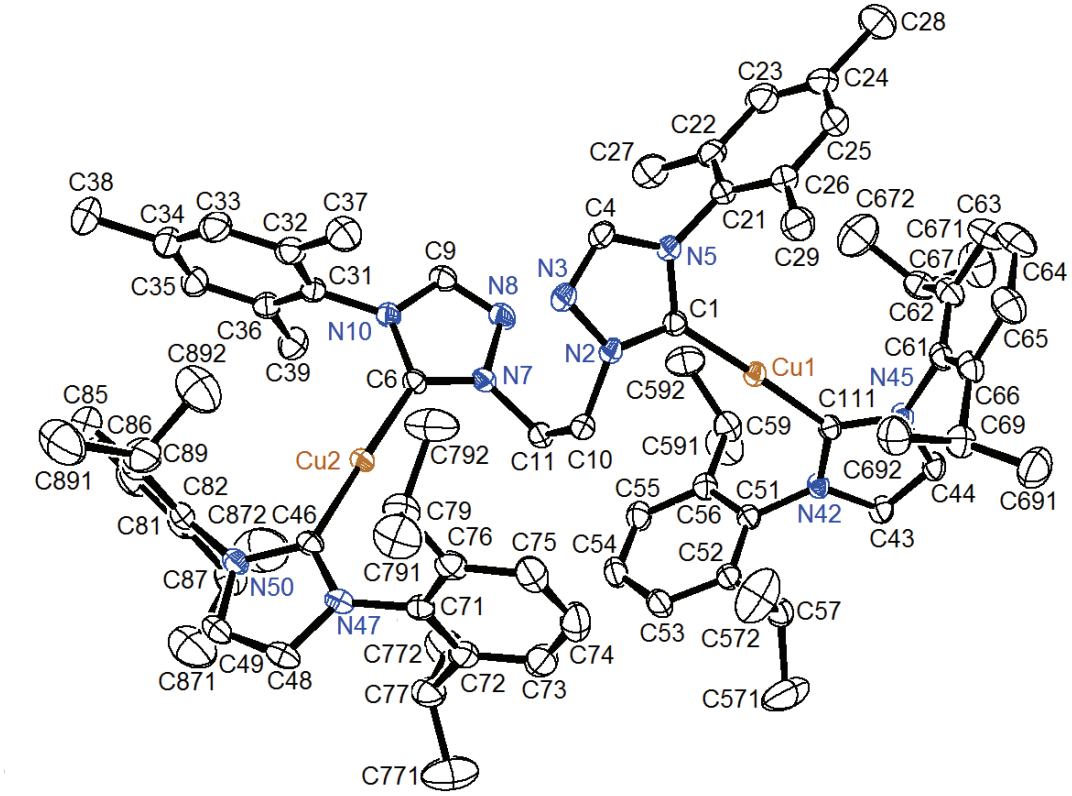

Figure 2.13.1: ORTEP plot of μ-{1,1'-(ethane-1,2-diyl)bis[4-(2,4,6-trimethylphenyl-1*H*-1,2,4-triazol-5-ylidene]}-$\kappa C,\kappa C'$-bis{[1,3-bis(2,6-diisopropylphenyl)imidazol-2-ylidene]copper(I)} bis-(hexafluorophosphate) (**81**) (hydrogen atoms, counterions and co-crystallized solvent molecules are omitted for clarity).[1]

2.14 μ-{1,1'-(Ethane-1,2-diyl)bis[4-(4-methylphenyl)-1*H*-1,2,4-triazol-5-ylidene}-$\kappa C,\kappa C'$-bis{[1,3-bis(2,6-diisopropylphenyl)imidazol-2-ylidene]copper(I)} Bis(hexafluorophosphate) (83)

Name: Regina Berg / Lena Hahn (AK Straub)
Sample: rb286
File Name: reb16.*
Operator: F. Rominger (AK Hofmann)
Instrument: Bruker APEX-II CCD

Table 2.14.1: Crystal data and structure refinement for reb16.

Identification code	reb16
Empirical formula	$C_{78}H_{98}Cu_2F_{12}N_{12}P_2$
Formula weight	1620.70
Temperature	200(2) K
Wavelength	0.71073 Å
Crystal system	triclinic
Space group	$P\bar{1}$
Z	1
Unit cell dimensions	*a* = 10.4897(12) Å α = 73.652(2) deg. *b* = 12.3247(15) Å β = 87.851(2) deg. *c* = 16.933(2) Å γ = 87.666(2) deg.
Volume	2098.1(4) Å^3
Density (calculated)	1.28 g/cm^3
Absorption coefficient	0.62 mm^{-1}
Crystal shape	polyhedron
Crystal size	0.28 x 0.17 x 0.05 mm^3
Crystal colour	colourless
Theta range for data collection	1.2 to 29.0 deg.
Index ranges	$-13\le h\le 14$, $-16\le k\le 16$, $-22\le l\le 23$
Reflections collected	41263
Independent reflections	10858 (*R*(int) = 0.0667)
Observed reflections	7318 ($I>2\sigma(I)$)
Absorption correction	Semi-empirical from equivalents
Max. and min. transmission	0.97 and 0.85
Refinement method	Full-matrix least-squares on F^2
Data/restraints/parameters	10858 / 399 / 544
Goodness-of-fit on F^2	1.02
Final *R* indices ($I>2\sigma(I)$)	*R1* = 0.056, *wR2* = 0.141
Largest diff. peak and hole	1.28 and -0.60 eÅ^{-3}

Table 2.14.2: Atomic coordinates and equivalent isotropic displacement parameters (Å^2) for reb16. (U_{eq} is defined as one third of the trace of the orthogonalized U_{ij} tensor.)

Atom	x	y	z	U_{eq}
Cu1	0.8209(1)	0.9629(1)	0.7098(1)	0.0320(1)
C1	0.9511(2)	0.8780(2)	0.6713(1)	0.0300(5)
N2	1.0315(2)	0.9121(2)	0.6061(1)	0.0333(5)

N3	1.1250(2)	0.8334(2)	0.5990(1)	0.0401(5)
C4	1.1009(3)	0.7476(2)	0.6626(2)	0.0361(6)
N5	0.9983(2)	0.7708(2)	0.7080(1)	0.0309(4)
C6	0.7087(2)	1.0588(2)	0.7521(2)	0.0312(5)
N7	0.6268(2)	1.0348(2)	0.8178(1)	0.0351(5)
C8	0.5732(3)	1.1328(2)	0.8320(2)	0.0445(7)
C9	0.6223(3)	1.2201(2)	0.7734(2)	0.0437(7)
C10	1.0216(3)	1.0155(2)	0.5381(2)	0.0383(6)
N10	0.7045(2)	1.1740(2)	0.7250(1)	0.0347(5)
C11	0.9413(2)	0.6895(2)	0.7775(2)	0.0314(5)
C12	1.0201(3)	0.6122(2)	0.8307(2)	0.0377(6)
C13	0.9647(3)	0.5266(2)	0.8934(2)	0.0463(7)
C14	0.8340(3)	0.5187(3)	0.9036(2)	0.0494(7)
C15	0.7571(3)	0.5991(3)	0.8506(2)	0.0476(7)
C16	0.8096(3)	0.6846(2)	0.7869(2)	0.0406(6)
C18	0.7740(4)	0.4232(3)	0.9705(2)	0.0745(11)
C21	0.5975(2)	0.9215(2)	0.8681(2)	0.0344(5)
C22	0.6712(3)	0.8730(2)	0.9364(2)	0.0401(6)
C23	0.6366(3)	0.7665(3)	0.9861(2)	0.0517(8)
C24	0.5353(3)	0.7122(3)	0.9666(2)	0.0560(8)
C25	0.4661(3)	0.7614(3)	0.8977(2)	0.0519(8)
C26	0.4945(3)	0.8682(2)	0.8464(2)	0.0416(6)
C27	0.7859(3)	0.9294(3)	0.9583(2)	0.0555(8)
C29	0.4180(3)	0.9212(3)	0.7697(2)	0.0541(8)
C31	0.7694(3)	1.2395(2)	0.6508(2)	0.0352(6)
C32	0.6992(3)	1.2741(2)	0.5791(2)	0.0408(6)
C33	0.7603(3)	1.3427(2)	0.5092(2)	0.0518(8)
C34	0.8854(4)	1.3721(3)	0.5110(2)	0.0586(9)
C35	0.9532(3)	1.3337(3)	0.5817(2)	0.0576(9)
C36	0.8973(3)	1.2664(2)	0.6550(2)	0.0452(7)
C37	0.5640(3)	1.2365(3)	0.5745(2)	0.0495(7)
C39	0.9715(3)	1.2270(3)	0.7334(2)	0.0608(9)
C271	0.7612(5)	0.9569(6)	1.0398(3)	0.120(2)
C272	0.9057(4)	0.8563(5)	0.9604(4)	0.1057(17)
C291	0.2763(4)	0.8958(4)	0.7823(3)	0.0753(11)
C292	0.4737(4)	0.8804(4)	0.6973(2)	0.0701(10)
C371	0.4696(4)	1.3370(4)	0.5493(3)	0.0878(13)
C372	0.5595(4)	1.1619(4)	0.5174(3)	0.0952(16)
C391	0.9638(5)	1.3153(4)	0.7806(3)	0.0874(13)
C392	1.1105(4)	1.1955(5)	0.7175(4)	0.1028(17)
P1	0.6440(6)	0.5278(5)	1.2270(4)	0.0444(11)
F11	0.7673(7)	0.5073(7)	1.2842(6)	0.0655(19)
F12	0.5521(11)	0.4941(10)	1.3037(6)	0.123(3)
F13	0.6375(9)	0.6545(6)	1.2287(8)	0.110(3)
F14	0.5278(9)	0.5486(10)	1.1677(7)	0.111(3)
F15	0.7399(6)	0.5614(6)	1.1500(4)	0.090(2)
F16	0.6589(7)	0.4005(5)	1.2246(4)	0.0777(18)
P1B	0.6308(11)	0.5233(8)	1.2267(6)	0.059(2)
F11B	0.7607(12)	0.4975(13)	1.2732(10)	0.092(4)
F12B	0.6088(19)	0.3945(7)	1.2566(14)	0.167(6)
F13B	0.5647(14)	0.5385(16)	1.3079(6)	0.111(5)
F14B	0.4969(11)	0.5458(11)	1.1852(10)	0.084(3)
F15B	0.6511(14)	0.6541(8)	1.1969(8)	0.092(4)
F16B	0.6964(14)	0.5127(17)	1.1443(7)	0.125(5)
N40	0.8088(4)	0.7506(3)	0.5600(2)	0.0987(14)
C40	0.7767(3)	0.6638(3)	0.5935(2)	0.0581(8)
C41	0.7338(5)	0.5524(3)	0.6378(3)	0.0792(12)

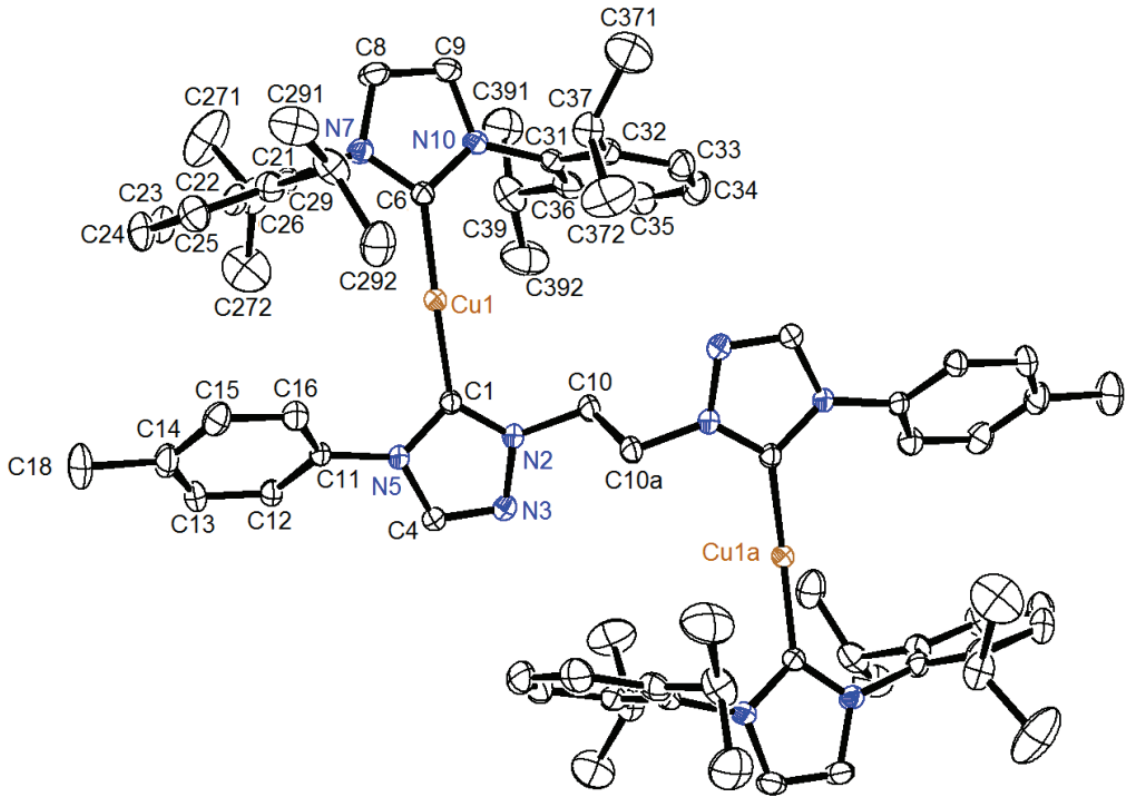

Figure 2.14.1: ORTEP plot of μ-{1,1'-(ethane-1,2-diyl)bis[4-(4-methylphenyl)-1*H*-1,2,4-triazol-5-ylidene}-κ*C*,κ*C'*-bis{[1,3-bis(2,6-diisopropylphenyl)imidazol-2-ylidene]copper(I)} bis(hexafluorophosphate) (**83**) (hydrogen atoms, counterions and co-crystallized solvent molecules are omitted for clarity).[1]

2.15 Bis(μ-acetato-κ*O*,κ*O'*)-μ-{1,1'-(ethane-1,2-diyl)bis[4-(2,4,6-trimethylphenyl)-1*H*-1,2,4-triazol-5-ylidene]-κ*C*,κ*C'*}dicopper(I) (91d)

Name:	Regina Berg (AK Straub)
Sample:	rb163
File Name:	reb8.*
Operator:	F. Rominger (AK Hofmann)
Instrument:	Bruker APEX

Table 2.15.1: Crystal data and structure refinement for reb8.

Identification code	reb8
Empirical formula	$C_{28}H_{34}Cu_2N_6O_4$
Formula weight	645.69
Temperature	200(2) K
Wavelength	0.71073 Å
Crystal system	monoclinic
Space group	$P2_1/c$
Z	4

Unit cell dimensions	a =9.569(2) Å	α = 90 deg.
	b = 18.170(4) Å	β = 102.822(6) deg.
	c = 17.100(4) Å	γ = 90 deg.
Volume	2899.0(12) Å^3	
Density (calculated)	1.48 g/cm^3	
Absorption coefficient	1.51 mm^{-1}	
Crystal shape	polyhedron	
Crystal size	0.26 x 0.06 x 0.05 mm^3	
Crystal colour	colourless	
Theta range for data collection	1.7 to 28.4 deg.	
Index ranges	$-12 \le h \le 12$, $-24 \le k \le 24$, $-22 \le l \le 22$	
Reflections collected	30742	
Independent reflections	7248 (R(int) = 0.0524)	
Observed reflections	5474 ($I > 2\sigma(I)$)	
Absorption correction	Semi-empirical from equivalents	
Max. and min. transmission	0.93 and 0.69	
Refinement method	Full-matrix least-squares on F^2	
Data/restraints/parameters	7248 / 0 / 369	
Goodness-of-fit on F^2	1.02	
Final R indices ($I > 2\sigma(I)$)	$R1$ = 0.043, $wR2$ = 0.090	
Largest diff. peak and hole	0.48 and -0.36 eÅ^{-3}	

Table 2.15.2: Atomic coordinates and equivalent isotropic displacement parameters (Å^2) for reb8. (U_{eq} is defined as one third of the trace of the orthogonalized U_{ij} tensor.)

Atom	x	y	z	U_{eq}
Cu1	0.0413(1)	0.0486(1)	0.1427(1)	0.0269(1)
Cu2	-0.1227(1)	0.1548(1)	0.1887(1)	0.0277(1)
C1	-0.0401(3)	-0.0441(1)	0.1554(2)	0.0250(5)
N2	-0.1665(2)	-0.0737(1)	0.1213(1)	0.0291(5)
N3	-0.1895(3)	-0.1431(1)	0.1488(2)	0.0434(6)
C4	-0.0734(3)	-0.1559(2)	0.2017(2)	0.0450(8)
N5	0.0195(2)	-0.0981(1)	0.2081(1)	0.0301(5)
C6	-0.3010(3)	0.1074(1)	0.1746(1)	0.0219(5)
N7	-0.3576(2)	0.0582(1)	0.1179(1)	0.0243(4)
N8	-0.4892(2)	0.0305(1)	0.1236(1)	0.0301(5)
C9	-0.5142(3)	0.0642(1)	0.1857(2)	0.0297(6)
N10	-0.4053(2)	0.1107(1)	0.2181(1)	0.0236(4)
C10	-0.2707(3)	-0.0472(1)	0.0514(2)	0.0309(6)
C11	-0.2979(3)	0.0344(1)	0.0512(2)	0.0255(5)
C21	0.1605(3)	-0.0947(1)	0.2591(2)	0.0285(6)
C22	0.1740(3)	-0.0841(2)	0.3409(2)	0.0364(6)
C23	0.3109(4)	-0.0803(2)	0.3873(2)	0.0436(8)
C24	0.4312(3)	-0.0867(2)	0.3565(2)	0.0423(7)
C25	0.4127(3)	-0.0971(2)	0.2752(2)	0.0386(7)
C26	0.2776(3)	-0.1012(2)	0.2249(2)	0.0319(6)
C27	0.0441(4)	-0.0773(2)	0.3764(2)	0.0587(10)
C28	0.5791(4)	-0.0835(2)	0.4104(2)	0.0676(11)
C29	0.2603(3)	-0.1107(2)	0.1363(2)	0.0461(8)
C31	-0.4029(3)	0.1546(1)	0.2885(2)	0.0247(5)
C32	-0.3070(3)	0.1368(1)	0.3594(2)	0.0286(6)
C33	-0.3139(3)	0.1781(2)	0.4266(2)	0.0323(6)
C34	-0.4147(3)	0.2328(2)	0.4251(2)	0.0336(6)
C35	-0.5066(3)	0.2487(2)	0.3534(2)	0.0327(6)
C36	-0.5030(3)	0.2112(1)	0.2833(2)	0.0278(5)
C37	-0.2003(3)	0.0753(2)	0.3647(2)	0.0390(7)

C38	-0.4224(4)	0.2730(2)	0.5010(2)	0.0505(8)
C39	-0.6042(3)	0.2306(2)	0.2060(2)	0.0358(6)
C41	0.0984(4)	0.2437(2)	0.0180(2)	0.0489(8)
C42	0.0409(3)	0.1919(2)	0.0720(2)	0.0328(6)
O42	0.0742(2)	0.1251(1)	0.0690(1)	0.0387(5)
O43	-0.0344(2)	0.2184(1)	0.1158(1)	0.0433(5)
C44	0.2432(3)	0.1249(2)	0.3803(2)	0.0436(7)
C45	0.1503(3)	0.1242(2)	0.2968(2)	0.0303(6)
O45	0.1875(2)	0.0844(1)	0.2460(1)	0.0348(4)
O46	0.0389(2)	0.1633(1)	0.2851(1)	0.0397(5)

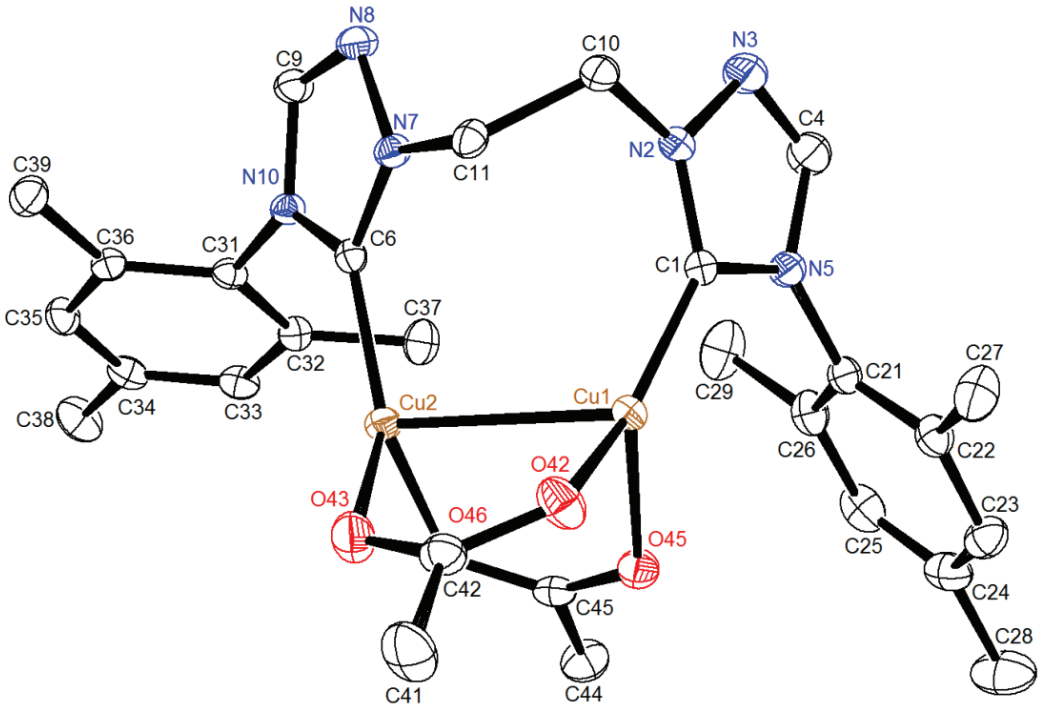

Figure 2.15.1: ORTEP plot of bis(μ-acetato-κ*O*,κ*O*')-μ-{1,1'-(ethane-1,2-diyl)bis[4-(2,4,6-trimethylphenyl)-1*H*-1,2,4-triazol-5-ylidene]-κ*C*,κ*C*'}dicopper(I) (**91d**) (hydrogen atoms are omitted for clarity).[1]

2.16 Bis{μ-[1,1'-(ethane-1,2-diyl)bis(4-(2,4,6-trimethylphenyl)-1*H*-1,2,4-triazol-5-ylidene)]-κ*C*,κ*C*'}dicopper(I) Bis(hexafluorophosphate) (111)

Name:	Regina Berg (AK Straub)
Sample:	rb221
File Name:	reb13.*
Operator:	F. Rominger (AK Hofmann)
Instrument:	Bruker APEX-II Quazar

Table 2.16.1: Crystal data and structure refinement for reb13.

Identification code	reb13	
Empirical formula	$C_{54}H_{68}Cu_2F_{12}N_{12}O_2P_2$	
Formula weight	1334.22	
Temperature	200(2) K	
Wavelength	0.71073 Å	
Crystal system	triclinic	
Space group	$P\bar{1}$	
Z	1	
Unit cell dimensions	*a* =9.8196(16) Å	α = 111.611(3) deg.
	b = 12.399(2) Å	β = 98.387(3) deg.
	c = 13.631(2) Å	γ = 90.094(3) deg.
Volume	1523.7(4) Å^3	
Density (calculated)	1.45 g/cm^3	
Absorption coefficient	0.84 mm^{-1}	
Crystal shape	polyhedron	
Crystal size	0.21 x 0.15 x 0.04 mm^3	
Crystal colour	colourless	
Theta range for data collection	1.6 to 28.4 deg.	
Index ranges	$-13\le h\le 13$, $-16\le k\le 16$, $-18\le l\le 17$	
Reflections collected	16125	
Independent reflections	7523 (R(int) = 0.0291)	
Observed reflections	5701 ($I>2\sigma(I)$)	
Absorption correction	Semi-empirical from equivalents	
Max. and min. transmission	0.97 and 0.84	
Refinement method	Full-matrix least-squares on F^2	
Data/restraints/parameters	7523 / 399 / 451	
Goodness-of-fit on F^2	1.03	
Final R indices ($I>2\sigma(I)$)	*R1* = 0.045, *wR2* = 0.101	
Largest diff. peak and hole	0.44 and -0.22 eÅ^{-3}	

Table 2.16.2: Atomic coordinates and equivalent isotropic displacement parameters (Å^2) for reb13. (U_{eq} is defined as one third of the trace of the orthogonalized U_{ij} tensor.)

Atom	x	y	z	U_{eq}
Cu1	0.6416(1)	0.6192(1)	0.6452(1)	0.0298(1)
C1	0.7508(2)	0.4906(2)	0.5861(2)	0.0270(4)
N2	0.8099(2)	0.4533(2)	0.4974(1)	0.0288(4)
N3	0.8750(2)	0.3510(2)	0.4805(2)	0.0366(4)
C4	0.8563(2)	0.3260(2)	0.5622(2)	0.0357(5)
N5	0.7831(2)	0.4072(2)	0.6278(1)	0.0287(4)
C6	0.5104(2)	0.3162(2)	0.2833(2)	0.0275(4)
N7	0.6307(2)	0.3707(2)	0.2888(1)	0.0293(4)
N8	0.7196(2)	0.3029(2)	0.2252(2)	0.0392(5)
C9	0.6503(2)	0.2043(2)	0.1800(2)	0.0402(5)
C10	0.8101(2)	0.5089(2)	0.4201(2)	0.0321(5)
N10	0.5243(2)	0.2070(2)	0.2123(1)	0.0321(4)
C11	0.6727(2)	0.4926(2)	0.3490(2)	0.0324(5)
C21	0.7445(2)	0.4081(2)	0.7264(2)	0.0288(4)
C22	0.8240(2)	0.4785(2)	0.8220(2)	0.0345(5)
C23	0.7839(3)	0.4793(2)	0.9161(2)	0.0409(6)
C24	0.6705(3)	0.4125(2)	0.9151(2)	0.0435(6)
C25	0.5946(3)	0.3441(2)	0.8184(2)	0.0435(6)
C26	0.6306(2)	0.3386(2)	0.7216(2)	0.0339(5)
C27	0.9500(3)	0.5495(2)	0.8258(2)	0.0522(7)

C28	0.6330(4)	0.4135(3)	1.0197(2)	0.0681(10)
C29	0.5499(3)	0.2601(2)	0.6172(2)	0.0492(6)
C31	0.4196(2)	0.1131(2)	0.1687(2)	0.0321(5)
C32	0.4192(3)	0.0290(2)	0.2134(2)	0.0443(6)
C33	0.3187(3)	-0.0614(2)	0.1668(2)	0.0492(7)
C34	0.2215(3)	-0.0697(2)	0.0798(2)	0.0403(6)
C35	0.2264(3)	0.0164(2)	0.0387(2)	0.0403(5)
C36	0.3245(2)	0.1090(2)	0.0812(2)	0.0368(5)
C37	0.5229(4)	0.0373(3)	0.3093(3)	0.0775(11)
C38	0.1145(3)	-0.1695(2)	0.0310(3)	0.0581(8)
C39	0.3278(4)	0.2014(3)	0.0346(2)	0.0646(9)
O40	0.7261(2)	0.7591(2)	0.6041(2)	0.0638(6)
C40	0.8267(4)	0.8296(2)	0.6377(2)	0.0655(10)
C41	0.8388(6)	0.9177(4)	0.5899(3)	0.130(2)
C42	0.9345(4)	0.8292(3)	0.7238(3)	0.0798(11)
P1	0.8594(6)	0.7855(7)	1.2598(5)	0.0445(11)
F11	0.7432(7)	0.8463(7)	1.3232(5)	0.092(3)
F12	0.8703(16)	0.8849(10)	1.2159(10)	0.077(3)
F13	0.7453(8)	0.7156(6)	1.1623(4)	0.093(3)
F14	0.9730(9)	0.7206(7)	1.1957(9)	0.124(4)
F15	0.8516(13)	0.6846(10)	1.3055(11)	0.076(2)
F16	0.9702(8)	0.8535(5)	1.3597(6)	0.089(2)
P1B	0.8654(7)	0.8027(7)	1.2568(5)	0.0478(13)
F11B	0.8461(11)	0.9086(5)	1.3611(4)	0.113(3)
F12B	0.8826(13)	0.8947(8)	1.2022(8)	0.0550(16)
F13B	0.7059(4)	0.7930(8)	1.2163(7)	0.105(3)
F14B	0.8834(10)	0.7047(5)	1.1502(4)	0.097(2)
F15B	0.8467(16)	0.7135(11)	1.3125(12)	0.104(4)
F16B	1.0258(5)	0.8141(6)	1.2963(7)	0.090(2)

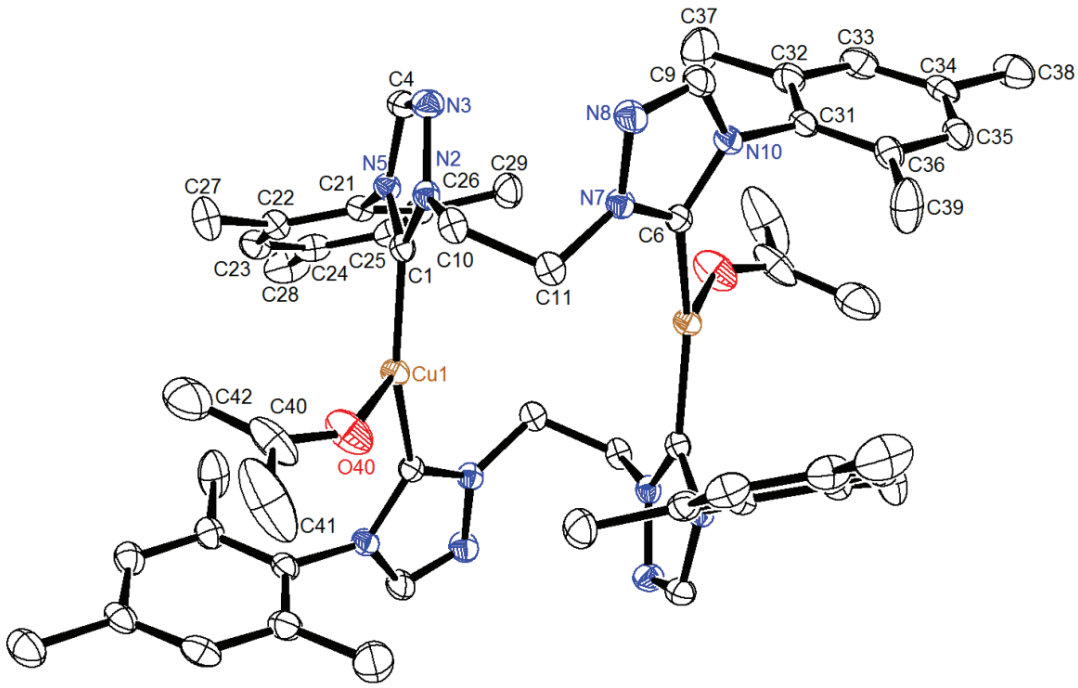

Figure 2.16.1: ORTEP plot of bis{μ-[1,1'-(ethane-1,2-diyl)bis(4-(2,4,6-trimethylphenyl)-1*H*-1,2,4-triazol-5-ylidene)]-κC,κC'}dicopper(I) bis(hexafluorophosphate) with two associated acetone molecules (**111** • 2 acetone) (hydrogen atoms are omitted for clarity).[1]

2.17 Bis(μ-acetato-κO,κO')-μ-{1,1'-(ethane-1,2-diyl)bis[4-(3,5-dimethylphenyl)-1*H*-1,2,4-triazol-5-ylidene]-κC,κC'}dicopper(I) (92p)

Name: Regina Berg (AK Straub)
Sample: rb340
File Name: reb19.*
Operator: F. Rominger (AK Hofmann)
Instrument: Bruker APEX-II Quazar

Table 2.17.1: Crystal data and structure refinement for reb19.

Identification code	reb19
Empirical formula	$C_{31}H_{37.50}Cu_2N_{8.50}O_4$
Formula weight	720.28
Temperature	200(2) K
Wavelength	0.71073 Å
Crystal system	monoclinic
Space group	$P2_1/n$
Z	4
Unit cell dimensions	*a* = 13.0903(15) Å α = 90 deg. *b* = 13.1366(14) Å β = 94.839(3) deg. *c* = 20.261(2) Å γ = 90 deg.
Volume	3471.7(7) Å^3
Density (calculated)	1.38 g/cm^3
Absorption coefficient	1.27 mm^{-1}
Crystal shape	needle
Crystal size	0.70 x 0.06 x 0.05 mm^3
Crystal colour	colourless
Theta range for data collection	1.8 to 25.4 deg.
Index ranges	$-14 \le h \le 15$, $-15 \le k \le 15$, $-23 \le l \le 24$
Reflections collected	35181
Independent reflections	6317 (*R*(int) = 0.0725)
Observed reflections	4063 ($I > 2\sigma(I)$)
Absorption correction	Semi-empirical from equivalents
Max. and min. transmission	0.94 and 0.47
Refinement method	Full-matrix least-squares on F^2
Data/restraints/parameters	6317 / 102 / 457
Goodness-of-fit on F^2	1.06
Final *R* indices ($I > 2\sigma(I)$)	*R1* = 0.075, *wR2* = 0.187
Largest diff. peak and hole	1.18 and -0.49 eÅ^{-3}

Table 2.17.2: Atomic coordinates and equivalent isotropic displacement parameters ($Å^2$) for reb19. (U_{eq} is defined as one third of the trace of the orthogonalized U_{ij} tensor.)

Atom	x	y	z	U_{eq}
Cu1	0.1529(1)	0.7663(1)	0.2126(1)	0.0422(3)
Cu2	0.1624(1)	0.5937(1)	0.2838(1)	0.0441(3)
C1	0.2842(5)	0.8150(4)	0.1972(3)	0.0340(14)
N2	0.3764(4)	0.8208(4)	0.2360(2)	0.0373(12)
C3	0.4477(5)	0.8624(5)	0.1993(3)	0.0420(16)
N4	0.4113(4)	0.8847(4)	0.1405(3)	0.0473(14)
N5	0.3102(4)	0.8535(4)	0.1403(2)	0.0375(12)
C5	0.2407(5)	0.8791(5)	0.0838(3)	0.0414(16)
C6	0.2976(5)	0.5464(5)	0.2973(3)	0.0375(15)
N7	0.3775(4)	0.5384(4)	0.2562(3)	0.0422(13)
C8	0.4607(6)	0.4981(5)	0.2915(4)	0.0512(18)
N9	0.4428(4)	0.4782(4)	0.3517(3)	0.0486(15)
N10	0.3432(4)	0.5112(4)	0.3541(3)	0.0382(12)
C10	0.2913(5)	0.4904(5)	0.4142(3)	0.0412(16)
C11	0.3935(5)	0.7930(5)	0.3046(3)	0.0419(16)
C12	0.4903(5)	0.7558(5)	0.3270(3)	0.0468(17)
C13	0.5093(6)	0.7304(5)	0.3937(4)	0.056(2)
C14	0.4315(7)	0.7424(5)	0.4361(3)	0.057(2)
C15	0.3362(6)	0.7782(5)	0.4132(3)	0.0486(17)
C16	0.3179(5)	0.8051(5)	0.3460(3)	0.0400(15)
C17	0.6137(7)	0.6883(8)	0.4190(4)	0.087(3)
C18	0.2521(7)	0.7899(6)	0.4598(4)	0.067(2)
C21	0.3746(6)	0.5664(5)	0.1872(3)	0.0503(18)
C22	0.4638(7)	0.6037(6)	0.1631(4)	0.070(2)
C23	0.4652(9)	0.6250(8)	0.0969(5)	0.095(4)
C24	0.3773(10)	0.6127(7)	0.0563(4)	0.092(4)
C25	0.2863(8)	0.5792(6)	0.0784(4)	0.070(3)
C26	0.2881(6)	0.5536(5)	0.1467(4)	0.0542(19)
C27	0.5643(11)	0.6659(13)	0.0716(6)	0.161(7)
C28	0.1904(9)	0.5659(7)	0.0333(4)	0.092(3)
C31	0.0223(6)	0.5981(6)	0.1647(4)	0.056(2)
O31	0.0558(4)	0.6845(4)	0.1491(2)	0.0603(14)
O32	0.0494(4)	0.5504(4)	0.2153(3)	0.0629(15)
C32	-0.0563(8)	0.5478(8)	0.1157(5)	0.101(4)
C33	0.0350(5)	0.7570(6)	0.3283(4)	0.0530(18)
O33	0.0507(4)	0.8050(4)	0.2768(3)	0.0615(14)
O34	0.0753(4)	0.6726(4)	0.3446(2)	0.0565(13)
C34	-0.0342(7)	0.8055(8)	0.3741(5)	0.087(3)
N40	0.7104(14)	0.783(2)	0.2321(11)	0.147(9)
C40	0.7695(12)	0.8077(14)	0.1931(10)	0.072(5)
C41	0.8447(19)	0.824(3)	0.1571(13)	0.087(8)
N42	0.6757(15)	0.9858(19)	0.0520(10)	0.113(7)
C42	0.5907(16)	0.988(2)	0.0261(11)	0.105(7)
C43	0.5004(19)	1.031(3)	0.0138(11)	0.107(10)
N44	0.7443(18)	0.9451(16)	0.0709(9)	0.111(6)
C44	0.7915(16)	0.8778(16)	0.1002(11)	0.090(6)
C45	0.842(2)	0.809(3)	0.1349(11)	0.083(8)
N46	-0.1544(9)	0.5770(11)	0.3026(8)	0.177(6)
C46	-0.2307(14)	0.562(2)	0.2648(9)	0.312(15)
C47	-0.2813(19)	0.490(3)	0.2324(12)	0.40(2)

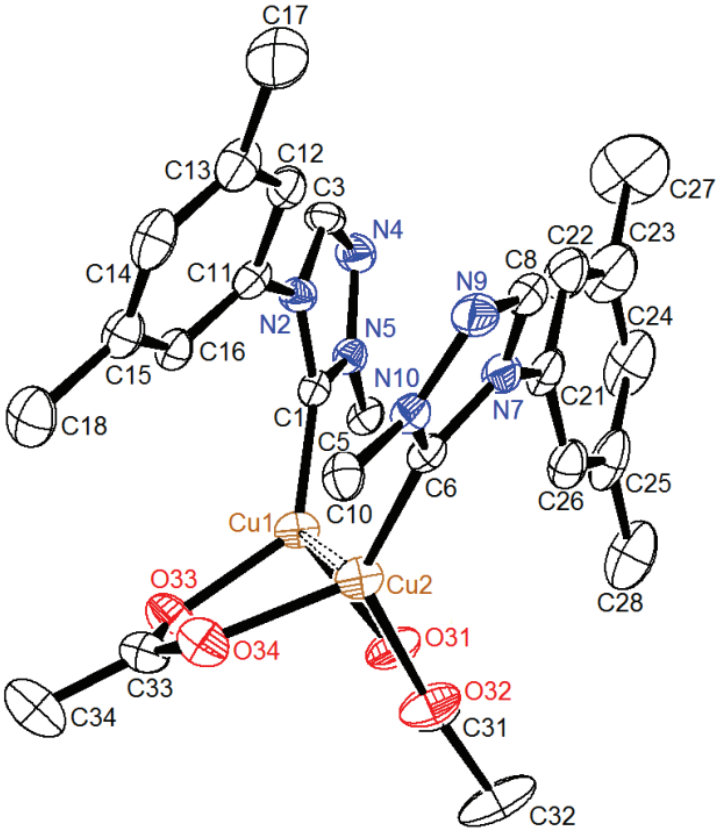

Figure 2.17.1: ORTEP plot of an excerpt from the coordination polymer of bis(μ-acetato-κ*O*,κ*O*')-μ-{1,1'-(ethane-1,2-diyl)bis[4-(3,5-dimethylphenyl)-1*H*-1,2,4-triazol-5-ylidene]-κ*C*,κ*C*'}dicopper(I) (**92p**) (hydrogen atoms are omitted for clarity).[1]

2.18 $[(ICy)_2Cu]PF_6$ (123)

Name:	Regina Berg (AK Straub)
Sample:	rb250
File Name:	reb15.*
Operator:	F. Rominger (AK Hofmann)
Instrument:	Bruker APEX-II CCD

Table 2.18.1: Crystal data and structure refinement for reb15.

Identification code	reb15
Empirical formula	$C_{34}H_{56}CuF_6N_4OP$
Formula weight	745.34
Temperature	200(2) K
Wavelength	0.71073 Å
Crystal system	monoclinic
Space group	$P2_1/n$
Z	4
Unit cell dimensions	*a* = 10.1187(11) Å α = 90 deg.

	b = 18.1662(19) Å β = 95.786(2) deg.
	c = 20.410(2) Å γ = 90 deg.
Volume	3732.6(7) Å^3
Density (calculated)	1.33 g/cm^3
Absorption coefficient	0.69 mm^{-1}
Crystal shape	polyhedron
Crystal size	0.15 x 0.14 x 0.06 mm^3
Crystal colour	colourless
Theta range for data collection	1.5 to 25.9 deg.
Index ranges	$-12 \le h \le 12$, $-22 \le k \le 22$, $-24 \le l \le 25$
Reflections collected	48953
Independent reflections	7223 (R(int) = 0.0404)
Observed reflections	5430 ($I > 2\sigma(I)$)
Absorption correction	Semi-empirical from equivalents
Max. and min. transmission	0.96 and 0.90
Refinement method	Full-matrix least-squares on F^2
Data/restraints/parameters	7223 / 476 / 453
Goodness-of-fit on F^2	1.03
Final R indices ($I > 2\sigma(I)$)	$R1$ = 0.046, $wR2$ = 0.114
Largest diff. peak and hole	0.65 and -0.30 eÅ^{-3}

Table 2.18.2: Atomic coordinates and equivalent isotropic displacement parameters (Å^2) for reb15. (U_{eq} is defined as one third of the trace of the orthogonalized U_{ij} tensor.)

Atom	x	y	z	U_{eq}
Cu1	0.5670(1)	0.8148(1)	0.1812(1)	0.0333(4)
C1	0.6408(8)	0.8766(5)	0.1191(4)	0.0332(19)
N2	0.7035(8)	0.8522(4)	0.0676(4)	0.0396(18)
C3	0.7519(12)	0.9104(6)	0.0340(5)	0.056(3)
C4	0.7185(11)	0.9719(6)	0.0638(5)	0.053(3)
N5	0.6514(8)	0.9507(4)	0.1164(4)	0.0388(18)
C6	0.5147(8)	0.7464(5)	0.2446(4)	0.0337(19)
N7	0.4534(7)	0.6805(4)	0.2330(4)	0.0358(16)
C8	0.4451(10)	0.6426(5)	0.2909(5)	0.044(2)
C9	0.5007(10)	0.6850(5)	0.3399(5)	0.044(2)
N10	0.5429(7)	0.7483(4)	0.3111(4)	0.0366(17)
C11	0.7173(10)	0.7733(5)	0.0518(5)	0.043(2)
C12	0.7082(14)	0.7603(7)	-0.0216(5)	0.068(3)
C13	0.7256(16)	0.6773(7)	-0.0357(7)	0.082(4)
C14	0.8531(14)	0.6478(7)	-0.0001(8)	0.083(5)
C15	0.8583(14)	0.6614(7)	0.0722(7)	0.075(4)
C16	0.8437(11)	0.7427(6)	0.0871(6)	0.058(3)
C21	0.5881(10)	1.0020(5)	0.1591(5)	0.040(2)
C22	0.4682(10)	1.0385(6)	0.1221(6)	0.051(3)
C23	0.4019(12)	1.0914(6)	0.1665(7)	0.065(3)
C24	0.5005(14)	1.1483(6)	0.1964(7)	0.070(4)
C25	0.6202(15)	1.1126(6)	0.2332(6)	0.070(4)
C26	0.6868(11)	1.0590(6)	0.1893(5)	0.052(3)
C31	0.4083(9)	0.6524(5)	0.1669(4)	0.0354(19)
C32	0.5042(10)	0.5954(7)	0.1455(5)	0.056(3)
C33	0.4582(11)	0.5676(8)	0.0761(6)	0.068(3)
C34	0.3217(12)	0.5352(6)	0.0733(6)	0.061(3)
C35	0.2248(10)	0.5911(6)	0.0948(6)	0.057(3)
C36	0.2684(9)	0.6215(6)	0.1639(5)	0.050(3)
C41	0.6088(9)	0.8096(5)	0.3493(4)	0.037(2)
C42	0.7496(9)	0.8218(6)	0.3328(5)	0.048(2)
C43	0.8142(11)	0.8835(6)	0.3750(6)	0.058(3)

C44	0.7338(11)	0.9538(6)	0.3679(6)	0.058(3)
C45	0.5926(11)	0.9412(6)	0.3831(6)	0.056(3)
C46	0.5272(10)	0.8794(5)	0.3409(5)	0.045(2)
P1	0.2591(4)	0.8162(2)	0.0187(2)	0.0472(12)
F11	0.1493(15)	0.8764(7)	0.0143(6)	0.138(6)
F12	0.3695(14)	0.8780(5)	0.0285(6)	0.133(6)
F13	0.2561(19)	0.8067(7)	0.0944(4)	0.122(5)
F14	0.3735(9)	0.7564(6)	0.0223(5)	0.094(3)
F15	0.1541(11)	0.7536(6)	0.0053(4)	0.094(4)
F16	0.2681(13)	0.8253(7)	-0.0580(4)	0.079(3)
P1B	0.240(6)	0.813(3)	0.024(3)	0.21(8)
F11B	0.094(5)	0.826(4)	0.002(3)	0.06(2)
F12B	0.261(7)	0.892(3)	0.048(3)	0.037(19)
F13B	0.202(7)	0.788(4)	0.091(3)	0.04(2)
F14B	0.390(5)	0.804(5)	0.039(4)	0.09(4)
F15B	0.239(8)	0.733(3)	-0.003(3)	0.06(2)
F16B	0.233(12)	0.840(5)	-0.047(3)	0.13(10)
O51	0.3750(13)	0.4661(6)	0.2862(7)	0.136(5)
C52	0.2729(15)	0.4197(7)	0.2660(9)	0.097(5)
C53	0.3256(18)	0.3493(10)	0.2470(10)	0.107(5)
C54	0.4477(19)	0.3442(13)	0.2828(12)	0.135(7)
C55	0.483(2)	0.4176(12)	0.3112(13)	0.162(11)

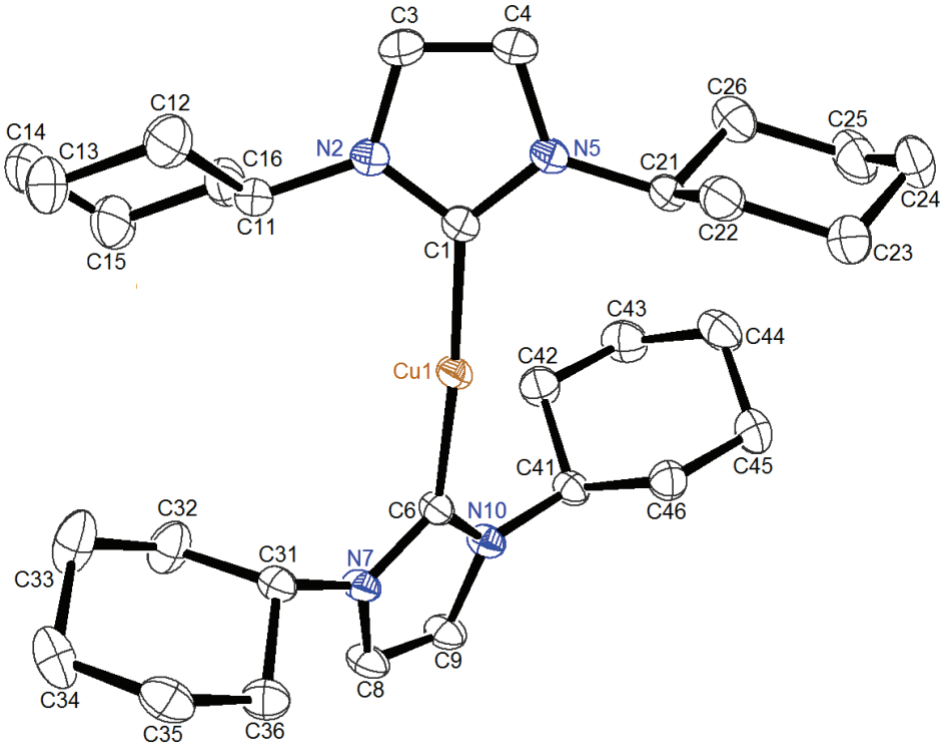

Figure 2.18.1: ORTEP plot of $[(ICy_2)Cu]PF_6$ (**123**) (hydrogen atoms and the counterion are omitted for clarity).

3 Gas Chromatographic Data

3.1 Determination of Response Factors

General Procedure: In separate experiments, different quantities of dodecane and the analyte in question were weighed into 1.5 ml clear glass vials by Shimadzu, which were then filled up with dichloromethane, closed with a screw cap equipped with a septum and subjected to the same GC method as the corresponding reaction mixture. The GC instrument was operated in the split mode with a split ratio of ten. Injection was carried out by an autosampling unit. The injection volume was always 1 µl of sample solution. The following temperature programs were used for GC analyses (Table 3.1.1).

Table 3.1.1: Temperature programs used for GC measurements.

Method 1

rate [°C min^{-1}]	temperature [°C]	hold time [min]
–	60	3.50
8.00	260	8.00
40.00	300	3.00

Method 2

rate [°C min^{-1}]	temperature [°C]	hold time [min]
–	60	3.50
10.00	250	3.00

Method 3

rate [°C min^{-1}]	temperature [°C]	hold time [min]
–	60	3.50
10.00	250	10.00
15.00	295	5.00

For quantitation, all peak areas in the chromatogram were measured. In order to compensate for varying sample volumes, the analytes' peak areas were divided by the peak area of the internal standard, whose concentration was constant for all samples.

The results of all calibration measurements are summarized below (Table 3.1.2).

Table 3.1.2: Response factors for analytes with respect to dodecane.

substance	method	response factor
benzyl azide	*1*	1.8271
benzyl azide	*2*	1.8494
1-benzyl-4-phenyl-1*H*-1,2,3-triazole	*1*	0.8044
1-benzyl-4-ethanoat-1*H*-1,2,3-triazole	*2*	1.5633
1-benzyl-4-hexyl-1*H*-1,2,3-triazole	*2*	1.1662
2-(1-benzyl-1*H*-1,2,3-triazol-4-yl)propan-2-ol	*2*	1.4774
4,4'-(azidomethylene)bis(methylbenzene)	*3*	1.2893
1-(di-4-tolylmethyl)-4-phenyl-1*H*-1,2,3-triazole	*3*	1.3338
ethyl-1-(di-4-tolylmethyl)-1*H*-1,2,3-triazole-4-carboxylate	*3*	2.1949

3.1.1 Response Factors for Benzyl Azide

weighted samples

No.	*m* (benzyl azide) [mg]	*n* (benzyl azide) [mmol]	*m* (dodecane) [mg]	*n* (dodecane) [mmol]	$\frac{n\text{ (benzyl azide)}}{n\text{ (dodecane)}}$
0	0.00	0.00000	0.00	0.00000	0.00
1	1.23	0.00924	1.92	0.01127	0.82
2	1.35	0.01014	1.91	0.01121	0.90
3	2.49	0.01870	1.92	0.01127	1.66
4	1.55	0.01164	1.87	0.01098	1.06
5	0.40	0.00300	2.44	0.01432	0.21
6	0.99	0.00744	1.90	0.01115	0.67
7	0.15	0.00113	1.81	0.01063	0.11
8	1.74	0.01307	1.84	0.01080	1.21
9	1.93	0.01449	1.84	0.01080	1.34

10	3.05	0.02291	1.91	0.01121	2.04
11	2.35	0.01765	1.88	0.01104	1.60
12	2.74	0.02058	1.90	0.01115	1.84

integral measurements with GC method *1*

No.	integral (benzyl azide) [a.u.] t_R = 9.716 min	integral (dodecane) [a.u.] t_R = 11.809 min	$\frac{\text{integral (benzyl azide)}}{\text{integral (dodecane)}}$
0	0.0000	0.0000	0.00
1	0.4923	1.1802	0.42
2	0.5417	1.1307	0.48
3	1.0307	1.1317	0.91
4	0.6300	1.1056	0.57
5	0.1408	1.2277	0.11
6	0.3848	1.1441	0.34
7	0.0451	1.0656	0.04
8	0.7112	1.0869	0.65
9	0.7961	1.1023	0.72
10	1.3032	1.1393	1.14
11	0.9794	1.1183	0.88
12	1.1273	1.0971	1.03

linear fit: y = 1.8271 x, R^2 = 0.9977

weighted samples

No.	*m* (benzyl azide) [mg]	*n* (benzyl azide) [mmol]	*m* (dodecane) [mg]	*n* (dodecane) [mmol]	$\frac{n \text{ (benzyl azide)}}{n \text{ (dodecane)}}$
0	0.00	0.00000	0.00	0.00000	0.00
1	1.23	0.00924	1.92	0.01127	0.82
2	1.35	0.01014	1.91	0.01121	0.90
3	2.49	0.01870	1.92	0.01127	1.66
4	1.55	0.01164	1.87	0.01098	1.06
5	0.40	0.00300	2.44	0.01432	0.21
6	0.99	0.00744	1.90	0.01115	0.67
7	0.15	0.00113	1.81	0.01063	0.11
8	1.74	0.01307	1.84	0.01080	1.21
9	1.93	0.01449	1.84	0.01080	1.34

10	3.05	0.02291	1.91	0.01121	2.04
11	2.35	0.01765	1.88	0.01104	1.60
12	2.74	0.02058	1.90	0.01115	1.84

integral measurements with GC method *2*

No.	integral (benzyl azide) [a.u.] t_R = 8.676 min	integral (dodecane) [a.u.] t_R = 10.345 min	$\frac{\text{integral (benzyl azide)}}{\text{integral (dodecane)}}$
0	0.0000	0.0000	0.00
1	0.4774	1.1387	0.42
2	0.5268	1.1114	0.47
3	0.9892	1.1029	0.90
4	0.6185	1.0906	0.57
5	0.1431	1.2118	0.12
6	0.3793	1.1318	0.34
7	0.0448	1.0580	0.04
8	0.6769	1.0457	0.65
9	0.7561	1.0441	0.72
10	1.2443	1.1097	1.12
11	0.9337	1.0800	0.86
12	1.0873	1.0729	1.01

linear fit: y = 1.8494 x, R^2 = 0.9985

3.1.2 Response Factor for 1–Benzyl-4-phenyl-1*H*-1,2,3–triazole

weighted samples

No.	*m* (triazole) [mg]	*n* (triazole) [mmol]	*m* (dodecane) [mg]	*n* (dodecane) [mmol]	$\frac{n\text{ (triazole)}}{n\text{ (dodecane)}}$
0	0.00	0.00000	0.00	0.00000	0.00
1	0.58	0.00247	1.41	0.00828	0.30
2	0.99	0.00421	1.49	0.00875	0.48
3	1.24	0.00527	1.49	0.00875	0.60
4	1.59	0.00676	1.44	0.00845	0.80
5	2.32	0.00986	1.74	0.01022	0.97

6	1.75	0.00744	1.42	0.00834	0.89
7	2.06	0.00876	1.38	0.00810	1.08
8	2.65	0.01126	1.32	0.00775	1.45
9	3.12	0.01326	1.45	0.00851	1.56
10	0.31	0.00132	1.73	0.01016	0.13
11	0.16	0.00068	1.44	0.00845	0.08
12	0.75	0.00319	1.42	0.00834	0.38

integral measurements with GC method *1*

No.	integral (triazole) [a.u.] t_R = 27.759 min	integral (dodecane) [a.u.] t_R = 11.802 min	$\frac{\text{integral (triazole)}}{\text{integral (dodecane)}}$
0	0.0000	0.0000	0.00
1	0.8390	0.3028	0.36
2	0.9018	0.5469	0.61
3	0.8153	0.6261	0.77
4	0.8062	0.7919	0.98
5	0.9647	1.1276	1.17
6	0.7843	0.8817	1.12
7	0.7500	1.0234	1.36
8	0.7381	1.3060	1.77
9	0.8035	1.5802	1.97
10	0.9539	0.1448	0.15
11	0.7699	0.0514	0.07
12	0.7938	0.3872	0.49

linear fit: y = 0.8044 x, R^2 = 0.9988

3.1.3 Response Factor for 1-Benzyl-4-ethanoat-1*H*-1,2,3-triazole

weighted samples

No.	*m* (triazole) [mg]	*n* (triazole) [mmol]	*m* (dodecane) [mg]	*n* (dodecane) [mmol]	$\frac{n\text{ (triazole)}}{n\text{ (dodecane)}}$
0	0.00	0.00000	0.00	0.00000	0.00
1	0.09	0.00078	1.64	0.01004	0.05
2	0.29	0.00510	1.50	0.01022	0.19
3	1.04	0.00195	1.63	0.01010	0.64
4	0.51	0.00381	1.50	0.01016	0.34
5	1.58	0.01085	1.44	0.01010	1.10
6	1.23	0.00774	1.50	0.01215	0.82
7	2.07	0.00973	1.51	0.01016	1.37
8	2.50	0.00627	1.50	0.00951	1.67
9	2.99	0.01319	1.46	0.00998	2.05
10	2.83	0.00921	1.51	0.00910	1.87
11	1.75	0.00026	1.48	0.01016	1.18
12	0.80	0.01176	1.48	0.01004	0.54

integral measurements with GC method *2*

No.	integral (triazole) [a.u.] t_R = 21.040 min	integral (dodecane) [a.u.] t_R = 10.332 min	$\frac{\text{integral (triazole)}}{\text{integral (dodecane)}}$
0	0.0000	0.0000	0.00
1	0.0249	0.9236	0.03
2	0.1170	0.8490	0.14
3	0.3810	0.9627	0.40
4	0.1728	0.8788	0.20
5	0.5465	0.7764	0.70
6	0.4493	0.8269	0.54
7	0.7047	0.8221	0.86
8	0.8633	0.812	1.06
9	1.0086	0.7988	1.26
10	1.0112	0.8099	1.25
11	0.6243	0.8101	0.77
12	0.2785	0.7901	0.35

linear fit: y = 1.5633 x, R^2 = 0.9972

3.1.4 Response Factor for 1-Benzyl-4-hexyl-1*H*-1,2,3-triazole

weighted samples

No.	*m* (triazole) [mg]	*n* (triazole) [mmol]	*m* (dodecane) [mg]	*n* (dodecane) [mmol]	$\frac{n\text{ (triazole)}}{n\text{ (dodecane)}}$
0	0.00	0.00000	0	0	0.00
1	0.08	0.00078	1.69	0.01004	0.05
2	0.47	0.00510	1.77	0.01022	0.27
3	1.01	0.00195	1.85	0.01010	0.55
4	1.98	0.00381	1.82	0.01016	1.09
5	0.70	0.01085	1.81	0.01010	0.39
6	1.73	0.00774	1.71	0.01215	1.01
7	2.94	0.00973	1.78	0.01016	1.65
8	1.59	0.00627	1.64	0.00951	0.97
9	2.46	0.01319	1.65	0.00998	1.49
10	2.24	0.00921	1.64	0.00910	1.37
11	1.27	0.00026	1.61	0.01016	0.79
12	0.26	0.01176	1.83	0.01004	0.14

integral measurements with GC method *2*

No.	integral (triazole) [a.u.] t_R = 21.329 min	integral (dodecane) [a.u.] t_R = 10.340 min	$\frac{\text{integral (triazole)}}{\text{integral (dodecane)}}$
0	0.0000	0.0000	0.00
1	0.0699	0.9463	0.07
2	0.2456	0.9790	0.25
3	0.4635	1.0303	0.45
4	0.9301	1.0121	0.92
5	0.3212	1.0420	0.31
6	0.8446	0.9464	0.89
7	1.3614	1.0046	1.36
8	0.7491	0.8932	0.84
9	1.1882	0.897	1.32

10	1.1161	0.9518	1.17
11	0.6492	0.934	0.70
12	0.1099	1.0052	0.11

linear fit: y = 1.1662 x, R^2 = 0.9965

3.1.5 Response Factor for 2-(1-Benzyl-1*H*-1,2,3-triazol-4-yl)propan-2-ol

weighted samples

No.	*m* (triazole) [mg]	*n* (triazole) [mmol]	*m* (dodecane) [mg]	*n* (dodecane) [mmol]	$\frac{n\text{ (triazole)}}{n\text{ (dodecane)}}$
0	0.00	0.00000	0.00	0.00000	0.00
1	0.11	0.00051	1.78	0.01004	0.06
2	0.73	0.00336	1.83	0.01022	0.40
3	0.24	0.00110	1.75	0.01010	0.14
4	1.08	0.00497	1.73	0.01016	0.62
5	2.00	0.00921	1.79	0.01010	1.12
6	1.79	0.00824	1.83	0.01215	0.98
7	3.03	0.01395	1.82	0.01016	1.66
8	2.31	0.01063	1.65	0.00951	1.40
9	1.58	0.00727	1.83	0.00998	0.86
10	2.55	0.01174	1.70	0.00910	1.50
11	2.77	0.01275	1.75	0.01016	1.58
12	0.49	0.00226	1.78	0.01004	0.28

integral measurements with GC method *2*

No.	integral (triazole) [a.u.] t_R = 18.696 min	integral (dodecane) [a.u.] t_R = 10.338 min	$\frac{\text{integral (triazole)}}{\text{integral (dodecane)}}$
0	0.0000	0.0000	0.00
1	0.0461	1.0349	0.04
2	0.2636	1.0213	0.26
3	0.0962	0.9799	0.10
4	0.4049	0.9529	0.42
5	0.7286	0.9959	0.73

6	0.7025	1.0225	0.69
7	1.1150	0.9797	1.14
8	0.8789	0.9357	0.94
9	0.6142	1.0200	0.60
10	0.9964	0.9718	1.03
11	0.9971	0.9520	1.05
12	0.1934	0.9989	0.19

linear fit: y = 1.4774 x, R^2 = 0.9987

3.1.6 Response Factor for 4,4'-(Azidomethylene)bis(methylbenzene)

weighted samples

No.	*m* (azide) [mg]	*n* (azide) [mmol]	*m* (dodecane) [mg]	*n* (dodecane) [mmol]	$\frac{n\text{ (azide)}}{n\text{ (dodecane)}}$
0	0.00	0.00000	0.00	0.00000	0.00
1	1.56	0.00657	1.80	0.01004	0.87
2	0.19	0.00080	1.82	0.01022	0.10
3	0.62	0.00261	1.79	0.01010	0.35
4	1.31	0.00552	1.80	0.01016	0.73
5	1.65	0.00695	1.74	0.01010	0.95
6	1.07	0.00451	1.77	0.01215	0.60
7	2.00	0.00843	1.86	0.01016	1.08
8	2.44	0.01028	1.92	0.00951	1.27
9	2.16	0.00910	1.91	0.00998	1.13
10	2.71	0.01142	1.96	0.00910	1.38
11	3.19	0.01344	1.98	0.01016	1.61
12	0.80	0.00337	1.93	0.01004	0.41

integral measurements with GC method *3*

No.	integral (azide) [a.u.] t_R = 18.635 min	integral (dodecane) [a.u.] t_R = 9.873 min	$\frac{\text{integral (azide)}}{\text{integral (dodecane)}}$
0	0.0000	0.0000	0.00
1	0.6739	1.0172	0.66
2	0.0593	0.9921	0.06
3	0.2601	0.9445	0.28
4	0.5776	1.0467	0.55
5	0.7383	0.9844	0.75
6	0.4833	0.9994	0.48
7	0.8965	1.0672	0.84
8	1.0690	1.0752	0.99
9	0.9484	1.0920	0.87
10	1.1576	1.0836	1.07
11	1.3729	1.0967	1.25
12	0.3108	1.0807	0.29

linear fit: y = 1.2893 x, R^2 = 0.9986

3.1.7 Response Factor for 1-(Di-4-tolylmethyl)-4-phenyl-1*H*-1,2,3-triazole

weighted samples

No.	*m* (triazole) [mg]	*n* (triazole) [mmol]	*m* (dodecane) [mg]	*n* (dodecane) [mmol]	$\frac{n\text{ (triazole)}}{n\text{ (dodecane)}}$
0	0.00	0.00000	0.00	0.00000	0.00
1	0.16	0.00047	1.89	0.01004	0.08
2	0.51	0.00150	1.75	0.01022	0.29
3	2.25	0.00663	1.85	0.01010	1.22
4	1.20	0.00354	1.94	0.01016	0.62
5	0.10	0.00029	2.02	0.01010	0.05
6	1.78	0.00524	1.95	0.01215	0.91
7	1.48	0.00436	2.00	0.01016	0.74
8	0.97	0.00286	1.85	0.00951	0.52
9	1.98	0.00583	2.24	0.00998	0.88

10	2.91	0.00857	1.99	0.00910	1.46
11	2.82	0.00831	1.80	0.01004	1.57

integral measurements with GC method *3*

No.	integral (triazole) [a.u.] t_R = 31.811	integral (dodecane) [a.u.] t_R = 9.869	$\frac{\text{integral (triazole)}}{\text{integral (dodecane)}}$
0	0.0000	0.0000	0.00
1	0.0818	1.0985	0.07
2	0.2067	1.0118	0.20
3	0.9100	1.0283	0.88
4	0.4824	1.1176	0.43
5	0.0557	1.1117	0.05
6	0.6981	1.0486	0.67
7	0.632	1.1040	0.57
8	0.4137	1.0245	0.40
9	0.8088	1.2407	0.65
10	1.2433	1.1159	1.11
11	1.2676	1.0609	1.19

linear fit: y = 1.13338 x, R^2 = 0.9978

3.1.8 Response Factor for Ethyl-1-(di-4-tolylmethyl)-1*H*-1,2,3-triazole-4-carboxylate

weighted samples

No.	*m* (triazole) [mg]	*n* (triazole) [mmol]	*m* (dodecane) [mg]	*n* (dodecane) [mmol]	$\frac{n\text{ (triazole)}}{n\text{ (dodecane)}}$
0	0.00	0.00000	0.00	0.00000	0.00
1	2.21	0.00659	1.87	0.01004	1.18
2	0.25	0.00075	1.87	0.01022	0.13
3	2.77	0.00826	1.88	0.01010	1.47
4	1.00	0.00298	1.95	0.01016	0.51
5	1.52	0.00453	1.89	0.01010	0.80
6	0.04	0.00012	1.79	0.01215	0.02

7	1.71	0.00510	1.94	0.01016	0.88
8	0.71	0.00212	1.83	0.00951	0.39
9	0.45	0.00134	1.72	0.00998	0.26
10	1.21	0.00361	1.81	0.00910	0.67
11	2.45	0.00730	1.88	0.00910	1.30
12	1.98	0.00590	1.92	0.01004	1.03

integral measurements with GC method *3*

No.	integral (triazole) [a.u.] t_R = 25.665 min	integral (dodecane) [a.u.] t_R = 9.870 min	$\frac{\text{integral (triazole)}}{\text{integral (dodecane)}}$
0	0.0000	0.0000	0.00
1	0.5961	1.1368	0.52
2	0.0639	0.9691	0.07
3	0.7360	1.0802	0.68
4	0.2496	1.0816	0.23
5	0.3877	1.039	0.37
6	0.0162	0.9378	0.02
7	0.4405	1.1113	0.40
8	0.1833	0.9739	0.19
9	0.1268	1.0029	0.13
10	0.2989	1.0358	0.29
11	0.5752	0.9743	0.59
12	0.5011	1.0489	0.48

linear fit: y = 2.1949 x, R^2 = 0.9984

3.2 Catalytic Test Reactions

3.2.1 Variation of Catalyst

*3.2.1.1 Reaction of Phenylacetylene and Benzyl Azide with 0.5 mol-% of Catalyst Complex **91***

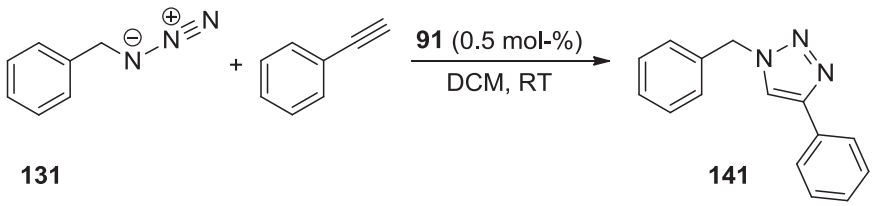

131 **141**

time [min]	alkyne t_R = 4.796 integral [a.u.]	azide t_R = 9.681 integral [a.u.]	dodecane t_R = 11.754 integral [a.u.]	triazole t_R = 27.712 integral [a.u.]	alkyne norm. integral [a.u.]	azide norm. integral [a.u.]	triazole norm. integral [a.u.]
0	0.2034	0.1783	0.1862	0.0000	1.0924	0.9576	0.0000
1	0.0696	0.0565	0.0683	0.0055	1.0190	0.8272	0.0805
3	0.0591	0.0457	0.0627	0.0162	0.9426	0.7289	0.2584
5	0.0581	0.0456	0.0700	0.0322	0.8300	0.6514	0.4600
7	0.0470	0.0373	0.0672	0.0415	0.6994	0.5551	0.6176
10	0.0461	0.0362	0.0786	0.0618	0.5865	0.4606	0.7863
15	0.0346	0.0234	0.0744	0.0899	0.4651	0.3145	1.2083
20	0.0235	0.0149	0.0734	0.1032	0.3202	0.2030	1.4060
25	0.0157	0.0087	0.0737	0.1192	0.2130	0.1180	1.6174
30	0.0093	0.0052	0.0741	0.1348	0.1255	0.0702	1.8192
35	0.0053	0.0029	0.0761	0.1505	0.0696	0.0381	1.9777
40	0.0035	0.0010	0.0685	0.1396	0.0511	0.0146	2.0380
45	0.0027	0.0005	0.0692	0.1398	0.0390	0.0072	2.0202
50	0.0010	0.0004	0.0816	0.1697	0.0123	0.0049	2.0797
55	0.0000	0.0001	0.0790	0.1687	0.0000	0.0013	2.1354
60	0.0000	0.0000	0.0819	0.1746	0.0000	0.0000	2.1319
65	0.0000	0.0000	0.0767	0.1703	0.0000	0.0000	2.2203

Correction with response factors

time [min]	azide *f* = 1.8271 [a.u.]	triazole *f* = 0.8044 [a.u.]	conversion [%]
0	1.7496	0.000	0.0
1	1.5114	0.065	4.1
3	1.3317	0.208	13.5
5	1.1902	0.370	23.7
7	1.0141	0.497	32.9
10	0.8415	0.632	42.9
15	0.5747	0.972	62.8
20	0.3709	1.131	75.3
25	0.2157	1.301	85.8
30	0.1282	1.463	91.9
35	0.0696	1.591	95.8
40	0.0267	1.639	98.4
45	0.0132	1.625	99.2
50	0.0090	1.673	99.5
55	0.0023	1.718	99.9
60	0.0000	1.715	100.0
65	0.0000	1.786	100.0

*3.2.1.2 Reaction of Phenylacetylene and Benzyl Azide with 0.5 mol-% of Catalyst Complex **92***

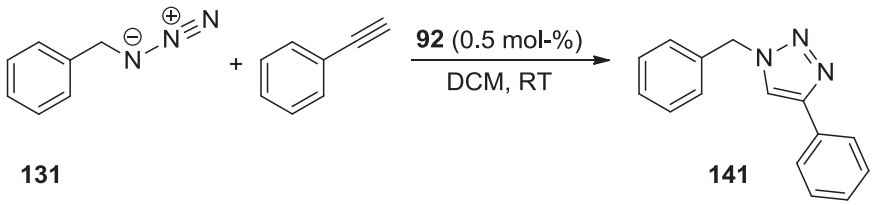

131 **141**

time [min]	alkyne t_R = 4.848 integral [a.u.]	azide t_R = 9.745 integral [a.u.]	dodecane t_R = 11.773 integral [a.u.]	triazole t_R = 27.731 integral [a.u.]	alkyne norm. integral [a.u.]	azide norm. integral [a.u.]	triazole norm. integral [a.u.]
0	0.0431	0.0370	0.0473	0.0000	0.9112	0.7822	0.0000
1	0.0522	0.0414	0.0515	0.0071	1.0136	0.8039	0.1379
3	0.0478	0.0403	0.0520	0.0101	0.9192	0.7750	0.1942
5	0.0490	0.0417	0.0558	0.0143	0.8781	0.7473	0.2563
7	0.0384	0.0328	0.0474	0.0199	0.8101	0.6920	0.4198
10	0.0360	0.0312	0.0496	0.0257	0.7258	0.6290	0.5181
15	0.0243	0.0232	0.0464	0.0399	0.5237	0.5000	0.8599
20	0.0147	0.0157	0.0477	0.0627	0.3082	0.3291	1.3145
25	0.0115	0.0094	0.0497	0.0847	0.2314	0.1891	1.7042
30	0.0071	0.0042	0.0454	0.0864	0.1564	0.0925	1.9031
35	0.0041	0.0022	0.0487	0.0961	0.0842	0.0452	1.9733
40	0.0000	0.0010	0.0472	0.0963	0.0000	0.0212	2.0403
45	0.0000	0.0000	0.0472	0.1034	0.0000	0.0000	2.1907
50	0.0000	0.0000	0.0477	0.1075	0.0000	0.0000	2.2537
55	0.0000	0.0000	0.0465	0.1068	0.0000	0.0000	2.2968
60	0.0000	0.0000	0.0457	0.1032	0.0000	0.0000	2.2582
65	0.0000	0.0000	0.0533	0.1205	0.0000	0.0000	2.2608
70	0.0000	0.0000	0.0481	0.1132	0.0000	0.0000	2.3534

Correction with response factors

time [min]	azide *f* = 1.8271 [a.u.]	triazole *f* = 0.8044 [a.u.]	conversion [%]
0	1.4292	0.0000	0.0
1	1.4688	0.1109	7.0
3	1.4160	0.1562	9.9
5	1.3654	0.2061	13.1
7	1.2643	0.3377	21.1
10	1.1493	0.4168	26.6
15	0.9136	0.6917	43.1
20	0.6014	1.0574	63.7
25	0.3456	1.3709	79.9
30	0.1690	1.5308	90.1
35	0.0825	1.5873	95.1
40	0.0387	1.6412	97.7
45	0.0000	1.7622	100.0
50	0.0000	1.8129	100.0
55	0.0000	1.8475	100.0
60	0.0000	1.8165	100.0
65	0.0000	1.8186	100.0
70	0.0000	1.8931	100.0

*3.2.1.3 Reaction of Phenylacetylene and Benzyl Azide with 0.5 mol-% of Catalyst Complex **93***

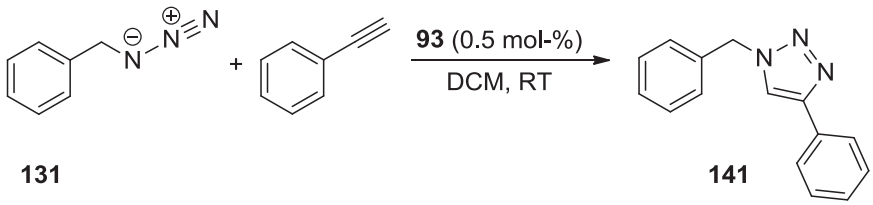

131 **141**

time [min]	alkyne t_R = 4.798 integral [a.u.]	azide t_R = 9.631 integral [a.u.]	dodecane t_R = 11.750 integral [a.u.]	triazole t_R = 27.702 integral [a.u.]	alkyne norm. integral [a.u.]	azide norm. integral [a.u.]	triazole norm. integral [a.u.]
0	0.1500	0.1308	0.1376	0.0000	1.0901	0.9506	0.0000
5	0.0582	0.0442	0.0582	0.0102	1.0000	0.7595	0.1753
10	0.0468	0.0346	0.0559	0.0328	0.8372	0.6190	0.5868
15	0.0335	0.0225	0.0530	0.0504	0.6321	0.4245	0.9509
20	0.0241	0.0161	0.0600	0.0785	0.4017	0.2683	1.3083
25	0.0134	0.0070	0.0532	0.0843	0.2519	0.1316	1.5846
30	0.0071	0.0040	0.0562	0.1044	0.1263	0.0712	1.8577
35	0.0041	0.0019	0.0565	0.1104	0.0726	0.0336	1.9540
40	0.0022	0.0006	0.0553	0.1112	0.0398	0.0108	2.0108
45	0.0022	0.0002	0.0580	0.1241	0.0379	0.0034	2.1397
50	0.0000	0.0000	0.0589	0.1186	0.0000	0.0000	2.0136
55	0.0000	0.0000	0.0608	0.1251	0.0000	0.0000	2.0576
60	0.0000	0.0000	0.0597	0.1270	0.0000	0.0000	2.1273

Correction with response factors

time [min]	azide f = 1.8271 [a.u.]	triazole f = 0.8044 [a.u.]	conversion [%]
0	1.7368	0.0000	0.0
5	1.3876	0.1410	9.2
10	1.1309	0.4720	29.4
15	0.7757	0.7649	49.7
20	0.4903	1.0524	68.2
25	0.2404	1.2746	84.1
30	0.1300	1.4943	92.0

35	0.0614	1.5718	96.2
40	0.0198	1.6175	98.8
45	0.0063	1.7211	99.6
50	0.0000	1.6197	100.0
55	0.0000	1.6551	100.0
60	0.0000	1.7112	100.0

3.2.1.4 Reaction of Phenylacetylene and Benzyl Azide with 2.0 mol-% of *Catalyst Complex **71***

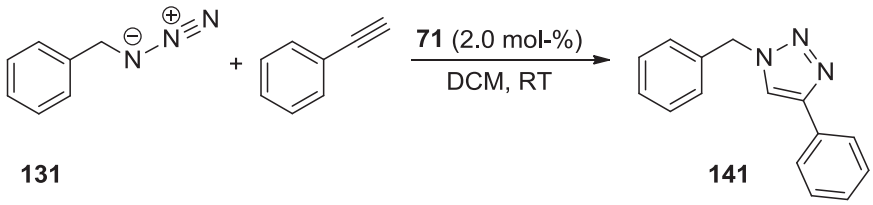

131 **141**

time [h]	alkyne t_R = 4.790 integral [a.u.]	azide t_R = 9.679 integral [a.u.]	dodecane t_R = 11.753 integral [a.u.]	triazole t_R = 27.709 integral [a.u.]	alkyne norm. integral [a.u.]	azide norm. integral [a.u.]	triazole norm. integral [a.u.]
0	0.2458	0.2259	0.2320	0.0000	1.0595	0.9737	0.0000
1	0.0729	0.0600	0.0705	0.0000	1.0340	0.8511	0.0000
2	0.0786	0.0656	0.0761	0.0000	1.0329	0.8620	0.0000
16	0.0673	0.0551	0.0667	0.0046	1.0090	0.8261	0.0690
20	0.0766	0.0677	0.0706	0.0036	1.0850	0.9589	0.0510
24	0.1143	0.0986	0.1103	0.0057	1.0363	0.8939	0.0517
42	0.0917	0.0810	0.0800	0.0040	1.1463	1.0125	0.0500
48	0.1031	0.0929	0.0939	0.0031	1.0980	0.9894	0.0330
72	0.1369	0.1338	0.1569	0.0270	0.8725	0.8528	0.1721
88	0.1198	0.1371	0.2351	0.1784	0.5096	0.5832	0.7588
94	0.0711	0.1281	0.3776	0.3706	0.1883	0.3392	0.9815
112	0.0000	0.0000	0.0310	0.0633	0.0000	0.0000	2.0419

Correction with response factors

time [min]	azide f = 1.8271 [a.u.]	triazole f = 0.8044 [a.u.]	conversion [%]
0	1.7791	0.000	0.0
1	1.5550	0.000	0.0
2	1.5750	0.000	0.0
16	1.5093	0.055	3.5
20	1.7520	0.041	2.3
24	1.6333	0.042	2.5
42	1.8499	0.040	2.1
48	1.8076	0.027	1.4
72	1.5581	0.138	8.2
88	1.0655	0.610	36.4
94	0.6198	0.789	56.0
112	0.0000	1.643	100.0

3.2.1.5 Reaction of Phenylacetylene and Benzyl Azide with 2.0 mol-% of *Catalyst Complex **81***

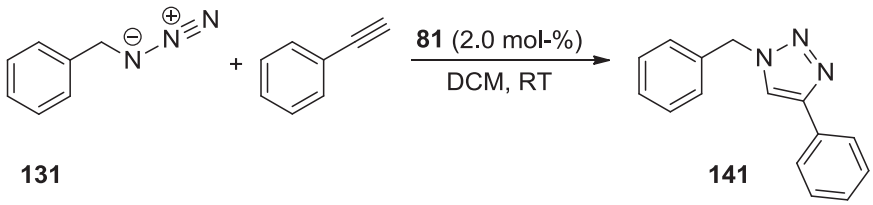

131 **141**

time [h]	alkyne t_R = 4.946 integral [a.u.]	azide t_R = 9.816 integral [a.u.]	dodecane t_R = 11.875 integral [a.u.]	triazole t_R = 27.810 integral [a.u.]	alkyne norm. integral [a.u.]	azide norm. integral [a.u.]	triazole norm. integral [a.u.]
0	0.0858	0.0795	0.0801	0.0000	1.0712	0.9925	0.0000
1	0.0629	0.0531	0.0576	0.0000	1.0920	0.9219	0.0000
2	0.0512	0.0421	0.0514	0.0000	0.9961	0.8191	0.0000
4	0.0507	0.0418	0.0480	0.0000	1.0563	0.8708	0.0000
27	0.0677	0.0541	0.0621	0.0000	1.0902	0.8712	0.0000
48	0.0754	0.0733	0.0844	0.0000	0.8934	0.8685	0.0000
72	0.0875	0.0699	0.0946	0.0000	0.9249	0.7389	0.0000

96	0.1074	0.1025	0.1068	0.0217	1.0056	0.9597	0.2032
104	0.0687	0.0623	0.0809	0.0271	0.8492	0.7701	0.3350
120	0.0897	0.0991	0.1592	0.1146	0.5634	0.6225	0.7198
129	0.0319	0.0419	0.1184	0.1369	0.2694	0.3539	1.1563
144	0.0029	0.0187	0.1314	0.1627	0.0221	0.1423	1.2382
152	0.0022	0.0088	0.0673	0.1463	0.0327	0.1308	2.1738
154	0.0000	0.0093	0.0781	0.1682	0.0000	0.1191	2.1536

Correction with response factors

time [h]	azide *f* = 1.8271 [a.u.]	triazole *f* = 0.8044 [a.u.]	conversion [%]
0	1.8134	0.0000	0.0
1	1.6844	0.0000	0.0
2	1.4965	0.0000	0.0
4	1.5911	0.0000	0.0
27	1.5917	0.0000	0.0
48	1.5868	0.0000	0.0
72	1.3500	0.0000	0.0
96	1.7535	0.1634	8.5
104	1.4070	0.2695	16.1
120	1.1373	0.5790	33.7
129	0.6466	0.9301	59.0
144	0.2600	0.9960	79.3
152	0.2389	1.7486	88.0
154	0.2176	1.7324	88.8

3.2.1.6 *Reaction of Phenylacetylene and Benzyl Azide with 2.0 mol-%* of *Catalyst Complex **83***

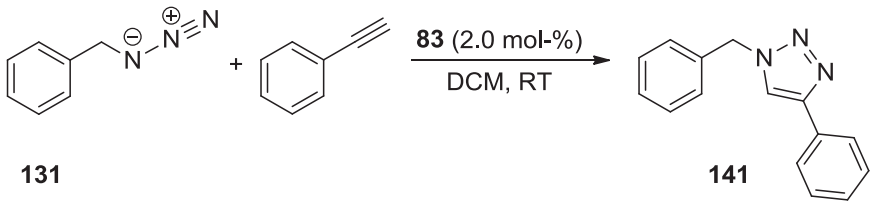

131 **141**

time [h]	alkyne t_R = 4.826 integral [a.u.]	azide t_R = 9.717 integral [a.u.]	dodecane t_R = 11.756 integral [a.u.]	triazole t_R = 27.713 integral [a.u.]	alkyne norm. integral [a.u.]	azide norm. integral [a.u.]	triazole norm. integral [a.u.]
0.25	0.0648	0.0500	0.0610	0.0000	1.0623	0.8197	0.0000
0.5	0.0621	0.0480	0.0596	0.0000	1.0419	0.8054	0.0000
1	0.0671	0.0534	0.0659	0.0000	1.0182	0.8103	0.0000
1.5	0.0748	0.0579	0.0732	0.0040	1.0219	0.7910	0.0546
2	0.0834	0.0659	0.0828	0.0099	1.0072	0.7959	0.1196
2.5	0.0801	0.0642	0.0844	0.0131	0.9491	0.7607	0.1552
3	0.0614	0.0475	0.0667	0.0131	0.9205	0.7121	0.1964
3.5	0.0583	0.0482	0.0702	0.0234	0.8305	0.6866	0.3333
4	0.0554	0.0431	0.0665	0.0254	0.8331	0.6481	0.3820
4.5	0.0687	0.0571	0.0920	0.0395	0.7467	0.6207	0.4293
5	0.0469	0.0373	0.0665	0.0358	0.7053	0.5609	0.5383
5.5	0.0506	0.0389	0.0739	0.0462	0.6847	0.5264	0.6252
6	0.0345	0.0268	0.0600	0.0417	0.5750	0.4467	0.6950
13	0.0219	0.0177	0.0716	0.0984	0.3059	0.2472	1.3743
14	0.0170	0.0117	0.0610	0.0939	0.2787	0.1918	1.5393
15	0.0159	0.0106	0.0706	0.1055	0.2252	0.1501	1.4943
16	0.0124	0.0086	0.0681	0.1173	0.1821	0.1263	1.7225
17	0.0123	0.0078	0.0734	0.1178	0.1676	0.1063	1.6049
18	0.0075	0.0034	0.0605	0.1095	0.1240	0.0562	1.8099
19	0.0042	0.0022	0.0522	0.0958	0.0805	0.0421	1.8352
20	0.0038	0.0021	0.0601	0.1119	0.0632	0.0349	1.8619
22	0.0046	0.0023	0.0826	0.1653	0.0557	0.0278	2.0012

Correction with response factors

time [h]	azide *f* = 1.8271 [a.u.]	triazole *f* = 0.8044 [a.u.]	conversion [%]
0.25	1.4976	0.0000	0.0
0.5	1.4715	0.0000	0.0
1	1.4805	0.0000	0.0
1.5	1.4452	0.0440	3.0
2	1.4542	0.0962	6.2
2.5	1.3898	0.1249	8.2
3	1.3012	0.1580	10.8
3.5	1.2545	0.2681	17.6
4	1.1842	0.3072	20.6
4.5	1.1340	0.3454	23.3
5	1.0248	0.4330	29.7
5.5	0.9618	0.5029	34.3
6	0.8161	0.5591	40.7
13	0.4517	1.1055	71.0
14	0.3504	1.2382	77.9
15	0.2743	1.2020	81.4
16	0.2307	1.3856	85.7
17	0.1942	1.2910	86.9
18	0.1027	1.4559	93.4
19	0.0770	1.4763	95.0
20	0.0638	1.4977	95.9
22	0.0509	1.6098	96.9

3.2.2 Variation of Substrates

*3.2.2.1 Reaction of Ethyl Propiolate and Benzyl Azide with 0.5 mol-% of Catalyst Complex **92***

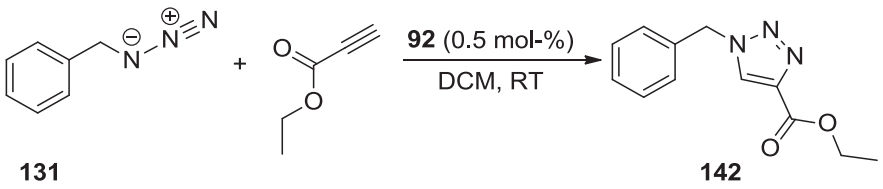

131 **142**

time [min]	alkyne t_R = 2.478 integral [a.u.]	azide t_R = 8.660 integral [a.u.]	dodecane t_R = 10.306 integral [a.u.]	triazole t_R = 21.008 integral [a.u.]	alkyne norm. integral [a.u.]	azide norm. integral [a.u.]	triazole norm. integral [a.u.]
0	0.0562	0.1259	0.1340	0.0000	0.4194	0.9396	0.0000
1	0.0167	0.0347	0.0519	0.0033	0.3218	0.6686	0.0636
3	0.0120	0.0250	0.0517	0.0166	0.2321	0.4836	0.3211
5	0.0060	0.0117	0.0418	0.0267	0.1435	0.2799	0.6388
7	0.0046	0.0088	0.0523	0.0474	0.0880	0.1683	0.9063
11	0.0033	0.0063	0.0681	0.0748	0.0485	0.0925	1.0984
13	0.0001	0.0021	0.0503	0.0636	0.0020	0.0417	1.2644
15	0.0000	0.0000	0.0452	0.0623	0.0000	0.0000	1.3783
17	0.0000	0.0000	0.0464	0.0672	0.0000	0.0000	1.4483

Correction with response factors

time [min]	azide f = 1.8494 [a.u.]	triazole f = 1.5633 [a.u.]	conversion [%]
0	1.7376	0.0000	0.0
1	1.2365	0.0994	7.4
3	0.8943	0.5019	35.9
5	0.5177	0.9986	65.9
7	0.3112	1.4168	82.0
11	0.1711	1.7171	90.9
13	0.0772	1.9767	96.2
15	0.0000	2.1547	100.0

3.2.2.2 Reaction of 1-Octyne and Benzyl Azide with 0.5 mol-% of Catalyst Complex ***92***

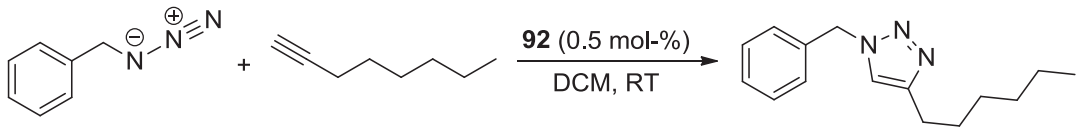

131 **143**

time [min]	alkyne t_R = 3.744 integral [a.u.]	azide t_R = 8.722 integral [a.u.]	dodecane t_R = 10.316 integral [a.u.]	triazole t_R = 23.315 integral [a.u.]	alkyne norm. integral [a.u.]	azide norm. integral [a.u.]	triazole norm. integral [a.u.]
0	0.0930	0.0823	0.0944	0.0000	0.9852	0.8718	0.0000
1	0.0435	0.0400	0.0503	0.0019	0.8648	0.7952	0.0378
3	0.0416	0.0340	0.0488	0.0057	0.8525	0.6967	0.1168
5	0.0403	0.0326	0.0499	0.0104	0.8076	0.6533	0.2084
7	0.0364	0.0299	0.0508	0.0171	0.7165	0.5886	0.3366
10	0.0264	0.0216	0.0407	0.0193	0.6486	0.5307	0.4742
15	0.0226	0.0175	0.0491	0.0427	0.4603	0.3564	0.8697
20	0.0131	0.0082	0.0448	0.0545	0.2924	0.1830	1.2165
25	0.0082	0.0077	0.0468	0.0734	0.1752	0.1645	1.5684
30	0.0033	0.0048	0.0448	0.0780	0.0737	0.1071	1.7411
35	0.0022	0.0027	0.0440	0.0830	0.0500	0.0614	1.8864
40	0.0000	0.0018	0.0477	0.0935	0.0000	0.0377	1.9602
45	0.0000	0.0012	0.0493	0.0983	0.0000	0.0243	1.9939
50	0.0000	0.0000	0.0430	0.0877	0.0000	0.0000	2.0395
55	0.0000	0.0000	0.0474	0.0975	0.0000	0.0000	2.0570

Correction with response factors

time [min]	azide f = 1.8494 [a.u.]	triazole f = 1.1662 [a.u.]	conversion [%]
0	1.6123	0.0000	0.0
1	1.4707	0.0441	2.9
3	1.2885	0.1362	9.6
5	1.2082	0.2431	16.7
7	1.0885	0.3926	26.5

10	0.9815	0.5530	36.0
15	0.6592	1.0142	60.6
20	0.3385	1.4187	80.7
25	0.3043	1.8290	85.7
30	0.1982	2.0304	91.1
35	0.1135	2.1999	95.1
40	0.0698	2.2859	97.0
45	0.0450	2.3253	98.1
50	0.0000	2.3785	100.0
55	0.0000	2.3988	100.0

*3.2.2.3 Reaction of 2-Methylbut-3-yn-2-ol and Benzyl Azide with 0.5 mol-% of Catalyst Complex **92***

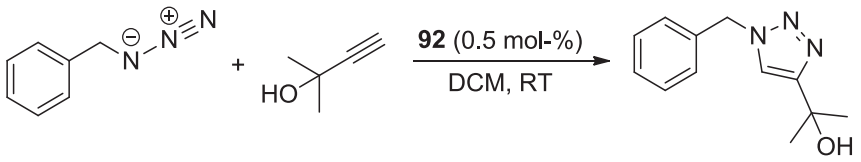

131 **144**

time [min]	alkyne t_R = 1.934 integral [a.u.]	azide t_R = 8.694 integral [a.u.]	dodecane t_R = 10.318 integral [a.u.]	triazole t_R = 18.641 integral [a.u.]	alkyne norm. integral [a.u.]	azide norm. integral [a.u.]	triazole norm. integral [a.u.]
0	0.0191	0.0511	0.0624	0.0000	0.3061	0.8189	0.0000
1	0.0259	0.0381	0.0529	0.0000	0.4896	0.7202	0.0000
3	0.0212	0.0352	0.0557	0.0074	0.3806	0.6320	0.1329
5	0.0226	0.0330	0.0593	0.0152	0.3811	0.5565	0.2563
7	0.0194	0.0279	0.0562	0.0203	0.3452	0.4964	0.3612
10	0.0158	0.0220	0.0526	0.0276	0.3004	0.4183	0.5247
15	0.0090	0.0160	0.0547	0.0390	0.1645	0.2925	0.7130
20	0.0079	0.0120	0.0535	0.0480	0.1477	0.2243	0.8972
25	0.0041	0.0083	0.0531	0.0517	0.0772	0.1563	0.9736
30	0.0053	0.0056	0.0552	0.0582	0.0960	0.1014	1.0543
35	0.0044	0.0060	0.0522	0.0608	0.0843	0.1149	1.1648
40	0.0025	0.0047	0.0537	0.0644	0.0466	0.0875	1.1993
45	0.0025	0.0033	0.0533	0.0672	0.0469	0.0619	1.2608
50	0.0021	0.0025	0.0551	0.0734	0.0381	0.0454	1.3321
55	0.0016	0.0019	0.0560	0.0775	0.0286	0.0339	1.3839

60	0.0000	0.0019	0.0527	0.0721	0.0000	0.0361	1.3681
65	0.0000	0.0004	0.0439	0.0613	0.0000	0.0091	1.3964
70	0.0000	0.0000	0.0526	0.0762	0.0000	0.0000	1.4487

Correction with response factors

time [min]	azide f = 1.8494 [a.u.]	triazole f = 1.4774 [a.u.]	conversion [%]
0	1.5145	0.0000	0.0
1	1.3320	0.0000	0.0
3	1.1687	0.1963	14.4
5	1.0292	0.3787	26.9
7	0.9181	0.5337	36.8
10	0.7735	0.7752	50.1
15	0.5410	1.0534	66.1
20	0.4148	1.3255	76.2
25	0.2891	1.4384	83.3
30	0.1876	1.5577	89.3
35	0.2126	1.7208	89.0
40	0.1619	1.7718	91.6
45	0.1145	1.8627	94.2
50	0.0839	1.9681	95.9
55	0.0627	2.0446	97.0
60	0.0667	2.0213	96.8
65	0.0006	2.0630	100.0
70	0.0000	2.1403	100.0

*3.2.2.4 Reaction of Phenylacetylene and 4,4'-(Azidomethylene)bis(methylbenzene) with 0.5 mol-% of Catalyst Complex **92***

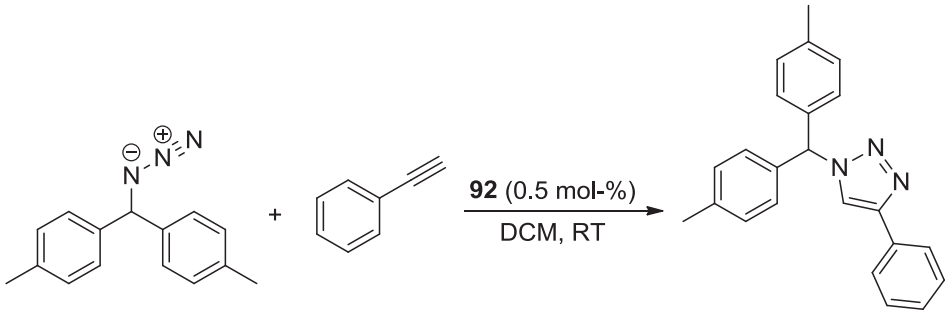

133 **145**

time [min]	alkyne t_R = 4.458 integral [a.u.]	dodecane t_R = 9.855 integral [a.u.]	azide t_R = 18.626 integral [a.u.]	triazole t_R = 31.832 integral [a.u.]	alkyne norm. integral [a.u.]	azide norm. integral [a.u.]	triazole norm. integral [a.u.]
0	0.1367	0.2155	0.2771	0.0000	0.7777	1.2858	0.0000
15	0.0482	0.0824	0.1059	0.0008	0.7781	1.2852	0.0097
30	0.0420	0.0765	0.0910	0.0047	0.8407	1.1895	0.0614
45	0.0400	0.0820	0.0867	0.0178	0.9458	1.0573	0.2171
60	0.0297	0.0815	0.0687	0.0371	1.1863	0.8429	0.4552
75	0.0224	0.0861	0.0533	0.0652	1.6154	0.6190	0.7573
90	0.0124	0.0781	0.0287	0.0759	0.1588	0.3675	0.9718
105	0.0063	0.0808	0.0191	0.0950	0.0780	0.2364	1.1757
120	0.0069	0.0808	0.0122	0.1093	0.0854	0.1510	1.3527
135	0.0039	0.0792	0.0074	0.1120	0.0492	0.0934	1.4141
150	0.0000	0.0850	0.0049	0.1225	0.0000	0.0576	1.4412
165	0.0000	0.0838	0.0025	0.1275	0.0000	0.0298	1.5215
180	0.0000	0.0875	0.0022	0.1328	0.0000	0.0251	1.5177
195	0.0000	0.0790	0.0014	0.1207	0.0000	0.0177	1.5278
210	0.0000	0.0821	0.0008	0.1293	0.0000	0.0097	1.5749
225	0.0000	0.0810	0.0000	0.1283	0.0000	0.0000	1.5840
240	0.0000	0.0890	0.0000	0.1417	0.0000	0.0000	1.5921

Correction with response factors

time [min]	azide *f* = 1.2893 [a.u.]	triazole *f* = 2.1949 [a.u.]	conversion [%]
0	1.6578	0.0000	0.0
15	1.6570	0.0129	0.8
30	1.5337	0.0819	5.1
45	1.3632	0.2895	17.5
60	1.0868	0.6072	35.8
75	0.7981	1.0100	55.9
90	0.4738	1.2962	73.2
105	0.3048	1.5682	83.7
120	0.1947	1.8043	90.3
135	0.1205	1.8862	94.0
150	0.0743	1.9222	96.3
165	0.0385	2.0293	98.1
180	0.0324	2.0243	98.4
195	0.0228	2.0378	98.9
210	0.0126	2.1006	99.4
225	0.0000	2.1127	100.0
240	0.0000	2.1236	100.0

*3.2.2.5 Reaction of Ethyl Propiolate and 4,4'-(Azidomethylene)bis(methylbenzene) with 0.5 mol-% of Catalyst Complex **92***

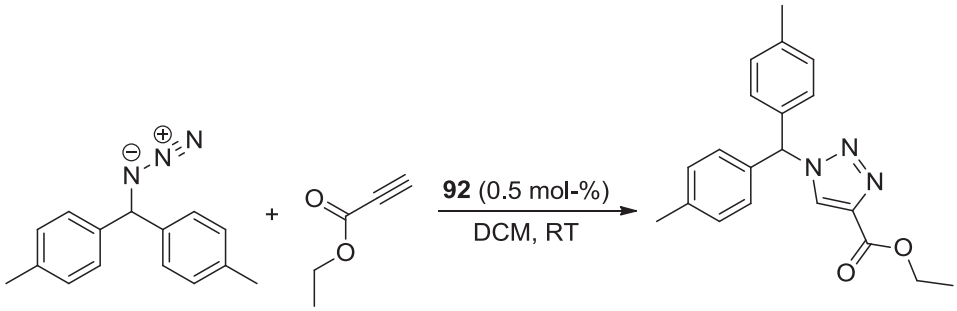

133 **146**

time [min]	alkyne t_R = 2.486 integral [a.u.]	dodecane t_R = 9.850 integral [a.u.]	azide t_R = 18.624 integral [a.u.]	triazole t_R = 25.600 integral [a.u.]	alkyne norm. integral [a.u.]	azide norm. integral [a.u.]	triazole norm. integral [a.u.]
0	0.0630	0.2199	0.3111	0.0000	0.2865	1.4147	0.0000
1	0.0205	0.0784	0.1081	0.0023	0.2615	1.3788	0.0293
3	0.0145	0.0758	0.0792	0.0163	0.1913	1.0449	0.2150
5	0.0087	0.0739	0.0426	0.0332	0.1177	0.5765	0.4493
7	0.0036	0.0803	0.0222	0.0593	0.0448	0.2765	0.7385
9	0.0000	0.0784	0.0070	0.0710	0.0000	0.0893	0.9056
11	0.0000	0.0601	0.0007	0.0661	0.0000	0.0116	1.0998
13	0.0000	0.0625	0.0000	0.0721	0.0000	0.0000	1.1536
15	0.0000	0.0712	0.0000	0.0805	0.0000	0.0000	1.1306
17	0.0000	0.0682	0.0000	0.0730	0.0000	0.0000	1.0704
20	0.0000	0.0641	0.0000	0.0703	0.0000	0.0000	1.0967

Correction with response factors

time [min]	azide f = 1.8494 [a.u.]	triazole f = 2.1949 [a.u.]	conversion [%]
0	1.8240	0.0000	0.0
1	1.7777	0.0644	3.5
3	1.3471	0.4720	25.9
5	0.7432	0.9861	57.0
7	0.3564	1.6209	82.0
9	0.1151	1.9877	94.5

11	0.0150	2.4140	99.4
13	0.0000	2.5320	100.0
15	0.0000	2.4816	100.0
17	0.0000	2.3494	100.0
20	0.0000	2.4072	100.0

3.2.3 Variation of Solvent

*3.2.3.1 Reaction of Phenylacetylene and Benzyl Azide in Tetrahydrofuran with 0.5 mol-% of Catalyst Complex **92***

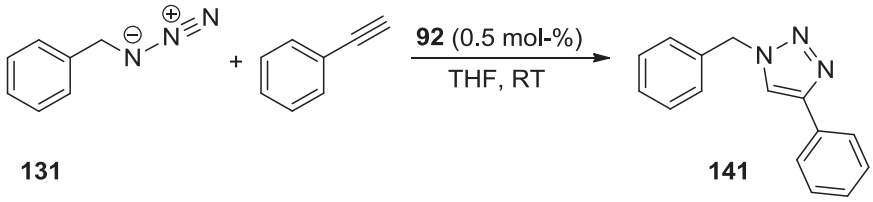

131 **141**

time [min]	alkyne t_R = 4.825 integral [a.u.]	azide t_R = 9.704 integral [a.u.]	dodecane t_R = 11.768 integral [a.u.]	triazole t_R = 27.713 integral [a.u.]	alkyne norm. integral [a.u.]	azide norm. integral [a.u.]	triazole norm. integral [a.u.]
0	0.1516	0.1197	0.1294	0.0000	1.1716	0.9250	0.0000
15	0.0594	0.0456	0.0605	0.0091	0.9818	0.7537	0.1504
30	0.0509	0.0367	0.0547	0.0165	0.9305	0.6709	0.3016
45	0.0478	0.0334	0.0564	0.0255	0.8475	0.5922	0.4521
60	0.0411	0.0290	0.0513	0.0286	0.8012	0.5653	0.5575
75	0.0274	0.0168	0.0373	0.0247	0.7346	0.4504	0.6622
90	0.0247	0.0149	0.0370	0.0258	0.6676	0.4027	0.6973
105	0.0378	0.0235	0.0589	0.0555	0.6418	0.3990	0.9423
120	0.0191	0.0092	0.0331	0.0290	0.5770	0.2779	0.8761
135	0.0293	0.0185	0.0569	0.0613	0.5149	0.3251	1.0773
150	0.0258	0.0146	0.0533	0.0711	0.4841	0.2739	1.3340
165	0.0186	0.0099	0.0456	0.0575	0.4079	0.2171	1.2610
180	0.0216	0.0120	0.0575	0.0755	0.3757	0.2087	1.3130
195	0.0168	0.0088	0.0541	0.0747	0.3105	0.1627	1.3808
210	0.0065	0.0019	0.0261	0.0332	0.2490	0.0728	1.2720
225	0.0103	0.0045	0.0533	0.0883	0.1932	0.0844	1.6567
240	0.0063	0.0020	0.0480	0.0808	0.1313	0.0417	1.6833
255	0.0051	0.0013	0.0677	0.1275	0.0753	0.0192	1.8833

270	0.0000	0.0000	0.0440	0.0830	0.0000	0.0000	1.8864
285	0.0000	0.0000	0.0541	0.1190	0.0000	0.0000	2.1996

Correction with response factors

time [min]	azide *f* = 1.8271 [a.u.]	triazole *f* = 0.8044 [a.u.]	conversion [%]
0	1.6901	0.000	0.0
15	1.3771	0.121	8.1
30	1.2259	0.243	16.5
45	1.0820	0.364	25.2
60	1.0329	0.448	30.3
75	0.8229	0.533	39.3
90	0.7358	0.561	43.3
105	0.7290	0.758	51.0
120	0.5078	0.705	58.1
135	0.5940	0.867	59.3
150	0.5005	1.073	68.2
165	0.3967	1.014	71.9
180	0.3813	1.056	73.5
195	0.2972	1.111	78.9
210	0.1330	1.023	88.5
225	0.1543	1.333	89.6
240	0.0761	1.354	94.7
255	0.0351	1.515	97.7
270	0.0000	1.517	100.0
285	0.0000	1.769	100.0

*3.2.3.2 Reaction of Phenylacetylene and Benzyl Azide in Acetonitrile with 0.5 mol-% of Catalyst Complex **92***

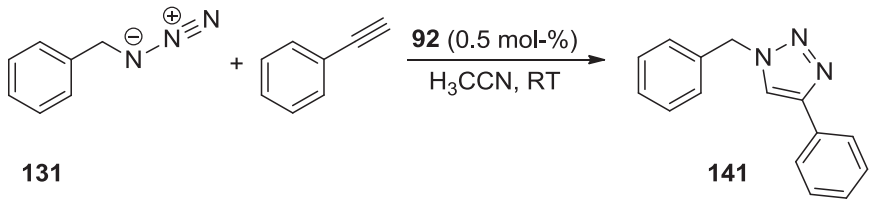

131 **141**

time [min]	toluene t_R = 3.019 integral [a.u.]	alkyne t_R = 4.827 integral [a.u.]	azide t_R = 9.720 integral [a.u.]	triazole t_R = 27.763 integral [a.u.]	alkyne norm. integral [a.u.]	azide norm. integral [a.u.]	triazole norm. integral [a.u.]
0	0.0787	0.0886	0.0843	0.0000	1.1258	1.0712	0.0000
5	0.0502	0.0375	0.0275	0.0183	0.7470	0.5478	0.3645
10	0.0470	0.0219	0.0188	0.0546	0.4660	0.4000	1.1617
15	0.0435	0.0146	0.0150	0.0483	0.3356	0.3448	1.1103
20	0.0568	0.0118	0.0129	0.0771	0.2077	0.2271	1.3574
25	0.0292	0.0035	0.0054	0.0429	0.1199	0.1849	1.4692
30	0.0525	0.0036	0.0043	0.0545	0.0686	0.0819	1.0381
35	0.0526	0.0000	0.0000	0.0610	0.0000	0.0000	1.1597
40	0.0404	0.0000	0.0000	0.0407	0.0000	0.0000	1.0074
45	0.0496	0.0000	0.0000	0.0548	0.0000	0.0000	1.1048

As dodecane is not miscible with acetonitrile, toluene was used as internal standard instead. The response factors could not be applied in this case, as they had been determined relative to dodecane as standard. Moreover, the product triazole precipitated during the course of the reaction. Thus, the concentration of the product triazole in the samples taken *via* syringe has always been too low and thus, a reliable time-conversion relationship could not be established.

3.2.3.3 *Reaction of Phenylacetylene and Benzyl Azide in Acetone with 0.5 mol-% of Catalyst Complex **92***

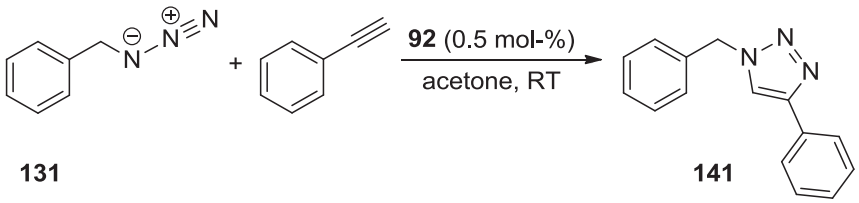

131 **141**

time [min]	alkyne t_R = 4.834 integral [a.u.]	azide t_R = 9.739 integral [a.u.]	dodecane t_R = 11.756 integral [a.u.]	triazole t_R = 27.712 integral [a.u.]	alkyne norm. integral [a.u.]	azide norm. integral [a.u.]	triazole norm. integral [a.u.]
0	0.1443	0.1282	0.1329	0.0000	1.0858	0.9646	0.0000
5	0.0425	0.0361	0.0434	0.0000	0.9793	0.8318	0.0000
15	0.0194	0.0155	0.0252	0.0054	0.7698	0.6151	0.2143
30	0.0160	0.0135	0.0301	0.0229	0.5316	0.4485	0.7608
45	0.0132	0.0109	0.0353	0.0403	0.3739	0.3088	1.1416
60	0.0110	0.0082	0.0336	0.0421	0.3274	0.2440	1.2530
75	0.0056	0.0075	0.0409	0.0596	0.1369	0.1834	1.4572
90	0.0047	0.0045	0.0541	0.0803	0.0869	0.0832	1.4843
105	0.0015	0.0009	0.0350	0.0404	0.0429	0.0257	1.1543
120	0.0000	0.0000	0.0480	0.0789	0.0000	0.0000	1.6438
135	0.0000	0.0000	0.0263	0.0355	0.0000	0.0000	1.3498

The product triazole precipitated during the course of the reaction. Thus, the concentration of the product triazole in the samples taken *via* syringe has always been too low and thus, a reliable time-conversion relationship could not be established.

*3.2.3.4 Reaction of Phenylacetylene and Benzyl Azide in Dimethyl Sulphoxide with 0.5 mol-% of Catalyst Complex **92***

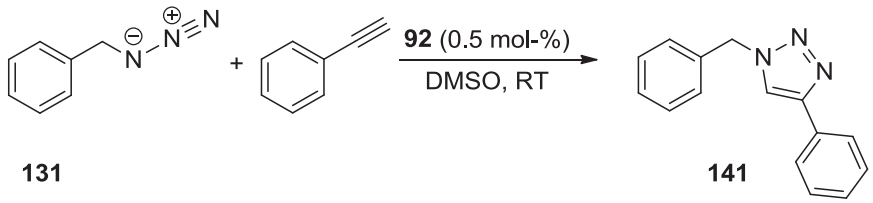

131 **141**

time [min]	toluene t_R = 3.026 integral [a.u.]	alkyne t_R = 4.816 integral [a.u.]	azide t_R = 9.693 integral [a.u.]	triazole t_R = 27.729 integral [a.u.]	alkyne norm. integral [a.u.]	azide norm. integral [a.u.]	triazole norm. integral [a.u.]
0	0.1465	0.1718	0.1423	0.0000	1.1727	0.9713	0.0000
30	0.0506	0.0653	0.0394	0.0000	1.2905	0.7787	0.0000
60	0.0513	0.0620	0.0414	0.0000	1.2086	0.8070	0.0000
120	0.0674	0.0758	0.0511	0.0127	1.1246	0.7582	0.1884
180	0.0470	0.0562	0.0355	0.0180	1.1957	0.7553	0.3830
240	0.0570	0.0609	0.0398	0.0219	1.0684	0.6982	0.3842
300	0.0479	0.0453	0.0264	0.0252	0.9457	0.5511	0.5261
360	0.0571	0.0496	0.0295	0.0368	0.8687	0.5166	0.6445
420	0.0539	0.0417	0.0254	0.0452	0.7737	0.4712	0.8386
480	0.0570	0.0399	0.0200	0.0464	0.7000	0.3509	0.8140
510	0.0458	0.0371	0.0178	0.0511	0.8100	0.3886	1.1157
540	0.0564	0.0388	0.0192	0.0665	0.6879	0.3404	1.1791
570	0.0514	0.0355	0.0121	0.0598	0.6907	0.2354	1.1634
600	0.0448	0.0000	0.0130	0.0486	0.0000	0.2902	1.0848
630	0.0481	0.0027	0.0111	0.0547	0.0561	0.2308	1.1372
660	0.0466	0.0033	0.0093	0.0617	0.0708	0.1996	1.3240
720	0.0490	0.0001	0.0082	0.0715	0.0020	0.1673	1.4592

As dodecane is not miscible with dimethyl sulphoxide, toluene was used as internal standard instead. The response factors could not be applied in this case, as they had been determined relative to dodecane as standard.

3.2.4 Variation of Catalyst Concentration

*3.2.4.1 Catalytic Reaction of Phenylacetylene and Benzyl Azide with 0.75 mol-% of Catalyst Complex **92***

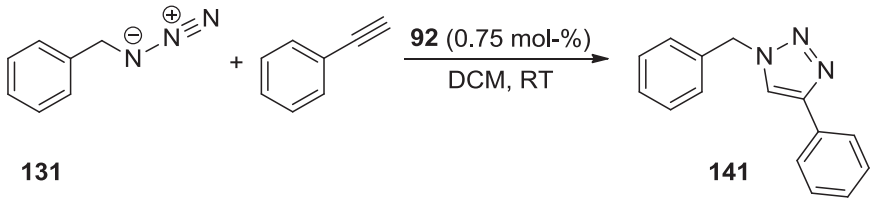

131 **141**

time [min]	alkyne t_R = 4.811 integral [a.u.]	azide t_R = 9.693 integral [a.u.]	dodecane t_R = 11.754 integral [a.u.]	triazole t_R = 27.710 integral [a.u.]	alkyne norm. integral [a.u.]	azide norm. integral [a.u.]	triazole norm. integral [a.u.]
0	0.1076	0.0947	0.1020	0.0000	1.0549	0.9284	0.0000
5	0.0531	0.0407	0.0551	0.0133	0.9637	0.7387	0.2414
10	0.0362	0.0257	0.0532	0.0429	0.6805	0.4831	0.8064
11	0.0285	0.0200	0.0490	0.0456	0.5816	0.4082	0.9306
12	0.0283	0.0200	0.0553	0.0547	0.5118	0.3617	0.9892
13	0.0205	0.0127	0.0448	0.0514	0.4576	0.2835	1.1473
15	0.0191	0.0120	0.0560	0.0808	0.3411	0.2143	1.4429
20	0.0084	0.0037	0.0576	0.1056	0.1458	0.0642	1.8333
25	0.0026	0.0006	0.0507	0.1058	0.0513	0.0118	2.0868
30	0.0000	0.0000	0.0535	0.1181	0.0000	0.0000	2.2075
35	0.0000	0.0000	0.0527	0.1170	0.0000	0.0000	2.2201

Correction with response factors

time [min]	azide f = 1.8271 [a.u.]	triazole f = 0.8044 [a.u.]	conversion [%]	integral triazole [%]
0	1.6963	0.0000	0.0	0.0
5	1.3496	0.1942	12.6	10.9
10	0.8826	0.6487	42.4	36.3
11	0.7458	0.7486	50.1	41.9
12	0.6608	0.7957	54.6	44.6
13	0.5180	0.9229	64.1	51.7
15	0.3915	1.1606	74.8	65.0

20	0.1174	1.4747	92.6	82.6
25	0.0216	1.6786	98.7	94.0
30	0.0000	1.7757	100.0	99.4
35	0.0000	1.7859	100.0	100.0

*3.2.4.2 Reaction of Phenylacetylene and Benzyl Azide with 0.62 mol-% of Catalyst Complex **92***

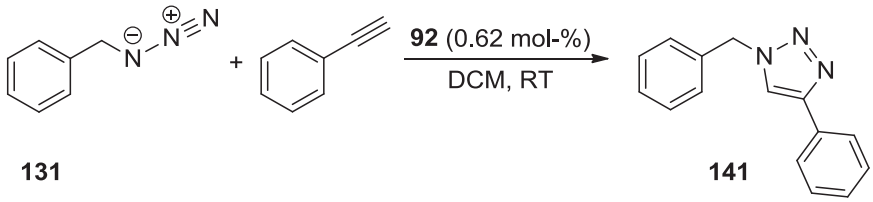

131 **141**

time [min]	alkyne t_R = 4.818 integral [a.u.]	azide t_R = 9.702 integral [a.u.]	dodecane t_R = 11.759 integral [a.u.]	triazole t_R = 27.717 integral [a.u.]	alkyne norm. integral [a.u.]	azide norm. integral [a.u.]	triazole norm. integral [a.u.]
0	0.1077	0.0895	0.0963	0.0000	1.1184	0.9294	0.0000
5	0.0571	0.0433	0.0543	0.0060	1.0516	0.7974	0.1105
10	0.0443	0.0326	0.0548	0.0288	0.8084	0.5949	0.5255
13	0.0369	0.0268	0.0578	0.0476	0.6384	0.4637	0.8235
15	0.0268	0.0180	0.0514	0.0506	0.5214	0.3502	0.9844
17	0.0230	0.0138	0.0496	0.0638	0.4637	0.2782	1.2863
19	0.0180	0.0106	0.0544	0.0760	0.3309	0.1949	1.3971
22	0.0126	0.0065	0.0580	0.0951	0.2172	0.1121	1.6397
25	0.0096	0.0043	0.0640	0.1240	0.1500	0.0672	1.9375
30	0.0045	0.0011	0.0601	0.1236	0.0749	0.0183	2.0566
35	0.0038	0.0006	0.0856	0.1786	0.0444	0.0070	2.0864
40	0.0000	0.0000	0.0872	0.1795	0.0000	0.0000	2.0585
45	0.0000	0.0000	0.0822	0.1704	0.0000	0.0000	2.0730

Correction with response factors

time [min]	azide f = 1.8271 [a.u.]	triazole f = 0.8044 [a.u.]	conversion [%]	integral triazole [%]
0	1.6981	0.0000	0.0	0.0
5	1.4570	0.0889	5.7	5.3
10	1.0869	0.4228	28.0	25.2
13	0.8472	0.6624	43.9	39.5
15	0.6398	0.7919	55.3	47.2
17	0.5083	1.0347	67.1	61.6
19	0.3560	1.1238	75.9	67.0
22	0.2048	1.3189	86.6	78.6
25	0.1228	1.5585	92.7	92.9
30	0.0334	1.6543	98.0	98.6
35	0.0128	1.6783	99.2	100.0
40	0.0000	1.6558	100.0	-
45	0.0000	1.6675	100.0	-

*3.2.4.3 Reaction of Phenylacetylene and Benzyl Azide with 0.50 mol-% of Catalyst Complex **92***

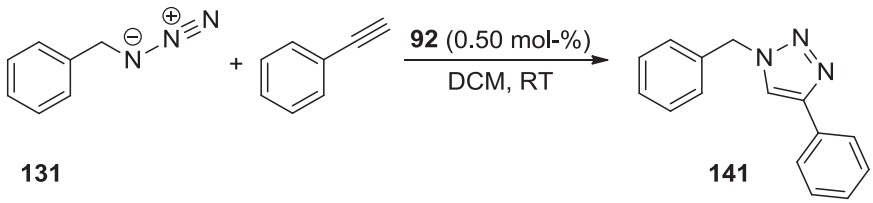

131 **141**

time [min]	alkyne t_R = 4.820 integral [a.u.]	azide t_R = 9.703 integral [a.u.]	dodecane t_R = 11.762 integral [a.u.]	triazole t_R = 27.721 integral [a.u.]	alkyne norm. integral [a.u.]	azide norm. integral [a.u.]	triazole norm. integral [a.u.]
0	0.1032	0.0843	0.0909	0.0000	1.1353	0.9274	0.0000
5	0.0692	0.0555	0.0674	0.0050	1.0267	0.8234	0.0742
10	0.0586	0.0459	0.0657	0.0206	0.8919	0.6986	0.3135
15	0.0446	0.0333	0.0645	0.0459	0.6915	0.5163	0.7116
16	0.0424	0.0317	0.0660	0.0568	0.6424	0.4803	0.8606
17	0.0410	0.0292	0.0677	0.0641	0.6056	0.4313	0.9468
18	0.0357	0.0265	0.0671	0.0703	0.5320	0.3949	1.0477

19	0.0348	0.0235	0.0651	0.0746	0.5346	0.3610	1.1459
20	0.0322	0.0230	0.0675	0.0791	0.4770	0.3407	1.1719
22	0.0264	0.0163	0.0627	0.0853	0.4211	0.2600	1.3604
25	0.0171	0.0097	0.0560	0.0922	0.3054	0.1732	1.6464
30	0.0114	0.0053	0.0610	0.1130	0.1869	0.0869	1.8525
35	0.0071	0.0026	0.0638	0.1260	0.1113	0.0408	1.9749
45	0.0000	0.0000	0.0622	0.1329	0.0000	0.0000	2.1367
50	0.0000	0.0000	0.0600	0.1323	0.0000	0.0000	2.2050
55	0.0000	0.0000	0.0671	0.1454	0.0000	0.0000	2.1669

Correction with response factors

time [min]	azide *f* = 1.8271 [a.u.]	triazole *f* = 0.8044 [a.u.]	conversion [%]	integral triazole [%]
0	1.6944	0.000	0.0	0.0
5	1.5045	0.060	3.8	3.4
10	1.2765	0.252	16.5	14.2
15	0.9433	0.572	37.8	32.3
16	0.8776	0.692	44.1	39.0
17	0.7881	0.762	49.1	42.9
18	0.7216	0.843	53.9	47.5
19	0.6596	0.922	58.3	52.0
20	0.6226	0.943	60.2	53.1
22	0.4750	1.094	69.7	61.7
25	0.3165	1.324	80.7	74.7
30	0.1587	1.490	90.4	84.0
35	0.0745	1.589	95.5	89.6
45	0.0000	1.719	100.0	96.9
50	0.0000	1.774	100.0	100.0
55	0.0000	1.743	100.0	-

3.2.4.4 *Catalytic Reaction of Phenylacetylene and Benzyl Azide with 0.37 mol-% of Catalyst Complex **92***

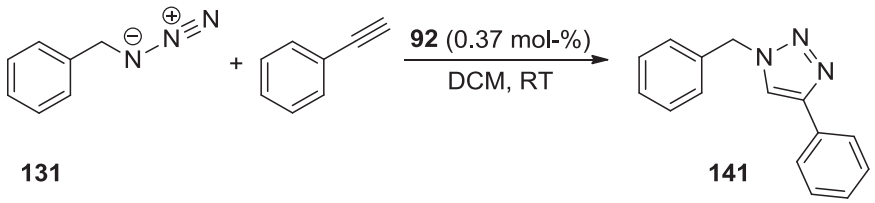

131 **141**

time [min]	alkyne t_R = 4.805 integral [a.u.]	azide t_R = 9.689 integral [a.u.]	dodecane t_R = 11.761 integral [a.u.]	triazole t_R = 27.711 integral [a.u.]	alkyne norm. integral [a.u.]	azide norm. integral [a.u.]	triazole norm. integral [a.u.]
0	0.2023	0.1707	0.1780	0.0000	1.1365	0.9590	0.0000
5	0.0606	0.0485	0.0610	0.0040	0.9934	0.7951	0.0656
10	0.0534	0.0417	0.0597	0.0169	0.8945	0.6985	0.2831
15	0.0465	0.0360	0.0628	0.0334	0.7404	0.5732	0.5318
17	0.0442	0.0325	0.0631	0.0440	0.7005	0.5151	0.6973
19	0.0391	0.0295	0.0649	0.0521	0.6025	0.4545	0.8028
20	0.0357	0.0257	0.0598	0.0533	0.5970	0.4298	0.8913
21	0.0306	0.0213	0.0544	0.0535	0.5625	0.3915	0.9835
22	0.0332	0.0235	0.0635	0.0688	0.5228	0.3701	1.0835
23	0.0294	0.0197	0.0590	0.0645	0.4983	0.3339	1.0932
25	0.0234	0.0148	0.0552	0.0704	0.4239	0.2681	1.2754
30	0.0132	0.0068	0.0489	0.0799	0.2699	0.1391	1.6339
35	0.0103	0.0048	0.0590	0.1105	0.1746	0.0814	1.8729
40	0.0066	0.0024	0.0605	0.1156	0.1091	0.0397	1.9107
45	0.0036	0.0006	0.0549	0.1124	0.0656	0.0109	2.0474
50	0.0025	0.0000	0.0572	0.1238	0.0437	0.0000	2.1643
55	0.0016	0.0000	0.0608	0.1304	0.0263	0.0000	2.1447
60	0.0000	0.0000	0.0657	0.1422	0.0000	0.0000	2.1644
65	0.0000	0.0000	0.0688	0.1505	0.0000	0.0000	2.1875
70	0.0000	0.0000	0.0608	0.1323	0.0000	0.0000	2.1760

Correction with response factors

time [min]	azide *f* = 1.8271 [a.u.]	triazole *f* = 0.8044 [a.u.]	conversion [%]	integral triazole [%]
0	1.7522	0.0000	0.0	0.0
5	1.4527	0.0527	3.5	3.0
10	1.2762	0.2277	15.1	12.9
15	1.0474	0.4278	29.0	24.3
17	0.9411	0.5609	37.3	31.9
19	0.8305	0.6458	43.7	36.7
20	0.7852	0.7170	47.7	40.7
21	0.7154	0.7911	52.5	45.0
22	0.6762	0.8715	56.3	49.5
23	0.6101	0.8794	59.0	50.0
25	0.4899	1.0259	67.7	58.3
30	0.2541	1.3143	83.8	74.7
35	0.1486	1.5065	91.0	85.6
40	0.0725	1.5370	95.5	87.3
45	0.0200	1.6469	98.8	93.6
50	0.0000	1.7410	100.0	98.9
55	0.0000	1.7252	100.0	98.0
60	0.0000	1.7410	100.0	98.9
65	0.0000	1.7596	100.0	100.0
70	0.0000	1.7504	100.0	-

3.2.4.5 *Reaction of Phenylacetylene and Benzyl Azide with 0.25 mol-% of Catalyst Complex **92***

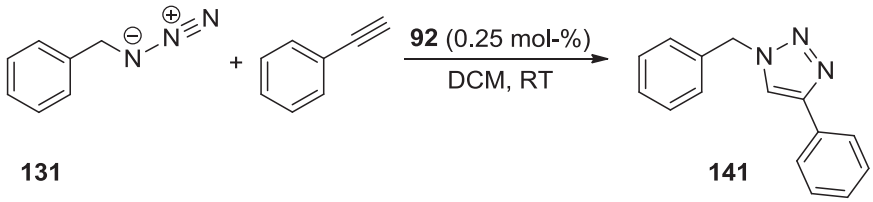

131 **141**

time [min]	alkyne t_R = 4.820 integral [a.u.]	azide t_R = 9.703 integral [a.u.]	dodecane t_R = 11.762 integral [a.u.]	triazole t_R = 27.721 integral [a.u.]	alkyne norm. integral [a.u.]	azide norm. integral [a.u.]	triazole norm. integral [a.u.]
0	0.1366	0.1092	0.1169	0.0000	1.1685	0.9341	0.0000
5	0.0625	0.0487	0.0590	0.0009	1.0593	0.8254	0.0153
10	0.0609	0.0470	0.0615	0.0086	0.9902	0.7642	0.1398
15	0.0526	0.0406	0.0609	0.0202	0.8637	0.6667	0.3317
20	0.0443	0.0341	0.0612	0.0357	0.7239	0.5572	0.5833
23	0.0374	0.0264	0.0549	0.0407	0.6812	0.4809	0.7413
25	0.0332	0.0235	0.0552	0.0436	0.6014	0.4257	0.7899
27	0.0306	0.0198	0.0529	0.0519	0.5784	0.3743	0.9811
29	0.0297	0.0206	0.0595	0.0633	0.4992	0.3462	1.0639
31	0.0268	0.0184	0.0607	0.0730	0.4415	0.3031	1.2026
33	0.0236	0.0150	0.0596	0.0797	0.3960	0.2517	1.3372
35	0.0211	0.0124	0.0590	0.0832	0.3576	0.2102	1.4102
45	0.0106	0.0050	0.0629	0.1194	0.1685	0.0795	1.8983
55	0.0052	0.0014	0.0640	0.1300	0.0813	0.0219	2.0313
65	0.0022	0.0002	0.0595	0.1251	0.0370	0.0034	2.1025
75	0.0017	0.0002	0.0871	0.1862	0.0195	0.0023	2.1378
80	0.0000	0.0000	0.0830	0.1803	0.0000	0.0000	2.1723
90	0.0000	0.0000	0.1028	0.2237	0.0000	0.0000	2.1761

Correction with response factors

time [min]	azide f = 1.8271 [a.u.]	triazole f = 0.8044 [a.u.]	conversion [%]	integral triazole [%]
0	1.7068	0.000	0.0	0.0
5	1.5081	0.012	0.8	0.7
10	1.3963	0.112	7.5	6.4
15	1.2181	0.267	18.0	15.2
20	1.0180	0.469	31.5	26.8
23	0.8786	0.596	40.4	34.1
25	0.7778	0.635	45.0	36.3
27	0.6839	0.789	53.6	45.1
29	0.6326	0.856	57.5	48.9
31	0.5538	0.967	63.6	55.3
33	0.4598	1.076	70.1	61.5
35	0.3840	1.134	74.7	64.8
45	0.1452	1.527	91.3	87.2
55	0.0400	1.634	97.6	93.3
65	0.0061	1.691	99.6	96.6
75	0.0042	1.720	99.8	98.2
80	0.0000	1.747	100.0	99.8
90	0.0000	1.750	100.0	100.0

3.2.4.6 *Reaction of Phenylacetylene and Benzyl Azide with 0.12 mol-% of Catalyst Complex **92***

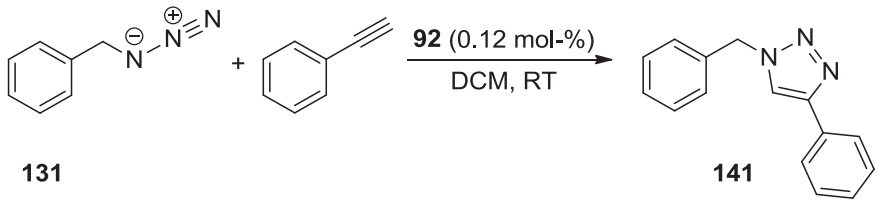

131 **141**

time [min]	alkyne t_R = 4.845 integral [a.u.]	azide t_R = 9.744 integral [a.u.]	dodecane t_R = 11.760 integral [a.u.]	triazole t_R = 27.716 integral [a.u.]	alkyne norm. integral [a.u.]	azide norm. integral [a.u.]	triazole norm. integral [a.u.]
0	0.0598	0.0497	0.0572	0.0000	1.0455	0.8689	0.0000
15	0.0699	0.0582	0.0751	0.0100	0.9308	0.7750	0.1332
30	0.0478	0.0361	0.0639	0.0402	0.7480	0.5649	0.6291
35	0.0495	0.0386	0.0767	0.0636	0.6454	0.5033	0.8292
37	0.0412	0.0310	0.0678	0.0569	0.6077	0.4572	0.8392
39	0.0409	0.0306	0.0711	0.0606	0.5752	0.4304	0.8523
41	0.0462	0.0341	0.0834	0.0801	0.5540	0.4089	0.9604
45	0.0356	0.0251	0.0707	0.0742	0.5035	0.3550	1.0495
47	0.0315	0.0215	0.0673	0.0763	0.4681	0.3195	1.1337
49	0.0314	0.0219	0.0721	0.0876	0.4355	0.3037	1.2150
51	0.0302	0.0207	0.0737	0.0926	0.4098	0.2809	1.2564
53	0.0283	0.0189	0.0737	0.0986	0.3840	0.2564	1.3379
55	0.0281	0.0179	0.0774	0.1081	0.3630	0.2313	1.3966
70	0.0146	0.0081	0.0759	0.1316	0.1924	0.1067	1.7339
90	0.0071	0.0025	0.0840	0.1611	0.0845	0.0298	1.9179
110	0.0030	0.0006	0.0883	0.1806	0.0340	0.0068	2.0453
120	0.0018	0.0002	0.0725	0.1608	0.0248	0.0028	2.2179
130	0.0000	0.0000	0.0965	0.2023	0.0000	0.0000	2.0964

Correction with response factors

time [min]	azide f = 1.8271 [a.u.]	triazole f = 0.8044 [a.u.]	conversion [%]	integral triazole [%]
0	1.5875	0.0000	0.0	0.0
15	1.4159	0.1071	7.0	6.0
30	1.0322	0.5061	32.9	28.4
35	0.9195	0.6670	42.0	37.4
37	0.8354	0.6751	44.7	37.8
39	0.7863	0.6856	46.6	38.4
41	0.7471	0.7726	50.8	43.3
45	0.6487	0.8442	56.5	47.3
47	0.5837	0.9120	61.0	51.1
49	0.5550	0.9773	63.8	54.8
51	0.5132	1.0107	66.3	56.6
53	0.4686	1.0762	69.7	60.3
55	0.4225	1.1235	72.7	63.0
70	0.1950	1.3947	87.7	78.2
90	0.0544	1.5427	96.6	86.5
110	0.0124	1.6452	99.3	92.2
120	0.0050	1.7841	99.7	100.0
130	0.0000	1.6863	100.0	-

*3.2.4.7 Catalytic Reaction of Ethyl Propiolate and Benzyl Azide with 0.74 mol-% of Catalyst Complex **92***

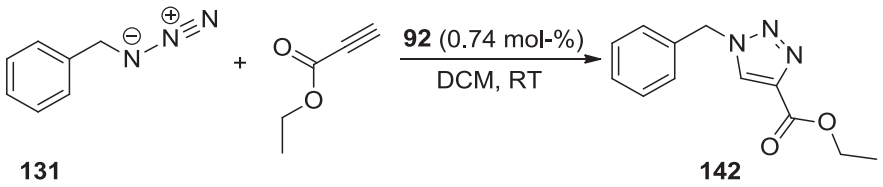

131 **142**

time [min]	alkyne t_R = 2.488 integral [a.u.]	azide t_R = 8.662 integral [a.u.]	dodecane t_R = 10.305 integral [a.u.]	triazole t_R = 21.003 integral [a.u.]	alkyne norm. integral [a.u.]	azide norm. integral [a.u.]	triazole norm. integral [a.u.]
0	0.0330	0.0905	0.0999	0.0000	0.3303	0.9059	0.0000
0.5	0.0163	0.0347	0.0508	0.0065	0.3209	0.6831	0.1280
1	0.0163	0.0340	0.0565	0.0156	0.2885	0.6018	0.2761
1.5	0.0081	0.0150	0.0354	0.0150	0.2288	0.4237	0.4237
2	0.0111	0.0230	0.0556	0.0295	0.1996	0.4137	0.5306
2.5	0.0073	0.0161	0.0503	0.0351	0.1451	0.3201	0.6978
3	0.0040	0.0064	0.0387	0.0315	0.1034	0.1654	0.8140
4	0.0024	0.0081	0.0513	0.0527	0.0468	0.1579	1.0273
5	0.0000	0.0000	0.0468	0.0596	0.0000	0.0000	1.2735

Correction with response factors

time [min]	azide f = 1.8271 [a.u.]	triazole f = 0.8044 [a.u.]	conversion [%]	integral triazole [%]
0	1.6754	0.0000	0.0	0.0
0.5	1.2633	0.2000	13.7	10.0
1	1.1129	0.4316	27.9	21.7
1.5	0.7836	0.6624	45.8	33.3
2	0.7650	0.8294	52.0	41.7
2.5	0.5920	1.0909	64.8	54.8
3	0.3058	1.2725	80.6	63.9
4	0.2920	1.6060	84.6	80.7
5	0.0000	1.9909	100.0	100.0

*3.2.4.8 Catalytic Reaction of Ethyl Propiolate and Benzyl Azide with 0.62 mol-% of Catalyst Complex **92***

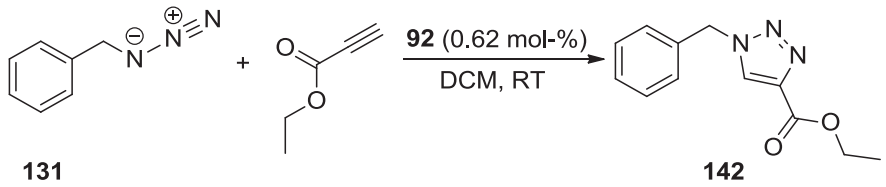

131 **142**

time [min]	alkyne t_R = 2.479 integral [a.u.]	azide t_R = 8.660 integral [a.u.]	dodecane t_R = 10.307 integral [a.u.]	triazole t_R = 21.004 integral [a.u.]	alkyne norm. integral [a.u.]	azide norm. integral [a.u.]	triazole norm. integral [a.u.]
0	0.0522	0.1244	0.1338	0.0000	0.3901	0.9297	0.0000
1	0.0149	0.0316	0.0494	0.0067	0.3016	0.6397	0.1356
2	0.0123	0.0261	0.0536	0.0173	0.2295	0.4869	0.3228
3	0.0083	0.0166	0.0562	0.0393	0.1477	0.2954	0.6993
5	0.0023	0.0047	0.0551	0.0524	0.0417	0.0853	0.9510
7	0.0000	0.0000	0.0485	0.0680	0.0000	0.0000	1.4021
9	0.0000	0.0000	0.0476	0.0700	0.0000	0.0000	1.4706
11	0.0000	0.0000	0.0515	0.0744	0.0000	0.0000	1.4447
13	0.0000	0.0000	0.0507	0.0709	0.0000	0.0000	1.3984

Correction with response factors

time [min]	azide f = 1.8271 [a.u.]	triazole f = 0.8044 [a.u.]	conversion [%]	integral triazole [%]
0	1.7195	0.0000	0.0	0.0
1	1.1830	0.2120	15.2	9.2
2	0.9005	0.5046	35.9	21.9
3	0.5463	1.0932	66.7	47.6
5	0.1578	1.4867	90.4	64.7
7	0.0000	2.1918	100.0	95.3
9	0.0000	2.2990	100.0	100.0
11	0.0000	2.2584	100.0	-
13	0.0000	2.1862	100.0	-

*3.2.4.9 Catalytic Reaction of Ethyl Propiolate and Benzyl Azide with 0.49 mol-% of Catalyst Complex **92***

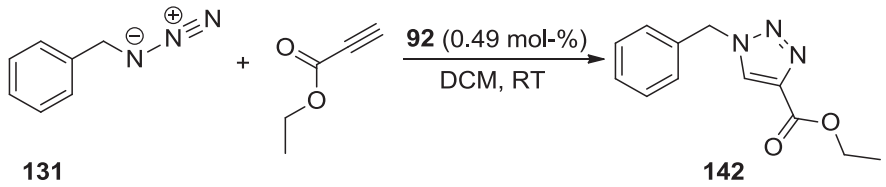

131 **142**

time [min]	alkyne t_R = 2.478 integral [a.u.]	azide t_R = 8.660 integral [a.u.]	dodecane t_R = 10.306 integral [a.u.]	triazole t_R = 21.008 integral [a.u.]	alkyne norm. integral [a.u.]	azide norm. integral [a.u.]	triazole norm. integral [a.u.]
0	0.0562	0.1259	0.1340	0.0000	0.4194	0.9396	0.0000
1	0.0167	0.0347	0.0519	0.0033	0.3218	0.6686	0.0636
3	0.0120	0.0250	0.0517	0.0166	0.2321	0.4836	0.3211
5	0.0060	0.0117	0.0418	0.0267	0.1435	0.2799	0.6388
7	0.0046	0.0088	0.0523	0.0474	0.0880	0.1683	0.9063
9	0.0033	0.0063	0.0681	0.0748	0.0485	0.0925	1.0984
11	0.0001	0.0021	0.0503	0.0636	0.0020	0.0417	1.2644
13	0.0000	0.0000	0.0452	0.0623	0.0000	0.0000	1.3783
15	0.0000	0.0000	0.0424	0.0605	0.0000	0.0000	1.4269
17	0.0000	0.0000	0.0464	0.0672	0.0000	0.0000	1.4483

Correction with response factors

time [min]	azide f = 1.8494 [a.u.]	triazole f = 1.5633 [a.u.]	conversion [%]	integral triazole [%]
0	1.7376	0.0000	0.0	0.0
1	1.2365	0.0994	7.4	4.4
3	0.8943	0.5019	35.9	22.2
5	0.5177	0.9986	65.9	44.1
7	0.3112	1.4168	82.0	62.6
9	0.1711	1.7171	90.9	75.8
11	0.0772	1.9767	96.2	87.3
13	0.0000	2.1547	100.0	95.2
15	0.0000	2.2307	100.0	98.5
17	0.0000	2.2641	100.0	100.0

*3.2.4.10 Catalytic Reaction of Ethyl Propiolate and Benzyl Azide with 0.37 mol-% of Catalyst Complex **92***

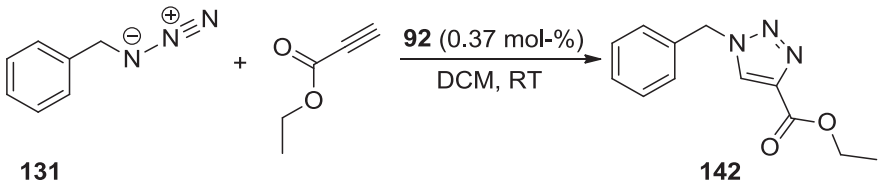

131 **142**

time [min]	alkyne t_R = 2.499 integral [a.u.]	azide t_R = 8.670 integral [a.u.]	dodecane t_R = 10.306 integral [a.u.]	triazole t_R = 21.004 integral [a.u.]	alkyne norm. integral [a.u.]	azide norm. integral [a.u.]	triazole norm. integral [a.u.]
0	0.0213	0.0596	0.0689	0.0000	0.3091	0.8650	0.0213
1	0.0169	0.0346	0.0483	0.0039	0.3499	0.7164	0.0169
2	0.0174	0.0355	0.0526	0.0068	0.3308	0.6749	0.0174
3	0.0153	0.0316	0.0514	0.0124	0.2977	0.6148	0.0153
4	0.0141	0.0275	0.0524	0.0181	0.2308	0.5248	0.0141
5	0.0120	0.0247	0.0520	0.0226	0.1740	0.4750	0.0120
7	0.0091	0.0184	0.0523	0.0329	0.1740	0.3518	0.0091
10	0.0052	0.0103	0.0513	0.0429	0.1014	0.2008	0.0052
15	0.0005	0.0028	0.0507	0.0602	0.0099	0.0552	0.0005
20	0.0000	0.0000	0.0511	0.0701	0.0000	0.0000	0.0000
25	0.0000	0.0000	0.0513	0.0715	0.0000	0.0000	0.0000

Correction with response factors

time [min]	azide f = 1.8494 [a.u.]	triazole f = 1.5633 [a.u.]	conversion [%]	integral triazole [%]
0	1.5998	0.0000	0.0	0.0
1	1.3248	0.1262	8.7	5.8
2	1.2482	0.2021	13.9	9.3
3	1.1370	0.3771	24.9	17.3
4	0.9706	0.5400	35.7	24.8
5	0.8785	0.6794	43.6	31.2
7	0.6506	0.9834	60.2	45.1
10	0.3713	1.3073	77.9	60.0
15	0.1021	1.8562	94.8	85.2

20	0.0000	2.1446	100.0	98.4
25	0.0000	2.1789	100.0	100.0

*3.2.4.11 Reaction of Ethyl Propiolate and Benzyl Azide with 0.25 mol-% of Catalyst Complex **92***

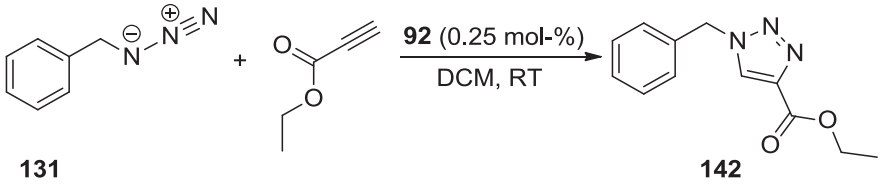

131 **142**

time [min]	alkyne t_R = 2.505 integral [a.u.]	azide t_R = 8.686 integral [a.u.]	dodecane t_R = 10.312 integral [a.u.]	triazole t_R = 21.008 integral [a.u.]	alkyne norm. integral [a.u.]	azide norm. integral [a.u.]	triazole norm. integral [a.u.]
0	0.0755	0.1670	0.1703	0.0000	0.4433	0.9806	0.0000
1	0.0190	0.0409	0.0507	0.0004	0.3748	0.8067	0.0079
3	0.0183	0.0383	0.0525	0.0052	0.3486	0.7295	0.0990
5	0.0174	0.0348	0.0530	0.0097	0.3283	0.6566	0.1830
7	0.0147	0.0323	0.0546	0.0158	0.2692	0.5916	0.2894
10	0.0131	0.0272	0.0542	0.0230	0.2417	0.5018	0.4244
13	0.0103	0.0213	0.0516	0.0286	0.1996	0.4128	0.5543
17	0.0078	0.0154	0.0513	0.0375	0.1520	0.3002	0.7310
20	0.0058	0.0111	0.0499	0.0422	0.1162	0.2228	0.8457
25	0.0034	0.0065	0.0538	0.0557	0.0632	0.1208	1.0353
30	0.0000	0.0030	0.0504	0.0606	0.0000	0.0595	1.2024
35	0.0000	0.0001	0.0499	0.0662	0.0000	0.0020	1.3267
40	0.0000	0.0000	0.0542	0.0764	0.0000	0.0000	1.4096
45	0.0000	0.0000	0.0492	0.0686	0.0000	0.0000	1.3943
50	0.0000	0.0000	0.0526	0.0739	0.0000	0.0000	1.4049

Correction with response factors

time [min]	azide *f* = 1.8494 [a.u.]	triazole *f* = 1.5633 [a.u.]	conversion [%]	integral triazole [%]
0	1.8136	0.0000	0.0	0.0
1	1.4919	0.0123	0.8	0.6
3	1.3492	0.1548	10.3	7.0
5	1.2143	0.2861	19.1	13.0
7	1.0941	0.4524	29.3	20.5
10	0.9281	0.6634	41.7	30.1
13	0.7634	0.8665	53.2	39.3
17	0.5552	1.1428	67.3	51.9
20	0.4121	1.3221	76.2	60.0
25	0.2234	1.6185	87.9	73.4
30	0.1101	1.8797	94.5	85.3
35	0.0037	2.0740	99.8	94.1
40	0.0000	2.2036	100.0	100.0
45	0.0000	2.1797	100.0	-
50	0.0000	2.1963	100.0	-

3.2.4.12 *Reaction of Ethyl Propiolate and Benzyl Azide with 0.12 mol-% of Catalyst Complex **92***

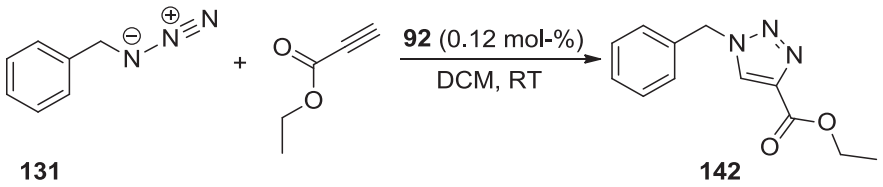

131 **142**

time [min]	alkyne t_R = 2.499 integral [a.u.]	azide t_R = 8.689 integral [a.u.]	dodecane t_R = 10.310 integral [a.u.]	triazole t_R = 21.006 integral [a.u.]	alkyne norm. integral [a.u.]	azide norm. integral [a.u.]	triazole norm. integral [a.u.]
0	0.0394	0.0912	0.0940	0.0000	0.4191	0.9702	0.0000
5	0.0191	0.0380	0.0505	0.0012	0.3782	0.7525	0.0238
10	0.0174	0.0352	0.0503	0.0034	0.3459	0.6998	0.0676
15	0.0170	0.0375	0.0538	0.0071	0.3160	0.6970	0.1320
20	0.0145	0.0275	0.0492	0.0091	0.2947	0.5589	0.1850
25	0.0136	0.0270	0.0481	0.0147	0.2827	0.5613	0.3056
30	0.0150	0.0285	0.0552	0.0257	0.2717	0.5163	0.4656
35	0.0112	0.0224	0.0493	0.0222	0.2272	0.4544	0.4503
40	0.0107	0.0213	0.0518	0.0279	0.2066	0.4112	0.5386
50	0.0073	0.0140	0.0472	0.0336	0.1547	0.2966	0.7119
60	0.0057	0.0120	0.0499	0.0417	0.1142	0.2405	0.8357
70	0.0041	0.0062	0.0499	0.0477	0.0822	0.1242	0.9559
80	0.0021	0.0041	0.0528	0.0561	0.0398	0.0777	1.0625
90	0.0000	0.0028	0.0514	0.0627	0.0000	0.0545	1.2198
100	0.0000	0.0007	0.0520	0.0691	0.0000	0.0135	1.3288
105	0.0000	0.0000	0.0474	0.0649	0.0000	0.0000	1.3692
110	0.0000	0.0000	0.0501	0.0688	0.0000	0.0000	1.3733
115	0.0000	0.0000	0.0496	0.0708	0.0000	0.0000	1.4274
120	0.0000	0.0000	0.0545	0.0777	0.0000	0.0000	1.4257

Correction with response factors

time [min]	azide *f* = 1.8494 [a.u.]	triazole *f* = 1.5633 [a.u.]	conversion [%]	integral triazole [%]
0	1.7943	0.0000	0.0	0.0
5	1.3916	0.0371	2.6	1.7
10	1.2942	0.1057	7.5	4.7
15	1.2891	0.2063	13.8	9.2
20	1.0337	0.2891	21.9	13.0
25	1.0381	0.4778	31.5	21.4
30	0.9549	0.7278	43.3	32.6
35	0.8403	0.7040	45.6	31.5
40	0.7605	0.8420	52.5	37.7
50	0.5486	1.1129	67.0	49.9
60	0.4447	1.3064	74.6	58.5
70	0.2298	1.4944	86.7	67.0
80	0.1436	1.6610	92.0	74.4
90	0.1007	1.9070	95.0	85.5
100	0.0249	2.0774	98.8	93.1
105	0.0000	2.1405	100.0	95.9
110	0.0000	2.1468	100.0	96.2
115	0.0000	2.2315	100.0	100.0
120	0.0000	2.2288	100.0	-

4 Computational Procedures

All computational results of this work were obtained by applying density functional theory methods (DFT)[3] using the program packages Jaguar 7.7 (release 107) and Jaguar 7.9 (release 23) with the graphical Maestro Molecular Modeling Interface by Schrödinger, LLC, on Intel Core i7 920 personal computers with an openSUSE operating system. For solving partial differential equations, the pseudo-spectral method available in the program Jaguar was always preferred over the purely analytical calculation in order to reduce the expenditure of time.[4]

Generally in quantum-chemical calculations, a set of mathematical functions, the so-called basis set, is used to describe the molecular orbitals Ψ_i by linear combinations of basis functions Φ_μ with the variational coefficients to be determined (LCAO method, Equation 1).[5] Minimal basis sets only contain atomic orbitals for the shells (partly) occupied in the ground state. However, the larger the number of basis functions Φ_μ, the more accurate the description of the molecule. In extended basis sets, a larger number of basis functions is used to give extra flexibility to the molecular orbital description and to allow for features such as anisotropic atomic shapes. In practical calculations, basis functions Φ_μ are fixed linear combinations of Gaussian-type orbitals (Equation 3).[6]

Equation 1: Linear combination of atomic orbitals Φ_μ for the construction of molecular orbitals Ψ_i.[5]

$$\Psi_i = \sum_\mu c_{\mu i} \Phi_\mu$$

Ψ_i	molecular orbital
$c_{\mu i}$	variational coefficient
Φ_μ	basis function

For geometry optimizations and frequency calculations in this work, the basis set LACVP** was applied. This basis set was developed by Hay and Wadt in the Los Alamos National Laboratories, which is why its denomination starts with the letters

LA. The letters C (standing for core) and V (standing for valence) indicate that both the valence shell (n) and the next shell (n-1) are explicitly considered in this basis set. For atoms with a higher number of protons than argon, calculations are simplified by combining the contributions of the nucleons and the core electrons (n-2 to n = 1) in a single, spherically symmetric potential called effective core potential (ECP). The ECP can be calculated by *ab initio* methods and has the mathematical structure of a Gaussian function with the distance to the nucleus as variable. For elements of the fourth and fifth period, relativistic effects are taken into account in the calculation of the ECP.[7] The only heavy atom in this work is copper. The copper atom has the electron configuration $1s^2 2s^2 2p^6 3s^2 3p^6 4s^1 3d^{10}$. In contrast to the classical definition of valence electrons, 19 electrons of the copper atom ($3s^2 3p^6 4s^1 3d^{10}$) are considered as valence electrons instead of eleven only. The construction of an ECP significantly reduces the electronic complexity of this system, as the single electron-electron interactions of ten electrons ($1s^2 2s^2 2p^6$) do not have to be calculated separately, but are integrated in the ECP.

For elements in the first to third row of the periodic table, no ECPs are applied. Instead, Pople's basis set 6-31G is used.[6] This is indicated by the last letter P in the basis set's name LACVP. In general, Gaussian functions (Equation 2) are greatly preferred in quantum-chemical calculations, although the exact solutions to the one-electron hydrogen atom are functions which decay exponentially with distance from the nucleus (r). However, these Slater-type functions (STO)[8] are very difficult to evaluate when it comes to the calculation of multi-electron molecular integrals, for example in the calculation of Coulomb or exchange energy. It is thus very convenient to approximately describe atomic orbitals by linear combinations of Gaussian functions (Equation 3),[6, 9] as these are much easier to integrate, so that computational efficiency is substantially increased. These contracted Gaussian functions can then be used as basis functions in the LCAO method (Equation 1).

Equation 2: Mathematical representation of primitive Gaussian atomic orbitals Φ^{GTO}.[9-10]

$$\Phi^{GTO}(r,x,y,z) = Nx^l y^m z^n e^{-\beta r^2}$$

Φ^{GTO}	primitive Gaussian-type orbital
N	normalization constant
r	distance of the electron from the nucleus
x, y, z	Cartesian coordinates
l, m, n, β	parameters for optimization
	s-orbital: l + m + n = 0
	p-orbital: l + m + n = 1
	d-orbital: l + m + n = 2

Equation 3: Contracted Gaussian atomic orbitals Φ^{CGTO} are constructed by linear combination of primitive Gaussian atomic orbitals Φ^{GTO}.[6, 9-10]

$$\Phi^{CGTO} = \sum_i d_i \Phi_i^{GTO}$$

Φ^{CGTO}	contracted Gaussian function
d_i	contraction coefficient

By adept choice of contraction coefficients d_i in the linear combination of primitive Gaussian-type orbitals (GTO) to contracted Gaussian orbitals (CGTO) (Equation 3), the form of the potential as a function of the distance to the nucleus can approximate the exponential function of Slater-type orbitals (STO). This is essential as the deviation of the primitive Gaussian functions (GTO) from the more realistic Slater functions (STO) is significant for $r \rightarrow 0$ (exponential STO function: first derivative $\rightarrow \infty$; GTO: first derivative = 0) and $r \rightarrow \infty$ (STO function: exponential decay; GTO function $\sim e^{-r^2}$, *i.e.* the GTO function falls off too rapidly in the tail region).[10] Generally, the higher the number of Gaussian functions contributing to the linear combination, the higher the accuracy in the description of the orbitals.

As the valence electrons influence the chemical characteristics much more than the core electrons, these two classes of electrons are treated differently.[6] In a split valence basis set, every valence orbital is represented by two contracted Gaussian functions (double zeta), which are in turn composed of a fixed linear combination of

primitive Gaussian functions. This strategy allows the atoms to adapt their spatial extent appropriate to the particular molecular environment, especially to different net atomic charges. In the basis set 6-31G, the first representation for each valence orbital is made up by linear combination of three primitive Gaussian functions (“inner” valence orbital, less spatial extent), whereas the contracted Gaussian functions of the second representation of each valence orbital is equivalent to one primitive Gaussian function except for a factor (“outer” valence orbital, higher spatial extent).[6, 10] The relative weighting of the inner and outer part in the linear combination of the LCAO method (Equation 1) gives the molecular orbital Ψ_i some spatial flexibility. On the other hand, the core atomic orbitals are each composed of six primitive Gaussian functions. For example, first row elements are described by nine functions, one contracted Gaussian function for the 1s orbital and two contracted Gaussian functions for each of the orbitals 2s, $2p_x$, $2p_y$, and $2p_z$. For hydrogen, there is only one 1s orbital, which is represented by two functions, an inner function Φ'_{1s} and an outer function Φ''_{1s}.[6]

In all calculations carried out in this work, the LACVP basis set was expanded by polarization functions (LACVP**). This means that Gaussian functions of unoccupied atomic orbitals with higher angular quantum number are also included in the linear combinations.[11] The inclusion of d-type functions on main-group elements is marked by a single asterisk (*), the additional inclusion of p-type functions on hydrogen atoms by a second asterisk (**). As these orbitals of higher angular quantum number contain more nodal planes, the basis set is more flexible now and a much better adaptation of the electron distribution to the real molecular environment can be accomplished because the difference between the electron density distribution in free atoms as compared to the atoms’ electron distribution in the molecule can be taken into account. Generally speaking, the admixing of orbitals of higher angular quantum number with more nodal planes allows for the (spherically asymmetric) displacement of electron density away from the nuclear positions. For example, the basis set 6-31G* is constructed from 6-31G by admixing a set of d-type polarization functions that are expressed by a single contracted Gaussian function for each non-hydrogen atom.[11b] This means that six primitive Gaussian functions representing the d-orbitals are used for polarization of the main group elements’ p-orbitals. Analogously, f-type functions are added to a basis set with d-type orbitals. The basis set 6-31G** is identical to 6-

31G* for all elements except hydrogen. The double asterisk indicates that three p-orbitals on each hydrogen atom are admixed for polarization of the 1s orbital.[11a, 12]
For single point calculations with higher accuracy, the basis set LACV3P**++ has been used. The LACV3P basis set is a triple-zeta contraction of the LACVP basis set developed and tested at Schrödinger, Inc.. The basis set LACV3P**++ applies Pople's 6-311++G** basis set for main group elements. As indicated by nomenclature, the 6-311G** basis set is a single zeta core, triple zeta valence basis set with polarization functions on all atoms.[13] This means that there is one contracted Gaussian function for each inner shell orbital, and each of these contracted Gaussian functions itself is constructed by linear combination of six primitive Gaussian-type orbitals. Each valence shell orbital, on the other hand, is represented by three contracted Gaussian functions, two of which are equivalent to a primitive Gaussian-type orbital (except for a factor) and the third one is constructed by linear combination of three primitive Gaussian functions. The "+" in a basis set's name indicates that diffuse functions are added to all atoms except hydrogen and helium; "++" indicates that diffuse functions are used on all atoms.[14] Diffuse functions are especially important when the electron density is widely spread out and the electron density has a long "tail" far away from the nuclei. To model this correctly, Gaussian-type orbitals with small exponents are added, which are very shallow and outstretched themselves. Normally, these diffuse Gaussian-type functions are added in their primitive form and not combined to a contracted Gaussian function.

The semi-empirical hybrid functional B3LYP containing local-spin-density, gradient, and exact-exchange terms was used to take into account exchange interaction and correlation energy. The exchange-correlation functional B3LYP contains Becke's three parameter exchange-only density correction[15] and the Lee-Parr-Young gradient-corrected correlation functionals.[16] The exchange energy is calculated exactly by using the Hartree-Fock method.

Equation 4: B3LYP exchange-correlation energy.[17]

$$E_{XC}^{B3LYP} = (1 - a)\, E_X^{LSD} + a\, E_{XC}^{\lambda=0} + b\, E_X^{B88} + c\, E_c^{LYP} + (1 - c)\, E_c^{LSD}$$

a,b,c	empirical parameters
E_{XC}^{B3LYP}	energy correction for exchange and correlation of electrons
E_X^{LSD}	local spin density exchange energy
$E_{XC}^{\lambda=0}$	energy correction in a system without electron-electron interactions ($\lambda = 0$), exchange part of the Slater determinant
E_X^{B88}	exchange-only density-gradient correction, Becke88 exchange functional
E_c^{LYP}	gradient-corrected correlation functional
E_c^{LSD}	local spin density correlation energy

Calculations of thermodynamical data were carried out on the assumption of an ideal gas at standard conditions (T = 298.15 K, p = 1atm), if not explicitly stated otherwise.
In some cases, the solvent environment was modelled by using the Poisson-Boltzmann continuum solvent model[18] as integrated in the Jaguar program. First, the program calculates the wave function in the gas phase, which is then applied to determine the charge distribution in the molecule. This result is used to construct a sheath of point charges on the molecular surface by numerically solving the Poisson-Boltzmann equation. This layer of point charges on the molecule's surface shall represent the solvent environment. Taking into account this solvent layer of point charges, the molecule's wave function is calculated anew. This two-step process of re-ordering the point charges on the molecular surface and then calculating a new wave function is repeated until self-consistency is reached, *i.e.* until further re-organization of the point charges does not lead to a further gain in energy.[19] For dichloromethane as solvent, the following default parameters were applied: dielectric constant – 8.93 F m^{-1}, molecular weight – 84.93 g mol^{-1}, density – 1.3266 g cm^{-3}, probe radius – 2.33 Å.
The more accurate LACV3P**++ basis set was employed for single point calculations of geometries obtained with the smaller basis set LACVP**. Geometry optimizations and frequency calculations were not carried out with this larger basis set as this would have been too time-consuming. However, the Gibbs free energy can be esti-

mated by adding the difference between SCF energy and Gibbs free energy as calculated with the LACVP** basis set to the SCF energy calculated with the larger basis set. It is assumed that the summand X = ZPE + U + pV – TS does not vary much when changing from LACVP** to LACV3P**++. An analogous procedure was applied for calculations with the PBF solvent model.

Equation 5: Estimation of the Gibbs free energy for calculations with basis set LACV3P**++ or with basis set LACVP** and PBF solvent model based on calculations including frequency evaluations with the smaller basis set LACVP**.

$$G_{tot}^{LACVP^{**}} = SCFE^{LACVP^{**}} + ZPE + U + pV - TS = SCFE^{LACVP^{**}} + X^{LACVP^{**}}$$

$$G_{tot}^{LACV3P^{**}++} \approx SCFE^{LACV3P^{**}++} + X^{LACVP^{**}}$$

$$G_{tot}^{LACVP^{**}/PBF} \approx SCFE^{LACVP^{**}/PBF} + X^{LACVP^{**}}$$

Except for distance scans, all geometry optimizations were carried out without constraints. Minimum structures were confirmed by the absence of imaginary frequencies in the corresponding Hesse matrix.

Transition states were mostly found by carrying out a distance scan, in the course of which the atomic distance was thus constrained that with every subsequent optimization the substrates' geometries approached the geometry of the product complex. The structural arrangement with the highest energy on the pathway between substrate and product complex was subjected to the standard transition state search implemented in the Jaguar program. This method strives for 1) maximization of the energy content along the eigenvector with the minimal frequency in the Hessian, and 2) minimization of the energy along all other coordinates. Alternatively, LST (linear synchronous transit) and QST (quadratic synchronous transit) transition state searches were carried out.[20] For the LST option, the structures of the starting material and the product need to be known to allow for a transition state search by intrapolation of these two structures. For the QST search, a good guess for the desired transition state needs to be uploaded as well. This allows the program to search for the correct transition state on the trajectory which leads from the starting material to the transition state guess and from there to the product structure. Having found the point of maximum energy on this curve, the program deviates from this path and searches

the correct transition state structure from there on. All three options for transition state search were equally applicable in this project, but due to its simplicity, the standard search was generally preferred. The transition states found by one of these methods were confirmed by three criteria: 1) existence of one, and only one, imaginary frequency in the Hesse matrix, 2) visualization of the vibration belonging to this negative frequency to check whether it belonged to the reactive coordinate, and 3) minute changes in the atomic distances of the bond-forming or bond-breaking atoms to check whether the substrate and product structures can be reached starting from the calculated transition state.
All structures that have been modelled by quantum-chemical calculations are named by the letter **C** (indicating a calculated structure) plus a number.

All structures that have been modelled by quantum-chemical calculations are named by the letter **C** (indicating a calculated structure) plus a number. The computational data can be found on a CD, which is part of this dissertation.

5 Bibliography

[1] a) L. Farrugia, *J. Appl. Crystallogr.* **1997**, *30*, 565; b) ORTEP plot: by way of exception thermal ellipsoids are drawn at the 30 % probability level.

[2] ORTEP plot: thermal ellipsoids are drawn at the 50 % probability level.

[3] a) P. Hohenberg, W. Kohn, *Phys. Rev.* **1964**, *136*, B864-B871; b) W. Kohn, L. J. Sham, *Phys. Rev.* **1965**, *140*, A1133-A1138.

[4] Schrödinger LLC, *Jaguar 7.5 User Manual* **2008**, 32-33.

[5] C. C. J. Roothaan, *Rev. Mod. Phys.* **1951**, *23*, 69-89.

[6] a) R. Ditchfield, W. J. Hehre, J. A. Pople, *J. Chem. Phys.* **1971**, *54*, 724-728; b) W. J. Hehre, R. Ditchfield, J. A. Pople, *J. Chem. Phys.* **1972**, *56*, 2257-2261.

[7] P. J. Hay, W. R. Wadt, *J. Chem. Phys.* **1985**, *82*, 299-310.

[8] J. C. Slater, *Phys. Rev.* **1930**, *36*, 57-64.

[9] a) E. Clementi, D. R. Davis, *J. Chem. Phys.* **1966**, *45*, 2593-2599; b) E. Clementi, D. R. Davis, *J. Computational Phys.* **1966**, *1*, 223-244.

[10] W. Koch, M. C. Holthausen, *A Chemist's Guide to Density Functional Theory*, 2nd ed., Wiley VCH, Weinheim, **2000**, pp. 97-101.

[11] a) W. J. Hehre, *A Guide to Molecular Mechanics and Quantum Chemical Calculations*, Wavefunction Inc., **2003**, pp. 39-46; b) P. C. Hariharan, J. A. Pople, *Mol. Phys.* **1974**, *27*, 209-214; c) A. Rauk, L. C. Allen, E. Clementi, *J. Chem. Phys.* **1970**, *52*, 4133-4144; d) J. T. H. Dunning, R. M. Pitzer, S. Aung, *J. Chem. Phys.* **1972**, *57*, 5044-5051.

[12] a) P. C. Hariharan, J. A. Pople, *Theoret. Chim. Acta* **1973**, *28*, 213-222; b) M. M. Francl, W. J. Pietro, W. J. Hehre, J. S. Binkley, M. S. Gordon, D. J. DeFrees, J. A. Pople, *J. Chem. Phys.* **1982**, *77*, 3654-3665.

[13] R. Krishnan, J. S. Binkley, R. Seeger, J. A. Pople, *J. Chem. Phys.* **1980**, *72*, 650-654.

[14] a) M. J. Frisch, J. A. Pople, J. S. Binkley, *J. Chem. Phys.* **1984**, *80*, 3265-3269; b) D. E. Woon, J. T. H. Dunning, *J. Chem. Phys.* **1993**, *98*, 1358-1371; c) T. Clark, J. Chandrasekhar, G. W. Spitznagel, P. V. R. Schleyer, *J. Comput. Chem.* **1983**, *4*, 294-301.

[15] A. D. Becke, *Physical Review A* **1988**, *38*, 3098-3100.

[16] C. Lee, W. Yang, R. G. Parr, *Phys. Rev. B* **1988**, *37*, 785-789.

[17] a) W. Koch, M. C. Holthausen, *A Chemist's Guide to Density Functional Theory*, 2nd ed., Wiley VCH, Weinheim, **2000**, pp. 78-85; b) P. J. Stephens, F. J. Devlin, C. F. Chabalowski, M. J. Frisch, *J. Phys. Chem.* **1994**, *98*, 11623-11627.

[18] a) D. J. Tannor, B. Marten, R. Murphy, R. A. Friesner, D. Sitkoff, A. Nicholls, B. Honig, M. Ringnalda, W. A. Goddard, *J. Am. Chem. Soc.* **1994**, *116*, 11875-11882; b) B. Marten, K. Kim, C. Cortis, R. A. Friesner, R. B. Murphy, M. N. Ringnalda, D. Sitkoff, B. Honig, *J. Phys. Chem.* **1996**, *100*, 11775-11788.

[19] Schrödinger LLC, *Jaguar 7.5 User Manual* **2008**, 51-52.

[20] Schrödinger LLC, *Jaguar 7.5 User Manual* **2008**, 78-79.

Statutory Declaration

Eidesstattliche Versicherung gemäß § 8 der Promotionsordnung der Naturwissenschaftlich-Mathematischen Gesamtfakultät der Universität Heidelberg

1. Bei der eingereichten Dissertation zu dem Thema “Highly Active Dinuclear Copper Catalysts for Homogeneous Azide-Alkyne Cycloadditions“ handelt es sich um meine eigenständig erbrachte Leistung.
2. Ich habe nur die angegebenen Quellen und Hilfsmittel benutzt und mich keiner unzulässigen Hilfe Dritter bedient. Insbesondere habe ich wörtlich oder sinngemäß aus anderen Werken übernommene Inhalte als solche kenntlich gemacht.
3. Die Arbeit oder Teile davon habe ich bislang nicht an einer Hochschule des In- oder Auslands als Bestandteil einer Prüfungs- oder Qualifikationsleistung vorgelegt.
4. Die Richtigkeit der vorstehenden Erklärungen bestätige ich.
5. Die Bedeutung der eidesstattlichen Versicherung und die strafrechtlichen Folgen einer unrichtigen oder unvollständigen eidesstattlichen Versicherung sind mir bekannt.

Ich versichere an Eides statt, dass ich nach bestem Wissen die reine Wahrheit erklärt und nichts verschwiegen habe.

_____ _____

Ort und Datum Unterschrift R. Berg